Vol. I

Plasma Physics and Controlled Nuclear Fusion Research

CONFERENCE PROCEEDINGS, NOVOSIBIRSK, 1-7 AUGUST 1968

INTERNATIONAL ATOMIC ENERGY AGENCY, VIENNA, 1969

PLASMA PHYSICS AND CONTROLLED NUCLEAR FUSION RESEARCH

VOL. I

The following States are Members of the International Atomic Energy Agency:

AFGHANISTAN
ALBANIA
ALGERIA
ARGENTINA
AUSTRALIA
AUSTRIA
BELGIUM
BOLIVIA
BRAZIL
BULGARIA
BURMA
BYELORUSSIAN SOVIET SOCIALIST REPUBLIC
CAMBODIA
CAMEROON
CANADA
CEYLON
CHILE
CHINA
COLOMBIA
CONGO, DEMOCRATIC REPUBLIC OF
COSTA RICA
CUBA
CYPRUS
CZECHOSLOVAK SOCIALIST REPUBLIC
DENMARK
DOMINICAN REPUBLIC
ECUADOR
EL SALVADOR
ETHIOPIA
FINLAND
FRANCE
GABON
GERMANY, FEDERAL REPUBLIC OF
GHANA
GREECE
GUATEMALA
HAITI
HOLY SEE
HUNGARY
ICELAND
INDIA
INDONESIA
IRAN
IRAQ
ISRAEL
ITALY
IVORY COAST
JAMAICA
JAPAN
JORDAN
KENYA
KOREA, REPUBLIC OF
KUWAIT
LEBANON
LIBERIA
LIBYA
LUXEMBOURG
MADAGASCAR
MALI
MEXICO
MONACO
MOROCCO
NETHERLANDS
NEW ZEALAND
NICARAGUA
NIGERIA
NORWAY
PAKISTAN
PANAMA
PARAGUAY
PERU
PHILIPPINES
POLAND
PORTUGAL
ROMANIA
SAUDI ARABIA
SENEGAL
SIERRA LEONE
SINGAPORE
SOUTH AFRICA
SPAIN
SUDAN
SWEDEN
SWITZERLAND
SYRIAN ARAB REPUBLIC
THAILAND
TUNISIA
TURKEY
UGANDA
UKRAINIAN SOVIET SOCIALIST REPUBLIC
UNION OF SOVIET SOCIALIST REPUBLICS
UNITED ARAB REPUBLIC
UNITED KINGDOM OF GREAT BRITAIN AND NORTHERN IRELAND
UNITED STATES OF AMERICA
URUGUAY
VENEZUELA
VIET-NAM
YUGOSLAVIA

The Agency's Statute was approved on 23 October 1956 by the Conference on the Statute of the IAEA held at United Nations Headquarters, New York; it entered into force on 29 July 1957. The Headquarters of the Agency are situated in Vienna. Its principal objective is "to accelerate and enlarge the contribution of atomic energy to peace, health and prosperity throughout the world".

Printed by the IAEA in Austria
January 1969

PROCEEDINGS SERIES

PLASMA PHYSICS AND CONTROLLED NUCLEAR FUSION RESEARCH

PROCEEDINGS OF THE THIRD
INTERNATIONAL CONFERENCE ON PLASMA PHYSICS
AND CONTROLLED NUCLEAR FUSION RESEARCH
HELD BY THE
INTERNATIONAL ATOMIC ENERGY AGENCY
AT NOVOSIBIRSK, 1 - 7 AUGUST 1968

In two volumes

VOL.I

INTERNATIONAL ATOMIC ENERGY AGENCY,
VIENNA, 1969

PLASMA PHYSICS AND CONTROLLED NUCLEAR FUSION RESEARCH
(Proceedings Series)

ABSTRACT. Proceedings of the Third Conference on this matter convened by the IAEA and held at Novosibirsk, 1-7 August 1968. The meeting was attended by more than 400 participants from 24 countries.

Contents: (Vol.I) Summary of the Conference (4 papers); Shock waves (8 papers); Toroidal confinement I (Tokamak, Zeta, etc.) (11 papers); Toroidal confinement II (Multipoles, etc.) (9 papers); Toroidal confinement III (Stellarators) (9 papers); Drift waves and non-linear phenomena (15 papers); Toroidal confinement IV (Theory), Laser-produced plasmas, Astron (9 papers).

(Vol.II) Plasma focus, Confinement by neutral gas, Instabilities and waves (16 papers); Open-ended systems I (Mirrors) (11 papers); HF heating, confinement and stabilization (13 papers); Open-ended systems II (Theta pinch)(12 papers); Turbulent heating, Beam-plasma interaction (10 papers).

Each paper is in its original language (80 English, 37 Russian and 10 French) and is preceded by an abstract in English with one in the original language if this is not English. The discussions are in English.

(Vol.I: 998 pp., Vol.II: approx. 980 pp., 16 × 24 cm, paper-bound, 968 figures; 1968)

Price: Vol.I: US $23.00; £9.11.8

PLASMA PHYSICS AND CONTROLLED NUCLEAR FUSION RESEARCH
IAEA, VIENNA, 1969
STI/PUB/192

FOREWORD

As has often been stated, the achievement of controlled fusion would be the ultimate solution of the earth's energy problems. Thus it is one of the most important scientific quests of our time, or perhaps of all time.

The International Atomic Energy Agency has shared in this quest by sponsoring international conferences on fusion in 1961 at Salzburg and in 1965 at Culham, following the first open exchange of information at the 1958 Geneva Conference on the Peaceful Uses of Atomic Energy. In 1961 the Agency also founded the journal Nuclear Fusion. In accordance with its continued strong interest in this subject, it recently sponsored the Third Conference on Plasma Physics and Controlled Nuclear Fusion Research, which was held in Novosibirsk, USSR, on 1-7 August 1968. The Conference, attended by more than 400 participants from 24 countries, took place with the full cooperation and support of the government of the USSR and the Institute of Nuclear Physics of the Siberian Academy of Sciences. The present two-volume publication contains the complete proceedings of the Novosibirsk Conference, including the discussions. The texts of the 123 topical papers, from 14 countries, are here published in the original languages. The 34 papers presented here in Russian will be published in English translation in Nuclear Fusion early in 1969.

Current research on fusion ranges from basic plasma physics studies, which provide a foundation for fusion research as well as constituting a scientific discipline in their own right, to work on the large experimental devices such as Tokamaks, stellarators, pinches, wherein perceptible progress is being made toward the main objective: longer containment of hot plasma. The programme of the Novosibirsk Conference reflects this range of research effort and provides a balanced presentation of the current progress in the various approaches. Sincere thanks are due to the authors and the scientific institutions they represent, and gratitude is expressed to the USSR authorities for their hospitality and their help in arranging the meeting.

EDITORIAL NOTE

The papers and discussions incorporated in the proceedings published by the International Atomic Energy Agency are edited by the Agency's editorial staff to the extent considered necessary for the reader's assistance. The views expressed and the general style adopted remain, however, the responsibility of the named authors or participants.

For the sake of speed of publication the present Proceedings have been printed by composition typing and photo-offset lithography. Within the limitations imposed by this method, every effort has been made to maintain a high editorial standard; in particular, the units and symbols employed are to the fullest practicable extent those standardized or recommended by the competent international scientific bodies.

The affiliations of authors are those given at the time of nomination.

The use in these Proceedings of particular designations of countries or territories does not imply any judgement by the Agency as to the legal status of such countries or territories, of their authorities and institutions or of the delimitation of their boundaries.

The mention of specific companies or of their products or brand-names does not imply any endorsement or recommendation on the part of the International Atomic Energy Agency.

CONTENTS OF VOL. I

SUMMARY OF CONFERENCE

SHOCK WAVES (Session A)

TOROIDAL CONFINEMENT I (TOKAMAK, ZETA, etc.) (Session B)

TOROIDAL CONFINEMENT II (MULTIPOLES, etc.) (Session C)

TOROIDAL CONFINEMENT III (STELLARATORS) (Session D)

DRIFT WAVES AND NON-LINEAR PHENOMENA (Session E)

TOROIDAL CONFINEMENT IV (THEORY), LASER-PRODUCED PLASMAS, ASTRON (Session F)

SUMMARY OF CONFERENCE

The papers on pages 11, 33 and 43 are English translations of the preceding papers.

ОБЗОР ПО ЗАМКНУТЫМ ПЛАЗМЕННЫМ СИСТЕМАМ

Л.А.АРЦИМОВИЧ
ИНСТИТУТ АТОМНОЙ ЭНЕРГИИ
им. И.В.КУРЧАТОВА, МОСКВА,
СОЮЗ СОВЕТСКИХ СОЦИАЛИСТИЧЕСКИХ
РЕСПУБЛИК

При распределении тематики между участниками данной дискуссии на мою долю достался обзор экспериментов по замкнутым плазменным системам.

Следует отметить, что при анализе различных экспериментальных программ не всегда удается провести строгое различие между замкнутыми и открытыми системами. Так, например, системы типа тета-пинча, которые обычно относятся к классу открытых, при определенных условиях приобретают такую структуру магнитного поля, что в них образуется замкнутая плазменная конфигурация. Ввиду такой неопределенности я постараюсь еще больше ограничить предмет обзора и буду касаться только замкнутых систем с относительно небольшой величиной β. К этой категории относятся стеллараторы, различные типы так называемых мультиполей, тороидальные установки с аксиальной симметрией и омическим нагревом (наиболее известными представителями которых являются Зета и Токамак), а также некоторые другие системы, как, например, винтовой тороидальный тета-пинч.

Моя основная задача заключается в том, чтобы дать краткий обзор развития экспериментальных исследований по замкнутым системам за последние три года. Таким образом, фоном для сравнения будет служить состояние проблемы в том виде, как оно представлялось во время конференции в Калэме в 1965 году. Такое сравнение полезно для того, чтобы лучше оценить общие тенденции развития и удельный вес различных направлений исследований. Заметим, что даже яркие результаты, достигнутые ранее, блекнут, если дальнейшее движение тормозится. И наоборот, непрерывное и успешное продвижение вперед может вновь привлечь интерес к тем направлениям экспериментов, которые ранее казались потерявшими значения. Напомним вкратце ситуацию, которая существовала в выбранный нами исходный момент времени. Начнем со стеллараторной программы. Итогом экспериментальных исследований, проведенных на различных моделях стеллараторов в Принстоне, в 1965 году явилось подтверждение формулы Бома для скорости ухода частиц из плазмы. Результаты измерений времени жизни частиц в широком интервале изменения основных параметров процесса (плотность, температура, напряженность магнитного поля) находились в очень хорошем согласии с этой знаменитой формулой. Однако, причины быстрого ухода частиц из плазмы оставались неясными. Этот уход мог быть обусловлен действием различных форм неустойчивости. Тем не менее, нельзя было полностью исключить предположение о том, что аномально большой коэффициент диффузии в системах с такой сложной геометрией поля, как стелларатор, может объясняться также несовершенством магнитной структуры, т.е. разрушением магнитных поверхностей (заметим, что существование настоящих магнитных поверхностей в стеллараторе никогда не было математически доказано).

Естественно, что такая ситуация должна была обязательно привести к разработке новой широкой программы исследований. Эта программа, конечная цель которой заключается в выяснении физического механизма аномальной диффузии в замкнутых магнитных системах, складывается из следующих главных пунктов:

1. Изучение свойств стелларатора как магнитной ловушки для отдельных заряженных частиц.

2. Исследование процессов диффузии в так называемых Q-машинах, в которых с помощью термической ионизации металлических паров создается квазистационарная низкотемпературная плазма, не возмущаемая прохождением тока.

3. Изучение влияния геометрии магнитного поля на диффузионные процессы в плазме с помощью установок, получивших название мультиполей.

В таких системах с внутренними проводниками, подвешенными в плазме, можно в широких пределах изменять две основные характеристики магнитного поля, которые должны определять, согласно теории, устойчивость плазменных конфигураций. Эти характеристики – глубина магнитной ямы и величина шира. Кроме того, естественно, нужно было продолжать изучение существовавших стеллараторных установок с целью получения более подробной информации о зависимости между скоростью диффузии и основными параметрами системы.

Результаты работ по указанной программе занимают значительное место в тематике данной конференции. Прежде чем говорить об этих результатах, однако, нужно сказать несколько слов о том, в каком положении три года назад находились другие элементы рассматриваемой проблематики.

Тороидальная установка Зета в течение ряда лет изнемогала под тяжким бременем крупномасштабных магнитогидродинамических неустойчивостей, и большинству из нас излечение этой болезни казалось безнадежным. На конференции в Калэме появились, однако, первые указания на то, что в некоторых режимах амплитуда высокочастотных колебаний и скорость ухода частиц из плазмы в этой установке резко уменьшаются. Такой результат стимулировал дальнейшее развитие работ на установке Зета.

На установках семейства Токамак была подтверждена магнитогидродинамическая устойчивость системы при выполнении критерия Крускала-Шафранова, но потери энергии оставались аномальными. Запас накопленной экспериментальной информации был недостаточен для того, чтобы установить какие-либо количественные закономерности, связывающие время удержания энергии в плазме с параметрами процесса. Тем не менее, уже на этой стадии было поднято знамя борьбы за освобождение от формулы Бома и удалось превзойти бомовские времена в несколько раз. Направление дальнейших разработок по программе Токамак было достаточно ясным. Нужно было расширять диапазон изменения основных параметров, использовать более разнообразные диагностические методики и перейти к более систематическому накоплению экспериментального материала.

Я не буду останавливаться на характеристиках других замкнутых плазменных ловушек, поскольку в 1965 году результаты исследований, проведенных на них, не укладывались в достаточно определенную картину.

После рассмотрения общей характеристики начальных условий и тенденций развития экспериментов перейдем к обсуждению итогов данной конференции. Это обсуждение снова начнем со стеллараторов, затем обратимся к мультиполям и закончим системами с аксиальной симметрией.

Отметим прежде всего эксперименты с тритием, проведенные в Калэме на тщательно изготовленной стеллараторной установке "Класп". В этих экспериментах впервые было показано, что стелларатор, при надлежащем исполнении магнитной системы, является хорошей ловушкой для отдельных заряженных частиц. Вместе с тем было выяснено, при каких нарушениях правильной геометрии поля начинается резкое уменьшение времени удержания. Мне кажется, что в дальнейшем было бы желательно провести аналогичные опыты и на других существующих стеллараторах для проверки качества магнитной структуры.

На стеллараторе Физического института им. П.Н.Лебедева АН СССР была установлена четкая связь между структурой магнитного поля и временем удержания плазмы. Когда при изменении угла вращательного преобразования возникает резонансное расщепление магнитных поверхностей, то одновременно резко уменьшается время удержания.

В Гархинге в течение ряда лет ведутся работы по удержанию в стеллараторе низкотемпературной плазмы, получаемой методом термической ионизации. Результаты этих работ заслуживают внимания, так как в них впервые для плазмы получены времена удержания, близкие к тем, которые предсказываются классической теорией диффузии (и более чем на порядок величины превосходящие бомовские времена). Эксперименты, из которых следует этот вывод, представляются достаточно убедительными. В особенности это относится к опытам с бариевой плазмой, проводимым на новом стеллараторе "Вендельштейн II". Однако следует с осторожностью относиться к экстраполяции этих результатов для случая высокотемпературной плазмы.

Интересные эксперименты с плазмой низкой плотности были выполнены на Новосибирском стеллараторе. В этих экспериментах была исследована зависимость скорости диффузии от напряженности магнитного поля как в бесстолкновительном режиме, так и в режиме с малой длиной пробега заряженных частиц. Установлено, что скорость диффузии всегда изменяется обратно пропорционально квадрату напряженности магнитного поля, причем для случая, когда столкновения играют существенную роль, абсолютная величина скорости диффузии приближается к величине, которую дает классическая теория. Результаты измерений в Новосибирске хорошо сходятся с закономерностями, найденными в Гархинге.

Очень большая программа экспериментов была выполнена в Принстоне на большом стеллараторе С. Для плазмы, изготовляемой самыми различными методами, изучалась зависимость удержания от основных параметров. Новые измерения показывают, что при некоторых условиях времена удержания τ могут значительно превосходить величины, предсказываемые формулой Бома. Однако до сих пор еще не удалось установить однозначное соотношение между отношением τ/τ_B и параметрами системы. На стеллараторе С впервые была предпринята попытка найти связь между удержанием плазмы и флуктуациями концентрации и электрического поля в плазме. Результаты этого исследования, по-видимому, можно сформулировать следующим образом: если отношение продольной дрейфовой скорости электронов u_e (при наличии тока) и тепловой скорости ионов v_i превосходят единицу, то наблюдается прямая связь между флуктуациями и скоростью ухода частицы с плазмы. В противном случае, т.е. при $u_e/v_i < 1$, корреляция между скоростью ухода частиц и амплитудой флуктуации отсутствует. Интересным физическим эффектом является обнаружение на стеллараторе С аномального сопротивления плазмы. Данные, полученные при исследовании этого явления, смыкаются с результатами аналогичных исследований, выполненных на установках Токамак (при бо́льших напряженностях электрического поля).

Перечисленные экспериментальные результаты выбраны мной с известным произволом, и на их основе можно получить лишь поверхностное впечатление об общем состоянии вопроса. Однако, если привлечь для рассмотрения всю совокупность фактов из различных работ, то, к сожалению, все же не удастся составить достаточно определенную картину процессов, от которых зависит удержание плазмы в стеллараторах. Даже чисто феноменологические закономерности, касающиеся времени удержания плазмы в стеллараторах, нельзя считать сейчас однозначно установленными для широкого интервала изменения параметров.

Приходится поэтому констатировать, что для создания прочного научного фундамента стеллараторной программы нужны дальнейшие усилия. Развитию работ в этом направлении будет способствовать ввод в строй новых стеллараторных установок. В связи с этим следует отметить, что недавно в Харькове была введена в действие большая установка "Ураган", рассчитанная на различные методы создания горячей плазмы. Характерная особенность магнитной системы "Ураган" состоит в том, что величина шира может достигать относительно больших значений (до 0,1).

Наряду с непосредственным "физическим" экспериментированием, большое значение в дальнейшем могут приобрести "математические" эксперименты с плазмой как коллективом частиц на электронных вычислительных машинах. Надо приветствовать первые успехи, достигнутые в этом направлении в Принстоне.

Программа исследований на мультиполях первоначально казалась очень многообещающей, поскольку в таких системах можно в широких пределах изменять параметры, влияющие на устойчивость плазмы. Однако приходится признать, что наши ожидания пока еще не сбылись. На существующих мультипольных системах не удалось установить однозначные закономерности, связывающие время удержания с геометрией магнитного поля. Неожиданную неудачу потерпели также попытки установить в мультипольных устройствах связь между флуктуациями и скоростью ухода частиц. По-видимому, в существующих системах из-за наличия подвесок, проходящих через плазму, или же из-за наличия сильных электрических полей при индукционной подвеске внутренних проводников эквипотенциальные и магнитные поверхности не совпадают друг с другом, и это вызывает дополнительный уход частиц. В настоящее время остается надежда на то, что положение радикально изменится после перехода к сверхпроводящим мультиполям (с индукционным удержанием). Очевидно, что разработка этой новой техники займет продолжительное время, а поэтому новые результаты появятся только к следующей международной конференции.

Обратимся теперь к тороидальным установкам с аксиальной симметрией. Прежде всего нужно отметить очень важные и обнадеживающие результаты, полученные на Зете при детальном изучении так называемых "спокойных"("quiescent") режимов, обнаруженных несколько лет тому назад. Проведенные эксперименты показали, что при определенных начальных условиях в системе на некоторой стадии процесса самопроизвольно создается такая конфигурация магнитных полей, которая обеспечивает магнитогидродинамическую стабильность, и как следствие — высокое время удержания энергии и эффективный нагрев плазмы. Длительность "спокойной" фазы, по-видимому, связана со скин-временем для внешней оболочки плазменного шнура. Достигаемые в спокойных режимах времена удержания измеряются несколькими миллисекундами и во много раз превосходят бомовские времена.

Вполне возможно, что в дальнейшем при переходе к бо́льшим магнитным полям и бо́льшим силам тока в установках типа Зеты удастся значительно увеличить длительность "спокойного" периода и в результате получать плазму с очень высокими параметрами.

На установках Токамак основные усилия были направлены на выяснение закономерностей нагревания плазмы и, в частности, на изучение зависимости времени удержания энергии и времени удержания частиц от основных физических параметров. Установлено, что время удержания τ_E быстро растет с возрастанием силы тока в плазме и не зависит от напряженности продольного магнитного поля. По-видимому, также можно считать, что τ_E увеличивается с повышением температуры, поскольку мы наблюдаем возрастание τ_E во время процесса при почти постоянной величине H_φ. Таким образом, в Токамаках пока не наблюдается ухудшения термоизоляции с ростом температуры, предсказываемым формулой Бома. Отношение τ_E/τ_B в режимах с высокой температурой и высокой плотностью на установках Токамак достигает величины порядка 30. Приведенные результаты создают уверенность в том, что при дальнейшей интенсификации процессов в системах Токамак можно будет продвинуться значительно дальше по пути получения все более высоких температур и все бо́льших времен удержания плазмы. При этом не исключено (хотя и не доказано), что при достаточно высоких температурах уход частиц и потери энергии в Токамаках будут определяться чисто классическими механизмами диффузии и теплопроводности на так называемых запертых частицах. Если бы это оказалось справедливым, то можно было бы сказать, что физические процессы в Токамаках в основных чертах поняты. Вполне возможно, однако, что какая-либо из многочисленных неустойчивостей может развеять эти надежды.

При оценке дальнейших перспектив разработки кольцевых систем с омическим нагревом плазмы нельзя забывать о том, что при высоких температурах этот метод нагрева очень неэффективен, и даже при самых оптимистических ожиданиях вряд ли удастся с помощью простого омического нагрева поднять температуру плазмы выше нескольких киловольт. Поэтому одной из важнейших задач на будущее является разработка новых методов нагревания плазмы в таких системах, как Зета и Токамак.

Мой обзор подходит к концу, и поэтому я бы хотел сделать несколько замечаний общего характера. У меня нет намерения нарушать границы сфер влияния, добровольно установленные участниками данной дискуссии. И все же хотелось бы сказать несколько слов о таком деликатном вопросе, как взаимоотношение между теорией и экспериментом, и о том, в частности, какой характер носят эти взаимоотношения в вопросах устойчивости плазменных конфигураций. За время разработки нашей проблемы, т.е. за 10-15 лет, теоретический анализ дал ряд сильных результатов, которые могут восприниматься не только количественно, но даже грубо качественно, так как использование этих результатов позволяет установить отчетливые границы перехода между существенно разными состояниями плазмы. Сюда относятся: критерий Крускала-Шафранова, идея минимума В, идея о подавлении крупномасштабных плазменных деформаций широм, условия перехода электронов в режим ускорения и развития пучковых неустойчивостей. Эти достижения теории вошли в плоть и кровь современной физики высокотемпературной плазмы и стали рабочим инструментом экспериментаторов. За последние годы главным направлением теоретических исследований стал анализ чрезвычайно многочисленных и трудно различимых форм различных слабых дрейфовых и резистивных неустойчивостей с относительно небольшими инкрементами нарастания. Практически весь этот анализ ведется в линейном приближении. Следует прямо сказать, что здесь теория пока еще не находит должной поддержки в эксперименте и, вероятно, не найдет до тех пор, пока теоретики не перейдут к синтезу полученных ими частных результатов, но уже на значительно более высоком нелинейном уровне.

При современном состоянии экспериментов, когда мы в основном работаем с несовершенной магнитной геометрией, с плазменными конфигурациями, для которых характерна неопределенность граничных условий и сильное взаимодействие со стенками, можно всегда в громадной картотеке неустойчивостей найти ту, которая нам больше всех других придется по вкусу. С таким же успехом вы отыщете и желательный всем стабилизирующий механизм. А в общем экспериментатор должен относиться к теории как к хорошенькой женщине: с благодарностью принимать то, что она ему дает, но не доверять ей безрассудно.

Мое второе замечание сводится к следующему. Затруднения, с которыми мы сейчас встречаемся при анализе физических процессов в замкнутых плазменных системах, отчасти связаны с тем, что экспериментальная программа в своем развитии была недостаточно последовательной. Следовало уделять больше внимания плазменным системам с возможно более простой конфигурацией и возможно более высокой симметрией, прежде чем изучать сложные несимметричные геометрии. Поэтому мне представляется, что в дальнейшем нужно сосредоточить больше усилий на исследовании таких относительно простых систем, как Зета, Токамак, Левитрон, круглый стелларатор. В этих системах имеются широкие возможности для изменения геометрии полей при неизменной симметрии.

Теперь я попытаюсь совершить диверсию в сторону другой сферы влияния. Часто задают вопрос: какая плазменная система лучше – замкнутая ловушка или зеркальная машина? Окончательный ответ на этот вопрос будет получен, вероятно, очень не скоро, так как обе системы этих двух классов имеют свои достоинства и недостатки. И, наконец, есть третий класс систем, в которых создаются плазменные сгустки с очень большой плотностью и очень малым временем существования. Возможно, что именно они в конечном счете одержат победу в тройном соревновании. Представляется полезным, однако, отметить одно обстоятельство. Допустим, что сравниваются две системы – замкнутая и открытая – с одинаковой плотностью плазмы и одинаковой температурой ионов. В какой из этих систем время удержания плазмы больше? Выберем в качестве открытой ловушки самую наилучшую, т.е. такую, в которой подавлены все виды неустойчивостей. В идеальной открытой ловушке длительность удержания плазмы будет порядка одного интервала времени между двумя ион-ионными столкновениями. Таким образом, соотношение между временами удержания плазмы в замкнутой системе и идеальной зеркальной ловушке по порядку величины будет просто равно числу кулоновских столкновений, которые испытывает ион в первой из этих систем за то время, пока он в ней находится. Примером может служить установка Т-3, принадлежащая к семейству Токамак. При плотности плазмы порядка $5\cdot 10^{13}$ см$^{-3}$ и температуре ионов водорода $\sim$0,5 кэв ион за время своей жизни в установке совершает несколько десятков столкновений. Таким образом, даже отнюдь не идеальная замкнутая ловушка по времени удержания в десятки раз превосходит идеальную (и еще неосуществленную) зеркальную машину. Конечно, надо честно признаться, что температура ионов еще низковата. Однако, у нас есть надежда на ее дальнейшее повышение.

Приведенное здесь сравнение отнюдь не преследует цели подкопа под программу разработки открытых ловушек. На данном этапе необходимо мирное сосуществование между различными направлениями развития исследований, посвященных проблеме управляемых термоядерных реакций. И я бы сказал больше – не только мирное сосуществование, но активное сотрудничество в рамках международного научного содружества.

Наконец, еще два слова. Чего же мы достигли по сравнению с Калэмом? Мне кажется, что один, по крайней мере, действительно важный результат был достигнут. Мы освободились от мрачного призрака громадных потерь, воплощенного в формуле Бома, и открыли путь для дальнейшего повышения температуры плазмы с выходом на физический термоядерный уровень.

Разрешите мне теперь принести искренние извинения авторам многих очень интересных работ, не упомянутых в моем обзоре по той причине, что я не обладаю способностью абсорбировать и переварить за несколько дней такой огромный объем научной информации.

SURVEY ON CLOSED PLASMA SYSTEMS

L. A. ARTSIMOVICH
I. V. KURCHATOV INSTITUTE OF ATOMIC ENERGY
MOSCOW, UNION OF SOVIET SOCIALIST REPUBLICS

In the allotment of subjects to the speakers participating in this Panel Discussion I have been assigned the task of reviewing experiments on closed plasma systems.

I should like to start by pointing out that when one is analysing various experimental programs it is not always possible to make a rigorous distinction between closed and open systems. For example, systems of the theta-pinch type, which we usually consider to be open systems, acquire under certain conditions a magnetic field structure which is such that a closed plasma configuration is formed. In view of this uncertainty I shall try to confine my review to closed systems with relatively low β - for example, stellarators, different types of the so-called multipoles, toroidal devices with axial symmetry and ohmic heating (the best known of which are Zeta and the Tokamak devices), and a number of other systems such as the helical toroidal theta-pinch.

My main task is to survey briefly the experimental studies of closed systems performed over the past three years. As a basis for comparison, I shall therefore take the state of the problem as we saw it in 1965 at the time of the Culham conference. Such a comparison is useful in that it enables one to evaluate more accurately the general trends and the relative importance of the various lines of research. It is worth bearing in mind that brilliant results achieved in the past fade if subsequent progress is slow; by the same token, a succession of advances can revive interest in lines of research which appeared to have lost their meaning.

Let us recall briefly the situation as it was at our chosen reference date, beginning with the stellarator programs. By 1965, experiments at Princeton with various stellarator models had confirmed the validity of Bohm's formula for the rate of particle escape from the plasma. Particle lifetime measurements for a wide range of parameter values (density, temperature, magnetic field strength) were found to be in very good agreement with this well-known formula. However, the reasons for the rapid escape of particles from the plasma remained obscure. It might be due to various types of instability, but one could not exclude completely the possibility that the anomalously high diffusion coefficient for systems with such a complex field geometry as that of the stellarator was also associated with imperfections in the magnetic structure, i.e. with magnetic surface destruction (it is worth noting that the existence in stellarators of real magnetic surfaces has never been proved mathematically).

This naturally led to an extensive new program of investigations, with the ultimate objective of discovering the physical mechanism of anomalous diffusion in closed magnetic systems. The principal components of the program were:

1. Study of the properties of the stellarator as a magnetic trap for individual charged particles;

2. Investigation of diffusion processes in Q-machines, in which thermal ionization of metal vapours produces quasi-stationary low-temperature plasma that is not perturbed by the passage of current;
3. Multipole studies of the influence of the magnetic field geometry on diffusion processes in the plasma.

In such systems, with internal conductors suspended in the plasma, it is possible to vary within broad limits both magnetic well depth and shear - the magnetic field characteristics which, according to theory, play a principal role in determining the stability of plasma configurations.

Naturally it was also considered necessary to pursue the study of existing stellarator devices with a view to obtaining more detailed information about the relationship between the diffusion rate and the main parameters of the system.

The results of the work performed as part of this program have been prominent at the present Conference. Before discussing these results, however, I should say a few words about the position three years ago with regard to other aspects of the subject we are considering.

For a number of years Zeta had been weighed down by the heavy burden of large-scale magnetohydrodynamic instabilities, and most of us felt that the complaint was an incurable one. At Culham, however, we saw the first indications that under certain conditions the amplitude of the high-frequency oscillations and the rate of particle escape from the plasma could be reduced drastically. These results stimulated further work with Zeta.

In devices of the Tokamak family confirmation had been obtained of the magnetohydrodynamic stability of the system when the Kruskal-Shafranov criterion was satisfied, but the energy losses remained anomalous. The amount of experimental data was insufficient to establish any quantitative connection between the duration of energy containment in the plasma and the parameters of the process.

Nevertheless, even at that stage investigators were struggling to liberate themselves from Bohm's formula and had succeeded in exceeding the Bohm times by a substantial factor. The line to follow in the Tokamak program was fairly obvious: it was necessary to extend the range of variations in the basic parameters, to use more varied diagnostic methods and to accumulate experimental data on a more systematic basis.

I shall not dwell on the characteristics of other closed plasma traps, since in 1965 the results of investigations performed with such traps did not fit into a sufficiently well-defined picture.

Having considered in general terms the initial situation and the prospective trends, let us look at the results of the present conference. I shall again start with stellarators, go on to multipoles, and finally discuss systems with axial symmetry.

Let us take the tritium experiments performed in the carefully designed "Clasp" stellarator at Culham. In these experiments it has been shown for the first time that, if the magnetic system is of suitable design, a stellarator is a good trap for individual charged particles. In addition, this work has shown which departures from the correct field geometry give rise to an abrupt decline in containment time. I think it would be useful to conduct similar experiments in other existing stellarators with a view to verifying the quality of the magnetic structure.

The precise relationship has been established, using the stellarator of the P.N. Lebedev Physics Institute, between magnetic field structure and plasma containment time. When resonance disintegration of the magnetic surfaces occurs as a result of a change in the rotational transform angle, it is accompanied by a sharp decline in the containment time.

Over a number of years, investigators at Garching have been working on the containment in a stellarator of a low-temperature plasma produced by thermal ionization. They have achieved noteworthy results, obtaining for the first time plasma containment times close to those predicted by classical diffusion theory (and more than an order of magnitude greater than the Bohm times). The experiments on which this conclusion is based are fairly convincing - particularly those performed with a barium plasma in the new Wendelstein II stellarator. However, we should be careful about extrapolating these results to high-temperature plasmas.

Interesting low-density plasma experiments have been performed with the Novosibirsk stellarator. The purpose of these experiments has been to investigate the dependence of the diffusion rate on magnetic field strength both under collisionless conditions and in a regime where the charged particles have a short path length. It has been found that the diffusion rate always varies in inverse proportion to the square of the magnetic field strength, the absolute diffusion rate approaching the value given by classical theory when collisions are significant. The measurements made in Novosibirsk are in good agreement with the results obtained at Garching.

A major experimental program has been carried out with the Model-C stellarator at Princeton. The dependence of containment on the main parameters is being studied for a plasma produced by variety of methods. Recent measurements show that under certain conditions the containment times τ significantly exceed those predicted by Bohm's formula. However, it has not yet proved possible to establish a clear relationship between the ratio τ/τ_B and the parameters of the system. First attempts to establish a correlation between plasma containment on one hand and plasma concentration and electric field fluctuations on the other have been made with the Model-C stellarator. The results of this study would appear to be the following: if the ratio of the longitudinal drift velocity of the electrons $\boldsymbol{v}_e$ (in the presence of current) to the thermal velocity of the ions v_i exceeds unity, a direct correlation is observed between the fluctuations and the rate of particle escape from the plasma. If it is less than unity, there is no correlation between the rate of particle escape and the amplitude of the fluctuations. An interesting physical phenomenon observed in the Model-C stellarator is anomalous resistance of the plasma. The data relating to this phenomenon tally with the results of similar Tokamak experiments performed with stronger electric fields.

The experimental results have been singled out by me in a somewhat arbitrary manner and give only a superficial impression of the general state of the problem. However, even if one considers all the results obtained in the relevant investigations, it is unfortunately still impossible to draw a sufficiently clear picture of the processes on which plasma containment in stellarators depends. Even the purely phenomenological pattern to which the containment time of plasmas in stellarators conforms cannot yet be considered as definitely established for major parameter variations.

We must therefore conclude that further efforts are needed to create a firm scientific basis for the stellarator research program. Work along these lines will probably result in the construction of new stellarator devices. In this connection, I would mention that a large device, the "Uragan" ("Hurricane"), designed for the production of hot plasma by various methods, recently went into operation at Kharkov. A special feature of Uragan's magnetic system is that relatively high (up to 0.1) shear values can be achieved.

In addition to direct "physical" experiments, "mathematical" computerbased experiments with the plasma considered as a body of particles may acquire considerable importance in the future. The workers at Princeton are to be congratulated on the first advances in this direction.

At first, the program of research on multipoles seemed very promising, since the parameters affecting plasma stability can be varied over a wide range in such systems. However, expectations have not yet been fulfilled. In the existing multipole systems it has not proved possible to establish a definite relationship between containment time and magnetic field geometry. Attempts to establish a relationship between fluctuations and particle escape rate in multipole devices have also unexpectedly failed. It would appear that, due to the presence of supports passing through the plasma, or to the presence of strong electric fields when the internal conductors are inductively suspended, the equipotential and magnetic surfaces do not coincide in the existing systems, and this gives rise to additional particle escape. There remains the hope that the position will change radically when superconducting multipoles (with induction containment) are adopted. However, it is obvious that, since it will take a considerable time to develop these techniqués, new results will start appearing only towards the time of the next international conference.

Let us now consider toroidal devices with axial symmetry. I should first like to draw attention to the very important and encouraging results obtained with Zeta in detailed investigations of the quiescent regimes discovered some years ago. Experiments have shown that for certain initial conditions the magnetic field configuration which ensures magnetohydrodynamic stability - and consequently long energy containment times and efficient plasma heating - is created spontaneously within the system at some stage in the process. The duration of the quiescent phase appears to be associated with the skin-time for the outer sheath of the plasma column. The containment times achieved under quiescent conditions are several milliseconds in duration and exceed the Bohm times by a substantial factor. With stronger magnetic fields and currents, it is quite possible that the duration of the quiescent period will be increased in devices of the Zeta type and that plasmas with very high parameter values will be produced.

The main effort in Tokamak experiments has been directed at investigating the plasma heating process and the dependence of energy and particle containment times on the basic physical parameters. It has been established that the energy containment time τ_E increases as the current in the plasma rises and is independent of the strength of the longitudinal magnetic field. The energy containment time may well also increase with rising temperature; we observe an increase in τ_E during experiments at almost constant H_φ. Thus, we have not yet observed in Tokamak devices the deterioration in thermal insulation with rising temperature predicted by Bohm's formula. In high-temperature and high-density regimes, the ratio τ_E / τ_B in these machines attains a value of the order of 30. In the light of the above-mentioned results we are confident that, through further investigation of the processes occurring in Tokamak systems, substantial progress will be made towards obtaining increasingly high temperature and increasingly long plasma containment times; and it is quite possible (although this has not been proved) that, at sufficiently high temperatures, energy losses and the escape of particles in Tokamak devices will be determined by the purely classical mechanisms of diffusion and heat conduction associated with trapped particles. If this proved to be the case, one could say that the basic features of the physical processes occurring in Tokamak devices have been understood. However, any one of numerous instabilities might easily dispel these hopes.

When assessing the future prospects of annular systems with ohmic heating, one should not forget that at high temperatures this method of heating is very inefficient, and even if our most optimistic expectations are realized it is hardly likely that the plasma temperature will be raised above a few kilovolts by simple ohmic heating. One of the main tasks for the future will therefore be to devise new methods of plasma heating in Zeta, Tokamak and similar systems.

Since I am approaching the end of this review, I should like to make a few general comments. I do not intend to transgress the boundaries of the spheres of influence established for those participating in this Panel Discussion. However, I should like to say a few words about the extremely delicate question of the relationship between theory and experiment, and in particular about the nature of this relationship as it affects the stability of plasma configurations.

Over the past 10-15 years theoretical analysis has yielded significant results, which we are able to interpret not only quantitatively by also in a crudely qualitative manner, since they enable us to establish clearly the boundaries between significantly different plasma states. I am thinking here of the Kruskal-Shafranov criterion, the minimum-B concept, the idea of suppressing large-scale plasma deformations by means of shear, and the conditions for the transition of electrons to an acceleration regime and for the development of beam instabilities. These achievements in the field of theory have become part of the flesh and blood of contemporary high-temperature plasma physics and the tool of the experimentalists. In recent years, however, theoretical studies have been directed principally towards the analysis of the very numerous and barely distinguishable forms of the various weak drift and resistive instabilities with relatively small growth rates. Such analyses are performed almost entirely in the linear approximation. We have to admit that in this field the theory has not yet been confirmed experimentally and that it probably will not be until the theoreticians have synthesized their various results at a significantly higher, non-linear level.

In the present state of experimental research - in which we are working essentially with an imperfect magnetic geometry and with plasma configurations that are characterized by vagueness of the boundary conditions and strong interaction with the walls - it is always possible to find in the great instability catalogue the particular instability which is most to one's liking; and with the same ease one can find the stabilizing mechanism, which suits everyone. As a general principle, we may say that the experimentalist should treat theory as he would a beautiful woman: accept with gratitude what she has to offer, but avoid trusting her completely.

My second comment concerns the difficulties which we are now encountering in our attempts to analyse the physical processes which occur in closed plasma systems. These difficulties are due partly to the fact that the conduct of the experimental program has been insufficiently consistent. Before studying complex non-symmetric geometries we should have paid more attention to plasma systems with the simplest possible configuration and the greatest possible symmetry. I therefore feel that we should in future concentrate on relatively simple systems such as Zeta, Tokamak, Levitron and the circular stellarator. In these systems there are many ways of varying the field geometry while keeping the symmetry unchanged.

I shall now attempt to create a diversion near another sphere of influence. The question is often asked as to which plasma system is better - the closed trap or the mirror machine. It is unlikely that a final answer to this question will be obtained in the near future, since both systems have their advantages and drawbacks. There is, moreover, a third system in which plasma blobs of very high density and very short lifetime are produced, and this system may eventually win the three-sided contest.

However, there is one important point which should not be overlooked. Let us assume that we are comparing two systems - a closed and an open system with identical plasma densities and identical ion temperatures. Which of these systems will give the longer plasma containment time? Let us take as our optimum an open trap in which all types of instability are suppressed. In this ideal open trap the plasma containment time would be of the order of the interval between two ion-ion collisions. Thus, the ratio of the containment time of a plasma in a closed system to that of a plasma in an ideal mirror trap would be of the same order of magnitude as the number of Coulomb collisions experienced by an ion while it is in the former system. Let us take by way of example the third device of the Tokamak family. At a plasma density of the order of 5×10^{13} cm^{-3} and a hydrogen ion temperature of the order of 0.5 keV, the ion would experience several dozen collisions while it is in the device. Thus, the containment time of a closed trap that is by no means ideal is many times greater than that of an ideal (and as yet non-existent) mirror machine. Of course, it must be admitted that the ion temperature is still rather low; but we are hoping to raise it further.

The purpose of this comparison was in no way to undermine the open trap research program. At the present stage, it is essential that there be peaceful co-existence between the various lines of controlled nuclear fusion research; in fact, I would go as far as to say: not simply peaceful co-existence, but active collaboration within the framework of international scientific collaboration.

What, then, have we accomplished since Culham? In my opinion, at least one really important result has been achieved: we have rid ourselves of the gloomy spectre of the enormous losses embodied in Bohm's formula and have opened the way for further increases in plasma temperature leading to the physical thermonuclear level.

Allow me to express my sincerest apologies to the authors of those many interesting papers which have not been mentioned in my review - for the simple reason that I am not capable of absorbing and digesting within a few days such an enormous amount of scientific information.

SUMMARY REMARKS

S. J. BUCHSBAUM
SANDIA CORPORATION, ALBUQUERQUE, NEW MEXICO,
UNITED STATES OF AMERICA

In these remarks I want to summarize those papers which deal with "low-beta" systems (high-frequency heating; acceleration and stabilization, and laser plasmas), "high-beta" systems (plasma focus), and the Astron.

Let me start with the Astron. As you know, the aim of the Astron Program is to create a cylindrical shell of rotating relativistic particles (electrons) at a sufficient level of intensity to produce a magnetic well with closed lines of force which confines the plasma. The energy of the relativistic electrons is sufficient to heat the plasma to thermonuclear energies. The most recent results from the Astron group, both theoretical and experimental, are encouraging. On the theoretical side, theorists at LRL have found, in an initial calculation, that if and when such a closed configuration is achieved, the stability of a plasma in this well is rather favourable, provided a special hollowed-out E-layer distribution can be provided. Experimentally, an injection of 300 amperes of 4 MeV electrons was achieved. This resulted in a field reversal of 6% from an E-layer having a length of about 2 metres. Moreover, at this intensity, the E-layer precessed stably and rigidly, in a sense and at a frequency which were predicted by theory. This, I believe, is an important result. The idea that a 2-metre long shell of electrons precessed like a rigid body, I (for one) find a little incredible. Now this value of 6% is some 10 times greater than what was achieved at Culham. But many problems remain, such as understanding what happens during injection; how to tailor the distribution of the E-layer particles to suit one's fancy or need; how to achieve trapping in a vacuum rather than a residual gas, and many other problems. Not the least among those other problems is how to proceed ultimately from MeV electrons to GeV protons. But, Dr. Christofilos assures me that by the time of the next conference, three years from now, the 6% which I quoted will have become at least 60% or very close to the value needed for field reversal.

I should like now to touch on high-beta research. I think that high-beta research has come of age in the last few years. Let me explain what I mean by this statement. Until very recently, all or nearly all experiments in this field were <u>with</u> high-beta plasma. The plasma was not stable long enough for meaningful experiments to be performed <u>on</u> the plasma. Now the situation is different. Reports are presented at this conference on experiments on theta-pinch devices, in which the plasma is stable for sufficiently long times (10 or 20 microseconds) for the high-beta plasma to be regarded as just another plasma column - not quite the plasma column of a Q-machine, but a plasma column nonetheless. On such a plasma column one can do experiments. Specifically, by an ingenious method an $\ell = 0$ bump of controllable amplitude was able to be induced in the plasma, and the growth or the absence of growth of the stability induced by this bump could be studied experimentally. It was studied in a beautiful experiment at Culham, in which the growth of this Haas-Wesson instability was observed to be in agreement with theory. The Culham experiment was on collisional plasma; that is, one in which the mean free path was short compared to the eight-metre length of the column. In the Los Alamos machine a similar experiment was done on a collisionless plasma. Here, no growth was observed for reasons not quite understood. Conditions in this experiment were such that the experimentor was able to do experiments on effects of turbulent heating and on the excitation of the Kruskal-Shafranov modes.

Returning to the Culham experiments, there is one very significant result, I think. In these experiments radial losses were measured to be at least 200 times smaller than the calculated Bohm loss, when the sheath was diffuse, and they were in the order of Bohm losses when the sheath was very thin. Now, in a thin sheath one can expect turbulence because of the electron-ion acoustic-wave instabilities. So, this result perhaps is not so surprising. But the fact that the losses are observed to be nearly classical when the sheath is diffuse is, I think, very encouraging.

Turning to closed high-beta systems, we also learn of a possible way of stabilization of a short toroidal theta pinch, i.e. a theta pinch which is formed by trapping a reversed-bias field. This is done by passing a hard core through the pinch which carries a heavy current. The current returns, not through the plasma, but through conductors which are located outside the plasma. As Dr. Kolb points out, there are very interesting similarities between this device and the Tokomak. They have similar properties of shear, well-depth, etc. In the Jutphaas experiments, a toroidal screw pinch, it was discovered that a cold "pressureless" plasma outside the pinch can provide some stabilization against the Kruskal-Shafranov modes.

I think the most ambitious undertaking in this field is that of the Los Alamos group, and that is the very large toroidal device, Scyllac. Scyllac will ultimately become a fast toroidal pinch with a diameter of about five metres. In such a device, one has to worry about equilibrium, and one has to worry about whether or not dynamic stabilization is necessary. In a size of Scyllac, dynamic stabilization is difficult and expensive. A group at New York University presents a theoretical analysis of a certain configuration for which equilibrium may be assured without dynamic stabilization (paper C-24/K-6). If dynamic stabilization is necessary, there are papers (especially from the Leningrad group) stating that such stabilization should be possible, because it appears to work on lower-beta systems, both toroidal and linear.

A very interesting little gadget in high-beta research is the plasma focus. From a specially shaped co-axial gun a small-volume plasma is produced which is stable during a radial collapse. It is of a very high density (10^{19} cm^{-3} or more), has a very high temperature, lasts a very short time (a small fraction of a microsecond), but puts out very copious neutrons. This device, whose plasma contains more than 10^{17} particles at temperatures of a few keV, seems to me a good injector for low-beta open systems in lieu of some of the other injection devices being used today. There has been much work on this system as measured by five papers from five different groups. Very thorough measurements have been done: spectroscopic studies, neutron measurements, X-rays and so on. The predominant, but not unanimous, opinion has it that the neutrons originate from a thermal plasma which is moving longitudinally at a velocity of 10^7 to 10^8 cm/s while it is collapsing radially. An interesting off-shoot of this work is that described by Dr. Morozov. He has introduced the important idea of "isomagnetic flow" which can stabilize the most dangerous (m = 0) instability of a z-pinch. The possibility therefore arises of a continuous, flow-stabilized z-pinch with some reactor possibilities. Some of these ideas have been tested experimentally. By pulsing the neutral gas, the stability time was extended from fractions of microseconds to a few tens of microseconds, although at a considerable reduction in density and in temperature of the plasma.

I now turn to low-beta research. At the Culham Conference it was shown beyond any doubt that Ioffe was right and that in a minimum-B configuration all dangerous modes are suppressed, that is, all modes of low frequency such that the magnetic moment of the particles is conserved. But at Culham there were also the first papers on the loss-cone instability. The subject of the loss instability has been with the mirror people ever since, both theoretically and experimentally, and will be with them for a considerable time to come. But this is nothing to be disheartened about. Again, judging from the papers and discussions in this conference, very considerable progress has been made both in the theoretical understanding of loss-cone instabilities and in the experimental elucidation of these instabilities. I am not going to discuss theory here, except to say that, in spite of the fact that some new instabilities are discussed here (in particular, the so-called modified or average-negative-mass instability), I think that this subject is rather well understood so far as the onset of instabilities is concerned – understood theoretically, that is. If any new surprises appear, they are not going to be shocking surprises. What is not understood is how these instabilities grow to the non-linear regime and how they affect the particle loss from the device.

The mirror machine is a simple machine. It is flexible, unlike many of the toroidal devices – even the axially symmetric toroids. It is accessible to diagnostics. One can control plasma parameters much more readily than in a toroidal machine. Whether or not these devices have reactor possibilities is not, I believe, that important to-day when there is so much yet to be learned about the plasma in a magnetic field. What one learns about mirror machines will be of interest to many devices – not just open-ended devices, and because of flexibility of the mirror machine, the various loss-cone instabilities can be studied one by one, unlike the situation in toroidal machines.

We are shown at least two very beautiful examples of this point. The modified or average-negative-mass instability has been studied in a very nice experiment in the DCX-2 machine at Oak Ridge and possibly identified in Ioffe's PR-5 machine and in the DECA experiment. In the Phoenix machine in a really beautiful experiment the Harris instability (modified by finite geometry) has been studied very thoroughly as a function of a variety of experimental parameters, their effect on the growth rate, and so on. I think this is just the beginning. I think that many, if not all of those modes, will fall to the experimentor sooner or later. However, many puzzles remain. For example, what has happened to the drift cyclotron instability which was supposed to be so prevalent? At Culham, Dr. Ioffe discussed the results of the PR-5 experiment and suggested that this was the instability that was possibly responsible for the very fast decay time which he observed early when the density was high. So he built a larger machine (PR-6) in which he could vary the strength of the magnetic field. Theory says that the threshold for the instability goes up very rapidly in the magnetic field. Unfortunately, he did not observe the theoretically predicted result. What he did observe was that the decay-rate varied as a function of the radial well depth, for reasons which are not yet clear.

There are other puzzles. The 2X machine and the MTSE machine yield different results. They use similar magnetic fields; they have similar plasma parameters: high temperature, high density, beta of a few per cent. By the way, this is the reason why I put quotation marks around the word "low-beta": a few per cent is not really low. They use guns, although different guns, for injection. Yet in the MTSE machine the loss is apparently classical, except for some anomalous electron cooling, while in the 2X machine it remains anomalously high. There are experimental differences which the experimentalist waves his hand about. He states that in the MTSE the trapping is very fast so that not all the gun plasma is trapped. It may move around the machine and provide some line-tying or warm plasma stabilization. This is not so in the 2X machine. In the 2X machine purity is achieved by coating its walls with titanium while in the MTSE machine purity is achieved by just moving the walls away. These experimental differences are frustrating. After all, we ought to ultimately wind up with a standard plasma in a standard mirror machine whose properties and characteristics are determined by the plasma parameters within the machine and not by its history.

As there are puzzling things there are also heartening things. In a 2X machine the decay rate is lower the higher the initial density, for reasons not quite understood, but there it is. While the classical loss in MTSE is hard to understand, there it is.

In the beam-injected plasmas there are heartening things. The decay of the plasma after the beam is turned off is stable, as a result of the energy broadening which the turbulence of the instability prior to beam shut-off induced in the ion distribution. There is evidence that if one broadens the beam energy distribution prior to injection the density threshold for the instability goes up. There is evidence both from the Phoenix experiment and the Alice experiment that one can suppress some of the rf activity connected with the instability by heating the electrons with microwaves. (This heating will bring me to my next subject.) There is evidence that one can fool the instability (i.e. by adjusting cleverly the boundary conditions and/or by feedback as in the Ogra experiment), and suppress its amplitude by better than an order of magnitude. Those working on the Ogra succeeded in suppressing a flute instability and a cyclotron resonance instability at the fundamental. So there are things that the experimentalist has up his sleeve which I am sure he will bring out in the next few years.

The question of heating of the electrons in a mirror machine brings me to my next point. At this conference there are many experimental and theoretical papers on high-frequency heating, acceleration, and stabilization of plasmas in open systems. I think that there is not enough communication between the two sets of people, the "mirror-machine" people and the "high-frequency" people. If the mirror-machine people are to do good experiments, they have to know and understand exactly what happens when they apply a microwave field to their machine, and I do not think that they understand now. The heating experiments discussed in this conference are of very great variety. They are concerned primarily with collisionless heating, relying either on resonance absorption or on stochastic heating. Conversion of energy from the electro-magnetic wave to the plasma can occur because of density gradients, magnetic field gradients, etc. I have no time to discuss all results, but I want to select two examples which strike me as being the most important.

When one applies a microwave field to a plasma, the largest density normally reached is such that the plasma frequency is of the order of the microwave frequency. It is very hard to go beyond this because of cutoff conditions. Yet it was shown here in a formal paper from the Ioffe Institute and in an informal remark from Brussels, that densities which are by two orders of magnitude above the critical density can be achieved if the experimental conditions are suitably arranged. Also, in the past, plasmas produced by microwave fields were unstable at low pressures (pressures lower than 10^{-5} torr). This result, of course, is not good if microwave plasmas are to be used in mirror machines. In a paper from Oak Ridge it is shown that, by producing the plasma in a minimum-B geometry, the instability disappears and plasmas at pressures as low as 5×10^{-7} can be produced stably, although the highest density that they could achieve so far was about a factor of 10 lower than the critical density. This is an interesting plasma for use as a target for injection of a high-energy atomic beam because of additional trapping that the plasma produces and because of the additional stabilization that Landau damping by hot electrons produces. I still think, however, that not enough is known and understood about the properties of a microwave-heated plasma, where one gets two classes of electrons, one at high energy and one at low energy, and where one does not know the real distribution in space and energy. I am sure that these things will come in time.

Many papers on acceleration by rf fields are discussed. The one that strikes my fancy is that from France, where a plasma produced by a relatively small laser is accelerated by the application of microwave fields with suitable gradients. Again these devices can be used for injection into mirror machines to get around some of the difficulties one has with guns, especially the purity difficulty.

Let me conclude by talking about the laser plasmas. We have learned that by using a laser pulse on a small particle – a laser pulse of the order of 5 to 50 joules with a duration of 5 to 50 nanoseconds - plasmas with a total number of particles of 10^{15} to 10^{17} can be obtained at temperatures on the order of 100 electron volts. These are interesting plasmas for their own sake, but they are still not of great interest for thermonuclear research. If one had a laser with an energy of 100 joules and a pulse duration of 10^{-10} seconds to 10^{-11} seconds (at a peak power of 10^{12} to 10^{13} watts), there would be efficient heating before the plasmas had time to expand. Then 10^{17} or so particles would be available at energies of 1 to 2 kilovolts. Such plasmas would be of great interest for injection into mirror machines, or indeed into stellarators or other toroidal machines. It is fortunate that this is the direction in which this research is going. Such a laser already exists in the Lebedev Institute, where Professor Basov is working. Unfortunately, he is not a participant in this conference. Let me point out that the peak power of 10^{12} watts is five times greater than the total average electrical output of the United States. That just goes to show how short a time of 10^{-10} seconds is.

Finally, I find it quite interesting to note that throughout this Conference only two speakers refer directly or indirectly to the Lawson criterion. This does not mean that we do not have the ultimate goal of CTR in mind. It does mean, I think, that we have chosen to reach this goal through a thorough understanding of the behaviour of a plasma in the magnetic field. This is progress.

THEORIE ET PHENOMENES DE BASE

M. TROCHERIS
CEA FONTENAY-AUX-ROSES, FRANCE

Le sujet de cet exposé a été défini, en fait, par différence avec les deux autres rapports qui traitent essentiellement des configurations fermées et des configurations ouvertes. Je tenterai donc de résumer les résultats apportés par les communications théoriques et par les communications expérimentales qui ne traitent pas directement du confinement magnétique, c'est-à-dire celles qui étudient les phénomènes de base, tels que les processus dissipatifs sans collisions, les ondes et les micro-instabilités.

A vrai dire cette division des sujets ne s'applique pas bien aux communications théoriques. Une partie de ces communications traite directement de l'équilibre ou de la stabilité du plasma dans les configurations fermées ou ouvertes et je commencerai par les rappeler brièvement.

A. THEORIE

La proportion de communications théoriques apparaît moins grande que dans les conférences précédentes. Mais il y a surtout un changement dans la nature des travaux. Par exemple, il y a très peu d'instabilités vraiment nouvelles. Par contre, un effort très important a été fait pour étendre les résultats théoriques à des géométries réalistes. C'est le cas en particulier dans les communications théoriques sur les configurations fermées.

1. Théorie des configurations fermées

Le thème général de ces communications est l'étude de l'équilibre et de la stabilité du plasma en tenant compte très en détail de la configuration magnétique réelle.

Pour réaliser une configuration du genre Stellarator, par exemple, le premier souci est d'avoir de bonnes surfaces magnétiques et nous avons appris par une étude numérique que des perturbations très faibles du champ magnétique pourraient donner lieu à des effets de résonance et détruire les surfaces magnétiques. Ce résultat n'est qu'un aspect des difficultés présentées par le problème de l'équilibre du plasma dans des configurations fermées. Nous avons déjà été avertis par les mathématiciens de la difficulté de ce problème; le professeur Grad est même d'avis qu'il faudrait abandonner et il a proposé une solution de rechange. Si toutefois on persévère, on rencontre les difficultés sous une forme physique: il apparaît des champs électriques « self-consistent » qui peuvent avoir des formes compliquées et gênantes. Ces champs électriques peuvent être liés à l'équilibre lui-même, ou être entraînés par le mode de formation du plasma ou les défauts de la configuration magnétique. Leurs conséquences sont étudiées de façon approfondie dans une communication présentée par M. Furth à partir de l'hypothèse de conservation du second invariant adiabatique J. Un champ électrique dont le potentiel est constant sur les surfaces magnétiques n'est pas gênant, mais un champ irrégulier peut entraîner des déplacements importants des particules et donner lieu à des cellules de convection qui sont spécialement dangereuses dans les multipoles sans champ toroïdal.

L'influence de la forme exacte du plasma ou du champ magnétique sur la stabilité apparaît également dans plusieurs communications. Dans le domaine de la stabilité MHD l'influence de la forme de l'axe magnétique est discutée. Mais un facteur encore plus important pour la stabilité est la forme des sections des surfaces à pression constante. En particulier, des sections circulaires au voisinage de l'axe magnétique ont l'avantage de supprimer la limite de β imposée par les «ballooning modes» à l'ordre le plus bas.

L'étude des instabilités à partir de l'équation de Vlasov et à l'aide d'invariants adiabatiques est appliquée dans plusieurs communications à la géométrie symétrique de révolution et à celle du Stellarator droit, dans le domaine des instabilités de basse fréquence et en considérant spécialement l'instabilité due aux particules piégées. Les résultats obtenus sont particulièrement importants pour les configurations multipolaires, mais beaucoup s'appliquent à toutes les configurations fermées.

2. Théorie des configurations ouvertes

La théorie des configurations ouvertes, telle qu'elle était connue à la Conférence de Culham, prédisait l'existence de deux modes électrostatiques instables particulièrement dangereux, qui peuvent tous deux être stabilisés par des conditions imposées aux dimensions de la bouteille magnétique. L'instabilité convective de cône de perte peut être éliminée si la longueur de la bouteille magnétique n'est pas trop grande et l'instabilité de dérive cyclotronique demande que le rayon du plasma soit assez grand. La condition est donc de faire des machines à miroirs grosses et courtes avec des dimensions longitudinales et transversales de l'ordre de 100 rayons de giration des ions dans les conditions thermonucléaires. Ceci signifie aussi que la vérification expérimentale de la théorie n'est pratiquement possible que dans des dispositifs assez grands et coûteux. Aussi un gros effort théorique a été fait pour rechercher tous les moyens de stabilisation possibles. On ne peut pas en fait supprimer complètement les instabilités, mais on peut au moins rendre les conditions de stabilité moins sévères.

Dans ce but, on a d'abord repris en détail l'analyse de la stabilité du plasma infini avec une distribution de cône de perte dans un champ magnétique uniforme. En plus des modes déjà mentionnés, une instabilité absolue apparaît au voisinage des harmoniques de la fréquence cyclotronique ionique. On a étudié l'influence de la température des électrons, de la distribution en énergie des ions, et de l'addition d'un plasma froid ou tiède. Il est possible de supprimer complètement les modes résonnants absolus au moyen d'un plasma tiède, mais au prix de densités et de températures inacceptables. Par contre, on peut obtenir assez facilement des conditions de stabilité moins sévères avec quelques pour cent de plasma tiède. Des résultats importants ont été obtenus en tenant compte de l'inhomogénéité du champ magnétique, et en particulier la stabilisation des nouveaux modes résonnants.

Malheureusement, une instabilité nouvelle est apparue. Elle est décrite par Kadomtsev et Pogutse, et également dans une communication sur le DCX-2; on peut la considérer comme une instabilité de masse négative modifiée. Un mécanisme analogue à l'instabilité de masse négative devient possible du fait qu'une particule oscillant entre deux miroirs voit une fréquence cyclotronique moyenne qui dépend de son énergie.

Un autre mécanisme important est celui des instabilités explosives qui peuvent résulter de l'interaction non linéaire de deux modes, l'un d'énergie positive et l'autre d'énergie négative, ou de l'interaction non linéaire des ondes avec les particules. Ces effets non linéaires déstabilisants montrent qu'on ne doit pas s'attendre, dans les configurations ouvertes, à une turbulence faible qui s'établit à un niveau stationnaire. Le développement explosif prédit par la théorie peut correspondre aux chutes brusques de densité, avec éjection de plasma, qui sont observées expérimentalement et qui pourraient s'accompagner d'une relaxation du plasma vers un état plus stable.

3. Communications théoriques diverses

Un ensemble de huit communications diverses ne peut être classé dans aucune de ces deux théories (configurations ouvertes ou fermées). Les effets non linéaires sont le premier sujet par ordre d'importance, puisque trois communications y sont consacrées, dont deux sur l'étude non linéaire des ondes de dérive. On sait déjà que la stabilisation des ondes de dérive par le cisaillement (shear) ne peut pas être étudiée uniquement avec les modes localisés. Il est nécessaire de tenir compte de paquets d'onde qui peuvent se propager en s'amplifiant dans une zone instable jusqu'à atteindre une zone stable où ils sont amortis. L'amplitude stationnaire qui en résulte peut être calculée à partir des fluctuations thermiques. On a mis également en évidence un mécanisme de réflexion non linéaire des ondes qui permet une amplification et rend l'instabilité beaucoup plus dangereuse. Le critère de stabilité a été précisé en tenant compte de ce mécanisme.

Les autres sujets traités vont de la mécanique statistique, avec l'étude numérique d'un plasma unidimensionnel, aux problèmes théoriques de confinement par gaz neutre.

Si ces comptes rendus n'apportent pas de nouveauté fondamentale dans le domaine théorique, on ne peut pourtant pas parler d'un ralentissement de l'effort des théoriciens. Il faut au contraire se réjouir de voir que leurs efforts, toujours aussi soutenus, ont été consacrés à adapter de mieux en mieux la théorie aux conditions expérimentales réelles. Je pense en effet que l'un des principaux progrès enregistrés est l'accord de plus en plus général et de plus en plus quantitatif entre la théorie et l'expérience. Cet accord se manifeste certainement dans les résultats obtenus sur le confinement du plasma, mais il est plus facile à obtenir dans les expériences dont le but est l'étude des phénomènes de base. Ces expériences vont faire l'objet de la suite de ce rapport.

B. ETUDE DES PHENOMENES DE BASE

Parallèlement à l'étude directe du confinement dans les configurations ouvertes ou fermées, de nombreuses expériences sont faites dans le but de comprendre les phénomènes d'importance fondamentale pour les recherches sur la fusion contrôlée. Ces phénomènes sont d'abord les effets dissipatifs sans collisions, qui se traduisent par la diffusion accélérée, la résistivité anormale et le chauffage turbulent, et également l'étude expérimentale des micro-instabilités et des interactions non linéaires des ondes.

1. Phénomènes dissipatifs sans collisions

Les effets dissipatifs sans collisions sont étudiés dans trois catégories d'expériences dont les résultats sont présentés: les ondes de choc sans collisions, le chauffage turbulent et la diffusion anormale.

a) Ondes de choc sans collisions

Les expériences de striction azimutale (θ-pinch), en particulier, permettent de produire de fortes ondes de choc à l'aide d'un piston magnétique dans un plasma initial dont les paramètres physiques peuvent varier largement. C'est une idée déjà ancienne que de chercher à produire une telle onde de choc dont le front ait une épaisseur très inférieure au libre parcours moyen des particules. On sait maintenant que la clé du problème n'est pas de trouver une longueur caractéristique qui remplace le libre parcours moyen, mais de disposer d'un mécanisme de dissipation anormal à l'intérieur du front de l'onde. L'épaisseur du front δ est alors déterminée par la condition que l'énergie dirigée puisse être dissipée dans la traversée du front. Connaissant cette épaisseur, on peut calculer la résistivité effective qui est nécessaire à cette dissipation et qui est proportionnelle à l'épaisseur du front et à sa vitesse: $\eta_{\text{eff}} \sim \delta u$. Des ondes de choc sans collisions dans lesquelles η_{eff} est très supérieur à η_{normal} sont déjà connues, en particulier par les expériences de Paul à Culham sur Tarantula.

Les résultats présentés ici montrent tous clairement l'existence de telles ondes de choc nettement détachées du piston. Ils peuvent être classifiés schématiquement suivant la valeur du nombre de Mach magnétique M_A.

<u>$M_A < 2$ ou 3.</u> Il y a une sub-division par un nombre de Mach critique au-dessus duquel apparaissent les effets dissipatifs anormaux.

$M_A < M_{\text{crit}}$. La théorie prédit une structure oscillante de longueur caractéristique:

$$\lambda \sim \frac{c}{\omega_{pe}} \qquad \text{pour les ondes droites}$$

$$\lambda \sim \frac{c}{\omega_{pi}}\,\theta \qquad \text{pour les ondes obliques.}$$

Ces structures ont été observées à Novosibirsk, à Juliers et de manière particulièrement spectaculaire sur des ondes de choc obliques à l'Université du Texas.

$M_A > M_{\text{crit}}$. Le mécanisme de dissipation apparaît et la structure du front devient apériodique. Ces conditions ont été réalisées à l'Université de Maryland, à Garching et à Novosibirsk. La communication présentée par M. Sagdeev montre clairement que l'épaisseur du front dépend de la masse des ions, et confirme l'hypothèse du rôle joué par les ondes ioniques dans la dissipation.

$\underline{M_A > 3}$. Il faut alors faire intervenir d'autres mécanismes de dissipation qu'une simple résistivité. Dans ces conditions, il apparaît un phénomène important, le chauffage des ions, qui a été observé à Novosibirsk et à Garching.

b) Chauffage turbulent

Le chauffage turbulent représente le plus évident des processus dissipatifs anormaux. La perspective de pouvoir l'utiliser pour le chauffage d'un plasma thermonucléaire lui donne aussi une grande importance.

Les communications sur le chauffage turbulent sont publiées ici et je m'abstiendrai d'y revenir. En particulier, je ne chercherai pas à faire un résumé du rapport présenté par M. Berezin sur l'interaction faisceau-plasma.

Je voudrais seulement souligner l'importance des résultats obtenus. L'intensité des effets dissipatifs obtenus est impressionnante. Ils se traduisent en particulier par les densités d'énergie de l'ordre de 5×10^{16} eV/cm^3 observées sur les expériences TN5 et NPR2 dans le laboratoire du professeur Zavoisky, ainsi que les valeurs élevées du rendement global atteignant 25% dans NPR2. Le chauffage des ions a été aussi clairement obtenu. L'explication théorique qui fait intervenir les ondes ioniques a également reçu plusieurs confirmations.

Les performances bien connues, et en progrès constant, des expériences «burnout» d'Oak Ridge sont aussi très intéressantes. Mais la nature du phénomène est différente puisqu'il semble s'agir d'une instabilité de faisceau d'électrons. Le chauffage des ions est néanmoins observé de façon spectaculaire.

c) Diffusion anormale

On observe dans de nombreuses expériences des fluctuations de densité ou de potentiel électrique et, en même temps, des pertes anormales de plasma. Il est bien établi expérimentalement que des fluctuations importantes, par exemple de 10% sur la densité, peuvent apporter une contribution à la fuite des particules. Mais il n'existe encore que très peu d'expériences où une relation quantitative ait été établie entre les fluctuations et la diffusion anormale.

Une mesure directe du flux moyen de particules associé à la diffusion a été mise au point à Princeton. Cette mesure a été faite en particulier sur un plasma de césium en présence d'instabilités de dérive. On a constaté un accord qualitatif avec les prédictions théoriques d'un modèle non linéaire de l'instabilité. Par contre, la comparaison avec le taux de perte globale du plasma n'a pas été donnée. La difficulté de déterminer les causes exactes de perte dans les expériences sur les plasmas de césium apparaît d'ailleurs clairement dans les communications. L'analyse des processus de diffusion et de recombinaison faite sur l'expérience Barbara de Garching diffère sensiblement des résultats obtenus sur une expérience semblable à Princeton.

Sur la colonne de plasma Daphnis de Saclay, la mesure directe de la diffusion transversale a été comparée à un coefficient de diffusion calculé à partir du temps de corrélation et de l'amplitude des fluctuations: les deux résultats sont du même ordre de grandeur et décroissent de façon semblable avec le champ magnétique.

La comparaison des fluctuations avec les pertes de plasma a été faite dans tous les multipoles, malheureusement avec le résultat général que les pertes étaient dues en majeure partie à d'autres causes, dont en particulier les mouvements convectifs entraînés par des champs électriques stationnaires, résultant, par exemple, d'imperfections de la configuration ou de la méthode de formation du plasma.

Il y a donc encore très peu de résultats expérimentaux quantitatifs sur la relation entre les fluctuations et la diffusion. Pourtant ce problème est au moins aussi important que la comparaison entre la diffusion observée et celle de Bohm, et il devrait faire l'objet d'efforts importants dans l'avenir.

En résumé, l'étude expérimentale des mécanismes dissipatifs sans collisions apparaît comme un domaine en plein developpement. L'accord avec la théorie est encore semi-quantiatif et les modèles théoriques utilisés sont peut-être encore incertains, mais les résultats obtenus sont très encourageants.

2. Ondes et micro-instabilités

Les travaux expérimentaux sur les ondes et les micro-instabilités présentés ici portent principalement sur les observations d'instabilités de dérive effectuées sur des plasma de césium et sur des études d'effets non linéaires particuliers.

a) Instabilités de dérive

Les premières observations d'ondes de dérive faites à Princeton ont été confirmées. L'étude de la relation de dispersion a été complétée par celle de l'amplitude de l'onde en fonction du champ magnétique en accord qualitatif avec un modèle théorique non linéaire.

Un point important dans l'identification des ondes de dérive est le rôle joué par les champs électriques, qui sont très difficiles à éviter complètement dans un plasma de césium. Une étude systématique de ce point a été entreprise à Frascati avec un dispositif spécialement conçu pour créer un champ électrique localisé et contrôlable. Les résultats montrent l'apparition d'un mode instable du genre flûte lié au champ électrique et, par ailleurs, une instabilité de dérive dans une région de fort gradient de densité. L'influence du champ électrique a également été étudiée à Princeton et une parfaite continuité a été observée entre les modes avec champ électrique et les instabilités de dérive sans champ électrique.

La stabilisation des ondes de dérive par le cisaillement a été observée en accord qualitatif avec la théorie. Par contre, la diminution des fuites du plasma par le cisaillement est compliquée par le phénomène de convection. Une exploration très fine du potentiel du plasma a montré en effet que le cisaillement modifiait la forme du champ électrique et réduisait la convection.

Un effet de stabilisation d'une onde de dérive par un champ électrique alternatif a été observé à l'Institut de physique des plasmas de Nagoya.

b) Effets non linéaires

L'accord entre la théorie et l'expérience dans l'étude des ondes de dérive est très encourageant, mais il reste encore semi-quantitatif. Un accord plus précis peut être obtenu dans l'étude de phénomènes plus simples et je voudrais en donner deux exemples, qui portent sur l'étude d'effets non linéaires.

Le premier est l'observation de la désintégration non linéaire d'une onde de plasma dans l'expérience EOS de Fontenay-aux-Roses. La vérification de la théorie a porté sur les règles de sélection satisfaites par les ondes produites, sur le seuil d'instabilité non linéaire lié à l'amortissement de l'onde et sur la longueur de désintégration. On a montré en particulier que la longueur de désintégration était inversement proportionnelle à l'amplitude de l'onde à 10% près, ce qui est une bonne vérification du modèle théorique. Il est rassurant de voir qu'on peut comprendre quantitativement un phénomène qui joue certainement un rôle fondamental dans le développement non linéaire des instabilités et dans l'apparition de la turbulence.

Un autre exemple, dans lequel l'accord entre la théorie et l'expérience est particulièrement remarquable, est l'étude détaillée de l'amortissement de Landau au laboratoire de la Gulf General Atomic à San Diego. La connaissance des ondes linéaires est suffisamment bonne pour permettre de mesurer la densité et la température des électrons à partir de la relation de dispersion avec une précision de 5%. Le flux cohérent d'électrons recueilli à une distance supérieure à la longueur d'amortissement a été comparé aux prévisions théoriques, et les principales caractéristiques, intensité du courant, valeur du maximum, sont en bon accord. Les résultats constituent donc une bonne vérification quantitative de la théorie quasi-linéaire.

Il est clair que les deux expériences qui viennent d'être citées ne sont que des exemples et qu'un accord quantitatif entre la théorie et l'expérience est obtenu dans des domaines très divers de la physique des plasmas. On peut citer l'exemple bien connu de l'accord entre les nombreuses mesures de densité électronique dans le Stellarator C.

En conclusion, il me semble que ces comptes rendus n'apportent pas seulement des résultats très encourageants sur le confinement magnétique des plasmas, mais qu'ils sont aussi le reflet d'un progrès très important dans la compréhension générale des phénomènes. Nous disposons maintenant d'une base physique solide pour les recherches sur la fusion contrôlée.

THEORY AND BASIC PHENOMENA

M. TROCHERIS
CEA FONTENAY-AUX-ROSES, FRANCE

The subject of my talk can best be defined by saying that it concerns questions not covered by the other two speakers, whose talks deal essentially with closed and open configurations. I shall attempt to summarize the results presented in the theoretical and experimental papers which do not relate directly to magnetic confinement - that is to say, those which concern basic phenomena such as collisionless dissipative processes, waves and microinstabilities.

Actually, this division into subjects is not a very convenient one as far as the theoretical papers are concerned. Some of these papers deal directly with plasma equilibrium or stability in closed or open configurations, and I shall begin by referring to them briefly.

A. THEORY

There appears to have been a smaller proportion of theoretical papers at this Conference than at preceding ones. Moreover, there has been a change in the nature of the work reported. For example, there are very few really new instabilities. On the other hand, considerable efforts have been made to extend the theoretical results to realistic geometries. This is particularly so in the case of the theoretical papers on closed configurations.

1. Theory of closed configurations

The general theme of these papers is the study of plasma equilibrium and stability with detailed consideration of the actual magnetic configuration.

The primary prerequisite for achieving a configuration of the stellarator type, for example, is to have good magnetic surfaces. However, a numerical study has shown that very weak perturbations of the magnetic field could give rise to resonance effects and destroy the magnetic surfaces. This is only one aspect of the difficulties presented by the problem of plasma equilibrium in closed configurations. We have been warned by the mathematicians of the difficulty of this problem; Mr. Grad is even of the opinion that this approach should be dropped, and proposes an alternative solution. If one nevertheless persists with this approach, one encounters difficulties of a physical nature: there appear self-consistent electric fields which may have complicated and awkward shapes. These electric fields may be associated with the equilibrium itself, or result from the way in which the plasma is produced or from faults in the magnetic configuration. The consequences of such faults have been studied thoroughly in a paper presented by Mr. Furth, who takes as his starting point the hypothesis of conservation of the second adiabatic invariant J. An electric field whose potential is constant at the magnetic surfaces does not cause any trouble; however, an irregular field may cause substantial particle movement and give rise to convection cells, which are particularly dangerous in multipoles without toroidal field.

The influence of the exact shape of the plasma or of the magnetic field on stability is also brought out by several authors. In the field of MHD stability, the influence of the shape of the magnetic axis has been discussed. However, an even more important factor from the point of view of stability is the shape of the cross-sections of the constant-pressure surfaces. In particular, circular cross-sections near the magnetic axis offer the advantage of suppressing the limit on β imposed by the ballooning modes to the lowest order.

In several papers, instability studies based on the Vlasov equation and on the use of adiabatic invariants have been carried out for the symmetrical geometry of revolution and for that of the straight stellarator; the authors consider low-frequency instabilities and pay special regard to the trapped-particle instability. The results are especially important for multipole configurations, but many of them are applicable to all closed configurations.

2. Theory of open configurations

The theory of open configurations, as it was understood at Culham, predicted the existence of two particularly dangerous unstable electrostatic modes, both of which can be stabilized by imposing certain conditions on the dimensions of the magnetic mirror trap. The convective loss oone instability can be eliminated if the magnetic trap is not too long, while the cyclotron drift instability requires that the plasma radius be fairly large. The answer would therefore be to build large but short mirror machines with longitudinal and transverse dimensions of the order of 100 ion gyration radii under thermonuclear conditions. This means virtually that the experimental verification of the theory would be possible only in fairly large and expensive devices. Accordingly, considerable theoretical effort has gone into studying all possible stabilization methods. One cannot in fact suppress instabilities completely, but one can at least render the stability conditions less rigorous.

With this object in mind, the analysis of the stability of an infinite plasma with a loss cone distribution in a uniform magnetic field was first resumed and pursued in greater detail. In addition to the modes already mentioned, an absolute instability appears near the harmonics of the ion cyclotron frequency. The influence of electron temperature, ion energy distribution, and the addition of a cold or warm plasma has been studied. It is possible to suppress the absolute resonant modes completely by means of a warm plasma, but only at the cost of unacceptable densities and temperatures. On the other hand, it is fairly easy to obtain less rigorous stability conditions with a few per cent of warm plasma. Improved results have been obtained by taking into account the non-uniformity of the magnetic field, and in particular the stabilization of the new resonant modes.

Unfortunately, a new instability has appeared on the scene. It is described by Kadomtsev and Pogutse, and was also reported in a paper on DCX-2; it may be considered as a modified negative-mass instability. A mechanism like negative-mass instability becomes possible because a particle oscillating between two magnetic mirrors acquires a mean cyclotron frequency which is dependent on its energy.

Another important mechanism is that of explosive instabilities, which may result from the non-linear interaction of two modes (a positive-energy and a negative-energy mode) or from the non-linear interaction of waves with particles. These destabilizing non-linear effects show that in open configurations one cannot expect the establishment of a weak turbulence at a steady-state level. The explosive development predicted by theory may correspond to the abrupt decreases in density (with plasma ejection) which are observed experimentally and which might be accompanied by relaxation of the plasma towards a more stable state.

3. Various theoretical papers

A varied collection of eight papers deals neither with open nor closed configuration theory. Non-linear effects are the principal subject; three of the papers deal with such effects, two of them relating to the non-linear study of drift waves. We know already that the stabilization of drift waves by shear cannot be studied solely with localized modes. It is necessary to take into account wave packets which propagate during build-up into an unstable zone, being damped when they reach a stable zone. The resulting steady-state amplitude may be calculated on the basis of the thermal fluctuations. A non-linear wave reflection mechanism has also been discovered; it permits build-up of waves and renders the instability much more dangerous. This mechanism has been taken into account in defining the stability criterion.

The other subjects discussed the range from statistical techniques (with the numerical study of a one-dimensional plasma) to the theoretical problems of confinement by a neutral gas.

While this Conference does not produce any fundamentally new developments in the field of theory, it cannot be said that the theoreticians are flagging in their endeavours. On the contrary, it is gratifying to note that their continuing efforts have been directed towards adapting theory more and more closely to actual experimental conditions. I think that one of the principal advances recorded at this Conference has been the increasingly widespread and increasingly quantitative agreement between theory and experiment. This agreement can certainly be seen in the plasma confinement results, but it is easier to achieve it in experiments relating to the study of basic phenomena. These experiments will be the subject of the next part of my talk.

B. STUDY OF BASIC PHENOMENA

In addition to the direct study of confinement in open or closed configurations, many experiments have been directed at gaining an understanding of the phenomena which are of fundamental importance to controlled fusion research. These phenomena are: (i) the collisionless dissipative effects which result in accelerated diffusion, anomalous resistivity, and turbulent heating, and (ii) micro-instabilities and non-linear wave interactions.

1. Collisionless dissipative phenomena

Collisionless dissipative effects have been studied in three types of experiments, the results of which are being presented at this Conference; collisionless shock waves, turbulent heating and anomalous diffusion.

(a) Collisionless shock waves

Theta-pinch experiments, in particular, enable one to produce powerful shock waves by means of a magnetic piston in an initial plasma whose physical parameters may vary considerably. The idea of attempting to produce a shock wave of this type, with the thickness of the wave front much less than the mean free path of the particle, is an old one. We now know that the key to the problem is not to find a characteristic length which will replace the mean free path, but to have an anomalous dissipation mechanism within the wave front. The thickness of the wave front is then determined by the condition that the directed energy should be dissipated across the wave front. Knowing the thickness of the wave front, it is possible to calculate the effective resistivity which is necessary for this dissipation and which is proportional to the thickness of the wave front and its velocity: $\eta_{eff} \sim \delta u$. Collisionless shock waves in which η_{eff} is much greater than η_{normal} are already known, particularly through the experiments carried out by Paul on the Tarantula device at Culham.

The results presented at the Conference demonstrate clearly the existence of such shock waves, which are distinctly detached from the piston. They can be classified schematically by the value of the magnetic Mach number M_A.

$\underline{M_A < 2 \text{ or } 3}$. In this case one has a sub-division relating to a critical Mach number above which anomalous dissipative effects make their appearance:

$M_A < M_{crit.}$. The theory produces an oscillating structure of characteristic length

$$\lambda \sim c/\omega_{pe} \qquad \text{for straight waves}$$
$$\lambda \sim c/\omega_{pi} \qquad \text{for oblique waves.}$$

Such structures have been observed at Novosibirsk and Jülich and, in a particularly spectacular manner, in the oblique shock waves at the University of Texas.

$M_A > M_{crit.}$. The dissipation mechanism makes its appearance and the structure of the wave front becomes aperiodic. These conditions have been achieved at the University of Maryland, Garching and Novosibirsk. The paper presented by Mr. Sagdeev showed clearly the dependence of the thickness of the wave front on the ion mass and confirmed the hypothesis concerning the role played by ionic waves in the dissipation process.

$\underline{M_A > 3}$. In this case one has to introduce dissipation mechanisms other than simple resistivity. An important phenomena (heating of the ions) occurs under these conditions and has been observed at Novosibirsk and Garching.

(b) Turbulent heating

Turbulent heating is the most obvious of the anomalous dissipative processes. It is also of considerable importance in view of the possibility of its being used in heating a thermonuclear plasma.

The reports on turbulent heating are published in this book and I shall therefore not repeat them at this point. In particular, I shall not attempt to summarize the report presented by Mr. Berezin on the beam-plasma interaction.

I should merely like to stress the importance of the results obtained. The intensity of the dissipative effects obtained is most impressive, in particular, the energy densities of the order 5×10^{16} eV/cm^3 observed in the TN5 and NPR2 experiments carried out in Mr. Zavoisky's laboratory and the high overall efficiency (25%) achieved in the NPR2 device. It is clear that ion heating was achieved. The theoretical explanation involving ionic waves has also received substantial confirmation.

The well known and steadily improving results of the "burnout" experiments at Oak Ridge are also extremely interesting. But the nature of the phenomenon is different since it seems to be an electron beam instability. Heating of the ions on a spectacular scale is nevertheless observed.

(c) Anomalous diffusion

Density or electric potential fluctuations are observed in several experiments, together with anomalous plasma losses. It has been established experimentally that substantial density fluctuations (for example, 10%) can contribute to the loss of particles. There have so far been very few experiments in which a quantitative relationship has been established between fluctuations and anomalous diffusion.

The main particle flux associated with diffusion has been measured directly at Princeton. These measurements were performed in a caesium plasma in the presence of drift instabilities. There is qualitative agreement with theoretical predictions of a non-linear model of the instability. On the other hand, the comparison with the amount of total plasma loss was not reported. The difficulty in determining the exact causes of losses in caesium plasma experiments emerges clearly from the papers presented at this Conference. The results of the analysis of diffusion and recombination in the Barbara experiment at Garching differ noticeably from those obtained in a similar experiment at Princeton. Direct measurements of the transfer diffusion in the Daphnis plasma column at Saclay have been compared with a diffusion coefficient calculated on the basis of the correlation time and the amplitude of the fluctuations. The two sets of results are of the same order of magnitude and decrease in a similar fashion with the magnetic field.

A comparison of fluctuations with plasma losses has been made for all multipoles, unfortunately with the general result that the losses were due to other causes - in particular, convective movements induced by steady-state electric fields resulting from, for example, imperfections of the configuration or from the method of plasma production.

We there still have very few quantitative experimental results for the relationship between fluctuations and diffusion, although this problem is at least as important as the comparison between observed diffusion and Bohm diffusion. This question should be thoroughly studied.

In summary, the experimental study of collisionless dissipative mechanisms appears to be well under way. Agreement with theory is still only semi-quantitative and the theoretical models used are perhaps still rather tentative. However, the results obtained are very encouraging.

2. Waves and micro-instabilities

The experimental papers on waves and micro-instabilities presented at this Conference contain primarily observations of drift instabilities in caesium plasmas and studies of various non-linear effects.

(a) Drift instability

The initial observations of drift waves made at Princeton have been confirmed. In addition to the dispersion relation, wave amplitude as a function of magnetic field (in qualitative agreement with a non-linear theoretical model) has become a subject for study.

An important aspect of the identification of drift waves is the role played by electric fields, which are extremely difficult to avoid completely in a caesium plasma. This point has been studied systematically at Frascati in a device designed especially for the production of a localized and controllable electric field. In this study, an unstable mode of the flute type and associated with electric field has been observed, as has a drift instability in a region with a great density gradient. The influence of the electric field has also been studied at Princeton and perfect continuity has been observed between the modes with electric field and the drift instabilities without electric field.

The stabilization of drift waves by shear has been observed, in qualitative agreement with theory. On the other hand, the reduction of plasma losses by shear is complicated by convection. A detailed investigation of the plasma potential has shown that shear modifies the shape of the electric field and reduces convection.

Stabilization of a drift wave by an alternating electric field has been observed at the Institute of Plasma Physics, Nagoya.

(b) Non-linear effects

The agreement between theory and experiment in the study of drift waves is very encouraging, but remains only semi-quantitative. More precise agreement can be obtained in the study of simpler phenomena, and I should like to give two examples relating to the study of non-linear effects.

The first is the observation of the non-linear disintegration of a plasma wave in the EOS experiment at Fontenay-aux-Roses. Verification of the theory has proved the selection rules satisfied by the resulting wave, the non-linear instability threshold associated with wave damping, and the disintegration length. It has been shown that the disintegration length is inversely proportional (to within 10%) to the wave amplitude, which provides good confirmation of the theoretical model. It is reassuring to see that a quantitative understanding has been obtained of a phenomenon which undoubtedly plays a fundamental role in the non-linear development of instabilities and in the appearance of turbulence.

Another example of particularly remarkable agreement between theory and experiment is the detailed study of Landau damping at the laboratory of Gulf General Atomic in San Diego. The information accumulated about linear waves is sufficient to permit measurements of the electron density and temperature on the basis of the dispersion relation; such measurements are accurate to within 5%. The coherent electron flux at a distance greater than the damping length has been compared with theoretical predictions and the principal characteristics (current intensity and maximum value) are in agreement. The results thus provide satisfactory quantitative confirmation of the quasi-linear theory.

Clearly, the two experiments just referred to are only examples; quantitative agreement between theory and experiment is obtained in many different areas of plasma physics - for example, the agreement between the many measurements of electron density in Stellarator C.

In conclusion, I feel that these reports not only produce encouraging results concerning the magnetic confinement of plasmas, but also extremely important advances towards a general understanding of the phenomena involved. We now possess a sound physical basis for controlled fusion research.

ЗАКЛЮЧИТЕЛЬНОЕ СЛОВО

Г.И.БУДКЕР
ИНСТИТУТ ЯДЕРНОЙ ФИЗИКИ
СО АН СССР, НОВОСИБИРСК,
СОЮЗ СОВЕТСКИХ СОЦИАЛИСТИЧЕСКИХ
РЕСПУБЛИК

Мне кажется, что за последние годы в науке произошли изменения, открывшие новые возможности, на которых я хотел бы остановиться. Я хочу напомнить, что в 1951 году мы начали работы по физике плазмы и термоядерным реакциям. У нас была уверенность, что мы решим эту проблему с ходу, сразу. Мне было поручено обеспечивать регулирование будущего термоядерного реактора, чтобы тот не очень "разогнался" и не вышел из-под контроля. Сейчас это поручение напоминает историю о том, как один хотел изобрести вечный двигатель и взял патент на то, чтобы тот не разгонялся до бесконечных скоростей... Большие успехи в разработке "взрывчатых термоядерных реакторов", которые были созданы за очень короткое время, породили у физиков уверенность в то, что они могут сделать все и сделать быстро. Однако очень скоро жизнь показала, что этим делом нужно заниматься не как конструированием, а как наукой, что надо развивать плазменную науку, и мы приступили к работе по изучению физики плазмы, которая длится уже более десяти лет.

Эта работа привлекла к себе новых людей с новой философией и новой идеологией. Мне кажется, что успехи, достигнутые за прошедший период физиками в данной области, заставляют нас вернуться к идее создания термоядерного реактора. Физику не обязательно начинать дело только тогда, когда он будет знать все. Чтобы вступить в бой, ему не обязательно ждать, когда будет пришита последняя пуговица к шинели последнего солдата. Физику достаточно лишь очень тщательно изучить то, что принципиально в данном деле, и найти решение по определению неизвестных. Подобной была ситуация и при создании первого атомного (уран-графитового) реактора.

Это не означает, что мы должны приостановить работу по физике плазмы. Наоборот, работы по ядерной физике только тогда получили бурное развитие, когда заработал первый ядерный реактор. Но мне кажется, что количество накопленных знаний о плазме достаточно, чтобы те, кто тесно связан с этой проблемой, переключили свое внимание на создание термоядерного реактора, оставив исследовательскую работу тем, кто любит исследовать физические проблемы. На это могут возразить: как же можно начать и выполнить эту работу, если нет новых идей? Но идеи появятся в процессе работы. Если же мы не изменим нашу философию, то будем напоминать софиста, который утверждал, что не залезет в воду, пока не научится плавать.

Очень часто ставится вопрос о том, как скоро будет создан термоядерный реактор. Ответ на этот вопрос аналогичен известной истории с путником и мудрецом. Однажды к мудрецу подошел путник и спросил, как долго ему идти до ближайшего города. Мудрец сказал: "Иди, иди вперед!". Путник недоуменно пожал плечами, но мудрец повторил: "Иди, тогда я тебе скажу". Тот пошел, потом обернулся. Тогда мудрец сказал: "Иди, не оборачивайся". И путник пошел прямо вперед. "Вот теперь я могу сказать, как долго тебе идти, – изрек мудрец. – Теперь я знаю, как быстро ты ходишь"... Когда мы рассмотрим всю проблему в целом и будем знать, сколько на ее решение отводится материальных средств, людских ресурсов и какое уделяется ей внимание, тогда мы сможем ответить на вопрос, как долго будет создаваться термоядерный реактор.

Еще один вопрос: кто первым придет к цели? Первым придет к цели тот, кто пойдет по этой дороге. Чтобы достичь цели, надо отправиться в путь. Во всяком случае, кто бы ни пришел первым, он достигнет цели в результате труда многих ученых и государственных деятелей, а также всех тех, кого объединяют наши постоянные конференции. Это будет результат международного научного сотрудничества всех стран земного шара.

Проблема термоядерной реакции – это не обычная физическая проблема. Это проблема, которая должна преобразовать общество и мир. Наше поколение, которое дало людям атомную энергию и термоядерную энергию в взрывном виде, несет ответственность перед человечеством за решение основной энергетической задачи – получения энергии из воды. Люди ждут решения этой проблемы. Наш долг – решить ее при жизни нашего поколения, и поэтому мы должны вступить на этот путь.

CONCLUDING REMARKS

G. I. BUDKER
INSTITUTE OF NUCLEAR PHYSICS
SIBERIAN DEPARTMENT OF THE
USSR ACADEMY OF SCIENCES, NOVOSIBIRSK
UNION OF SOVIET SOCIALIST REPUBLICS

I feel that the changes which have taken place in science in the last few years open up new possibilities, about which I should like to say a few words. In 1951 we began work on thermonuclear reactions in the confident belief that we would solve the problem with a rush and immediately. I was assigned the task of ensuring that our future thermonuclear reactor would not get too much out of hand. It was like the story of the man who wished to invent a perpetual motion machine and had taken out a patent on a method for keeping it under control. This attitude stemmed from the successes in developing "explosive thermonuclear reactors", a task which was achieved within a very short period of time, leaving physicists with the impression that they could do everything - and do it fast. However, experience soon showed that here we had a scientific rather than a technological problem and that it would be necessary to study in detail the physics of plasmas - which we have now been doing for over ten years.

The work in this field attracted new people with a new philosophy and a new ideology. Now, I feel that the progress achieved by the physicists during this period justifies our again thinking in terms of building a thermonuclear reactor. The physicist is not obliged to embark upon a project only when he is in possession of all the facts; he does not have to wait until the last button is sewn onto the tunic of the last soldier before engaging battle. He needs only to study carefully the underlying principles and then to find a solution which will reveal the unknowns. Such was the situation in the case of the first atomic (uranium-graphite) reactor.

That does not mean that we should give up plasma research - quite the contrary in fact; it should be remembered that nuclear physics really got under way only after the first atomic reactors had been built. However, I feel that the amount of data accumulated is now sufficient for some of those working in the field of plasma physics to direct their attention to the construction of a thermonuclear reactor, leaving the research to those who prefer to study physics problems. If it is objected that no new ideas have been advanced as to how this should be done, my answer would be that ideas materialize in the course of work and that, if we do not change our philosophy, we shall resemble the sophist who said that one should not enter the water until one had learned to swim.

The question is often asked as to how long it will take to build a thermonuclear reactor. The answer to this question is reminiscent of the story about the wise man who was asked by a traveller how long it would take him to reach a town. The wise man replied "Walk on! Walk on!". The traveller was nonplussed and shrugged his shoulders, but the wise man said "Walk on, and then I shall tell you". The traveller walked a little way and then turned round and looked at the wise man, who said "Keep walking, dont't look round". So the traveller continued walking straight ahead. At length the wise man said "Now I can tell you how long it will take you to reach your destination - now I know how fast you walk". When we have considered the problem as a whole and ascertained what material and human resources are being expended, we shall be able to answer the question how long it would take to build a thermonuclear reactor.

There is another question: Who will first reach the goal? Those who first take the road towards the practical realization of our objective will be the first to reach it. One thing is certain, whoever reaches the goal will do so by virtue of the work of a great many scientists and statesmen, the work of the people concerned with this series of conferences. The results of these labours will be the fruit of international scientific co-operation between countries in all continents.

The problem of the thermonuclear reaction is an unusual problem of physics, and one which will transform human society and the world. Our generation, which gave the world atomic energy and thermonuclear energy in explosive form, now is responsible towards Mankind to solve the main problem - obtaining energy from water. The world expects it of us, and it is our duty towards mankind. It is a task which our generation must accomplish, and to do so we must now set forth on the road.

SHOCK WAVES

(Session A)

Chairman: W. E. DRUMMOND

Papers A-2 to A-6 were presented by E. HINTZ as Rapporteur.

РАЗВИТИЕ ПРОГРАММЫ ПО УДАРНЫМ ВОЛНАМ БЕЗ СТОЛКНОВЕНИЙ

С.Г.АЛИХАНОВ, Н.И.АЛИНОВСКИЙ,
Г.Г.ДОЛГОВ-САВЕЛЬЕВ, В.Г.ЕСЕЛЕВИЧ,
Р.Х.КУРТМУЛЛАЕВ, В.К.МАЛИНОВСКИЙ,
Ю.Е.НЕСТЕРИХИН, В.И.ПИЛЬСКИЙ,
Р.З.САГДЕЕВ и В.Н.СЕМЕНОВ
ИНСТИТУТ ЯДЕРНОЙ ФИЗИКИ СО АН СССР, НОВОСИБИРСК,
СССР

Abstract — Аннотация

DEVELOPMENT OF A COLLISIONLESS SHOCK WAVE PROGRAM. The authors generalize results obtained in investigations of the different types of collisional shock wave found in a plasma. For a wide range of plasma parameters they investigate in experimental devices virtually all the types of laminar wave occurring in a dilute plasma. They look into the nature of the turbulent processes which can occur inside a collisionless shock wave front under different conditions. The measured thickness of the wave front is found to agree with theoretical predictions based on turbulence models. The electron and ion components of the plasma behind the wave front are measured.

РАЗВИТИЕ ПРОГРАММЫ ПО УДАРНЫМ ВОЛНАМ БЕЗ СТОЛКНОВЕНИЙ. Обобщаются результаты исследования различных типов бесстолкновительных ударных волн в плазме. На экспериментальных установках охвачена широкая область параметров плазмы и исследованы фактически все типы волн ламинарной структуры, существующие в разреженной плазме. Проведены исследования по выяснению природы турбулентных процессов, которые могут возникать внутри бесстолкновительного ударного фронта в различных условиях. Экспериментально измеренная толщина фронта в этом случае согласуется с величиной, предсказанной теоретически на основе конкретных моделей турбулентности. Проведены измерения электронной и ионной компонент плазмы за фронтом волны.

I. ВВЕДЕНИЕ

На конференции 1965 года в Калэме было доложено о первом экспериментальном исследовании бесстолкновительной ударной волны в разреженной плазме [1] (см. также [2]), распространяющейся поперек магнитного поля.

Уже эти экспериментальные результаты подтвердили предсказание теории [3] о многообразии типов структуры фронта, зависящем от параметров начального состояния плазмы и волны. Это многообразие явлений и критические условия, при которых происходит смена типов бесстолкновительного ударного фронта (в дальнейшем БУФ), явились предметом детального исследования [4], результаты которого обобщаются в настоящем докладе.

Широкий диапазон параметров БУФ потребовал создания ряда лабораторных устройств, основные характеристики которых сведены

Таблица I. ЭКСПЕРИМЕНТАЛЬНЫЕ УСТАНОВКИ ПО ИССЛЕДОВАНИЮ УДАРНЫХ ВОЛН В РАЗРЕЖЕННОЙ ПЛАЗМЕ

Название установки	Тип ударной волны	Способ генерации ударной волны	Характерные размеры L = длина D = диаметр	Температура плазмы (T_0 – в невозмущенном состоянии, T_1 – за фронтом волны).	Плотность плазмы
I	2	3	4	5	6
УН-4	Поперечные и косые к Но(2500гс)	"Магнитный поршень" в геометрии θ-пинча	L = 100 см D = 16 см.	$T_0 \sim 1 \div 10$ эв $T_1 \sim 1000 \div 50000$ эв	$5 \cdot 10^{10} \div 10^{14}$ см$^{-3}$
ПУММ	Косые и вдоль Но ($\lesssim 400$ гс)	Налетание сверхзвукового потока плазмы на тело или магн. диполь	L = 250 см D = 40 см	$T_0 \sim 1 \div 5$ эв $T_1 \sim 100$ эв	$10^{14} \div 10^{16}$ см$^{-3}$
"Волна"	В неизотермической плазме без магнитного поля ($T_e \gg T_i$)	Электростатический поршень, создаваемый системой проволочек	L = 120 см D = 90 см	$T_e \sim 5 \div 10$ эв	$10^6 \div 5 \cdot 10^7$

I	2	3	4	5	6
УН-5	$H_0 \sim 5000$ гс	Быстрый магнитный поршень ($\tau \sim 5 \times 10^{-8}$ сек) $H_\sim \sim 20$ кгс			
УН-6	Вдоль магнитного поля $H_0 \lesssim 1000$ гс	Магнитный поршень, создаваемый коническим витком	$L = 300$ см $D = 40$ см	$T \sim 10 \div 100$ эв	10^{14} см$^{-3}$

в таблицу I. Как видно из таблицы, использование этих устройств позволило перекрыть широкую область параметров плазмы от $n_0 \sim 10^6 см^{-3}$ до $n_0 \sim 10^{16} см^{-3}$. Содержание настоящего доклада, в основном, базируется на результатах, полученных на трёх первых установках табл.I, а работы на двух последних находятся в начальной стадии.

П. УДАРНЫЕ ВОЛНЫ, РАСПРОСТРАНЯЮЩИЕСЯ ПОПЕРЁК МАГНИТНОГО ПОЛЯ

Исследования БУФ в этом случае проводились на установке УН-4, где с помощью магнитного поршня генерировались цилиндрические ударные волны.

Анализ экспериментов показывает, что характерный пространственный размер δ БУФ зависит от плотности, магнитного поля, отношения массы ионов к массе электронов, числа Маха в водородной плазме. Нижняя ветвь этой зависимости согласуется с представлением о ламинарной осцилляторной структуре течения при малой плотности, когда микронеустойчивости не успевают развиться. Характерный масштаб переднего скачка и последующих осцилляций порядка c/ω_0 *) и не зависит от массы ионов при изменении атомного веса на 2 порядка (D, He, Ar, Xe). Типичная осциллограмма магнитного поля в волне этого типа, возбужденной в аргоновой плазме, приведена на рис.2. Такой характер течения внутри БУФ сохраняется вплоть до определенной критической плотности n_c, выше которой осцилляции исчезают, а толщина переходной области Δ становится много больше (третья ветвь, рис.1). Значение n_c зависит от начального магнитного поля H_0 и возрастает примерно как H_0^2 (рис.3; при $H_0 \sim (0,5 - 1).10^3$ гс $n_c \leqslant 10^{12} см^{-3}$). Типичный вид БУФ в режиме больших плотностей плазмы ($n_0 \sim 10^{13} - 10^{14} см^{-3}$) приведен на рис.4. При макроскопическом описании в магнитной гидродинамике подобная структура БУФ может быть объяснена либо существованием аномально низкой проводимости плазмы, либо аномально высокой её вязкостью, т.к. частоты парных соударений пренебрежимо малы. То обстоятельство, что профиль магнитного поля опережает профиль электрического потенциала как раз

---

*) Как следует из теории [3], при весьма малых плотностях $m_e n c^2 \leqslant \frac{H^2}{8\pi}$ характерный масштаб осцилляций должен быть $H/4\pi ne \cong V_a/\Omega_0$. По-видимому, самые левые экспериментальные точки на рис.I.(относящиеся к разреженной ксеноновой плазме) нужно интерпретировать именно так.

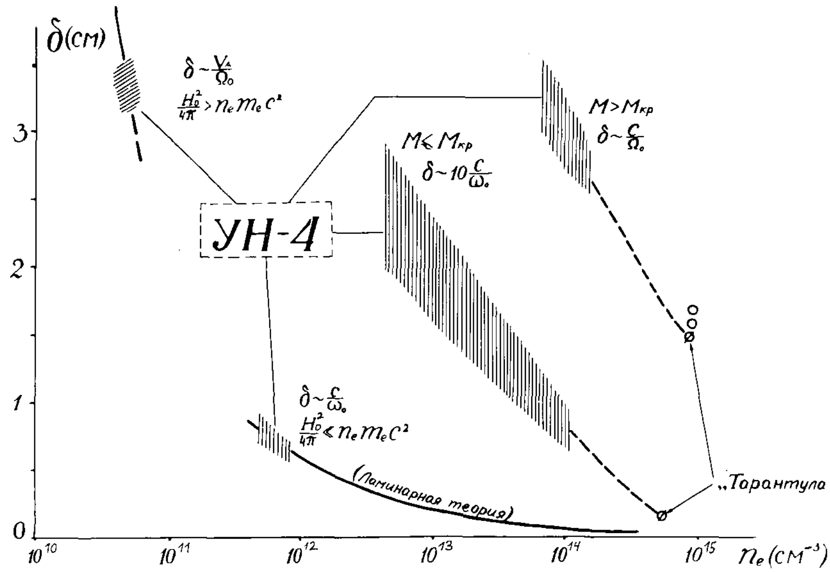

Рис.1. Ширина фронта ударной волны в зависимости от начальной плотности плазмы и других параметров.

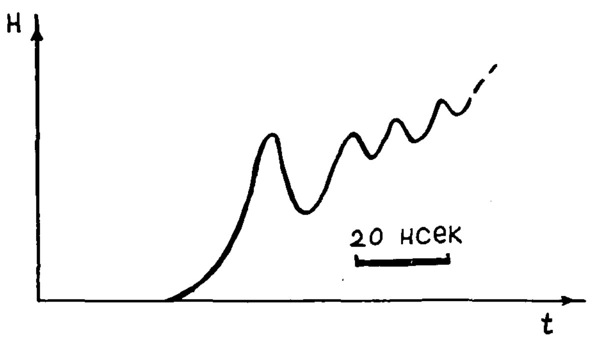

Рис.2. Структура БУФ при ламинарном течении (аргон, $n_0 \sim 10^{12}$ см$^{-3}$).

на величину порядка толщины БУФ, показывает, что $\sigma_{eff} \sim \frac{c^2}{4\pi \Delta U}$ и достаточно для объяснения диссипации внутри БУФ.

Какова же микроскопическая природа этой аномальной проводимости? Наиболее правдоподобными являются гипотезы об аномальном сопротивлении из-за: а) раскачки ионно-звуковых колебаний [3] ; б) электромагнитных волн с частотой $\frac{\omega_r}{2\pi}$ ("свисты") [6] . Предпочтительность первой гипотезы подтверждают следующие дополнительные экспериментальные данные.

I. Зависимость Δ от атомного веса A (рис.5); этот эффект зависимости "сверхсопротивления" плазмы внутри БУФ можно трактовать как своего рода аналог "изотопического эффекта" в

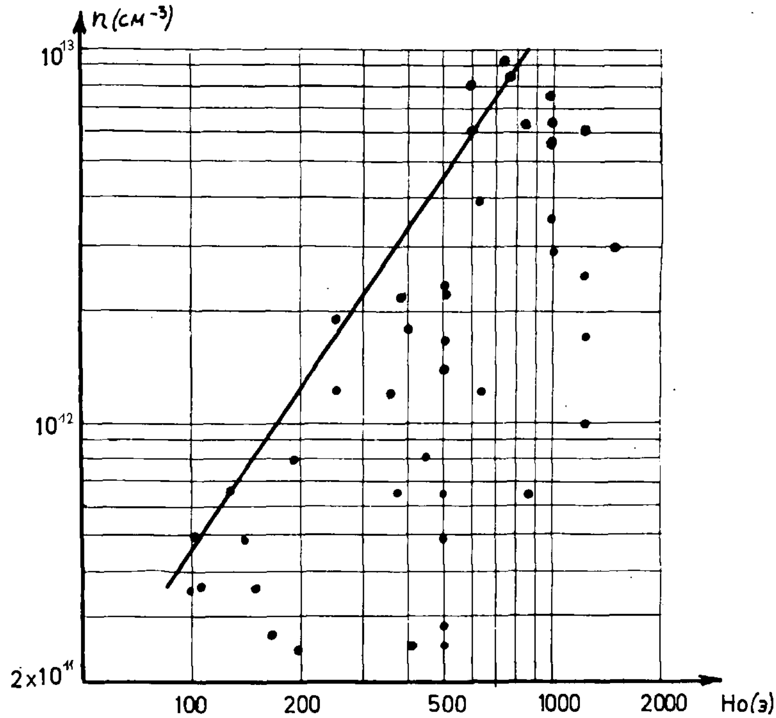

Рис.3. Граница ламинарности в аргоне (точки соответствуют экспериментальным значениям n_0, H_0, при которых регистрировалась осцилляторная структура БУФ).

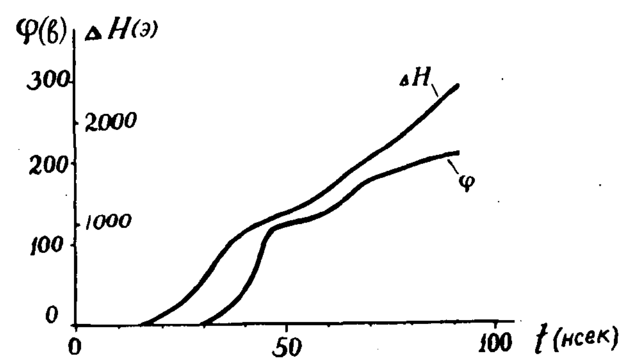

Рис.4. Профили H, φ при апериодической структуре БУФ (водород, $n_0 \sim 5 \cdot 10^{13}$ см$^{-3}$).

сверхпроводниках, получившего свое объяснение в фононной (т.е. фактически ионно-звуковой) модели сверхпроводимости. Более того, зависимость Δ от A на рис.5 не противоречит закону $\Delta \sim \left(\frac{m_i}{m_e}\right)^{1/3}$, полученному из приближенной нелинейной теории ионно-звуковой неустойчивости в плазме [5].

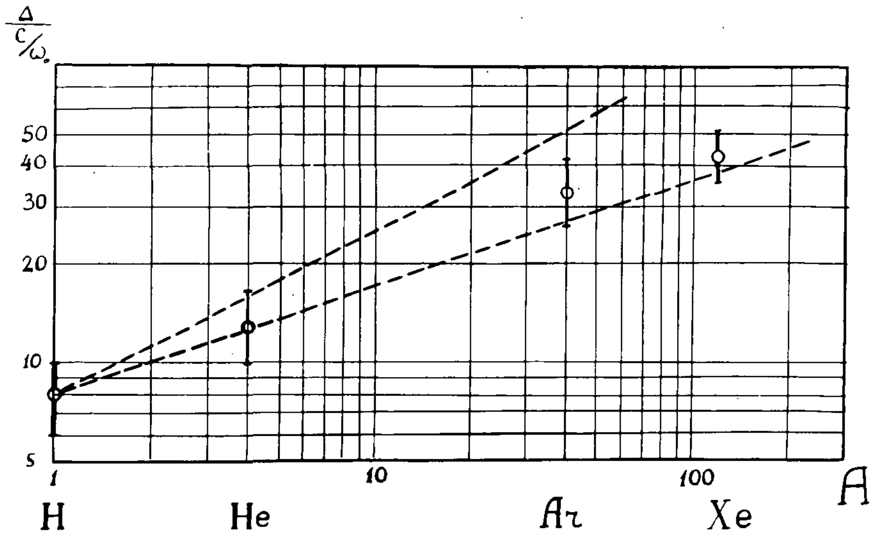

Рис.5. Зависимость ширины БУФ от массы ионов.

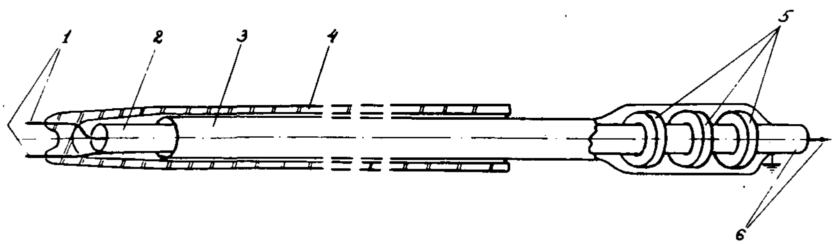

Рис.6. Конструкция электрического зонда: 1 – антенны; 2 – коаксиал; 3 и 5 – внешний экран и ферритовые кольца для защиты от помех; 4 – стеклянный изолятор; 6 – коаксиальный выход.

2. Зависимость n_c от H_c. В терминах ионно-звуковой неустойчивости переход от ламинарного к турбулентному режиму происходит тогда, когда $\nu\tau > \ln \varphi/\varphi_c$, где $\nu \sim \Omega_0$ – инкремент неустойчивости, $\tau \sim \frac{c/\omega_0}{V_a}$ – характерное время, а $\ln \varphi/\varphi_c$ – порядка кулоновского, если амплитуда флуктуаций φ_0 порядка равновесной. Это даёт неравенство $\omega_0 > 10\omega_H$, согласующееся с экспериментальной зависимостью, приведенной на рис.3.

3. Непосредственное измерение спектра микрофлуктуаций электромагнитного поля внутри БУФ. Для этой цели использовался миниатюрный двойной электрический зонд, конструкция которого приведена на рис.6. Экспериментально было установлено, что при $n > n_c$ внутри БУФ наряду с регулярными колебаниями $\tilde{E}$, соответствующими профилю волны, возникают высокочастотные стохасти-

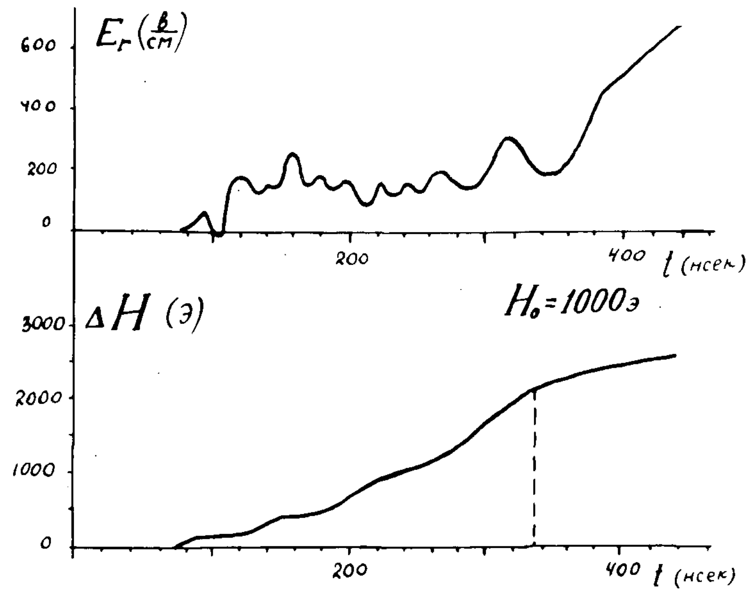

Рис.7. Распределение H, E_r, $\widetilde{E}$ внутри БУФ при $M > M_c$ (аргон, $n_0 \sim 10^{13}$ см$^{-3}$).

ческие колебания электрического поля (рис.7). Для анализа этих колебаний использовалось отличие длин волн ионного звука ($\lambda \sim 2\pi r_D$) и "свистов" ($\lambda \sim \Delta$). При изменении расстояния между антеннами в 10 раз (0,5 - 5 мм) средняя амплитуда флуктуационного сигнала с зонда практически не изменялась, что с достаточной убедительностью исключает "свистовую" природу этих колебаний ($\lambda \sim \Delta \sim$ 1 см). В пользу ионно-звукового механизма свидетельствует также близость частоты колебаний и ионно-звуковой ($\frac{\omega}{2\pi} \sim$ 100 ÷ 150 Мгц, $n_0 \sim 3 \cdot 10^{13}$см$^{-3}$).

Оценка флуктуаций потенциала внутри плазмы по зондовому сигналу затруднена тем обстоятельством, что диаметр антенны ($d \sim$ 0,2 мм) и длина её части, контактирующей с плазмой ($\ell \sim$ 0,5-1 мм) превосходят характерный масштаб колебаний ($r_D \sim 10^{-2} - 10^{-3}$ см в типичных условиях эксперимента $n \sim 10^{13}$см$^{-3}$, $T_e \sim$ 1 кэв), поэтому в оценку величины $\widetilde{\varphi}$ должен входить фактор $\frac{\ell}{2\pi r_D} \cdot \frac{d}{r_D}$. Различные способы учёта этого фактора дают для эффективной частоты столкновений, оцениваемой согласно [5] $\nu_{eff} \sim \frac{k^3 \widetilde{\varphi}^2}{4\pi m_e v_e n}$, значения, лежащие в пределах одного порядка с экспериментальными, найденными из формулы [5]:

$$\nu_{eff} \sim \frac{4\pi n e^2 u \Delta}{c^2 m_e}$$

4. Исследование спектра магнитных флуктуаций. Весьма тщательные измерения, проведенные в широком диапазоне частот (10–500 Мгц), миниатюрными магнитными зондами показали, что магнитное поле внутри БУФ обычно носит монотонный апериодический характер. Колебания $\tilde{H}$ удается регистрировать преимущественно в плазме тяжелых газов на начальной стадии формирования фронта. Они могут представлять собой как слабые магнито-звуковые возмущения, вызванные переходными процессами, так и "свисты" (измеренные частоты близки к $\frac{\omega}{2\pi} = \frac{\sqrt{\omega_H \Omega_H}}{2\pi}$).

Однако малость амплитуды ($\tilde{H} \sim 0.1 H_0$) делает пренебрежимым их вклад в турбулентное сопротивление плазмы. Эффективная частота столкновений, оцененная по измерениям $\tilde{H}$, оказывается на один-два порядка меньше требуемой для обеспечения наблюдаемой величины Δ .

Экспериментально найденные значения $\sigma \sim 10^{12}$-10^{13} $CGSE$, $j \sim 10^3$ а/см^2 внутри фронта позволяют оценить турбулентный нагрев j^2/σ и температуру T_e за фронтом. В условиях рис.7. ($n \sim 3.10^{13}$см$^{-3}$, $H_0 \sim 10^3$ гс) $T_e \sim 1$ кэв, что согласуется со значениями, полученными из измерений диамагнетизма плазмы за БУФ и из решения волновой задачи на ЭВМ. Таким образом, вся совокупность изложенных данных о макроструктуре БУФ и микроструктуре электромагнитных флуктуаций в волне с $M < M_c$ не противоречит представлениям о резистивном механизме диссипации, обусловленном "фононным трением".

Рассмотрим результаты, относящиеся к сильной волне ($M > M_c$).

Ранее было наблюдено резкое изменение структуры БУФ (образование "подножия", уширение до значения $\Delta \sim c/\Omega_0$) при $M > M_c \sim 3 \div 4$ [1, 2].

Последующие опыты были направлены на выяснение относительной роли в этом процессе механизмов дисперсии, сопротивления и вязкости.

1. Дисперсионный механизм уширения, возможный при возникновении перекоса фронта θ относительно H_0 был надежно исключен, поскольку было экспериментально показано $\theta = 0$ при $M > M_c$. Типичная осциллограмма магнитного поля в прямой волне при $M > M_c$ приведена на рис.8.

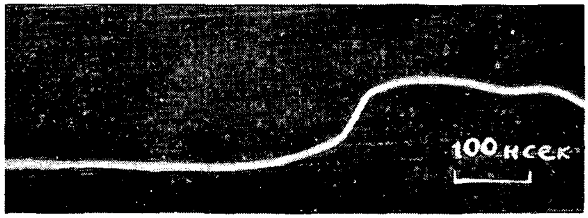

Рис.8. Профиль фронта H при $M > M_c$ (водород, $n_0 \sim 5 \cdot 10^{13}$ см$^{-3}$).

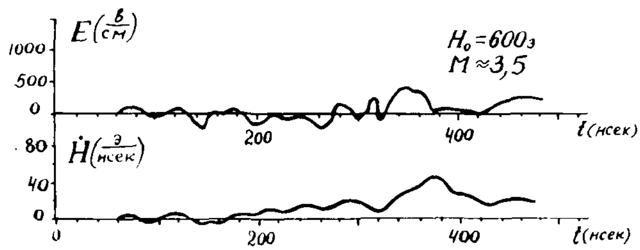

Рис.9. Флуктуации электрического и магнитного полей внутри БУФ при $M > M_c$(аргон, $n_0 \sim 10^{13}$ см$^{-3}$).

2. Предположение о возрастании сопротивления при $M > M_c$, как причине уширения фронта, противоречит наблюдаемому в эксперименте исчезновению запаздывания профиля φ относительно профиля H.

3. Одновременная регистрация профилей H и n установила при $M > M_c$ существование явления типа "изомагнитного скачка" плотности, что можно рассматривать как результат нарушения баланса между резистивной диссипацией и возрастающей нелинейностью в сильной волне, ведущего к её опрокидыванию и образованию многопотокового течения [4].

4. Электромагнитные флуктуации во фронте при переходе через критическое число Маха изменяют характер: область их локализации перемещается к подножию, одновременно регистрируются колебания с частотами $f \sim \frac{\sqrt{\omega_H \Omega_H}}{2\pi} M$ (рис.9).

Методом, описанным выше, показано, что характерный масштаб этих колебаний $\lesssim c/\omega_0$.

5. Выяснению микропроцессов внутри БУФ может послужить исследование энергетического спектра ионов и его зависимости от параметров волны. Измерения проводились с помощью дифференциального электростатического анализатора энергии ионов, получен-

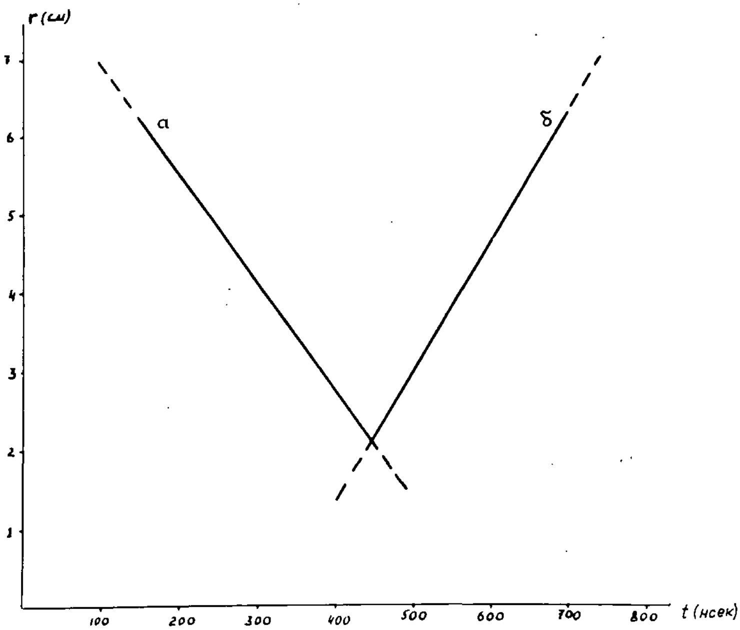

Рис.10. Диаграмма, определяющая место и время "старта" нейтралов перезарядки (а – движение фронта к оси; б – движение нейтралов с энергией $W \sim 150$ эв к периферии; водород, $n_0 \sim 4 \cdot 10^{14}$ см$^{-3}$, $M > M_c$).

ных при обдирке нейтралов, испускаемых нагретой плазмой. Одновременно использовались два анализатора,ориентированные соответственно поперек и вдоль фронта.

Зная расстояние от оси трубы до анализатора, положение магнитных зондов, скорости волны и регистрируемых ионов, можно построить диаграмму, устанавливающую место и время "старта" перезаряженных нейтралов (рис.10). Наиболее важным является экспериментальный результат, показывающий, что при $M > M_c$ нейтралы эмитируются "назад" относительно движения волны еще до её кумуляции на оси, что может быть объяснено лишь возникновением взаимопроникающих потоков (рис.10,11).

Средняя "температура" T_i, найденная из энергетического спектра ионов в области "подножия" волны $\sim \frac{mU^2}{2}$. При $M < M_c$ нейтралы эмитируются лишь из осевой области после кумуляции волны, которая также сопряжена с взаимопроникающими потоками и раскачкой колебаний $\tilde{E}$ и $\tilde{H}$.

6. Измерение скачка электрического потенциала на БУФ показывает, что величина $\frac{\varphi}{m_i(U^2 - v_i^2)}$ начинает падать в области

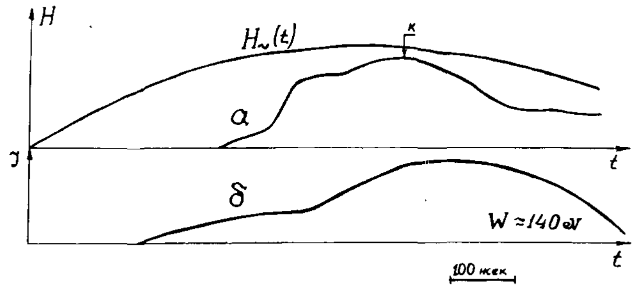

Рис.11. Профиль H во фронте (а) и интенсивность выхода нейтралов (б) при $W \sim 150$ эв. Начало движения частиц на периферию – до прихода волны на зонд, r= 2 см.

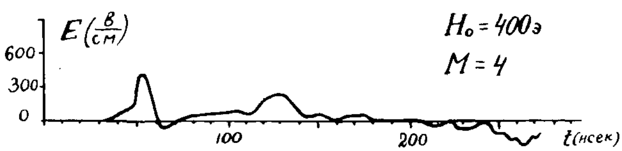

Рис.12. Распределение электрического поля E_r вдоль возмущенного слоя плазмы при $M > M_c$ (последовательные пики E_r: во фронте, в области "поршня", во фронте отраженной волны).

$M \sim M_c$ и при $M > M_c$ уменьшается примерно вдвое относительно исходного. Это может быть объяснено появлением и нарастанием при $M > M_c$ ионного давления во фронте.

7. По-видимому, этой же причиной обусловлен тонкий эффект, обнаруженный с помощью электрического зонда: появление при $M > M_c$ второго скачка E_r в области магнитного поршня. Это поле E_r должно компенсировать градиент ионного давления (рис.12).

8. Измерения диамагнетизма электронов плазмы показали уменьшение относительного нагрева электронной компоненты nT_e при $M > M_c$ (при $M < M_c$ величина nT_e согласуется с адиабатой Гюгонио).

Обобщая изложенные результаты, можно выдвинуть следующую картину развития физических процессов внутри БУФ при $M > M_c$. При возрастании амплитуды волны резистивная диссипация перестает компенсировать нелинейное укручение профиля n, что приводит к нарушению однопотоковости и последующему развитию ион-ионной неустойчивости с частотами порядка $\frac{\omega}{2\pi} \sim M \frac{\sqrt{\omega_H \Omega_H}}{2\pi}$ и $\lambda \sim c/\omega_0$. Оценка турбулентной вязкости по амплитуде колебаний $\tilde{E}$, $\tilde{H}$ приводит к значению ширины фронта, по порядку, близкому к c/Ω_0. Однако, проведенные измерения не позволяют считать исключенным вклад ионного звука, возбуждаемого неустойчивостью ионных потоков после опрокидывания, в вязкостное уширение фронта. Это обусловлено тем, что амплитуда колебаний $\tilde{E}$, достаточная для объяснения наблюдающихся толщин БУФ, ниже чувствительности использованной аппаратуры.

Ш. УДАРНЫЕ ВОЛНЫ, РАСПРОСТРАНЯЮЩИЕСЯ ПОД УГЛОМ К МАГНИТНОМУ ПОЛЮ

Закон дисперсии плазменных колебаний весьма чувствителен к направлению их распространения относительно магнитного поля [3]. Поэтому структура БУФ в волне, распространяющейся под углом θ к H_0, представляет убегающий относительно основного скачка шлейф осцилляций с характерным размером $\frac{c}{\Omega_0}\theta$, что было впервые экспериментально подтверждено в [1]. Последующие исследования "косых" волн проводились в двух экспериментальных схемах, различавшихся условиями возбуждения и параметрами начального состояния: I) подвижный "магнитный поршень" (УН-4), 2) плазменный поток, налетающий на препятствие (ПУММ). Параметры эксперимента на установке УН-4 указаны выше (гл.I, II). Наклон поршня к Но создавался благодаря неоднородности внешнего поля $H_\sim$ на краю ударного витка. С помощью системы 6 зондов, размещенных по координатам r, z, непосредственно измерялись угол наклона фронта θ, компоненты скорости U_r, U_z, компоненты поля H_r, H_z, H_φ. Основное внимание было уделено следующим вопросам: а) влияние на структуру БУФ угла θ; б) условия диссипативного подавления осцилляций; в) возможность разрушения фронта при больших числах Маха.

Эксперимент показал, что при непрерывном изменении от 0 до 45^0 происходит непрерывная перестройка БУФ от вида рис.2 до вида рис.13.

Турбулентное сопротивление, о существовании которого, в частности, свидетельствуют шумовые измерения, не нарушает характерного осцилляторного профиля, что можно объяснить большим размером осцилляции: $\frac{c}{\Omega_0}\theta > 10\, c/\omega_0$. По этой же причине влияние парных столкновений обнаруживается лишь при весьма низких степенях ионизации $\alpha \sim 10^{-3}$. Особый интерес представляет экспериментальное исследование зависимости структуры БУФ от амплитуды, поскольку аналитически не установлено существование критического числа Маха, а трудность качественного рассмотрения обусловлена существованием убегающих осцилляций, затрудняющих укручение фронта.

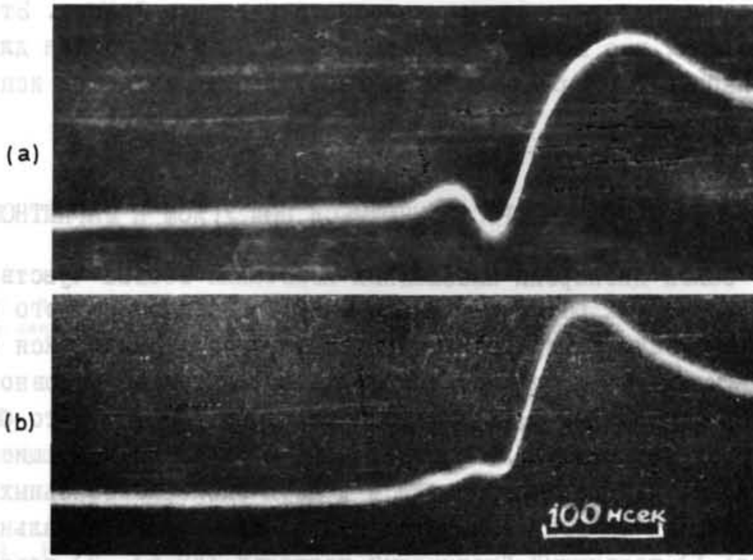

Рис.13. Структура БУФ при $\theta \sim 30°$, когда: а) $M < M_c$; б) $M > M_c$.

Результаты эксперимента, проведенного с постоянной ре - гистрацией θ, показали, что с возрастанием амплитуды первона - чально исчезают убегающие осцилляции, а затем оставшийся основной скачок перестраивается подобно тому, как это происходит в прямой волне (образование "подножия" и т.д., рис.13).

Решение задачи на ЭВМ показало весьма близкий к экспериментальному характер переходных процессов при приближении к $M \sim 5 \div 6$. Резюмируя, можно сказать, что в косой волне дисперсионный эффект не подавляется турбулентной диссипацией, однако, он не может предотвратить нарушения однопотоковости и разрушение осцилляторного профиля при больших амплитудах волны.

Любопытный тип косых ударных волн генерировался на установке "ПУММ". В этом случае ударный фронт формировался в результате взаимодействия плазменного потока с телом или с магнитным полем дипольной конфигурации.

Выбранный метод генерации ударных волн позволяет получить квазистационарный БУФ. В условиях эксперимента "ПУММ" (см.табл.I) фронт не является чисто БУФ, т.к. большую роль играют и диссипативные процессы типа вязкости и джоулевой диссипации. Однако, дисперсионные эффекты и здесь достаточно велики, чтобы привести к осцилляторной структуре фронта ударной волны. На рис. 4 пока -

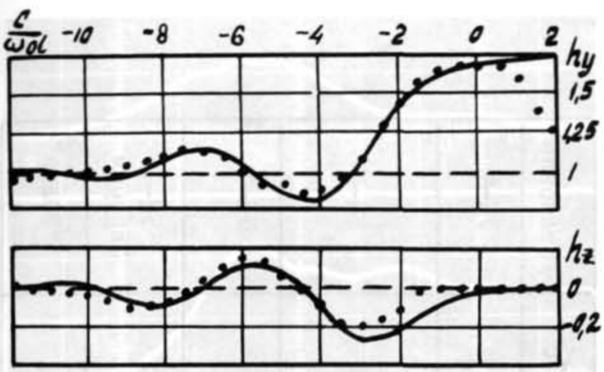

Рис.14. Профиль магнитного поля в косой волне $n_0 \sim 2 \cdot 10^{14}$ см$^{-3}$, $M_{off} = 2$. Сплошные кривые – расчет, точки – эксперимент.

заны экспериментальные и расчётные данные, полученные при учёте вязкости и джоулевой диссипации. Сопоставление расчётных и экспериментальных данных позволяет сделать вывод, что критическим параметром для возникновения осцилляций на фронте является степень замагниченности электронов $\omega_H \tau_e$. При $\omega_H \tau_e \gtrsim 1$ наблюдаются осцилляции, если же $\omega_H \tau_e < 1$, осцилляции подавлены и профиль волны становится апериодическим.

Вопрос о возможности существования БУФ, распространяющегося вдоль магнитного поля ($\Theta \sim \frac{\pi}{2}$), остается открытым.

Параметры установки УН-6 (таблица I) должны позволить приподнять завесу над мистерией БУФ в этом случае.

IУ. УДАРНЫЕ ВОЛНЫ В ПЛАЗМЕ БЕЗ МАГНИТНОГО ПОЛЯ

Одна из возможностей существования БУФ в плазме без магнитного поля связана с вопросом о нелинейных ионно-звуковых колебаниях в неизотермической плазме ($T_e \gg T_i$) [3]. Неизотермическая плазма представляет собой пример сильно диспергирующей среды с малым поглощением. В такой среде возможно распространение нелинейных устойчивых элементарных волн, например, солитонов сжатия, а любое гладкое начальное возмущение, вообще говоря, с течением времени будет распадаться на совокупность таких элементарных колебаний с длинами волн порядка характерной длины дисперсии (дебаевский радиус в данном случае).

На установке "Волна" (таблица I) поставлен эксперимент, в котором удалось наблюсти, как первоначально гладкое возмущение

Таблица 2. ТИПЫ И ХАРАКТЕРНЫЕ РАЗМЕРЫ БУФ

Тип БУФ		δ - в ламинарном случае	Δ - турбулентное	M_c	Установка
$\perp H$ при $\frac{H^2}{8\pi} < n m_e c^2$	$n < n_c$	$\frac{c}{\omega_0}$			УН-4
	$n > n_c$		$10 \div 30 \frac{c}{\omega_0}$ при $M < M_c$ $\sim \frac{c}{\Omega_0}$ при $M > M_c$	~ 3	УН-4
$\perp H$ при $\frac{H^2}{8\pi} > n m_e c^2$		$\frac{V_A}{\Omega_0}$			УН-4
Косой БУФ $\theta > \theta_c$		$\frac{c}{\Omega_0}\theta$			УН-4 "ПУММ"
$H=0$, $T_e \gg T_i$		r_D			"Волна"

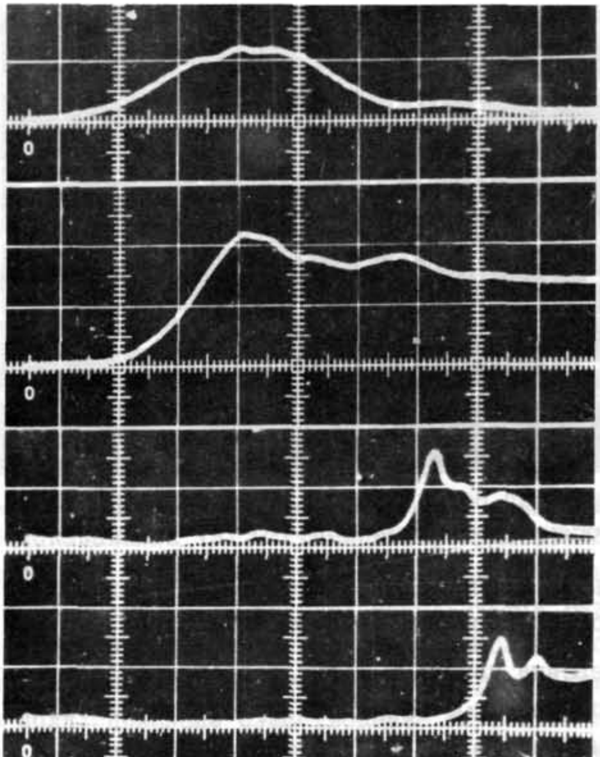
Рис.15. Осциллограммы сигналов с поглотителя на расстояниях (сверху вниз): 1, 3, 12, 19 см от источника. Масштаб времени и концентрации – соответственно 20 мксек и $2 \cdot 10^5$ см$^{-3}$ на большое деление.

большой амплитуды в неизотермической плазме, в результате нелинейной деформации, распадается на элементарные колебания с характерным пространственным размером порядка дебаевского радиуса, т.е. появление осцилляторной структуры.

Плазма образовывалась в металлической цилиндрической камере (диаметром 90 см, длиной I20 см) ионизацией газа потоком электронов от накаленного катода (Iк $\simeq$ I0 ма). Опыты проводились в инертных газах: ксеноне, аргоне и гелии при давлении 0,5 – I.I0^{-4} мм рт.ст. Температура и концентрация электронов в такой плазме определялись из зондовых характеристик. Для создания волны возмущения в "спокойной" плазме был использован специально разработанный для этой цели источник плазмы, представляющий собой цилиндр диаметром 80 см и длиной 20 см, набранный из последовательно включенных плоских сеток (4) ("электростатичес-

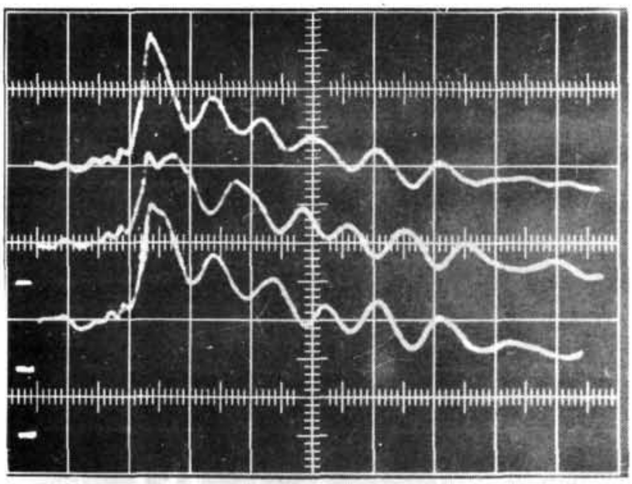

Рис.16. Сигналы с зонда, полученные в последовательные моменты времени. Масштаб времени и концентрации – соответственно 10 мксек и $2\cdot10^{6}$ $см^{-3}$ на большое деление.

кий поршень"). К центральной сетке прикладывался положительный потенциал с регулируемым фронтом нарастания.

Измерение потока в волне регистрировалось с помощью поглотителя плазмы, состоящего из набора параллельных пластинок, установленных вдоль движения волны. Приложенное к ним напряжение рассасывало плазму, и сигнал, пропорциональный току, подавался на вход дифференциального усилителя. Частотная характеристика измерительной цепи была линейной вплоть до I мггц.

На рис.15 приведены осциллограммы при некоторых положениях измерителя, показывающие эволюцию формы волны в ксеноновой плазме по мере её распространения. Скорость фронта равна 3.10^5 см/сек, что соответствует числу Маха $M \sim 1{,}5$. Видно, как по мере распространения волны происходит уменьшение ширины фронта вплоть до некоторого уровня порядка 2 см, что примерно равно дебаевскому радиусу, а за фронтом возникают колебания с длиной волны порядка дебаевского размера. С помощью электростатического зонда, перемещающегося перпендикулярно распространению волны, было установлено, что отклонение от плоской формы по всему фронту не более I см.

Характер регистрируемых на установке "Волна" сигналов совершенно меняется при увеличении амплитуды "электростатического поршня" (рис.16). Колебания за фронтом волны в этом случае становятся хаотическими. Их частота, по-прежнему, порядка Ω_0.

Трудно предположить здесь какой-либо иной механизм возбуждения, кроме пучковой неустойчивости взаимопроникающих ионных потоков, возникающих после опрокидывания фронта нелинейного возмущения. Длина корреляции таких колебаний оказывается приблизительно на порядок больше дебаевского радиуса. Эта длина, к сожалению, ненамного меньше характерных размеров плазменного потока в установке "Волна". Поэтому наблюдённую картину еще нельзя считать картиной установившегося БУФ.

У. ЗАКЛЮЧЕНИЕ

Таким образом, на установках табл.I удалось исследовать практически все типы ламинарных структур БУФ, возможные в разряженных плазмах. При этом достигнуто хорошее согласие с теоретическими предсказаниями [3] . Границы перехода от ламинарного к турбулентному БУФ также достаточно удовлетворительно описываются теоретическими моделями, в которых используются различные неустойчивости (удобно подытожить всё это с помощью табл.2). Наиболее детально исследован при этом БУФ, распространяющийся поперёк магнитного поля. Доказано существование аномально низкой электропроводности внутри такого БУФ, причиной чему является ионно-звуковая турбулентность [5] . Механизмы, связанные со "свистами" [6] , не проходят из-за слишком низкой интенсивности флуктуаций, которые можно было бы отождествить с волнами типа "свистов". Однако само присутствие таких флуктуаций (пусть даже малой интенсивности) может свидетельствовать о том, что внутри БУФ неустойчивость этого типа сосуществует с ионно-звуковой (хотя и играет второстепенную роль). Далее показано, что при числах Маха, больших критического, главную роль начинает играть не аномальное сопротивление, а вязкость. Происходящий при этом эффективный нагрев ионов указывает на то, что следует искать ионный механизм этой вязкости. Критическое число Маха $M_c \sim 3 \div 4$, что совпадает с границей появления изомагнитного скачка (для стационарной плоской волны $M_c = 2{,}8$ при $\gamma = 5/3$). Более того, показано, что при приближении M к M_c профиль плотности внутри БУФ становится круче магнитного. Теперь все это можно согласовать с опрокидыванием фронта плотности и появлением многопотокового движения ионов при $M > M_c$. Тогда наблюденные электромагнитные флуктуации с $\omega \sim (\omega_H \Omega_H)^{1/2}$ и $K \sim \frac{\omega_0}{c}$ естественно связывать с неустойчивостью взаимопроникающих потоков ионов, движущихся поперёк магнитного поля [3]. Длина размешивания здесь порядка

$\Delta \sim \frac{c}{\omega_0}\left(\frac{m_i u^2}{e\tilde{\varphi}}\right)^2$ или $\frac{c}{\omega_0}\left(\frac{H_0}{\tilde{H}}\right)^2$ (естественно предположить, что при максимальных амплитудах турбулентности $e\varphi \sim m_i u^2$, $H_\sim \sim H_0$, размешивание происходит на расстоянии порядка длины волны неустойчивости). Измеренные величины $\tilde{\varphi}$ и $\tilde{H}$ приводят к Δ как раз на два порядка больше c/Ω_0.

СПИСОК ОБОЗНАЧЕНИЙ

m_e, m_i – массы электрона и иона

e – заряд электрона

c – скорость света

n – концентрация плазмы

ω_0, Ω_0 – электронная и ионная плазменные частоты

ω_H, Ω_H – электронная и ионная циклотронные частоты

$\omega_г = \sqrt{\omega_H \Omega_H}$ – гибридная частота

r_D – дебаевский радиус

H – магнитное поле

E_r, E_φ – радиальная и азимутальная компоненты электрического поля

φ – электрический потенциал

$\tilde{\varphi}, \tilde{H}, \tilde{E}$ – амплитуда флуктуаций потенциала, магнитного и электрического полей

u – скорость волны

V_a – альфвеновская скорость

V_1 – скорость плазмы за фронтом волны

M – число Маха

$\frac{\pi}{2}-\theta$ – угол распространения волны по отношению к начальному магнитному полю

Δ, δ – пространственная ширина фронта

τ – временная ширина фронта

σ_{eff} – эффективная проводимость плазмы

ν_{eff} – эффективная частота столкновений

τ_e – время свободного пробега электронов

T_e, T_i – электронная и ионная температуры

j – плотность тока

λ – длина волны колебаний

$f = \frac{\omega}{2\pi}$ – частота колебаний

k – волновой вектор колебаний

d – диаметр антенны электрического зонда

l – длина антенн электрического зонда

L – длина установки

D – диаметр установки

ЛИТЕРАТУРА

[1] КУРТМУЛЛАЕВ, Р.Х., НЕСТЕРИХИН, Ю.Е., ПИЛЬСКИЙ, В.И., САГДЕЕВ, Р.З., Plasma Physics and Controlled Nuclear Fusion Research, II, CN-21/218, IAEA, Vienna, 1966, p.367;
ИСКОЛЬДСКИЙ, А.М., КУРТМУЛЛАЕВ, Р.Х., НЕСТЕРИХИН, Ю.Е., ПОНОМАРЕНКО, А.Г., ЖЭТФ 47 (1964) 774.

[2] PAUL, J.M., HOLMS, L.S., PARKINSON, M.J., SHEFFIELD, J., Report, Int. Conf. on Phenomena in Ionized Gases, Belgrade, 1965;
ЗАГОРОДНИКОВ, С.П., СМОЛКИН, Г.Е., ШОЛИН, Г.Н., Доклад на Межд. конф. по ионизованным газам, Белград, 1965.

[3] САГДЕЕВ, Р.З., Вопросы теории плазмы 4 Атомиздат, М., 1964, стр.20;
САГДЕЕВ, Р.З., ЖТФ 31 (1961) 1955; БЕРЁЗИН, Ю.А., КУРТМУЛЛАЕВ, Р.Х., НЕСТЕРИХИН, Ю.Е., Физика горения и взрыва 1 1966, стр.3.

[4] БЕРЕЗИН, Ю.А., КУРТМУЛЛАЕВ, Р.Х., Физика горения и взрыва 3 1966, стр.3;
ЕСЕЛЕВИЧ, В.Г., КУРТМУЛЛАЕВ, Р.Х., ПИЛЬСКИЙ, В.И., Письма ЖЭТФ 5 (1967) 9, 311; КУРТМУЛЛАЕВ, Р.Х., МАСАЛОВ, В.Л., МЕКЛЕР, К.И., ПИЛЬСКИЙ, В.И., Письма ЖЭТФ 7 (1968) 65; ЕСЕЛЕВИЧ, В.Г., КУРТМУЛЛАЕВ, Р.Х., МАСАЛОВ, В.Л., МЕКЛЕР, К.И., ПИЛЬСКИЙ, В.И., Доклад на Межд. конф. по физике ударных волн, Новосибирск, 1967.

[5] SAGDEEV, R.Z., GALEEV, A.A., Lecture on the Non-linear Theory of Plasma, Trieste, Sept. 1966.

[6] CAMAC, M., KANTROWITZ, A.R., LITVAK, M.M., PATRICK, R.M., PETSCHEK, H.E., Int. Conf. on Plasma Physics and Controlled Nuclear Fusion Research, Salzburg, paper CN-10/132, 1961;
РУДАКОВ, Доклад на Межд. конф. по физике ударных волн, Новосибирск, 1967.

DISCUSSION

S.D. FANCHENKO: Was the spectrum of the microwave oscillations which you detected by means of an electric probe monochromatic or broad?

R.Z. SAGDEEV: It was a broad, disordered spectrum. However, it cannot be interpreted quantitatively since the dimensions of the oscillations may be much less than those of the probe.

S.D. FANCHENKO: Can one identify the oscillation type?

R.Z. SAGDEEV: The oscillations in question have a wavelength less than ten Debye radii, and we do not know of any oscillations (except ion-sound oscillations) in this range.

EXPERIMENTAL RESULTS ON THE GENERATION AND STRUCTURE OF COLLISIONLESS SHOCKWAVES

E. HINTZ
INSTITUT FÜR PLASMAPHYSIK DER KERNFORSCHUNGSANLAGE JÜLICH,
FEDERAL REPUBLIC OF GERMANY

Abstract

EXPERIMENTAL RESULTS ON THE GENERATION AND STRUCTURE OF COLLISIONLESS SHOCK-WAVES. Investigations on shockwaves generated in z-pinches and θ-pinches at low densities have previously shown that under certain conditions the structure of the wave front is determined by collective interactions. First experiments have been performed in a narrow parameter range. More experimental evidence on the dependence of the wave structure on shock parameters M_A, β_0, α and θ is needed. Here $M_A^2 = U_0^2 4\pi n_0 m_i/B_0^2$; $\beta_0 = 8\pi n_0 k T_0/B_0^2$, $\alpha = B_0^2/8\pi n_0 m_e c^2$; θ is the angle between B_0 and the wave front. B_0 is the initial magnetic field, n_0 the initial density, T_0 the initial temperature, m the particle mass, and U_0 the shock velocity.

An investigation of the dependence of the structure of collision-free shockwaves on β_0 (between 0.02 and 1) and M_A (between 1.3 and 10) with $\alpha << 1$ and $\theta << 1$ was one main objective of the experiments reported here. Another main purpose was to examine the conditions under which "steady-state" shockwaves can be generated in a θ-pinch, and to develop an experimental technique for the generation of such shockwaves.

The appearance of Rayleigh-Taylor instabilities in the plasma boundary is also discussed.

1. INTRODUCTION

Most of the experiments on collisionless shockwaves have been performed in z-pinch [1, 7] and θ-pinch [2-6] devices of cylindrical geometry with the driving current being generated by simple LC-circuits. Shockwaves obtained under such conditions are time-dependent. In case of θ-pinches the diameter of the discharge tubes has, in addition, usually been too small to allow a distinct separation of wave front and piston and to exclude the possibility of the observed shock structure being influenced by the piston. The existing difficulties may be enhanced if the initial plasma does not fill the tube and if the distribution of plasma density and plasma temperature is strongly non-uniform. As a result, a comparison of the experiments with theory, which is usually done for steady-state conditions, is difficult and an unambiguous interpretation of the measurements and an identification of the collisionless dissipation mechanism may be impossible.

To obtain better results it is not sufficient to use discharge tubes of larger diameter; it is necessary to choose carefully the electrical circuit parameters and to examine and control the properties of the initial plasma for each case under study. If we take into consideration the conclusions from a simplified model it is found experimentally that shockwaves can be generated in a θ-pinch (tube diameter 20 cm) which appear to be stationary for an appreciable period of time and the macroscopic properties of which are in agreement with the model.

Detailed studies of collisionless shockwaves [1-7] have so far been confined to the parameter range $\beta_0 \ll 1$; $\theta \ll 1$; $\alpha \ll 1$; $2 < M_A < 4$. Although there remains much to be learned under these conditions, it appears desirable to study shockwaves in other parameter ranges where new structures and different dissipation mechanisms will occur. In our laboratory we have first made an effort to generate large-amplitude waves at smaller Alfvén Mach-numbers; in addition, we have started investigations at larger values of β_0 ($\beta_0 \approx 1$) partly motivated by the fact that the magnetospheric bow shock occurs under such conditions. We have extended these studies to the limiting case $B_0 = 0$. This case is of practical interest since it is under this condition that θ-pinches have been successful in producing high-density plasmas with ion temperatures in excess of 5 keV. We expect that a detailed experimental investigation will show that ion acoustic shocks [8] are responsible for the observed heating.

2. EXPERIMENTAL PROCEDURES

For the generation of the shockwaves a θ-pinch [9] device was used. A diagram of the electrical circuit and the typical shape of the current pulse in the compression coil are shown in Fig. 1. The initial plasma is generated by means of an electrodeless discharge. After the formation of a fully ionized plasma of about 2 eV temperature, the preheater bank is shortcircuited and a slowly rising magnetic field is switched on, which keeps the plasma away from the walls and at the same time compresses

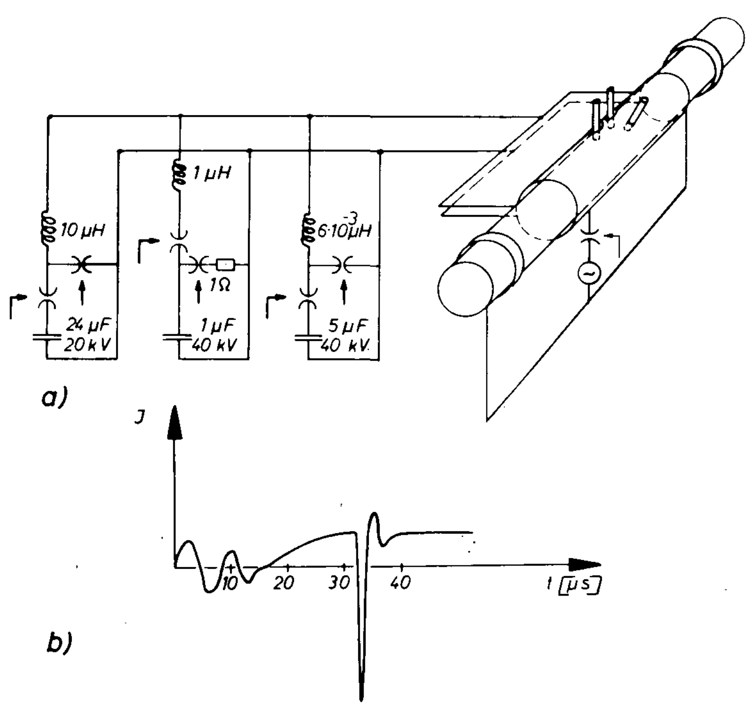

FIG. 1. a) Electrical circuit diagram; b) shape of current pulse in compression coil.

the plasma more or less strongly, depending on its final magnitude. This current is crowbarred at its maximum and then the main compression field is switched on. This field has a rise time of about 0.8 μs and its magnitude can be varied between 1.5 and 7 kG. The compression coil is 45 cm long and has a diameter of 20 cm. In general, deuterium at 3.5×10^{-3} Torr was used as a filling gas. In one case we used argon at 2×10^{-3} Torr. The electron density was measured by means of a microwave probe [10] of high space- and time resolution in combination with a 2 mm microwave interferometer. The magnetic field was measured with a particularly small and fast magnetic probe. The electron temperature in the initial plasma was determined by standard spectroscopic methods.

The electron temperature in the shock front is obtained by using the light scattering technique [6, 7]. These measurements are difficult at small densities and first results have just been obtained.

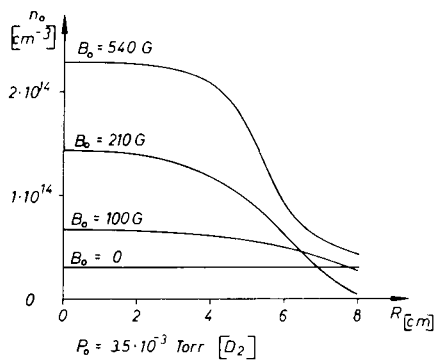

FIG. 2. Radial density distributions shortly before start of compression for different magnetic bias fields.

3. PROPERTIES OF THE INITIAL PLASMA

Figure 2 shows density distributions at the time when the compression pulse is applied to the coil, the magnitude of the magnetic bias field being varied between 0 and 540 G. The density variation along the tube axis was less than 20%. Figure 3 shows the development of the electron temperature during the pre-heating phase. The variation of the electron temperature along the axis was negligible. The ion temperature was not measured but it can be assumed that it is equal to the electron temperature. A more complete description of the apparatus and of the measurements during the pre-heating phase is found in Ref. [11].

4. MACROSCOPIC PROPERTIES OF SHOCKWAVES IN θ-PINCHES

Questions connected with the generation of stationary shockwaves in θ-pinches are discussed in more detail in Ref. [11]. Here we will summarize only the results of this discussion.

If a simple LC-circuit is used for the generation of the compression pulse and if L_0 is the inductance of the circuit before the plasma in the coil starts moving and L_c the vacuum inductance of that part of the coil which is initially occupied by the plasma, then $L_0/2\,L_c \ll 1$ is one requirement to obtain a "steady state" shock. The cylindrical convergence of the wave can be neglected as long as $(R_p-R_s)/R_0 \ll 1$, R_0 being the initial radius of the plasma and the subscripts p and s referring to the piston and the shock front, respectively.

To obtain a distinct separation between piston and shock front we have to demand $\Delta/(R_p-R_s) \ll 1$ and $d/(R_p-R_s) \ll 1$. Here d is the penetration depth of the magnetic field into the shocked plasma and Δ the shock thickness. For resistive shocks with sufficiently high Alfvén-Mach number the last inequality is equivalent to $\Delta/(R_0-R_s) \ll (1/(\eta^2)\cdot(\sigma_p/\sigma_s)$ with η being the compression ratio across the shock front and σ the plasma conductivity.

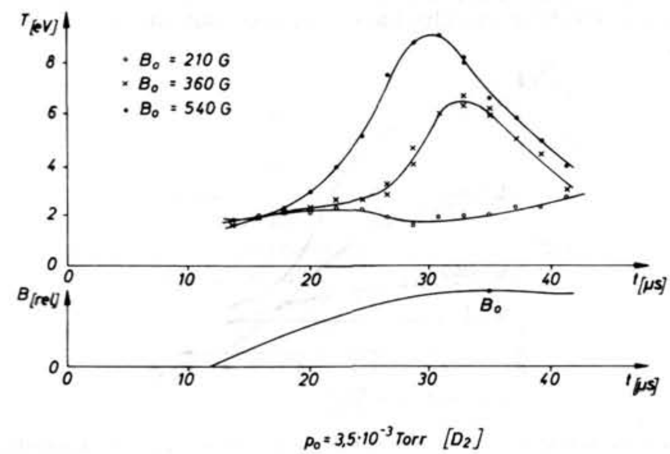

FIG. 3. Electron temperature as function of time for different magnetic bias fields.

Since $\eta^2 \approx 10$ for strong shocks, we need tube radii of at least 10 cm if we want to resolve the shock front and if $\sigma_p \approx \sigma_s$. The restrictions are relaxed if $\sigma_p \gg \sigma_s$, as may be the case if the polarity of the driving magnetic field is opposite to that of the bias field.

In that region of the tube where the shock can be considered as plane the following relations hold:

$$U_p = \frac{1}{(1+\gamma)^{1/4}}\;\frac{1}{(\mu_0 n_0 m_i)^{1/4}}\,E_p^{1/2}$$

$$B_p = (1+\gamma)^{1/4}\,(\mu_0 n_0 m_i)^{1/4}\;E_p^{1/2}$$

where U_p is the piston velocity, E_p the electric field at the piston, and γ is the ratio of the specific heats.

In Fig. 4 a typical magnetic field signal is reproduced for a shockwave in deuterium with a negative bias field of 360 G. About 200 ns after the start of the discharge the wave front arrives at the probe. The magnetic field in the plasma is compressed by the shock in about 40 ns, remains constant for 200 ns except for some fluctuations and is then reversed as the piston arrives. The shock width can be taken from the B-signal and corresponds to 10 c/ω_{pe}.

Shock and piston velocity are approximately constant through a region of about 4 cm and the magnitudes of the piston velocity and of the driving magnetic field agree with the values calculated from the above formulae to within 15%. It is seen that the magnetic field of the piston is indeed practically constant.

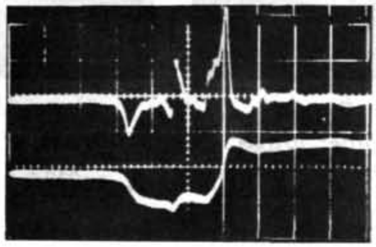

FIG.4. Magnetic probe signal in case of "steady-state" shock wave propagating into plasma with negative bias field.

All results presented in this report have been obtained with negative bias fields. If the bias field has the same polarity as the piston field it is more difficult to obtain stationary shocks, however the shock width does not change [11].

The main difficulties encountered in generating "steady state" shock-waves were due to the appearance of instabilities. Two types of instabilities have been observed:

a) Rayleigh-Taylor type instabilities (Fig. 5)

This instability, which is often observed, starts in the acceleration phase of the piston. After the piston has obtained a constant velocity, the amplitudes do not grow any more. The observed growth rate γ is consistent with wavelength and acceleration ($\gamma = \sqrt{k \cdot g}$) [12]. On the basis of the existing data it cannot be decided by what processes the observed wavelength of maximum growth is determined; viscous damping [13] as well as density gradient [14] of the boundary layer might be important. With high initial temperatures ($T_e \geq 5$ eV) and an initial magnetic field antiparallel to the compressing field the instability is not observed. In case of parallel fields the instability always appears although wavelength and amplitude depend on the initial parameters.

b) Instabilities due to the magnetic field passing through zero

This instability is observed only at later times when the piston has reached a constant velocity and has not been investigated in detail.

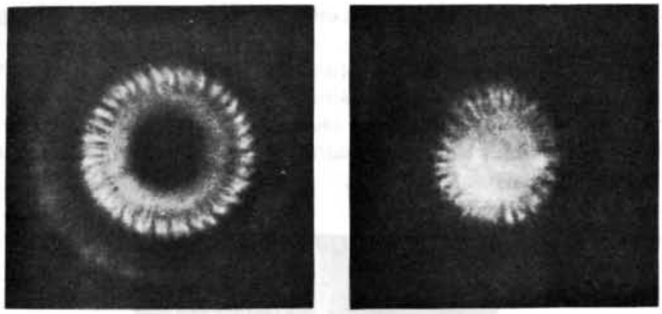

FIG.5. Development of Rayleigh-Taylor instabilities during implosion of plasma.

5. RESULTS ON SHOCKWAVE STRUCTURES

1. Large amplitude compression waves with oscillatory structure

Waves with oscillatory structure can only be expected if the damping due to Coulomb collisions is sufficiently small and the Alfvén Mach-number is small enough for electrostatic instabilities to be unimportant [15]. For technological reasons we could not generate steady-state collisionless shockwaves of small Mach number. It was, however, expected that at the beginning of the discharge, during the acceleration of the shockwave, regular oscillations would be excited in the wave front. This was indeed observed in several cases. Figure 6 b shows oscillograms of the voltage at the coil, of the magnetic field and of the dB/dt at R = 4 cm. The electron density at this point of space was $n \approx 5 \times 10^{13}$ cm^{-3}. The magnetic field signal shows the formation of a small amplitude shockwave ($M_A \approx 1.3$) immediately after the voltage has reached its maximum. Since the initial field and the compression field are of opposite polarity, the compression wave is clearly recognizable. The damped oscillation is more evident in the B-signal. From an analysis of the oscillogram a wavelength of 10 c/ω_{pe} is obtained. This is in agreement with theoretical expectations [15] ($\lambda = 2\pi\, c/\sqrt{(M-1)}\omega_{pe}$). By withdrawing the probe to R = 6 cm one can observe the wave at an earlier stage. As shown in Fig. 6 a the wave has the shape of a solitary pulse. The half-width is about 5 c/ω_{pe}. A quantitative comparison with theory is not possible since the accuracy of the measurements is not good enough and the waves are non-steady.

2. Shockwaves with monotonic structure at small β_0

Shockwaves were also studied under conditions similar to those obtained in various other laboratories [1-7], i.e. at $\beta_0 = 0.1$ and $M_A \approx 2.5$. For this case radial magnetic field distributions were measured and gave a shock thickness of 5 mm corresponding to $\Delta \approx 10\ c/\omega_{pe}$ in agreement with observations by other authors. The thickness of resistive shocks derived from hydromagnetic theory is [15]:

$$\Delta = \frac{c^2}{4\pi\sigma U_0 (M-1)} = \frac{c^2}{\omega_p^2} \quad \frac{V_{eff}}{U_0} (M-1)$$

A comparison of this thickness with the measured shock thickness shows that the effective conductivity in the shock front is by a factor of 25 lower than the conductivity of the initial plasma. For the effective collision frequency we obtain $\nu_{eff} = 5 \times 10^9 \ s^{-1}$ which is approximately $0.5\,\omega_{pi}$.

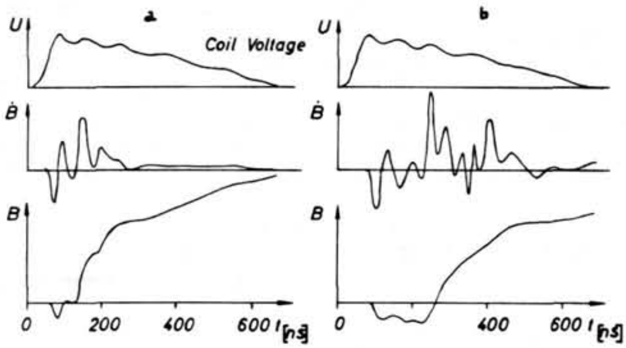

FIG. 6. Oscillatory wave structures in early phase of shock formation; a) solitary wave ($n_0 = 3.10^{13}$ cm^{-3}, R = 6 cm); b) shock wave at M_A 13-15; ($n_0 = 5.10^{13}$ cm^{-3}, R = 4 cm). $T_{eo} \approx 8$ eV, $B_0 \approx -600$G.

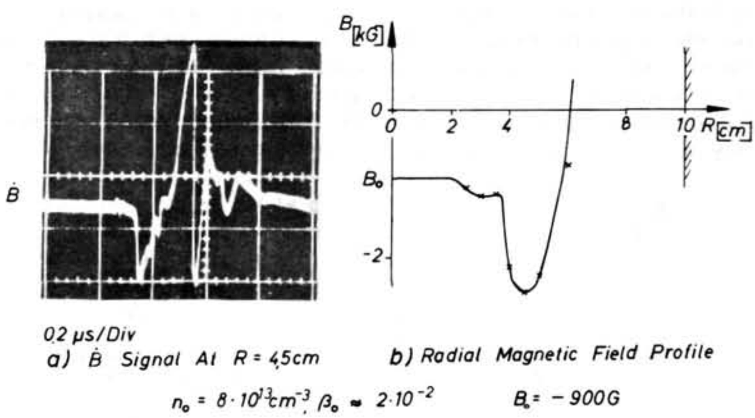

FIG. 7. Shock wave in argon at $M_A = 3.1$.

To check whether the effective collision frequency is proportional to the ion plasma frequency, we repeated the experiment with argon. Figure 7 b shows a shockwave profile in an argon plasma at $\beta_0 = 0.02$ and $M_A \approx 3.1$ at an initial density of $n_0 = 8 \times 10^{13}$ cm^{-3}. Unfortunately, the Alfvén Mach-number is a little higher than the critical Mach number [16] at which purely resistive shocks with a monotonic structure fail to dissipate a sufficient amount of energy, and another dissipation mechanism must be present. It is generally believed that the double structure of the shock front at Alfvén-Mach numbers above 3, as was observed in other laboratories (see Refs [5, 7, 17]), is due to this effect. Here we observe a similar double structure, consisting of a broad and a narrow part. The broad part occurs at a later time and changes with time. Most of the effective Joule heating occurs in the narrow part, which has a thickness of about 3 mm. From this we again obtain $\nu_{eff} \approx 1/2\ \omega_{pi}$. One of the theoretical models for resistive shocks in this Mach number range assumes that the shock front starts as a solitary wave [15]. Owing to the increasing gradient of the magnetic field, the electrons acquire a drift velocity sufficient to start an electron two-stream instability which randomizes the drift velocity and results in an increase of the electron temperature. An ion wave instability, which heats the electrons further can be excited. If this were true one would expect sudden changes in the magnetic field gradient. This has not been observed so far. However, an examination of the B-signal in the shock front of the argon case, Fig. 7 a, shows that the magnetic field gradient first is rather steep and then flattens. Simultaneously, small amplitude fluctuations are observed with a frequency of about $5 \times 10^7\ s^{-1}$ ($\approx 0.1\ \nu_{eff}$). Fluctuations at higher frequencies would probably not be detected because of the frequency response of the measuring system. The drift velocity of the electrons in the shock front is about 3×10^8 cm s^{-1}, which is much larger than the initial thermal velocity.

3. Shockwave structures at large β_0

Further results on shockwave structures have been obtained at larger values of β_0 ($\beta_0 \approx 0.5$ and $\beta_0 = 1$) and at Alfvén-Mach numbers between 2 and 9.

Fig. 8 shows a radial magnetic field profile for a shockwave at $M_A = 2.7$. From the shock profile we obtain $\Delta = 10\ c/\omega_{pe}$ and $\nu_{eff} \approx 0.3\ \omega_{pi}$, as in the low-$\beta$ cases. Immediately behind the front, large magnetic field fluctuations were observed. The fluctuations have also a B_θ-component with an amplitude about equal to that of the B_z fluctuations. The observed frequency is about 10 times the local ion cyclotron frequency ω_{ci}.

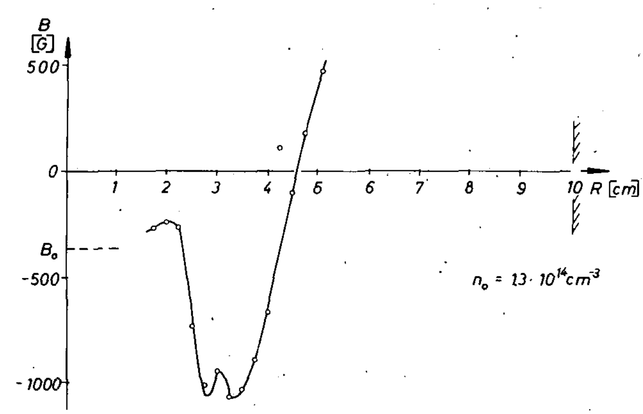

FIG. 8. Shock wave in deuterium at $M_A = 2.7$, $\beta_0 = 0.6$.

For a shock under very similar conditions T_e was measured in the middle of the shock front. We obtained $T_e = 19$ eV $\pm 30\%$.

Fig. 9 shows the radial magnetic field profiles for an Alfvén Mach-number of 4.4. The shock front is considerably broader than for $M_A = 2.7$; however, the double structure observed for small β_0 at such high Mach numbers does not appear. This may be connected with the high initial β.

The magnetic field is not monotonic. Therefore it may well be that the dissipation in the shock is mostly resistive, although the Alfvén Mach-number is well above critical. Similar shock structures have been observed by Heppner [18] in the earth's bow shock, when owing to fluctuations of the interplanetary magnetic field, β_0 and M_A were abnormally low. In this case a shock width is observed which is within a factor of two equal to c/ω_{pi}. In Fig. 9 $\Delta \approx 0.3\ c/\omega_{pi}$ or $\Delta \approx 20\ c/\omega_{pe}$.

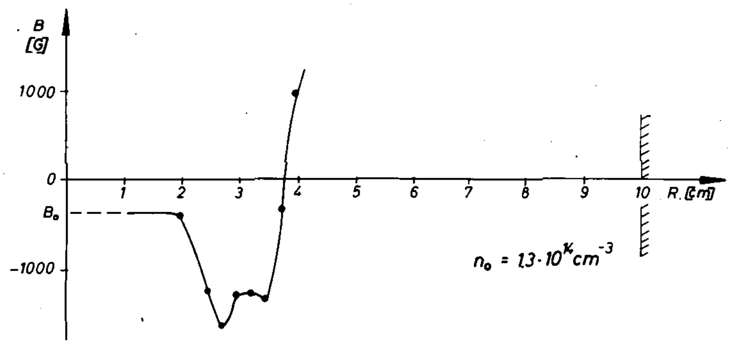

FIG. 9. Shock wave in deuterium at $M_A = 4.5$, $\beta_0 = 0.6$.

The 2 mm microwave probe was used to observe the density variation in the shock front. The density jump appears simultaneously with the jump in the magnetic field. For high β_0 there is no indication for a double structure up to Alfvén Mach-numbers of 6.5. The interferometer signal is highly damped. If we assume that the attenuation is due to "collisional" damping we obtain for the effective collision frequency $0.03 < \nu_{eff}/\omega < 0.1$, where $\omega = 8.5 \times 10^{11}$ rad/s. It is clear that the correct interpretation of the observed attenuation may be more complicated.

By increasing E_p a Mach number $M_A = 8.7$ was obtained at the same initial β. The shock structures did not change very much $\Delta \approx 20\,c/\omega_{pe}$. The structure changes considerably when $\beta_0 = 1$: for $M_A = 8.4$ the shock front gets very broad and turbulent as is shown in Fig. 10. The shock thickness approaches $\Delta \approx c/\omega_{pi}$.

4. Plasma compression at $B_0 = 0$

Some preliminary results have been obtained on plasma acceleration and plasma compression for $B_0 = 0$. Sheath formation and radial implosion of the plasma were observed by measuring the radial magnetic field distribution as a function of time. The initial electron density had a value $n_0 = 2 \times 10^{13}\ \mathrm{cm}^{-3}$, the electron temperature in the plasma was $T_e = 1.8$ eV. Some magnetic field measurements are presented in Fig. 11. The sheath thickness is $\Delta \approx 10\ c/\omega_{pe}$ and $U_p \approx 3 \times 10^7\ \mathrm{cm\ s^{-1}}$. The implosion velocity and the thickness of the current sheath are approximately constant. No magnetic field fluctuations are observed in the current sheath; however, the electron drift velocities deduced from the current density should be sufficiently high to excite two stream instabilities ($v_d \approx 6 \times 10^8$ cm s^{-1}). This should result in a rapid heating of the electrons in the plasma boundary.

At the end of the first implosion the radius of the plasma cylinder is only about 1.5 cm. In contrast to this, the "free particle" model predicts a radius of about 5.5 cm, which means that this model is inapplicable for a description of the plasma implosion. After the first maximum compression the plasma expands to a radius of about 2.5 cm. At this time the average perpendicular energy of the ions is estimated to be about 600 eV and $B_p \approx 3$ kG. Owing to the high drift velocities the electron current should be unstable and provide rapid heating of the boundary layer. The temperature in the layer should diffuse across the plasma radius in a time smaller than the acceleration time of the plasma boundary. If we use the effective conductivity obtained before to calculate the heating rate, we obtain $dT_e/dt \approx 3 \times 10^{14}$°Ks^{-1}.

The main effect is that T_e is much larger than T_i before the actual plasma implosion starts. This means that ion acoustic shocks can be formed. These shock waves would explain the observed rapid heating of the collisionless plasma during the first implosion. Indications exist that such shocks are produced.

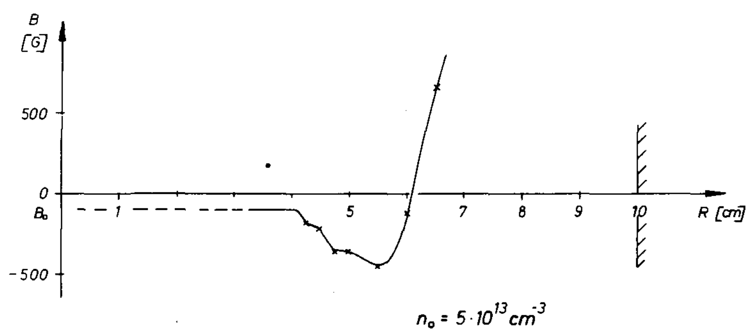

FIG.10. Shock wave in deuterium at $M_A = 8.7$, $\beta_0 \approx 1$.

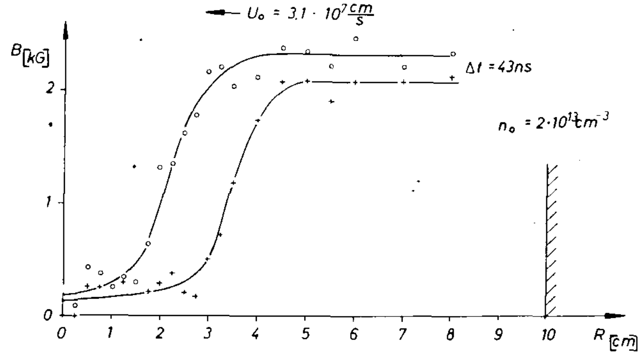

FIG.11. Magnetic field profiles during plasma implosion for $B_0 = 0$.

6. CONCLUSIONS AND SUMMARY

The experimental technique described allows collisionless shockwaves to be generated which at least in some cases appear to be stationary. Macroscopic properties of the observed shockwaves are in agreement with the estimates obtained from a simplified model. Most of the problems encountered in generating stationary shocks seem to be due to interactions of the shocked plasma with the vacuum magnetic field. Instabilities in the plasma vacuum boundary layer can have a dominant effect. In addition, magnetic field diffusion and plasma heating due to strong currents seem to be of importance.

In case the Alfvén Mach-number and the electron-ion collision frequency are sufficiently small ($\gamma_{ei} < (\omega_{ce}\,\omega_{ci})^{1/2}$), large amplitude waves with oscillatory structure are observed during the formation of the shock-wave. The observed wavelengths agree approximately with theoretical predictions.

Collisionless shockwaves were first generated in deuterium at $\beta_0 = 0.1$, and $M_A = 2.5$. The shock width was about $\Delta \approx 10\ c/\omega_{pe}$ as observed in other laboratories. Shockwaves in argon at $\beta_0 = 2.3 \times 10^{-2}$ and $M_A = 3.1$ showed a double structure with a broad and a narrow part. The narrow part is 2 to 3 mm broad, and an effective collision frequency $\nu_{eff} \approx 0.3\ \omega_{pi}$ is deduced; the broad part is probably not stationary and its instantaneous width has therefore no simple theoretical significance.

Increasing the β_0 from 0.1 to 0.5 does not change the shock structure at smaller Mach numbers ($M_A \approx 2.7$). A fluctuating magnetic field is now observed in the plasma behind the shock. For $M_A > 3$ and $\beta_0 = 0.5$ the double structure mentioned before is not always observed. The shock width becomes typically broader by a factor of two ($\Delta \approx 20\ c/\omega_{pe}$). If the Alfvén Mach-number is varied between 3.8 and 8.7 the shock width does not change appreciably.

The value of the initial β was increased to one. For $M_A = 8.4$ the shock front is much broader than before and approaches $\Delta = c/\omega_{pi}$. In contrast to the other cases the magnetic field in the shock front is now fluctuating. The change in β_0 seems to be responsible for this fact.

Investigations of plasma implosion for $B_0 = 0$ showed that, although the mean free path for ion-ion collisions and the ion cyclotron radius are large, the plasma motion cannot be described by the "free-particle" model. The magnetic field in the piston does not fluctuate. Ion acoustic shocks with $\gamma = 5/3$ would explain the observed plasma behaviour. Because of the large electron drift velocities observed in the current sheath, small-scale electrostatic turbulence should be generated and the electron temperature should rise rapidly. Large-amplitude ion acoustic waves should be excited. Such waves would explain plasma heating in low density θ-pinches.

ACKNOWLEDGEMENTS

The author wants to thank Dr. F. Waelbroeck for his great interest in this work, H. Hartwig for the performance of the microwave measurements, and Dr. P. Testa and E. Fassotte for their efforts in connection with the light scattering measurements. The assistance of E. Brandt and E. Noczinski in building up and operating the experiment is gratefully acknowledged.

REFERENCES

[1] PAUL, J.W.M. et al., Nature 208 (1965) 133.
[2] KURTMULLAEV, R.Kh. et al., in Plasma Physics and Controlled Nuclear Fusion Research, (Proc. Conf. Culham, 1965) 2 IAEA, Vienna (1966) 367.
[2a] ZAGORODNIKOV, S.P., Soviet Phys. JETP 25 (1967) 783.
[3] ASCOLI-BARTOLI, U. et al., in Plasma Physics and Controlled Nuclear Fusion Research, (Proc. Conf. Culham, 1965) 2 IAEA, Vienna (1966).
[4] GOLDENBAUM, G.C., HINTZ, E., Phys. of Fluids, 8 (1965) 211.
[5] GOLDENBAUM, G.C., Physics Fluids 10 (1967) 1894.
[6] DE SILVA, A.W., STAMPER, J.A., Phys. Rev. Lett. 19 (1967) 1027.
[7] PAUL, J.W.M. et al., Nature 216 (1967) 5113.
[8] TIDMAN, D.A., Physics Fluids 10 (1967) 547.
[9] Nuclear Fusion 1962, Supplement - Part 2, pp. 497-621.
[10] HARTWIG, H., Dielektrische Leiter und Antennen..., Berichte der Kernforschungsanlage Jülich GmbH; Jül-473-PP (1967).
[11] HINTZ, E., Berichte der Kernforschungsanlage Jülich GmbH (1968) (under press).
[12] KRUSKAL, M., SCHWARZSCHILD, M., Proc. Roy. Soc. A., 223 (1954) 348.
[13] GREEN, T.S., NIBLETT, B., Nucl. Fusion 1 (1960) 42.
[14] VEDENOV, A.A. et al., Soviet Phys. Usp. 4 (1961) 332.
[15] SAGDEEV, R.Z., Review Paper, in "Reviews of Plasma Physics", 4 (1966) 23.
[16] WOODS, L.C., Critical Alfvén-Mach-numbers, Culham Report CLM-P 153 (1967).
[17] KURTMULLAEV, R.Kh. et al., Symp. Collisionless Shockwaves, Novosibirsk (1967).
[18] HEPPNER, J.P. et al. OGO-A Magnetic Field Observations NASA, Report T-M-X 55740.

DISCUSSION

S.J. BUCHSBAUM: Could you comment, please, on your measurement of ν_{eff} by means of the 2-mm interferometer? The value of $\nu_{eff} \approx 2\omega_{pi}$ seems rather high.

E. HINTZ: In addition to turbulent resistivity, the observed attenuation may be caused by effects such as refraction of the microwaves in a medium with a non-uniform refraction index.

S.D. FANCHENKO: What was the effective collision frequency?

E. HINTZ: Effective collision frequencies between 5×10^8 and $5 \times 10^9\ s^{-1}$ were observed.

INVESTIGATION OF ENERGY DISSIPATION IN COLLISIONLESS SHOCK WAVES

R. CHODURA, M. KEILHACKER, M. KORNHERR AND H. NIEDERMEYER,
INSTITUT FÜR PLASMAPHYSIK, GARCHING, MUNICH,
FEDERAL REPUBLIC OF GERMANY

Abstract

INVESTIGATION OF ENERGY DISSIPATION IN COLLISIONLESS SHOCK WAVES. Strong magnetic compression waves are generated in a plasma with the electron density varying from 10^{12} to 5×10^{14} cm^{-3} by means of a fast theta-pinch discharge (dB/dt = 3.5×10^{10} G/s, coil length 60 cm, coil diameter 16 cm). The fast-rising magnetic field playing the part of the piston reaches 12 kG in 0.5 μs, a quasi-stationary field can be superimposed. The working gas (H_2, D_2, He, Kr, Ar) is pre-ionized up to 20% ($n_e \approx 10^{12}$ - 2×10^{13} cm^{-3}) by a pulse of strong ultraviolet radiation emitted by two z-pinches placed at both ends of the discharge tube. This pre-ionization can be followed, or at pressures above 5 μ H_2 can be substituted, by a fast theta-pinch discharge which produces a highly ionized plasma of density $1\text{-}5 \times 10^{14}$ cm^{-3}. In both cases conditions for collisionless shock waves can be achieved.

The width and structure of the shock waves have been investigated by means of multiple magnetic probes. At electron densities $> 10^{14}$ cm^{-3} and a plasma $\beta > 1$ shock waves with velocities between 2 and 4×10^7 cm/s are being observed for both parallel and antiparallel initial fields. They show a well-defined shock front of width 0.5 to 1 cm, corresponding to 10 to 40 c/ω_p, and a clear separation between front and piston. By properly adjusting the initial values of electron density and magnetic field, Alfvén Mach-numbers can be varied between 1 and 4. Their influence on the width of shock profiles and on heating rates is discussed. The energy spectrum of ions which are lost along the axis of the theta-pinch is measured by means of an electrostatic energy analyzer. Typical mean parallel energies are in the range of 200 - 500 eV.

At densities between 10^{12} and 10^{13} cm^{-3} and a plasma with $\beta \ll 1$ non-stationary shock waves with velocities between 5×10^7 and 10^8 cm/s and a width of 5 to 10 c/ω_p are observed. The mean ion energies are a few keV.

Experimental profiles of magnetic field are compared with calculations based on a two-fluid model containing a collisionless friction term, which roughly describes the action of a two-stream instability by limiting the electron velocity to a critical value. Thereby this critical velocity is determined to be about 1/4 to 1/2 of the local rms velocity of electrons.

1. INTRODUCTION

This paper describes an experimental investigation of collisionless shock waves produced by a fast theta-pinch discharge in a tube of 14 cm inner diameter. The work aims at studying the structure of collisionless shock fronts and the mechanisms of energy dissipation within them under various experimental conditions. The former is done by multiple magnetic probes, the latter by means of an electrostatic energy analyser measuring the energy spectrum of electrons and ions lost along the axis of the theta-pinch. It is hoped that the results of these experiments will be extended by a 90° laser scattering experiment, currently under way, in which both the radial and azimuthal electron velocity distributions will be measured.

Much care is taken to produce the shock waves in a plasma of homogeneous and well-known initial density and magnetic field and to vary these quantities over a wide range. Therefore two kinds of pre-ionization are used. At filling pressures below 5 mtorr H_2 the gas is first ionized to about

10% (n_e + 10^{12} - 2×10^{13} cm^{-3}) by strong ultraviolet radiation emitted by a Z-pinch placed at one end of the discharge tube. This pre-ionization can be followed, or at pressures above 5 mtorr H_2 can be substituted, by a fast theta-pinch discharge which brings the degree of ionization to 70-80% ($n_e = 5 \times 10^{13}$ - 5×10^{14} cm^{-3}). In the first case (pre-ionization by UV-radiation) the plasma β (= ratio of particle pressure to magnetic pressure ≈ ratio of sound velocity to Alfvén velocity squared) of the initial plasma is in the range of 10^{-4} to 10^{-1}, whereas in the second case (theta-pinch pre-ionization) it varies between 10^{-1} and 10.

Most of the results reported here are for transverse shock waves with Mach numbers between 1.5 and 4. A clear separation between shock and piston can be observed only for low Mach numbers.

2. TURBULENCE HEATING EXPERIMENT

A fast theta-pinch discharge is used to generate strong magnetic compression waves in a tube of 14 cm inner diameter. The details of construction and technical data of the different capacitor banks employed are summarized in [1]. The fast-rising magnetic field playing the part of the piston is produced in a double-fed coil of 60 cm length and 15.8 cm diameter by two 40 kV capacitor banks connected in series. The magnetic field reaches 12 kG in 0.5 μs. Special components of the bank system are: two low-inductance collectors of the sandwich type connected in series, pressurized combined start and crowbar spark gaps, and suppressor units at the collector for reducing line reflections.

One sixth of the main bank can be charged and triggered separately and can thus be used for theta-pinch pre-ionization of the plasma. A second pre-ionization system consists of a Z-pinch placed at one end of the discharge tube and driven by a 0.84 μF, 120 kV capacitor. The pinched plasma emits strong ultraviolet radiation, thus photo-ionizing the plasma.

A bias field of either polarity can be produced by a slow bank which feeds a separate multiturn coil surrounding the theta-pinch coil. Thus the bias field can be kept homogeneous at the ends of the theta-pinch coil, making it possible to generate oblique shock waves at a well defined angle in this region of the coil.

3. PRE-IONIZATION OF PLASMA

3.1. Photo-ionization by strong ultraviolet radiation

Pre-ionization of a plasma by a pulse of strong radiation has some important advantages, e.g. purity and homogeneity of the plasma, and easy control of the trapped magnetic field. For hydrogen at pressures below a few millitorr it even seems to be the only possible pre-ionization. We therefore developed a light source [2, 3] which emits a very intense radiation pulse at wavelengths just below 800 Å (≅ 15.4 eV = ionization energy of H_2). The light source is a fast Z-pinch which is filled dynamically with hydrogen or rare gases of density ≈ 10^{18} cm^{-3} by means of a pulsed gas inlet. The Z-pinch is placed at one or both ends of the theta-pinch tube, as shown in Fig. 1, with no windows in between. In the approximation of a point source

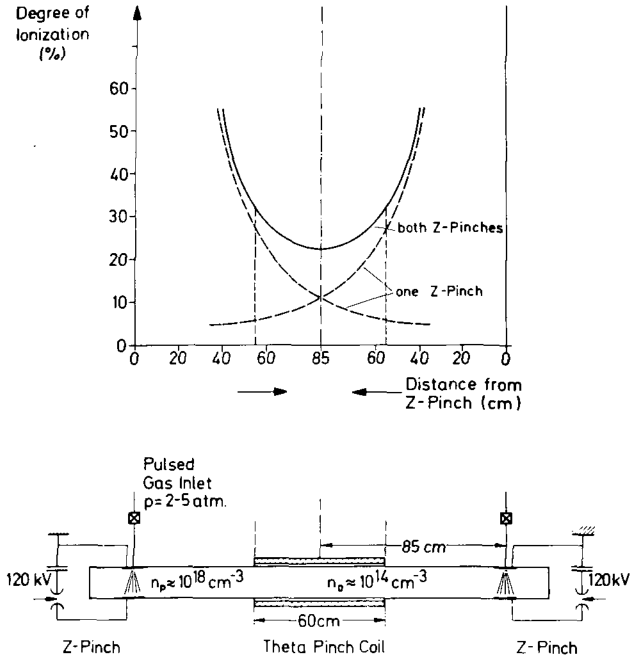

FIG.1. Experimental arrangement of UV-preionization and measured degree of ionization in 4 mtorr hydrogen.

the radiation density decreases with the distance z from the pinch proportional to $z^{-2} \exp(-z \sigma n_0)$, with n_0 = neutral particle density and σ = cross-section for photo-ionization (for $\lambda \leq 803$ Å). The degree of ionization $\alpha = n_e/(n_0 + n_e) \approx n_e/n_0$ has the same dependence on z and n_0. It therefore increases – all other quantities kept constant – with decreasing neutral particle density n_0, indicating that this method is especially suited to pre-ionize gases at low filling pressures. Figure 1 shows the axial distribution of α for 4 mtorr H_2 for the cases of one and two Z-pinches, respectively. The absolute value of α has been measured, and is controlled at each discharge, using an 8 mm micro-wave interferometer. It can be varied over a range of at least two orders of magnitude (0.2 to 20% for pressures below 10 μH_2) by choosing different gases for the Z-pinch filling and varying the delay time between start of gas filling and ignition of Z-pinch or the time between ignition of Z-pinch and theta-pinch discharge. Figure 2 shows α and n_e as functions of time after the ignition of the Z-pinch. Among the various gases used so far in the Z-pinch the best results with respect to a high degree of ionization have been obtained with xenon [3], which has therefore been used in most of the experiments described in this paper.

Since the relaxation time for electrons of density 10^{13} cm^{-3} and energies below 100 eV is small compared with the duration of the radiation pulse, the electrons in the photo-ionized plasma assume a temperature T_e, which according to Ref. [2] should be a few electron volts. The ions are gradually heated by collisions with the electrons. At an electron density of

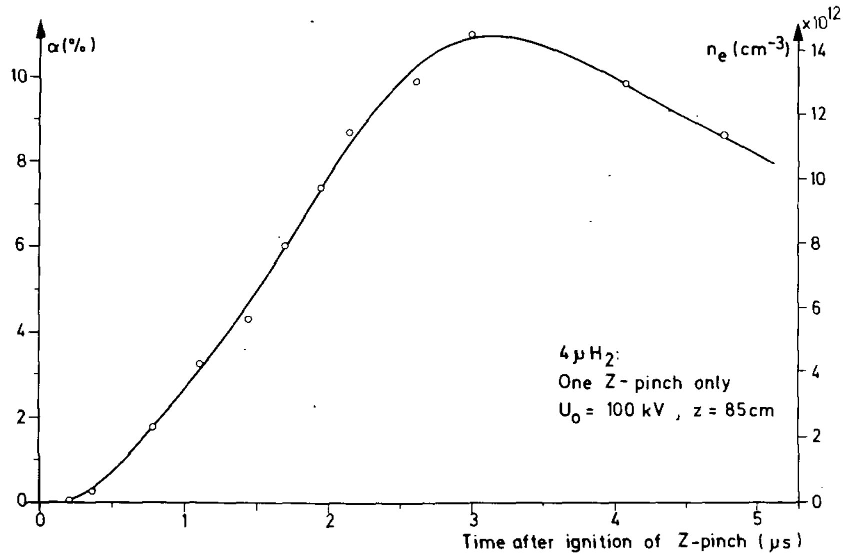

FIG.2. Time-dependence of measured electron density n_e in 4 mtorr hydrogen exposed to strong UV-radiation.

$n_e = 10^{13}\,cm^{-3}$ and a temperature of $T_e = 2$ eV the equipartition time [4] is 20 μs. It decreases inversely proportional to n_e.

3.2. Theta-pinch pre-ionization

To increase further the density and temperature of the initial plasma, the UV-radiation pre-ionization can be followed by a fast theta-pinch pre-ionization discharge, which breaks down the gas in the first half-cycle and produces an almost fully ionized plasma of a few tens of electronvolts. At filling pressures above 5 mtorr in hydrogen the theta-pinch on its own produces a well reproducible initial plasma although breakdown occurs only in later half-cycles.

Figure 3 shows the time dependence of plasma density n_e and ion temperature T_i in the pre-ionization theta-pinch for 10 mtorr H_2. The values were determined spectroscopically by recording the line profiles of H_α(Doppler-broadened) and H_δ (mainly Stark-broadened) and defolding the measured profiles with respect to the different line broadening effects. The results plotted are mean values along the line of sight, i.e. along the discharge axis in end-on observation and along a major diameter in side-on observation. The slight differences in end-on and side-on temperature could be due to directed plasma velocities, radial velocities at early times, and streaming out of the theta-pinch coil at later times. The decrease in ion temperature after a few microseconds could indicate a heating of the electrons by electron-ion collisions, since the equipartition time is less than 1 μs. Measurements at 5 mtorr H_2 gave results similar to that at 10 mtorr H_2, but with slightly higher temperatures.

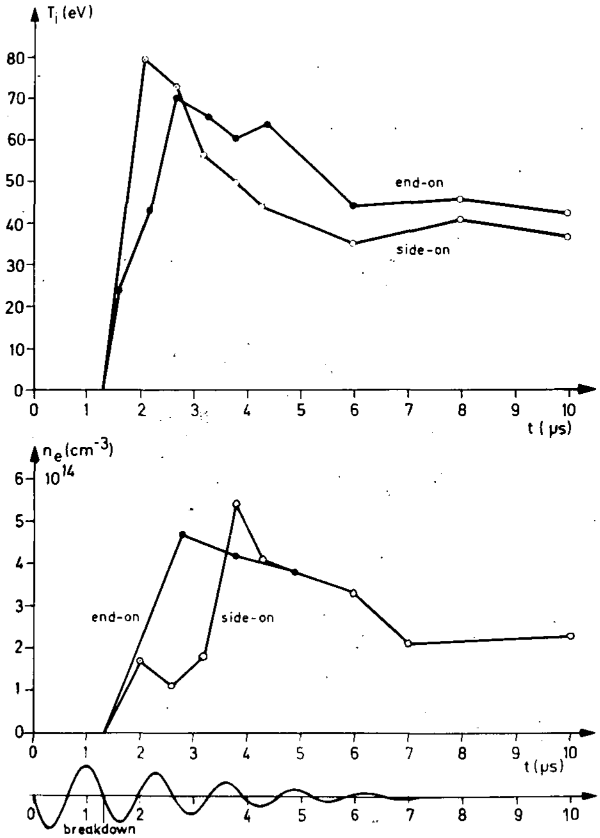

FIG. 3. Ion temperature T_i and density n_e in 10 mtorr hydrogen (= 6.7×10^{14} cm^{-3}) preionized by a fast theta pinch discharge.

4. SHOCK WAVES FOR $\beta > 1$ AND WITH MACH NUMBERS BETWEEN 1.5 AND 4

The initial plasmas produced by the two above-mentioned pre-ionization methods differ greatly with respect to density and temperature, and therefore also in the plasma β. It therefore seems reasonable to discuss the experimental results for the two cases separately.

First we want to report on shock wave observations in a plasma formed by the theta-pinch pre-ionization. Typical values for this initial plasma are: $n_e = n_i = 2$ and 4×10^{14} cm^{-3} at filling pressures of 5 and 10 mtorr H_2, respectively (degree of ionization up to 80%), $T_i \approx 40$ eV, $T_e \lesssim T_i$, $\beta \approx 5$. This means that, for the magnetic fields used, the sound velocity v_S is greater than the Alfvén velocity v_A, and that the Mach number M, defined as

$$M = \frac{u}{\sqrt{v_A^2 + v_S^2}}$$

with u being velocity of shock front, is mainly determined by v_S.

4.1. Parallel bias field

Figures 4a and 5 show typical probe traces of the magnetic field at different radii for a discharge in hydrogen with the abovementioned initial conditions and a parallel bias field of 350 G. The magnetic field was measured with multiple magnetic probes consisting of six multiturn coils (diameter 0.8 mm), 3 or 12 mm apart. The probes were shielded by a brass tube and embedded in a quartz jacket (diameter 3 mm). For detailed measurements on fast shock structures a single turn loop covered with quartz and a dimension in the direction of shock propagation of 1 mm was used in connection with a Tektronix 519 oscilloscope (0.35 ns risetime).

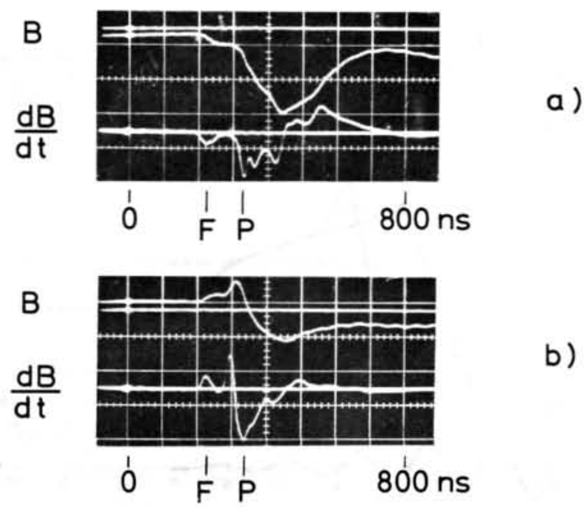

FIG.4. Probe traces of B and dB/dt at 3.2 cm radius showing structure of collisionless shock waves in hydrogen of density $4 \times 10^{14}\,cm^{-3}$. F = front, P = magnetic piston.
a) B_0 = +350 G, $n_{eo} = 4 \times 10^{14}\,cm^{-3}$, 10 mtorr H_2
b) B_0 = -440 G, $n_{eo} = 3 \times 10^{14} cm^{-3}$, 7.5 mtorr H_2.

The signals of Fig. 4a show a well-defined shock front (F) and a clear separation between front and magnetic piston (P). The separation steadily increases with time, as can be seen from Fig. 5, which shows more probe traces of the same shot. At about half the tube radius, the shock wave is almost stationary and has the following values which are typical of these conditions: $u = 3.0 \times 10^7$ cm/s, jump in magnetic field $B/B_0 = 2.7$, width of shock front D = 0.6 to 0.8 cm. For our initial temperature $T_e + T_i$ = 75 eV and three degrees of freedom this gives a Mach number M = 2.6. The pure Alfvén Mach-number $M_A = u/v_A$ would be 7.8. From the conservation relations one gets the following values behind the shock front: $T_e + T_i$ = 230 eV, $n = 10.8 \times 10^{14}\,cm^{-3}$.

By increasing the bias field strength, shock waves with smaller Mach numbers could be generated. Typical values for a shock wave observed in 5 mtorr H_2(e.g. Fig. 6) with a parallel bias field of 500 G are: $u = 2.5 \times 10^7$ cm/s, B/B_0 = 2.4 to 2.6, and D = 0.4 to 0.5 cm. In this case the Mach number M is 1.9, and M_A is 3.2.

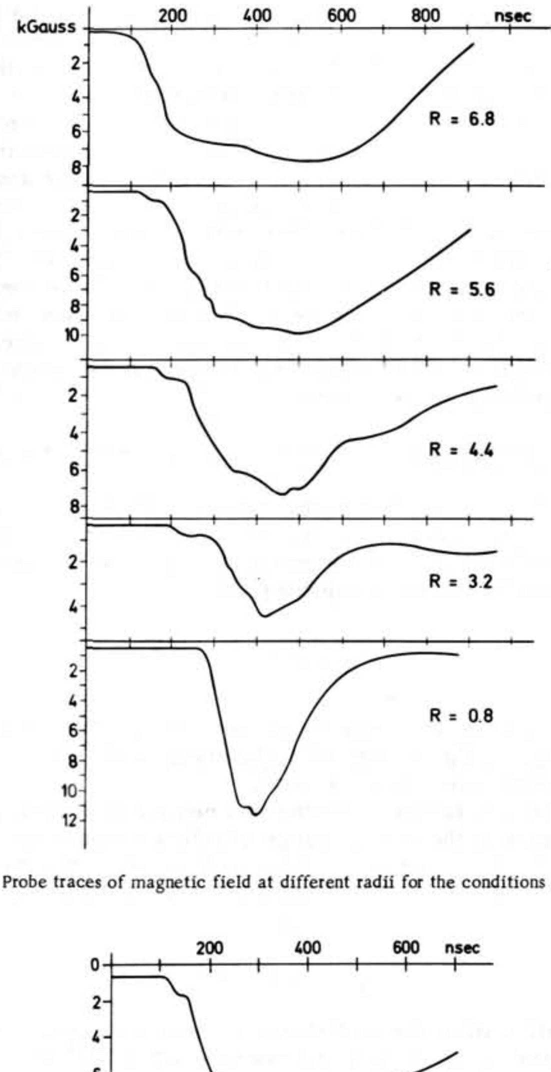

FIG. 5. Probe traces of magnetic field at different radii for the conditions of Fig. 4a.

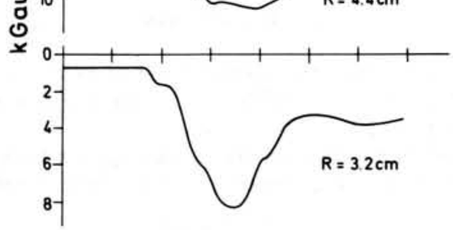

FIG. 6. Probe traces of magnetic field at 4.4 cm and 3.2 cm radius. B_0 = 500 G, $n_{eo} = 2 \times 10^{14}$ cm^{-3}, 5 mtorr H_2.

A comparison of the measured shock widths D with the collisionless skin depth c/ω_p (c = velocity of light, ω_p = electron plasma frequency) shows that for shocks with $M < 2$, $D \approx 12\ c/\omega_p$, and for shocks with M = 2.5 to 3, $D \approx 30\ c/\omega_p \approx 1\ c/\Omega_p$ (Ω_p = ion plasma frequency). Similar observations – though for plasmas with smaller β – have also been made by other authors [5-7]. One possible interpretation of this broadening of the shock front above a critical Mach number is overturning of the shock front followed by ion two-stream instabilities which lead to enhanced heating of the ions. For a hot plasma Sagdeev [8] predicts in this case a shock thickness of c/Ω_p. In our experiment strong ion heating is observed. The energy distribution of the ions lost along the theta-pinch axis is measured by an electrostatic particle energy analyser [9] placed on axis, with its aperture about 30 cm away from the end of the theta-pinch coil. For the above-mentioned conditions the spectrum has a maximum at a few 100 eV during the first compression of the plasma.

4.2. Estimate of the absence of collision processes in the shock front

It shall now be shown that under these conditions the shock fronts are collisionless. The condition that a particle r is not appreciably deflected by binary collisions with particles s during its passage through the shock front can be expressed by the following inequality

$$\nu_{rs} = n_s < \sigma v_{rs} > < \frac{u}{D} \qquad (1)$$

where ν_{rs} is the collision frequency of particles r with particles s, v_{rs} their relative velocity, n_s the density of background particles s, and σ the appropriate total collision cross-section.

For collisions between electrons and neutral hydrogen the product σv is almost constant in the energy range of interest and is equal to $1 \times 10^{-7}\ cm^3\ s^{-1}$ [10]. Using this value and inserting the measured values $u = 3 \times 10^7$ cm/s and D = 0.6 cm into Eq.(1) we get for the density of neutral hydrogen n_n

$$n_n < 5 \times 10^{14}\ cm^{-3}$$

A similar consideration for collisions between hydrogen ions and neutral hydrogen, setting v_{rs} equal to u and taking $\sigma = 2 \times 10^{-15}\ cm^2$ (the charge exchange cross-section at 1 keV, corresponding to $u = 3 \times 10^7$ cm/s, is $4 \times 10^{-16}\ cm^2$ in H_2 [11] and $2 \times 10^{-15}\ cm^2$ in H [10] yields

$$n_n < 8 \times 10^{14}\ cm^{-3}$$

These values are higher than the background of neutral hydrogen present in the experiment, which was $1 \times 10^{14}\ cm^{-3}$ in discharges at 10 mtorr and $5 \times 10^{13}\ cm^{-3}$ at 5 mtorr H_2.

For the electron-ion collision frequency ν_{ei} we take the reciprocal of the deflection time defined in [4]. Inserting the corresponding expression into Eq.(1) we obtain

$$n_e < 2.4 \times 10^5\ \frac{T_e^{3/2}(eV)}{\ln \Lambda}\ \frac{u}{D}$$

Using again the measured values for u and D and a mean temperature before and behind the shock front (about 80 eV in this case) the condition becomes $n_e < 7.4 \times 10^{14}\ cm^{-3}$. This condition is just met for the discharges in 10 mtorr H_2, but is better fulfilled for the discharges in 5 mtorr H_2 ($n_{eo} = 2 \times 10^{14}\ cm^{-3}$).

4.3. Antiparallel bias field

Figures 4b and 7 show typical magnetic field profiles for conditions similar to that discussed before, but with the initial field in a direction opposite to the driving field. Again a shock front F travels ahead of the magnetic piston P, as can be seen best on the dB/dt trace of Fig. 4b. The shock formation in discharges with antiparallel bias field differs from that with parallel bias field in that the magnetic pressure at the plasma boundary first decreases, causing the plasma to expand. Only after a time interval $\Delta t \approx 2\ B_0/(dB/dt)$ (B_0 = bias magnetic field, dB/dt = rise of magnetic field) does the magnetic pressure start to compress the plasma. In our experiment for antiparallel bias fields the shock waves did not become quite stationary. Typical values for shock waves similar to those shown in Fig. 4b are (at about half the tube radius): $u = 3$ to 3.5×10^7 cm/s, $M = 3$ and $D \approx 1.0$ cm $\approx c/\Omega_p$, which is rather similar to the results with parallel bias field. A strong damping of the discharge circuit indicates a high transfer of energy to the plasma.

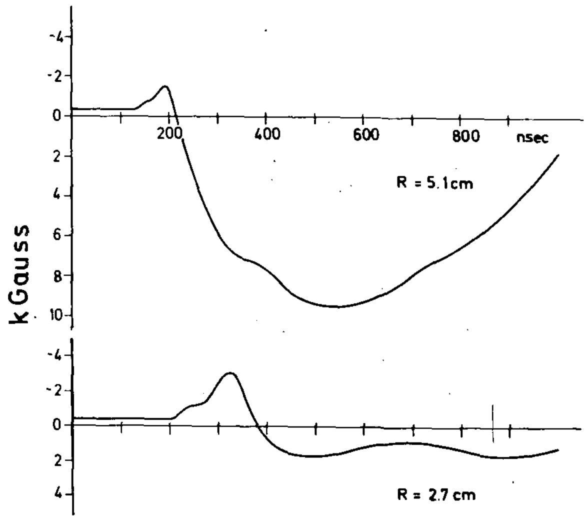

FIG. 7. Probe traces of magnetic field at 5.1 cm and 2.7 cm radius for conditions similar to that of Fig. 4b.

5. SHOCK WAVES FOR $\beta \ll 1$

5.1. Experimental results

Now we want to discuss shock waves in a plasma of lower density formed by a strong pulse of UV-radiation. These results are especially suited for comparison with theory since the initial density is almost homogeneous across the tube diameter and can be measured accurately. Also, the strength of the bias field can be varied as one wishes. Typical values of this initial plasma are $n_e = n_i = 10^{12}$ to 2×10^{13} cm^{-3}, $T_e \approx 2$ eV, $T_i \leq 2$ eV, $\beta = 10^{-2}$. Under these conditions the Mach number is determined exclusively by the Alfvén velocity, i.e. $M = u/v_A$. With respect to collision processes, for electron ion collisions the inequality (1) is fulfilled for these conditions, whereas for collisions between electrons and neutral hydrogen it is only valid for pressures below ≈ 8 μ H_2.

Figure 8b shows a typical probe trace for these conditions with anti-parallel bias field. The shock structure is similar to the corresponding case at $\beta > 1$, but the shock velocities are higher, and the shock front is formed only relatively close to the axis and is non-stationary. The width of the shock front is about 1.8 cm (that is, about $10\ c/\omega_p$), and the velocity is $u = 6 \times 10^7$ cm/s, corresponding to a Mach number $M = 1.6 < M^*$.

An earlier and better separation between piston and shock front, but again no stationary shock, is obtained for shock waves in heavier gases, e.g. argon or krypton. Typical values for a shock observed in 1 mtorr krypton are; $u \approx 5 \times 10^7$ cm/s, $M \approx 20$ and $D \approx 1.2$ cm $\approx 10\ c/\omega_p \approx 1/40\ c/\Omega_p$.

Figure 8a shows a shock wave in 4 mtorr H_2 with a small parallel bias field. The Mach number is about 3, $D \approx 5\ c/\omega_p$. The energy spectrum of the ions as determined with the electrostatic analyser in a similar discharge at 4 mtorr D_2 has a maximum at 600 to 800 eV. In discharges at 2 mtorr D_2, the maximum is at about 1200 eV with detectable intensities extending to 4-6 keV.

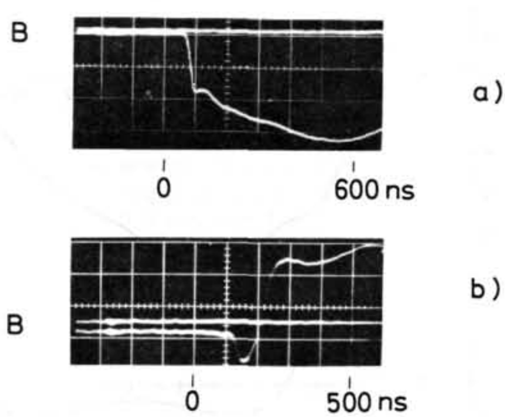

FIG. 8. Probe traces of B at 2.0 cm radius showing collisionless shock waves in hydrogen of density 10^{13} cm^{-3}.
a) $B_0 = +200$ G, $n_{eo} = 8 \times 10^{12}$ cm^{-3}, 4 mtorr H_2
b) $B_0 = -1000$ G, $n_{eo} = 1.5 \times 10^{13}$ cm^{-3}, 7.5 mtorr D_2.

5.2. Comparison with numerical calculations

To get an idea of the dissipation process in the front of the compression wave we compared our experimental results with a numerical model. This model [12] describes the motion of ions and electrons by time-dependent two-fluid equations, including electron inertia. It admits dissipation of ordered motion for the electrons only and is limited to compression waves of moderate strength in which no overturning occurs. As a rough description of the action of a two-stream instability the azimuthal velocities of electrons relative to the ions are limited by a friction force to a critical value $\lambda\ v_{eth}$ where v_{eth} is the local rms velocity of electrons and λ is a constant parameter. As long as the electromagnetic forces try to enlarge the value of the azimuthal velocity above this critical value the friction force is acting. When the azimuthal acceleration ceases in the course of compression the friction force is switched off. The power produced by the electron motion against the friction force is assumed to raise the internal energy of the electrons, thereby in turn changing the critical velocity.

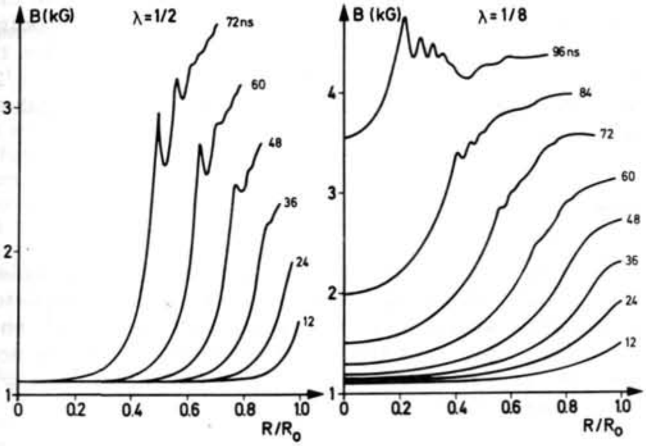

FIG. 9. Calculated profiles of magnetic field for two values of λ (λ = ratio of drift velocity of electrons to their thermal velocity). B_0 = 1100 G, $n_{eo} = 1 \times 10^{13}$ cm^{-3}, deuterium.

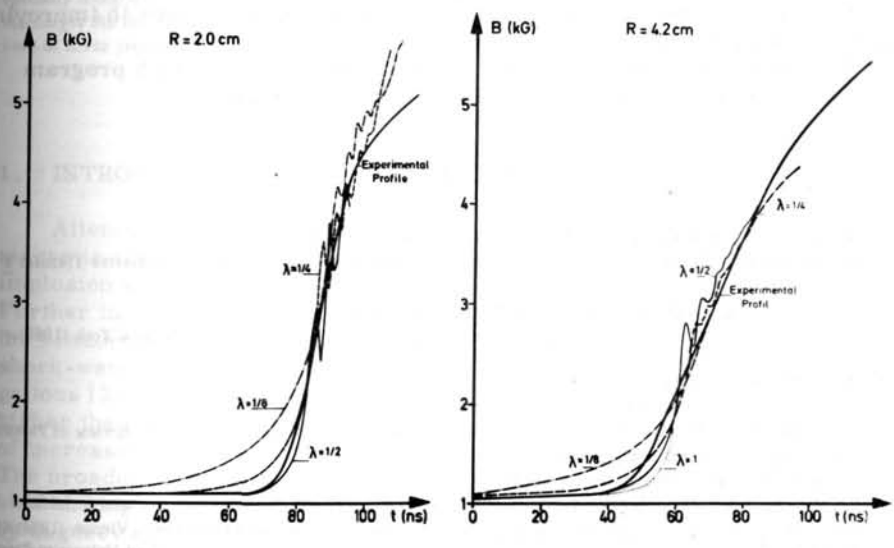

FIG. 10. Experimental and calculated (with λ varying between 1/8 and 1) profiles of magnetic field at 2.0 and 4.2 cm radius for the conditions of Fig. 8.

Calculations were done for different values of λ in order to get information about the electron friction by adjusting the calculated profiles to the experimental ones. Figure 9 shows calculated profiles of the magnetic field for different instants of time for $\lambda = 1/2$ and $1/8$, respectively. In Fig. 10 calculated profiles of the magnetic field at two fixed radial positions (R = 2.0 and R = 4.2 cm) are compared with experimental profiles measured with magnetic probes. The calculated profiles are for different values of λ, varying between 1/8 and 1. A comparison of the initial rise of the magnetic field indicates (the oscillations in the calculated profiles following this first rise could not be observed with the magnetic probes) that the critical velocity of the electrons is of the order of their thermal velocity (1/4 to 1/2 v_{eth}). This is a fairly low friction which does not broaden the front very much. On the other hand, the calculations show that for $\lambda > 1/2$ the front breaks after travelling about half of the tube radius. Then other dissipation mechanisms will set in.

6. SUMMARY

Summarizing we can say that almost stationary, collisionless shock waves with $M \approx 3$ and a clear separation between shock and piston have been observed for plasmas with $\beta > 1$. The shock width is $\approx c/\Omega_p$ and strong ion heating is observed. For conditions with $\beta \ll 1$ the waves are non-stationary and the front thickness is 5-10 c/ω_p, in agreement with the results of the numerical model.

ACKNOWLEDGEMENT

We are indebted to Prof. E. Fünfer and Prof. A. Schlüter for their interest and support during the course of these experiments. We also greatly acknowledge the help of Drs Pecorella and G. C. Vlases in improving the UV-radiation pre-ionization.

This work has been performed as part of the joint research program of EURATOM and the Institut für Plasmaphysik, Garching.

REFERENCES

[1] HERPPICH, G., KNOBLOCH, A., MÜLLER, G., IPP-Rep. IPP 4/50 (1968).
[2] HOFMANN, G., IPP-Rep. IPP 1/43 (1966) and J. of Quantitative Spectroscopy and Radiative Transfer 8 (1968) 729.
[3] PECORELLA, F., VLASES, G., Phys. Rev. Lett. (to be published).
[4] SPITZER, L., Jr., Physics of Fully Ionized Gases, 2nd Edn., Interscience Publishers, New York (1965).
[5] PAUL, J.W.M. et al., Nature 208 (1965) 133 and Nature 216 (1967) 363.
[6] KURTMULLAEV, R.Kh. et al., Zh.éksp.teor.Fiz. Pis'ma 7 (1968) 65.
[7] ZAGORODNIKOV, S.P. et al., Soviet Phys. JETP 25 (1967) 783.
[8] SAGDEEV, R.Z., "Cooperative phenomena and shock waves in collisionless plasmas", Review of Plasma Physics, 4, Consultants Bureau, New York (1966) 85.
[9] NIEDERMEYER, H., IPP-Rep. IPP 1/66 (1967).
[10] DELCROIX, J.L., "Données de base de la physique des gaz ionisés", Survey of Phenomena in Ionized Gases (Proc. 8th Int. Conf. Phenomena Ionized Gases, Vienna, 1967), Invited Papers, IAEA, Vienna (1968) 611.
[11] MASSEY, H.S.W., BURHOP, E.M.S., Electronic and Ionic Impact Phenomena, Oxford University Press, London (1956) 526.
[12] CHODURA, R., Physics Fluids 11 (1968) 400.

MEASUREMENTS OF THE ION ENERGY DISTRIBUTION FUNCTION AND THE DENSITY PROFILE IN STRONG SHOCK WAVES

U. SCHUMACHER,
INSTITUT FÜR PLASMAPHYSIK, GARCHING, MUNICH,
FEDERAL REPUBLIC OF GERMANY

Abstract

MEASUREMENTS OF THE ION ENERGY DISTRIBUTION FUNCTION AND THE DENSITY PROFILE IN STRONG SHOCK WAVES. In a theta pinch discharge a strong implosion wave is produced by a rapidly rising magnetic field ($dB/dt \geq 10^{11}$ G/s, zero bias field), resulting in ion energies in the keV region at the first maximum compression. This compression wave in deuterium is investigated spectroscopically to get information about the density profile and the velocity distribution function of the ions inside the imploding sheath. Because of the relatively low electron temperature (compared with the high ion energies) measurements of the Balmer line broadening are possible. The electron density profile is obtained from the Stark broadening of D_β. At filling pressures of $p_0 \leq 20$ mtorr D_2 a very broad density profile is found with maximum electron densities of some 10^{15} cm^{-3} in the outer parts of the imploding sheath. The electron density reaches a peak of 10^{16} cm^{-3} at the end of the first implosion, as has also been found from laser scattering. At a filling pressure of 60 mtorr the maximum electron density is reached in the inner parts of the imploding layer. These measurements of the width of the impldoing sheath are in agreement with those made with magnetic probes for the current-carrying layer. Time- and space-resolved measurements (side-on and end-on) of the Doppler broadening of D_α gave information about an anisotropic velocity distribution of the deuterons. For a 20 mtorr discharge (for example, in the density maximum of the imploding sheath) an undirected motion of nearly 400 eV was found to be superimposed on the radially directed imploding motion with kinetic energies of 550 eV. The ion energies parallel to the magnetic field, however, have a thermal component of only 120 eV and a mean kinetic part of about 60 eV. These results for the space-resolved ion velocity distribution function agree well with the data obtained from the spatially integrated measurements of the neutron emission at the end of the first implosion. For 60 mtorr discharges the thermal energies in the perpendicular and parallel directions do not differ as much as in the case of lower pressures.

1. INTRODUCTION

Attempts have already been made to achieve high ion temperatures by magnetic compression in theta-pinch devices by producing a very strong implosion wave, which can be obtained by a fast-rising magnetic field [1, 2]. Further ion heating in the low-pressure regime is limited, however, by the broadening of the current-carrying layer [1]. This broadening of the shock-wave profile has also been observed in several experimental investigations [3-6] at supercritical Mach numbers. It is an order of magnitude higher than in low Mach-number profiles and has been explained in terms of increased electron friction [3-5], resulting in large electron heating. The broadening has also been ascribed by Zagorodnikov et al.[6] to an overturning of the ion sheath followed by ion-ion instabilities, as described by Sagdeev [7]. This mechanism would lead to enhanced heating and thermalization of the ions. Numerical two-dimensional calculations of strong shock waves by Kilb [8] also show an overturning of the ion layer at very early stages of the theta-pinch implosion, and an effective entropy increase from ion-gyration phase mixing is obtained. To decide whether the electrons or ions are preferentially heated and to what degree the ions are thermalized by instabilities, we made measurements of the ion energy distribution function and the density profile in very strong shock waves. For these strong implosion waves (without bias field) we also found a very broad current-carrying layer [1, 2].

The purpose of the experimental investigations was to determine the ratio of the transverse thermal ion energy to the kinetic energy and the relationship between the longitudinal and the transverse thermal energies.

2. APPARATUS AND DIAGNOSTICS

A detailed description of the theta-pinch apparatus has already been given by Wilhelm [1]. In a divided coil of 14 cm length and 7 cm diameter an electric field strength of 1.6 kV/cm and a magnetic field rise of more than 10^{11} G/s (without plasma) can be reached.

For pre-ionization a 120 kV Z-pinch with a single current pulse [9] was used. It produces a field-free plasma with a mean degree of ionization of about 50 percent at deuterium filling pressures of 20 mtorr.

Under these conditions the collisionless skin depth $C/\omega_{pe} \approx 2 \times 10^{-2}$ cm is less than the mean ion gyrodius and the mean free path of resonant charge exchange of approximately 1 cm. The self-collision time of ions (1 μs) is much longer than the time of observation. But electron-electron and electron-ion collisions may be important, because of the relatively low electron temperature.

During the implosion phase of the main discharge the electron temperature is very much lower than the mean ion energy. At the end of the first maximum compression, for example, the electron temperature measured by Laser scattering [10] reaches a value of only (80 ± 20) eV, while the mean ion energy at this time is higher by one order of magnitude [1, 2].

Broadening measurements at Balmer lines can thus be performed during the implosion phase[1]. The Doppler broadening of D_α in end-on and side-on observation is influenced neither by Stark nor by Zeeman broadening under our experimental conditions. From space-resolved measurements, information on the ion energy distribution function can be obtained in this manner.

The broadening of D_β in end-on observation is mainly produced by the Stark effect [11], thus giving the electron density. The Doppler broadening of D_β in the longitudinal direction is not completely negligible. For this reason the Doppler broadening of D_β (found from D_α) was folded with theoretical Stark profiles [11], corresponding to different densities. The numerical comparison of the resulting curves with the measured profiles gave the electron density and its error.

As an example, Fig.1 gives the measured profile of D_β 160ns after the ignition of the main discharge in 20 mtorr D_2 for the axial region as a function of the distance $\Delta\lambda$ (Å) from the line centre. For comparison some of the theoretical Stark profiles folded with the Doppler profile of a parallel mean ion energy of $kT_\parallel$ = 160 eV are plotted.

[1] The upper levels of the Balmer lines are above the collision limit [11].

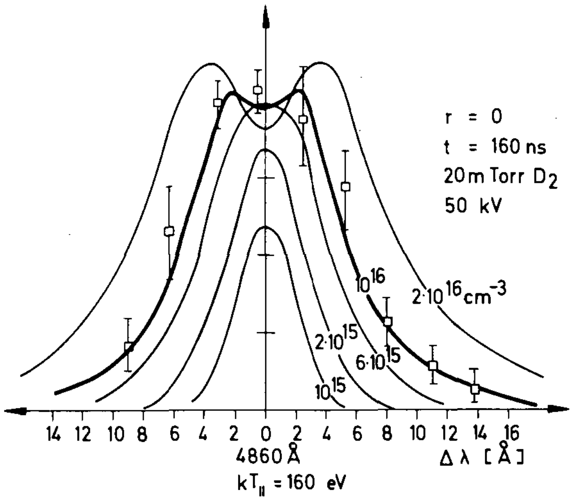

FIG. 1. Measured line profile of D_β with Stark profiles of several electron densities folded with Doppler profile of $kT_{\|}$ = 160 eV.

The curve of 10^{16} electrons/cm^3 seems to fit the measured points best in this example.

The measurements of line broadening were performed with a 10-channel monochromator in Littrow arrangement [12] with (f/6) and with 3.2 Å, 2.8 Å or 1.05 Å wavelength intervals per channel. The radiation was detected photoelectrically.

The reproducibility of the discharges was checked by measurements of the diamagnetic signal [1] and the neutron production. The local magnetic field was measured by direct magnetic probes, which are discussed in Ref. [1].

3. MEASUREMENTS

The radial electron density distribution during the implosion phase was determined from the profile measurements of D_β. The results for two different initial pressures are plotted in Fig.2. The density profiles, especially for the higher pressure, show a rather steep front. The width of the profiles, however, is rather extended. Magnetic probe measurement [1, 2] had already shown a comparably large width for the current-carrying layer.

Figure 3 gives a sketch of the time behaviour of the imploding layer. The hatched region indicates those parts of the layer where the electron density is higher than 20% of its maximum value, the position of which is given by the heavily drawn line. The thin line shows the front of the plasma, characterized by the density jump. The dashed line is the spatial curve of the magnetic field rise [1, 2]. For 20 mtorr discharges the magnetic field and the electron density rise at almost the same point. The whole plasma of the imploding sheath is mixed with the magnetic field. For the higher pressure, however, there exists (in front of the magnetic piston) a small field-free plasma region.

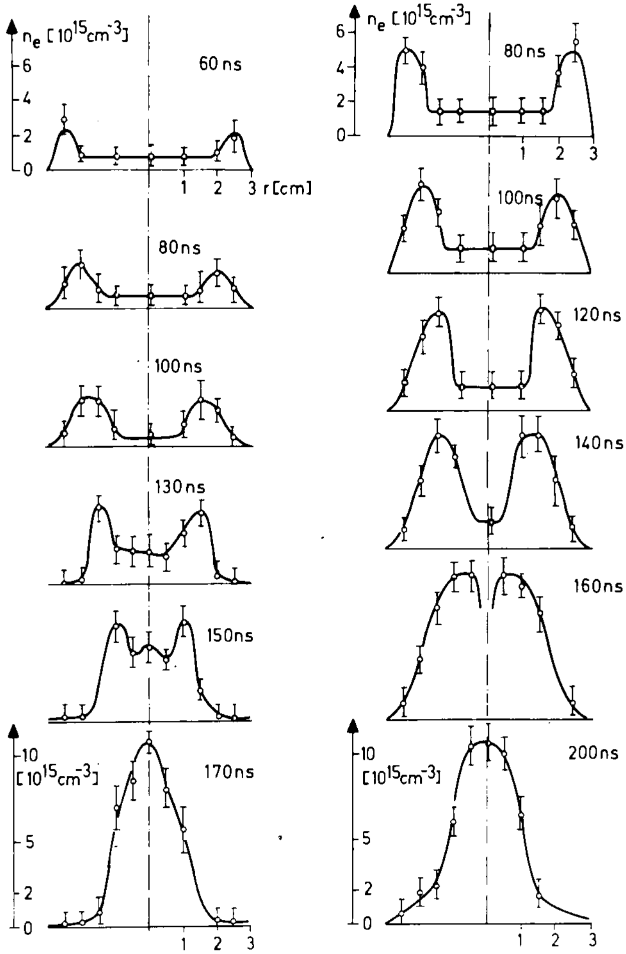

FIG.2. Electron density distribution for 20 mtorr (left) and 60 mtorr (right).

The profile measurements of the Balmer line D_α in end-on and side-on observation show strong anisotropy of the ion energy[2]. This can be roughly demonstrated in Fig.4. The upper part of the figure shows the side-on Doppler-profile of 20 mtorr discharges. The end-on profile is drawn below. It has a mean width nearly three times smaller. Therefore, the mean ion velocities in the transverse direction seem to be considerably higher compared with the longitudinal motion.

The end-on profile of D_α can be approximated by a Doppler profile with a Maxwellian distribution with $kT_\parallel = 160$ eV. Experimental separation

[2] Doppler profile measurements at impurity lines do not give the deuteron energies because the impurities are not in equilibrium with the deuterons under these collisionless conditions.

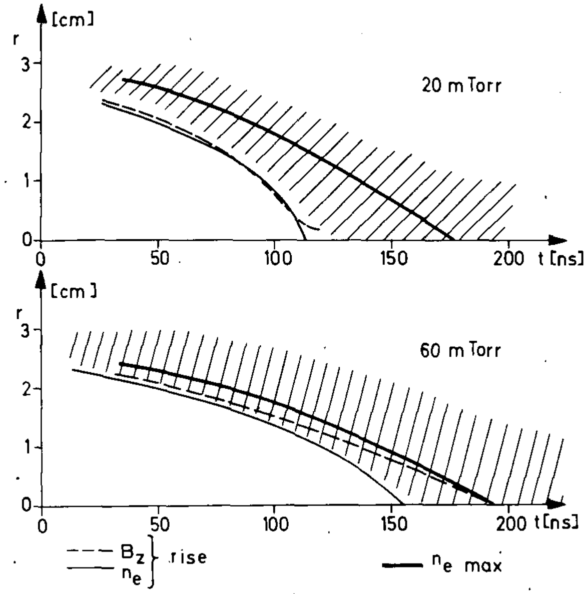

FIG. 3. Density and current layer as a function of time.

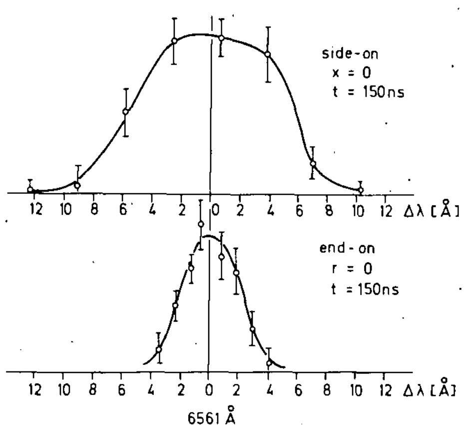

FIG. 4. Comparison of Doppler broadening of D_α in end-on and side-on observation.

of the directed motion in the longitudinal direction gave a thermal (undirected) ion energy component of $kT_\parallel = 120$ eV.

In the side-on observation there is folding over several space regions with an undirected (thermal) component superposed on a radial directed motion. This may be assumed isotropic in the plane perpendicular to the magnetic field with a Maxwellian distribution of the temperature $kT_\perp$.

Then the intensity I (x, $\Delta\lambda$) at a distance x from the discharge axis and the wavelength difference $\Delta\lambda$ from the line centre at λ_0 is given by

$$I(x,\Delta\lambda) = \int_{|x|}^{R} \epsilon(r)\left(\frac{m}{2\pi kT_{\perp}(r)}\right)^{\frac{1}{2}} \frac{c}{\lambda_0}\left[\exp\left(-\frac{m\left(\frac{c}{\lambda_0}\Delta\lambda - v_r(r)\sqrt{1-\left(\frac{x}{r}\right)^2}\right)^2}{2kT_{\perp}(r)}\right) + \exp\left(-\frac{m\left(\frac{c}{\lambda_0}\Delta\lambda + v_r(r)\sqrt{1-\left(\frac{x}{r}\right)^2}\right)^2}{2kT_{\perp}(r)}\right)\right]\frac{r\,dr}{\sqrt{r^2-x^2}} \quad (1)$$

where $\epsilon(r)$ is the line emission coefficient at radius r, and $v_r(r)$ is the directed radial ion velocity and R is the plasma (or tube) radius.

The solution of this integral equation was found by an approximation method. The velocities $v_r(r)$ and temperatures $kT_{\perp}(r)$ resulted when the minimum sum of the square of the errors between the measured intensities and the values $I(x,\Delta\lambda)$ from Eq.(1) was reached. The number of measurements was nearly one order of magnitude higher than the number of resulting values $v_r(r)$ and $kT_{\perp}(r)$.

With a parabolic undirected distribution function instead of the Maxwellian, similar results are obtained.

Some results for 20 mtorr discharges at 120 ns after ignition of the main discharge are plotted in Fig.5. The upper part shows the spatial distribution of the thermal energies perpendicular ($kT_{\perp}(r)$) and parallel ($kT_{\parallel}(r)$) to the magnetic field. The kinetic energies $E_{kin\perp}(r) = (1/2)m_i v_r^2(r)$ are drawn below. For comparison, the local magnetic field B(r) and the electron density $n_e(r)$ are also plotted.

The thermal and kinetic ion energies in the transverse direction are nearly of the same order of magnitude. But the thermal energies in the longitudinal direction are lower than the thermal transverse energies by more than a factor of two.

The ion energy distribution is strongly anisotropic. Only in the outer parts, where the electron density is small, are the thermal energies approximately equal. Ion heating in the transverse direction occurs in the very broad region where the magnetic field increases.

To obtain information on the relationship between the directed and the isotropic components of the ion distribution function, the energies were folded with the density to give

$$\overline{E} = \frac{1}{N_L}\int_0^R n_e(r)E(r)\, 2\pi r\,dr$$

N_L is the line density and E(r) is the respective energy component. The resulting averaged energies $\overline{E}$ are plotted in Fig.6 for 20 mtorr discharges. Addition of the transverse thermal energy to the kinetic energy of radial

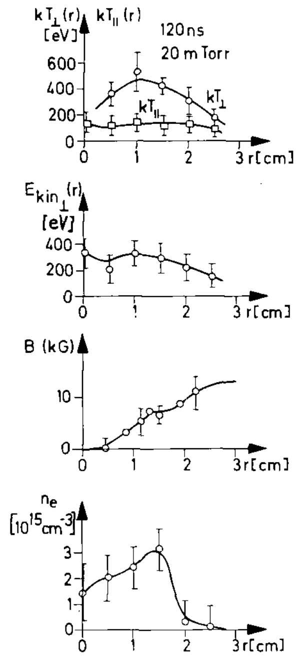

FIG. 5. Local distribution of thermal and kinetic energies, magnetic field, and electron density for 20 mtorr. Time: 120 ns.

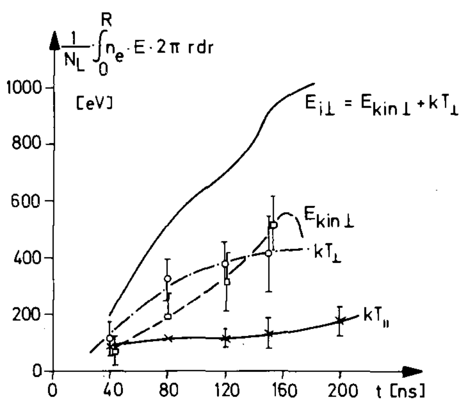

FIG. 6. Time development of ion energy components.

motion results in the transverse ion energy $E_{i\perp} = E_{kin\perp} + kT_\perp$. From this figure it can also be seen that the thermal energy $kT_\parallel$ parallel to B is very much smaller than $kT_\perp$.

The mean kinetic energies in the longitudinal direction are only 40-60 eV.

These 20 mtorr discharges show very strong anisotropy of the ion energies during the implosion phase. At a filling pressure of 60 mtorr the anisotropy is not so pronounced. Here $kT_\perp \approx 380$ eV, $kT_\parallel \approx 200$ eV, and $E_{kin\perp}$ rises to 300 eV.

The spectroscopically determined ion energies can be checked by comparison of the neutron emission calculated from the measured ion energy distribution and the density profile with the measured neutron yield.

At the first maximum compression a pronounced neutron peak of nearly 10^{10} neutrons/s was measured [2]. On the other hand, the neutron flux N was calculated from the spectroscopically measured ion velocity distribution and the density profile with

$$N = l \int_0^R n_i^2(r)\, \pi r \langle \sigma(g) g \rangle (r) dr \tag{2}$$

where l is the plasma length, R the plasma radius, g the relative velocity, $\sigma(g)$ the cross-section for neutron production, and $\langle\sigma(g)g\rangle$ the neutron rate averaged over the energy distribution function. With the measured ion energy distribution from Eq.(2), a value of $N = (7 \pm 5) \times 10^9$ neutrons/s was found. This is in good agreement with the measured neutron flux because the neutron rate $\langle \sigma(g)g \rangle$ is a very sensitive function of energy in the low keV region.

4. DISCUSSION OF RESULTS

The basic experimental results, especially in the case of low-pressure discharges (20 mtorr), show a very broad density profile of the imploding sheath, a pronounced ion energy anisotropy, and a rather high energy of the transverse undirected motion relative to the kinetic energy. These results can be interpreted in terms of an overturning [7] of the ion sheath and gyration phase mixing in the transverse plane as calculated by Kilb [8]. The transverse thermal energy $kT_\perp$ can thus rise to values as large as the kinetic energy $E_{kin\perp}$. This thermalization cannot be explained in terms of ion-ion instabilities due to counterstreaming ion layers [6,7][3], because in our experiments the electron temperature is much lower than the mean ion energy. For the onset of these instabilities, however, $T_e \gg T_i$ is required.

Because of the long self-collision times of ions the relaxation from transverse ion velocity components to longitudinal components by Coulomb collisions is very unlikely: only less than 10 eV of the ion energy parallel to the magnetic field can be explained in this way.

But, because of the high anisotropy of the ion energy, there may be instabilities leading to enhanced relaxation of ions. The condition for the onset of mirror instabilities [7] with $E_{i_\perp}/E_{i_\parallel} - 1 > 1/\beta_\perp$ is fulfilled for a large part of the sheath. $E_{i\perp}$ and $E_{i\parallel}$ are the ion temperature moments perpendicular and parallel to the magnetic field, and $\beta_\perp$ is the ratio of perpendicular gaskinetic pressure to magnetic pressure. The condition may be modified for experimental cases with finite boundary conditions and non-vanishing ion gyroradii. The growth times in our experimental conditions are of the order of more than 30 ns and so filling of the longitudinal ion energy component by mirror instabilities may be expected.[4]

[3] The experiments in Ref. [6] have been carried out with non-zero bias field.

[4] HF oscillations on the diamagnetic signal [1] may probably be indications of these instabilities.

But the anisotropy of the thermal energies is not lowered by this mechanism because during the growth time of the mirror instabilities the perpendicular ion energies are increased by approximately 150 eV.

A similar instability due to ion energy anisotropy is proposed by Kennel and Wong [13] and may also play a role in these strong shocks. But the conditions for the onset of these instabilities are only fulfilled in small regions near the front of the implosion wave.

ACKNOWLEDGEMENTS

The author would like to thank Prof.Dr.E.Fünfer for the opportunity of conducting this experiment and Dr.H. Zwicker for his interest and encouragement. He is especially indebted to Dr.R.Wilhelm for his valuable collaboration.

This work was performed as part of the joint research program between the Institut für Plasmaphysik, GmbH, Garching and Euratom.

REFERENCES

[1] WILHELM, R., to be published in Z.Phys., IPP Report under preparation.
[2] SCHUMACHER, U., WILHELM, R., ZWICKER, H., APS Topical Conference on Pulsed High Density Plasmas (Proc. Conf. Los Alamos) LA-3770-D 1 (1967).
[3] GOLDENBAUM, G.C., HINTZ, E.A., Physics Fluids 8 (1965) 2111, GOLDENBAUM, G.C., Physics Fluids 10 (1967) 1897.
[4] PAUL, J.W.M et al., Nature 208 (1965) 133; Culham Lab. Report CLM-P 142 (1967).
[5] KURTMULLAEV, P.Kh., NESTERIKHIN, Yu.E., PILSKY, V.I., SAGDEEV, R. Za, in Plasma Physics and Controlled Nuclear Fusion Research (Proc. Conf. Culham, 1965) 2, IAEA (Vienna, 1966) 367.
[6] ZAGORODNIKOV, S.P. et al., Soviet Phys. JETP 25 (1967) 783.
[7] SAGDEEV, R.Z., Soviet Phys. Techn. Phys. 6 (1962) 867; Reviews of Plasma Physics 4, Consultants Bureau (New York, 1966) 23.
[8] KILB, R.W., Gen. Electric Res. Lab. Report 67-C-166 (1967).
[9] SCHUMACHER, U., WILHELM, R., Phys. Verhandl. 5 (1966).
[10] GRUND, P., IPP Report under preparation, Phys. Verhandl. 6 (1968) 426.
[11] GRIEM, H.R., Plasma spectroscopy, McGraw Hill, New York (1964).
[12] GLOCK, E. in Conference Phen. Ion Gases (Proc. 7th Int. Beograd) 3 (1966) 194.
[13] KENNEL, C.F., WONG, H.V., Phys. Rev. Letters 17 (1966) 245.

DISCUSSION

A.G. PONOMARENKO: Can you explain in greater detail the difference between the transverse and the longitudinal energy of the ions in low-density θ-pinch experiments?

U. SCHUMACHER: Ion-ion collisions can be excluded as a reason for this difference: if there were no collective dissipation process and no charge exchange collisions, all the energy would be in the radial motion. Ion two-stream instabilities can probably also be excluded, although the mean free path for charge exchange is such that this process could be significant. It would explain the sheath broadening and the ion temperature anisotropy. The time scales are such that gyration phase mixing may also play a role.

EXPERIMENTS ON COLLISIONLESS SHOCK WAVES IN PLASMAS

C. YAMANAKA, S. NAKAI, T. YAMANAKA, Y. IZAWA AND K. KASUYA
FACULTY OF ENGINEERING, OSAKA UNIVERSITY, HIGASHINODA,
OSAKA, JAPAN
AND
Y. SAKAGAMI
NARA TECHNICAL COLLEGE,
YAMATO-KORIYAMA, JAPAN

Abstract

EXPERIMENTS ON COLLISIONLESS SHOCK WAVES IN PLASMAS. The structure of collisionless shock fronts which is determined by the mechanisms of energy dissipation is one of the most interesting problems of recent plasma research. We used three different approaches. The first method is to produce the shock waves in a pre-ionized collisionless magnetized plasma by a super-Alfvénic disturbance from a plasma gun. A strong linear pinch discharge of peak currents of 100 kA in rarefied gases was used to produce a plasma. The properties of the pre-ionized plasma were evaluated by the cut-off of the transmission of three different microwaves and the data from electric double probes. With a gas pressure of 10^{-3} torr, the degree of ionization was found to be about 90%. The initial electron temperature was up to 15 eV; the ion temperature estimated from the pinch velocity was also 15 eV. A conical gun was fired at a peak current of 200 kA in this collisionless plasma to drive the shock wave. By means of a magnetic probe a sharp front was observed, the thickness of which was much smaller than the mean free path. The Alfvén Mach-number was varied from 1 to 4. In a certain domain of the plasma parameter, defined by the three axes initial number density, the magnetic field and the atomic weight of the gas, the shock front had an oscillatory structure. This was markedly influenced by the Alfvén Mach-number. A Rogowski probe was used to detect the electron drift current flowing along the shock front across the magnetic field. When the electron drift velocity exceeded the thermal one, an intense soft X-ray burst was observed by a Be-foil CsI(Tl) scintillator. These results seem to confirm the existence of a collisionless turbulent dissipation at an Alfvén Mach-number of about 3.

The second method consists of forming a standing shock wave with a transverse magnetic field in a fast collisionless caesium plasma flow produced by a plasma generator analogous to the ion rocket engine. The diminution of the pre-existent oscillation was very important.

The last method is to produce the shock wave in a magnetized plasma by irradiating the target with an intense laser beam. Various configurations of the magnetic field are used to study the dissipation processes and also to simulate a sunflare phenomenon.

1. INTRODUCTION

The existence of shock waves in high-temperature collisionless plasmas in a super-high velocity flow depends upon the following three factors: a steepening effect due to a non-linearity, a dispersive wave property, and some collisionless dissipative mechanism [1]. The balancing of the first two effects, which is described by the Kortweg-de Vrier equation produces a steady solitary wave. If non-collisional dissipation which is assumed to be due to micro-instabilities in the plasma is introduced, the characteristic profile of a steady flow begins to change and forms a wave train tending to a shock wave. These energy conversion processes which dissipate the energy of a flow to non-linear wave motions are among the most interesting problems in plasma physics; besides, they provide a heating mechanism in fusion research.

To clarify the properties of collisionless shock waves we performed three different approaches. The first method [2] is to produce a shock wave perpendicular to the magnetic field in a pre-ionized collisionless magnetized plasma by a super-Alfvénic disturbance from a plasma gun. The main object of this experiment is to determine the shock structure for various Alfvén Mach-numbers and to find the instabilities responsible for shock formation.

The second method [3] is to form the shock waves in a laser-produced magnetoplasma by irradiating it with another intense laser pulse. In this case we can use various configurations of the magnetic field and examine the stable regions of existence of the shock wave including an oblique form [4].

The third method is to form a standing shock wave against a transverse magnetic field by a super-Alfvénic continuous flow of caesium plasma from a hot-plate plasma generator [5]. This experiment aims at determining the characteristic fluctuations around the domain of the shock front. In this superhigh-velocity plasma tunnel we are also expecting to study the possibility of collisionless shock waves due to the ion acoustic instability without a magnetic field [6]. In Table I the typical plasma parameters of these three experiments are shown for comparison. These approaches to obtain information on collisionless shock waves seem very effective. In our experiments, there is a definite domain of plasma parameters where collisionless shock waves can be shown to exist.

2. GUN DRIVE EXPERIMENT

In the usual shock-wave experiments [7-10] symmetrical configurations of the magnetic fields were adopted. But we want to have a rather long interaction region of the waves and, therefore, use a gun drive system.

2.1. Experimental arrangement

A schematic view of the apparatus is shown in Fig. 1. The inner diameters of the discharge tubes were 6.7 cm and 17 cm; the length was 50 cm. The diameter of a magnet was 20 cm; its magnetic field was up to 3 500 G. The base pressure was less than 5.0×10^{-5} torr. The working gases were hydrogen, helium, argon, nitrogen and air which were passed through a vessel under pressures ranging from 5×10^{-4} to 1×10^{-1} torr. After a transverse magnetic field had been applied by an electromagnet the gas was ionized by a linear Z-pinch discharge. The current was up to 100 kA, its duration was about 60 μs, the discharge energy was about 640 J, 20 kV, 3.2 μF. A quiet magnetoplasma was used as a working medium; its electron temperature was varied by a time decay from the period of pre-ionization. The electron density n_e and the degree of ionization α were estimated by measuring the cut-off times of microwave transmissions (three frequencies: 4 GHz, 10 GHz, and 70 GHz). The electron temperature T_e was measured by pulse electric double probes, a mm-wave interferometer [11] and a method making use of the spectral line intensity. The ion temperature T_i was estimated from the converging velocity of the linear

TABLE I. TYPICAL PLASMA PARAMETERS OF THREE EXPERIMENTS

Parameter	Gun drive experiment	Laser plasma experiment	Cs flow experiment
Working plasma species	Nitrogen *	Carbon	Cesium
Density (cm^{-3})	7×10^{13}	3×10^{12}	$10^7 - 10^9$
Electron temperature T_e (eV)	15	3	0.2 - 2
Ion temperature T_i (eV)	15		0.2
Magnetic field B (G)	0-500	0-1000	0-6200
Ion Larmor radius R_L (cm)	4.8	2	15
Ion-ion(electron-electron) mean free path λ_1 (cm)	7.6	7.2	17
Electron-ion mean free path λ_2 (cm)	5.4	5.2	
Alfvén velocity V_m (cm/s)	2×10^6 (300G)	1.5×10^7 (500G)	-
Sound velocity V_a (cm/s)	2×10^6 (γ=2)	1×10^6 (γ=2)	7.8×10^4 (γ=2)
Wave velocity V (cm/s)	6×10^6	3×10^7	8.4×10^6
$\frac{1}{2}$ nmv^2 (erg/cm^3)			
ahead of front	3×10^3	3.1×10^4	7.8
behind front	7.5×10^2		
2 nkT (erg/cm^3)			
ahead of front	3.4×10^3	9.6	6.4×10^{-4}
behind front	—	—	—
$B^2/8\pi$ (erg/cm^3)			
ahead of front	3.6×10^3	4×10^4	-
behind front	14.4×10^3	6×10^4	
Characteristic lengths			
$2\pi v/\Omega_{ci}$ (cm)	180	4.7×10^2	$7.3 \times 10^5/B$
$2\pi v/\Omega_{ce}$ (cm)	2.2×10^{-3}	3.4×10^{-1}	3/B
$2\pi v/\Pi_i$ (cm)	1.28×10^{-2}	0.29	14.8
$2\pi v/\Pi_e$ (cm)	8×10^{-5}	1.9×10^3	$3 \times (10^{-1}-10^{-2})$
$2\pi v/\sqrt{\Omega_{ce}\Omega_{ci}}$ (cm)	0.63	12.6	$1.47 \times 10^3/B$
c/Π_e (cm)	6.4×10^{-2}	0.1	$1.7 \times (10 \sim 10^2)$
Magnetic Reynolds number R_m	2.7×10^2 (L=6cm)	1.98×10^2 (L=6cm)	60 (L=20cm)

* Hydrogen, helium, argon and air were also used.

Z-pinch measured by an image-converter camera and the Doppler width of radiation. Figure 2 shows a typical example of magnetoplasmas with an initial pressure of 1×10^{-3}torr. In the case of air the electron density was $7.0 \times 10^{13}/cm^3$, at the onset of the afterglow, and the plasma was almost fully ionized. The electron and ion temperatures were 15 eV. The electron density and temperatures decreased exponentially with time constants of

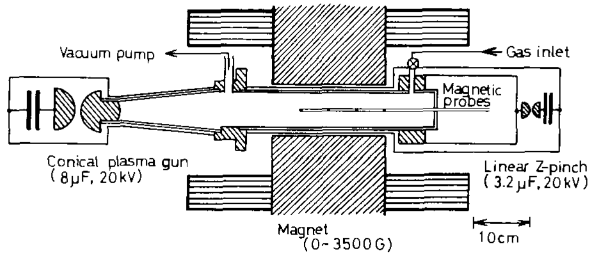

FIG. 1. Schematic diagram of experimental apparatus of gun-drive experiment.

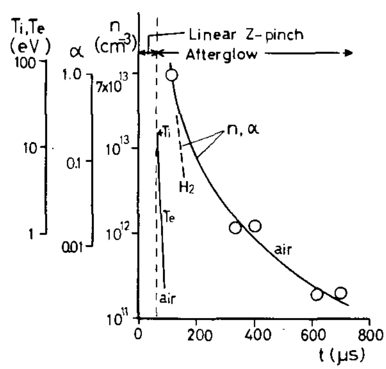

FIG. 2. Number density n, degree of ionization α and temperatures T_e, T_i of working plasma produced by a linear Z-pinch discharge in air and hydrogen at initial pressure of 1.0×10^{-3} torr.

100 μs and 10 μs, respectively. The mean free path of collision was 8 cm. The ion Larmor radius at 3 500 G was 0.48 cm, and the electron radius was 2.9×10^{-3} cm. The characteristic scale of the magneto-acoustic waves c/Π_e was 6×10^{-2} cm, where Π_e is the electron plasma frequency. The magnetic Reynolds number R_m was 2.7×10^2 which shows that the magnetic flux is frozen.

As the mass of the working plasma atoms was increased, (i.e. going from hydrogen to helium, air and argon), the experimental conditions of different Alfvén velocities were introduced. In a region where the mean free path was longer than the other characteristic lengths of the plasma, a super-Alfvénic flow was applied to perform a collisionless shock-wave experiment.

A conical gun was used to drive a shock wave. The maximum current of the gun was 200 kA, the discharge energy was 1.6 kJ, 20 kV, 8 μF. In a transverse magnetic field, only a fast magneto-acoustic mode can exist in a stable manner.

2.2. Observation of the shock front

The propagation of magnetohydrodynamic disturbances was measured by a set of four small and movable magnetic probes. Figure 3 shows the wave propagation behaviour of a wave front and a gun-driven plasma. A typical propagation velocity v was about 3 to 6×10^6 cm/s in hydrogen

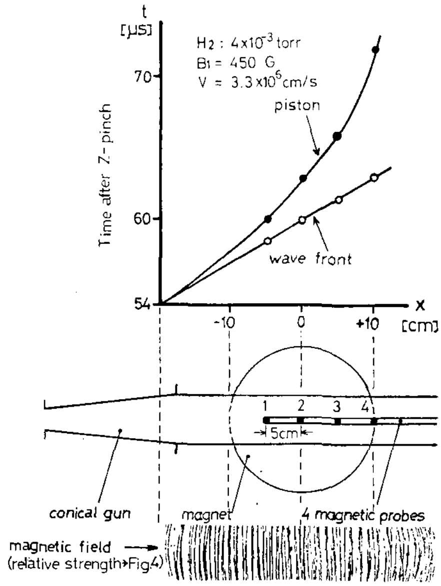

FIG. 3. Time of flight wave propagation in hydrogen by gun-drive and a magnetic field distribution pattern.

plasma of an initial pressure of 4×10^{-3} torr under a magnetic field of 450 G.

The magnetic Mach number M_m was varied from 1 to 4 according to the applied magnetic field intensity and also to the density of the plasmas.

The plasma light radiated at the instant of arrival of the shock front was observed by a photomultiplier. The bremsstrahlung gives an information on the plasma density. From the data from the magnetic probes and the light signals we see that the magnetic field and the plasma density show a jump at the same time. In Fig. 4 the wave forms in hydrogen measured by the magnetic probes are shown for various magnetic Mach numbers, where the probe positions are indicated. The propagation of the fronts and their deformation were observed. In the case of weak magnetic fields and also at the first probe position the gun plasma shows a diamagnetic response just after the wave front.

As to the formation of the shock waves, the dispersion of the magneto-acoustic waves and the dissipation mechanism are important. When the wavelength of these waves decreases to the order of c/Π_e, the dispersion property is responsible for retaining the steepening of the front. The shock width of our experimental results was about 30 c/Π_e. In Fig. 5 we see a particular oscillation which was introduced just after the front of the air plasma. The width of the shock front was about 2 cm which was smaller than the mean free path of collision in a range of $M_m < 3$. At the high magnetic Mach number $M_m > 3$, the wave front became broad and showed a two-step structure. As the plasma became collisionless the cooperative motions of the plasma predominated in exciting the oscillations, the frequency of which was approximately equal to the electron-ion hybrid frequency. These oscillations were not observed in the case of collisional magnetohydrodynamic shock waves. In Fig. 6 the region where the oscillatory structure was observed is shown in a parameter volume composed of

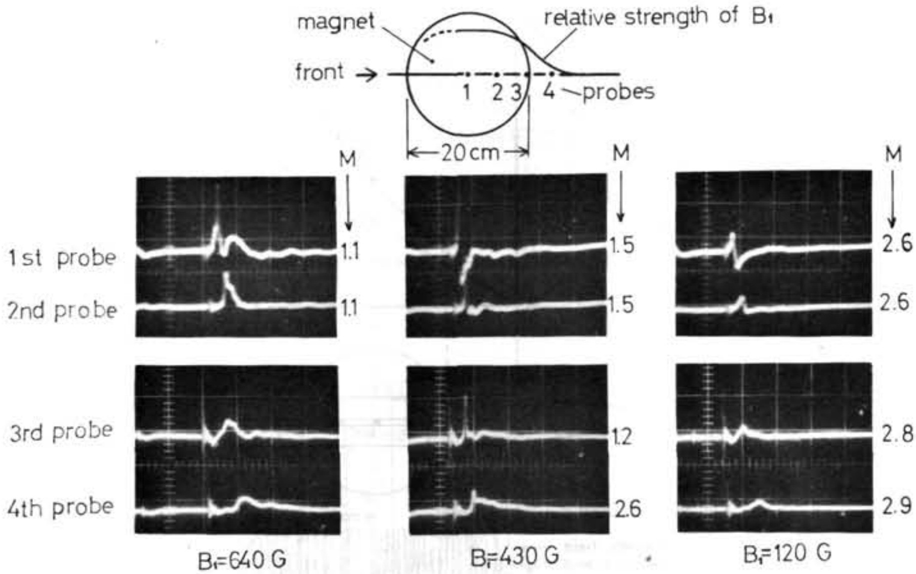

FIG. 4. Wave forms measured by magnetic probes in various Mach numbers in hydrogen plasma (the gun was driven after 50 μs of Z-discharges); initial pressure $\sim 4 \times 10^{-3}$ torr, 80 G/div., 10 μs/div.

the three axes initial gas pressure P_1, magnetic field B_1 and mass number of atom A. This region corresponds almost to the collisionless shock domain, where the x plane indicates the condition $M_1 = 1$ and the y plane shows the condition that the mean free path of collision is equal to the ion Larmor radius.

2.3. Dissipation mechanism

The study of the collisionless dissipative processes is very interesting. Many models which seem suitable to describe the process in a weak shock condition have been proposed [12 - 15]. For high Mach numbers, however, the situation remains unclear. We measured a current in the front by a Rogowski probe with a diameter of 1 cm. Figure 7 shows a current wave form in hydrogen plasma which seems to be due to the drift electrons crossing the magnetic field in the surface of the shock front.

The positive signal coming afterwards corresponds to a reverse current flowing in the surface of a piston plasma. Assuming the initial plasma density to be $7 \times 10^{13}/\text{cm}^3$, the electron drift velocity is up to 4.5×10^8 cm/s which is greater than the thermal electron velocity of 2.6×10^8 cm/s at a temperature of 15 eV. According to a theory of two-stream instabilities [16], the instability is introduced, when the velocity of the drift electrons exceeds the thermal velocity of the electrons behind the front. The threshold magnetic Mach number of this instability [1] is given by $M_m = 1 + (3/8)(8\pi n k T_e/B^2)^{1/3}$. In our experiment of Fig. 7, the flow velocity exceeds this threshold of $M_m = 1.26$, $B_0 = 350$ G and tends to be dissipative.

To check the existence of beams in a front we used an ion-sensitive probe [17]. As is well known, if a surface of the ion-sensitive probe is

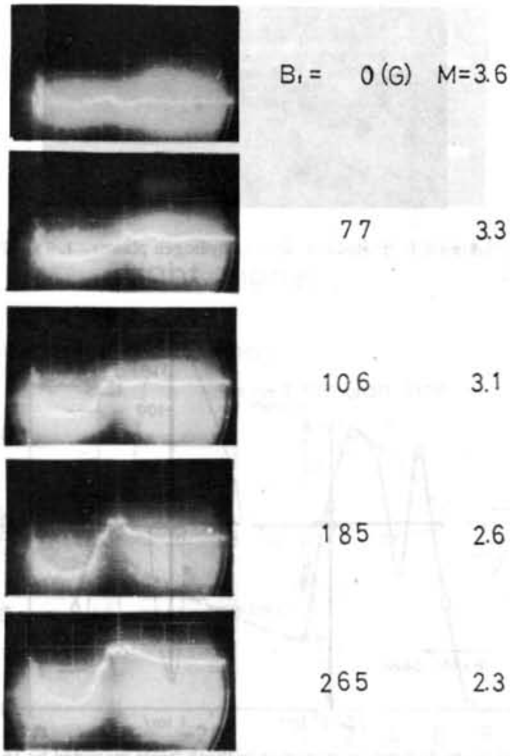

FIG. 5. Oscillation of the front structure in air plasma 130 G/div., 2 μs/div; initial pressure 1 × 10⁻³ torr.

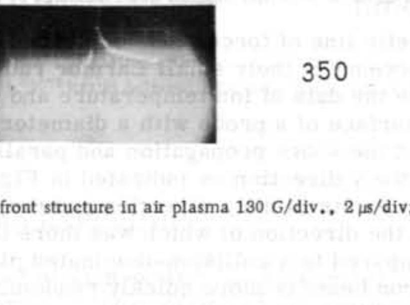

FIG. 6. Observed region of oscillatory shock structure and collisionless domain in the three axes representing plasma pressure, magnetic field and atomic number.

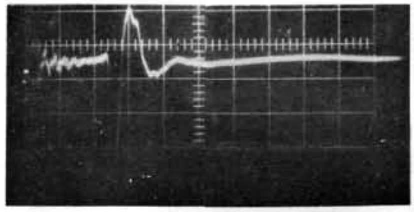

FIG. 7. Current in shock front by drifted electrons in hydrogen plasma, 1.0×10^{-3} torr.; 1600 A/div., 2μs/div., B_1 = 350 G.

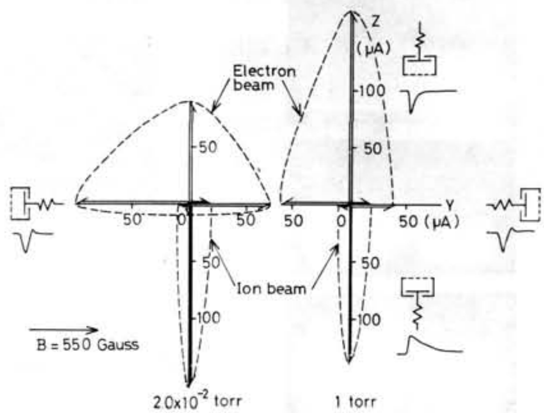

FIG. 8. Directional beam distribution properties in shock fronts measured by an ion sensitive probe.

put parallel to a magnetic line of force, less energized electrons cannot reach a collector on account of their small Larmor radius while the ions easily get there to give the data of ion temperature and density. In the hydrogen plasma the surface of a probe with a diameter of 10 mm, was set along the x direction of the shock propagation and parallel or perpendicular to the line of force in the y direction as indicated in Fig. 8. These data show that the ion beam exists in the z direction and the energized electron beam was observed, the direction of which was more divergent in a collisionless case compared to a collision-dominated plasma. This confirms the fact that the electron beam is more quickly randomized by the two-stream instability than by the collisional thermalization.

In helium plasma, the variation of the electron temperatures across the shock front was measured by the spectral intensity ratio of the HeI 4713 Å and 4921 Å lines (Fig. 9b). The results are shown in Fig. 9a.

The electrons were heated very rapidly in a turbulent state. The growth rate of the two-stream instability, estimated from a linear analysis, is $\gamma_{max} = \pi i (m_i/m_e)^{1/6}$ [15]; in the case of hydrogen we obtained $\gamma = 3 \times 10^{10}$/s. Then we measured the soft X-rays from the shock front using a CsI (Tl) scintillator. The scintillator, of 45 mm diameter and 3 mm thickness, was covered by a 150-μm-thick Be plate. In Fig. 10, the X-ray burst in the hydrogen plasma is shown when the front arrives at a given position of the detector. This indicates the existence of a few keV-electrons in the plasma. The two-stream instability in the front surface seems to be responsible for the turbulent dissipation of the collisionless plasma.

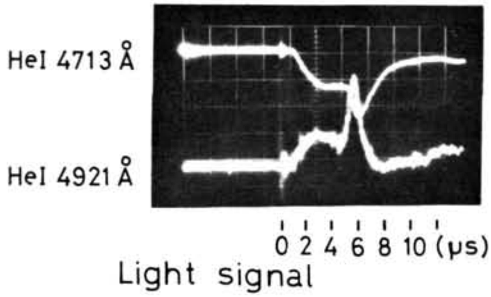

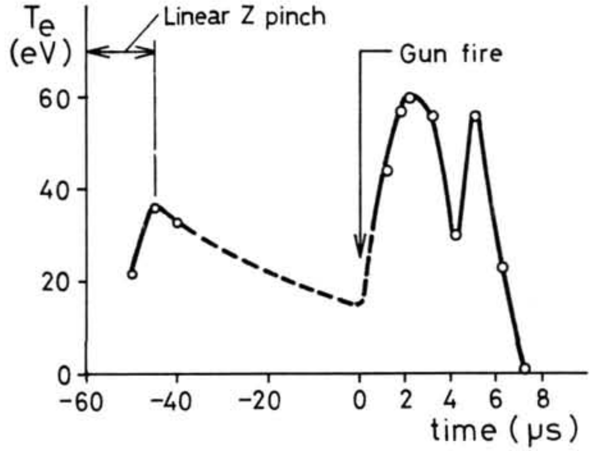

FIG.9(a). Electron temperature T_e vs. time estimated by line intensity ratio HeI 4921Å/HeI 4713Å. The initial pressure was 5.0×10^{-3} torr in helium. The initial field was 320 G. The magnetic Mach number was 1.5.

3. LASER PLASMA EXPERIMENT

The development of high-power lasers enables us to produce an isolated, hot, neutral and impurity-free plasma at any desired point in the vacuum environment. We tried to drive a laser-produced carbon plasma immersed in a magnetic field by another laser-produced LiH plasma.

3.1. Experimental apparatus

We used two glass lasers with diameters of 20 mm and 10 mm and lengths of 30 cm and 15 cm, respectively, supplying powers of 50 MW and 20 MW of a 30 ns-pulse in Q-switched mode, respectively. The irradiated targets were a carbon plate and a LiH crystal. The laser beams were collimated through a lens. The experimental setup is shown in Fig. 11 where the direction of the magnetic field is perpendicular to the laser beams. Two magnetic probes were used to investigate the front structures.

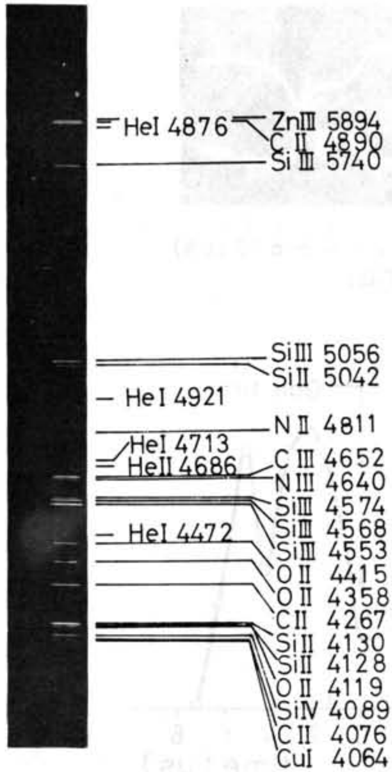

FIG. 9(b). Spectrum in gun-drive experiment.

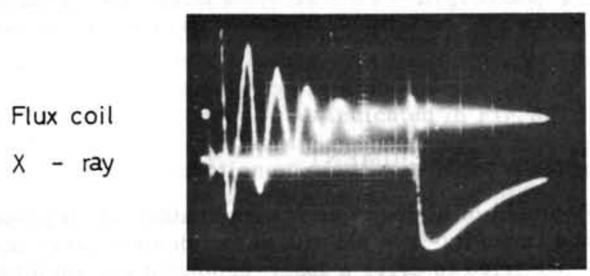

FIG. 10. Soft X-ray burst from shock wave in hydrogen plasma, 1.0×10^{-3} torr, $B_1 = 300$ G, 10 μs/div.

3.2. Experimental results

The carbon working plasma was measured by electric double probes, a particle detector and Thomson scattering of the ruby laser light. The results are shown in Fig. 12. The directional distributions of plasma are shown in Fig. 13 [18]. In the transverse magnetic field, the shock-front structures were observed at different Mach numbers by changing the magnetic field intensity as shown in Fig. 14. A carbon working plasma, the

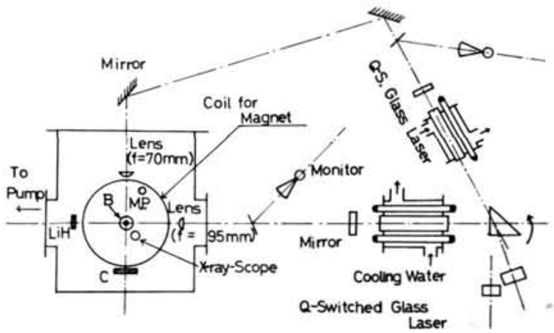

FIG. 11. Experimental setup of the laser experiment.

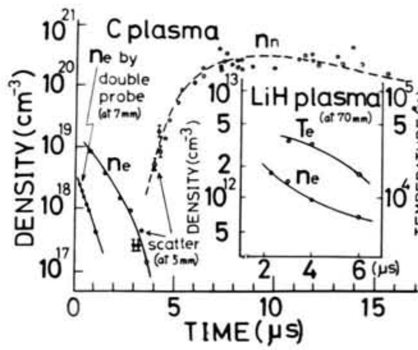

FIG. 12. Density and temperature of laser-produced plasma.

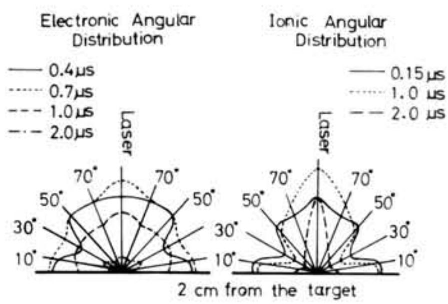

FIG. 13. Directional distribution of plasma from the carbon target without magnetic field.

density of which was $10^{13}/cm^3$ 4 μs after its production, was driven by a LiH plasma of the second laser. In this period a burst of soft X-rays was observed as shown in Fig. 15. When the Mach number is higher the shock front seems to be broad and the driving plasma penetrates into the field as in the high-β case.

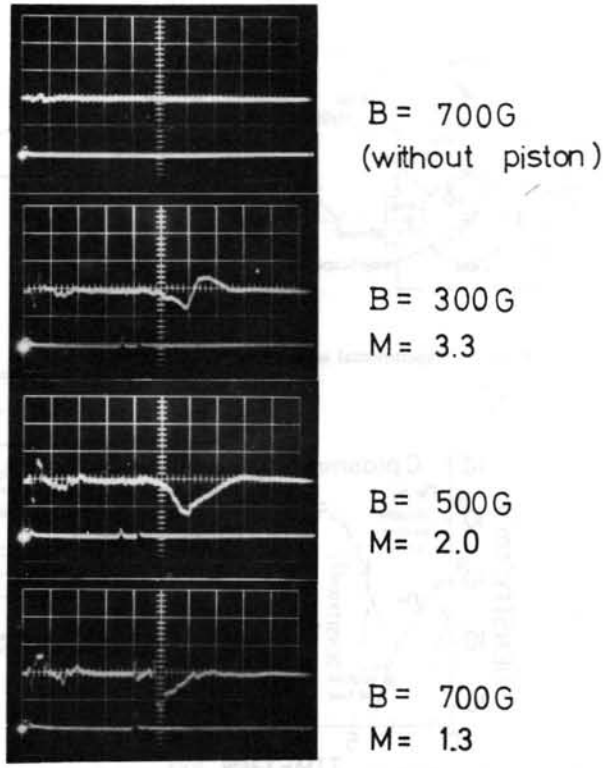

FIG. 14. Shock structures of laser plasma in collisionless state. Sweep speed 1 μs/div. The upper trace is the magnetic field (32 G/div) and the lower trace is the laser pulse.

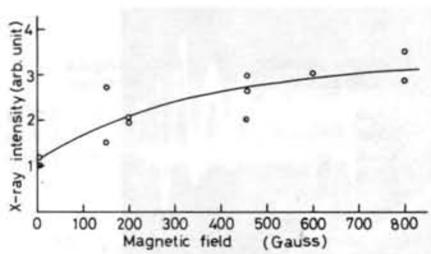

FIG. 15. Soft X-ray intensity with magnetic field in laser plasma.

4. CAESIUM PLASMA EXPERIMENT

A steady supersonic alkali plasma flow was injected into a straight transverse magnetic field to study the collisionless standing shock waves.

4.1. Experimental arrangement

A schematic diagram of the experimental apparatus is shown in Fig. 16. We ionized Cs atoms from a reservoir by passing them through a hot

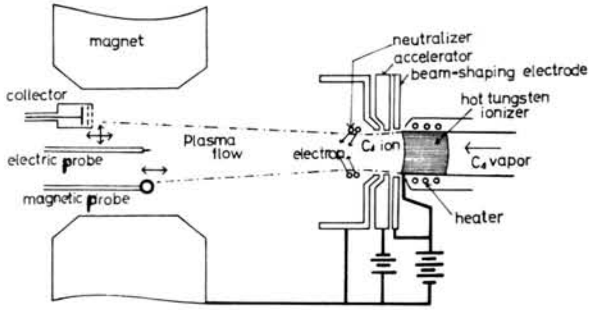

FIG.16. Schematic diagram of experimental apparatus of Cs plasma flow.

tungsten ionizer (1800°K). The ions from the ionizer were accelerated electrostatically through a Pierce-type electrode (0-5000V) and neutralized by thermal electrons from a hot filament sitting around the ion beam. The beam shape and its density were observed by a movable small collector. The velocity was measured by an electrostatic deflection-type energy analyser. The local plasma density and temperature were measured by movable Langmuir probes. The oscillations were picked up by electric and magnetic probes and displayed on a spectral analyser.

The beam diameter was about 15 mm. The typical beam current density was 3 mA/cm^2 at an acceleration voltage of 5000 V, the beam velocity was about 10^7 cm/s, and the ion density was about 2×10^9 /cm^3. The transverse magnetic field strength was up to 6200 G and decreased with the distance as $1/r^3$.

In the neutralization process, electron mixing was freely accomplished and positive space charge was almost neutralized. The electron temperature

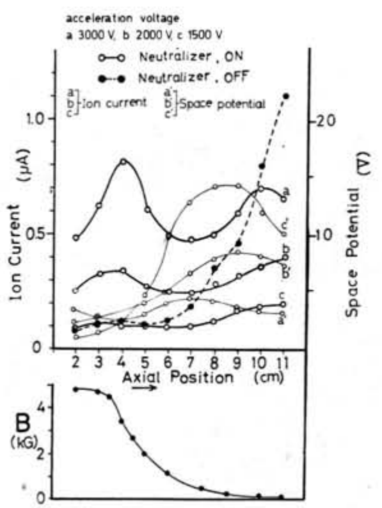

FIG.17. Characteristic structure of plasma density along the beam and magnetic field configuration. 1.0 cm/unit, Acceleration voltage a) 3000V, b) 2000 V, c) 1500 V.

could be controlled injecting energetic electrons. In this case the beam induced a low-frequency oscillation. The neutralization by electrons of lower energy showed a decrease in intensity.

4.2. Experimental results

When the injected plasma beam was very tenuous, no characteristic structure was observed around the magnetic field. As the beam density increased, the ion distribution shows humps along the beam. They are shown in Fig. 17 with the configuration of the magnetic field and the space potentials. The electron temperatures around the positions 10 and 5 were 2 eV and 0.2 eV, respectively. When the unneutralized ion beam was injected, the characteristic structure disappeared. This density structure seems to be caused by the charge separation effect due to different Larmor radii of ions and electrons. The condition of dynamic pressure balance

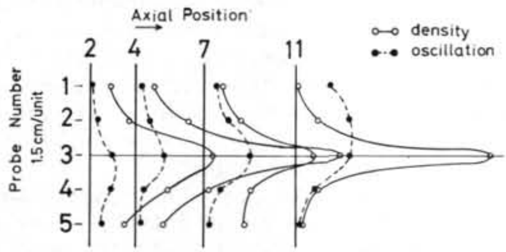

FIG. 18. Radial distribution of low frequency oscillation and density at various axial positions.

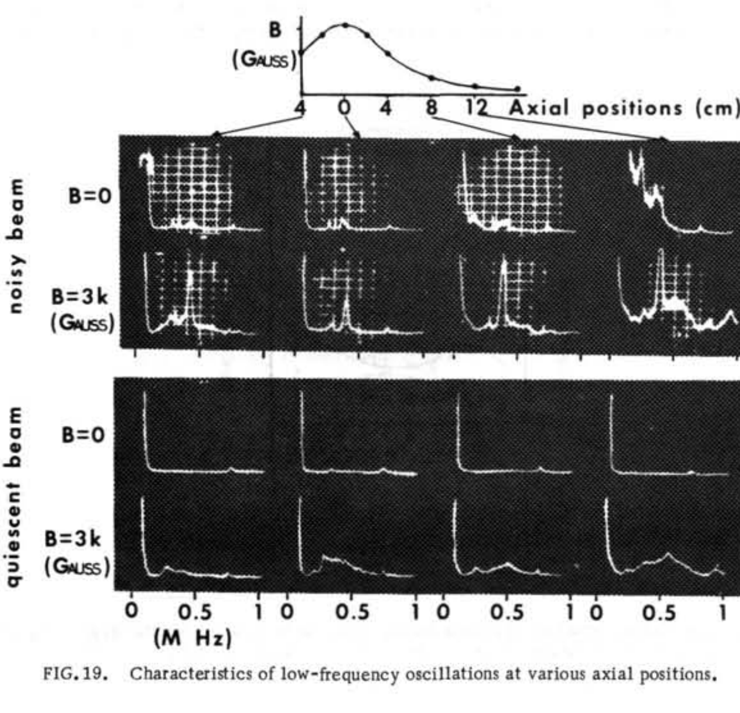

FIG. 19. Characteristics of low-frequency oscillations at various axial positions.

($B^2/8\pi = (1/2)nmv^2$) was nearly satisfied at the axial position 11-12 where the ion density showed a maximum.

Together with the appearance of a density structure, low- and high-frequency oscillations began to take place. The low-frequency oscillation was of the order of several 100 kHz localized to a forward position. In Fig. 18 this spatial distribution of the amplitude of the low-frequency oscillation is shown with a radial distribution of the ion density. The high-frequency oscillation was enhanced by a magnetic field whose frequency range was about 15 MHz. Figure 19 shows the spectra of these oscillations. When the electron temperature of the beam rose, the amplitude of the oscillations was increased, and the spectrum became noisy at the low-frequency side of the peak. This may suggest that the ion acoustic wave instability plays the role of a collisionless mechanism randomizing the flow energy.

5. CONCLUSIONS

The three different approaches of a gun drive, a laser plasma and Cs flow experiments are of a complementary significance in the investigation of the collisionless shock waves. In the magnetic Mach number range of 1-4, we ascertained the simultaneous jumps of the magnetic field and the density in the shock front. In this case we often noticed oscillations in the front. The rise of the front seems to be the steepest for a magnetic Mach number of about 2. Measured shock-front widths are shown in Fig. 20.

The dissipative mechanism of the two-stream instability was assumed to be a very important process for shock formation in our case. The drift electrons in the front were observed in detail.

A soft X-ray burst indicates turbulent electron heating up to a few keV.

The dissipative mechanisms caused by the ion acoustic and decay instabilities are still being studied.

We want to express our gratitude to Dr. M. Yokoyama and Messrs T. Sasaki, R. Shimaki and M. Onishi for their help in our experiments.

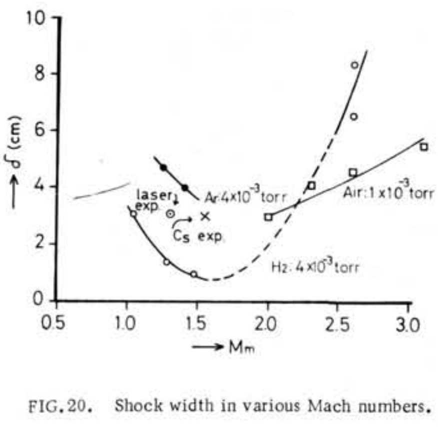

FIG. 20. Shock width in various Mach numbers.

REFERENCES

[1] SAGDEEV, R.Z., in Reviews of Plasma Physics, (LEONTOVICH, M.A., Ed.) 4 Consultants Bureau, New York (1966).

[2] SAKAGAMI, Y., YAMANAKA, C., Report Ionosphere, Space Research Japan 20 (1966) 45; Technol. Repts Osaka Univ. 16 (1966) 153.

[3] YAMANAKA, C., YAMANAKA, T. et al., COSPAR, Symp. on Solar Flares and Space Research A: 5.7 (1968), Jap. J. appl. Phys. 7 (1968) 84.

[4] KAKUTANI, T., TANIUTI, T. et al., J. phys. Soc. Japan 24 (1968) 1159; SAFFMAN, P.G., J. Fluid Mech. 11 (1961) 552.

[5] YAMANAKA, C., NAKAI, S. et al., IPPJ-44 (1965) 75.

[6] COLGATE, S.A., Physics Fluids 10 (1967) 1288.

[7] PAUL, J.W.M. et al., Nature 208 (1965) 133; 216 (1967) 363.

[8] KURTMULLAEV, R.Kh., NESTERIKHIN, Yu.E., PILSKY, V.I., SAGDEEV, R.Z., in Plasma Physics and Controlled Nuclear Fusion Research (Proc. Conf. Culham, 1965) 2, IAEA, Vienna (1966) 367.

[9] ASCOLI-BARTOLI, U., MARTELLUCCI, S., MARTONE, M., in Plasma Physics and Controlled Nuclear Fusion Research (Proc. Conf. Culham, 1965) 1, IAEA, Vienna (1966) 275.

[10] GOLDENBAUM, G., Physics Fluids 8 (1965) 2111.

[11] YAMANAKA, C. et al., J. phys. Soc. Japan 22 (1967) 1306.

[12] KENNEL, C.T., SAGDEEV, R.Z., J. geophys. Res. 72 (1967) 3303.

[13] TIDMAN, D.A., Physics Fluids 10 (1967) 547.

[14] NIU, K., HUNG, R-J., phys. Soc. Japan 23 (1967) 436.

[15] MORAWETZ, C.S., Physics Fluids 5 (1962) 1447.

[16] STIX, T.H., The Theory of Plasma Waves, McGraw-Hill, New York (1962).

[17] KATSUMATA, I. et al., Jap. J. appl. Phys. 6 (1967) 123.

[18] YAMANAKA, C. et al., 1st Int. Conf. Laser Application (1967).

DISCUSSION

S. D. FANCHENKO: How were the oscillations at frequency ω_{pe} detected?

C. YAMANAKA: The oscillation signals were detected by a movable probe connected to a spectrum analyser.

OBLIQUE HYDROMAGNETIC SHOCK WAVES

A. E. ROBSON AND J. SHEFFIELD
UNIVERSITY OF TEXAS, AUSTIN, TEXAS, UNITED STATES OF AMERICA

Abstract

OBLIQUE HYDROMAGNETIC SHOCK WAVES. An experiment is described in which shock waves are propagated in a magnetized hydrogen plasma with Alfvén Mach numbers up to $M_A = 5$ and at angles α to the magnetic field from 90° to 40°.

The plasma of density $\sim 5 \times 10^{14}$ cm^{-3} and temperature ~ 1 eV is created in a pyrex chamber of 45 cm diameter and 93 cm length by means of an oscillatory z-discharge. The initial magnetic field is 500-1000 G. A curved magnetic piston is driven into the plasma by exciting a rapidly rising θ-current in a single-turn loop of short axial length arranged round the tube on its midplane. A curved shock front propagates ahead of the piston in the manner of a bow wave.

Magnetic and electric probes are used to study the development and structure of the shock front. On the midplane the front has the monotonic field jump typical of propagation perpendicular to the field, but for propagation at an angle to the field a radically different structure is seen. Ahead of the main jump in field and density there is a large-amplitude, circularly polarized oscillation which is identified as a high-frequency Alfvén ("whistler") wave propagating at the same speed as the shock. The wavelength λ is given by

$$\lambda \approx \frac{2\pi \cos\alpha}{(M_A^2 - 1)^{\frac{1}{2}}} \cdot \frac{c}{\omega_{pi}}$$

The results are compared with numerical computations of shock structure using hydromagnetic equations. To account for the observed structure, it is necessary to invoke collisionless effects.

INTRODUCTION

Compared with the extensive work on shock waves propagating perpendicular to the magnetic field in a magnetized plasma, shocks propagating at oblique angles have received relatively little attention. In this paper we describe an experiment specifically designed to study the oblique shock.

Oblique shocks differ from perpendicular shocks in that the component of magnetic field normal to the shock front allows electron motion parallel to the field to play a dominant role in determining the structure when the angle of deviation from the perpendicular exceeds $\sim (m_e/m_i)^{\frac{1}{2}}$. Whereas the perpendicular shock jump has a characteristic length $\sim c/\omega_{pe}$, and may be followed by a train of oscillations of similar wavelength, it is predicted that the oblique shock should be preceded by a train of oscillations in the magnetic field having a wavelength $\sim (c/\omega_{pi}) \cos\alpha$, where α is the angle between the direction of propagation and the field [1,2,3]. A precursor oscillation of this kind was observed by Martone [4] at the end of a theta-pinch experiment, although the angle was not measured. More recently, Eselevich et al. [5] have studied shocks deviating from the perpendicular by up to 10° and have observed the increase in wavelength with increasing deviation.

For larger angles ($\alpha \sim 1$) the characteristic length of an oblique shock becomes $\sim (m_i/m_e)^{\frac{1}{2}}$ times the corresponding length of a perpendicular shock, and to study the oblique shock one must work at relatively high plasma density, or in large apparatus. The approach which has been adopted in the present work is to do both.

THE APPARATUS

A schematic diagram of the apparatus is shown in Fig. 1. The plasma is produced by an oscillatory z-discharge through hydrogen in a pyrex glass tube 45 cm in diameter and 93 cm long, in which a uniform axial magnetic field of up to 1000 gauss has first been established by means of an external coil system. The filling pressure is 20 mtorr, and the preheating current is a damped oscillation of 100 kA peak and 80 μsec half-period. This arrangement is identical in all important respects to the preheating system of Paul et al. [6]. The plasma density, measured by a four-pass infrared interferometer, is $\sim 5.10^{14}$ cm^{-3}, $T_e + T_i \approx 2$ eV from the diamagnetic signal; and the degree of ionisation, by analogy with [6] is $\sim 90\%$. For these conditions, the characteristic length c/ω_{pi} is 1 cm.

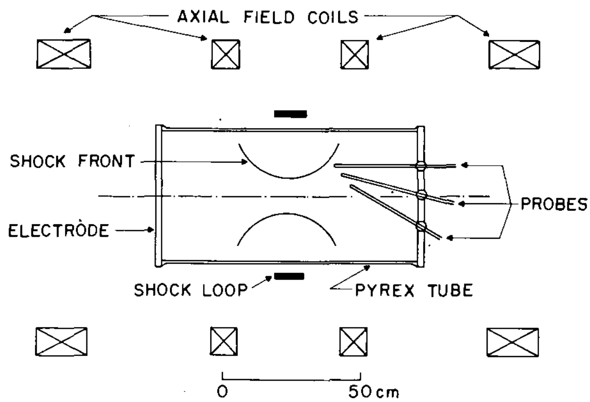

FIG.1. Schematic diagram of the apparatus.

A magnetic piston is produced by a single-turn loop, 50 cm diameter and 10 cm axial length, wrapped round the discharge tube in its midplane. The loop is fed at four symmetrical points, each of which is connected to a 2 μF capacitor through a low-inductance transmission line and spark gap switch. With the capacitors charged to 60 kV, the voltage round the loop is 200 kV, and the current rises to 190 kA in a quarter-period of 1.0 μsec. The magnetic piston is convex to the plasma, and as it drives radially inwards, a shock propagates ahead of it in the manner of a bow wave. With the exception of a short region on the midplane, the shock is everywhere oblique to the field in the plasma.

The strongest shocks are produced when the field of the piston is in the same direction as the field in the plasma, and the apparatus is normally operated in this condition.

EXPERIMENTAL RESULTS

The motion and structure of the shock front are studied with magnetic and electric probes inserted through the end electrode via sliding and swivelling vacuum seals. Each magnetic probe consists of 10 turns of 0.05 mm dia. wire, wound on a former 0.3 mm dia. and enclosed in a glass tube 1 mm o.d. The electric probes consist of platinum spheres, 1 mm dia., on the end of 0.5 mm dia.

wires sheathed in 1 mm dia. pyrex tube. The response time of both systems is better than 10 nsec.

The best region for study is between 14 and 6 cm radius, since here the shock appears to have reached steady flow conditions, and the effect of cylindrical convergence is not yet significant. The shock arrives in this region about 1.0 μsec after firing the shock bank, and the time of arrival at any point is usually within ±15 nsec. The reproducibility of the system allows the motion of the shock to be mapped out using only two moveable probes and collecting data from a large number of shots. Fig. 2 shows the progress of a typical shock, velocity $u_S \sim 2.10^7$ cm/sec (Alfvén Mach number $M_A \sim 4$). When the incident shock hits the axis, a reproducible reflected shock propagates outwards.

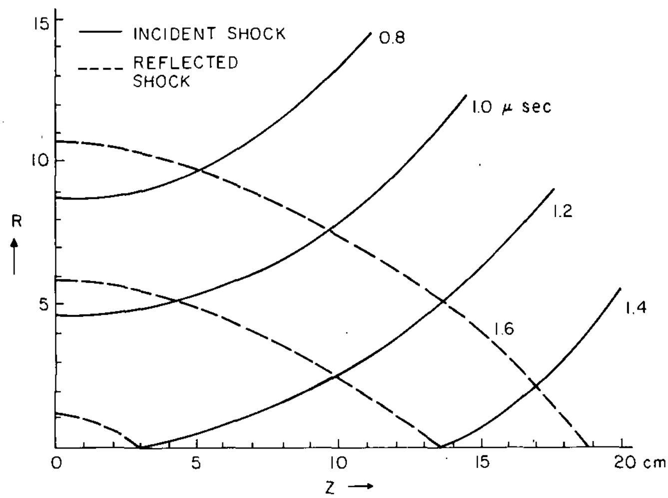

FIG.2. Progress of the shock front. Times in microseconds after firing the shock bank.

At r = 10 cm, z = 12 cm, the incident shock is propagating at 45° to the field. In Fig. 3a we show the integrated signals from two magnetic probes at this position, one measuring the field in the (r,z) plane and the other measuring the field in the azimuthal (θ) direction. The field in front of and behind the shock is in the (r,z) plane, as would be expected from axial symmetry, and the component parallel to the shock, $B_{\parallel}$, increases by a factor 3.6 across the shock, in agreement with the Rankine-Hugoniot relations for these flow conditions. Within the shock front an oscillatory θ-component is generated, and from the relative phases of the components we see that the field vector rotates several times through the shock, in the direction of electron gyration in the initial magnetic field (Fig. 3b). The magnetic field jump thus has the character of a large amplitude, damped, "whistler" wave.

By making similar measurements along the shock front, we can construct a two-dimensional picture of the instantaneous spatial structure. In Fig. 4 we show the variation of the quantity $(dB_\theta/dt)/u$ where u is the shock speed, in the direction normal to the shock at different positions along the front. This quantity is proportional to the current density in the (r,z) plane responsible for the generation of the θ-component of field. From these measurements we deduce that the density of current flowing across the broken lines to maintain div $\vec{j} = 0$ is only a few percent of the principal current densities. The interaction between parts of the shock front at different angles is therefore likely to be small, and we are justified in considering local regions of the front as plane.

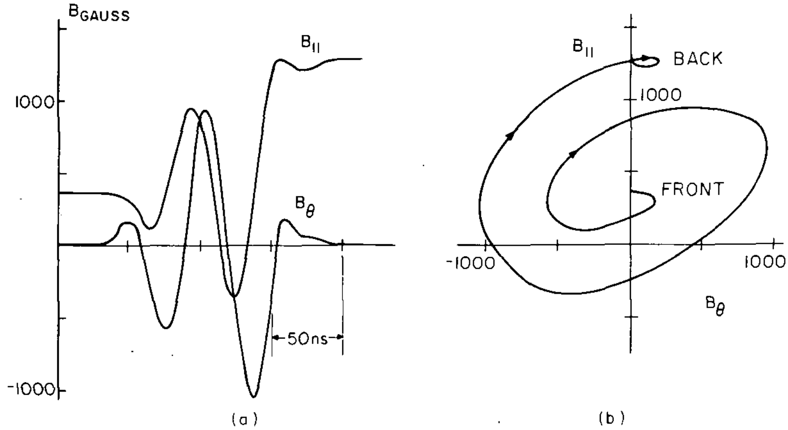

FIG.3. a) Integrated magnetic probe traces at r = 10 cm, z = 12 cm; b) $B_\parallel$ versus B_θ. Conditions: $\alpha = 45°$, $B_0 = 500$ G, $n = 5 \times 10^{14}$ cm^{-3}, $u_s = 2 \times 10^7$ cm/s ($M_A = 4.0$).

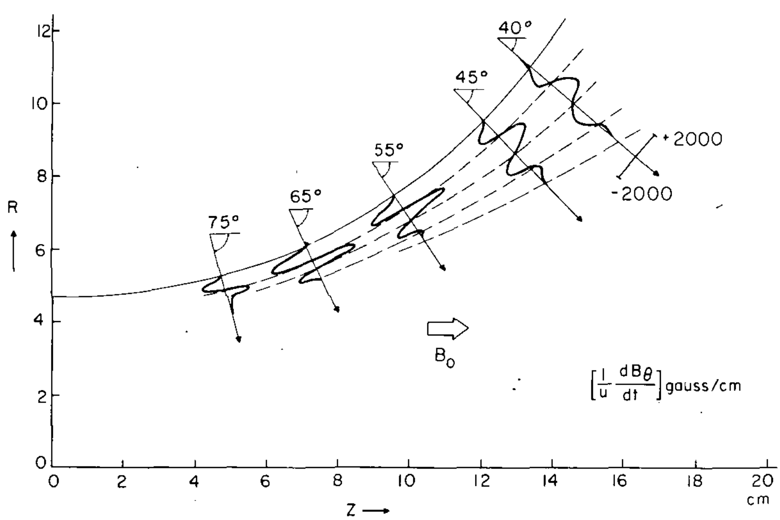

FIG.4. Spatial structure of the incident shock derived from measurements of B_θ along the shock front.

The dispersion relation for whistler waves is [7]

$$\omega^2 = c_A^2 k^2 \left(\frac{c_A^2 k^2 \cos^2 \alpha}{\Omega_i^2} + 1 \right) \tag{1}$$

where c_A is the Alfvén speed. The wavelength λ of a whistler having phase velocity $\omega/k = M_A c_A$ is then

$$\lambda = \frac{2\pi \cos \alpha}{(M_A^2 - 1)^{\frac{1}{2}}} \cdot \frac{c}{\omega_{pi}} \tag{2}$$

In Fig. 5, we plot the measured wavelength in units of c/ω_{pi} against the quantity $2\pi \cos \alpha/(M_A^2 - 1)^{\frac{1}{2}}$. Included in this plot are results in hydrogen at 20 mtorr ($c/\omega_{pi} \sim 1$ cm), deuterium at 12 mtorr ($c/\omega_{pi} \sim 2$ cm), $\alpha = 75°$ to $40°$, $M_A = 2.8 - 5.2$. Also shown are points derived from numerical calculations to be described later. The points lie close to the line representing equation (2), which confirms that the magnetic jump in an oblique shock indeed occurs through a whistler wave. It is a fortunate property of this wave that the dispersion relation (1) is only slightly modified at large amplitudes.

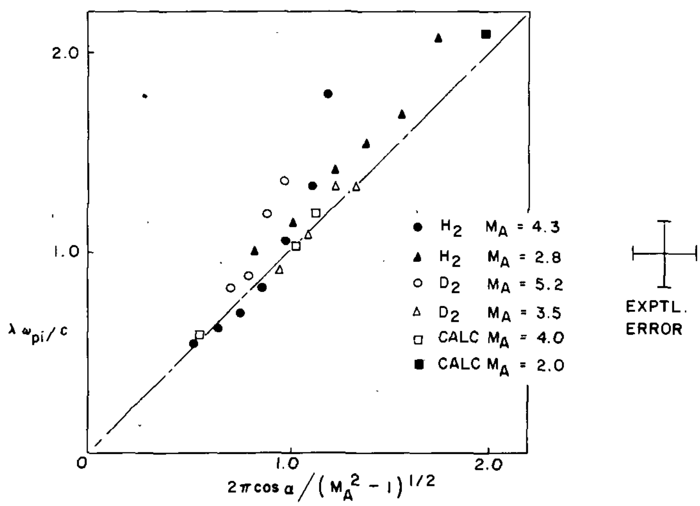

FIG. 5. Comparison of measured wavelengths with whistler dispersion relation.

Signals from an electric probe at various positions round the shock front of Fig. 4 are shown in Fig. 6. On the midplane, the signal shows the characteristic double structure of a large-Mach-number perpendicular shock [6]. For oblique angles, the potential shows precursor oscillations of the same wavelength as the magnetic structure, followed by a sharp rise at the back of the shock. The synchronization of electric and magnetic probe signals is indicated by the arrows on Fig. 6 which correspond to the solid line in Fig. 4.

The magnetic and electric structures of $M_A = 3.5$, $\alpha = 45°$ shocks in hydrogen at 20 mtorr and deuterium at 10 mtorr are compared in Fig. 7. The unintegrated magnetic signals are shown, since these reveal more clearly a fine structure in deuterium which is absent in hydrogen. For these two cases the one-fluid descriptions are identical (mass density, Alfvén speed, shock velocity), but in deuterium the characteristic length c/ω_{pi} and the energy per particle are twice their respective values for hydrogen. The whistler wavelength and the total potential jump in deuterium are twice the values for hydrogen, but the profiles are closely similar. The bumpiness of the deuterium traces increases with increasing M_A, and appears to be an incipient instability, since for $M_A \geqslant 4.5$ the structure of the deuterium shock becomes somewhat irreproducible.

The magnetic structure of the reflected shock in hydrogen is shown in Fig. 8 for the same conditions as Fig. 4. Compared to the strongly damped structure of the incident shock, a longer wave train is seen in which shorter wavelengths appear to be propagating first, in the manner of a true "whistler." However, we find the structure does not change appreciably as the shock moves outwards, and so all wavelengths are apparently propagating at the same speed. It is difficult to establish the exact flow conditions at each point along the reflected shock front, since the reflected shock is propagating into a moving plasma in which the magnetic field has been strongly modified by the incident shock. Here $n \sim 1.7 \times 10^{15}$ cm^{-3}, $T_e + T_i \sim 60$ eV, $B \sim 1350$ gauss, $\beta \sim 2.3$. The structure of the reflected shock in deuterium is irreproducible and appears to be unstable.

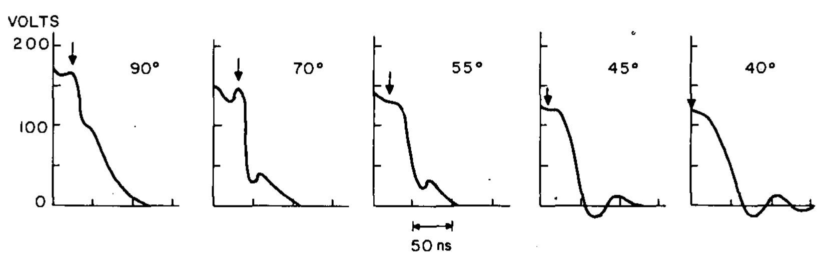

FIG.6. Electric probe traces at positions along the shock front (cf. Fig.4).

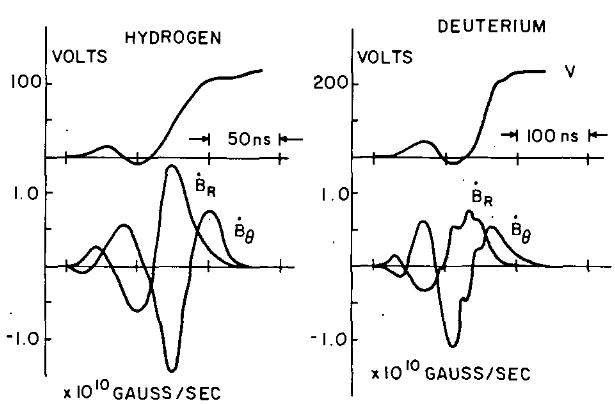

FIG.7. Magnetic and electric probe signals at r = 10 cm, z = 12 cm. Conditions: α = 45°, B_0 = 500 G, n = 5 × 10^{14} cm^{-3}(hydrogen), n = 2.5 × 10^{14} cm^{-3}(deuterium), u_S = 1.7 × 10^7 cm/s (M_A = 3.5).

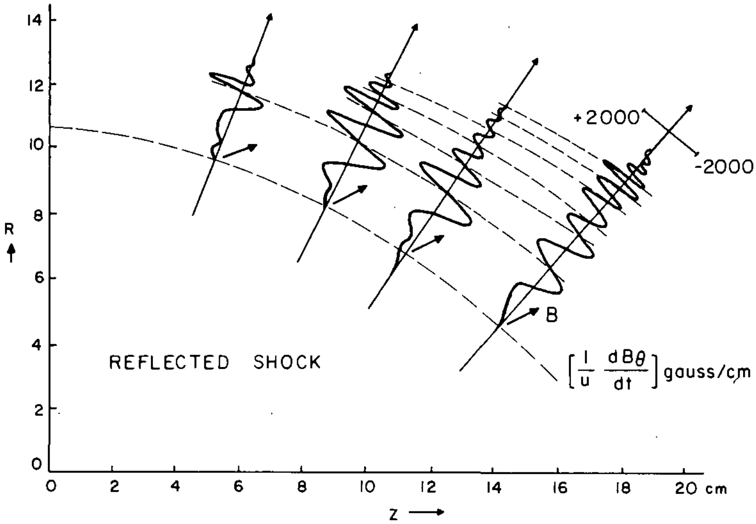

FIG.8. Structure of reflected shock in hydrogen derived from measurements of B_θ along shock front. Initial conditions as in Fig.4. The short arrows indicate the estimated direction of the magnetic field.

NUMERICAL CALCULATIONS

We consider a model of a plane shock wave described by the two-fluid hydromagnetic equations in which the only dissipative effects are resistivity η and ion viscosity μ_i. Thermal conductivity, electron viscosity, thermoelectric effects and electron inertia are neglected. This model was suggested by Bickerton [8].

The shock is taken to be at rest in the y-z plane, the upstream flow is in the x direction, and the magnetic field upstream and downstream is in the x-y plane. The equations are then:

$$\begin{aligned}
&nm_i v_x \vec{v}' = \vec{j}\times\vec{B} - \hat{x}\,(p_e + p_i + \mu_i v_x')' \\
&\vec{E} + \vec{v}\times\vec{B} = \eta\vec{j} + (\vec{j}\times\vec{B} - \hat{x}\,p_e')/ne \\
&\frac{n^\gamma v_x}{\gamma - 1}\,(p_{e,i}\,n^{-\gamma})' = \begin{cases} \eta j^2 & \text{electrons} \\ \mu_i (v_x')^2 & \text{ions} \end{cases} \\
&\text{curl}\,\vec{B} = 4\pi\vec{j} \qquad \text{curl}\,\vec{E} = 0 \qquad p_{e,i} = nT_{e,i} \qquad \gamma = 5/3
\end{aligned} \tag{3}$$

where the primes indicate d/dx. These equations are solved on a computer for the six variables, B_y, B_z, T_e, T_i, n, and E_x.

For flow conditions corresponding to Fig. 3 (M_A = 4.0, $\alpha = 45^\circ$), with η given by the Spitzer-Harm formula and with μ_i the collisional viscosity coefficient, the solution is a broad, monotonically increasing structure with only a vestigial whistler at the front. However, by reducing μ_i by a factor $\sim$ 5 (which is equivalent to artificially reducing the mean-free path λ_{ii} by this factor) we obtain a solution (Fig. 9) in which a resistively damped whistler, of wavelength $\lambda_\omega = 1 \cdot 1\, c/\omega_{pi}$ is followed by a region of viscous compression of width $\sim\lambda_{ii}$. The condition for a whistler solution appears to be $\lambda_{ii} \leqslant 0.2\lambda_\omega$, and provided that this is satisfied, the whistler structure is independent of λ_{ii}.

The wavelength of the computed whistler agrees well with observations, but the observed structure is somewhat more strongly damped. When we attempt to simulate the shock in deuterium the discrepancy is much greater. Not only is it necessary to reduce μ_i by ~ 40 to obtain a whistler solution, but the structure shows a very long wavetrain because the higher electron temperature in deuterium results in less resistive damping (Fig. 10a). To account for the observed strongly damped structure we have to invoke a non-collisional resistivity.

Throughout most of the whistler $v_D/c_S \sim 5$, where v_D is the local electron drift velocity and c_S the local ion-sound speed. Under these conditions, anomalous resistivity can arise through the excitation of ion-sound waves. Following Sagdeev and Galeev [9] we take

$$\eta = \frac{mc^2}{ne^2} \cdot \nu^* \qquad \text{where} \quad \nu^* = A\left(\frac{v_D}{c_S}\right)\left(\frac{T_e}{T_i}\right)\omega_{pi} \tag{4}$$

and we find that we can compute solutions in good agreement with the results in deuterium by taking $A = 0.001$ (Fig. 10b).

The computed total electric potential across the shock, normalized to $m_i u_S^2/2e$ is shown in Fig. 11a as a function of M_A. The upper curve is computed on the assumption that the viscous heating goes into the electrons rather than the ions. The experimental points lie closer to the lower curve. The computed temperature ratio $T_e/(T_e+T_i)$ behind the shock corresponding to this case is shown in Fig. 11b. In

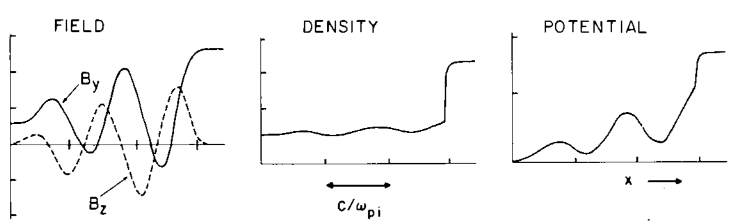

FIG. 9. Computed structure of shock in hydrogen, $M_A = 4.0$, $\alpha = 45°$, initial $\beta = 0.16$.

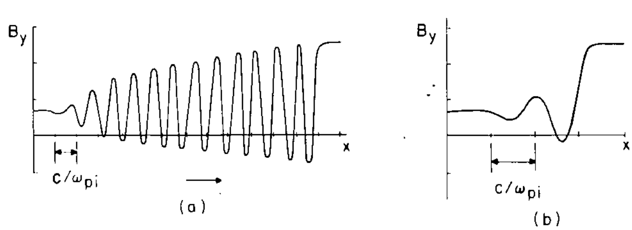

FIG. 10. Computed magnetic structure of shock in deuterium; a) With collisional resistivity only; b) With anomalous resistivity, $A = 0.001$.

our model electrons are heated by resistive dissipation and adiabatic compression in the whistler, and by adiabatic compression in the viscous region. The ions are heated predominantly in the viscous region by viscous dissipation and adiabatic compression.

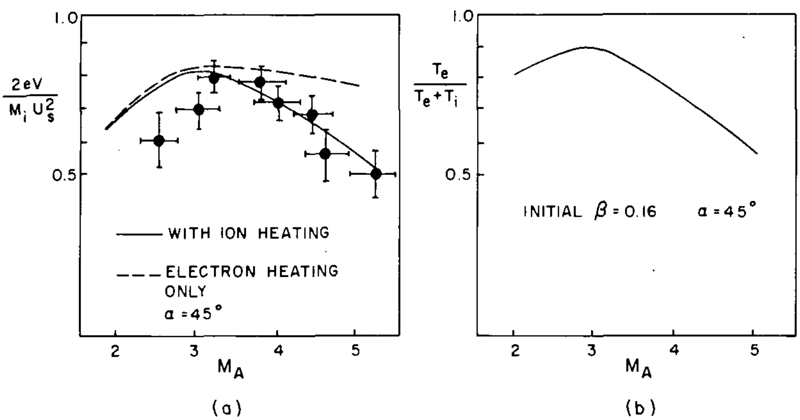

FIG. 11. a) Measurements of total electric potential across the shock compared with two theoretical models; b) Computed ratio $T_e/(T_e+T_i)$ behind the shock, assuming viscous heating of the ions.

DISCUSSION

Although our initial plasma is collision dominated ($\lambda_{ee} \sim \lambda_{ii} \sim 10^{-3}$cm, $\omega_{ce}\tau_{ei} \sim 0.2$), in the hot plasma at the back of the shock $\lambda_{ee} \sim 1$ cm in hydrogen and ~ 8 cm in deuterium. As we have seen, it is clearly necessary to invoke collisionless resistivity to account for the damping of the whistler in deuterium, while in hydrogen it appears to be of the same order as the collisional resistivity. With the coefficient $A \sim 10^{-3}$, the effective collision frequency $\nu^* \sim \nu_{pi}$ towards the rear of the shock, but more experimental data are needed to determine whether (4) is a valid representation of the observed collisionless resistivity. Also, the theoretical model needs to be improved, notably to include the tensor nature of the resistivity and the effect of heat flow. Note, however, that the reduction of the effective mean free path by microturbulence preserves the validity of the fluid equations, at least for the electrons.

It is an important feature of the oblique shock, which is not shared by the perpendicular shock, that the ion compression is not strongly coupled to the field compression, and so the viscous region may be considered separately from the whistler region. The point of separation is where the local acoustic Mach number goes through unity. Above the critical Mach number $M_A^* \approx 2.5$, ions leave the back of the whistler with directed velocity in excess of their final flow velocity; for our $M_A = 4$ shocks they would slow down by Coulomb collisions in ~ 0.6 cm in hydrogen and ~ 4 cm in deuterium. Ion-neutral collisions are unimportant since residual neutrals in the initial plasma will be ionized by the hot electrons in the whistler before reaching the back of the shock. Although we found it necessary to artificially reduce λ_{ii} to obtain a whistler-type solution, this does not necessarily imply that collisionless viscous effects are present. The calculation neglects ion gyration which will probably be important here since v_x/Ω_i behind the shock is 0.5 cm in hydrogen and 1 cm in deuterium. A small magnetic perturbation of approximately this length is seen at the back of the shock (the "pigs tail" in Fig. 3b). The electric probe also frequently shows a distinctive feature here (Fig. 7), but we cannot positively identify this as the double structure predicted by the calculation (Fig.9). More detailed study of this region is necessary to determine the processes operative there.

Below the critical Mach number it is unnecessary to introduce viscosity at all [10], and the oblique shock is then simply a resistively damped whistler wave in which compression of the ion flow is achieved by the electric field in the shock front.

ACKNOWLEDGMENTS

We are indebted to Dr. R. J. Bickerton for suggesting this experiment and for much valuable advice, to Mr. J. E. Goebel for his contribution to the engineering of the apparatus and to Mr. L. Lenamon for assistance with the computations. We also acknowledge many stimulating discussions with Dr. A. B. Macmahon.

This work was supported in part by the Texas Atomic Energy Research Foundation and in part by the United States Atomic Energy Commission.

REFERENCES

[1] MORTON, K.W., Phys. Fluids 7 (1964) 1800.
[2] SAGDEEV, R.Z., "Co-operative phenomena and shock waves in collisionless plasmas", Reviews of Plasma Physics (LEONTOVITCH, M.A., ed.) Vol. 4, Consultants Bureau, New York (1966).
[3] CAVALIERE, A. and ENGLEMAN, F., Nucl. Fusion 7 (1967) 137.
[4] MARTONE, M., Phys. Letters 22 (1966) 73.
[5] ESELEVICH, V.G. et al., JETP Letters 5 (1967) 255.
[6] PAUL, J.W.M. et al., Proc. 7th Int. Conf. on Phenomena in Ionized Gases, Beograd (1966) Vol. 2, 819.
[7] STRINGER, T. E., Plasma Physics JNE Pt C 5 (1963) 89.
[8] BICKERTON, R. J., Private communication.
[9] SAGDEEV, R. Z. and GALEEV, A. A., Lectures on the non-linear theory of plasma, IAEA Report IC/66/64 (1966).
[10] WOODS, L. C., Phys. Fluids (1968) to be published.

СТРУКТУРА БЕССТОЛКНОВИТЕЛЬНЫХ УДАРНЫХ ВОЛН И ДИССИПАЦИЯ СИЛЬНЫХ ПЕРЕМЕННЫХ МАГНИТНЫХ ПОЛЕЙ В ПЛАЗМЕ

М.В.БАБЫКИН и Г.Е.СМОЛКИН
ИНСТИТУТ АТОМНОЙ ЭНЕРГИИ им.И.В.КУРЧАТОВА,
МОСКВА,
СССР

Abstract — Аннотация

STRUCTURE OF COLLISIONLESS SHOCK WAVES AND THE DISSIPATION OF STRONG ALTERNATING MAGNETIC FIELDS IN A PLASMA. Various collisionless plasma heating mechanisms are investigated by studying the structure of the front of straight shock waves as a function of the initial magnetic field and by studying the turbulence of the current layer in an experiment of the theta pinch type. Collisionless shock waves are excited by trapezoidal pulses of a magnetic field having an amplitude of 1 - 1.5 kOe and a rise time of (3-5) $\times 10^{-8}$ s. The authors investigate the case where the pulsed field $\tilde{H}$ is parallel to the quasi-stationary field H_1. They measure the electron temperature and study the nature of the propagation of probing magneto-acoustic perturbations in the plasma behind the shock wave front for small and large Alfvén-Mach numbers M_A. The results indicate that in both cases there is collisionless heating of the electrons, and for large M_A a strong irreversible process apparently caused by the appearance of energetic ions in the plasma is also observed. In an experiment with anti-parallel $\tilde{H}$ and H_1 fields the experimental conditions exclude the formation of a shock wave. In this experiment the authors use a plasma in the form of a hollow cylinder. The external magnetic field H, with an amplitude of 3 kOe and a frequency f = 0.84 Mc/s, is produced by a broad winding. The authors observe the formation of a cylindrical current layer in the region of zero magnetic field. For plasma densities below 4×10^{13} cm^{-3} there is effective heating of the plasma electrons accompanied by intense noise emission at wavelength λ = 3 cm and a sharp decline in the lifetime of the trapped magnetic field. This indicates turbulent heating of the plasma in the current layer.

СТРУКТУРА БЕССТОЛКНОВИТЕЛЬНЫХ УДАРНЫХ ВОЛН И ДИССИПАЦИЯ СИЛЬНЫХ ПЕРЕМЕННЫХ МАГНИТНЫХ ПОЛЕЙ В ПЛАЗМЕ. Различные механизмы бесстолкновительного нагрева плазмы исследовались путем изучения структуры фронта прямых ударных волн в зависимости от начального магнитного поля, а также путем изучения турбулентного режима токового слоя в эксперименте типа θ-пинча. Бесстолкновительные ударные волны возбуждались трапецеидальными импульсами магнитного поля с амплитудой $1 \div 1{,}5$ кэ и временем нарастания $(3 \div 5) \cdot 10^{-8}$ сек. Исследовался случай, когда импульсное поле $\tilde{H}$ было параллельно квазистационарному полю H_1. Измерялась электронная температура, изучался характер распространения зондирующих магнитно-звуковых возмущений в плазме за фронтом ударной волны при малых и больших числах Альфвена-Маха (M_A). Полученные результаты свидетельствуют о том, что в обоих случаях имеет место бесстолкновительный нагрев электронов, а при больших (M_A) наблюдается также сильный необратимый процесс, обусловленный, по-видимому, появлением энергичных ионов в плазме. Проведен эксперимент с антипараллельными $\tilde{H}$ и H_1 полями, условия которого исключали образование ударной волны. Для этого специально использовалась плазма в виде полого цилиндра. Внешнее магнитное поле H (с амплитудой до 3 кэ и частотой $f = 0{,}84$ Мгц) создавалось широким витком. Наблюдалось образование цилиндрического токового слоя в области нулевого магнитного поля. При плотности плазмы ниже $4 \cdot 10^{13}$ см$^{-3}$ был обнаружен эффективный нагрев электронов плазмы, сопровождаемый интенсивным шумовым излучением на длине волны λ=3 см и резким сокращением времени жизни захваченного магнитного поля. Все это, по-видимому, свидетельствует о том, что наблюдался турбулентный нагрев плазмы в токовом слое.

1. ВВЕДЕНИЕ

В 1961 году [1] было обнаружено сильное поглощение прямых магнито-звуковых волн большой амплитуды, возбуждавшихся в разреженной замагниченной плазме внешним высокочастотным контуром. Поглощение энергии контура сопровождалось эффективным нагревом электронного компонента плазмы в условиях, когда можно было пренебречь парными столкновениями частиц. Наблюдаемое явление авторы связывали с возникновением в плазме мелкомасштабной токовой неустойчивости, которая должна приводить к резкому увеличению эффективности рассеяния электронов. В соответствии с этим метод нагрева плазмы был назван турбулентным.

В работе [2], посвященной спектроскопическому исследованию турбулентно нагретой плазмы, была осуществлена скоростная развертка диаметра плазменного столба в свете линии HeII 4686Å и показано, что процесс турбулентного нагрева распространяется на всю глубину плазменного столба со скоростью, близкой к альфвеновской. При этом электронная температура на фронте возмущения возрастает от начального значения $T_{e1} \approx 0{,}1$ эв до максимальной величины $T_{e2} \geq 100$ эв за время, равное приблизительно 1/4 периода колебаний высокочастотного контура.

В упомянутых экспериментах [1, 2] направление внешнего магнитного поля $\widetilde{H}$ на границе плазменного объема периодически изменялось во времени относительно направления поля H_1 в невозмущенной плазме. При этом возбуждались следующие друг за другом волны сжатия и разрежения. Интересно было выделить и исследовать раздельно обе эти противоположные фазы процесса: фазу сжатия, когда поле $\widetilde{H}$ параллельно полю H_1, и фазу разрежения, когда поля $\widetilde{H}$ и H_1 антипараллельны.

Программа для первого случая явилась причиной возникновения проблемы возбуждения и исследования в лабораторных условиях стационарных бесстолкновительных ударных волн, распространяющихся поперек магнитного поля. Эта программа требовала создания трапецеидальных импульсов магнитного поля $\widetilde{H}$, обладающих достаточно большой амплитудой и удовлетворяющих условию $\tau_0 \ll \Delta t < T$, где τ_0 и T – время нарастания и длительность импульса соответственно, а Δt – время распространения волны вдоль радиуса плазменного столба. Такого рода магнитный "поршень" был осуществлен с помощью высоковольтной искусственной линии специальной конструкции. Это позволило провести первые измерения ширины фронта прямых бесстолкновительных ударных волн в условиях, близких к стационарным [3]. Измеренная длительность фронта волны в плазме с плотностью $n_1 \approx (1 \div 3) \cdot 10^{13}$ см$^{-3}$ оказалась равной приблизительно $2C\sqrt{mM}/eH_1 \approx 6C\sqrt{mM}/e(H_1 + \widetilde{H})$, а соответствующая ширина фронта $\delta_e \approx 6C/\omega_{pe}$ – меньше длины свободного пробега относительно парных столкновений и меньше ларморовского радиуса ионов в волне (см. также [5, 17 – 19]).

Программа для второго случая, когда поле $\widetilde{H}$ антипараллельно полю H_1, разбивается на две различные по динамике волновых процессов области. При $|\widetilde{H}| < 2|H_1|$ в плазме образуется перепад магнитного поля, характерный для волны разрежения. Образование ударных волн в этом случае исключено. Плазма, расширяясь, опирается на стенку разрядной камеры и остывает на ней, а магнитное поле со скоростью этого остывания выходит из плазменного объема. При $|\widetilde{H}| > 2|H_1|$ в плазме может существовать квазистационарная конфигурация встречных магнитных полей. Исследование такого образования представляет самостоятельный интерес, поскольку в токовом слое, разделяющем встречные магнитные поля, можно осуществить условия, необходимые для турбулентного нагрева плазмы [4]. Эффективность бесстолкновительных диссипативных процессов еще больше должна возрасти при $|\widetilde{H}| \gg |H_1|$, поскольку в данном случае плотность тока в промежуточном слое все время поддерживается на более высоком уровне, чем в квазистационарном случае, и кроме того, впереди токового слоя может образоваться бесстолкновительная ударная волна.

В данной работе описываются эксперименты по исследованию бесстолкновительных ударных волн при различных числах Альфвена-Маха и по изучению механизма диссипации в квазистационарном токовом слое, разделяющем магнитные поля.

2. ИССЛЕДОВАНИЕ БЕССТОЛКНОВИТЕЛЬНЫХ УДАРНЫХ ВОЛН В ПЛАЗМЕ

2.1. Описание эксперимента

Опыты проводились на экспериментальной установке УВ-2, подробно описанной в работе [5]. Плазма предварительной ионизации создавалась током прямого электродного разряда. В качестве рабочего газа использовались водород и гелий. Сходящиеся цилиндрические ударные волны возбуждались в плазме послесвечения, когда ток предварительной ионизации полностью прекращался. Момент старта волны задавался величиной регулируемой задержки $t_з$ относительно тока предварительной ионизации.

По спектрам рекомбинации было установлено, что в течение первых $50 \div 100$ мксек гелиевая плазма состоит из однозарядных и двухзарядных ионов в отношении, равном приблизительно 5/1.

Для возбуждения ударных волн использовались трапецеидальные импульсы магнитного поля $\widetilde{H}$, которые создавались цилиндрическим витком ударного контура шириной 40 см. Импульсы поля $\widetilde{H}$ имели время нарастания $\tau_0 = (3 \div 5) \cdot 10^{-8}$ сек, длительность $T = (2{,}5 \div 5) \cdot 10^{-7}$ сек и амплитуду $|\widetilde{H}| = (1 \div 1{,}5)$ кэ. Осциллограммы импульсов поля $\widetilde{H}$ и производной $d\widetilde{H}/dt$ представлены на рис.1.

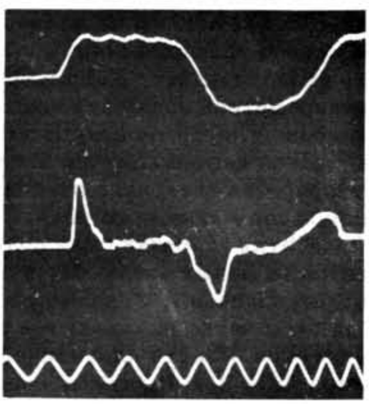

Рис.1. Осциллограммы импульсов магнитного поля $\widetilde{H}$ и производной $d\widetilde{H}/dt$. Период калибровочного сигнала 10^{-7} сек.

2.2. Методы диагностики

Для исследования ударных волн и плазмы предварительной ионизации использовались дифференцирующие магнитные зонды [3, 5] и кинетика спектральных линий в плазме [2, 6]. Для получения разрешенных во времени спектров плазмы применялись многокаскадные электронно-оптические преобразователи (ЭОП). Обычно использовался участок спектра в диапазоне от ~ 4400 Å до ~ 5100 Å.

Электронная температура измерялась по отношению интенсивностей линий нейтрального и ионизированного гелия. Плотность плазмы в области от 10^{12} до $5 \cdot 10^{13}$ см$^{-3}$ измерялась с помощью радиоинтерферометров [7], а в области выше $5 \cdot 10^{13}$ см$^{-3}$ – по штарковскому уширению бальмеровской линии H_β[6,7]. Обе эти методики позволяли получить временную зависимость концентрации распадающейся в магнитном поле плазмы. По этой кривой и задержке $t_з$ определялась плотность плазмы n_1 перед фронтом ударной волны.

2.3. Экспериментальные результаты

2.3.1. Результаты зондовых измерений

Ранее [3, 5] магнитный зонд использовался для измерения профиля магнитного поля в ударной волне. Было показано, что в плазме плотностью $\sim 3 \cdot 10^{13}$ см$^{-3}$ при числах Альфвена-Маха $M_A = 1{,}7$ ширина переходного участка $\delta_e \approx 10C/\omega_{pe}$. При числах $M_A = 4$ ширина фронта в гелиевой плазме возрастала примерно на порядок величины. Последующие эксперименты показали, что в тех же условиях ширина фронта в водородной плазме имеет заметно меньшую величину. Возможное объяснение этому факту будет дано в разделе 2.4. Здесь же важно отметить следующее. Увеличение числа M_A достигалось уменьшением постоянного магнитного поля H_1 в невозмущенной плазме при фиксированной амплитуде поля $\tilde{H}$. Это, однако, приводило к увеличению скорости распада плазмы послесвечения. Поэтому в экспериментах с большими M_A для получения заданной концентрации n_1 необходимо было пользоваться значениями задержек, лежащими в области $t_з < 50 \div 100$ мксек.

В данной работе, помимо измерения профиля магнитного поля, магнитный зонд использовался для получения дополнительной информации о свойствах плазмы за фронтом ударной волны, в условиях, когда вслед за первой ударной волной возбуждалась вторая, зондирующая, волна. Очевидно, характер распространения этой второй волны будет зависеть от параметров плазмы, возникающих под действием предыдущего возмущения и, в частности, от давления $p = nT_e + nT_i + H^2/8\pi$. Для получения такой информации мы воспользовались тем, что ударный контур генерировал несколько идущих друг за другом и чередующихся по знаку импульсов магнитного поля.

В этих условиях были получены следующие результаты. При относительно малых числах M_A в первом полупериоде поршня, когда поля H_1 и $\tilde{H}$ параллельны, в плазме распространяется ударная волна с $\delta_e \approx 10C/\omega_{pe}$ [5]. При этом четко наблюдаются эффекты кумуляции и отражения волны в приосевой области плазменного столба. Во втором полупериоде поршня, когда поля H_1 и $\tilde{H}$ антипараллельны, магнитное поле выходит из плазменного объема. При этом в сторону оси разрядной камеры распространяется возмущение с перепадом магнитного поля, характерным для волны разрежения. В третьем полупериоде поля $\tilde{H}$, когда поршень снова становится сжимающим, в плазме возбуждается вторая, зондирующая волна. Амплитуда ее приблизительно равна амплитуде первой волны. Характерный для описанного случая профиль магнитного поля, полученный интегрированием сигналов магнитного зонда в приосевой области плазменного столба в водороде ($n_1 \approx 3 \cdot 10^{13}$ см$^{-3}$; $H_1 = 1500$ э; $M_A = 1{,}5$), представлен кривой 1 на рис.2.

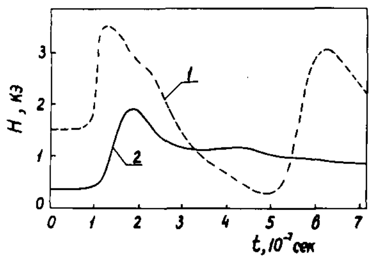

Рис.2. Профили магнитного поля в ударной волне, полученные в приосевой области плазменного столба: 1) $M_A = 1{,}5$; 2) $M_A = 4$.

При больших числах M_A характер волновых процессов существенно отличается. Помимо эффекта уширения фронта волны наблюдался специфический необратимый процесс [8]: магнитное поле $\tilde{H}$, проникая с ударной волной в плазму, вмораживалось в ней и во втором полупериоде не выходило из плазменного объема. При этом полное давление $p = nT_e + nT_i + H^2/8\pi$ возрастало настолько, что вторая, зондирующая, волна не могла проникать в плазму или проникала с малой амплитудой. Характерный для этого случая профиль магнитного поля в приосевой области плазменного столба в водороде ($n_1 \approx 3 \cdot 10^{13}$ см$^{-3}$, $H_1 = 300$ э и $M_A \approx 4$) представлен кривой 2 на рис.2.

2.3.2. Результаты спектроскопических наблюдений

На рис.3 представлены фотографии разрешенного во времени спектра гелиевой плазмы в процессе работы ударного контура для двух значений числа M_A: $M_A = 1{,}5$ и $M_A = 4$. Прежде всего, следует отметить, что эти спектрограммы также свидетельствуют об увеличении давления в плазменном объеме при увеличении числа M_A. По интенсивности линий, особенно линии He II 4686 Å, имеющей потенциал возбуждения 51 эв, видно, что в первом случае возбуждается три, следующие друг за другом, ударные волны с одинаковой примерно амплитудой. Во втором случае только первая волна является достаточно энергичной.

Наиболее яркими примесными линиями на выбранном участке спектра оказались линия H_β и неразрешенные относительно друг друга линии O II 4649 и O II 4642 Å. Интенсивность их практически не зависит от числа M_A.

Скорость разгорания спектральных линий гелия, особенно линии He II 4686 Å, падает с увеличением числа M_A, тогда как максимальное значение отношения интенсивностей линий He II 4686 Å и He I 5016 Å возрастает. Как показали измерения, это значение равно $\sim 1{,}5$ при $M_A = 1{,}5$ и ~ 6 при $M_A = 4$. В условиях нашего эксперимента распределение атомов по возбужденным уровням можно считать подчиняющимся режиму мгновенного высвечивания. При этом наблюдающееся отношение интенсивностей линий He II 4686 Å и He I 5016 Å может быть объяснено только увеличением температуры электронов на фронте волны до величины $T_e \geq 100$ эв. Действительно, степень ионизации плазмы перед фронтом волны была около 50%. При такой степени ионизации измеренное отношение интенсивностей можно было бы объяснить, если бы приписать электронам бесконечно большую температуру. Поэтому следует предположить, что на фронте волны происходит дополнительная ионизация. Однако, необходимый прирост n_e при фиксированной плотности нейтральных атомов и длительности фронта возможен тогда, когда T_e практически мгновенно возрастает до величины порядка 100 эв.

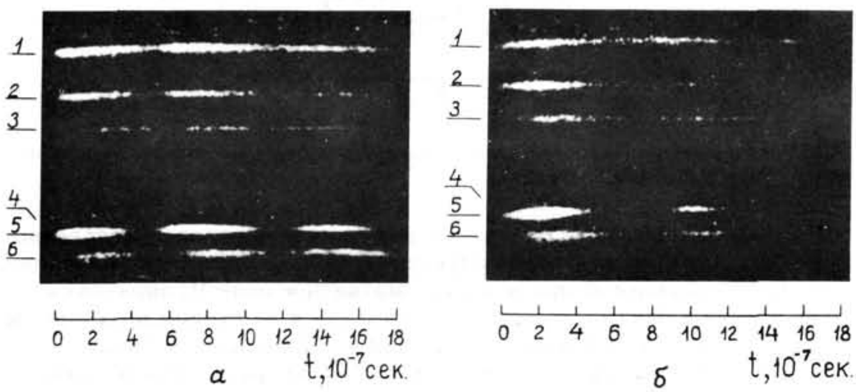

Рис.3. Фотографии разрешенного во времени спектра гелиевой плазмы в процессе работы ударного контура: а) $M_A = 1{,}5$; б) $M_A = 4$.
1 – He I 5016Å; 2 – He I 4922Å; 3 – H_β; 4 – He I 4713Å; 5 – He II 4686Å; 6 – O II 4649Å и O II 4642Å.

2.4. Обсуждение

Спектроскопические измерения приводят, как мы видели, к электронной температуре за фронтом волны $T_e \geq 100$ эв. Такое значение T_e не может быть объяснено на основе механизма парных соударений. Действительно, дрейфовая скорость электронов на фронте волны $V_{\text{др}} = \tilde{H}C/\delta 4\pi n_1 e$ составляет в наших экспериментах $(2 \div 3)\cdot 10^8$ см/сек. Вследствие парных кулоновских столкновений T_e на фронте может возрасти только на величину порядка 20 эв. Измеренное значение $(T_e)_{max} \geq 100$ эв может быть объяснено только, если эффективная частота столкновений $\nu > 10^9$ сек$^{-1}$, что почти в сто раз превышает среднюю частоту парных кулоновских соударений при $T_e \approx 20$ эв и $n_1 < 10^{14}$, а также частоту всех других столкновительных процессов. Разумно предположить, что эта аномально высокая частота столкновений имеет коллективную природу и обусловлена неустойчивостью движения электронов на фронте волны [1, 2, 9].

В то же время наблюдается существенная разница в характере проникновения зондирующих возмущений в плазму, образующуюся за фронтом волны при малых M_A и больших M_A. Это можно объяснить различным характером диссипативных процессов в указанных двух областях чисел M_A. В случае малых M_A в качестве основного механизма диссипации теория [10, 11] привлекает механизм токовой неустойчивости, при котором должны нагреваться преимущественно электроны. Во втором случае в плазме, по-видимому, могут появляться быстрые ионы, поскольку согласно двухжидкостной теории уединенных волн [10 – 12] при $M_A = M_A^* = 2$ должно наступать отражение ионов в поле разделения зарядов на фронте волны[1] и развитие неустойчивости ион-ионного типа, рассмотренного в [13]. Но электроны в этом случае, как показывает эксперимент, также нагреваются, что явно указывает на наличие турбулентности в плазме.

Рассмотрим теперь поведение плазмы, образующейся за фронтом волны при $M_A < M_A^*$ и $M_A > M_A^*$ во втором полупериоде поршня. В первом случае плазма, расширяясь, опирается на стенку камеры горячими электронами и остывает в течение нескольких электронных циклотронных периодов. Такой отрезок времени значительно меньше τ_e, поэтому магнитное поле во втором полупериоде поршня выходит из плазменного объема. Соответственно вторая, зондирующая, волна проникает в плазму. Во втором случае, если помимо горячих электронов имеется значительное количество быстрых ионов, остывание плазмы, следовательно и размораживание силовых линий магнитного поля, должно затянуться, по крайней мере, на промежуток времени, равной ларморовскому периоду ионов T_{Hi}. Поскольку $T_{Hi} > 2T$ полное давление $p = nT_e + nT_i + H^2/8\pi$ в плазменном объеме, обусловленное возросшим β и захваченным магнитным полем, не успевает снизиться заметным образом к моменту возбуждения второй, зондирующей, волны. Поэтому последняя при $M_A > M_A^*$ не может проникать в плазму.

Процесс отражения ионов на фронте ударной волны, вообще говоря, должен приводить к перераспределению поля разделения зарядов на расстояние порядка ларморовского радиуса ионов R_{Hi} или, другими словами, – к расширению фронта волны до размеров C/ω_{pi}. Этот процесс, однако, в полной мере может развиться лишь в условиях, близких к стационарным. Легко показать, что такие условия достигаются лишь при удовлетворении довольно жесткого условия $R > 10^8\sqrt{2A/n_1}$, где A – массовое число иона. Например, при $n_1 = 10^{14}$ см$^{-3}$ и A = 1 радиус плазменного столба R должен превышать 10 см.

В условиях данных экспериментов это требование не удовлетворялось, поэтому полного расширения фронта ударной волны в водороде не должно было наблюдаться. Интересно, что условие (2) для гелиевой плазмы более жестко, чем для водородной. Между тем, расширение фронта волны в первом случае было больше, чем во втором. Это, по-видимому, можно объяснить существованием в плазме предварительной ионизации однозарядных и двухзарядных ионов гелия. В такой плазме разность потенциалов, образующаяся из-за разделения зарядов на фронте волны, должна сообщить двухзарядным ионам скорости в два раза большие, чем однозарядным. При этом отражение двухзарядных ионов может наступить при меньшем числе M_A, чем в случае с ионами одного сорта. Вообще говоря, такая же ситуация должна возникать в плазме, состоящей из ионов с одинаковым зарядом, но с разными массами. В подобных случаях возникает относительное движение ионов с разными Ze/M,

[1] В реальной плазме с низким β, вследствие аномального сопротивления, связанного с неустойчивостью тока, критическое число M_A^* должно возрасти до значения, превышающего 3.

которое может прекратиться только в результате трения между этими потоками. При отсутствии парных столкновений эффективное трение может быть обеспечено развитием неустойчивости ионных потоков с разными Ze/M, аналогичной неустойчивости во встречных потоках одинаковых ионов, которая исследована в работе [13].

3. ЭКСПЕРИМЕНТЫ ПО ТУРБУЛЕНТНОМУ НАГРЕВУ ПЛАЗМЫ ПРИ АННИГИЛЯЦИИ ВСТРЕЧНЫХ МАГНИТНЫХ ПОЛЕЙ

3.1. Описание эксперимента

Условия, необходимые для осуществления турбулентного нагрева в токовом слое, разделяющем встречные магнитные поля, были рассмотрены в работе [4]. В той же работе приводится обширная библиография по вопросу аннигиляции встречных полей. Эксперименты проводились на установке, получившей название "ДИМПОЛ" (диссипация магнитных полей). Чтобы уменьшить возможность образования ударной волны и ее влияние на конечное состояние плазмы, предварительная плазма создавалась в виде полого цилиндра диаметром 14 см и толщиной слоя плазмы $0{,}5 \div 0{,}6$ см. Внутренний диаметр вакуумной камеры равен 17 см.

Для создания плазмы использовался пеннинговский разряд с горячими электродами в виде колец. Ток разряда в большинстве экспериментов составлял 30 а (в некоторых случаях достигал $40 \div 50$ а). Постоянное магнитное поле имело форму магнитной ловушки с пробочным отношением, равным 2, и создавалось двумя катушками диаметром 1 м, установленными на расстоянии 1,2 м друг от друга. Кольцевые катоды пеннинговского разряда диаметром 100 мм устанавливались в магнитных пробках.

Переменное магнитное поле с амплитудой до 4 кэ создавалось разрядным контуром с частотой 0,84 Мгц. Цилиндрическая катушка контура длиной 30 см и диаметром 20 см имела в средней части разрез шириной 6 см для диагностических целей.

Предварительный разряд зажигался при непрерывном протоке нейтрального газа. Основная часть экспериментов проводилась на водороде; в ряде контрольных опытов применялись аргон и ксенон. Концентрация нейтрального газа устанавливалась от $5 \cdot 10^{12}$ см$^{-3}$ до 10^{14} см$^{-3}$. Концентрация заряженных частиц в предварительно ионизованной плазме измерялась интерферометром на длине волны $\lambda = 8$ мм. При токе разряда 30 а она слабо зависит от давления нейтрального газа и меняется от $5 \cdot 10^{12}$ см$^{-3}$ до 10^{13} см$^{-3}$.

3.2. Результаты эксперимента

Как указано в работе [4], должно существовать пороговое значение концентрации, при котором токовая скорость электронов может превысить некоторую критическую величину и может возникнуть неустойчивость. При этом проводимость плазмы из-за турбулентности должна стать очень низкой,и захваченное в плазму поле должно быстро диссипировать. Это явление должно сопровождаться сильным нагревом плазмы.

Первые же опыты показали, что действительно существует критическое значение концентрации, которое разделяет два принципиально различных режима работы, отличающихся поведением магнитного поля внутри плазмы на втором и последующих полупериодах переменного магнитного поля. При плотности нейтрального водорода в камере больше $4 \cdot 10^{13}$ см$^{-3}$ и концентрации предварительной плазмы порядка 10^{13} см$^{-3}$ на втором полупериоде разряда осевой магнитный зонд регистрирует захват магнитного поля первого полупериода (рис.4), которое удерживается в плазме в течение 3 − 5 полупериодов переменного поля, т.е. 2 ÷ 3 мксек.

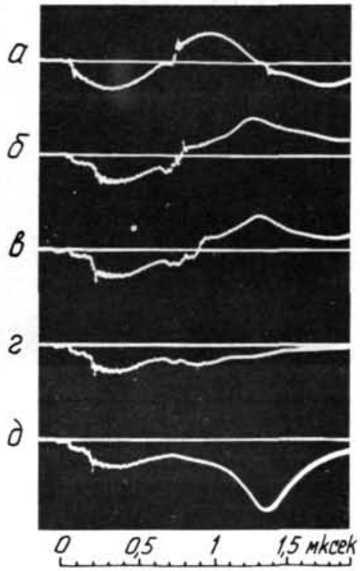

Рис.4. Осциллограммы магнитного зонда, иллюстрирующие зависимость времени жизни вмороженного магнитного поля на втором полупериоде от концентрации нейтрального газа. Ток пеннинговского разряда 34 а, амплитуда переменного магнитного поля $\tilde{H} = 3,5$ кэ, зонд с L,R − интегрированием:
а − $n_0 = 10^{13}$ см$^{-3}$, $H_0 = 175$э; б − $4 \cdot 10^{13}$ см$^{-3}$, 1400 э; в − $4 \cdot 10^{13}$ см$^{-3}$, 1225 э; г − $5 \cdot 10^{13}$ см$^{-3}$, 1400 э; д − $7,5 \cdot 10^{13}$ см$^{-3}$, 1400 э.

При снижении концентрации ниже $4 \cdot 10^{13}$ см$^{-3}$ поле также захватывается, но быстро диссипирует (за время порядка 0,2 ÷ 0,3 мксек). Во время перехода внешнего магнитного поля через ноль, на осциллограммах магнитного зонда (рис.5) появляются колебания высокой частоты в диапазоне от 10 до 100 Мгц, свидетельствующие о появлении неустойчивости, сопровождающей быструю диссипацию магнитного поля. В результате диссипации энергии магнитного поля плазма нагревается, о чем свидетельствует появление быстрых электронов, регистрируемых сцинтилляционным датчиком в пробках (рис.6). При концентрации выше $4 \cdot 10^{13}$ см$^{-3}$ поле долго существует в плазме и высокочастотные колебания отсутствуют. На рис.5 показаны осциллограммы магнитных зондов, измеряющих dH_z/dt: верхняя − с зонда, расположенного в 2 см от стенки камеры, нижняя − с центрального зонда. Из приведенных осциллограмм видно, что частота колебаний падает с ростом плотности плазмы.

Через широкую кольцевую щель в витке контура проводились измерения микроволнового излучения из плазмы на длинах волн 3,2; 1,6 и 0,8 см. Рупоры приемных антен были ориентированы так, что вектор $\overline{E}$ в них был перпендикулярен магнитному полю контура. Проводились также измерения рентгеновского излучения из плазмы.

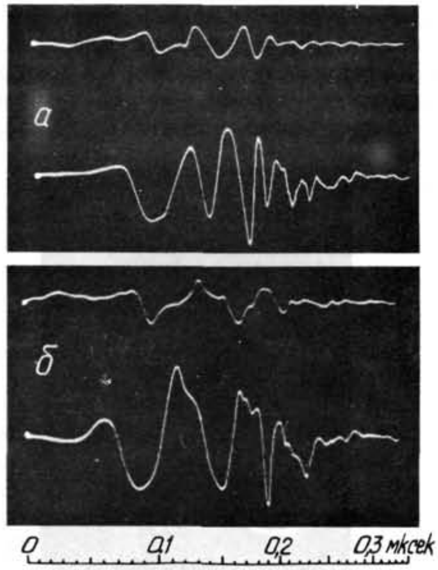

Рис.5. Осциллограммы магнитных зондов, регистрирующих dH_z/dt в начале второго полупериода. Верхние осциллограммы – зонд на расстоянии 2 см от стенки, нижние – осевой зонд. $\tilde{H}$ = 4 кэ, H_0 = 700 э. Амплитуда высокочастотных колебаний магнитного поля достигает 100÷150 эрстед:
а) $n_0 = 10^{13}$ см$^{-3}$, б) $n_0 = 2\cdot10^{13}$ см$^{-3}$.

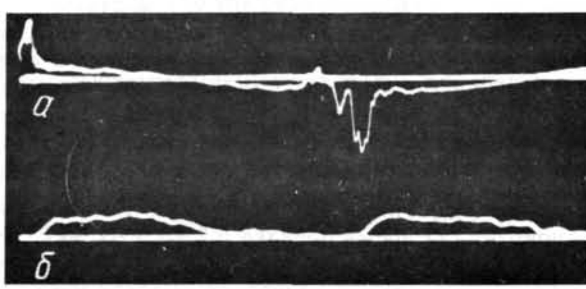

Рис.6. Осциллограммы осевого магнитного зонда (вверху) и сцинтилляционного датчика, регистрирующего появление горячих электронов в пробках на первом и втором полупериодах.

Предварительные измерения показали, что интенсивного жесткого рентгеновского излучения, выходящего через стенки разрядной камеры (6 мм стекла), не наблюдается. Сцинтилляционный датчик, расположенный на оси камеры в магнитной пробке, регистрирует появление электронов с энергиями порядка 5 ÷ 10 кэв (кристалл CsJ был закрыт алюминиевой фольгой толщиной 9 мк). Как видно из осциллограмм рис.6, быстрые электроны появляются одновременно с развитием высокочастотных колебаний, в то время как СВЧ-шумы в диапазоне 3,2 см и 1,6 см запаздывают на несколько десятков наносекунд (рис.7). Это запаздывание увеличивается с уменьшением значения переменного магнитного поля. СВЧ-излучения в диапазоне 8 мм обнаружено не было.

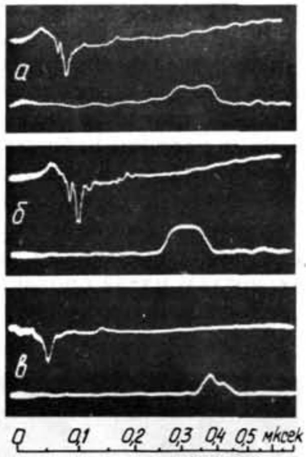

Рис.7. Осциллограммы осевого магнитного зонда (верхняя в каждой паре) и огибающей СВЧ-шумов:
а) λ = 1,6 см, H_0 = 700 э, $n_0 = 10^{13}$ см$^{-3}$, $\tilde{H}$ = 4 кэ;
б) λ = 3,2 см, H_0 = 700 э, $n_0 = 10^{13}$ см$^{-3}$, $\tilde{H}$ = 4 кэ;
в) λ = 3,2 см, H_0 = 700 э, $n_0 = 10^{13}$ см$^{-3}$, $\tilde{H}$ = 1,3 кэ.

3.3. Обсуждение результатов

1. Наблюдаемая на опыте пороговая зависимость времени существования захваченного поля от концентрации может быть обусловлена развитием неустойчивости, приводящей к быстрой диссипации вмороженного магнитного поля. По критериям работы [4] можно оценить пороговые значения плотности, при которых токовые скорости не превышают соответственно тепловой скорости электронов и скорости ионного звука, предполагая при этом, что плазма холодная (5 – 10 эв). При максимальных значениях встречных полей (4 кэ с каждой стороны слоя) токовая скорость становится меньше тепловой скорости электронов, когда плотность больше $5 \cdot 10^{13}$ см$^{-3}$, и остается больше скорости ионного звука при плотности до 10^{15} см$^{-3}$ (предполагается, что плазмой такой плотности заполнено все сечение камеры). Пороговое значение плотности, при котором токовая скорость перестает превышать тепловую, совпадает с наблюдаемым на опыте. Однако, этому совпадению не следует придавать абсолютного значения, так как на втором полупериоде могло происходить заметное увеличение плотности плазмы в результате десорбции газа со стенок. Кроме того, оценки делались для холодной плазмы, тогда как на первом полупериоде происходит сильный нагрев плазмы. Чтобы окончательно решить, с каким типом неустойчивости связана наблюдаемая на опыте пороговая зависимость, необходимо измерить плотность и температуру плазмы на втором полупериоде.

2. Появление интенсивных колебаний при смене знака переменного магнитного поля отмечалось и ранее в работах ряда авторов [14, 15], где они хорошо объяснялись возбуждением собственных колебаний плазменной оболочки в магнитном поле или магнито-звуковым резонансом. В данном случае такое объяснение нельзя признать удовлетворительным по следующим причинам:

а) согласно расчету, период собственных магнито-звуковых колебаний $\tau = 2\pi\sqrt{M}/H$, где M — масса на единицу длины оболочки. Подставляя сюда магнитное поле в плазме H, которое существует к моменту возникновения колебаний ($\sim 10^3$), и минимальное значение концентрации $5 \cdot 10^{12}$ см$^{-3}$, получим верхний предел возможной частоты колебаний $\sim 10^7$ гц, что существенно ниже частоты наблюдаемых колебаний;

б) из приведенных осциллограмм, снятых одновременно с двух магнитных зондов (рис.8) и помещенных на разном расстоянии друг от друга вдоль оси камеры, видно, что масштаб колебаний по Z для высокочастотной части спектра существенно меньше размера ударного контура (сигналы отличаются полярностью из-за соответствующего подключения зондов). Различие в осциллограммах проявляется уже при расстоянии между зондами порядка 4,5 см;

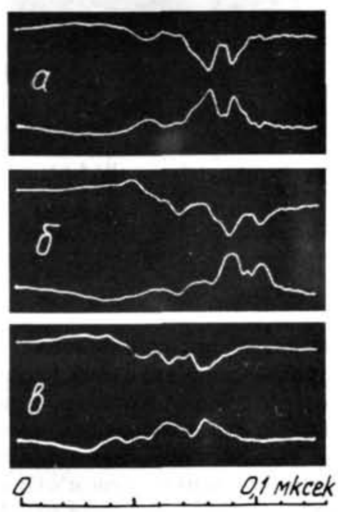

Рис.8. Зависимость корреляции продольной составляющей высокочастотных колебаний от расстояния между магнитными зондами, сдвинутыми вдоль оси камеры (без интегрирования): H_0 = 700 э; $\tilde{H}$ = 4 кэ; $n_0 = 10^{13}$ см$^{-3}$.
а) l = 0 см; б) 4,5 см; в) 9 см.

в) контрольные эксперименты, выполненные на более тяжелых газах (аргоне и ксеноне), показывают, что частоты колебаний практически не зависят от массы ионов.

Изложенные результаты говорят за то, что в данном случае, по-видимому, возбуждается не магнито-звуковая волна. Одним из возможных типов колебаний, которые могут здесь развиваться, являются колебания типа "свистящих атмосфериков". Расчет неустойчивости такого типа приведен в докладе Арефьева, Гордеева и Рудакова на данной конференции. Согласно этой теории, длина волны возмущений по Z порядка толщины токового слоя, умноженной на 2π, уменьшается с увеличением частоты колебаний.

3. В работе [16] также наблюдались в разряде типа θ-пинча СВЧ-шумы из плазмы на длинах волн 8 мм и 4 мм, но их условия несколько отличались от наших условий. Характерной особенностью этих шумов является, как и в данном случае, запаздывание появления СВЧ-сигналов

по отношению к перемене знака магнитного поля в плазме. Это излучение авторы вышеупомянутой работы объясняют возбуждением кинетической неустойчивости на гармониках электронной циклотронной частоты в результате анизотропии функции распределения электронов по скоростям (большие поперечные скорости у электронов). При этом для частоты излучения должно выполняться условие: $\omega = n\omega_{He} \leq \omega_{pe}$. В наших экспериментах при напряжении на контуре 30 кв максимальная напряженность переменного магнитного поля равнялась 4 кэ, чему соответствует электронная циклотронная частота $f = 1{,}1 \cdot 10^{10}$ гц. Следовательно, наблюдаемое в данных экспериментах излучение может соответствовать первой и второй гармоникам электронной циклотронной частоты.

Появление шумов в диапазонах 3,2 и 1,6 см примерно сопадают по времени, что также говорит в пользу объяснения, приведенного в работе [16]. Возможно также развитие других неустойчивостей, возникающих из-за анизотропии функции распределения, например, "конусной".

В заключение можно сделать следующие выводы:

1. При плотности плазмы ниже некоторой критической величины аннигиляция встречных магнитных полей происходит очень быстро и сопровождается нагревом электронов плазмы.

2. В плазме развиваются интенсивности колебания как ВЧ-диапазона (до 100 Мгц), так и в диапазоне до $2 \cdot 10^{10}$ гц, свидетельствующие о проявлении коллективных процессов. Колебания в диапазоне $10 \div 100$ Мгц можно связать с раскачкой волн типа "свистящих атмосфериков".

Материалы, изложенные в разделе 2 данного доклада, были получены при участии С.П.Загородникова, Е.А.Стригановой, Г.В.Шолина; в разделе 3 – при участии А.И.Жужунашвили и С.С.Соболева. Всем им авторы выражают искреннюю благодарность. Авторы пользуются случаем выразить свою признательность Е.К.Завойскому, постоянное внимание и ценные советы которого способствовали выполнению данной работы, и поблагодарить А.В.Гордеева и Л.И.Рудакова за многочисленные обсуждения.

ЛИТЕРАТУРА

[1] БАБЫКИН, М.В., ЗАВОЙСКИЙ, Е.К., РУДАКОВ, Л.И., СКОРЮПИН, В.А., Ядерный синтез, Дополнение 3 (1962) 1073.
[2] ЗАГОРОДНИКОВ, С.П., СМОЛКИН, Г.Е., ШОЛИН, Г.В., ЖЭТФ 45 (1963) 1850.
[3] ЗАГОРОДНИКОВ, С.П., РУДАКОВ, Л.И., СМОЛКИН, Г.Е., ШОЛИН, Г.В., ЖЭТФ 47 (1964) 1717; Письма в редакцию ЖЭТФ 2 вып.5 (1965) 238.
[4] БАБЫКИН, М.В., ЖТФ 38 4(1968) 603.
[5] ЗАГОРОДНИКОВ, С.П., СМОЛКИН, Г.Е., ШОЛИН, Г.В., ЖЭТФ 52 (1967) 1178.
[6] ЗАГОРОДНИКОВ, С.П., СМОЛКИН, Г.Е., ШОЛИН, Г.В., Теплофизика высоких температур 6 2(1968).
[7] БЛИНОВ, П.И., ЗАГОРОДНИКОВ, С.П., СМОЛКИН, Г.Е., ШОЛИН, Г.В., ЖЭТФ 48 (1965) 61.
[8] ЗАГОРОДНИКОВ, С.П., СМОЛКИН, Г.Е., ШОЛИН, Г.В., Доклад на Межд. конф. по ударным волнам в плазме, 1 – 5 августа 1967, Новосибирск, СССР.
[9] БАБЫКИН, М.В., ГАВРИН, П.П., ЗАВОЙСКИЙ, Е.К., РУДАКОВ, Л.И., СКОРЮПИН, В.А., ЖЭТФ 43 (1962) 411.
[10] ВЕДЕНОВ, А.А., ВЕЛИХОВ, Е.П., САГДЕЕВ, Р.З., Ядерный синтез 1 (1961) 92.
[11] САГДЕЕВ, Р.З., в сб. "Вопросы теории плазмы", вып.4, Атомиздат, 1964.
[12] ADLAM, J.H., ALEEN, J.E., Phil. Mag. 3 (1958) 488.
[13] КАДОМЦЕВ, Б.Б., в сб. "Физика плазмы и проблема управляемых термоядерных реакций" 4 Изд. АН СССР, 1958, стр.364.
[14] GREEN, T.S., Nucl. Fusion 2 (1962) 92.

[15] БОРОДИН, А.В. и др. ЖЭТФ 41 (1961) 317.
[16] EL-KHALAFAWY, T.A., et al., Plasma Phys. 10 2 (1968) 117.
[17] ИСКОЛЬДСКИЙ, А.М., КУРТМУЛЛАЕВ, Р.Х., НЕСТЕРИХИН, Ю.Е., ПОНОМАРЕНКО, А.Г., ЖЭТФ 47 (1964) 774; КУРТМУЛЛАЕВ, Р.Х., НЕСТЕРИХИН, Ю.Е., ПИЛЬСКИЙ, В.И., САГДЕЕВ, Р.З., Доклад 21/218 на II Межд. конф. по физике плазмы, Калэм, 1965, Conf. Proc. VII, 367.
[18] PAUL, J.M., HOLMS, L.S., PARKINSON, M.J., SHEFFIELD, J., Report on Int. Conf. on Phenomena in Ionized Gases, Belgrad 22-27 August 1965.
[19] GOLDENBAUM, G.C., HINTZ, E.A., Phys. Fluid 8 (1965) 2111.

COLLISIONLESS SHOCK WAVES AND TURBULENT HEATING IN HIGH VOLTAGE THETA PINCHES*

A. W. DESILVA, D. F. DÜCHS, G. C. GOLDENBAUM, H. R. GRIEM,
E. A. HINTZ, A. C. KOLB**, H. -J. KUNZE AND I. M. VITKOVITSKY**
UNIVERSITY OF MARYLAND, COLLEGE PARK, MD.,
UNITED STATES OF AMERICA

Abstract

COLLISIONLESS SHOCK WAVES AND TURBULENT HEATING IN HIGH VOLTAGE THETA PINCHES. Based on preceding experiments with smaller systems, a large (46 cm diameter, 100 cm length) theta pinch has been constructed which is driven by a Blumlein-type transmission line (~0.4Ω) capable of generating a 1 MV pulse (open circuit) of 100 ns duration. For the experiments described herein, it was operated at 40% of design voltage. The corresponding peak field is 3.2 kG, and a strong shock wave (5×10^7 cm/s) is generated in the initial plasma containing a (parallel or antiparallel) bias field. This initial plasma is prepared in typically 5 m Torr D_2 by a sequence of auxiliary discharges through the theta-pinch coil. Shock structure and field-vacuum interface are investigated (mainly by magnetic probes). These measurements, besides being compared directly with theoretical predictions, also yield current densities required for the determination of effective (turbulent) electrical conductivities from measured electron heating rates (using X-ray emission). Ion energies are estimated from neutron yields. Indications are that there is an anomalous ion heating mechanism, in addition to anomalous electron heating, as observed in preceding experiments from Thomson scattering measurements. In parallel with these laboratory investigations, a computer simulation program has been developed which permits quantitative discussion of the influence of non-stationarity and cylindrical convergence on the experimental results and of the deviations from classical results caused by anomalous transport processes (with coefficients either estimated theoretically from growth rates of expected microinstabilities or chosen to fit the experimental results).

Introduction

Previous work at this laboratory [1,2,3,4] and others [5,6,7,8] has established the possibility of heating a low density plasma by means of a fast rising current. Plasma heating occurs directly as a result of the induced plasma current or by shock waves produced by the current. Under the conditions of interest the observed heating rates cannot be explained by two particle collisions. At low densities however, the particle drifts are of sufficient magnitude to excite instabilities which, according to their nature, may heat the electrons, ions, or both. Some questions of interest are:

1) How efficient can the coupling between an external energy source and the plasma thermal energy be?
2) What are the important dissipation mechanisms?
3) Does thermal energy go into electrons or ions preferentially, and under what conditions?
4) Can a study of shocks provide basic information on growth rates, turbulence levels, wave energy spectra, etc. associated with various instabilities?

---

* Work performed under the auspices of a Joint Program in Plasma Physics between the U.S. Naval Research Laboratory and the University of Maryland.

** US Naval Research Laboratory, Washington, D.C., USA.

In order to provide a means to answer these and related questions, a number of Θ-pinch type shock devices have been operated. Indications of strong electron [2], and ion [3,4] heating have been reported, and experience gained with these machines has led to the device described herein, which is basically a large-bore Θ-pinch driven by a high-voltage pulse line.

The objective of the experiment is the creation and investigation of high-energy plasmas by imploding high-voltage theta pinch sheaths, under conditions where the external energy source is rather closely coupled to the plasma. Good coupling is achieved by matching the generator impedance to the effective plasma resistance $R_{eff} = \frac{dL}{dt}$, due to motion of the plasma boundary. This resistance increases both with plasma radius and plasma boundary velocity, and reaches about one ohm at r = 20 cm for v_B = 8×10^7 cm/sec. Construction of pulse lines at impedances much less than one ohm is difficult. Accordingly, a tube of 46 cm inside diameter was chosen for the work. This will lead to initial values of R_{eff} in the range $\lesssim$ 1 ohm, and provides long paths for shock travel to allow investigations of broad shock structures.

In the following, we will describe the apparatus and procedure for establishing an initial plasma. Certain experimental conditions will next be described, leading to a variety of wave types. Finally, we will attempt to interpret the observed behavior in terms of existing shock theory.

Initial Plasma Generation

Plasma currents are generated by a fast-rising current pulse in a single turn coil one meter long surrounding the 46 cm diameter tube. Prior to this, a plasma is created in the tube by a ringing discharge into the same coil, and a bias magnetic field is provided by a quasi-static current, also in the same coil.

The plasma tube is pyrex, 3 meters long, evacuated to a base pressure of 5×10^{-6} Torr. Typical fillings are deuterium at 5 to 10 mTorr. The initial plasma is created by a 100 KHz discharge into the coil from a 0.85μF capacitor charged to 70 kV (Fig. 1). This current damps away in about 150 μsec, after which the bias magnetic field is switched on. This field is provided by a 56 μF capacitor bank at 11 kV, and is crowbarred at peak current, leaving a slowly changing field that damps out with a time constant of 70 μsec. The fast current pulse is switched on sometime during the decay of this field.

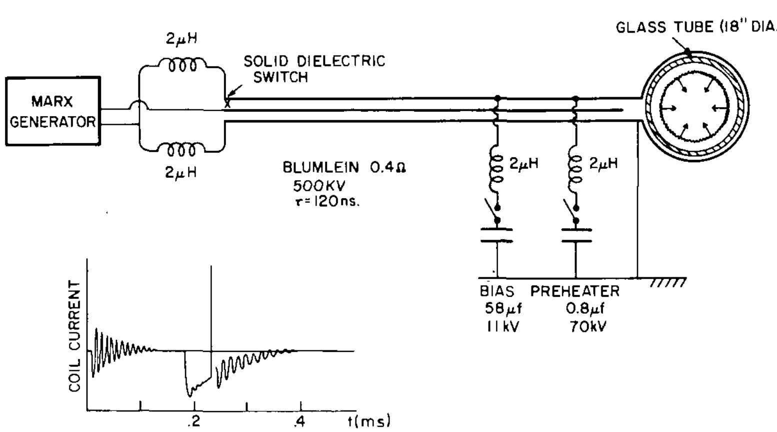

FIG. 1. Schematic diagram of electrical circuit.

High-Voltage Pulse Line

The fast current pulse is provided by a Blumlein type parallel-plate pulse line, of characteristic impedance 0.4 Ω and electrical length 120 nsec (Fig. 2). The line is constructed of three copper sheets, each 0.25 mm thick, with Mylar dielectric 4 mm in thickness, and measures 4 meters wide by 7 meters long. The two outer copper sheets are connected at one end through a short taper section to a 2 meter long by 1 meter wide line that couples to the coil, while the middle sheet in the sandwich is isolated, ending 2 meters short of the coil. The whole assembly is immersed in a bath which is a weak solution of copper sulfate ($\rho = 10^3$ ohm-cm) in water. This solution acts to evenly grade potentials at the edges of the line, preventing local accumulations of charge that would lead to surface arcing or corona. The center plate can be resonance charged to a design voltage of 500 kV by a separate Marx generator. In the initial experiments described in this paper, the line was operated at a charge voltage of 200kV (energy ≈ 10kJoule).

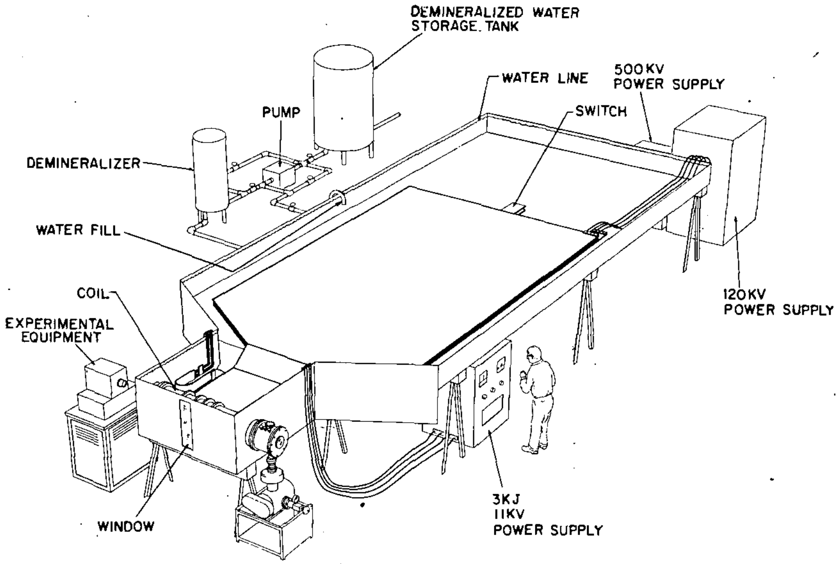

FIG. 2. *Experimental layout.*

The line is switched between the top and middle plates by means of a single solid dielectric switch at the midpoint of the end of the line opposite the coil. This is a sheet of polyethylene, needle-stabbed to a depth that will lead to its breakdown just as the line reaches full voltage while charging. Since the resonance charging takes only 4 μsec, the line is in fact not charged until after the initial plasma has been generated and the bias field established. Breakdown of the solid dielectric switch then generates a wave which propagates toward the coil. On arriving at the discontinuity representing the end of the center plate, the potential between the top and middle plates reverses abruptly, now adding to the potential between bottom and middle plates, and placing twice the charge voltage on the coil.

The coil current rises rapidly until the wave reflected from the far end of the line returns about 120 nsec later. After this time the electrical circuit begins to behave more like a simple lumped L-C circuit than a pulse line feeding an inductance, and the magnetic field in fact continues to increase slowly to a peak of about 3.5 kGauss at about 240 nsec, returning slowly to zero about 360 nsec later.

Plasma-circuit Coupling

For about the first 120 nsec, the generator appears to the load as a resistive source, and the current risetime depends on the ratio of load inductance to source resistance. The rise time constant assuming an applied square waveform is $L_o/(Z_o+R_{eff})$, and the peak current to be expected is $2V_o/(Z_o+R_{eff})$, where $R_{eff}=dL/dt$ is the effective plasma resistance due to motion of the boundary, V_o the charge voltage, and L_o is the inductance of the plasma-filled coil. In practice, the applied voltage from the Blumlein is not square, primarily due to the internal reflections within the line arising from the single point switching[1]; consequently, the current rise time is greater than predicted for an ideal pulse line. The initial current development also depends strongly on L_0, and it is necessary that the coil be well filled with plasma to obtain high currents before the plasma moves appreciably.

During the current pulse, the plasma boundary moves inward, causing an increase in L_o. Thus, when the first line reflection arrives at the coil, it sees a large inductance, and the current in the coil is not strongly affected. We obtain a current pulse in this way that rises rapidly and lasts much longer than the line transit time.

The Initial Plasma

Conditions in the initial plasma have been determined by spectroscopic measurements (line intensity ratios, line to continuum ratio, absolute line intensities, line intensity time history) and through analysis of small amplitude magnetosonic waves induced at the plasma boundary. The 100 KHz initial discharge ionizes and heats the gas to a temperature of a few eV. The gas rapidly cools to about 1.5 eV as the discharge current damps away, as evidenced by disapperance of D_β line radiation. In addition, the gas rapidly expands out the ends of the coil, reducing the density. This axial expansion proceeds with a time constant of order 50 μsec. The bias field is turned on about 150 μsec after the preheater discharge, and rises to its peak in 15 μsec. The currents induced by this field penetrating the plasma again heat the gas, and a temperature of 5 to 6 eV obtains, again rapidly decreasing as the field becomes steady after being crow-barred. The plasma is pinched toward the tube axis by the bias field, and leaves a strongly non-uniform density distribution. The fast discharge is usually delayed until the bias field has decayed by a factor 2 or more to allow the plasma to expand somewhat. It is likely that neutrals diffuse into the test section during these delays. However, at the very low density used the neutrals are probably not effectively coupled to the shocked plasma.

A lower limit to the initial plasma density near the tube wall, where the speed of the magnetosonic wave is too large to measure, may be inferred from the observed current density there, coupled with the observation that the electron cyclotron radius in the driving field must be less than the tube radius. This leads, e.g. to a density $n_e \gtrsim 10^{10}$ cm^{-3} near the tube wall in case I.

Neutral Background

The appearance of a constant intensity of line emission of neutral deuterium in the region behind the shock shows the continuing presence of neutral atoms. On these time scales, the failure of neutral atoms to burn out is to be expected, since ionization cross sections are of order

1. There is provision for multiple switching in later experiments.

$10^{-17}cm^2$, so the ionization time is of order 10^{-4} sec, assuming an electron density n_e=$10^{13}cm^{-3}$. Ions interact with the neutral background through change exchange with a cross section $\sigma \gtrsim 10^{-15}cm^{-3}$. If the neutral density is $\lesssim 5 \times 10^{13}cm^{-3}$ however, the ion mean free path is greater than the tube radius.

Diagnostics

The wave magnetic field B_z is monitored by a magnetic probe 0.4 mm in diameter protruding about 10 cm radially from an axial support rod. It may be traversed across the tube radius. Visible light output is monitored axially along a narrow pencil 8 cm off the tube axis, as well as side-on through a slot in the coil. An image-converter camera allows streak photography of gross plasma effects. The soft x-ray emission is measured by means of scintillators placed behind thin metallic foils of Al, Au or Pb. Four such channels [9] are collimated to look along the axis at the central 20cm diameter, and allow an estimate of the x-ray spectrum on a single shot.

The neutron output is monitored by a pair of lead-shielded scintillation counters placed at two positions off the end of the tube. Neutrons may not be detected side-on due to the shielding effect of the water surrounding the coil. These counters, in addition to responding to neutrons, are sensitive to gamma rays in the energy range about 0.5 MeV. (Lead shields used are 3 or 6 mm in thickness). Both neutrons and gammas appear in short pulses of the order of 100 nsec wide, so neutrons are easily distinguished by their time of flight delay. No spatial resolution was attempted for either neutrons or gammas.

Experimental Results

Case I

A filling of 5 mTorr deuterium was used with a 300 Gauss anti-parallel bias field, resulting in the density distribution shown in Fig. 3 at the time the fast field was turned on. Magnetic field profiles from the probe are shown in Fig. 4, and typical time histories of B_z, neutrons, x-rays and T_e are shown in Fig. 5.

Examining the magnetic field profiles we see that there are two distinct regimes of interaction of driving field with the plasma - the region r > 10 cm, in which the initial density $n_e \lesssim 2 \times 10^{12}$; and the region r $\lesssim$ 10 cm, where the initial density $n_e \approx 1 \times 10^{13}$.

In the outer (r > 10 cm) region, the field penetration appears to be due to a diffusive process, leading to no compression of the initial field. The width of the front is about 10 cm, which is about equal to c/ω_{pi} and is much greater than a resistive (binary collision) skin depth, and suggests the presence of a microinstability leading to enhanced effective resistivity. The probe traces in the outer region are characterized by strong fluctuations in B_z near peak field at a frequency of 50 MHz, which is the upper limit of probe response. This frequency also corresponds to the local lower hybrid frequency in the region of the oscillations.

The conditions that an electron-ion two-stream instability be excited in the current stream when $T_e = T_i$ are (1) $\omega_{pe} > \omega_{ce}$ and (2) $v_D > v_{th}$, where v_D is the electron drift velocity relative to the ions, and v_{th} is the electron mean thermal velocity. The first condition is satisfied throughout the experiment, except perhaps in the very early stages near the tube wall. Electron drift velocities deduced from measured current densities in the outer region are well above initial thermal velocities while the field is penetrating, and could reach relativistic values in the low density regions near the tube wall. The two-stream instability develops with a growth rate about equal to ω_{pi}. The time $2\pi/\omega_{pi}$ has been used as an

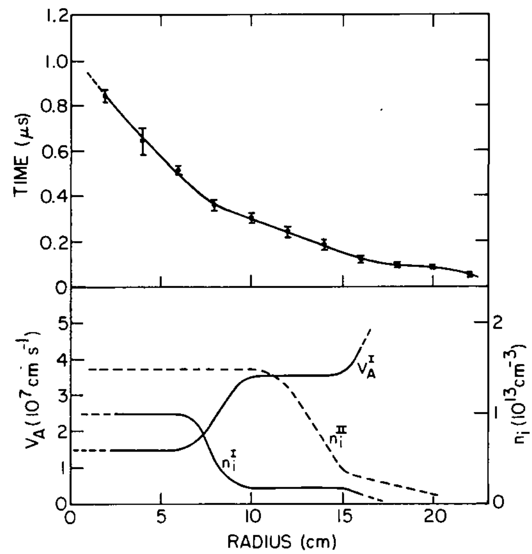

FIG. 3. Initial plasma measurements. Upper curve shows x-t plot of small amplitude magnetosonic wave peak for 5 mTorr D_2 filling, 300 G bias. Curves labeled (I) are Alfvên speed V_A and ion density n_i deduced from above. Dotted curve labeled (II) is ion density deduced in similar manner with 10 mTorr D_2 filling, 450 G bias field.

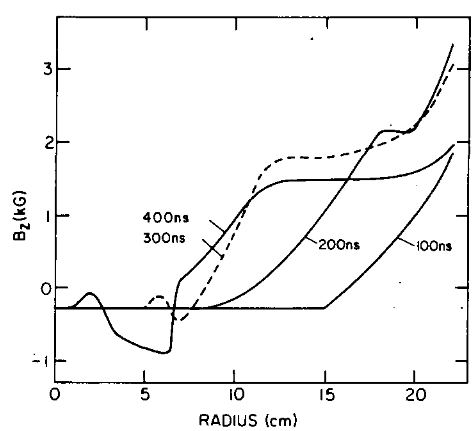

FIG. 4. Magnetic field profiles from probe for case 1 (see text). Tube wall is at 22.8 cm.

effective collision time in a code calculation (described in a following section) which reproduces the rapid diffusion-like penetration of the magnetic field profile (Fig. 6), and predicts electron temperatures $T_e \approx 20$ KeV. (Use of the conventional Spitzer-Härm resistivity in the code leads to strongly relativistic drift velocities and very narrow profiles.) Although the code calculation shows the field penetrating with a velocity about 10^8 cm/sec, it also shows the plasma radial velocity to be only about 5×10^6 cm/sec.

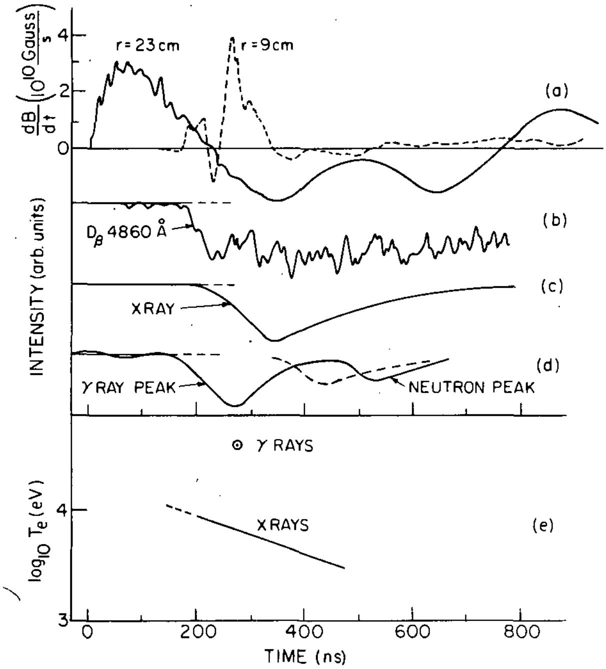

FIG. 5. Time histories fro case I. (a) dB/dt from probes at tube wall and at a radius of 9 cm. (b) D_β emission at r = 8cm. (c) X-ray intensity seen through Al foil 0.13 mm thick. (d) Output of neutron detector. Large peak is due to γ-rays, smaller peak to neutrons. Dotted curve shows neutron peak shifted to correct for time-of-flight delay. (e) Electron temperature deduced from soft x-ray measurements. The γ-ray point is T_e assuming γ's are produced by electrons on tail of Maxwellian distribution.

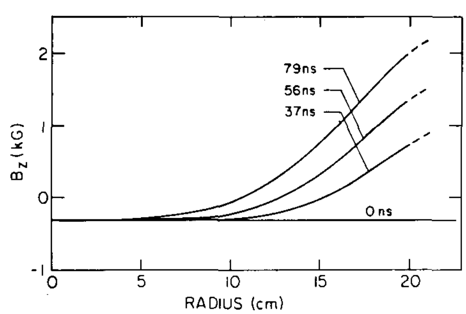

FIG. 6. Magnetic field B_z from numerical code calculation, using initial density from Fig. 3(I) and observed external current, with "collision frequency" $\omega_{pi}/2\pi$.

Soft x-ray measurements show an electron temperature decreasing from about 10 keV from the first appearance at r < 10 cm at 160 nsec, about the time the earliest magnetic disturbance comes into view of the detector at r ≈10 cm. Emission of γ-rays with energies above 0.5 MeV is seen to begin about the same time as x-ray emission, though the observable volume was not restricted to r ≲ 10 cm as in the case of the x-rays. The γ's peak about 70 nsec before the observed x-ray peak, i.e. about the time the piston field encounters the steep density gradients near $r \gtrsim 9$ cm. It is interesting to assume the observed γ-flux being produced by electrons far out on the tail of a Maxwellian velocity distribution: the necessary electron temperature would be of the order of 40 keV. This suggests a non-Maxwellian distribution out on the tail since the soft x-rays indicate a temperature of only 7 keV for the same time. Absolute intensity measurements show that the observed x-ray flux can only be explained if it is produced by all the electrons, i.e. it is not possible that only a small fraction of the electrons have the temperature quoted above.

The neutron emission is of the order of 10^5 neutrons emitted with a duration of about 200 nsec, which corresponds to a peak neutron flux of 10^{12} neutrons/sec. The neutrons peak at about 430 nsec, before the magnetic disturbance has reached the tube axis. If we assume this flux is generated by D-D reactions in the total coil volume with a mean ion density $n = 10^{13}\text{cm}^{-3}$ this would require an ion temperature of $T_i \gtrsim 6$ keV. The actual emitting plasma volume will, of course, be smaller so the above ion temperature will be an underestimate. If, for example, the effective volume were 15% of the total coil volume at the same density the temperature estimate increases by a factor of 2. Any reasonable deviation from a Maxwellian velocity distribution should not change this mean energy by more than a factor of 2. Detectable neutron emission from D-D reactions does not begin until the wave encounters the denser plasma around $r \gtrsim 10$ cm; however the lack of detectable neutrons arising earlier is completely consistent with the lower density in the region $r > 10$ cm, and does not necessarily mean the ions are cold there.

Image converter photographs of the plasma taken axially show a sharply defined luminosity moving toward the tube axis. This light seems to be associated with the field reversal region where $B_z \gtrsim 0$. D_β light was observed from an axial pencil at $r = 8$ cm and is seen to rise sharply about the time the first magnetic disturbance appears there, increasing to a peak intensity in the vicinity of B_z reversal. The persistence of D_β line emission for hundreds of nanoseconds after passage of the current sheet is further evidence for a high density neutral background, weakly coupled to the plasma through infrequent collisions.

Shots taken at lower initial density show much more intense x-and γ-ray emission, and the magnetic field shows violent high frequency oscillations even near the axis. The implication is that at lower density the drift velocities are higher, leading to a higher level of turbulence.

In the inner region, $r \lesssim 10$ cm, a compressional wave forms, accompanied by pronounced steepening of the leading edge of the driving field. In this region, even though the gradients are larger, owing to the high initial density the electron drift velocity is low and the two-stream instability should not occur. The leading edge of the compression front travels at $M_A \approx 3$. The shock conservation equations for $\gamma = 5/3$ predict a compression ratio $\eta \approx 2.8$ for a $M_A = 3$ shock, which is about what is observed. By the time this compression forms at 300 nsec, the x-rays have reached peak intensity, γ-rays are nearly gone, and neutrons are increasing towards a peak at 430 nsec.

Case II

We have also investigated the conditions at higher fill pressures (10 m Torr D_2) and 450 gauss bias field. The initial density, deduced again from a study of small amplitude magnetosonic waves, appears in this case to be higher everywhere than in case I, but not by a factor of two (Fig.3). Measurements were made with the bias and compressing field both parallel and antiparallel. The two situations seem to be vastly different; the parallel field arrangement leading to shock-like compression waves and the antiparallel to the same diffusive type field penetration as in the 5mTorr case.

(a) Antiparallel bias field

The antiparallel field geometry gives no magnetic compression at $r \gtrsim 16$cm and only small compression at $r<16$ cm with no structure resembling a stationary shock wave. Although the electron density did not simply increase by a factor of two over the 5 mTorr case, the observed maximum electron temperature from the x-ray measurement appeared to be only about 1 keV, measured at the time of peak intensity. Earlier than this, the data were too irreproduceable to obtain a temperature. This low temperature may be interpreted as due to larger particle density and hence, lower drift velocity near the walls.

Neutron flux in this case is about 5×10^{11} sec^{-1} at peak, lower by a factor of two than in case I. Since the estimate of T_i is insensitive to small changes in ion density and neutron flux, we conclude that T_i is about 4 keV.

(b) Parallel bias field

The parallel bias field situation leads to a sharp front moving into the plasma at about $M_A \cong 2.5$ in the outer 10 cm of the plasma and then slowing down to $M_A \cong 1$ in the central 13 cm. The sharp leading edge has a width of about 7 mm which is 3.5 c/ω_{pe} (initial plasma). The electron drift velocity in the middle of the shock front, assuming the electron density is compressed at the same rate as the magnetic field, is about 5×10^8 cm/sec. This is about ten times the initial plasma thermal velocity. Assuming a resistive shock, the effective collision time deduced from the expression $\Delta \approx \left(\frac{c}{\omega_{pe}}\right)^2 \frac{1}{u_0 \tau_c}$, where Δ is shock thickness, u_0 is shock velocity, and τ_c is effective collision time; is about $6/\omega_{pi}$. The numerical code computation using as a collision time $2\pi/\omega_{pi}$ when drift velocities exceed thermal velocities, gives a sharp shock with width $\Delta \cong 4\, c/\omega_{pe}$. As shown in Fig. 7, two regions of changing magnetic field are observable; the one on the c/ω_{pe} scale length followed by a constant field, then a field increase on the c/ω_{pi} scale (initial plasma) which is about the same as the diffusion length in the antiparallel case. The electron temperature is again about 1 keV but the absolute x-ray intensity is about a hundred times lower than in the 10 m Torr antiparallel case. This may be in part due to the decrease in the emitting volume. No neutrons were observed in the parallel case. The large magnetic compression ratio of about four and the low x-ray intensity may also result from a loss of electron energy along the field lines.

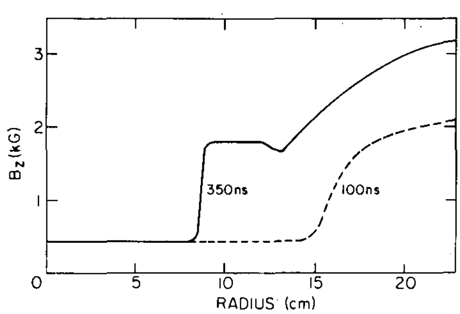

FIG.7. Magnetic field profiles from probe for case II, with bias and driving fields parallel.

Numerical Code Simulation

In a first attempt the low density plasma is described by a two-fluid model. The effects of viscosity, heat conduction, coupling of electron and ion kinetic energies and electrical resistance are taken into account.

Electron and ion pressure are considered to be scalars and all the coefficients for the mentioned effects are "classical" (except as noted). In Ohm's law, the electron inertia terms are included. The set of partial differential equations is solved numerically by an implicit method in order to avoid too small time steps in this low-density and high velocity regime. As initial conditions, measured plasma density profiles are used. Results corresponding to experimental case I are shown in Fig. 6.

Summary

Under the conditions of our experiment, two types of magnetic disturbance occur: one by a diffusion-like penetration of the induced current into the plasma and the other by a shock wave disturbance in front of the induced current.

Comparision of experimental observations with computer calculations implies that in the antiparallel bias field configuration rapid diffusion of the applied current into the plasma occurs with tne penetration length determined by an enhanced resistivity characteristic of an electron-ion streaming instability (effective collision frequency $\nu_c \approx \omega_{pi}/2\pi$). With an initial filling of 5mT D_2 we observed electron temperatures up to about 7 keV and ion energies of the same order. The peak neutron emission occurs before the current stream reaches the axis and also before the ions undergo one gyroperiod. Larmor radii of the hot ions are greater than tube dimensions.

In the parallel bias field configuration a ($M_A \approx 2.5$) whock wave develops, well separated from the piston. The narrow ($3.5\ c/\omega_{pe}$) front thickness is consistent with simple resistive shock estimates using an enhanced resistivity determined by an electron-ion streaming instability. The observed electron temperatures are about the same as in the antiparallel case but the x-ray intensity is about one hundred times smaller, presumably due to a small volume of hot plasma. No neutrons were observed in the parallel bias case.

Acknowledgements

We are grateful for stimulating discussions with N. A. Krall and D. A. Tidman. Much of the design of the device was performed by J. M. Frame of the Naval Research Laboratory. The advice of W. H. Lupton and J. D. Shipman of the Naval Research Laboratory on high voltage pulse technique was invaluable. We are indebted to R. C. Elton, also of the Naval Research Laboratory, for the design of the x-ray unit [9] and for making x-ray transmission curves available prior to publication. Technical support by M. P. Young, K. R. Diller, F. W. Knouse and N. L. Bretz is gratefully acknowledged.

REFERENCES

[1] G. C. Goldenbaum and E. A. Hintz, Phys. Fluids 8 2111 (1965).
[2] G. C. Goldenbaum, Phys. Fluids 10 1897 (1967).
[3] A. W. DeSilva and J. A. Stamper, Phys. Rev. Lett. 19 1027 (1967); 20 528 (1968).
[4] A. W. DeSilva and H.-J. Kunze, J. Appl. Phys., 39 2454 (1968).

[5] J. W. M. Paul, L. S. Holmes, M. J. Parkinson, and J. Sheffield, Nature 208 133(1965).
[6] R. C. Kurtmullaev, Yu. E. Nesterikhin, V. I. Pil'skii, R. Z. Sagdeev, Plasma Physics and Controlled Fusion Research, Vol. II, 367 (I.A.E.A. Vienna, 1966).
[7] E. A. Hintz, unpublished.
[8] I. M. Vitkovitsky, International Conference on Collisionless Shock Waves and Nonlinear Phenomena in Plasmas, Novosibirsk, U.S.S.R., July 29-Aug. 5 1967 (Unpublished).
[9] R. E. Elton and N. V. Roth, Appl. Opt. 6 2071 (1967).

DISCUSSION

S.J. BUCHSBAUM: Could you please explain why, in the antiparallel case, the shock has no time to develop?

A.W. DESILVA: Although we do not know for certain the cause of the difference between magnetic profiles in the two cases, we believe that it is due to a difference in the ratio of acceleration time of the plasma boundary to field diffusion time. If this ratio is small, one may expect a shock to form; if it is large, a diffusion profile may form. In the field reversal region accompanying the antiparallel case, neutral gas present near the tube walls will ionize, loading and slowing the piston, and at the same time leading to increased losses and to a shorter diffusion time.

TOROIDAL CONFINEMENT I
(TOKAMAK, ZETA, etc.)

(Session B)

Chairman: M. SEIDL

Papers B-4 to B-8 were presented
by R. PEASE as Rapporteur.

ЭКСПЕРИМЕНТАЛЬНЫЕ ИССЛЕДОВАНИЯ НА УСТАНОВКАХ ТОКАМАК

Л.А.АРЦИМОВИЧ, Г.А.БОБРОВСКИЙ,
Е.П.ГОРБУНОВ, Д.П.ИВАНОВ, В.Д.КИРИЛЛОВ,
Э.И.КУЗНЕЦОВ, С.В.МИРНОВ, М.П.ПЕТРОВ,
К.А.РАЗУМОВА, В.С.СТРЕЛКОВ и Д.А.ЩЕГЛОВ
ИНСТИТУТ АТОМНОЙ ЭНЕРГИИ им.И.В.КУРЧАТОВА,
МОСКВА,
СССР

Abstract — Аннотация

EXPERIMENTS IN TOKAMAK DEVICES. The authors describe the results of recent investigations carried out with magnetic fields of 9-35 kG in the Tokamak devices T-3 and TM-3, presenting new data on the conditions of plasma column equilibrium, the energy balance and the containment time of particles in the plasma column. The total ion and electron temperature is determined by measuring the diamagnetism of the plasma and the radiointerferometric broadening of the plasma density. The electron temperature is estimated independently by measuring the soft X-ray emission spectrum, and the ion temperature by analysing the energy spectrum of the charge-exchange atoms. The density of the plasma electrons varies between 10^{12} and 5×10^{13} cm^{-3}. The electron temperature lies within the range 100-2000 eV, while the ion temperature reaches ~300 eV. The authors give the energy containment time τ_E characterizing the confinement of the plasma. An attempt is made to find an emipirical formula linking τ_E with the basic parameters characterizing the state of the plasma. It is shown that τ_E increases with the amplitude of the discharge current pulse and is independent of the longitudinal magnetic field as long as the plasma column is magnetohydrodynamically stable. The maximum value of τ_E is ~10 ms. At high temperatures τ_E differs significantly (by a factor of up to 50) from the value given by Bohm's formula. Anomalously high plasma resistance is observed in cases of large currents and low electron densities. The charged particle containment time is determined by measuring the rate of ionization of the neutral hydrogen atoms entering the plasma column during the discharge and the variation in plasma electron density over time. It is found to be several times greater than the energy containment time τ_E.

ЭКСПЕРИМЕНТАЛЬНЫЕ ИССЛЕДОВАНИЯ НА УСТАНОВКАХ ТОКАМАК. Изложены результаты последних исследований на тороидальных установках Токамак: Т-3 и ТМ-3. Приведены новые данные об условиях равновесия плазменного шнура, энергетическом балансе и времени удержания частиц в плазменном шнуре. Эксперименты проводились в диапазоне магнитных полей от 9 до 35 кгс. Суммарная температура ионов и электронов определялась на основании измерений диамагнетизма плазмы и радиоинтерферометрических измерений ее плотности. Независимо электронная температура оценивалась по результатам измерения спектра мягкого рентгеновского излучения, а ионная температура — по результатам анализа энергетического спектра атомов перезарядки. Концентрация электронов в плазме варьировалась в пределах от 10^{12} до $5{\cdot}10^{13}$ см$^{-3}$. Электронная температура была в пределах от 100 до 2000 эв, а ионная температура достигала величины ~300 эв. Приводится величина энергетического времени удержания τ_E, характеризующая термоизоляцию плазмы. Сделана попытка найти эмпирическую формулу, связывающую τ_E с основными параметрами, характеризующими состояние плазмы. Показано, что величина τ_E возрастает с увеличением амплитуды импульса разрядного тока и не зависит от величины продольного магнитного поля в пределах обеспечения магнитогидродинамической устойчивости плазменного шнура. Максимальное значение τ_E достигает величины ~10 мсек. При больших значениях температуры величина τ_E значительно (до 50 раз) отличается от величины, определяемой формулой Бома. При больших токах и малых концентрациях электронов наблюдалось аномально высокое сопротивление плазмы. Время удержания заряженных частиц определялось на основании измерений скорости ионизации нейтральных атомов водорода, поступающих в плазменный шнур в течение разряда, и временного хода концентрации электронов в плазме. Это время оказывается в несколько раз больше времени удержания энергии τ_E.

Цель экспериментальной программы, выполняемой на установках Токамак, заключается в том, чтобы получить возможно более полную информацию о свойствах кольцевого плазменного шнура с током, стабилизируемого с помощью сильного продольного магнитного поля. В докладе изложены результаты исследований, проведенных по этой программе на установках ТМ-3 и Т-3 в 1967 - 1968 гг. В таблице 1 указаны геометрические размеры установок и интервалы значений основных параметров (начальное давление p_0, напряженность продольного магнитного поля H_z, сила тока J), в пределах которых производились измерения.

ТАБЛИЦА 1. ГЕОМЕТРИЧЕСКИЕ РАЗМЕРЫ УСТАНОВОК ТМ-3 И Т-3 И ИНТЕРВАЛЫ ЗНАЧЕНИЙ ОСНОВНЫХ ПАРАМЕТРОВ

Установка	a_0 [а] см	R [б] см	p_0 мм рт.ст. H_2	J ка	H_z кэ
Т-3	15	100	$8\cdot10^{-5} - 10^{-3}$	25-120	17-34
ТМ-3	8	40	$10^{-4} - 2\cdot10^{-3}$	10-40	10-25

[а] a_0 – радиус диафрагм.
[б] R – большой радиус тора.

Ранее было установлено, что в установках Токамак для обеспечения магнитогидродинамической устойчивости плазменного шнура необходимо, чтобы величина $q(a)=H_z \cdot a/H_J(a) \cdot R$ (где H_J – напряженность поля на границе плазмы и a – радиус поперечного сечения плазменного шнура) превышала 2-3 [1]. Во всех экспериментах указанное условие выполнено. Заметим, что оно допускает простую интерпретацию. Запас устойчивости $q(r) = H_z \cdot r/H_J(r) \cdot R$ есть функция r – радиуса поперечного сечения тороидальной магнитной поверхности в плазменном шнуре. Отношение между величинами запаса устойчивости на границе плазменного шнура и его осевой линии зависит от распределения тока по сечению плазменного шнура. При естественных предположениях о характере этого распределения (оно, очевидно, должно иметь колоколообразную форму) находим, что отношение $q(a)/q(0)$ лежит в пределах от 2 до 3. Поэтому условие $q(a) > 2-3$ означает, что $q(0)$ должно превышать единицу. Смысл этого результата очевиден: критерий устойчивости Крускала-Шафранова для желобковых деформаций и первой моды ($m = 1$) винтовых возмущений должен выполняться во всем объеме плазмы.

В описываемых измерениях получены новые данные об условиях равновесия плазменного шнура, об энергетическом балансе и о времени удержания частиц в плазменном шнуре.

Рассмотрим сначала результаты измерений, относящихся к условиям равновесия.

Согласно теории равновесия, развитой Шафрановым [2], горизонтальное смещение центра магнитной поверхности плазменного шнура относительно центра поперечного сечения медной оболочки камеры равно $\delta_0+\delta_H$, где:

$$\delta_0 = \frac{b^2}{2R}\left\{\ln\frac{b}{a} + \left(1 - \frac{a^2}{b^2}\right)\left(\beta_J + \frac{l_i - 1}{2}\right)\right\} \qquad (1)$$

и

$$\delta_H = c\frac{b^2 H_\perp}{2J} \qquad (2)$$

В этих выражениях $\beta_J = 8\pi\overline{p}/H_J^2(a)$ ($\overline{p}$ – средняя величина давления плазмы), l_i – внутренняя индуктивность плазменного шнура на единицу длины и $H_\perp$ – напряженность поперечного управляющего магнитного поля, создаваемого с помощью специальных контуров с током. При постоянных значениях а, l_i и β_J смещение должно быть линейной функцией $H_\perp$. На рис.1 показана зависимость измеренного экспериментально смещения δ от величины δ_H при двух различных значениях начального давления водорода в камере на установке ТМ-3. При начальном давлении, равном $2{,}8\cdot10^{-4}$ мм рт. ст. H_2, данные измерений подтверждают линейную зависимость δ от δ_H (с угловым коэффициентом, равным 1). Однако, при начальном давлении $\approx 1\cdot10^{-3}$ мм рт. ст. H_2 наблюдается резкое отклонение экспериментальных данных от предсказанной теории.

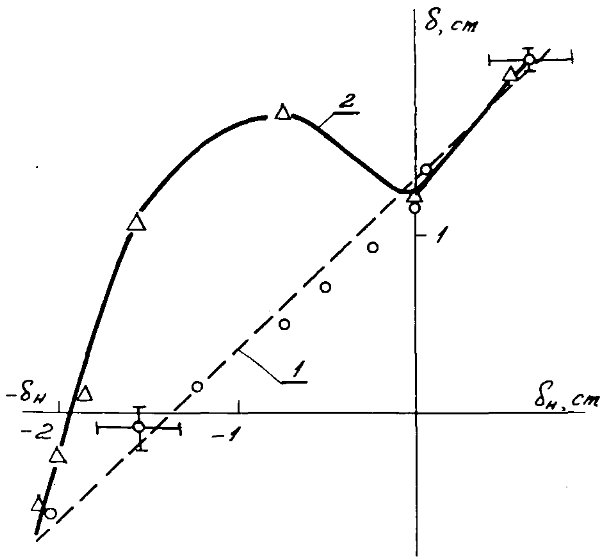

Рис.1. Зависимость измеренного на установке ТМ-3 смещения δ от δ_H (положительным величинам δ и δ_H соответствуют смещения к внешней части тора).
Режим разряда: J – 28 ка; H_z = 18 кэ:
Кривая 1 – $p_0 = 2{,}8\cdot10^{-4}$ мм рт.ст. H_2.
Кривая 2 – $p_0 = 9\cdot10^{-4}$ мм рт.ст. H_2.

В указанном случае вертикальное внешнее поле Н перестает выполнять ту основную функцию, для которой оно предназначено. Это поле оказывается не способным уменьшить смещение плазменного шнура наружу в широком интервале изменения величины $H_\perp$. Обнаруженная аномалия начинает проявляться при тем больших значениях начального давления газа, чем больше сила тока в плазме. Нарушение обычных условий равновесия при больших начальных давлениях газа (т.е. в плазме с высокой электронной концентрацией) наблюдается также и в опытах на установке Т-3. Происхождение этого эффекта пока еще не установлено. Для его объяснения a priori можно было бы выдвинуть следующие предположения:

1. Наличие большой продольной скорости у ионной компоненты плазмы. В этом случае в уравнении равновесия нужно учитывать влияние центробежной силы.

2. Увеличение внутренней индуктивности плазмы (т.е. величины l_i) вследствие того, что в некотором слое плазменного шнура ток меняет знак. При сильном влиянии скин-эффекта такое явление, в принципе, может иметь место.

Подтверждением первого предположения могло бы служить изменение контура спектральной линии за счет Допплер-эффекта при наблюдении вдоль оси плазменного шнура. Изучение контура линии однократно ионизованного гелия показало, что у ионной компоненты нет большой направленной скорости[1]. Второе предположение трудно подвергнуть прямой экспериментальной проверке. Поэтому в настоящее время его нельзя исключить.

Изучение энергетического баланса плазмы представляет собой один из наиболее важных элементов данной экспериментальной программы. Измерение диамагнитного эффекта позволяет определить запас энергии. Принимая определенный закон распределения температуры по сечению плазменного шнура и используя данные радиоинтерферометрического измерения концентрации, можно из измерений диамагнетизма найти среднюю величину суммарной температуры ионов и электронов, т.е. величину $\overline{T}_e + \eta\overline{T}_i = \overline{T}$, где η — отношение концентрации ионов к концентрации электронов (для водородной плазмы $\eta = 1$). Фактически выбор конкретного вида функции $T(r)$ слабо сказывается на вычисляемой средней температуре. В данных вычислениях обычно принимается параболический закон зависимости $T(r)$.

В качестве независимого метода оценки электронной температуры можно использовать результаты измерений спектра мягкого рентгеновского излучения плазмы. Такие измерения были проведены на установке ТМ-3 при концентрации плазмы порядка нескольких единиц 10^{12} см$^{-3}$ [3]. Спектр рентгеновского излучения определялся путем амплитудного анализа импульсов в пропорциональном газовом счетчике. Оценки электронной температуры на основе таких измерений находятся в хорошем согласии с результатами определения T_e по диамагнитному эффекту (в исследованных режимах $\overline{T}_i \ll \overline{T}_e$, и поэтому $\overline{T} \approx \overline{T}_e$).

Для измерения ионной температуры применяется метод, основанный на анализе энергетического спектра атомов перезарядки [4]. Этот метод,в принципе, дает возможность определить максимальную величину ионной температуры в шнуре.

На рис. 2 показан энергетический спектр протонов в установке Т-3 для различных моментов времени. На рис. 3 приведены также результаты измерения энергетического спектра дейтонов на установке Т-3 (верхняя кривая снята при $H_z = 32$ кэ, $J = 120$ кА и $\overline{n}_e \sim 4 \cdot 10^{13}$ см$^{-3}$). В опытах с дейтериевой плазмой при достаточно больших значениях силы тока J индикатором ионной температуры может служить также нейтронное излучение плазмы.

---

[1] Измерения проводились при разрядах в водороде с добавкой гелия.

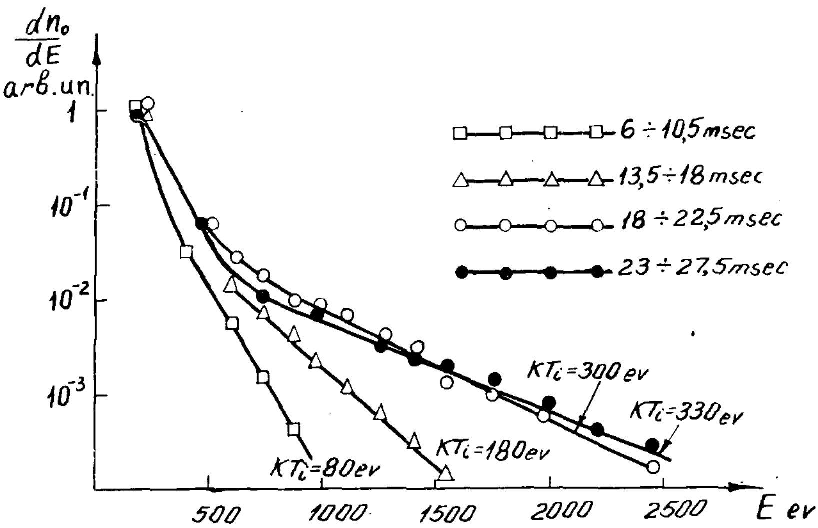

Рис.2. Энергетический спектр протонов в зависимости от времени, измеренный на установке Т-3.

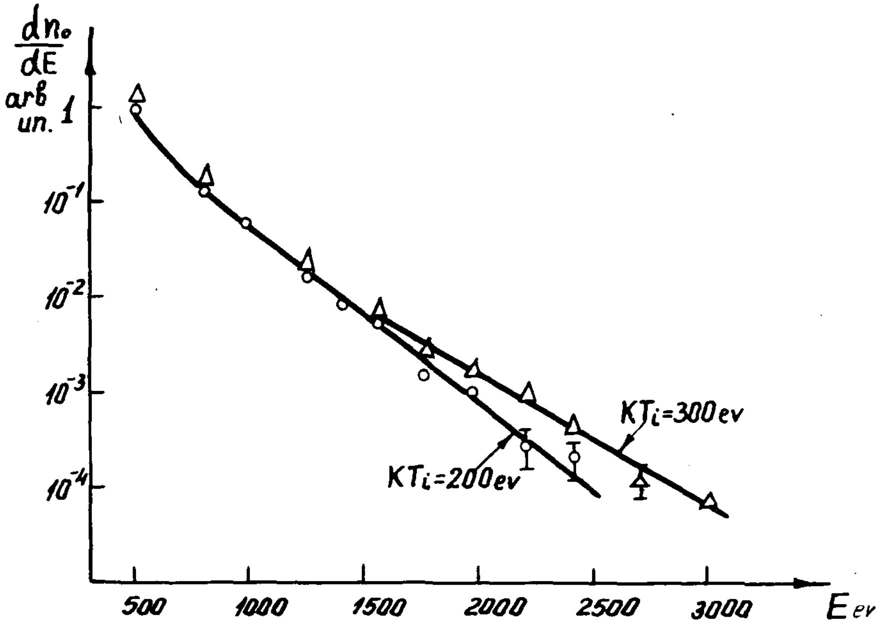

Рис.3. Энергетический спектр дейтонов, измеренный на установке Т-3. Нижняя кривая снята при тех же условиях разряда, что и верхняя кривая на рис.2.

Используя осциллограммы тока, напряжения и показания магнитных зондов, определяющих положение шнура в разрядной камере, совместно с данными о величине диамагнитного эффекта и радиоинтерферометрическими измерениями концентрации, можно составить систему уравнений процессов, с помощью которых, кроме суммы температур $\overline{T}$ и средней электронной концентрации, определяются также радиус шнура a и средняя величина электропроводности $\overline{\sigma}$. Решение уравнений процесса производится с помощью электронной вычислительной машины, и все указанные выше параметры вычисляются в функции от времени. На рис. 4 приведены результаты таких расчетов для типичного режима разряда на установке Т-3. Видно, что сумма температур $\overline{T}$ возрастает в течение процесса. Этот рост продолжается и после того, как ток в плазме проходит через максимальное значение.

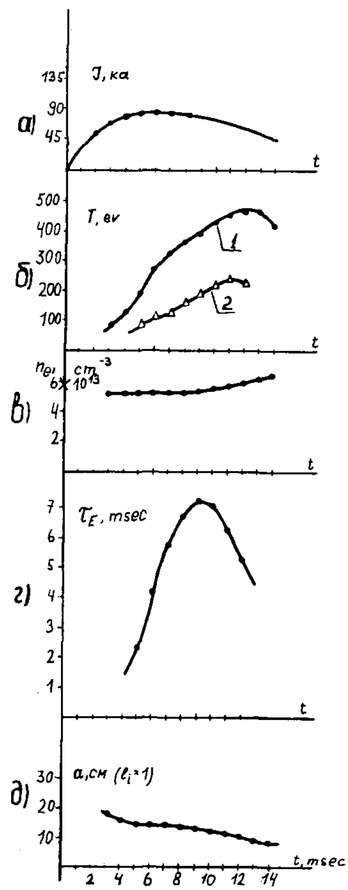

Рис.4. Результаты расчета параметров плазменного шнура на установке Т-3 при H_z = 30 кэ:

а) ток разряда (осциллограмма);

б) кривая 1 – сумма температур $\overline{T}$, вычисленная по диамагнитному эффекту, кривая 2 – температура электронов, вычисленная по электропроводности, $\overline{T}_{eo}$;

в) концентрация электронов;

г) время удержания энергии τ_E ;

д) радиус шнура, вычисленный в предположении параболического распределения плотности тока по сечению шнура.

Если электропроводность плазмы определяется кулоновскими соударениями, то справедлива классическая формула $\sigma = AT_e^{3/2}$, где A для исследуемого интервала значений n_e и T_e и чистой водородной плазмы можно установить равным $\approx 1 \cdot 10^7$ (σ – в единицах CGSE, T_e – в градусах). Исходя из этого соотношения, можно попытаться определить из электропроводности среднюю по сечению плазменного шнура электронную температуру. В дальнейшем она обозначается $\overline{T}_{e\sigma}$. Изменение $\overline{T}_{e\sigma}$ во время процесса показано на рис. 4 (кривая b2). Видно, что в рассматриваемом частном случае (при относительно высокой электронной концентрации n_e) отношение $\overline{T}/\overline{T}_{e\sigma}$ находится в пределах от 2 до 2,3 (при статистической ошибке в измерении отношения около 20-30%). При больших энерговкладах на частицу, т.е. при больших значениях E/n_e, где E – напряженность электрического поля в плазме, величина $\overline{T}/\overline{T}_{e\sigma}$ резко возрастает.

На установке ТМ-3 величина отношения $\overline{T}/\overline{T}_{e\sigma}$ измерялась в широких пределах изменений параметров. Оказалось, что все экспериментальные результаты, полученные как при различных параметрах разряда, так и в различные моменты времени на протяжении одного процесса, можно представить в виде одной зависимости, если использовать некоторые безразмерные координаты. Такая зависимость приведена на рис. 5. По оси ординат отложена величина $(\overline{T}_e/\overline{T}_{e\sigma})^{3/2}$, равная σ/σ_{exp}, где σ – электропроводность, вычисленная с помощью классической формулы при температуре T_e, σ_{exp} – измеренное значение электропроводности. По оси абсцисс отложено отношение E/E_c, где E_c – так называемая критическая напряженность поля по Дрейсеру ($E_c \approx 10^{-8} n_e/T_e$).

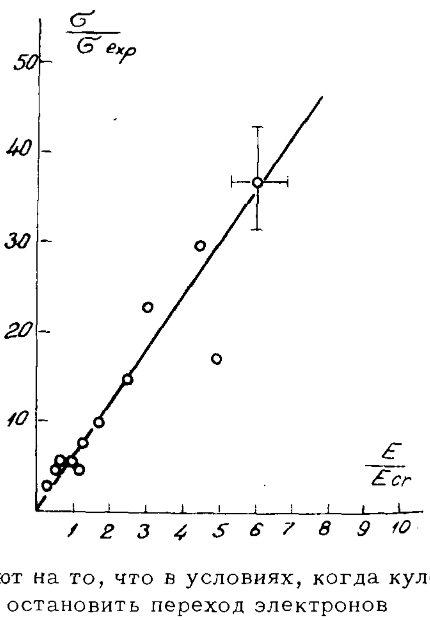

Рис.5. Зависимость отношения σ/σ_{exp} от E/E_{cr} для установки ТМ-3.

Полученные результаты указывают на то, что в условиях, когда кулоновские столкновения не в состоянии остановить переход электронов плазмы в режим непрерывного ускорения электрическим полем, появляется другой механизм торможения, обусловленный, по-видимому, взаимодействием ускоренных электронов с волнами в плазме. С этим процессом связано нагревание электронов плазмы за счет перехода энергии продольного движения электронов в энергию поперечного движения. Теория этого эффекта была развита Кадомцевым и Погуце [5]. Результаты измерений на установке ТМ-3 можно рассматривать как качественное подтверждение этой теории. Энергетический баланс плазменного шнура может быть представлен в форме следующего равенства:

$$\frac{dW}{dt} = Q - \frac{W}{\tau_E} \qquad (3)$$

Здесь W – запас энергии в плазме, Q – тепло, выделяемое током в единицу времени, τ_E – интегральная характеристика термоизоляции плазмы, которая обычно называется временем удержания энергии в плазме. В величине τ_E учитываются все возможные виды потерь энергии: за счет диффузии, теплопроводности, излучения и перезарядки (а также, в принципе, за счет ухода частиц вдоль силовых линий при резонансном разрушении магнитных поверхностей). Исследования энергетического баланса плазмы на установках Т-3 и ТМ-3 при различных значениях начальных параметров разряда и в разные моменты времени привели к установлению следующих фактов:

1. Время удержания энергии τ_E в режимах разряда с $n_e > 1 \cdot 10^{13}$ см$^{-3}$ в пределах точности измерений не зависит от напряженности продольного магнитного поля, если обеспечена магнитогидродинамическая устойчивость шнура по Крускалу-Шафранову.

2. Величина τ_E, измеренная в определенный момент времени после начала разрядного импульса, возрастает с увеличением концентрации (см. рис.6).

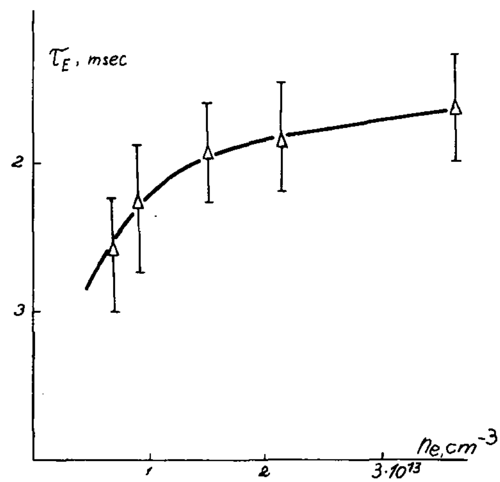

Рис.6. Зависимость времени удержания энергии τ_E от концентрации электронов n_e на установке Т-3. Режим разрядов: J_{max} = 40 ка; H_z = 25 кэ.

3. При $n_e > 1 \cdot 10^{13}$ см$^{-3}$ и сохранении формы импульса разрядного тока величина τ_E возрастает с ростом силы тока в плазме в пределах соблюдения критерия Крускала-Шафранова (рис.7).

Сделана попытка путем обработки экспериментального материала, накопленного при работе на установках Т-3 и ТМ-3, найти эмпирические формулы, связывающие τ_E с основными параметрами, характеризующими состояние плазмы. Одна из полученных эмпирических формул имеет вид:

$$\frac{a^2 n_e \overline{T}^{3/2}}{\tau_E} = \text{const} \qquad (4)$$

Она удовлетворительно описывает экспериментальные данные в интервале изменения n_e от $2\cdot10^{12}$ до $5\cdot10^{13}$ см$^{-3}$, $K\bar{T}$ – от 100 до 1000 эв, a – от 8 до 17 см и H_z – от 12 до 35 килоэрстед при $q(a)>2$. Учитывая, что τ_E представляет условную интегральную характеристику теплового баланса, а также принимая во внимание, что термоизоляция плазмы может в большой степени определяться условиями на границе плазменного шнура и может зависеть также от распределения тока по сечению шнура, мы не должны переоценивать значение найденного соотношения между τ_E, n_e и T_e. Для интерполяционных оценок при установившемся режиме можно пользоваться также формулой $\tau_E \sim a^2 H_J n^{\alpha}$, где $\alpha \sim 1/3$.

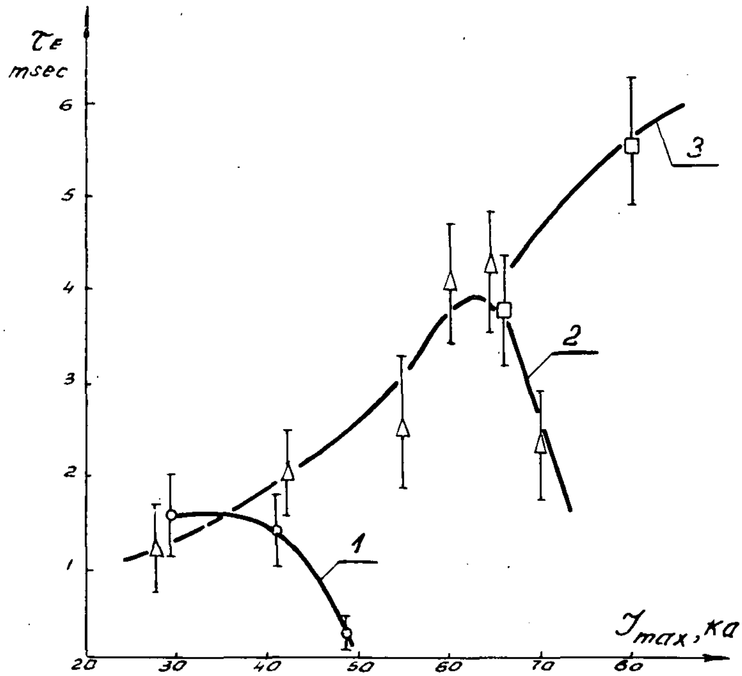

Рис.7. Зависимость τ_E от силы разрядного тока на установке Т-3 при $n_e \approx 2\cdot10^{13}$ см$^{-3}$:
Кривая 1 – H_z = 17 кэ;
Кривая 2 – H_z = 26 кэ;
Кривая 3 – H_z = 34 кэ.

При интерпретации эмпирических формул необходимо помнить, что в Токамаке плазма удерживается только во время протекания тока, т.е. в данных условиях нет возможности изучать термоизоляцию плазмы без непрерывного выделения в ней энергии. Поэтому трудно определить, является ли улучшение термоизоляции следствием повышения температуры плазмы или наоборот. Однако, независимо от того, как интерпретировать найденную зависимость τ_E от основных физических параметров процесса, следует признать установленным, что термоизоляция плазмы в установках Токамак, в исследованных нами режимах, не ослабляется с ростом температуры. Поэтому величины потерь энергии при достаточно высокой температуре оказываются во много раз меньшими, чем те значения, кото-

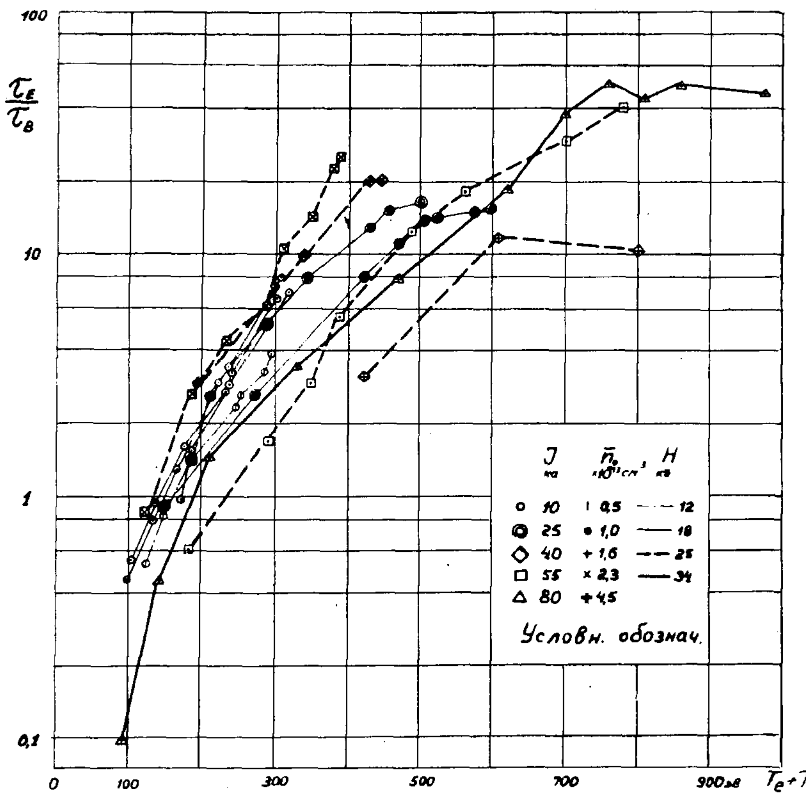

Рис.8. Зависимость отношения τ_E к бомовскому времени τ_B от $\overline{T}$.

рые вычисляются на основе применения формулы Бома. На рис.8 для широкого интервала изменений основных параметров процесса даны отношения измеренных значений τ_E к величинам τ_B, вычисленным по формуле $\tau_B = 3a^2eH_z/cKT_e$. Величины τ_E/τ_B приводятся здесь в функции температуры. Видно, что при $K\overline{T} \approx 10^3$ эв отношение τ_E/τ_B превышает 30. Вместе с тем, при $K\overline{T} < 100$ эв, это отношение может быть значительно ниже единицы. На несоответствие между результатами измерений на установках Токамак и формулой Бома было впервые указано на конференции в Калэме в 1965 году [6], и это было встречено тогда с заметным чувством недоверия. В настоящее время уже никто не высказывает удивления по этому поводу, так как вера в универсальный характер фомулы Бома полностью подорвана.

В настоящее время мы не располагаем экспериментальными данными, с помощью которых можно было бы однозначно разъяснить вопрос о механизме потерь энергии в установках Токамак. Однако, можно сделать замечания по этому поводу.

Измерения ионнной температуры показывают, что она быстро возрастает с увеличением n_e (см. рис.9) [4]. Наблюдаемая зависимость T_i от n_e, а также результаты измерений ионной температуры в водороде и дейтерии при одинаковых значениях n_e, J, H_z, находятся в согласии с предположением о кулоновском характере передачи энергии от электронов к ионам. При этом предположении можно заключить, что потери энергии из плазмы не связаны, в основном, с ионной компонентой плазмы. В справедливости этого вывода можно убедиться на основе следующих рассуждений.

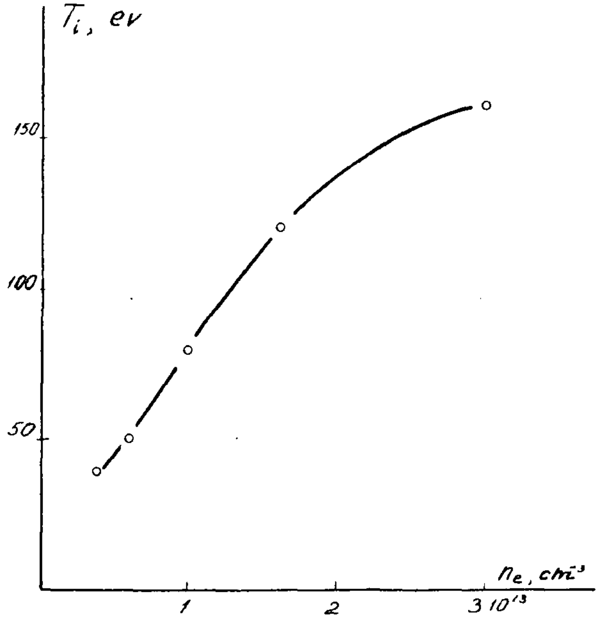

Рис.9. Зависимость T_i от n_e для установки ТМ-3.

Допустим, что основная часть энергии, уходящей из плазмы, переносится ионами. В таком случае в установившемся режиме для водородной плазмы должно было бы соблюдаться условие:

$$\frac{3}{2}K\frac{T_e+T_i}{\tau_E} = 1{,}2\cdot 10^{-17} n_e \frac{T_e - T_i}{T_e^{3/2}} \tag{5}$$

В правой части этого равенства стоит величина энергии, которую ион получает в единицу времени в результате столкновений с электронами. Из (5) следует:

$$T_e^{3/2} < 6\ 10^{-2} n_e \tau_E \tag{6}$$

Пусть $n_e = 1\cdot 10^{13}$ см$^{-3}$ и $\tau_E = 1{,}5\cdot 10^{-3}$ сек. При этом величина электронной температуры, согласно неравенству (6), должна быть значительно меньше $1\cdot 10^6$ град., т.е. KT_e ниже 100 эв. Вместе с тем, при указанных значениях n_e и τ_E получаем на установке ТМ-3 плазму с температурой до 1000 эв. Поэтому потеря энергии через ионную компоненту не может принадлежать к числу основных механизмов, ответственных за охлаждение плазмы в установках Токамак (в исследованных до сих пор режимах опытов). В дополнение к этому следует отметить, что потери энергии на излучение и перезарядку также не могут объяснить наблюдаемую скорость охлаждения плазмы. По-видимому, должен существовать некоторый механизм аномальной теплопередачи, который осуществляется за счет энергии электронной компоненты. Баланс числа частиц в плазменном шнуре, в принципе, легче интерпретировать, так как при этом нужно принимать во внимание только два главных процесса: потерю частиц благодаря диффузии и появление новых частиц вследствие ионизации нейтральных атомов, проникающих в плазму из окружающего пространства (десорбция со стенок). Уравнение баланса, учитывающее оба указанных процесса, имеет вид:

$$\frac{dn}{dt} = -\frac{n}{\tau_n} + I \qquad (7)$$

где n – концентрация частиц в плазменном шнуре, τ_n – среднее время жизни заряженной частицы, I – приток частиц извне (число актов ионизации в единицу времени). В этом уравнении n и dn/dt определяются из интерферограммы. Для того чтобы найти время жизни частиц, нужно знать также число актов ионизации I.

Подавляющая часть потока нейтральных частиц, проникающих в плазменный шнур, обусловлена десорбцией водорода со стенок. Поэтому можно попытаться определить величину I путем измерения абсолютной величины интенсивности свечения линий бальмеровской серии. На опыте были выбраны линии H_α и H_β. Измерения абсолютной интенсивности излучения линий были проведены на установке ТМ-3. На рис.10 приведены данные радиоинтерферометрических измерений и измерений абсолютной интенсивности излучения линии H_α для типичного режима работы установки ТМ-3. Поскольку в любом элементе объема число актов ионизации k_i и число актов излучения k_r пропорционально концентрации нейтральных частиц, то между ними должно существовать соотношение $k_i = \xi k_r$, где коэффициент пропорциональности ξ является функцией электронной температуры T_e и электронной концентрации n_e. В.А.Абрамовым, Э.И.Куз-

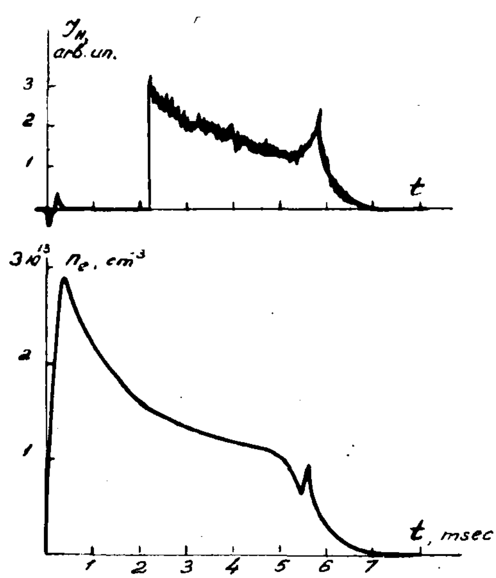

Рис.10. Осциллограмма свечения линии H_α и временной ход концентрации электронов в процессе разряда на установке ТМ-3. Режим разряда: $p_0 = 4{,}6\cdot10^{-4}$ мм рт.ст. H_2, $J = 40$ ка, $H_z = 24$ кэ. Регистрация линии H_α начинается иа третьей миллисекунде.

нецовым и В.И.Коганом было выполнено вычисление величины ξ как функции от T_e и n_e в предположении, что нейтральные частицы, проникающие в плазму извне, в основном, представляют собой атомарный водород. Из указанных вычислений следует, что в довольно широком интервале изменения T_e коэффициент ξ изменяется лишь незначительно. Зависимость ξ от n_e при $n_e \approx 10^{13}$ также довольно слабая. Поэтому, усредняя соотношение $k_i = \xi k_r$ по объему плазмы, можно записать, что $I = \xi J_H$, где J_H — полное число квантов данной линии, излученных плазмой, а величина ξ берется для средних значений T_e и n_e. При измерении на установке ТМ-3 были определены значения I и найдены средние времена жизни частиц в плазме. На рис.11 приведены для сравнения результаты вычисления τ_n с учетом и без учета притока нейтральных частиц в плазму. Как показывают эти данные, учет величины I в уравнении баланса изменяет величину τ_n не более чем на 20%. Некоторый элемент произвола в эту поправку вносит сделанное предположение о том, что в плазму проникает только атомарный водород.

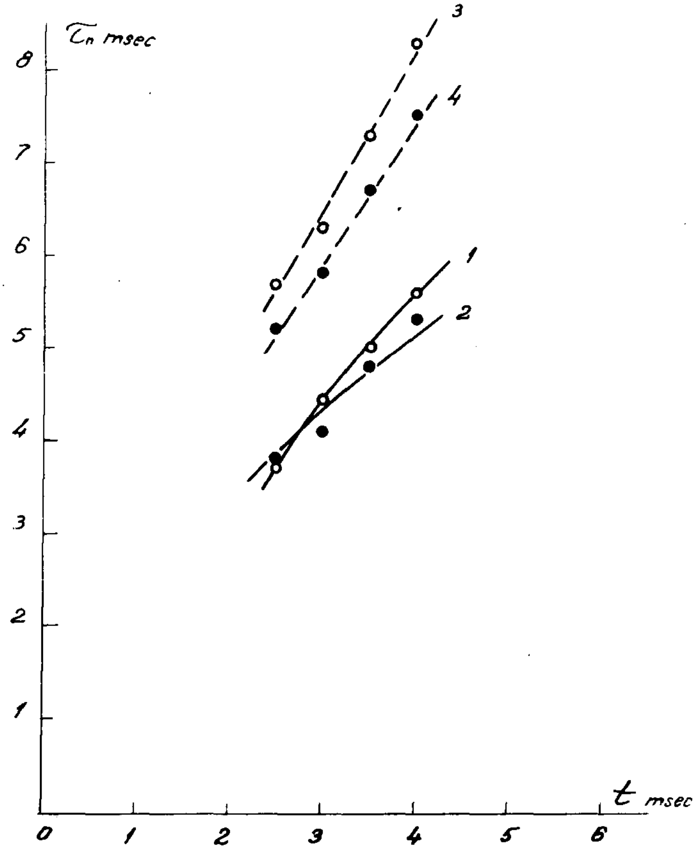

Рис.11. Изменение времени жизни частиц τ_n в течение разряда. Режим разряда: $p_0 = 4{,}6 \cdot 10^{-4}$ мм рт. ст. H_2, J= 40 ка, H_z = 24 кэ.
Кривая 1 — вычисление τ_n с учетом притока нейтральных атомов по линии H_α;
Кривая 2 — то же для линии H_β;
Кривые 3 и 4 — величины τ_n без учета притока электронов для режимов, в которых измерялись линии H_α и H_β соответственно.

Из данных, приведенных на рис.12 и 13, следует, что время жизни заряженных частиц в плазменном шнуре на установке ТМ-3, вычисленное с поправкой на приток извне, превышает среднее время сохранения энергии τ_E более чем вдвое и в оптимальных режимах достигает 6 мсек.

На установке Т-3 аналогичные измерения не производились. Можно только заметить, что, если соотношение между $\tau_п$ и τ_E приблизительно одинаково для обеих установок Токамак, то в оптимальных режимах эксперимента на Т-3 длительность удержания частиц должна составлять не менее 20-30 мсек (что соответствует отношению $\tau_п/\tau_B$ от 50 до 70).

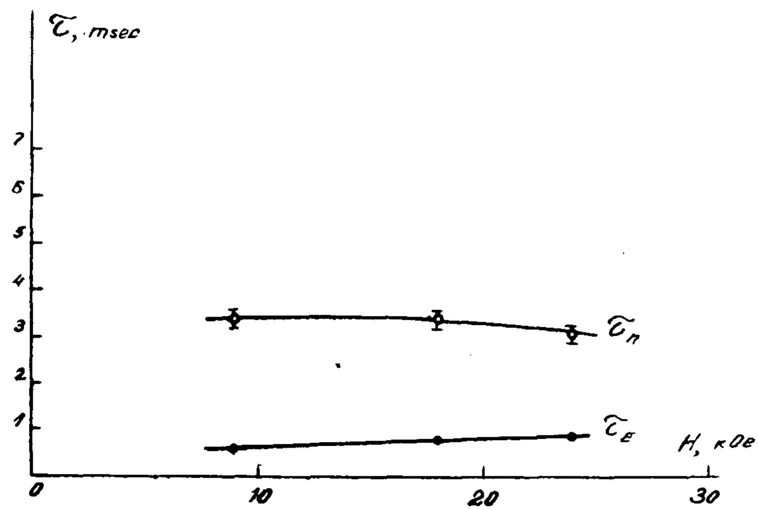

Рис.12. Зависимость времен удержания от продольного магнитного поля H_z для момента разряда t= 4 мсек. Режим разряда: $p_0 = 3{,}7\cdot 10^{-4}$ мм рт. ст. H_2, J = 16 ка.

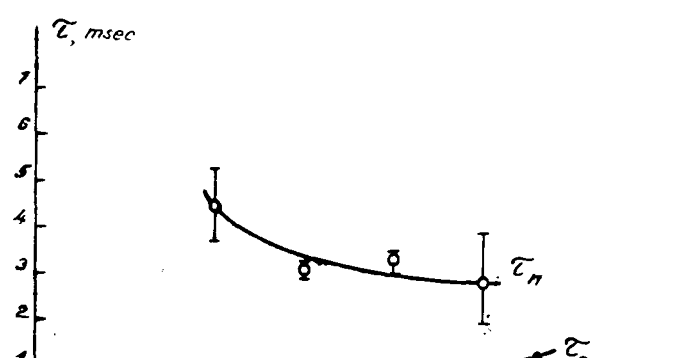

Рис.13. Зависимость времени удержания от начального давления водорода в камере p_0, для момента разряда t = 4 мсек. Режим разряда: J= 40 ка, H_z = 24 кэ.

ВЫВОДЫ

1. Для обеспечения гидромагнитной устойчивости в установках Токамак условие $q > 1$ должно выполняться в каждой точке объема плазменного шнура.

2. В режимах с $q(a) > 2$-3 и $\overline{T}_e/\overline{T}_{e\sigma} \approx 1$ интегральная характеристика термоизоляции плазмы τ_E :

   а) не зависит от напряженности продольного магнитного поля H_z при соблюдении условия Крускала-Шафранова;

   б) возрастает с увеличением концентрации плазмы;

   в) возрастает с увеличением силы тока в плазме.

3. Термоизоляция плазмы в установках Токамак не ослабляется с ростом температуры.

4. При больших значениях температуры τ_E значительно (до 50 раз) отличается от характерной величины времени удержания, определяемой известной формулой Бома.

5. В большинстве режимов потери энергии, в основном, связаны с электронной компонентой плазмы и не могут быть объяснены аномальными ионными потерями, если принять кулоновский механизм передачи энергии от электронов к ионам.

6. Предположение о кулоновском механизме теплообмена подтверждается измерением зависимости τ_i от параметров разряда в водороде и дейтерии.

7. Измерения скорости ионизации нейтральных атомов водорода и временного хода концентрации электронов плазмы позволяют определить время удержания заряженных частиц. Оно оказывается в несколько раз больше времени удержания энергии τ_E .

Основное заключение, к которому мы сейчас приходим, анализируя экспериментальную информацию, полученную при работе по программе Токамак, можно сформулировать следующим образом.

В системах Токамак при достаточно высокой напряженности продольного магнитного поля можно в настоящее время получать плазму с концентрацией порядка $5 \cdot 10^{13}$ см$^{-3}$, электронной температурой до 0,7 кэв, максимальной ионной температурой до 0,5 кэв (в водороде). При этом плазменный шнур обладает очень высокой устойчивостью (время жизни заряженных частиц в оптимальных условиях превышает, по-видимому, 20 мсек).

Полученные результаты позволяют с уверенностью рассчитывать на то, что в рамках программы Токамак удастся продвинуться значительно дальше и выйти на уровень ионной температуры порядка киловольта и выше при временах удержания энергии, измеряемых десятыми долями секунды.

ЛИТЕРАТУРА

[1] АРЦИМОВИЧ, Л.А., МИРНОВ, С.В., СТРЕЛКОВ, В.С., Атомная энергия 17 (1964) 170.

[2] ШАФРАНОВ, В.Д., Атомная энергия 13 (1962) 521.

[3] ЩЕГЛОВ, Д.А., ЖЭТФ, Письма в редакцию 6 (1967) 949.

[4] АФРОСИМОВ, В.В., ПЕТРОВ, М.П., ЖТФ 37 (1967) 1995.

[5] КАДОМЦЕВ, Б.Б., ПОГУЦЕ, О.П., ЖЭТФ 53 (1967) 2025.

[6] АРЦИМОВИЧ, Л.А., и др., Plasma Physics and Controlled Nuclear Fusion Research 2 (Conf. Proc., Culham, 1965), Vienna, IAEA, 1965, p. 595.

DISCUSSION

B. COPPI: The Tokamak experiments, aimed at evaluating the electron temperature and revealing the presence of anomalous resistivity, have been followed by similar ones on the Princeton stellarator. The latter experiments, in which the temperature was precisely measured by laser light scattering, have shown the existence of anomalous resistivity at very low electric fields much smaller than the runaway threshold and, since it was possible to observe the transition from normal to anomalous resistivity, they have led to studies of the nature of this anomalous resistivity by observing the dependence of its onset on various physical parameters.

We propose an explanation of the stellarator experiments which does not involve the effects of runaway electrons. This differs from the one which is mentioned in your paper and which relates to the high electric field regimes of the Tokamak experiments. What is missing now is a detailed interpretation which will link the two regimes.

S.D. FANCHENKO: Perhaps I might be allowed to make a comment in this connection. In 1963, our group found anomalous resistivity in a toroidal discharge with very strong electric fields (far in excess of the Dreicer field). This anomalous resistivity was due to ion sound excitation at lower fields and to Langmuir oscillation excitation at higher fields.

These results are supported by the work of Hamberger and collaborators at Culham (paper CN-24/D-8).

L.A. ARTSIMOVICH: With regard to Mr. Coppi's comment, it is possible that our interpretation is not the correct one – we were simply pointing to one of the possibilities indicated by Kadomtsev.

In this connection I should like to point out that the relationship between the measured and theoretical electrical conductivity in our low-density plasma is also a function of the magnetic field strength. The presence of a magnetic field in the system is therefore of considerable importance. If one plotted a curve showing this relationship as a function of the ratio of Larmor radius to Langmuir frequency, one would find substantial differences between the experimental and theoretical values when the Larmor radius was significantly greater than the Langmuir frequency. This is a further indication of the importance of the longitudinal magnetic field; if there is no strong longitudinal magnetic field, the difference between the experimental and theoretical values is relatively small.

In this sense, the regime in our experiments differs from that obtained in the experiments of Lavoisky, Fanchenko and co-workers, who did not employ strong magnetic fields. Nevertheless, Kadmotsev's theory provides an interpretation of the dependence in question.

J.L. TUCK: You ascribe the continued emission of H_α, H_β from your hot (T_i = 0.5 - 1.0 keV) plasmas to the entry of cold hydrogen desorbing from the walls. In the case of our Scylla θ-pinch, we find such an effect to be more a symptom of enhanced diffusion; and a θ-pinch is, after all, not unlike a short segment of a Tokamak. No H_α or H_β emission from our plasma is observed when conditions favour stability, although our plasma is hotter (T_i = 2 - 5 keV) and denser, and the walls are much nearer (3.5 cm). On the other hand, when the θ-pinch is deliberately allowed to become unstable (by lowering the temperature), a wave of plasma comes in from the wall. A flux of cold hydrogen into a Tokamak plasma, where the ion temperature is determined by transfer from Joule-heated electrons, might have a most complex effect - even raising the ion temperature. Do you have any idea of the magnitudes of any such effects?

L.A. ARTSIMOVICH: The ion temperature is not limited by the gas flux from the walls, but by ohmic heating of the electrons and by heat transfer from the electrons to the ions. The role of atoms penetrating from outside the system is secondary.

G. VON GIERKE: Could you say something about the fluctuations in Tokamak devices?

L.A. ARTSIMOVICH: Unfortunately, I cannot. Fluctuation measurements have not yet played an important part in our experimental work.

ОБ УСТОЙЧИВОСТИ ПЛАЗМЫ В ЗАМКНУТЫХ СИСТЕМАХ

Л.С.СОЛОВЬЕВ, В.Д.ШАФРАНОВ и
Э.И.ЮРЧЕНКО
ИНСТИТУТ АТОМНОЙ ЭНЕРГИИ им.И.В.КУРЧАТОВА,
МОСКВА,
СССР

Abstract — Аннотация

PLASMA STABILITY IN CLOSED SYSTEMS. The authors investigate the stability of closed plasma configurations using the general geometric criterion of local stability developed by Mercier and co-workers. To render in an explicit form the equilibrium configuration parameters on which the stability of the configuration depends, the general geometric criterion is transformed by expanding with respect to the deviation from the magnetic axis. In the resulting criterion the terms describing the ballooning mode and plasma stabilization through deepening of the magnetic well due to the toroidal magnetic surface displacement associated with the plasma pressure are rendered explicitly. For circular magnetic surface cross-sections these terms cancel out exactly and the stability condition is found to be independent of the plasma pressure. In the case of elliptical magnetic surface cross-sections, the effect of the ballooning instability predominates over deepening of the magnetic well. In this case the plasma pressure, which is critical for stability, is limited. The resulting stability criterion is applied to a number of toroidal systems. The authors consider the conditions for stability in closed systems with a spatial magnetic axis and in systems with a circular magnetic axis of the two-turn and three-turn stellarator type. They also consider the effect of the longitudinal current on plasma stability in such systems. In closed magnetic traps without longitudinal current, plasma stabilization is relatively simple in the presence of a shallow magnetic well. The critical value of $\beta = 2p/B^2$ may exceed the relative depth of the vacuum magnetic well $\Phi V''/V'$ by an order of magnitude. When there is a longitudinal current, there appear additional factors that affect the stable containment of the plasma.

ОБ УСТОЙЧИВОСТИ ПЛАЗМЫ В ЗАМКНУТЫХ СИСТЕМАХ. Исследуется устойчивость замкнутых плазменных конфигураций. При этом используется общегеометрический критерий локальной устойчивости Мерсье и др. Для выделения в явном виде параметров равновесной конфигурации, от которых зависит ее устойчивость, общегеометрический критерий преобразуется методом разложения по отклонению от магнитной оси. В полученном таким образом критерии явно выделены слагаемые, описывающие балонную моду неустойчивости и стабилизацию плазмы за счет углубления магнитной ямы из-за тороидального смещения магнитных поверхностей, связанного с давлением плазмы. Для круглых сечений магнитных поверхностей эти слагаемые в точности компенсируются, и условие устойчивости оказывается не зависящим от давления плазмы. В случае эллиптических сечений магнитных поверхностей эффект балонной неустойчивости преобладает над углублением магнитной ямы. В этом случае критическое для устойчивости давление плазмы ограничено.

Полученный критерий устойчивости применяется к некоторым конкретным тороидальным системам. Рассматриваются условия устойчивости в замкнутых системах с пространственной магнитной осью, а также в системах с круговой магнитной осью типа двухзаходного и трехзаходного стеллараторов. Рассматривается также влияние продольного тока на устойчивость плазмы в таких системах. В замкнутых магнитных ловушках без продольного тока стабилизация плазмы сравнительно легко осуществляется при наличии неглубокой магнитной ямы. Критическое значение $\beta = 2p/B^2$ может на порядок превышать относительную глубину вакуумной магнитной ямы $\Phi V''/V'$. При наличии продольного тока появляются дополнительные факторы, влияющие на устойчивое удержание плазмы.

1. ПОСТАНОВКА ЗАДАЧИ

Состояние теории гидромагнитной устойчивости плазмы в приближении бесконечной проводимости в настоящее время позволяет произвести детальный анализ особенностей замкнутых систем для удержания плазмы. Мы будем иметь ввиду системы, не содержащие проводников с током внутри плазмы, т.е. системы типа стелларатора и Токамака, но не левитрона и октуполя. При этом мы ограничимся рассмотрением однородных конфигураций, у которых магнитное поле на оси постоянно, а сечения магнитных поверхностей вблизи оси представляют собой эллипсы с постоянным отношением полуосей. Общей основой для рассмотрения таких систем может служить предложенный Мерсье [1] метод разложения по расстоянию от магнитной оси.

Как известно, равновесие и устойчивость плазмы зависят от числа вращения силовых линий $\mu = d\chi/d\phi$, от производной $\mu' = d\mu/d\phi$, характеризующей перекрещенность силовых линий (шир) и от производной $V'' = d^2V/d\phi^2$, характеризующей крутизну усредненой магнитной ямы (при $V'' < 0$) или магнитного бугра ($V'' > 0$). Здесь через χ и ϕ обозначены поперечный и продольный потоки магнитного поля, а через V - объём, ограниченный магнитной поверхностью, через которую проходит поток ϕ. Все упомянутые величины, вообще говоря, не постоянны. Расчеты систем, обладающих симметрией, показывают, что значения μ, μ', V'' на крайних магнитных поверхностях вблизи сепаратрисы могут сильно отличаться от значений этих величин в центральной части системы (в окрестности магнитной оси). Однако в реальных системах, не обладающих строгой симметрией, магнитные поверхности на периферии, как раз в той области , где μ, μ', V'' изменяются круто, оказываются разрушенными. Пригодной для удержания плазмы является лишь центральная часть системы. Это обстоятельство и оправдывает применение к расчету тороидальных систем с достаточно плавной магнитной осью метода разложения в окрестности магнитной оси. Независимо от способов создания системы для удержания плазмы её свойства в основном зависят от значений μ, μ', V'' в окрестности магнитной оси.

Для определения μ и V'' в окрестности оси достаточно задания шести геометрических параметров, зависящих от длины дуги s , отсчитываемой вдоль магнитной оси

$$k(s),\ \varkappa(s),\ \varepsilon(s),\ \delta(s),\ q_1(s),\ q_2(s)$$

Здесь k и $\varkappa$ - кривизна и кручение магнитной оси ; ε параметр эллиптичности,связанный с отношением полуосей ℓ_1 , ℓ_2 , эллиптического сечения магнитных поверхностей вблизи магнитной оси :

$$\varepsilon = (\ell_1^2-\ell_2^2)/(\ell_1^2+\ell_2^2) \tag{1}$$

Наряду с ε удобно использовать также параметр η , связанный с ε соотношением

$$e^{\eta} = \sqrt{(1+\varepsilon)/(1-\varepsilon)} \tag{2}$$

$\delta(s)$ - угол между главной нормалью к оси и малой полуосью эллипса, так что $\delta(L)/2\pi = n$ определяет число оборотов, которое совершает сечение магнитной поверхности при прохождении вдоль замкнутой системы с длиной оси L ; параметры $q_1(s)$, $q_2(s)$ характеризуют асимметрию сечения магнитных поверхностей (третью гармонику), которая наиболее заметно проявляется при удалении от оси.

Производная μ' при $\varepsilon \neq 0$ требует для своего определения знания ещё двух параметров, характеризующих четвертую гармонику магнитных поверхностей. Однако в критерий устойчивости μ' входит в более высоком приближении разложения по отклонению от оси. Поэтому для описания равновесия и устойчивости плазмы в окрестности магнитной оси достаточно задания указанных выше шести параметров. В методе разложения по степеням расстояния ρ от магнитной оси это соответствует ограничению третьим приближением разложения.

При расчете устойчивости плазмы в замкнутых системах необходимо принимать во внимание искажение магнитных поверхностей, связанное с наличием плазмы. При конечном давлении плазменный шнур подобно накаченному балону стремится растянуться. При этом внутренние магнитные поверхности оказываются смещенными наружу относительно внешних поверхностей в сторону более слабого тороидального магнитного поля. Благодаря этому возникает углубление магнитной ямы. Этого углубления достаточно для компенсации существенной доли эффекта балонной неустойчивости замкнутого плазменного шнура. Такая самостабилизация плазмы в замкнутой системе весьма существенно повышает критическое отношение давления плазмы к давлению магнитного поля $\beta = 2p/B^2$, при котором плазма устойчива (в приближении идеальной гидродинамики) благодаря наличию вакуумной магнитной ямы.

Для расчета искажений магнитных поверхностей под влиянием плазмы необходимо задавать внешние граничные условия. В условиях большинства существующих экспериментальных тороидальных систем в качестве граничных условий необходимо задание внешнего магнитного поля. Однако решение задачи с таким условием требует расчета магнитного поля вне области, занятой плазмой, что при некруглой форме сечения магнитных поверхностей представляет собой достаточно сложную задачу. Более проста для решения задача с другим условием, соответствующим наличию идеально проводящего кожуха профилированного сечения,фиксирующего форму крайней внешней магнитной поверхности. Мы ограничимся здесь именно этой постановкой задачи.

В третьем приближении разложения по расстоянию ρ от магнитной оси, достаточном для описания основных характеристик равновесной конфигурации и параметров, влияющих на устойчивость, уравнение семейства магнитных поверхностей имеет вид

$$\psi = \frac{B_0}{\sqrt{1-\varepsilon^2}}\left[\rho^2(1+\varepsilon\cos 2u)+\rho^3(\alpha_1\cos u+\alpha_2\sin u+\alpha_3\cos 3u+\alpha_4\sin 3u\right]=\mathrm{const} \quad (3)$$

Здесь B_0 - магнитное поле на магнитной оси, взятой за координатную ось, u - фаза эллиптического сечения вблизи оси

$$u = \theta + s \quad (4)$$

θ - азимутальный угол, отсчитываемый от главной нормали к магнитной оси ; α_1 , α_2 , α_3 , α_4 - параметры третьего приближения магнитных поверхностей. Эти параметры связаны двумя соотношениями, так что независимыми являются только два из них [2].

Сечения $s = \mathrm{const}$ магнитных поверхностей представляют собой семейство несимметричных замкнутых кривых. Целесообразно ввести понятие геометрической оси заданной магнитной поверхности. Определим её так, чтобы в системе координат, связанной с геометрической осью и деформированной так, чтобы эллипсы вблизи оси превратились в "окружности" $\rho_0 = const$, уравнение магнитной поверхности в третьем приближении не содержало бы гармоник $\cos u$, $\sin u$:

$$\psi = \rho_0^2 + 2\left(q_1 e^{-1/2}\cos 3u + q_2 e^{1/2}\sin 3u\right)\rho_0^3 = const = a^2 \tag{5}$$

В недеформированной системе координат, связанной с геометрической осью, это уравнение имеет тогда вид

$$\psi = \frac{B_0}{\sqrt{1-\varepsilon^2}}\left\{(1+\varepsilon\cos 2\tilde{u})\tilde{\rho}^2 + q_1\left[(2-\varepsilon)\cos 3\tilde{u} + 3\varepsilon\cos\tilde{u}\right]\tilde{\rho}^3 + \right.$$
$$\left. + q_2\left[(2+\varepsilon)\sin 3\tilde{u} + 3\varepsilon\sin\tilde{u}\right]\tilde{\rho}^3\right\} = B_0 a^2 \tag{6}$$

где $\tilde{\rho}$, $\tilde{u}$ – расстояние от оси и фаза сечения магнитной поверхности в новой системе координат.

Одну из этих поверхностей примем за поверхность идеально проводящего кожуха

$$\psi(\tilde{\rho}, \tilde{u}, s) = B_0 a_k^2 \tag{7}$$

Задав кожух, мы тем самым фиксируем параметры ε, q_1, q_2. Заданным значениям этих параметров соответствует семейство кожухов, сечения которых изображены на рис.1. Значение ψ на сепаратрисе при $q_2 = 0$ равно

$$\psi_s = B_0 a_s^2 = B_0 e^{1/2}/27 q_1^2 \tag{8}$$

Для определения магнитных поверхностей $\psi = B_0 a^2$ при заданном кожухе достаточно знать смещения $\Delta_1 = \xi_1 a^2$, $\Delta_2 = \xi_2 a^2$ их геометрических осей по нормали и бинормали к магнитной оси. Эти смещения однозначно выражаются через заданные параметры ε, q_1, q_2 с помощью уравнений равновесия [3]. Параметры q_1, q_2, ξ_1, ξ_2 связаны с α_1, α_2, α_3, α_4 соотношениями

$$\begin{aligned} \alpha_1 &= 3\varepsilon q_1 - (2+\varepsilon)e^{1/2}\xi_1, \\ \alpha_2 &= 3\varepsilon q_2 - (2-\varepsilon)e^{-1/2}\xi_2, \\ \alpha_3 &= (2-\varepsilon)q_1 - \varepsilon e^{1/2}\xi_1, \\ \alpha_4 &= (2+\varepsilon)q_2 - \varepsilon e^{-1/2}\xi_2. \end{aligned} \tag{9}$$

Заметим, что в выражение для V'' параметры α_1, α_2, α_3, α_4 входят в комбинациях $(2-\varepsilon)\alpha_1 - 3\varepsilon\alpha_3$, $(2+\varepsilon)\alpha_2 - 3\varepsilon\alpha_4$. Как видно из формул (7) первая из них равна $-4(1-\varepsilon)e^{1/2}\xi_1$, а вторая $-4(1+\varepsilon)e^{1/2}\xi_2$. Таким образом, магнитная яма в соответствии с качественными соображениями зависит непосредственно от смещения магнитных поверхностей. Поскольку в смещении есть часть, зависящая от давления плазмы, то и в магнитной яме можно выделить чисто геометрическую часть и часть, связанную с давлением плазмы

$$V'' = V_0'' + V_p'' \tag{10}$$

В свою очередь геометрическая часть магнитной ямы состоит из вакуумной магнитной ямы и ямы, созданной током, текущим по плазме.

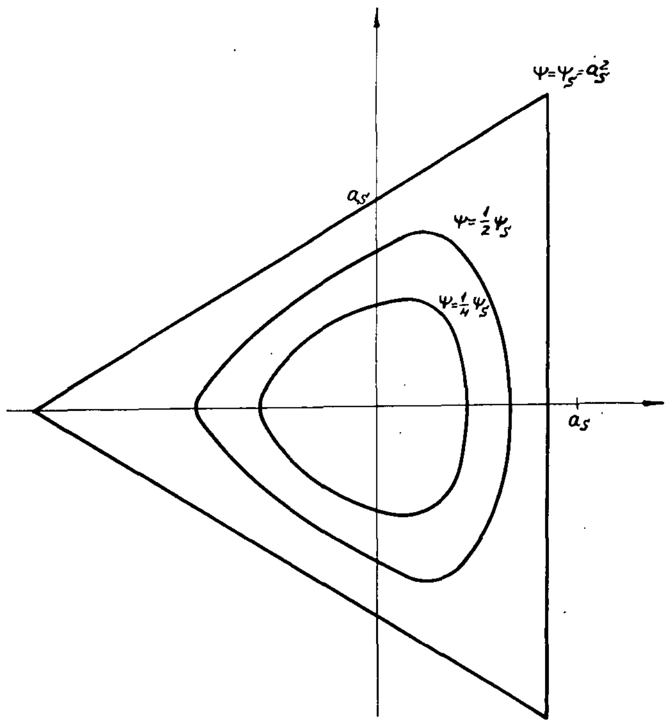

Рис.1. Семейство возможных сечений кожуха с заданным параметром $q_1 = 1^{\eta/2}/3\sqrt{3}\,a_s$ в "скругленной" системе координат. При переходе к нормальной системе координат следует ось у растянуть, а ось х сжать в $\sqrt[4]{(1+\epsilon)(1-\epsilon)}$ раз.

Общий критерий гидромагнитной устойчивости плазмы относительно локальных возмущений [4 – 7] состоит в основном из четырех членов [8, 9].

$$S + C + B + W \geq 0 \tag{11}$$

Первый член $S \sim \mu'^2$ характеризует стабилизирующую роль шира, второй $C \sim p'$ – перестановочную неустойчивость, связанную с продольным током, третий $B \sim p'^2 k^2$ – балонную моду неустойчивости, связанную с непостоянством кривизны силовых линий, четвертый

$W \sim p'V''$ – стабилизирующую роль магнитной ямы. В окрестности оси слагаемое S выпадает, так как оно более высокого порядка малости по ρ, чем остальные слагаемые.

В соответствии с разделением магнитной ямы на две части можно написать

$$W = W_0 + W_p \tag{I2}$$

Расчет показывает, что при $\varepsilon = 0$ углубление магнитной ямы, связанное с давлением плазмы, полностью компенсирует балонную неустойчивость $(W_p = -B)$. В общем случае, $\varepsilon \neq 0$,

$$W_p + B \sim -\varepsilon^2 p'^2 \tag{I3}$$

Таким образом,роль балонной моды неустойчивости уменьшается с уменьшением ε . Однако в ряде систем для удержания плазмы глубина вакуумной магнитной ямы также падает с уменьшением ε . Поэтому существуют оптимальные значения параметра ε , дающие максимальное критическое значение β по устойчивости в конкретных тороидальных ловушках.

2. СИСТЕМЫ С КРУГЛЫМ СЕЧЕНИЕМ МАГНИТНЫХ ПОВЕРХНОСТЕЙ

Рассмотрим сначала системы, в которых внешнее магнитное поле есть поле соленоида, ось которого представляет собой замкнутую кривую с кривизной $k(s)$ и кручением $\varkappa(s)$. При $\varkappa = 0$ для обеспечения равновесия в таких системах необходим ток. При $\varkappa \neq 0$ равновесие возможно и без продольного тока, однако, при этом плазма неустойчива. Продольный ток приводит к смещению магнитных поверхностей в область ослабленного тороидального магнитного поля и созданию усредненной "вакуумной" ямы ($V_0'' < 0$), обеспечивающей гидромагнитную устойчивость плазмы. Критерий устойчивости плазмы в таких системах при однородной плотности тока и параболическом распределении давления получен и исследован в работах Мерсье [1] .Возможно обобщение этого критерия на случай произвольных распределений давления и тока по радиусу плазменного шнура. Соответствующий критерий выглядит как обобщение критерия Сайдема на случай замкнутого плазменного шнура [8]:

$$\frac{1}{4}\left(\frac{\mu'}{\mu}\right)^2 + \frac{2p'}{\tau B_s^2}\,\frac{\mu_J^2}{\mu^2}\,(1-F) \geq 0 \tag{I4}$$

Здесь $\mu = \mu_J + \mu_0$, μ_J - число вращения, обусловленное током

$$\mu_J = \frac{B_\theta L}{B_s 2\pi r} \equiv \frac{1}{q}, \tag{15}$$

а μ_0 - число вращения, связанное с кручением магнитной оси

$$\mu_0 = -\frac{L}{2\pi}\int_0^L \varkappa\, ds \equiv -\frac{\varkappa_0 L}{2\pi} \tag{16}$$

Функция F связана с вакуумной магнитной ямой

$$F = -\frac{B_0^2 L}{4\pi \mu_J^2} V_0'' = \frac{1}{\mu_J^2}\sum_{n=-\infty}^{\infty} \frac{\mu_J - \mu_0 - n}{\mu_J + \mu_0 + n} |k_n|^2 \left(\frac{L}{2\pi}\right)^2 \tag{17}$$

В этой формуле k_n - фурье-компоненты относительной кривизны

$$K(s) = k(s) \exp -i\left(\varkappa_0 s - \int_0^s \varkappa\, ds\right) \tag{18}$$

Заметим, что

$$\sum_{n=-\infty}^{\infty} |k_n|^2 = \overline{k^2} = \frac{1}{L}\int_0^L k^2 ds \tag{19}$$

При $J = 0$ критерий (14) принимает вид

$$\frac{L}{4}\left(\frac{\mu'}{\mu}\right)^2 + \frac{2p'}{r B_s^2}\frac{\overline{k^2}}{\varkappa_0^2} \geqslant 0 \tag{20}$$

Устойчивость при $p' < 0$ возможна только за счет шира ($\mu' \neq 0$).

При $J \neq 0$ коэффициент F может превышать единицу, так что критерий устойчивости выполнится даже при $\mu' = 0$. В частности, для плазменного шнура с круговой магнитной осью (Токамак),когда $k_n L/2\pi = \delta_{n0}$, $\mu_0 = 0$, коэффициент $F = 1/\mu_J^2$, и условие устойчивости выполняется в области достаточно малых токов [1]

$$\mu_J^2 < 1 \tag{21}$$

В системах типа рейстрека эта область устойчивости сужается и исчезает, когда длина прямолинейных участков сравнивается с длиной закруглений. Но зато появляются дополнительные области устойчивости (щели Мерсье). Диаграмма устойчивости в рейстреке приведена на рис.2.

На рис.3 приведена диаграмма устойчивости в восьмёрке Спитцера, составленной из дуг одинакового радиуса. Характерным здесь является то, что попасть в область устойчивости при наращивании тока нельзя, не проходя области неустойчивости. Этим восьмёрка с током принципиально отличается от системы Токамак.

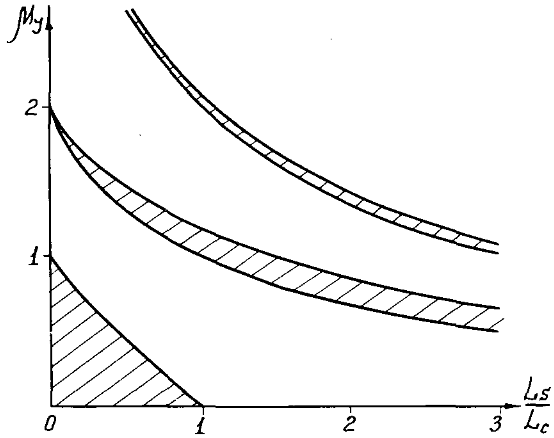

Рис.2. Диаграмма устойчивости плазмы в Токамаке, имеющем форму рейстрека: L_s, L_c – длины прямого и закругленного участков, соответственно, $\mu_J = 1/q = LB_\Theta/2\pi aB_0$.

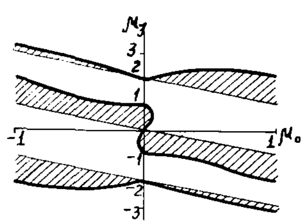

Рис.3. Диаграмма устойчивости плазмы в восьмерке Спитцера при наличии продольного тока. μ_0 – поделенный на 2π собственный угол вращательного преобразования, связанный с геометрическим углом восьмерки α соотношением $\mu_0 = 1 - 2\alpha/\pi$, $\mu_J = LB_\Theta/2\pi aB_0$. Из рисунка видно, что центральная область устойчивости соответствует примерно условию $-1 < \mu < 0$ при $\mu_J < 0$ и условию $0 < \mu < 1$ при $\mu_J > 0$; ($\mu = \mu_0 + \mu_J$).

3. СИСТЕМЫ С НЕКРУГЛЫМ СЕЧЕНИЕМ МАГНИТНЫХ ПОВЕРХНОСТЕЙ

В системах с некруглым сечением магнитных поверхностей расчёт устойчивости нетрудно произвести в предположении, соответствующем примерно однородному распределению тока и параболическому распределению давления плазмы [1], [7]. Системы с принципиально некруглым сечением - это системы стеллараторного типа, в которых вращательное преобразование создаётся поперечным мультипольным магнитным полем. Однако и в тех системах, где вращательное преобразование создается за счёт тока или кручения оси, деформация сечений магнитных поверхностей может способствовать углублению ямы и, тем самым, повышению устойчивости плазмы.

Сначала мы рассмотрим именно такие системы, так как они могут обладать осевой и винтовой симметрией.

а) Токамак с некруглым сечением кожуха

Условие устойчивости плазмы в осесимметричном Токамаке может быть записано в виде [3, 7]

$$\mu_J^2 < f_1(\varepsilon) + q_1 f_2(\varepsilon) - \beta_J f_3(\varepsilon) \qquad (22)$$

где

$$f_1 = 1 - \frac{3\varepsilon}{2}\,\frac{1+\varepsilon}{2+\varepsilon}\,, \quad f_2 = 12\varepsilon\,\frac{1-\varepsilon}{2+\varepsilon}\,,$$

$$f_3 = \frac{4\varepsilon^2\sqrt{1-\varepsilon^2}}{(1+\varepsilon)(2+\varepsilon)^2\left[1+\sqrt{1-\varepsilon^2} - \varepsilon^2/(2+\varepsilon)\right]} \qquad (23)$$

$$\mu_J = \frac{j_0 R}{2B_0}\sqrt{1-\varepsilon^2}\,, \quad \beta_J = 2\langle p\rangle/(J/2\pi a)^2 \qquad (24)$$

Последнее слагаемое в (22) характеризует роль балонной моды неустойчивости.

Из критерия устойчивости видно, что если при $\varepsilon = 0$ (круглое сечение) плотность тока ограничена условием

$$j_0^2 R^2/4B_0^2 < 1 \qquad (25)$$

то при $\varepsilon \neq 0$, $q_1 \neq 0$ предел тока может стать выше (особенно при $\varepsilon < 0$, $q_1 < 0$, что соответствует сплюснутому в направлении оси симметрии сечению с заострением, направленном внутрь тора). Например, при ε = 0,8 , $q_1 R$ = 0,5

$$j_0^2 R^2/4B_0^2 < 1{,}56 - 0{,}2\beta_J \qquad (26)$$

а при ε = - 0,8 , $q_1 R$ = - 0,5

$$j_0^2 R^2/4B_0^2 < 23{,}4 - 14\beta_J \qquad (27)$$

Для нагрева плазмы выгодно иметь большое j^2 , однако если при этом сечение сильно сплюснуто, то возникают большие градиенты температуры и сильные потери тепла, зависящие от $\nabla^2 T$. При фиксированной тороидальности кожуха (т.е. при заданном отношении горизонтальной полуоси ℓ_t к радиусу R)

$\nabla^2 T \sim T(1+\ell_r^2/\ell_z^2)/\ell_r^2 = 2T/\ell_r^2(1+\varepsilon)$. Таким образом, температура будет тем выше, чем больше $j^2(1+\varepsilon)$. Оптимальным с точки зрения нагрева плазмы будет условие, при котором максимальна безразмерная функция

$$Q = \frac{R^2 j^2}{4B_0^2}(1+\varepsilon) = \frac{M_J^2}{1-\varepsilon} = \frac{f_1}{1-\varepsilon} + \frac{12\varepsilon}{2+\varepsilon} q_1 - \beta_J \frac{f_3}{1-\varepsilon} \qquad (28)$$

Для круглого сечения кожуха ($\varepsilon = 0$) Q = I. Графики зависимости функций $f_1/(1-\varepsilon)$ и $f_3/(1-\varepsilon)$ показаны на рис.4. На рис.5 (кривая "а") представлена функция Q при чисто

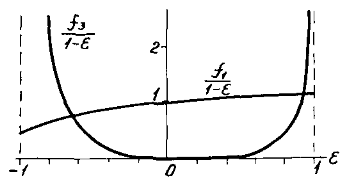

Рис.4. Зависимость функций $f_1/(1-\epsilon)$ и $f_3/(1-\epsilon)$ от ϵ. Первая из них характеризует магнитную яму в Токамаке чисто эллиптического сечения, вторая – роль баллонной моды.

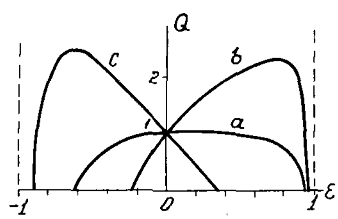

Рис.5. Зависимость функции Q, характеризующей влияние формы кожуха на нагрев плазмы в Токамаке, от ϵ при $\beta_J = 1$ и разных значений параметра ассимметрии сечения q_1:
a) $q_1R = 0$; b) $q_1R = 0{,}5$; c) $q_1R = -0{,}5$.

эллиптическом сечении кожуха ($q_1 = 0$) с β_J = I. Как видно из этого рисунка, Q имеет максимальное значение при круглом сечении ($\varepsilon = 0$). В случае несимметричных сечений величина Q изменяется на $12\varepsilon q_1/(2+\varepsilon)$. С ростом $|q_1|$ уменьшается средний радиус сепаратрисы семейства кожухов с заданным значением q_1 и, соответственно, отношение поперечного размера плазменного шнура к его длине. Поэтому следует выбрать q_1 не слишком большим. Для достаточно крутого тора с q_1R= 0,5 и q_1R = – 0,5 функция $Q(\varepsilon)$ показана на том же рис.5 (кривые b , c). Здесь имеется два максимума при $\varepsilon = \pm$ 0,7. Значение Q в этих максимумах в два с небольшим раза превышает значение Q при ε = 0. Форма сечения кожухов с $q_1R = 0,5$; $\varepsilon = 0,7$ и $q_1R = -0,5$, $\varepsilon = -0,7$ показана на рис.6. Действительный же выигрыш, связанный с изменением формы кожуха, зависит от закона, по которому реальный коэффициент теплопроводности связан с температурой плазмы и не может быть оценен в рамках данной работы.

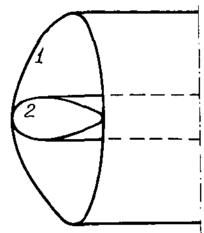

Рис.6. Возможная форма кожуха в Токамаке, соответствующая кривым b и с на рис.5.

б) Пространственная система с магнитной ямой

Пространственной системой мы для краткости будем называть систему, ось которой представляет собой пространственную кривую, обладающую кривизной k и кручением $\varkappa$. Пространственные системы с круглым сечением магнитных поверхностей, как следует из раздела 2, имеют магнитную яму только при наличии продольного тока конечной величины. Добавление второй и третьей гармоник магнитного поля позволяет создать пространственную систему, обладающую магнитной ямой и в отсутствие тока [2]. Простейшей пространственной системой является система с винтовой симметрией, имеющая вид винтового соленоида. Если винтовой соленоид обвивает тор, кривизна которого мала по сравнению с кривизной винта, то мы получаем замкнутую систему, мало отличающуюся от системы с винтовой симметрией.

Условие устойчивости плазмы в системе с винтовой симметрией выглядит так ($R = L/2\pi = 1/\sqrt{k^2+\varkappa^2}$)

$$\frac{R^2}{a^2}\beta < \frac{\mu^4(1+e^4)}{2(1-\sqrt{1-\varepsilon^2})}\left[\frac{\mu_J-\mu_0}{\mu_J+\mu_0} + \frac{3\varepsilon}{4} - \frac{(2+\varepsilon)(\mu_J^2+\varepsilon^2\varkappa^2R^2)}{2(1-\varepsilon)k^2R^2} + 6\varepsilon\frac{q_1}{k}\right] \qquad (29)$$

В отсутствие продольного тока ($\mu_J = 0$) стабилизация возможна, если произведение $\varepsilon q_1/k$ превышает некоторое критическое значение. На рис.7 показана зависимость $\beta R^2/a^2$ от ε

при фиксированном значении q_1 для винтового плазменного шнура с углом подъема 45° ($k = \varkappa$). Следует иметь ввиду, что средний радиус сечения плазменного шнура можно считать независимым от q_1 и равным среднему радиусу сечения кожуха $a = a_k$ лишь при $q_1 a_k < e^{1/2}/3\sqrt{3}$, когда размер сепаратрисы семейства магнитных поверхностей с данным q_1 больше размера кожуха. При фиксированных размерах системы при увеличении q_1 сепаратриса попадает внутрь камеры. В этом случае макси-

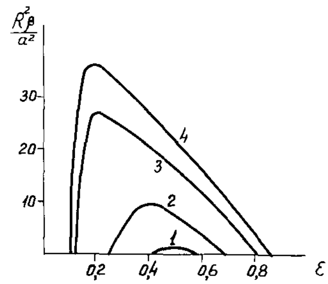

Рис.7. Зависимость критического по устойчивости давления плазмы от ϵ и q_1 в винтовом плазменном шнуре:
1 – q_1R = 0,3; 2 – q_1R = 0,5; 3 – q_1R = 1,0; 4 – q_1R = 1,2.

мальный размер шнура ограничен размером сепаратрисы $a_{max} = e^{1/2}/3\sqrt{3}q_1$.Поэтому несмотря на то, что функция $\beta R^2/a^2$ растет с увеличением q_1, граничное значение β в данной системе сначала растет с q_1, достигает максимума при $q_1 \simeq e^{1/2}/3\sqrt{3}\,a_k$ и затем падает. Зависимость β_{max} от q_1 при фиксированной тороидальности R/a_k представлена на Рис.8. Как видно из этого рисунка, при соответствующем выборе параметров системы ограничения на давление плазмы с точки зрения гидромагнитной устойчивости практически нет ($\beta_{max} \sim 1$). Заметим, что глубина ямы при этом невелика (~ 4 %).

В системе с вакуумной магнитной ямой можно пропускать ток, не нарушая равновесия и устойчивости плазмы. Если ток имеет такое направление, что числа вращений μ_J и μ_0 одного знака, то он оказывает стабилизирующее действие. Малый обратный ток ($|\mu_J| < |\mu_0|$, $\mu_J \mu_0 < 0$) оказывает дестабилизирующее действие. Его максимально допустимая величина зависит от глубины вакуумной магнитной ямы. Достаточно сильный обратный ток, при котором изменяется знак суммарного вращательного преобразования, ($|\mu_J| > |\mu_0|$), оказывает также стабилизирующее действие.

Диаграмма устойчивости винтового плазменного шнура с максимальной вакуумной магнитной ямой ($\varepsilon \approx 0{,}3$; $q_1^R \approx 1$) представлена на рис.9. Как видно из рисунка, по плазме можно пропускать также и переменный ток, не выходя из области устойчивости.

Рассмотренная пространственная система с винтовой симметрией может служить грубой моделью замкнутых систем типа пространственных восьмёрок.

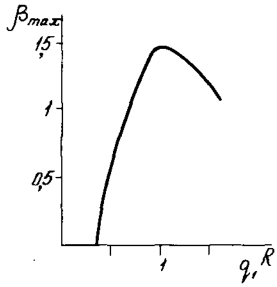

Рис.8. Зависимость критического давления от q_1 при оптимальном значении ϵ в винтовой системе с фиксированной тороидальностью $R/a_k = 4$.

в) Двухзаходный стелларатор

Под двухзаходным стелларатором обычно подразумевается система, в которой поперечное магнитное поле изменяется по закону $\exp 2i(\theta + h\zeta)$, где $\zeta = 2\pi s/L$. Благодаря эффекту кривизны, которая входит с множителем $\exp(\pm i\theta)$ к любому двухзаходному стелларатору всегда подмешиваются гармоники поля $\exp i(\theta + 2h\zeta)$ и $\exp i(3\theta + 2h\zeta)$. При этом параметры q_1 , q_2 магнитных поверхностей имеют вид

$$q_1 = q_{10} \cos h\zeta \quad , \quad q_2 = q_{20} \sin h\zeta \tag{30}$$

Оказывается, что примесные гармоники даже при малой амплитуде довольно сильно влияют на форму магнитной оси и на крутизну магнитной ямы. Искусственным добавлением примесных гармоник можно существенно расширить возможности двухзаходного стелларатора. Поэтому будем считать амплитуды q_{10} , q_{20} произвольными.

Чувствительность магнитной ямы к полю третьей гармоники усложняет применение критерия устойчивости к конкретным установкам. Поэтому мы ограничимся здесь выяснением принципиального вопроса о возможностях двухзаходного стелларатора, полагая, что магнитная ось при наличии плазмы является окружностью радиуса R. Так как оптимальные условия устойчивости достигаются при малой эллиптичности, то мы запишем критерий устойчивости двухзаходного стелларатора, полагая $\varepsilon^2 \ll 1$:

$$\frac{R^2}{q^2}\beta < \frac{h^2\varepsilon^2}{2}\left[\frac{3}{2} - h^2\varepsilon^2 + \frac{4(q_{10}+q_{20})R}{\varepsilon}\right] \tag{31}$$

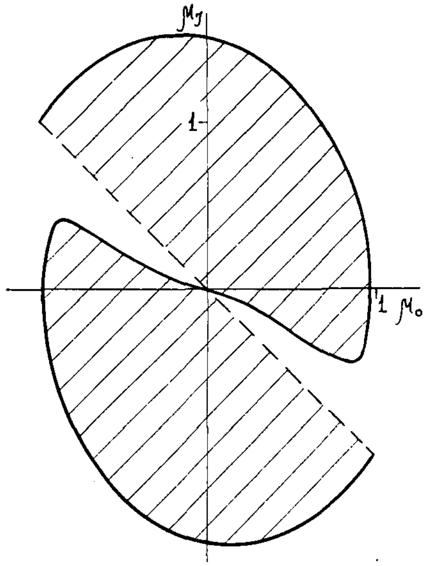

Рис.9. Диаграмма устойчивости винтового плазменного шнура с максимальной вакуумной магнитной ямой ($\epsilon \approx 0{,}3$); $q_1 R \approx 1$) при наличии продольного тока ($\mu_J \neq 0$).

Из этого условия следует, что в случае чисто эллиптических сечений магнитных поверхностей ($q_{10} = q_{20} = 0$) плазма устойчива лишь при $\varepsilon^2 < 3/2h^2$. При этом максимальное критическое давление равно $\beta_{max} = 9q^2/32R^2$ и достигается оно при $\varepsilon^2 = 3/4h^2$.

Добавление третьей гармоники существенно изменяет условие устойчивости. На рис.10 приведены графики функции $R^2\beta/q^2$ для стелларатора с $h = 7$ при $q_{10} = q_{20} = q$. На рис.11 изображена зависимость β_{max} от параметра третьей гармоники при фиксированной тороидальности кожуха $R/q_k = 6$. Эта кривая построена аналогично кривой рис.8 для винтового плазменного шнура с той разницей, что размер шнура принимается равным половине размера сепаратрисы, поскольку в системах, не обладающих симметрией магнитные поверхности вблизи сепаратрисы разрушены. Как и в случае винтового шнура, в двухзаходном стеллараторе при соответствующем выборе его параметров нет ограничения по давлению плазмы. Однако определенным практическим недостатком его является отмечавшаяся выше чувствительность к весьма малым изменениям формы равновесной конфигурации.

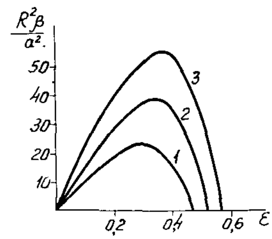

Рис.10. Зависимость критического по устойчивости давления плазмы от ϵ и q_1 в двухзаходном стеллараторе с n= 7:
1 – q_1R= 0,5; 2 – q_1R= 0,75; 3 – q_1R= 1,0.

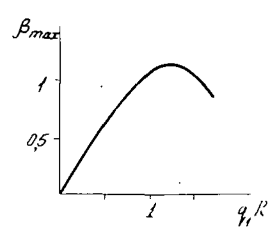

Рис.11. Зависимость критического давления от q_1 при оптимальном значении ϵ в двухзаходном стеллараторе с n= 7, $R/a_к$= 6.

г) Резонансный характер трехзаходного стелларатора

Трехзаходный стелларатор выпадает из общей схемы рассмотрения, использованной в настоящей работе, из-за равенства нулю угла прокручивания на магнитной оси ($\mu(0) = 0$). Случай μ = 0 относится к числу резонансных. Малое поперечное однородное магнитное поле $B_\perp$ приводит к существенному искажению конфигурации в окрестности магнитной оси. Характер этого искажения легко уяснить, рассмотрев задачу о влиянии поперечного поля $B_y = B_\perp$ на семейство круглых магнитных поверхностей $r^2 = x^2 + y^2 = const$. Для m -заходного стелларатора $\mu = \mu_1 \cdot r^{2(m-2)}$. В этом случае, как нетрудно показать, возмущенные магнитные поверхности описываются уравнением

$$\Psi = \int \mu \, d r^2 + \frac{2B_\perp}{B_0} R x =$$

$$= \frac{\mu_1}{m-1}\left[r^{2(m-1)} + \frac{2(m-1) R B_\perp}{\mu_1 B_0} x \right] = const.$$

Магнитная ось этого семейства имеет координаты $x = x_0$, $y = 0$, где

$$x_0^{2m-3} = -\frac{R B_\perp}{\mu_1 B_0}$$

Из-за корневой зависимости смещения от возмущающего поля ($x_0 \sim B_\perp^{1/(2m-3)}$) величина смещения даже при малом возмущении оказывается достаточно большой. Вблизи оси сечения эллиптические, причем параметр эллиптичности и отношение полуосей равны, соответственно

$$\varepsilon = \frac{m-2}{m-1} \quad , \quad \frac{\ell_y}{\ell_x} = \sqrt{2m-3}$$

Искажение начальной формы магнитных поверхностей перестает сказываться лишь при значительном удалении от оси $r \gg |x_0|$.

В трехзаходном стеллараторе ($m = 3$) отношение полуосей эллипсов вблизи оси равно $\ell_y/\ell_x = \sqrt{3}$. На рис.12 показана форма магнитных поверхностей при $\mu = 400\, r^2/R^2$, $B_\perp/B_0 = 10^{-4}$. Как видно, уже простая модель показывает очень большую чувствительность приосевой области к возмущающему однородному полю.

Численные расчеты магнитных поверхностей в трехзаходном стеллараторе [10, 11] подтверждают эти заключения. Более детальные расчеты показывают, что отношение полуосей не постоянно. По мере продвижения вдоль магнитной оси оно слегка меняется. При этом сам эллипс слегка покачивается, но не проворачивается вокруг оси полностью.

Путем тщательного регулирования можно добиться обращения однородного поперечного магнитного поля на оси в нуль. Однако уже незначительные изменения параметров плазмы (например, давления) вновь приводят к искажению приосевой области. В случае трехзаходного стелларатора поперечное поле связано с давлением соотношением $B_\perp \sim \beta B_0 / \mu_{max}$.

Это резонансное свойство трехзаходного стелларатора требует специального подхода к расчету критического давления плазмы с точки зрения гидромагнитной устойчивости.

ПРИЛОЖЕНИЕ I

В работах [4 – 6] был получен общегеометрический необходимый критерий устойчивости равновесной идеально проводящей плазмы, относительно локальных возмущений. При этом под локальными возмущениями понимаются малые смещения плазмы относительно положения равновесия, имеющие произвольную форму на рассматриваемой магнитной поверхности и малую протяженность в направлении нормали к магнитной поверхности.

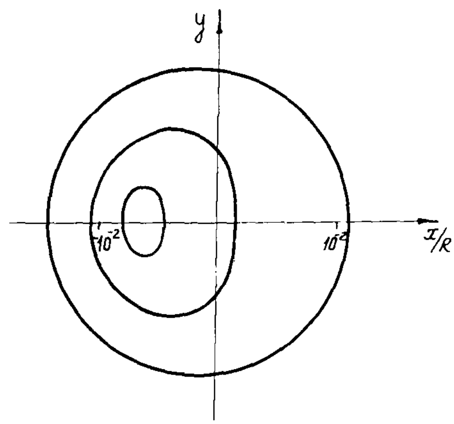

Рис.12. Иллюстрация неустойчивости приосевой области трехзаходного стелларатора на модели цилиндрически-симметричной конфигурации с $\mu = \mu_1 r^2$. Принято $\mu_1 = 400/R^2$, где R – радиус воображаемого тора. Возмущающее поперечное поле составляет $10^{-2}\%$ от продольного ($B_\perp/B_0 = 10^{-4}$).

Для равновесной плазмы, описываемой уравнениями

$$\nabla p = [\vec{j}\vec{B}] , \quad \vec{j} = \mathrm{rot}\,\vec{B} , \quad \mathrm{div}\,\vec{B} = 0 \tag{I.1}$$

соответствующий критерий устойчивости можно представить в виде [7]:

$$\frac{1}{4} S^2 + F - G \geq 0 \tag{I.2}$$

где

$$F = -\Omega \left\langle \frac{\vec{B}^2}{|\nabla V|^2} \right\rangle + S \left\langle \frac{\vec{j}\vec{B}}{|\nabla V|^2} \right\rangle \tag{I.3}$$

$$G = \left\langle \frac{\vec{j}^2}{|\nabla V|^2} \right\rangle \left\langle \frac{\vec{B}^2}{|\nabla V|^2} \right\rangle - \left\langle \frac{\vec{j}\vec{B}}{|\nabla V|^2} \right\rangle^2 \tag{I.4}$$

Величины Ω и S, также как и давление p, являются поверхностными функциями, зависящими только от текущего объема V, заключенного внутри рассматриваемой магнитной поверхности. Они выражаются через производные по объему V от продольного и азимутального магнитных потоков ϕ и χ и продольного и азимутального токов J и I

$$p' = I'\phi' - J'\chi', \quad \Omega = I'\phi'' - J'\chi'', \quad S = \chi'\phi'' - \phi'\chi'' \tag{I.5}$$

угловыми скобками обозначено усреднение по объему, заключенному между двумя соседними магнитными поверхностями, или, что эквивалентно, усреднение по замкнутой магнитной силовой линии, лежащей на рациональной магнитной поверхности

$$\langle f \rangle = \frac{d}{dV}\int f\, d\tau = \oint f \frac{dl}{B} \Big/ \oint \frac{dl}{B} \tag{1.6}$$

Член $S^2/4$ характеризует стабилизацию широм, величина F - описывает стабилизирующее действие магнитной ямы ($\min \bar{B}$), а величина G описывает дестабилизацию, связанную с конечным давлением плазмы.

Как показано в работе [9], критерий (I.2) без члена $S^2/4$ является достаточным условием устойчивости для плазмы, удерживаемой квазиоднородным магнитным полем. При этом условие квазиоднородности предполагает малость магнитного поля, создаваемого токами в плазме, по сравнению с внешним магнитным полем.

В окрестности магнитной оси s плазменной конфигурации критерий (I.2) без члена $S^2/4$ можно преобразовать к виду [9]

$$p'\frac{V''}{V'} - \left\langle \frac{p'^2}{B_s^2} \right\rangle - \left\langle \frac{B_s^2 \left(\rho \frac{\partial}{\partial \rho} \frac{j_s}{B_s}\right)^2}{|\nabla\phi|^2} \right\rangle \geq 0 \tag{I.7}$$

где ρ - расстояние от магнитной оси, а штрихами обозначены производные по продольному потоку ϕ. Здесь характеристикой магнитной ямы является V'', а остальные члены описывают дестабилизацию, связанную с наличием токов в плазме. Для устойчивости при спадающем давлении $p'(V) < 0$ необходимо $V'' < 0$.

Величину V'' в окрестности магнитной оси можно представить в виде контурного интеграла по магнитной оси :

$$V'' = -\frac{1}{\pi}\oint \frac{ds}{B_0^2}\Big\{\Big[\frac{k^2}{2}(1-\varepsilon\cos 2\delta) - \varepsilon^2(\delta' - \varkappa)^2 - \frac{\eta'^2}{4} - \frac{3B_0'^2}{4B_0^2} + \frac{\varepsilon\eta' B_0'}{B_0}\Big]\operatorname{ch}\eta -$$
$$- \frac{\pi p'}{B_0} - \frac{\dot{j}_0^2}{4B_0^2\operatorname{ch}\eta} - 2kB_0^{1/2}\left(\alpha_1 e^{-\eta/2}\cos\delta + \alpha_2 e^{\eta/2}\sin\delta\right)\Big\} \tag{I.8}$$

где $k(s)$ и $\varkappa(s)$ -кривизна и кручение магнитной оси, $\varepsilon(s) = th\,\eta$ - параметр эллиптичности приосевых нормальных сечений магнитных поверхностей, $\delta(s)$- угол малой полуоси эллипса с нормалью к магнитной оси, $B_0(s)$ и $j_0(s)$ - поле и плотность тока на магнитной оси, $p' = p'(\psi)$, $\alpha_1(s)$ и $\alpha_2(s)$ - параметры магнитных поверхностей, уравнение которых в скругляющей системе координат r, ϑ, s, проворачивающейся вокруг магнитной оси s вместе с приосевыми сечениями магнитных поверхностей, имеет вид

$$\psi = r^2 + r^3(\alpha_1\cos\vartheta + \alpha_2\sin\vartheta + \alpha_3\cos 3\vartheta + \alpha_4\sin 3\vartheta) + \dots = const. \qquad (I.9)$$

Член, пропорциональный p', в выражении (I.8) в общем случае сокращается при подстановке V'' и $V' = \oint \frac{ds}{B_0}$ в критерий устойчивости (I.7), который в результате также может быть представлен в виде контурного интеграла на магнитной оси s

$$-p'\oint\frac{ds}{B_0}\Big\{\Big[\frac{k^2}{2}(1-\varepsilon\cos 2\delta) - \varepsilon^2(\delta'-\varkappa)^2 - \frac{\eta'^2}{4} - \frac{3B_0'^2}{4B_0^2} + \frac{\varepsilon\eta' B_0'}{B_0}\Big]ch\,\eta -$$

$$-\frac{j_0^2}{4B_0^2 ch\,\eta} - 2kB_0^{1/2}(\alpha_1 e^{-\eta/2}\cos\delta + \alpha_2 e^{\eta/2}\sin\delta) + \pi p' B_0^2 V'^2\Big(\frac{\gamma_1^2}{1+e^{-\eta}} + \frac{\gamma_2^2}{1+e^{\eta}}\Big)\Big\} \geq 0 \qquad (I.10)$$

Входящие сюда параметры γ_1 и γ_2 определяются стандартной системой уравнений

$$\left.\begin{aligned} \gamma_1' + v'\gamma_2 &= -\frac{2ke^{-\eta/2}}{V'B_0^{3/2}}\cos\delta \\ \gamma_2' - v'\gamma_1 &= -\frac{2ke^{\eta/2}}{V'B_0^{3/2}}\sin\delta \end{aligned}\right\} \qquad (I.11)$$

где

$$v' = \frac{1}{ch\,\eta}\Big(\delta' - \varkappa + \frac{j_0}{2B_0}\Big) = \sqrt{1-\varepsilon^2}\Big(\delta' - \varkappa + \frac{j_0}{2B_0}\Big) - \qquad (I.12)$$

- угол прокручивания магнитных силовых линий в окрестности магнитной оси.

Уравнения для параметров α_1 и α_2 имеют такой же вид как и (I.II), однако в правые части этих уравнений входят также и параметры γ_1 и γ_2. Поэтому целесообразно представить α_1 и α_2 в виде сумм

$$\alpha_1 = \bar\alpha_1 + \tilde\alpha_1 \quad , \quad \alpha_2 = \bar\alpha_2 + \tilde\alpha_2 \qquad (I.13)$$

таким образом, чтобы $\tilde{\alpha}_1$ и $\tilde{\alpha}_2$ удовлетворяли уравнениям

$$\left.\begin{aligned} \tilde{\alpha}_1' + v'\tilde{\alpha}_2 &= \frac{2\pi p'V'}{e^{\psi}+3e^{-\psi}}\gamma_1 \\ \tilde{\alpha}_2' - v'\tilde{\alpha}_1 &= \frac{2\pi p'V'}{e^{-\psi}+3e^{+\psi}}\gamma_2 \end{aligned}\right\} \qquad \text{(I.14)}$$

При этом критерий устойчивости (I.10) можно преобразовать так, чтобы в него не входили $\tilde{\alpha}_1$ и $\tilde{\alpha}_2$:

$$-p'\oint\Big\{\Big[\frac{k^2}{2}(1-\varepsilon\cos 2\delta)-(\delta'-\varkappa)^2\varepsilon^2-\frac{\psi'^2}{4}-\frac{3B_0'^2}{4B_0^2}+\frac{\varepsilon B_0'\psi'}{B_0}\Big]\frac{\operatorname{ch}\psi}{B_0^2}- \qquad \text{(I.15)}$$
$$-\frac{j_0^2}{4B_0^4\operatorname{ch}\psi}-2kB_0^{-3/2}\left(\tilde{\alpha}_1 e^{-\psi/2}\cos\delta+\tilde{\alpha}_2 e^{\psi/2}\sin\delta\right)+2\pi p'V'^2\frac{\operatorname{sh}^2\psi/2}{\operatorname{ch}\psi/2}\left(\frac{\gamma_1^2 e^{3\psi/2}}{3+e^{2\psi}}+\frac{\gamma_2^2 e^{-3\psi/2}}{3+e^{-2\psi}}\right)\Big\}dl\geqslant 0$$

Как показывает выражение (I.15),условие устойчивости конфигураций с круглыми приосевыми сечениями магнитных поверхностей, когда $\varepsilon=0$, сводится, при $p'<0$, к требованию $V''\leqslant 0$, где в выражении V'' отброшен член, пропорциональный p' .

Для получения уравнений для параметров магнитных поверхностей $\bar{\alpha}_1$ и $\bar{\alpha}_2$ ограничимся решением граничной задачи при заданной форме нормального сечения внешней магнитной поверхности Σ . В общем виде семейство магнитных поверхностей, каждую из которых можно принять за внешнюю поверхность Σ , можно в рассматриваемом приближении записать в смещенной системе координат

$$\begin{aligned} x_1 &= r_1\cos\vartheta_1 = x_0+x \\ y_1 &= r_1\sin\vartheta_1 = y_0+y \end{aligned} \qquad \text{(I.16)}$$

в виде

$$r_1^2+r_1^3\left(b_1\cos\vartheta_1+b_2\sin\vartheta_1+b_3\cos 3\vartheta_1+b_4\sin 3\vartheta_1\right)=a^2 \qquad \text{(I.17)}$$

где $a=\mathrm{const}$, а $b_i(l)$ - заданные функции. При этом функция магнитных поверхностей представляется в виде

$$\psi=\left[1+r_1(\Delta_1\cos\vartheta_1+\Delta_2\sin\vartheta_1)\right]\left[r_1^2+r_1^3(b_1\cos\vartheta_1+b_2\sin\vartheta_1+\right.$$
$$\left.+b_3\cos 3\vartheta_1+b_4\sin 3\vartheta_1)-a^2\right]+a^2 \qquad \text{(I.18)}$$

Сравнивая это выражение с выражением (I.9) для функции ψ в координатах $x = r\cos\vartheta$, $y = r\sin\vartheta$, получим при малых Δ_1 и Δ_2 :

$$\Delta_1 = 2x_0/a^2 \quad , \quad \Delta_2 = 2y_0/a^2 \tag{I.19}$$

$$\alpha_1 = \Delta_1 + b_1 \ , \quad \alpha_2 = \Delta_2 + b_2 \ , \quad \alpha_3 = b_3 \ , \quad \alpha_4 = b_4 \tag{I.20}$$

Функции $b_i(s)$ могут быть заданы произвольно, при этом только следует иметь в виду, что семейство (I.17) имеет сепаратрису, размеры которой зависят от b_i . Если ограничиться случаем симметричных относительно оси y профилей сечений магнитных поверхностей, то $\Delta_2 = b_2 = b_4 = 0$, и остаются два произвольных параметра несимметричности сечений b_1 и b_3 . В тексте доклада мы ограничились случаем $b_1 = 0$. В общем случае параметры $\bar{\alpha}_1$ и $\bar{\alpha}_2$, входящие в критерий устойчивости (I.15), удовлетворяют стандартной системе уравнений

$$\left.\begin{aligned} \bar{\alpha}_1' + v'\bar{\alpha}_2 &= \frac{g_1(b_3' + 3v'b_4) - \mathcal{P}_1}{2g_0 + g_1} \\ \bar{\alpha}_2' - v'\bar{\alpha}_1 &= \frac{g_1(b_4' - 3v'b_3) - \mathcal{P}_2}{2g_0 - g_1} \end{aligned}\right\} \tag{I.21}$$

Здесь $\mathcal{P}_1$ и $\mathcal{P}_2$ соответственно равны

$$2\mathcal{P}_1 = -(3g_0 + g_1)(c_1' - v'c_2) + (g_0' - g_1')c_1 - \left(\frac{6u'}{B_0} + \frac{j_0}{B_0^2}\right)c_2 \tag{I.22}$$

$$2\mathcal{P}_2 = -(3g_0 - g_1)(c_2' + v'c_1) + (g_0' + g_1')c_2 + \left(\frac{6u'}{B_0} + \frac{j_0}{B_0^2}\right)c_1$$

и введены следующие обозначения : $u' = \delta' - \varkappa$,

$$g_0 = \frac{ch\,\eta}{B_0} \ , \quad g_1 = -\frac{sh\,\eta}{B_0} \ , \tag{I.23}$$

$$c_1 = kB_0^{-1/2}e^{-\eta/2}\cos\delta \quad , \quad c_2 = kB_0^{-1/2}e^{\eta/2}\sin\delta \tag{I.24}$$

Таким образом, входящие в критерий устойчивости параметры $\bar{\alpha}_1$, $\bar{\alpha}_2$ и γ_1 , γ_2 определяются системами уравнений (I.21) и (I.11) с известными правыми частями. Решения этих уравнений можно представить в виде рядов Фурье, что в основном и использовалось в тексте доклада. Однако, в ряде случаев представляется более удобным использовать интегральное решение [1], которое для стандартной системы уравнений

$$\left.\begin{aligned} z_1' + v' z_2 &= f_1 \\ z_2' - v' z_1 &= f_2 \end{aligned}\right\} \qquad (I.25)$$

может быть записано в виде

$$z = \frac{i e^{iv(L)/2} e^{iv}}{2\sin v(L)/2} \int_0^L e^{-iv} f\,ds + e^{iv} \int_0^s e^{-iv} f\,ds \qquad (I.26)$$

где $z = z_1 + i z_2$, $f = f_1 + i f_2$, L - длина магнитной оси конфигурации , $v = v(s) = \int_0^s v' ds$.

ЛИТЕРАТУРА

[1] MERCIER, C., Nucl. Fusion 3 (1963) 89.
[2] СОЛОВЬЕВ, Л.С., ШАФРАНОВ, В.Д., Вопросы теории плазмы под ред.М.А.Леонтовича, Госатомиздат, Москва 5 1967, стр.3.
[3] SHAFRANOV, V., YURCHENKO, E., Nuclear Fusion, to be published 4 (1968).
[4] MERCIER, C., Inter. Conf. Plasma Phys. and Control. Nucl. Fusion, Salzburg, Sept. 1961.
[5] BINEAU, M., Inter. Conf. Plasma Phys. and Contr. Nucl. Fusion, Salzburg, Sept. 1961.
[6] GREEN, J.M., JOHNSON, U.L., Phys. Fluids 5 (1962) 510.
[7] СОЛОВЬЕВ, Л.С., ЖЭТФ 53 вып.8(1967).
[8] SHAFRANOV, V.D., Nuclear Fusion, to be published 3 (1968).
[9] СОЛОВЬЕВ, Л.С., ЖЭТФ 53 вып.12 (1967).
[10] GREEN, J.M., JOHNSON, J.L., Phys. Fluids 4 (1961) 875.
[11] VUILLEMIN, M., GOURDON, C., Association CEA Fur - CEA - Fc.393 (1966).

DISCUSSION

R.S. PEASE: What is the limit on β for stability in Tokamak systems?

L.S. SOLOVYEV: There is no limit on β in the formula $p'(4/R^2 - j^2/\beta^2) > 0$. If one drops the assumption that the transverse cross-sections of the magnetic surfaces near the magnetic axis are circular, the width of the stability region becomes dependent both on the plasma pressure and on the ellipticity and non-symmetry (pear shape) of the magnetic surface cross-sections.

M.S. RABINOVICH: In your presentation you stated that, if no magnetic well was employed, hydrodynamic stability was impossible however great the shear. Did I understand you correctly?

L.S. SOLOVYEV: Yes, you did. Since Mercier's generalized geometric criterion is an essential condition for stability, while the magnetic well is a fundamental stabilizing factor in this criterion, there is – generally speaking – an unstable region in the vicinity of the magnetic axis when there is no magnetic well.

M.S. RABINOVICH: To what extent are your calculations applicable? For example, there is apparently no dependence on β in Tokamak devices in your approximation, whereas there is in the next approximation.

L.S. SOLOVYEV: For a toroidal system with a longitudinal current (Tokamak) and with magnetic surfaces having circular transverse cross-sections, the pressure-dependent terms in the stability criterion cancel out. The dependence of the stability region on pressure is extremely weak in such a case – from the point of view, naturally, of the generalized geometric criterion for local hydromagnetic stability.

PROPRIETES DES PLASMAS TOROIDAUX A β FINI

J.-C. ADAM ET C. MERCIER
ASSOCIATION EURATOM-CEA, FONTENAY-AUX-ROSES, FRANCE

Abstract — Résumé

PROPERTIES OF TOROIDAL PLASMAS WITH FINITE β. There are particular values $(\iota/2\pi)_0$ of the rotational transform on the magnetic axis in the vicinity of which the plasma is strongly perturbed. If the plasma has a plane magnetic axis defined by its curvature, $1/R(s) = \Sigma a_k \exp(i2k\pi s/L)$ a value of $(\iota/2\pi)_0 = k$ corresponds to each Fourier coefficient $a_k \neq 0$.

There are two possible methods for studying these deformations and their effect on plasma stability: expansion in the vicinity of a magnetic axis; and the helicoidal approximation, which is applied particularly to the type of configuration whose rotational transform is due to the longitudinal current.

This approximation reduces the problem to one of solving equations for a helicoidal plasma and simplifies analysis.

The paper is a fairly general study of the equilibria predicted in devices of the Tokomak and Harmonica types. The authors show how the various equilibrium characteristics (displacement of the magnetic axis, mean magnetic well - V", and shear) vary as a function of parameters such as $\langle\iota/2\pi\rangle$ and $\beta = \langle 2p/B^2\rangle$ and those parameters characterizing the current and pressure distributions.

The above quantities increase substantially as $(\iota/2\pi)_0$ is approached, until the simple-topology (one magnetic axis) equilibrium breaks down.

Models describing the behaviour of a plasma with several magnetic axes are studied and tend to prove that, when one passes the point where $(\iota/2\pi)_0 = k$, there results either strong turbulence of the plasma or states involving several magnetic axes.

The equilibrium can be studied experimentally by measuring the flux passing through a loop formed by two diametrically opposed conductors wound several times around the torus. The plasma displacement and formulas giving this flux as a function of the plasma parameters are established and compared with the experimental results.

The MHD stability is studied with the localized criterion. The high $V'' < 0$ and the strong shear calculated near $(\iota/2\pi)_0$ favour non-MHD instability.

PROPRIETES DES PLASMAS TOROIDAUX A β FINI. On sait qu'il existe des valeurs particulières $(\iota/2\pi)_0$ de la transformation rotationnelle sur l'axe magnétique au voisinage desquelles le plasma est fortement perturbé. Si le plasma présente un axe magnétique plan défini par sa courbure $1/R(s) = \Sigma a_k \exp(i2k\pi s/L)$, à chaque coefficient de Fourier $a_k \neq 0$ correspond un $(\iota/2\pi)_0 = k$.

Pour étudier ces déformations et leurs conséquences sur la stabilité, deux méthodes sont possibles: le développement au voisinage d'un axe magnétique et l'approximation hélicoïdale qui s'applique principalement au type de configuration dont la transformée rotationnelle est due au courant longitudinal.

Cette approximation réduit le problème à la résolution des équations pour un plasma hélicoïdal et permet des études analytiques plus simples.

Le mémoire présente une étude relativement générale des équilibres prévus dans les appareils du type Tokomac et Harmonica. Il montre, en fonction de paramètres tels que $\langle\iota/2\pi\rangle$, $\beta = \langle 2p/B^2\rangle$ et de ceux qui caractérisent la répartition du courant et de la pression, comment varient les diverses caractéristiques de l'équilibre: déplacement de l'axe magnétique, puits magnétique moyen (V") et cisaillement. Ces quantités sont très fortement augmentées à l'approche de $(\iota/2\pi)_0$ jusqu'à la rupture de l'équilibre de topologie simple (un axe magnétique).

Les auteurs étudient des modèles de comportement du plasma avec plusieurs axes magnétiques; ces modèles tendent à prouver que le franchissement de $(\iota/2\pi)_0 = k$ conduit soit à une turbulence forte du plasma, soit à des états comportant plusieurs axes magnétiques.

L'étude expérimentale de l'équilibre peut se faire en particulier par la mesure du flux passant à travers une boucle formée par deux conducteurs diamétralement opposés dans une section et tournant plusieurs fois le long du tore. Les auteurs établissent des formules donnant ce flux en fonction des paramètres du plasma ainsi que le déplacement de ce dernier.

Ils étudient la stabilité MHD avec le critère localisé. Le fort $V'' < 0$ et le fort cisaillement calculé près de $(\iota/2\pi)_0$ sont par ailleurs favorables aux instabilités non MHD.

Pour étudier les propriétés des plasmas toroïdaux plusieurs méthodes sont possibles, qui peuvent se compléter pour obtenir les renseignements nécessaires à la compréhension des divers phénomènes [1], [2], [3], [4]. Parmi ces méthodes nous rappellerons le développement au voisinage d'un axe [1] et la représentation hélicoïdale du plasma torique [2].

La première méthode a permis de mettre en évidence certaines valeurs particulières des paramètres caractérisant la transformation rotationnelle sur l'axe magnétique au voisinage desquelles le plasma est fortement perturbé. Si l'axe magnétique est plan, on peut le définir par sa courbure $\frac{1}{\mathcal{R}(s)} = \sum a_k \exp i \frac{2k\pi s}{L}$ et à chaque $a_k \neq 0$ correspond un $\left(\frac{\iota c}{2\pi}\right)_o = k$.

La déformation du plasma est alors due aux effets de courbure et dépend fortement de β. A cette déformation sont liées des propriétés intéressantes telles que la formation de puits magnétiques moyens ($V'' < 0$) et l'augmentation des effets de cisaillement (shear). L'inconvénient de la méthode précédente est qu'elle relie difficilement les propriétés près de l'axe magnétique à la géométrie totale du plasma (plasma, vide , coque, champs magnétiques extérieurs appliqués) et cesse d'être applicable quand $\left(\frac{\iota c}{2\pi}\right)$ tend vers K. Dans ce dernier cas, la méthode hélicoïdale s'applique très bien et permet d'étudier le plasma dans son ensemble en étudiant un problème de type plasma hélicoïdal, l'image hélicoïdale du plasma étant différente suivant la singularité k étudiée. Dans la suite de cet article nous exposerons certaines études de configurations fermées planes (axe magnétique plan) dont la transformation rotationnelle est due au courant longitudinal I. Les résultats seront en particulier applicables aux appareils du type Tokamac et Harmonica :

- avec k = 0 axe magnétique circulaire - (Tokamac , Harmonica 0),
- avec k = 2 axe magnétique donné par $\frac{1}{\mathcal{R}(s)} = \frac{2\pi}{L}\left(1+2\cos\frac{4\pi s}{L}\right)$ (Harmonica II).

Dans la partie 1 nous étudierons les propriétés générales des équilibres avec un seul axe magnétique au voisinage de $\left(\frac{\iota c}{2\pi}\right)_o = k$.

La partie 2 étudie la stabilité MHD de ces équilibres.

La partie 3 expose quelques modèles de plasma de topologie plus complexe qui peuvent se présenter quand les conditions requises pour les équilibres de topologie simple ne sont pas remplies.

1. PROPRIETES DANS L'APPROXIMATION HELICOIDALE DES PLASMAS EN EQUILIBRE

1.1. Calcul général

Dans un travail précédent [2] sur la méthode hélicoïdale nous avons établi les équations suivantes pour un plasma MHD

$$\vec{B} = f\,\vec{u} + \vec{u} \wedge \operatorname{grad} F \qquad (1)$$

f et F fonctions uniquement de ρ et $t = \theta + \frac{2k\pi s}{L}$

f et la pression p sont fonctions arbitraires de F qui est donné par :

$$\mathcal{L}F - \frac{2Kf}{g} + \frac{1}{2}\frac{df^2}{dF} + g\frac{dP}{dF} = 0 \qquad (2)$$

$$\mathcal{L} = g \operatorname{div}\left(\frac{1}{g}\operatorname{grad} F\right) \qquad g = (1-a_k\rho\cos t)^2 + k^2\rho^2$$

$$K = \frac{2k\pi}{L} \qquad \vec{u} = \frac{(1-a_k\rho\cos t)\vec{e_s} - k\rho\,\vec{e_\theta}}{g}$$

Pour des questions de simplicité nous limiterons p(F) et f(F) à des fonctions quadratiques. Nous poserons alors sans perte de généralité

$$\begin{cases} f^2 = f_o^2 - \dfrac{\mu^2}{R^2} F^2 = f_o^2 - \lambda^2 F^2 \\ P = p_2 F^2 + p_1 F + p_o \end{cases} \tag{3}$$

Nous supposerons en outre que le champ magnétique longitudinal appliqué est fort et qu'il est peu perturbé par le plasma . On peut alors développer l'opérateur $\mathscr{L}$ suivant les puissances successives de $(a\rho) \sim (k\rho) \sim \varepsilon$ en écrivant $F = F_1(\varepsilon) + F_2(\varepsilon)$ et $f = f_o + O(\varepsilon^2) = B_S + O(\varepsilon)$. L'opérateur $\mathscr{L}$ s'écrit :

$$\mathscr{L} F = \left[\nabla_c^2 + \frac{1}{2} \operatorname{grad}_c \frac{1}{g} \operatorname{grad}_c \right] F \tag{4}$$

l'indice "c" indique que l'on doit écrire les opérateurs en coordonnées cylindriques ρ et t . Pour un tore à section circulaire , la solution générale à l'ordre ε^2 s'écrit :

$$\frac{F}{Rf_o} = \frac{G}{f_o} - \frac{X}{4} E(x,t) = \frac{G}{f_o} - \left(E_{SY} + (a_k R) E_{NS} \cos t \right) \frac{X}{4} \tag{5}$$

$$E(x,t) = \frac{I_o - I_o(\mu' x)}{2 I_2} - \frac{(a_k R)}{4} \frac{I_o}{I_2} \left(\frac{I_1(\mu' x)}{I_1} - x \frac{I_o(\mu' x)}{I_o} \right) \cos t \tag{6}$$

$$+ \frac{(a_k R)}{X} \frac{8}{\mu'^2} \left(\frac{XYE_1}{2} + 2kR \right) \left(x - \frac{I_1(\mu' x)}{I_1} \right) \cos t \tag{7}$$

$$+ \frac{(a_k R)}{2} \cdot \frac{y}{(\mu'^2 I_2)} \left[\mu' I_1(\mu' x)(1 - x') - 4 I_o \left(x - \frac{I_1(\mu' x)}{I_1} \right) \right] \cos t$$

avec $\rho = Rx \quad y = p_2 R^2 \qquad \mu'^2 = \mu^2 - 2y \qquad X$ = constante d'intégration

$$E_1 = \frac{2}{XY} \left[\frac{p_1 R}{f_o} \left(1 + \frac{2y}{\mu'^2} \right) + \frac{xy}{4 I_2} \cdot I_o - \frac{4(kR)y}{\mu'^2} \right]$$

$$I_n = I_n(\mu') \tag{8}$$

Pour obtenir cette solution nous avons tenu compte du fait qu'à l'approche des singularités p_1 et p_2 croissent et peuvent devenir d'ordre $\frac{1}{\varepsilon}$ et qu'alors des termes comme $(a_k\rho)\, p_1$ ou $(a_k\rho)\, p_2$ doivent être considérés comme d'ordre zéro. Par contre, nous avons négligé des termes comme $(a_k\rho)^2 p_1$, qui ne sont pas déterminants pour les propriétés au voisinage de la singularité. La connaissance de F permet alors de calculer toutes les quantités intéressant le plasma.

Les quatre paramètres X, Y, μ'^2, E, contenus dans F peuvent être reliés à des quantités physiques globales telles que le courant total longitudinal I et la pression moyenne P_M. Ces quantités seront introduites dans les calculs par les quantités sans dimension :

$$\frac{\iota_M}{2\pi} = -\left(\frac{I}{2\pi R}\right)\left(\frac{L}{2\pi R}\right)\frac{1}{f_o} = k + \eta \tag{9}$$

$$\beta = \frac{2 P_M}{f_o^2} \tag{10}$$

$\frac{\iota_M}{2\pi}$ étant une valeur globale de la transformation rotationnelle dans le plasma. Compte tenu de la condition de confinement du plasma, c'est-à-dire de la nullité de la pression P pour $\rho = R$ on obtient :

$$\beta_\ell = \frac{2P}{f_o^2} = \frac{1}{8}\, y x^2\, E\,(E - 2E_1) \tag{11}$$

d'où l'on tire par intégration en négligeant les termes en ε^2

$$\beta = \frac{1}{8}\, y x^2 \left[E_o - E_1\right] \tag{12}$$

avec $E_o = \frac{1}{2 I_2^2}\left(I_o I_2 - I_1^2/2\right)$, variant de 0,36 à 0,25 lorsque μ'^2 varie de J_{o1}^2 à $+\infty$.

Pour que la pression soit partout positive nous devons imposer plusieurs conditions:

a) $(y E_1) < 0$

b) $\left(\frac{\partial E}{\partial x}\right)_{\substack{x=1\\ t=0}} \leqslant 0$

c) $E_1 > \frac{1}{2} E_{MAX}$ si $E_1 > 0$

La condition b) s'écrit $\nu \leqslant 1$ avec :

$$\frac{\nu}{a_k R} = \frac{1}{2}\left(1 - \frac{I_o I_2}{I_1^2}\right) - \frac{32}{X \mu'^2}\,\frac{I_2^2 (kR)}{I_1^2} + \frac{8 I_2^2}{\mu'^2 I_1^2}\, Y (E_o - E_1) \tag{13}$$

Remarquons que le cas limite $E_1 = 0$ n'impose pas la condition b) mais que si $\nu > 1$ la topologie de l'équilibre est complexe avec 2 axes magnétiques (cf. § 3).

<u>Calcul des courants</u> : Il se fait sans difficulté à partir de :

$$\begin{aligned} \vec{J} &= j_u\, \vec{u} - \vec{u} \wedge \operatorname{grad} f = j_u\, \vec{u} + \frac{\mu^2}{R}\, \vec{u} \wedge \operatorname{grad} F \\ j_u &= \mathscr{L} F - \frac{2kf}{g} = \left(\mu^2 - 2gy\right)\frac{F}{R^2} - g P_1 \end{aligned} \tag{14}$$

On trouve le courant total à partir de la composante longitudinale j_S ; il vient :

$$-\frac{\iota_M}{2\pi} = \frac{I}{2\pi R}\,\frac{1}{f_o}\left(\frac{L}{2\pi R}\right) = \left(\frac{L}{2\pi R}\right)\frac{\mu'^2}{2}\left[\frac{G}{f_o} - \frac{x}{8} - \frac{P_1 R}{f_o \mu'^2}\right] = -k - \eta \qquad (15)$$

d'où

$$X = -2\left(\frac{2\pi R}{L}\right)\left(\frac{4 I_2}{\mu I_1}\right)\eta \qquad (16)$$

En utilisant cette expression le courant j_S s'écrit

$$\frac{-R j_S}{2 f_o}\left(\frac{L}{2\pi R}\right) = k + \eta + \frac{\mu'^2 \eta}{8}\left(\frac{4 I_2}{\mu I_1}\right)\left(1 - 2 E_{SYM}\right)$$

$$+\left(a_k R\right) x \cos t \left\{ k + \eta + \frac{\mu'^2 \eta}{8}\left(\frac{4 I_2}{\mu I_1}\right)\left(1 - 2 E_{SYM} - 2\,\frac{E_{NS}}{x}\right)\right. \qquad (17)$$

$$\left. + 2\left(\frac{\mu' I_1}{4 I_2}\right)\left(\frac{L}{2\pi R}\right)^2 \frac{\beta}{\eta}\;\frac{E_1 - E_S}{E_o - E_1} \right\}$$

A l'aide de (12) et (16) on peut exprimer y en fonction de E,

$$y = 2\left(\frac{\mu' I_1}{4 I_2}\right)^2\left(\frac{L}{2\pi R}\right)^2 \frac{\beta}{\eta^2}\;\frac{1}{E_o - E_1} \qquad (18)$$

L'expression de ν (13) s'écrit alors

$$\frac{\nu}{a_k R} = \frac{1}{2}\left(1 - \frac{I_o I_2}{I_1^{\,2}}\right) + \frac{k}{\eta}\left(\frac{4 I_2}{\mu' I_1}\right) + \left(\frac{L}{2\pi R}\right)^2 \frac{\beta}{\eta^2} \qquad (19)$$

La partie symétrique de j_S montre clairement que le paramètre μ'^2 caractérise la forme de la répartition de courant : si $\mu'^2\,\eta < 0$, j_S aura un maximum et un minimum si $\mu'^2\,\eta > 0$. Lorsque $\mu'^2 \rightarrow 0$ la répartition du courant ne diffère d'une constante que par sa partie antisymétrique proportionnelle à la courbure. Ces effets deviennent très forts quand $\eta \rightarrow 0$ particulièrement pour les termes contenant β comme le montre (17) ou (19) . Cependant , η ne peut devenir trop petit sans qu'on viole la condition $\nu \ll 1$. Nous terminerons en donnant les expressions finales pour le calcul de $E(x,t)$

$$E_{SYM} = \frac{I_o - I_o(\mu' x)}{2 I_2} \qquad (20)$$

$$E_{NS} = -\frac{I_1^2}{2 I_2^2} \frac{\nu}{(a_k R)} \cdot \left(x - \frac{I_1(\mu' x)}{I_1} \right) + \mathcal{E}_{NS} \qquad (21)$$

$$\mathcal{E}_{NS} = -\frac{1}{4} \frac{I_0}{I_2} \left[\frac{I_1(\mu' x)}{I_1} - \frac{x I_0(\mu' x)}{I_0} + \left(1 - \frac{I_1^2}{I_0 I_2}\right)\left(x - \frac{I_1(\mu' x)}{I_1}\right) \right]$$

$$+ \frac{y}{\mu'^2 I_2} \left[\mu' I_1(\mu' x)(1 - x^2) - \frac{2 I_1^2}{I_2} \left(x - \frac{I_1(\mu' x)}{I_1}\right) \right] \qquad (22)$$

E_S et le premier terme de E_{NS} sont indépendants de E_1, E_{NS} reste petit ne présentant pas d'amplification pour η petit analogue au terme en ν. Notons également que $\left(\frac{\partial \mathcal{E}_{NS}}{\partial x}\right)_{x=1} = 0$

L'expression de la répartition de pression est donnée par

$$\frac{\beta_\ell}{\beta} = \frac{E\,(E - 2E_1)}{E_0 - E_1} \qquad (23)$$

expression qui met bien en évidence le rôle de E_1 sur cette répartition.

Une dernière caractéristique importante de ces configurations au voisinage d'une singularité ($\eta \longrightarrow 0$) est le déplacement qui peut être très important de l'axe magnétique par rapport au centre du plasma. Pour avoir la position x_M de l'axe magnétique qui se trouve sur l'axe $t = 0$ (ou η) on cherche les racines de $\left(\frac{\partial E}{\partial x}\right)_{t=0} = 0$. Nous la donnerons explicitement dans l'un des cas particuliers que nous traiterons par la suite .

Remarquons enfin qu'au voisinage de $\frac{\iota_c}{2\pi} = k$ la représentation hélicoïdale k est prépondérante et l'axe magnétique tourne k fois autour de l'axe central du plasma par grand tour de tore.

1.2. Cas particulier

a) Champ magnétique dans le cas du vide entourant le plasma

$$f = f_0$$

$$F = F_0 + \alpha_0 \log\rho + \frac{k f_0}{2}\rho^2 + \cos t \left| -\frac{\alpha_0 a_k \rho}{2} \log\rho + \alpha.\rho + \right.$$
$$+ \frac{\beta_1}{\rho} + \frac{3}{8} a_k\, k f_0\, \rho^3 \qquad (24)$$

on en déduit

$$\vec{B} = \left[-\frac{\alpha_0 a_k \log\rho}{2} + \alpha_1 + \frac{\beta_1}{\rho^2} + \frac{3}{8} a_k\, k f_0 \rho^2 \right] \sin t\; \vec{e}_\rho \qquad (25)$$
$$+ \left[\frac{\alpha_0}{\rho} + \cos t \left(\frac{a_k \alpha_0}{2} - \frac{\alpha_0 a_k}{2} \log\rho + \alpha_1 - \frac{\beta_1}{\rho^2} + \frac{1}{8} a_k\, k f_0 \rho^2 \right) \right] \vec{e}_\theta$$
$$+ \left[f_0 (1 + a_k\, \rho \cos t) + \alpha_0 k \right] \vec{e}_s$$

b) $\mu' \# 0$

Cette limite a l'avantage de simplifier considérablement les expressions analytiques. Elle permet en outre de découpler les effets de répartition de courant des effets de courbure en s'affranchissant des premiers pour ne dégager que les effets physiques importants qui sont amplifiés par l'approche de la singularité $\eta = 0$. $E(x,t)$ s'écrit alors :

$$E(x,t) = (1-x^2)\left[1 - \nu x \cos t + \frac{\gamma(a_k R)}{6}(1-x^2)\cos t\right] \qquad (26)$$

$(a_k R)\gamma$ restant toujours petit devant ν. Dans les mêmes conditions ν s'écrit :

$$\nu = (a_k R)\left[\frac{1}{4} + \frac{k}{\eta} + \left(\frac{L}{2\pi R}\right)^2 \frac{\beta}{\eta^2}\right] \qquad (27)$$

Comme mentionné précédemment on obtient facilement l'expression du déplacement de l'axe magnétique (sur l'axe $t=\pi$)

$$x_M = \frac{-1 \pm \sqrt{1+3\nu^2}}{3\nu}$$

x étant compris entre -1 et +1, dans le cas $\nu \leqslant 1$ on voit qu'il n'y aura qu'une seule valeur de x_M alors qu'on en trouve 2 pour $\nu > 1$. Le déplacement maximum de l'axe pour les topologies avec un seul axe est $x_M = \frac{1}{3}$ $(\nu = 1)$; il s'écrit au contraire $x_M \simeq \frac{\nu}{2}$ pour ν petit.

c) Cas $E_1 = \infty$ et $E_1 = 0$

Le cas $E_1 = \infty$ correspond à la loi linéaire pour P : $p_2 = 0$, la répartition de pression correspondant à ce cas étudié en détail dans /2/

$$\beta_\ell = 2\beta\, E(x,t)$$

Le cas $E_1 = 0$ donne au contraire : $\beta_\ell = 2\beta \dfrac{E^2}{E_o}$

On voit que quelle que soit la valeur de ν la pression est strictement positive. Ce cas est étudié dans le § 3.

1.3. Cisaillement des lignes magnétiques (shear)

Une propriété importante des configurations en relation avec la stabilité MHD et non MHD est l'effet stabilisant de la variation de la transformation rotationnelle en fonction de la surface magnétique.

Selon la réf. /2/ nous écrirons :

$$\frac{\iota_c}{2\pi} = k - \mathcal{L}\frac{dF}{d\Psi} = k - (a_k R)\left(\frac{4 I_2}{\mu' I_1}\right)\eta\, x \;\frac{1}{\frac{1}{\eta}\int_{\mathcal{C}} \frac{x\,dx}{E_{NS}\sin t}} \qquad (28)$$

l'intégrale étant prise sur la courbe définie dans une section droite par E=Cte.

Pour simplifier les calculs et faciliter l'interprétation, nous calculerons le "shear" dû à la répartition des courants indépendamment des effets de courbure ($a_k R = 0$) et celui calculé avec $\mu' = 0$ et entièrement lié aux effets de courbure.

$$\text{Si } (a_k R) = 0 : \frac{\iota_c}{2\pi} = k + \frac{I_1(\mu' x)}{x\, I_1} \eta \tag{29}$$

Pour $\mu' = 0$ et $(a_k R) \neq 0$ on obtient

$$\frac{\iota_c}{2\pi} = k + \frac{\pi}{2} \frac{\sqrt{a-c}}{K(\varphi)} \eta \nu \quad \varphi = \sqrt{\frac{a-b}{a-c}} \tag{30}$$

a,b,c, racines de $\nu^2 t^3 + (1-\nu^2) t^2 - 2Et + E^2 = 0$

$K(\varphi)$ fonction elliptique complète.

Sur le bord du plasma (E=0) ou sur son axe ($E=E_M$) cette expression se simplifie et donne :

$$\left(\frac{\iota}{2\pi}\right)_{axe} = k + \eta \sqrt{\frac{\sqrt{1+3\nu^2}}{3} \left(2 + \sqrt{1+3\nu^2}\right)} \tag{31}$$

$$\left(\frac{\iota}{2\pi}\right)_{bord} = k + \eta \sqrt{1-\nu^2} \tag{32}$$

Cette dernière expression $\left(\frac{\iota}{2\pi}\right)_{bord}$ est tout à fait générale comme on peut le montrer en étudiant (28) pour $E \longrightarrow 0$. Il est intéressant de remarquer que si le courant a un maximum les deux shears (cylindrique et de courbure) sont de même signe, ($\eta > 0$), de signes opposés si le courant est minimum. Nous verrons dans la partie 2 que pour les termes de stabilisation liés à V" c'est le contraire qui se produit.

1.4. Equilibre à deux milieux : plasma-vide

1.4.1. Plasma et vide avec coque conductrice circulaire et champ transverse appliqué

Pour simplifier les calculs, nous supposerons dès le départ que le plasma a une section circulaire décentrée de la distance δ par rapport au centre de la coque circulaire ($\delta > 0$ signifie que le déplacement est vers l'extérieur pour $s = 0$). Le mouvement du plasma par rapport à l'axe de la coque est analogue au mouvement de l'axe magnétique par rapport à l'axe géométrique du plasma. Il tourne k fois si $\left(\frac{\iota}{2\pi}\right)_M \sim k$. Une étude plus poussée utilisant les coordonnées bipolaires a permis de montrer que l'approximation circulaire est seulement valable si $\nu < 1$.

Pour calculer δ il est commode de poser R=1. On écrit à l'aide de (24) que la coque de rayon b serait surface magnétique si le champ magnétique extérieur B n'était pas appliqué .

$$\delta\left[\frac{\alpha_0}{b} + kf_0\, b\right] = -\alpha_0\, a_k\, b \log b + \frac{3}{8}(a_k \quad)\, kf_0\, b^3 + (\alpha_1 - B_\perp)\, b + \frac{\beta_1}{b}$$

Pour calculer α_0, α, β il suffit d'écrire que la surface du plasma de rayon R=1 est surface magnétique pour le champ dans le vide ainsi que les 2 équations de continuité des champs magnétiques sur cette surface. Finalement :

$$\frac{\delta}{b} = -\frac{k+\eta}{k+\eta-\frac{k\,b^2}{r^2}} \cdot \frac{a_k R}{2}\,\frac{b}{R}\left\{\log\frac{b}{R} + \left(1-\frac{R^2}{b^2}\right)\frac{\eta}{\eta+k}\left[\frac{\nu}{a_k R} - \frac{1}{2} + \frac{k}{4\eta}\left(\frac{3b^2}{R^2}-5\right)\right]\right\}$$
$$+ \frac{b/R \quad B_\perp}{\left(\frac{2\pi R}{L}\right) f_0\left[k+\eta-\frac{k\,b^2}{R^2}\right]} \tag{33}$$

Remarque : dans /5/ on introduit la self induction interne d'une unité de longueur du cordon de plasma

$$l_i = \frac{1}{\pi a^2 B_{\theta\,(x=1)}^2} \int_0^R B_\theta^2\, \rho\, d\rho\, d\theta \tag{34}$$

ce qui donne à $\mathcal{E}^2$ près dans notre cas

$$l_i = \frac{1}{2}\left[1 + \frac{(2\bar{l}_i - 1)\eta^2}{(k+\eta)^2} - \frac{2k\eta}{k+\eta}\;\frac{I_3}{I_1}\right] \qquad \bar{l}_i = 1 - \frac{I_0 I}{I_1^{\,2}} \tag{35}$$

pour k=0 $l_i = \bar{l}_i$. Si on écrit alors

$$\frac{\nu}{a\,R} = \frac{l_i}{2} + \frac{k}{\eta}\left(\frac{4 I_2}{\mu I}\right) + \left(\frac{L}{2\pi R}\right)^2 \frac{\beta}{\eta^2} \tag{36}$$

il est facile de voir que pour k=0 l'expression de δ est identique à la formule (48) de la réf. /5/ .

Un moyen de diagnostic très bien adapté à ces phénomènes consiste à mesurer le flux k passant à travers un ruban faisant k tours le long du tore, dont les bords seront disposés symétriquement par rapport à l'axe central de la coque (distance $2\,l$) et disposés dans le milieu vide pour ne pas perturber le plasma .

Ce flux K est proportionnel à $F(\ell,\pi) - F(\ell,\theta)$ et nous le définirons en introduisant un champ magnétique transverse moyen $B_\perp$ tel que

$$K = 2\,L\,\ell\,B_\perp \tag{37}$$

On trouve

$$\frac{B_\perp}{\left(\frac{2\pi R}{L}\right)f_o}\;\frac{\ell/R}{(k+\eta)-\frac{k\ell^2}{R^2}} = \frac{\delta_b-\delta_\ell}{\ell} + \frac{B_\perp}{\frac{2\pi R}{L}f_o}\cdot\frac{b}{\ell}\cdot\frac{b/R}{\left(k+\eta-\frac{kb^2}{R^2}\right)} \tag{38}$$

où δ_b est donné par (33) avec $B_\perp = 0$
et δ_ℓ est la même expression que δ_ℓ avec ℓ à la place de b.

1.4.2. Plasma-vide en l'absence de coque conductrice

Le problème consiste à évaluer le champ magnétique $\vec{B}_{ee}$ que l'on doit créer de l'extérieur pour que le plasma précédemment étudié soit en équilibre.

Pour cela nous devons calculer le champ extérieur $\vec{B}_e$ au voisinage du plasma puis lui retrancher le champ créé par les courants intérieurs au plasma $\vec{B}_{ei}$

$$\vec{B}_{ee} = \vec{B}_e - \vec{B}_{ei} \tag{39}$$

Dans le cas k=0 , symétrie de révolution , le calcul est analytiquement simple. Pour les cas plus compliqués, seul un calcul approximatif est possible sans trop de complication. Pour les champs extérieurs, comme nous voulons étendre un peu la validité du calcul à des valeurs de $\frac{\iota_c}{2\pi}$ non nécessairement très proches de k , nous prendrons les formules (25) pour B_{ext} en sommant sur k . Dans cette sommation , η doit être remplacé par $\left(\frac{\iota_c}{2\pi} - k\right)$; de même, pour le courant j_s (17) , qui nous permettra de calculer approximativement le champ créé par les courants intérieurs , nous ajouterons une sommation sur k dans les mêmes conditions.

Cette généralisation n'est pas rigoureusement exacte et cela tient au fait que les expressions trouvées représentent une solution adaptée au mode k dominant . Ceci est visible en remarquant que même pour $a_k R = 0$ la solution choisie dépend de l'image hélicoïdale envisagée. Cependant si on pose que $\mu'^2\eta = \mu_k'^2\left(\frac{\iota_c}{2\pi} - k\right)$ est une quantité indépendante de k , la généralisation proposée est valable dans la mesure où les expressions qui interviennent dans les calculs tels que $\left(\frac{4I_2}{\mu' I_1}\right)$ dépendent peu de μ' .

Cette généralisation étant admise pour déterminer le champ extérieur produit par les courants intérieurs sans calculs lourds et sans intérêt compte tenu des approximations faites, nous remplacerons le calcul de ce champ dans la section d'abscisse curviligne par le champ produit par le tore circulaire de même courbure en s et parcouru par le courant j_s calculé en s .

On peut montrer que cette approximation revient à calculer exactement le terme en $\frac{1}{\rho}$ et en $\log \rho$ dans un développement du champ au voisinage d'un conducteur, le terme constant suivant n'étant pas évalué exactement .

Ce calcul donne pour le champ

$$\begin{aligned}\vec{B}_{ei} = \sum_k \Bigg\{ & \left[-\frac{\alpha_o a_k \log\rho}{2} + \frac{\beta_1}{\rho^2}\right]\sin\left(\theta + \frac{2k\pi s}{L}\right)\vec{e}_\rho \\ & + \left|\frac{\alpha_o}{\rho} + \left[\frac{a_k\alpha_o}{2} - \frac{\alpha_o a_k \log\rho}{2} - \frac{\beta_1}{\rho^2}\right]\cos\left(\theta + \frac{2k\pi s}{L}\right)\vec{e}_\theta\right\} \\ & + \left(\frac{2\pi R}{L}\right)\left(\frac{R}{2\mathcal{R}(s)}\right)\left(\frac{\iota_c}{2\pi}\right)\log\frac{R}{8\mathcal{R}(s)}\left[\sin\theta\,\vec{e}_\rho + \cos\theta\,\vec{e}_\theta\right]\end{aligned} \tag{40}$$

d'où B_{ee} que l'on décomposera

$$\vec{B}_{ee} = \vec{B}_{\perp e} + \vec{B}_{2t} + \vec{B}_{\perp plan} + \vec{B}_s \tag{41}$$

$\vec{B}_{\perp e}$ est un champ transverse qui tourne k fois le long du tore. Il a pour valeur :

$$\vec{B}_{\perp e} = f_o \sum_k -\left(\frac{2\pi R}{L}\right)(a_k R)\left[k + \frac{\eta}{4} + \frac{\eta}{2}\,\frac{\nu}{a_k R} - \frac{k x^2}{4}\right]\left[\vec{\ell}_\rho \sin t + \vec{\ell}_\theta \cos t\right] \tag{42}$$

$\vec{B}_{2t}$ est un champ transverse qui tourne 2k fois autour du tore

$$\vec{B}_{2t} = f_o \sum_k \frac{1}{8}\left(\frac{2\pi R}{L}\right)(a_k R)\, k x^2 \left(\vec{\ell}_\rho \sin t - \vec{\ell}_\theta \cos t\right) \tag{43}$$

$B_{\perp plan}$ est un champ transverse perpendiculaire au plan de l'axe magnétique. Son module dépend de s

$$B_{\perp plan} = -f_o \left(\frac{2\pi R}{L}\right) \frac{R}{2\mathcal{R}(s)} \left(\frac{\iota}{2\pi}\right) \mathcal{L}og\left(\frac{R}{8\mathcal{R}(s)}\right)\left[\sin\theta\, \vec{e}_\rho + \cos\theta\, \vec{e}_\theta\right] \tag{44}$$

si k=0 , on a simplement :

$$\vec{B}_{ee} = \left(\frac{2\pi R}{L}\right)^2 \left(\frac{\iota}{2\pi}\right)\left[\mathcal{L}og\,\frac{8L}{2\pi R} - \frac{1}{2} + \frac{\nu}{a_o R}\right] \tag{45}$$

2. ETUDE DE LA STABILITE

Nous utiliserons le critère de Suydam généralisé /6/ sous la forme donnée dans /1/ .

$$\left[\frac{1}{2}\frac{d}{d\Psi}\left(\frac{\iota}{2\pi}\right) + \int_s \vec{B}.\vec{Q}\,\frac{ds}{|grad\Psi|^3}\right]^2 + \int_s \frac{B^2 ds}{|grad\Psi|^3}\left[\left(\frac{\iota}{2\pi}\right)^2 \frac{dp}{d\Psi}\,\frac{d^2V}{d\Psi^2} - \int_s |Q|^2 \frac{ds}{|grad\Psi|^3}\right] \geqslant 0 \tag{46}$$

Comme dans /2/ et pour les mêmes raisons , nous avons particulièrement étudié la 2ème partie du critère lié au V" et aux effets de pression (ballooning) . Pour comparer ces 2 parties , on peut écrire de façon très schématique ce critère en négligeant les termes de pression liés au shear et au V":

$$\left[\frac{d}{dE}\left(\frac{\iota_c}{2\pi}\right)\right]^2 + 2\left(\frac{L}{2\pi R}\right)\frac{\beta}{E_n - E}\cdot\frac{d}{dE}\,\mathcal{L}og\, U \geqslant \text{(termes de pression)} \tag{47}$$

où $U = \dfrac{dV}{d\Psi}$

Vers l'axe magnétique $E \neq E_M$, donc le terme de shear ne joue pas.

Près de la singularité, si β n'est pas trop petit , $\nu \# (a_k R)^2 \frac{\beta}{\eta^2}$ ce qui donne en ordre de grandeur:

$$(\Delta S)^2 + \frac{2}{(a_k R)} \Delta \log U \gg \text{(termes de pression)} \tag{48}$$

$$S = \frac{1}{\sqrt{\nu}} \frac{1}{\eta} \left(\frac{\iota_c}{2\pi} - k \right)$$

Dans le cas $\mu' = 0$, S ne dépend que de ν (voir fig. 1 et 8).

Pour $\nu = 1$ $\Delta F = \sqrt{\frac{8}{3}}$ et si $(a_k R) = 0{,}1$ la fig. 5 donne $\Delta \log U \# 0{,}1$, les 2 termes sont du même ordre dans le critère , quel que soit β pas trop petit .

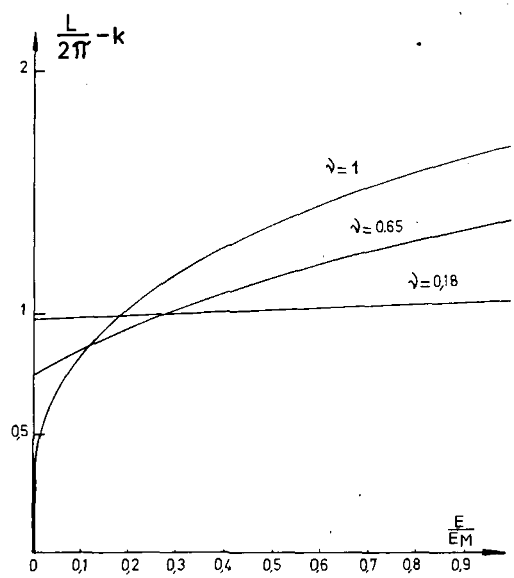

FIG. 1. Variation de l'angle de transformation rotationelle en fonction de E/E_M.

Les études sur ce critère (46) ont été faites, soit analytiquement (au voisinage de l'axe magnétique par exemple) , soit numériquement. Sans connaissance précise sur la répartition de pression, nous avons étudié le cas linéaire ($E_1 = \infty$ $p_2 = 0$).

Les Fig.2,3 et 4 montrent les domaines d'équilibre stable à un axe magnétique pour k=0 et k=2 ($\frac{a_2}{a_0} = 1$, cas Harmonica 2) et k=4 avec valeur variable de a_4 / a_0 . La courbe $\nu = 1$ sépare les régions représentant des configurations à un axe magnétique des régions représentant des configurations à topologie plus complexe (3ème partie) . Les courbes μ =Cte séparent les domaines stables et instables pour les régions du plasma voisines de l'axe magnétique. Ce sont les régions les plus difficiles à stabiliser et où l'effet du terme shear, de toute manière, ne joue pas .

Il est à remarquer que le domaine de stabilité diminue quand μ^2 décroît et devient négatif, c'est-à-dire lorsque le courant tend à se concentrer

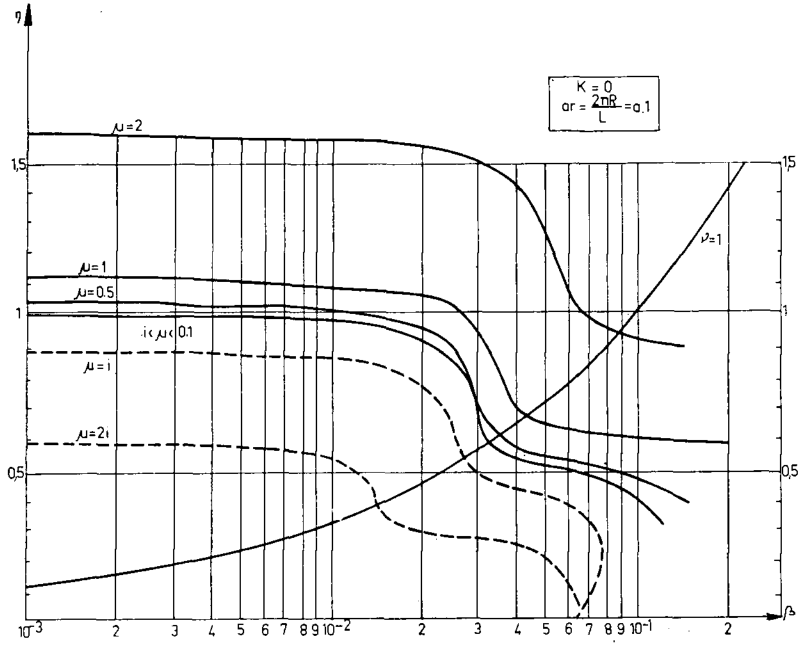

FIG. 2. Domaines maximum de stabilité pour les machines du type Harmonica 0 pour differentes valeurs de μ.

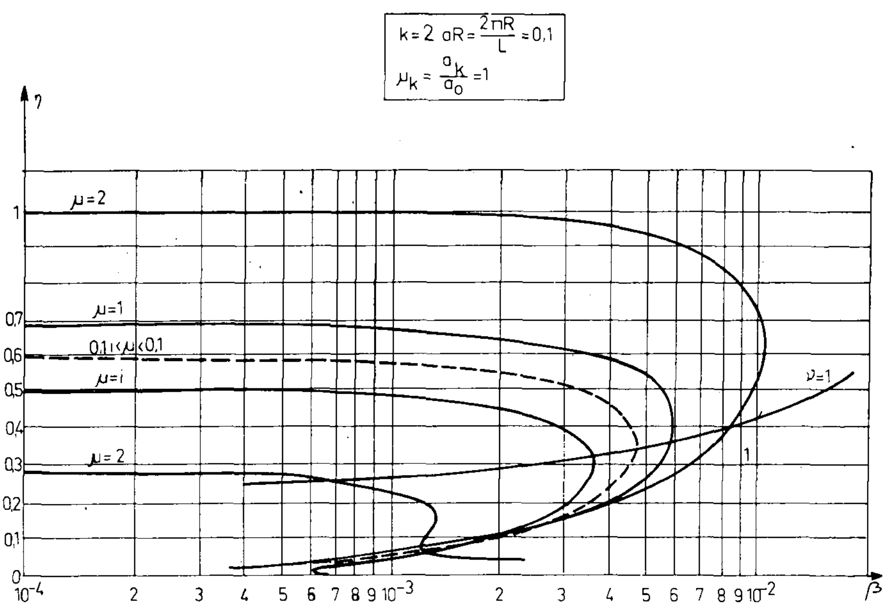

FIG. 3. Domaines maximum de la stabilité pour les machines du type Harmonica 2 pour differentes valeurs de μ.

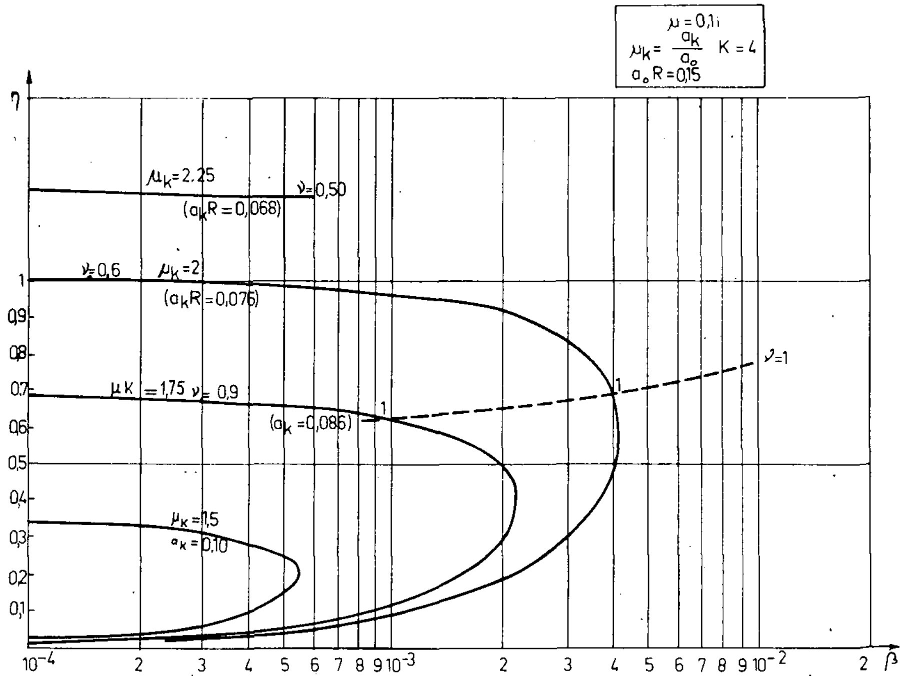

FIG. 4. Influence du rapport a_k/a_0 sur le domaine de stabilité. Machine type Harmonica 4.

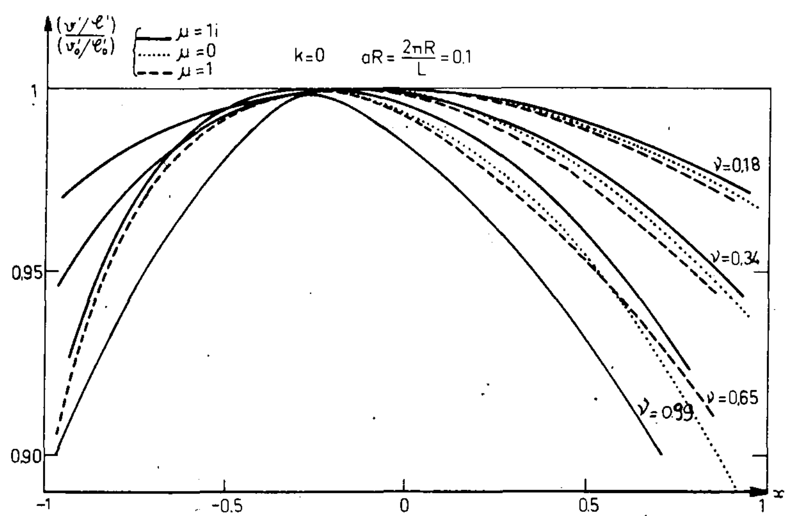

FIG. 5. Profondeur moyenne de puits; influence de μ.

dans le plasma (maximum de courant) . Cet effet est plus accentué pour k=2 que pour 0 car la courbe $\nu = 1$ est plus haute. Plusieurs expériences font penser que μ'^2 serait négatif et de l'ordre de quelques unités pour $\eta \gg 0$. Si la valeur devenait assez négative , on ne pourrait trouver une configuration à la fois stable sur l'axe magnétique et de topologie simple. Nous examinerons ce cas plus loin (§ 3).

Effet du β . Quelque soit β, on constate sur les figures que des courbes de stabilité, après être restées relativement indépendantes de β pour β petit, chutent assez brutalement pour des β variant de 1/1000 à 1/100. Or, les calculs au voisinage d'un axe magnétique montrent que si les surfaces magnétiques sont des petits cercles au premier ordre, ces courbes seraient indépendantes de β : l'effet constaté ici provient du déplacement de l'axe magnétique qui se traduit aussi par une déformation importante des surfaces magnétiques près de l'axe qui ne restent plus circulaires. Il y a donc un grand intérêt à étudier des plasmas de limite extérieure non circulaire et tels qu'après déplacement à l'approche d'une singularité les surfaces magnétiques soient des cercles au voisinage de l'axe magnétique, région particulièrement difficile à stabiliser.

La Fig. 5 montre en fonction de ν , qui est le vrai paramètre de déformation du milieu plasma, le puits magnétique moyen qui se crée. L'influence de μ' est faible .

La Fig. 8 montre de même en fonction de ν dans le cas $\mu' = 0$, la variation de $\frac{\iota_c}{2\pi} - \frac{1}{\eta}$

Pour $\nu = 1$, limite d'équilibre, le puits moyen et le shear atteints sont importants. On obtient des puits de l'ordre de 10%. Si l'on caractérise le shear par $\Delta = \left(\frac{\iota}{2\pi}\right)_{max} - \left(\frac{\iota}{2\pi}\right)_{bord}$ les effets de courbure seuls ($\mu' = 0$) permettent d'obtenir des valeurs de $\Delta = \sqrt{\frac{8}{3}}\,\eta \sim 0{,}8$ (pour $\eta = 0{,}5$) et les effets liés à la répartition de courant ($\mu' \neq 0$) conduisent pour des valeurs de μ' trouvées expérimentalement ($\mu' \sim 2{,}4\,i$) à $\Delta \sim 0{,}6\,\eta \sim 0{,}3$.

Sans entrer dans la discussion des instabilités non MHD, notons que ces facteurs (V" et shear) sont favorables à la stabilité .

Quant aux instabilités "kink" que nous n'avons pas envisagées dans ce travail, elles doivent être étudiées en connexion avec les effets de courbure qui changent certains ordres de grandeur au voisinage des singularités , ce qui ne permet pas a priori d'utiliser les résultats classiques dans ce domaine.

3. PLASMA A TOPOLOGIE COMPLEXE

Nous avons vu au cours des parties précédentes qu'à partir d'une certaine valeur $\nu = 1$ les équilibres étudiés présentaient 2 régions possédant chacune leur axe magnétique (Fig. 6 et 7). De plus, en général , une des régions est à pression négative si on continue à supposer la pression nulle sur le bord du plasma.

L'étude des états du plasma qui correspondraient à $\nu > 1$ est importante pour plusieurs raisons:

a) Si , comme nous l'avons vu au § 2 , la valeur de μ'^2 est très négative, on ne pourra pas éviter particulièrement pour les équilibres à k élevé (Harmonica 2, 4, ...) des configurations de ce type.

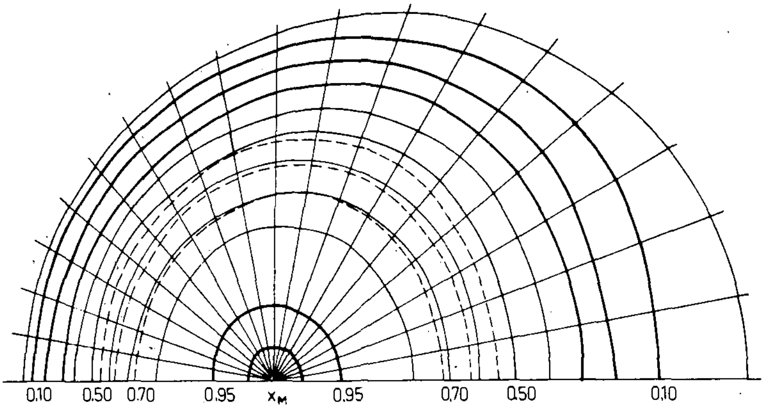

FIG. 6. Etude de la forme des surfaces E(x, t) pour $\beta = 0,002$, $k = 2$, $\mu = 1,21$, $\eta = 0,3$, $aR = \frac{2\pi R}{L} = 0,1$.

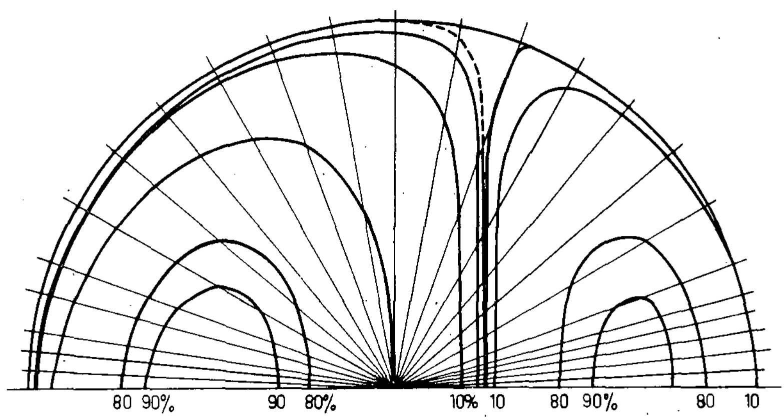

FIG. 7. Etude de la forme des surfaces E(x, t) pour $\beta = 0,002$, $\mu = 1$, $k = 2$, $\eta = 0,1$, $aR = \frac{2\pi R}{L} = 0,1$.

b) Par ailleurs, dans la phase transitoire de création de la configuration cherchée, il est probable que l'on devra franchir plus ou moins rapidement ces domaines à topologie complexe. Si le franchissement est rapide, il faut étudier les propriétés dynamiques du système; si le franchissement est assez lent pour pouvoir considérer que le système passe par une série de quasi-équilibres, on peut tenter de prévoir le comportement des systèmes avec des modèles simples.

Remarquons d'abord que $\left|\frac{\iota_c}{2\pi} - k\right|$ est minimum sur le bord du plasma et lorsque $\left(\frac{\iota_c}{2\pi}\right)_{bord} = k$, $\nu = 1$ (32). Si ν augmente, alors les 2 régions du plasma sont enveloppées par une surface magnétique qui conserve $\frac{\iota_c}{2\pi} = k$, comme on peut s'en persuader en notant que la ligne magnétique commune aux 2 régions sur cette surface tourne k fois.

Deux cas ont été étudiés [7] :

a) $E_1 = 0$

Cas simple à pression toujours positive. Ce cas ne permet pas le franchissement de la singularité.

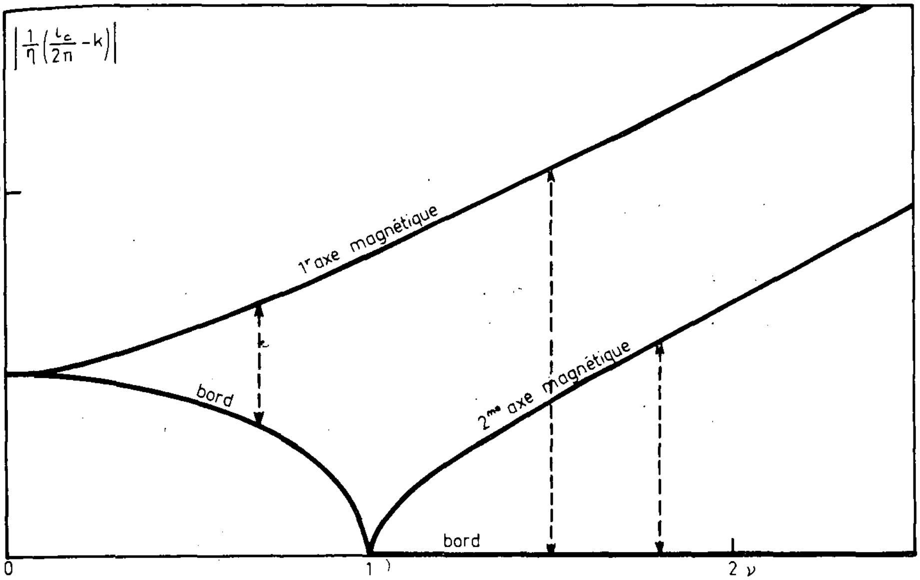

FIG. 8. Variation de l'angle de transformation rotationelle en fonction de ν.

b) $E_1 \neq 0$

On ne peut avoir de pression positive dans les 2 régions du plasma qu'en prenant des valeurs de E_1 différentes dans chacune d'elles et on ne peut atteindre $\frac{\iota_c}{2\pi} = k$ qu'en introduisant une couche de courant à la séparation. Même dans ce cas, on n'obtient pas réellement le franchissement de la singularité k car la suite continue des configurations de topologie simple et franchissant la singularité k sont des suites distinctes : par exemple , les répartitions des courants sont différentes pour les mêmes η .

On est donc tenté de conclure que la création de 2 axes magnétiques obtenue en augmentant $\left(\frac{\iota_c}{2\pi}\right)_M$ ne s'achève pas en configuration à topologie simple , la valeur k ayant été franchie, à moins que des effets dynamiques (instabilités, turbulence ....) ne viennent complètement perturber les phénomènes.

REFERENCES

[1] MERCIER, C., Nucl. Fusion 4 (1960) 213.

[2] MERCIER, C., in Plasma Physics and Controlled Nuclear Fusion Research (Proc. Conf. Culham, 1965) I, IAEA, Vienna (1966) 417.

[3] SHAFRANOV, V.D., SOLOVIEV, L.S., Closed Magnetic Configurations in Plasma Physics and the Problem of Controlled Nuclear Reactions (LEONTOVICH, M.A., Ed.) 4, Moscow.

[4] Advances in Theoretical Physics (BRUECKNER, K.A., Ed.) 2, New York, Academic Press (1967).

[5] SHAFRANOV, V.D., Atomn. Energ. 13 (1962) 521.

[6] MERCIER, C., Nucl. Fusion, 1962 Supplement, Part 2 (1962) 801; C. r. hebd. Séanc. Acad. Sci. Paris 252 (1961) 1577.

[7] ADAM, J.C., Rapport CEA R-3490 (1968).

DISCUSSION

M.S. RABINOVICH: What is the difference between your approach and that of Solovyev and co-workers?

C. MERCIER: There are two methods for studying the characteristics of toroidal plasmas: expansion near the magnetic axis (the general case - C. Mercier, Nucl. Fusion 3 (1963) 89; C. Mercier, Nucl. Fusion 4 (1964) 213; C. Mercier, Problems in the study of toroidal configurations, EUR-CEA-FC-397, 1966) and expansion near the singularities ($\iota/2n = 0$ for Tokamak, $\iota/2n = 2$ for Harmonica II - C. Mercier, on Plasma Physics and Controlled Nuclear Fusion Research 1 (Proc. 2nd Conf.) 1 (1966) 417). The former method, which has been used by Solovyev and co-workers, has the disadvantage that (for convergence questions) it does not permit the study of properties near the singularities or of the magnetic surfaces far from the magnetic axis.

In our paper, we used the latter method. It is less general, but applies throughout the plasma, enabling one to study the approach of singularities and even the more complex configurations (several magnetic axes) which may then arise.

The difference between the two methods may be illustrated by the following example. With the first method, if the magnetic surfaces are circles near the axis, no ballooning effect limits β. On the other hand, the second method places a limitation on β, although the external plasma retains a circular cross-section. This limitation is due to displacement of the magnetic axis, which may be substantial and which may result in non-circular magnetic surfaces near the axis.

BEHAVIOUR OF OHMICALLY HEATED PLASMA IN A HELIOTRON MAGNETIC FIELD

KOJI UO, RYOHEI ITATANI, AKIHIRO MOHRI, HIROSHI OSHIYAMA, SEIICHI ARIGA AND TAISEI UEDE
PLASMA PHYSICS LABORATORY, KYOTO UNIVERSITY, KYOTO, JAPAN

Abstract

BEHAVIOUR OF OHMICALLY HEATED PLASMA IN A HELIOTRON MAGNETIC FIELD. The behaviour of a plasma produced by ohmic heating in a corrugated toroidal magnetic field with circular cusp trains near the wall – the *heliotron field* – is studied experimentally. Rogowski-coil and directional-probe measurements show that the current column is well confined inside the separatrix without contacting the wall of the vacuum vessel and seems to be stable with respect to Kruskal instabilities as could be expected. The effect of the vertical magnetic field B_V on the plasma equilibrium is examined. The cross-section area, where the equipotential surfaces of the static electric field across the plasma column are closed, becomes maximum for optimum B_V and fills up the region inside the separatrix. When B_V is not optimum the area is small and some of the equipotential surfaces inside the separatrix are not closed. Experimentally observed optimum values of B_V are by more than a factor of 2 smaller than the theoretically calculated values; changing the heliotron field to the Tokamak-type field makes little difference although the plasma parameters remain almost the same in both cases. Periodically intensified B_V in space corresponding to the period of the corrugated field remarkably improves the maximum current. Anomalous plasma loss through the ring cusp is observed. It results from the cusp split due to strong pulsive azimuthal current flowing through the cusp. This pulsive current is the azimuthal component of a spiral plasma current string rotating around the minor axis. The period of the rotation or of the pulsive current increases with increasing magnetic field intensity and plasma density, and finally the rotation ceases. When this current flows through the cusp, the cusp splits into two parts and the magnetic lines of force, formerly confined inside the separatrix, move outside and cross the wall resulting in an anomalous plasma loss. It seems that, under the present experimental conditions, the plasma in the heliotron field hardly forms the necessary plasma density profile required for stability against interchange, and the plasma becomes unstable for interchange of m = 1. The rotation is due to the radial electric field.

1. INTRODUCTION

This paper consists of two parts. In the first part, the behaviour of a plasma produced by ohmic heating in a corrugated toroidal magnetic field with circular cusp trains near the wall [1-4], i.e. the heliotron field, is studied. Recently, plasma confinement by modified heliotron fields was proposed in order to overcome defects of the heliotron field. [5, 6]. The second part of this paper describes an experiment on one of these modified heliotron fields, the poloidal heliotron field having a poloidal conductor buried inside the plasma. While the ohmically heated plasma in the heliotron-C machine is noisy and shows an anomalous cusp loss, the plasma injected from a gun into the poloidal heliotron field is extremely quiescent and has very long life-time corresponding to about 20 times of the Bohm confinement time.

2. THE HELIOTRON-C EXPERIMENT

The magnetic field configuration of the heliotron-C machine is shown in Fig.1. This field provides an equilibrium of the plasma inside the separatrix, and the plasma with an appropriate density profile is stable with respect to the flute instability [2]. The heliotron-C machine shown in Fig.2 is designed such as to eliminate the U-bend drift by the azimuthal drift due to the corrugated field and such as to produce the uniform electric field needed for the ohmic heating by distributing the 16 iron cores of the coupling transformer around the torus. The major radius is 1.02 m, the tube radius 7 cm, the magnetic field on the axis under the negative coil 0.1 Wbm^{-2}, the mirror ratio on the axis 3.5-8, the radius of the neutral line 2 cm and the loop voltage 500 V. The basic pressure is about 10^{-6} Torr; hydrogen is used as the gas.

The observed values of the optimum vertical field B_V, which is necessary for the equilibrium of a current-carrying toroidal plasma, are by a factor of 2-3 smaller than the theoretically predicted values [7, 8] as shown in Fig.3. Replacing the heliotron field by a Tokamak-type field makes little difference on the B_V-I_{OH} relation although the plasma parameters remain almost the same in both cases. The substitution of a stainless aperture limiter by a glass limiter requires larger B_V for optimization since the stainless limiter has some short-circuit effect for the charge separation. The heliotron field being corrugated, it seems to be effective to superpose the corrugated vertical field B_w upon the uniform vertical

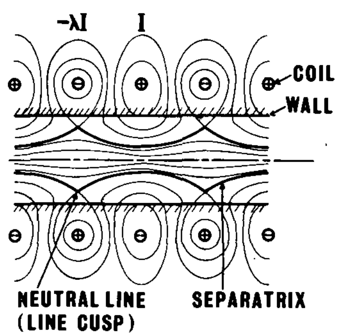

FIG.1. The heliotron-C magnetic field.

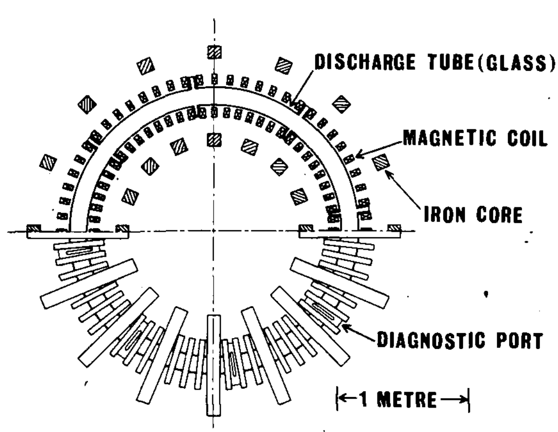

FIG.2. The heliotron-C machine.

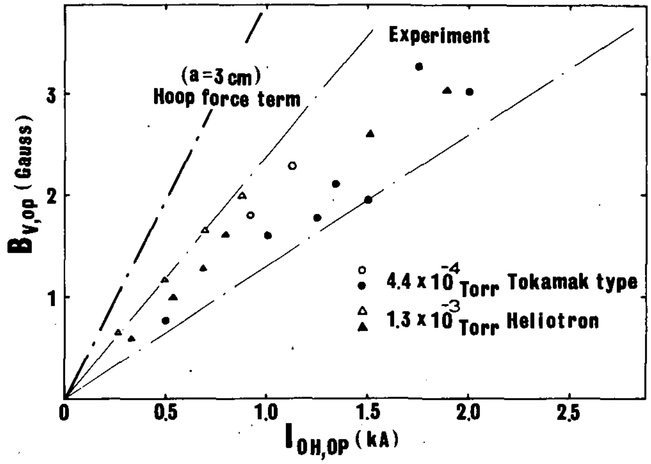

FIG. 3. Optimum vertical field B_V for the ohmic heating current I_{OH}.
The thick chain line is the hoop force term of B_V calculated theoretically. If we include the pressure term of B_V, the deviation from the experimental value becomes larger.

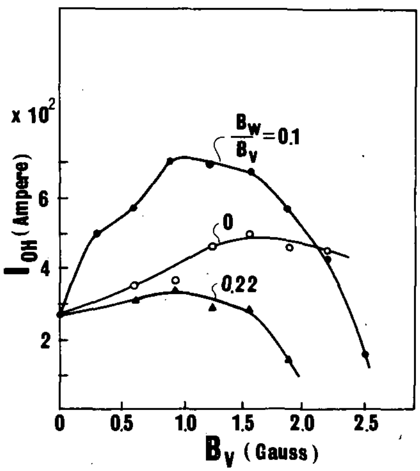

FIG. 4. The effect of the superposition of corrugated vertical field B_W on the uniform vertical field.

field B_V corresponding to the period of the confining field. Figure 4 shows that the appropriate superposition of B_W improves the maximum I_{OH} by about 40%.

The electric potential in the cross-section of the plasma column is produced both by the perpendicular charge separation due to the U-bend drift and the radial charge separation due to the radial density gradient and the difference in the ion and electron Larmor radii. In the heliotron plasma, the equipotential surfaces are closed in the region inside the separatrix when B_V is optimum. If B_V is not optimum, the region where the surfaces are closed becomes narrow and the potential gradient becomes steeper. T_i/T_e is equal to 1 for the heliotron discharge and equal to 2/3 for the Tokamak-type discharge although other plasma parameters are almost the same in both cases. This result suggests the existence of a thermalization effect due to the corrugated field. The ohmic heating current is confined to the region inside the separatrix. Outside the separatrix, I_{OH} is zero. The plasma density is about 10^{20} m^{-3} on the axis, and the plasma is quite noisy. $\Delta n/n$ is about 20% on the axis and about 100% on the separatrix.

In the discharge we observed a helical current string rotating around the axis. The pitch of the helix changes in the axial direction and is shortest near the neutral line. In the plane including a neutral line where B = 0, the azimuthal component of this helical current is concentrated in the region near the neutral line. When I_{OH} = 2 kA, E_{OH} = 80 Vm^{-1}, T_e = 6 eV, $n \approx 10^{19}$ m^{-3} and B = 0.1 Wbm^{-2} on the axis under the neutral line, the helical current near the neutral line is about 600 A according to the measurement with the Rogowski coil whose inner diameter is 1.5 cm. Since the helix rotates the signal observed by the Rogowski coil is pulsive and its frequency is about 50 kHz which agrees with the frequency of rotation of the $\vec{E}_r \times \vec{B}$ drift. This phenomenon seems to be closely connected with the anomalous loss mechanism of the heliotron discharge. The azimuthal component of the above-mentioned large helical current breaks the magnetic surface of the separatrix pulsively and moves the plasma inside the separatrix toward the wall. We observe the strong pulsive plasma flow outside the separatrix. The decay time of the afterglow plasma is about 30 μs.

3. MINIMUM $\bar{B}$ HELIOTRON FIELD

From the experimental results, it is concluded that the normal cusp loss and the anomalous loss due to the cusp split quickly remove the plasma on the separatrix, and the plasma inside the separatrix cannot satisfy the density profile necessary for stability against interchange [2]. To overcome this effect, modified heliotron fields putting the negative coils of the heliotron field inside the vacuum vessel were proposed [5, 6]. The field configuration of the poloidal heliotron field is shown in Fig.5, which is the same as already proposed by Kadomtsev [1]. The buried conductors and the magnetic surfaces of the helical heliotron field are shown in Fig.6. These fields form magnetic wells of the potential $U = -\int dl/B$, and the bottom of the well is on the separatrix which is the surface woven by the lines of force passing the points where $B_z = B_r = 0$. It is interesting that the plasma inside the separatrix has no contact with the supports of the buried conductors; it is stable as far as the region

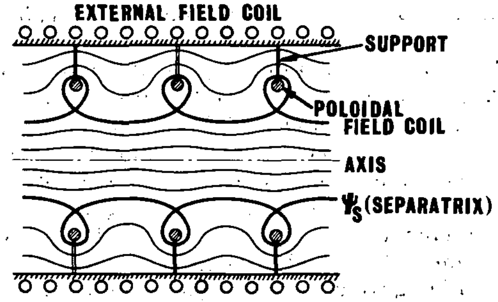

FIG. 5. The poloidal heliotron field.

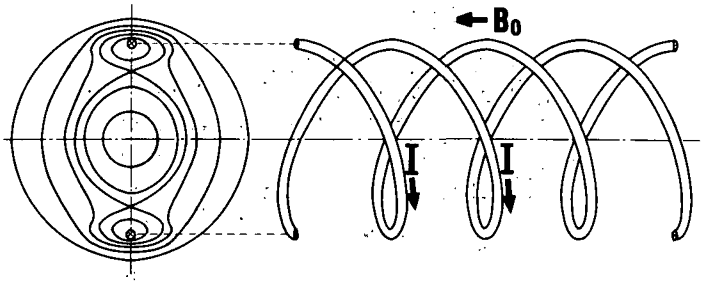

FIG.6. Buried conductors and the magnetic surfaces of the helical heliotron field.

just outside the separatrix is filled with the plasma [1, 2]. When the plasma fills the region inside the maximum U surface, it is stable with respect to flute instability. The plasma outside the separatrix will be lost gradually because of the support loss. When the plasma density just outside the separatrix becomes sufficiently low, the plasma inside the separatrix starts to leak out owing to the instability. However, we can decrease the effective loss rate by making the region inside the separatrix sufficiently large compared with the size of the support. Moreover, if we compensate the plasma loss due to the supports by injection or other means and keep the plasma density constant just outside the separatrix, the plasma inside the separatrix will be confined stably, and the confinement time will be extended considerably. The substitution of the old plasma by the newly injected one will take place only in the region outside the separatrix, but not inside it.

4. MINIMUM $\overline{B}$ HELIOTRON EXPERIMENT

As in the preliminary experiment on the plasma confinement by a poloidal heliotron field, the plasma behaviour in a mirror field with a buried poloidal conductor is investigated. The experimental device is shown in Fig.7. The buried copper ring with an inner diameter of 9 cm is placed inside the vacuum tube of 15 cm diameter in the mid plane of the mirror field. The current of the ring is supplied externally through the support of 1.0 cm diameter. The radius of the neutral line with B = 0 is 2.5 cm. The mirror ratio of the field inside the separatrix is 9 on the axis. The field intensity is 2.2×10^{-2} $\mathrm{Wbm^{-2}}$ on the axis under the buried conductor. Thus, the maximum B on the axis is 0.2 $\mathrm{Wbm^{-2}}$. The base pressure is 4×10^{-6} Torr. The plasma is produced by a coaxial gun and injected into the field through a glass aperture limiter of 3 cm diameter which makes it possible to reduce the neutral influx produced by the gun firing into the confining region. To cut the tail of the plasma streaming into the confining region as quickly as possible, a short circuit controlling the current width through the gun in the range between 15 and 60 μs, is applied to the gun. The gas is helium.

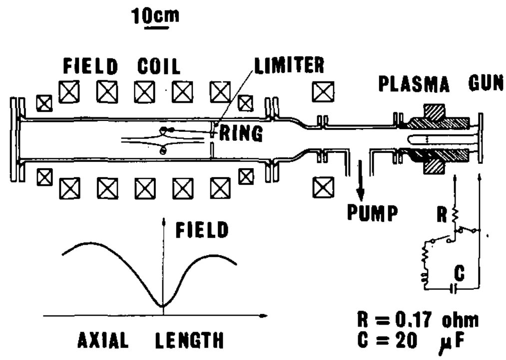

FIG. 7. Preliminary experimental device of the poloidal heliotron.

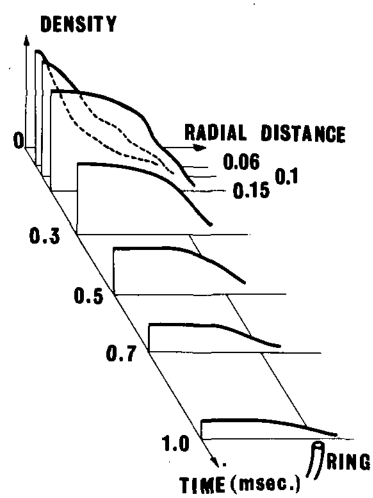

FIG. 8. The time variation of the radial density distribution of the plasma injected into the poloidal heliotron field.

The time variation of the radial density distribution near the buried conductor is shown in Fig.8. The figure shows that the plasma quickly spreads in radial direction with an average speed of 1.5×10^3 ms^{-1}. 0.4 ms after gun firing the profile becomes flat inside the separatrix, and the density decays, keeping this profile. In this state, the observed time constant of the density decay is 0.45 ms as shown in Fig.9, and the plasma is very quiescent.

The factors contributing to the plasma decay in this system could be the support loss, the end loss and the radial-diffusion loss. If we designate by τ_0 the decay time in the absence of support loss, and by τ_s the decay time due to the existence of two supports, the total decay time τ_N due to the existence of 2N supports can be written approximately as $\tau_N^{-1} = \tau_0^{-1} + (N/\tau_s)$. Observation of τ_N for different N gives τ_s = 1.7 ms and τ_0 = 0.62 ms. Since τ_0 consists of the time constant of the end loss, τ_m, and that of the radial diffusion loss, τ_r, we have $\tau_0^{-1} = \tau_m^{-1} + \tau_r^{-1}$. The computed value of τ_m is 3.4 ms for n = 10^{17} m^{-3}, T_i = 23 eV and T_e = 15 eV.

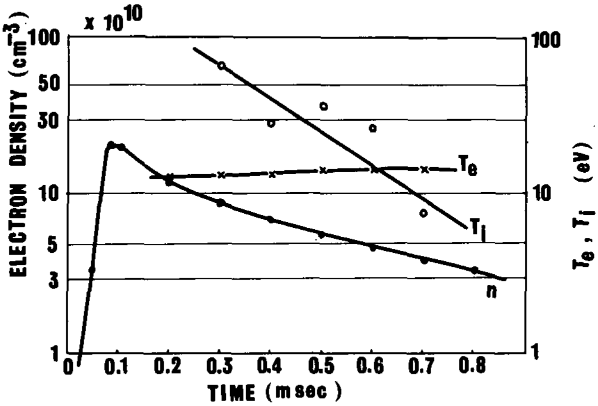

FIG. 9. The decay curves of the density n, the ion temperature T_i and the electron temperature T_e of the plasma confined in the poloidal heliotron field.

Then, we have τ_r of 0.76 ms. This is about 22 times the Bohm confinement time, $\tau_B = 2.8Br_p{}^2T_e^{-1}$ (eV), where $B = 0.11$ Wbm^{-2} , $r_p = 4 \times 10^{-2}$ m and $T_e = 15$ eV. Even the observed confinement time of 0.45 ms is still 13 times τ_B . It is interesting that, if we assume that each particle of the plasma can touch the support, the calculated loss time for two supports, $\tau_s^* = V(v_iS)^{-1}$, is 0.25 ms, which is much shorter than the measured τ_s of 1.7 ms. This time is about one third of the observed radial diffusion time τ_r , 0.76 ms, and about one half even of the observed total confinement time 0.45 ms. As shown in Fig.9, the ion temperature decreases with a decay time of some 0.2 ms. There is neutral gas flowing through the aperture from the gun. This neutral gas pressure is 6.6×10^{-5} Torr at 0.5 ms after the initiation of the gun injection; it coincides well with the decay time of the charge transfer of ions with neutral atoms. The electron temperature T_e is almost constant. These curves are quite similar to those of the experiment on the toroidal octupole [9]. When we produce the heliotron-C-type field by inserting a glass tube of 7.5 cm outer diameter and destroy the condition of min $\bar{B}$, a strong oscillation takes place in the plasma.

REFERENCES

[1] KADOMTSEV, B. B., in Plasma Physics and the Problem of the Controlled Thermonuclear Reactions (LEONTOVICH, M.A., Ed.), Pergamon Press (1960) 417.
[2] UO, K., J. phys. Soc. Japan 16 (1961) 1380.
[3] UO, K., Kakuyūgō-kenkyū 1 (1958) 1.
[4] UO, K., Physics Fluids 5 (1962) 1293.
[5] UO, K., Kakuyūgō-kenkyū 20 (1968) 193.
[6] MOHRI, A., MATSUDA, S., Kakuyūgō-kenkyū 20 (1068) 165.
[7] SHAFRANOV, V.D., J. nucl. Energy, Part C, 5 (1962) 251.
[8] YOSHIKAWA, S., et al., MATT-155 (Dec., 1962).
[9] OHKAWA, T., et al., CN-21/115 (1965).

О СПЕКТРЕ ТУРБУЛЕНТНЫХ ФЛЮКТУАЦИЙ ПАРАМЕТРОВ ПЛАЗМЫ СИЛЬНОТОЧНОГО ТОРОИДАЛЬНОГО РАЗРЯДА

М.М.ЛАРИОНОВ, В.А.РОДИЧКИН,
В.В.РОЖДЕСТВЕНСКИЙ и А.М.ТИМОНИН
ФИЗИКО-ТЕХНИЧЕСКИЙ ИНСТИТУТ
им.А.Ф.ИОФФЕ, ЛЕНИНГРАД,
СССР

Abstract — Аннотация

SPECTRUM OF TURBULENT FLUCTUATIONS OF PLASMA PARAMETERS IN A HIGH-CURRENT TOROIDAL DISCHARGE. The turbulent fluctuations of various plasma parameters are investigated in a high-current toroidal discharge stabilized by a weak longitudinal magnetic field (the "Alpha" device). The authors study voltage fluctuations at double probes, fluctuations in the signals from magnetic probes and fluctuations in the power of a microwave signal in the 4-mm range passing through the plasma. Using equipment for the correlation analysis of electrical signals, they determine the mean squares of the amplitudes and the power spectra of the above fluctuations over the range 50 kc/s - 2 Mc/s. In addition, they investigate the spatial correlation of the signals from the double and magnetic probes. It is established that the power density of the fluctuations of all the signals in the range considered falls monotonically as the frequency rises. No characteristic frequencies are found in the spectra. It may be assumed that the voltage fluctuations at the double probes are associated with random movement of the plasma surrounding the probes across the lines of force of the magnetic field. It is then possible to calculate from the voltage fluctuations the characteristic velocity of such motion; this is found to be of the order of 10^6 cm/s. On this assumption, the voltage fluctuation spectrum coincides with the velocity spectrum of the transverse plasma motion; it is found that the velocity spectrum of the plasma motion is similar to the velocity spectrum of hydrodynamic turbulence.

Velocity fluctuations in the presence of a mean density gradient lead to plasma density fluctuations. Study of the fluctuations of the microwave signal passing through the plasma confirms the presence of density fluctuations of the order of 10% of the mean density value.

The turbulent motion across the magnetic field also leads to an increase in the plasma diffusion rate. The particle lifetime calculated from the coefficient of turbulent diffusion is found to be close to the measured energy lifetime.

О СПЕКТРЕ ТУРБУЛЕНТНЫХ ФЛЮКТУАЦИЙ ПАРАМЕТРОВ ПЛАЗМЫ СИЛЬНОТОЧНОГО ТОРОИДАЛЬНОГО РАЗРЯДА. В сильноточном тороидальном разряде, стабилизированном слабым продольным магнитным полем (установка "Альфа"), исследовались турбулентные флюктуации различных параметров плазмы. Изучались флюктуации напряжения на двойных зондах, флюктуации сигналов магнитных зондов, флюктуации мощности СВЧ-сигнала 4-х миллиметрового диапазона, проходящего через плазму. При помощи аппаратуры для корреляционного анализа электрических сигналов определялись средние квадраты амплитуд и спектры мощности флюктуаций указанных величин в диапазоне 50 кгц – 2 мгц. Исследовалась пространственная корреляция сигналов с двойных и магнитных зондов. Установлено, что плотность мощности флюктуаций всех сигналов в исследованном диапазоне монотонно падает с ростом частоты. Каких-либо характерных частот в спектрах не обнаружено. Можно предположить, что флюктуации напряжения на двойном зонде связаны с хаотическим движением окружающей зонд плазмы поперек силовых линий магнитного поля. Тогда по величине флюктуаций напряжения можно вычислить характерную скорость такого движения, которая оказывается порядка 10^6 см/сек. Спектр флюктуаций напряжения в этом предположении совпадает со спектром скоростей поперечного движения плазмы. При этом оказывается, что спектр скоростей движения плазмы подобен спектру скоростей гидродинамической турбулентности. Флюктуации скорости при наличии градиента средней плотности приводят к флюктуациям плотности плазмы. Исследование флюктуаций проходящего СВЧ-сигнала подтверждает наличие флюктуаций плотности порядка 10% от среднего ее значения. Турбулентное движение поперек магнитного поля приводит также к увеличению скорости диффузии плазмы. Время жизни частиц, вычисленное по величине коэффициента турбулентной диффузии, оказывается близким к измеренному энергетическому времени жизни.

Эксперименты с сильноточными разрядами, стабилизированными слабым продольным магнитным полем и проводящим кожухом, показали, что плазма в таких разрядах находится в турбулентном состоянии. Эта турбулентность проявляется в интенсивных флюктуациях с частотами порядка сотен килогерц как интегральных характеристик разряда (производной тока, яркости свечения спектральных линий, мощности проходящего через плазму СВЧ-сигнала), так и локальных параметров в любой точке внутри плазмы (сигналы с электрических и магнитных зондов).

Причиной развития турбулентности, вероятно, является магнитогидродинамическая конвективная неустойчивость, приводящая к возможности обмена силовыми трубками магнитного поля с плазмой между центральными и периферическими областями разряда. В работе Кадомцева [1] исследованы условия возникновения конвективной неустойчивости в разряде рассматриваемого типа. Исходя из критерия устойчивости Сайдема, показано, что конвекция развивается, если давление плазмы на оси разряда превосходит некоторую величину, определяемую начальным стабилизирующим полем H_0 и параметром $\eta = \frac{4J}{aH_0}$, где J – ток разряда, a – радиус стабилизирующего кожуха. Давление устойчиво удерживаемой плазмы в таком разряде не может превосходить четырех процентов от давления магнитного поля на оси.

На установке "Альфа" [2] в последнее время проводилось изучение явлений, связанных с турбулентностью. Имелась возможность оценить условия в разряде с точки зрения выполнения критерия Сайдема. По известным току разряда и распределению магнитных полей в сечении шнура было вычислено максимально возможное давление устойчивой плазмы. Имелись сведения о плотности и температуре плазмы, полученные разными методами (зондирование пучком нейтральных атомов, измерение радиационной температуры в СВЧ-диапазоне, измерения с помощью многосеточного анализатора энергий заряженных частиц). По этим данным было вычислено газокинетическое давление $P = nK(T_e + T_i)$. Оказалось, что это давление в 3–4 раза превышает максимально допустимое с точки зрения критерия Сайдема. Таким образом, условия для развития конвективной неустойчивости являются благоприятными.

На установке "Альфа" в одинаковых режимах работы исследовались различные флюктуационные явления: измерялись среднеквадратичные значения и спектры сигналов двойных электрических и магнитных зондов и колебаний мощности проходящего через плазму СВЧ-сигнала. Кроме того, изучалась пространственная корреляция зондовых сигналов. Для анализа сигналов был построен прибор, блок-схема которого изображена на рис.I [3]. Прибор преобразует подаваемые на вход флюктуационные электрические сигналы X_1 и X_2 в напряжение, пропорциональное их коэффициентам корреляции или автокорреляции:

$$K_{12} = \frac{1}{T}\int_0^T X_1(t)\, X_2(t+\tau)\, dt$$

$$K_{11} = \frac{1}{T}\int_0^T X_1(t)\, X_2(t+\tau)\, dt$$

где $X(t)$ - значение сигнала в момент t, $X(t+\tau)$ - значение сигнала в момент $t+\tau$, τ - время задержки, T - время усреднения.

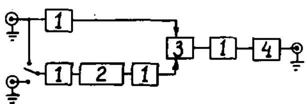

Рис.1. Блок-схема корреляционного анализатора: 1 – усилители; 2 – регулируемая линия задержки; 3 – перемножающая ячейка; 4 – интегратор.

Величина K_{11} при $\tau = 0$ представляет собой среднеквадратичное значение сигнала X_1. Зависимости коэффициентов корреляции от времени задержки представляют собой корреляционные функции исследуемых сигналов $B_{12}(\tau)$ и $B_{11}(\tau)$. Спектр мощности флюктуаций сигнала X_1 вычисляется по его автокорреляционной функции путем преобразования Фурье:

$$W_1(\omega) = \frac{1}{2\pi}\int_{-\infty}^{\infty} e^{-i\omega\tau} B_{11}(\tau)\, d\tau$$

В нашей работе это вычисление выполнялось на ЭВМ.

В корреляционном анализаторе, с которым проводились измерения, линия задержки допускала исследование сигнала при задержках от 0 до 20 мксек ступенями через 0,2 мксек. Это определяло анализируемый диапазон частот в спектре сигнала - от 50 кгц до I Мгц. Исследуемый разряд имел импульсный характер, длительность его составляла 3 мсек. Это ограничивало допустимое время усреднения величиной, равной 0,5 мсек. Сигнал с выхода корреляционного анализатора регистрировался импульсным осциллографом, обычно вместе с сигналом тока разряда, и позволял определить изменение коэффициента корреляции в течение разряда. Так как воспроизводимость усредненных параметров от разряда к разряду была хорошей, функцию корреляции можно было построить, используя значения ряда коэффициентов корреляции, полученных при разных временах задержки в последовательных разрядах. Ниже приводятся функции корреляции, относящиеся к моменту максимума разрядного тока. Состояние плазмы в этот момент можно было считать стационарным в течение времени усреднения анализатора.

Ранее было обнаружено, что между электродами двойного зонда, находящимися под плавающим потенциалом в плазме сильноточного разряда, развивается значительное напряжение флюктуационного характера [4]. Предполагается, что оно отражает флюктуации напряженности электрического поля внутри плазмы. Для изучения этого явления на установке "Альфа" применялась зондовая система, состоящая из 8 двойных зондов, размещенных на одной кварцевой трубке, которая вводилась через вакуумное уплотнение по радиусу разрядной камеры. Электроды каждого двойного зонда были расположены так, что регистрировалась составляющая поля, перпендикулярная оси трубки. Они представляли собой платиновые проволочки диаметром I и длиной 5 мм, вваренные в трубку на расстоянии 8мм друг от друга. Расстояние между соседними парами электродов равнялось IOмм. Выводы от каждого зонда были тщательно экранированы от электрических и магнитных наводок. Сигналы с двойных зондов через разделительные трансформаторы подавались на вход корреляционного анализатора, и по осциллограммам напряжения на его выходе строились корреляционные и автокорреляционные функции флюктуаций.

В измерениях, описываемых в докладе, зондовую систему устанавливали вблизи оси разряда и ориентировали так, что регистрировалась перпендикулярная оси составляющая электрического поля. Так как магнитное поле в этом месте направлено вдоль оси разряда, то зонд регистрировал перпендикулярную силовым линиям компоненту электрического поля.

Флюктуации магнитного поля изучались при помощи системы магнитных зондов, состоящей из 8 катушек, помещенных внутри кварцевой трубки. Расстояние между соседними катушками равнялось IO мм, а их оси были перпендикулярны оси трубки. Каждая катушка имела диаметр около 5мм и состояла из 70 витков. Система зондов была экранирована от электростатических наводок. Резонансная частота магнитного зонда вместе с его кабелем составляла 2 Мгц, поэтому на более низких частотах напряжение, снимаемое с зонда, было пропорционально производной магнитного потока сквозь его катушку. При измерениях система зондов помещалась вблизи оси разряда и ориентировалась таким образом, что регистрировалась перпендикулярная оси разряда составляющая магнитного поля.

Режим работы установки "Альфа" при всех измерениях, описанных в докладе, характеризовался следующими параметрами:

Давление водорода в разрядной камере P_0 = 4.10^{-4}мм рт.ст.
Стабилизирующее поле H_0 = 360 эрст.
Напряжение на конденсаторной батарее U_0 = 7,5 кв
Амплитудное значение тока разряда J_{max} = 90 кА.

Измерения относятся к моменту максимума разрядного тока.

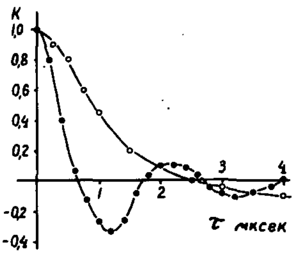

Рис.2. Автокорреляционные функции флюктуаций в интервале 0÷4 мксек:
○ – электрического поля;
● – производной магнитного поля.

На рис.2. приведены функции автокорреляции флюктуаций напряжения на двойном зонде и сигнала с магнитного зонда в зависимости от времени задержки τ. Мы предполагаем, что они совпадают с функциями автокорреляции флюктуаций поперечных составляющих электрического поля и производной магнитного поля.

На рис.3 приведены спектры мощности флюктуаций электрического поля, $\overline{E_\omega^2} = f(\omega)$, магнитного поля, $\overline{H_\omega^2} = f(\omega)$ и его производной $\overline{H_\omega'^2} = f(\omega)$. Спектры вычислены по соответствующим функциям корреляции. Спектр для магнитного поля был вычислен по спектру его производной, учитывая, что $H'_\omega = \omega H_\omega$. Кроме того, в другой серии измерений сигнал с магнитного зонда подавался на вход корреляционного анализатора после электрического интегрирования. Таким образом, сразу анализировались флюктуации магнитного поля. Спектр, полученный на основе этих измерений, близок к рассчитанному по спектру флюктуаций производной поля.

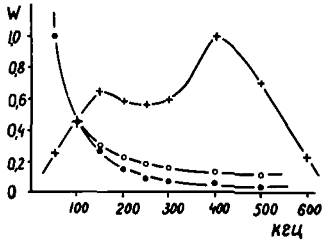

Рис.3. Спектры мощности флюктуаций:
○ – электрического поля;
● – магнитного поля;
+ – производной магнитного поля.

Измерялись среднеквардатичные величины флюктуаций электрического и магнитного поля. Они имеют величину:

$$(\overline{E}^2)^{1/2} \cong 30\ в/см,\ (\overline{H}^2)^{1/2} \cong 40\ эрст.$$

Для определения линейного масштаба флюктуации полей были выполнены опыты по изучению взаимной корреляции сигналов с двух зондов. Сигналы с двух двойных или с двух магнитных зондов, находящихся на различном расстоянии друг от друга, подавались на два входа корреляционного анализатора, и по осциллограммам строились пространственные корреляционные

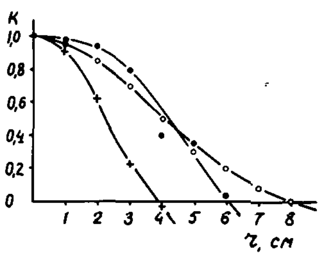

Рис.4. Пространственные функции корреляции флюктуаций:
○ – электрического поля;
● – магнитного поля;
+ – производной магнитного поля.

функции. На рис.4 эти функции приведены для флюктуаций электрического поля $B_{EE}(r)$, флюктуаций магнитного поля $B_{HH}(r)$ и его производной $B_{H'H'}(r)$. Пространственный масштаб корреляции для двух первых функций близок к 5см.

В том же режиме работы, что и зондовые измерения, выполнялись исследования флюктуаций мощности СВЧ-сигнала, прошедшего сквозь турбулентную плазму. Это явление описано в работах [5, 6]. Можно предполагать, что оно является результатом рассеяния электромагнитной волны на неоднородностях коэффициента преломления в турбулентной плазме и интерференции рассеянных волн в точке приема. Флюктуации мощности сигнала, прошедшего сквозь турбулентную среду, широко изучались в связи с проблемой распространения радиоволн в ионосфере. Теория, разработанная для этого случая [7, 8], применима и к явлениям в плазме сильноточного разряда.

СВЧ-зондирование производилось в 4-мм диапазоне длин волн. Плотность плазмы по данным измерений с помощью пучка нейтральных атомов водорода составляет 2.10^{13} $1/см^3$. Таким образом, плазма прозрачна для СВЧ-сигнала, и отношение частоты сигнала к плазменной частоте равно двум. Влиянием магнитного поля на распространение сигнала можно пренебречь, так как частота сигнала значительно выше циклотронной.

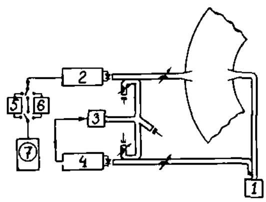

Рис.5. Блок-схема аппаратуры для исследований флюктуаций мощности СВЧ-сигнала: 1 – сигнальный клистронный генетатор; 2 – УПЧ приемника; 3 – гетеродинный клистронный генератор; 4 – блок автоматической подстройки частоты; 5 – корреляционный анализатор; 6 – блок резонансных фильтров; 7 – осциллограф.

Блок-схема СВЧ-аппаратуры приведена на рис.5. Сигнал проходил между передающей и приемной рупорными антеннами, расстояние между которыми равно 90см. Характерной особенностью супергетеродинного приемника сигналов является наличие системы мгновенной автоматической регулировки усиления, благодаря чему приемник имеет логарифмическую зависимость выходного напряжения от мощности сигнала. Это обеспечивает большой динамический диапазон при исследовании флюктуаций мощности сигнала, достигающий 30 дб. Логарифмирование сигнала удобно также и по другой причине. Теория распространения волн в среде со случайными неоднородностями дает выражение для величины, называемой флюктуацией уровня сигнала $\chi = \ln \frac{A}{A_o}$, где A - мгновенное значение амплитуды сигнала, A_o - ее среднее значение. Сигнал на выходе логарифмического приемника пропорционален флюктуации уровня, что облегчает обработку результатов измерений.

Флюктуационный сигнал с выхода приемника регистрировался непосредственно на экране осциллографа, а также исследовался при помощи корреляционного анализатора и при помощи набора резонансных фильтров в диапазоне 100 кгц - 2 Мгц.

Обработка осциллограмм сигнала показала, что закон распределения флюктуаций логарифма мощности сигнала близок к нормальному. Это соответствует предсказаниям теории. Средняя величина флюктуации логарифма мощности составляет ± 7 дб от среднего уровня. Наблюдается также общее ослабление проходящего сигнала, составляющее в рассматриваемом режиме 3-5 дб.

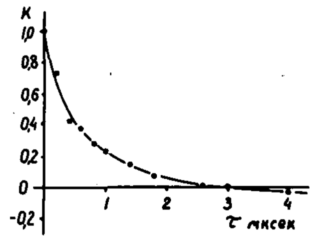

Рис.6. Автокорреляционная функция флюктуаций уровня СВЧ-сигнала в интервале 0÷4 мксек.

Функция автокорреляции сигнала приведена на рис.6. Она близка по форме к функции автокорреляции флюктуаций напряжения на двойном зонде. Однако она имеет более резкий спад в начальном участке, что указывает на большую амплитуду высокочастотных составляющих в спектре.

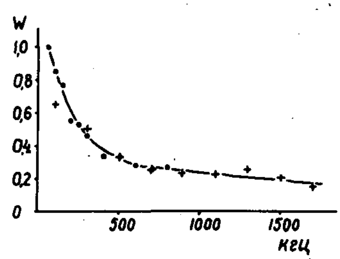

Рис.7. Спектр мощности флюктуаций уровня СВЧ-сигнала:
●– корреляционный анализатор;
+– резонансные фильтры.

Спектр мощности флюктуаций уровня, рассчитанный по функции автокорреляции, изображен на рис.7. Там же нанесены точки, полученные путем статистической обработки осциллограмм сигнала, пропущенного через резонансные фильтры.

Таким образом, все исследованные флюктуации (электрического и магнитного полей и проходящего СВЧ-сигнала) имеют сходный характер. Времена корреляции всех процессов близки к 2 мксек. Плотность мощности в спектрах всех флюктуаций монотонно убывает с ростом частоты, хотя и имеется некоторое различие в частотной зависимости. Быстрее всего убывает с частотой мощность флюктуаций магнитного поля, медленнее всего - СВЧ-сигнала. Каких-либо характерных частот в диапазоне 50кгц - 2 Мгц в спектрах не обнаружено.

Следует отметить, что флюктуации яркости свечения спектральных линий, исследовавшиеся ранее в работе [9], также имеют случайный характер, и время корреляции их составляет несколько мксек. Однако тщательный анализ их спектра не проводился.

Вероятно, все флюктуации имеют общую причину и связаны с магнитогидродинамической турбулетностью разряда. Можно попытаться по имеющимся данным определить величины, характеризующие эту турбулентность.

Теория распространения волн в среде со случайными неоднородностями дает выражение для среднеквадратичной флюктуации уровня [7]:

$$\overline{\chi^2} = \overline{\left(\ln\frac{A}{A_0}\right)^2} \cong 35\, \overline{\Delta\mathcal{N}^2}\, \frac{\ell L}{\lambda^2} \left(1 - \frac{\operatorname{arctg} D}{D}\right)$$

где $\mathcal{N}$ - коэффициент преломления среды, $\Delta\mathcal{N}$ - его флюктуация, ℓ - масштаб корреляции неоднородностей, L - толщина слоя турбулентной среды, λ - длина волны сигнала в среде, $D = \frac{2}{\pi}\frac{L\lambda}{\ell^2}$ - волновой параметр.

Выражение справедливо для $\mathcal{N} \cong 1$, $\overline{\Delta\mathcal{N}^2} \ll 1$. Подставив сюда измеренную величину $\overline{\chi^2}$ и приняв по данным зондовых измерений $\ell \cong 5$ см, оцениваем величину флюктуаций коэффициента преломления $\overline{\Delta N^2} \cong$ $\cong 10^{-3}$. Отсюда вычисляем величину флюктуаций электронной плотности в плазме:

$$\sqrt{\overline{\left(\frac{\Delta n}{\bar{n}}\right)^2}} \cong 0{,}15$$

Если причиной флюктуаций плотности являются коллективные движения в плазме при наличии градиента средней плотности от оси разряда к стенкам разрядной камеры, то величину флюктуаций плотности можно оценить по формуле:

$$\frac{\Delta n}{\bar{n}} \cong \ell\, \frac{\operatorname{grad} n}{\bar{n}} \cong \frac{\ell}{R}$$

где ℓ - масштаб коллективных движений, R - радиус разрядной камеры.

Подставляя ℓ = 5см, R = 50см, получаем $\frac{\Delta n}{\bar{n}} \cong 0{,}1$, что согласуется с величиной, определенной по флюктуациям мощности СВЧ-сигнала.

Данные о частотном спектре флюктуаций уровня позволяют сделать некоторые выводы о спектре флюктуаций плотности [7, 8]. Можно утверждать, что в спектре флюктуаций плотности отсутствуют какие-либо характерные частоты в исследованном диапазоне, так как в противном случае эти частоты появились бы и в спектре СВЧ-сигнала. Очевидно также, что с ростом частоты интенсивность флюктуаций плотности монотонно убывает. Однако определение точной зависимости от частоты затруднительно. Ряд причин, известных из теории, приводит к тому, что в спектре СВЧ-сигнала увеличивается мощность флюктуации в высокочастотной области по сравнению со спектром флюктуаций плотности. Одна из этих причин - влияние многократного рассеяния СВЧ-сигнала на неоднородностях.

Флюктуации разности потенциалов между электродами двойного зонда, по-видимому, отражают флюктуации напряженности электрического поля в плазме. Последние, в свою очередь, должны быть связаны с хаотическим движением плазмы поперек силовых линий магнитного поля. Действительно, если плазма в месте расположения зонда движется поперек силовых линий со скоростью $\vec{v}$, в системе координат, связанной с зондом, должно существовать поле $\vec{E}=[\vec{v}\,\vec{H}]$. Так как флюктуации магнитного поля малы, $\frac{\Delta H}{\overline{H}} \ll 1$, можно считать $\vec{E}=[\vec{v}\,\overline{\vec{H}}]$, где $\overline{H}$ - усредненное магнитное поле в точке, где расположен зонд. Таким образом, по величине напряжения на зонде можно оценить среднее значение поперечной составляющей скорости плазмы, а функция корреляции и спектр флюктуаций напряжения и поперечной составляющей скорости совпадают.

Наблюдаются флюктуации напряженности порядка 30 в/см. При магнитном поле 10^3 эрст. это соответствует флюктуациям скорости 3.10^6 см/сек. Разделив масштаб корреляции флюктуаций напряженности - 5см на характерное время корреляции - 2мксек, получаем ту же величину. Скорость коллективных движений, оцененная таким образом, составляет заметную долю от тепловой скорости ионов, имеющей при T_i = 50эв величину 10^7см/сек. Интересно отметить, что автокорреляционная функция флюктуаций напряжения на двойном зонде очень близка по форме к экспериментально наблюдаемым функциям корреляции пульсаций скорости в турбулентном потоке газа [10]. Таким образом, экспериментально наблюдаемые факты можно объяснить, предположив, что в плазме сильноточного тороидального разряда существует развитая магнитогидродинамическая турбулентность. Она характеризуется величиной поперечных скоростей коллективных движений порядка 3.10^6см/сек, масштабом корреляции скоростей $\ell \cong$ 5см, временем корреляции $\tau \cong$ 2мксек и весьма широким спектром - от десятков килогерц по, крайней мере, до 500 кгц, а возможно и выше. Флюктуации скорости плазмы сопровождаются флюктуациями плотности порядка 10% и флюктуациями магнитного поля. Можно оценить коэффициент турбулентной диффузии:

$$\mathcal{D}_T = \frac{\ell^2}{\tau}$$

Он оказывается равным 10^7 см^2/сек. Время диффузии частиц из центра разряда на стенку при этом составляет 100 мксек.

Это время можно сравнить с энергетическим временем жизни в рассматриваемом режиме разряда:

$$t_e = \frac{V n K (T_i + T_e)}{U J}$$

где J - ток разряда, U - напряжение на обходе камеры в момент максимума тока, V - объем плазмы.

Энергетическое время жизни в момент максимума разрядного тока составляет 60 мксек. Сравнение энергетического времени и времени диффузии подтверждает установленный ранее факт, что уход частиц на стенки вследствие турбулентности является главной причиной охлаждения плазмы в рассматриваемом режиме работы.

ЛИТЕРАТУРА

[1] КАДОМЦЕВ, Б.Б., Конференция по исследованиям в области физики плазмы и управляемого ядерного синтеза, Зальцбург, 1961, Доклад CN-10/227.

[2] ГЛУХИХ, В.А., КОМАР, Е.Г., ЛАРИОНОВ, Б.А., МАЛЫШЕВ, И.Ф., МОНОСЗОН, Н.А., СТОЛОВ, А.М., СТРЕЛЬЦОВ, Н.С., ЖТФ 30 (1960) 1394.

[3] РОДИЧКИН, В.А., СЕРЕБРЕНЫЙ, Г.А., ТИМОНИН, А.М., Сб. "Диагностика плазмы" (в печати).

[4] RUSBRIDGE, M.G., LEES, D.J., SAUNDERS, P.A.H., Конференция по исследованиям в области физики плазмы и управляемого ядерного синтеза, Зальцбург, 1961, Доклад CN-10/58.

[5] WORT, D.J.H., HEALD, M.A., J. Nucl. En. pt. C 7 (1965) 79.

[6] ЛАРИОНОВ, М.М., РОЖДЕСТВЕНСКИЙ, В.В., ЖТФ 38 (1968) 279.

[7] ЧЕРНОВ, Л.А., Распространение волн в среде со случайными неоднородностями, Изд. АН СССР, Москва, 1958.

[8] ТАТАРСКИЙ, В.И., Распространение волн в турбулентной атмосфере, Изд. "Наука", Москва, 1967.

[9] БЕРЕЗИН, А.Б., ЗАЙДЕЛЬ, А.Н., МАЛЫШЕВ, Г.М., РАЗДОБАРИН, Г.Т., СКИДАН, В.В., Конференция по исследованиям в области физики плазмы и управляемого ядерного синтеза, Зальцбург, 1961, Доклад CN-10/239.

[10] БЭТЧЕЛОР, Дж., Теория однородной турбулентности, Изд. ин. лит., Москва, 1955.

СВОЙСТВА ПЛАЗМЫ В КОМБИНИРОВАННОМ СИЛЬНОТОЧНОМ РАЗРЯДЕ

И.Ф.КВАРЦХАВА, Г.Г.ЗУКАКИШВИЛИ,
Ю.С.ГВАЛАДЗЕ, Ю.В.МАТВЕЕВ, Н.А.РАЗМАДЗЕ,
З.Д.ЧКУАСЕЛИ, В.К.ОРЕШКИН и И.Я.БУТОВ
ФИЗИКО-ТЕХНИЧЕСКИЙ ИНСТИТУТ
ГОСУДАРСТВЕННОГО КОМИТЕТА ПО
ИСПОЛЬЗОВАНИЮ АТОМНОЙ ЭНЕРГИИ СССР,
СУХУМИ,
СССР

Abstract — Аннотация

PROPERTIES OF A PLASMA IN A COMBINED HIGH-CURRENT DISCHARGE. The authors consider the results of experiments relating to the properties of the combined discharge which occurs when a Θ-pinch and a z-pinch are produced simultaneously in the same space, and new data concerning Θ-pinches and z-pinches separately. It is established that in this combined system the plasma is significantly more stable than in the individual pinches: the positive processes which are typical of the individual pinches and which promote plasma heating and containment are preserved and intensified, whereas the negative processes vanish or are substantially attenuated. For example, the hydromagnetic instabilities which occur in z-pinches ($m = 0$ and $m = 1$ modes) or in Θ-pinches (cumulative ejection of plasma streams through the containing magnetic field) are not observed. Similarly, there is no repeated discharge along the chamber walls, which is typical of z-pinches and which substantially limits heating of the compressed plasma since most of the discharge current thereby flows through the boundary region. In a combined pinch, the plasma maintains its stable state even when the longitudinal current flowing through it is several times in excess of the Kruskal-Shafranov limit. The authors discuss the observed effect of the initial stage in the development of the z-pinch discharge on the behaviour of the plasma and on the distribution of the magnetic field in the combined pinch: pre-ionization of the gas and the superposition of an anti-parallel initial magnetic field improve the conditions for the formation of a skin layer and increase the efficiency of plasma compression and heating. The authors also present data showing that there is a definite optimum relationship between the temperature of the electron component of the plasma in a combined pinch and the length of the period between the triggering of the Θ-pinch and the z-pinch. Ideas of a thermodynamic nature are put forward and the conclusion drawn that, from the point of view of achieving a thermonuclear reaction under laboratory conditions, systems with $\beta \approx 1$ should offer significant advantages over systems with $\beta \ll 1$.

СВОЙСТВА ПЛАЗМЫ В КОМБИНИРОВАННОМ СИЛЬНОТОЧНОМ РАЗРЯДЕ. Рассматриваются результаты экспериментов по исследованию свойств комбинированного разряда, возникающего при совместном зажигании тета- и зет-пинчей в одном и том же объеме, а также новые данные, относящиеся к тета- и зет-пинчам в отдельности. Установлено, что в получаемой таким путем комбинированной системе плазма значительно более стабильна, чем в отдельных пинчах. При этом сохраняются или усиливаются процессы положительного характера, свойственные отдельным пинчам и способствующие нагреву и удержанию плазмы. В то же время процессы противоположного характера исчезают или в значительной мере ослабевают. Так, например, в комбинированном пинче не наблюдаются гидромагнитные нестабильности, возникающие в зет-пинчах (моды $m = 0$ и $m = 1$) или в тета-пинчах (коммулятивные выбросы плазменных струй через удерживающее магнитное поле); отсутствуют повторные зажигания разряда вдоль стенок камеры, характерные для зет-пинчей и существенно ограничивающие возможность нагрева сжатой плазмы, так как основная доля разрядного тока при этом протекает в пристеночной области. В комбинированном пинче плазма сохраняет стабильное состояние и в том случае, когда протекающий по ней продольный ток в несколько раз превышает известный предел Крускала-Шафранова. Обсуждается наблюдаемое влияние начальной стадии развития разряда в зет-пинче на поведение плазмы и на распределение магнитного поля в комбинированном пинче. При этом, предварительная ионизация газа и наложение антипараллельного начального магнитного поля улучшают условия формирования скин-слоя и увеличивают эффективность сжатия и нагрева плазмы. Приводятся данные, показывающие наличие определенного оптимума в зависимости между температурой электронной компоненты плазмы комбинированного пинча и величиной промежутка времени между моментами зажиганий тета- и зет-пинчей. Высказываются соображения термодинамического характера, на основе которых делается вывод о том, что с точки зрения возможности осуществления термоядерной реакции в лабораторных условиях опыта, системы с $\beta \approx 1$ должны обладать значительным преимуществом по сравнению с системами, в которых $\beta \ll 1$.

ВВЕДЕНИЕ

В настоящее время исследование плазмы с $\beta \approx 1$ ведется в основном по трем направлениям:

1. Эксперименты по плазменному фокусу.

Опыты проводятся на зет-пинчах специальной конструкции [1] и коаксиальных пушках [2].

Благодаря фокусировке плазмы вблизи центрального электрода удается получить в малом объеме, в течение короткого промежутка времени, очень высокие значения концентрации и температуры плазмы.

2. Эксперименты с тета-пинчами.

В этих опытах для нагрева и удержания плазмы используются быстронарастающие во времени магнитные поля, создаваемые в одновитковых катушках [3].

3. Эксперименты с комбинированными разрядами [4].

Комбинированные разряды представляют совмещенные в одном объеме зет- и тета-пинчи. Как будет показано ниже, есть основание полагать, что в комбинированных разрядах удастся использовать положительные качества каждого из разрядов (удобный метод нагрева плазмы, высокие плотности и т.д.) и подавить нежелательные (магнитогидродинамические неустойчивости, повторные пробои у стенок разрядной камеры в зет-пинче и т.д.).

Кроме того, комбинированные разряды удобны и тем, что удерживающие магнитные поля можно создавать токами, протекающими на самой плазме.

В докладе изложены результаты экспериментов, полученные на установке "Комбинированный пинч". Предпосылкой для создания такой установки послужили исследования, проведенные с зет- и тета-пинчами, в результате которых выяснилось, что, наряду с известными магнитогидродинамическими и мелкомасштабными нестабильностями плазмы, существенное влияние на развитие сильноточного разряда оказывают ее структурные особенности, а также повторные зажигания разряда в зет-пинче [5, 6].

Основные выводы этих исследований сводятся к следующему:

1) Как в тета-, так и в зет-пинчах сжимающийся слой плазмы распадается на периодическую систему Е-волокон, ориентированных вдоль электрического поля и представляющих собой элементарные зет-пинчи (рис.1, ряды 1, 2, 3, 5). Теоретические исследования двумерной модели плазмы [7, 8] приводят к выводу, что структуры с Е-волокнами являются энергетически более выгодными, чем однородная структура той же мощности.

2) Кроме Е-волокон, возникает периодическая система Н-волокон, ориентированных вдоль магнитного поля и, по-видимому, представляющих собой элементарные тета-пинчи (рис.1, ряд 6). Очевидно, эти структуры также являются энергетически более выгодными.

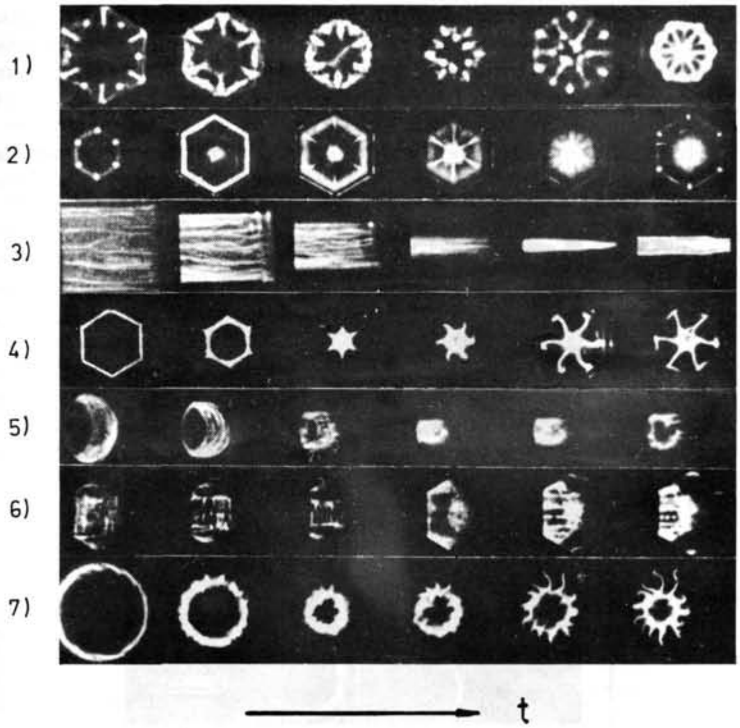

Рис.1. Фотографии Е- и Н-волокон в зет- и тета-пинчах:
1) зет-пинч I_z = 200 ка;
2) зет-пинч I_z = 1000 ка;
3) зет-пинч I_z = 240 ка (фотография сбоку);
4) тета-пинч I_φ = 370 ка;
5) и 6) тета-пинч I_φ = 300 ка (фотография под углом 10° к оси разрядной камеры);
7) тета-пинч I_φ = 400 ка.
Экспозиция каждого кадра 0,5 мксек. Временной интервал между кадрами 2 мксек.

3) При сжатии плазмы в тета-пинчах столкновения Н-волокон стимулируют возбуждение плазменных струй, движущихся наружу, поперек магнитного поля, и достигающих стенок камеры (рис.1, ряды 4, 7). При этом струи в направлении к оси камеры сильно тормозятся. Причиной такого торможения является наличие захваченного магнитного поля, быстро нарастающего по мере сжатия плазмы. При достаточно быстром нарастании магнитного поля между плазмой и катушкой могут, по-видимому, отсутствовать и наружные струи.

4) На образование волокнистых структур существенное влияние оказывает начальное магнитное поле. Оно стимулирует развитие параллельных ему волокон, одновременно подавляя перпендикулярные волокна (рис.2 (1), зет-пинч в аксиальном магнитном поле; рис.2 (2), тета-пинч в азимутальном магнитном поле).

5) Важная особенность развития разряда в зет-пинчах состоит в том, что скорость накопления энергии в плазме ограничивается главным образом не магнитогидродинамическими нестабильностями, как это считалось раньше, а повторными зажиганиями разряда у стенок камеры (рис.1, ряд 2).

Естественным следствием перечисленных результатов явилась идея "Комбинированного пинча". Так как в зет- и тета-пинчах токи взаимно перпендикулярны, то совместное зажигание их в одном разрядном объеме приведет к тому, что зет-пинч окажется в продольном магнитном поле тета-пинча, а тета-пинч в азимутальном магнитном поле зет-пинча. Это должно привести к ослаблению структурных неоднородностей сжимающегося слоя и к повышению стабильности плазмы.

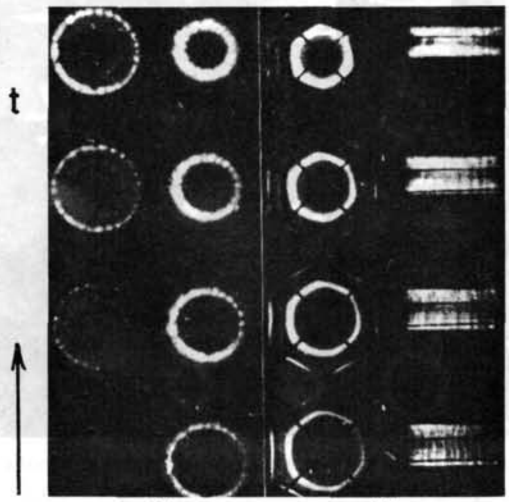

Рис.2. Фотографии зет- и тета-пинчей, показывающие влияние начального магнитного поля на структуру плазмы:
1) зет-пинч в аксиальном магнитном поле; 2) тета-пинч в азимутальном магнитном поле. Экспозиция каждого кадра 0,5 мксек. Временной интервал между кадрами 0,5 мксек.

ЭКСПЕРИМЕНТАЛЬНАЯ УСТАНОВКА И МЕТОДЫ ИЗМЕРЕНИЯ

Первые опыты проводились на разрядной камере, изготовленной из органического стекла и имеющей в радиальном сечении шестигранную форму [5, 6]. Диаметр камеры – 30 см, длина межэлектродного промежутка – 50 см. Максимальный ток в зет-пинче достигает ~400 ка с полупериодом $T/2 = 12$ мксек, а катушке тета-пинча достигает ~800 ка с полупериодом $T/2 = 16$ мксек. Тета-пинч можно было включить после зет-пинча с регулируемой задержкой. Рабочий газ – He. Конструкция электродов и магнитной катушки позволяла фотографировать разряд одновременно с торца и сбоку. На рис.3 приведена принципиальная схема второй установки. В качестве разрядной камеры использовалась алундовая (Al_2O_3) или кварцевая труба длиной 57 см и внутренним диаметром 6 см. На концах разрядной камеры имелись демпферные объемы. Они предназначались для ослабления разрушающего влияния аксиальных плазменных струй на торцовые окна, изготовленные из оптического стекла. Электроды линейного пинча представляли собой полые цилиндры. Межэлектродное расстояние – 33 см. Аксиальное магнитное поле создавалось в одновитковой медной катушке длиной 35 см и внутренним диаметром

7,8 см. Предварительная плазма создавалась апериодическим разрядом емкости ($C_1 = 12$ мкф, $V = 30$ кв, $I = 60$ ка) на межэлектродный промежуток. Для питания зет-пинча использовалась емкость C_2($C_2 = 12$ мкф, $V = 30$ кв, $I = 140$ ка) с полупериодом разряда $T/2 = 7{,}5$ мксек. К катушке тета-пинча через коллекторные пластины прямоугольной формы подсоединялись две батареи конденсаторов. Первая предназначалась для создания быстронарастающего магнитного поля ($C_4 = 215$ мкф, $V = 30$ кв, $H_z = 50$ кгс, $T/2 = 10$ мксек). Вторая батарея конденсаторов ($C_3 = 2000$ мкф, $V = 5$ кв, $H_{z0} = 3$ кгс, $T/2 = 200$ мксек) служила для создания квазипостоянного магнитного поля. Последовательность срабатывания разрядных контуров для комбинированного пинча с предионизацией и антипараллельным магнитным полем показана на рис.4. Через 80 – 90 мксек после включения квазипостоянного магнитного поля срабатывала батарея предионизации. Когда ток предварительного разряда спадал почти до нуля (через 10 – 13 мксек), включались зет- и тета-пинчи, причем, как правило, первым включался зет-пинч, а потом, с регулируемой задержкой в пределах 0 – 5 мксек, включался тета-пинч. Такая схема позволяла изучать в отдельности зет-пинч, тета-пинч и "Комбинированный пинч". В качестве рабочего газа использовался водород. Диапазон рабочих давлений – $2{\cdot}10^{-1} \div 10^{-2}$ мм рт.ст.

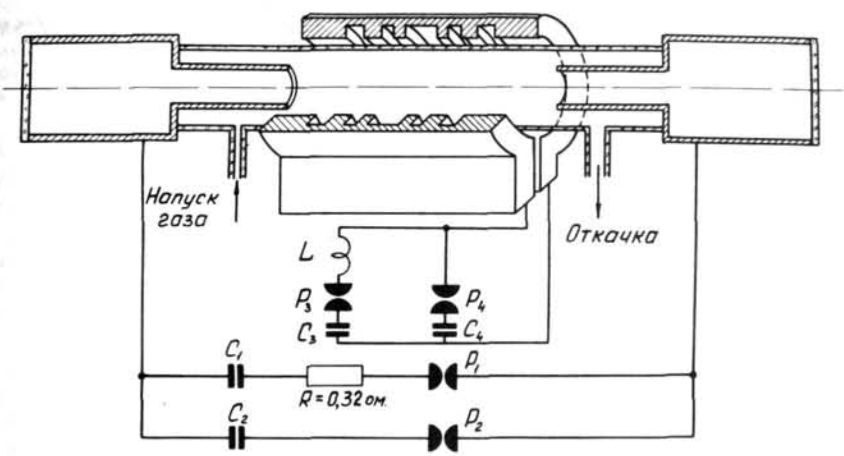

Рис.3. Принципиальная схема второй установки "Комбинированный пинч".

. Токи в разрядных контурах измерялись интегрирующими поясами Роговского. Напряжение на электродах линейного пинча и на вводах магнитной катушки измерялось с помощью малоиндуктивных низкоомных делителей. Фотографирование разряда производилось с помощью "СФР-2М" в режиме кадровой съемки со скоростью $2{\cdot}10^6$ кадров/сек. Распределение магнитных полей в разрядном объеме получено на основании зондовых измерений. Отклонение аксиального тока от оси разрядной камеры регистрировалось с помощью двух магнитных зондов, расположенных диаметрально на внешней стороне разрядной камеры и включенных таким образом, чтобы сигнал с них был равен нулю, когда ток протекает по оси разрядной камеры. Появление сигнала, отличного от нуля, свидетельствует об отклонении плазменного шнура от оси разрядной камеры. Временные характеристики жесткого рентгеновского излучения исследовались с помощью сцинтиллятора NaJ и ФЭУ. Пространственные характеристики излучения определялись по фотографиям разряда в рентгеновских лучах. Энергия γ-квантов оценивалась по поглощению излучения в свинцовых и медных экранах.

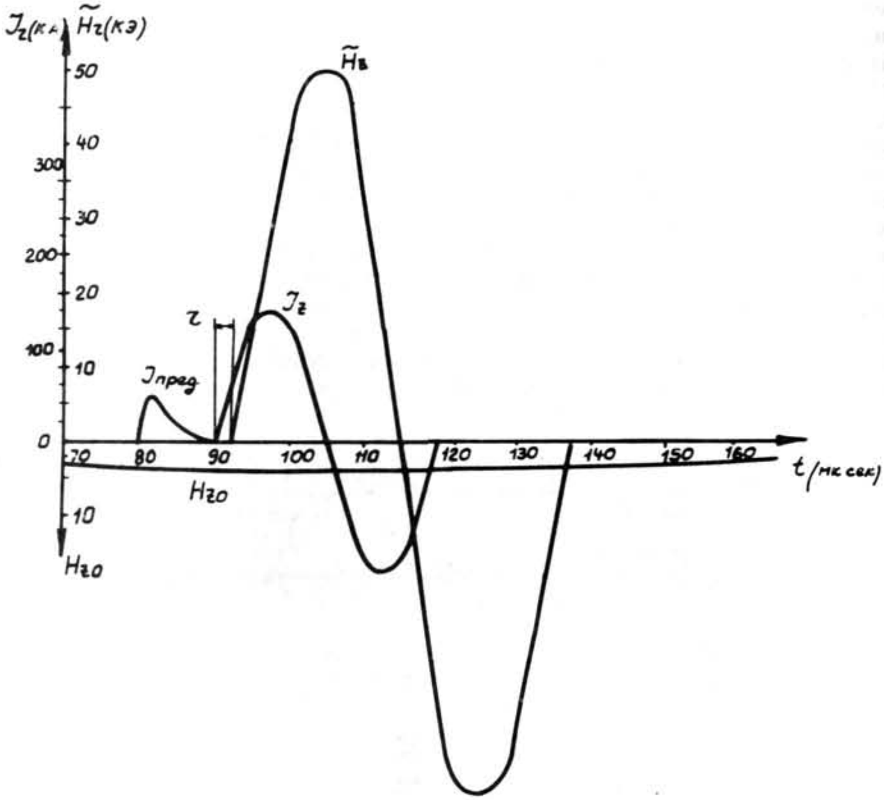

Рис.4. Временная последовательность включения разрядных контуров комбинированного пинча.

Электронная температура до 100 эв определялась из отношения интенсивностей примесных спектральных линий трижды ионизованного углерода. Для надежного измерения интенсивностей линий углерода в разрядную камеру напускался метан CH_4, концентрация которого не превышала 1% концентрации водорода. Электронная температура выше 100 эв оценивалась по тормозному излучению плазмы в области мягкого рентгена.

РЕЗУЛЬТАТЫ ЭКСПЕРИМЕНТОВ

На рис.5 (ряды 4, 5, 6) приведены СФР-граммы разряда в комбинированном пинче. Ряды 4 и 5 представляют собой две проекции, с торца и сбоку, одного и того же разряда. Ток зет-пинча – 300 ка, ток в катушке

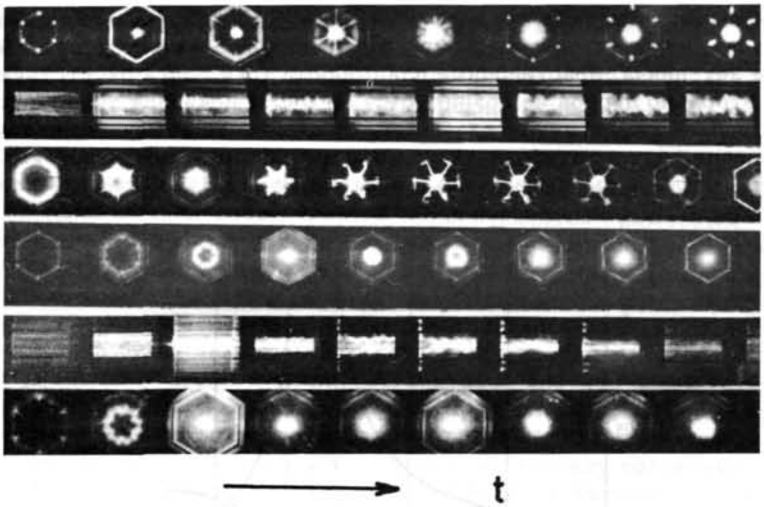

Рис.5. 1) Зет-пинч (фотография с торца); 2) зет-пинч (фотография сбоку); 3) тета-пинч (фотография с торца); 4) и 5) комбинированный пинч (фотография одного и того же разряда с торца и сбоку), ток в зет-пинче – 300 ка, ток в катушке тета-пинча – 420 ка; 6) комбинированный пинч (фотография сбоку), ток в зет-пинче – 400 ка, ток в катушке тета-пинча – 750 ка. Начальное давление гелия $p = 10^{-1}$ мм рт. ст. Экспозиция каждого кадра 0,5 мксек. Временной интервал между кадрами 2 мксек. Зет-пинч включался на 2 мксек раньше тета-пинча.

тета-пинча – 420 ка. В случае ряда 6 ток зет-пинча равен 400 ка, а в катушке тета-пинча – 750 ка. Тета-пинч включался на 2 мксек позже зет-пинча.

Торцовые фотографии показывают, что плазменный шнур в обоих случаях имеет достаточно четкую границу и устойчив в течение всего полупериода разрядного тока; повторные пробои у стенок разрядной камеры отсутствуют. Для сравнения на этом же рисунке приведены фотографии отдельных зет- и тета-пинчей, на которых видны характерные для них неустойчивости (ряды 1, 2, 3). Если предположить, согласно приведенным фотографиям, что весь ток зет-пинча сосредоточен в столбе радиусом 4,5 см, то коэффициент устойчивости $K = (H_z/H_\varphi)(2\pi a/L)$ будет больше единицы только в течение двух микросекунд (рис.6) в области, где ток зет-пинча в конце первого полупериода переходит через нуль; в остальное время он меньше единицы. Таким образом, несмотря на то, что условие устойчивости Крускала – Шафранова [9] по существу не выполняется, плазменный шнур устойчив в течение всего первого полупериода разряда.

Объяснение этому факту, видимо, следует искать в структуре токового слоя и связанной с ней геометрией магнитных полей. Действительно, на боковых фотографиях разряда видно, что плазменный шнур представляет собой жгут скрученных токовых волокон. Магнитными зондами было измерено распределение азимутальной и аксиальной составляющей магнитного поля вдоль радиуса разрядной камеры. На основании этих измерений можно сделать следующие заключения. Аксиальное магнитное поле на оси разрядной камеры больше вакуумного поля тета-пинча в течение всего первого полупериода разрядного тока, что указывает на наличие спиральной деформации токового шнура и согласуется с боковыми фотографиями разряда. Обработка зондовых измерений показала, что в том случае, когда тета-пинч включается через 0,5 ÷ 1 мксек после зет-пинча, пристеночные плазменные токи почти отсутствуют, т.е. вторично пробои не возникают. На рис.7 показана зависимость электронной температуры плазмы T_e от сдвига Δt между моментом включения зет- и тета-пинчей. Она достигает максимума (14 эв) при $\Delta t = 0{,}5$ мксек и уменьшается в два раза при $\Delta t = 1{,}5$ мксек. Точность

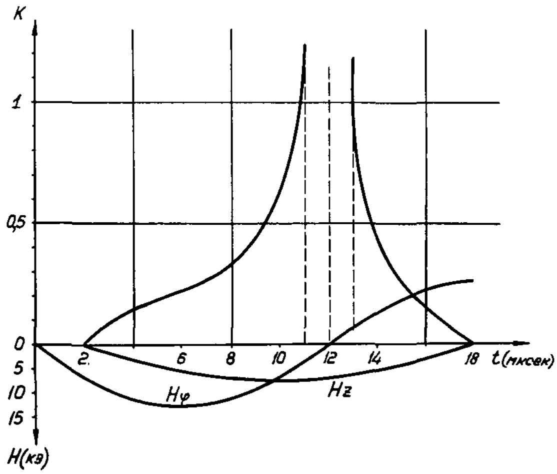

Рис.6. Зависимость коэффициента устойчивости $K = H_z/H_\varphi \cdot 2\pi a/L$ от времени; построена для условий рис.5(4) и (5).

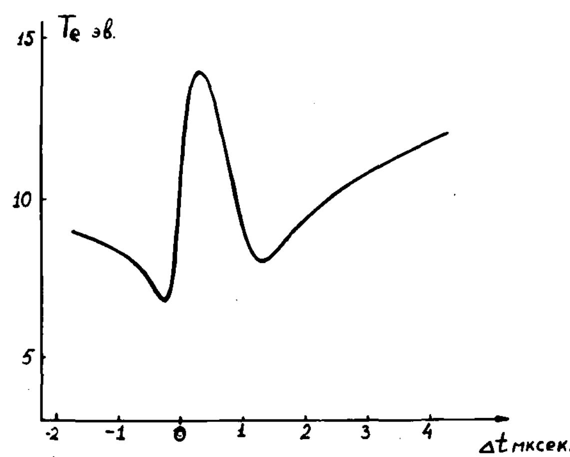

Рис.7. Зависимость электронной температуры плазмы в комбинированном пинче от сдвига по фазе Δt между зет- и тета-пинчами.

определения температуры составляет ±1,0 эв. Для того чтобы понять такую сильную зависимость электронной температуры от сдвига по фазе, рассмотрим последовательные стадии развития зет-пинча: первая стадия – пробой межэлектродного промежутка и образование скин-слоя у стенок разрядной камеры; вторая стадия – завершение формирования волокнистой структуры плазменной оболочки; третья стадия – быстрое радиальное сжатие плазмы под действием нарастающего магнитного давления; четвертая стадия — повторный пробой у стенок разрядной камеры.

Для того чтобы получить разряд с высоким значением $\beta \approx 1$, тета-пинч следует включить на первой стадии развития зет-пинча, когда уже образовался скин-слой. В этом случае тета-пинч зажигается по оболочке зет-пинча. Аксиальное магнитное поле проникает в плазму только на толщину скин-слоя. Сжатие осуществляется суммарным магнитным давлением зет- и тета-пинчей. Этот режим соответствует примерно $\Delta t = 0{,}5$ мксек и дает максимальную электронную температуру. Если тета-пинч включается раньше, чем образовался скин-слой зет-пинча, то аксиальное магнитное поле заполнит весь объем плазмы и после образования скина будет захвачено. В результате,степень сжатия и температура плазмы будут меньше, чем в первом случае. Если тета-пинч включается на второй стадии зет-пинча, когда уже имеется развитая волокнистая структура, то и в этом случае аксиальное магнитное поле, видимо, может легко проникнуть через щели между волокнами в плазму и по мере сжатия токовой оболочки будет захвачено. Этот режим соответствует $\Delta t \approx 1{,}5$ мксек. При включении тета-пинча на четвертой стадии зет-пинча пристеночный плазменный ток, возникший в результате вторичного пробоя, будет экранировать аксиальное магнитное поле. Температура центральной области плазмы в этом случае будет полностью определяться зет-пинчем, по которому течет относительно малый ток. Этот случай соответствует $\Delta t > 3$ мксек.

В зависимости от условий разряда (размеров разрядной камеры, материала стенок и степени их обезгаженности, начального давления, рода газа, скорости нарастания тока) длительности перечисленных стадий разряда зет-пинча могут меняться. Кроме того, в зависимости от начальных условий может измениться сам процесс развития разряда.

Описанные выше результаты получены в условиях, когда в плазме присутствуют примеси ионов тяжелых атомов и напряженности магнитных полей сравнительно малы. Поэтому естественно, что электронная температура плазмы не превышает 20 эв.

В дальнейшем опыты проводились на установке, показанной на рис.3. За счет уменьшения разрядного объема были увеличены напряженности магнитных полей. Созданы более чистые вакуумные условия. Измерения в комбинированном пинче проводились в основном в двух режимах. В первом режиме отсутствовало начальное квазипостоянное магнитное поле. Во втором режиме на разряд накладывалось начальное антипараллельное магнитное поле напряженностью $H_{z0} = 2$ кгс. Начальное давление водорода 10^{-1} мм рт.ст.

На рис.8 приведены осциллограммы азимутального и аксиального магнитных полей на оси разрядной камеры и на расстоянии 13 мм от оси, а также сигнал с компенсированного магнитного зонда. Измерения проведены в первом режиме. Зет- и тета-пинчи включаются одновременно. На оси разрядной камеры аксиальное магнитное поле больше вакуумного поля тета-пинча и по форме близко к синусоиде. На расстоянии 13 мм от оси аксиальное поле совпадает с вакуумным полем. Сигнал с компенсированного зонда является большим. Эти факты указывают на то, что имеет место спиральная деформация плазменного тока. Оценки показывают, что шаг спирали — порядка длины межэлектродного расстояния. Из характера приведенных осциллограмм видно также, что толщина скин-слоя больше радиуса разрядной камеры ($R = 3$ см).

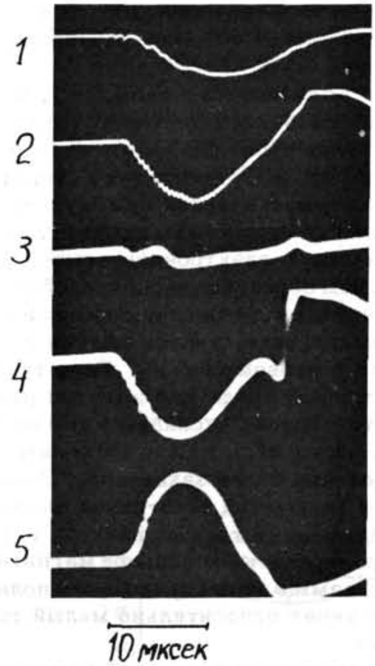

Рис.8. Комбинированный пинч $\Delta t = 0$:
1 и 2 – магнитные поля H_φ и H_z на расстоянии 13 мм от оси разрядной камеры; 3 и 4 – магнитные поля H_φ и H_z на оси разрядной камеры; 5 – сигнал с компенсированного зонда.

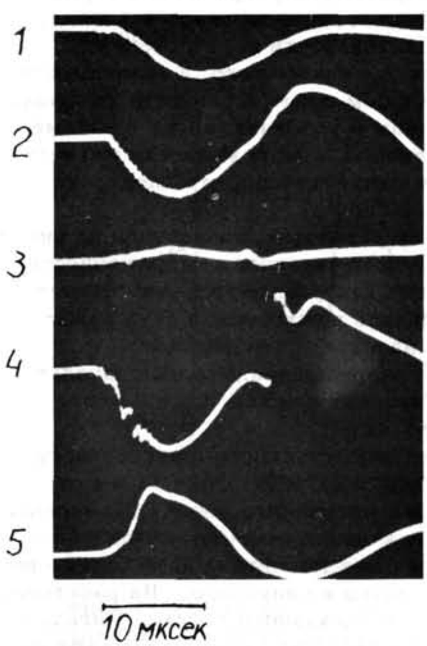

Рис.9. Комбинированный пинч с антипараллельным начальным магнитным полем H_{z0} = 2 кгс, $\Delta t = 0$:
1 и 2 – магнитные поля H_φ и H_z на расстоянии 13 мм от оси разрядной камеры; 3 и 4 – магнитные поля H_φ и H_z на оси разрядной камеры; 5 – сигнал с компенсированного зонда.

На рис.9 приведена осциллограмма для второго режима. Зет- и тета-пинчи, как и в первом случае, включаются одновременно. Качественно картина развития разряда соответствует рис.8, только амплитуда сигнала с симметричного зонда несколько меньше, а на фронте аксиального магнитного поля в приосевой области камеры появляются высокочастотные колебания. При этом, вначале магнитное поле нарастает медленнее, чем вакуумное; толщина скин-слоя, видимо, сравнима с радиусом разрядной камеры.

На рис.10 приведена осциллограмма для первого режима. Тета-пинч включался на 1 мксек позже зет-пинча. До полного сжатия плазмы аксиальное магнитное поле на оси равно нулю. В момент сжатия оно быстро (за $2\cdot10^{-7}$ сек) нарастает и становится больше вакуумного магнитного поля тета-пинча. На расстоянии 13 мм от оси аксиальное магнитное поле равно вакуумному полю. Таким образом, толщина скин-слоя при $\Delta t = 1$ мксек меньше радиуса разрядной камеры и равна приблизительно 2 см. Интересно отметить, что величина сигнала с компенсированного зонда гораздо меньше, чем в первых двух случаях. Спиральная деформация тока имеет место и в этом случае, так как величина аксиального магнитного поля на оси после сжатия плазмы больше вакуумного поля, но радиус плазменного столба меньше, чем $\Delta t = 0$.

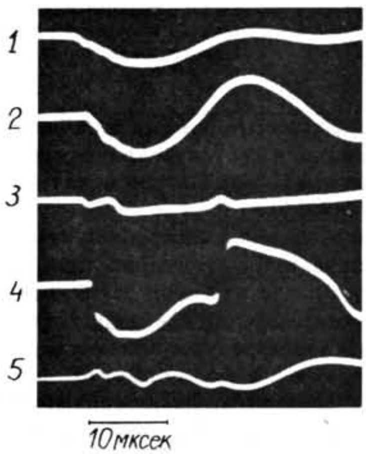

Рис.10. Комбинированный пинч $\Delta t = 1$ мксек:
1 и 2 – магнитные поля H_φ и H_z на расстоянии 13 мм от оси разрядной камеры;
3 и 4 – магнитные поля H_φ и H_z на оси разрядной камеры;
5 – сигнал с компенсированного зонда.

На рис.11 приведены осциллограммы магнитных полей для второго режима. Тета-пинч включался на 1 мксек позже зет-пинча. Такого сдвига во времени между зет- и тета-пинчами уже достаточно, чтобы плазменной оболочкой захватывался антипараллельный магнитный поток. К началу третьей микросекунды плазма уже сжата к оси. После завершения фазы сжатия антипараллельное магнитное поле из приосевой области исчезает, но появляется азимутальное магнитное поле. В это же время компенсированный зонд регистрирует отклонение продольного тока от оси к стенке камеры. В последующий момент времени зонды, расположенные на расстоянии 13 мм от оси, регистрируют прохождение плазменного шнура с обратным захваченным магнитным полем. Сигнал с компенсированного зонда в это время уменьшается до нуля, так как плазменный шнур располагается симметрично относительно зондов. В дальнейшем сигнал с компенсированного зонда меняет полярность, что свидетельствует о том, что плазменный шнур находится по другую сторону от оси разрядной камеры.

Интересной особенностью этого режима является то, что плазменный цилиндр, скручиваясь в спираль, несет в себе захваченное антипараллельное магнитное поле. Время развития спиральной неустойчивости составляет $2 \div 3$ мксек. Шаг спирали, оцененный по величине аксиального магнитного поля, порядка 13 см.

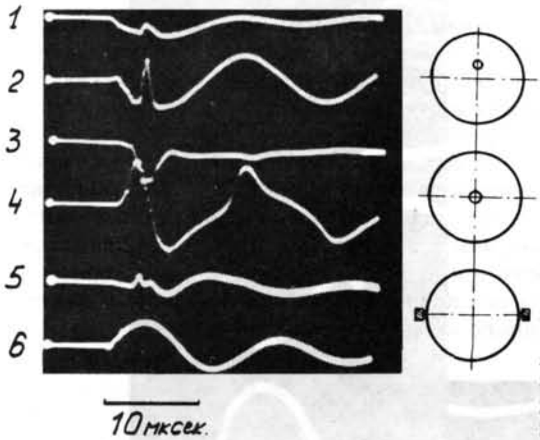

Рис. 11. Комбинированный пинч с антипараллельным магнитным полем $H_{z0} = 2$ кгс, $\Delta t = 1$ мксек:
1 и 2 – магнитные поля H_φ и H_z на расстоянии 13 мм от оси разрядной камеры;
3 и 4 – магнитные поля H_φ и H_z на оси разрядной камеры; 5 – сигнал с компенсированного зонда; 6 – ток в зет-пинче.

Следует отметить, что во всех описанных опытах в начале второго полупериода разрядного тока тета-пинча имеется захваченное обратное магнитное поле, которое после сжатия плазмы быстро исчезает. Температура плазмы в это время максимальна.

На рис.12 приведены графики изменения электронной температуры во времени, при наличии антипараллельного магнитного поля, для трех значений Δt. Для первой кривой $\Delta t = 0$, для второй – $\Delta t = 0{,}3$ мксек и для третьей – $\Delta t = 0{,}8$ мксек. Вакуумное магнитное поле тета-пинча равно 20 кгс. Зависимость электронной температуры плазмы в первом полупериоде от Δt качественно такая же, как и в экспериментах с шестигранной камерой (рис.5) и согласуется с зондовыми измерениями магнитных полей. В случае первой кривой захватывается большой поток магнитного поля (рис.8), поэтому степень сжатия и температура плазмы соответственно малы. В случае второй кривой поток обратного захваченного магнитного поля мал или вообще отсутствует (подобная картина наблюдается и в комбинированном пинче без антипараллельного магнитного поля, но при $\Delta t = 1$ мксек (рис.10).

Третьей кривой соответствуют осциллограммы магнитного поля, приведенные на рис.11. Резкий спад температуры плазмы на пятой микросекунде объясняется развитием винтовой деформации плазменного шнура и его уходом из приосевой области, в которой проводятся наблюдения.

Во всех описанных опытах на второй установке было зарегистрировано рентгеновское излучение с энергией порядка 15 кэв, которое возникает всегда одновременно с током зет-пинча. Длительность излучения составляет $1{,}5 \div 2$ мксек.

Таким образом, характерными особенностями развития разряда в комбинированном пинче без предионизации газа являются:

1) При нулевом сдвиге между моментами зажигания зет- и тета-пинчей ($\Delta t = 0$) толщина скин-слоя больше или сравнима с радиусом разрядной камеры.

2) При увеличении Δt до одной микросекунды, толщина скин-слоя уменьшается до 2 см.

3) Наложение антипараллельного магнитного поля всегда уменьшает толщину скин-слоя.

4) Наиболее благоприятным режимом для комбинированного пинча является режим, когда захваченный плазмой магнитный поток отсутствует.

5) В начальной стадии разряда наблюдается жесткое рентгеновское излучение.

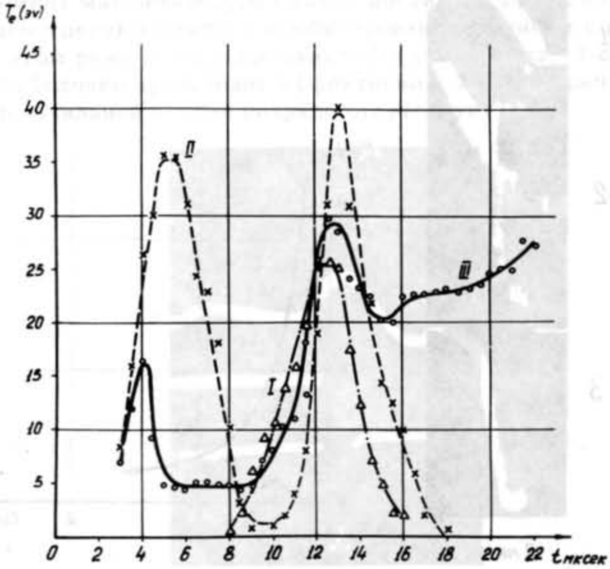

Рис.12. Зависимость электронной температуры плазмы в комбинированном пинче с антипараллельным магнитным полем (H_{z0} = 2 кгс, I. $\Delta t = 0$; II. $\Delta t = 0{,}3$ мксек; III. $\Delta t = 0{,}8$ мксек) от времени.

Для того чтобы выяснить, какой вклад вносит в процессы, развивающиеся в комбинированном пинче, каждая из компонент, были проведены аналогичные измерения на зет- и тета-пинчах в отдельности.

На рис.13 приведены осциллограммы тока, напряжения, рентгеновского излучения и омического сопротивления плазмы в зет-пинче без предварительной ионизации. На начальной стадии разряда видны высокочастотные колебания напряжения. Они всегда сопровождаются излучением жесткого рентгена, интенсивность которого однородно распределена по длине разрядной камеры. Сопротивление разряда определялось по падению напряжения между электродами и полному разрядному току с вычетом реактивного сопротивления. В начале разряда оно порядка одного ома и много больше реактивного сопротивления. Через 1 ÷ 2 мксек колебания напряжения срываются, рентгеновское излучение исчезает, а активное сопротивление плазмы становится меньше индуктивного.

Полагая (на основании зондовых измерений магнитных полей и фотографий разряда), что плазма занимает весь объем разрядной камеры, можно вычислить проводимость плазмы. В начале разряда она составляет $\sigma \simeq 10^{12}$CGSE, а в момент срыва неустойчивого режима достигает $\sigma \simeq 5 \cdot 10^{13}$CGSE. При этом толщина скин-слоя $\delta = (C/4\pi\sigma\omega)^{1/2}$ должна уменьшиться от 15 см до 2 см. Как было показано выше, в тех режимах, когда тета-пинч включался через 1 мксек после зет-пинча, толщина скин-слоя не превышала 2 см (рис.10). При смещениях $\Delta t < 1$ мксек, в отсутствии антипараллельного магнитного поля, толщина скин-слоя становится больше радиуса разрядной камеры (рис.8).

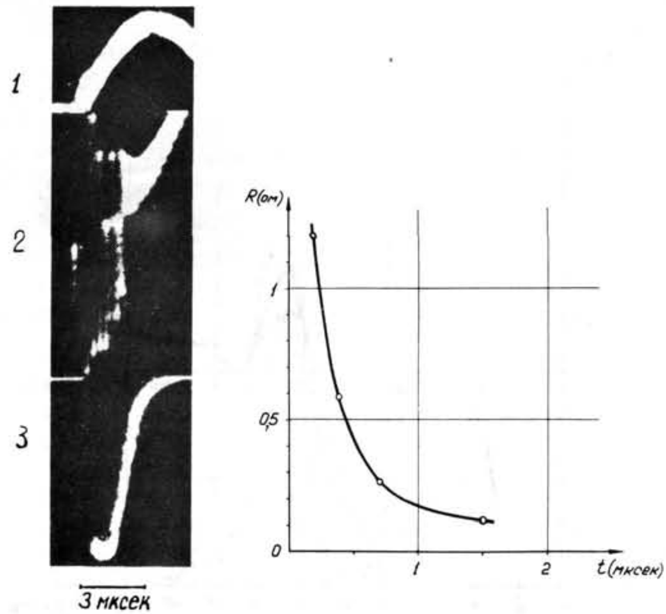

Рис.13. Зет-пинч: 1 – осциллограмма тока; 2 – напряжение на межэлектродном промежутке; 3 – осциллограмма рентгеновского излучения. Справа – график зависимости активного сопротивления разрядного промежутка от времени.

Оценки показывают, что при температуре электронов в начальной фазе развития зет-пинча $T_e \simeq 5$ эв, отношение эффективной частоты взаимодействия электронов с плазмой $\nu_{эф} \simeq ne^2/\sigma m_e$ к классической частоте $\nu = 25n/T^{3/2}$ составляет величину порядка 50. После срыва нестабильного режима это отношение становится порядка единицы. Таким образом, в начальной стадии зет-пинча, видимо, развивается коллективная нестабильность [10], приводящая к увеличению толщины скин-слоя в плазме.

В случае использования предварительной ионизации газа, колебания напряжения и рентгеновское излучение отсутствуют. Толщина скина становится меньше радиуса разрядной камеры. В момент максимального сжатия плазмы регистрируется мягкое рентгеновское излучение. Оценка электронной температуры по этому излучению дает значение порядка 100 – 150 эв.

Были проведены также измерения на отдельном тета-пинче. В режиме без предионизации, при начальном давлении 10^{-1} мм рт.ст., в первом полупериоде разряд не зажигается. Во втором полупериоде появляется жесткое рентгеновское излучение с энергией около 100 – 150 кэв.

При этом магнитное поле совпадает с вакуумным. В третьем полупериоде формируется нормальный пинч. С уменьшением давления разряд зажигается в более поздних полупериодах. В режиме с предионизацией жесткое рентгеновское излучение отсутствует, а разряд зажигается во втором полупериоде.

При наложении на тета-пинч с предионизацией антипараллельного магнитного поля, разряд зажигается в первом полупериоде. Причем интенсивность мягкого рентгена возрастает на порядок по сравнению с тета-пинчем без предионизации и начального поля. Электронная температура в момент максимального сжатия достигает 150 − 200 эв.

Проведены первые опыты с комбинированным пинчем с предионизацией. В этом режиме толщина скин-слоя составляла ≈1 см. Сжатие плазменной оболочки происходит эффективно. Жесткое рентгеновское излучение в начальной стадии разряда отсутствует.

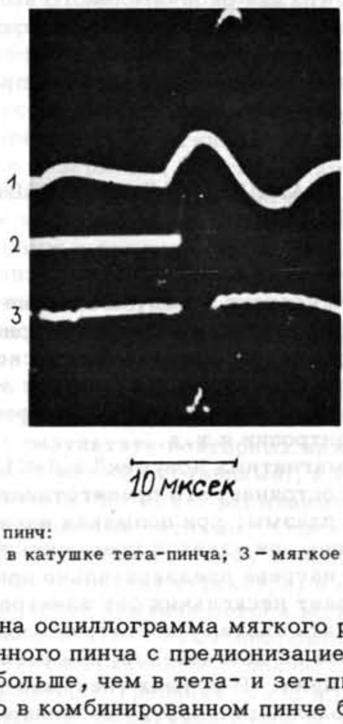

Рис.14. Комбинированный пинч:
1 − ток в зет-пинче; 2 − ток в катушке тета-пинча; 3 − мягкое рентгеновское излучение.

На рис. 14 показана осциллограмма мягкого рентгеновского излучения из комбинированного пинча с предионизацией. Длительность излучения в два раза больше, чем в тета- и зет-пинчах в отдельности. Следует отметить, что в комбинированном пинче без предионизации мягкое рентгеновское излучение отсутствует.

ВЫВОДЫ

1. Установлено, что плазма в комбинированном пинче более устойчива, чем в зет- или тета-пинчах в отдельности.

2. На динамику плазмы в комбинированном пинче существенное влияние оказывает начальная стадия развития зет-пинча. В течение первых 1 ÷ 2 мксек в зет-пинче развивается коллективная неустойчивость, которая приводит к увеличению толщины скин-слоя. Применение предварительной ионизации позволяет подавить эту нестабильность.

3. Начальное антипараллельное магнитное поле улучшает условия скинирования тока.

4. Исследована зависимость электронной температуры в комбинированном пинче от временного смещения между зет- и тета-пинчами. В случае разрядной камеры большого радиуса ($R = 16$ см) в режиме без предионизации оптимальное смещение равно 0,5 мксек. В случае разрядной камеры малого радиуса ($r = 3$ см) в режиме с предионизацией $\Delta t = 0$.

В дальнейшем основное внимание будет уделено изучению устойчивости плазмы в комбинированном пинче в режиме с предварительной ионизацией. С помощью лазерной методики предполагается провести измерение радиального градиента электронной плотности и ионной температуры плазмы. Будет измерено абсолютное значение электронной концентрации по штарковскому уширению спектральных линий и т.д.

Следует отметить, что для окончательного выяснения вопроса стабильности плазмы в комбинированном пинче необходимо провести опыты в тороидальной геометрии или в линейных пинчах большой длины, так как в коротких пинчах время жизни плазмы, как правило, ограничивается быстрыми концевыми потерями.

НЕКОТОРАЯ ТЕРМОДИНАМИЧЕСКАЯ ТРАКТОВКА ПОЛУЧЕННЫХ РЕЗУЛЬТАТОВ

Отличительная черта плазменных систем, используемых в термоядерных экспериментах, состоит в том, что они не достигают состояния термодинамического равновесия: в них всегда присутствуют градиенты температуры, плотности частиц, распределения скоростей, электрического и магнитного полей и др. и связанные с этими градиентами потоки энергии (тепловой, механической и электромагнитной), массы, количества движения, энтропии и т.д.

В системах типа "магнитных ловушек" с $\beta \ll 1$ очень быстро наступает стационарное состояние, что препятствует достижению необходимых параметров плазмы: при попытках накопить в системе заранее "нагретые" частицы не удается превысить значения концентрации $10^{10} \div 10^{11}$ см$^{-3}$; при нагреве предварительно приготовленной плазмы температура не превышает нескольких сот электронвольт. При $\beta \simeq 1$, напротив, трудно удержать систему достаточно долго в стационарном состоянии: оно или вовсе не достигается, или реализуется в течение слишком короткого времени. В лучших системах такого типа (например, в "Сцилле IV") продолжительность стационарного состояния не превышает 5 мксек.

В термодинамике необратимых процессов для характеристики эволюции системы используется величина σ – внутреннее производство энтропии (или обобщенной энтропии) в единицу времени, представляющая собой сумму обобщенных мощностей – произведений от термодинамических сил (градиентов) X_i и вызываемых ими потоков (термодинамических скоростей) J_i

$$\sigma = \sum_i X_i J_i$$

Для необратимых процессов всегда $\sigma > 0$. Общий критерий эволюции, сформулированный Пригожиным [11 – 13], приводит к выводу, что если система, взаимодействующая с окружающей средой, обладает выраженной индивидуальностью и подчинена граничным условиям, не зависящим от времени, σ может только уменьшаться. Это означает, что подобные системы развивают тенденцию к упорядочению внутренней эволюции путем повышения эффективности к.п.д. термодинамических процессов. Подобная тенденция сохраняется и в том случае, когда в системе, наряду с необратимыми диссипативными явлениями, происходят и обратимые механические явления. Теорема Пригожина гласит, что при соблюдении некоторых условий эти системы в конечном итоге достигают стационарного состояния, при котором σ приобретает минимальное значение, определяемое условиями (мощностью) взаимодействия с с окружающей средой.

Теорема Пригожина находит много интересных приложений [14]. В частности, для стационарной дуги она приводит к известному принципу Штеенбека [15], согласно которому падение напряжения принимает минимальное значение для заданной силы тока и при фиксированных внешних условиях. Как известно, это свойство характерно почти для всех видов сильноточных разрядов. Аналогичная ситуация возникает и в пинчевых разрядах после завершения сжатия плазмы. Это указывает на возможность применения упомянутого критерия и к такого рода системам. Попытаемся на этой основе сделать некоторые выводы по отношению к рассмотренным в предыдущих разделах результатам экспериментов.

Опыт показывает, что,хотя согласно критерию Пригожина отдельные зет- и тета-системы должны стремиться к стационарному состоянию, в действительности же они или не достигают его, или пребывают в нем в течение очень короткого времени (например, система "Сцилла IV"). Из предыдущего рассмотрения следует, что в зет-пинчах это происходит, главным образом, в результате повторных зажиганий разряда (образуется новая плазма с новыми границами), а также из-за возмущающего влияния плазменных струй, выбрасываемых с поверхностей электродов катодными и анодными пятнами. Они усиливают нестабильности сжатой плазмы. В тета-пинчах этому способствуют начальные неоднородности плазмы (волокнистая структура) и наличие однородного удерживающего поля, медленно изменяющегося во времени (выбросы плазмы желобкового типа и т.д.). В комбинированных пинчах причины, приводящие к нарушениям граничных условий, значительно ослаблены. В результате хорошего "сгребания" газа и наличия "шира" магнитного поля, здесь повторные зажигания разряда затруднены; отсутствует влияние приэлектродных процессов и ослаблены эффекты, вызываемые начальной неоднородностью плазмы; наличие "шира" магнитного поля улучшает гидромагнитную стабильность пинча, а скрученность составляющих его волокон удлиняет пути аксиального движения плазмы. Это указывает на то, что комбинированная система более устойчива, чем отдельные пинчи. В ней сохраняются или усиливаются свойства отдельных пинчей, способствующие нагреву и удержанию плазмы, а свойства, приводящие к развитию нестабильностей, подавляются.

Таким образом,из приведенного рассмотрения следует, что для достаточной стабильности стационарного состояния плазменной системы существенное значение имеют не только свойства самой плазмы, но и "прочность" граничных условий. Поскольку достижение термоядерных параметров потребует дальнейшего наращивания мощности разряда, мы будем встречаться с усиливающимися трудностями в сохранении граничных условий неизменными. Поэтому комбинированные системы, видимо, будут иметь определенные преимущества по сравнению с простыми системами.

ЛИТЕРАТУРА

[1] ФИЛИППОВ, Н.В., ФИЛИППОВА, Т.Н., Ядерный синтез 2 (1966) 405.

[2] MATHER, I.W., Phys. Fluids 9 (1966) 2080.

[3] QUINN, W.E., LITTLE, E.M., RIBE, F.L., SAWYER, G.A., Plasma Physics and Controlled Nuclear Fusion Research (Proc. Conf. Culham, 1965) 1 IAEA, Vienna (1966) 237.

[4] VAN DER LAAN, P.C.T., VAN DONSELAAR, M.F., MEWE, R., Препринт доклада I.R. 67/02 на Европ. конф. по термоядерному синтезу и физике плазмы, август 1967, Стокгольм.

[5] КВАРЦХАВА, И.Ф., КЕРВАЛИДЗЕ, К.Н., ГВАЛАДЗЕ, Ю.С., ЗУКАКИШВИЛИ, Г.Г., Ядерный синтез 5 (1965) 181.

[6] КВАРЦХАВА, И.Ф., КЕРВАЛИДЗЕ, К.Н., ЗУКАКИШВИЛИ, Г.Г., ГВАЛАДЗЕ, Ю.С., Ядерный синтез 3 (1963) 286.

[7] КОМАРОВ, Н.Н., КВАРЦХАВА, И.Ф., ФАДЕЕВ, В.М., Ядерный синтез 5 (1965) 192.

[8] ФАДЕЕВ, В.М., КВАРЦХАВА, И.Ф., КОМАРОВ, Н.Н., Ядерный синтез 5 (1965) 202.

[9] ШАФРАНОВ, В.Д., Атомная энергия 5 (1956) 38.

[10] СУПРУНЕНКО, В.А., СУХОМЛИН, Е.А., ВОЛКОВ, Е.Д., РУДНЕВ, Н.И., ЖТФ 31 (1961) 1057.

[11] PRIGOGINE, I., Physica 31 (1965) 719.

[12] LANSDORFF, P.G., PRIGOGINE, I., Physica 33 (1967) 351.

[13] ПРИГОЖИН, И., Введение в термодинамику необратнмых процессов, пер. с англ., Москва, 1960.

[14] ФИНКЕЛЬБУРГ, В., МЕККЕР, Г., Электрические дуги и термическая плазма, пер. с немецк., Москва, 1961.

[15] STEENBECK, M., Phys. Z. 33 (1932) 809.

DISCUSSION

F.L. RIBE: Does a fast-growing kink instability develop in the second apparatus? If so, how does it depend on the presence of a reversed trapped field?

G.G. ZUKAKISHVILI: In the combined pinch in the second apparatus, a helical instability also exists when there is a reversed trapped magnetic field in the plasma column, which twists into a helix and entrains the reversed field. As the reversed trapped field diminishes, the radius of the spiral decreases, while the plasma temperature rises accordingly. Helical instability appears to develop because the Kruskal-Shafranov stability condition is not satisfied. On the other hand, stabilization by the conducting sheath is not possible since the radius of the plasma is much less than that of the conducting sheath (the role of which could be played by the theta-pinch coil).

H.A.B. BODIN: Regarding the maximum electron temperature achieved with a reversed trapped field, is the measured value in agreement with the value calculated or estimated theoretically on the basis of resistive and compression heating with no energy losses or cooling, or is the temperature held down by radiation or other losses?

G.G. ZUKAKISHVILI: The maximum temperature values calculated on the basis of compression heating are near the measured values. Since the system which we were studying was a short one with open ends, the decrease in plasma energy after maximum compression may be attributed mainly to end losses.

THE POLYTRON: A TOROIDAL DISCHARGE WITH PULSED MAGNETIC CUSPS

A. E. DANGOR, G. J. PARKINSON, R. M. DUNNETT, M. G. HAINES AND R. LATHAM
IMPERIAL COLLEGE, LONDON, UNITED KINGDOM

Abstract

THE POLYTRON: A TOROIDAL DISCHARGE WITH PULSED MAGNETIC CUSPS. An experiment is described in which an axial current is produced in a toroidal plasma with many large superposed cusp magnetic fields and also a small axial magnetic field. The effects of preheating the discharge are given. It is shown that the presence of the magnetic fields modifies the discharge as follows: (1) $\omega\tau$ for the electrons is much greater than unity and the axial current is very much smaller than the axial current with no cusp fields; (2) A Hall current is produced by electrons drifting azimuthally in the cusp regions; this is verified by measurements of the axial magnetic field and of the total flux across the cross-sectional area; (3) The Larmor radius for the ions is greater than the separation of the cusps and the axial current is mainly composed of ions, thus motion of the plasma's centre of mass is predicted.

For the experimental conditions used the maximum ion velocity is limited by the periodic variation of the electric field rather than by collisions with trapped electrons. Spectroscopic measurements of the Doppler shift in an argon plasma made tangentially to the axis of the torus are given, together with measurements of the directed ion motion made with Faraday-cup-type probes. A computer study of a time-varying MHD model of the experiment has been performed. Comparisons between computed and experimental results are given with predictions of the conditions necessary for a stable ion-current regime.

1. INTRODUCTION.

The "Polytron" device is a toroidal discharge configuration on which is superimposed multiple cusp shaped magnetic fields as shown in Fig. 1. The radial component of each cusp field, B_r, interacts with the axial current density, i_z, to give rise to an azimuthal Hall current. This in turn interacts with B_r to produce an $\vec{i} \times \vec{B}$ force in the z direction independent of the sign of B_r. (For convenience we are using the terminology of cylindrical coordinates). Provided the ion Larmor radius is sufficiently large, this force preferentially accelerates the ions, whereas the electrons, having much smaller Larmor radii, tend to remain trapped within the cusps. If the ion velocity so produced is greater than the ion thermal speed, the radial leakage out of the cusps will be prevented. Besides providing the acceleration mechanism, the cusp field if dominant should provide stability. The cusp fields are stronger on the outside of the torus and this is necessary to balance in equilibrium the strong centrifugal force of the ion current.

The system was first proposed by Haines [1] who determined the necessary operating criteria on the basis of a hydromagnetic model. Dunnett [2] has subsequently analysed the Hall acceleration in more detail.

2. EXPERIMENTAL DETAILS.

A schematic diagram of the assembly is shown in Fig. 1. The discharge vessel is a quartz torus of 50cm major diameter and 4.6cm minor diameter. The firing sequence together with details of typical working parameters is given in Fig. 2. The toroidal magnetic field, used to assist pre-ionization, is small and does not appear to disturb the system. Experiments have been done in hydrogen and helium but the most comprehensive results have been obtained with argon.

Diagnostics have been confined to the following: The axial plasma current and current in the induction rods were measured with Rogowski coils; current distributions in the plasma have been measured with conventional magnetic field probes and the asymmetric Hall currents have been measured with external loops positioned in the null region between cusp coils; time-resolved photographs and line spectra of the plasma have been obtained; finally a Faraday-cup probe [3] has been used to detect axial ion velocity. The properties of the preionizer discharge have been examined using a 4mm microwave interferometer and Langmuir probes.

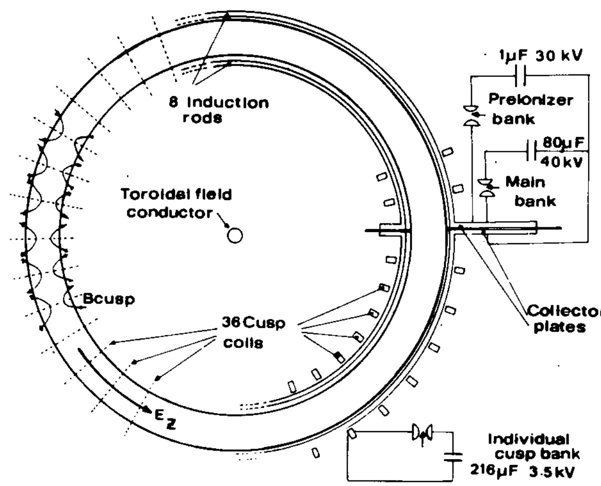

FIG.1. Schematic diagram of the Polytron.

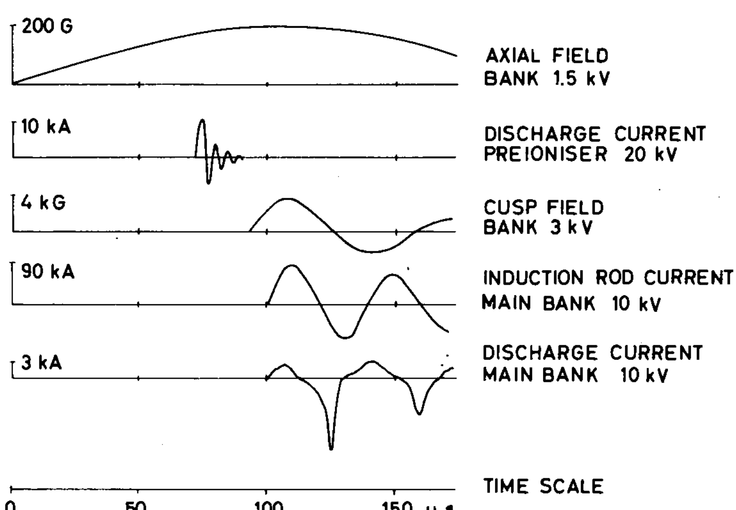

FIG.2. The firing sequence.

3. RESULTS.

3.1. Current waveforms

Current waveforms clearly indicate the existence of two regimes as may be seen in Fig. 3. At a low main bank voltage (7.5 kV) the discharge current is drastically reduced by the presence of the cusp fields, whereas at a higher voltage (25 kV) the plasma current is unaffected by the cusps and remains large. Also shown in the figure is an intermediate case. Note that in the low current regime the waveform exhibits a large current spike at the time when $B_{cusp} = 0$. The division between the two regimes depends on other parameters such as the magnitude of the cusp field and the gas filling pressure (see Fig. 8). In general the low current regime is favoured by low main bank voltages, high cusp fields and low initial filling density. Further discussion is given in section 4.

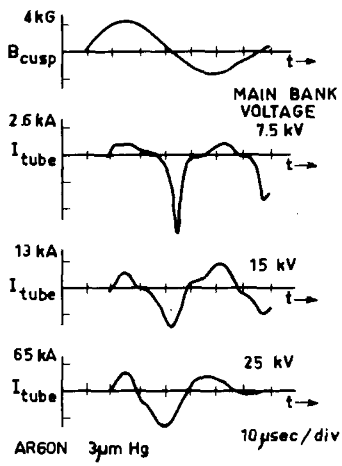

FIG. 3. Axial current waveforms.

3.2. Magnetic field measurements

The acceleration mechanism is entirely dependent on azimuthal Hall currents. The magnetic fields produced by these currents can be measured by a loop or probe in the midplane between cusps. These can clearly be seen from the dependence of the loop signals on the polarity of cusp banks and main bank as shown in Fig. 4. Over a wide range of experimental conditions, the Hall current signal was proportional to the main bank voltage and inversely proportional to the cusp field for $\omega\tau \gg 1$ (see Fig. 8). It was found that the gas pressure was critical in determining the duration of the Hall current. For an argon plasma, at pressures below 20 μm Hg, the Hall current lasted for the whole of the current first half-cycle but showed oscillations which depended on the size of the axial electric field. Between 20 μm Hg and 500 μm Hg pressure, the Hall current lasted for 2 to 4 μsec before disappearing completely. Above 500 μm Hg pressure, the Hall current lasted throughout the discharge and was smoother (see Fig. 5). The behaviour of discharges in hydrogen and helium at pressures up to 100 μm Hg was similar to argon at pressures below 20 μm Hg.

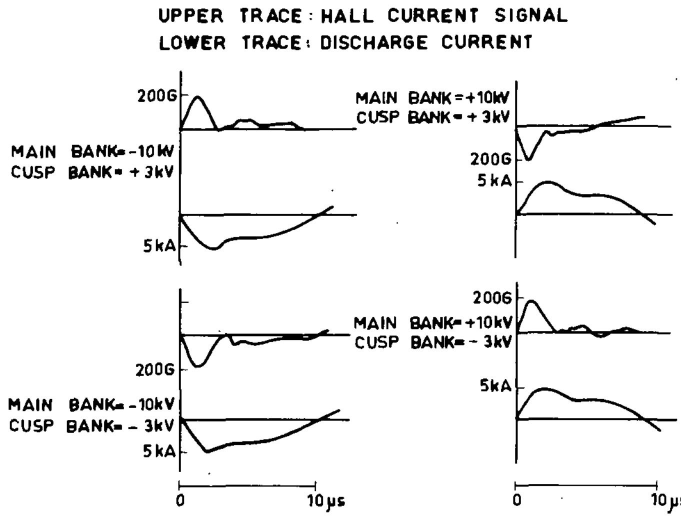

FIG. 4. Variation of Hall current with bank polarity.

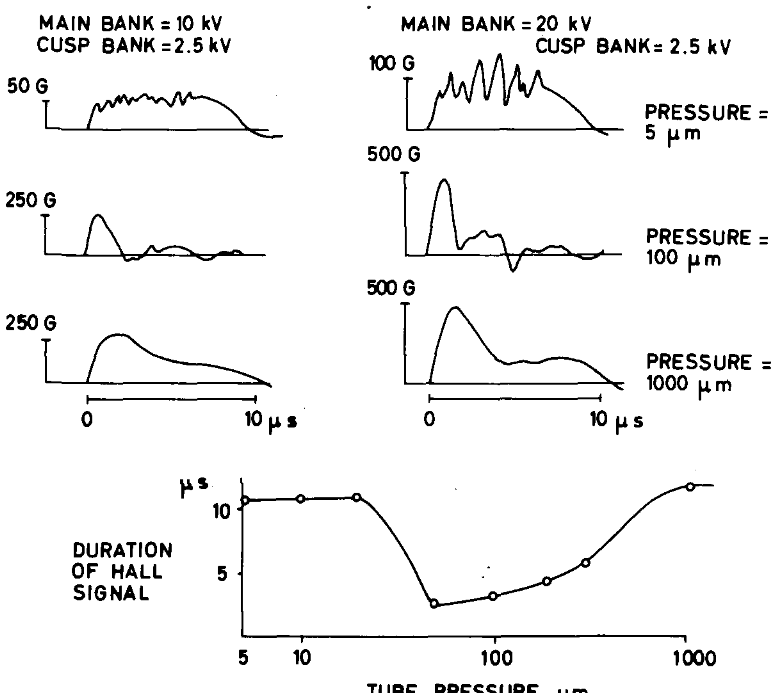

FIG. 5. Variation of Hall current with pressure and electric field.

Analysis of magnetic field profiles across the discharge showed that the axial current was confined mainly to a region 2 cm diameter around the centre of the tube at pressures up to 20 μm Hg whereas at pressures greater than 100 μm Hg the current density was almost uniformly distributed across the whole tube. Even very modest cusp fields prevented the implosion of a current sheet. The radial distribution of the Hall current showed a displacement towards the inside of the torus probably due to the inward displacement of the magnetic axis through toroidal effects.

3.3 Spectroscopic measurements

The achievement of a centre-of-mass axial velocity is central to the Polytron concept and spectroscopic work was concentrated therefore on Doppler shift measurements of the principal ion species involved. The line profile was measured photoelectronically using a Hilger and Watts medium quartz spectrometer, the radiation being sampled tangentially to the axis of the torus. The ion motion was expected to be in the direction of the applied electric field and comparison was therefore made of the profile measured with the electric field in one direction and then reversed. Fig. 6 shows a Doppler shift of Argon IV λ2809Å corresponding to a directed velocity of 1.1 x 10^6 cm sec^{-1} with respect to the laboratory frame. This was measured in a low current regime in which Hall acceleration was expected. A Doppler shift of the same order was obtained from another region of the discharge. Here the shift was measured with respect to the profile obtained in both the preionizer discharge and in the main bank discharge at the time when B_{cusp} = 0 when no ion currents were expected.

An estimate of the electron temperature has been obtained from the time history of line radiation from successive ionization stages in the argon discharge. An analysis similar to McWhirter and Kolb [4] indicates an electron temperature of the order of 20 eV for a discharge in the low current regime (10 kV main bank voltage, 4 kG cusp field, 5 μm Hg pressure). The measurement was obtained about 1 μsec after initiation of the main discharge which is before wall interactions occur (see section 3.5). At higher pressures the electron temperature is lower.

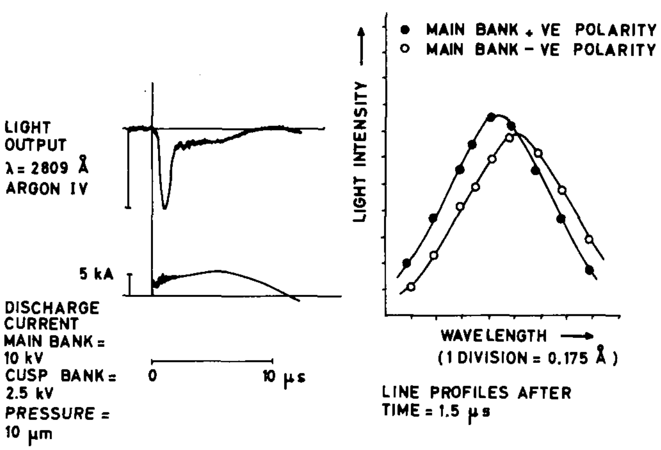

FIG.6. Line profile showing Doppler shift.

3.4. Ion probe measurements

Further confirmation of ion currents was obtained by the insertion of a Faraday cup probe into the discharge. The probe was positioned to receive particles travelling parallel to the axis of the tube and a radial scan was made from the outside wall to the axis. Measurements were made parallel and antiparallel to the applied electric field. The experiment was then repeated with the polarity of the main bank changed to eliminate spurious results. Typical probe traces and results are shown in Fig. 7. During the first half cycle of the discharge at peak cusp field it was found that the plasma noise was large on the tube axis and small away from the axis. This was probably due to the presence of high-energy electrons in the region where B_r is small. At a later time when $B_{cusp} = 0$ the plasma noise was excessive and arcing frequently occurred in all regions of the discharge.

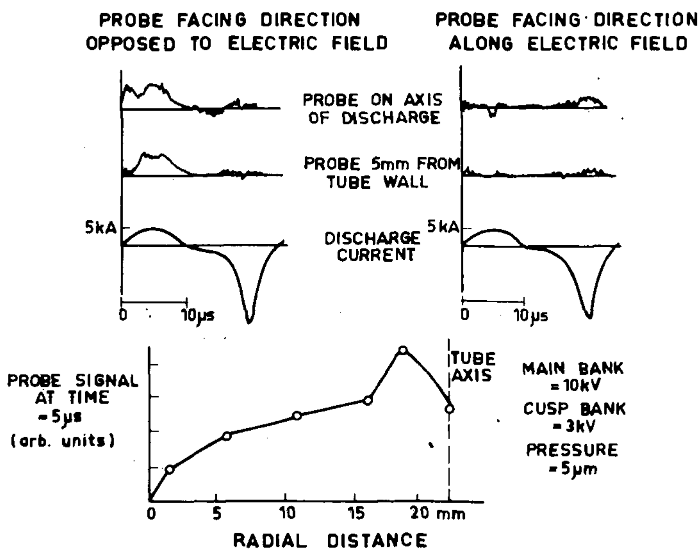

FIG. 7. Ion probe signals.

3.5. Photography

Image converter camera pictures clearly show the leakage of plasma to the walls at the centre of the cusps at times greater than 1 µsec from initiation of the main discharge. At pressures below 20 µm Hg for argon this appears to be the only cause of loss of plasma. For intermediate pressures of 50-500 µm Hg the cusp shaped plasma remains stationary for 1 to 4 µsec and then there is a displacement of the cusp shape in the direction of the applied field. After a further 0.5 to 1 µsec the plasma breaks up. At pressures above 500 µm Hg the plasma is slightly cusp shaped and fills most of the tube. No break up of plasma is observed. There is a good time correlation between the presence of the Hall current and the cusp shaped appearance of the plasma.

Associated with the observed plasma leakage to the wall in the cusp regions there is a drop in electron temperature, and at low pressures oscillations occur in the Hall currents.

4. COMPARISON WITH THEORY

Computer calculations have been performed on a magnetohydrodynamic model [2] in which the electric and magnetic fields are given realistic time variation. Current waveforms so derived have shown the same behaviour as Fig. 3. In the low current regime the computations indicated that the axial current was carried wholly by the ions, whereas the high current regime corresponded to an electron axial current. This changeover from axial ion current to an electron current occurred in the theoretical model when the induced azimuthal currents had grown large enough to remove the applied cusp field from the plasma region.

The computer program has been run for a variety of conditions and amplitude variations of axial plasma current and azimuthal Hall current are compared with experiment in Fig. 8. Certain plasma parameters were assumed in the computations, and so the main significance is the qualitative agreement with the experimental results.

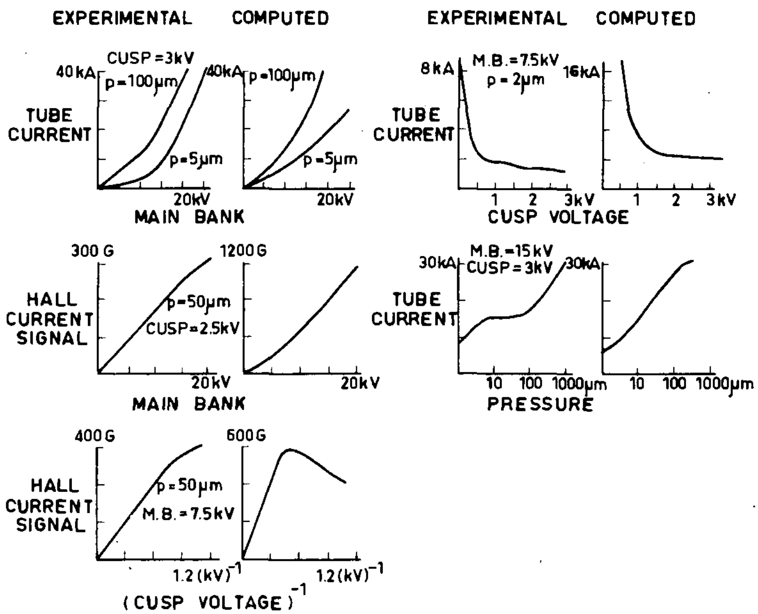

FIG. 8. Comparison of experiment with MHD model calculations.

5. CONCLUSIONS

Two discharge regimes characterised by very different axial currents have been obtained and the Hall current observed. These observations are in agreement with a numerical MHD model. Directed ion motion has been found by Faraday cup and Doppler shift measurements. These results are taken as evidence for the existence of the basic ion acceleration mechanism.

However, cusp leakage has not been eliminated. This could be due to inadequate acceleration of the ions. An additional factor in the present experiment is that the cusp coils are large compared with the tube diameter and this prevents the attainment of a strong radial magnetic field in the plasma. Theoretical considerations show that higher ion velocities will be obtained if the discharge is operated at lower number densities and higher electric fields. Modifications are at present being made to improve the effectiveness of the cusp system and to enable preionization at lower filling pressures.

Acknowledgements

The authors are grateful to Mr. D.A. Brown who has been associated with some of the work presented. Mr. P. Garnett gave technical assistance. The experiment is partly financed by the Science Research Council.

REFERENCES

[1] HAINES, M.G. Nuclear Fusion 1962 Supp. Pt 3 1122 (Abstract only). See also 6th Int. Conf. Ionization Phenomena in Gases. Paris (1963) 4 477.

[2] DUNNETT, R.M., Nuclear Fusion 8 4 (1968).

[3] ASHBY, D.E.T.F., AVIS, B.E., J. Nucl. Energy Pt C 8 (1966) 1.

[4] KOLB, A.C., McWHIRTER, R.W.P., Phys. Fluids 7 4 (1964) 519.

FACTORS INFLUENCING THE PERIOD OF IMPROVED STABILITY IN ZETA

D. C. ROBINSON AND R. E. KING
UKAEA, CULHAM LABORATORY, ABINGDON, BERKS, UNITED KINGDOM

Abstract

FACTORS INFLUENCING THE PERIOD OF IMPROVED STABILITY IN ZETA. Further experimental and theoretical studies have been made of the period of improved stability in Zeta.

Measurements, by Thomson scattering, show that the electron temperature, T_e, at the start of the period is about 100 eV. Studies have also been made of T_e during this period. Detailed measurements have been made of the plasma parameters (N_e, T_e) at the edge of the discharge. Measurements of the axial field at a pinch parameter of 1.8 show that this field is reversed by about 20% of the initial axial field B_0 at the start of the period. This reversal disappears after 1 ms when the improved stability ceases. At a pinch parameter of 2.9 the reversal is 80% of B_0 and the period is extended to 3 ms. The degree of reversal is constant round the major axis of the torus.

A reversed axial electric field at the edge of the plasma is always observed during the period. The dependence of stability on this field has been studied further by modifying the machine so that the field can be controlled externally.

The observations of the field configuration in the outer regions during the period of stability are consistent with the requirements of MHD theory. However, residual fluctuations are still observed and an analysis has been made of the possible instabilities which might cause these fluctuations. The MHD stability close to the magnetic axis for localized modes with vanishing pressure gradient has been studied and compared with experiment. Resistive instabilities, in particular the tearing mode and the possibility of stabilization by ion viscosity, have been analysed for the measured configurations. Estimates have been made of the growth times. The trapped particle modes are predicted not to be serious during this period and calculations have been made of the shear stabilization of drift modes.

1. Introduction

Attempts to produce stable plasmas in toroidal pinch geometry [1-3,33] have shown that certain pinch configurations are more favourable than others. In Zeta [5,6], stability is observed for periods of up to 3 msec in spite of a markedly unstable phase beforehand. A typical result for the rate of change of current fluctuations is shown in Fig.1. In Tokamak [4] hydromagnetic stability is apparently obtained with strong toroidal curvature but a much weaker rotational transform than in Zeta. The theoretical requirements for stability have been studied extensively [6,7,8,9] and from these results it has been concluded that the observed improved stability in Zeta is attributable to a combination of a reversed axial electric and magnetic field (E_φ, B_φ - Fig.3) in the outer regions, as indeed was found in a small programmed experiment [3].

In this paper we compare the theoretical requirements for stability with the observed field configurations both near the wall and the magnetic axis. New measurements of the electron temperature and density as a function of time, suggest that the particle and energy containment times are appreciably longer than obtained previously.

Experiments have been made on the effect of a programmed longitudinal electric field (E_φ) on stability. The origin of the period and the

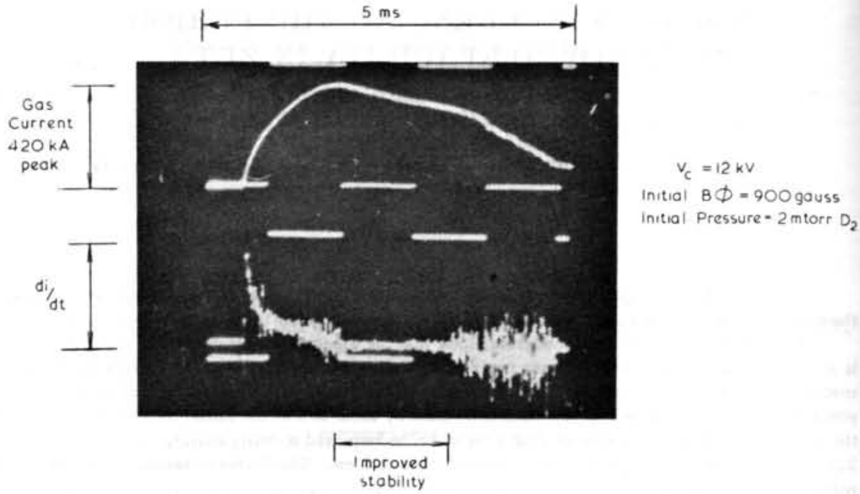

FIG. 1. Gas current and rate of change of current showing the period of improved stability.

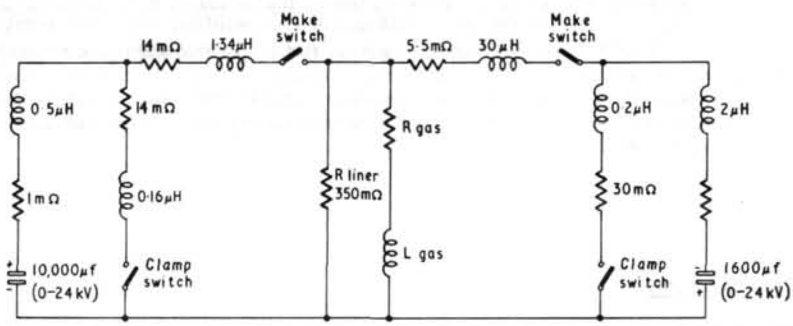

FIG. 2. Modified ZETA equivalent circuit, May 1968.

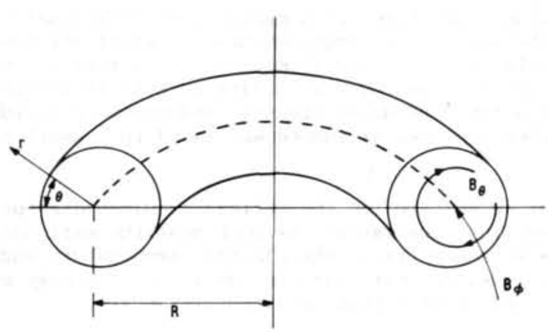

FIG. 3. Co-ordinate system and field components.

factors which determine its lifetime and the residual fluctuations are discussed.

2. Apparatus and Parameters

The torus assembly and power supply is essentially as described by previous workers [32]. The present equivalent circuit is shown to the left in Fig.2, and to this has been added a 0·5 MJ capacitor bank which provides additional control of the longitudinal electric field. The primary windings have been split, two thirds being powered by the large capacitor bank and the remaining third, with either polarity, by the smaller bank. The timing of the discharge of the small bank with respect to the first, is variable. Stabilizing magnetic fields of up to 2 kG are used.

The range of gas currents used in these experiments is 400–700 kA and initial deuterium gas pressures are 1·5–3 mtorr. The paramagnetic magnification of the stabilizing field produces central B_φ fields of up to 6 kG. Periods of improved stability lasting up to 3 msec are observed, when the pinch configuration parameter θ, is greater than 1·8. (θ is the ratio of the azimuthal field B_θ at the walls to the initial stabilizing field $B_{\varphi o}$). The coordinate system and field components are shown in Fig.3.

3. Electron Temperature

Previous measurements [6] of the electron temperature and density, by 90° Thomson scattering, have been extended into the period of improved stability. This has been achieved by increasing the sensitivity of the system by a factor of ten using a larger exit aperture and two passband filters - 6893Å, 6800Å, whose widths are 27 and 41Å respectively. The new results agree to within the errors (15%) with the previous measurements, which were made with a six channel system, at earlier times when the temperature is relatively low (60 eV). The measured scattered signal at 6800Å, shown in Fig.4, is relatively flat during the period, and falls later when the plasma is lost. The scattered and Doppler shifted signal at 6893Å also shown in Fig.4, falls steadily throughout the period. These results, which show that during the period the density remains almost constant and the electron temperature rises, - are summarized in Fig.5. The magnitude of this rise is about 50–100 eV, but it is difficult to estimate accurately due to uncertainties in the magnitude of the 6893Å signal. These results are consistent with earlier microwave measurements [10] which indicated a rise of 40 eV with the density remaining constant. The density falls rapidly at the end of the period.

Taking a temperature of 90 eV at the start of the period, the observed central current densities (Section 5), a density of 5×10^{13}e cm^{-3}*, classical resistivity and neglecting radiation and conduction losses, an electron temperature rise of 110 eV in 800 μsec is calculated from ohmic heating. This rise will be somewhat less if ion-electron thermalisation is included; it is slightly affected by considering an average ohmic heating rate in a minor cross section. This is consistent with the observed temperature rise, and indicates a relatively low loss by radiation and conduction. The use of classical resistivity is jusitified because the ratio of the drift speed of electrons to the sound speed is 1·2. Previous [32] and recent [11] experimental results have established

*This value for the electron density is obtained from relative density measurements by laser scattering, and observations previously reported [6].

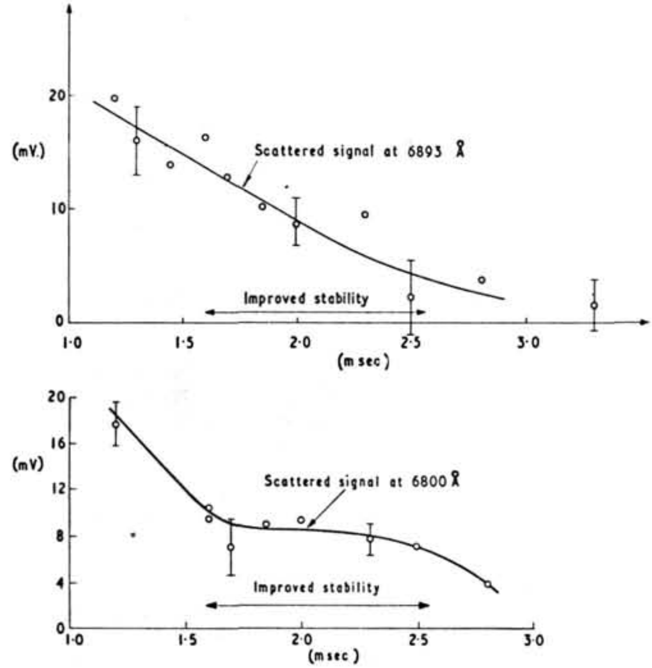

FIG.4. 90°-scattered light from a ruby laser (6943 Å) at two wavelengths as a function of time.

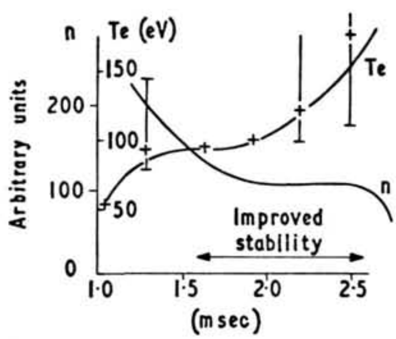

FIG.5. The electron temperature and density during the relatively stable period.

that unless this ratio significantly exceeds unity there should be no anomalous resistivity.

During the longer period of improved stability scattered signals comparable with those of Fig.4 are obtained. There is no observable scattered signal at 6800Å, if the conditions for the period are not satisfied.

These results suggest that the energy containment times are at least 3·5 msec, and the value deduced from the observed parameters is 10 msec. As the temperature is increasing and the density remains constant, an energy balance calculation shows that the particle containment time exceeds 3·5 msec. The calculated Bohm diffusion time is about 1 msec.

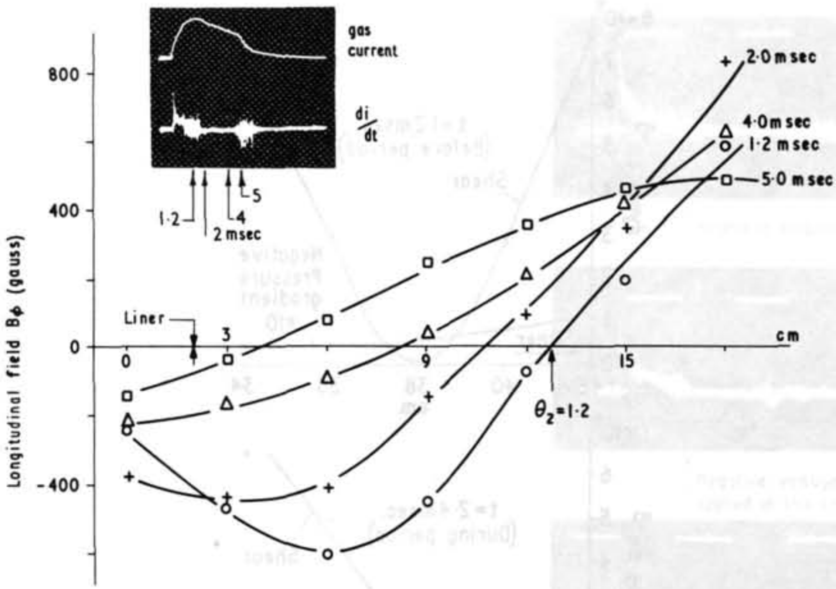

FIG. 6. Longitudinal magnetic field at various times as a function of radius in the outer regions.

Previous measurements of the particle containment time in helium discharges [12] gave values up to 2 msec, but in that case the current was lower and the plasma less stable.

It has been assumed that $T_i = T_e$, because the turbulent phase before the period preferentially heats the ions [13] and during the period, the equipartition time is 1·4 msec. With this assumption, the central value of β $(8\pi nkT/B^2(0))$ at the end of the period is about 10%, whereas shortly before the period it is 6%.

4. Outer Field Configuration

Suydam's necessary criterion for the stabilization of localised modes, requires that the shear $- B_\varphi \mu'/\mu$, where $\mu = B_\theta/rB_\varphi$, should be everywhere non-zero. Even discharges with vanishing pressure gradient are unstable where the shear vanishes [15]. As

$$B_\varphi \frac{\mu'}{\mu} = - \frac{2B_\varphi}{r} + \frac{4\pi j_\parallel B}{B_\theta} > 0 \quad \text{for stability,} \tag{1}$$

where $B^2 = B_\theta^2 + B_\varphi^2$ and $j_\parallel$ is the current density along the magnetic field, then a confined plasma with $j_\parallel \to 0$ near the walls, will require a reversal in the sign of B_φ. To ensure $j_\parallel B$ remains positive, a reversed j_φ in the outer regions is also desirable but, theoretically, does not seem to be necessary. A reversed axial magnetic field is observed throughout the shorter periods of improved stability (~ 1 msec) [6]. The measured axial field distribution for a period starting after 2 msec and lasting for 3 msec is shown in Fig.6. The normalised shear parameter, $\theta_2 = 2\pi r^2 \, d/dr \, . \, B_\theta/rB_\varphi$, whose magnitude is of interest when considering the stability of microinstabilities, is calculated to be 1·2 at the field reversal position. The reduction in the reversed axial field close to the liner at $t = 1{\cdot}2$ msec is due to flux being

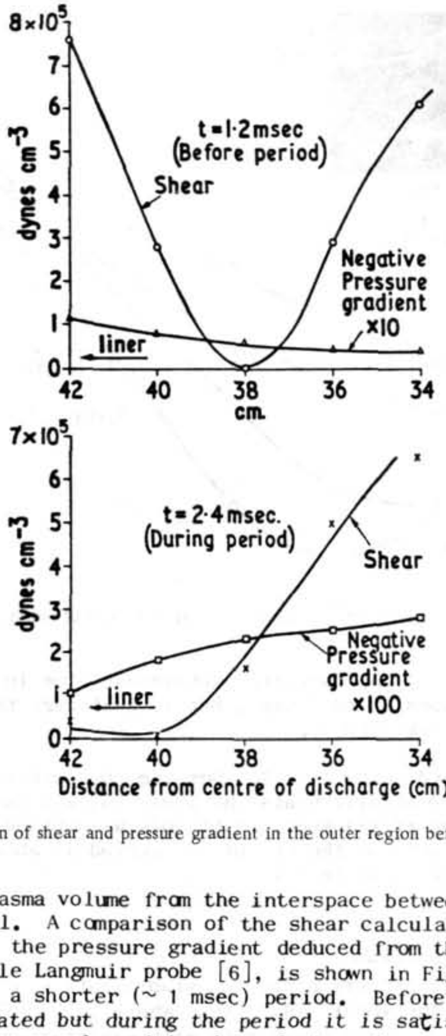

FIG. 7. Comparison of shear and pressure gradient in the outer region before and during the period.

drawn into the plasma volume from the interspace between the liner and the aluminium wall. A comparison of the shear calculated from the field distributions and the pressure gradient deduced from the ion saturation current to a double Langmuir probe [6], is shown in Fig.7, for times before and during a shorter (~ 1 msec) period. Before the period the *criterion is violated but during the period it is satisfied everywhere* and at the field reversal position by a factor of over a hundred.

The requirements for a reversed j_φ and B_φ satisfy the sufficient condition

$$j_\parallel B_\varphi B_\theta < 0 \quad \text{everywhere,} \tag{2}$$

for the stability of the non-localised kink mode. A reversed E_φ is always closely correlated with the start and finish of the period of improved stability. The experimental necessity for this reversal has been verified by controlling the axial electric field as described in Section 2. The results, in terms of the effect on the rate of change of current fluctuations, are shown in Fig.8.

(a) shows a normal period of improved stability,

(b) application of the reversed voltage at the conditions shown in (a) and

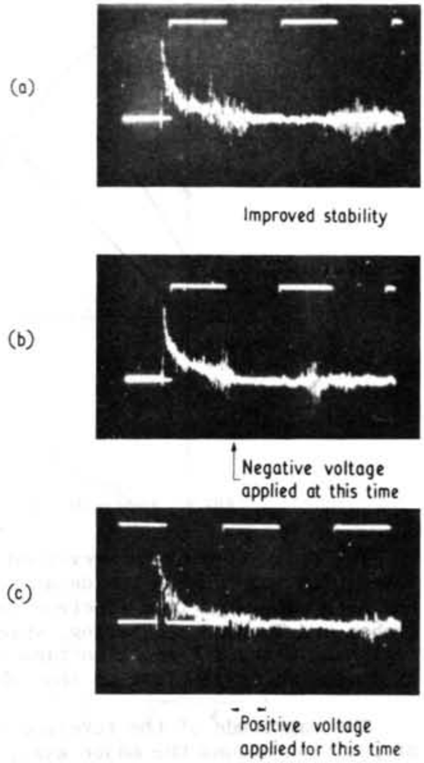

FIG. 8. Effect on rate of change of current fluctuations of applied voltage.

(c) application of a positive axial electric field at the condition shown in (a) which has previously been noted [5].

The creation and destruction of the period of improved stability clearly shows the necessity for the axial electric field reversal. Applying the reverse voltage at a much later time has little effect on the abrupt termination of the period. This could be due to the plasma being well isolated from the walls during the period or that the reversed axial magnetic field vanishes at this time and is not influenced by the second applied voltage.

Distributions possessing these field reversal properties can be obtained analytically by writing $j_{\parallel} = \sigma_{\parallel} E_{\parallel}$, $j_{\perp} = \sigma_{\perp} E_{\perp}$, $\underline{E} = (0, E_{\theta}, E_{\varphi})$. A range of such configurations has been shown to be stable against <u>all</u> modes by the Newcombe criterion [17] for field reversals of 30% and β's of 20%. An example of a stable configuration is shown in Fig.9, where the fields are shown as a function of normalised radius.

The reverse B_{φ} arises from the instabilities during the current rise and it is possible to show that it can be generated by a finite amplitude kink mode, though turbulent fluctuations can also give such a reversal [18].

The observations that B_{φ} and E_{φ} (j_{φ}) reverse in the outer regions during the period thus satisfy the requirements of infinite conductivity hydromagnetic stability theory.

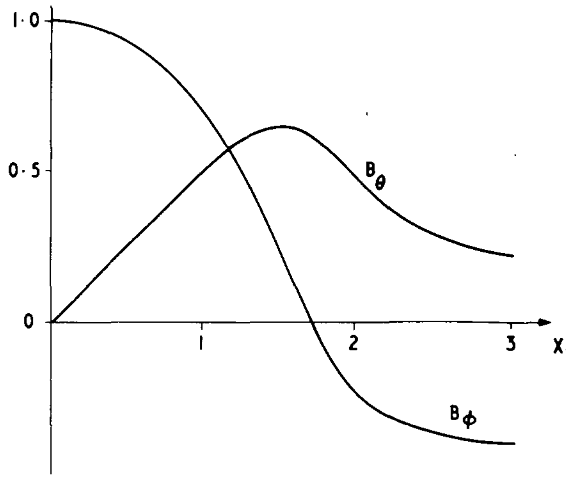

FIG.9. Field configuration for $E_\theta = 0.6\ X/E_\varphi(0)$ and $\sigma_\perp/\sigma_\parallel = 0.01$.

The decay time of the reversed field layer in Fig.6, has been calculated. In this region the decay time is determined by $\sigma_\parallel$ [31] and this has been estimated from electron temperature measurements by Langmuir probes and Thomson scattering, which give $T_e \sim 20$ eV in these outer regions. Using a Bessel function model for the field gives a decay time of 4 msec which is close to that observed for the reversed field.

The magnitude of the reversed field has been found to be independent of position around the major axis, suggesting that no asymmetry effects are associated with the period. This symmetry of the initial applied magnetic field has been destroyed by reversing one of the fifty coils generating this field. This reduces the applied field by 40% near the reversed coil and completely destroys the period of improved stability.

5. Central Field Configurations

Measurements of the field configuration close to the magnetic axis have been made by means of a multi-coil probe, for a few discharges, in conditions where the period of improved stability was not destroyed. Measurements of B_φ, B_θ, B_r have been made with an accuracy of better than ½%. The variation of B_φ as a function of distance from the centre of the minor cross section before and during the period is shown in Fig.10. The variation of all three components is shown in Fig.11. The uniform B_r variation indicates that the magnetic centre is situated 2·5 cm above the probe at this time, this distance decreases steadily during the period and reaches zero when it ends.

By expanding about the magnetic centre, the variations of the field components for vanishing pressure gradient are found to be

$$B_r = \frac{r^2 C}{8R}\sin\theta + O(r^3)$$

$$B_\theta = Cr - \frac{r^2 C5}{8R}\cos\theta + O(r^3) \qquad (3)$$

$$B_\varphi = B_\varphi^o - \frac{r}{R}\cos\theta\ B_\varphi^o + \frac{r^2}{R^2} B_\varphi^o \cos^2\theta - \frac{C^2 r^2}{B_\varphi^o} + \frac{C^2 r^3}{RB_\varphi^o}\,\frac{3}{4}\cos\theta - \frac{r^3}{R^3}\cos^3\theta\ B_\varphi^o + O(r^4)$$

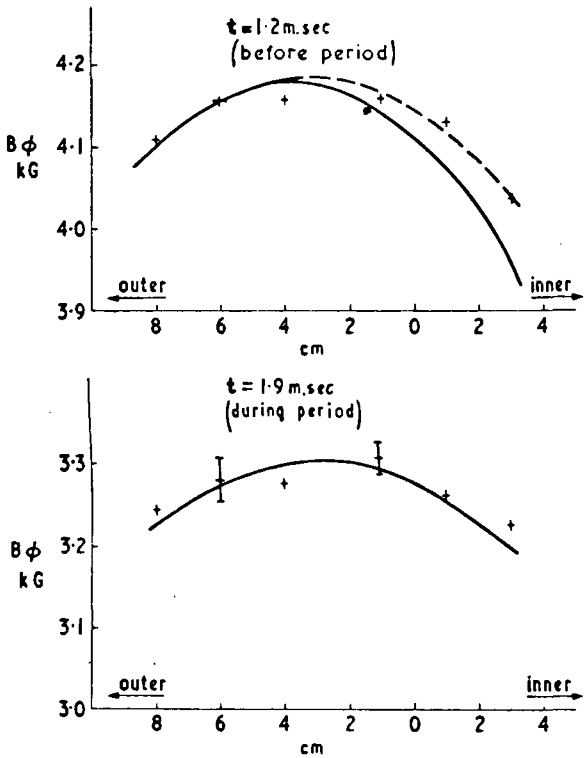

FIG. 10. Central longitudinal field B_φ; solid line as calculated from Eq. 3, dotted line includes a correction for pressure gradient.

The theoretical curves are shown in Fig. 10 and observations during the period give a vanishing pressure gradient at the centre. Prior to the period a negative pressure gradient is observed. The magnitude can be obtained from a modified form of (3) which gives $1/r \cdot dp/dr = -6{\cdot}1 \times 10^2$ dynes.cm^{-4}. If the pressure profile is assumed to be similar to that given by the model configuration in the last section, then the estimated value of β is 20%. This is consistent with $T_i > T_e$ at this time.

The Suydam criterion in a toroid is [19]

$$\frac{r}{4} B_\varphi^2 \left(\frac{\mu'}{\mu}\right)^2 + 8\pi \frac{dp}{dr} (1 - q^2) > 0 \qquad (4)$$

where $q = rB_\varphi/RB_\theta$; as $q < 1$ the measured configuration is locally unstable at the centre before the period. A stability analysis close to the magnetic axis of a toroid using the theory of Newcombe [17] for the case of vanishing dp/dr in this region, shows that the field configuration is always stable, independent of the value of q. Consequently the field configuration at the later time is believed to be stable to local perturbations near the centre. The vanishing pressure gradient could be due to the ohmic heating being greater off the central axis, as we would expect from strong reverse field configurations.

Calculation of the toroidal displacement, taking into account the observed pressure and field reversal, using the theory of Shafranov [20],

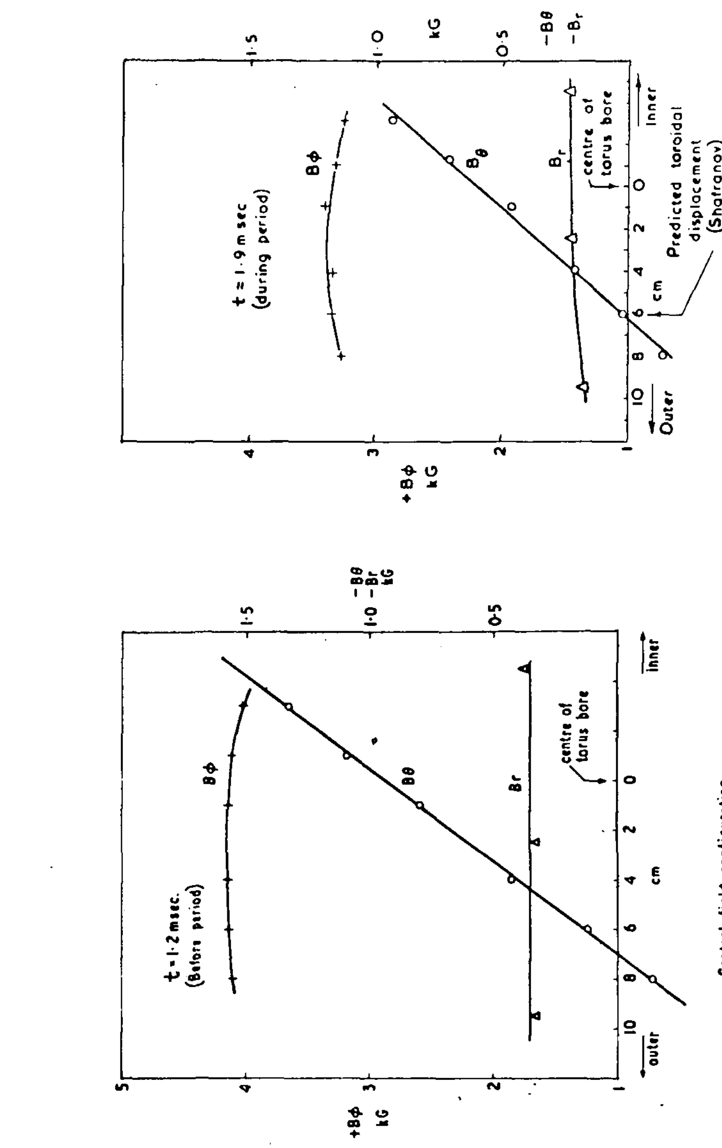

FIG.11. Central field configurations, before and during the period.

gives a horizontal displacement of 6 cm which is comparable to that observed. The initial vertical displacement is not understood.

6. Central Fluctuations

Infrared laser transmission experiments have been performed to study the density fluctuations at the centre of the discharge [21], using a shadowgraph technique [22] which is sensitive to the second derivative of the density. The observed intensity fluctuations are related to the magnitude of the density fluctuations, their spectral index and the large and small correlation lengths. No marked change in the level of the intensity fluctuations is observed from before to during the period, but the fluctuations are noticably slower. Correlation measurements show that the length correlation increases from 2.5 cm to 4.0 cm. From these observations we deduce that the random velocities fall by a factor of about two. Microwave measurements by Wort [10] on the larger scale density inhomogeneities show a reduction by a factor of five. These results therefore indicate that the larger eddies are suppressed during the period, which implies a gross form of stabilisation, as we might expect from the suppression of a kink instability. Correspondingly the Reynolds number is reduced and thus the measured length scale will increase, as is observed. On the basis of these considerations and the fact that the mean density falls from peak current into the period, it is apparent that the level of the density fluctuations at the centre remains the same. As previously noted [6] the level of the density fluctuations in the outer region is considerably reduced.

7. Discussion

We have interpreted the improved stability in terms of infinite conductivity hydromagnetic stability theory and have also considered the effect of other modes of instability, in particular resistive ones. The residual fluctuations in the centre of the plasma indicate that there remains some form of instability.

The tearing mode has recently been studied [24] for a configuration similar to that shown in Fig.6. It was shown that resistivity hardly affects the stability of the $m = 1$ mode, and it has been established [25] that this mode is the most dangerous.

For the experimental parameters, finite conductivity pressure driven flutes (g-mode) will be affected by ion-ion collisions and the electron pressure gradient in Ohm's law [26]. In the central regions, where the radius of curvature is large and the shear weak, there will be stability for negative pressure gradients if $T_e > 80$ eV, which is probably marginally satisfied. However in the outer regions where the radius of curvature is smaller, much higher temperatures are necessary for complete stabilisation (300 eV), even though the shear is strong; however, the growth rate is reduced by ion-ion collisions.

Consideration has also been given to the trapped particle instabilites [27] in a system with a large azimuthal field, and here shear turns out to be relatively unimportant and collisional stabilization will occur.

If we now consider the overheating effect [23], then the time taken to heat the plasma ohmically to some critical value of β (20%), obtained from the known parameters, is $\sim$ 10 msec. The expression is sensitive to β so that a critical β of 10% gives a time of 2·1 msec. However the local overheating effect may be more serious than this because, if the current density is peaked near the centre, negative pressure gradients will be created which will violate the Suydam criterion at the centre [28]. This violation will move out in radius until the plasma is lost. This effect suggests a possible explanation for the residual instabilities at the centre of the discharge. Because the density is constant and the temperature increasing, the 'runaway' condition is not approached [29].

8. Conclusions

To achieve kink stability in these diffuse discharges where the field configuration approaches a vacuum field at the edge, reversal of the B_φ field in this outer region is necessary. The reversal of the electric field does not appear theoretically to be essential in all circumstances, but experiments using direct control of E_φ show that it is necessary in the circumstance of the present experiments. These results are in good agreement with those obtained on a small scale experiment where both E_φ and B_φ were programmed [3]; in the present experiment, the reverse B_φ is generated, apparently, by instabilities of the discharge during the current rise.

During the period of improved stability, the electron temperature rises from 90 eV to 150-200 eV, in approximate accord with the ohmic heating rate calculated from the collisional resistivity formulae, and the density, measured by light scattering at the centre remains constant. These results suggest energy confinement times exceeding about 3 msec.

The field structure in the centre of the discharge at the end of the period agrees with toroidal equilibrium theory for a vanishing pressure gradient. Although there is a small unexplained vertical displacement at the outset, these measurements preclude a marked helical equilibrium structure at the centre.

Fluctuations of density in the central regions show changes indicative of a gross stabilization during the quiet period, but no overall major reduction in amplitude. Local overheating effects leading to violation of Suydam's criterion - might be important in the low shear regions. The major reduction in the fluctuations occurs in the outer high shear regions [6], but there are nevertheless residual fluctuations in these regions which are not accounted for.

9. Acknowledgements

We are grateful to Dr R.S. Pease for helpful discussions, Dr A.N. Gondhaleker for the infrared scattering measurements; to Mr B.C. Boland for his invaluable assistance in the Laser Scattering measurements; and the Zeta operations team without whom this work would not have been possible.

10. References

[1] E.P. Butt, et al., Proc. 2nd UN Conf. PUAE 32 (1958) 42.

[2] S.A. Colgate, et al., Proc. 2nd UN Int. Conf. PUAE 32 129.

[3] T. Ohkawa, et al., Phys. Fluids 66 (1963) 846.

[4] G.A. Bobrovskii, et al., Kurchatov Report IAE 1408 (1967).

[5] E.P. Butt, et al., Proc. Conf. on Plasma Physics and Controlled Nuclear Fusion Research, Culham, 2 (1965) 751.

[6] D.C. Robinson, et al., 2nd European Conf. on Controlled Fusion and Plasma Physics, Stockholm (1967) (Abstract in Plasma Physics 10 4 (1968) 469).

[7] M.N. Rosenbluth, et al., Proc. 2nd UN Conf. PUAE 31 (1958) 85.

[8] B.B. Kadomtsev. Nuclear Fusion 1 (1961) 286.

[9] K.J. Whiteman. Plasma Physics (J. Nucl. Energy Pt.C) 7 (1965) 293.

[10] D.J.H. Wort. Culham Report CLM-R 40 (1965)

[11] D. Dimock and E. Mazzucato. E., Phys. Rev. Letters 20 (1968) 713.

[12] A. Gibson, et al., Plasma Physics (J. Nucl. Energy Pt. C) 9 (1967) 1.

[13] M.G. Rusbridge. Plasma Physics, to be published.

[14] B.R. Suydam. Proc. 2nd UN Conf. PUAE 31 157.

[15] D.C. Robinson, to be published.

[16] A.A. Ware. Phys. Fluids 7 12 (1964) 2006.

[17] W.A. Newcomb. Annals of Physics 10 (1960) 232.

[18] D.C. Robinson. Ph.D. Thesis, Manchester University (1966).

[19] A.A. Ware and F.A. Haas. Phys. Fluids 9 5 (1966) 956.

[20] V.D. Shafranov. Nuclear Fusion 3 (1963) 183.

[21] A.N. Gondhalekar. Ph.D. Thesis, Manchester University (1968)

[22] V.I. Tatarskii. 'Wave Propagation in Turbulent Media', McGraw-Hill (1961).

[23] E.P. Butt and R.S. Pease. Culham Report CLM-R 30 (1965)

[24] D. Gibson and K.J. Whiteman, to be published.

[25] B.R. Suydam, private communication.

[26] T.E. Stringer. Phys. Fluids 10 2 (1967) 418.

[27] A. Kent and T.E. Stringer, private communication.

[28] M.G. Rusbridge. Culham Report CLM-R 41 (1964).

[29] H. Dreicer. Proc. 2nd UN Conf. PUAE 31 57.

[30] B. Coppi, et al., Nuclear Fusion 6 (1966) 261.

[31] G.D. Hobbs. Culham Preprint CLM-P 19 (1963).

[32] W.M. Burton, et al., Nuclear Fusion Suppl. Pt.3, (1962) 903.

[33] J.P. Commer, et al., Proc. 2nd UN Int. Conf. PUAE <u>32</u> 297.

DISCUSSION

S. J. BUCHSBAUM: In the stable Zeta, how many Bohm times does the 3-ms confinement time represent?

R. S. PEASE: I must emphasize that the 3-ms energy confinement time is based on the assumption of Spitzer resistivity. However, our measurements of anomalous resistivity published in 1961 suggest that this is a good assumption. The figure is the minimum consistent with it and with the experimental data, and represents about four Bohm times.

V. D. SHAFRANOV: Could one improve the stability in Zeta by programming the negative longitudinal magnetic field?

R. S. PEASE: I expect that we could lengthen the period of stability if we had direct control over the longitudinal field in the outer regions. Perhaps, also, we could improve the configuration. However, the present construction of Zeta precludes such control.

ИССЛЕДОВАНИЕ СЖАТИЯ ПЛАЗМЫ НА УСТАНОВКЕ "ТУМАН"

В.Е.ГОЛАНТ, И.П.ГЛАДКОВСКИЙ, В.А.ИПАТОВ,
М.Г.КАГАНСКИЙ, С.Г.КАЛМЫКОВ, А.И.КИСЛЯКОВ,
В.А.ОВСЯННИКОВ, Л.В.СОКОЛОВА и С.С.ТЮЛЬПАНОВ
ФИЗИКО-ТЕХНИЧЕСКИЙ ИНСТИТУТ им.А.Ф.ИОФФЕ,
ЛЕНИНГРАД,
СССР

Abstract — Аннотация

PLASMA COMPRESSION STUDIES IN THE "TUMAN" DEVICE. The paper describes experiments relating to the ohmic heating and adiabatic compression of a plasma by a magnetic field in the "Tuman" device. A conducting liner is installed in the toroidal sections of the dielectric discharge chamber, leading to an increase in plasma temperature and in the degree of plasma ionization. The plasma is compressed by a magnetic field which rises to a maximum of 10 kOe in 20 μs. By means of u.h.f. location it is found that compression is accompanied by effective detachment of the plasma column from the walls of the discharge chamber and the diaphragm. The plasma density near the diaphragm is less than 5×10^{12} cm^{-3} during compression. Outward displacement of the plasma column in the toroidal drift direction is found to occur during compression. Compression is accompanied by substantial plasma heating; when the amplitude of the compressing field is 10 kOe the plasma conductivity rises by a factor of 5 - 8, which corresponds to an increase in electron temperature from 7 - 10 eV to 30 - 40 eV. The increase in plasma temperature is due to adiabatic compression and to an increase in the efficiency of ohmic heating. When the plasma is compressed the energy containment time increases by a substantial factor to 20 - 40 μs. This is accompanied by a sharp decrease in the intensity of the H_β line, indicating a decrease in the neutral concentration, which is estimated at $\sim 2 \times 10^{12}$ cm^{-3} during compression for a plasma density $\sim 10^{15}$ cm^{-3}.

ИССЛЕДОВАНИЕ СЖАТИЯ ПЛАЗМЫ НА УСТАНОВКЕ "ТУМАН". Описываются опыты по омическому нагреву и адиабатическому сжатию плазмы магнитным полем в установке "Туман". В тороидальных участках диэлектрической разрядной камеры был установлен проводящий лайнер. Это привело к повышению температуры плазмы и степени ее ионизации. Сжатие плазмы осуществляется магнитным полем, нарастающим до максимального значения 10 кэ за 20 мксек. С помощью СВЧ-локации установлено, что при сжатии происходит эффективный отрыв плазменного шнура от стенок разрядной камеры и диафрагмы. Вблизи диафрагмы концентрация плазмы при сжатии меньше $5 \cdot 10^{12}$ см$^{-3}$. Обнаружено смещение шнура при сжатии наружу, в сторону тороидального дрейфа. При сжатии обнаружен существенный нагрев плазмы. При амплитуде сжимающего поля 10 кэ проводимость плазмы возрастает в 5 – 8 раз, что соответствует увеличению электронной температуры от 7 – 10 до 30 – 40 эв. Увеличение температуры плазмы происходит за счет адиабатического сжатия и повышения эффективности омического нагрева. При сжатии время удержания энергии увеличивается в несколько раз и составляет 20 – 40 мксек. Интенсивность линии H_β при этом резко уменьшается, что указывает на уменьшение концентрации нейтрали. Оценка концентрации нейтрали при сжатии дает значение $\sim 2 \cdot 10^{12}$ см$^{-3}$ при концентрации плазмы $\sim 10^{15}$ см$^{-3}$.

1. ВВЕДЕНИЕ

Адиабатическое сжатие плазмы в тороидальной магнитной ловушке нарастающим магнитным полем может быть использовано для получения равновесного шнура плотной и горячей плазмы, изолированного от стенок и диафрагм разрядной камеры. В течение нескольких лет в ЛФТИ проводятся опыты по изучению адиабатического сжатия на установке "Туман".

Первые эксперименты [1] показали, что несовершенная геометрия магнитного поля в установке препятствует омическому нагреву плазмы в сильном продольном магнитном поле. После улучшения конструкции установки и подбора поперечного магнитного поля, составляющего $\sim 10^{-3}$ от продольного, удалось значительно улучшить параметры плазмы, получаемой при омическом нагреве [2]. Эксперименты по сжатию плазмы, полученной при омическом нагреве ($n - 10^{-14}$ см$^{-3}$, $T_e = 5 - 10$ эв) магнитным полем, нарастающим до амплитудного значения за 20 мксек показали [3], что при сжатии концентрация внутри шнура существенно возрастает, а вблизи диафрагмы резко уменьшается. Так, при концентрации внутри шнура $\sim 10^{15}$ см$^{-3}$, вблизи диафрагмы концентрация менее 10^{13} см$^{-3}$. Однако, заметного нагрева плазмы при сжатии не наблюдалось. Оценки показали, что причиной быстрого охлаждения плазмы являлась резонансная перезарядка.

В экспериментах, описываемых в данной работе, в тороидальные участки разрядной камеры был введен металлический лайнер из нержавеющей стали, толщиной 0,1 мм. В соответствии с данными работы [4], при наличии металлического лайнера, из-за закорачивания полей разделения зарядов, существенно замедляется уход плазмы на стенки при нарушении равновесия.

2. ОМИЧЕСКИЙ НАГРЕВ

Схема установки и расположение применявшихся средств диагностики приведены на рис.1. Проводились измерения напряжения на обходе разрядной камеры и тока разряда, смещения оси тока с помощью магнитных зондов, фотографирование разряда с помощью СФР, зондирование плазмы пучком быстрых нейтральных атомов [5], СВЧ-локация плазмы [3], измерение относительной интенсивности спектральной линии водорода — H_β, измерение рентгеновского излучения, измерение диамагнетизма плазмы в прямых участках в период омического нагрева.

Как и в предыдущих опытах, для улучшения равновесия плазменного шнура в тороидальных участках создавались дополнительные поперечные поля. Однако, их влияние на проводимость плазмы при наличии проводящего лайнера было не таким сильным, как в опытах с диэлектрической разрядной камерой [3].

Сначала возбуждается квазистационарное продольное магнитное поле; его полупериод составляет ~2 мсек. Одновременно включается дополнительное поперечное магнитное поле, имеющее такой же период, что и продольное магнитное поле. Когда продольное магнитное поле достигает амплитудного значения, с помощью ВЧ-импульса длительностью 30 мксек осуществляется предварительная ионизация. Затем проводится омический нагрев, длительность которого составляет ~250 мксек. При омическом нагреве наблюдается рентгеновское излучение. Оно излучается в основном из области диафрагм. Энергия квантов достигает 1 — 2 Мэв. Наличие жесткого рентгена показывает, что грубые возмущения магнитного поля в установке отсутствует, так как для получения необходимой энергии электроны должны ускоряться на протяжении нескольких тысяч оборотов. Эксперименты проводились в водороде в диапазоне давлений $(1 - 20) \cdot 10^{-3}$ мм рт.ст. Работа производилась при непрерывном протоке водорода. Измерениям предшествовала тренировка разрядной камеры 30 — 50 разрядами.

Квазистационарное магнитное поле составляло в тороидальных участках от 12 до 24 кэ. Соотношение полей в прямых и тороидальных участках в период омического нагрева составляло 1 : 20. Ток омического нагрева обычно составлял от 1 до 3 ка, что соответствовало запасу устойчивости по Крускалу-Шафранову $q = 1 - 3$.

На рис.2 приведены осциллограммы тока разряда, напряжения на обходе разрядной камеры и интенсивности спектральной линии водорода $- H_\beta$, полученные при давлении $2 \cdot 10^{-3}$ и $20 \cdot 10^{-3}$ мм рт.ст. Расчет проводимости дает значение $\sim 1{,}2 \cdot 10^{15}$ CGSE при давлении $10 - 20 \cdot 10^{-3}$ мм рт. ст. (при продольном поле в тороидальных участках 18 кэ). С уменьшением давления проводимость несколько уменьшается; при давлении $2 \cdot 10^{-3}$ мм. рт.ст. и квазистационарном поле в узких частях 18 кэ и 24 кэ составляет $4 \cdot 10^{14}$ CGSE и $6 \cdot 10^{14}$ CGSE соответственно. С уменьшением давления ниже $1 \cdot 10^{-3}$ мм рт.ст. проводимость быстро падает.

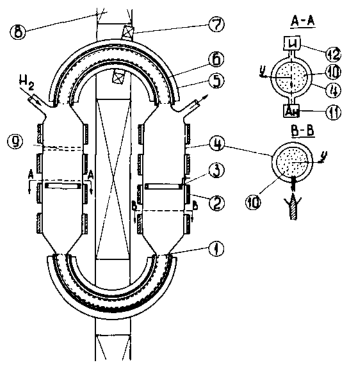

Рис.1. Схема установки "Туман":
1 – металлический лайнер; 2 – катушка продольного магнитного поля в прямых участках; 3 – диафрагма; 4 – разрядная камера; 5 – катушка продольного магнитного поля в тороидальных участках; 6 – медный кожух; 7 – пояс Роговского; 8 – трансформатор омического нагрева; 9 – щель для снимков СФР; 10 – плазма; 11 – анализатор проходящего пучка нейтральных атомов; 12 – источник пучка нейтральных атомов.

Измерение концентрации плазмы с помощью пучка нейтральных атомов показали, что концентрация достигает максимума после максимума тока (приблизительно через 100 – 150 мксек после начала омического нагрева). На рис.3 показана зависимость максимальной концентрации плазмы от давления. Как видно из рис.3, максимальная концентрация линейно растет с давлением, причем величина ее приблизительно соответствует концентрации атомов водорода перед разрядом. При давлении $1 \cdot 10^{-3}$ мм рт.ст. и более низких давлениях концентрация плазмы значительно ниже, чем концентрация нейтральных атомов.

Диамагнитный сигнал измерялся с помощью катушки, намотанной на прямой участок разрядной камеры. При расчете диамагнетизма учитывался вклад парамагнитного эффекта. Парамагнитный сигнал, за исключением начального периода времени, был в несколько раз меньше диамагнитного. Диамагнитный сигнал достигает максимума несколько позже, чем ток, и составляет при давлении $2 \cdot 10^{-3}$ мм рт.ст. и квазистационарном поле в узких частях 18 кэ $nT = (1{,}0 \div 1{,}5) \cdot 10^{15}$ эв. см$^{-3}$. При концентрации $n = 1{,}4 \cdot 10^{14}$ см$^{-3}$ это дает для электронной температуры $T_e = 7 - 10$ эв, согласующееся с температурой, вычисленной из проводимости плазмы.

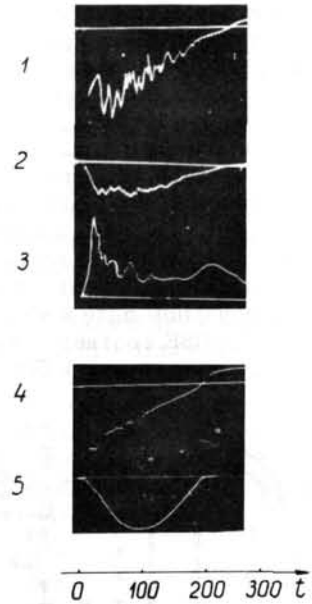

Рис.2. Осциллограммы: 1,2,3 – осциллограммы напряжения на обходе камеры, разрядного тока и интенсивности линии H_β соответственно, полученные при омическом нагреве при давлении $2\cdot10^{-3}$ мм рт. ст.; 4,5 – осциллограммы напряжения на обходе и разрядного тока соответственно при давлении $2\cdot10^{-2}$ мм рт. ст. Напряженность магнитного поля в тороидальных и прямых участках – H_T = 18 кэ, H_0 = 0,9 кэ соответственно. Начальное напряжение на обходе разрядной камеры U_0 = 750 в.

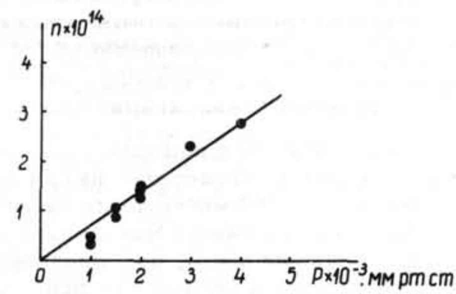

Рис.3. Зависимость максимальной концентрации плазмы от начального давления водорода в разрядной камере. H_T = 18 кэ, H_0 = 0,9 кэ, U_0 = 750 в.

Уже отмечалось, что с ростом давления проводимость плазмы растет. Это связано с тем, что при омическом нагреве мощность выделяется, в основном, в тороидальных участках установки, которые имеют малое сечение, а основной объем плазмы находится в прямых участках. Из-за конечной температуропроводности температура плазмы в тороидальных и в прямых участках может существенно отличаться. Оценка времени выравнивания температуры $t_T \approx \chi^2/\eta$, где χ – расстояние между областями с перепадом температуры, а η – коэффициент температуропроводности, дает $t_T = 20$ мксек при $T_e = 10$ эв, $n = 5\cdot10^{14}$ см$^{-3}$, $\chi = 50$ см. Низкая температуропроводность плазмы может приводить к тому, что в прямых участках температура ниже, чем в тороидальных. Этот эффект усиливается с ростом концентрации, чем, по-видимому, обусловлен факт роста проводимости с ростом давления (проводимость определяется, в основном, сопротивлением тороидальных участков).

При омическом нагреве расчет энергетического времени жизни

$$\tau_E = \frac{3nk(T_e + T_i)}{2W} \tag{1}$$

где W — мощность нагрева, определяемая по осциллограммам, а $nk(T_e + T_i)$ — определяется из диамагнитных измерений, дает значение $\tau_E \sim 5 - 8$ мксек. Это время соответствует времени передачи энергии от электронов к ионам — τ_B.

$$\tau_B = \frac{3}{8\sqrt{2\pi}e^4 L_K} \cdot \frac{M}{\sqrt{m}} \cdot \frac{(KT_e)^{3/2}}{n} \tag{2}$$

где M и m — масса иона и электрона соответственно, e — заряд электрона, K — постоянная Больцмана, L_K — кулоновский логарифм. Расчет дает для наших условий ($n = 1{,}4 \cdot 10^{14}$ см$^{-3}$, $T_e = 10$ эв) $\tau_B = 10$ мксек. Это, по-видимому, указывает, что охлаждение электронов происходит через ионную компоненту плазмы. Достаточно присутствие в плазме 5 — 10% нейтралей, чтобы обеспечить требуемую высокую скорость охлаждения плазмы за счет резонансной перезарядки. Время перезарядки ионов

$$\tau_n = \frac{1}{n_0 V_c \sigma} \tag{3}$$

где n_0 — концентрация нейтральных атомов, V_c — скорость ионов, σ — сечение резонансной перезарядки. При $n_0 = 1 \cdot 10^{13}$ см$^{-3}$ из соотношения (3) $\tau_n = 4$ мксек.

3. СЖАТИЕ ПЛАЗМЫ

Сжатие плазмы осуществлялось быстрым увеличением продольного магнитного поля в прямых участках установки. Обычно сжатие начиналось спустя 120 мксек после начала омического нагрева. Период сжимающего магнитного поля составлял 82 мксек. Таким образом, время сжатия составляло ~20 мксек. После сжатия происходило расширение плазмы, затем продольное магнитное поле в прямых участках уменьшалось до нуля; при этом происходил интенсивный контакт плазмы со стенками, в плазму попадало большое количество примесей [3]. Поэтому исследовались только процессы, происходящие в первом полупериоде сжимающего поля, т.е. при сжатии и расширении плазмы. На рис.4 приведены осциллограммы, полученные при амплитуде сжимающего магнитного поля 10 кэ. Как видно из осциллограмм, с нарастанием сжимающего магнитного поля начинается рост тока в плазме. При этом возрастание тока происходит несмотря на быстрое уменьшение $U_{обх}$ и на уменьшение сечения шнура. Таким образом, при сжатии наблюдается нагрев плазмы. Отметим, что возрастание тока при сжатии получено лишь в этой серии опытов; в опытах [3] без металлического лайнера ток в плазме уменьшался. Это, по-видимому, связано с более высокой степенью ионизации плазмы в этих опытах. Однако, увеличение тока происходит лишь при давлениях водорода меньше $5\cdot10^{-3}$ мм рт.ст. На рис.4 показаны также осциллограммы тока и напряжения на обходе разрядной камеры, полученные при давлении $2\cdot10^{-2}$ мм рт.ст. Видно, что наложение сжимающего магнитного поля практически не меняет характера изменения тока разряда. Здесь же виден вклад в напряжение на обходе индуктивного члена IL, связанного с изменением индуктивности шнура L при его сжатии и расширении. Отметим, что при давлении $2\cdot10^{-3}$ мм рт.ст. ток вдвое меньше, чем при $2\cdot10^{-2}$ мм рт.ст. Соответственно меньше и роль индуктивного члена.

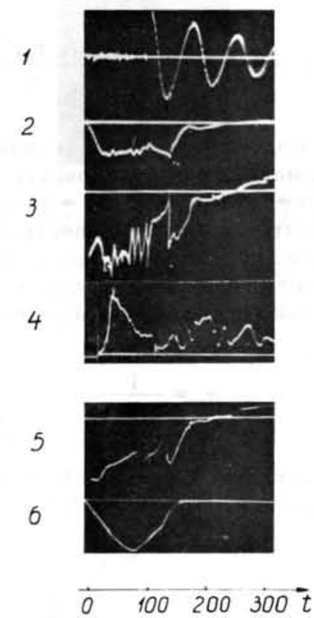

Рис.4. Осциллограммы, полученные при сжатии плазмы:
1 – производная сжимающего магнитного поля; 2,6 – ток омического нагрева при давлениях $2\cdot10^{-3}$ мм рт. ст. и $2\cdot10^{-2}$ мм рт. ст. соответственно; 3,5 – напряжение на обходе разрядной камеры при $2\cdot10^{-3}$ и $2\cdot10^{-2}$ мм рт. ст. соответственно; 4 – интенсивность линии H_β.
H_T = 18 кэ, H_0 = 0,9 кэ, U_0 = 750 в. Амплитуда сжимающего магнитного поля H_c = 10 кэ.

При сжатии наблюдается существенное уменьшение интенсивности свечения спектральной линии водорода H_β (рис.4 – 4). Очевидно, это связано с резким уменьшением концентрации нейтрального водорода при нагреве плазмы. Это подтверждается и фотографированием плазменного шнура с помощью СФР. На рис.5 приведена фоторазвертка свечения плазменного шнура. С началом сжатия свечение шнура резко ослабляется и остается очень слабым вплоть до момента времени, когда при расширении шнура плазма касается стенок.

Изменение проводимости при сжатии показано на рис.6. При расчете проводимости ток и напряжение на обходе плазменного витка были получены с помощью осциллограмм, аналогичных показанным на рис.4.

При этом предполагалось, что сечение канала тока в прямых участках определяется изменением магнитного поля $S_c = S_0(H_0/H_c)$, где S_c и S_0, H_c и H_0 сечение токового шнура и напряженность магнитного поля при сжатии и в период омического нагрева. Расчеты приведены для амплитуд сжимающего поля 3,5 и 10 кэ. Видно, что с ростом амплитуды сжимающего поля растет проводимость плазмы. Однако, максимальная проводимость достигается значительно позже максимума сжимающего магнитного поля. Кроме того, после расширения проводимость плазмы

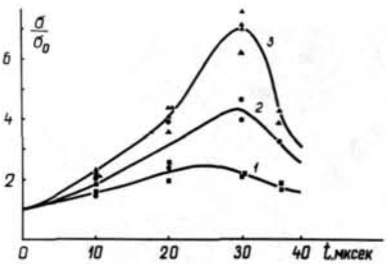

Рис.5. Изменение проводимости плазмы в период сжатия и расширения плазмы ($p = 2\cdot10^{-3}$ мм рт. ст., $H_T = 18$ кэ, $H_0 = 0{,}9$ кэ, $U_0 = 750$ в):
1 – H_c = 3 кэ; 2 – H_c = 5 кэ; 3 – H_c = 10 кэ.
σ_0 – проводимость плазмы перед началом сжатия.

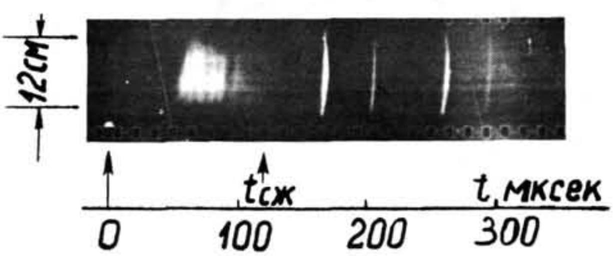

Рис.6. Снимок свечения плазмы в прямом участке камеры, сделанный через щель шириной 4 мм с помощью СФР. Показаны границы диафрагмы. Стрелками указаны начало разряда и начало сжатия.

значительно выше, чем перед сжатием. Помимо факта увеличения проводимости при сжатии, следует обратить внимание на резкое уменьшение амплитуды колебаний тока с момента начала сжатия.

Локация плазмы СВЧ-излучением проводилась в сечении ВВ прямого участка (рис.1). На рис.7 показана осциллограмма, полученная при локации на 8 мм. Отражение СВЧ-излучения происходит при этом от слоя с концентрацией $1{,}7\cdot10^{13}$ см$^{-3}$. По набегу фазы можно определить, на какое расстояние перемещается слой плазмы с такой концентрацией. Это расстояние растет с ростом сжимающего магнитного поля и составляет 3 – 4 см при сжимающем поле 10 кэ. Примерно такое же расстояние получается при зондировании на 16 см. Это показывает, что при сжатии происходит эффективный отрыв плазменного шнура от стенок и диафрагм разрядной камеры. При концентрации в сжатом шнуре $\sim10^{15}$ см$^{-3}$ вблизи диафрагмы концентрация меньше, чем $5\cdot10^{-12}$ см$^{-3}$ (критическая концентрация для 16 мм СВЧ-излучения).

На рис.7 приведены величины набега фаз, полученные при локации шнура с внутренней и с наружной стороны разрядной камеры. Приведенные результаты представляют усредненные значения, полученные в ряде разрядов при амплитуде сжимающего поля 3 кэ и 10 кэ. Видно, что при сжатии происходит смещение плазменного шнура наружу, в сторону тороидального дрейфа, примерно на 1 см (на уровне концентрации $1{,}7 \cdot 10^{13}$ $см^{-3}$). Отметим, что имеющиеся данные показывают то, что и в процессе омического нагрева наблюдается некоторое смещение шнура. Таким образом, суммарное смещение при сжатии, видимо, несколько более

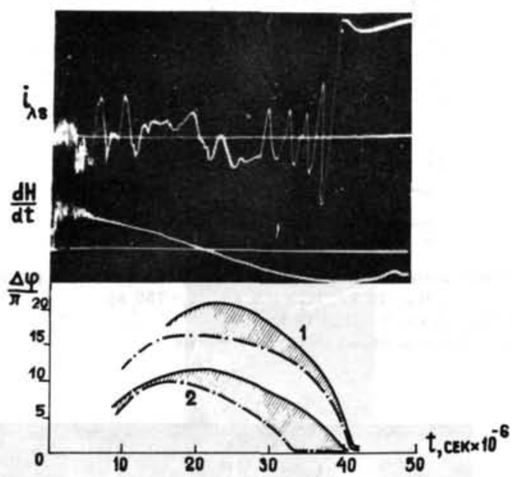

Рис.7. СВЧ-локация плазменного шнура излучением, с длиной волны 8 мм ($p = 5 \cdot 10^{-3}$ мм рт. ст., $H_T = 18$ кэ, $H_0 = 0{,}9$ кэ, $U_0 = 750$ в):
$i_{\lambda 8}$ – осциллограмма интерференционного сигнала при $H_c = 3$ кэ; dH/dt – осциллограмма производной сжимающего магнитного поля; 1 и 2 – набег фазы при сжатии и расширении шнура соответственно при $H_c = 10$ кэ и $H_c = 3$ кэ; Сплошная кривая – локация с внутренней стороны разрядной камеры; пунктирная кривая – локация с наружной стороны разрядной камеры.

1 см. Измерение концентрации показало, что плотность плазменной мишени $\overline{nL}$ при сжатии почти не меняется. В то же время расчет дает увеличение произведения $\overline{nD}$ (D – диаметр плазменного шнура) в 2 раза при отсутствии потерь частиц. Это может быть связано со смещением сжатого плазменного шнура, при котором зондирование происходит не по его диаметру, а по хорде, отстоящей от центра шнура на расстоянии 1 – 1,5 см.

Основным результатом, полученным в работе, является эффективный нагрев плазмы при сжатии. При амплитуде сжимающего поля 10 кэ проводимость увеличивается в 5 – 8 раз, что соответствует увеличению температуры электронов примерно в 4 раза, от 7 – 10 до 30 – 40 эв. Увеличение проводимости при адиабатическом сжатии при отсутствии потерь должно быть примерно таким же. Однако, тот факт, что максимальная температура достигается значительно позже максимума сжимающего поля и после расширения плазмы значительно выше, чем перед сжатием, показывает, что роль омического нагрева в повышении температуры плазмы также существенна.

Эффективный нагрев при сжатии соответствует, по оценкам, увеличению энергетического времени жизни до 20 – 40 мксек. Это, по-видимому, связано с тем, что при сжатии происходит резкое уменьшение концентрации нейтрали в плазме. На этот факт указывает как резкое уменьшение интенсивности линии H_β (рис.4 – 4), так и СФР-фоторазвертка (рис.5). Уменьшение количества нейтрали в плазме происходит из-за уменьшения потока нейтрали со стенок и диафрагм при сжатии шнура. Кроме того, при увеличении плотности нейтраль поглощается в более тонком поверхностном слое плазмы. Резкое уменьшение количества нейтрали в плазме соответственно увеличивает время перезарядки. Если время перезарядки становится больше времени обмена энергии между электронами и ионами, то время удержания энергии определяется временем перезарядки. Отметим, что время перезарядки 20 – 40 мксек в соответствии с уравнением (3) соответствует концентрации нейтральных атомов (1 – 2) 10^{12} см$^{-3}$. При этом, поскольку $\tau_n > \tau_B$ становится возможным нагрев ионов. Нагрев при сжатии не наблюдается при давлениях водорода выше $5 \cdot 10^{-3}$ мм рт.ст. С повышением давления, как отмечалось выше, быстро увеличивается концентрация нейтрали в плазме и, соответственно, уменьшается время перезарядки τ_n. При сжатии время удержания энергии остается малым, и нагрев плазмы отсутствует. Снимки СФР, сделанные при большом давлении, показывают, что при сжатии сечение плазмы остается довольно интенсивным. Это указывает на то, что в плазме остается большое число нейтралей.

Существенным является наблюдаемое при сжатии смещение плазменного шнура наружу, в сторону тороидального дрейфа. Пока имеются лишь данные, полученные с помощью СВЧ-локации, о смещении периферийных областей плазмы с концентрацией, значительно меньшей концентрации шнура ($n \sim 10^{15}$ см$^{-3}$). Для выяснения смещения центра шнура будет проведен эксперимент по зондированию пучком быстрых нейтральных атомов по нескольким каналам.

В заключение авторы пользуются случаем, чтобы выразить искреннюю благодарность А.Б.Березину, Л.В.Васильевой, Г.М.Малышеву, В.Е.Мисюку и В.Л.Паутову за помощь в работе.

ЛИТЕРАТУРА

[1] ГОЛАНТ, В.Е., КАГАНСКИЙ, М.Г., ОВСЯННИКОВ, В.А., Доклад CN-21/208, Конф. по физике плазмы и исследованиям в области управляемого ядерного синтеза, Калэм, 1965.

[2] КАГАНСКИЙ, М.Г., ОВСЯННИКОВ, В.А., ЖТФ 38 вып.6 (1968).

[3] БЕРЕЗИН, А.Б., ИПАТОВ, В.А., КАГАНСКИЙ, М.Г., КАЛМЫКОВ, С.Г., КИСЛЯКОВ, А.И., МАЛЫШЕВ, Г.М., ОВСЯННИКОВ, В.А., СОКОЛОВА, Л.В., ТЮЛЬПАНОВ, С.С., Доклад на II-й Европ. конф. по управляемому синтезу и физике плазмы, Стокгольм, 1967.

[4] YOSHIKAWA, S., HARRIES, W.L., SINCLAIR, R.M., Phys. Fl. 6 (1963) 1506.

[5] АФРОСИМОВ, В.В., ИВАНОВ, Б.А., КИСЛЯКОВ, А.И., ПЕТРОВ, М.П., ЖТФ 36 (1966) 102.

PROPERTIES OF A TOROIDAL SCREW PINCH SURROUNDED BY A CONSTANT-PITCH MAGNETIC FIELD

C. BOBELDIJK, R. J. J. VAN HEIJNINGEN, P. C. T. VAN DER LAAN,
L. Th. M. ORNSTEIN, W. SCHUURMAN AND R. F. DE VRIES
ASSOCIATION EURATOM-FOM, FOM-INSTITUUT VOOR PLASMA-FYSICA,
RIJNHUIZEN, JUTPHAAS, NETHERLANDS

Abstract

PROPERTIES OF A TOROIDAL SCREW PINCH SURROUNDED BY A CONSTANT-PITCH MAGNETIC FIELD. In the screw pinch a toroidal plasma is produced by a fast-rising helical magnetic field. Experimentally this plasma is found to be in equilibrium, showing complete reproducibility during the 7 μs that the confining field is present (C. Bobeldijk et al., Plasma Physics 9 (1967) 13). The behaviour of the screw pinch is strongly influenced by force-free currents flowing in the low-density plasma outside the central column. If the conductivity of this plasma is high enough and if near the wall field lines of constant pitch are applied, a constant pitch will result throughout the outside region. Experimentally, this constancy has been observed.

The plasma column is in equilibrium because the outward drift is counteracted by the compression of the B_θ-field against metal shells surrounding the torus. Calculations on the equilibrium position show that a pinch surrounded by a constant-pitch magnetic field is more easily kept in equilibrium than a pinch surrounded by vacuum. Also the stability is markedly improved by the presence of the constant-pitch region; a normal mode analysis shows that a $\beta = 0$ screw pinch is stable for all m and k. For high β unstable modes with k-numbers around the interchange value appear; the growth rates may be limited by a proper choice of the pitch and of the circumference of the torus.

Apart from the arrangement mentioned above, a small device (R = 16 cm, r = 4 cm) is in operation. A combination of capacitor banks applies initially a fast-rising and then a low-frequency clamped field. This allows a study at higher temperatures and during longer confinement times. In a third experiment a torus of the same size as in the first assembly (R = 36 cm, r = 6 cm) and a 75 kJ clamped capacitor bank are used.

Our diagnostics include holographic plasma interferometry and miniaturized dielectric-filled waveguide probes.

1. Introduction

Experiments carried out at Rijnhuizen as part of a study on toroidal pinched plasmas have led to the discovery of an unexpectedly stable configuration. In this configuration, the "screw pinch", the plasma column is produced by a rapidly rising helical magnetic field.

As is well known, such a plasma can be in equilibrium in a torus if the discharge tube is surrounded by a conducting shell. The plasma column is then forced to a position, slightly eccentric in the tube, where the outdriving force is balanced by the force arising from the compression of the B_θ-field*) between the plasma and the metal wall. In our experiments this equilibrium is observed.

*) Cylindrical coordinates r, θ, z are used; the z-direction coincides with the axis of the column.

Since our first measurements on the screw pinch in 1963 [1,2] its enhanced stability has been very intriguing. In an earlier paper [3] estimates for the growth time of an m=1 instability were given; according to existing theories this kink instability should develop rapidly, as soon as the longitudinal current surpasses the Kruskal-Shafranov limit, as it does in our experiments.

We have realized only recently that the discharge is strongly influenced by force-free currents flowing in the low-density plasma outside the central column. In most pinch experiments, this low-density plasma has a good conductivity so that it moves as if frozen to the field. Following the initial implosion of the pinch, field lines of (in general) helical shape move radially inward with the low-density plasma. These field lines cannot be further twisted if they are tied at the ends of the system, or if the system is endless (toroidal). The pitch of a helical field line is then constant in a coordinate frame moving with the plasma (compare Sec. 2.1 and the proof given by Colgate et al. [4]). In the screw pinch the field lines at the wall are applied with a constant pitch; consequently throughout the outside region a constant pitch is to be expected.

The magnetic field distribution thus formed (Sec. 2.1) differs strongly from the vacuum-field configuration. This modifies considerably the existing theories for toroidal equilibrium [5] and for stability [6]. A brief outline of the modified theory for the equilibrium is given in Sec. 2.2; more details can be found in [7,8]. Similarly an outline of a modified normal mode stability analysis is given in Sec. 3 and in [8]; the detailed theory will be published [9].

The influence of "pressureless plasma" on stability has been discussed previously [10]; however, in the configurations considered the pressureless plasma carried current in the perturbed state only; the equilibrium field had a vacuum configuration.

The constant-pitch configuration around the screw pinch is due to the relatively fast formation - the field rises to its maximum in 3 or 12 μs - and to the constancy of the pitch at the wall. In both these respects the screw pinch is different from other helical field systems like the Tokamak and the Stellarator. Moreover in these two systems the flow of currents in the outside region is unlikely because of the lower density and the presence of a limiter or divertor.

In a paper by Colgate et al. on the screw-dynamic pinch [4] the existence of the constant-pitch region was already demonstrated. Since the pitch in that experiment was much shorter than in ours (6 mm compared to 1 m) a different-looking field distribution was found. At that time no modification of the existing stability theory was considered.

2. Equilibrium

2.1 Field distribution in linear geometry

We consider a plasma column compressed to a radius r_o, in a cylinder with radius r_1. A pressureless plasma occupies the region $r_o<r<r_1$. If the electron temperature and the density of this plasma exceed certain limits [11] the magnetic field lines are constrained to move with the plasma. Suppose that the

pitch $h \equiv 2\pi r B_z/B_\theta$ of a helical field line varies when the line moves radially. The field line is then either further twisted or unwound, which implies that the low-density plasma rotates around the axis with a z-dependent speed. This situation may occur if the lines of force when leaving the system do not intersect with conductors. However, if the lines are tied at the ends or if the system is toroidal such a differential rotation is impossible. Then the pitch of the field line should be constant for an observer moving with the plasma, that is

$$dh/dt = 0 \tag{1}$$

Eq. (1) can also be derived from the conservation of flux in loops moving with the plasma [4,11] . However, in these derivations the essential role of the ends is less clearly shown. The importance of the ends is also evident if we consider the currents flowing along the field lines (compare Eq. (3)).

Since all the plasma behind the snowplow has come from the region just in front of the wall, the pitch distribution in space can be derived from the time variation of the pitch at the wall. In the screw pinch $h(r_1)$ is constant in time, so everywhere outside the column $h(r,t)$ is constant. For mathematical convenience we introduce the parameter $\mu \equiv 2\pi/h$.

If the density of the plasma in the outside region is low the currents in the plasma are predominantly force-free: $\vec{j} \times \vec{B} = 0$. Using curl $\vec{B} = \mu_0 \vec{j}$ and μ = constant we calculate the fields and the current densities

$$B_z = C(1 + \mu^2 r^2)^{-1} \qquad B_\theta = \mu r C(1 + \mu^2 r^2)^{-1} \tag{2}$$

$$\mu_0 j_z = 2\mu C(1 + \mu^2 r^2)^{-2} \qquad \mu_0 j_\theta = 2\mu^2 r C(1 + \mu^2 r^2)^{-2} \tag{3}$$

The integration constant C can be expressed in the B_z-field at the wall: $C = (1 + \mu^2 r_1^2) B_z(r_1)$. The field and current distributions are plotted in Fig. 1 as a function of the dimensionless parameter μr. Only the part between μr_0 and μr_1 applies to the experiment; in our case the values of μr are less than 1, which

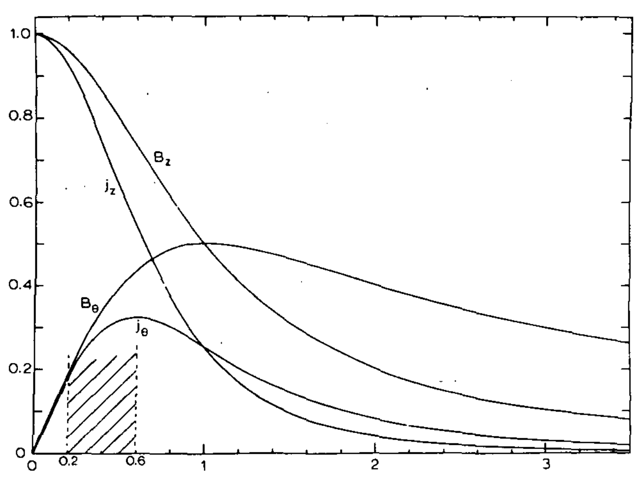

FIG. 1. Magnetic field components and current densities in a cylindrically symmetric force-free field of constant pitch. The hatched area $0.2 < \mu r < 0.6$ corresponds to the outside region under typical experimental conditions. The curves for B_z and j_z are normalized at the axis.

means that B_θ rises with r, rather than falling off as 1/r like in vacuum. In Colgate's experiment [4] μr ranged between 1 and 10; there B_θ decreases with r and the B_z-curve has a concave shape.

2.2 Equilibrium in toroidal geometry [7,8].

The plasma column with radius r_o, confined by the constant-pitch magnetic field within a conducting shell of radius r_1, is now bent to form a torus with major radius R. The plasma then experiences three out-driving forces, associated with the plasma pressure, the inhomogeneity of the B_z-field and the longitudinal current (hoop force). An outward motion of the column causes a compression of the B_θ-field between the plasma and the wall. The hoop force is then reversed and increases until at a displacement Δ of the column an equilibrium is obtained. The magnitude of Δ clearly depends on the B_θ-field distribution.

We follow the calculation by Shafranov [5] in which the toroidal effects are expressed as first-order corrections of the cylindrical solution. At a certain stage of this derivation the displacement of a magnetic surface at radius r can be found from.

$$d\Delta(r)/dr = \{\tfrac{1}{2}r\langle B_\theta^2\rangle_r - 2\mu_o rp + 2\mu_o r\langle p\rangle_r\}/RB_\theta^2 \tag{4}$$

where a quantity between triangular brackets is to be averaged over a cross-section with radius r.

In Shafranov's paper the zero-order B_θ-field is then assumed to be proportional to 1/r (a vacuum field), which leads to the displacement $\Delta(r_o) = \Delta$ of the column itself

$$\Delta_{vac} = \frac{r_1^2}{2R}\left\{\ln\frac{r_1}{r_o} + (\Lambda + \tfrac{1}{2})\left(1 - \frac{r_o^2}{r_1^2}\right)\right\} \tag{5}$$

The parameter Λ depends on the pressure and field distribution inside the column:

$$\Lambda + 1 = \{\tfrac{1}{2}\langle B_\theta^2\rangle_{r_o} + 2\mu_o\langle p\rangle_{r_o}\}/B_\theta^2(r_o) \tag{6}$$

In our situation the B_θ-field distribution of the constant-pitch configuration, given in Eq. (2) is to be inserted in Eq. (4). The general solution for Δ is complicated [8]; for the small values of μ^2r^2 in our experiments Δ can be approximated as

$$\Delta_{cp} = \frac{r_1^2}{2R}\left(1 - \frac{r_o^2}{r_1^2}\right)\left\{\frac{r_o^2}{r_1^2}(\Lambda+\tfrac{3}{4}) + \tfrac{1}{4}\right\} + \frac{\mu^2 r_o^4}{R}\Lambda\left\{2\ln\frac{r_1}{r_o} - \left(1 - \frac{r_o^2}{r_1^2}\right)\right\} \tag{7}$$

The values of Δ obtained from Eq. (7) are considerably smaller than those obtained from Eq. (5), as is illustrated in the following table, valid for a homogeneous plasma column with skin currents and for $\mu = 10\ m^{-1}$, $r_o = 0.02$ m, $r_1 = 0.06$ m and R = 0.36 m (compare Fig. 2).

β	Λ	Δ_{vac} (cm)	Δ_{cp} (cm)
0.0	-1	0.33	0.09
0.1	1.6	1.48	0.24
0.2	4.2	2.64	0.36

For larger values of β, i.e. the ratio of the plasma pressure to the magnetic pressure just outside the column, the assumption $\Delta \ll r_1$ which has been used to derive Eq. (4) is no longer true for Δ_{vac}; the eccentricity Δ_{cp} of the plasma in the tube remains pleasantly small for the constant-pitch field.

3. Stability [8,9]

In the equilibrium calculation, given in Sec. 2.2, the outward displacement of the column was found to be smaller for a column surrounded by a constant-pitch field than for a column surrounded by a vacuum field. A similar improvement might be expected for the stability; since in the constant-pitch case more B_θ-flux has to be compressed against the wall, the restoring force on the perturbation will be larger.

To check this supposition a normal mode analysis has been carried out for a linear homogeneous plasma column with skin currents surrounded by the constant-pitch magnetic field given in Eq. (2), within a conducting cylinder (see Fig. 2). If the equilibrium is perturbed, the total current density in the outside region remains force-free, that is parallel to the total B-field. A differential equation for e.g. B_{1r} (the radial perturbed field) can then be derived. In the case where the outside region is a vacuum, the corresponding equation can be solved analytically [6]; in our case computer calculations are necessary. The solutions in the outside and the central region have to be matched at the perturbed boundary of the column by means of the surface equations. These equations are in this case consistent with the requirement that the component of the material velocity normal to the surface should be continuous.

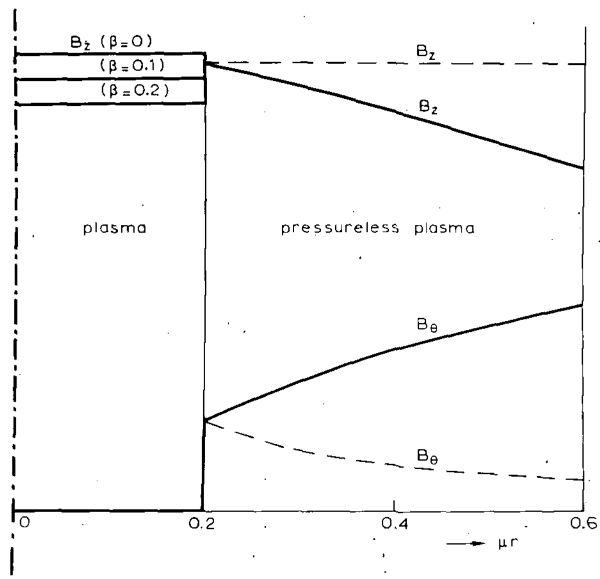

FIG.2. Magnetic field configuration as used in the calculations. The B_z-field inside the column depends on β. The field components outside the column are shown for the constant-pitch model (full lines) and for the vacuum model (dashed lines). The parameters are: $\mu = 10\ m^{-1}$, $r_1 = 0.02$ and $r_0 = 0.06$ m.

The procedure outlined above leads to a dispersion relation; real roots ω of this equation indicate instability. We write the equation in the form $L \equiv (1-\beta)f(\omega) = R$. The function $f(\omega)$ is a monotonic increasing function of ω [12]; the right-hand side R is independent of ω. Factors determining L and R are the wave numbers of the perturbation, m and k, the pitch of the applied field, given as the parameter μ, the plasma parameters and the dimensions of the system. If the value L for $\omega = 0$ exceeds R, stability is ensured; if it is less an instability grows at a rate ω to be found from the equation $L(\omega) = R$.

In Fig. 3, L and R are plotted as a function of k for $m = 1$; L is given for $\omega = 0$ and $\beta = 0$. Apart from R_{cp} calculated for the constant-pitch field, also R_{vac}, the right-hand side of the corresponding dispersion equation for a pinch surrounded by vacuum is shown. The values of μ, r_o, and r_1 correspond to typical experimental parameters.

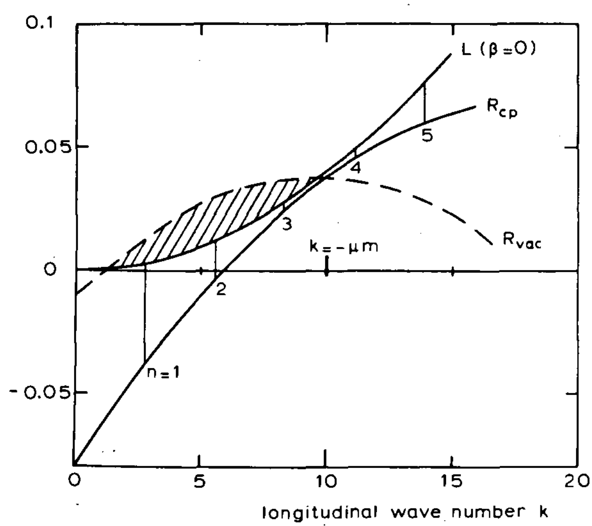

FIG. 3. Stability diagram for the m = 1 mode. In the constant-pitch model the $\beta = 0$ screw pinch is stable ($L > R_{cp}$). The same column in vacuum is unstable in the shaded area ($L < R_{vac}$). The indicated values of n correspond to modes fitting the circumference of the torus with R = 0.36 m. The other parameters are as in Fig. 2.

It is evident from Fig. 3 that the constant-pitch field causes a marked improvement of the stability; for $\beta = 0$ the pinch turns out to be stable for all k. At higher values of β the curve L comes down and at a critical value β_c the curves L and R touch. In the given example $\beta_c = 3\ \%$, at still higher β an instability will grow at about the value of k where the perturbation is parallel to the field, that is for $k + \mu m = 0$. All computer runs made thus far, indicate that the shortest distance between L and R is found at about this value of k. If we generalize these results, a simple calculation for this particular mode would predict stability for all values of μ and r_o at $\beta = 0$. For small μr_o the value of β_c goes to zero.

In the experiment the instability has to fit the circumference $2\pi R$ of the torus. Therefore the only k-values permitted are given by $k = nm/R$, where n is an integral number. The vertical lines in the figure indicate these values for R = 0.36 m. The modes at these k-values turn unstable at a β larger than or equal to the β_c defined above.

The same plasma column, with the same fields at its boundary, but confined in a vacuum field, is unstable, even at

$\beta = 0$ since in the hatched region $R_{vac} > L$. The only possibility to avoid the instability in this case is to choose μ (or R) such that the first possible mode for n = 1 occurs at the right of this area. This means that the longitudinal current has to be below the Kruskal-Shafranov limit. If the field outside the column has a constant-pitch, such a limit does not exist.

Note that the curves R_{cp} and R_{vac} intersect when $k + \mu m = 0$. A perturbation parallel to the magnetic field does not disturb the field, therefore the type of field distribution does not influence the stability of this mode.

Calculations on the stability of modes with m = 0, 2 and 3 have shown that the m = 1 mode is the most dangerous one. The m = 0 mode is stable for any β; the m = 2 and 3 modes are stable up to critical β-values larger than that for m = 1.

The stability against local interchanges in a skin of finite thickness is discussed in [8]; it appears that at least in some of our experiments the skin thickness is such as to give enough shear to satisfy Suydam's criterion. Local interchanges could also be present in the outside region, where, according to the model used above, the shear is zero. However, the destabilizing pressure gradient is also small in this region. Furthermore, slow-growing modes might be suppressed because of the finite length of the torus, unless the lines of force close on themselves.

4. Experimental methods

The screw pinch is studied in four toroidal set-ups, of which several parameters are given in the following table

Device	I		Ia		II		III	
R and r_1 (cm)	36	6	36	6	16	4	36	6
coilsystem	2 orthogonal coils				one helical coil			
energy (kJ)	15		15		2.5/12.5		75	
$\hat{B}_z$ (Wb/m^2)	0.6		0.6		1.5		2	
$\dot{B}_z$ (V/m^2)	2.6×10^5		2.6×10^5		10^6		2.5×10^5	
1/4-period (μs)	3.5		3.5		12		12	

In all systems the quartz torus is surrounded by a copper shell of 1 to 3 mm thickness. The gaps in this shell are covered by insulated overlapping metal strips; the primary coils are wound outside the shell. The devices I and Ia, which are very similar in construction, were originally intended for work on the alternating pinch [11]. Two primary coils can produce z- and θ-pinches, either simultaneously, as in the screw pinch, or with any desirable phase difference. The two primary systems have both a ringing frequency of 70 kHz. Device I is more extensively described in [3].

The devices II and III, which recently have been put in operation, are equipped with one helical coil, so that only screw pinches can be studied. The maximum value of the field has been raised and clamp switches have been added to allow a study of the discharge during longer times. In device II a fast capacitor bank, damped by resistors, applies initially a fast-rising B-field. At the first current maximum of the fast bank, a slow capacitor bank is switched. The resulting waveform of the primary field should lead to a fast implosion of the plasma, followed by a prolonged period of confinement.

In all experiments a pre-discharge is applied in the form of a low-power screw pinch. Usually the pitch of the field in this discharge is chosen equal to that of the main discharge, to avoid a time variation of the pitch during the early stages of the main discharge.

Density measurements have been performed by means of a microwave reflection probe [13,14]. Densities well above the critical density are found from the phase angle of the reflected wave, which is measured interferometrically. So far the measurements have been done with an 8-mm waveguide probe, insulated at the outside and closed by an alumina window of $\lambda/4$ thickness. This probe might perturb the plasma, especially if it is moved into the central core. Thin dielectric-filled 8 mm probes as well as a set-up at 4 mm are being prepared.

5. Measurements

Magnetic field distributions of a screw pinch are shown in Fig. 4. The measured quantities are clearly in much better agreement with the constant-pitch model than with the vacuum model; in the region outside the column B_θ rises with r (vacuum: $B_\theta \propto 1/r$); B_z has a convex distribution (vacuum: constant); $|B_\theta|/B_z$ is linear in r (vacuum: $\propto 1/r$); the pitch h is constant (vacuum: $\propto r^2$).

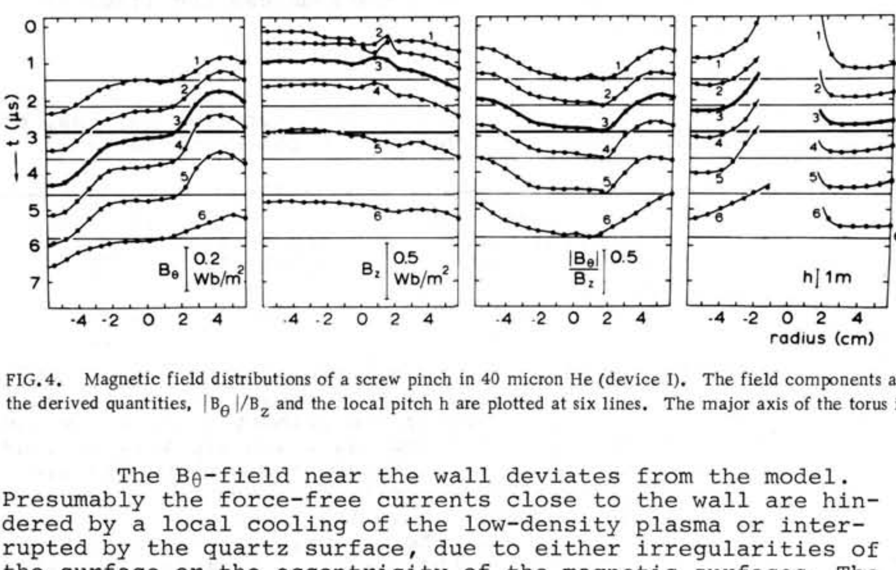

FIG.4. Magnetic field distributions of a screw pinch in 40 micron He (device I). The field components and the derived quantities, $|B_\theta|/B_z$ and the local pitch h are plotted at six lines. The major axis of the torus is left.

The B_θ-field near the wall deviates from the model. Presumably the force-free currents close to the wall are hindered by a local cooling of the low-density plasma or interrupted by the quartz surface, due to either irregularities of the surface or the eccentricity of the magnetic surfaces. The convex B_z-distribution is tilted as a result of the toroidal geometry. The bounces of the pinch cause oscillations of the B_z-field in the column. In the outside region B_z is enhanced by force-free currents. Although the column may exclude some B_z-field a net increase in B_z-flux is to be expected. Consequently, the discharge behaves paramagnetically as we have verified with a compensated loop system.

The local pitch h depends on the position of the magnetic axis, that is the point where B_θ is zero. Inaccuracies in the B_θ measurements influence the pitch curves, especially near the centre. The displaced column compresses B_θ at the outside. This causes the local pitch to be shorter at the outside than at the opposite side of the column.

In the devices I and Ia the duration of the confinement is 7 μs, the length of the first half period. During this time the discharge is completely reproducible and apparently stable. In the devices II and III the confining field lasts longer allowing the growth of an instability, presumably of the $m = 1$ type. In Fig. 5 a streak picture of a screw pinch in device III is shown. The magnetic field distributions in device II have been measured; both for slow and fast rising fields, distributions similar to those in Fig. 4 have been found. No precise measurement of β is available, but we estimate it to be 10 to 20%. This would mean that the critical β (Sec. 3) for $m = 1$ is exceeded.

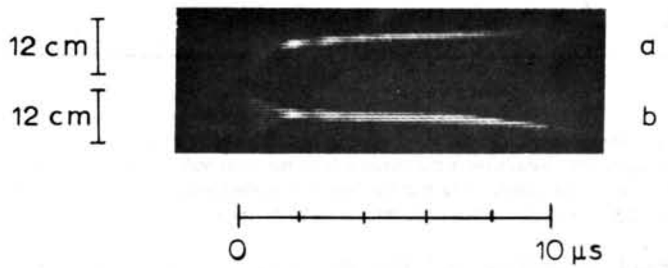

FIG. 5. Streak picture of a screw pinch in 40 micron He (device III). The two pictures are taken from mutually perpendicular directions, in part a slow outward motion can be seen, simultaneously a downward motion is registered in part b.

Densities obtained from measurements with a microwave reflection probe are shown in Fig. 6 as a function of time at three positions close to the wall. Outside the pinch the density is 2 to 5 $\times 10^{13}$ el/cm^3 compared to a density of $\geq 2 \times 10^{16}$ el/cm^3 inside the column; at the end of the half cycle when the field goes to zero the plasma moves outward. Because of the orientation of the probe window fast inward moving plasma could not be detected. Earlier measurements with a coaxial electrostatic double probe showed also a dense core at the same position, but could not give quantitative information about the density outside the pinch. Densities will also be measured by means of interferometric holography [15, 16]; results are not yet available.

The electron temperature has been estimated from the decay time of the He II λ 4686 Å line; in device I or Ia the temperature is 15 eV at 20 micron He filling pressure. This estimate is in good agreement with the temperature determined from the outward drift in toroidal θ-pinches, and with energy calculations for the screw pinch. In these calculations the energy input during the implosion and the energy loss by electrons necessary for exitation and ionization of He^+-ions are taken into account [17].

6. Discussion

A pinched plasma is surrounded by a dilute plasma of a density which is less than the density in the core by a factor 100 to 1000 (compare Fig. 6). Large force-free currents may flow in this medium if the lines of force either are contained in a closed system or intersect with conductors when leaving the system. The currents then conserve the pitch of the field lines, thereby modifying the field distribution and influencing

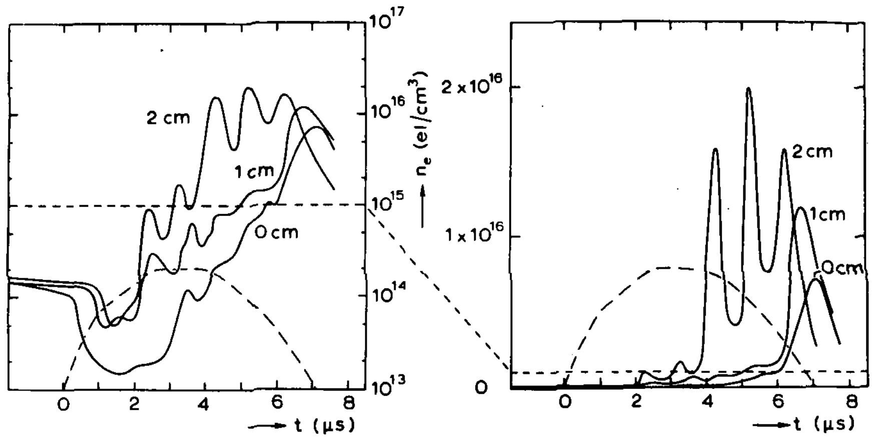

FIG.6. The density measured with the microwave reflection probe as a function of time at three positions in the outside region (the parameter is the distance from the outer wall). The course of the primary current is indicated by the dashed curve. Note that the density is plotted both on a logarithmic and on a linear scale. The discharge is a screw pinch in 60 micron He in device I.

the overall behaviour of the column. These currents flow in any type of pinch with the exception of the pure z- and the pure θ-pinch. In the screw pinch a constant pitch is applied at the wall and therefore the pitch of the field in the outside region is constant in time and space.

At high current densities in the dilute plasma the drift velocity of the electrons exceeds their thermal velocity. Instabilities might then allow the field lines to leak through the plasma; however since the resulting "turbulent heating" will raise the thermal velocity the instabilities are probably quenched. In our present experiments these effects are not yet to be expected. Also the resistive decay of the currents is not important on the present time scale.

Preliminary experiments in the new devices show a slow-growing instability, which is probably excited because the maximum admissible β is exceeded. Calculations are in progress to optimize this β beyond its present value of about 6% by a proper choice of r_1, μ, and the length of the system 2πR. In the experiments we attempt to lower β by changing the initial conditions and the time dependence of the main fields.

Acknowledgements

The authors are indebted to Professor C.M. Braams for his stimulating interest and his valuable comments. They gratefully acknowledge the assistance of Messrs. D.J. Maris, W. Kooijman, C.T. van Driel, P.J. Bouman, C.A.J. Hugenholtz, H.C.W. Gundlach and J. Roos.

This work was performed as part of the research program of the association agreement of Euratom and the "Stichting voor Fundamenteel Onderzoek der Materie" (FOM) with financial support from the "Nederlandse Organisatie voor Zuiver-Wetenschappelijk Onderzoek" (ZWO) and Euratom.

References

[1] RIETJENS, L.H.Th., VAN DER LAAN, P.C.T., BOBELDIJK, C., Bull. Am. Phys. Soc. 9 (1964) 335.
[2] VAN DER LAAN, P.C.T., Rijnhuizen Report 64-16 (1964).
[3] BOBELDIJK, C. et al., Plasma Physics 9 (1967) 13.
[4] COLGATE, S.A. et al., Proc. 2nd UN Int. Conf. PUAE 32 (1958) 140.
[5] SHAFRANOV, V.D., Nucl. Fusion 4 (1964) 232.
[6] KRUSKAL, M.D., TUCK, J.L., Proc. Roy. Soc. London A245 (1958) 222.
[7] BOBELDIJK, C., Plasma Physics 10 (1968) 567.
[8] BOBELDIJK, C., Rijnhuizen Report 68-45 (1968).
[9] SCHUURMAN, W., BOBELDIJK, C., DE VRIES, R.F., to be published.
[10] KRUSKAL, M.D. et al., Phys. Fluids 1 (1958) 421.
[11] VAN DER LAAN, P.C.T., Proc. Coll. Interaction of Electromagnetic Fields with a Plasma, Saclay-France (1968).
[12] BOBELDIJK, C., Rijnhuizen Report 67-39 (1967).
[13] TAKEDA, S., TSUKISHIMA, T., J. Phys. Soc. Japan 18 (1963) 3.
[14] HERMANSDORFER, H., Z. Naturforsch. 21a (1966) 1471.
[15] JAHODA, F.C., JEFFRIES, R.A., SAWYER, G.A., Applied Optics 6 (1967) 1407.
[16] KÜPPER, F.P., private communication.
[17] MEWE, R., private communication.

DISCUSSION

F.L. RIBE: What is your estimated value of β?

P.C.T. van der LAAN: Between 10% and 20%. Accurate measurements of β are to be made, and we hope to reduce it below the critical value predicted by theory.

F.L. RIBE: What is the relationship between the electron drift velocity and the electron thermal velocity in your experiments?

P.C.T. van der LAAN: The drift velocity is about 10% of the thermal velocity. This is not a precise estimate because the electron temperature of the low-density plasma is not known.

TRAPPED PARTICLE INSTABILITY IN AXISYMMETRIC TOROIDAL SYSTEMS

A. KENT AND T. E. STRINGER
UKAEA, CULHAM LABORATORY, ABINGDON, BERKS,
UNITED KINGDOM

Abstract

TRAPPED-PARTICLE INSTABILITY IN AXISYMMETRIC TOROIDAL SYSTEMS. We examine the trapped-particle instability of low β plasmas in toroidal fields with large aspect ratio and nearly-cylindrical symmetry. This problem was considered by Kadomtsev and Pogutse for Tokamak fields where the component B_θ about the minor axis is small. We find that when B_θ is not small, as in pinch-like systems, the instability has a qualitatively different behaviour.

The instability arises in systems with large B_θ only if the local radial density variation at some point is much stronger than that of the magnetic field strength, and does not arise at all in a magnetic well. Shear of the magnetic field lines is not important.

The presence of a radial electric field in Tokamak systems is known to change the nature of the instability, but has no effect on large B_θ system except to cause a frequency shift. Collisions have a stabilizing effect. The conclusion is that devices with large B_θ are less prone to the trapped-particle instability than Tokamaks.

1. INTRODUCTION

The trapped-particle instability has been studied by Kadomtsev and Pogutse [1] and Galeev et al. [2] for Tokamak fields with large ratio of major to minor toroidal radius (i.e. large aspect ratio R/a) and small ratio of azimuthal to longitudinal magnetic field (viz. $B_\theta \approx (a/R)B_\zeta$). In this work we remove the restriction $B_\theta \approx (a/R)B_\zeta$, which is valid for Tokamak and Stellarator studies. We examine the trapped-particle instability for general toroidal systems with large aspect ratio and nearly cylindrical symmetry, including, for example, levitrons or low-β toroidal pinches.

In section 2 the single particle paths are discussed for Tokamak and pinch systems. In certain circumstances of experimental interest [3] the Tokamak analyses [1, 2] hold for a Stellarator. In section 3 we examine the electrostatic oscillations of a low-β plasma, by means of the linearized Vlasov equation. It turns out that the trapped-particle flute modes are unstable only in radial positions where the logarithmic density gradient greatly exceeds the logarithmic magnetic field gradient ($n'/n \gtrsim +(a/R)^{-\frac{1}{2}} B_0'/B_0$). If n'/n and B_0'/B_0 have opposite signs, the flute modes are stable.

In section 4 it is shown that when the collision frequency reaches a particular order of magnitude it may modify the growth rate of the instability, but never alters its order of magnitude. (This contrasts with Tokamak systems where a critical collision rate enhances the instability.) Further increase of the collision rate completely removes the instability in both systems.

The presence of a radial electric field merely causes a frequency shift, whereas in Tokamak systems the trapped particle instability is quenched, and a new one arises [2].

2. SINGLE-PARTICLE BEHAVIOUR

The single-particle analysis shows the existence of trapped particles whose guiding centre motion is a relatively rapid oscillation between magnetic mirror points and a slower drift off the magnetic field lines. The single particle paths (2.4) below will be used to integrate the Vlasov equation in section 3.

The co-ordinates used to describe the toroidal system are plane polars (r, θ) measured perpendicular to the minor axis, which is taken to coincide with the magnetic axis or axis of the buried conductor in a levitron. The position of the (r, θ) planes on the minor axis is fixed by the angular co-ordinate ζ. These co-ordinates differ slightly from Kadomtsev and Pogutse's, where the magnetic surfaces have the simple equation ρ = constant, and consequently ρ is curvilinear. Here, the magnetic surface equations are less simple, but the co-ordinates have the simple metric

$$ds^2 = dr^2 + r^2 d\theta + (R - r\cos\theta)\, d\zeta^2$$

where R is the major radius.

We study axially symmetric toroidal magnetic fields $\vec{B} = (B_r, B_\theta, B_\zeta)$ where

$$\begin{aligned} B_r &= \epsilon\, b_1(r) \sin\theta \\ B_\theta &= B_2(r) + \epsilon\, b_2(r) \cos\theta \\ B_\zeta &= B_3(r) + \epsilon\, b_3(r) \cos\theta \end{aligned} \tag{2.1}$$

where $\epsilon = r/R$ is small. These fields are symmetric about the major axis (independent of ζ) and nearly symmetric about the minor axis (weakly dependent on θ). The functions $B_2(r)$, $B_3(r)$, $b_3(r)$ are arbitrary, but the requirement div $\vec{B} = 0$ implies $(r^2 b_1)' = r(b_2 - B_2)$. The fields (2.1) include a fairly wide class, including currents of arbitrary radial dependence, but weak θ-dependence. For example, the explicit form of (2.1) due to a hardcore current I_1 on the minor axis, and a straight current I_0 on the major axis is

$$\begin{aligned} B_r &= -\frac{\mu_0}{2\pi}\frac{I_1}{r}\frac{1}{2}\epsilon(\ell+2)\sin\theta \\ B_\theta &= \frac{\mu_0}{2\pi}\frac{I_1}{r}\left(1 - \frac{1}{2}\epsilon(\ell+1)\cos\theta\right) \\ B_\zeta &= \frac{\mu_0}{2\pi}\frac{I_0}{r}(1 + \epsilon\cos\theta) \end{aligned} \tag{2.2}$$

where $\ell(r) = \log \epsilon/8$, and the expressions are in MKS units. An electric field may be present, normal to the magnetic surfaces. To zero order in ϵ this field will be represented by the potential $\Phi(r)$.

The guiding centre equations in general form are

$$\frac{d\vec{r}}{dt} = \frac{v_\parallel \vec{B}}{|\vec{B}|} + \frac{\vec{E}\times\vec{B}}{|\vec{B}|^2} + \frac{m v_\parallel^2}{e|\vec{B}|^4}\vec{B}\times\vec{B}\cdot\nabla\vec{B} + \frac{m v_\perp^2}{2e|\vec{B}|^3}\vec{B}\times\nabla|\vec{B}| \qquad (2.3)$$

where the velocity $\vec{v} = (v_\parallel, v_\perp)$ has been resolved parallel and perpendicular to the magnetic field. Substituting the field (2.1) in expression (2.3), we obtain:

$$\frac{dr}{dt} = \epsilon\frac{v_\parallel b_1}{B_0}\sin\theta + \frac{V^2+v_\parallel^2}{2\Omega r}\epsilon\frac{b_0}{B_0}\sin\theta$$

$$r\frac{d\theta}{dt} = \frac{v_\parallel B_2}{B_0} + \frac{1}{\Omega}\left(\frac{B_3}{B_0}\frac{e\Phi'}{m} + \frac{V^2+v_\parallel^2}{2}\frac{B_3 B_0'}{B_0^2}\right) + \frac{V^2+v_\parallel^2}{2\Omega}\epsilon\frac{(rb_0)'}{rB_0}\cos\theta \qquad (2.4)$$

$$R\frac{d\zeta}{dt} = \frac{v_\parallel B_3}{B_0} - \frac{1}{\Omega}\left(\frac{B_2}{B_0}\frac{e\Phi'}{m} + \frac{V^2+v_\parallel^2}{2}\frac{B_2 B_0'}{B_0^2}\right)$$

where $|\vec{B}| = B_0 + \epsilon b_0 \cos\theta$, $B_0 = (B_2^2 + B_3^2)^{\frac{1}{2}}$ and $B_0 b_0 = B_2 b_2 + B_3 b_3$. The terms included in Eqs (2.4) are of zero order and first order in the inverse gyrofrequency $1/\Omega = m/eB_0$. We assume $e\Phi/m \lesssim V^2$, where $V^2 = v_\perp^2 + v_\parallel^2$, so that the electrostatic energy is comparable with the thermal energy. The two terms containing the factor ϵ/Ω are important in the Tokamak case where $B_0 \approx$ const. Remaining terms of order $(v_\perp/a\Omega)\epsilon$ have been omitted.

To zero order, the first two equations can be rewritten

$$\frac{1}{r}\frac{dr}{d\theta} = \frac{\epsilon b_1}{B_2}\sin\theta \qquad (2.5)$$

$$\frac{d\theta}{dt} = \frac{VB_2}{rB_0}\sqrt{1 - \frac{\mu}{V^2}|\vec{B}(r_p)|} \qquad (2.6)$$

The projected guiding centre position $r_p(\theta)$ to be used in Eq.(2.6) is obtained by integrating Eq.(2.5). The result $r_p = r - (rb_1/B_2)\,\epsilon\cos\theta$ gives the displacement of the magnetic surfaces from circles centred on the magnetic axis. From Eq.(2.6), expanding $|\vec{B}|$, we obtain

$$\frac{d\theta}{dt} = \frac{VB_2}{rB_0}\sqrt{\epsilon}\,h(r)\sqrt{2x^2 - 1 \mp \cos\theta} \qquad (2.7)$$

where $2x^2 - 1 = (1 - \mu B_0/V^2)/h^2\epsilon$ and $h^2(r) = \left|\frac{b_0}{B_0} - \frac{b_1}{B_2}\frac{rB_0'}{B_0}\right|$. The minus sign in Eq.(2.7) corresponds to $(b_0/B_0) > (b_1/B_2)(rB_0'/B_0)$, and the plus sign to the opposite inequality. In Tokamaks, $h = +1$ and the minus sign applies. The variable x is a label for the particles. Decreasing x corresponds to smaller longitudinal velocity $v_\parallel$, and to zeros of $d\theta/dt$ (trapping) close to $\theta = \pi$. The value $x = 1$ is the boundary between trapped and untrapped particles. If $b_0 > (rb_1/B_2) B_0'$ the trapped particle orbits lie on the outer half of the torus as in Fig. 1a, whereas for $b_0 < rb_1/B_2 B_0'$ they lie on the inner half of the torus as in Fig. 1b. In both cases the collective behaviour of the trapped particles is the same. The first case is the normal one, and the following analysis applies to this case. The second case, which corresponds to larger field strength on the outer half of a magnetic surface, is uncommon. It might occur, for instance, in a levitron in which magnetic surfaces were displaced inwards relative to the central conductor by applying a vertical field[1]. If the magnitude of the vertical field were so adjusted that $h(r) = 0$ in the region of maximum density gradient, and small at other radii, the trapped particle instability should be very much weakened.

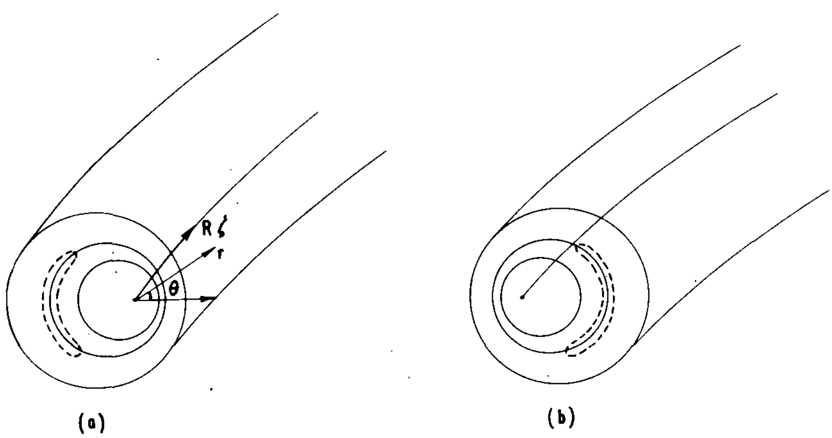

FIG. 1. Toroidal coordinates with (r, θ)-origin on the minor axis. The broken lines show the (r, θ)-projections of the trapped particle orbits when (a) $b_0 > \frac{rb_1}{B_2} B_0'$, (b) $b_0 < \frac{rb_1}{B_2} B_0'$, where $b_0 B_0 = B_2 b_2 + B_3 b_3$ and $B_0 = (B_2^2 + B_3^2)^{1/2}$.

The trapped particles have $v_\parallel \lesssim V\sqrt{\epsilon}$. This conclusion is not modified by the presence of the electric field drifts, as it is in Tokamaks [2].

The quantity $\xi = \zeta - q\theta$, where $q = (r/R)(B_3/B_2)$ measures the particle drift off the field line. From Eq. (2.4) we get

$$\frac{d\xi}{dt} = -\frac{V^2 + v_\parallel^2}{2\Omega R}\frac{B_0'}{B_2} - \frac{1}{\Omega R}\frac{B_0}{B_2}\frac{e\Phi'}{m} - \frac{V^2 + v_\parallel^2}{2\Omega R}\left(\frac{(rb_0)'}{rB_0} q\cos\theta + \frac{b_0}{B_0} q'\,\theta\sin\theta\right) \quad (2.8)$$

In Tokamaks, where $(B_2/B_3) = O(\epsilon)$, $rB_0'/B_0 = O(\epsilon)$ and $q = O(1)$, the first term is negligible and the drift depends on θ. The direction of the ξ-drift can be altered, for some particles at least, by altering q'/q. Hence, shear has an important influence on the trapped particle instability. But for

[1] This was pointed out to the authors by P.H. Rebut.

general fields of type (2.1), where $q = O(\epsilon)$ the first term in Eq.(2.8) is the dominant one, and the ξ drift has the same sign (that of $-(1/\Omega)\,(B'/B)$ for all θ. Shear has no significant effect on the trapped-particle instability.

The oscillation time τ of the trapped particles is important in the analysis of collective effects (section 3). From Eq.(2.7) we obtain

$$\tau = \frac{4}{V\sqrt{\epsilon}}\,\frac{rB_0}{B_2 h}\int_{\theta_0(x)}^{\pi}\frac{d\theta}{\sqrt{2x^2 - 1 - \cos\theta}}$$

$$= \frac{4}{V\sqrt{\epsilon}}\,\frac{rB_0}{B_2 h}\,\sqrt{2}\,K(x) \tag{2.9}$$

where $K(x)$ is the complete elliptic integral of the first kind. The expression (2.9) is valid for $0 < x < 1$, that is for the trapped particles. When $x > 1$, $\tau(1/x)$ is the time taken for two circuits of the minor axis by the untrapped particles. From the r-equation in Eqs (2.4) the maximum radial displacement from a magnetic surface has the very small value $\Delta r \approx \sqrt{\epsilon}\; V/\Omega$. In Tokamak fields $\tau \approx \epsilon^{-3/2}\; r/V$ and $\Delta r \approx \epsilon^{-1/2}\; V/\Omega$. These larger values account for the enhanced diffusion coefficients predicted for Tokamak systems by Galeev and Sagdeev [4]. No such effect could occur in pinch systems.

We conclude this section by noting that the Tokamak analysis of Kadomtsev and Pogutse [1] can be used intact for stellarators of the type discussed by Gibson and Taylor [3], where the helical field components have small magnitudes characterized by $\epsilon_h \sim \epsilon$, in the form $(\epsilon_h b_r,\ \epsilon_h b_\theta,\ \epsilon\epsilon_h b_\xi)$. The small value of the helical ξ-component leads to the Tokamak forms of Eqs. (2.7) and (2.8). Physically, the helically trapped particles (or 'localized particles' [3], or bananas [5]) have very small $V_\parallel \approx V\epsilon_h$ and are negligible. The toroidally trapped particles ('blocked particles' [3]) have $v_\parallel \approx V\sqrt{\epsilon_h}$ and behave as in Tokamaks, being only weakly affected by the helical field. Since an $\ell = 3$ helical winding gives $q'/q = -2$, it invariably satisfies the criterion for shear stabilization deduced by Kadomtsev and Pogutse [1].

3. COLLECTIVE BEHAVIOUR

As in the Tokamak analysis [1], the equilibrium distribution function $f_j^{(0)}(\vec{v}, \vec{r})$ is nearly Maxwellian. To first order in Ω^{-1},

$$f_j^{(0)} = f_{0j} + \frac{1}{\Omega_j}(\vec{B}\times\vec{V})\cdot\left(\nabla f_{0j} + \frac{e_j}{kT_j} f_{0j}\nabla\Phi\right) \tag{3.1}$$

where $f_{0j} = n_0(r)(m_j/2\pi kT_j)^{3/2}\exp(-m_j V^2/2kT_j)$, and $\Phi(r)$ is the equilibrium electrostatic potential.

The solution of the linearized Vlasov equation may be written in the form

$$f_j^{(1)} = \frac{e_j}{m_j}\int_{-\infty}^{t}\nabla\phi^{(1)}\,\frac{\partial f_j^{(0)'}}{\partial\vec{V}}\,dt' \tag{3.2}$$

where integration is over the guiding centre paths in the unperturbed fields. Because the system is independent of ζ and periodic in θ, $\phi^{(1)}$ may be written

$$\phi^{(1)} = \phi(r,\theta)\ \exp[-i(\omega t+\ell\zeta)] \tag{3.3}$$

where ϕ is periodic in θ, and ℓ is an integer.

Integrating the solutions $f_j^{(1)}$ over velocity space yields the perturbed density of electrons and ions. Using the quasi-neutrality condition, valid for low frequency distrubances, we have

$$\left(\frac{1}{T_e}+\frac{1}{T_i}\right)n_0\phi = -i\sum_j \frac{1}{T_j}\int d\vec{v}\ f_{0j}\int_{-\infty}^{0} dt'\left[\left(\left(\omega-\omega_{*j}-\omega_E\frac{B_2^2}{B_0^2}\right)\phi(\theta')\right.\right.$$
$$\left.+\frac{i}{\ell}\left(\omega_{*j}+\omega_E B_2^2/B_0^2\right)\frac{R}{r}\frac{B_3}{B_2}\frac{\partial\phi}{\partial\theta}\right]\exp[-i(\omega t'+\ell\zeta')) \tag{3.4}$$

where $\zeta' = \zeta(t')$ is the single-particle path, the T_j are the ion and electron temperatures, and

$$\omega_{*j} = \frac{\ell}{R}\frac{kT_j}{m_j}\frac{1}{\Omega_j}\frac{f_{0j}'}{f_{0j}}\frac{B_2}{B_0};\quad \omega_E = \frac{\ell}{R}\frac{\phi'}{B_2}$$

The function $\phi(r,\theta)$ is now written as a Fourier series

$$\phi(r,\theta) = \sum_{m=-\infty}^{\infty}\phi_m(r)\,e^{im\theta} \tag{3.5}$$

Equation (3.4) may be averaged over the fast oscillation time τ of the trapped or untrapped particles, provided $\omega \ll \tau^{-1}$. This is achieved to first approximation by replacing the rapidly oscillating part of the integrand by its average over a single period. The integration $\int_{-\infty}^{0} dt'$ can then be carried out, since the average drift velocities remaining in the exponential are constant. It follows that

$$\left(\frac{1}{T_e}+\frac{1}{T_i}\right)n_0\sum_{m=-\infty}^{\infty}\phi_m e^{im\theta} = e^{i\ell q\rho}\sum_j\frac{1}{T_j}\int_T d\vec{v}\ f_{0j}$$

$$\times\sum_{m=-\infty}^{\infty}\phi_m(r)\ \frac{\omega-\left(\omega_{*j}+\omega_E\dfrac{B_2^2}{B_0^2}\right)\left(\dfrac{m}{\ell q}\dfrac{B_3^2}{B_2^2}+1\right)}{\omega-\omega_E-\omega_{Dj}}\ \frac{1}{\tau_j}\int_{-\tau_j}^{0} dt'\,e^{-i(m-\ell q)\theta'} \tag{3.6}$$

where

$$\omega_{Dj} = \frac{\ell}{R}\,\frac{V^2}{2\Omega_j}\,\frac{B_0'}{B_2} \tag{3.7}$$

and $\int_T d\vec{v}$ is now over the trapped particles only. The contribution of the untrapped particles to the integral is negligible, because for them the denominator is $\omega - \omega_E - \omega_{Dj} - (m - \ell q)\,(B_2/rB_0)v_{\|}$ which is larger than the numerator provided $|m - \ell q| > \omega_{*j}\,\tau/v_{\|}$.

Equation (3.6) is simplified by putting $T_e = T_i$ and writing the operators

$$\int_{-\tau}^{0} \frac{dt'}{\tau} = \int_{\theta_0(x)}^{2\pi - \theta_0(x)} \frac{d\theta'}{2\sqrt{2}\,K(x)\,\sqrt{2x^2 - 1 - \cos\theta'}}$$

and

$$\int d\vec{v} = 2\pi \int_0^\infty v_\perp\, dv_\perp \int_{\sim -\sqrt{\epsilon}V}^{\sim +\sqrt{\epsilon}V} dv_{\|}$$

$$= 2\pi h\sqrt{\epsilon} \int_0^\infty V^2\, dV \int_{x_0(\theta)}^{1} \frac{dx^2}{\sqrt{2x^2 - 1 - \cos\theta}}$$

where $x_0^2 = (1/2)(1 + \cos\theta)$; $\cos\theta_0 = 2x^2 - 1$. Then from Eq. (3.6), inverting the Fourier transform, and changing the order of the $d\theta$ and dx integrals

$$\phi_m(r) = \pi\sqrt{2\epsilon}\; h \int_0^\infty V^2\, dV \frac{f_0}{n_0}$$

$$\times \sum_{m'=-\infty}^{\infty} \frac{\bar{\omega}\left[\omega - \omega_E \dfrac{B_2^2}{B_0^2}\left(1 + \dfrac{m'}{\ell q}\,\dfrac{B_3^2}{B_2^2}\right)\right] - \omega_* \,\omega_D\left(1 + \dfrac{m'}{\ell q}\,\dfrac{B_3^2}{B_2^2}\right)}{\bar{\omega}^2 - \omega_D^2}$$

$$\times\, \phi_{m'} \int_0^1 \frac{dx^2\, C_{m-\ell q}\, C_{m'-\ell q}}{K(x)} \tag{3.8}$$

where $\bar{\omega} = \omega - \omega_E$, and

$$C_n = \int_{\theta_0(x)}^{2\pi-\theta_0(x)} \frac{\cos n\theta d\theta}{\sqrt{2x^2 - 1 - \cos\theta}}$$

It is pointed out in Ref. 2 that $C_n(x) = \pi/\sqrt{2}\, P_{n-\frac{1}{2}}(1 - 2x^2)$ where P is the Legendre function. The quantities in (3.8) now refer to the ions. For flute modes, with slowly varying phase along the filed lines, we choose $m \approx \ell q$. Since C_n decreases rapidly as n increases, a pure flute mode with a single fixed m number is approximately described by

$$1 = -\pi\sqrt{2\epsilon}\, h \int_0^\infty V^2 dV \frac{f_0}{n_0} \frac{B_0^2}{B_2^2} \frac{\omega_*}{\omega_D} \cdot \frac{\omega_D^2}{\bar{\omega}^2 - \omega_D^2} \int_0^1 \frac{dx^2\, C_0^2(x)}{K(x)} \tag{3.9}$$

where

$$\frac{B_0^2}{B_2^2} \frac{\omega_*}{\omega_D} = \frac{2kT}{MV^2} \frac{f_0'/f_0}{B_0'/B_0}$$

Replacing the velocity-dependent terms in Eq.(3.9) by their average, we have

$$\left(\frac{\bar{\omega}}{\omega_D}\right)^2 = 1 - \lambda\sqrt{\epsilon}\, \frac{n_0'/n_0}{B_0'/B_0} \tag{3.10}$$

where the positive number λ is given by

$$\lambda = \sqrt{2}\,\pi\, h \int_0^1 \frac{dx^2\, C_0^2(x)}{K(x)}$$

It may be seen from Eq.(3.10) that the trapped-particle instability occurs only if the density gradient is much steeper than the gradient in magnetic field strength, i.e. $\epsilon^{\frac{1}{2}}\, n_0'/n_0 \gtrsim B_0'/B_0$.

An equilibrium electric field produces a Doppler shift in the frequency, but does not affect the stability criterion. In the Tokamak ordering scheme an important effect of the electric field is the displacement of the centre of the band of trapped velocities from $v_\parallel = 0$ to $v_\parallel = (\Phi'/B_0)(B_\zeta/B_\theta) = 0(\Phi'/\epsilon B_0)$. Hence a modest electric field may displace the trapping band to the tail of the ion distribution [2]. The condition that the displacement of the band of trapped $v_\parallel$ shall be negligible is

$$\frac{\langle v_\parallel \rangle}{v_{th,i}} = \left(\rho_{Li} \frac{\Phi'}{\Phi}\right)\left(\frac{e\Phi}{kT_i}\right)\left(\frac{B_\zeta}{B_\theta}\right) << 1$$

where ρ_{Li} is the ion Larmor radius. Since the first factor is much less than unity, this condition is satisfied if $B_\theta = O(B_\zeta)$ and $e\Phi \lesssim kT_i$. The instability will not occur if B'/B and n'/n have opposite sign, i.e. if particles are trapped in a magnetic well region such as can be produced in a levitron with a vertical magnetic field.

The physical origin of the stabilization may be explained as follows. Consider a sinusoidal density perturbation, initially neutron. If $(B'/B)/(n'/n) > 0$, the resulting radial $\vec{E} \times \vec{B}$ convection increases the density perturbation. However, when the charge separation distance exceeds a half wavelength of the sinusoidal perturbation, the ions and electrons begin to come in phase again and neutralize each other. If the time taken to drift one half wavelength is less than the initial e-folding time, the perturbations will not grow significantly. The condition for this is $\gamma < \omega_D$. This can occur in the large-B_θ case, but not in Tokamaks, as can be seen from Eq.(3.10). The growth rate of the instability, if it occurs, is of order $\gamma \sim \epsilon^{1/4}(\omega_* \omega_D)^{1/2}$. In a Tokamak, $\omega_D \approx \epsilon\, \omega_*$ so $\gamma \approx \epsilon^{3/4}\omega_* > \omega_D$. In the large-$B_\theta$ case, if $B'/B > \epsilon^{1/2} n'/n$ i.e. $\omega_D > \epsilon^{1/2}\omega_*$, the natural growth rate is less than ω_D and so the above stabilization effect occurs.

4. THE EFFECT OF COLLISIONS

The effective collision frequency for the scattering of particles out of the narrow cone in velocity space corresponding to trapping, whose angular width is $O(\epsilon^{1/2})$, is ν_j/ϵ where ν_j is the frequency for large-angle scattering. Inclusion of a collision term $(\partial f/\partial t)_{coll} = -(\nu_j/\epsilon) f^{(1)}$ on the right-hand side of the linearized Vlasov equation (3.2) causes ω to be replaced by $\omega + i\nu_j/\epsilon$ in the dispersion relation (3.6). Including only the electron collisions, Eq.(3.6) may be written in order of magnitude as

$$O(1) \approx -\frac{\sqrt{\epsilon}\,\omega_*}{\omega - \omega_D} + \frac{\sqrt{\epsilon}\,\omega_*}{\omega + \frac{i\nu_e}{\epsilon} + \omega_D} \qquad (4.1)$$

i.e.

$$\omega^2 + \frac{i\nu_e}{\epsilon}\omega + \left\{ \frac{i\nu_e}{\epsilon}(\omega_D + \sqrt{\epsilon}\,\omega_D) + (\sqrt{\epsilon}\,\omega_*\omega_D - \omega_D^2) \right\} \approx 0 \qquad (4.2)$$

The nature of the solutions of this quadratic equation for ω depends on the order of magnitude of its coefficients, without reference to numerical factors, which have been omitted. When $\nu_e/\epsilon \ll \omega_D \approx \epsilon^{1/2}\omega_*$ the collisionless analysis holds. When $\nu_e \approx \epsilon\omega_D$, which is the growth rate of the collisionless instability, the value of ω is modified, but its order of magnitude remains unchanged. When $\nu_e \gg \epsilon\omega_D$ the last term in Eq.(4.2) is negligible, and no instability occurs.

In Tokamak systems [2] the collisionless analysis holds for $\nu_e \ll \epsilon^{3/2}\omega_*$, enhanced instability occurs when $\nu_e \approx \epsilon^{3/2}\omega_*$, and complete stability for $\nu_e \gg \epsilon^{3/2}\omega_*$.

The conclusion is that the collisionless trapped-particle instability of section 3 is stabilized by collision rates $\nu_e >> \epsilon\omega_D$, while collision rates $\nu_e \lessapprox \epsilon\omega_D$ are unimportant.

5. CONCLUSIONS

Asymptotic analysis for small $\epsilon = a/R$ leads to the conclusion that configurations with $B_\theta = O(B_\zeta)$ are less prone to the trapped-particle instability, because it occurs only in regions of large density gradients where $\epsilon^{1/2} n_0'/n_0 \gtrsim B_0'/B_0$ and is not enhanced by collisions. When ϵ is very small, this is a stringent condition. Thus large aspect ratio tori should be stable. However, if the asymptotic analysis is applied to practical systems, where a/R is frequently not very small, the above condition for the occurrence of the trapped-particle instability can be satisfied. When it does occur, the instability growth rate is $\epsilon^{1/2}\omega_*$, which is rather faster than the Tokamak growth rate of $\epsilon^{3/4}\omega_*$. Electric fields such that $e\Phi \lesssim kT$ do not affect the stability condition.

REFERENCES

[1] KADOMTSEV, B.B., POGUTSE, O.P., Zh. eksp. teor. Fiz. 51 (1966) 1734; Soviet Phys. JETP 24 (1967) 1172.

[2] GALEEV, A.A., SAGDEEV, R.Z., WONG, H.V., Physics Fluids 10 (1967) 1535.

[3] GIBSON, A., TAYLOR, J.B., Physics Fluids 10 (1967) 2653.

[4] GALEEV, A.A., SAGDEEV, R.Z., Zh. eksp. teor. Fiz. 53 (1967) 348, Soviet Phys. JETP 26 (1968) 233.

[5] GALEEV, A.A., SAGDEEV, R.Z., FYURS, G.P., Novosibirsk Report CTO/489 (Nov. 1967).

DISCUSSION

B. COPPI: What is your explanation for the fact that, with the collisional trapped-particle instability, there is no peak in the growth rate when the pinch ordering is considered?

T.E. STRINGER: The growth rate of the collisional trapped-particle instability attains its maximum value when collisions first become important, and then falls off with increasing frequency as ν_e^{-1}. The order of magnitude of the maximum growth rate is $\epsilon^{\frac{1}{2}}$ d (lnn)/d(lnB) times the growth rate of the collisionless instability. For a Tokamak this factor is $O(\epsilon^{-\frac{1}{2}})$, so that the maximum growth rate of the collisional mode always exceeds that of the collisionless mode. For the pinch ordering this is generally not the case. The collisional mode starts with a growth rate comparable with the collisionless mode, and its growth rate decreases with increasing collision frequency.

A.B. MIKHAILOVSKY: How does Tokamak differ from a pinch discharge?

T.E. STRINGER: The most important difference between Tokamak and pinch-like fields lies in the ratio between the magnetic drift and the diamagnetic drift velocities. In Tokamak this ratio is always of order ϵ, and consequently in our Eq. (3.10) the second term would be of order $\epsilon^{-\frac{1}{2}}$.

Hence, ω is always imaginary. In a pinch-like geometry this ratio is not determined by the aspect ratio, but depends on the details of the radial field distributions.

A.B. MIKHAILOVSKY: Is there no MHD instability in pinch discharges?

T.E. STRINGER: The growth rate of the trapped-particle instability is much less than that for MHD instabilities, and we have tacitly assumed that the configurations studied are MHD-stable and that the collision frequency is too low for resistive instabilities. The existence of stable MHD pinch configurations has been demonstrated by Kadomtsev and by Whiteman, and levitron configurations should certainly be MHD-stable.

P.L. HUBERT: I should like to mention the Stator II device constructed at our laboratory by Mr. Rebut. It is a kind of levitron in which there is a slight outward displacement of the central ring, so that one can achieve uniformity of the field along a line of force to within a few per cent. Do you think that this degree of precision is enough to avoid trapped-particle instabilities?

T.E. STRINGER: The variation of magnetic field strength around the magnetic surfaces is proportional to $[1+\epsilon h^2(r) \cos\theta]$. Thus, if the parameters are adjusted in such a way that the field strength is nearly constant over the magnetic surfaces, h(r) is much less than unity, and from Eq.(3.10) the plasma is stable up to much higher density gradients; i.e. $(n'/n) < (B'/B)\epsilon^{-\frac{1}{2}} h^{-1}$. A uniformity in field strength over surfaces to within a few per cent should permit relative density gradients that are an order of magnitude more rapid than the gradient in field strength.

A.A. RUKHADZE: What assumption did you make regarding the potential difference across the plasma radius?

T.E. STRINGER: We assumed that it was less than, or comparable with, the plasma temperature; i.e. $e\Phi(0) \lesssim kT$.

A.A. RUKHADZE: Which collisions lead to stabilization of the instability considered by you – electron or ion?

T.E. STRINGER: The collisions which reduced the growth rate were the electron collisions, which first affected the solution when $\nu_e \sim \epsilon\omega$. At higher collision rates the ion collisions also became important, completely stabilizing this mode.

TOROIDAL CONFINEMENT II
(MULTIPOLES, etc.)

(Session C)

Chairman: C. BRAAMS

PLASMA CONFINEMENT IN A TOROIDAL OCTUPOLE MAGNETIC FIELD

H. FORSEN, D. KERST, D. LENCIONI, D. MEADE, F. MILLS,
A. MOLVIK, J. SCHMIDT, J. SPROTT AND K. SYMON
UNIVERSITY OF WISCONSIN, MADISON, WIS.,
UNITED STATES OF AMERICA

Abstract

PLASMA CONFINEMENT IN A TOROIDAL OCTUPOLE MAGNETIC FIELD. The confinement of low-density ($n = 10^9\ cm^{-3}$) collisionless plasmas with $T_i \simeq 40$ eV, $T_e \doteq 10$ eV produced by gun injection or with $T_e \simeq 1$ eV, $T_i < 1$ eV produced by microwave heating was studied to determine the mechanisms for plasma loss from an inductively excited, mechanically supported toroidal octupole. The decay time for the hot ion plasma was $\simeq 700\,\mu s$ while the lifetime for the cold ion plasma was about 3 times longer. Particle collector measurements indicated that most of the particles were lost on the hoops and their supports for both types of plasma. Direct measurements of the radial particle loss to the outside wall using a large azimuthally symmetric screened collector outside the MHD stable region indicated that roughly 15% of the hot ion plasma and $\leqslant$ 2% of the cold ion plasma was lost radially during the quiescent confinement period. The amplitude of the fluctuations (1 kHz to 1 MHz) in the MHD stable region implied a turbulent diffusion coefficient; the order of 10^{-3} of the Bohm diffusion coefficient which was not large enough to produce the observed radial loss. Studies were also made to determine the importance of low-frequency fluctuations or convective cells which may have been produced by injection, magnetic field perturbations or azimuthal density variations. The addition of a toroidal magnetic field decreased the lifetime slightly and generated large-scale convective cells in the shearless layer near the plasma surface. Currents parallel to the magnetic field have been observed which must be considered in determining the cause of increased fluctuation with the increase of the toroidal field. The mechanical supports were also guarded with magnetic dipoles in the manner proposed by Lehnert. The plasma flux to one of the supports was reduced for the hot ion plasma by an order of magnitude when there was one ion gyroradius between the mechanical support and the guard field separatrix. However, the plasma flux along the guard field separatrix increased to the value of the original support flux and there was a negligible ($\leqslant$ 20%) improvement of the lifetime. An inductively excited, magnetically force-free octupole is being assembled with transiently withdrawn supports to eliminate the plasma loss to hoop supports. The device will provide at least 10 msec of experimental time during which only 5% of the magnetic flux diffuses into the internal hoops. 100 eV protons will have 15 gyroradii on each side of the separatrix.

Introduction

Toroidal multipoles have been studied extensively starting with the low β analysis of equilibrium and flute stability by Kadomtsev [1] and the high β ballooning stability of Ohkawa and Kerst [2]. Previous experimental results [3,4,5] have dealt with the overall properties of gun injected plasmas in mechanically supported toroidal octupoles such as injection and filling by $\vec{E} \times \vec{B}$ motion and quiescent confinement as the ions were lost at a rate proportional to their velocity. The overall confinement properties in these experiments were consistent with the loss of plasma due to the thermal flow of plasma into the supports. In the experiments described here, plasma losses to the supports, hoops and vacuum vessel walls were determined from the measurements of currents to particle collectors in an attempt to determine the intrinsic confinement properties of an octupole without

* Work supported by the US Atomic Energy Commission.

supports. The observations indicate that the losses were not mainly on the supports but rather on the current-carrying hoops. Observations indicate that low frequency (≈ 100 Hz) phenomena are responsible since high frequency (10 kHz to 1 MHz) fluctuations were not consistent with the observations. The effect of obstacles similar to supports, static and magnetically-guarded, insulated and conducting, were studied for subtle effects on confinement.

APPARATUS

The magnetic field was a pulsed half sine wave of 5 msec duration which was produced by inductively coupling a 6 kJ capacitor bank to the four internal hoops. The total current induced in the copper hoops was 3 x 10^5 A. The primary winding was placed as close as physically possible to the insulated gap and was distributed to match the required current density in the wall of the vacuum vessel thereby avoiding large field perturbations [6].

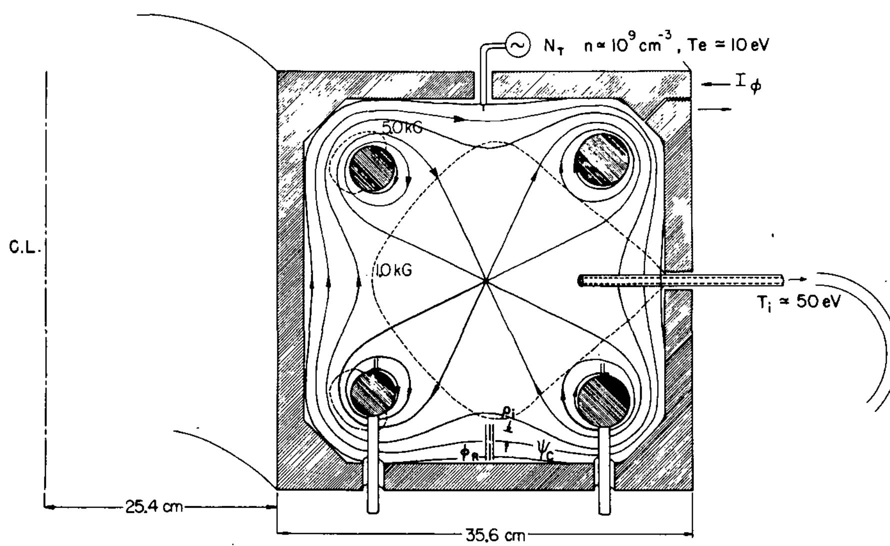

FIG. 1. General toroidal octupole apparatus showing field lines, |B| contours, positions of the hoop supports, particle collectors on the hoops and wall and other diagnostic equipment.

Each of the four hoops was held in place by three beryllium copper supports as shown in Fig. 1. Each hoop support was constructed from a 1 cm diameter beryllium copper rod with a 4 mm wide slot cut along the length of the rod to form a current loop for magnetic guarding. Each support could be energized to 2 x 10^4 A by a separate pulse transformer which was driven either by the current in the primary of the main octupole transformer or by a 1 msec long square pulse from a separate delay line which permitted varying the guard field strength relative to the octupole field and allowed the guard field to be applied after the plasma had been injected. This insured that the guard field did not affect the injection and filling processes.

The pulsed magnetic field diffused into the copper hoops and the aluminum vacuum vessel due to their finite electrical conductivity. The location of the field lines near the metal surfaces at the peak of the magnetic field was determined with an electron beam. Field line positions were calculated for a superconducting wall one skin depth (0.7 cm) behind the physical wall to simulate magnetic field diffusion. Calculated positions agreed closely with the electron beam measurements and are shown in Fig. 1. The magnetic field will be specified in terms of $N_{\rho i}$, the minimum number of 40 eV proton gyroradii between ψ_s (separatrix) and ψ_c (the $\oint d\ell/B$ stability limit). For the gun injection plasma the parameters were $n_e \approx 10^9$ cm^{-3}, $T_i \approx 40$ eV, $T_e \approx 5$ eV and $N_{\rho i} \leq 5.0$. Cold ion plasmas ($T_i < 1$ eV, $T_e \approx 2$ eV, $n \lessapprox 10^9$ cm^{-3}) were produced in a background gas of hydrogen at 10^{-4} torr by a 140 μsec long 5 kW pulse of 3.2 GHz microwaves when electron cyclotron resonance occurred in the magnetic field. Typical resonance zones are shown in Fig. 1.

DIAGNOSTICS

The density was inferred from the ion saturation current to a single Langmuir probe. Electric fields and floating potentials in these low density plasmas could be measured only with balanced resistive [7] or capacitive [8] attenuator probes which had an input resistance of 2 MΩ and an input capacitance of 0.5 pF. Energetic ions were extracted from the center of the toroidal octupole through a high permeability tube and then analyzed with an electrostatic energy analyzer. Also, with a miniature analyzer mounted in the tip of the extracting tube, the ion distribution function was found [9] to be given by $f \approx \exp -[(mv^2/kT_i) + \alpha P_\theta]$. This implies an isotropic velocity distribution. Calculations indicated that nonadiabatic effects can produce a large scattering in velocity space [10].

The total number of electrons in the confinement region was determined by using a microwave cavity perturbation technique. Microwaves at a frequency of 24 GHz were used to excite the entire aluminum vacuum chamber in a high order mode. When $\omega^2 \gg \omega_p^2$ and the spatial variation of microwave electric field is much shorter than the density variation, we have $\delta f/f = (\int n\, d\vec{x})/n_c \int d\vec{x} = N_T/n_c V_T$ where $4\pi n_c e^2/m = \omega^2$ and N_T is the total number of electrons in the cavity of volume V_T.

Particle collectors of various types were used to estimate the magnitude of the plasma losses from the toroidal octupole. Several systematic checks were made to determine the extent to which particle collectors were disturbing the plasma. An individual hoop and its three supports were electrically connected but could be biased with respect to the other hoop assemblies and the vacuum chamber wall. Method #1 of estimating the total flux to the hoops and supports was to operate the internal hoop assemblies as a large floating double probe with adjacent hoops oppositely biased. The total number of particles collected on the hoops and supports, 4×10^{14}, agreed with the 3×10^{14} particles inferred from microwave diagnostics. Since the other losses from the device were found to be small, this indicated that the hoop and support current measurement was not grossly in error. However, I-V characteristics for the hoops did not saturate at $V = 2kT_e/e$ indicating that hoop voltages were capable of pulling plasma out of the confinement region. This was verified by pulsing on an 80 volt bias on the hoops with respect to the vacuum chamber walls at t = 2.5 msec for a magnetic field of $N_{\rho i} = 2.5$ which caused a more rapid decay of the plasma. There was no noticeable increase in decay rate for a 40 volt bias at $N_{\rho i} = 5.0$. Due to the lack of saturation, the actual loss was estimated by extrapolating, the I-V characteristic to zero voltage as shown in Fig. 2. Because of this difficulty the collector measurements may be in error by as much as a factor of 2.

Method #2 for determining hoop loss was to insulate the hoop supports from the plasma with mylar insulators and to operate the hoops as floating double probes. Method #3 used azimuthally symmetric particle collectors operated as floating double probes which were constructed from printed circuit board with 0.02 mm thick copper sheet which did not disturb the 100 Hz magnetic field. These collectors, which were mounted as shown in Fig. 1, had the advantage that they could collect ions and electrons from the same magnetic field line. The collector for the inner hoop extended $2.3\rho_i$ out from the last field line touching the inner hoop leaving $3.9\ \rho_i$ between the density peak and the collector tip. The outer hoop collector extended $1.5\rho_i$ out from the last field line touching the hoop leaving $2.1\rho_i$ between the density peak and the collector tip. Method #4 used a double probe which consisted of two strips of 0.02 mm brass foil with a width of 5 cm along the hoop mounted tightly on the hoop surfaces. All of these techniques gave qualitatively the same results but quantitative measurements of better than a factor of 2 were difficult due to the lack of voltage saturation. The H_β light was unaffected as the bias voltage was applied to the hoops indicating that ionization due to hoop bias was absent. Two copper cylinders which had the same size as real hoop supports were placed at the same azimuthal position, one above an inner hoop and one above the outer hoop in a position similar to that of a real support. In method # 5, these cylinders were biased as a floating double probe to estimate the losses to a real support.

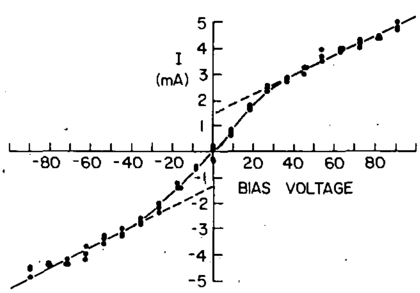

FIG. 2. The current-voltage characteristic for the inner hoops with supports insulated, operated as a floating double probe as in method 2. The characteristic was taken at t = 2.5 ms for the gun-injected plasma.

Method #6 was used to estimate the plasma flux to the outer vacuum wall from the current drawn to a collector placed near the vacuum wall(Fig. 1). This azimuthally symmetric collector had an outer screen electrode with ~40% optical transparency and could be operated as a floating double probe. The central conductor, constructed from a printed circuit board with 0.02 mm copper plating, was divided into independent inner and outer collectors. Each of the collectors was in turn subdivided into 36 equal sections to test for azimuthal variation of radial particle loss. Small circular plate collectors placed on the vacuum wall were used to detect localized loss and to detect wall loss before and after the radial collector was installed. Ion saturation was observed in the I-V characteristic of the screened collector for bias voltages greater than 20 volts. The bias voltage on this detector placed near the wall was observed to have a negligible effect on the plasma. The collector extended into the plasma so that its tip was $3\rho_i$ from the conducting wall, $2\rho_i$ from the last field line in the wall and $1\rho_i$ inside ψ_c. The particle loss to the upper ring (nearest the plasma) of the collector was roughly 14 times larger than the particle loss to the lower ring indicating that the wall loss collector was acting as a limiter. Some particles were still observed to hit the wall with the wall loss collector in place so the wall loss collector current was taken only as a lower limit of particle flux being lost on the walls. Similar collectors have been used previously to measure plasma losses in other plasma devices [11].

Results

General Plasma Properties

The overall time behavior of the plasma parameters at the center of the confinement region is given in Fig. 3. The lifetime of an ion has been found to be proportional to the reciprocal of the ion velocity [3]. The density decay time at peak magnetic field for the gun injected plasma was roughly 1 msec as compared to ≈ 3 msec for the microwave produced plasma.

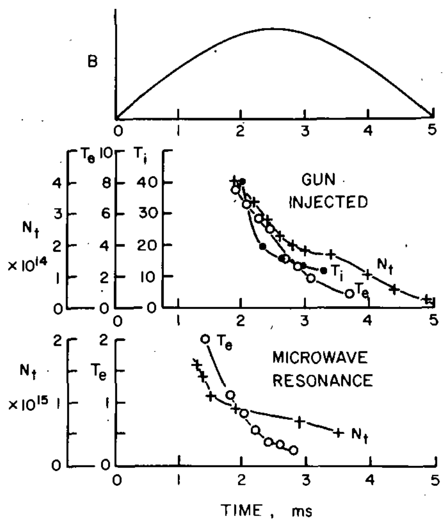

FIG. 3. Time decay of the plasma parameters at the centre of the toroidal octupole.

The density profile (Fig. 4) as determined from an ion saturation current profile assuming a constant temperature has shown that the density was constant along a field line to within an experimental accuracy of 20%. The experimental uncertainty arises since the effect of the magnetic field on the probe collection efficiency is not known. The azimuthal variation of the plasma was studied by placing five single probes collecting ion saturation current at azimuthal angles, θ = 50°, 100°, 180°, 243°, 310°. The probes were individually calibrated by placing them 10 cm from a standard probe in the plasma. The rms deviation of the five probe currents from the mean divided by the mean measured in the zero field region at 500 μsec after plasma production was 0.03 for the gun injected plasma and 0.21 for the microwave produced plasma.

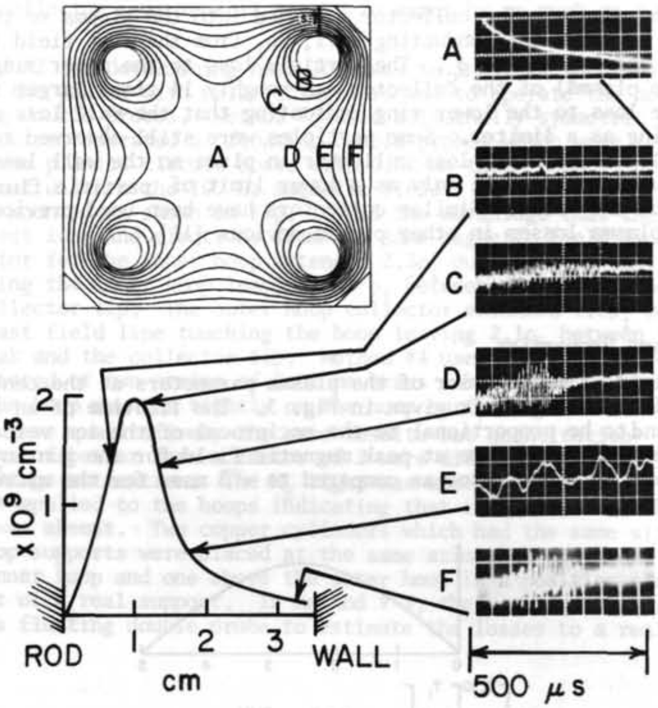

FIG. 4. Typical density fluctuations are exhibited for various positions on the density profile. These positions are also labelled on the flux plot. The density profile is for the gun-injected plasma at t = 2.2 ms taken along a line marked S between the rod and wall. A typical ion saturation current trace is shown at A. The remaining traces are filtered to remove the quiescent density signal. Trace A has an amplitude of 2×10^9 cm^{-3} div^{-1}. All remaining traces have an amplitude of 2×10^8 cm^{-3} div^{-1}. ψ_C is at 2.8 cm.

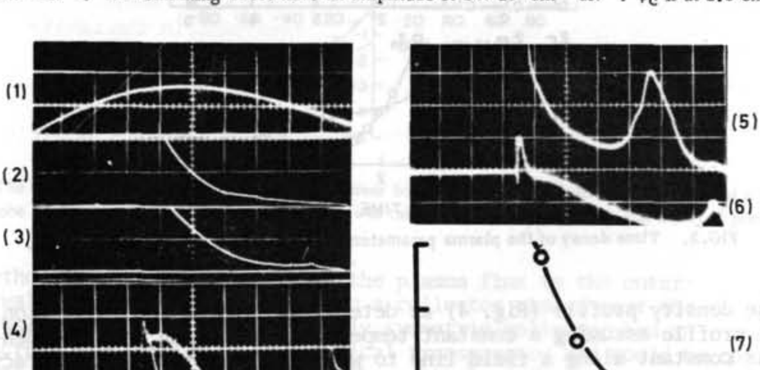

FIG. 5. Currents to plasma collectors biased to 45 V for the gun-injected plasma: 1) magnetic field; 2) total support current, 6 mA/div; 3) outer hoop current method 3, 10 mA/div; 4) inner hoop current, method 2, 4 mA/div; 5) wall collector current method 6, 2 mA/div; 6) all hoops plus supports method 1, 20 mA/div; 7) total number of electrons, microwave diagnostics, 10^{14} particles/div.

Plasma Loss Measurements

The currents to various particle collectors are shown in Fig. 5 for a gun injected plasma with $N_{\rho i} = 5.0$. The injection and filling period lasts from 1.7 to 2.0 msec, the confinement period from 2.0 msec to 3.0 msec and plasma ejection due to the magnetic field decay starts at 3.0 msec. The total number of ions collected on the wall loss collector was roughly 10% of the total collected on the hangers, hoops and the wall loss collector during the confinement period. A very pessimistic upper limit for the wall loss can be obtained from the ejection of plasma at the end of the magnetic field pulse. The lifetime of the plasma due to the wall loss at $t_1 = 3.5$ msec is given by

$$\tau_W = [\int_{t_1}^{\infty} \alpha_H(I_H)\ dt + \int_{t_1}^{\infty} \alpha_W(I_W)\ dt]/\alpha_W I_W$$

where α_H, α_W are the hoop and wall collection efficiencies, I_H and I_W are the ion currents to the hoops and wall collectors respectively. Now assuming that α_W was independent of time, we find

$$\tau_W > [\int_{t_1}^{\infty} I_W\ dt]/I_W = 3.0 \text{ msec.}$$

This still represents an upper limit if more particles hit the wall at late times due to large gyroradius. The lifetime of the plasma at this point was roughly 1 msec. Therefore, the wall loss was less than 30% of the total loss.

The loss of particles as detected by the particle collector on the hoops decayed smoothly in time (Fig. 5). If the hoop loss were due entirely to field diffusion, the loss should stop abruptly at t = 3.75 msec when the electric field at the surface of the hoop reverses. The integrated flux from t = 2.2 msec to 4.0 msec to the inner collector was 3×10^{13} which corresponds to ≈10% of the total number of particles in the machine at t = 2.2 msec. The integrated flux over the same period of time for the outer hoop collector corresponds to ≃50% of the total number of particles. The loss rates at peak field to various regions of the machine for the gun plasma are presented in Table I. These rates are estimated from the currents drawn to the collectors with 45 V bias which did not perturb the gross properties of plasma and may be in error by a factor of two due to the lack of voltage saturation.

However the numbers are internally consistent and the sum of all the fluxes corresponds quite closely to the flux required to produce the observed density decay observed by the microwave diagnostic system. Previous estimates of the support loss assuming thermal flow of plasma into the supports predicts a total support loss of roughly 10^{17} particles/sec which is a factor of 3 larger than the observed losses to the supports [4].

The azimuthal variations of the hoop loss and the loss to the outer wall were also studied. The azimuthal variation of the wall losses (Fig. 6) for the gun plasma show a 6-peak variation. Some of these peaks can be identified with azimuthal perturbations in the device such as the three supports, the insulated gap, and the two pump ports. However, the physical causes for these azimuthal variations which persist near the edge of the plasma arenot known. Note that at t = 4.0 msec when the magnetic field was leaving the machine through the insulated gap, the wall loss of plasma increased at this position. The azimuthal symmetry of the hoop losses was investigated by dividing the hoop loss collector into six segments. Segments centered on θ = 0° and 180° each received 22% of the total hoop loss, 18% was collected on each of the segments centered at ±60° and 10% was collected on the segments centered at θ = ±120° indicating that hoop losses were greater near supports. However,no increased local losses were observed near small obstacles which were extended into the plasma.

The plasma losses are tabulated in Table I for the microwave produced plasma at the time of peak magnetic field. The rates were determined from the currents drawn to the collectors with 36 volt bias and may be in error by as much as a factor of 2 due to the lack of voltage saturation.

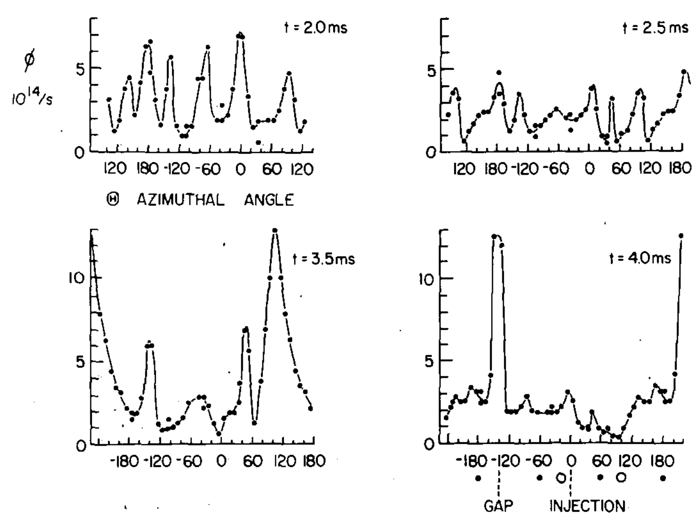

FIG. 6. Azimuthal distribution of wall losses for the gun-injected plasma. The wall loss collector had 36 segments each of 7.5 cm length. Solid circles at θ = ± 60°, 180° represent the positions of the hoop supports. Open circles at θ = - 20°, + 100° represent the positions of the pump ports.

TABLE I

Summary of Collector Measurements at Peak Field

	Method	Flux (10^{16} particles/sec) Gun Plasma	Microwave Plasma
Inner hoops	#3	5.0	-
Inner hoops	#2	4.0	6.6
Outer hoops	#3	8.8	-
Outer hoops & supports	#1	10.0	13.0
Supports	#5	3.0	3.8
Outer wall	#6	1.3	0.1
All hoops & supports	#1	20.0	-
Observed decay.	N_T/τ =	17.0	16.0

Particle Loss Mechanisms

Since the plasmas studied were collisionless and had $\beta < 10^{-6}$, the plasma could move across the magnetic field region only by means of an $\vec{E} \times \vec{B}$ drift. The electric fields which could give rise to the observed loss rates to the hoops and walls originate from at least five sources: fluctuations, field line diffusion into the walls and hoops, inductive electric fields due to the time varying magnetic fields, rotating convective cells produced during the injection phase and low frequency electric fields arising from obstacles such as hoop supports and probes or from azimuthal perturbations in the magnetic field.

The fluctuations in the octupole have been extensively analyzed and reported [4,12,13]. The flute instabilities (F of Fig. 4) outside ψ_c had little effect on particle containment since they were outside the main body of the plasma. The probe induced oscillations (C and D of Fig. 4) should have little effect on plasma containment since they only arose when a probe or baffle was inserted into the plasma. The low frequency fluctuations (E of Fig. 4) observed in the $\oint d\ell/B$ stable region at $\theta = 150°$ had $k_{\parallel} \simeq 0$, $\lambda_{\perp} \simeq 6$ cm with δn and δV essentially in phase. The amplitude of this fluctuation was largest near $\theta = 150°$ and was decreased by an order of magnitude at $\theta = -50°$. The maximum flux to the wall in a region of azimuthal width $\Delta\theta$ near $\theta = 150°$ is given by $\phi = \int \langle\delta n\delta V\rangle\, dA = 2\pi\, \Delta\theta R(\delta n\delta V/\lambda_{\perp})(\oint d\ell/B)\, \sin\alpha \simeq 1.3\text{x}10^{17}\Delta\theta\sin\alpha$ where R is the distance from the major axis to the point where $\lambda_{\perp}$ was determined and α is the phase angle between δn and δV. Experimentally $\alpha < 10°$ which gives an upper limit of $\phi \leq 2 \times 10^{16}\, \Delta\theta$ compared to a measured particle flux of $0.5 \times 10^{16}\, \Delta\theta$. Therefore, this fluctuation may have been the cause of plasma loss near $\theta = 150°$ but at other azimuths such as $\theta = -50°$ other processes are required to produce the observed loss. This fluctuation may have been caused by a lack of equilibrium produced during injection or it may be an indication of an instability such as the flute-like modes [14] produced by resonant particles.

Fluctuations near the outer hoops which had $\delta n/n \lesssim 10^{-2}$ and $\delta eV/kT_e \lesssim 10^{-2}$ were capable of producing a flux to the outer hoops of $\phi < 5 \times 10^{15}$ or roughly 5% of the observed loss.

Magnetic flux measurements show that a maximum of 23% of the total magnetic flux in the octupole had diffused into the outside hoops at the time of peak magnetic field. Measurements of electric field at the surface of the outer hoop indicate that 7% of the magnetic flux diffused into the hoop in 1 msec near peak field. This corresponds to a volume extending out from the hoop a distance of 2 mm on the density plot of Fig. 4 which contains only 0.6% of the total number of particles. An upper limit was obtained by extending this volume by one ion gyroradius (5mm) which gives an upper limit of 6% of the total number of particles that could strike both outer hoops.

The motion of plasma arising from these time varying magnetic fields has been studied, and agrees well with the expected transport of plasma. At the end of the multipole magnetic field pulse, large amounts of plasma were observed hitting the wall near the insulated gap (Fig. 6). However, since the plasma was injected near peak field when only a small amount of field line motion takes place, the electric fields arising from this motion did not cause the observed plasma loss to the outside walls or to the hoops at the time of peak field.

It has been previously reported that the gun injected plasma fills the toroidal octupole by developing large vortices with electric fields of $\approx 10^4$ V/m. These electric fields were observed to be correlated with losses to the wall during injection [15]. These electric fields were reduced to the order of a few V/m after $\approx$ 100 μsec. Observations on the azimuthal variation (Fig. 6) show greater losses to the hoops and outer wall at the injection $\theta = 0°$, and collision $\theta = 180°$ azimuthally suggesting that the initial convective cell persists for several msec.

A fifth loss mechanism is the generation of low frequency electric fields by obstacles due to the lack of equilibrium near hoop supports and probes which penetrate the plasma. These electric fields have been measured around a wide variety of artificial obstacles as well as around the hoop supports themselves. Figure 7 shows the floating potential across a model support. These potentials were strongly dependent on the coordinate ψ and essentially constant along a field line. A model has been proposed to explain the potential field structure observed. The average magnetic field gradient drifts of ions and electrons are in opposite directions which produce a charge separation due to the slight decrease in density at the support with the electric field at the support pointing in the direction of the ion drift. Measurements of the floating potentials around obstacles are in good qualitative agreement with this simple model. Since this electric field is curl free the potential structure produced by the three sets of hoop supports will be a three peaked saw tooth with sharp gradients existing at the position of the supports and small reverse gradients between the support positions.

The maximum flux to the outer hoops given by the local flux toward the hoop at the supports is roughly $\phi = nAE/B \cong 4 \times 10^{17}$ where A is the area over which the electric field exists. This flux was 4 times the observed flux. Since the plasma in regions between supports was flowing away from the hoops, the density profile in the azimuthal direction must be known to calculate the net plasma loss.

Magnetic Guarding

The hoop supports were guarded with magnetic dipoles in the manner proposed by Lehnert [16] to determine the efficiency of magnetically guarding supports in a plasma. Previously it has been reported [17] that magnetic guarding of all 12 hoop supports gave a negligible increase in plasma lifetime. The measurement of plasma lifetime was not a sensitive test for magnetic guarding since the particle collector measurements indicated that the support losses were a small fraction of the total losses. The support losses were measured by a particle collector which covered the surface of one of the supports. Collectors mounted on the surface of the hoop and the outer vacuum wall intercepted the null lines of the guard field and were used to measure the loss of plasma along the nulls (Fig. 8). All collectors were operated as single probes biased at -45V with respect to the vacuum wall. At the time of the guarding experiments the ion temperature was 20 eV. When the current through the guarded support was increased to provide six 20 eV gyroradii between the support and the guard field null, the flux to the support decreased by an order of magnitude indicating that magnetic guarding of the support was effective. However, the flux of plasma to the hoop and to the outer wall increased to roughly the same value as the original flux to the support as shown in Fig. 9.

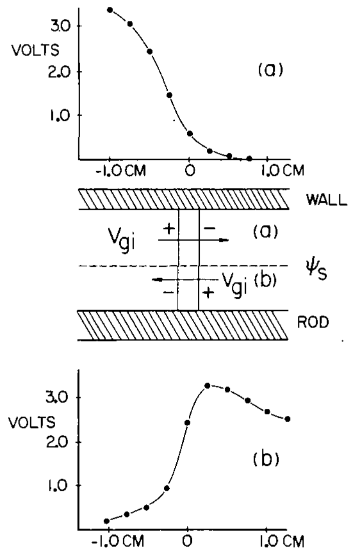

FIG. 7. The floating potential variation around a 0.625 cm diam. obstacle is shown for flux surfaces lying inside and outside the separatrix. Also shown is a schematic of these regions with the ∇B drifts for the ions and the expected charge separation due to particle losses on the obstacle.

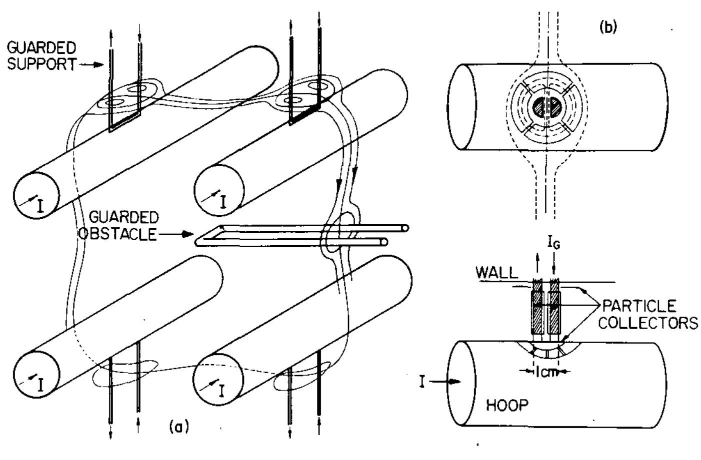

FIG. 8. Magnetic guarding apparatus: (a) perspective view of the octupole showing the positions of the guarded supports and the guarded obstacle; (b) side and top view of a guarded support showing the positions of the particle collectors used to measure support loss, wall loss and hoop loss.

The increased wall loss cannot be caused by field lines spiralling out of the octupole since all of the field lines are still closed after one transit around the minor cross-section due to reflection symmetry about the midplane of the octupole.

The outward loss of plasma has been estimated by Lehnert [18] assuming that single particles undergo a random walk near the null of the guard field resulting in ambipolar diffusion which produces a total flux out of the confinement region given by $\phi \cong 4\pi N V_e \rho_e{}^3 \nabla n \approx 10^{13}$ particles/sec where N = 12 is the number of guarded supports, V_e = 2×10^8 cm/sec is the electron thermal velocity and $\rho_e = 8 \times 10^{-3}$ cm is the electron gyroradius. The observed flux corresponds to 3×10^{16}/sec which cannot be explained by Lehnert's model. Recently a magnetohydrodynamic model [19] has been developed which treats the initial acceleration of a slab of plasma along the null of a guard field or along the null of a multipole. This model, which is based on the lack of magnetohydrodynamic equilibrium since $p \neq p(\oint d\ell/B)$ near a guarded support, predicts that the plasma on a field line initially accelerates outward with an acceleration given by

$$a(\psi) = - \frac{k(T_i + T_e)}{M} \frac{\nabla n}{n} \frac{u(\psi) - u(\psi_1)}{u(\psi)}$$

where $u = \oint d\ell/B$ and $a(\psi_1) = 0$. The effective size of the hole through which plasma accelerates outward with a free acceleration a_o = $[k(T_i+T_e)\nabla n]/nM$ is roughly $6\pi d^2$ where 2d is the spacing between the two leads of the guarded support. The effective loss area, $6\pi d^2$, is roughly the same as the area of the unguarded support and therefore this model predicts that guarding should not affect the total loss rate appreciably which is in qualitative agreement with the experimental results.

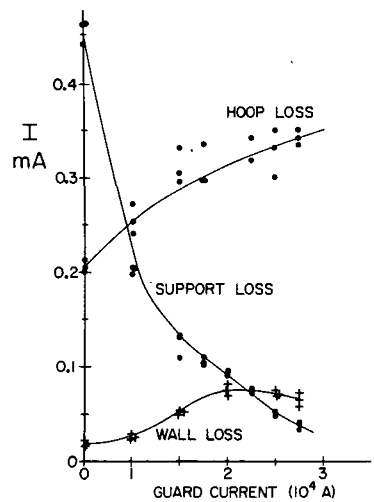

FIG. 9. Variation of losses near a guarded support as a function of guard current. The positions of the collectors are described in Fig.8. A guard current of 3×10^4 A corresponds to 6 gyroradii for 20 eV ions between the support and the guard field null.

Also, experiments have been done on the effect of placing dipole obstacles into the center of the machine in the midplane of the octupole (Fig. 8). The U-shaped dipole obstacles were constructed from 9 mm diameter hard copper rods with a center to center leg spacing of 1.5 cm and were extended from the outer wall to the center of the octupole in the same position as the iron pipe shown in Fig. 1. Three obstacles were placed at azimuths of $\theta = 50°, 180°, 310°$ and each could be pulsed with up to 2×10^4 A using the same circuits that were used for energizing the guarded supports. This provided 5 gyroradii for 32 eV protons between the support and guard field null. Measurements of the lifetimes of 32 eV ions and of ion saturation current to a Langmuir probe near the null field region showed that the plasma lifetime decreased to one-half when the dipole obstacles were inserted into the center of the octupole and then recovered when the obstacles were energized. There was no significant difference between the dipole obstacles forward guarded with the magnetic field inside the dipole opposing the octupole field, or with reverse or with transverse guarding in agreement with results obtained earlier at General Atomic [20]. All field lines in the octupole remain closed after one transit around the minor cross-sections for forward and reverse guarding of the dipole obstacle due to the reflection symmetry about the midplane.

The loss of plasma to the dipole obstacle as measured by the ion saturation current to the dipole obstacle decreased by an order of magnitude when there was 3 gyroradii between the hairpin and the separatrix at the outer wall. The loss to a wall collector increased but remained one order of magnitude below the original unguarded obstacle loss (Table II). The increase in wall loss for the dipole obstacles was almost an order of magnitude greater than the increase in wall loss for the guarded supports.

Therefore, the increase in lifetime due to guarding the dipole obstacles that extend into the zero field region of the octupole does not imply that magnetic guarding was effective since there was an associated outward loss which for realistic supports in the high field region would be comparable to the original support loss.

Discussion

The experiments indicate that low frequency electric fields with a period comparable to the confinement time associated possibly with the presence of hoop supports or the injection process were responsible for the plasma loss as observed by the particle collectors. An effective Bohm time has been defined [12] for a toroidal multipole by assuming that the Bohm diffusion coefficient was valid locally and that the density was constant along a field line during the diffusion. The observed loss rates for the gun injected plasma, indicated that loss across the minimum average B stable region to the outer wall was ~2% of the Bohm rate and the flux across the minimum B stable region to the hoops was ~20% of the Bohm rate. However, the equivalent Bohm rate

TABLE II

Summary of Loss Measurements near a Guarded Support

	Flux (10^{16}/sec)	
	Model Support	Obstacle
Direct Loss		
Unguarded	0.40	7.0
Guarded	0.06	0.7
Local Wall Loss		
Unguarded	0.015	0.18
Guarded	0.06	1.0
Local Hoop Loss		
Unguarded	0.14	
Guarded	0.28	

for a multipole was derived using the assumption that $D \propto B^{-1}$ along a field line. If the losses were due to $k_{\parallel} = 0$ fluctuations or convective cells, $D \propto B^{-2}$ along a field line and the previous analysis is not valid.

When the hoop supports were magnetically guarded the associated plasma loss along the null region was comparable to the original support loss indicating that magnetic guarding would be intolerable in a full scale fusion machine if this loss scaled as the support area. Experiments are in progress to determine the scaling for the null loss rate.

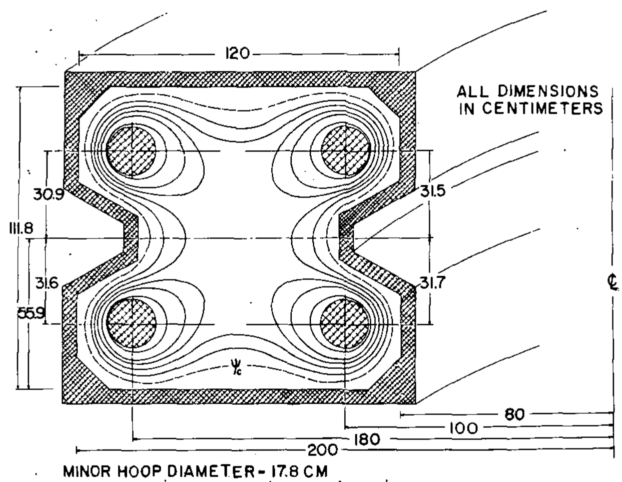

FIG.10. Computed magnetic field pattern and relevant dimensions for the magnetically force-free toroidal octupole under construction.

An inductively excited, magnetically force-free octupole is being assembled with transiently withdrawn supports to eliminate the effect of hoop supports on plasma confinement which complicates study of the intrinsic confinement properties of the toroidal octupole. The 5 cm thick aluminum wall which carries the return current was shaped to provide a magnetically force-free configuration for the 4 solid aluminum hoops as shown in Fig. 10. The total current in the hoops is a sine wave with a peak of 1.4×10^6 A and a half period of 50 msec, which will provide a minimum of 12 gyroradii for 100 eV protons between ψ_s and ψ_c and allows 10 msec of experimental time during which 5% of the magnetic flux diffuses into the internal hoops. A typical operating cycle will consist of

a) withdrawing the 16 supports;
b) triggering the capacitor bank for multipole field;
c) plasma injection, and
d) repositioning of the hoop supports.

References

[1] B. B. Kadomtsev, Plasma Physics and the Problem of Controlled Thermonuclear Reactions (Pergamon Press, Inc., N.Y. 1960) IV p. 417.

[2] T. Ohkawa and D. W. Kerst, Phys. Rev. Letters 7 41 (1961); Nuovo Cimento 22 784 (1961).

[3] D. W. Kerst, R. A. Dory, W. E. Wilson, D. M. Meade and C. W. Erickson, Phys. Rev. Letters 15 396 (1965).

[4] R. A. Dory, D. W. Kerst, D. M. Meade, W. E. Wilson, and C. W. Erickson, Phys. Fluids 9 997 (1966).

[5] T. Ohkawa, A. A. Schupp Jr., M. Yoshikawa and A. G. Voorhies, Plasma Physics and Controlled Nuclear Fusion Research (International Atomic Energy Agency, Vienna, 1966) II 719.

[6] A. A. Schupp Jr., H. K. Forsen and D. W. Kerst, J. Nucl. Energy C5 161 (1963).

[7] J. C. Sprott, Rev. Sci. Instr. 37 897 (1966).

[8] J. A. Schmidt, to be published in Rev. Sci. Instr. Sept. 1968.

[9] C. W. Erickson, to be submitted to Phys. Fluids.

[10] J. E. Howard, to be published in Phys. Fluids July 1968.

[11] E. Berkl, D. Eckhartt, G. von Gierke, and G. Grieger, Phys. Rev. Letters 17 906 (1966); R. Palladino and S. Yoshikawa, submitted to Phys. Fluids.

[12] D. M. Meade, Phys. Rev. Letters 17 677 (1966).

[13] D. E. Lencioni, J. W. Poukey, J. A. Schmidt, J. C. Sprott and C. W. Erickson, Phys. Fluids 11 1115 (1968).

[14] P. H. Rutherford and E. A. Frieman, Phys. Fluids 11 569 (1968).

[15] C. W. Erickson and D. M. Meade, Bull. Am. Phys. Soc. 10 235 (1965); G. O. Barney and J. C. Sprott, submitted to Phys. Fluids.

[16] B. Lehnert, J. Nucl. Energy C1 40 (1959).

[17] H. K. Forsen, A. W. Molvik and J. C. Sprott, Bull. Am. Phys. Soc. 13 266 (1968); A. W. Molvik, Bull. Am. Phys. Soc. 13 869 (1968).

[18] B. Lehnert, Plasma Physics 10 207 (1968).

[19] D. M. Meade, submitted to Phys. Fluids.

[20] T. Ohkawa and N. Rostocker, Physics today 20 48 (1967).

DISCUSSION

B. LEHNERT: The plasma loss in the direction along the guarded supports can be interpreted in a different way. In your configuration, the dimension of the plasma in the direction along the supports is comparable with the distance between the supports. Thus, when magnetic guarding is switched on, the surfaces of the average guiding centre drift of ions and electrons become strongly deformed and a considerable part of the plasma drifts out to the walls at the supports. In your device, this should also apply to the experiment with the hairpin-shaped obstacle, but to a smaller extent, since the transverse dimension of the plasma is greater at the obstacle than at the supports. In fact, the total loss in the obstacle experiment also decreases by almost an order of magnitude when magnetic guarding is switched on. Therefore, your results for magnetic guarding are not necessarily negative. I would say that they are encouraging and that further research on this problem is necessary.

D. MEADE: From a general point of view, the existence of single-particle drift surfaces which leave the machine is in reality simply the microscopic picture of the lack of MHD equilibrium described in the paper. Some classes of particles with drift surfaces leaving the machine will always be present, regardless of the spacing of the magnetic guards. These particles produce a self-consistent electric field which causes the particles to leave the machine by an $\vec{E} \times \vec{B}$ drift. We find experimentally that, for a guarded support which has $a/2d \simeq 3$ (where a is the plasma thickness and 2d is the spacing of the supports), the local flux to the wall near the support increases by 0.04×10^{16} particles/s, when the support guarding is energized (Table 2). The local loss to the wall near the guarded obstacle, where $a/2d \simeq 11$, increases by 0.8×10^{16} particles/s. This larger loss is in disagreement with your suggestion that the loss for the guarded obstacle should be reduced because of the greater ratio of plasma thickness to support spacing.

It is important note that the guarding of an obstacle really does not have any direct relevance to the guarding of an actual support, since the obstacle need not penetrate the toroidal plasma; but a support must penetrate the plasma, thereby destroying its toroidal properties.

In spite of what Mr. Lehnert has just been kind enough to say, I find the present experiments very discouraging. However, we shall reach a final conclusion when the experiments to determine the scaling of the loss rate as a function of B and T are completed.

PLASMA INSTABILITIES IN GULF GENERAL ATOMIC MULTIPOLE DEVICES*

T. OHKAWA, M. YOSHIKAWA AND A. A. SCHUPP
GULF GENERAL ATOMIC INC., SAN DIEGO, CALIF.,
UNITED STATES OF AMERICA

Abstract

PLASMA INSTABILITIES IN GULF GENERAL ATOMIC MULTIPOLE DEVICES. The plasma instabilities are studied in both the octopole and quadrupole configurations. A typical set of parameters is a plasma density of 10^{10} cm^{-3}, an ion temperature of 100 eV, and an electron temperature of 10 eV. In both devices the difference of the vector potential between the separatrix and the wall or the stability limit corresponds to about five gyroradii for 100 eV hydrogen ions.

In the octopole configuration, three types of fluctuations are recognized. The first type of fluctuation has a zero wave number parallel to the magnetic field and propagates along the diamagnetic current with a wave number comparable to the reciprocal of the ion gyroradius. The amplitude of the potential fluctuation is about 50 mV and increases rapidly as the octopole field is decreased. The fluctuation is suppressed by applying a toroidal field of a few gauss or by lowering the ion temperature. The results of the fluctuation measurement and the transmission experiment agree with the theoretical dispersion relation for drift cyclotron instability.

The second type is observed at the plasma density below 3×10^{8} cm^{-3} with a toroidal field larger than 40 G. The mode is identified as the electron-driven drift cyclotron instability with finite parallel wave number.

The third type is observed in the plasma with a density below 3×10^{-8} cm^{-3} only when the ion temperature is lowered. A toroidal field of a few gauss suppresses the fluctuation. The amplitude is approximately uniform and no phase shift is observed along the magnetic line of force. This mode is interpreted as the ion-driven instability due to the modulation of the magnetic field along the line of force.

Large-amplitude (20%) fluctuations are found inside the stability limit in the quadrupole device. The frequency spectrum is 10 kHz to 500 kHz. The wave number parallel to the magnetic field line is zero. The phase velocity is in the direction of and less than the ion diamagnetic drift velocity. These characteristics are consistent with an interchange instability due to finite gyroradius of ions. The absence of this type of instability in the octopole device is expected from the theory.

I. INTRODUCTION

It has been shown by several experiments that mhd type instabilities may be controlled in toroidal configurations and that the plasma is confined for a much longer period than the mhd time scale. The next step then is to study and eventually to control the microinstabilities.

Three parameters are considered important for controlling the microinstabilities. They are the magnetic well, magnetic shear, and connection length between the good curvature and the bad curvature region. Quantitative information on the effects of these parameters are necessary to arrive at a configuration for thermonuclear plasma. In multipole configurations, the shear may be changed by superposing a toroidal magnetic field. The depth of the magnetic well and the connection length may be varied by changing the number of poles, for example, an octopole to a quadrupole.

* The work reported herein was supported in part under a joint General Atomic-Texas Atomic Energy Research Foundation program on controlled thermonuclear reactions and in part by the US Atomic Energy Commission under Contract No. AT(04-3)167, Project Agreement 38.

The fluctuations in both the Gulf General Atomic octopole[1,2,3] and quadrupole device[4] are measured. Plasma parameters are kept as close as possible in comparing the two configurations. The measurements are made for a wide range of parameters, such as the plasma dielectric constant and the ratio of temperatures.

Three types of fluctuations are found in the octopole configurations. They are all at a low level; less than 1% in density modulation amplitude. By reducing the magnetic field, the amplitude is increased to about 5%. The measurements are performed at the increased fluctuation level. Two types are observed in the quadrupole configuration. The amplitude is larger than 15% and weakly dependent on the magnetic field.

The summary of the experimental observations and the theoretical interpretations of these fluctuations will be discussed in this article.

II. PLASMA PARAMETERS

The Gulf General Atomic octopole device has been described previously.[1] It has been converted to a quadrupole configuration. The magnetic field strength in both configurations give about three gyroradii between the multipole axis and the critical flux line for 100 eV hydrogen ion. The magnetic well depth, defined by $\{\oint ds/B \text{ (at } \psi=\psi_c/2) - \oint ds/B \text{ (at } \psi=\psi_c)\}/\oint ds/B \text{ (at } \psi=\psi_c)$ where ψ is the flux function and ψ_c is the value at the critical line, is 10% for the octopole and 3% for the quadrupole configuration. The flux surface where the magnetic shear vanishes is within 1 mm of the $\psi=\psi_c$ surface because of the large aspect ratio of the device.

The plasma is produced by a coaxial gun in both cases. The plasma density is varied from 10^{11} cm^{-3} to 10^8 cm^{-3}. The corresponding dielectric constants are 1000 and 1. The ion temperature is approximately 100 eV and the electron temperature is 10 eV.[5] The ion temperature may be lowered by introducing either hydrogen or oxygen gas into the device. The ratio of the plasma pressure to the magnetic field pressure β is smaller than the mass ratio of an electron and a hydrogen ion.

The decay of magnetic field, plasma density, and temperatures is negligible during the sampling time, typically $100 \sim 200$ μsec, of the fluctuation measurements. A toroidal field of up to a tenth of the average multipole field may be applied. Because of the magnetic shear, it is possible to examine both regimes $\omega \gtrless k_\parallel v_e$ by changing the toroidal field.

Langmuir probes are used to study the properties of the fluctuations. The frequency range studied is 20 kc $\sim$ 500 kc. The experimental methods are described in detail in Reference [3].

III. FLUCTUATIONS IN THE TOROIDAL OCTOPOLE

The fluctuation level in the octopole configuration is low, less than 1% with a normal set of parameters ($n \sim 10^{10}$ cm^{-3}, $T_i \sim 100$ eV and 5 gyroradii to the wall) as reported previously.[2,3] By reducing the magnetic field by a factor of 2, the fluctuation level was increased by nearly an order of magnitude. This type of fluctuation is called Mode I.

The characteristics of the fluctuations change when parameters such as plasma density, ion temperature and toroidal field are varied. Figure 1

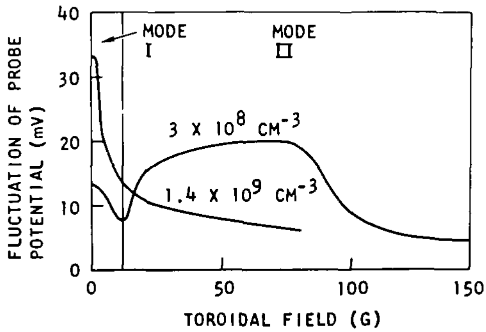

FIG. 1. Potential fluctuations in the octopole as a function of the toroidal magnetic field with plasma density as a parameter.

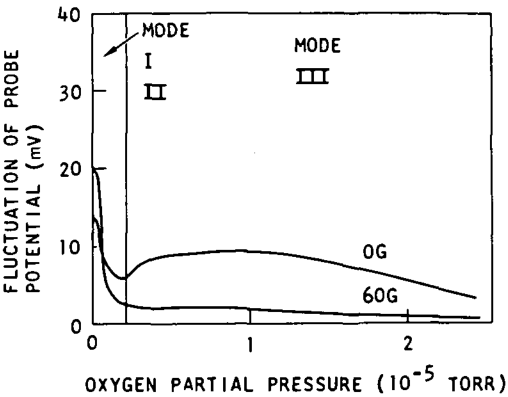

FIG. 2. Potential fluctuations in the octopole as a function of the oxygen pressure in vacuum chamber with toroidal field as a parameter.

shows the fluctuation amplitude as a function of the toroidal field with plasma density as a parameter. At all densities, Mode I becomes undetectable above 10 G of the toroidal field. At densities lower than 10^9 cm^{-3}, a new type of fluctuation appears with a toroidal field of several tens of gauss as shown in Fig. 1. This mode is called Mode II.

Figure 2 shows the fluctuation amplitude as a function of the oxygen pressure introduced in the vacuum chamber with the toroidal field as a parameter. The abscissa can be considered a measure of ion temperature since the ion temperature decreases as the oxygen pressure increases. Above 2×10^{-6} Torr, Mode I and Mode II become undetectable. A new mode appears in the range of oxygen pressure from 2×10^{-6} Torr to 2×10^{-5} Torr, if the plasma density is below 10^9 cm^{-3}. This mode is called Mode III.

The summary of the experimental results are tabulated in Table I. In the following each mode will be discussed separately.

3.1 Mode I

All the characteristics of this mode are consistent with the drift cyclotron instability.[6,7,8] Other types of instabilities have one or more properties in disagreement with the experimental observations. Reference[3] describes this instability in detail.

The superposition of a toroidal field produces a shear in the magnetic field and produces a finite parallel wave number. For a toroidal field B_t much smaller than the average multipole field B_M, the parallel wave number $k_\parallel$ is given approximately by $k_\parallel \sim k_\perp (B_t/B_M)$, where $k_\perp$ is the perpendicular wave number. A finite parallel wave number introduces a motion of electrons along the flux line due to the electric field. The inertia of electrons due to this motion affects the real part of the frequency of the wave and the Landau damping affects the imaginary part of the frequency. Both are stabilizing. The inertial effects are independent of the electron temperature while Landau damping depends on the electron temperature. With the parameters of this experiment, the inertial effects give a smaller critical $k_\parallel$, hence a smaller toroidal field, for the stabilization of the mode than the critical values due to Landau damping. The theoretical prediction agrees with the experimental observation.

TABLE I. EXPERIMENTAL RESULTS FOR OCTOPOLES.

	OCTOPOLE	MODE I	MODE II	MODE III
Plasma Parameters	(1) n_i (cm^{-3})†	$> 10^9$	$< 5 \times 10^8$	$< 5 \times 10^8$
	(2) T_i (eV)	~ 100	~ 100	~ 10
	(3) T_e (eV)	~ 6	~ 6	~ 6
	(4) Toroidal field (G)	0 - 2	10 - 120	0 - 2
Amplitude	(5) Potential fluctuation (V)	0.3-0.4	0.5-0.7	0.3-0.4
	(6) Density fluctuation (%)	~ 5 at reduced B	~ 5 at reduced B	~ 5 at reduced B
Fluctuation Properties	(7) Frequency (kHz)	~ 100	~ 100	~ 50
	(8) $k_\parallel$	0	finite	0
	(9) Phase velocity (cm/sec)‡ parallel to diamagnetic velocity of	3×10^5 ions	(2.5×10^5) electrons	(2×10^5) ions
	(10) Phase angle between potential and density fluctuations (deg)	180	0	-

†The density is at 8 cm vertically from the axis.

‡The phase velocities in brackets have not been corrected for the $E \times B$ drift.

The drift cyclotron instability has a density threshold. The condition for instability is given by[6,7]

$$R_i^2/R^2 > 8\ (\Omega_i^2/\omega_{pi}^2 + m_e/m_i) \tag{1}$$

where R_i is the ion gyroradius and $R = n(dn/dr)^{-1}$. With the experimental parameters, Eq. (1) gives $1 \times 10^9\ \mathrm{cm}^{-3}$ as the threshold density. This is consistent with the experimental results.

3.2 Mode II

This mode is observed only with a plasma density below $5 \times 10^8\ \mathrm{cm}^{-3}$ and a toroidal field larger than 10 G. The experimental results show a finite parallel wave number and propagation in the direction of the electron diamagnetic drift which suggest the universal drift instability. However, the mode disappears when the ion temperature is lowered. This and the presence of Mode I indicate the importance of an ion cyclotron wave.

Cyclotron waves, one (Mode IIA) propagating in the direction of the ion diamagnetic drift[6] and the other (Mode IIB) propagating in the opposite direction[14] may become unstable with a finite $k_\parallel$. The growth rate is computed digitally for these instabilities using the dispersion equation given by[9]

$$1 + \frac{T_e}{T_i} + (k_\perp^2 + k_\parallel^2)\lambda_{Di}^2 - \frac{\omega - k_\perp v_{ce}}{k_\parallel v_e}\frac{T_i}{T_e} Z\left(\frac{-\omega + k_\perp v_{ge}}{\omega_\parallel v_e}\right)$$

$$- \frac{1}{\sqrt{2\pi b}}\frac{\omega - k_\perp v_{ci}}{k_\parallel v_i} Z\left(\frac{-\omega + \Omega_i + k v_{gi}}{k_\parallel v_i}\right) = 0 \tag{2}$$

where

$$Z(\zeta) = (1/\sqrt{\pi}) \cdot \int_{-\infty}^{\infty} \exp(-y^2)(y-\zeta)^{-1}\,dy \quad \text{and} \quad b = k_\perp^2\ T_i/m_i\Omega_i^2 \quad ,$$

v_{ce} and v_{ci} are the electron and ion diamagnetic velocity, and v_{ge} and v_{gi} are the guiding center velocities of electrons and ions.

Mode IIA is reduced to Mode I with $k_\parallel = 0$. As $k_\parallel$ is increased to about $k_\parallel \sim (\omega/v_e)(T_e/T_i)^{\frac{1}{2}}$, the mode becomes stable due to the parallel motion of electrons. A further increase in $k_\parallel$, to values much larger than (ω/v_e), makes the mode unstable again, if the electron temperature is much smaller than the ion temperature. The real part of the frequency stays almost constant with various $k_\parallel$.

Mode IIB also becomes unstable for $k_\parallel$ larger than (ω/v_e). However, this mode is stabilized with a small electron to ion temperature ratio in contrast to Mode IIA.

The observed dependence of the amplitude on the toroidal field and on the ion temperature may be expalined by either mode. However, the observed direction of the propagation seems to favor Mode IIB, assuming the Doppler shift due to $E \times B$ drift is not large enough to reverse the direction of propagation. Without further tests, for example, varying electron temperature, a definite discrimination between two modes is not possible.

3. Mode III

This mode is observed only with plasma densities below 3×10^8 cm^{-3} and with oxygen pressures above 2×10^{-6} Torr. The amplitude has a broad maximum around an oxygen pressure of 1×10^{-5} Torr. At this pressure the lifetime of 100 eV ion is about 100 μsec. This agrees with the value calculated from charge exchange cross section. The fluctuations are measured at 200 μsec after injection when the ion temperature may be about 10 eV. With this oxygen pressure, the ion temperature cannot be measured accurately, because the relation between the ion energy in the plasma and at the detector is not known at energies comparable to the electron temperature.

The characteristics of the Mode III fluctuation are similar to those of the fluctuation observed in the quadrupole configuration, except they only appear when the ion temperature is comparable to the electron temperature.

Several calculations have been made on interchange instabilities recently. These instabilities are due to (1) ions staying for a long time in the bad region[10], (2) a large ion gyroradius making an average drift velocity in the bad direction[4], (3) resonance between the ion bouncing frequency along a flux line and the drift wave frequency[11], (4) resonance between the drift wave and the ion drift motion[12,13], and (5) the effect of the curvature modulation along a flux line[14,15]. A low density or a nonisotropic temperature is required for all modes.

The presence of Mode III, only when the electron and ion temperature are about equal, suggests instability (3) or (5). These instabilities require that the drift wave resonantes with the ion transit time between the good and the bad region.

$$k_\perp v_{ci} \sim (2\pi/L)\ v_i$$

where L is the connection length. They also require that the electron Landau damping does not overcome the resonant ion contribution. This sets a lower limit on the ion temperature for instability. The experimental observation appears to agree qualitatively with either instabilities (3) or (5). The discrimination between (3) and (5) is not possible from the available experimental data.

IV. FLUCTUATIONS IN THE TOROIDAL QUADRUPOLE PLASMA

Fluctuations of larger amplitude were observed in the toroidal quadrupole plasma.[4] The fluctuation amplitude does not decrease by increasing the multipole field. The amplitude distribution on the median plane from the rings to the wall is shown in Fig. 3. The amplitude is much larger outside the separatrix than inside, where the absolute minimum B condition is satisfied. The toroidal field does not affect the amplitude appreciably. However, it changes the character of the fluctuation from a flute mode ($k_\parallel = 0$) to a drift mode ($k_\parallel \neq 0$). The critical field for the transition is about 4 G. At this field, the relation $\omega/(k_\parallel v_e) = 1$ is approximately satisfied. The summary of the experimental results is tabulated in Table II.

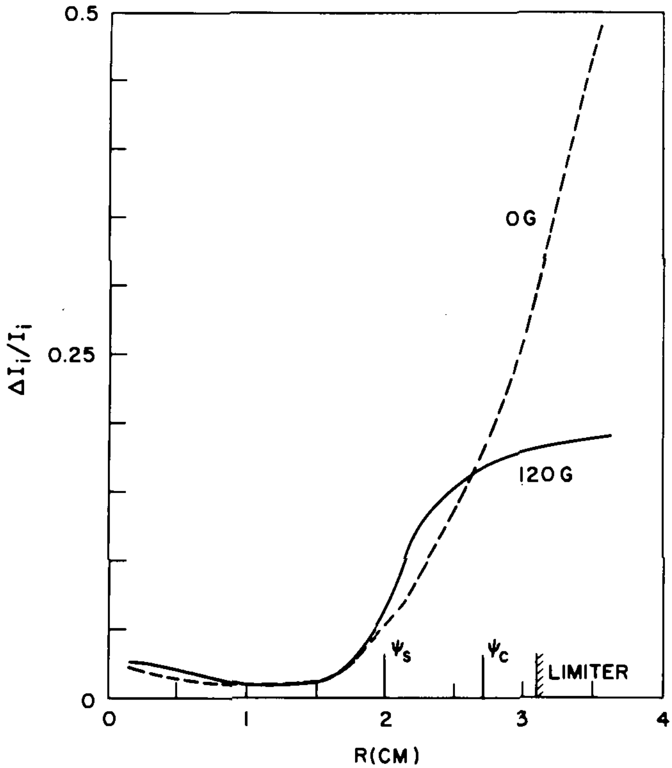

FIG. 3. Distribution of the quadrupole fluctuation ΔI_i of the ion collection current normalized to the average current I_i at 1 ms. The distance is measured from the surface of the outer ring towards the wall. The position of the separatrix, the stability limit, and the flux line at the edge of the limiter is at 2 cm, 2.7 cm, and 3.1 cm, respectively.

The magnetic well of the quadrupole configuration is much shallower than that of the octopole. Therefore the instabilities (2), (3), and (4) mentioned in Mode III section become important. In the multipole configuration the field is weak where the field curvature is favorable and is strong where the curvature is unfavorable. The ions in the "good" region do not participate effectively in the drift motion due to the flute electric field as the ions in the "bad" region do. This puts more weight on the contribution from the "bad" region and may destabilize the mode. As shown in Reference[4] the instability (2) should be present in the quadrupole if $k^2\lambda_{Di}^2 > \langle 1/BR\rangle/\langle I_0(b)e^{-b}/R_cB\rangle$, where $\langle A\rangle = \int A\,ds/B/\int ds/B$. For the quadrupole the instability condition is satisfied even inside the mhd stability limit, when the ion gyroradius is finite.

The instability (4) is due to some particles drifting in the bad direction although the "average" drift velocity is in the good direction. The instability occurs if the drift wave resonates with the particles drifting in the bad direction. Since the drift velocity of the particles is ordinarily smaller than the phase velocity of the drift wave, either a small plasma density or nonuniform temperature is required for the instability. The stability condition is given by[12]

$$k^2\lambda_{Di}^2 + (1-I_0(b)e^{-b})(T_{\parallel i}/T_{\perp i} - 1) > \langle v_{gi}\rangle/v_{ci} \tag{3}$$

where $v_{ci} = cT_i(n'/n - T_i'/2T_i)/eB$. $\langle v_{gi}\rangle$ is v_{gi} averaged over the orbits of all particles. The condition for instability (3) is also given by Eq. (3).[13] The number of particles in resonance with the wave and hence the growth rate are proportional to $\exp[-\omega/k_\perp v_{gi}^*] \approx \exp[v_{ci}/v_{gi}^*]$, where v_{gi}^* is the drift velocity in the bad region. In an average magnetic well, $\langle v_{gi}\rangle$ is much smaller than v_{gi}^*. Therefore, the condition for instability may be satisfied with a significant growth rate. The exponential factor is of the order of $e^{-(5 \sim 10)}$.

The high ion temperature has a destabilizing effect, because the ratio between the average drift $\langle v_{gi}\rangle$ and the diamagentic velocity becomes smaller due to the finite gyroradius effect. In the large gyroradius limit, $\langle v_{gi}\rangle$ is proportional to the gradient of $\oint ds$ rather than on $\oint ds/B$. Then the instability condition, Eq. (3), can be satisfied in the quadrupole even at higher densities.

With a toroidal field larger than 5 G which corresponds to the condition $\omega \sim k_\parallel v_e$, the instability changes to a universal drift instability. The measured properties are in agreement with the theory.

TABLE II. EXPERIMENTAL RESULTS FOR QUADRUPOLE PLASMAS

QUADRUPOLE		Without Toroidal Field	With Toroidal Field
Plasma Parameters	(1) n_i $(cm^{-3})^\dagger$	2×10^9	2×10^9
	(2) T_i (eV)	~ 100	~ 100
	(3) T_e (eV)	~ 6	~ 6
	(4) Toroidal field (G)	0	5 - 120
Amplitude	(5) Potential fluctuation (V)	1.5 - 2	1.5 - 2
	(6) Density fluctuation (%)	15 - 20	15 - 20
Fluctuation Properties	(7) Frequency (kHz)	20 - 500	20 - 500
	(8) $k_\parallel$	0	finite
	(9) Phase velocity (cm/sec) parallel to diamagnetic velocity of	1.5×10^5 ions	0.3×10^5 electrons
	(10) Phase angle between potential and density fluctuations (deg)	180	0

†The density is at 3.5 cm vertically from the axis.

V. SUMMARY

Three types of fluctuations are observed in the toroidal octopole plasma. The first type is observed at densities above 10^{10} cm^{-3} on the axis. It was identified as the drift cyclotron instability. At densities below 5×10^9 cm^{-3} on the axis, and with a toroidal field larger than 10 G, the second type, the electron-driven drift cyclotron instability appears. The third type is observed at low densities when the ion temperature is lowered. The fluctuation level of these instabilities is low and it is not responsible for the observed plasma loss.

Fluctuations of large amplitude were found in the quadrupole device. The amplitude is 30 times larger than in the octopole. They are tentatively idientified as residual interchange instabilities. The superposition of a toroidal field does not affect the amplitude of the fluctuation, but induces a transition from the interchange instability to the drift instability. The observed plasma loss may be due to these instabilities.

The deeper magnetic well in the octopole configuration avoids the interchange instabilities and may account for the overall lower fluctuation level.

REFERENCES

[1] OHKAWA, T., SCHUPP, A. A., VOORHIES, H. G., and YOSHIKAWA, M., Plasma Physics and Controlled Nuclear Fusion Research (International Atomic Energy Agency, Vienna) II (1966) 531.

[2] OHKAWA, T. and YOSHIKAWA, M., Phys. Rev. Letters 17 13 (1966) 685.

[3] OHKAWA, TIHIRO and YOSHIKAWA, MASAJI, "Observation of Fluctuations in the Plasma Confined in the Toroidal Octopole," Gulf General Atomic Report No. GA-8337 (submitted for publication in Phys. Fluids).

[4] OHKAWA, T. and YOSHIKAWA, M., Phys. Rev. Letters 19 24 (1967) 1374.

[5] YOSHIKAWA, MASAJI, OHKAWA, TIHIRO, and SCHUPP, ARTHUR A., "Plasma Confinement in General Atomic Toroidal Octopole," Gulf General Atomic Report No. GA-8141 (submitted for publication in Phys. Fluids).

[6] MIKHAILOSKII, A. B., Nucl. Fusion 5 2 (1965) 125.

[7] KRALL, N. A. and FOLWER, T. K., Phys. Fluids 10 7 (1967) 1526.

[8] BHADRA, D. K., Phys. Rev. 161 1 (1967) 126.

[9] BHADRA, D. K., "Effect of Toroidal Magnetic Field on Low-Frequency Plasma Instabilities in a Multipole Machine," Gulf General Atomic Report No. GA-8348 (to be published in Phys. Rev. July 1968).

[10] ROSENBLUTH, M. N., Phys. Fluids 11 4 (1968) 869.

[11] ROSENBLUTH, M. N., "Present Status of Low-Beta Toroidal Confinement Research," invited paper presented at the Division of Plasma Physics Meeting of the American Physical Society, Austin, Texas, November 8-11, 1967.

[12] OHKAWA, T., "Low Frequency Interchange Instability in an Average Well," Gulf General Atomic Report No. GA-8575, dated March 5, 1968 (submitted for publication in the Kakuyugo-Kenkyu).

[13] HORTON, C. W., Jr., COPPI, B., and ROSENBLUTH, M. N., "Stability and Nonlinear Evolution of the Ion Flute Mode," paper presented at the Annual Sherwood Theoretical Aspects of Controlled Thermonuclear Fusion Meeting, held at Berkeley, May 6-7, 1968.

[14] OHKAWA, T., "Plasma Fluctuations Observed in Multipole Devices," paper presented at the International Symposium on Fluctuations and Diffusion in Plasmas held at Princeton Plasma Physics Laboratory, January 26-30, 1967.

[15] COPPI, B. and OSSAKOW, S., "Low-Density Modes in Multipole Devices," Princeton Plasma Physics Laboratory Report MATT-567, dated November, 1967.

DISCUSSION

B. COPPI: What is your view regarding the anomalous particle losses in the quadrupole and octopole configurations in the absence of fluctuations?

T. OKHAWA: In the quadrupole configuration, the loss is to the wall. The loss in the octopole configuration is due to the presence of the supports and is not related to the plasma fluctuations.

Cs-PLASMA IN THE GARCHING OCTOPOLE W V

C. W. ERICKSON, G. v. GIERKE, G. GRIEGER, F. RAU AND H. WOBIG
INSTITUT FÜR PLASMAPHYSIK, GARCHING, MUNICH,
FEDERAL REPUBLIC OF GERMANY

Abstract

Cs-PLASMA IN THE GARCHING OCTOPOLE W V. In the Octopole a Cs plasma in the density range of typically some 10^8 cm^{-3} is produced by contact ionization with an ion input flux of the order of $\Phi = 10^{15}$ s^{-1}. The influence of an applied azimuthal magnetic field is studied. In accordance with a previous experiment an improvement in density by a factor of 10 is found, when superimposing $B_\varphi = 65$ G. Axial density profiles show a maximum near the lower small separatrix. No appreciable azimuthal density gradient is found, however a large density gradient parallel to the magnetic field towards the rings is to be concluded. n proportional to Φ is found. The experimental confinement time is $\tau_\varphi \approx 20$ ms for $B_\varphi = 65$ G and $\tau_0 = 2$ ms for $B_\varphi = 0$. The confinement is discussed in terms of a collisionless model where non-conservation of magnetic moment and large Larmor radii lead to recombination of particles at the rings.

Introduction

Preliminary results on the Octopole were reported [1] in 1965, at the Culham Conference. After several technical improvements regarding the current-carrying rings the investigation of the confinement of a Cs plasma in the Octopole has been resumed. For the sake of continuity as well as to check the possible influence of the abovementioned changes on the physics in this machine the experimental conditions are chosen in the same range of operation as in 1965. In this paper, however, we concentrate on experiments where the main magnetic field as well as the temperature of the plasma source, is kept constant.

Apparatus

A description of the apparatus is already given in ref. [1]. Here we only list the main features and give details of certain changes made in the meantime.

When energizing appropriately a system of two pairs of inner rings along with outer reverse windings a meridional field as shown in fig. 1 is produced. The maximum magnetic field at the big separatrix, $B_0 = 2.3$ kG, is near the inner ring at $z \approx 15$ cm, near the outer ring there is $B = 0.84$ kG. Vertically between the crossing

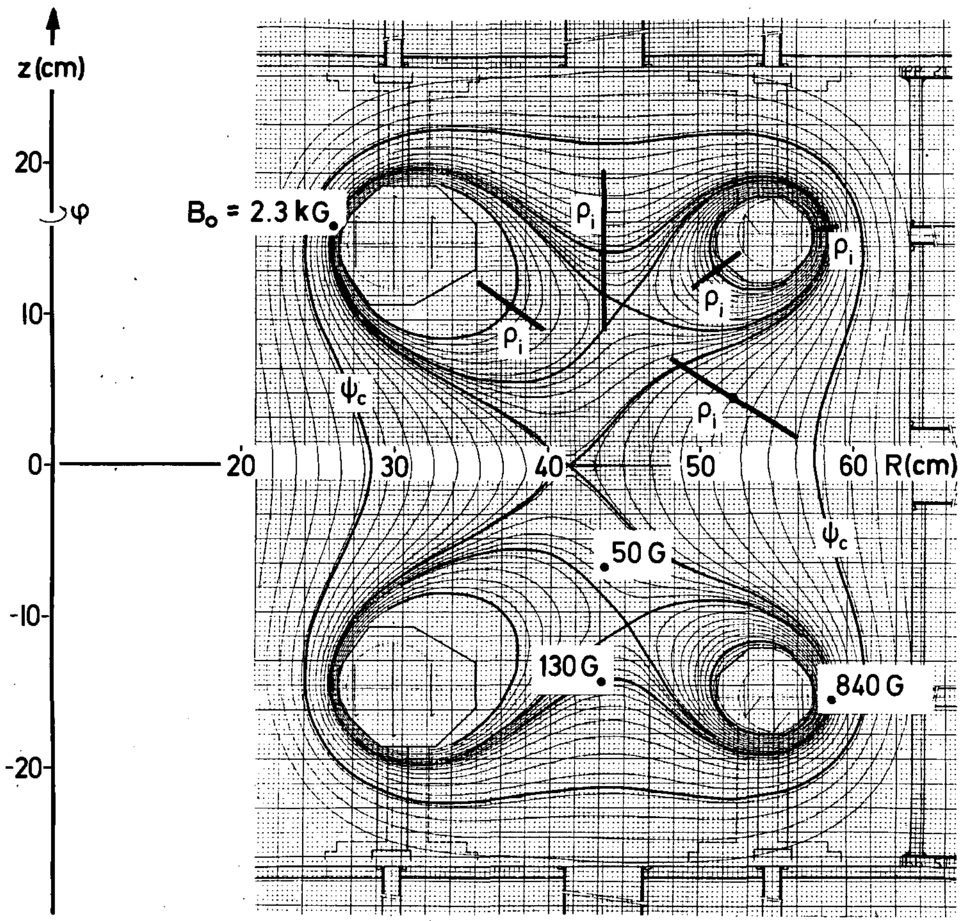

FIG. 1. Magnetic field plot of octopole W V.

points of the separatrices there is B ≈ 50 G. The theoretical limit of a flute-stable confinement, ψ_c, is inside the vacuum tank. Considering Cs ions with energy of 0.2 eV there are about 3.3 Larmor radii ρ_i between ψ_c and the big separatrix in the plane z = 0. Near the outer ring, however, there is only one Larmor radius between the shell of the ring and the small separatrix. Generally, ρ_i is of the order of a scale length in the magnetic field.

These statements also were valid for the experiment described in ref. [1]. In the meantime more rigid structures of the shells around the coils with also three supports for each ring were constructed. Care was taken to keep the new shells inside the same magnetic flux lines as were those described in ref. [1]. The dimensions of the

supports have been increased slightly, the long sides still being parallel to the field lines of the meridional field. The surfaces of the supports are insulated by silicon paint, the shells of the coils are connected electrically with the vacuum tank.
The magnetic field is switched on for two seconds, this time being long compared to the experimental confinement time as well as to the rise time of current in the inner rings. An azimuthal magnetic field B_φ up to several hundred gauss can be superimposed upon the meridional field.
We use contact ionization of Cs-vapour which is directed vertically from the bottom of the machine towards a hot conical spiral of about 2 cm diameter and 1.6 cm height, made of 2 mm dia tantalum wire. The tip of the cone is pointing downward. The spiral is heated by d.c. up to 2500 $^{\circ}$K. The heating is switched off during the pulse time of the magnetic field. As the spiral is well insulated it can assume its floating potential. The plasma source is placed at the same azimuth as the big supports of the rings in order to have a maximum of azimuthal symmetry in the machine. We use single Langmuir probes and special double-double probes as described in ref. [2] as diagnostic tools. The single probes are of 0.5 mm diameter and 2 mm length biased with respect to the spiral. Ion density is calculated the usual way. An empirical correction factor of 2.5, see e.g. ref. [3, 4], is applied.
The probe signals are evaluated at t = 1 s. At this time the spiral is cooled down from 2500 $^{\circ}$K to about 2300 $^{\circ}$K. No corrections regarding recombination at the probe itself and at the shaft are made.

Experiments

We first investigate the influence of an applied azimuthal magnetic field B_φ on the density of the Cs plasma in this machine. In the previous experiment, ref. [1], an increase of nearly one order of magnitude in peak density was reported when superimposing a weak magnetic field $B_\varphi \approx 50$ G on the main meridional field. In fig. 2 we give the results of our investigation. Using an ion input flux $\Phi = 10^{15}\ s^{-1}$ the density n vs azimuthal field $\pm B_\varphi$ is measured at azimuthal position $\varphi = 180^{\circ}$ with respect to the plasma source, at several points of the big separatrix, as indicated in the insert. There is a close agreement with the 1965 results when normalizing the 1965 data at the maximum of the curve. With increasing B_φ the density rises monotonically up to a factor of 10 as compared to the density at $B_\varphi = 0$. The maximum of the curve is reached near $B_\varphi = 65$ G; beyond this maximum there is a slow decrease. The same behaviour is found when measuring axially at R = 30 cm above the inner ring.

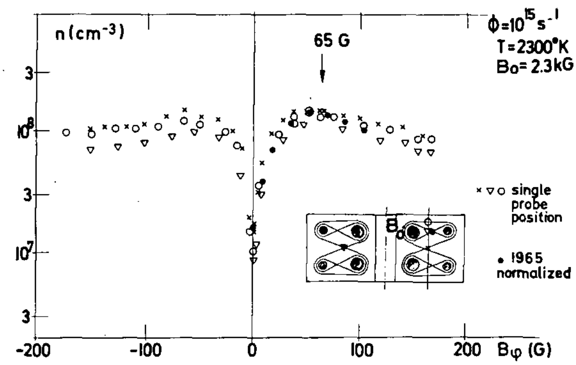

FIG.2. Density versus azimuthal magnetic field B_φ. Probe position indicated in insert.

In fig. 3 we give axial and radial profiles of Cs ion density n in the Octopole. The data of these curves is gained during several days of experiments where the ion input flux Φ was varying from $9 \cdot 10^{14}$ to $3.4 \cdot 10^{15}$ s^{-1}. Corresponding to the result of the following fig. 4 (n proportional to Φ) we normalized the profiles to $\Phi = 1 \cdot 10^{15}$. The vertical profiles at azimuthal angles $\varphi = 60^{\circ}$ and 180° are taken with the identical probes, the vertical profile at $\varphi = 180^{\circ}$ is measured with double-double and with single probe, resp. The radial profiles are obtained with two different single probes. All these profiles are taken with an azimuthal field $B_\varphi = 65$ G; with $B_\varphi = 0$ we only show a vertical profile at $\varphi = 180^{\circ}$. The relative agreement of the 4 different probes used is within a factor of 2.

We note the following details of the profiles:

i) with $B_\varphi = 65$ G and $B_\varphi = 0$ we find in the axial profiles a maximum of density in the lower half of the machine, peaked around the lower small separatrix.

This asymmetry is not changed when using the reverse polarity of the currents which produce the meridional field.

ii) the radial profiles are rather flat-topped and centered around the big separatrix.

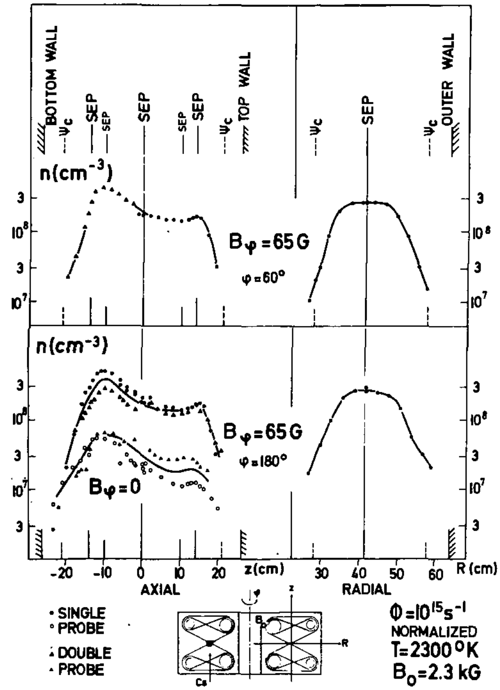

FIG.3. Axial and radial density profiles.

iii) the density at the big separatrix is approximately constant at the different points in the profiles shown. However, when measuring axial profiles above the rings at an azimuth of 180° we find peak densities of about one order of magnitude lower than those as given in fig. 3. This information is obtained with another double-double probe of the same construction and dimensions as were used in the profiles shown. Assuming the same sensitivity this means that a remarkable density gradient parallel to the magnetic lines is to be concluded.

iv) apparently there is no appreciable azimuthal density gradient to be observed.

A comparison of confinement mechanisms as predicted by theoretical considerations with the experimental data can be undertaken by a study of a n vs Φ plot, e.g. as shown in fig. 11 of ref. [1].

In fig. 4 we present our data obtained by single and double-double probes at several points of the big separatrix. The bulk of the experimental points follows the relation n proportional to Φ. Vertically above the upper rings, however,but still near the separatrix we find the density to be an order of magnitude lower. The density above the inner ring (x) appears to be higher by about a factor of 2 as compared to the density above the outer ring (+).

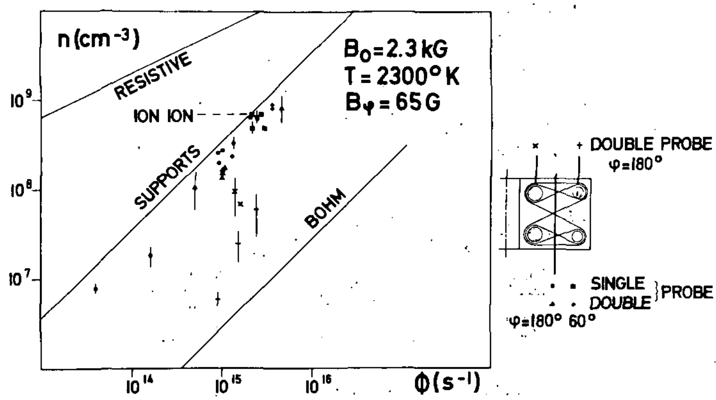

FIG.4. Density at large separatrix-versus-ion input flux and theoretical particle losses.

Discussion

In fig. 4 three theoretical curves (straight lines) are reproduced from fig. 11 of ref. [1], corresponding to resistive and Bohm-type diffusion and to recombination at the supports, resp., as predominant loss processes. In order to take into account our changes in the size of the supports we shifted the line "SUPPORTS" by a factor of 1.5 towards lower densities.The curve "RESISTIVE" also is adjusted to a magnetic field higher by a factor of 2 as compared to the corresponding line in fig. 11 of ref. [1].

The dashed line marked ION-ION is taken from a report of GRAWE [5].

1) Resistive diffusion

Resistive diffusion as the predominant loss process in the Octopole W V is not to be expected.

ii) Bohm diffusion

This type of loss mechanism yields n proportional to Φ. However, the bulk of the experimental points is found to be about a factor of 60 higher in density than predicted by this model. Furthermore, the experimental radial profile is not as broad as the Bohm profile (ref.[6]).

iii) Support losses

Recombination of the ions at the supports of the Octopole was concluded to be the predominant loss process in the 1965 experiment [1]. Similar statements were made e.g, by OHKAWA et.al. [7] and KERST et.al, [8], Our experimental data obtained axially above the rings at the same radii where the supports are situated, however, do not yield constant density along the big separatrix, but typically show one order of magnitude less density than in the region of low magnetic field. Consequently this would shift the curve SUPPORTS of fig. 4 higher by the same amount beyond the experimental error of the measured n(Φ) curve. Therefore it is to be concluded that - assuming unchanged probe sensitivity as mentioned above - in the Octopole with magnetic fields as used in this experiment the confinement of a Cs plasma of 0.2 eV mean thermal energy is not governed by recombination at the supports.

iv) Like particle diffusion

This was considered by GRAWE [5] using the experimental data of the 1965 experiment [1]. Numerically he solved a transport equation and succeeded in a nearly perfect fit of the vertical density profile given in ref.[1], fig. 10. The res[illegible] of his calculation, however, was very insensitive with respect to a variation of the ion input flux Φ; as shown in fig. 4 of this paper, dashed curve, marked "ION ION" . Since in 1965 n proportional to Φ was found, GRAWE concluded that like particle diffusion is not likely to be predominant.

In our present investigation the meridional field was higher by a factor of 2 as compared to the conditions of fig. 10 in ref. [1]. As the probability of like particle diffusion is proportional to $\rho_i^{\ 4}$ [9] (ρ_i..ion Larmor radius), we are of opinion that like particle diffusion is to be excluded as the main loss process.

Collisionless model with large Larmor radii

Following the procedure as described in ref. [8] to evaluate the absolute confinement zones we calculate a vertical density profile by integration over the distribution function of the Cs ions. This was taken to be Maxwellian with a mean thermal energy of 0.2 eV at the source. The losses due to recombination at the supports are taken into account. Electric fields which should be present in the machine are neglected. According to the energy dependence of the confinement zones the confinement of particles with energy higher than 0.2 eV should be poor. This profile is shown in the middle part of fig. 5, (bold curve), adjusted at the mid plane to fit the experimental curve taken with $B_\varphi = 65$ G at $\varphi = 180^\circ$ (light curve).

Due to the magnetic flux between the big and the small separatrix the calculated profile shows a marked dip at the small separatrix. Experimentally, this dip is not observed. However, at the lower small separatrix there is a maximum of density, the origin of which has to be studied in the future.

In the case of a toroidal multipole with a collisionless plasma the energy H and the momentum p_φ are conserved, see e.g. ref. [8]. Whenever a charged particle penetrates the zone of low magnetic field the magnetic moment μ may change. This may be regarded as an elastic collision where the momentum vector is rotated about some angle in velocity space.

In the case of a superimposed perpendicular field this statement also holds true, as can be seen in the upper part of fig. 5. There, for a linear quadrupole we calculate numerically the path of a charged particle with given Larmor radius and starting direction. One percent of the maximum magnetic field at the separatrix is superimposed.

In this connection we now discuss a loss mechanism which might be applicable to this experiment. This model yields a

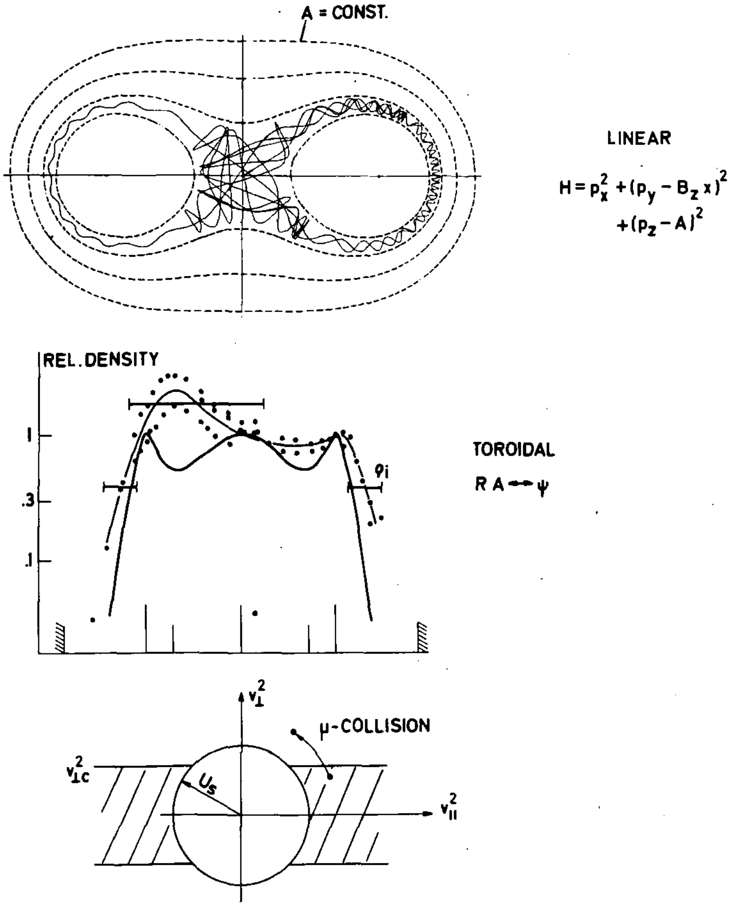

FIG. 5. Collisionless model with non-conservation of magnetic moment and large Larmor radii.

relation of n proportional to Φ. Qualitatively the improvement of the confinement by applying the azimuthal field B_φ can be shown, however no prediction can be made with respect to the reduction of particle density beyond the optimum value of $B_\varphi \approx 65$ G.

Since in the Octopole between the outer ring and the small separatrix the distance is only one Larmor radius ρ_i of a 0.2 eV Cs ion those particles having by chance a larger radius of gyration than this distance are lost by recombination at the shell. This effect depletes the velocity distribution beyond a critical perpendicular velocity $v_{\perp c}$. Whenever a Cs ion is passing near the zone of lower field at a rate $\nu \approx 4 \frac{v_{ith}}{L} \approx 2 \cdot 10^3\ s^{-1}$ ($L \approx 1$ m being the length of the big separatrix), μ might change. There is a probability $c < 1$ that this change transfers part of the parallel velocity to perpendicular velocity beyond the critical value.

In order to calculate the losses in stationary state we have to balance the input flux Φ and the losses $\Phi = c\ \nu\ n\ V$; n being an average density in the confinement volume $V \approx 10^5\ cm^3$.

Inserting the experimental values of the measurement without azimuthal field (see fig. 3) we find $c_o = 0.2$ corresponding to a confinement time $\tau_o \approx 2$ ms. This time is short as compared to ion-electron or ion-ion collision times, respectively.This value reduces to $c_\varphi \approx 0.02$ when considering the results of the measurement with optimal B_φ. Since in the case with azimuthal field (non-zero-min-B-device) μ is a better adiabatic constant, the confinement should be improved.
Particles with energy $E < \frac{m}{2} v_{\perp c}^2$ cannot leave the plasma in the model discussed above. Those low velocities, presumably do not exist in the Octopole at the conditions of this experiment. With a Ta-spiral at about T = 2300 ^oK and at densities of typically $10^8\ cm^{-3}$ there exists an electron sheath with sheath voltage U_s large as compared to 0.2 V. In the collisionless regime the distribution function (assumed to be at the source half-Maxwellian with temperature T) is accelerated in the sheath+).
Thus the distribution of velocities in this experiment might well be as asymmetric as shown in the lower part of fig. 5, with only the shaded area of the velocity space being populated.

In the loss model discussed here characteristic distances in the machine are compared with local Larmor radii of a 0.2 eV Cs ion. Considering the influence of the sheath acceleration one might argue that larger Larmor radii have to be taken into account.
Up to now we have totally neglected effects of electrical fields which at least are caused by the large factor between

+) In accordance with ref. [3] this introduces no marked error in our evaluation of probe signals.

ion and electron Larmor radii. Taking into account the gradient of the measured floating potential, however, leads to the conclusion that the Larmor radius of an Cs ion can be reduced up to a factor of 2. This counteracting effect might balance part of the increase of Larmor radii caused by energy gain in the sheath in front of the emitter.

Conclusion

From the experimental data and the results of a simple collisionless model of particle losses taking non-conservation of magnetic moment as well as effects of Larmor radii into account we believe that confinement of Cs ions in this experiment on the Octopole is governed mostly by recombination at the surfaces of the rings.

To test this model more experiments are to be made, especially those using smaller Larmor radii and an emitter with less sheath voltage. The decrease of density beyond the optimum value of $B_\varphi \approx 65$ G is to be investigated further. Up to now no explanation of this feature is given.

This work was performed under the terms of the agreement between the Institut für Plasmaphysik GmbH, Munich-Garching, and Euratom to conduct joint research in the field of plasma physics.

References

[1] Eckhartt, D. et.al. Proceedings of the Culham Conf. 1965, Vol.II,718,paper CN 21/50.

[2] D'Angelo, N. et.al. VI ICPIG Paris, 1963, paper III c, 9.

[3] Hashmi, M. et.al. Proc. of Conf. on Phys. of Quiescent Plasmas, Frascati 1967, paper I, 1.

[4] Hashmi, M. et.al. 2nd Eur.Conf.on Controlled Fusion and Plasma Phys., Stockholm 1967, paper Wa BI.

[5] Grawe, H. Report IPP 6/61, 1967.

[6] Eckhartt, D. et.al. Report MIP/PAE/PL 6/65.

[7] Ohkawa, T. et.al. Proc.of the Culham Conf. 1965, Vol. II, 531, paper CN 21/115.

[8] Kerst, D.W. et.al. Phys.Fl. 9, 997 (1966).

[9] Simon, A. Ph.Rev. 100, 1557 (1955).

DISCUSSION

J. L. TUCK: In Fig. 3, the two peaks are of unequal height. Is there any asymmetry in the geometry of the apparatus to which this inequality can be related?

F. RAU: As I mentioned in my oral presentation, the device has two independent quadrupoles, and asymmetries in plasma production can lead to preferred filling of one of the two quadrupoles even when the conical spiral is located near the mid-plane of the device.

J. L. TUCK: When you say "recombination of particles at the rings" are you implying something different from "loss to the rings"? Once an ion has reached the rings, it is a loss as regards confinement, whether it chooses to recombine or not.

F. RAU: Of course, there is a sheath near the surface of the rings. By "surface recombination" we simply mean that particles are lost at the surface of solid materials.

S. J. BUCHSBAUM: At the temperatures obtained in your experiment, how did the thickness of the sheath compare with the Larmor radius?

F. RAU: The sheath thickness, which is governed by the Debye length, was about 0.3 mm. This is small compared with the Larmor radius, especially when one bears in mind that the magnetic field is high at the surface of the ring.

F. F. CHEN: Does the toroidal field needed for a tenfold increase in density correspond to that which gives a sufficient pitch of the lines of force for the injected ions to miss the filament on the first turn?

F. RAU: It gives a much larger pitch.

ORNL LEVITATED TOROIDAL MULTIPOLE PROGRAM*

M. ROBERTS, I. ALEXEFF, R. A. DORY, W. HALCHIN AND W. L. STIRLING
OAK RIDGE NATIONAL LABORATORY, OAK RIDGE, TENN.,
UNITED STATES OF AMERICA

Abstract

ORNL LEVITATED TOROIDAL MULTIPOLE PROGRAM. We are studying confinement of gun-injected and microwave-produced plasmas in a levitated toroidal quadrupole in which internal hoop supports are not present to limit plasma confinement. Electromagnetic levitation is made possible by reducing the 60 Hz skin depth in the copper walls with liquid nitrogen cooling. The cooling also increases the magnetic field lifetime so that an e-folding time of 17 ms was measured after crowbarring. Computations indicate that in a properly designed, larger device, an e-folding time of 100 ms can be reached.

Washer-gun hydrogen plasmas and Bostick-type lithium gun plasmas were injected into the levitated quadrupole with typical parameters: $B \geq 3$ kG, $T_e \approx 3$ eV, $n_i \approx 10^9$ cm^{-3}, and $1 < T_i < 30$ eV. The hydrogen plasma lifetime increased as the probe area decreased, and extrapolated to about 30 times Bohm. The longest observed e-folding lifetime was about 1 ms. Surprisingly long-persisting localized fluctuations in the 300 kHz range appear azimuthally opposite the plasma-producing H or Li gun.

Electron-cyclotron resonance (with 40 W at $\lambda = 12$ cm) was used to produce hydrogen plasmas with parameters: $n_i \approx 10^{10}$cm^{-3}, $T_e \approx 30$ eV, and $\tau/\tau_{Bohm} \approx 30$. Density fluctuations ($\Delta n/n$) in the region of good field curvature were less than 0.05 and in the region of bad curvature 0.10-0.25. With the removal of the magnetic well (by removing the inner hoop), τ/τ_{Bohm} and n_i each dropped a factor of 4 and $\Delta n/n$ became greater than 0.25.

Recent experiments using 200 W at $\lambda = 3$ cm have produced plasmas with higher densities ($n > 10^{11}$ cm^{-3} assuming $T_e \approx 100$ eV), higher temperatures ($T_e \approx 100$ eV) and longer lifetimes ($\tau \approx 80$ μs ≈ 40 τ_{Bohm}) than in the $\lambda = 12$ cm experiments. Detailed probe measurements of density and temperature are consistent with models for plasma behaviour based on computed magnetic field plots. Probe data show clear evidence of the changes in heating zones during the variation of the sinusoidal magnetic field and a large obstacle intercepting all flux lines effectively prevents the formation of the plasma.

We are also studying a levitated helical hexapole, whose advantages over the quadrupole are a better ratio of connection length to radius of bad curvature and more confinement volume.

1. INTRODUCTION

An exciting development in fusion physics has been the production of a stable plasma, usable for detailed studies, in the toroidal multipole magnetic field configuration. One important limitation of the toroidal multipole plasma containment experiments of Kerst [1], Ohkawa [2], and Eckhartt [3] is the presence of mechanical supports holding the internal conducting hoops that generate the multipole magnetic field; these supports can be a dominant plasma loss mechanism and apparently effective shielding is not yet possible [4].

One scheme to eliminate these obstacles to the plasma is to use electromagnetic levitation to support the internal conductors. The earlier toroidal multipole experiments [1,2,3] had used octupole configurations (4 hoops) with internal supports; the early levitron [5] experiments utilized levitation but of only a single hoop (dipole).

---

* Research sponsored by the US Atomic Energy Commission under contract with the Union Carbide Corporation.

The ORNL toroidal multipole program is involved with experiments of plasma confinement in two magnetic geometries with levitated internal conductors; the quadrupole and the hexapole.

2. LEVITATION

2.1 Basic Concept

Operation of the quadrupole is accomplished by inducing hoop currents (I_s) and allowing the quadrupole field (ϕ_s) of these hoop currents to induce, in turn, eddy currents (I_e) in the walls surrounding the hoops (see Fig.1). The multipole field then does both the plasma confining and the levitating. If the magnetic pressure of the plasma confining field is transmitted from hoop surface to wall surface, then levitation is achieved when the hoops are sufficiently below the center position so that the force of gravity is equal to the difference in magnetic forces acting on the hoops.

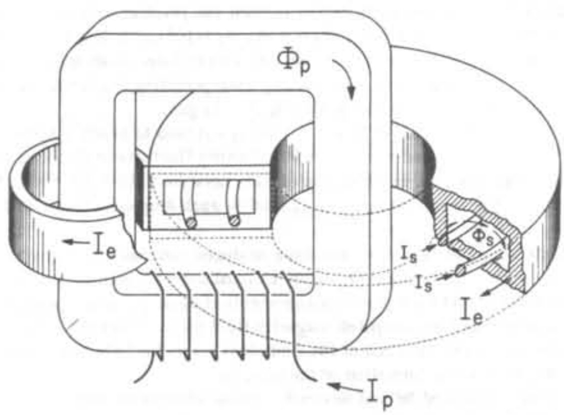

FIG. 1. Schematic drawing of the ORNL levitated toroidal quadrupole showing the primary (I_p), secondary (I_s), and eddy (I_e) currents and the primary (ϕ_p) and secondary (ϕ_s) fluxes.

The extent of the magnetic force at the wall depends on the surface current whose magnitude is a function of the eddy current impedance. For a given frequency and geometry, the eddy currents vary roughly as (resistivity)$^{-1/2}$ which means for copper that a reduction in temperature from +20°C to -190°C reduces the resistivity a factor of 10 and yields a threefold increase in levitation force at the wall, presuming a resistive eddy-current impedance. As the impedance for our quadrupole is resistive at room temperature, cooling the bars as well as the walls results in a generally higher field level at each point in addition to the reduction of the rate of magnetic field diffusion into the walls.

For the wall to carry current in the direction opposite to that for the hoop currents, it must not form a closed loop threading the transformer. A radial cut placed in the copper shell for this reason is oriented to be between the poles of the iron core (see Fig.2) and forces the eddy-current path to include both the inner and outer surfaces of the torus. The path can be shortened, the impedance reduced, and the magnitude of the current increased by placing jumpers around the outer leg of the core connecting the two split edges together. By placing a sufficient number of these connections on the torus, it is possible to reduce the local field errors (at the cut) that would result from local radial currents going to a single point-contact jumper. The bottom half of the quadrupole is shown in Fig.2 with levitated hoops. Without the repulsive forces from the top half, the inner, lighter hoop will rise higher than the outer, heavier hoop.

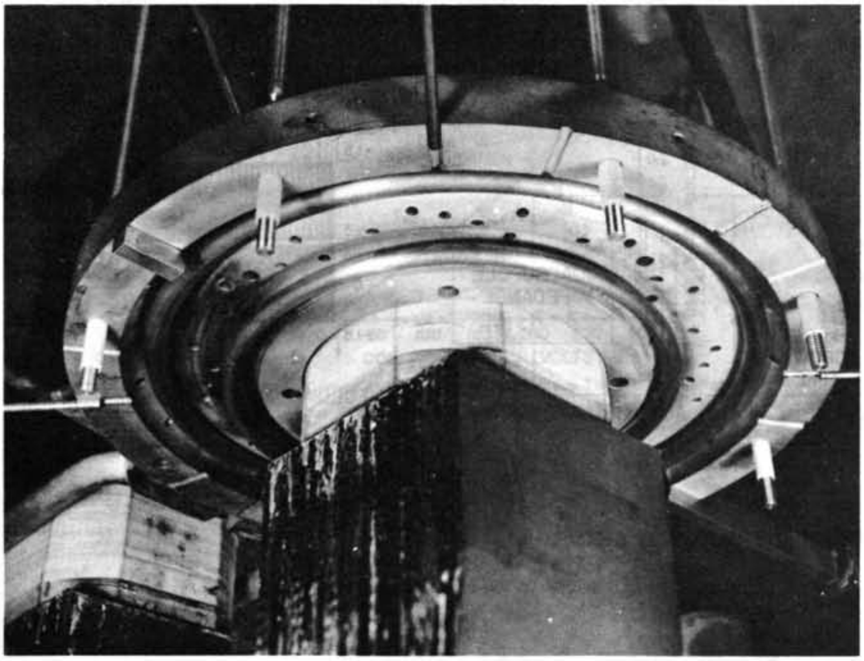

FIG.2. Levitated hoops in the bottom half of the quadrupole.

2.2 Importance of Hoop-Wall Geometry and Cooling

The new effect present when one levitates two hoops rather than a single one (see the early levitron work [5]) is the strong attractive force between the hoops; this force must be balanced by repulsive wall forces acting on both hoops at all other azimuths.

For plane geometry, one could represent the wall currents by image currents within the wall a distance equal to the hoop-to-wall spacing plus the skin depth. With this model, equilibrium occurs for zero skin depth with a hoop-to-wall spacing less than or equal to one-half of the hoop-to-hoop distance. Since the room temperature 60 Hz skin depth is 0.83 cm, the liquid nitrogen 60 Hz skin depth is $10^{-1/2} \times 0.83$ cm, and as the relevant spacings are of order 1-2 centimeters, it should be possible to observe significant changes in the balance of forces as a function of temperature. Using a small test model with a simple rectangular internal cross-section, one does see a dramatic change from no equilibrium to an azimuthally symmetric equilibrium (with slowly growing oscillations) below a temperature of about -100°C.

2.3 Excitation of the Coil and Crowbarring

The quadrupole forms the inductive part of a series resonant circuit (as in Fig.3) that reduces the reactive current drain on the source. Reliance on series resonance also enhances the oscillation of the hoops as the circuit tries to reduce the stored energy. The 17 msec crowbarred magnetic field e-folding time (see Fig.3) is proportional to L/R where L and R are the inductance and resistance of the quadrupole. L scales as the radius and R scales as $f^{-1/2}$ where f is the excitation frequency. Thus by scaling up in linear size three times and scaling down in frequency from 60 Hz to 15 Hz, the e-folding time should be more than 100 msec.

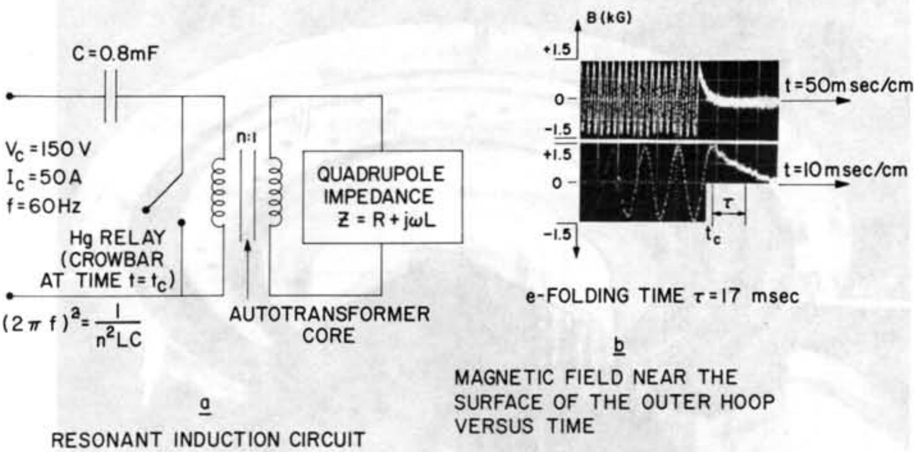

FIG.3. Excitation and crowbarring of magnetic field.

2.4 Core Saturation

In the test model experiments, the entire device (made of copper slabs and a split autotransformer core) was immersed in a liquid nitrogen bath. An equilibrium is possible at the cryogenic temperature with the presence of the liquid required to stabilize the hoops against the weak resonant circuit effects, apparently through viscous damping. Excitation of the core into saturation greatly increased the oscillation amplitude, driving the hoops into the top and bottom of the container in the buildup time shown in Fig.4.

2.5 Vacuum System

Throughout these multipole experiments, a large cylindrical vacuum tank encloses each apparatus being used. In a vacuum tank shaped to fit around or be the torus, it would be necessary to provide multiply-connected, insulated, and cryogenic high-vacuum seals because of the cryogenic temperatures and radial cuts in the torus. Installing the multipole and iron core in the (4 ft diam.) tank allows ease of operation and flexibility to the extent of changing the entire configuration in a short time. Background pressure using a 10-inch diffusion pump and baffle (at -50°C) and the torus cold is $p < 3 \times 10^{-7}$ torr. In addition, the large tank absorbs gas pulses (produced from gun injection) with little pressure rise. Cooling of the hoops in the multipole is accomplished by the use of four steel pins attached to remotely controlled air cylinders that can be lowered, after each operation, to press each hoop against the liquid-nitrogen-cooled torus. The hoops can be cooled from above room temperature to liquid nitrogen temperature in about 15 minutes.

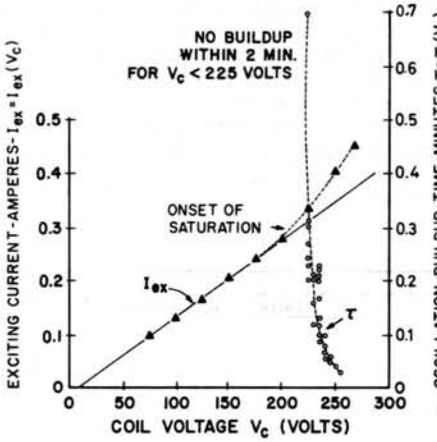

Exciting Current and Hoop-Oscillation Buildup Time vs. Coil Voltage
for Test Quadrupole Immersed in Liquid Nitrogen

FIG. 4. Correlation of hoop oscillation with iron core saturation.

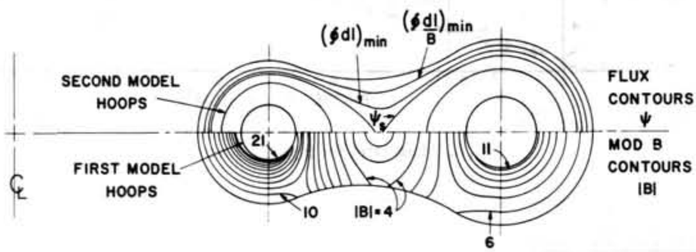

FIG. 5. Computed magnetic field plots.

3. QUADRUPOLE EXPERIMENTS

3.1 Magnetic Flux Properties

The magnetic characteristics of this particular quadrupole were computed [6] for zero skin depth and are described in Fig.5. Nearly 80% of the flux encircling each bar is enclosed within the separatrix. The present bars are shown by the two innermost circles, and the design for new hoops, which would place the separatrix (ψ_s) and its density maximum equidistant from wall and hoop, is also indicated. At present, microwave heating zones (at $\lambda = 12$ cm and $\lambda = 3$ cm) encircle each of the bars (corresponding to $I_s \approx 18$ kA) and with the newer hoops, $\lambda = 3$ cm heating zones will be within the well region.

3.2 Diagnostic Techniques

The principal diagnostic tools have been floating double probes placed at various positions in the cross section and at many azimuthal locations. Inductive current pickups are used to measure probe current thus maintaining electrostatic isolation of the probes from ground. Densities are inferred from the ion saturation current measurements, assuming the ion velocity is given by $v_i = (3kT_e/m_i)^{1/2}$. Time dependent electron temperatures are then obtained from the probe characteristics. The double probe signals are also analyzed to make use of the buildup time, the decay time, and the time dependence of the saturation current. In addition, diagnostic tools include photographic emulsions to detect x-rays, photomultipliers at different cross-sectional locations, and a solid state x-ray counter for time resolved energy measurements.

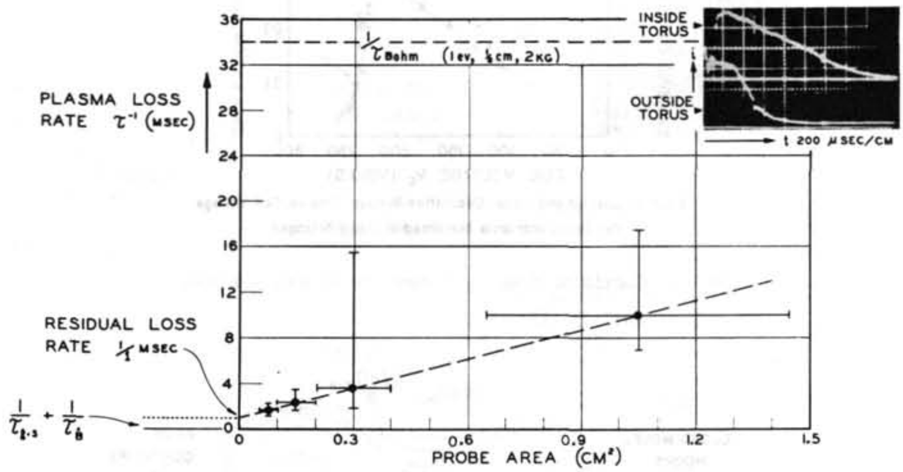

FIG. 6. Loss rates for injected plasmas.

3.3 Warm Ion Plasmas

3.3.1 Lifetime Experiments

Plasma production is accomplished by either a hydrated titanium washer gun or a Bostick-type lithium gun. The use of lithium was prompted by the fact that the charge-exchange cross section for Li^+ on background H_2 or N_2 is less than $10^{-18}cm^2$ [7]. The guns are at different azimuths, but each is located so as to fire directly up toward the field zero and can be triggered to fire at any specified phase of the magnetic field. The principal set of experiments conducted with the injected gun plasmas involve measuring the e-folding decay times as a function of total probe area in the device at peak magnetic field strength. The best measured values for the decay time were on the order of 1 msec; the Bohm diffusion time is calculated to be about 30 microseconds or 1/30 the measured time. The filled-in circles in Fig.6 represent the average values of the decay rates from many events and the spread of values is indicated by the vertical error bars. Uncertainty in the effective area of the probes is the reason for the horizontal spread. The pressure rise in the large vacuum tank, about 400 liters in volume, is up to 6×10^{-6} torr so that the instantaneous neutral pressure in the torus, which has a volume of about 1 liter, could be as high as 10^{-3} torr at the time of firing of the gun; in which case the neutral gas scattering time is of order 1 ms. In addition, the sinusoidal 60 Hz magnetic field has an approximate e-folding time of 3 ms. There is also a diffusion of the magnetic field into the wall which, at a speed 1 mm/ms, would have an effective e-folding time of about 3 ms. In addition, the classical Coulomb scattering time is much greater than 100 times the measured value.

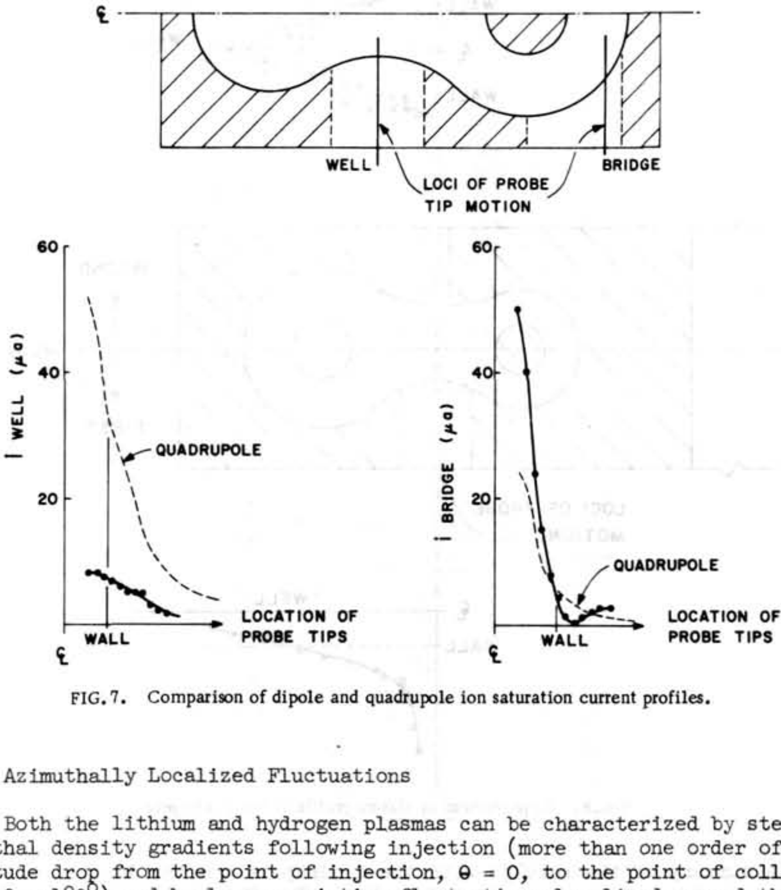

FIG. 7. Comparison of dipole and quadrupole ion saturation current profiles.

3.3.2 Azimuthally Localized Fluctuations

Both the lithium and hydrogen plasmas can be characterized by steep, azimuthal density gradients following injection (more than one order of magnitude drop from the point of injection, $\theta = 0$, to the point of collision, $\theta = 180^{\circ}$) and by long persisting fluctuations localized around the collision point. These results in the levitated toroidal quadrupole [8] demonstrate that long persisting, localized fluctuations do exist in the absence of hoop supports and are indicative of the filling properties of the azimuthally symmetric quadrupole magnetic field.

3.4 Hot Electron Plasmas

3.4.1 Resonant Heating with 40 W of $\lambda = 12$ cm Microwave Power

Since filling is more uniform and production on a specified Mod B surface is possible with microwave heating, we began to use the easily generated electron-cyclotron resonance plasmas in a filling pressure of 8×10^{-5} torr. We have been investigating the effect of the quadrupole magnetic well by removing the inner noop, so we can measure plasma properties with and without the magnetic well, i.e., in a quadrupole and in a dipole. The ion saturation current profiles for plasma in the dipole and for comparison in the quadrupole are presented in Fig.7. Plasma is detected up to and through the wall because there is a large access hole which allows the 1-1/2 kG magnetic field to leak out a considerably long distance. A probe current of 50 μA indicates a density of 10^{10}cm^{-3}, when the ion velocity is taken to be $(3kT_e/m_i)^{1/2}$ with T_e = 30 eV.

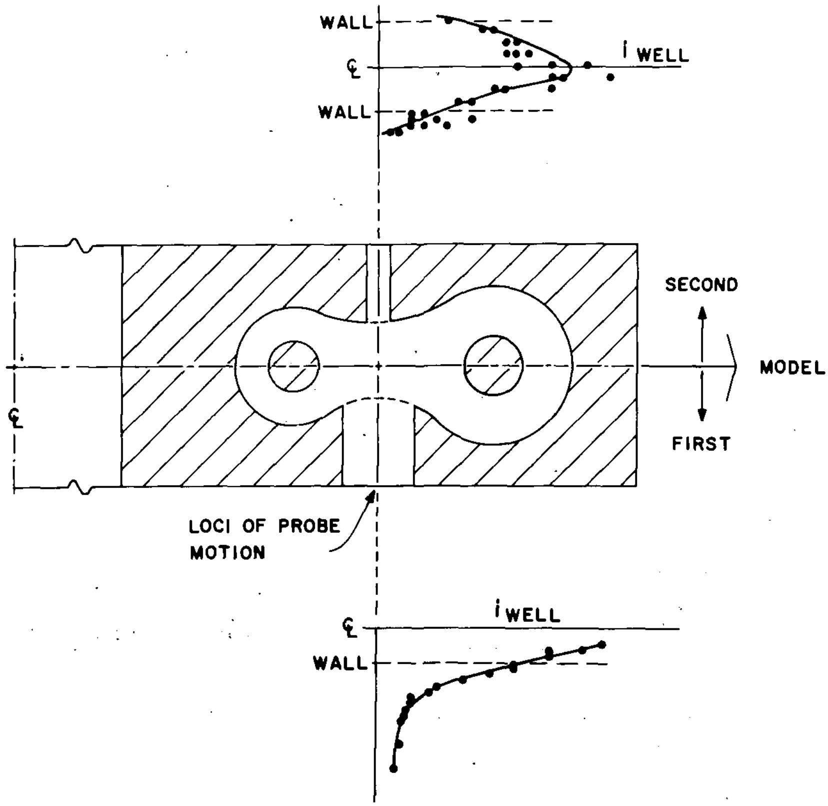

FIG.8. Improvement of plasma profile in the quadrupole.

A summary of the results with the quadrupole and the dipole for the λ = 12 cm hydrogen plasma is listed in Table I. The fluctuation level in the quadrupole is a constant (0.05) in the well region along the probe's line of motion but varies in the bridge region from 0.10 near the center line to 0.25 near the wall, corresponding to the crossing from stable region to unstable region.

A comparison of plasma profiles between two quadrupoles with λ = 12 cm microwave plasma is indicated in Fig.8. The First Model was used for early experiments and the Second Model is presently in use for λ = 3 cm experiments. The differences are two: first the access holes which were 3/4" diam. in the lower case are now 1/4" in the upper case, greatly reducing the leakage of the magnetic field and the plasma; and secondly, the protruding hump in the bottom case has been flattened out considerably in the upper case.

3.4.2 Resonant Heating with 200 W of λ = 3 cm Microwave Power

Hot electron ($T_e \gg T_i$) hydrogen plasmas produced by λ = 3 cm microwave heating are being studied in the levitated toroidal quadrupole. Considerable emphasis has been placed on making a reliable estimate of T_e. Table II summarizes these results.

When resonant microwave heating is pulsed on, the probe current e-folding buildup time is of order 20 μs. From the growth rate $dn_i/dt = n_g n_e \sigma_{ionization} v_{electron}$ and using $n_e = n_i$, σv is about 5×10^{-8} cm^3/sec, the highest value σv can have; this determination gives a lower limit to the electron temperature of order 100 eV.

Table II

Plasma Electron Temperature Determination

A.	X-ray Emulsion Absorption	$\approx$ 1-3 keV
B.	Double Probe Characteristics	> 100 eV
C.	Probe Current Buildup Time	$\gtrsim$ 100 eV
D.	4 Gyroradii Across Flux Bridge	< 3 keV
E.	Incident Microwave Power Fully Used	$\approx$ 0.3-3 keV

Table I

Comparison of λ = 12 cm Microwave Plasmas in Two Magnetic Configurations

		Quadrupole	Dipole
T_e (eV)		30	15
τ (μs)		30	15
τ/τ_{Bohm}		30	8
n (cm^{-3})		$8 \cdot 10^9$	$2 \cdot 10^9$
$\Delta n/n$	well	0.05	>0.25
	bridge	0.10-0.25	>0.25

The characteristic curves on the double probes placed near the heating zones show essentially straight line behavior up to the maximum applied bias voltage of 300 V, implying that T_e > 150 eV. On the left hand curve in Fig.9, it is clear that breakdown is occurring over 200 V. These data were taken with microwave power on; at the microwave turnoff, however, the signal amplitudes do not drop rapidly, but have smooth decays indicating that at least for the first half e-folding time the temperature remains reasonably constant. From the analysis of probe signal decays after microwave turnoff, it is clear that the decay time constant is 80-100 μs in the magnetic well and is over 200 μs in back of the outer bar. The decay measurement is made when the heating takes place at the inner bar, so that the longer decay accompanies the measured lower temperature in the non-resonant zone.

Considering $dE/dt = n_g \sigma_{excitation} v_{electron} \Delta E_{excitation}$, the 80 μs decay of T_e (shown on the right side of Fig.9) is consistent with cooling on the background gas by excitation or ionization processes. In fact, after microwave turnoff, increases in the probe current are frequently measured after a 10-15 μs delay.

The broad band light signals have nearly the same decay time constant as the probe signals do, further corroborating the fact that electrons with $T_e > 13.6$ eV do exist after microwave turnoff. After the initial buildup of light and probe signals, the light flux is constant indicating a constant production rate of plasma particles. Since the current probe signals limit after buildup, this suggests there is an increase in the loss rate at higher densities.

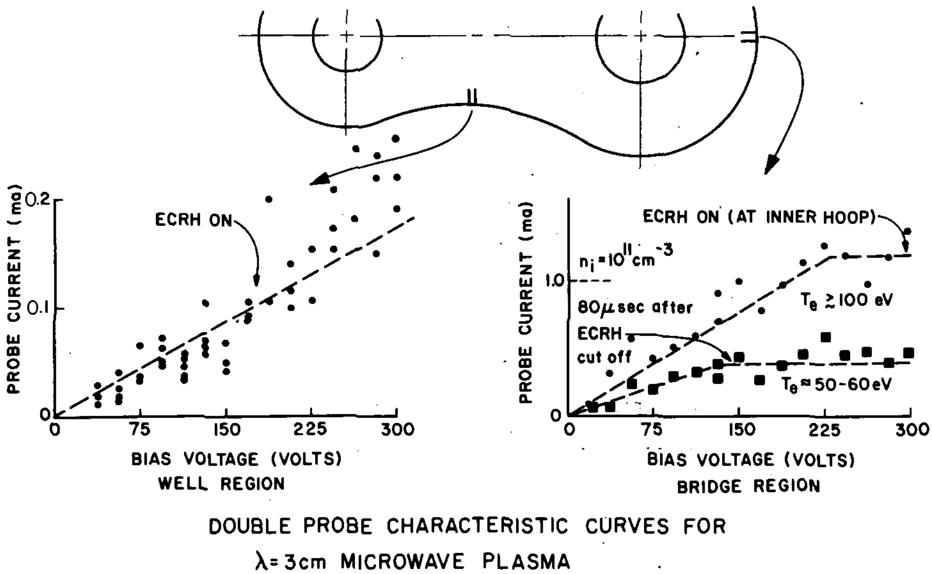

FIG. 9. Electron temperature measurements in the magnetic well and in the flux bridge.

An upper limit to the electron energy can be made by studying the x-ray spectrum using personnel monitoring type x-ray film. In a graded absorption measurement, it was possible to bracket the energy of the x-rays (and, hence, the electrons) causing the image to be on the order of 1-3 kV.

Calculating that all the incident microwave power (≈ 100 W) put into the cavity goes into heating ($n_e \approx 10^{11} cm^{-3}$) plasma electrons (in 40 μs), then an upper limit is placed of order 300 eV, or 3 keV if $n_{e\ hot} = 0.1 n_e$ total.

The final determination of the upper limit is made in terms of the gyroradius of hot electrons. With 1 cm of space between hoop and wall at the bridge and an average of 2 kG magnetic field, 15 keV electrons could have two gyroradii on each side of the separatrix.

These five determinations seem to bracket the electron temperature during the heating and for at least a short time after the heating is off in the range between 100 and 1000 eV. Using the lower, more pessimistic number and the average value for the magnetic flux as determined by Hobbs and Taylor [9], the Bohm time is about 2 μs. Since the decay time is on the order of 80 to 100 μs, the conservative τ/τ_{Bohm} is on the order of 40.

3.4.3 Change in Heating Zone

The computed Mod-B contour plots shown in Fig.5 indicate that as the magnitude of the hoop currents increases there will be a heating zone first encircling the inner bar and then, secondly, an additional zone encircling the outer hoop. The appearance of the second zone comes when the inner hoop resonance zone is near the cavity wall and is essentially confined to a vertical line spaced between the inner hoop and the field zero.

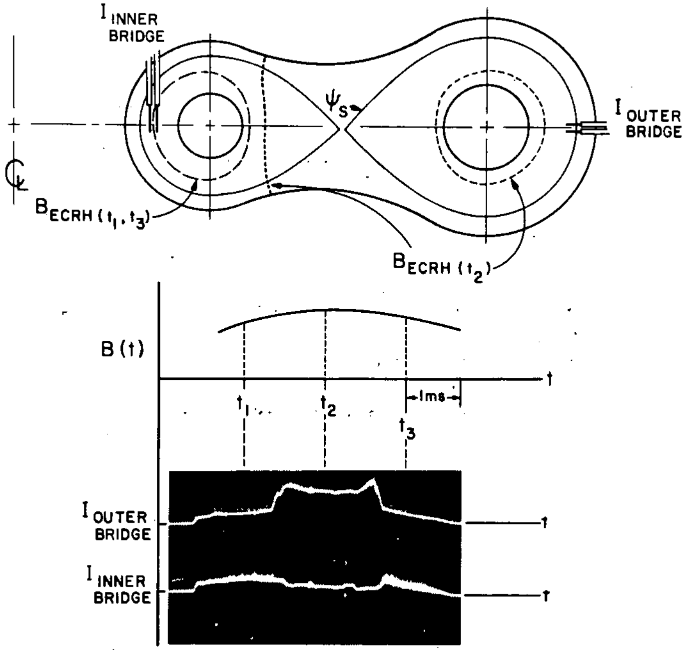

CHANGE OF HEATING ZONES WITH TIME

FIG.10. Probe currents showing the effects of changing the microwave resonance zones.

Fig.10 illustrates the positions of the heating zones and a clear example of the plasma signals in each of the bridge regions appearing out of phase with each other. A probe in the magnetic well region seems to indicate an average (or sum) of the two outer probes, plus transients at the times of heating zone change.

Light signals were measured in the well region and in a bridge region. As the magnetic field varied, the light in the well region took on the same shape as the well probe. The outer bridge light occurred only when the heating zone was encircling the outer bar.

Thus, it appears that a probe in each of the resonance regions (within the separatrix) sees mostly that plasma contained on the self flux. The two regions are connected, however, by the 20% mutual flux, and current from the plasma in the neighboring bar's zone does appear on the probe curves as a smaller signal. The time constant for the density in the outer heating zone to drop when the heating zone vanishes into the bar is on the same order of magnitude as the decay time when the microwave power is pulsed off.

Statistical evidence from x-ray films exposed to various (upper) parts of the cross section at many azimuths indicates that most of the x-ray production is in the region directly above and to each side of the bars but not in the center, the magnetic well region. This implies that the hot electrons are confined to the resonance zones and produce x-rays there.

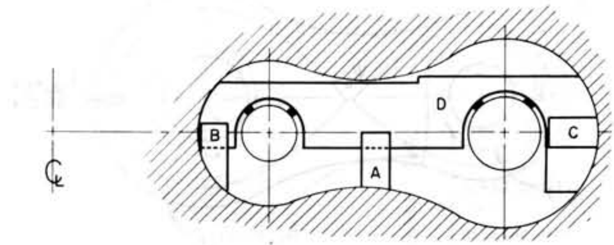

EFFECT OF VARIOUS OBSTACLES ON $\lambda = 3$ cm MICROWAVE PLASMA

A. Little effect

B + (C) Alters production rate locally:

$$\text{at probe}\left\{\begin{array}{l}< 1\text{cm}\\ \approx 3\text{cm}\\ = 8\text{cm}\end{array}\right\}\text{ from obstacle, probe current is }\left\{\begin{array}{l}\text{decreased}\\ \text{increased}\\ \text{unchanged}\end{array}\right\}$$

D. Prevents formation of plasma

FIG. 11. Different conducting obstacles placed in the magnetic field.

3.4.4 Fluctuations

The fluctuation amplitude appears to accompany the heating zone, i.e., the outer bridge probe shows high frequency noise when a heating zone encircles the outer bar and not when it is around the inner bar and vice versa for the probe around the inner bridge (see probe currents in Fig.10).

3.4.5 Obstacle Experiments in the Microwave Generated Plasma

With a 1/4" diam. bar or obstacle located at B (Fig.11) the current signal on a fixed position double probe placed directly above the obstacle was measured as a function of the bar's vertical position. Resonance heating was taking place around the inner hoop when the microwave power was cut off, and the probe amplitude readings were normalized with respect to another probe placed in the wall 105° in azimuth away minimizing the effects of shot-to-shot fluctuations.

There is no significant decrease in plasma lifetime caused by the introduction of the obstacles at B or C. This implies that the presence of the bar is affecting only the plasma production rate or the microwave field pattern as manifested by the steady state current amplitude and not the loss rate as determined from the plasma lifetime. Since this effect is strongest in the immediate vicinity of the bar, one concludes that the production by microwave resonance is a local phenomenon occurring uniformly around the machine.

As a second experiment, a similar bar (C) was pushed in to touch the outer hoop as a dummy support. Once more the effect of the bar on the steady-state amplitude was maximum in the neighborhood of the disturbance.

A 1 cm thick conducting obstacle (insulated from the hoops) shown as D in Fig.11 was placed 180° from the microwave port and 90° from a set of probes. The plasma is prevented from forming and then forms alternately with the frequency of vibration of the hoops ($f_v \approx 16$ Hz) as the hoops are and are not touching the obstacle. With the obstacle cutting all flux lines, the plasma-forming hot electrons can live at most one or two machine transits, a time (a few microseconds) that is less than the exponentiation buildup time (40-50 μs).

Another, even more drastic, step with even clearer results is the experiment performed by pressing the hoops against the bottom of the cavity with the resonance field energized. No plasma is detected on any probes in this case.

4. HELICAL HEXAPOLE

In addition to the levitated toroidal quadrupole, another device, the levitated helical hexapole is also under study. The helical hexapole (Fig. 12) is structurally a single piece although at any radial cross section it appears to be a conventional hexapole configuration (the other three "poles" carrying the return currents are in a continuous copper wall (not shown) surrounding the three conductors). This device has the advantage over the quadrupole of a better ratio of connection length to

FIG. 12. The helical hexapole (made from a 1-in diam. copper bar).

radius of bad curvature and more confinement volume; the built-in shear will require the addition of an external toroidal field for comparison purposes. It is necessary to design the hexapole to withstand the magnetic compression forces by its torsional strength; the present structure having 1-1/2" diam. copper tubes of 0.3" wall thickness (work hardened) with 21" mean major diam. appears to be sufficiently strong for preliminary investigation and has been levitated.

5. SUMMARY

Electromagnetic levitation of a toroidal quadrupole is being used to study various types of plasmas in the absence of hoop supports. Levitation is made possible when the quadrupole is liquid-nitrogen cooled to reduce the skin depth below the size of the relevant hoop-to-wall spacings.

The experiments with a gun injected hydrogen plasma show that the loss rate of the sampled plasma was linearly proportional to the area of the measuring probe. In addition, gun plasma experiments showed the peculiar nature of the axisymmetric quadrupole magnetic field itself (without hoop supports) during the filling process in which localized fluctuations persisted at the collision point for the duration of the experiment.

The introduction of low power $\lambda = 12$ cm microwave fields into the quadrupole facilitated the direct comparison of a quadrupole and a dipole, showing that the magnetic well reduced the fluctuation level and resulted in both a higher temperature and density, as well as a longer decay time.

With higher power $\lambda = 3$ cm microwave fields available, the electron temperature was increased to between 100 eV and 1000 eV. The observed heating of the electrons is consistent with expectations based on the computed flux plots and the observed behavior of the plasmas in the presence of the obstacles is also consistent with a two-component electron plasma - one, the hot electrons in and near the heating zones and two, those electrons less than 100 eV away from the heating zones. The drift time around the machine for this second component is comparable to the observed lifetime so that this component would not be affected by the presence of obstacles.

We are continuing these experiments with emphasis on measuring hoop support effects, the comparison between the two ratios of mutual-to-self flux in two quadrupoles and the comparison between hexapole and quadrupole plasmas.

REFERENCES

[1] DORY, R.A. et al., Phys. Fluids 9 997 (1966).
[2] OHKAWA, T. et al., Plasma Physics and Controlled Nuclear Fusion Research (IAEA, Vienna, 1966) Vol. II, p.531.
[3] ECKHARTT, D. et al., Plasma Physics and Controlled Nuclear Fusion Research (IAEA, Vienna, 1966) Vol. II, p.719.
[4] FORSEN, H.K. et al., Bull. Am. Phys. Soc. 13 266 (1968).
[5] COLGATE, S.A. and FURTH, H.P., UCRL-5392 (1958) Lawrence Radiation Lab., Livermore, California.
[6] We would like to acknowledge the help of G. D. Hobbs and Culham Laboratory in providing the magnetic field computations.
[7] McNALLY, J.R., Jr., ORNL-4063 (1966) p.60, Oak Ridge National Laboratory, Oak Ridge, Tennessee - to be published.
[8] ROBERTS, M. et al., Physics Letters 26A 590 (1968).
[9] HOBBS, G.D. and TAYLOR, J.B., Plasma Physics 10 207 (1968).

DISCUSSION

F.F. CHEN: How did you compute the Bohm time?

M. ROBERTS: We used the integral properties of the magnetic field in the manner prescribed by Hobbs and Taylor in Plasma Physics 10 (1968) 207.

A.F. KUCKES: Are your microwave-generated plasmas fully ionized? If not, how do you reconcile your electron temperature of several hundred electron volts with a plasma rise time of 25 μs? I think the ionization time must be much shorter for this electron temperature.

M. ROBERTS: The plasma density is about equal to the neutral density. Our calculations, based on $\sigma v = 5 \times 10^{-8}$ cm^3/s, show that the build-up time of 25 μs is consistent with an electron temperature of 100 eV.

P.L. HUBERT: Could your helical hexapole be made force-free by appropriate contouring of the outer chamber, in a manner similar to that proposed for the University of Wisconsin's octopole?

M. ROBERTS: At present, we are using the torsional strength of the copper hoops to balance the magnetic forces, but on a larger scale we would probably have to contour the walls.

LOW-FREQUENCY STABILITY OF AXISYMMETRIC TORUSES

P. RUTHERFORD, M. ROSENBLUTH,† W. HORTON,† E. FRIEMAN AND B. COPPI†
PLASMA PHYSICS LABORATORY, PRINCETON UNIVERSITY,
PRINCETON, N.J., UNITED STATES OF AMERICA

Abstract

LOW-FREQUENCY STABILITY OF AXISYMMETRIC TORUSES. The low-frequency stability of low-β collisionless plasma in axisymmetric toroidal configurations such as multipoles with and without applied toroidal fields is studied in some detail. Defining the "bounce" frequency $\omega_b = (\int d\ell/v_\parallel)^{-1}$ modes are investigated with $\omega > \omega_{be}$, $\omega_{bi} < \omega < \omega_{be}$, and $\omega < \omega_{bi}$. Three classes are found: (1) flute modes, (2) ballooning and drift modes, and (3) trapped particle modes.

Stability of the flutes requires, without a toroidal field, favourable $\int d\ell/B$, and with a toroidal field a new generalization of the V" criterion. Even with these criteria satisfied residual flute instabilities occur depending on resonant particle effects. Two modes are found: an electron flute with $\omega/\omega_{*e} > 0$ destabilized if $\omega_{bi} < \omega < \omega_{be}$ by electron resonances provided $T_i/T_e < L^2/rR$, and an ion flute with $\omega/\omega_{*i} > 0$ destabilized if $\omega \lesssim \omega_{bi}$ by ion resonances requiring finite Debye length and $k_\perp^2 \lambda_{Di}^2 > (1 + T_e/T_i)r/\bar{R}$, though having an exponentially small growth rate if $(1 + T_e/T_i)\, 4\pi\rho c^2/B^2 > r\bar{R}/L^2$. Here $\omega_{*i,e}$ are the diamagnetic drift frequencies, r the density scale length, R the average radius of curvature, and L the connection length.

For systems unstable to the generalized V" criterion, the residual ion instability occurs at all densities and is insensitive to shear. Slight anisotropy or temperature gradient also affects the stability of the residual ion flute, but quasi-linear calculations indicate that the non-linear formation of a sufficient stabilizing anisotropy is slow.

The drift ballooning mode local to a bad curvature region and the drift universal mode are unstable for $\omega_{bi} < \omega < \omega_{be}$ provided $T_i/T_e < L^2/rR$ and $T_i/T_e < L/r$, respectively. An eikonal procedure provides the effect of shear on the ballooning mode including geodesic curvature.

Trapped particle models have $\omega < \omega_{bi}$. Curvature-driven modes, insensitive to shear but stable in maximum-J configurations, are also stabilized if r/R is not too small, and criteria are given but can be very restrictive. For large $k_\perp$ a new overstable mode relatively insensitive to shear, independent of curvature, and not involving resonant particles is found requiring terms of order $(\omega/\omega_{bi})^2$ and $k_\perp^2 a_i^2$, where a_i is the ion Larmor radius: instability occurs if $k_\perp^2 a_i^2 > (1 + T_i/T_e)r/L$.

1. INTRODUCTION

This paper treats low-frequency instabilities of low-β collisionless plasmas magnetically confined in axisymmetric toroidal configurations, particularly multipoles, both with and without toroidal field. The analysis is based on the Vlasov equation solved in this geometry for perturbations with perpendicular wavelengths permitted to be of the order of the Larmor radius. The magnetic field strength is allowed to vary finitely along the field so that trapped-particle effects are included. Only electrostatic modes are considered, but the theory includes the interchange or flute modes, drift modes, and trapped-particle modes.

The analysis with only a poloidal field is presented in some detail in Sec. II. Defining the "bounce" frequency $\omega_b \sim v_T/L$ for each

---

† Also Institute for Advanced Study, Princeton, New Jersey.

species, the discussion of the instabilities is divided into three regimes, namely, $\omega < \omega_{bi}$, $\omega_{bi} < \omega < \omega_{be}$, and $\omega > \omega_{be}$. In Sec. III some results on the effect of a toroidal field and the associated shear are presented; limitations of space do not permit a detailed discussion of this case. In Sec. IV the main results and conclusions are summarized.

2. POLOIDAL FIELD ONLY

The equilibrium axisymmetric poloidal vacuum magnetic field may be written

$$\vec{B} = \nabla\chi = \nabla\psi \times \nabla\theta \tag{1}$$

thus defining an orthogonal set of spatial coordinates (ψ, θ, χ), ψ being the magnetic flux and θ the angle about the axis of symmetry. For velocity space coordinates, we use the energy and magnetic moment per unit mass, namely,

$$\varepsilon = v^2/2 + e\phi/m \quad , \quad \mu = v_\perp^2/2B$$

together with a coordinate ζ denoting the azimuthal angle of the velocity vector about the field line. In terms of these coordinates, the parallel velocity is

$$q = [2(\varepsilon - \mu B - e\phi/m)]^{1/2}$$

and the volume element in velocity space is $d^3v = Bd\mu d\varepsilon d\zeta/q$, contributions from positive and negative parallel velocities being added. The equilibrium is assumed to vary on a scale r much larger than a Larmor radius a, and to lowest order in a/r the equilibrium distribution function is $F = F(\varepsilon, \mu, \psi)$ which will normally be taken to be Maxwellian, i.e., $F = N(\psi)\, F^M(\varepsilon) = N(\psi)\,(2\pi v_T^2)^{-3/2} \exp(-\varepsilon/v_T^2)$, without temperature gradient or equilibrium electric potential. Perturbations are Fourier analyzed, e.g., for the perturbed electric potential

$$\phi = \phi(\psi, \chi)\, \exp(-i\omega t + i\ell\theta)$$

but, except in treating the shear problem in Sec. II, the ψ dependence of the eigenfunctions is neglected (local analysis). Frequencies ω are assumed to be much less than a gyro-frequency Ω, but perpendicular wavelengths $k_\perp^{-1}$ may be of order a gyro-radius a; specifically we treat the case where

$$\frac{\omega}{\Omega} \sim \frac{a}{r} \sim k_\parallel a \sim \epsilon, \quad k_\perp a \sim 1 \tag{2}$$

All the usual low-frequency modes, namely, interchange or flute modes, drift waves, and trapped-particle modes, may be recovered in limiting cases of this ordering. A formal treatment of such perturbations in a general magnetic field configuration has recently been presented [1]: the Vlasov equation for the perturbed distribution f is solved iteratively using the ordering (2), and for the lowest-order distribution averaged over the azimuthal velocity angle ζ we obtain an expression

$$\langle f\rangle_\zeta = \frac{e}{m}\,\phi\left[\frac{\partial F}{\partial \varepsilon} + \left(1-J_o^2\right)\frac{\partial F}{B\partial\mu}\right]$$

$$-\frac{e}{m}\left(\frac{\partial F}{\partial \varepsilon} + \frac{\ell m}{e\omega}\frac{\partial F}{\partial \psi}\right)J_o H \qquad (3)$$

Here $J_o = J_o(\ell v_\perp/R_o\Omega)$ where R_o is the major radius, and the quantity H is given by an orbit integral taken along a guiding-center orbit, namely,

$$H = -i\omega\int^t J_o\phi\,dt' \qquad (4)$$

satisfying the equation

$$\left(\omega - \omega_D \pm iq\frac{\partial}{\partial s}\right) H = \omega J_o\phi \qquad (5)$$

where s is the length along a field line, $ds = d\chi/B$, and ω_D is a frequency formed from the particle gradient and curvature drifts, namely,

$$\omega_D = \frac{\ell m}{eB}\,(2\varepsilon - \mu B)\left.\frac{\partial B}{\partial\psi}\right|_\chi \qquad (6)$$

A rigorous derivation of Eqs. (3) and (5) has been given in Ref. [1] and limitations of space prohibit its reproduction here. However, an intuitive derivation may be given based on guiding-center orbit theory. The first term in Eq. (3) clearly arises from the transformation to the total energy ε as a variable; the third (orbit integral) term arises from the perturbations $\delta\varepsilon$ and $\delta\psi$ accumulated following the particle orbit. The energy changes according to

$$\frac{d\varepsilon}{dt} = \frac{e}{m}\frac{\partial\langle\phi\rangle}{\partial t}$$

and the guiding-center orbit is determined by

$$\frac{d\psi}{dt} = -\frac{\partial\langle\phi\rangle}{\partial\theta}\,,\quad \frac{d\theta}{dt} = \vec{v}_D\cdot\nabla\theta + \frac{\partial\langle\phi\rangle}{\partial\psi}\,,\quad \frac{ds}{dt} = q$$

the terms in $\langle\phi\rangle$ on the right being the electric drift terms expressed in the ψ, θ coordinate system. Here the expression $\langle\phi\rangle$ denotes the average potential seen by a particle in its gyration about a guiding center at θ_{GC}, i.e.,

$$\langle\phi\rangle = \langle\phi(\theta_{GC} - \vec{v}\times\vec{B}\cdot\nabla\theta/\Omega B)\rangle$$

$$= \phi_{GC}\langle\exp(+i\ell v_\perp\cos\Omega t/R_o\Omega)\rangle_t = J_o\phi_{GC}$$

Integrating along guiding-center orbits we obtain expressions for the changes $\delta\varepsilon$ and $\delta\psi$, and hence an expression for the perturbed guiding-center distribution, namely,

$$f_{GC} = - \delta\varepsilon \frac{\partial F}{\partial \varepsilon} - \delta\psi \frac{\partial F}{\partial \psi}$$

$$= -\frac{e}{m}\left(\frac{\partial F}{\partial \varepsilon} + \frac{\ell m}{e\omega}\frac{\partial F}{\partial \psi}\right) H$$

where H is as given in Eq. (4); furthermore, we have

$$\langle f \rangle_\zeta = \langle f_{GC}(\theta + \vec{v}\times \vec{B}\cdot\nabla\theta/\Omega B)\rangle_\zeta$$

$$= f_{GC}\langle \exp(i\ell v_\perp \cos\zeta/R_o\Omega)\rangle_\zeta = J_o f_{GC}$$

which completes the derivation of the orbit integral term in Eq. (3). The term in $\partial F/\partial\mu$ in Eq. (3) arises naturally in the formal theory [1] but is difficult to obtain intuitively; it expresses the constancy of a generalized μ invariant [2], namely,

$$\mu + \frac{e}{mB}\,(\phi - \langle\phi\rangle)$$

For a Maxwellian distribution without temperature gradient, Eq. (3) reduces to

$$\langle f \rangle = -\frac{eF}{T}\left[\phi - \left(1 - \frac{\omega_*}{\omega}\right) J_o H\right] \tag{7}$$

where

$$\omega_* = \frac{\ell T}{Ne}\frac{dN}{d\psi}$$

is the diamagnetic drift frequency. The perturbed distributions $\langle f \rangle$ are to be substituted into the Poisson equation

$$8\pi^2 \sum e \int B d\mu d\varepsilon \langle f \rangle / q = \ell^2 \phi / R_o^2 \simeq 0 \tag{8}$$

usually in the latter approximate form (quasi-neutrality). The difficulty lies in Eq. (5) where solution involves a complicated orbit integral along the field. We consider two limiting cases for which simple solutions may be obtained, namely, $\omega < \omega_b$ and $\omega > \omega_b$.

For $\omega < \omega_b$ we have to lowest order $\partial H/\partial s = 0$, i.e., H = constant, this constant being determined by the requirement that the next-order term in H be periodic over the closed orbit; dividing by q and integrating around we obtain the solution to lowest order in ω/ω_b, namely,

$$H = \frac{\overline{J_o\phi}}{1-\overline{\omega}_D/\omega} \simeq \overline{J_o\phi} \left(1 + \frac{\overline{\omega}_D}{\omega}\right) \tag{9}$$

where $\overline{J_o\phi}$ and $\overline{\omega}_D$ denote time averages along the orbit, e.g.,

$$\bar{\phi} = \oint \frac{\phi ds}{q} \Big/ \oint \frac{ds}{q}$$

the second form of Eq. (9) being for $\omega_D < \omega$. Using Eq. (6) it may easily be shown that

$$\overline{\omega}_D = -\frac{\ell m}{e} \left(\frac{\partial}{\partial\psi} \oint q ds\right) \Big/ \oint \frac{ds}{q} \tag{10}$$

Certain instabilities depend on corrections to this lowest-order solution of Eq. (5) and these may be calculated by iteration. Terms of first order in ω/ω_b clearly cancel in the velocity space integration (summing over $\pm$ contributions); the second-order term in the solution for H is found to be (for untrapped particles, with a slightly different form for trapped particles)

$$H^{(2)} = \omega^2 \left(\int^s \frac{ds'}{q'} - \frac{1}{\oint ds/q} \oint \frac{ds}{q} \int^s \frac{ds'}{q'}\right)^2 (\phi - \bar{\phi})$$

where we have neglected ω_D and set $J_o = 1$, both approximations being valid in cases where this term is employed. A more convenient form of the solution results from a Fourier analysis in a variable

$$t = \int^s ds/q$$

over the period $\tau = 2\pi/\omega_b = \oint ds/q$. Writing

$$\left.\begin{matrix}\phi \\ H\end{matrix}\right\} = \sum \begin{Bmatrix}\phi_n \\ H_n\end{Bmatrix} e^{2\pi int/\tau}$$

we obtain immediately from Eq. (5) the solution $H_n = \omega\tau\phi_n/(\omega\tau \mp 2\pi n)$, and to second order

$$H_n^{(2)} = -\frac{\omega^2\tau^2}{(2\pi n)^2} \phi_n \tag{11}$$

For $\omega > \omega_b$ a solution of Eq. (5) may easily be obtained by iterations, treating the derivative term as small; keeping terms of first order in ω/ω_D and terms of second order in the derivatives (the first-order terms cancel in the velocity space integration, summing over $\pm$) we obtain

$$H = J_o\phi + \frac{\omega_D}{\omega} J_o\phi \mp \frac{iq}{\omega} \frac{\partial J_o\phi}{\partial s} - \frac{q}{\omega}\frac{\partial}{\partial s}\left(\frac{q}{\omega} \frac{\partial J_o\phi}{\partial s}\right) \tag{12}$$

Even if one or the other of the approximate solutions (9) and (12) is valid for the majority of the particles of one species, there will be certain particles, in particular resonant particles, for which the approximate solution fails. These resonant particles give rise to Landau damping or growth; instabilities which depend on them will be termed residual. Treating all such resonance terms as small, the growth rate of a residual instability may be evaluated by standard perturbation methods. Defining linear operators L and R by

$$\left.\begin{matrix} L(\omega) \\ R(\omega) \end{matrix}\right\} \phi = \sum e \int \frac{d\mu d\varepsilon}{q} \begin{cases} \langle f \rangle & \text{non-resonant} \\ \langle f \rangle & \text{resonant} \end{cases}$$

the quasi-neutrality condition (8) is $L(\omega)\phi + R(\omega)\phi = 0$. It will be found that for both of the approximations (9) and (12) the expression $\int \phi^* L\phi ds$ is real for real ω, so that the growth rate γ is given by

$$\gamma \int \phi^* \frac{dL}{d\omega} \phi ds = - \operatorname{Im} \int \phi^* R\phi ds$$

The expression on the right may be calculated by solving Eq. (5) exactly (integrating along field lines using an integrating factor [1]); alternatively, the method of Fourier analysis described above may be used. We obtain

$$\operatorname{Im} \int \phi^* R\phi ds = - \pi \sum \frac{e^2}{T} (\omega - \omega_*) \int F\tau d\mu d\varepsilon \cdot \sum_n \delta(\omega - \bar{\omega}_D - n\omega_b) \left|\overline{J_o\phi I}\right|^2 \tag{13}$$

with $\tau = 2\pi/\omega_b = \oint ds/q$, and where $I = \exp(\pm i \int^s (\omega - \omega_D) ds/q$ for untrapped particles and $I = \cos \int_{s_o} (\omega - \omega_D) ds/q$ for trapped particles with turning point s_o. This expression is a sum of terms representing resonances between $\omega - \bar{\omega}_D$ and harmonics of the "bounce" frequency ω_b. Often ω is much larger than the drift frequency ω_D for a typical thermal particle so that the n = 0 term is exponentially small, arising only from high-energy particles with large ω_D. Similarly, if ω is much larger than a typical ω_b the $n \neq 0$ terms are also exponentially small, again arising from high-energy particles. Thus the largest resonances occur if $\omega < \omega_b$; here the first few terms n = 1, 2, ... dominate and a contribution of order $(\omega/\omega_b)^3$ is found. This contrasts with the well-known result for a straight uniform field where for small phase velocities resonance terms of order ω/kv_T arise; the different orders of magnitude arise from the different volumes of velocity phase space involved in the resonance: here we require small ω_b and hence small energy, whereas for a uniform field we require merely small parallel velocity. Clearly the result that the resonant terms are of order $(\omega/\omega_b)^3$ is related to the existence of the non-divergent non-resonant term of order $(\omega/\omega_b)^2$ calculated above; the velocity space integral of this term diverges for a uniform field. At this point we may note that the sign of the resonance terms for one species is entirely determined by the sign of the factor $\omega - \omega_*$; hence instability conditions may be inferred without investigating the detailed structure of the resonances, provided the dangerous species can be identified.

2.1 The case $\omega < \omega_{bi}$

Here we use the approximate solution (9) for both ions and electrons. A real quadratic form (which may be used as a variational principle at least for real ω) is obtained by multiplying the charge neutrality condition (8) by ϕ/B and integrating over s, giving

$$\sum \frac{1}{T} \int F\tau \, d\mu d\varepsilon \left(\overline{\phi^2} - \frac{\omega - \omega_*}{\omega - \bar{\omega}_D} \overline{J_o \phi}^2 \right) = 0 \tag{14}$$

Assuming $\omega > \omega_D$, expanding $J_o = 1 - b/2$ where $b = \ell^2 v_\perp^2 / 2R_o^2 \Omega^2$, and keeping terms of order ω_D/ω and of order b, we have

$$\sum \frac{1}{T} \int F\tau d\mu d\varepsilon \left[\overline{\phi^2} - \bar{\phi}^2 + \left(1 - \frac{\omega_*}{\omega}\right) \overline{\phi b \phi} + \frac{\omega_* \bar{\omega}_D}{\omega^2} \bar{\phi}^2 \right] = 0 \tag{15}$$

The contribution from terms of order $(\omega/\omega_b)^2$ to the quadratic form may be obtained from the solution for $H^{(2)}$ given in Eq. (11). We obtain a contribution

$$\sum \frac{\omega^2}{T} \left(1 - \frac{\omega_*}{\omega}\right) \int F\tau d\mu d\varepsilon \sum_n \frac{\tau^2 |\phi_n|^2}{(2\pi n)^2} \tag{16}$$

and, inverting the Fourier transforms,

$$\sum \frac{\tau^2 |\phi_n|^2}{(2\pi n)^2} = \oint \oint dt\, dt' \, \phi(t) \, \phi(t') \sum_n \frac{1}{(2\pi n)^2} e^{-2\pi i n (t-t')/\tau}$$

$$= \oint \oint dt\, dt' \, \phi(t) \, \phi(t') \left[\frac{1}{12} - \frac{|t-t'|}{2\tau} + \frac{(t-t')^2}{2\tau^2} \right]$$

$$= \int \int \frac{ds}{q} \frac{ds'}{q'} \phi(s) \, \phi(s') \, K(s, s') \tag{17}$$

where for the untrapped particles we have

$$K(s, s') = \frac{1}{12} - \frac{1}{2\tau} |t - t'| + \frac{1}{2\tau^2} (t - t')^2 \tag{18}$$

and for the trapped particles (the s, s' integrations in Eq. (17) by convention being taken only one way between the turning points)

$$K(s, s') = \frac{1}{3} - \frac{1}{\tau} (|t - t'| + t + t') + \frac{2}{\tau^2} (t^2 + t'^2) \tag{19}$$

where $t = \int_{s_o}^{s} ds/q$ (with s_o a turning point for trapped particles). The kernels $K(s, s')$ are positive definite.

2.1.1 The ion flute instability

If $\omega \sim \omega_* > \omega_D$, the largest term on the left in Eq. (15) is

$$\sum \frac{1}{T} \int F\tau d\mu d\varepsilon \, (\overline{\phi^2} - \bar{\phi}^2) \tag{20}$$

which is always positive by the Schwartz inequality except for $\phi = \bar{\phi} =$ constant, which is therefore the lowest-order solution for the eigenfunction, i.e., a flute mode. The dispersion relation may be found by keeping correction terms of order ω_D/ω and terms of order b (for the ions), and putting ϕ = constant in these correction terms. Varying (15) with respect to ϕ, integrating the resulting equation over s, and performing the velocity space integrations we obtain a dispersion relation

$$\left(1 - \frac{\omega_{*i}}{\omega}\right) \langle b_i \rangle + \frac{\omega_{*i}^2}{\omega^2} \left(1 + \frac{T_e}{T_i}\right) \langle \kappa \rangle = 0 \tag{21}$$

where $b_i = \ell^2 v_{T_i}^2 / R_o^2 \Omega_i^2$, $\langle \cdot \rangle$ denotes an average over s, i.e., $\langle b \rangle \int ds/B = \int b ds/B$, and $-\langle \kappa \rangle$ is the average favorable curvature, i.e., $-\langle \kappa \rangle \int ds/B = (d/d\ell nN) \int ds/B$. Equation (21) has two real roots of opposite signs. In this regime, namely, $\omega < \omega_{bi}$, the largest resonances are the terms like $(\omega/\omega_b)^3$ from the ions. Employing the perturbation technique described above we find that for these to be destabilizing we require $0 < \omega/\omega_{*i} < 1$, and clearly (21) does not have such a root. However, if the Poisson equation rather than quasi-neutrality is used (i.e., finite Debye length terms included) there is a further term on the left in (21), namely, $\langle d_i \rangle$, where $d_i = \ell^2 \lambda_{Di}^2 / R_o^2 \Omega_i^2$, and this term can lead to a residual instability. The condition for instability can be found from the marginal case where $\omega = \omega_{*i}$ and is

$$\langle d_i \rangle > - \left(1 + \frac{T_e}{T_i}\right) \langle \kappa \rangle \, . \tag{22}$$

Unless the density is very low, this condition is satisfied only for very short perpendicular wavelengths (large ℓ). The condition that $\omega < \omega_{bi}$ at the marginal case $\omega = \omega_{*i}$ for perpendicular wavelengths short enough to satisfy (22) requires

$$\frac{B^2}{4\pi N M_i c^2} > \left(1 + \frac{T_e}{T_i}\right) \frac{L^2}{r\bar{R}} \tag{23}$$

where r is the density scale length, L a typical connection length along the field ($\omega_b \sim v_T/L$), and $\bar{R} \sim -\langle \kappa \rangle^{-1}$. If (23) is violated the instability will have $\omega > \omega_{bi}$, and hence an exponentially small growth rate. Inspection of the quadratic form (14) for $J_o \sim 1$ shows that, provided $T_e < T_i$ and $|\omega| > |\omega_{*e}|$, flute modes of this type may exist even for $b_i \gtrsim 1$; for in this case the electron contribution to (20) dominates and remains of the same form as before, so that a flute mode occurs. Here the dispersion relation obtained as before reduces to

$$\left\langle \left[1 - \frac{\omega_{*i}}{\omega} (1-\kappa)\right] \left(1 - I_o(b_i) e^{-b_i}\right) \right\rangle + \frac{\omega_{*i}^2}{\omega^2} \left(\left\langle \kappa I_o(b_i) e^{-b_i} \right\rangle + \langle \kappa \rangle \frac{T_e}{T_i} \right) = 0 \tag{24}$$

where $\kappa = 2(\partial \ell nB/\partial \ell nN)_\chi$ is the local curvature. It has been noted [3] that the average ion curvature appropriate to this case, namely, $\langle \kappa I_o(b_i) \exp(-b_i)\rangle$, is different from the average in the sense of $\int ds/B$; indeed, for $b_i > 1$ it essentially involves the variation of $\int ds$ rather than $\int ds/B$. However, even if this average is unfavorable an unstable root of (24) does not occur (even with small T_e/T_i) if

$$\left\langle (1-\kappa)^2 \left[1 - I_o(b_i)e^{-b_i}\right]\right\rangle > 4 \left\langle \kappa I_o(b_i)e^{-b_i}\right\rangle$$

which (typically) holds for all values $b_i \gtrsim 1$. Furthermore, it may be noted that the above theory of the residual instability is unaffected; for the condition for residual instability is obtained from the marginal case $\omega = \omega_{*i}$, and here the value of b_i is irrelevant since the whole term involving J_o vanishes. Thus the condition (22) for residual instability remains good independent of b_i, and the average curvature term therein (coming only from the electrons) remains as before, i.e., in the sense of $\int ds/B$.

Unless the density is very small this mode has $\omega \sim \omega_{*i}$, and hence its stability is sensitive to small effects so far neglected. We have considered two such effects, namely, a small anisotropy ($T_\parallel \neq T_\perp$) and a small temperature gradient. Anisotropy is included by replacing the Maxwellian equilibrium distribution by

$$F(\varepsilon,\mu) \sim \exp\left[-\frac{\varepsilon}{v_{T_\parallel}^2} - \mu B_o\left(\frac{1}{v_{T_\perp}^2} - \frac{1}{v_{T_\parallel}^2}\right)\right]$$

where B_o is some constant reference value; this distribution is everywhere locally a two-temperature Maxwellian but of course the anisotropy varies along the field. Defining ω_{*i} in terms of $T_\parallel$, the sign of the ion resonance terms [these involve only $\partial F/\partial\varepsilon$ and $\partial F/\partial\psi$, see Eq. (3)] is still determined by the sign of $\omega - \omega_{*i}$. However, the terms in $\partial F/\partial\mu$ in Eq. (3) for the ions contribute to the real part of the dispersion relation, and the instability condition (22), obtained from the marginal case $\omega = \omega_{*i}$, becomes

$$\langle d_i\rangle + \left\langle \frac{B_o}{B}\left(\frac{T_\parallel}{T_\perp} - 1\right) b_i\right\rangle > -\left(1 + \frac{T_e}{T_i}\right)\langle\kappa\rangle$$

provided $b_i < 1$, otherwise the term b_i is replaced by $1 - I_o(b_i)\exp(-b_i)$. Thus anisotropy is stabilizing if $T_\parallel < T_\perp$, destabilizing if $T_\perp < T_\parallel$. A similar effect occurs due to a temperature gradient. The ion resonance terms involve slow particles; their sign is given by $\omega - \omega_{*i}$ as before provided we define ω_{*i} in terms of $\partial \ell n(N/T^{3/2})/\partial\psi$ instead of $\partial \ell nN/\partial\psi$. There is a temperature gradient contribution to the real part of the dispersion relation, and the instability condition (22), obtained from $\omega = \omega_{*i}$, becomes

$$\langle d_i\rangle - \frac{5}{2}\frac{\partial \ell nT}{\partial \ell nN}\langle b_i\rangle > -\left(1 + \frac{T_e}{T_i}\right)\langle\kappa\rangle$$

so that a small positive $\partial \ell nT/\partial \ell nN$ is stabilizing. Adding both small effects, the condition that $\omega < \omega_{bi}$ at $\omega = \omega_{*i}$ for perpendicular wavelengths short enough for instability gives a final instability criterion replacing (23), namely,

$$\frac{B^2}{4\pi N M_i c^2} + \frac{T_\parallel}{T_\perp} - 1 - \frac{5}{2}\frac{\partial \ell nT}{\partial \ell nN} > \left(1 + \frac{T_e}{T_i}\right)\frac{L^2}{r\bar{R}} \tag{25}$$

In an initially Maxwellian plasma with a density below the threshold density a spectrum of flute waves grows with the waves taking energy from the bouncing motion of the ions, thereby reducing the parallel temperature of the ions. We have constructed a quasi-linear theory which shows that as a consequence the spectrum of waves produces an anisotropy with $T_\perp > T_\parallel$ which tends to stabilize the mode. However, time-scale estimates show that the time for energy exchange between the waves and particles is longer by a factor L^2/r^2 than the time scale for spatial diffusion. Consequently, the particles can diffuse out of the system before quasi-linear stabilization occurs unless the initial density is close to threshold. These conclusions arise from a study of the quasi-linear equation for the slow variation of the background ion distribution $F(\varepsilon, \mu, \psi, t)$, namely,

$$\frac{\partial F}{\partial t} = \frac{e^2}{m^2}\sum_{\ell, n}\left[\frac{\ell m}{e}\frac{\partial}{\partial \psi} + \left(\bar{\omega}_D + n\omega_b\right)\frac{\partial}{\partial \varepsilon}\right]\frac{|\phi_\ell|^2\,\gamma_\ell\,J_n^2\left(\frac{\tilde{\omega}_D}{\omega_b}\right)}{\left|\omega_\ell - \bar{\omega}_D - n\omega_b\right|^2 + \gamma_\ell^2}$$

$$\cdot\left[\frac{\ell m}{e}\frac{\partial F}{\partial \psi} + \left(\bar{\omega}_D + n\omega_b\right)\frac{\partial F}{\partial \varepsilon}\right]$$

the functions J_n^2 arising from the variable part of the curvature drift $\tilde{\omega}_D$. The largest terms are the n = 0 non-resonant ψ-derivative terms leading to diffusion on a time scale $\tau_D^{-1} \sim \Sigma\, e^2\, \phi_\ell^2\, \gamma_\ell/T^2$. Computing by a moment equation the rate of loss of parallel energy from the resonant particles to the waves (principally the $\omega = \omega_b$ resonance), we obtain a time scale for creation of anisotropy, namely, $\tau_E^{-1} \sim \Sigma\, b_i\, e^2\, \phi_\ell^2\, \gamma_\ell/T^2 \sim b_i\, \tau_D^{-1}$, and $b_i \sim r^2/L^2$ for the most unstable modes ($\omega \sim \omega_{bi} \sim \omega_{*i}$).

2.1.2 The trapped particle instability

Returning to the quadratic form (15) and considering non-flute solutions, taking $\omega^2 \sim \omega_* \omega_D$ and neglecting the term of order b, we have

$$\sum \frac{1}{T}\int F\tau\, d\mu\, d\varepsilon\,(\overline{\phi^2} - \bar{\phi}^2) + \sum \frac{1}{T}\int F\tau\, d\mu\, d\varepsilon\, \frac{\omega_* \bar{\omega}_D}{\omega^2}\,\bar{\phi}^2 = 0\,. \tag{26}$$

If there are particles with time-averaged drifts such that $\omega_* \bar{\omega}_D > 0$, i.e., $J = \int q ds$ increasing outwards, see Eq. (10), then instabilities are possible. Such an instability has been discussed by Kadomtsev and Pogutse [4] considering trapped particles in a Tokamak configuration, and by Rosenbluth [5] considering particles in a multipole which mirror close to B_{max} where the curvature is unfavorable, using trial functions for ϕ. An alternative to the method of trial functions is a WKB approximation for the eigenfunctions, presumably good at least for high-order modes. We write

$$\phi = \hat{\phi}\, e^{i\int k ds} + \hat{\phi}^{*}\, e^{-i\int k ds} \tag{27}$$

By steepest descents around the particle mirror point where $q = 0$ (treating both q and the phase $\int kds$ as rapidly varying) we find

$$\left(\int \frac{\phi ds}{q}\right)^2 = \left(\frac{\pi f_1 |\hat{\phi}|^2}{\varepsilon |\partial \ell n B/\partial s|\,|k|}\right)_{s_o} \tag{28}$$

where s_o is the mirror point given by $\varepsilon = \mu B(s_o)$, and where f_1 is a quantity determined by the symmetry of the mode about B_{min}: $f_1 = 2$ for an even mode, $f_1 = 0$ for an odd mode, $f_1 = 1$ if the configuration is not symmetric about B_{min}. Substituting (27) into the variational principle (26) using (28) to calculate $\bar{\phi}^2$, varying $\hat{\phi}$ and k to produce equations for k and $\hat{\phi}$, respectively, there results

$$|k(s)| = \frac{3\pi f_1 T_e \omega_{*i}^2}{2T_i \omega^2} \left[\frac{\partial}{\partial \ell n N} \int ds\ (1 - \lambda B)^{1/2}\right] \Big/ \left(\int \frac{ds}{(1 - \lambda B)^{1/2}}\right)^2_{\lambda B(s)=1}$$

$$\hat{\phi}^2(s) \propto B\,|k(s)|$$

The instability has $\omega^2 < 0$ and is localized to the region encompassing the mirror points of trapped particles which have $\bar{\omega}_D \omega_* > 0$; WKB turning points occur at the "null" points, defined to be the mirror points of trapped particles with $\bar{\omega}_D = 0$. The dispersion relation is obtained from the phase integral condition $(n + 1/2)\pi = \int kds$, the integral being taken between the nulls. In a multipole the nulls occur very close to B_{max} and "bounce" periods of particles involved are logarithmically large; if $2L_o$ is the (short) length between the nulls the phase integral condition gives a growth rate $\gamma^2 \sim \omega_{*i}^2\ (T_e/T_i)(rL_o/RL)(\ell nL/L_o)^{-1}$.

If the growth rate is small enough, the assumption $\omega > \omega_D$ breaks down; with $\omega \sim \omega_D$ the mode can be stabilized. To calculate this effect, we return to the unexpanded quadratic form given in Eq. (14) (again setting $J_o = 1$). A variational principle for ω^2 may be found for the case $T_e = T_i$ by summing over species; we obtain

$$\int F\tau d\mu d\varepsilon \left(\overline{\phi^2} - \bar{\phi}^2 + \frac{\omega_* \bar{\omega}_D - \bar{\omega}_D^2}{\omega^2 - \bar{\omega}_D^2}\, \bar{\phi}^2\right) = 0$$

Considering the marginal mode $\omega = 0$, we find that instability occurs if (carrying out the velocity space integrals where possible).

$$\int \frac{ds}{B} \phi^2 < -\frac{1}{2} \int d\lambda \left(\int \frac{\phi ds}{(1-\lambda B)^{1/2}} \right)^2 \Big/ \frac{\partial}{\partial \ell n N} \int ds\,(1-\lambda B)^{1/2} \tag{29}$$

where $\lambda = \mu/\mathcal{E}$. If this inequality cannot be satisfied for any trial function ϕ, the mode is stable. Clearly, trial functions which maximize the right-hand side of (29) are localized near the null point on the unstable side, where the denominator in the integral is small and negative; the WKB solution for this case gives eigenfunctions peaked in this way: specifically at $\omega = 0$ we find $k(s) \sim \hat{\phi}(s)^2 \sim (s-s_o)^{-1}$ where s_o is the null point. Strictly the WKB solution fails for such sharply peaked eigenfunctions but it suggests the trial function to use in (29), namely, $\phi \sim (s-s_o)^{-1/2}$, confirmed by a more careful analysis. Choosing such a trial function we may evaluate both sides of (29). In evaluating the right-hand side, two cases must be distinguished, namely, (i) where the field is increasing towards the unfavorable region, as in multipoles, and (ii) where the field is decreasing towards the unfavorable region, as in Tokamaks. In (i), only particles with positive $\omega_* \overline{\omega}_D$ contribute significantly, namely, those which mirror just on the unfavorable side of the null; in (ii), particles with both signs of $\overline{\omega}_D$ contribute, namely, those which mirror close to the null on either side. Surprisingly, the same result is obtained for both cases. After a straightforward calculation which need not be reproduced here, we find for stability

$$\left(\frac{1}{B^2} \frac{\partial B}{\partial s} \right)_{s_o} \frac{\partial}{\partial \lambda} \left(\frac{\partial}{\partial \ell n N} \int ds \left| 1 - \lambda B \right|^{1/2} \right)_{\lambda_o} > \pi^2 \tag{30}$$

where $\lambda_o B(s_o) = 1$. For a multipole configuration this reduces to

$$\frac{rL}{RL_o} > \pi^2$$

where L is defined by $B \simeq B_{max}(1 - s^2/L^2)$, $s = L_o$ is the null, with r and R evaluated at B_{max}(i.e., $r/R = \partial \ell n B/\partial \ell n N$ at B_{max}).

The instabilities discussed above do not occur in "maximum-J" configurations [5] where all the time-averaged drifts are favorable.

2.1.3 The ion drift trapped particle instability

For short perpendicular wavelengths the terms of orders b_i and $(\omega/\omega_{bi})^2$ may no longer be neglected. When both are included, we find a new trapped-particle instability essentially independent of field curvature, and hence occurring even in maximum-J configurations. Assuming

$(\omega_* \omega_D)^{1/2} < \omega < \omega_{*i}$, the variational principle (15) including the contribution order $(\omega/\omega_{bi})^2$ given in Eqs. (16)-(18) is

$$\left(1 + \frac{T_i}{T_e}\right) \int F\tau d\mu d\varepsilon\, (\overline{\phi^2} - \bar{\phi}^2)$$

$$- \int F_i \tau d\mu d\varepsilon \left[\frac{\omega_{*i}}{\omega} \overline{\phi} \overline{b \phi} + \omega \omega_{*i} \int\int \frac{ds\, ds'}{q \quad q'} \phi \phi' K(s, s') \right] = 0 \qquad (31)$$

Inspection of this quadratic equation for ω (the kernel K is positive definite) reveals that instabilities (almost purely growing) can occur if b_i is sufficiently large (see Fig. 1a), specifically if in order of magnitude $b_i^{1/2}\, \omega_{*i}/\omega_{bi} > 1 + T_i/T_e$, which may be written, using $\omega_{*i} = b_i^{1/2} v_{T_i}/r$,

$$b_i > \frac{r}{L} \left(1 + \frac{T_i}{T_e}\right) \qquad (32)$$

and the growth rate is $\gamma \sim b_i^{1/2}\, \omega_{bi}$. For $b_i > 1$ the assumption $\omega < \omega_{bi}$ breaks down and the instability does not occur. For b_i too small to satisfy (32), residual instability [i.e., from the ion resonance terms like $(\omega/\omega_{bi})^3$] occurs in the lower branch of the dispersion relation (see Fig. 1a), i.e., the branch with $\omega \sim \omega_{*i}\, b_i/(1 + T_i/T_e)$.

A detailed analysis of this mode has been carried out by two methods; (i) solving the variational principle (31) using the WKB approximation (27), and (ii) using simple trial functions (the variational principle is good for real ω and may be thought of as a maximum principle for b_i, providing the largest b_i for stability). In (i) we use the result (28) for ϕ, and compute the integral over K for trapped particles in (31) by the same steepest descents method around q = 0 used to obtain (28). Varying ϕ we obtain an equation for k(s), namely,

$$\left(1 + \frac{T_e}{T_i}\right) |k(s)| = \frac{3\pi f_1}{4} \frac{\omega_{*i} b_i}{\omega} \Bigg/ \int \frac{ds'}{(1-B'/B)^{1/2}} + \frac{\pi f_2}{2 v_{T_i}^2} \omega_{*i} \omega \int \frac{ds'}{(1-B'/B)^{1/2}}$$

where f_2 is another symmetry factor, namely, 1/6 for an even mode, 1/2 for an odd mode, and 1/3 if no symmetry occurs. In multipoles this instability occurs for the even mode, i.e., even about B_{min}, and the dispersion relation is obtained from the phase integral condition, $\int$ kds = 2πn, taken around the field line. Setting to zero the discriminant of the resultant quadratic equation for ω to determine the marginal case, we find instability (for n = 1) if

$$\frac{\omega_{*i}^2}{v_{T_i}^2} \left(\int \frac{b ds}{\int ds'/(1-B'/B)^{1/2}} \right) \left(\int ds \int \frac{ds'}{(1-B'/B)^{1/2}} \right) > 8 \left(1 + \frac{T_i}{T_e}\right)^2 \qquad (33)$$

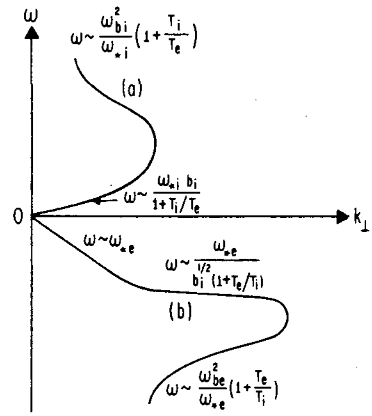

FIG. 1. Dispersion curves for (a) ion drift trapped-particle mode; (b) electron drift trapped-particle mode.

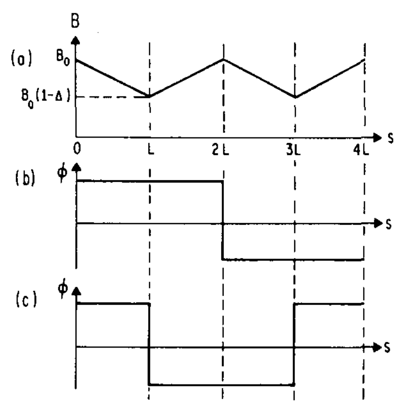

FIG. 2. (a) Quadrupole field model; (b) trial function for ion drift trapped-particle mode; (c) trial function for electron drift trapped-particle mode.

Evaluating these integrals for the saw-tooth model of a quadrupole field shown in Fig. 2a for small field modulation (small Δ), we find instability if (32) is satisfied with an extra numerical factor of $\sqrt{6}/4$ on the right. For large field modulation the condition is little changed, the number $\sqrt{6}/4$ being replaced by $1/\sqrt{2}$; here b_i and r are to be evaluated at B_{min}. Since the WKB solution may fail for the lowest-order mode (n = 1), calculations have been done for the same saw-tooth model using method (ii), i.e., trial functions. The square-well trial function shown in Fig. 2b was used. Calculating the integrals involved, the variational principle (31) becomes (for small Δ), only untrapped particles contributing to the $(\omega/\omega_b)^2$ term.

$$1 + \frac{T_i}{T_e} - \frac{\Delta^{1/2}\omega_{*i}\, b_i}{\omega} - \frac{8}{15}\,\frac{\omega\omega_{*i} L^2}{\Delta^{1/2} v_{T_i}^2} = 0$$

giving an instability condition similar to (32) with a numerical factor $\sqrt{15/32}$ on the right, very close to the WKB result. One general feature should be noted: as the field modulation becomes small the condition for instability remains approximately unchanged [this may be seen in the general case by inspection of (33)]. However, the growth rate is reduced, i.e., $\gamma \sim \Delta^{1/2} b_i^{1/2} \omega_{bi}$.

2.2 The case $\omega_{bi} < \omega < \omega_{be}$

Here we use the approximate solutions (9) for the electrons and (12) for the ions. A variational principle is again constructed by multiplying the neutrality condition (8) by ϕ/B and integrating over s, giving

$$\frac{T_i}{T_e}\left(1-\frac{\omega_{*e}}{\omega}\right)\int 2\pi F_e \tau d\mu d\varepsilon \left[\overline{\phi^2} - \bar{\phi}^2\left(1+\frac{\overline{\omega}_{De}}{\omega}\right)\right]$$
$$+\left(1-\frac{\omega_{*i}}{\omega}\right)\int \frac{ds}{B}\left\{\left[1-I_o e^{-b_i}\left(1+\frac{\omega_{*i}}{\omega}\kappa\right)\right]\phi^2 - \frac{v_{T_i}^2}{\omega^2}\left(\frac{\partial}{\partial s} I_o e^{-b_i}\phi\right)^2\right\} \tag{34}$$

where $\kappa = 2(\partial \ell nB/\partial \ell nN)_\chi$ and the ion velocity space integration has been carried out. Where $b_i \lesssim 1$ and $\kappa < 1$, the first term in (34) is the largest and must vanish to lowest order, giving two possibilities, namely, $\phi = \bar{\phi} =$ constant (flute mode) or $\omega \simeq \omega_{*e}$ (drift mode).

2.2.1 The electron flute instability [1, 6]

The flute mode dispersion relation is obtained by varying (34) with respect to ϕ, putting ϕ = constant in the small terms, and integrating over s. We obtain the same dispersion relation as for the ion flute, i.e., Eq. (21). But here the largest resonances are from the electrons [either the $(\omega/\omega_{be})^3$ terms, or the n = 0 resonances where $\omega = \overline{\omega}_{De}$]. The perturbation technique shows these to be destabilizing if $0 < \omega/\omega_{*e} < 1$, and hence from Eq. (21) there is a residual electron flute instability if

$$1 > \langle b_i \rangle > -\frac{T_i}{T_e}\langle \kappa \rangle$$

If $b_i \gtrsim 1$, a flute mode occurs only if $T_e < T_i$ and $\omega > \omega_{*e}$ and so the electron flute instability does not occur.

2.2.2 The electron drift instabilities [1, 6, 7]

Putting $\omega = \omega_{*e}$ in the small terms the variational principle (34) shows that residual instability (again arising if $\omega/\omega_{*e} < 1$) occurs if, for $b_i < 1$,

$$\int \frac{ds}{B}\left(b_i + \frac{T_i}{T_e}\kappa\right)\phi^2 > \frac{v_{T_i}^2}{\omega_{*e}^2}\int \frac{ds}{B}\left(\frac{\partial \phi}{\partial s}\right)^2 \tag{35}$$

Maximizing the left-hand side, we find modes localized around κ_{max} for $b_i < \kappa$ (drift ballooning mode) and around b_{max} for $b_i > \kappa$ (drift universal mode), satisfying (35) if $b_i \gg (T_i/T_e)\, rR/L^2$ and $b_i > (T_i/T_e)\, r/L$, respectively, where r and R are to be evaluated at the respective mode locations. A more complete discussion may be found elsewhere [1, 6, 7].

2.2.3 The electron drift trapped-particle instability

For very short perpendicular wavelengths, i.e., large b_i, the electron drift mode has ω/ω_{*e} small. For one of the modes, namely, the odd mode, the terms of order $(\omega/\omega_{be})^2$ become important, and with these included a new almost purely growing electron drift instability is found, contrasting with the results of plane geometry calculations where only residual instabilities are found except for $\omega \gtrsim \omega_{be}$. For the mode odd about B_{min}, we have $\bar{\phi} = 0$; neglecting all curvature terms in (34), taking $\omega < \omega_{*i}$ and $b_i > 1$, and adding the electron term of order $(\omega/\omega_{be})^2$ given in Eqs. (16) - (18), we have

$$\left(1 + \frac{T_i}{T_e}\right) \int \frac{ds}{B}\, \phi^2 + \frac{\omega_{*i}}{\omega} \int \frac{ds}{B}\, \frac{\phi^2}{(2\pi b_i)^{1/2}}$$

$$+\, \omega\omega_{*i} \int 2\pi F_e \tau\, d\mu\, d\varepsilon \iint \frac{ds}{q}\, \frac{ds'}{q'}\, \phi\phi'\, K(s, s') = 0$$

Inspection of this quadratic equation for ω (see Fig. 1b) shows that instabilities (almost purely growing) can occur if $\omega_{*i}^2/\omega_{be}^2 > b_i^{1/2} \times (1 + T_i/T_e)^2$, i.e., if

$$b_i^{1/2} > \left(\frac{r}{L}\right)^2 \frac{T_e}{T_i}\, \frac{M}{m} \left(1 + \frac{T_i}{T_e}\right)^2 \qquad (36)$$

and have growth rates $\gamma \sim \omega_{be}/b_i^{1/4}$. For b_i too small to satisfy (36), residual instability [i.e., from the electron resonance terms like $(\omega/\omega_{be})^3$] occurs in the branch with smaller $|\omega|$ (see Fig. 1b), i.e., the branch with $\omega \sim \omega_{*e}/b_i^{1/2}\, (1 + T_e/T_i)$, merely the large b_i limit of the usual drift instability. The result (36) holds only for $b_e < 1$; putting $b_e \sim 1$, the limiting value, in (36) we obtain a stability condition $T_i/T_e > (m/M)\, (L/r)^4$ if $T_i > T_e$. A detailed analysis of this mode has been carried out by the same two methods used for the ion drift trapped-particle mode; namely, (i) a WKB approximation and (ii) simple trial functions, applied to the saw-tooth quadrupole model shown in Fig. 2a. The odd square-well trial function shown in Fig. 2c was used [here both trapped and untrapped particles contribute to the $(\omega/\omega_b)^2$ term]. For small field modulations, the methods provided numerical factors of $3\sqrt{2\pi\Delta}/16$ and $15\sqrt{2\pi\Delta}/64$ for the right-hand side of (36); growth rates are of order $\gamma \sim \Delta^{1/4}\, \omega_{be}/b_i^{1/4}$.

The case $\omega > \omega_{be}$ is less interesting and is not discussed here, since for $\omega \lesssim \omega_*$ extremely short perpendicular wavelengths are required, except for very large L. Residual flute and drift instabilities do occur in this regime but growth rates are exponentially small.

3. POLOIDAL AND TOROIDAL FIELDS

With a toroidal field B_T added to the poloidal field $B_\perp$ the stability problem becomes much more complicated since, because of the shear, it is, in general, necessary to calculate the ψ-dependence of the eigenfunctions. The analysis is further complicated by the presence of radial drifts due to geodesic curvature. We write for perturbed quantities

$$\phi = \hat{\phi}(\psi, \chi) \exp\left[-i\omega t + i\ell\left(\theta - \int^{\chi} B_T d\chi / R_o B_\perp^2\right)\right] \tag{37}$$

the phase being constant along a field line; the matching condition is then $[\ell n \phi] = i \ell \iota' \psi$, where $[\ ]$ denotes the jump going once around in χ, $\iota(\psi) = \oint B_T d\chi / R_o B_\perp^2$, and ψ is measured from some rational surface where $\ell \iota = 2\pi n$. The function $\hat{\phi}(\psi, \chi)$ is to be determined. The analysis is lengthy and will be presented elsewhere. We confine ourselves here to a statement of some of the essential results.

3.1 Flute modes

For $\omega < \omega_{bi}$ these are localized within $\ell \iota' \psi < \omega / \omega_{be}$. We find the average curvature $\left[\text{replacing } (\int ds/B)'\right]$ to be given by a new generalization of the quantity V'', namely,

$$V^{\dagger\dagger} = \frac{\partial}{\partial\psi}\int \frac{d\chi}{B_\perp^2} - \frac{3}{2}\left(\int \frac{d\chi}{B_\perp^2}\right)\left(\frac{\partial}{\partial\psi}\int \frac{B^2 d\chi}{B_\perp^2}\right)\int_o^{1/B_{max}} d\lambda \Bigg/ \int \frac{B d\chi}{B_\perp^2 (1-\lambda B)^{1/2}}$$

which may be compared with the result of a finite resisitivity fluid theory [8], namely,

$$V^{**} = \frac{\partial}{\partial\psi}\int \frac{d\chi}{B_\perp^2} - \left(\int \frac{d\chi}{B_\perp^2}\right)\frac{\partial}{\partial\psi}\, \ell n \int \frac{B^2 d\chi}{B_\perp^2}$$

A Schwartz inequality shows that

$$\frac{3}{2}\int d\lambda \Bigg/ \int \frac{B d\chi}{B_\perp^2 (1-\lambda B)^{1/2}} < \left(\int \frac{B^2 d\chi}{B_\perp^2}\right)^{-1}$$

which relates $V^{\dagger\dagger}$ and V^{**} as follows: if the average toroidal curvature is favorable, i.e., $\partial/\partial\psi \int B^2 d\chi / B^2 > 0$, (e.g., in spherators) then $V^{\dagger\dagger} > V^{**}$ so that the condition $V^{\dagger\dagger} < 0$ is stronger than the condition $V^{**} < 0$; if, however, the average toroidal curvature is unfavorable then the

$V^{**} < 0$ condition is the stronger. Essentially, in the $V^{\dagger\dagger}$ criterion the toroidal curvature contribution comes only from the untrapped particles, and is therefore reduced. The flute modes are easily stabilized by shear [shear $\sim (m/M)^{1/2}$], except if $V^{\dagger\dagger} > 0$ when a residual ion flute instability remains, highly localized but not shear stabilized. For $\omega > \omega_{be}$ the average curvature is found to be given by V^{**}; for $\omega_{bi} < \omega < \omega_{be}$ the appropriate quantity has not been determined.

3.2 Trapped-particle instabilities

These are not highly localized ($\ell \iota' \psi > \omega/\omega_{bi}$) and the untrapped particles (which cause most of the difficulty in the analysis) are not significantly involved [5]. The analysis in Sec. II remains good provided in integrals over s we write $ds = B d\chi / B_\perp^2$. The maximum-J condition becomes

$$\frac{\partial J}{\partial \psi} = \frac{\partial}{\partial \psi} \int \frac{q B d\chi}{B_\perp^2} < 0$$

It has been noted [4] that having $B_\perp$ increase outwards in stellarator or Tokamak configurations reduces the number of trapped particles with $\partial J/\partial \psi > 0$, though there always remain some (namely, those trapped on the outside very close to B_{min}). A "null" where $\partial J/\partial \psi = 0$ always occurs, and hence we can apply the stability criterion (30) which now becomes

$$\frac{B_\perp^2}{B^3} \frac{\partial B}{\partial \chi} \frac{\partial}{\partial \lambda} \left(\frac{\partial}{\partial \ell n N} \int \frac{B d\chi}{B^2} (1 - \lambda B)^{1/2} \right) > \pi^2$$

We have applied this condition to a Tokamak configuration, but find it difficult to satisfy; it becomes

$$\frac{d}{d \ell n r} \ell n \left(\frac{B_\perp}{r^{3/2}} \right) > \frac{\pi^2 R r}{r_o^2}$$

in the most favorable case where the left-hand side is very large; here r is the minor radius and r_o the density gradient scale.

3.3 Geodesic curvature ballooning modes

The toroidal field provides geodesic curvature; here we look for possible drift ballooning instabilities, i.e., with $\omega_{bi} < \omega < \omega_{be}$, driven by it. We use the form (37) so that the χ-dependence of ϕ describes the whole variation along the field, with $B d\chi / B_\perp^2 = ds$; we take a WKB form in both s and ψ, i.e., $\phi \sim \exp(i \int k_\psi d\psi + i \int k_s ds)$, giving

$$\frac{T_i}{T_e} \left(1 - \frac{\omega_{*e}}{\omega}\right) + \left(1 - \frac{\omega_{*i}}{\omega}\right) \left(b_i - \frac{\omega_{Di}}{\omega} - \frac{\omega_{Gi}}{\omega} - \frac{k_s^2 v_{T_i}^2}{\omega^2}\right) = 0 \quad (38)$$

where

$$\omega_D = \ell \, \vec{v}_D \cdot \nabla(\theta + \int^{\chi} B_T d\chi / R_o B_\perp^2)$$

$$\omega_G = k_\psi \, \vec{v}_D \cdot \nabla\psi$$

$$b = a^2 \, (\ell^2 B^2 / R_o^2 B_\perp^2 + k_\psi^2 |\nabla \psi|^2)$$

$$= b_\theta + b_\psi$$

We have here neglected one term in b which describes the effect of the shear, namely, a term in $(\partial/\partial\psi)\int^{\chi} B_T d\chi / R_o B_\perp^2$, but this is relatively negligible for modes localized in χ. We treat the second group of terms in (38) as small and put $\omega = \omega_{*e}$ in these terms. Imposing the condition $\partial\omega/\partial k_\psi = 0$ for non-convection of the mode in ψ, we find $k_\psi |\nabla\psi|^2 = \vec{v}_{Di} \cdot \nabla\psi / 2\,\omega_{*e} a_i^2$. Substituting back into (38) we find

$$\frac{T_i}{T_e}\left(1 - \frac{\omega_{*e}}{\omega}\right) = \left(1 + \frac{T_i}{T_e}\right)\left[-b_{i\theta}^2 + \frac{\omega_{Di}}{\omega_{*e}} + \frac{(v_{Di} \cdot \nabla\psi)^2}{4\omega_{*e}^2 a_i^2 |\nabla\psi|^2} + \frac{k_s^2 \, v_{T_i}^2}{\omega_{*e}^2}\right]$$

which shows (at least for modes of this type) that the geodesic curvature is in fact stabilizing (particularly for small ℓ), since it tends to make $1 - \omega_{*e}/\omega > 0$. The point of localization in s is where $\partial k_s/\partial s = 0$, i.e., from (38) where

$$\frac{\partial}{\partial s}\left(b_i - \frac{\omega_{Di}}{\omega_{*e}} - \frac{\omega_{Gi}}{\omega_{*e}}\right) = 0$$

together with a condition that the second derivative be negative. This shows that the geodesic curvature can alter the mode location and (particularly at small ℓ) this seems to be its dominant effect.

These conclusions do not apply to values of k_ψ such that $\partial\omega/\partial k_\psi \neq 0$, where the mode will be convected out by the geodesic curvature effect before it has time to grow as long as $\gamma < \omega - \omega_{*e}$ as calculated above.

4. CONCLUSIONS

The principal new contributions of the present work are as follows:

(i) A fairly comprehensive theory has been given of the low-frequency stability of low-β collisionless plasmas in axisymmetric toruses, in which the variation of the field strength along the field is rigorously treated. Modes previously discovered in simpler geometries (i.e., electron flute, ion flute, electron drift and ballooning) have been found, and stability criteria given.

(ii) The ion flute mode has been considered in some detail, and, in $\int d\ell/B$ stable configurations, shown to be residually unstable only at low density; stabilization due to slight anisotropy or temperature gradient has been demonstrated.

(iii) The curvature driven trapped-particle mode has been shown to be stabilized by a finite curvature effect; the criterion seems attainable in multipoles.

(iv) Two new instabilities have been found, termed ion and electron drift trapped-particle modes. The ion mode is a specific consequence of the trapped particles and can be almost purely growing. The electron mode is similar to the usual drift waves, but can be almost purely growing even for $\omega < \omega_{be}$ this being a specific consequence of the finite variation of the field strength along the field.

(v) For the case with toroidal field, a new generalized V'' criterion is presented essentially involving the correct orbit for trapped and untrapped particles.

(vi) An eikonal method for treating geodesic ballooning modes is presented; non-convective modes driven directly by geodesic curvature do not seem to occur.

ACKNOWLEDGMENT

This work was performed under the auspices of the U.S. Atomic Energy Commission, Contract No. AT(30-1)-1238.

REFERENCES

[1] RUTHERFORD, P.H., FRIEMAN, E.A., Phys. Fluids 11 (1968) 569.

[2] TAYLOR, J.B., Phys. Fluids 10 (1967) 1357.

[3] OHKAWA, T., YOSHIKAWA, M., Phys. Rev. Letters 19 (1967) 1374.

[4] KADOMTSEV; B., POGUTSE, O., Zh. Eksp. Teor. Fiz. 51 (1966) 1734 [Sov. Phys.--JETP 24 (1967) 1172].

[5] ROSENBLUTH, M. N., Phys. Fluids 11 (1968) 869.

[6] COPPI, B., LAVAL, G., PELLAT, R., ROSENBLUTH, M. N., Plasma Phys. 10 (1968) 1; see also COPPI, B., OSSAKOW, S., Princeton University report MATT-567 (1967) for a similar treatment of the ion flute mode.

[7] COPPI, B., ROSENBLUTH, M.N., YOSHIKAWA, S., Phys. Rev. Letters 20 (1968) 190.

[8] JOHNSON, J. L., GREENE, J. G., Plasma Phys. 9 (1967) 611.

NON-ADIABATIC BEHAVIOUR OF PARTICLES IN INHOMOGENEOUS MAGNETIC FIELDS

R.J. HASTIE, G.D. HOBBS AND J.B. TAYLOR
UKAEA, CULHAM LABORATORY, ABINGDON, BERKS, UNITED KINGDOM

Abstract

NON-ADIABATIC BEHAVIOUR OF PARTICLES IN INHOMOGENEOUS MAGNETIC FIELDS. The results are presented of a numerical study of charged particle orbits in linear multipole fields. This study includes, in particular, the breakdown of adiabatic behaviour in regions of weak magnetic field. The breakdown, which is confined to comparatively short lengths of an otherwise adiabatic orbit in the vicinity of the field minima, results in abrupt step-like changes in the particle's magnetic moment μ. The circumstances in which this occurs have been analysed and a theory is presented which predicts, and is in agreement with, the observed dependence on the various parameters of the particle trajectory (energy, pitch, phase for example).

1. INTRODUCTION

It has been known for some time [1,2] that the magnetic moment of a particle orbiting in an inhomogeneous magnetic field suffers its largest variations as the trajectory passes through a local minimum in the field, i.e., where $\partial B/\partial \ell = 0$; $\partial^2 B/\partial \ell^2 > 0$. Garren et al. [1], in numerical studies of particle trajectories in axisymmetric mirror fields, found $\mu_0 = v_\perp^2/2B$ to be approximately constant over the greater part of the trajectory, but to change rapidly from one constant value to another as the particle crossed the mid-plane of the mirror field. They also showed that these jumps $(\Delta\mu)$ in μ have an exponential dependence on the particle velocity: $\Delta\mu = Ae^{-B/v}$, and are periodic in the Larmor phase φ_0, with which the particle crosses the mid-plane. More recently Howard [3] has studied orbits in a linear Octopole field and has found similar non-adiabatic phenomena.

In the Russian literature several efforts [4,5,6], have been made to devise analytic expressions for the non-adiabatic change $\Delta\mu$ but none of these is particularly suitable for comparison with numerical calculations in real fields and their derivation is frequently lengthy and indirect.

In this paper we derive an analytic expression for the non-adiabatic jumps in μ by a method which is applicable to magnetic fields of arbitrary complexity. This is then compared with numerical results from a wide variety of orbits in linear multipole fields.

Work on adiabatic invariants has established both the first order correction (μ_1) to μ_0 [7], and the second order correction (μ_2) in axisymmetric fields [8] and in arbitrary vacuum fields [9]. Using these results we may write the magnetic moment invariant, correct to second order, in a linear multipole field as:

$$\hat{\mu} = \mu_0 + \mu_1 + \mu_2 \tag{1.1}$$

with

$$\mu_0 = \frac{v_\perp^2}{2B} \tag{1.2}$$

$$\mu_1 = -\frac{v_\perp}{B}\frac{1}{\omega_c}\left\{(v_\parallel^2+\frac{1}{2}v_\perp^2)\,\rho_1\sin\varphi+\frac{1}{4}v_\parallel v_\perp\,\rho_2\sin 2\varphi\right\} \tag{1.3}$$

$$\mu_2 = \sum_{n=0}^{4} C_n\cos n\varphi \tag{1.4}$$

$$C_o = \frac{1}{2B}\frac{1}{\omega_c^2}\left\{v_\parallel^4\,\rho_1^2 - v_\parallel^2 v_\perp^2\left(\frac{\partial\rho_2}{\partial\ell}+\frac{7}{8}\rho_2^2\right)-v_\perp^4\left(\frac{3}{8}\frac{\partial\rho_2}{\partial\ell}+\frac{7}{16}\rho_2^2-\frac{3}{8}\rho_1^2\right)\right\} \tag{1.5}$$

$$C_1 = \frac{v_\parallel v_\perp}{2\omega_c^2 B}\left\{\frac{3}{4}v_\perp^2\left(\frac{\partial\rho_1}{\partial\ell}+3\rho_1\rho_2\right)+v_\parallel^2\left(2\frac{\partial\rho_1}{\partial\ell}+3\rho_1\rho_2\right)\right\} \tag{1.6}$$

$$C_2 = \frac{v_\perp^2}{8\omega_c^2 B}\left\{v_\perp^2\left(\frac{\partial\rho_2}{\partial\ell}+\frac{3}{2}\rho_2^2-\rho_1^2\right)+3v_\parallel^2\left(\frac{\partial\rho_2}{\partial\ell}+\rho_2^2\right)\right\} \tag{1.7}$$

$$C_3 = \frac{v_\parallel v_\perp^3}{24\omega_c^2 B}\left(\rho_1\rho_2-\frac{\partial\rho_1}{\partial\ell}\right) \tag{1.8}$$

$$C_4 = \frac{v_\perp^4}{64\omega_c^2 B}\rho_2^2 \tag{1.9}$$

and $\rho_2 \equiv -1/B(\partial B/\partial\ell)$; $\rho_1 = 1/R_c$ the curvature, and $v_\parallel$, $v_\perp$ have their usual meaning. The phase angle φ is defined by $\tan\varphi = v_z/v_n$ where v_n is the component of velocity normal to the flux surfaces of the multipole field, and v_z is the component in the direction of symmetry.

When a B_z field is added these expressions must be replaced by the more complicated expressions given in [9]*.

In Section 2 the expression for $\hat{\mu}$ correct to zero, first and second order, i.e.,

$$\hat{\mu}_n = \sum_{o}^{n}\mu_r\ ;\ n=0,1,2$$

are computed along orbits in a quadrupole field and their qualitative behaviour described. This shows, in agreement with the earlier calculations, that over large parts of the orbit $\hat{\mu}_o$, $\hat{\mu}_1$ and $\hat{\mu}_2$ oscillate, with successively smaller amplitudes, about a constant value. However in the neighbourhood of the minimum field along an orbit $\hat{\mu}_n$ may undergo a sudden change from one almost constant value to another.

In Section 3 we derive an analytic formula for these abrupt changes $\Delta\mu$ in $\hat{\mu}$ and in Section 4 this formula is compared with the computed values of $\Delta\mu$ over a range of phase, pitch and energy of the particle. It is found that the analytic formula gives good agreement with the numerical calculations.

2. NUMERICAL RESULTS

In this section we consider the results of numerical calculations of $\hat{\mu}_n$ along particle trajectories in a quadrupole field. There are basically two types of orbit, mirror orbits in which the particle is confined

*There is an error in the sign of c_o in reference [9]; with c_o replaced by $-c_o$ the formula given is correct.

to one section of the quadrupole field and passing orbits which pass completely round the system. Both types of orbit show non-adiabatic changes in $\hat{\mu}$ as the energy of the particle is increased.

The basic multipole field can be represented by

$$B = \frac{2I}{aq}\,(1 + 2\,q\,\mathrm{Cos}\,\Phi + q^2)^{\frac{n-1}{2n}} \tag{2.1}$$

where q labels the different field lines, Φ is the magnetic potential and $2a$ is the separation between the current filaments producing the field. A full discussion of the field is given by Hobbs & Taylor [10]. For a quadrupole $(n = 2)$ the field line $q = 1$ passes through the zero of B while $q = 1{\cdot}19$ is the critical $\int d\ell/B$ line and $q = 2{\cdot}0$ is a line on which the curvature ρ_1 is zero at the 'weak field' plane of symmetry. This 'weak field' plane of symmetry corresponds to $\Phi = \pi$ while $\Phi = 0$ is the 'strong field' plane of symmetry.
The particle orbit is characterised by

φ the phase angle $= \tan^{-1} v_z/v_n$
ψ the pitch angle $= \tan^{-1} v_\perp/v_\parallel$
r the larmor radius $= mv/eB(o)$ where $B(o)$ is the field strength at the particle's starting point.

(a) <u>Mirror Trapped Particles</u>

<u>Abiabatic Orbits</u>

Fig.1 shows the time variation of the three successive approximations $\hat{\mu}_0$, $\hat{\mu}_1$, $\hat{\mu}_2$ to the invariant, for a typical adiabatic particle.

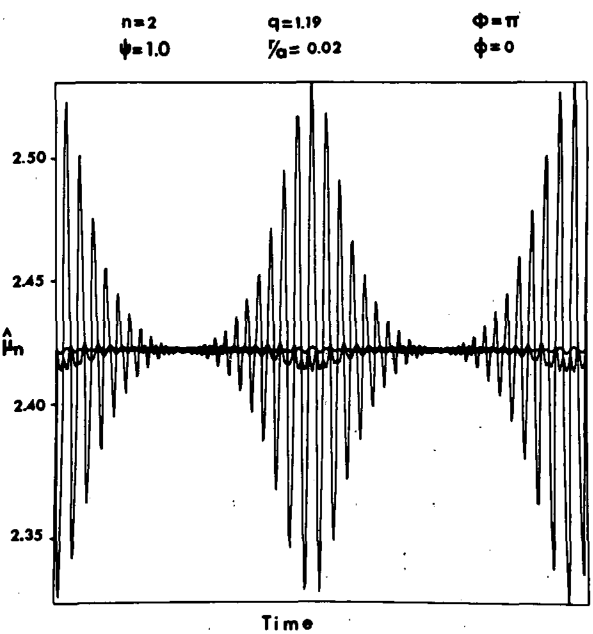

FIG.1. Variation of $\hat{\mu}_n \Big/ \frac{v^2}{2B_m}$ versus time; $n = 2$, $q = 1.19$, $\Phi = \pi$, $\psi = 1.0$, $r/a = 0.02$, $\varphi = 0$.

In all figures $B_m = B(\Phi = 0)$, the maximum value on a field line.

Its trajectory starts on the critical $\int d\ell/B$ line i.e., $q = 1\cdot19$ in the weak-field ($\Phi = \pi$) plane of symmetry and has been followed through two reflections and two transits of the weak field plane. The zero order approximation $\hat{\mu}_0$ oscillates at the gyrofrequency with small amplitude, while $\hat{\mu}_1, \hat{\mu}_2$ oscillate with still smaller amplitudes, about a constant value.

Non-Adiabatic Orbits

In Fig.2 the $\hat{\mu}_n$ are shown for a particle of smaller pitch, and larger energy. The behaviour between crossings of the $\Phi = \pi$ plane is very similar to that of an adiabatic particle, but distinct jumps in $\hat{\mu}_n$ occur over a short interval, of order a few gyro-periods, as the particle crosses this plane.

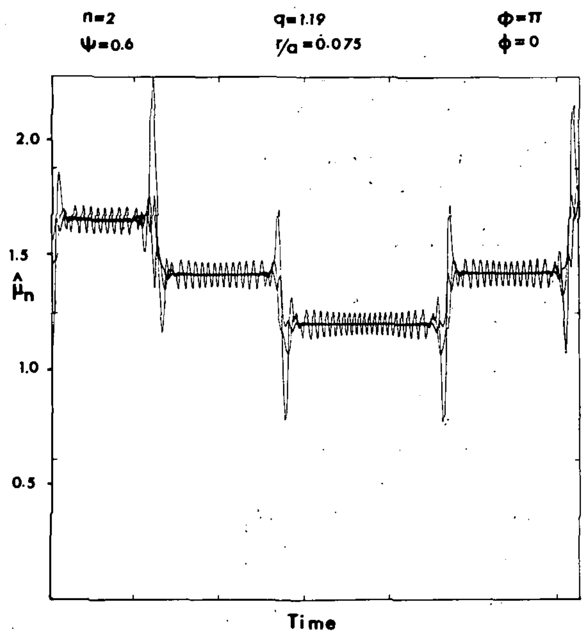

FIG.2. Variation of $\hat{\mu}_n / \frac{v^2}{2B_m}$ versus time; $n = 2$, $q = 1.19$, $\Phi = \pi$, $\Psi = 0.6$, $r/a = 0.075$, $\varphi = 0$.

In Fig.3 these results are shown in more detail using separate (and different) scales for $\hat{\mu}_0$, $\hat{\mu}_1$ and $\hat{\mu}_2$. This figure shows quite clearly that the particle behaves adiabatically over the greater part of its orbit and that in this adiabatic region $\hat{\mu}_0$, $\hat{\mu}_1$, $\hat{\mu}_2$ again represent successively better approximations to a true invariant.

In Fig.4 the same particle is followed through many transits of the $\Phi = \pi$ plane, during which the magnetic moment changes in random fashion, and in fact the particle changes from a 'mirror' ($\hat{\mu}>1$) to a 'passing' ($\hat{\mu}<1$) particle and back again several times.

(b) Passing Orbits

The behaviour of passing particles near the field line $q = 1\cdot19$ is not qualitatively different from that of mirror particles described above.

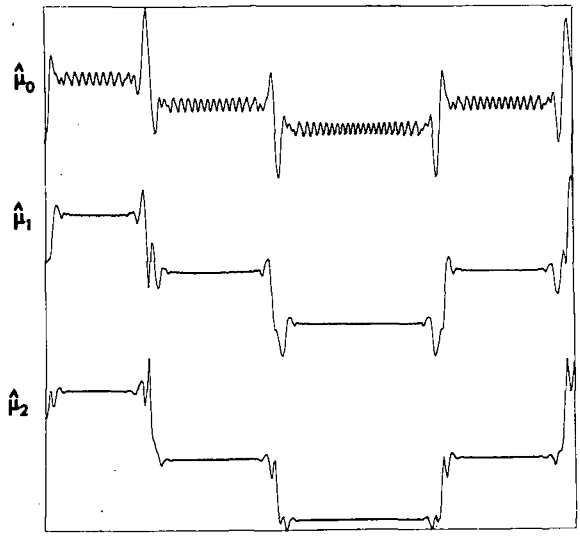

FIG.3. $\hat{\mu}_0$, $\hat{\mu}_1$, $\hat{\mu}_2$ separately, versus time; n = 2, q = 1.19, $\Phi = \pi$, $\Psi = 0.6$, r/a = 0.075, $\varphi = 0$.

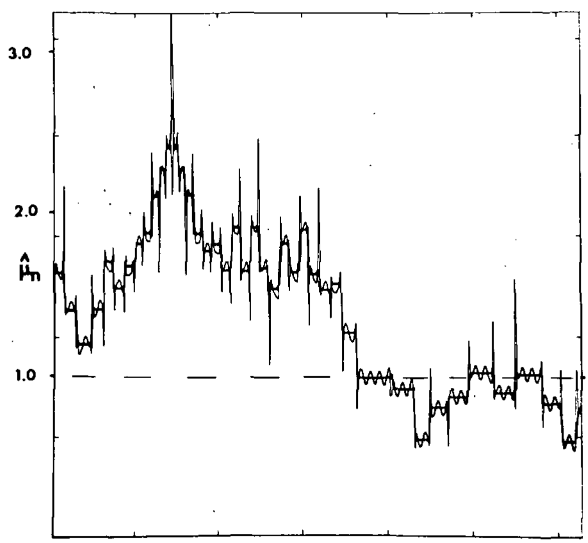

FIG.4. Variation of $\hat{\mu}_n / \frac{v^2}{2B_m}$ versus time, followed through many transits of the weak field; n = 2, q = 1.19, $\Phi = \pi$, $\Psi = 0.6$, r/a = 0.075, $\varphi = 0$.

At small energy they behave adiabatically with $\hat{\mu}_n$ oscillating about a constant value while at larger energy the $\hat{\mu}_n$ undergo sudden changes near the field minimum. Consequently we do not show examples of the type of passing orbit. Instead we concentrate on passing particles near the line q = 2. The behaviour of $\hat{\mu}_n$ for such a particle is shown in Fig.5.

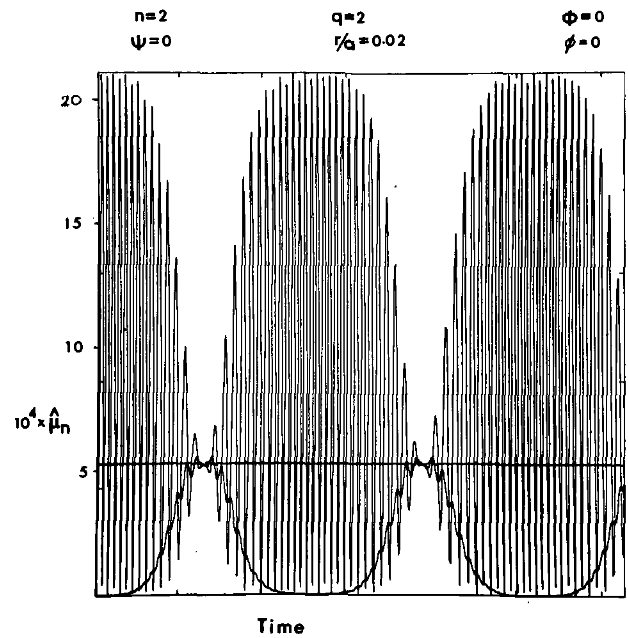

FIG. 5. Variation of $\hat{\mu}_n / \frac{v^2}{2B_m} \times 10^4$, versus time; n = 2, q = 2.0, Φ = 0, Ψ = 0, r/a = 0.02, φ = 0.

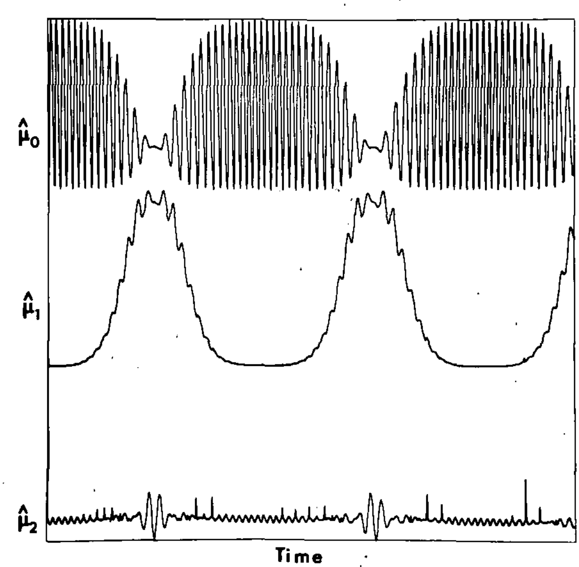

FIG. 6. $\hat{\mu}_0$, $\hat{\mu}_1$, $\hat{\mu}_2$ separately versus time; n = 2, q = 2.0, Φ = 0, Ψ = 0, r/a = 0.02, φ = 0.

The field line q = 2 has zero curvature in the Φ = π, weak field plane. This explains why $\hat{\mu}_0$ has its smallest oscillations in this region for these oscillations are principally due to variation in B around the orbit and B is nearly constant when the curvature is zero. At first sight this might indicate that the non-adiabatic behaviour in the neighbourhood of $\Phi = \pi$ would also disappear. However inspection of Fig.6 (in which the $\hat{\mu}_n$ curves are separated and shown on different scales) shows that the oscillations of $\hat{\mu}_2$, unlike those of $\hat{\mu}_0$, are a maximum in this region. This in turn suggests that at higher energies non-adiabatic jumps in $\hat{\mu}$ will occur as the particle passes through the $\Phi = \pi$ plane. This is confirmed by Fig.7 which shows the behaviour of a particle with five times larger Larmor radius than that of Fig.6. These observations suggest that abrupt changes in the invariant near the mid-plane region depend more on the parallel variation in the field than in the transverse variation.

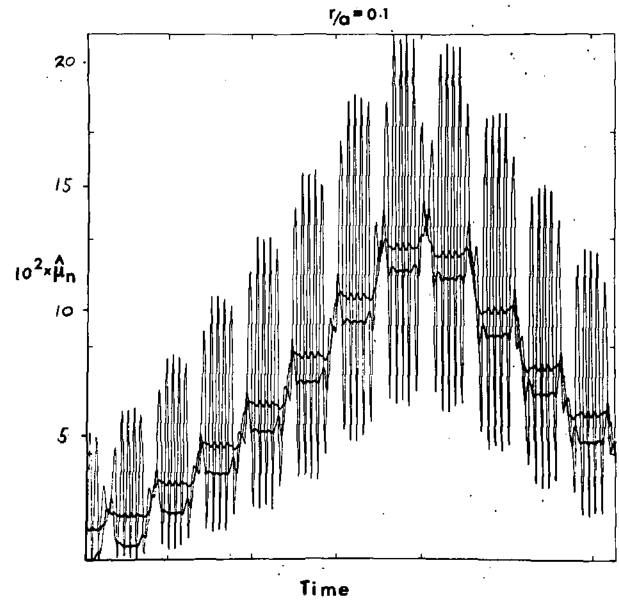

FIG.7. Variation of $\hat{\mu}_n / \frac{v^2}{2B_m}$ × 10^2 versus time; n = 2, q = 2.0, $\Phi = 0$, $\Psi = 0$, r/a = 0.1, $\varphi = 0$.

3. ANALYTIC APPROXIMATION FOR $\Delta\mu$

We outline here a method for obtaining an analytic formula for the non-adiabatic mid-plane jumps $\Delta\hat{\mu}$ in $\hat{\mu}$ observed in the previous section. In essence it involves integrating the time derivative of μ_0 along an approximate orbit in the neighbourhood of the mid-plane. The method is applicable to trajectories in magnetic fields of arbitrary form, but for simplicity we treat only the linear multipole in detail

We first note that the overall change of $\hat{\mu}_n$ in one transit is essentially given by $\Delta\hat{\mu}_0$ since $\hat{\mu}_1$ and $\hat{\mu}_2$ are small in the adiabatic region on either side of the jump. For $\hat{\mu}_0$ we have the exact equation

$$\frac{d\mu_0}{dt} = -\frac{v_\perp}{B}\left\{\left(v_\parallel^2 + \frac{1}{2}v_\perp^2\right)\rho_1 \cos\varphi + \frac{v_\parallel v_\perp}{2}\rho_2 \cos 2\varphi\right\} \qquad \ldots (3.1)$$

where ρ_1, ρ_2, φ are defined in paragraph 2, and $v_\parallel$, $v_\perp$ have their usual meaning. Then

$$\Delta\mu_0 = \int_{-t}^{t} \frac{d\mu_0}{dt}\, dt \qquad \ldots (3.2)$$

where $t = 0$ is the time of arrival at the plane $\Phi = \pi$.

(a) Transformation to Averaged Variables

The observed non-adiabatic effects are confined to a narrow region about the $\Phi = \pi$ plane which suggests that the integral can be evaluated by expanding the orbit about this plane. In the small larmor radius limit however, φ is a rapidly rotating phase, $d\varphi/dt = O(\omega_c)$, and higher order time derivatives of all quantities get progressively larger as the order is increased, so that the range of validity of a direct expansion of φ, $v_\parallel$ and $v_\perp$ shrinks to zero as the expansion proceeds.

To overcome this difficulty we first transform to 'averaged variables' discussed by Bogoliubov and Zubarev [11]. These have the property that time derivatives of all quantities do not depend on the phase and so higher order time derivatives remain of zero order in the expansion parameter which is effectively $1/\omega_c$. Regarding this parameter as small, the transformation to first order is

$$\begin{aligned}
\varphi &= \bar{\varphi} + \frac{1}{\bar{\omega}_c}\left[\left(\frac{\overline{v^2\rho_1}}{v_\perp}\right)\cos\bar{\varphi} + \left(\frac{\overline{v_\parallel\rho_2}}{4}\right)\cos 2\bar{\varphi}\right] \\
v_\parallel &= \bar{v}_\parallel - \frac{\bar{v}_\perp}{\bar{\omega}_c}\left[(\overline{v_\parallel\rho_1})\sin\bar{\varphi} + \left(\frac{\overline{v_\perp\rho_2}}{4}\right)\sin 2\bar{\varphi}\right] \\
v_\perp &= \bar{v}_\perp + \frac{\bar{v}_\parallel}{\bar{\omega}_c}\left[(\overline{v_\parallel\rho_1})\sin\bar{\varphi} + \left(-\frac{\overline{v_\perp\rho_2}}{4}\right)\sin 2\bar{\varphi}\right] \\
\underset{\sim}{r} &= \bar{\underset{\sim}{r}} + \frac{\bar{v}_\perp}{\bar{\omega}_c}\left[\cos\bar{\varphi}\,\underset{\sim}{e}_z - \sin\bar{\varphi}\,\bar{\underset{\sim}{e}}_n\right]
\end{aligned} \tag{3.3}$$

and the time derivatives of the averaged variables are given by

$$\begin{aligned}
\frac{d\bar{\varphi}}{dt} &= -\bar{\omega}_c \quad ; \quad \frac{d\bar{v}_\perp}{dt} = -\frac{\bar{v}_\parallel\bar{v}_\perp}{2}\bar{\rho}_2 \\
\frac{d\bar{v}_\parallel}{dt} &= \frac{\bar{v}_\perp^2\bar{\rho}_2}{2} \quad ; \quad \frac{d\bar{r}}{dt} = \bar{v}_\parallel\,\bar{\underset{\sim}{e}}_1 + \frac{1}{\bar{\omega}_c}\left(\bar{v}_\parallel^2 + \frac{1}{2}\bar{v}_\perp^2\right)\bar{\rho}_1\, e_z
\end{aligned} \tag{3.4}$$

Using the transformation to averaged variables in lowest order $\Delta\hat{\mu}_o$ may be written

$$\Delta\mu_o = -\mathrm{Re}\int_{-t}^{t} dt\left\{v_\perp(v_\parallel^2 + \tfrac{1}{2}v_\perp^2)\,\frac{\rho_1}{B}\,e^{i\varphi}\right\} \quad . \tag{3.5}$$

where we have dropped the bar superscripts for convenience. We have also omitted terms in $\exp 2i\varphi$ as these would lead to exponentially smaller contributions to $\Delta\mu$ than terms in $\exp i\varphi$. This expression (3.5) is of the form

$$I = \int_c \chi(z)\, e^{\frac{1}{\varepsilon}f(z)}\, dz \tag{3.6}$$

with $\varepsilon \ll 1$ which is normally evaluated by the steepest descent method, expanding $f(z)$ about the point ζ where $f'(\zeta) = 0$. However in (3.5) the function $\chi(z)$ has a pole at ζ so that before applying the saddle point method we must rewrite (16) as

$$\Delta\hat{\mu}_o = -\mathrm{Re}\int \frac{v_\perp}{B_o}\left(v_\parallel^2 + \frac{1}{2}v_\perp^2\right)\rho_1\, e^{i\varphi - \log B/B_o}\, dt \tag{3.7}$$

We now carry out a Taylor expansion about the mid-plane and obtain $\Delta\mu_0$ in the form 3.6 with

$$\frac{1}{\varepsilon}f(z) = -i\omega_{co}\left[z + \frac{B_0''}{B_0}\frac{z^3}{6}\right] - \log\left(1 + \frac{B_0''}{B_0}\frac{z^2}{2}\right) + i\varphi_0 \tag{3.8}$$

$$\chi(z) = \left[v_\perp\left(v_\parallel^2 + \frac{1}{2}v_\perp^2\right)\frac{\rho_1}{B}\right]_0 + \frac{z^2}{2}\left[\frac{v_\perp}{2}\left(v_\parallel^2 - \frac{1}{2}v_\perp^2\right)\frac{B''}{B}\rho_1 + \frac{v_\perp}{B}\left(v_\parallel^2 + \frac{1}{2}v_\perp^2\right)\rho_1''\right]_0 \tag{3.9}$$

and where $B_0'' = \left[v_\parallel^2\frac{\partial^2 B}{\partial\ell^2}\right]_{t=0}$; $\rho_1'' = \left[v_\parallel^2\frac{\partial^2\rho_1}{\partial\ell^2}\right]_{t=0}$

and c is a contour in the complex plane connecting $-t$ and t.

The saddle point $z = \zeta$, of $f(z)$ is given by

$$-i\omega_{co}\left[1 + \frac{B_0''}{B_0}\frac{z^2}{2}\right] - \frac{\frac{B_0''}{B_0}z}{1 + \frac{B_0''}{B_0}\frac{z^2}{2}} = 0 \tag{3.10}$$

whose solution may be written

$$\zeta_\pm = -i\sqrt{\frac{2B_0}{B_0''}} \pm \frac{i}{\sqrt{\omega_{co}}}\left(\frac{B_0}{2B_0''}\right)^{1/4} + O(\varepsilon) \tag{3.11}$$

where the + sign in 3.11 must be taken so that the path of integration does not cross the branch cut from the singularity at $z_0 \equiv -\sqrt{2B_0/B_0''}$.

Finally, $\Delta\mu_0$ is given, in terms of the averaged variables as

$$\Delta\mu_0 = A\,\mathrm{Cos}\,\varphi_0 e^{-\alpha/\varepsilon} \tag{3.12}$$

where

$$A = -\frac{(\pi e)^{1/2}}{4}\left[\frac{v_\perp\rho_1}{B}\left(v^2 + \frac{1}{2}v_\perp^2\right) - \frac{v_\perp\rho_1''}{B''}\left(v^2 + v_\parallel^2\right)\right]_0\left(\frac{2B_0}{B_0''}\right)^{1/2} \tag{3.13}$$

and

$$\alpha/\varepsilon = \frac{2}{3}\,\omega_c\left(\frac{2B_0}{B_0''}\right)^{1/2} \tag{3.14}$$

To compare this with the numerical results, we must return from the averaged to the local variables. The inverse transformation, since it introduces $o(\varepsilon)$ corrections, need only be applied to the exponential term. The result is

$$\Delta\mu_0 = A\,\mathrm{Cos}\,\varphi_0 e^{-\alpha/\varepsilon}\, e^{\beta\,\mathrm{Sin}\,\varphi_0} \tag{3.15}$$

where

$$\beta = \frac{1}{3}\rho_1 v_\perp\left(\frac{2B_0}{B_0''}\right)^{1/2}\left(1 + \frac{\rho_1''}{\rho_1}\frac{B}{B''}\right) \quad \text{and} \quad A,\ \alpha/\varepsilon \tag{3.16}$$

are as given in 3.13 and 3.14.

The method outlined above can also be applied to the more complicated case of a multipole field with a superimposed constant B_z.

4. DISCUSSION AND COMPARISON OF ANALYTIC AND NUMERICAL RESULTS

In the previous section we derived a theoretical expression for the non-adiabatic jumps discussed in paragraph 2. In this section we investigate the dependence of this expression, on the velocity and field variables, and compare the predicted jumps with those obtained numerically.

(a) Dependence on Phase Angle

The analytic formulae (3.15 and 3.17) show that the dependence of $\Delta\hat{\mu}$ on the phase φ_0 is a distorted cosine with zeros at $\varphi = \pi/2$, $3\pi/2$ but with maxima displaced from 0, and π. The zeros at $\pi/2$, $3\pi/2$, corresponding to trajectories with $v_n = 0$ at $t = 0$, are a consequence of the symmetry - any change in $\hat{\mu}$ in one half of the trajectory being cancelled in the other. The displacement of the maxima arises from the factor $\exp(\beta \sin \varphi)$ introduced by the transformation from average (or guiding centre) variables to particle variables. It reflects the fact that for a given guiding centre position orbits with negative v_n penetrate nearer to the field zero than do orbits with positive v_n.

Fig.8 shows a direct comparison of the phase dependence of $\Delta\hat{\mu}$ (broken line) with the numerical calculations (solid line). There is a discrepancy in amplitude which will be discussed later; however the dependence on phase is very accurately predicted as can be seen from Fig.9 where the curves have been normalised to a common amplitude.

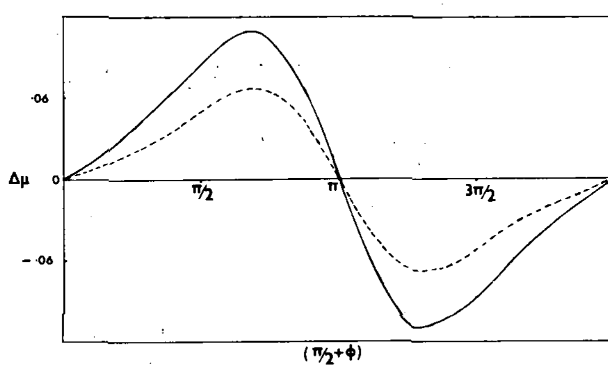

FIG.8. Variation of $\Delta\hat{\mu}$ against phase; $n = 2$, $q = 1.19$, $\Psi = 0.8$, $r/a = 0.075$.

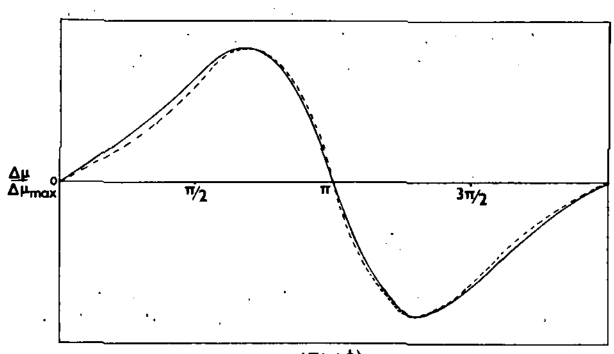

FIG.9. Variation of $\Delta\hat{\mu}/\Delta\hat{\mu}_{max}$ against phase. [Renormalized version of Fig.8]; $n = 2$, $q = 1.19$, $\Psi = 0.8$, $r/a = 0.075$.

(b) Dependence on Pitch Angle

Fig.10 shows the comparison of the pitch dependence of $\Delta\hat{\mu}$ from theory with that from the numerical calculations. The numerical values of $\Delta\hat{\mu}$ become increasingly difficult to define as $v_{\parallel} \to 0$ ($\psi \to \pi/2$) because the orbit does not then penetrate far enough into the mirrors for a steady value of $\hat{\mu}$ to be defined.

Such, nearly planar orbits are of some interest in that the quantity $\int p_n\, dn$ is then an invariant . It can also be shown that if $v_{\parallel} = 0$ the infinite series for $\hat{\mu}$ can be summed and is a true constant. In other words if the magnetic moment series is regarded as being a double expansion in $\varepsilon_{\perp} = v_{\perp}/L_{\perp}\,\omega_c$ and $\varepsilon_{\parallel} = v_{\parallel}/L_{\parallel}\,\omega_c$ then when $\varepsilon_{\parallel} \to 0$ the $\varepsilon_{\perp}$ series can be summed and tends to a true constant of motion - albeit a trivial one. However as $\varepsilon_{\perp} \to 0$ the magnetic moment still exhibits abrupt changes, proportional to $\exp^{-1/\varepsilon_{\parallel}}$, which cannot be represented by a power series in $\varepsilon_{\parallel}$.

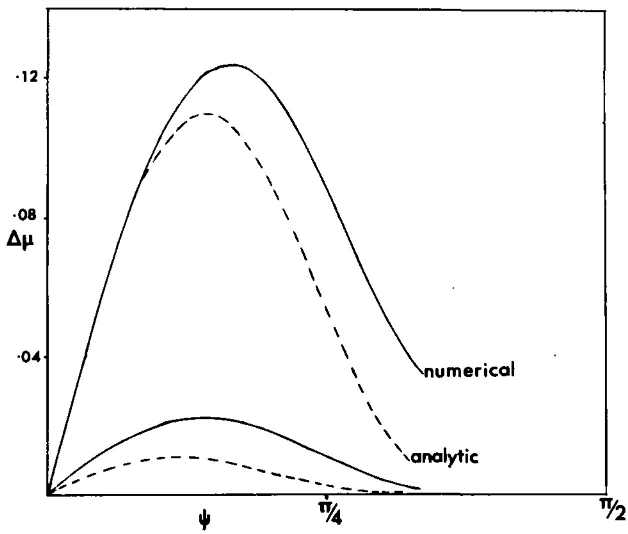

FIG.10. Variation of $\Delta\hat{\mu}$ against pitch; n = 2, q = 1.19, r/a = 0.075, r/a = 0.05, φ = 0.

(c) Dependence on Energy

The comparisons made so far confirm that eq.(3.15) gives the correct phase and pitch dependence for $\Delta\hat{\mu}$ but have revealed a consistent discrepancy in the magnitude of $\Delta\hat{\mu}$. This is also illustrated in Fig.11 where the variation of $\log \Delta\hat{\mu}$ is shown as a function of a/r_L (which is proportional to $1/v$) for a particle of pitch $\psi = 0{\cdot}75$ in a quadrupole field. The theoretical curve again gives the correct qualitative behaviour but the slope is somewhat too large. The dependence of this slope, i.e., of $d(\log \Delta\hat{\mu})/d(1/v)$, on pitch angle is shown in Fig.12 for orbits in both quadrupole and octopole. It will be seen that the theoretical curves (a) lie consistently above the numerical curve (c).

We believe this discrepancy is primarily due to the Taylor expansion of the magnetic field rather than to the use of the averaged orbit equations. That this is so is indicated by the improvement shown when this

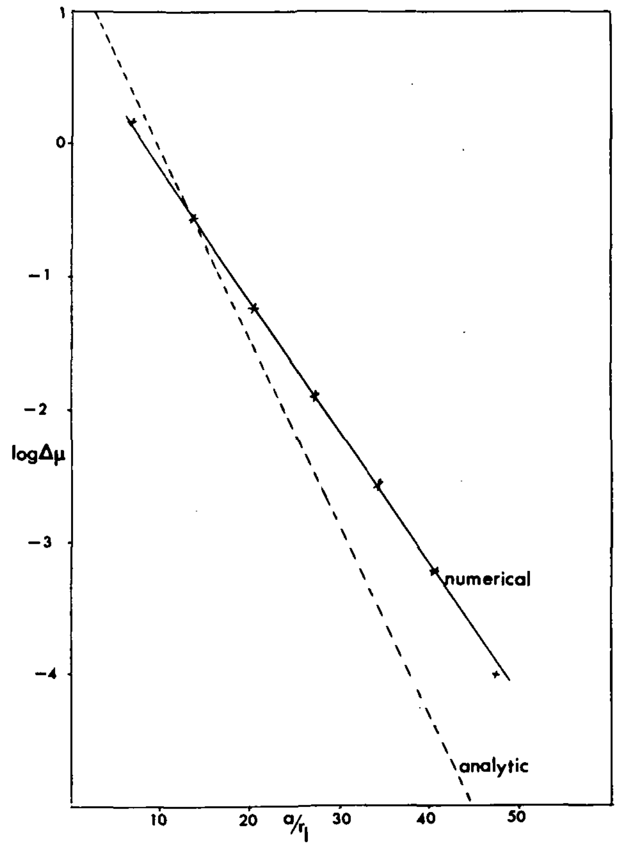

FIG. 11. Variation of log $\Delta\mu$ against $a/r_L = \frac{a\,eB_0}{mv}$; $n = 2$, $q = 1.19$, $\Psi = 0.75$, $\varphi = 0$. Here $B_0 = 2B(q = 2,\ \Phi = \pi) = 2I/a$.

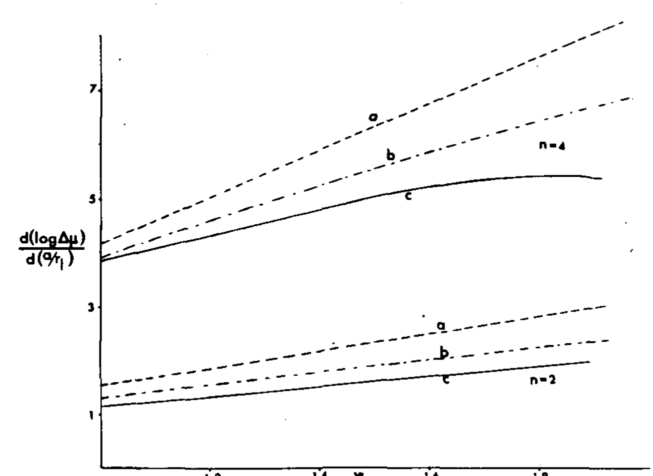

FIG. 12. Variation of $d(\log \Delta\mu)/d(a/r_L)$ against $v/v_\parallel$ for quadrupole ($n = 2$) and octopole ($n = 4$).

expansion is carried out to higher order (fifth order instead of third). The effect of this improvement is to multiply the exponential in eq.(3.15) by

$$\frac{3\sqrt{3}}{5} Q^{\frac{1}{2}} (2-Q)$$

where

$$Q = \frac{\left[1 + \frac{2}{3}\left(\Upsilon + \frac{2v_\perp^2}{v_\parallel^2}\right)\right]^{\frac{1}{2}} - 1}{\left(\Upsilon + \frac{2v_\perp^2}{v_\parallel^2}\right)}$$

and

$$\Upsilon = \frac{7-n}{n-1} + \frac{n}{(n-1)} \frac{(q-1)^2}{q}$$

The result of this change is shown in the modified theoretical curves (b). These show that the improvement in the representation of the field has significantly improved the agreement between the theoretical value and the numerical calculations.

REFERENCES

[1] GARREN, A., et al. 2nd Int. Conf. Peaceful Uses Atom. Energy (Proc. Conf. Geneva 31 (1958).

[2] GRAD, H., van NORTON, R., Nuclear Fusion Supp. Part 1 (1962) 61.

[3] HOWARD, J.E., Bull. Am. Phys. Soc. 13 (1968) 267.

[4] DYKHNE, A.M., POKROVSKY, V.L., Soviet Physics JETP 12 (1961) 264.

[5] DYKHNE, A.M., CHAPLIK, A.V., Soviet Physics JETP 13 (1961) 465.

[6] BALEBANOV, V.M., SEMASHKO, N.N., Nuclear Fusion 7 (1967) 207.

[7] KRUSKAL, M.D., Princeton Univ. Rep. PM-S-33 (1958)

[8] GARDNER, C.S., Phys. Fluids 9 (1966) 1997.

[9] HASTIE, R.J., TAYLOR, J.B., HAAS, F.A., Ann. Phys. 41 (1967) 302.

[10] HOBBS, G.D., TAYLOR, J.B., Culham Rep. CLM-R 95.

[11] BOGOLIUBOV, N.N., ZUBAREV, D.N., Ukrainian Mathematical Journal VII, (1955).

DISCUSSION

D.G. BARATOV: What type of magnetic field did you use?

R.J. HASTIE: We used linear multipole fields - both octopole and quadrupole.

P.L. HUBERT: A statistical theory first proposed by Robson and Taylor leads to the conclusion that, in a system such as the one which you are studying, the equilibrium particle distribution corresponds to a uniform density throughout the accessible phase space. It would be interesting to verify this prediction on the basis of your calculations if the computed variations in μ or the analytical formulas could be used for very long times.

R.J. HASTIE: To follow actual particle orbits on the computer would require too much time, but if the analytical formula for $\Delta\mu$ were used to predict successive values of μ, what you propose should be possible.

E. CANOBBIO: In your oral presentation you spoke of two analytical methods for approximating $\Delta\mu$. Do they both have the same expansion parameter?

R.J. HASTIE: The only difference between the two methods lies in the approximation of the orbit integration: there is mid-plane expansion in one case and not in the other. The small parameter is the same in each case, namely the adiabatic parameter ϵ.

LINEAR MULTIPOLE AND SPHERATOR EXPERIMENTS

S. YOSHIKAWA, M. BARRAULT,* W. HARRIES, D. MEADE,†
R. PALLADINO AND S. VON GOELER
PLASMA PHYSICS LABORATORY, PRINCETON UNIVERSITY,
PRINCETON, N.J., UNITED STATES OF AMERICA

Abstract

LINEAR MULTIPOLE AND SPHERATOR EXPERIMENTS. Plasma containment and fluctuations are being studied in magnetic field configurations with strong stabilizing and symmetry properties. For this purpose, a multipole device with linear conductors (LM-1), and a toroidal single-ring device (spherator) have been constructed.

The LM-1 facility has been operated as a quadrupole, generally in the collisionless regime, with $n = 10^{10} - 10^{12}$ cm^{-3} and $T = 1 - 10$ eV. Plasma production by rf ohmic heating and resonant microwave heating has been used for $T_i \ll T_e$; and gun injection for $T_i \gtrsim T_e$.

Both high-frequency fluctuations with $k_\parallel \neq 0$, and low-frequency, $k_\parallel = 0$ modes have been observed inside the $\int d\ell/B$ - stable region. The structure of the high-frequency mode fits the theory of drift-type ballooning. It is suppressed by a weak axial field. The low-frequency fluctuation, which may be related to the trapped-particle mode, is suppressed by $T_i \gtrsim T_e$. The plasma profile on the minimum-B (conductor) side is always quiescent.

The observed confinement times (typically 1-2 ms) are limited mainly by radial (outward) plasma loss in the $T_i \ll T_e$ case, and mainly by axial loss in the $T_i \gtrsim T_e$ case. In the first case, the confinement time is typically ten times Bohm. In the second case, the confinement time as calculated from the radial loss corresponds to approximately fifty times Bohm.

The radial transport in LM-1 is not, in general, well correlated with the fluctuations, and one deduces the existence of additional loss mechanisms. Stationary convective cells have been identified in the case of ohmic heating, where the coil structure initiates and maintains a spatial periodicity. Their relevance to the anomalous transport is being studied.

The spherator experiments were performed in density and temperature ranges similar to LM-1. Fluctuations can be suppressed throughout the density profiles under certain conditions of plasma parameters. Plasma confinement times are measured to be 2-25 ms and the particle loss is mainly to supports of the centre ring under typical conditions. Under best conditions, support loss accounts for more than 95% of the total particle loss. In terms of Bohm confinement times, the typical confinement times calculated from the loss other than to supports are ten times Bohm, but under optimum conditions confinement times reach 40 times Bohm. A centre ring with reduced support area is being substituted and a superconducting ring has also been tested, for later operation.

1. INTRODUCTION

Toroidal devices with strongly stabilizing properties and azimuthal symmetry are expected to yield valuable information concerning equilibrium and stability of low-β toroidal plasmas. Encouraging results have been reported previously [1, 2, 3]. As a part of a project, which eventually leads to a superconducting levitated-ring device, we have initiated a study on multipole devices. Our objectives are manyfold: (1) to determine what processes are responsible for plasma loss, (2) to

* On leave from the University of Liverpool
† Now at the University of Wisconsin

investigate methods of heating, (3) to study fluctuations and to relate the observation to theory, and (4) to gain experiences which will be used to improve the design of the large levitated device (FM-1).

We have two devices in operation. The linear multipole device (LM-1) is composed of two parallel conductors of 5 m length, each conductor bundle carrying up to 60 kA turn. The small aspect-ratio single-ring conductor device similar to the Levitron [4], called the spherator [5] (SP-1), has a suspended-ring conductor of 65 cm diameter carrying up to 130 kA turn.

Plasmas have been produced and heated by (i) microwave electron resonance heating, (ii) ohmic heating, (iii) plasma gun, and (iv) hot filament discharge. The range of density is 10^{10} - 10^{13}/cc and the electron temperature T_e is less than 10 eV. The e-folding decay times are between 500 μsec and 2 msec in LM-1 and are typically between 2 and 30 msec in SP-1.

We shall discuss (a) LM-1 and (b) SP-1 experiments in that order.

2. LINEAR MULTIPOLE

2.1. Description of device

The linear multipole's two conductors are housed in a stainless steel casing, so that the displacement of the two conductors due to mutual attraction can be kept to the tolerable limit (Fig. 1). An axial magnetic field (parallel to the conductors) can be applied by the separate set of coils, as well as a mirror magnetic field to reduce the axial particle loss. The location of the plasma can be constrained by a set of limiters as shown in Fig. 1. Limiters also act as the particle loss detectors. Similar limiters are placed on one of the center conductors to measure the particle loss to the center conductor. Two sets of particle collectors are placed on both ends of LM-1 to determine the axial loss.

Plasmas are produced by microwave electron resonance heating at 12 cm and 3 cm wavelengths. By adjusting the center conductor current, we can change the resonance region, because the magnetic field varies from 0 to ~4 kG at the maximum current in the conductors. Ohmic heating at frequencies from 3 kc/sec to 200 kc/sec has also been tried. An electric field parallel to the magnetic field line can be applied by a set of coils placed 20 cm apart in the axial direction, inducing current in the plasma which acts as the secondary (Fig. 1). Plasmas also can be injected by a hydrogen-loaded titanium-washer gun placed facing perpendicular to the magnetic field. We also tried ion cyclotron resonance heating at 2.4 Mc/sec. The result so far obtained by this mode of heating is not encouraging. It is possible, however, that this result is due to the fact that high-energy ions are easily lost through the ends by lack of equilibrium.

Diagnostics chiefly used are Langmuir probes, magnetic probes, microwave interferometers, spectroscopy, and particle loss detectors.

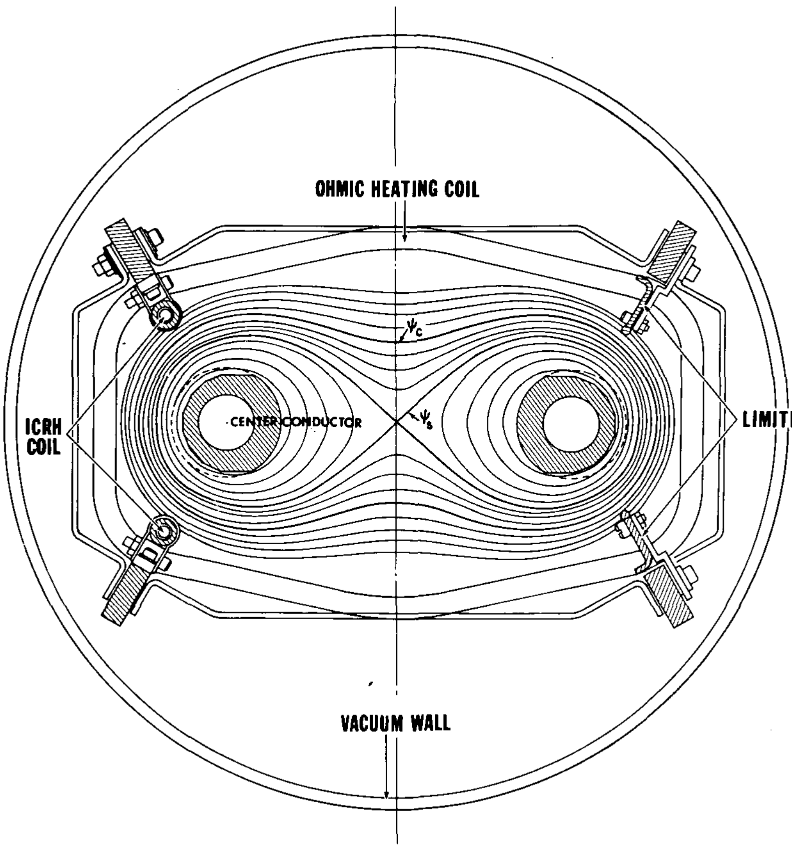

FIG.1. Cross-sectional view of the linear multipole device (LM-1). Ohmic heating coils as well as brackets to hold the assembly shown in the figure are spaced 20 cm apart. Stainless steel tubes to hold centre conductors (Q-lines) are shaped to follow a contour of a magnetic field line.

Electron temperature is determined by Langmuir probe characteristics, and plasma densities are determined both by probes and by interferometers. There is generally a satisfactory agreement between the two methods. Ion temperature is determined by spectroscopic methods and the particle energy analyzer. A detailed discussion of particle loss detectors is given in the Appendix.

2.2. Plasma production and heating

Radio-frequency heating can be used to preionize and heat the plasmas. Operating pressure of the system is typically 2×10^{-5} to 5×10^{-4} torr. With microwave heating, there is no indication of the production of high-energy electrons above 1 keV. The plasma is formed chiefly near the input port of the microwave and spreads slowly along the axis.

With ohmic heating, because the coil has a periodicity of 20 cm, the plasma is formed non-uniformly. Plasma temperature is higher just under the coil. Because the current flows along the confinement magnetic field lines and the alternating magnetic field is perpendicular to the current, the force $\vec{J} \times \vec{B}$ acts on the plasma similarly to the transverse magnetic field effect of a current-carrying torus [6]. The force tends to push the plasma inwards under the coil.

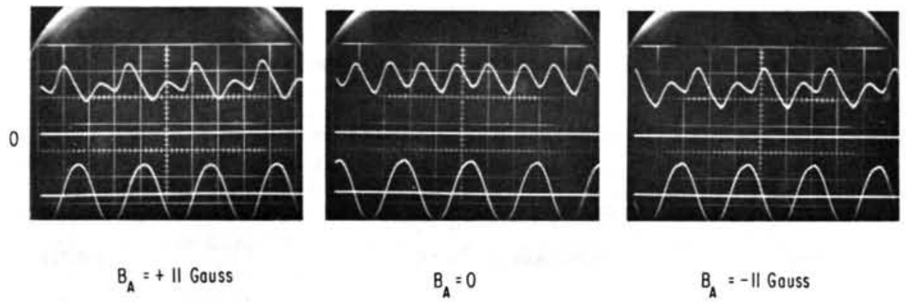

UPPER TRACE: Temporal variation of the ion saturation current I_{SAT} at the center of the machine for different values of the axial magnetic field B_A

(time scale 20μs/div; I_{SAT} 5 mA/div $\approx 4 \times 10^{11}$ e/cc/div).

LOWER TRACE: Proportional to the induced electric field.

FIG. 2. Ion saturation currents (which roughly reflect the density) vs time, when a periodic $\vec{E}$ field (ohmic heating) was applied parallel to $\vec{B}$. Line with 0 indicates the zero of the upper trace. Therefore, density changed up to 50% during one period of the ohmic heating.

An interesting effect of this $\vec{J} \times \vec{B}$ force is shown in Fig. 2. Since the current, $\vec{J}$, alternates, if we have a small uniform magnetic field superimposed on the axial directions, the force becomes either inwards or outwards depending upon the phase of the current which flows in the plasma. We expect that if the force is inwards, the plasma is well contained and if the force is outwards, the plasma is lost. In Fig. 2, the plasma density (the ion saturation current since the temperature is almost constant) is shown as a function of time for three cases of the axial magnetic field. In the absence of the axial magnetic field, the density has twice the frequency of the applied ohmic heating current, because the ionization is proportional to J^2. In applying a uniform field, the plasma density is less in the phase of the alternating current where the $\vec{J} \times \vec{B}$ force points outwards.

Using radial particle loss detectors, we can measure the confinement times even during the rf heating when the plasma is being formed by ionization. The confinement times thus deduced are typically 400 - 500 μsec and, taking the measured electron temperature of 3 - 4 eV, we conclude that the confinement time divided by the Bohm time is typically 10. However, our main measurement of the confinement times is taken in the afterglow, where the density distribution is peaked near the separatrix (ψ_s in Fig. 1) and is low near the critical surface (ψ_c in Fig. 1).

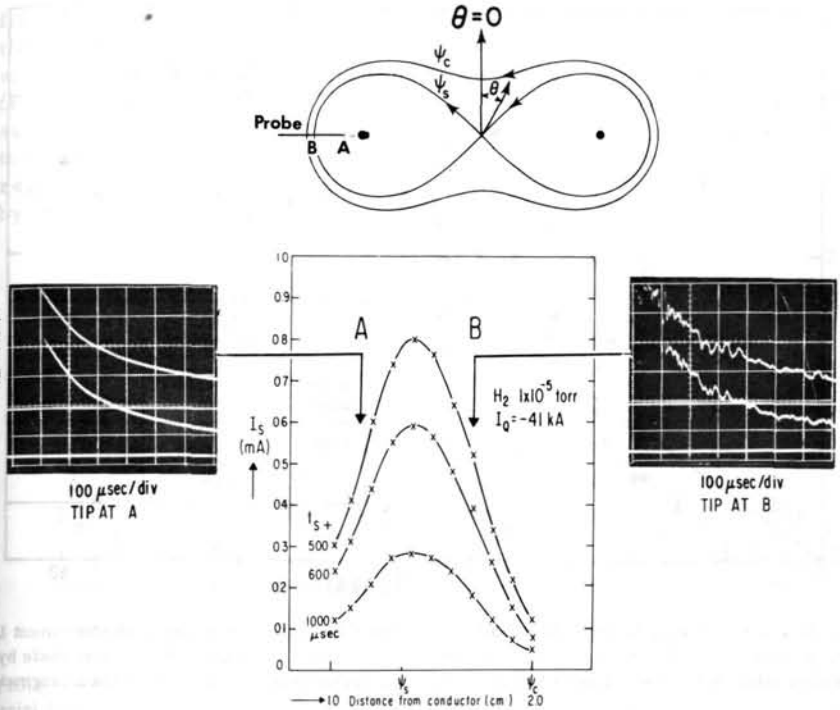

FIG. 3. Ion saturation currents vs time taken by a probe placed in the bad curvature section where $\nabla B^2 \cdot \nabla p > 0$. The oscilloscope pictures of approximately same average signals located on opposite sides of the density gradient are also shown.

2.3. Density distribution and particle loss times

The decay of the plasma as a function of time in the afterglow of rf-produced plasmas is shown in Fig. 3. We note that the plasma decays, maintaining its shape. We know by observation of electron temperature and plasma density that the particle loss is not due to recombination. By integrating the density distribution with proper geometric weighting, we can determine the particle loss times. The resultant confinement times vs the center conductor currents (I_Q) are shown in Fig. 4. The confinement times measured by the particle loss detectors also agree in general with this method. Confinement times thus calculated can be compared with the Bohm diffusion times using the formula first given by D. Meade [7]. Confinement times are approximately ten times the Bohm value.

Where the particles are lost, then, can be answered. It is obvious that, because the system is linear, a lack of equilibrium results in making particles escape from both ends of the device. The theoretical estimate, however, shows that the movement of particles along the axis is slow compared with the sound velocity of the plasma. In fact, the plasma loss detector measurements show that only approximately one tenth of the total particles are lost to both ends, and the main loss can be accounted for by the radial loss away from the center conductors as shown in Fig. 5.

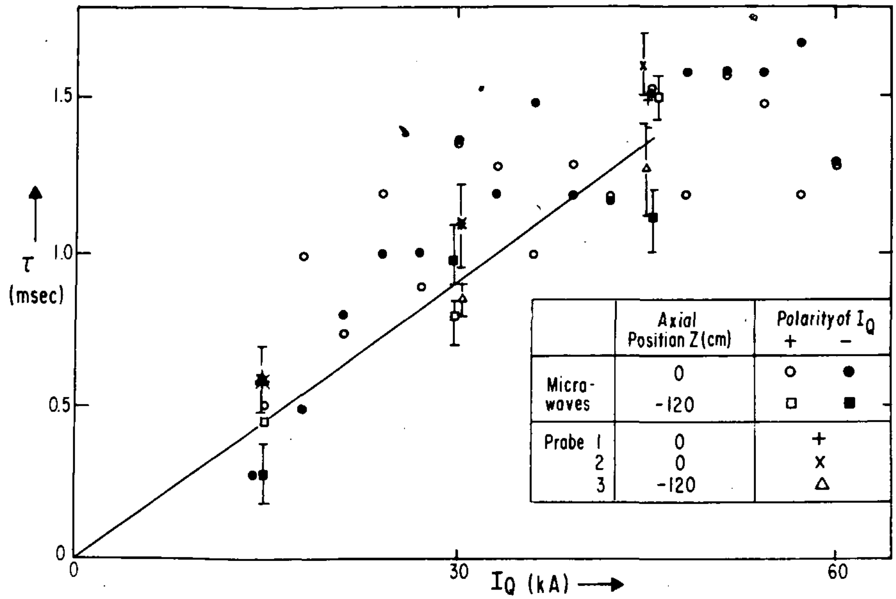

FIG. 4. Plasma confinement times τ (measured 1 ms after the rf heating) vs the centre conductor current I_Q for both polarities of I_Q. Electron temperature was approximately 1 eV. Measurements of τ were made by a microwave interferometer with 2 horns placed 12.0 cm apart in the axial direction and by three Langmuir probes.

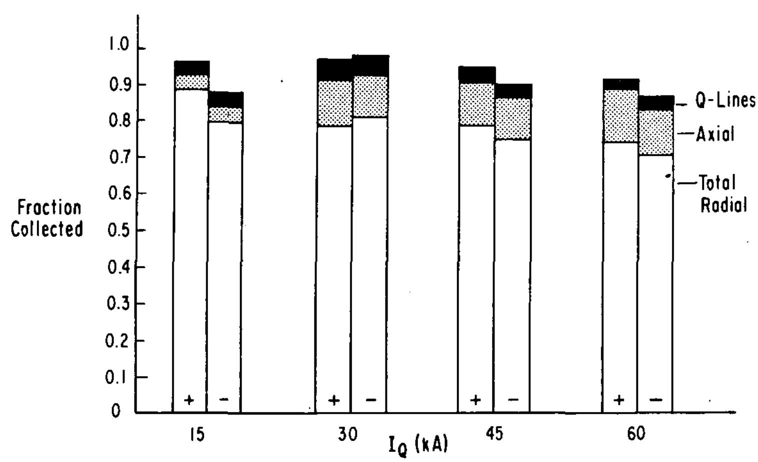

FIG. 5. Particle losses estimated from detectors, divided by the total number of particles contained in LM-1. Radial loss means the loss outwards away from centre conductors (Q-lines), whereas loss to centre conductors is indicated by Q-line loss.

2.4. Mechanisms of particle loss

The observation shows very clearly that the particles are lost across the magnetic field. The question then arises whether the loss is triggered by fluctuations in the range of drift frequencies. Although the fluctuation may account for the loss where the fluctuations exist, fluctuation alone cannot explain the transport of particles. In Fig. 3, two probe signals at the same average currents located at points towards and away from the center conductor are shown. We note that plasma decays at the same rate at both locations. Since we can neglect the particle loss to the ends and the center conductors, it follows that plasma in the stable region is somehow transported across the magnetic field and collected by the limiters.

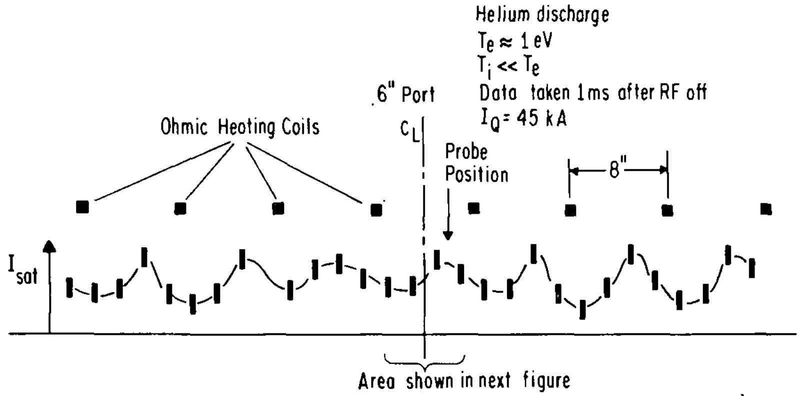

FIG. 6. Losses to limiters measured by small detectors placed 5 cm apart. Horizontal axis represents the axial dinstance (i.e parallel to Q-lines). Note that the loss was measured 1 ms after the ohmic heating was turned off.

One of the mechanisms which may explain this particle loss is the observation that plasmas are not uniform along the z direction. Instead, the plasma once formed by the ohmic heating keeps the periodic variation along z, even after the ohmic heating current is turned off. The particle loss outwards, for example, reflects the periodicity of the ohmic heating coil even after 1 msec (Fig. 6). Probe measurements also reflect the periodicity (Fig. 7). Any calculations based on the non-equilibrium of the plasma would predict that this kind of variation in density should disappear in the time of the order of 100 μsec.

Therefore, we are led to investigate the possibility that a stationary equilibrium with the plasma flow may exist. Under highly idealized conditions, solutions which have a density variation along the z direction exist if the plasma is allowed to rotate with a velocity comparable to $(|x/R|)^{1/2} v_i$, where x is the distance taken from ψ_c where $d/d\psi \oint d\ell/B = 0$, R is the radius of the curvature, and v_i is the sound velocity of the plasma [8]. Since the experiments were carried out in relatively low magnetic fields, the measured plasma potential $\sim kT_e/e$ is sufficient to provide the necessary rotational velocity.

The mechanism for this convective structure could also be caused by the anomalous conductivity across the magnetic field. The anomalous conductivity could start the polarization field and slow down the plasma expansion. Neutrals present in the device are not enough to let ions provide the necessary depolarization current through collisions.

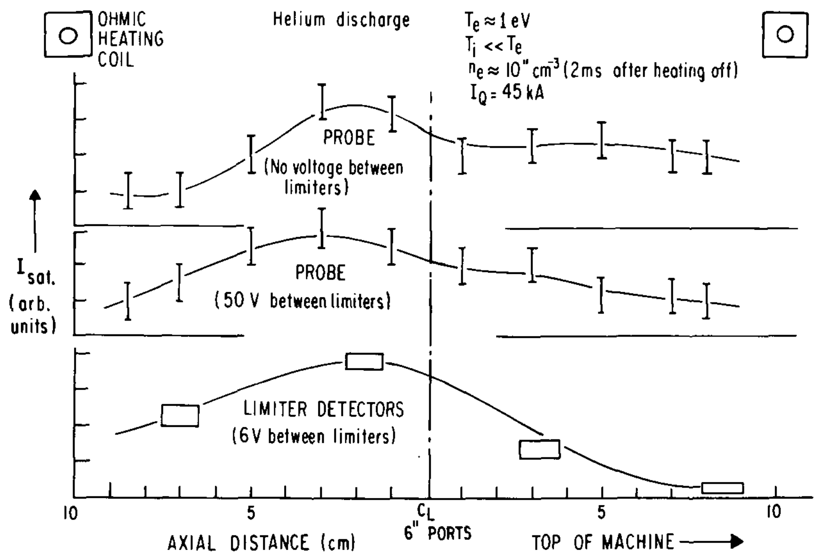

FIG. 7. Ion saturation current to probe near ψ_c and limiter detectors 2 milliseconds after ohmic heating was turned off. Notice that probe signal was not greatly influenced even when the bias voltage of 50 V was applied.

Periodic loss structures of approximately the same periodicity as the ohmic heating coil spacing are also observed after application of microwave heating. In order to see whether there is any relation between the two periodicities, a new, almost uniformly-wound coil is being substituted.

2.5. Gun-injected plasmas

We also injected plasmas created by a hydrogen-loaded titanium-washer gun. Electron temperatures measured by Langmuir probes ranged between 4 and 7 eV, and the density profiles (as interpreted from the ion saturation current) were more peaked than those of the rf-produced plasmas. The plasma density was typically 10^{10}/cc. The confinement of plasmas can be determined by the decay of the ion saturation current of Langmuir probes and independently through the integration of particle loss observed by detectors. Confinement times were typically 500 μsec. The particle loss to the axial detector is, contrary to rf-produced plasmas, typically about a factor two times greater than the particle loss to the radial detector. Data are summarized in Fig. 8. We note that if we take $T_e \approx$ 5 eV as measured by Langmuir single-probe characteristics, the confinement times are 50 times greater than Bohm time. Since the absolute confinement times are rather short, and the Langmuir probe temperature measurement may be in error, the results are to be treated with caution.

In another set of experiments, gun-injected plasma confinements are measured with the axial field which provides the shear to the magnetic field. Due to (presumably) the change in the gun performance, the electron temperature under this condition was approximately 2 eV and

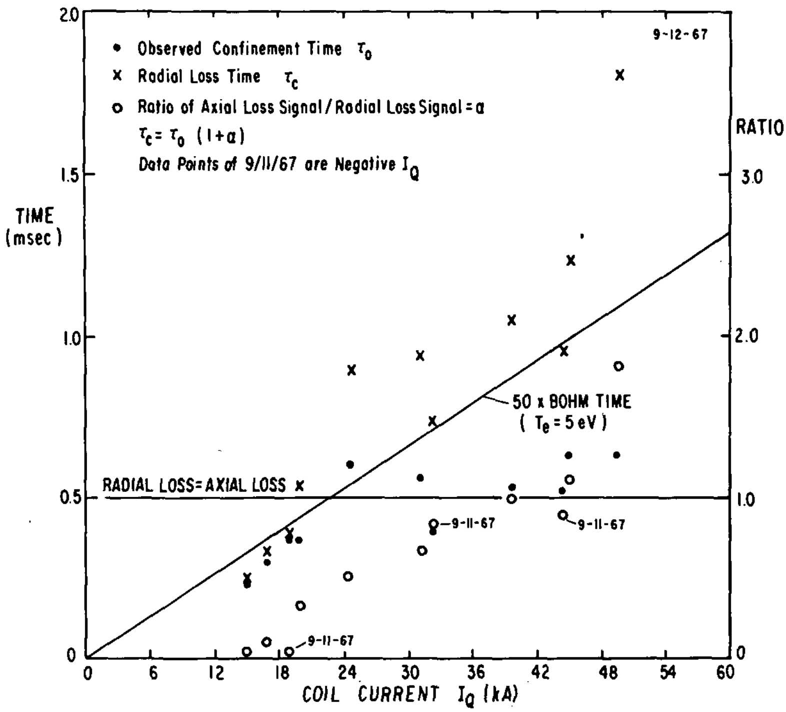

FIG. 8. Confinement time as a function of the centre conductor current, I_Q. Observed confinement times τ_0 saturate as I_Q is increased. The ratio of axial loss to Q-radial loss, α, however, increases with I_Q. If we estimate the radial loss time above, we find the confinement times, τ_c, actually increase with I_Q.

the plasma density was $\sim 3 \times 10^{10}$/cc. By applying a 3.6 times mirror field at both ends of the linear multipole, the confinement of plasmas as seen by ion saturation current and particle loss detectors was increased by approximately a factor of 1.5-2 above that of the plasma without mirror field. This experiment supports the inference drawn from the particle loss detector that the plasma is lost axially in the gun-produced plasma. In rf-produced plasmas, the application of the mirror field did not alter the confinement times as expected. The mirror field is not expected to be reduced because the aperture in the axial direction is restricted. (For the total integrated particle loss versus time see Fig. 9).

2.6. Fluctuations

Previously, it was reported that a ballooning type of oscillation [8] is observed in the LM-1 [9]. The frequency is $\sim$ 200 kc/sec, and the plasma could be stabilized against this instability by an application of small axial field which presumably stabilizes this instability by the effect of shear. In Fig. 10, ion saturation current traces taken from two Langmuir probes located on the same magnetic field lines are shown. In the region where $\nabla B \cdot \nabla p > 0$, we see that high-frequency oscillations were superimposed on the low-frequency oscillation. This high-frequency oscillation is interpreted as the oscillation produced by the ballooning

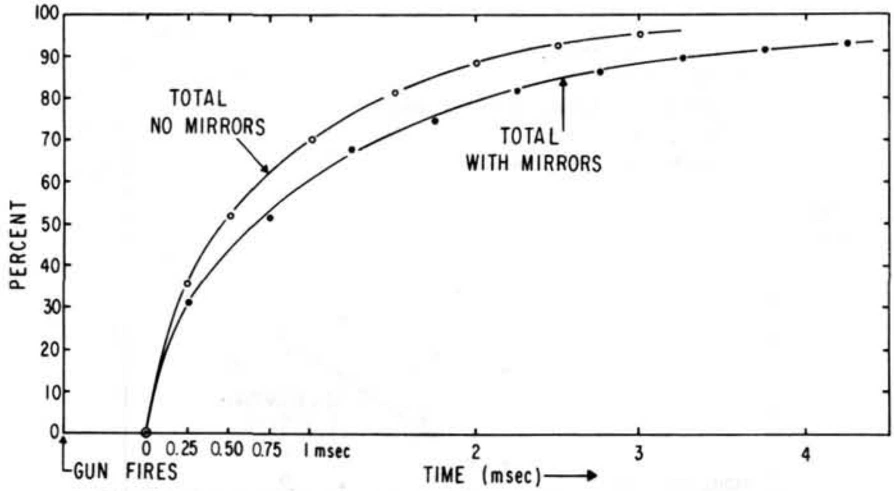

FIG. 9. Total integrated particle loss vs time. Since mirror fields were applied only at both ends, the plasma characteristic (in particular, injection processes) is not expected to change. We see a reduction in the particle loss with mirror fields on.

instability. The low-frequency oscillations have $k_{\parallel} = 0$ and appear only in the region between ψ_s and ψ_c, as is apparent from Fig. 3.

From a rather general consideration, it is expected that the $k_{\parallel} \neq 0$ mode can only be possible if the frequency is high enough so that $\omega/k_{\parallel}$ exceeds in thermal velocity. The observations are consistent with this consideration.

The mode $k_{\parallel} = 0$ appears to be a gravitational wave with the finite Larmor radius correction given by the relation [10]

$$\omega = 1/2 \left[\omega_{*i} \pm \sqrt{\omega_{*i}^2 + 4\kappa \frac{kT_i}{M} \frac{\bar{1}}{R} \left(1 + \frac{T_e}{T_i}\right)} \right]$$

where

$$\omega_{*i} = - \frac{kT_i}{eB} k_{\perp} \kappa$$

$$\kappa = - \frac{d}{dr} (\ell n \, n)$$

Here the curvature $1/R$ is averaged along a magnetic field line. In the $\oint d\ell/B$ stable region, $\overline{1/R}$ is positive. Thus, the frequency is real. The wave, however, can couple to electrons (if $T_e \gg T_i$) which are traveling perpendicular to the magnetic field with the phase velocity given by $-\omega/k_{\perp}$ moving in the direction opposite to the average electrons. Or in terms of the second invariant J, those electrons have the property that

$$\frac{\partial J}{\partial \psi} \cdot \frac{dP}{d\psi} < 0$$

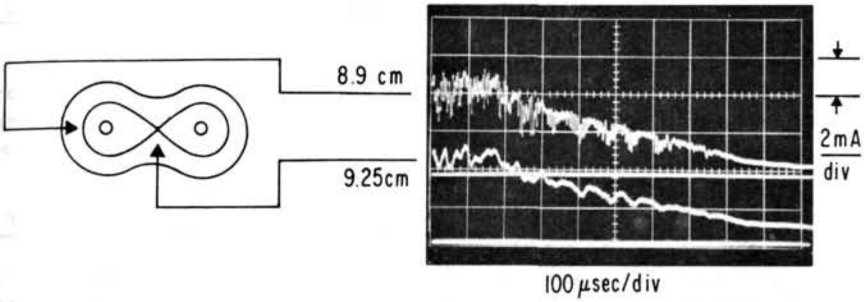

FIG. 10. Ion saturation currents in afterglow measured by two probes located on the same field line. Gas used was helium and I_Q = 45 kA.

Frequencies, perpendicular wavelengths, and resonant conditions agree with the above theoretical mechanism. Also, the instabilities are absent or very small with the gun-injected plasmas (where $T_i > T_e$), which is to be expected from the theory.

As has been stated previously, the fluctuations do not appear to be responsible for the anomalous particle loss observed in our device. However, it is quite conceivable that once we can eliminate the present particle loss mechanism, the fluctuations may be the limiting factor for the particle loss in the future.

3. SPHERATOR

3.1. Description of device

The magnetic configuration normally used for the experiment is shown in Fig. 11. The vacuum vessel is 1.5 m in diameter, the toroidal field coil is housed in 8.9 cm o.d. stainless tube, and the poloidal field coil has a minor diameter of 7.6 cm and a major diameter of 65 cm (Fig. 12). The poloidal field coil is suspended by six supports, and a current feed is attached from the side. In the first version, water-cooled conductors were used for the poloidal field coil. This required a current feed of 3 cm equivalent diameter. The supports were made of 1/8" stainless rods. The total surface area divided by the plasma volume, $1/L_f$, was approximately 1/10 m. That is, an average particle would hit the support or the current feed after the particle traveled a flight distance, L_f, of 10 m. In the second version, no water-cooled poloidal field coil was used. The current feed diameter is now reduced to 4 mm, and each of the six supports has a diameter of 1 mm. The flight distance is then increased by a factor of 6 and now is ~ 50 m. Eventually, a suspended and then a levitated superconducting coil is contemplated.

The current of the toroidal field coil can go up to 520 kA turn pulsed (72 kA steady) and the current of the poloidal field coil of the first version could go up to 130 kA turn pulsed (36 kA turn steady). The

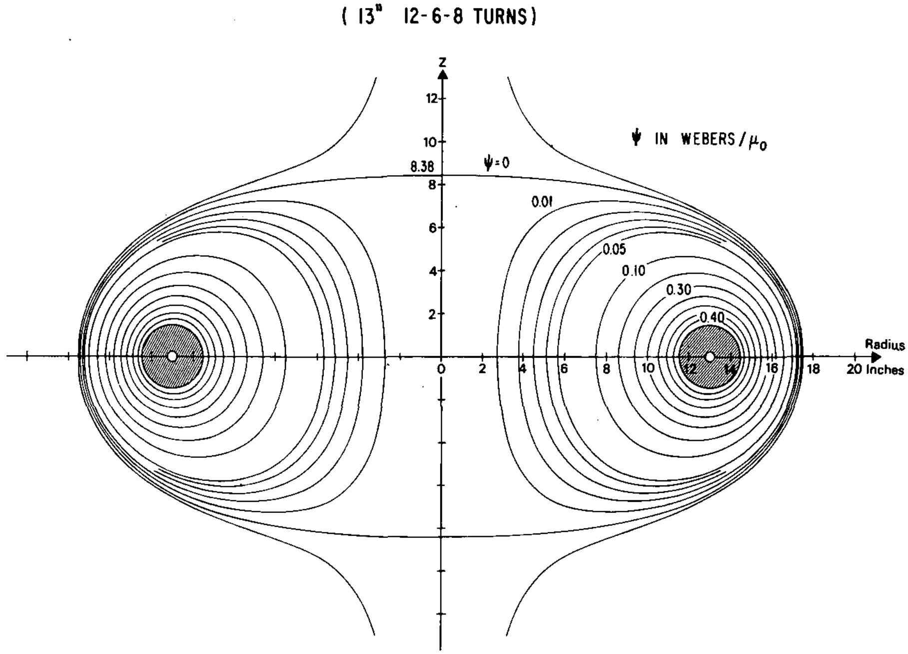

FIG. 11. Standard magnetic field configuration of spherator. The flux ψ refers to poloidal field current of 1 A.

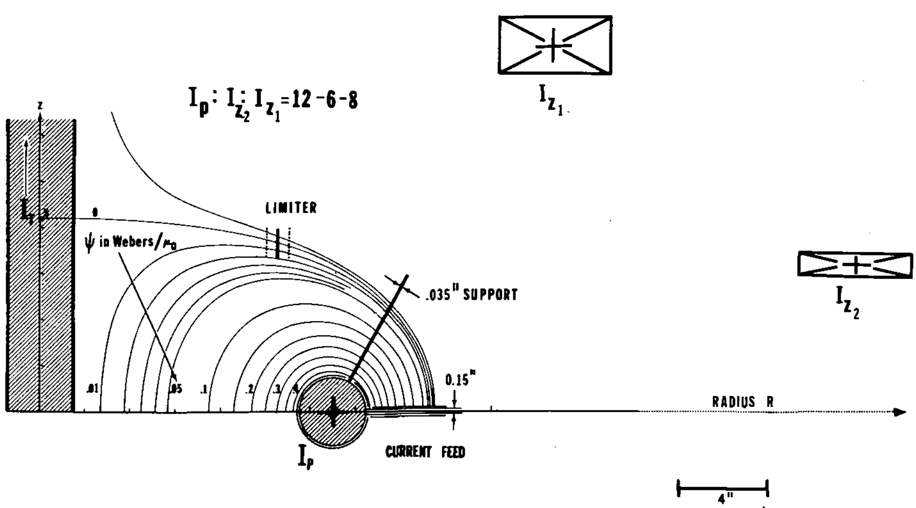

FIG. 12. Experimental configuration of spherator. Three sets of poloidal field coils (I_p, I_{Z_2}, I_{Z_1}) produce different magnetic field configurations, whereas toroidal field coil (I_T) changes shear and minimum average B property.

poloidal field coil of the second version has been tested up to 33 kA turn. The magnetic field strength is typically 1 kG at 33 kA turn for both toroidal and poloidal field currents.

3.2. Objectives of experiments

The objectives of the experiments with this supported version are to determine how the plasma is lost, to see whether the plasma is unstable, and to study the production and the generation of plasmas in the spherator geometry.

3.3. Plasma production and diagnostics

Plasmas could be produced in various ways. We have chiefly used 12 cm microwave electron resonance heating, but have also used 3 cm and 10 cm microwaves, ~ 1 kc and 200 kc ohmic heating, gun injection, and a filament discharge. The plasmas created are similar in characteristics to those in the LM-1. For the reasons stated before, we looked mainly at the decay of plasmas in the afterglow. The plasma densities of the experiments ranged between 10^{10} - 10^{12}/cc, and electron temperatures in the afterglow were typically 2 eV - 0.5 eV. The neutral density was typically 10^{12}/cc. The confinement times depended on the gases used, and ranged up to 40 msec, but at 1 eV or more the confinement times were limited so far to less than 30 msec.

Diagnostics used are a microwave interferometer, Langmuir probes, and a monochrometer. Since the surfaces of supports, poloidal field coil, toroidal field coil, and limiter are electrically isolated from ground, by simply biasing them negative with respect to ground, while grounding some of the supports, we can get an estimate of ions impinging on the surfaces in the absence of the bias (see Appendix). Often the plasma is influenced by the presence of biases. However, we can generally minimize the influence by adjusting biases, and a series of self-consistency checks indicates that our measurements cannot be off by more than a factor of 2. Since, in a perfectly confined system, particle loss to limiter and poloidal field coil surfaces would be almost zero (except for the classical diffusion term), any measurement of particles arriving on those surfaces implies the existence of anomalous particle loss.

The measurement of the loss to the limiter follows the principle used for the particle detection in the LM-1. A detailed description is given in the Appendix. The limiter can be moved vertically to limit the plasma at a desired radius. When the limiter is moved up completely, the toroidal field coil casing limits the plasma aperture.

3.4. Measurement of density profiles

Density profiles are measured by Langmuir probes biased negative with respect to ground (usually supports or poloidal field coil surfaces are grounded). Density profiles depend strongly on how the plasma is created. If a microwave is used, the plasma is first created at the resonance magnetic field and then the density peak shifts outwards, if the microwave is kept on (Fig. 13). Data of Fig. 13 were taken superimposing many pulses. The technique was described in detail by Harries elsewhere [11]. The plasma density usually reaches up to 10^{12}/cc, far above the density where the plasma frequency equals the microwave frequency.

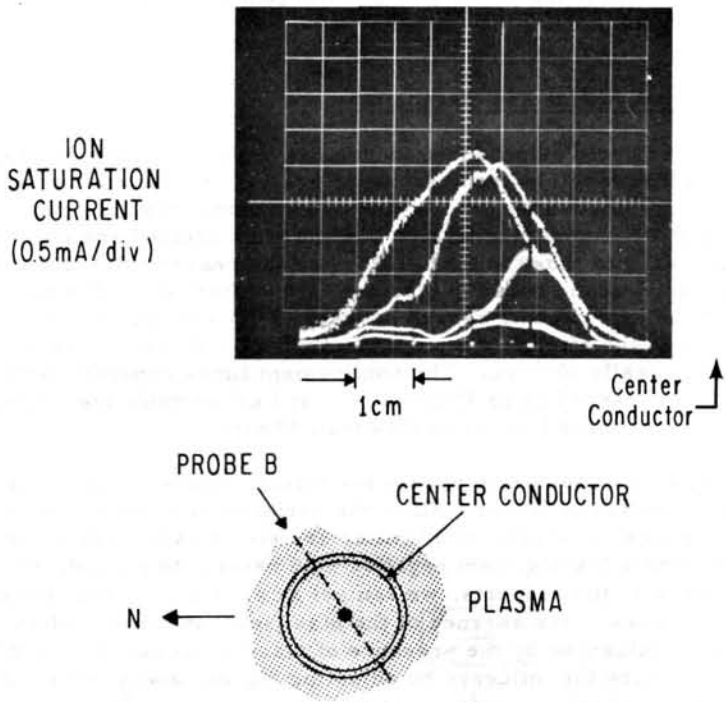

FIG. 13. Density profiles measured by a probe during microwave heating phase. Plasmas are created first near centre conductor (poloidal field coil) and the density peak gradually shifts outwards, at the same time the peak amplitude increases. Many shots (1 pulse per second,were used to make this profile.

Density profiles plotted vs the magnetic surfaces ψ are shown in Fig. 14. Ion saturation currents were measured by three probes. We note that the density for a given magnetic surface is nearly constant. A more careful study is shown in Fig. 15. Two probes placed diagonally opposite were used to determine the density profile. The agreement between the two probes indicates that the deviation of plasma density on a given magnetic surface cannot exceed more than 5%. Thus, the confinement measurement of plasmas can be considered to represent that of toroidal plasmas.

3.5. Particle loss time and cooling time

Since the density profiles do not change appreciably during the afterglow, it is reasonable to determine the confinement times through the decay times of the microwave interferometer signals. As electron temperatures cool in the afterglow, we measured the confinement time at T_e = 1 eV. In general, the confinement times change more slowly

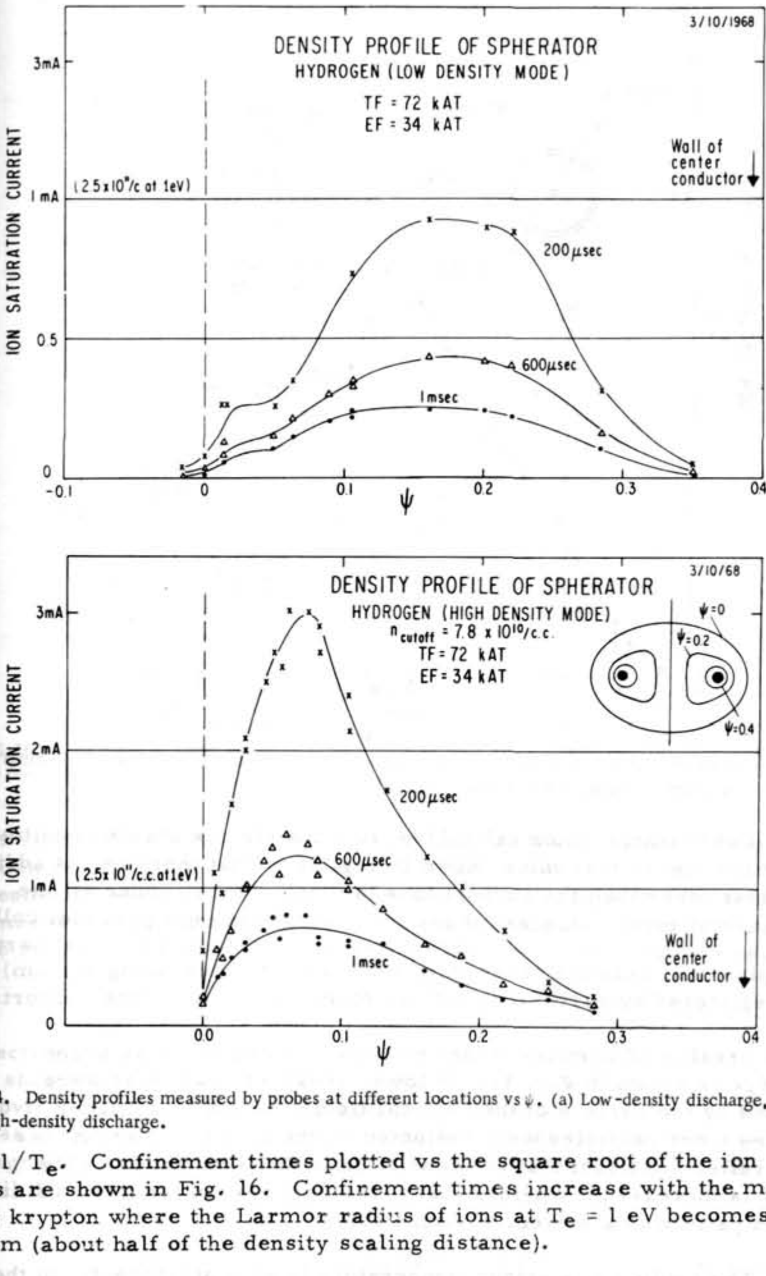

FIG. 14. Density profiles measured by probes at different locations vs ψ. (a) Low-density discharge, (b) high-density discharge.

than $1/T_e$. Confinement times plotted vs the square root of the ion mass are shown in Fig. 16. Confinement times increase with the mass up to krypton where the Larmor radius of ions at T_e = 1 eV becomes ~ 1 cm (about half of the density scaling distance).

Bohm confinement time was calculated by von Goeler et al. [12], using the extension of technique first used by D. Meade [7]. The calculation shows that, at the poloidal field current of 36 kA turn in the standard condition, the Bohm time at T_e = 1 eV should be ~ 2 msec. Since the magnetic field is somewhat lower in the case of Fig. 16, we arrive at $(\tau/\tau_B)_{max}$ = 18.

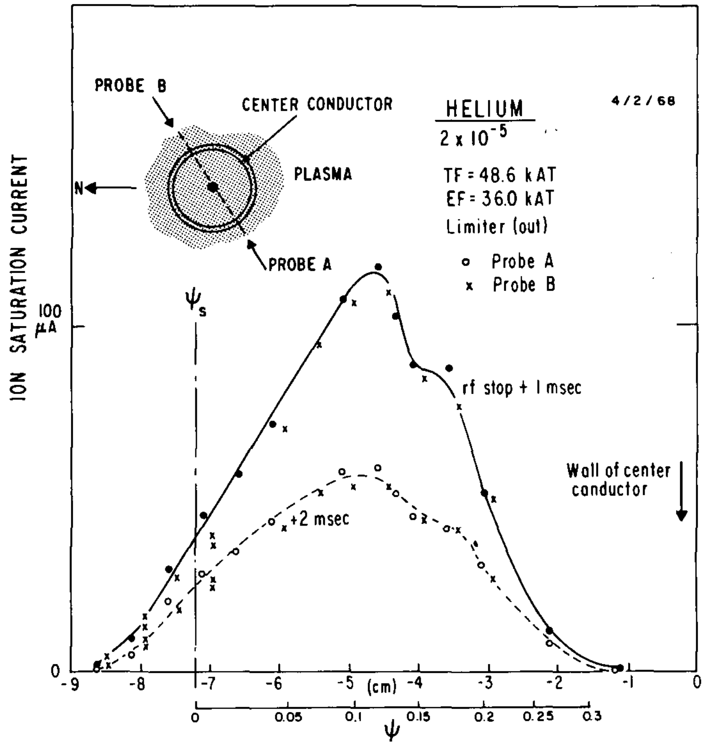

FIG. 15. Density profiles vs horizontal probe positions. Two probes at diagonally opposite locations were used. TF means toroidal field, and PF means poloidal field.

Confinement times calculated from the plasma sheath condition predict the theoretical value shown in Fig. 16. That there exists additional loss other than the support loss is clear, since, under all the experimental circumstances, more than half of the total particles collected (which, as stated earlier, does not necessarily imply half of the total particles in the plasmas, because of the interference of the measuring system) were registered by particle collectors other than those of the supports.

Breakup of particle losses collected vs density in an argon discharge is shown in Fig. 17. In lower densities, particles were collected by the surface of the poloidal field coil, while in higher densities more particles were collected by the limiter. Part of this result reflects the fact that the density peak shifts outwards as the density is increased. Whether that is the only reason for this shift in the loss pattern is a subject of future study.

The cooling of electron temperature is also of interest. In the regime of T_e = 1 - 2 eV in noble gas discharges, excitation and ionization of neutral atoms are negligible, whereas the recombination processes are too slow in the density range. Electrons are cooled by ions through Coulomb interaction and also can lose energy through the sheath effect to supports. The cooling times measured vs densities are shown in Fig. 18. Agreement between the theoretical Coulomb cooling

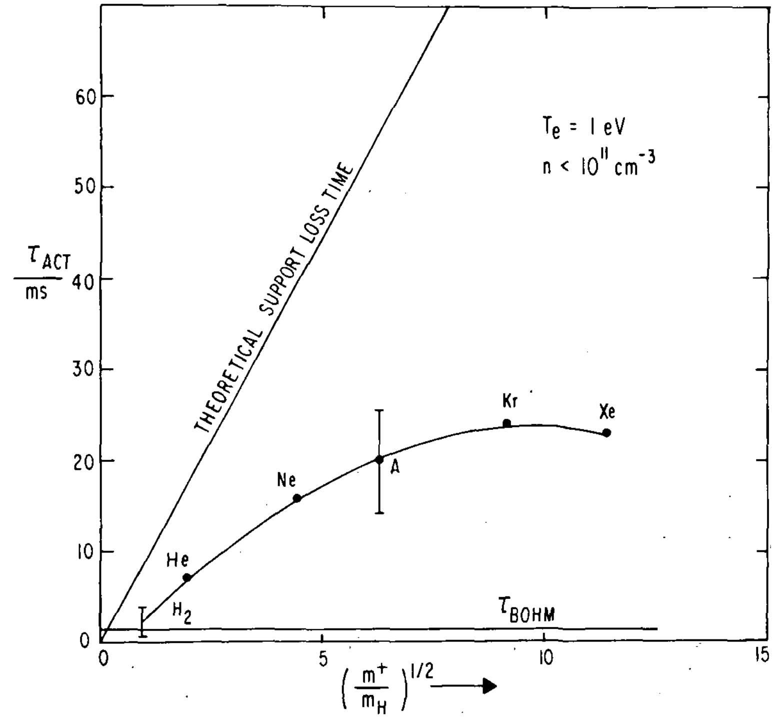

FIG.16. Confinement times measured at T_e = 1 eV vs ion mass. Confinement times are always less than the theoretical loss time to supports.

times and the plasma densities is good in the high-density regime, which gives credence to the determination of electron temperature by means of Langmuir probes. In the low-density regime, the cooling times deviate from the Coulomb cooling times and in general are in the range of 1/4 of the confinement times.

Since, from the sheath condition, we would expect high-energy electrons to be preferentially lost over the cold electrons, it is easy to show that the cooling time τ_T should be equal to $\tau/(\ell n(M/m)^{1/2} + 1)$, provided that the plasma temperature is uniform. The spatial uniformness of temperature requires an anomalous heat conductivity across the magnetic field. A detailed measurement of temperature distribution is still not available.

Confinement times were measured in different magnetic configurations. In general, there is no large difference in the confinement times. The ratio of loss to poloidal field coil and loss to the limiter could be altered by changing toroidal field strength. However, since the density profiles also change with the change in the magnetic configuration, as yet we cannot make any definite statement on the dependence on magnetic configurations.

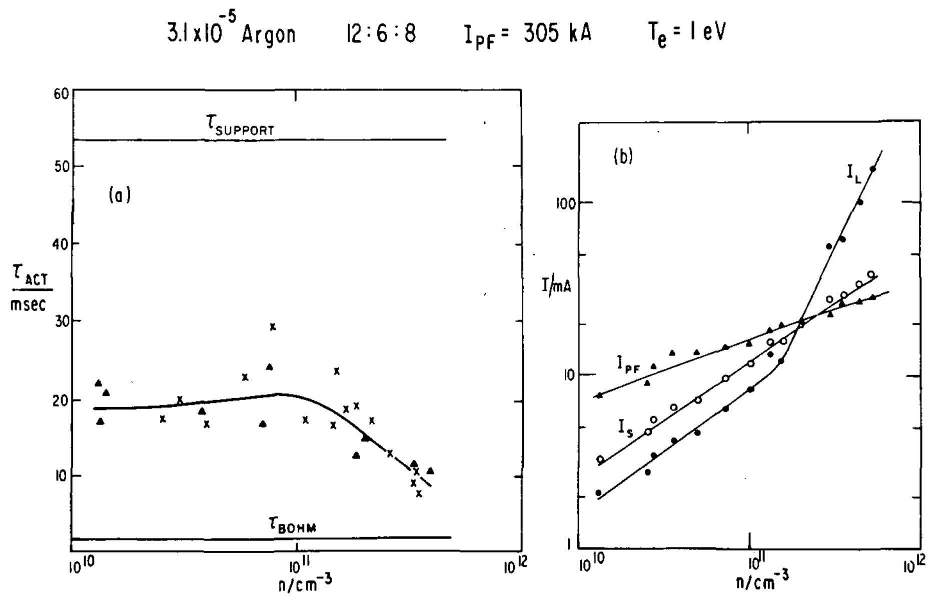

FIG. 17. (a) Actual confinement time vs plasma density determined from microwave interferometer; (b) We notice that particle loss to limiter increases at higher densities, at the same time confinement times decrease. The increase of loss to limiter partly reflects the fact that the density peak shifts outwards at higher densities (cf. Fig. 14), but probably also implies that the mean free path has some influence on confinement.

3.6. Fluctuations

Fluctuations of the plasma (between 1 kc/sec to 1 Mc/sec) were suppressed if the shear was high or if higher ion mass plasmas were used. If the toroidal field strength was low, and if a relatively high-density hydrogen plasma was used, fluctuations were observed in the regime towards ψ_s (Fig. 19) but the fluctuation can be reduced to an amplitude less than $\delta n/n = 1\%$ in higher toroidal fields. The frequency agrees with drift instabilities. Since even in the absence of the fluctuation there is an anomalous loss, we must seek another mechanism for the particle loss.

3.7. Possible mechanisms for particle loss

As in LM-1, we have two possibilities for particle loss. High-frequency instabilities could transport electrons across the magnetic field, and ions follow electrons because of large ion Larmor radius (e.g., by collision with neutrals). Another possibility is very low-frequency instability or lack of equilibrium. Since the present geometry with supports cannot be in toroidal equilibrium, plasmas could conceivably move across the magnetic field by $\vec{E} \times \vec{B}$ drift, the electric field $\vec{E}$ being developed by the presence of the support.

The shadow of the support could extend quite far along the magnetic field line. If we suppose that the density depression created

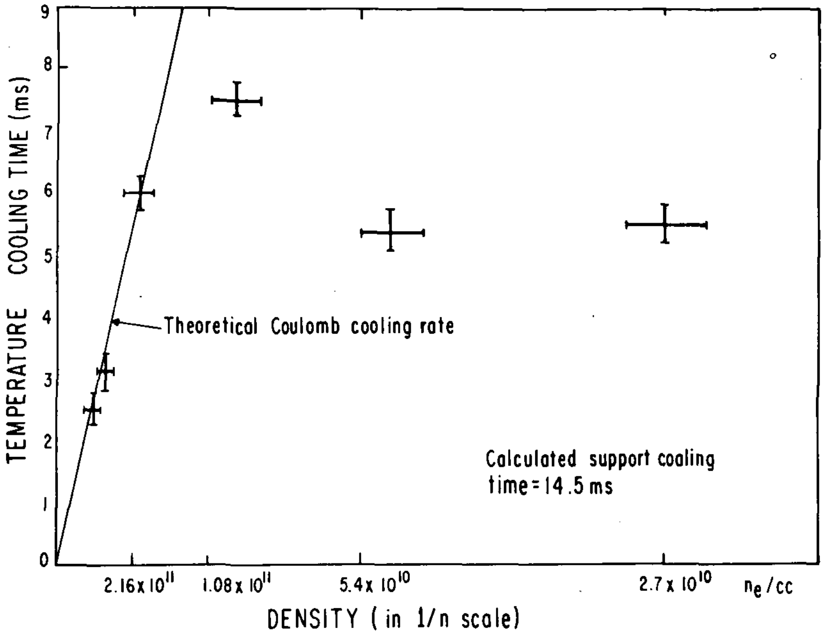

FIG. 18. Temperature cooling times measured from a single Langmuir probe characteristic vs 1/n. At high densities, cooling times agree with calculated Coulomb cooling times. Gas used was argon.

by the support along the magnetic field is filled by classical diffusion (D_{cl}) across the magnetic field, we must satisfy

$$\frac{\partial}{\partial z}(nv_z) - \frac{\partial}{\partial y} D_{cl} \frac{\partial}{\partial y} n = 0$$

where we have assumed that the support extends in the x direction, while the magnetic field is in the z direction. We expect v_z is of the order of the plasma sound-wave velocity and $\partial/\partial y$ is of the order of $2/\lambda$ where λ is the diameter of the support. The extent of the shadow in the z direction, $\mathcal{L}$, is then of the order of

$$\mathcal{L} = \frac{kT_e + kT_i}{M} \frac{\lambda^2}{4D_{cl}}$$

Taking $n = 10^{11}$/cc, $\lambda = 1$ mm, $T_e = 1$ eV, $T_i = 0$, $B = 1$ kG, and $M = 64 \times 10^{-24}$ kg (argon), we obtain $\mathcal{L} = 4$ m. Thus, this shadow could behave as a perturbation in otherwise equilibrium plasma (convective cell) and transport the plasma across the magnetic field. Experimentally, however, we have not observed an indication of this convective cell so far.

One possible outcome of this consideration is that the support could behave as if the size were increased by a factor that may depend

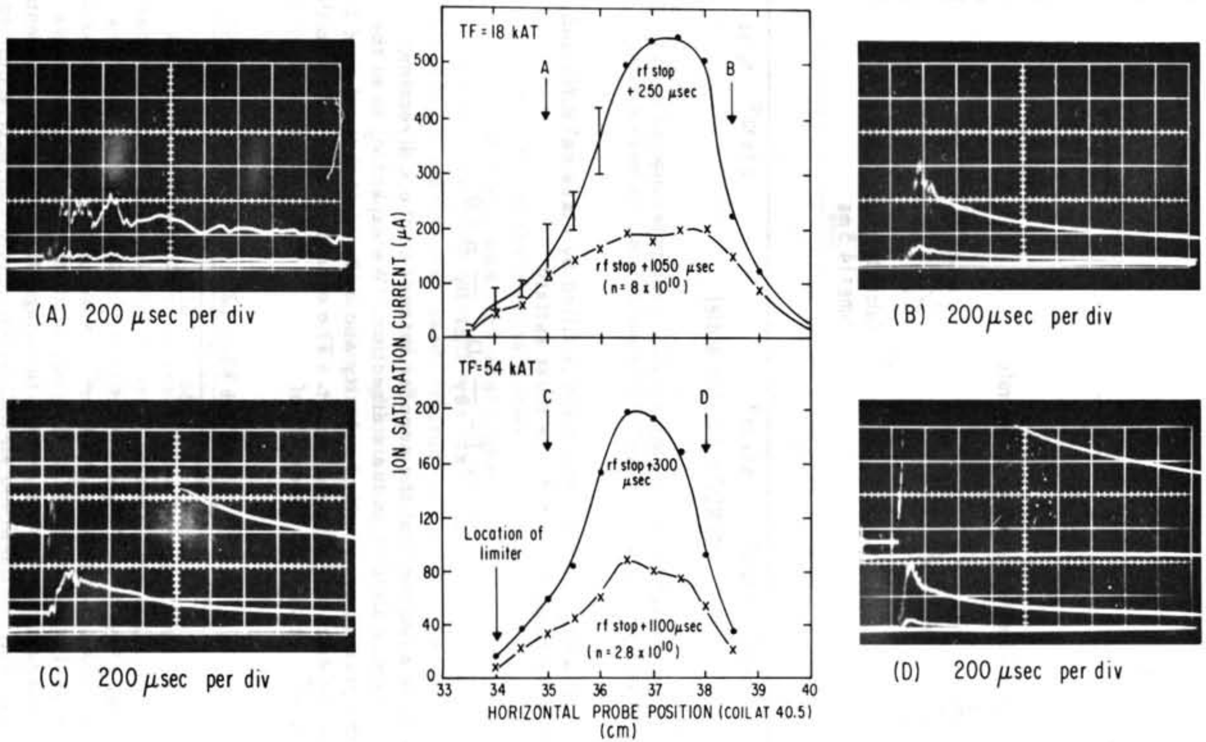

FIG. 19. Density profiles vs positions. The horizontal probe is located on the z = 0 plane as shown in inserts of Fig. 13 and Fig. 15. The bar shown is the peak-to-peak variation of the fluctuation. Two or three traces shown on oscilloscope pictures are the same probe signal at different gains.

on the strength of B (because of $\vec{E} \times \vec{B}$ drift). The experimental data of Fig. 16 are suggestive of this. The final test of this hypothesis, however, awaits a levitated ring.

4. CONCLUSIONS

In both the linear multipole device and the spherator, plasma confinement times were found to be limited to ~ 10 times Bohm time in the rf-produced plasmas where density and temperature were such that isotropic pressure distribution was expected. In the linear multipole device, plasma loss is mainly across the magnetic field, while in the spherator, plasma loss is roughly equally divided among limiter loss, support loss, and poloidal field coil loss.

With gun-injected plasmas in LM-1, the plasma loss to the end could be increased over that of the loss radially outwards, but the latter is still finite. If we make allowance for the end loss, the confinement times over the Bohm times could be increased up to ~ 50 times.

Fluctuations between 1 kc/sec - 1 Mc/sec were observed only in the limited portion of the density profiles (or sometimes none throughout the density profiles), yet the density profiles normalized at the peak density do not change appreciably with time. Hence, we conclude that we have an additional mechanism(s) of the plasma transport other than fluctuations.

The mechanism for this particle loss could lie in the equilibrium. In the case of LM-1, it was observed experimentally that the plasma pressure does not follow $p = p(\oint d\ell/B)$. A corresponding equilibrium solution was obtained theoretically. In the case of the spherator, within the experimental accuracy, $p = p(\psi)$, but it is still possible that convective cells, undetected, still exist. One possible hypothesis is that the existence of supports creates the perturbation which gives rise to cross-field convection. The fact that the confinement times depend on ion mass is highly suggestive of this hypothesis. The experiment to test this hypothesis awaits the levitated-ring experiment.

5. ACKNOWLEDGMENTS

Discussion with members of the Princeton Plasma Physics Laboratory were very helpful in carrying out the experiments. The Engineering groups have done considerable work to expedite the construction of the linear multipole (finished in six months), and of the spherator (finished in 16 months). The technicians group for LM-1 and spherator experiments have contributed to carrying out day-to-day experiments smoothly.

This work was performed under the auspices of the U. S. Atomic Energy Commission, Contract No. AT(30-1)-1238.

REFERENCES

[1] OHKAWA, T., KERST, D.W., Phys. Rev. Letters 7 (1961) 41.

[2] OHKAWA, T., SCHUPP, JR., YOSHIKAWA, M., VOORHIES, H.G., Plasma Physics and Controlled Nuclear Fusion Research (IAEA, Vienna, 1966), Vol. II, p. 531.

[3] DORY, R.A., KERST, D.W., MEADE, D.M., WILSON, W.E., ERICKSON, C.W., Phys. Fluids 9 (1966) 997.

[4] COLGATE, S.A., FURTH, H.P., Phys. Fluids 3 (1960) 982.

[5] YOSHIKAWA, S., CHRISTENSEN, U., Phys. Fluids 9 (1966) 2295.

[6] SINCLAIR, R.M., YOSHIKAWA, S., HARRIES, W.L., KESSLER, J.O., Phys. Fluids 6 (1963) 937.

[7] MEADE, D., Phys. Rev. Letters 17 (1966) 677.

[8] YOSHIKAWA, S., BARRAULT, M. (to be published).

[9] MEADE, D.M., YOSHIKAWA, S., Phys. Fluids 10 (1967) 2649.

[10] COPPI, B., ROSENBLUTH, M.N., Plasma Physics and Controlled Nuclear Fusion Research (IAEA, Vienna, 1966), Vol. I, p. 617.

[11] HARRIES, W.L., Rev. Sci. Instr. (in press).

[12] VON GOELER, S., CHRISTENSEN, U., FISHMAN, H., Princeton University, Plasma Physics Laboratory MATT-607 (1968).

APPENDIX

If a plasma is contained in the region characterized by magnetic surfaces ψ, the particle lost from that surface will go to the limiters and recombine. In general, ions and electrons arrive at the same rate to each limiter. Thus, electrons are repelled by the sheath. If we apply a potential, V, to opposing limiters, the ion current to two plates is essentially unchanged, whereas electron currents, Γ_e, to two plates are given by (like a double probe)

$$\Gamma_e \doteq \frac{I_s}{e}\left(1 \pm \tanh \frac{eV}{kT_e}\right) \qquad (A-1)$$

where I_s is the ion saturation current. Thus, if V is sufficiently high, the net electric current represents one-half of the total flux. We also note that the positive plate is very close to the floating potential of the plasma. This was observed experimentally.

With the spherator, the space requirement makes it impossible to mount two electrodes perpendicular to the magnetic field lines on the supports and the center conductor. Hence, those surfaces are biased negative to ground (while some supports are, for example, grounded) and the resulting ion saturation current is considered to be the measure of the particle loss in the absence of the bias. Plasmas are generally not very much (less than 20%) disturbed in density nor in density decay time.

The limiter of the spherator is made of a molybdenum ring of 56 cm diameter with two complete rings of mesh (about 50% in effective transparency) placed approximately 1.25 cm away in both sides. The mesh rings and molybdenum ring are electrically isolated. By applying potential flowing between the two mesh rings and the molybdenum ring, we can estimate the particle flux to the limiter.

DISCUSSION

R.S. PEASE: Could you summarize the effects observed when the magnetic configuration – particularly the stabilizing properties – is altered?

S. YOSHIKAWA: Containment times are generally unaffected by changes in magnetic field configuration (from minimum average B to maximum average B); they only have to be corrected for changes in the geometric dimensions (radius, etc.). The only exception is when the toroidal field is switched off: the confinement times are then reduced.

As for stability of the system with respect to the magnetic configuration, data on noise amplitude ($\delta n/n$) versus the ratio I_{TF}/I_{PF} for constant absolute magnitude of the magnetic field, indicate that the large shear ($L_s = 10$ cm when the plasma density gradient distance is 1-2 cm – both distances being measured at the probe) is effective in stabilizing the observed oscillation.

V.I. PISTUNOVICH: Do you observe a difference in plasma containment time when you use the ratio T_e/T_i?

S. YOSHIKAWA: There is some difference, but since the density profiles are different I would not like to make any statement at present regarding containment time differences for the spherator.

For LM-2, on the other hand, the figures show that there is a difference between the $T_i \ll T_e$ and the $T_i \gtrsim T_e$ cases.

I.S. SHPIGEL: Do you think that a contribution to the increase in the containment time of high-mass ions in the spherator may have been made by additional ionization through the plasma electrons?

S. YOSHIKAWA: Since our measurement of containment times was made at $T_e = 1$ eV, I do not think that ionization could have taken place. The containment times of both microwave-heated and ohmically heated plasmas are approximately the same. One does not expect mirror-trapped high-energy electrons in the latter case. Furthermore, the particle loss flux measurement agrees with the observed density decay rate to within a factor of two, and, in general, the total particle loss flux is smaller than the density decay rate.

PLASMA CONFINEMENT AND POTENTIAL FLUCTUATIONS IN A SMALL ASPECT RATIO LEVITRON

A. F. KUCKES*AND R. B. TURNER
UKAEA, CULHAM LABORATORY, ABINGDON, BERKS., UNITED KINGDOM

Abstract

PLASMA CONFINEMENT AND POTENTIAL FLUCTUATIONS IN A SMALL ASPECT RATIO LEVITRON. The magnetic confinement of a partially ionized, collisional plasma in a small aspect ratio levitron with considerable magnetic shear was studied. Plasmas produced in a purely poloidal field are observed to be very unstable, but with both poloidal and toroidal fields energized the plasma loss rate from the device is an order of magnitude slower than predicted by Bohm diffusion. Our observations are, however, consistent with plasma loss by diffusion at a rate inversely proportional to B. The plasma confinement does not vary explicitly with shear parameter θ between 0.05 and 0.15. Potential fluctuations are most pronounced on the outer density gradient of the plasma and have a well defined frequency which varies between 50 and 200 kHz. Their frequency is well correlated with that of drift oscillations ($\omega^* = k_\perp \kappa T_e/eB\ 1/n_e\ \partial n_e/\partial_x$) if $k_\perp$ is assumed to be the reciprocal of the plasma gradient length. The maximum rms value of these oscillations is about $0.05\ \kappa T_e/e$.

1. INTRODUCTION

Understanding the nature of plasma confinement by a static magnetic field is one of the outstanding problems of plasma physics today. Since a purely toroidal field does not provide plasma equilibrium one of the simplest closed magnetic surface systems in which to study plasma confinement is a combination of toroidal and poloidal fields [1]. This is the basis of the levitron, in which the poloidal field is generated by current in a ring which is immersed in the plasma, and the toroidal field by currents external to it. Tamm [2] showed that for axially symmetric magnetic fields all particle orbits are confined to within a Larmor radius (defined by the magnitude of the poloidal field) of the magnetic surfaces. Since the existence of a plasma equilibrium is assured, studies of its stability become meaningful. In the present study we are particularly concerned with the stabilization of plasma equilibrium by magnetic shear. In a levitron variation of the toroidal field magnitude relative to the poloidal field varies the shear considerably. Changing the magnetic shear in a stellarator also changes the shape of the magnetic surfaces while in a Tokomak the plasma heating current or confining field must be changed. Yoshikawa [3] pointed out that the addition of a uniform magnetic field along the axis of symmetry of a levitron can lead to a system with average minimum B properties. The parameters of this experiment give a positive value for V″ i.e. the present experiments do not investigate the question of stabilization by a magnetic well.

*On leave from Princeton University, Princeton New Jersey, U.S.A.

2. THE SPHINX DEVICE

SPHINX is a small aspect ratio, axially symmetric device with considerable magnetic shear. It is shown schematically in Fig.1. The discharge chamber is a spheroidal cavity 29 cm in diameter and 6·3 cm high. The toroidal field is generated by the combined effect of powered currents which flow in the 2 cm diameter center post and eddy currents in the wall of the cavity. The poloidal field is generated by a powered current inside the 23 cm diametre ring and eddy currents in the chamber wall. The ring is supported by three 0·4 mm diameter phosphor bronze wires and a 3 mm diameter stainless steel tube to enclose the wires which feed current to the ring. The plasma volume is defined by six symmetrically placed 0·2 mm thick stainless steel aperture limiters and is approximately 2×10^3 cm^3. Both the ring and toroidal field center post are electrostatically shielded; the ring and supports float electrically with respect to the rest of the chamber. The ring and center post are independently energized for approximately 2 msec by two, low loss, 4 section LC delay lines. The copper block is cooled to 76°K to provide cryogenic pumping and to increase its electrical conductivity ten fold. The base pressure of the device is 2×10^{-7} torr.

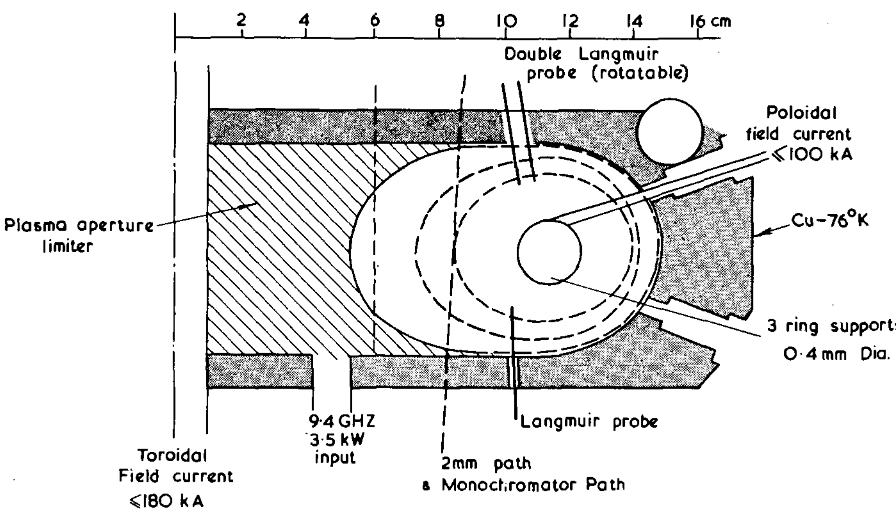

FIG.1. Schematic diagram of SPHINX experiment. The device is axially symmetric about the centre line.

The magnetic surfaces are determined solely by the poloidal field and are shown in Fig.2 together with the contours of the poloidal field modulus (B_p). Each magnetic surface is labelled by a parameter r_o which is the maximum distance between the center of the ring and the magnetic surface. We compute the rotational transform by noting the change in azimuthal angle $\Delta\theta$ which a field line makes in going once around the ring conductor. The total rotational transform ι once around the machine the 'long way' is $(2\pi)^2/\Delta\theta$ radians. We readily find

$$\Delta\theta = \oint \frac{B_t}{B_p} ds_p = \frac{I_t}{I_p} \oint \frac{ds_p}{b_p R^2} \tag{1}$$

where s_p is distance along a magnetic surface at fixed azimuth measured from the median plane, R the radial distance from the centre post, B_t, B_p, I_t, I_p, are the magnitude of the toroidal and poloidal fields and currents and b_p a function defined by the mod B_p contours shown in Fig.2. Fig.3 shows $\Delta\theta$ for SPHINX as a function of r_o.

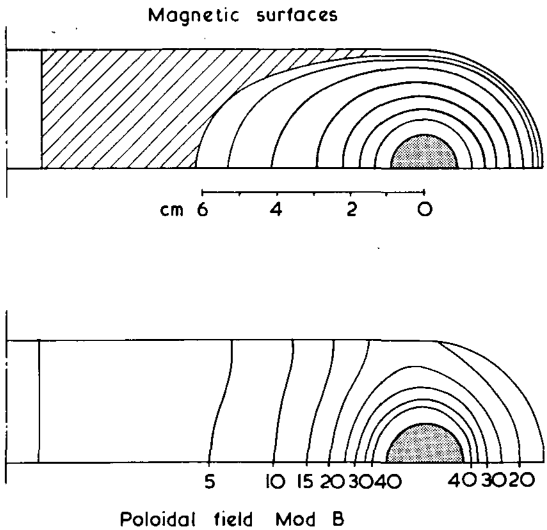

FIG. 2. Magnetic field surfaces and poloidal field modulus contours. The modulus B labels are relative field magnitudes with an arbitrary normalization.

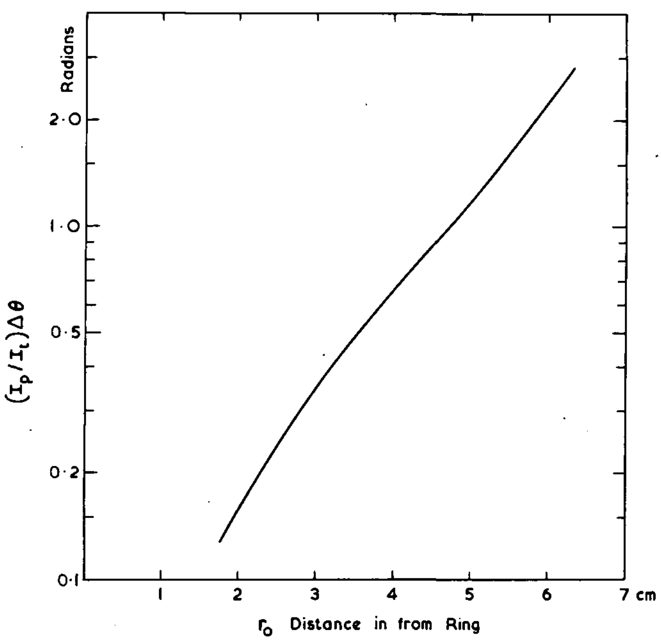

FIG. 3. Normalized azimuthal rotation of a magnetic field line in going once around poloidal field ring. Rotational transform $\iota = (2\pi)^2/\Delta\theta$.

To compute the shear, we calculated the twisting suffered by a ribbon defined by two adjacent field lines on neighbouring magnetic surfaces in going once around the ring conductor the short way, i.e. between two traversals of the center median plane. The shear length will be defined as the distance moved along the field lines for which this twist is 45^0 i.e. for the transverse displacement of the ribbon to equal the separation of the magnetic field surfaces. The shear length L_s presented below is an average value computed as if this twisting occurred uniformly. We obtain

$$L_s = \frac{s}{R(r_o)} \left(\frac{\partial(\Delta\theta)}{\partial r_o}\right)^{-1} \frac{B(r_o)}{B_p(r_o)} \qquad (2)$$

where s is the distance along the magnetic field line in going once around the ring. L_s is shown in Fig.4 as a function of magnetic field surface for several values of I_t/I_p.

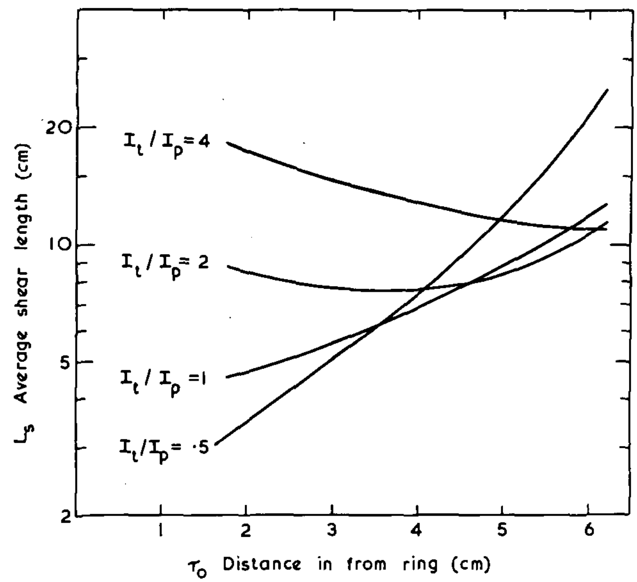

FIG.4. Average magnetic shear length.

3. PLASMA GENERATION

The plasma was generated by microwave discharge in low pressure H_2, D_2, He, or A. Neutral particle densities used were 1-5 $\times$ 10^{12} cm^{-3}, and the 9·4 GHz microwave power was supplied in the form of a square pulse, 1 msec maximum duration, 3·5 kW maximum power. In most of these experiments the electron cyclotron frequency in the discharge region was less than the microwave frequency, this corresponds to maximum currents of 35 kA in the ring and 100 kA in the center post. The gas usually breaks down within a few hundred microseconds after the heating is applied and the density rises to a steady value after a further few hundred microseconds.

All our observations are consistent with the conclusion that the discharge which we are studying are relatively cool and have electron temperatures of less than 10 eV. Although we are not now concerned with the details of the power absorption mechanism, considerations relating to collisional effects and the refractive properties of plasma near the upper hybrid resonance appear more relevant than those associated with simple electron cyclotron resonance. The present experiments produce discharges which are qualitatively quite different from pulsed, electron cyclotron resonance discharges [4] at low pressure in mirror geometry; in particular we have no evidence of a runaway electron component.

4. MEASUREMENTS

In a steady state discharge the rate of plasma loss must be balanced by the rate of production of new plasma by ionization. Hence by measuring the ionization rate we can find the particle containment time. To do this we measure the plasma density and the rate of excitation of an appropriate excited state as a function of time. By measuring the plasma accumulation, i.e., the plasma electron density and the total plasma production rate, we have made studies of the particle containment time.

We believe that both ionization and excitation result principally from electron collisions with atoms in their ground state. The ratio of the rate constant for ionization to that for the excitation of states near the ionization continuum is a rather insensitive function of electron temperature. The intensity of light from excited states, particularly those which are not influenced by resonant fluorescence, is thus proportional to the ionization rate. During the steady state period the value of the electron density n_e divided by the light intensity L in an appropriate spectral line is proportional to the particle containment time.

In addition to making relative light intensity measurements an absolute calibration of the apparatus was done in argon at 4200Å by noting the light production emitted by a current of electrons passing through a known pressure of argon gas. For this purpose a tetrode valve was suitably modified and mounted in the monochromator light path underneath the discharge chamber. The output current of the monochromator photomultiplier as a function of electron energy is shown in Fig.6. The argon ionization cross section [5] and the response shown in Fig.6 was integrated over velocity to determine the ratio of monochromator output to ionization rate as a function of electron temperature. This ratio varies by less than ± 15% as the electron temperature changes between 4 and 15 eV.

The mean electron density was measured by a 135 GHz interferometer. The system is subject to beam refraction and resonances in the discharge chamber which limit the overall accuracy to ± 15%.

The plasma profile was determined by double Langmuir probe measurements. The double probe consisted of two tungsten wire probe tips 0·4 mm diameter 0·8 mm long sleeved by alumina tubing with an outer diameter of 1·0 mm. The probes were integrally mounted in a holder to a separation of 6·3 mm at a common distance from the median plane. The entire assembly was rotatable and retractable, however most of our observations were made with the probe tips at a common radius from the center post. The circuitry used in conjunction with the double probe was suggested by D.J. Lees and is similar in design to that employed in the Proto-Cleo experiment [6]. The two probe tips are connected to windings on each of two small transformers connected in series in such a way to allow the double probes to float electrically with respect to the plasma. One transformer applies a 60 kHz sinusoidal voltage about 25 volts in amplitude between the two probes and the second transformer registers the current which the plasma carries. Comparison with 135 GHz interferometer signals indicates a linear relation during the heating phase between plasma density and double probe current.

Floating potentials and fluctuations thereof were measured with a single Langmuir probe which consisted of a tungsten wire tip 0·8 mm diameter, 1·6 mm long. The inactive portion of the probe was sleeved with a piece of alumina 2 mm in diameter. The total capacitance driven by the probe was 25 pf; in plasma potential measurements the input resistance of the measuring apparatus was 10^7 ohms. In the fluctuation measurements a high pass RC filter with $1{\cdot}2 \times 10^5$ ohms resistance and a time constant of 10^{-5} sec was inserted between the probe and the amplifier input. Plasma impedance measurements together with the capacitance seen by the probe indicate that the probe response should be a true measure of floating potential fluctuations up to about 700 kHz.

5. RESULTS

The preliminary studies were made using argon, because of the relative simplicity of measurement and interpretation to establish the nature of the discharge. Subsequent work using hydrogen gave similar results, despite the large difference in ionic mass.

(a) Experiments with Argon

A typical set of argon data is shown in Fig.5. An 800 μsec pulse of 9·4 GHz power was applied to the device after the magnetic field achieved a steady value. Breakdown occurs after a short delay, as shown by the interferometer and light intensity traces. After steady conditions are reached, both the light production and the electron density remained constant to within about 20%. Measurement with a rapidly responding ionization gauge showed that the gas pressure was also constant to within about 20% during discharge. After the heating power was shut off, the excitation light disappeared in 50 μsec and the plasma density decayed with about a 600 μsec time constant. Using argon we have not observed recombination light during the afterglow period though both hydrogen and helium discharges show considerable recombination glow. The density decay in the afterglow has shown considerable long-term irreproducibility.

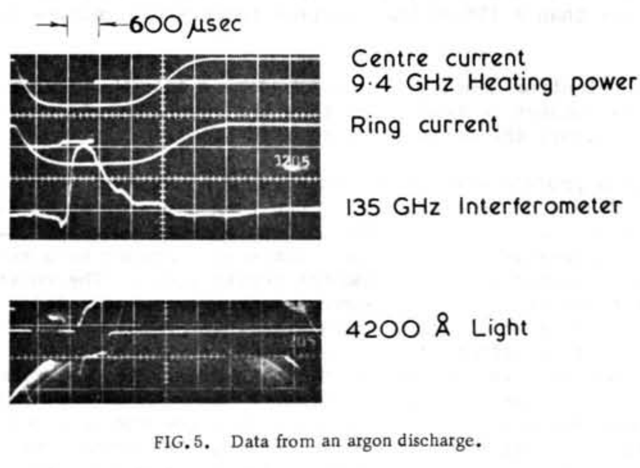

FIG. 5. Data from an argon discharge.

In Fig.7 the steady state light intensity at 4200 Å (L) and the ratio of electron density to light (n_e/L) are shown as a function of applied power and toroidal field. From the absolute light intensity, the electron density and the neutral gas pressure, a value of $\langle \sigma_i v_e \rangle$ was found which corresponds to an electron temperature of about 4 eV and an ionization time of about 600 μsec. An estimate of the containment time made from the rise of the electron density yields about half this value, which is within the precision of the absolute light measurements. These observations show quite unequivocally that the electron temperature is well

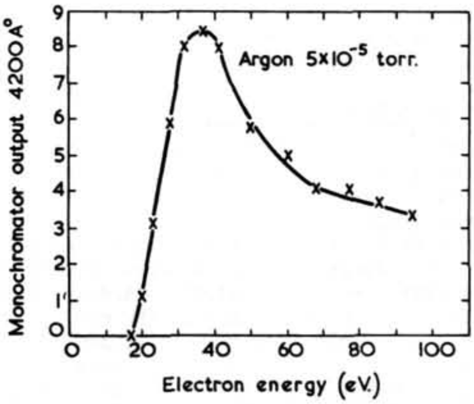

FIG. 6. Monochromator photomultiplier current as a function of electron energy at 4200 Å.

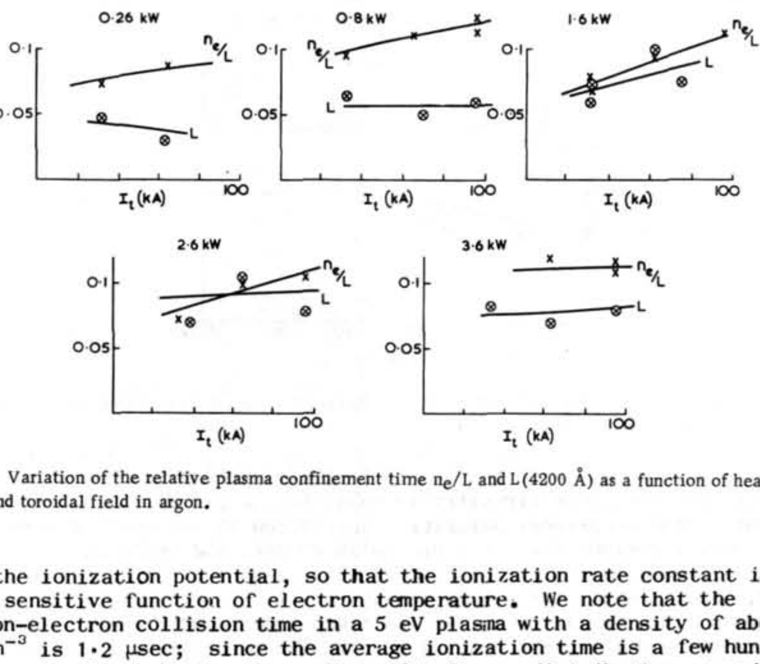

FIG. 7. Variation of the relative plasma confinement time n_e/L and L (4200 Å) as a function of heating power and toroidal field in argon.

below the ionization potential, so that the ionization rate constant is a very sensitive function of electron temperature. We note that the electron-electron collision time in a 5 eV plasma with a density of about 10^{12} cm^{-3} is 1·2 μsec; since the average ionization time is a few hundred microseconds the deviation from a Maxwell Boltzman distribution caused by ionization effects should not be very large. Small deviations from a thermal distribution caused by plasma heating effects are not expected to make any significant change to the ratio of the ionization and excitation rates.

The ratio of n_e/L, which is proportional to the plasma containment time, shows very little variation as the parameters of the discharge are changed with the exception of discharges with no toroidal field. In such discharges n_e/L is smaller by about a factor of 3 as shown in Fig.8. With no toroidal field the electron density decays after the heating power is turned off with a time constant of 70–90 μsec, whereas with toroidal field it decays in about 600 μsec. While this change in plasma containment is very dramatic we note that during the afterglow period the electron temperature may be rather low.

(b) Experiments with Hydrogen and Deuterium

Typical hydrogen data shown in Fig.9 indicates a great similarity to argon particularly during the initial gas break-down and steady state phases of the discharge, though the neutral gas operating pressure in hydrogen is somewhat higher than in argon. Figs.10 and 11 show the variation with the magnetic field parameters of the electron density, H_β light and their ratio during the steady state period of the discharge. The insensitivity of both the light production and the electron density to the magnetic field strength is apparent. The confinement times of deuterium and hydrogen are equal to within about 30%. While the chemical behaviour of hydrogen complicates the numerical ratio between the production of H_β light and the value of the ionization rate coefficient, the results show that the confinement time is essentially independent of both the magnetic shear and the magnitude of the magnetic field once the gross instability of plasma in a purely poloidal field is eliminated.

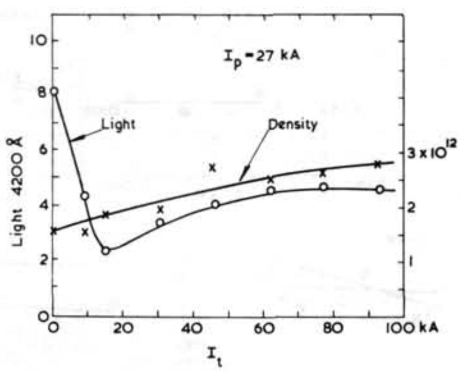

FIG.8. Variation of 4200 Å light intensity and electron density in argon showing increase in light production (decrease in containment) as $I_t \to 0$.

Observations made with the double Langmuir probe are shown in Fig.9. Unfortunately the probe circuitry is subject to a pickup signal which originates from occasional parasitic oscillation in the heating magnetron. During periods when this pickup is absent, the probe current signal is steady during the heating as well as during the afterglow period. Fig.12 shows the plasma density profile from double probe measurements. This family of curves was taken under conditions of constant gas pressure and microwave heating power. The peak electron density is independent of both poloidal and toroidal fields. The profile is also independent of the toroidal field; with increasing poloidal field the peak density moves to larger radii and the magnitude of the outer density gradient increases linearly. We have not resolved whether the steepening of the density gradient is primarily associated with a smaller plasma diffusion constant or whether it is more intimately connected with the mechanism governing the absorption of heating power.

The voltage-current response of a single Langmuir probe in the plasma has shown several perplexing features. During the heating phase, the probe current-voltage characteristic is linear between ± 90 V with a slope of $10^4 \Omega$. For larger voltages there is a slight saturation of the probe current. During the afterglow there is an apparently reasonable probe characteristic with some saturation of both electron and ion currents, the electron saturation current being some 12 times greater than that of the ions. However this response curve, indicates an electron temperature of several eV during a period when the plasma is recombining and is thus known to have an electron temperature of less than a few tenths of an eV [7]. These anomalies are not surprising since the probe current drawn represents the total ionization from more than a cubic centimeter of plasma which may severely disturb the plasma potential.

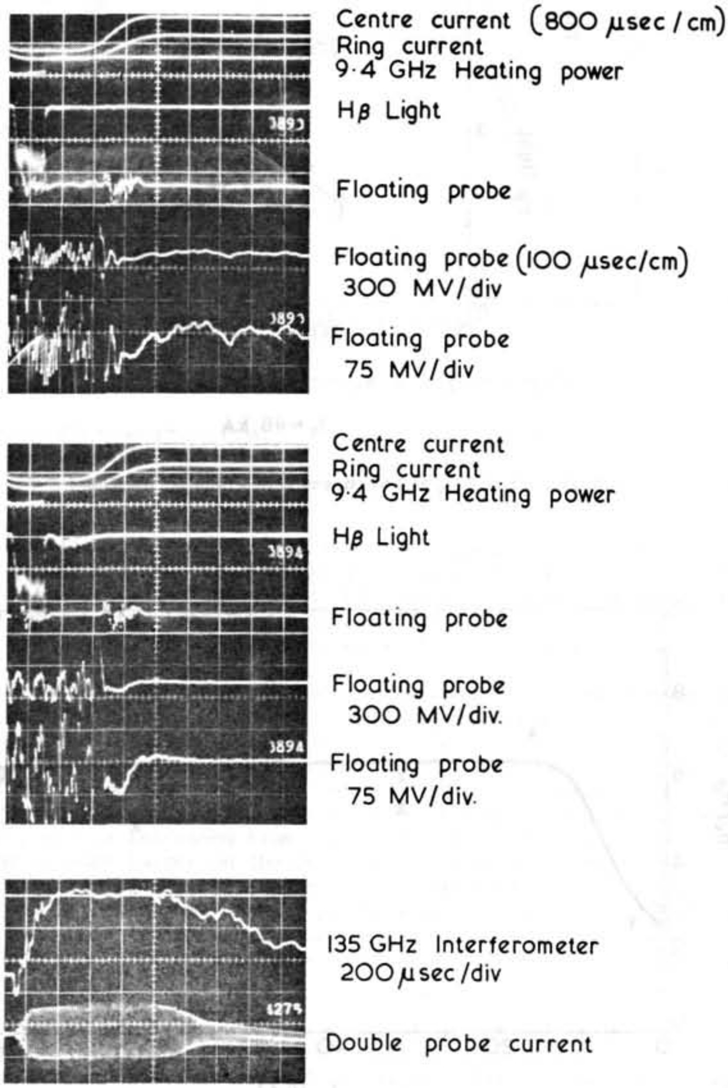

FIG. 9. Data from a hydrogen discharge. The fine structure in the 135 GHz interferometer time is instrumental – the step during the first 150 μs does not represent plasma density – it is pickup from the magnetron before gas breakdown. The fuzziness in the double probe current trace between 600 and 1000 μs is due to pickup and should be disregarded. The 135 GHz interferometer data and the double probe data are taken from a different discharge.

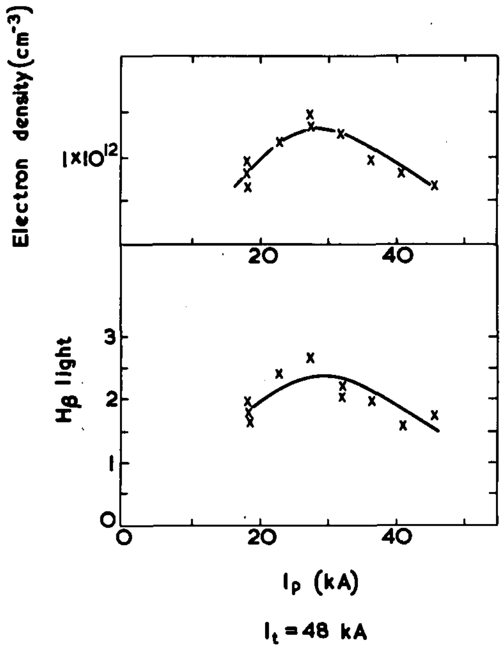

FIG. 10. n_e and H_β as a function of I_p in a hydrogen discharge.

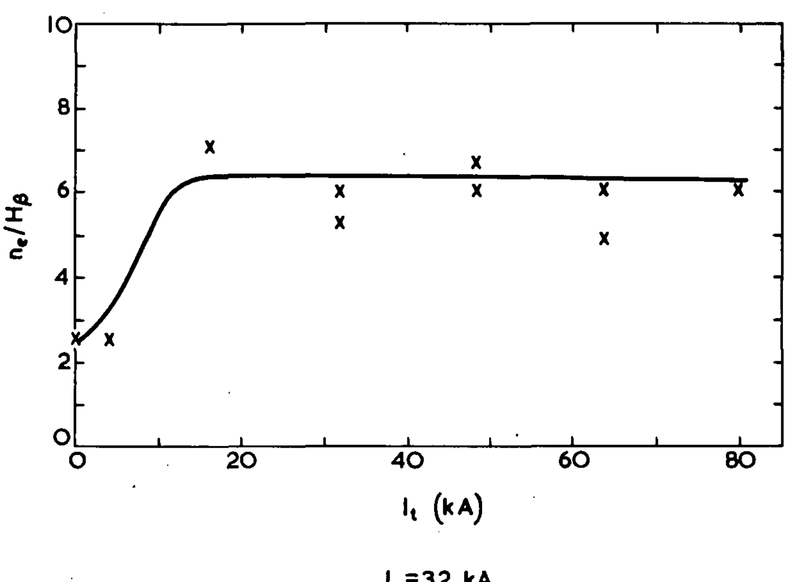

FIG. 11. n_e/H_β as a function of I_t in a hydrogen discharge.

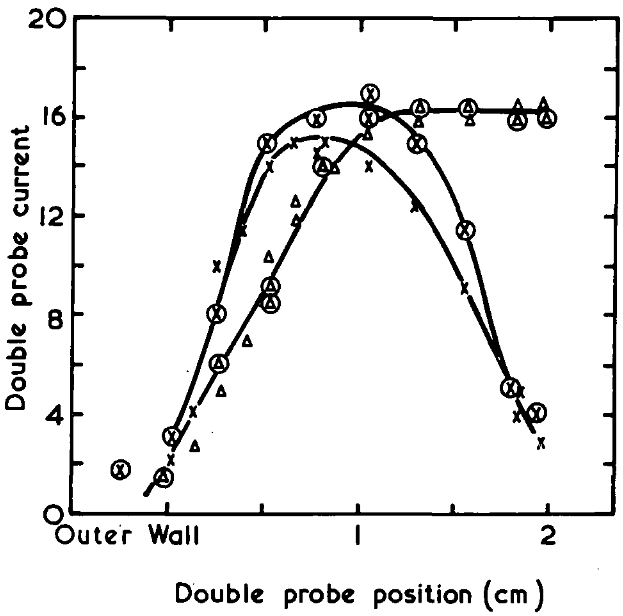

FIG. 12. Density profile measurements during heating from double Langmuir probe measurements. The probe current normalization of all data is the same. The poloidal and toroidal field currents are: X I_t = 16 kA, I_p = 36 kA; ⊗ I_t = 48 kA, I_p = 36 kA; △ I_t = 64 kA, I_p = 18 kA; ⊗ I_t = 48 kA, I_p = 18 kA.

The plasma floating potential is negative both during the heating period and the afterglow. In hydrogen it is about–15 volts during heating and is almost constant throughout the plasma. By contrast with both helium and argon we have observed a non-uniform floating potential considerably more negative near the outer wall of the discharge.

Fig.9 shows that the plasma potential fluctuations during the heating phase with both poloidal and toroidal fields energised are small. In agreement with the results of Birdsall et al. [8] the plasma is considerably noisier in the absence of a toroidal field. A large part of the potential fluctuation observed has a rather distinct frequency. The fluctuations are observed to slowly increase their frequency and amplitude as the heating power is increased from 0•25 to 3•6 kW. The amplitude of the fluctuations is much larger on the outside of the plasma. Two possible implications of Fig.13 are that the principal fluctuations are in the region defined by the plasma density gradient and are associated with the region of 'bad magnetic field curvature'. The frequency of the oscillations is found to increase linearly with poloidal field current as Fig.14 shows.

During the msec following complete turnoff of the microwave heating power the potential fluctuation observed with a Langmuir probe is very small, as indicated by discharge 3894 in Fig.9. After the heating power is shut off, the plasma goes into a period in which electron ion recombination is a dominant process as the H_β light trace shows. During this time the electron temperature is less than a few tenths of an eV [7] and the maximum rms potential fluctuations of only a few mvolts. Addition of about 4 Watts of 9•4 GHz power to the device is enough to stop the recombination as the H_β trace light in discharge 3893 shows. However,

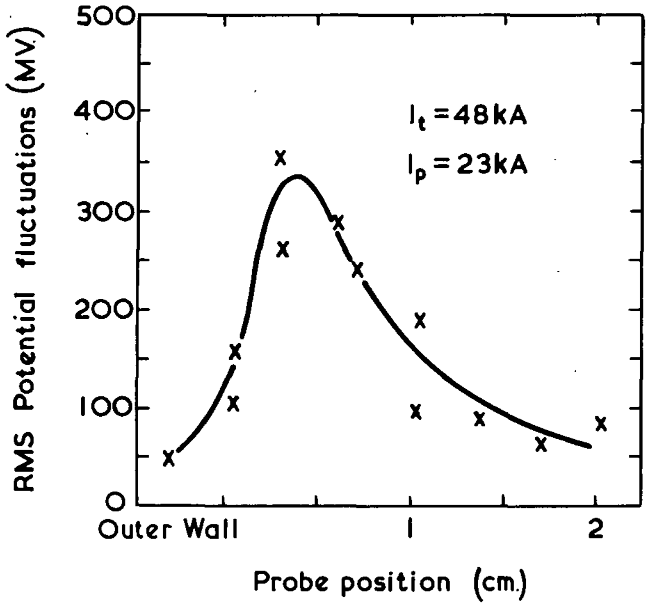

FIG. 13. RMS floating potential fluctuation magnitude during the heating as a function of probe position.

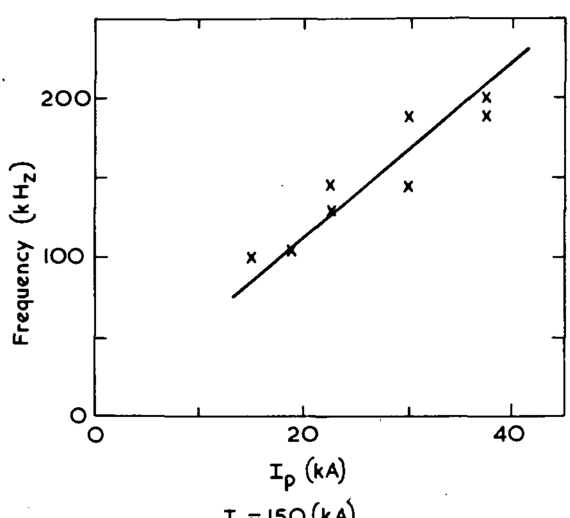

FIG. 14. Frequency of floating probe potential fluctuations as a function of poloidal field. These data were taken from a He discharge with a strong toroidal field I_t = 150 kA. Lower-field hydrogen plasma data is virtually identical.

even this small amount of heating is sufficient to increase the maximum rms level of the fluctuations tenfold to about 40 mvolts. The observation that recombination is the dominant process during the afterglow shows that state of the plasma is very quiescent. In particular, the currents which are driven in the plasma by the electric fields associated with the eddy currents in the walls of the chamber are very small.

Observation of the floating probe and H_β light traces during the decay of the magnetic confining field shows the effect of inducing a heating current in a recombining plasma. It is readily appreciated that one cannot heat a recombining plasma just a little by applying an ohmic heating electric field because of thermal runaway effects. When the plasma is heated a little, its electrical resistance decreases and more power is dissipated. The temperature then increases until an energy absorbing mechanism like excitation and ionization become important. This is observed during the decay of the magnetic confining field in Fig.9 where the plasma fluctuation level increases to a value comparable to that during the main heating pulse and a small amount of H_β light is generated. It is easily seen that the value of dB/dt required to make the effect of electric fields in the plasma dominant, is much larger than that which exists during the plateau period of the magnetic field.

The independence of the plasma confinement upon magnetic field strongly suggests that ring support losses are dominant. The computed plasma loss time found, assuming a flux of particles with an average velocity of $(\kappa T_e/\pi M)^{1/2}$ flowing to the surface area of the supports is 8·0 msec for argon and 1·25 msec for hydrogen (κT_e = 5 eV), whereas the observed confinement time is only a few hundred microseconds. Insertion of Langmuir probes into the discharge which effectively increases the support area by a factor of 1·75, show no significant effect on the production of H_β light or the 135 GHz interferometer signal. We therefore conclude that the simple loss of plasma to the ring supports does not make an important contribution to the loss of plasma from the device.

6. CONCLUSIONS AND DISCUSSIONS

A. Plasma Containment

During the steady state period of the discharge the particle containment and ionization times are equal. In a well contained plasma the ionization time becomes longer and longer by depletion of the neutral gas as the plasma becomes fully ionized. In a low temperature partially ionized plasma with relatively poor containment the electron temperature adjusts itself so that the average ionization rate constant becomes equal to the containment time. This leads to the anomalous conclusion that a poorly contained steady state plasma is hotter than a better contained one. In a microwave discharge of the kind which we are studying the power absorption of the plasma decreases as the plasma density increases due to wave evanescence effects. In the regime of low plasma temperatures the ionization rate constant is a very sensitive function of the electron temperature thus both the electron temperature and the plasma density adjust themselves so that a steady state condition is attained. In this experiment the electron temperature varies very little and is quite close to 5 eV. The fraction of the incident power absorbed by the plasma is between 2-8% and is not strongly dependent upon whether the magnetic field in the discharge chamber is above or below cyclotron resonance.

Our studies of plasma confinement during the heating phase are more reliable than those which were attempted during the afterglow. While an afterglow plasma is closer to equilibrium than one which is being heated the uncertainty of the plasma temperature and the importance of recombination effects is less clear. The observations with argon shown in Fig.7 which show confinement time essentially constant over a wide range of heating power suggests that heating effects are not a dominant parameter in determining the confinement time.

Assuming that the loss of plasma is a diffusive process, a diffusion constant D can be derived from the data. A convenient way of doing this is to note that the differential flux of plasma through an element of area dS is $d\varphi = D\nabla_{\perp}n\ dS$. The confinement time can be estimated by dividing the total plasma inside the surfaces of half maximum density by the total flux crossing them using the observed values for $\nabla_{\perp}n$ to compute φ. Assuming n constant on each magnetic surface and recalling that $\nabla B_p = 0$ the density gradient $\nabla_{\perp}n$ at any point on a surface is $\nabla_{\perp}n = B_pR/B_p(1)R(1)(\nabla_{\perp}n)$, where $B_p(1)$, $R(1)$ and $(\nabla_{\perp}n)_1$ are all evaluated at some point on the surface e.g. where $\nabla_{\perp}n$ is measured. The total flux leaving the system is

$$\varphi = \frac{2\pi}{B_p(1)\ R(1)}\ (\nabla_{\perp}n)_1 \oint D\ B_p\ R^2\ ds_p \tag{3}$$

The dominant part of the plasma loss in the integral (3) comes from the outer surface at large values of R. This occurs because (a) most of the surface area is at large R; (b) the density gradient of the plasma is larger at large R than small. The effect of increasing the toroidal field is to change the shear length considerably as Fig.4 shows, however its effect on changing the confinement time assuming diffusion proportional to $1/B$ is very small; changing I_t/I_p from 0·5 to 4 by increasing I_t increases the confinement time by 25%. In Fig.15 the ratio B_p/B is shown as a function of s_p. Note that by increasing I_t the diffusion constant is significantly reduced on a part of the surface where the diffusion loss is minimal i.e. toward the center of the device ($s_p = 0$).

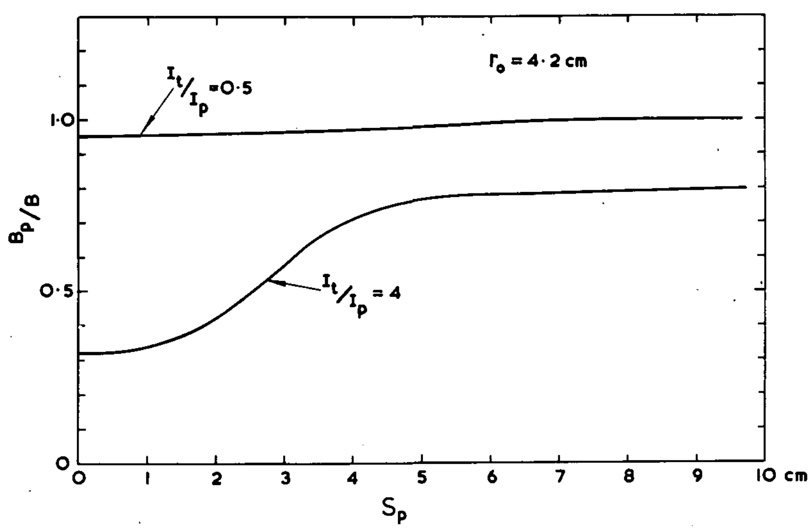

FIG.15. B_p/B as a function of s_p for the magnetic surface which intersects the median plane at $r_0 = 4.2$ cm.

The observation that the plasma containment is independent of I_t is an indication that the parameter [9] θ which is the ratio of the plasma gradient length to the shear length is not a dominant parameter in determining the plasma confinement in this experiment. The irrelevance of the exact magnitude of I_t provided it is not zero is one of the most reproducible features of the experiment. The range of the parameter θ in the region most prone to fluctuations is $0{\cdot}05 < \theta < 0{\cdot}15$.

The independence of the plasma confinement time on I_p is also consistent with a diffusive loss proportional to $1/B$ since the plasma density gradient is observed to steepen linearly with B_p. Assuming the Bohm diffusion constant $D = \kappa T_e/(16eB)$ and the density gradients and poloidal field corresponding to $I_p = 36$ kA the calculated confinement time varies from 22-28 μsec as I_t increases from 18 to 144 kA. The absolute magnitude of the confinement time observed was estimated from the rise time of the electron density, the value obtained is between 200-300 μsec.

B. Fluctuations

Excepting discharges with no toroidal field the fluctuations in plasma potential are observed to be small. The maximum rms value corresponds to about 5% of $\kappa T_e/e$. We have not yet attempted measurements and estimates to ascertain the magnitude of the plasma loss directly ascribable to fluctuation phenomena.

The oscillation frequencies observed are of the right order for drift waves i.e. $\omega^* = (k_\perp \kappa T_e/eB)\, \partial(\ell n\, n_e)/\partial x$ though the magnetic field dependence appears initially to be incorrect. The Doppler shift correction to the observed frequency for the E/B drift is not dominant. From Fig.13 we see that δ, the density gradient length, varies inversely with poloidal field; thus the assumption that $k_\perp \delta \approx 1$ clearly gives the observed magnetic field dependence and in fact also gives the correct magnitude for the frequency. For example using the observed density gradient, the magnetic field value 4 mm from the wall, an electron temperature of 5 eV, $I_p = 18$ kA and a frequency of 120 kHz implies $k_\perp = 3{\cdot}5$ cm^{-1}. The radial extent of the region in which the fluctuations are observed defines $\lambda_r/2 \approx 1$ cm which is about the same as δ. Thus we conclude that $k_r \approx k_\perp \approx 1/\delta$ for these oscillations. Correlation measurements to verify this conclusion have not yet been attempted.

7. ACKNOWLEDGEMENTS

The authors gratefully acknowledge discussion and critical revision of the manuscript by Dr R.J. Bickerton and Dr S.M. Hamberger.

8. REFERENCES

[1] B. Lehnert. J. Nucl. Energy C1, 40 (1959).

[2] I.E. Tamm. Plasma Physics and the Problems of Controlled Thermonuclear Fusion (1961) p.37.

[3] S. Yoshikawa and U.R. Christiansen. Phys. Fluids 9 2295 (1966).

[4] A.F. Kuckes and L.A. Ferrarri. Phys. Fluids 8, 2295 (1965).

[5] H.S.W. Massey and E.H.S. Burhop. Electronic and Ionic Impact Phenomena, Oxford Univ. Press London (1952) p.38.

[6] D.J. Lees. Private communication see also Adlam et al in Third Conference on Plasma Physics and Controlled Nuclear Fusion Research (I.A.E.A.· Vienna 1968) paper CN-24/D8.

[7] A.F. Kuckes , R.W. Motley, E. Hinnov and J.G. Hirschberg. Phys. Rev. Letters 6, 337 (1961).

[8] D.H. Birdsall, R.J. Briggs, S.A. Colgate, H.P. Furth and C.W. Hartman. Plasma Physics and Controlled Nuclear Fusion Research, (I.A.E.A. Vienna 1966), vol.II, p.291.

[9] B.B. Kadomtsev and O.P. Pogutze. In Plasma Physics and Controlled Nuclear Fusion Research, (I.A.E.A., Vienna 1966) vol.II, p.365.

DISCUSSION

D.A. PANOV: Did you observe a direct correspondence between particle lifetime and the level of potential fluctuation?

A.F. KUCKES: A direct evaluation of plasma loss by fluctuations requires study of the correlation of plasma density and potential fluctuations. Such correlated studies are planned for the near future.

D.A. PANOV: Is the scale of the fluctuations sufficient to explain the magnitude of the diffusion plasma flow?

A.F. KUCKES: The uncorrelated potential fluctuations seem a little too low to explain the loss observed. However, more detailed estimates are clearly required.

S.J. BUCHSBAUM: At what neutral pressure are the experiments performed?

A.F. KUCKES: About 10^{-4} mmHg.

S.J. BUCHSBAUM: I note that the density at which most of the measurements are made is about 10^{12} cm^{-3}, which is very near the critical density. What happens when the microwave power is reduced so that the density is lower?

A.F. KUCKES: The ratio of electron density to spectral light has been studied as a function of heating power, particularly in argon. At a heating power of a few hundred watts the plasma density is about 4×10^{11} cm^{-3}. Under these conditions the containment time is essentially the same as at higher power.

O.S. PAVLICHENKO: Have you any other confirmation of the fact that there is no dependence of the containment time on the longitudinal field, since the intensity of the H_β line may depend on many processes accompanying the injection of neutral particles (e.g. processes of the recycling type)?

A.F. KUCKES: Our experiments depend on the fact that recycling effects are dominant in the discharges studied. The neutral gas pressure does not change very much after the discharge is initiated. The many chemical effects which one may worry about in hydrogen are greatly minimized by the fact that our observations of light and plasma density change very little as conditions are varied. Also, argon, in which these effects should be absent, exhibits very similar behaviour.

PLASMA CONFINEMENT IN THE LEVITRON *

O. A. ANDERSON, D. H. BIRDSALL, C. W. HARTMAN AND E. J. LAUER
LAWRENCE RADIATION LABORATORY, UNIVERSITY OF CALIFORNIA
LIVERMORE, CALIF.,
AND
H. P. FURTH
PLASMA PHYSICS LABORATORY, PRINCETON UNIVERSITY,
PRINCETON, N. J., UNITED STATES OF AMERICA

Abstract

PLASMA CONFINEMENT IN THE LEVITRON. Confinement of gun-injected plasma and anisotropic hot electron plasma is investigated in the Levitron. Field configurations are employed which have strong shear ($L_s/r_p \approx 0.1 - 1$), reversible gradient in average B, and a local minimum $|B|$ mirror region of the Kadomtsev type embedded in the closed toroidal flux surfaces.

Gun plasma is produced by either a hydrogen washer source or a lithium "Bostick" gun. For broadly optimum field configurations with maximum shear and a stagnation point on the small major radius side of the floating ring, plasma injected across the separatrix spreads at the ion directed velocity (20 - 50 eV) to form a toroidal shell several cm thick with $n \approx 10^{10} - 10^{11}$ ions/cm^3, $T_e \approx 5 - 15$ eV. During the initial decay to $n \approx 10^9 - 10^{10}$ ions/cm^3 ($t \approx 100 - 300$ μs) the plasma profile shifts inward toward the ring, accompanied by fluctuations of several kilocycles ($\delta n/n \approx 0.1$) localized in the external density gradient on the large major radius side of the ring. Subsequently, $\delta n/n$ decreases and the decay time increases to 1 - 2 ms. Bohm confinement times are exceeded by 1 - 2 orders of magnitude. If the stagnation point is shifted to the large major radius side of the ring, strong shear is retained while destabilizing field gradients are increased; comparable decay times are again observed, suggesting dominantly shear-dependent confinement.

Hot electron plasma is formed by pulsed microwaves ($\lambda = 3$ cm, 5 - 20 kW, $\tau_H = 1 - 2$ msec) resonant in the minimum-$|B|$ mirror region. The initially anisotropic and mirror confined plasma ($n_{e\,hot} \approx 2 \times 10^{10}$, $T_{e\,hot} \approx 5 - 20$ keV) subsequently spreads around the ring along B by collisions with residual gas or by end-loss instability. Under optimum adjustment of parameters, the confinement time τ_c is established by either energy loss by collisions with background gas, probe collection, or decay of the pulsed confining field. Typically $\tau_c \approx 1 - 10$ ms, consistent with τ_c several orders of magnitude $> \tau_{Bohm}$. The degree to which isotropy is approached is limited by collection on stationary probes or by the slow scattering rate.

An ohmic heating current is observed for both gun and microwave produced plasmas. At 50-kA ring current, the weak ohmic current does not appreciably affect the decay of gun plasma. As the ring current is increased to 150 kA holding I_{ring}/I_z constant, a discharge forms causing a plasma density increase after gun injection or microwave heating to $n \approx 10^{11}$ to 10^{12} ions/cm^3 ($T_e \approx 20 - 30$ eV) in several ms which then decays with a time constant approaching the field decay, $\tau \approx 10$ ms. Induced ohmic current is inherent to an inductively excited resistive ring.

INTRODUCTION

The principal feature of the Levitron is an inductively excited ring which can be left unsupported for several tens of milliseconds. As a consequence, a variety of nearly axisymmetric, closed magnetic confinement configurations can be formed with the field of the truly floating ring and a toroidal field. Earlier experimental results [1] have been presented for Levitrons with a ring centered in the toroidal vacuum chamber (coil form) and with fixed external toroidal current distribution. In the present paper, experimental results are presented for a Levitron (Minimum B Levitron [2]) with an offset ring and segmented toroidal current poloidal field windings.

---

* Work performed under the auspices of the US Atomic Energy Commission.

The flexibility of toroidal current distribution allows shaping of the poloidal field, and consequently the flux surface shape, to obtain configurations with variable stabilizing properties. In particular, local mirror trapping regions with positive and negative ∇B can be formed, and the gradient in average B can be reversed for configurations with strong shear.

Experimental investigations of shear stabilization with the previous Levitron [1] were conducted with relatively dense (10^{12}-10^{13} cm^{-3}) collisional plasmas produced principally by ohmic and microwave heating. Fluctuations and enhanced plasma loss were observed over a broad range of conditions, and the results were not inconsistent with theoretically predicted instability when finite resistivity was taken into account [3]. In the experiments described here, extension of the plasma toward more collisionless regimes has been accomplished by two techniques, gun injection and electron-cyclotron-resonance heating at low pressure.

EXPERIMENTAL APPARATUS AND FIELD CONFIGURATION

A schematic cross section of the minimum B Levitron is shown in Fig. 1. The inductively excited, solid copper ring is supported by four retractable levitator rods (1.2-cm diameter) which are constructed out of hardened steel tubing. Levitation is accomplished by retracting the rods 15 cm for a period of about 20 msec. The stainless-steel toroidal chamber serves as a form for the toroidal and poloidal field windings, which are carefully contoured around a number of 2.5-cm maximum diameter access ports to minimize field perturbations. The chamber is evacuated to typical $(0.3\text{-}1) \times 10^{-6}$ torr base pressure.

Both the toroidal field winding and the poloidal field windings are energized by capacitor banks with 10-15 msec, 1/4-cycle time to provide ring current to I_r = 200 kA and toroidal field current to I_z = 1500 kA.

Three basic field configurations can be formed by adjusting the poloidal field winding current distribution:

(1) A minimum B configuration (1) shown in Fig. 2 with a stagnation (null in B_p) point positioned on the small major radius side of the ring;

(2) a reversed gradient configuration (2) shown in Fig. 2 with a stagnation point outside the ring; and

(3) a quasi-linear configuration for which the toroidal perturbation is minimized at a particular value of I_z/I_r.

Only preliminary results with configuration 3 have been obtained, and these will not be discussed here.

Configuration 1 has a well in $|B|$ as shown, and also a well in $\langle B^2 \rangle$ averaged over a poloidal flux tube volume, where

$$\langle B^2(\psi) \rangle = \oint B^2 \frac{d\ell}{B_p} \Big/ \oint \frac{d\ell}{B_p}$$

The local field curvature is fixed, stabilizing, and normal to the flux surface at the stagnation point ($B_t \neq 0$) and is given by $k_\perp = \hat{n} \cdot \nabla B/B = 1/R_{sp}$, $\hat{n} = \hat{\phi} x (\overline{B}_p/B_p)$. At point A, the curvature is also normal, but destabilizing

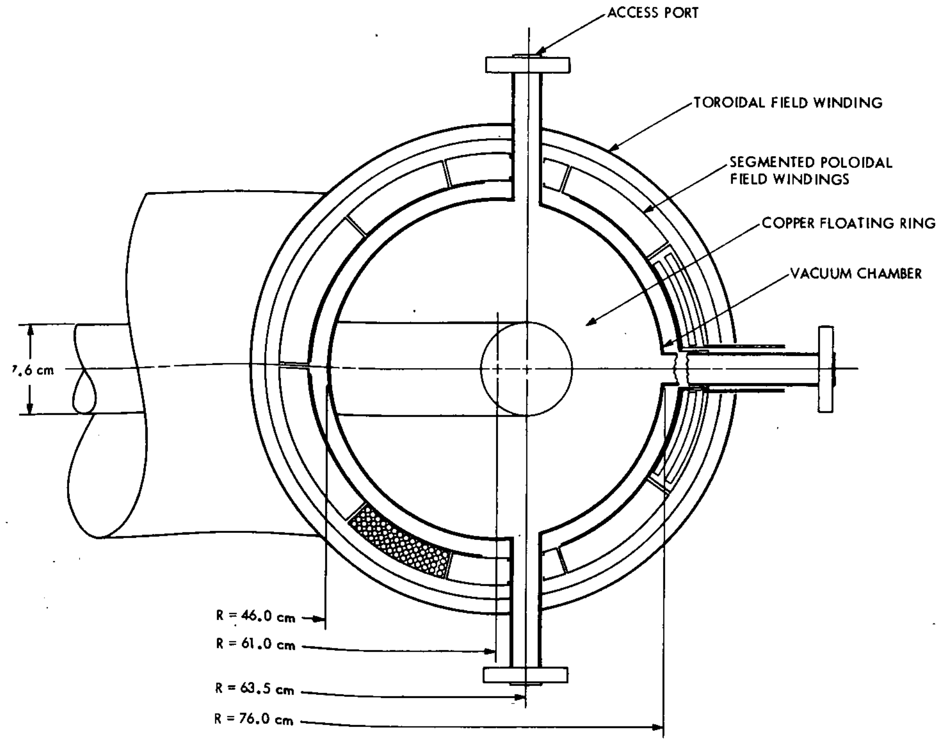

FIG. 1. Schematic cross-section of the Levitron. The floating ring is supported by four retractable levitator rods (not shown) and is offset from the toroidal shell centre by 2.5 cm. Each poloidal field winding segment consists of approximately 50 turns. Similar conductor is used in the toroidal field winding.

and varies from $K_{\perp} = \nabla B_p/B_p$ to $1/R$ as B_t increases from zero as shown. Between points SP and A, regions of geodesic curvature $K_{\parallel}$ are also present, as can be seen readily from contours of constant $|B|$ since $|K_{\parallel}| = (B_t \overline{B}_p/B\,B_p) \cdot \overline{\nabla} B/B$. Although a local and average well are present in principle for all values of $B_t > 0$, grad $\langle B \rangle$ is stabilizing over a region comparable to the density gradient distance only at relatively high values of I_z/I_r as shown in Fig. 2. In addition to variation of curvature, the local magnetic shear varies around the flux surface. The quantity θ shown is the local angle of rotation of B between the separatrix and a flux surface 1 cm closer to the ring at point A (typically $n/n' \approx 1$ cm).

Since θ varies appreciably, an appropriate average should be taken, depending on the instability mode considered. For nonlocalized drift modes, it might be expected that $\langle \theta \rangle \approx \theta_{max}$ because of the exponential dependence of ion Landau damping on θ.

Configuration 2 of Fig. 2 has similar confinement volume and shear. The gradients in $|B|$ and $\langle B \rangle$ are destabilizing except for large I_z/I_r where weak local stabilizing curvature is present near point A.

The stabilizing properties achieved by virtue of the effects of the stagnation point are diminished by nonsymmetrical field perturbations of ports, ring position errors, etc. which cause destruction of the surfaces

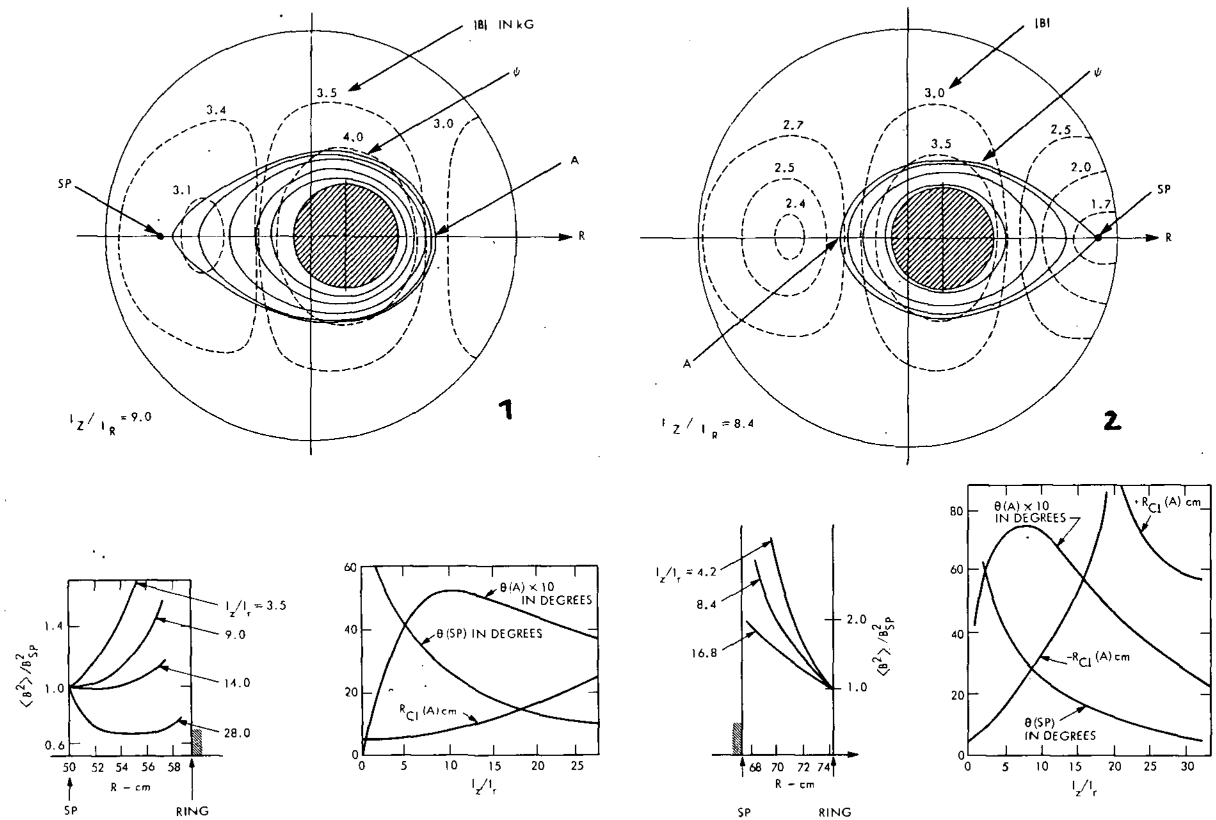

FIG. 2. Field configurations. Flux surface is indicated with solid lines and contours of constant $|B|$ are shown dashed. Configuration 1 ("Minimum B" Levitron) can be adjusted to have a local minimum $|B|$ mirror well as shown and, for increased toroidal field, a well in $\langle B\rangle$. Configuration 2 has similar confinement volume and shear but with reversed $|B|$, $\langle B\rangle$ gradients. Configuration 1 is shown for I_r = 90 kA, I_z = 800 kA, I_z/I_r = 9 and configuration 2 is shown for I_r = 73 kA, I_z = 615 kA, I_z/I_r = 8.4; $\langle B^2(\psi)\rangle$ is plotted against radius for the intersection of the flux surfaces between the ring and SP.

near SP. Preliminary numerical calculations show that if the ring is tilted 0.1 degree, surfaces are destroyed from SP to the point where the average rotational transform is $\langle i \rangle \approx 2\pi$.

GUN INJECTION STUDIES

Gun injection studies have been conducted with two sources; a hydrogen-loaded titanium washer source [4], and a lithium electrode Bostic-type [5] gun. Although similar results have been obtained with both sources (hydrogen gun plasmas tend to be more dense by a factor of 10) most detailed measurements have been conducted with a lithium gun, and the results given here are for this case. Typically, plasmas with $n \approx 10^9$ - 5×10^{10} ions/cm^3, $T_e \approx 5$ - 15 eV are obtained.

Plasma is injected with a gun positioned as shown in Fig. 3, or alternatively with the gun located directly above the ring but still outside the separatrix. Accelerated plasma crosses the magnetic field and enters the confinement zone by a process not well understood, but which involves polarization-induced drifts and appreciable $j \times B$ forces arising from the gun current and confining field. The properties of the plasma following injection depend critically on whether the ring is left supported or is levitated for large $I_r \gtrsim 90$ kA. The critical dependence arises from inductively driven ohmic heating currents, and this will be discussed more completely later. The following experimental results obtain if $I_r < 90$ kA, and are relatively insensitive to the presence or absence of support rods.

The arrival and subsequent decay of plasma at several radial positions is shown in Fig. 3, and density profiles at several times during the decay are shown in Fig. 4 for $I_r = 45$ kA, Configuration 1. Generally, the evolution of the plasma passes through three phases: (1) initial filling which lasts several hundred μsec and is characterized by nonreproducibility, large azimuthal asymmetries, and relatively dense plasma outside the separatrix; (2) an approximately azimuthally symmetric distribution which tends to be well-defined by the separatrix but peaked near it (Fig. 4, t = 200 μsec); and (3) a slower decay phase ($\tau_d \approx 1$ msec) as indicated by the profiles at t = 800, 1800 μsec in Fig. 4. The above characteristics are unchanged if the ring is levitated or supported. These data were taken with the ring supported.

The decay of plasma during phase 2 (200 μsec < t < 800 μsec) is accompanied by large amplitude ($\tilde{n}/n \approx 1$) fluctuations at about 10 kc which are localized outside the ring in the external density gradient of the plasma. These "ballooning" fluctuations are well-correlated with the rapid decay of density near the separatrix suggesting direct transport by the waves, although the rapid decay may also be due in part to continued symmetrization of the plasma.

Following phase 2, when the maximum external density gradient is decreased and displaced inward toward the ring, the fluctuation level decreases to $\tilde{n}/n < 0.1$ over most of the external gradient except near the separatrix where n is small and $\tilde{n}/n$ remains ≈ 1. At the beginning of phase 3, the density is typically 5×10^9 ions/cm^3 and $T_e \approx 10$ eV (T_e remains approximately constant throughout the decay). A determination of n and T_e has been made for several typical cases by iterative curve-fitting, using the low-density probe theory of Lafromboise [6] and curves obtained with a single probe biased to collect ion current and electron current of comparable magnitude.

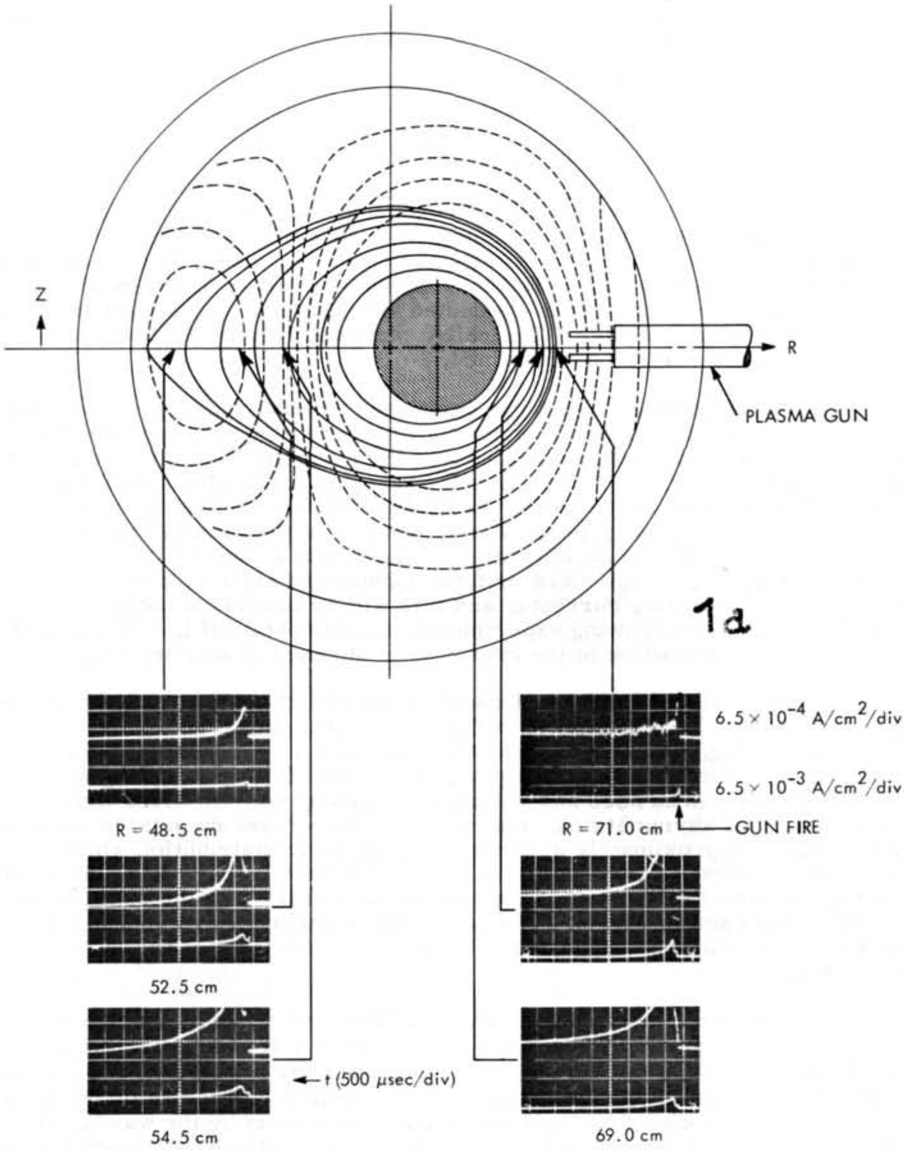

FIG. 3. Langmuir probe current vs position. Dual Langmuir probe current at fixed bias (80V) is shown as a function of time for several radial positions at the midplane (z=0). A collected current of 6.5×10^{-4} A/cm^2 corresponds to $n \approx 3 \times 10^9$ electrons/cm^3 and at t = 700μs after gun fire $T_e \approx 13$ eV. The field configuration shown (1a) is a variant of configuration 1 with $I_r = 45$ kA, $I_z = 200$ kA.

The decay time of phase 3 is remarkably insensitive to field configuration, I_z/I_r, fluctuation level, or the presence of support rods. It is only appreciably shortened (factor of 3) when $I_z/I_r < 1$, and then injection is inefficient and azimuthal symmetry is probably not approached. Attempts to relate the Langmuir probe decay time to an actual confinement time by direct measurement of the escaping flux have been unsuccessful. Several measurements have been performed, however, which suggest that $\tau_d \approx \tau_{confinement}$.

If the transient gas pressure during the decay is doubled by means of a pulsed gas value, the decay rate is not appreciably altered, suggesting that recycling is unimportant. Further data have been obtained with an ion energy analyzer [7]. With the acceptance energy set at 40 volts (well above the anticipated energy of recycled ions) the curves shown in Fig. 5 were obtained. When the ring is levitated, the decay rate is seen to be comparable to Langmuir probe decay shown earlier, while with the rod supported a more rapid decay is observed consistent with collection on the levitator rods. Since the bulk of the ion distribution is estimated to have $T_i \approx 1 - 5$ eV by use of a Larmor radius selection analyzer [8], the observed insensitivity to the presence of supports is also consistent with the observed τ_d.

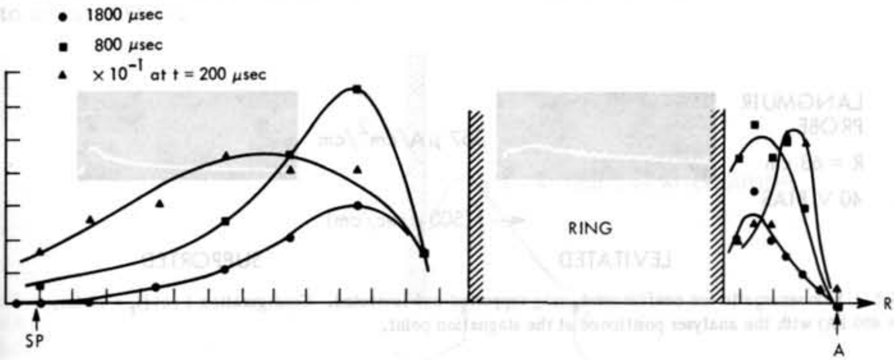

FIG.4. Midplane probe current profiles at t = 200, 800, 1800 μs after gunfire. The field configuration is shown in Fig.3. The probe bias is 80 V. Note the t = 200 μs curve is reduced by 10.

Assuming that $\tau_c = \tau_d$ and taking $T_e = 10$ eV, the normalized decay time ranges between 10 and 100 τ_{Bohm}, depending on B (in the range $I_r = 45\text{-}90$ kA) and the portion of the decay considered. Next, the effects of ohmic heating will be discussed.

Because of the finite resistivity of the floating ring the confining poloidal field is necessarily transient, and consequently inductive electric fields are present and, for $I_r = 45$ kA, $I_z = 200$ kA, $\overline{E} \cdot \overline{B}/B \approx 2 \times 10^{-3}$ volts/cm. In addition to ring resistivity, induction electric field can arise from time-changing current in the external windings. Generally, injection of plasma is timed to coincide with peak current in the windings.

Typical evidence of the onset of ohmic heating and recycling is shown in Fig. 6. At $I_r = 45$ kA, the decay after injection is nearly unchanged by the presence of the supports. The ballooning fluctuations evident at R = 71 cm are also relatively unchanged; however, low-frequency fluctuations are frequently induced near the ring as shown at R = 68.5 cm. If I_r and I_z are increased to 180 and 800 kA respectively, appreciable recycling appears when the rods are withdrawn. The effects of recycling are dependent on factors such as volatile gas evolution from the gun or surface cleanliness. Frequently the plasma density continues to increase after injection and then decays with a time constant approaching the field decay time $\tau_B \approx 20$ msec. In addition to recycling, high-frequency fluctuations ($f \approx 20 - 200$ kc) are excited.

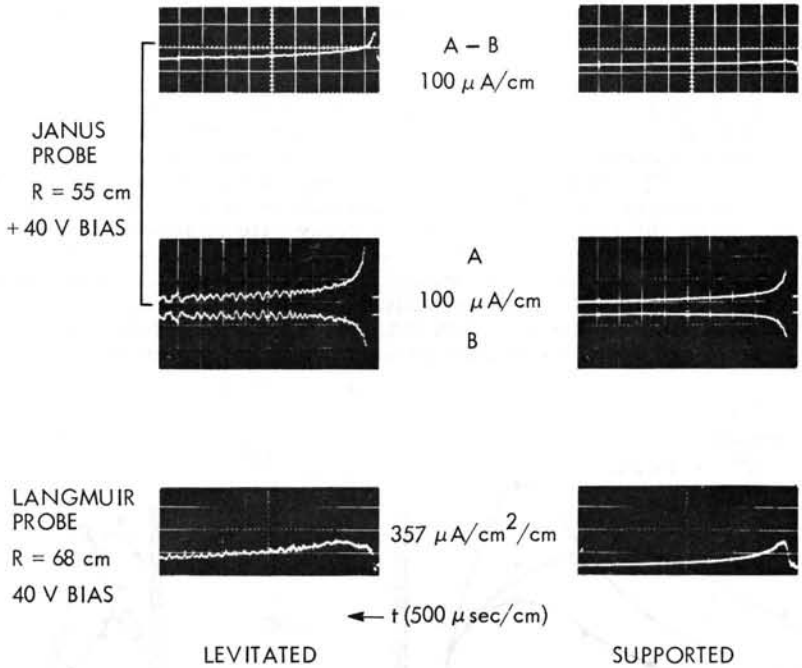

FIG. 5. Monoenergetic ion confinement, ring supported and levitated. Configuration 1 (a) (I_r = 90 kA, I_z = 400 kA) with the analyser positioned at the stagnation point.

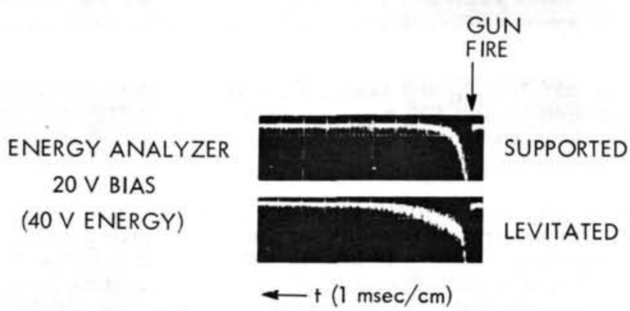

FIG. 6. Langmuir probe current at two positions for two field strengths, ring supported and levitated configuration 1(a). The probe bias is 40 V.

Measurements of the induced electron drift motion have been made with a symmetrical "Janus" probe which consists of two collection electrodes positioned behind 0.1-cm-diameter holes in an external tubular electrode. The holes are diametrically opposed, aligned with the magnetic field, and the electrodes are biased relative to the external electrode to collect the electron saturation current. The difference in collected current is a measure of the electron drift.

Typical results are shown in Fig. 7 for the ring supported and levitated. With the ring levitated the difference current (A - B) is comparable with the individual leg current, indicating appreciable drift ($v \approx v_{te}$) and consequent recycling as shown on the Langmuir probe trace. If the ring is left supported, the current decreases by ≈ 100, low-frequency fluctuations are greatly reduced, and a simple plasma density decay occurs.

Similar ohmic heating occurs for all configurations investigated thus far, provided B_t and B_p are roughly comparable and I_r is sufficiently large.

Fluctuations are observed for most of the duration of the plasma, although when ohmic heating is not important the decay rate in phase 3 is not appreciably affected by the fluctuation amplitude. Typical fluctuations observed in configuration 1 fall into two classes: (1) nonlocalized modes which appear when the ring is levitated, and (2) modes localized in the external density gradient region of the plasma. Class 2 modes may also be localized to certain regions of the flux surfaces as in the ballooning mode noted earlier. The spectrum of fluctuations extends from a few kilocycles to about 100 kc.

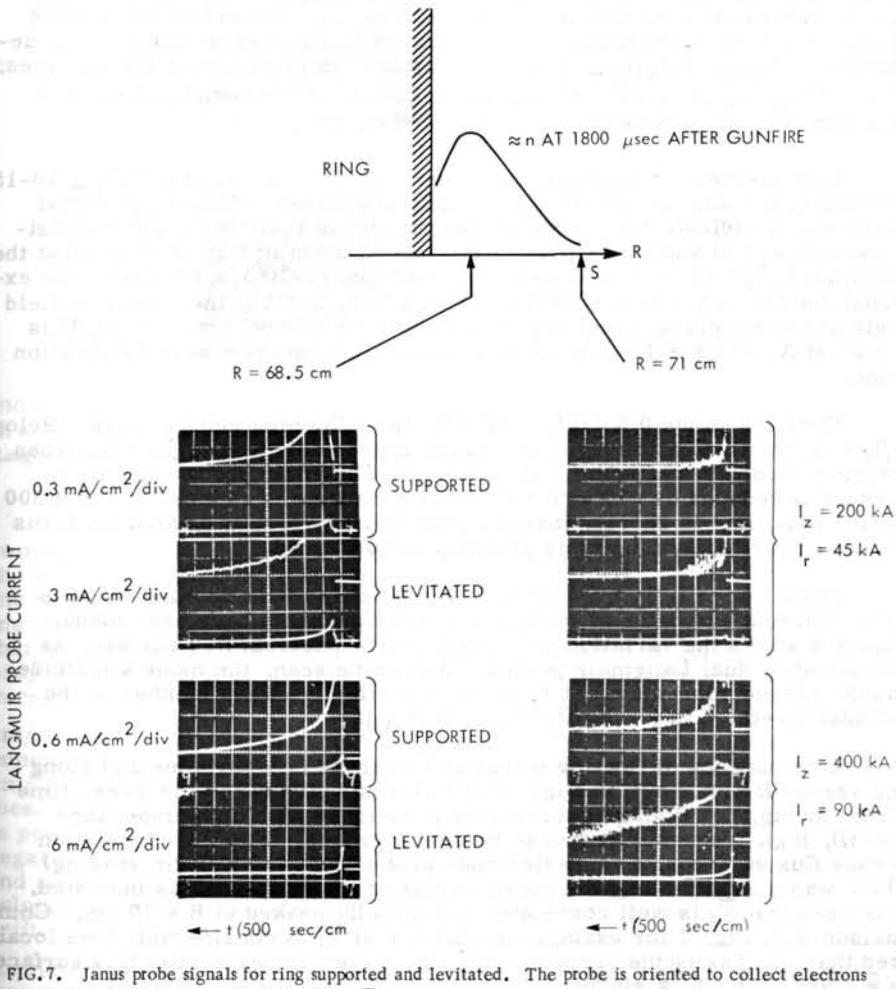

FIG.7. Janus probe signals for ring supported and levitated. The probe is oriented to collect electrons moving parallel (A) and antiparallel (B) to $\overline{B}$.

Two types of nonlocalized fluctuations are frequently observed: (1) a low-frequency (~2-5 kc) coherent "wobble" of the entire plasma (see Fig. 5, levitated for example); and (2) high-frequency (20-100 kc) fluctuations with short wavelength across B ($\lambda_\perp \lesssim 0.1$ cm). Both fluctuations appear to be excited by ohmic current and are most intense for $I_r > 90$ kA. However, because of lack of reproducibility, correlations have not yet been established.

Localized fluctuations are more reproducible and are relatively insensitive to the presence of levitator rods. These fluctuations appear almost entirely in the external density gradient region and are most intense near the low-density edge where typically $\tilde{n}/n \approx 0.1$. The internal gradient region near the ring, where plasma pressure is supported by an everywhere-stabilizing gradient in B, is nearly always quiescent ($\tilde{n}/n \lesssim 10^{-2}$) except under conditions of strongly excited nonlocalized modes.

The amplitude of localized fluctuations tends to be relatively insensitive to the magnetic field strength, although generally the frequency spectrum tends to shift upward as B is increased. A marked dependence of the amplitude distribution around constant flux surfaces is observed, depending on I_z/I_r. If $I_z/I_r \gtrsim 10$-15, fluctuations extend all over the surfaces; while for $I_z/I_r \lesssim 10$. localized ballooning occurs in the destabilizing field curvature region outside the ring, as noted earlier.

Only limited correlations have been made in the regimes $I_z/I_r \gtrsim 10$-15 because of the almost turbulent wave field developed. Floating potential correlations indicate the coherence length across $B, L_\perp$ is < 1 cm (consistent with $k_\perp a_i \approx 1$) and that $\lambda_{||}/L_\perp > 10$. Examination of Fig. 2 shows that the condition $I_z/I_r \approx 15$ corresponds to the condition $(\partial \langle B^2 \rangle / \partial\psi) \approx 0$ over the external density gradient region R = 51-56. At $I_z/I_r = 15$, the change in field angle at the midplane over the gradient distance n/n' (≈ 1 cm at point A) is $\theta = 5°$ at A, and $\theta = 17°$ for the flux surface intersection at the stagnation point.

Over the range $0.5 < I_z/I_r < 10$-15, the ballooning mode occurs. Below $I_z/I_r \approx 5$, the fluctuation level decreases appreciably until $I_z/I_r \approx 0.5$ when trapping becomes inefficient. If $I_z = 0$, the Langmuir probe saturation current is reduced by ~10 and the confinement time is reduced to about 500 μsec. This time is shorter than the grad B drift velocity around the torus so that azimuthal symmetry is probably not achieved.

In the range $I_z/I_r = 5$ - 10 ($I_r = 45$, 90 kA), the ballooning mode is quite coherent and detailed correlation measurements have been made. Figure 8 shows the variation of $\tilde{n}$ around the separatrix flux surface, as measured by dual Langmuir probes. As can be seen, the mode amplitude has decreased appreciably at B so that the effective wave number in the poloidal direction is $\bar{k} \cdot \bar{B}_p/B_p = k_p > \pi/2L_{AB}$.

Correlations of floating potential $\tilde{V}_f$ across flux surfaces and along and across B are shown in Figs. 9 and 10 respectively for the sweep time shown in Fig. 8. Both measurements were made with high-impedance ($10^7\,\Omega$), high-frequency response (~300 kc) probes. For the correlation across flux surfaces, a four-electrode probe was used (0.5 cm spacing) which was oriented along the major radius at the midplane, as indicated. It is seen that $\tilde{V}_f$ is well correlated and broadly peaked at $R \approx 70$ cm. Comparison with Fig. 7 for example indicates that $\tilde{V}_f$ is considerably less localized than $\tilde{n}$. Taking the variation of $\tilde{n}$, the wave number across flux surfaces is $\bar{k} \cdot \bar{\nabla}\psi/|\nabla\psi| = k_\psi \approx \pi(n'/n)$.

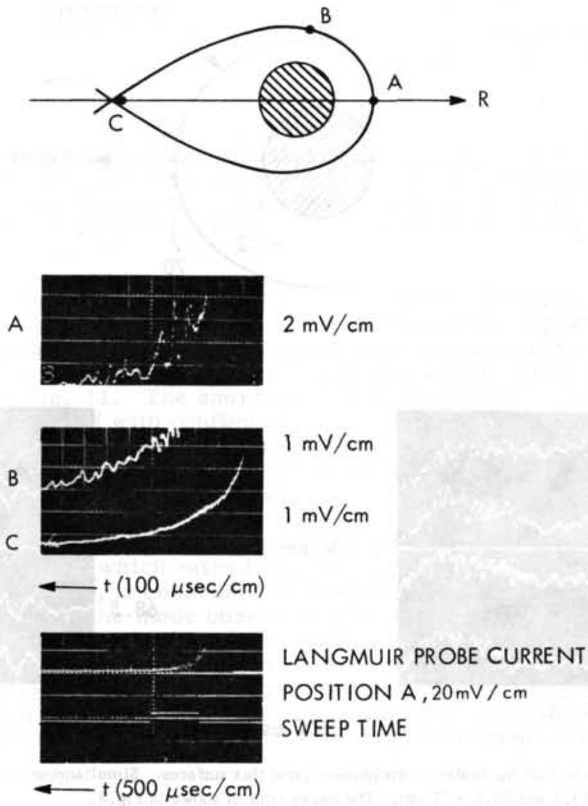

FIG.8. Variation of density fluctuations at a flux surface near the separatrix. Langmuir probes are positioned at A, B, C as shown for configuration 1. The sweep time is shown by the lower trace, along with the Langmuir probe current at position A (R = 70 cm, 80 V bias).

Correlations across and along B shown in Fig. 10 were taken with a two-electrode floating probe with variable separation and rotation and with the electrodes positioned at about the separatrix at the points shown. When the tips are aligned with B(A'B') well-correlated signals are seen, indicating that the lowest order variation in the poloidal direction is dominant so that $k_p \approx \pi/2\, L_{AB} \approx 0.16\ cm^{-1}$. With the tips at AB it is seen that phase propagation from A to B occurs, i.e., in the direction of the diamagnetic current or the ion grad B drift. The propagation velocity is $v_{p_\perp} \approx +0.34$ cm/μsec which yields $2\pi/k_\perp = \lambda_\perp \approx 33.5$ cm for the 10-kc component. For comparison, under the conditions shown, $f_{ci} \approx 250$ kc for Li, $v_{i\nabla n} = +0.35$ cm/μsec for $T_i = 2$ eV and $n'/n = 2\ cm^{-1}$, and $v_{i\nabla B} \approx +0.03$ cm/μsec. A local E/B velocity of ≈ -0.1 cm/μsec (electron diamagnetic drift direction) is present, as inferred from the gradient of V_f. (V_f is usually 3-5 volts negative at the maximum density point and increases to ≈ 0 near the ring and separatrix.) Consistent with experimental error, the propagation velocity is in the direction of and approximately at the ion diamagnetic drift. Attempts to determine the scaling of $v_{p_\perp}$ with Tn'/Bn have not yielded consistent results because of shot-to-shot variation. Increased B, however, increases roughly linearly the frequency of the dominant component.

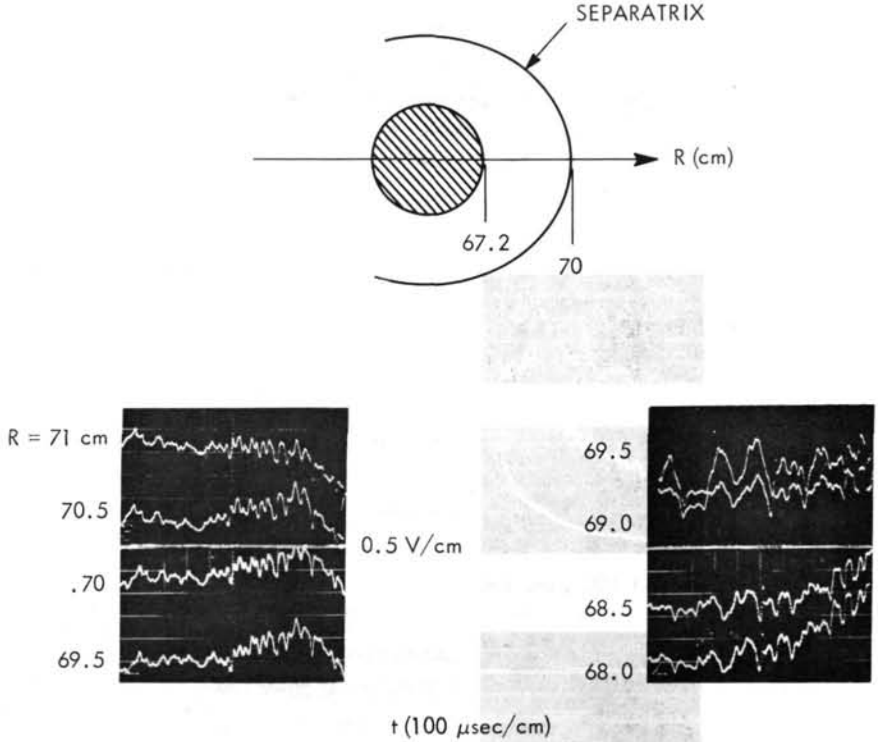

FIG. 9. Floating potential fluctuation correlations across flux surfaces. Simultaneous measurements are shown for R = 68 - 69.5 and 69.5 - 71 cm. The sweep time is shown in Fig. 8.

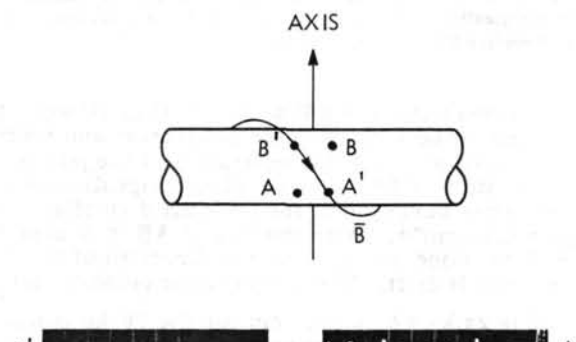

FIG. 10. Floating potential correlations for configuration 1. Correlations are shown for two probe orientations A, B, A', B' across and along $\overline{B}$ in the region outside the ring (R = 70 cm). The sweep time for the correlated signals is shown in Fig. 8.

Next, confinement and fluctuation observations with configuration 2 will be discussed. As noted earlier, the principal differences between configurations 2 and 1 are the strong reversal of grad $\langle B^2 \rangle$ and the gradient of B in the trapped particle zone.

The confinement characteristics of this configuration are similar to those noted earlier. For regimes in which ohmic heating is not important, comparable density and temperature plasma is trapped and after initial transients lasting ≈ 50 μsec a quiescent decay follows with $\tau_d \approx 1$ msec as before. Ohmic heating effects are observed which are similar to those described earlier.

One of the major differences in confinement when ohmic effects are unimportant is a pronounced shift of the external density gradient inward from the separatrix. This effect occurs early in the injection phase and persists during the remaining decay. Typical density and floating profiles are plotted in Fig. 11. The source of more rapid loss of plasma near the separatrix compared with configuration 1 has not been determined. In addition to plasma effects, it is likely that greater destruction of the magnetic surfaces occurs for this configuration because of the closer proximity of the stagnation point to port perturbations in the external windings.

Fluctuations similar to those described earlier are observed, including localized modes which extend over the entire flux surface at large I_z/I_r. In the case $I_z/I_r \lesssim 15$, a coherent low-frequency ballooning mode is observed which is similar to the mode observed with configuration 1 except that the frequency is lower and ballooning occurs near the stagnation point. Floating potential correlations of this mode are shown in Fig. 11. Comparison of probe positions AB and A'B' shows that propagation occurs across B in the direction of the ion diamagnetic drift. For the case shown, $v_{p\perp} \approx 0.12$ cm/μsec which roughly corresponds to the ion diamagnetic velocity at $(\tilde{n}/n)$ maximum.

HOT ELECTRON PLASMA STUDIES

The confinement of hot electron plasma has been investigated primarily with configuration 1 (or variant 1(a)) with $I_z/I_r \approx 9.0$ for which a minimum B mirror zone is formed as shown in Fig. 1. If the electron cyclotron frequency is adjusted so that resonance occurs in this region, a mirror-trapped hot electron plasma is produced which is stably confined against cross-field losses. During the subsequent decay, scattering or enhanced end losses relax the distribution toward isotropy.

Plasma is formed either by ionization of a low-pressure gas background at $p \approx 3 \times 10^{-7}$ (base) to 10^{-5} torr or by heating of gun-injected plasma. For $|B|$ adjusted for electron cyclotron resonance corresponding to contours $|B| = 3.2 - 3.8$ of Fig. 1, microwave power to 20 kW at 10.6 Gc is pulsed on for $\tau_h \lesssim 1$ msec to produce a plasma which consists of two electron energy components: mirror-trapped hot electrons with $T_{eh} \approx 5$-20 keV, $n_{eh} \lesssim 3 \times 10^{10}$; and cold electrons with $T_{ec} \approx 10$-20 eV, $n_{ec} \approx 10^{11} - 3 \times 10^{12}$. The upper limit of n_{ec} appears to be set by the cutoff condition $\omega_{pe} = \omega_h$. Hot electrons are measured with scintillation, thermocouple, and x-ray probes. Cold plasma is measured with Langmuir probes and an interferometer.

The achievement of dense, hot-electron regimes ($n_{eh} \approx 10^{10} - 3 \times 10^{10}$) is critically dependent on the resonance zone location and the buildup of cold plasma. The production of energetic electrons is strongly reduced when

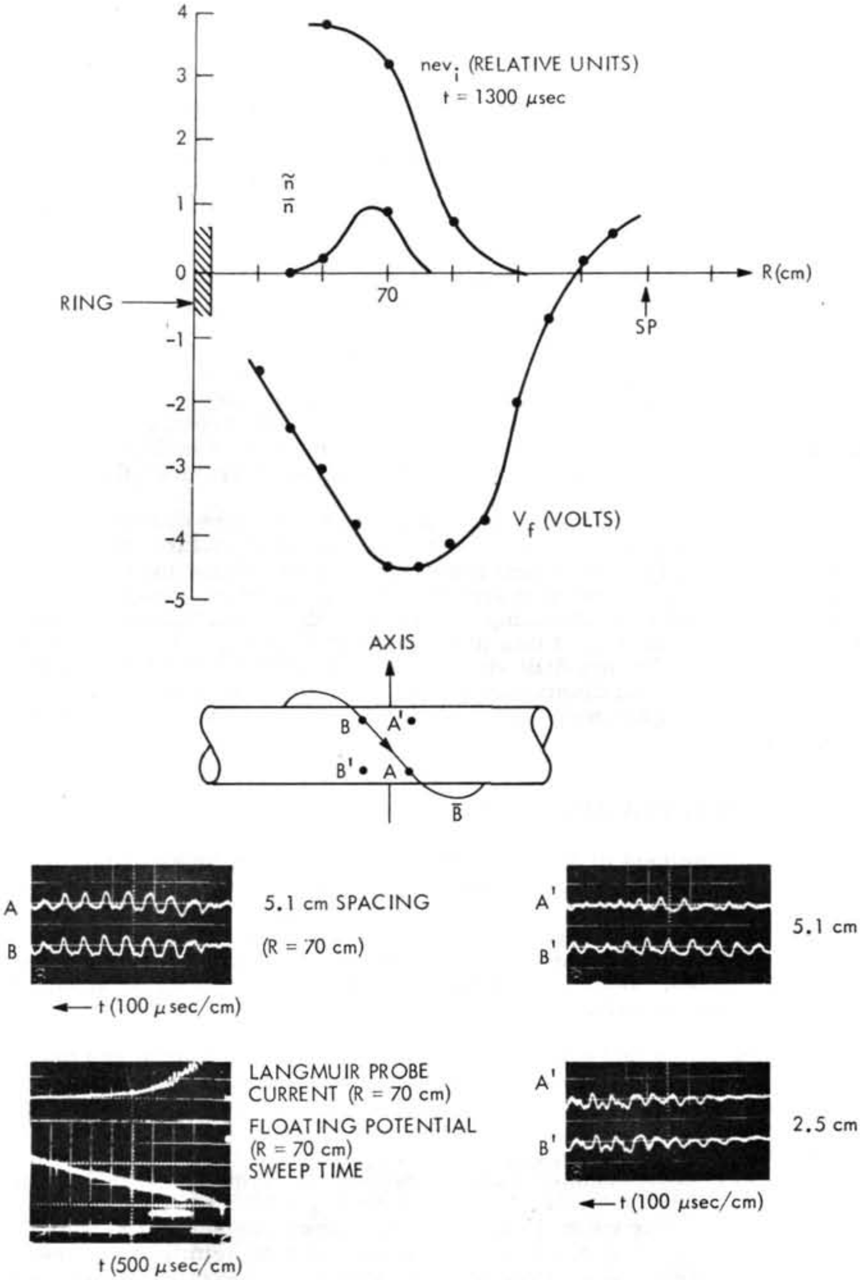

FIG.11. Langmuir probe current, density fluctuation, and floating potential vs radius and fluctuation correlations for configuration 2, I_r = 70 kA, I_z = 400 kA. Fluctuations in floating potential are shown for two probe positions AB, A'B' for spacings of 2.5 and 5.1 cm. The correlation sweep time is shown with Langmuir probe saturation current and floating potential at R = 70 cm.

n_{ec} is a small fraction (~10^{-1} to 10^{-2}) of the cutoff value. This critical dependence on n_{ec} suggests that heating by extraordinary wave propagation across B occurs where $\omega_h^2 = \omega_{ce}^2 + \omega_{pe}^2$. Because of the relatively shallow well in $|B|$, small ω_{pe}^2 can shift the heating zone out of the minimum B region.

The dependence of the plasma spatial distribution on the location of the resonance zone is shown in Fig. 12. A shift inward toward the ring is seen when I_r is reduced (I_z/I_r constant) consistent with the corresponding shift in the resonance zone. Sharp definition of the plasma boundary by the resonance zone has also been observed with microwave heating in a minimum B mirror device [9].

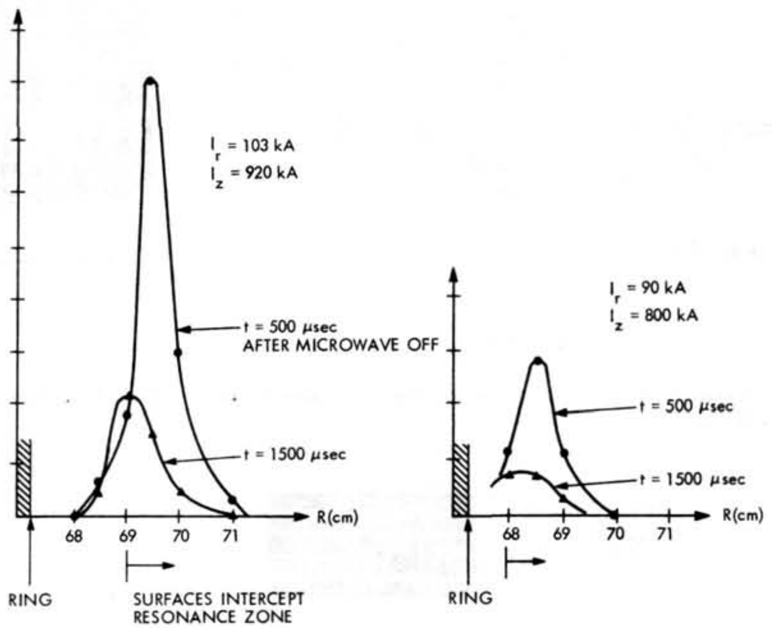

FIG. 12. Profiles of electron distribution taken with probe 3 for I_r = 90 kA, I_z = 800 kA. Probe 3 is a plastic scintillator sensitive to electrons with E ≳ 3 keV. Configuration 1 was used and the flux surfaces which intercept the resonance zone are indicated. The case I_r = 90 kA, I_z = 800 kA corresponds to resonance at B = 3.8 in Fig. 1. The vertical scale is relative.

Under optimum adjustment of parameters, the hot electron plasma is initially mirror-trapped and then spreads around the ring primarily by gas scattering, as shown in Fig. 13. Probe 1 in the mirror zone shows the direct flux of energetic electrons during heating and a rapid decay after microwave turn-off due to collection by the probe. Probes 2 and 3 show successively slower increases in signal, reflecting the gradual spreading of the plasma around the ring. Interception of a flux surface near Probe 1 reduces the signals on the same surface at positions 2 and 3 by 10-100, also consistent with mirror trapping.

Spreading around the ring is generally observed to be energy-dependent by x-ray measurement, and background gas pressure variation consistent with classical scattering. Figure 14 shows the loss rate to probe 3 for several pressures of argon and for pulsed argon introduced during the decay. The results are roughly consistent with scattering into the loss cone with $\tau_{scattering} \propto p^{-1}$, rapid loss of particles scattered into orbits which pass around the ring, and finally decay of the trapped population.

A cold plasma background is also present for which the density has roughly the same time-dependence as the visible light signal of Fig. 14. For the case shown $n_{ec} \approx 10^{10} - 10^{11}$, the density profile is similar to the gun plasmas described earlier, and similar fluctuations are present.

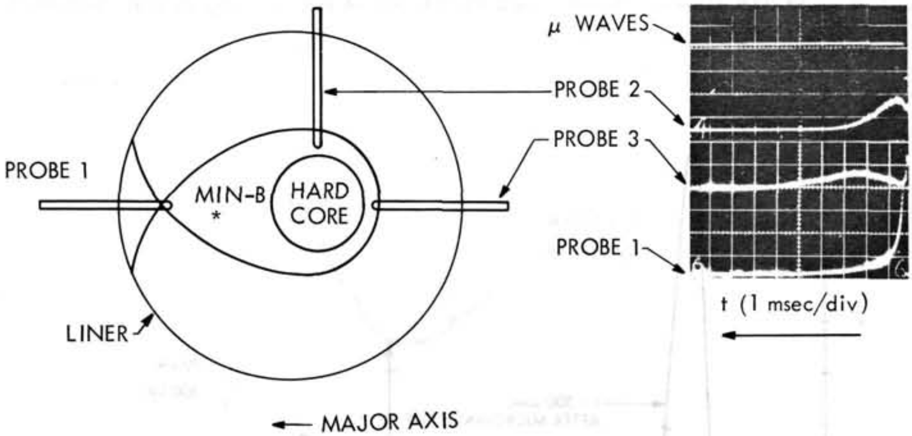

FIG. 13. Energetic electron signals received by scintillation probes positioned as shown for configuration 1(a)(Fig.3), I_r = 100 kA, I_z = 800 kA.

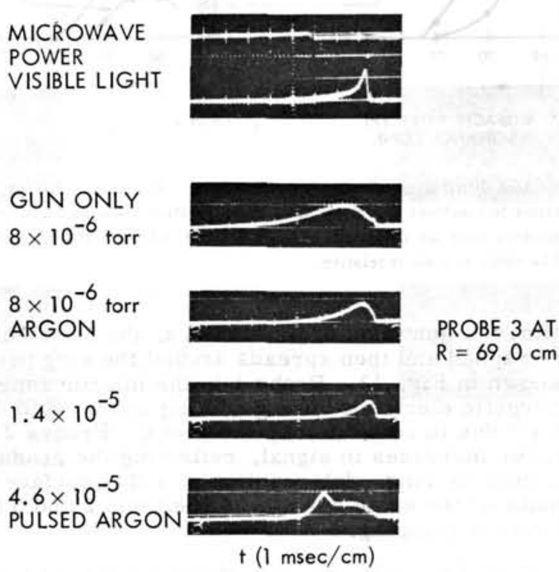

FIG. 14. Energetic electron signals received by probe 3 positioned at R = 69.0 cm for background pressures of 8×10^{-6} torr gun gas, and with 8×10^{-6} torr, 1.4×10^{-5}, and 4.6×10^{-5} (pulsed) argon.

Since the sweep-up time of passing electrons on the scintillation probes (0.3 cm diameter) is much shorter than the scattering rate ($\tau_{probe} \approx 5$ - 20 μsec) the above picture of mirror loss is expected. To determine the loss rate of passing particles in the absence of probes, the area of intercepting surfaces in the region of probe 3 was varied, with relatively little effect.

The relative insensitivity of the slower decay of more energetic electrons (10 - 30 keV) to varying obstacle size suggests that for this configuration the inherent loss rate of passing particles is considerably larger than the rate of scattering into the loss cone. This conclusion has also been tested with a moveable scintillation probe which can be inserted into the confinement region near probe 3 a distance 1 cm in 10^{-3} sec. If the probe is inserted during the usual slow decay shown in Figs. 13 and 14 an instantaneous signal is observed which corresponds roughly to the static signal with the probe fixed at the same position, thus indicating no appreciable confinement of passing particles. Inserting the probe 0.5-1 msec after the scattering time has been decreased to several hundred microseconds by pulsing in argon to $\approx 2 \times 10^{-4}$ torr pressure again fails to show an appreciable population of passing particles or any effect by fixed probes.

SUMMARY AND DISCUSSION

A clearly evident feature of gun-produced plasma is the appearance of strong ohmic heating and recycling at high ring current with the levitators withdrawn. The persistence of appreciable ohmic heating for constant current in the external windings stems from the resistive voltage drop which is virtually inavoidable with the present system.

A low ring current, or supported ring regime was identified where appreciable ohmic effects appear to be suppressed. In this regime nearly collisionless plasma with $n \approx 10^9$-10^{10} ions/cm^3, $T_e \approx 5$-15 eV is observed to decay over typically 10-100 τ_{Bohm} nearly independent of the detailed field configuration or field strength.

Several features of the near equilibrium of the decaying plasma bear discussion. Under most conditions where long-time confinement is observed, the floating potential is more negative by about $V_f \approx T_i$. Since it is expected (and approximately measured) that $T_e \approx$ constant, it appears reasonable that the space potential is also negative, implying good electron confinement and therefore closed magnetic surfaces. An additional consequence of negative space potential is the compression of ion drift surfaces to more closely coincide with flux surfaces, as is evident from consideration of conservation of canonical angular momentum and energy. Although the above conservation equations insure absolute confinement (provided a high degree of axisymmetry is present) ions need not be adiabatic. Since the transition energy at I_r = 45 kA is about 4 eV for Li^+, the estimated ion temperature of 2-5 eV is close to the nonadiabatic limit.

It is not clear what process establishes the decay time. Except during the early filling phase, the decay rate is relatively insensitive to the level of fluctuations between 5 and 100 kc, the poloidal field configuration (except near the stagnation point for configuration 2), or the ratio I_z/I_r. It is possible that low-frequency activity can account for the decay time. However, for frequencies of order 1 kc or less, the experimental determination of long wavelength potential variation is difficult and intimately associated with the degree of azimuthal symmetry achieved. Comparison of probes at several positions suggests that the plasma density is symmetric within $\pm 20\%$. This is well below the accuracy required to determine the importance of low-frequency "convective-like" processes which can account for the observed loss with average electric fields of order 10^{-2} volts/cm.

Fluctuations which appear to be associated with confinement are observed in the external density gradient while the internal density gradient is relatively quiescent. For both field configurations, low-frequency ($\omega \ll \omega_{ci}$) ballooning occurs in the region of maximum destabilizing field curvature and the phase velocity is at approximately the ion diamagnetic drift. These characteristics suggest the dissipative interchange instability [3]; however, because $k_{\parallel} \approx k_{\perp}$, and $\omega/k_{\parallel} v_{te} \ll 1$, propagation with the ion drift is inconsistent with equilibration of the electrons along B.

Several effects can alter the simple picture given above. First, for the reversed gradient configuration (2), the condition $\omega\tau_{Bi} \approx 0.5$ holds (τ_{Bi} is the bounce frequency of trapped ions) so that trapped particle effects can be important. Ballooning in the mirror-trapping region for this configuration would be consistent with predicted trapped particle instabilities [10], [11], [12]; however, there is no immediately evident reason why propagation should occur at $v_{\nabla ni}$. For the ballooning mode observed with the minimum B configuration (1), the frequency is higher and the ion bounce time is longer and varies considerably over the flux surfaces where the wave is localized so that $\omega\tau_{Bi} \approx 1 - 10$. As before, it appears that the detailed particle motion can be important; however, a direct correspondence with trapped-particle modes is difficult to establish. Finally, other effects which possibly can be important are that for the equilibrium $a_i\, n/n' \approx 2 - 4 >> (m/M)^{1/2}$, and a weak nonuniform electric field is present.

Hot electron plasma produced by ECR heating with $n_{eh} < 3 \times 10^{10}/cm^3$ and $T_{eh} = 5 - 20$ keV is observed to be confined for times many orders of magnitude longer than the Bohm time computed with T_{eh}. Although the Debye length is relatively short ($\lambda_D \approx 0.5$ cm) and the dielectric constant large ($\omega_{pi}^2/\omega_{ci}^2 \approx 10^2$), the degree of pressure isotropy attained during the decay is important and not yet precisely determined.

Preliminary indications are that anisotropy in the absence of intercepting probes remains high during the decay. Since the number of electrons in passing orbits does not increase appreciably with the probes removed, it appears that either the inherent loss time is less than the probe collection time ($\approx 10\ \mu$sec $= 10^2\ \tau_{Bohm}$) or that a selective loss of trapped electrons occurs when passing trajectories are approached. Such a selective loss needs to be only of the order of magnitude of scattering losses to agree with observation.

A number of possible loss mechanisms can occur either from single particle or collective effects, including modification of the energetic electron confinement by low-frequency fluctuations of the cold plasma. Also, considering single particle motion, electrons with energy $\lesssim 100$ keV remain adiabatic; however, excursions from flux surfaces increase with $v_{\parallel}/v_{\perp}$ and are largest for trapped particles which are marginally close to passing orbits. Conservation of canonical angular momentum may be used to estimate the excursion δ which is readily shown to be

$$\delta_{max} \approx 2\, a_{ep}$$

where $a_{ep} = v_\theta/(e/m)B_p$ is the electron gyroradius in the average poloidal field. Since $B_p \approx 4$ kG at the mirror points (Fig. 1) $a_{ep} \approx 0.3$ cm for a 20-keV electron at the separatrix above the ring and $a_{ep} \approx 2 - 4$ cm near the stagnation point. Thus a_{ep} is an appreciable fraction of the confinement volume near the stagnation point, and weak field inhomogenieties may lead to rapid loss of high-energy electrons.

ACKNOWLEDGMENT

The authors are indebted to Dr. J. Killeen and R. Freis for extensive magnetic field calculations (UCRL-50161, "Calculation of Toroidal Magnetic Field Configurations," J. Killeen, H. P. Furth, R. P. Freis), and to G. Orloff and D. Branum for assistance in performing the experiments.

REFERENCES

[1] BIRDSALL, D. H., BRIGGS, R. J., COLGATE, S. A., FURTH, H. P., HARTMAN, C. W., Plasma Physics and Controlled Nuclear Fusion Research, Vol. II (1966)

[2] KILLEEN, J., FURTH, H. P., ROSENBLUTH, M. N., Minimum-B and Minimum-Average-B configurations in the Levitron, Am. Phys. Soc. Plasma Phys. Div. 7th Annual Meeting, 1965, paper G7.

[3] FURTH, H. P., KILLEEN, J., ROSENBLUTH, M. N., Plasma Phys. and Controlled Nuclear Fusion Res. 1 (1966) 103.

[4] COENSGEN, F. H., CUMMINS, W. F., NEXSEN, W. E., Jr., SHERMAN, A. E., Phys. Fluids 9 (1966) 188.

[5] DICKINSON, H., Physics Fluids 3 (1960) 480.

[6] LAFRAMBOISE, J. G., Theory of spherical and cylindrical Langmuir probes in a collisionless, Maxwellian plasma at rest, Institute for Aerospace Studies (1966).

[7] KERST, D. W., DORY, R. A., WILSON, W. E., MEADE, D. M., ERICKSON, C. W., Phys. Rev. Letters 15 (1965) 396.

[8] AFROSIMOV, V. V., GLADKOVSKII, I. P., Sov. Phys.-Tech Phys. 12 (1968) 68.

[9] HARTMAN, C. W., Phys. Fluids 9 (1966) 821.

[10] KADOMTSEV, B. B., POGUTSE, O. P., Soviet Phys. JETP 24 (1967)

[11] ROSENBLUTH, M. N., Phys. Fluids 11 (1968) 869.

[12] COPPI, B., et al. (to be published in these Proceedings).

DISCUSSION

A. GIBSON: Have you attempted to produce plasmas by resistive microwave heating – i.e. with no resonance inside the tube?

C.W. HARTMAN: Yes, although no systematic studies have been conducted. Non-resonant heating of gun-injected plasma has been observed.

R.S. PEASE: What is the drift velocity along the lines of force due to inductive (and resistive) electric fields? Have you any information on the instabilities that may be produced thereby?

C.W. HARTMAN: Measurements with the Janus probe suggest that the drift velocity is comparable with the electron thermal motion when strong recycling occurs. However, quantitative interpretation of the probe characteristics is complicated by a wake, or shadow, which may be present under these conditions.

P.L. HUBERT: Does the induced electric field exceed the Dreicer limit for the production of runaway electrons?

C.W. HARTMAN: It is possible that runaway electrons are present, although X-ray measurements do not show any detectable intensity of photons with an energy greater than about 1 keV.

S.J. BUCHSBAUM: With regard to Mr. Hubert's question, your plasma is not fully ionized so that the runaway field is higher than the Dreicer field.

C.W. HARTMAN: Yes, I agree.

TOROIDAL CONFINEMENT III
(STELLARATORS)

(Session D)

Chairman: M. ROSENBLUTH

THE EXPERIMENTAL INVESTIGATION OF SINGLE-PARTICLE CONTAINMENT IN A HIGH-SHEAR STELLARATOR

A. GIBSON, J. HUGILL, G.W. REID, R.A. ROWE AND B.C. SANDERS
UKAEA, CULHAM LABORATORY, ABINGDON, BERKS, UNITED KINGDOM

Abstract

THE EXPERIMENTAL INVESTIGATION OF SINGLE-PARTICLE CONTAINMENT IN A HIGH-SHEAR STELLARATOR. A low-β toroidal reactor will only be feasible if ions with randomly directed velocities can be contained while they make more than 10^4 transits around the trap. However in a toroidal stellarator, because of the lack of symmetry, it has not been demonstrated that even the field lines are contained to this accuracy. This paper describes experiments to measure the confinement time for a distribution of single particles in a high shear stellarator. The method used is to populate the trap with β-particles from tritium gas and measure the equilibrium population by collecting all the trapped electrons on a moving scintillation probe, which is driven across the trap. The maximum containment time which can be measured in this way is set by the energy degradation time on the background gas and can correspond to more than 10^8 transits. Those particles born in the loss region of velocity space (i.e. on to orbits which intersect the wall in a few transits) are excluded from the measurement.

The trap is a stellarator with a toroidal $\ell = 3$ helical winding, minor radius 11.5 cm, major radius 30 cm, mean pitch angle 45°, there are 8 field periods on the torus. The limiter radius is 5.8 cm and the separatrix can be inside the limiter for toroidal fields of up to 1000 G. For this field the mean ratio of limiter to Larmor radius, for particles detected by the scintillator, is about 30. The windings are designed to produce a spatially accurate, quasi-d.c. ($\sim$ 10 s) field, it is possible deliberately to perturb the field and assess the effect on particle confinement.

Measurements with Hall probes on particular lines show that the field accuracy is in fact better than 0.3%, and electrons from guns ($V_{\parallel}/V_{\perp}$ large) lie on closed surfaces for at least 10 to 20 transits. Measurements, using tritium, show that there are regions of the trap where electrons are contained for more than 10^7 transits.

1. Introduction

A low β toroidal reactor will only be feasible if plasma particles can be contained while they make many transits of the trap. Currently envisaged parameters [1] for such a reactor imply that, in the absence of collisions, ions could make 10^4 to 10^5 transits of the trap, and electrons (4 to 40) $\times$ 10^5 transits. Knowledge of the single particle properties of a trap is thus an essential pre-requisite for understanding its behaviour and potentiality as a container for plasma.

Conservation theorms can be invoked [2] to show that particles are confined in axisymmetric systems, while in mirror machines single particle confinement, for more than 10^7 reflections, has been demonstrated experimentally. The situation is less satisfactory for stellarators. Thus magnetic surfaces are known to exist in straight stellarators with helical symmetry [3], and to exist in an asymptotic sense in certain other situations [4,5]; but in the general case of a toroidal stellarator it is not known whether the field lines generate magnetic surfaces or whether they behave ergodically. Furthermore, examples have been given of stellarator type fields which have no surfaces [6,7] or in which many of the surfaces are open [5]. The addition of perturbations can completely change the surfaces [8], and even very small perturbations [9] can cause surfaces near the separatrix to open.

Numerical examination of particle motion [10] in stellarator fields confirms that, if $V_{\parallel}/V_{\perp}$ (the ratio of the velocity components parallel to and transverse to the magnetic field) is not too small, then particles generate drift surfaces similar to but displaced from the magnetic surfaces; the displacement tends to zero with Larmor radius $(r_L)^{(1)}$. Particles with small $V_{\parallel}/V_{\perp}$ may be reflected in the gradients of the helical field and drift out of particular stellarators no matter how small the Larmor radius [10]. These particles, together with those whose drift surfaces intersect the walls because r_L is too large, form a loss region in velocity space. Experimental observations of the confinement of particles making many transits of a stellarator have been restricted to a small region of velocity space ($V_{\parallel}/V_{\perp}$ large). Experiments at Princeton [11] reveal the existence of runaway electrons which are inferred to be confined while they make more than 10^4 transits of the trap. Workers at the Lebidev Institute [12] have shown that electrons from guns (again with $V_{\parallel}/V_{\perp}$ large) are confined for more than 100 transits.

This paper described experiments to measure the confinement time of a random distribution of electrons in a high shear $\ell = 3$ stellarator. The trap is populated by radioactive decay, particles born in the loss region escape in a few transits and so do not contribute to the measurements. In our experiment because of the rather large Larmor radius of the particles (about 1/30 of the limiter radius) about 50% of the decays give rise to particles in the loss region.

2. Experimental Method

2.1 General Description

The method is similar to that used by Rodionov [13] in mirror machines. The trap is filled with tritium gas which populates the drift surfaces with β particles. The equilibrium population is measured by collecting all the electrons on a scintillation probe driven quickly across the trap so as to intersect each drift surface in turn. At sufficiently high tritium pressures the equilibrium density, determined by collisional interaction with the tritium gas, is independent of pressure and is about 4 β particles cm^{-3}. At lower pressures other processes, such as loss due to magnetic imperfections, cause the equilibrium population to fall. By observing the variation of equilibrium population with filling pressure the magnetic confinement time can be measured. Corrections have to be applied to the observed count on the moving probe to take account of the background count rate (photomultiplier noise and tritium adsorbed on the scintillator); and of particles, collected by the probe, which were born during the probe movement. This latter correction is pressure dependent and is evaluated, separately, by moving the probe slowly across the trap so that most of the particles collected are born during the movement.

2.2 Determination of confinement time

The generation rate of particles in the trap is:

$$\left[\frac{dn_{\beta}}{dt}\right]_{+} = G\, p_t\, f \tag{1}$$

(1)Defined in terms of the total energy.

Where

n_β is the number of β particles cm^{-3},
f is the fraction of particles born outside the loss region,
p_t is the partial pressure of tritium, in torr,
G is the decay rate of tritium [14], numerically equal to: $1{\cdot}26 \times 10^8$ sec^{-1} cm^{-3} $torr^{-1}$.

We will define the loss-rate of β-particles in terms of a characteristic time (τ_C) as,

$$\left[\frac{dn_\beta}{dt}\right]_- = \frac{n_\beta}{\tau_C} \qquad (2)$$

This can be divided into two parts:

$$\frac{1}{\tau_C} = \frac{1}{\tau_D} + \frac{1}{\tau_M} \qquad (3)$$

where τ_M is the average magnetic confinement time. τ_D is the mean time required for the background gas to degrade the energy of a β-particle to a value where it is no longer detectable, or is scattered into the loss-region in velocity space. It is related to the background gas pressure (mainly due to tritium and hydrogen) by

$$\frac{1}{\tau_D} = \sum_i \frac{p_i}{K_i} \qquad (4)$$

where p_i is the partial pressure of the i^{th} constituent
K_i is a constant depending on the gas, and the energy loss or deflection suffered by the β-particle.

In practice τ_M is so long that it is possible to determine τ_D, and hence K, experimentally. The trap is filled with tritium at such a pressure that $\tau_D \ll \tau_M$. The β-particle population then grows with time according to the formula:

$$n_\beta = n_{\beta_0}\left[1 - \exp\,(-t/\tau_D)\right]$$

Measurements of the build-up time give τ_D, and hence a value for K in hydrogen of $(7 \pm 3) \times 10^{-8}$ torr sec. This agrees with the value measured by Williams [15], if the mean degradation is about 2·5 keV.

The corrected count (see section 2.1) recorded by the fast moving probe is

$$C = \eta\, V_T\, n_\beta \qquad (5)$$

where η is the overall efficiency of the probe (counts per incident β-particle) and V_T is the volume of the trap, in cm^3.

In equilibrium the generation and loss rates given by (1) and (2) are equal. Combining these equations with (3), (4) and (5) gives:

$$(p_t + p_h) = (GfV_T\eta K).(p_t/C) - K/\tau_M \qquad (6)$$

where p_h is the partial pressure of hydrogen
A graph of $(p_t + p_h)$ against p_t/C has intercept $- K/\tau_M$; and slope, $(GfV_T\eta K)$. Thus τ_M is determined if K and the calibration of the pressure measuring device are known, (fV_T) can be found if, in addition, η is known

An independent method of finding τ_M depends on detecting particles escaping from the trap, by means of a stationary probe placed just outside the region to be investigated. If this probe intercepts a fraction α of the escaping flux, the count rate Γ will be $\alpha C/\tau_M$; where C is the count of trapped particles in the region, measured with the same probe. Generally there will be an additional term, proportional to the partial pressure of tritium, representing the flux of β-particles born on drift surfaces intersecting the probe at its stationary position. Thus,

$$\Gamma = \frac{\alpha C}{\tau_M} + Q\, p_t$$

or

$$\Gamma/C = Q(p_t/C) + \alpha/\tau_M \qquad (7)$$

The intercept on a graph of (Γ/C) against (p_t/C) is (α/τ_M), so that if α is known τ_M can be determined without knowledge of K, η, or the pressure calibration.

3. Possibility of Space Charge Effects

β-particles passing through the background gas produce a population of slow ions and electrons which may, in principle, give rise to space charge effects. The equilibrium level and corresponding growth time for this secondary population have been calculated on the assumption that each β-particle generates 200 ion pairs, and that these are lost by large angle scatter into the loss region of velocity space. For secondary electrons the equilibrium population is 10 per cm³ and the build up time is $\sim (2 \times 10^{-8}/p)$ sec , where p is the total hydrogen isotope pressure (torr); the corresponding values for ions are 2×10^4 per cm³ and $(3 \times 10^{-6}/p)$ sec. In the unlikely event that this space charge sets up an electric field such that the corresponding $\vec{E} \wedge \vec{B}$ drift is always radially inwards, a loss time of 10 msecs (2×10^5 transits) could conceivably be concealed. It is much more likely that the space charge will merely cause a very small modification of the particle transform. Consequently it is improbable that space charge effects can influence the confinement of the β-particles in the trap.

4. Apparatus

A schematic diagram of the trap (CLASP) used for our experiments is shown in Fig.1. It is a stellarator with a toroidal $\ell = 3$ winding, minor radius 11·5 cm , major radius 30 cm , mean pitch angle 45°; there are 8 field periods on the torus. The form of the helical winding is given by:

$$\varphi = -\frac{8}{3}\theta + \text{const}$$

where φ and θ are defined in Fig.2. The limiter radius is 5·8 cm and the separatrix can be inside the limiter for toroidal fields of up to 1000G, corresponding to a total current of 24×10^3 amperes in the helical winding. The windings are energised for about 10 sec , but in most of our experiments the interval between establishing the fields and measuring the population of the trap is about 2 seconds. The minimum energy of β-particles likely to be detected by our scintillator is around 2 keV [16] and the maximum energy possible for tritium β-particles is 18 keV, the corresponding spread in Larmor radius is from 0·1 to 0·3 cm . In this case we expect all the localised and most of the blocked particles [10] to be in the loss region, these particles comprise 40% to 50% of the total.

The trap [17,18] was designed to give accurate fields, the position of the conductors was carefully controlled and magnetic materials were excluded from the structure and the surroundings. The helical winding is continuous and consists of 34 turns of insulated, edge cooled, copper strip. The winding accuracy is such that the minor radius of the current centre is constant to within 0·25 mm, the ring axis of the winding is plane to within 0·6 mm and circular to within 0·1 mm. The 15 toroidal field coils are split so that they can be assembled about the completed load, they have a double pancake structure with helical crossovers. The major axis of the helical and toroidal windings are parallel to within $0{\cdot}1^{\circ}$ and coincident to within 1 mm. A uniform vertical field can be applied to modify the magnetic configuration. Computations [9] indicate that with no vertical field the rotational transform/field period (ι_K) is about 30° at the separatrix; the addition of a vertical field can increase this to about 52°. A typical value of the shear length (L_S) is 50 cm (2).

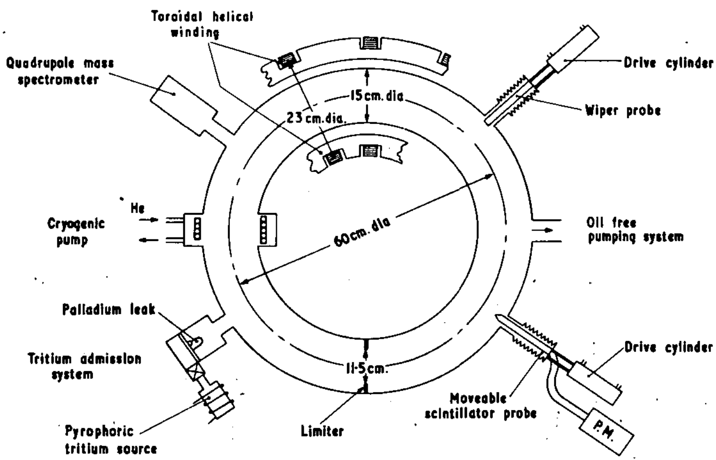

FIG.1. Schematic diagram of the CLASP apparatus.

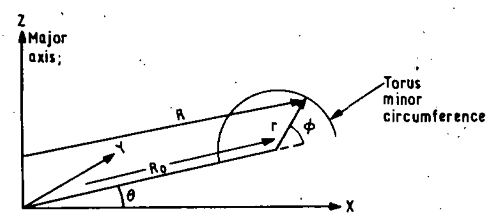

FIG.2. Co-ordinate system.

Tritium is introduced into the trap from a pyrophoric uranium source through a palladium leak. The tritium pressure is measured on an absolutely calibrated [19] mass spectrometer, the relative accuracy is better than 5% and absolute accuracy within 20%. During experiments the trap is pumped by a cryopump [20] inside the torus; the temperature of the pump is controlled so that it has a large pumping speed for impurities but very little speed for the isotopes of hydrogen. The only significant impurity in these circumstances is carbon monoxide, its partial pressure is less

(2) L_S is defined by: $L_S^{-1} = (r/L_K)\,d\iota_K/dr$
where r is a radius
and L_K the length of a field period

than 2×10^{-9} torr, so that the degradation time for the β-particles on impurities gases is more than two seconds (corresponding to about 4×10^7 transits).

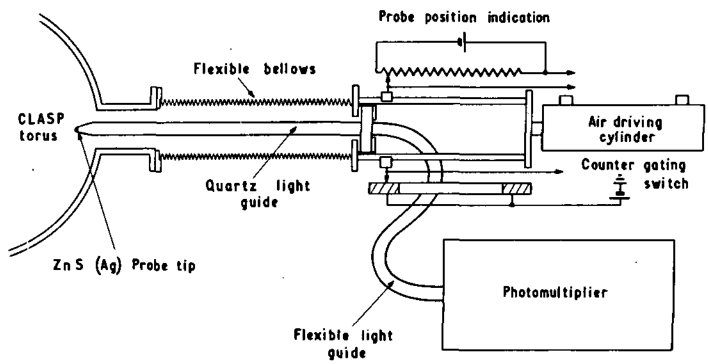

FIG. 3. Scintillation probe.

Fig.3 shows detail of the scintillation probe used to measure the equilibrium β population. The pneumatic cylinder can drive the probe across the trap in about 50 msec . The scintillator is constructed and calibrated, against a standard tritiated polymer source, as described by Powell [16]. The scintillator tip for these measurements is hemispherical so that electrons arriving in any direction are detected; it is small (0·03 cms^2) to minimise adsorption effects. The overall efficiency is about 1%. The photomultiplier noise gives a background of about 200 cps at room temperatures and adsorption of tritium on the probe tip increases this to about 350 cps; and β's released at the wall are unable to reach the probe tip when the fields are energised. An example of the variation of count rate with distance as the probe is driven across the trap is shown in Fig.5. It will be seen that electrons collected from different regions of the trap can be distinguished. The counting equipment can be gated so that the counts received from different radial regions are recorded separately, thus any variation of confinement time with radius can be measured.

After insertion the probe can be withdrawn to a specified radius to record the static count rate (see section 2). It is also possible to control the interval between the withdrawal of a 'wiper' probe, which intersects all the surfaces, and the insertion of the scintillation probe; in this way the growth time of the equilibrium population can be measured. In normal operations the wiper is withdrawn after the field configuration is established and the scintillation probe inserted after an interval of about 2 seconds. In this way any effects associated with switching on the fields are excluded.

5. Field Accuracy

The accuracy of the field produced by the coil systems has been assesed by Hall probes and electron guns. The toroidal field is found to be spacially accurate to ± 0·1% and the field lines close to within 0·4 mm. The magnetic field of the helical winding is measured along each of two lines passing across the aperture. The principal component of the field has the correct spacial dependence to within 0·2% of the total field.

The magnitude and pointing accuracy of the combined helical and toroidal fields agree with the computed field to within 1% of the total field on the two measured lines.

An electron gun has been used to obtain an indication of the drift surfaces. The finite size of the beam in the highly sheared field causes it to spread rapidly so as to fill the annular volume between two surfaces. The surfaces are plotted by probing this annulus. The beam can be followed for about 10 transits, and lies on closed nested surfaces. The largest surface which was fully mapped had a transform of 12°/field period, but a single beam followed once around the torus showed a transform of 240° in 8 field periods, equal to the maximum transform found by computation [9] . The position and shape of the surfaces was such as to suggest the presence of a stray vertical field of about 1% of the total field, this may have been due to a slight unbalance in the helical winding due to insulation difficulties. In all subsequent measurements precautions were taken to ensure that the winding was accurately balanced.

6. Experimental Results

6.1 A particular configuration

Computed properties of a particular configuration in CLASP are shown in Fig.4. This configuration has a vertical field (10G) applied to displace the magnetic surfaces towards the major axis. The transform at the magnetic separatrix, which intersects the limiter, is 52°/field period, and on the first magnetic surface which does not intersect the limiter is 19°/field period; the transform on the inner magnetic surfaces is approximately independent of radius and is about 10°/field period. Drift surfaces for two groups of particles moving in opposite directions around the torus are also shown, the displacements from the magnetic surfaces are appreciable. The nest of drift surfaces displaced towards the major axis is approximately shear free, while the nest displaced away from the major axis has a large shear. For this outer nest the transition from obviously open to apparently closed drift surfaces occurs within the limiter.

Fig.5 shows the counts received when the scintillator probe is driven across this configuration. The two sets of drift surfaces are clearly distinguished and their position agrees with the computed surfaces. The count received by the probe is found to be independent of pressure for hydrogen isotope pressures above 10^{-7} torr, using the value of K deduced in section 2, this immediately implies confinement of the β-particles for more than 10^7 transits. Experimental data is plotted in Figs 6 and 7, the counts have been corrected as described in section 2; the correction for probe background is typically less than 20% and the slow probe correction (section 2.1) less than 10%. The straight lines are least squares fits, for the case when both variables are in error [21]; the estimates of the errors of the slope and intercept are based soley on the scatter of the points about the fitted line. The results for this configuration are summarised in Table I, data from plots similar to Fig.6 are included for various regions of the trap together with the data from Fig.7 for one position of the static probe. The static probe result indicates that particles do not leave the trap by slowly spiraling out. The moving probe results indicate that electrons are confined for more than 10^7 transits in each region of the trap. The magnitude of the experimental errors and the possibility of base pressure effects are such that there is no reason to suppose, on the basis of these experiments, that there is any limit to the confinement of the β particles. The measured values of the effective volume (fV_T) suggest that most particles are confined if they are born onto drift surfaces, which according to computation, do not intersect the limiter.

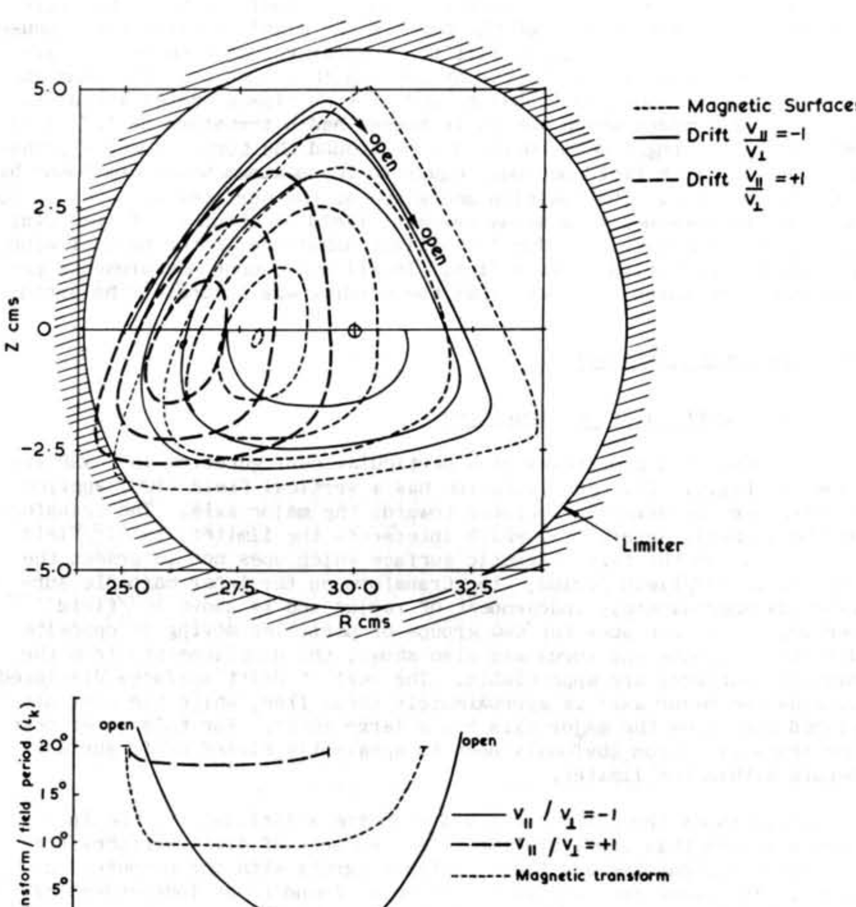

FIG.4. Computed drift and magnetic surfaces in CLASP together with the particle and magnetic transforms. The surfaces are plotted in a cross-section θ = const. A transverse field of 1% of the main field is used to displace the magnetic surfaces towards the major axis. The drift surfaces have $r_L = 0.26$ cm.

6.2 Radial Variation of Confinement

The radial resolution that can be obtained by using a gated counter to make plots like Fig.6 is limited by counting statistics. The example in Fig.5 is near the limit. In this case an outer annular region with shear length, based on the particle transform, of L_S = 30 cms, can be compared with an inner region (outer nest) with L_S = 70 cms, and with the inner nest of surfaces L_S > 1000 cm. The containment in each case is in excess of 10^7 transits.

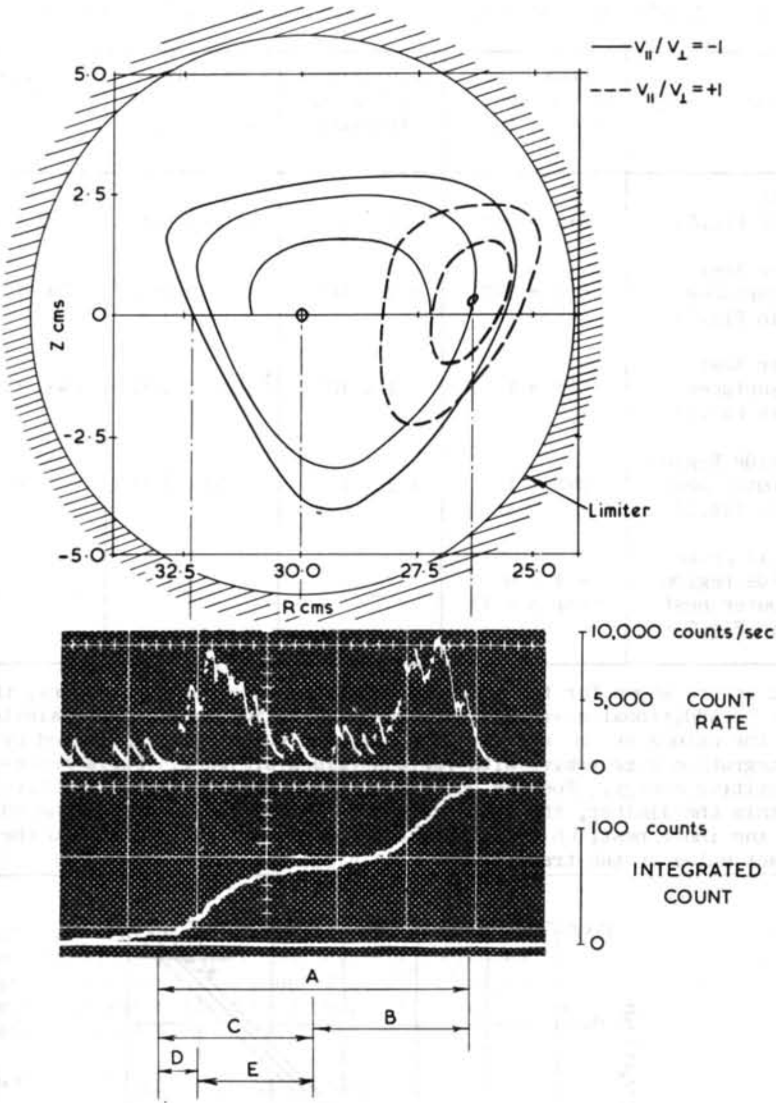

FIG. 5. Comparison of drift surfaces (from Fig. 4) with counts received by fast-moving scintillation probe. The various radial regions, for which results are given in Table I, are indicated.

The radial variation can also be examined by comparing the position at which a probe, moved quickly across the surfaces, begins to count; with that at which a probe moving slowly begins to count. The count on the fast probe can be predominantly due to trapped particles contained for 10^6 to 10^7 transits depending on the pressure, while the slow probe measures a population whose level is set by collisions with the probe, after typically 100 transits. We find that, if there is a region where the slow probe counts and the fast probe does not, then its thickness is less than 1 mm.

TABLE I. DATA ON A PARTICULAR CONFIGURATION IN CLASP

Region of Trap	Loss Rate ($1/\tau_M$) sec^{-1} ($K = 7 \times 10^{-8}$)	Equivalent Number of Transits	Measured fV_t ($K = 7 \times 10^{-8}$) ccs	Computed fV_t ccs
Total (A in Fig.5)	$0{\cdot}5 \rightarrow 0{\cdot}8$	$> 2 \times 10^7$	2800 ± 200	2300 ± 500
Inner Nest of surfaces (B in Fig.5)	$0{\cdot}4 \rightarrow 0{\cdot}7$	$> 2 \times 10^7$	1400 ± 200	700 ± 150
Outer Nest of surfaces (C in Fig.5)	$0{\cdot}4 \rightarrow 1$	$> 2 \times 10^7$	1500 ± 200	1600 ± 300
Outside Region of outer nest (D in Fig.5)	$0{\cdot}3 \rightarrow 1$	$> 2 \times 10^7$	450 ± 100	-
Static Probe inside region of outer nest (E in Fig.5)	$-1 \rightarrow 0$ (for $\alpha = 1$)	∞	-	-

The errors shown for the measured quantities are relative errors, there may be additional systematic errors of up to 50% due to uncertainties in the values of η and K. The computed volumes are estimated by integration over orbits with various values of $V_{\parallel}/V_{\perp}$ for a representitive energy. For the outer nest of surfaces, which are entirely within the limiter, the computed volume is well defined, but the volume of the inner nest, which intersect the limiter, is sensitive to the exact value of the transverse field.

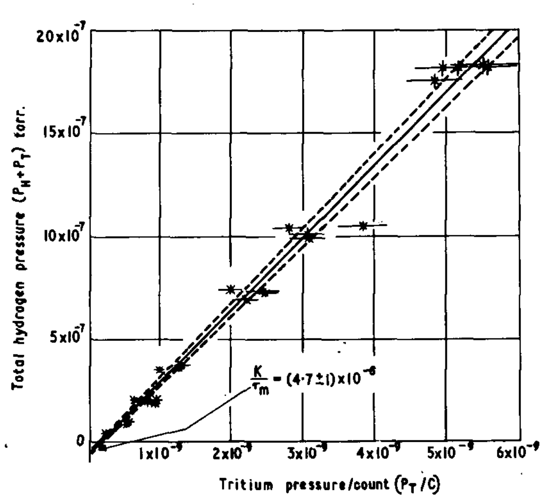

FIG. 6. *Determination of confinement time and effective trap volume from variation of equilibrium population with pressure* (Eq. (6)).

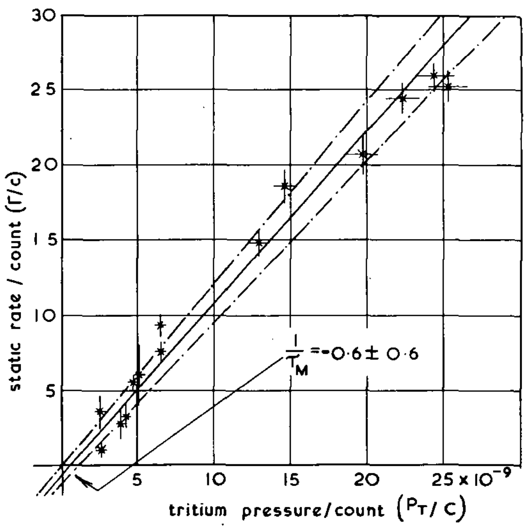

FIG. 7. Determination of confinement time from variation of static count rate and equilibrium population with pressure (Equ.(7)).

6.3 Other Configurations

We have also examined the following configurations.

(i) Magnetic separatrix inside limiter (no vertical field).

(ii) Both sets of drift surfaces approximately shear free (obtained by adding a vertical field of 25G).

(iii) Increased toroidal field (~ 2000G) giving maximum magnetic and particle transforms of 14° and 10°/field period.

In each case the observed confinement corresponds to more than 10^7 transits of the trap. We have deliberately increased the base pressure of nitrogen in the system to about 2×10^{-8} torr and in this case the confinement time was reduced to $1/\tau_M = 6 \pm 2$ sec^{-1} corresponding to confinement for $(2 \rightarrow 4) \times 10^6$ transits.

6.4 The Effect of Perturbations

The following perturbations have been applied to the field of the trap; a modulation of the toroidal field, a local vertical field, a local horizontal field due to a permanent magnet. The range of each of the fields was comparable with a helical field period and the magnetude was 10% of the main toroidal field. In each case the effect was merely to reduce the effective volume of the trap, the observed confinement time in the reduced volume remained in excess of 10^7 transits. The reduction in volume was apparent both as a change in the position at which the probe first receives β particles, and as a change in the slope of plots such as Fig.6.

The modulation of the toroidal field was produced by a single loop centred on the minor axis and in a radial plane. Computations show that this perturbation reduces the volume of the outward displaced nest of surfaces by about 30%, the volume of the inward displaced nest is unchanged(3). These computations follow the drift orbits for only one complete rotation about the minor axis (~ 30 field periods) and do not distinguish between surfaces which are truely open and those which are serrated or have an 'island' structure. The only effect revealed in the experiments is that the volume of the outward displaced nest is reduced by about 60%, the inward displaced nest is not affected and neither is the observed confinement time.

7. Conclusions

The intrinsic magnetic confinement time of particles, born outside the loss region, in all the configurations we have examined, is in excess of 0•6 secs., corresponding to more than 10^7 transits of the trap; we find no evidence that there is any limit to the confinement. Our experiment does not directly answer the question of whether or not closed magnetic surfaces exist, but it does show that the related drift surfaces are closed to high accuracy. This result applies both to configurations in which the drift surfaces are highly sheared, and to configurations in which they are nearly shear free. The observed position of the drift surfaces is in agreement with their computed position; the thickness of any transition region from the point where surfaces are closed for ~ 100 transits to where they are closed for ~10^7 transits in less than 1 mm. The degree of single particle confinement observed in these experiments is sufficiently large for any consequent loss to be acceptable in a fusion reactor. Thus from the point of view of confinement of particles not in the loss region, stellarators are as attractive as axisymmetric systems.

The principal effect of applying perturbations to the field system is to reduce the magnetic aperture, in a way that agrees qualitatively with computation. The confinement of particles on the drift surfaces which stay closed is unchanged. Thus in designing stellarator fields, it is sufficient to accept a field accuracy which gives an adequate aperture, as judged by computation. While each configuration must be separately assessed, this is likely to imply, for sheared fields, an accuracy of a few percent, rather than the few tenths of a per cent obtained in CLASP.

8. Acknowledgements

We are grateful to Drs R.J. Bickerton and R.S. Pease for much helpful discussion and encouragement, and to K.B. Axon, M.R. Barnes, L.J. Barrow, Mrs. M.E. Ellis and J.K. Mark for technical assistance.

9. References

[1] R. Carruthers. A study of some technological aspects and economic problems associated with a possible fusion reactor (Abstract of paper to Stockholm Conference, August 1967). Plasma Phys.(J. Nucl. Energy, Part C) 10 4 (1968) 441.
See also R. Carruthers, P.A. Davenport and J.T.D. Mitchell. The economic generation of power from thermonuclear fusion. Culham Report CLM-R 85 (October 1967).

(3) The volume of this nest is determined by the limiter, those surfaces which don't intersect the limiter are well inside the drift separatrix.

[2] I.E. Tamm. 'Theory of magnetic thermonuclear reactor (Part III), Drift and thermal conductivity of a plasma in a toroid in the presence of a stabilizing current'. Plasma Physics and the Problem of Controlled Thermonuclear Reactions (LEONTOVICH, M.A., Ed.) I 35. Pergamon, Oxford (1961).

[3] J.L. Johnson, C.R. Oberman , R.M. Kulsrud and E.A. Frieman. Some stable hydromagnetic equilibria. Phys. Fluids 1 4 (1958) 281.

[4] L. Spitzer. The stellarator concept. Phys. Fluids 1 4 (1958) 253.

[5] J.M. Greene and J.L. Johnson. Determination of hydromagnetic equilibria. Phys. Fluids 4 7 (1961) 875.

[6] I.M. Gel'fand, M.I. Graev, et al. An example of a toroidal magnetic field without magnetic surfaces. Soviet Phys.-Doklady 7 3 (1962) 223.

[7] A.I. Morozov and L.S. Solov'ev. Typical structure of a toroidal magnetic field. Soviet Phys.-JETP 18 3 (1964) 660.

[8] D.W. Kerst. The influence of errors on plasma-confining magnetic fields. Plasma Phys. (J. Nucl. Energy, Part C) 4 (1962) 253.

[9] A. Gibson. Trajectories of magnetic field lines in toroidal stellarators. Phys. Fluids 10 7 (1967), 1553.

[10] A. Gibson and J.B. Taylor. Single particle motion in toroidal stellarator fields. Phys. Fluids 10 12 (1967) 2653.

[11] W. Bernstein, F.F. Chen, M.A. Heald and A.Z. Kranz. 'Runaway' electrons and cooperative phenomena in B-1 stellarator discharges. Phys. Fluids 1 5 (1958) 430.

[12] G.M. Batanov, M.S. Berezhetskii, et al. Magnetic surfaces and containment of a plasma by spiral fields in a stellarator with external injection. Soviet Phys.-Doklady 10 2 (1965) 144.

[13] Rodionov, S.N. An experimental test of the behaviour of charged particles in an adiabatic trap. Plasma Phys.(J. Nucl. Energy, Part C) 1 (1960) 247.

[14] W.M. Jones. Half-life of tritium. Phys. Rev. 100 (1955) 124.

[15] E.J. Williams. Passage of α- and β-particles through matter and Born's theory of collisions. Proc. Roy. Soc. A135 (1932) 108.

[16] B.A. Powell. The counting efficiency for β-particles of ZnS(Ag) and glass scintillators and the adsorption of tritium on the scintillators and on stainless steel. Plasma Phys. 10 (1968) 79.

[17] R.A. Rowe, B.C. Sanders and G.L. Varley. Proc. 2nd International Conference on Magnet Technology, Oxford (1967).

[18] B.C. Sanders, R.A. Rowe and G.L. Varley. Some engineering aspects of the CLASP experiment. Paper presented at the 5th Symposium on Fusion Technology, Oxford (July 1968).

[19] M.B. Barnes and A. Gibson, Vacuum 18 8 (1968).

[20] W. Bachler, G. Klipping and G. Mascher. Cryogenic pump systems operating down to 2·5°K. Trans. 9th Nat. Vac. Symp., Amer. Vac. Soc. (1962) 216. Trans. (BANCROFT, G.H. Ed.,) Macmillan, New York (1962).

[21] J. Williamson, to be published in Can. J. Physics.

DISCUSSION

G. von GIERKE: If there were islands between the nested surfaces, they would not show up in your measurements as the statistical error is too large. While it is true that they would not affect the measurements of the electron lifetime in your experiment, they could on the other hand affect the plasma lifetime, so that your last conclusion regarding the accuracy with which a stellarator has to be constructed does not hold. In paper CN-24/F-2 it is shown that even very small perturbations can cause the formation of islands inside nested surfaces.

A. GIBSON: The measurements described show that the effect of a variety of perturbations is to reduce the volume of closed drift surfaces rather than to disrupt the entire set of surfaces. Furthermore, the observed reduction is in agreement with that computed on the basis of a few transits of the trap. This gives some confidence that stellarators can be designed on the basis of such computations. If significant islands exist they will be revealed by the computation.

C. GOURDON: I should like to make a comment in connection with Mr. von Gierke's question. In numerical calculations, we have observed - by following the magnetic lines for several hundred turns around the torus - that the lines remained confined within the magnetic configuration, even when quite large islands were formed. It is therefore possible that the presence of islands does not modify the lifetime measured by you to a noticeable extent.

In addition, I should like to ask two questions. First, is it possible to simulate structural defects by moving certain of the azimuthal field coils? Second, could one mask one side of the scintillator so as to detect only one of the two precession surface families at a time?

A. GIBSON: In reply to your first question, it is possible to move any of the azimuthal field coils for the purpose of comparison with computation, but such perturbations are of course relatively easy to avoid in practice. It is not possible to make any change to the helical winding in our experiment.

With regard to your second question, we have performed experiments with one side of the scintillator masked, so that only particles moving one way round the torus are detected. The results are similar to those reported here and are to be published in Physical Review Letters.

CONFINEMENT OF GUN-INJECTED HYDROGEN PLASMAS AND MICROWAVE-PRODUCED XENON PLASMAS IN THE C STELLARATOR

D. J. GROVE, * E. B. MESERVEY, W. STODIEK AND K. M. YOUNG
PLASMA PHYSICS LABORATORY, PRINCETON UNIVERSITY,
PRINCETON, N. J., UNITED STATES OF AMERICA

Abstract

CONFINEMENT OF GUN-INJECTED HYDROGEN PLASMAS AND MICROWAVE-PRODUCED XENON PLASMAS IN THE C STELLARATOR. Confinement times of gun-injected stellarator plasmas have been observed to be about five times the Bohm value. The confinement time is dependent on the current in the $\ell = 3$ helical windings. The major differences between these plasmas and those used in earlier experiments, where the density decay time was insensitive to helicla-winding current and agreed with the Bohm relation within a factor two, are the much longer mean free path, the high average ion energy, and the low neutral background density.

Titanium washer guns, located in the divertor, produce hydrogen plasmas of $n = 10^9$ to $4 \times 10^{10}\,cm^{-3}$, at $T_e \lesssim 10$ eV. Electron-ion mean free paths range up to several hundred machine lengths, contrasting with the earlier Bohm diffusion regimes (typically $n = 10^9\,cm^{-3}$, $T_e \sim 0.3$ eV to $n = 3 \times 10^{13}\,cm^{-3}$, $T_e \lesssim 100$ eV) where mean free paths were at best one machine length, and usually much less. The ratio of the observed confinement time to the Bohm value rises to a maximum of about 5 at $\ell = 3$ winding currents for which the rotational transform at the plasma boundary is approximately 2 radians. Thereafter, the ratio remains constant or decreases. The confinement time is approximately linear with B in the measured range from 1 to 40 kG.

In experiments with microwave-produced xenon plasmas of $n = 10^9\,cm^{-3}$ and $T_e \sim 0.3$ eV, the behavior of the confinement time is similar to the gun-plasma case in its dependence on helical-winding current. The maximum ratio of the observed confinement time to the Bohm value is again about 5.

In both experiments, there may be a considerable difference between the observed temperature obtained from the conductivity assuming a Maxwellian distribution and the actual temperature of the bulk of the particles. It is possible that experimentally observed electrons of relatively high energy are distorting the velocity distribution so that the conductivity yields an artificially high temperature. Because of this uncertainty, no detailed comparison of the experiment is made with theoretical predictions.

1. INTRODUCTION

In a number of earlier investigations of plasma confinement in stellarators [1-6], it has been shown that the Bohm formula gives an upper limit to the observed confinement time and correctly predicts the magnetic field and electron temperature dependence. Substantial increases in confinement time over that predicted by the Bohm formula have been reported for the experiments on thermal cesium plasmas by the Garching group [7] and for gun-injected plasmas by the Lebedev group [8]. More recently, Ellis and Eubank [9] have reported an order of magnitude improvement over the Bohm confinement time for gun-injected plasmas in the Etude stellarator and even larger factors for

---

* On loan from Westinghouse Research Laboratories, Pittsburgh, Pa.

such plasmas in the B-3 stellarator. Comparable improvements over the Bohm time have also been reported for experiments with toroidal multipoles, for example, by groups at Gulf General Atomic [10] and the University of Wisconsin [11] and in these cases also gun injection was used to produce the plasma.

The work described herein was performed on the C stellarator and consists of confinement studies of plasmas produced by gun injection into the divertor and of xenon plasmas produced by electron cyclotron resonance. The purpose of these experiments is to determine the importance of the electron collision frequency to the loss rate by working over a range of mean free paths around one machine length and to determine the importance of the ion mass.

Additionally, we look at the effect of varying magnetic shear or rotational transform for fixed plasma parameters. Related confinement experiments on the C stellarator for a different range of plasma parameters are described by Brown et al. [12].

The gun-injection experiments are described in Sec. 2, the xenon experiments in Sec. 3, and the conclusions in Sec. 4.

2. EXPERIMENTS WITH GUN-INJECTED PLASMAS

2.1 Experimental arrangement and diagnostics

Due to the short confinement times, plasmas of a high degree of ionization can be produced by collisional ionization only for electron densities greater than 1×10^{11} cm^{-3}. The remaining neutral gas cools the plasma rather rapidly if no heating is applied. If lower electron densities are to be obtained together with a low neutral background density, the plasma must be produced outside and then transferred to the confinement chamber. One such method is by injection from plasma guns. Filling a stellarator by plasma gun injection has been reported previously by Akulina et al. [8] and by Ellis and Eubank [9]. In this earlier work, the plasma from a titanium washer gun [13] was injected transverse to the main confining field and partially trapped. In the C stellarator, a plasma injected transversely must pass a considerable distance across the field before entering the confinement region and at fields greater than 3 kG the densities were low and the reproducibility usually bad.

If, instead, one or more guns are located in the divertor, it is possible to produce plasma densities up to 5×10^{10} cm^{-3} in magnetic fields ranging from 1 to 40 kG. The physical arrangement is given in Fig. 1, which is a simplified schematic of the C stellarator showing two guns located in the divertor. (Up to three guns were used in these experiments.) This arrangement differs from that reported by Zykov and Rudnev [14] where the guns are pulled well back from the curving field lines to introduce deliberately some cross-field trapping in an effort to purify the plasma. In that work, much higher densities were obtained (~ 10^{13} cm^{-3}) and detailed studies were made of the injection process. The divertor was not a part of a confinement device.

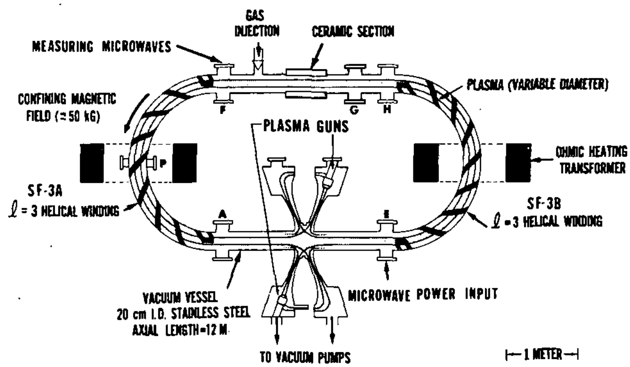

FIG. 1. Simplified schematic of the C stellarator as used for the experiments on the gun injection and microwave-produced xenon plasmas.

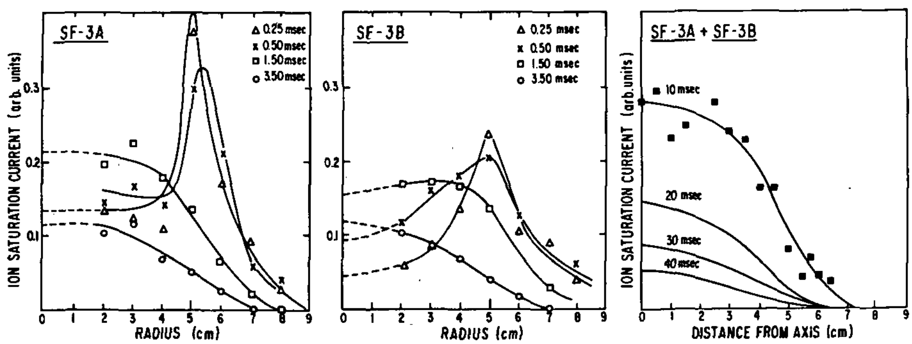

FIG. 2. Density profiles as a function of time as measured by probes. In about 2 ms the distribution has shifted from a concentration in the scrape-off to a bell-shaped one. The plasma radius was 5 cm. Note the differences at early times between the curve for the A winding and the B winding. The profiles at late times are taken from a different run than the early-time curves.

Injection into the divertor has a number of favorable aspects. First, the guns are immersed in an essentially axial magnetic field which is reported to increase the amount of plasma and the relative proton content [15]. Second, the plasma is guided by a longitudinal field most of the way to the main confinement area. Third, the plasma is injected near the stagnation point of the divertor and the field inhomogeneity should facilitate the trapping. Finally, most of the neutrals emitted by the guns tend to remain in the divertor.

We know little of the trapping mechanism, but very shortly after injection the plasma has filled the aperture and has taken up a density profile resembling that characteristic of a diffusion process, as can be seen in Fig. 2.

The composition of the trapped plasma is also not well known. Washer guns of this type have been investigated previously [15]. Usually more than half of the ions were protons of about 100 eV energy, the impurities being mainly oxygen and titanium. The base pressure generally corresponded to a neutral density of ~ 10^9 cm^{-3} and probably increased slightly as the guns were fired. The ion energy was obtained from retarding grid energy analyzers. One analyzer was located in the divertor at about the same radial distance from the axis as the guns but at a different azimuth. A second could be moved radially in and out of the plasma at location H (see Fig. 1) and was used to support the Langmuir probe result that the entire aperture was rather uniformly filled with plasma after a short time. These analyzers indicated that the initial ion energy was greater than 100 eV, but cooled in about 30 msec to 20 - 30 eV. From time of flight measurements, we conclude that a predominant fraction of the trapped ions are protons, but the amount of impurities depends on the voltages applied to the guns. This question is considered further in a subsequent section.

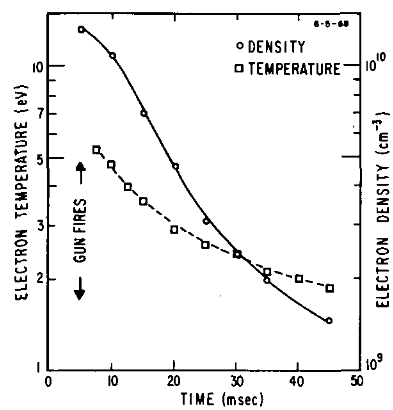

FIG. 3. The electron temperature determined by conductivity as a function of time. The density decay is also shown.

The electron density is determined as a function of time, using a high-sensitivity microwave interferometer. The electron temperature is determined from the conductivity. A Rogowskii coil measures the current produced when a small (typically 40 mV) 500 Hz voltage is induced around the plasma loop using the ohmic heating transformers shown in Fig. 1. Some representative measurements of density and temperature vs time are shown in Fig. 3. Most of the density decay rates were taken about 10 msec after the guns fired, at which time the electron temperature decay rates are 1/4 to 3/4 as large as the density decay rates taken at the same time. Electron temperatures were also measured by single, double, and triple Langmuir probes. These probe measurements gave temperatures 2 to 4 times higher than the conductivity for unknown reasons; in this paper only the conductivity values are used.

An important question which arises in any measurement of confinement times based on density decay rates is the extent to which ionization masks the true rate, yielding confinement times incorrectly large. Some evaluation of this effect can be obtained by observing the light emitted by the plasma as a function of position and time. Total light detectors using RCA 6342A photomultiplier tubes were placed to observe light emanating from the vessel axis at the center of the divertor and from viewing ports E, F, and H identified in Fig. 1.

Finally, we note from Fig. 1 that for these experiments two $\ell = 3$ helical windings were available, one on each end of the machine.

2.2 The experimental data

To explore the dependence of the confinement time on gun parameters, on density, and on temperature we have studied the decay time for a standard condition of the magnetic field. This condition is a confining field strength of 17 kG with both helical windings energized to produce a transform of 1.84 rad at the aperture of 5 cm radius.

In Fig. 4, the top graph shows the dependence of the confinement time on the electron density at a fixed time after the gun fires. These points come from many days' runs. We observe scatter of a factor of 3.5 in the confinement time for fixed density, but over the range of a factor 50 in density we find no density dependence. From this we conclude that the sactter in confinement time observed at nominally fixed density is not due to small changes in density.

In the center graph of Fig. 4 we plot the corresponding electron temperature derived from conductivity measurements assuming a Maxwellian velocity distribution. The squares are points from one particular day. Aside from these, we find the electron temperature scatters by about a factor of 2 over the range in density. So far we have not been able to change this temperature systematically by changing the gun parameters. Therefore we do not have data on the temperature dependence of the confinement time for a wide range of electron temperatures. The bottom graph of Fig. 4 shows the decay times normalized to the Bohm value where for the purposes of this paper we define, as customarily, the Bohm time in milliseconds as $\tau_B = 4 \times 10^{-2}\ r^2\ B/T$ where r is the radius in cm, B is in kG, and T is in eV. The temperature T is the electron temperature obtained from the measurement of conductivity assuming a Maxwellian velocity distribution. We find scatter of the data of about a factor of 3 but due to the wide range of density we can conclude that there is no definite dependence of the relative confinement on the electron density.

We have no detailed understanding of the large scatter of the relative confinement time. It is in general less for the same run than for different runs. We cannot account for it by instrumental errors, but must attribute it to irreproducibility in the gun operation or the trapping of the plasma.

The dependence of the observed confinement times on the confining field strength is plotted in Fig. 5. The observed confinement goes linearly with the magnetic field. Unfortunately, the strength

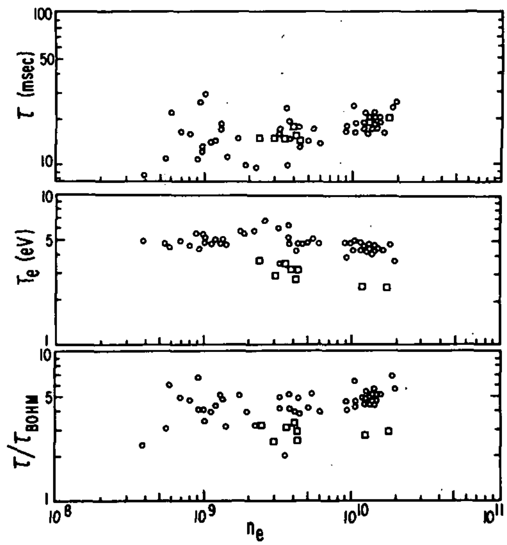

FIG.4. Electron temperature, observed confinement time, and relative confinement time, τ/τ_{Bohm} versus density; the squares indicate one particular run. Using the indicated temperatures, the mean free path for all these cases is greater than 1 machine length.

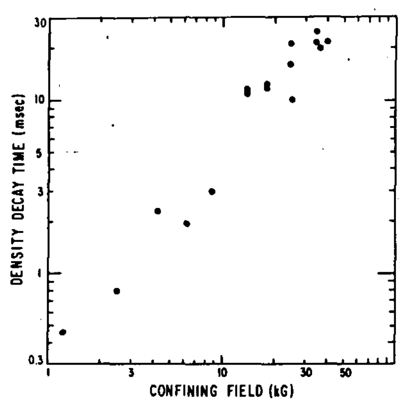

FIG. 5. Dependence of the confinement time on the confining field strength.

of the confining field influences the operation of the gun. The initial density varies by about a factor 2 and there could be a variation of the plasma temperature. At the low confining fields the temperature cannot be determined by ac current measurements because the confinement time is so short. We do not know, therefore, the temperature over the entire regime but at the higher values the temperature was about 5 eV. If we assume that the temperature is constant we find, from the observed actual confinement times, the linear dependence previously observed.

The dependence of the confinement on the helical field strength is given in Fig. 6. This figure represents all the points taken for the standard confining field of 17 kG plotted vs the angle of rotational transform with both helical windings energized. The ratio of the currents in the two helical windings was adjusted to give approximately equal transforms and equal maximum circularized radii.

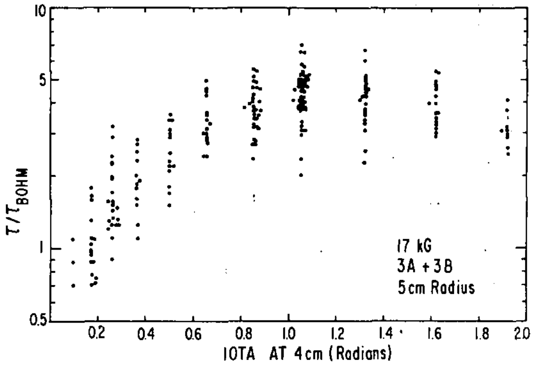

FIG. 6. Dependence of the relative confinement time on the rotational transform for A and B helical windings simultaneously energized.

Using the conductivity temperature, we find the confinement time relative to the Bohm value increasing with rotational transform followed by a slight decrease at high values of transform. For a transform of about 1 rad, corresponding to the standard condition of Fig. 4, we find a relative confinement time of about 4. An equivalent percentage increase with helical winding current has been found previously only at values of transform less than ~ 0.2 rad. We cannot give an explanation for this dependence on the helical field, but it is almost certain that this dependence is not a representation of the properties of the magnetic field configuration alone, but is somewhat influenced by a variation in plasma parameters.

To investigate this problem we have done a careful study of the dependence of the confinement on the transform when produced by each one of the helical windings alone and by the two in combination. The initial plasma density and the general appearance of the discharge were far more reproducible in this run than in most of our runs. The initial density was about 2×10^9 cm^{-3}; the confining field 17 kG. Figure 7 shows the electron temperature and the confinement time as a function of the transform for the various winding combinations. The data indicated that specifying the transform alone is not sufficient. It is likely that differences in trapping arise because of the slightly different design of the two windings, or a misalignment, either one producing a difference in the "scrape-off" area. For the B winding, we find a rather constant conductivity temperature as a function of the transform, possibly indicating that the plasma conditions were more nearly constant. The center and top graphs of Fig. 7 show that the confinement time and the relative confinement time are also rather independent of the transform.

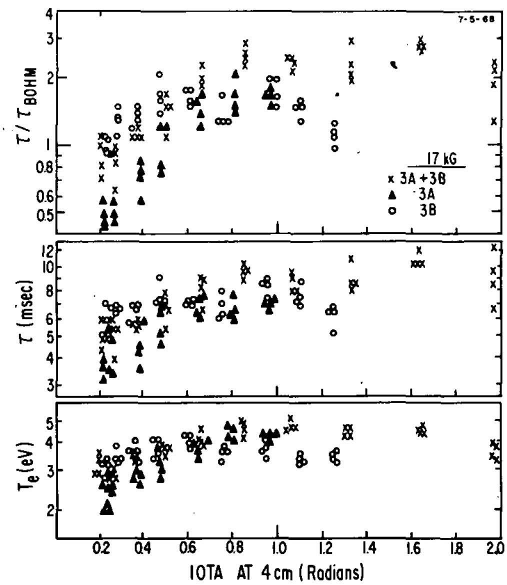

FIG. 7. Dependence of the electron temperature, confinement time, and relative confinement time on helical field for A and B windings energized separately and together.

For the A winding and the combined A and B windings we find again the dependence shown earlier in Fig. 6. As indicated by the differences in conductivity temperature, it cannot be excluded that the larger variation of the confinement observed with the A and A + B windings has other causes than differences in actual confinement properties of the magnetic field configuration.

2.3 Discussion of the results

The relative confinement time τ/τ_{Bohm} for low-density plasmas has been studied for a standard condition and for different confining fields, helical fields, and plasma densities. Taking the data given in the previous figures at face value, we have found for the gun-injected plasmas:

1) A linear dependence of the confinement on the magnetic field strength.

2) A dependence on the helical field, especially at low helical transforms.

3) No definite variation of the confinement with density has been observed over a range of densities of a factor of 50. For these data the mean free path ranged from 1 to 100 machine lengths.

4) The values of the relative confinement times vary from 2 to 5 for the standard condition.

5) An unusually large scatter of the data has been observed which cannot be accounted for by instrumentation errors.

The dependence on the electron temperature could not be determined due to the small range of temperatures available.

If the confinement of these discharges can be described by the Bohm formula the large scatter and systematic deviation must be accounted for by an incorrect interpretation or measurement of either the decay time or the electron temperature. If we can prove that both τ and T_e are correct, the confinement times cannot be described only in terms of the electron temperature but must depend on some other parameter such as plasma composition or ion temperature or initial trapping, which has not been measured and which is not very reproducible from shot to shot. The true rate of particle loss can only be falsified by ionization or by late influx of plasma either from the gun or from the divertor region. It is very unlikely that much plasma is trapped in the divertor bulge for a long time but this has not been definitely established. If all plasma ions were singly ionized titanium, we estimate from the rate coefficient that ionization to higher states could falsify the decay times by about 20%, assuming that the temperature of most of the electrons corresponds to the conductivity value.

Ionization of neutrals cannot be important if the total energy in the plasma can be roughly determined from the conductivity. If there is appreciable energy in fast particles, the ionization of neutrals may be important. We estimate that about 10% of the plasma injected by the gun is trapped; the untrapped part being neutralized at the walls would be available for ionization.

The plasma temperature has been determined from conductivity measurements assuming a Maxwellian distribution for the electrons and Z = 1. If because of impurities the effective Z is 2, we would underestimate the temperature by a factor of 1.5.

For the short confinement times provided by most devices (even the larger ones with high magnetic field) the condition of long electron mean free path is usually equivalent to having few collisions during a confinement time. Therefore, we cannot assume, as in the usual high-density discharges, that the electrons will have relaxed to a Maxwellian distribution from a non-Maxwellian initial distribution. This fact tremendously complicates the interpretation of this experiment from the experimental and theoretical point of view.

We have good evidence that the gun-injected plasmas in our experiment are at least initially non-Maxwellian. Titanium washer guns are known to produce fast electrons [15]. Electrons of energy greater than 200 eV have been observed immediately after injection, but we do not know their number density very well. Inserting a cylindrical rod 1.5 mm in diameter to the center of the discharge reduces the conductivity temperature more rapidly than would be expected for a Maxwellian. Furthermore, the floating potential (negative with respect to the wall) is found to be about 70 volts (20 times the conductivity temperature). We have observed cases in which a 3 mm diameter rod inserted to the center reduces the floating potential to about 6 volts and the conductivity temperature to about one-half the value in the absence of the probe without having much effect on the plasma decay time. If the electron velocity distribution is not Maxwellian, for example, if 10% of the electrons are at 200 eV in a cold main body, sufficient energy is available for some ionization. In some discharges we can definitely identify ionization during the first 10 milliseconds which is not present if the 3mm diameter rod is inserted.

Typically, phase angles of about 45° between the current and voltage are observed in our AC conductivity measurements at 500 Hz for densities of about $5 \times 10^9\ cm^{-3}$. A phase shift can arise from electron inertia effects in a Maxwellian distribution of an appropriate temperature. Since the density is known from the interferometer, the phase and real part over-determine the temperature and allow an experimental check. Alternatively, a fast group of particles moving through a cold Maxwellian can give a similar phase shift. If this fast group is assumed to contribute only inertial effects, no over-determination is available. For the single Maxwellian model, the density obtained from the phase measurements ranges from 1 to about 2 times the microwave density, the higher values suggesting that fast electrons are present. If we insert the 3 mm diameter rod, the phase angle becomes very small and the resistance increases by a factor of 2. We note that if the fast-group model is correct, the temperature of the Maxwellian cold group is reduced from the conductivity value by about 60% in the case of 45° phase shift.

At this stage of the experiment, we see two clear possibilities for explaining our observations. Firstly, the containment time of the bulk of the particles averages to about 4 times the normally accepted Bohm value. In this case, the scatter can only be explained by an additional variable. Alternatively, the temperature measurement by the conductivity does not describe the temperature of the bulk of the particles, and the scatter can be explained by different properties of a fast-particle group. On one plausible model, the relative containment is reduced by about 60%. To specify the actual reduction more clearly, additional information is needed on the details of the velocity distribution.

3. MICROWAVE-PRODUCED XENON PLASMAS

3.1 Motivation for the experiment

In contrast to the gun-injected plasmas discussed in the previous sections and the special cases described by Brown et al. [12], the plasmas produced in the C stellarator either by ohmic heating or by electron cyclotron resonance heating [5] generally have an electron-ion mean free path much less than one machine length. Under these conditions, the shear required to surpress the collisional instabilities in a hydrogen plasma is much higher than is available within good magnetic surfaces in the present

C stellarator. However, the theories [16] for the linear growth rates of both the collisional drift mode and the resistive interchange mode contain the factor $[(m_e/M_i)\nu_{ei}]^y$, where ν_{ei} is the electron-ion collision frequency, m_e and M_i are respectively the electron and ion masses, and y is of order one. For a plasma of high ion mass, the shear available should reduce the linear growth rates, provided the collision frequency is not too high (although still in the collisional regime).

We therefore investigated the confinement of a xenon plasma (M_i = 130) having an electron density of about 10^9 cm^{-3} and an electron temperature of about 0.3 eV. For these experiments the electron-ion collision mean free path was of the order of one-tenth of the machine length. These numerical values are close to those that were obtained for a contact-ionization alkali-metal plasma.

3.2 Experimental arrangement

The experimental arrangement for producing plasmas by electron cyclotron resonance in the C stellarator has been described in considerable detail elsewhere [5]. Briefly, there is a small region of the main discharge volume on either side of the midplane of the divertor over which the magnetic field is 3.8 kilogauss while the remainder of the machine is at 10 kilogauss. At location E (Fig. 1), 10 GHz microwave power is introduced, producing breakdown of the gas and resonance heating of the electrons in the low-field regions.

The initial neutral xenon pressure was typically 4×10^{-7} torr. Fast ion-gauge measurements showed that the percentage ionization was usually about 10%, but in some cases up to 50%, with peak densities ranging from 1 to 5×10^9 cm^{-3}. The measurements to be described were made in the afterglow.

The electron density and the electron temperature were determined in the same manner as in the gun experiment. The ion temperatures were not measured.

In these experiments the density decay rates were quite low and a relatively small amount of ionization could introduce serious errors in the determination of the confinement times. We have used three methods which indicate that ionization is not important in these experiments. First, total light detectors capable of measuring intensity ratios of more than 10^4 to 1 were placed to see light from the divertor and from port F (Fig. 1) on the far side of the machine. For ionization to falsify the results, light during the afterglow would have to be more than 1/800 of that during the initial ionization; less than 1/10,000 was observed. Second, if ionization were produced by a few runaway electrons in the remaining neutral gas, the introduction of a short burst of additional neutrals during the afterglow would produce both light and changes in density. Transient pressure increases of 10 to 100 times produced no effect. Third, if the power input to the plasma supplied by the 1 kHz conductivity-measuring current is as large as 10^{-4} watts, the temperature is observed to rise at a rate of about

0.3 eV/second. If ionization were an important factor in the decay rate observed, no temperature rise would be possible since the required power is much larger than is supplied, considering that about 50 eV is needed per ionization.

3.3 The experimental data

Two typical density decay curves are shown in Fig. 8. In one case, the current in the two $\ell = 3$ helical windings gave a value of $1.6 \times 10^{-3}\mathrm{cm}^{-1}$ for $1/L_s$ at 5.1 cm radius, where L_s is the shear length; $1/L_s \equiv (r/L_M)(d\iota/dr)$. The plasma radius is r, L_M is the machine length, and ι is the rotational transform. In the second case, $1/L_s$ was $3.6 \times 10^{-3}\mathrm{cm}^{-1}$, and in both cases, the microwave power was turned on at .04 and turned off at 0.1 seconds. The corresponding values of ι at 4 cm radius for the two cases are 0.43 and 0.97 radians. The electron temperature was slightly higher for the 250 ms decay curve, and here the confinement time was about 5 times the Bohm value, compared with 1.5 for the 90 ms curve.

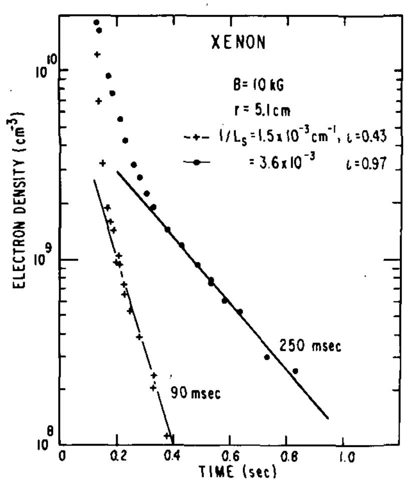

FIG.8. Electron density measured by microwave phase shift as a function of time for two values of helical winding current. The transform angles, iota, corresponding to the indicated reciprocal shear length at the boundary are 0.75 and 1.7 radians. The transform values given on the figure are for 4 cm radius.

The observed density decay times were measured as a function of the current in the helical windings for a 6.4 cm radius plasma and a 5.1 cm plasma. In Fig. 9, the relative confinement times are plotted against the value of $1/L_s$ at the plasma boundary. The same data are re-plotted in Fig. 10, but now as a function of the rotational transform computed at a point approximately 1 cm inside the plasma boundary. The data of Fig. 10 can be compared with the data from gun injection shown in Fig. 6. Two points taken using hydrogen rather than xenon are also shown. The hydrogen point at low transform was taken under high microwave power conditions. The hydrogen decay rate is somewhat faster than that of the xenon, but the difference in relative confinement time is mainly due to the hydrogen temperature.

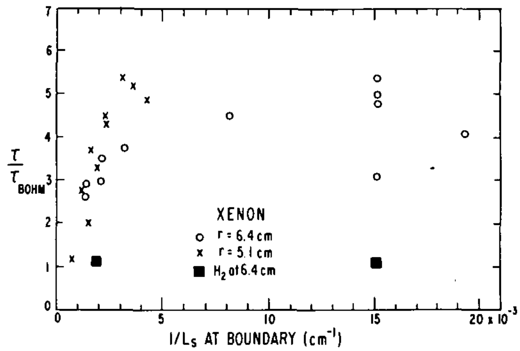

FIG. 9. Ratio of the observed density decay time to the Bohm time as a function of the reciprocal shear length ($1/L_s$ computed at the plasma boundary), for two values of plasma radius.

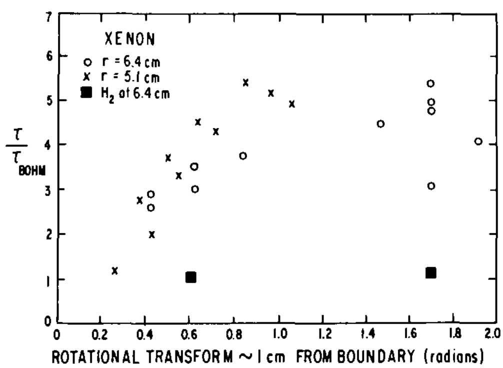

FIG. 10. The same data as in preceding figure now plotted as a function of the rotational transform, iota, computed at 1 cm inside the plasma boundary. These data can be compared with the gun injection data shown in Fig. 6.

The apparent relative confinement time for xenon is observed to rise with transform to a value of 4 to 5, then level off or decline slightly. We cannot ascribe the change in τ/τ_B preferentially to shear or transform.

3.4 Discussion

The considerable scatter in the data has not been entirely resolved. Because of background noise in the current measurement, the values of temperature calculated from the conductivity can be in error by as much as 30% at 0.2 to 0.3 eV for the smaller amplitude points. The error for the hydrogen points may be as high as 100%.

The data in the figures were selected for constancy of the conductivity, where the input power roughly matched the cooling. However, there are many examples, particularly for wide-aperture points, where the conductivity temperature falls, for example, by a factor of 4 from 0.2 eV to 0.05 eV, while the density decay time increases at most from 230 to 350 msec, a 50% change. As previously noted, the observed time constants for xenon are typically 1 to 2 times the hydrogen value. The significant differences in Figs. 9 and 10 arise mostly from the apparently colder temperature of the hydrogen. These results suggest the possibility that a fast electron component may be playing a role in distorting the conductivity measurement.

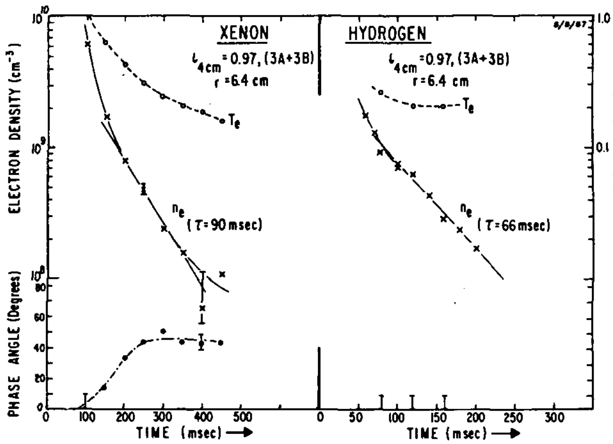

FIG. 11. Time rate of decay of the density in xenon and hydrogen plasmas after high power microwave heating for the same magnetic topology. The temperature computed from the conductivity, assuming no phase shift between current and voltage, and the phase shift observed at different times are also shown. Reading errors on typical points are indicated by vertical bars.

Figure 11 shows a comparison of two discharges at the same magnetic field conditions, one in xenon and one in hydrogen, both at higher microwave power than usual. (High powers, about 10 times the value used for most data, produced typically $1 \lesssim \tau/\tau_B < 2$ for xenon instead of $3 \lesssim \tau/\tau_B \lesssim 5$ characteristic of low power. There was no significant difference for hydrogen.) The density decay and the temperature computed from $|V|/|I|$ are shown in Fig. 11. Also shown is the phase shift in the 1 kHz current measuring system at different times during the pulse, which demonstrates a considerably higher phase correction for xenon than for hydrogen. Using the microwave interferometer-determined density of 5×10^8 cm^{-3} and the observed 45° phase shift between the current and voltage, we determine a temperature of 1.2 eV, which is inconsistent with the temperature of 0.31 eV computed from $|V|/|I|$, and also with the value 0.39 eV computed from $|V| \cos 45°/|I|$. This result suggests that there are fast particles at about 1.2 eV in the afterglow of the high-power discharges in xenon, but at the moment we have no theoretical model which accounts for the presence of these fast particles. The differences between the hydrogen and xenon data are not explained.

It may not be possible to extrapolate the interpretation of the high-power data to the low-power condition.

There is a possible alternative mechanism for the conductivity changing with time. In the case of a Maxwell-Boltzmann distribution the electrons may cool against protons, present as an impurity of 10 to 50%. The protons lose energy by charge-exchange collisions with molecular hydrogen or xenon atoms. At the present we, therefore, cannot definitely exclude either alternative and the scatter in Figs 9 and 10 is not well explained.

We do not yet know how the confinement depends on the conductivity; but during some discharges it appears to be independent.

We conclude that low-power microwave discharges in xenon produce apparent confinement times up to five times the Bohm value. There is a dependence on the current in the helical windings but it is not clear whether the shear or the transform is playing a role. Hydrogen discharges for the same field parameters give similar decay times. Their temperature is generally lower and they fit to the Bohm dependence independent of the transform. There is presently some doubt on the interpretation of the temperature measurement from the conductivity in the case of xenon. Until further measurements have been made, it is not possible to say by what amount the apparent increase in τ/τ_B is to be reduced for any particular data point.

4. SUMMARY AND CONCLUSIONS

In Secs 2.3 and 3.4 we have discussed the detailed results of our studies of gun-injected hydrogen plasmas and microwave-produced xenon plasmas in the C stellarator. In both cases there is an apparently longer confinement at high transforms than is given by the Bohm time characteristic of collisional plasmas. For both the gun plasmas and the xenon plasmas, the apparent relative confinement time increases at first, then levels off, or even decreases. We do not have an explanation for this except to note that the levelling off occurs for values of helical winding current at which computer calculations show that islands in the magnetic surfaces grow rapidly [17]. There is no experimental evidence directly connecting the presence of magnetic islands with the confinement.

We have pointed out, however, that there may be a considerable difference between the observed temperature obtained from the conductivity assuming a Maxwellian distribution, and the actual temperature of the bulk of the particles. In view of this ambiguity, we cannot usefully discuss our results in terms of resistive instabilities and their stabilization either by long mean free path effects or by effects due to ion inertia.

In summary, there are two principal alternative models to explain our observations: (1) the electron distribution is roughly Maxwellian, and the conductivity temperature thus provides something like the normal measure of mean kinetic energy which has been used in the Bohm formula in the standard collisional regime; or (2) the electron distribution has an enhanced high-energy tail, which dominates the conductivity, while the mean kinetic energy of the bulk of the distribution lies well below the conductivity temperature.

In case (1) the conclusion is that an improvement relative to Bohm, by a factor of 4 - 5, has been achieved. In case (2) we encounter an ambiguity in the definition of the Bohm time for non-Maxwellian velocity distribution. If we take the "temperature" used in the Bohm formula to refer to the bulk of the particles, we then conclude that the improvement over Bohm in the present regimes may be smaller than 4 - 5, or even entirely absent. This interpretation would imply that an enhanced high-energy tail can be present without impairing confinement: that is to say, the measure of electron energy which is relevant for anomalous diffusion is to be derived from a lower moment of the distribution function than gives the conductivity temperature.

Turning finally to the interpretation of the observed scatter in τ/τ_B, in case (1) this would be interpreted in terms of an undetermined plasma parameter other than the electron temperature affecting the confinement time; in case (2) the confinement time could still be a function only of the mean kinetic energy of the bulk of the electrons, and the scatter would arise from a variation of the ratio of this mean energy to the measured conductivity temperature, which has been used here to calculate τ_B.

5. ACKNOWLEDGMENTS

The authors acknowledge with pleasure the assistance of Elizabeth Cary in the analysis of the data. Our thanks also are extended to the stellarator operating crew led by J. M. Perron. Finally, we acknowledge with pleasure many profitable discussions of the results with H. P. Furth.

REFERENCES

[1] ELLIS, R. A., GOLDBERG, L. P., GORMAN, J. G., Phys. Fluids 3 (1960) 468.

[2] STODIEK, W., ELLIS, R. A., GORMAN, J. G., Nucl. Fusion Suppl. Pt. I (1962) 193.

[3] HINNOV, E., BISHOP, A. S., Phys. Fluids 9 (1966) 195.

[4] PEASE, R. S., YOSHIKAWA, S., EUBANK, H. P., Phys Fluids 9 (1966) 2059.

[5] STODIEK, W., GROVE, D. J., KESSLER, J. O., "Plasma Physics and Controlled Nuclear Fusion Research" (IAEA, Vienna, 1966), Vol. II, p. 687.

[6] D'ANGELO, N., DIMOCK, D., FUJITA, J., GRIEGER, G., HASHMI, M., STODIEK, W., "6th International Conference on Ionization Phenomena in Gases" (S.E.R.M.A., Paris, 1963), Vol. I, p. 399.

[7] BERKL, E., ECKHARTT, D., von GIERKE, G., GRIEGER, G., Phys. Rev. Letters 17 (1966) 906.

[8] AKULINA, D. K., BATANOV, G. M., BEREZHETSKY, M. S., GREBENSHCHIKOV, S. E., RABINOVICH, M. S., SBITNIKOVA, I. S., SHPIGEL, I. S., "Plasma Physics and Controlled Nuclear Fusion Research" (IAEA, Vienna, 1966), Vol. II, p. 733.

[9] ELLIS, R. A., EUBANK, H. P., Phys. Fluids 11 (1968) 1109.

[10] OHKAWA, T., SCHUPP, A.A., YOSHIKAWA, M., VOORHIES, H. G., "Plasma Physics and Controlled Nuclear Fusion Research" (IAEA, Vienna, 1966), Vol. II, p. 531.

[11] MEADE, D. M., Phys. Rev. Letters 17 (1966) 677.

[12] BROWN, I. G., DIMOCK, D. L., MAZZUCATO, E., ROTHMAN, M. A., SINCLAIR, R. M., YOUNG, K. M., Paper CN-24/D-3 this meeting.

[13] COENSGEN, F. H., CUMMINS, W. F., SHERMAN, A. E., Phys. Fluids 2 (1959) 350.

DISCUSSION

C. H. GOURDON: Are the rotational transform values plotted on the abscissa of the figure presented by you theoretical or experimental values?

D. J. GROVE: The actual numbers are from a computer calculation, but they have been checked in representative cases by electron beam techniques with good agreement up to $\iota_{4cm} \approx 1$ radian. Experimental checks have not been made for higher transforms.

O. S. PAVLICHENKO: Did you investigate the effectiveness of plasma trapping during injection from the gun through the divertor?

D. J. GROVE: No, we did not measure the effectiveness of trapping. It was estimated from work by other authors on the output of the gun and from the observed trapped density.

O. S. PAVLICHENKO: Did you observe oscillation of the gun-injected and the xenon plasma — as in the case of, for example, an ohmic hydrogen plasma?

D. J. GROVE: We did preliminary measurements on the fluctuations in density for both gun-injected and xenon plasmas. In both cases $\delta n/n$ was of the order of 10%. The frequencies are not inconsistent with the drift frequencies, but until further work is done on the potential fluctuations and the correlations we cannot relate these numbers to the confinement.

S. Yu. LUKYANOV: If the electron temperature was derived from the conductivity, what assumptions were made regarding the dependence of T_e on the radius of the plasma column?

D. J. GROVE: Since we had not measured the radial variation in T_e we assumed in the computation that it was constant across the aperture.

S. Yu. LUKYANOV: What is the reason for the different behaviour of the dependence of the plasma lifetime on the rotational transform angle for xenon and hydrogen?

D. J. GROVE: The difference in behaviour for xenon and hydrogen is qualitatively in accordance with the theory as presented in reference [16] of our paper. However, until mode identification has been achieved, the frequency dependence has been established, and other fluctuation measurements have been made, it is not possible to say that the observed difference is in fact related to the theory.

V. S. STRELKOV: One of the possible explanations advanced by you for the difference between the observed plasma lifetime and that obtained from the Bohm formula is that the electron temperature deduced from the electrical conductivity is higher than the true electron temperature. As far as I remember, however, in all earlier stellarator experiments the opposite applied: the true electron temperature was higher than that deduced from the electrical conductivity. How do you explain this?

D. J. GROVE: In such cases, which are described in paper CN-24/D-3, the ratio of the electron drift velocity to the thermal velocity was greater than 0.02 and resulted from the fact that induced electric fields were driving the current.

In the gun-injected plasma and xenon plasma experiments, we consider cases with no (or very small) applied electric fields and concern ourselves only with a situation in which the bulk of the electrons are at some lower temperature and a few much hotter electrons seriously affect the conductivity measurement. Whether the conductivity and the temperature corresponding to the bulk of the electrons are the correct ones from which to calculate τ_B is not known.

A. GIBSON: Do you have results for direct cross field injection?

D. J. GROVE: With direct cross field injection we obtained usable plasmas only for fields up to 3 kG; even these were of low density and poor reproducibility. The few results which we obtained did not differ significantly from those obtained with divertor injection.

EXPERIMENTAL STUDIES OF ANOMALOUS RESISTIVITY AND THE ASSOCIATION OF FLUCTUATIONS AND COLLISION FREQUENCY WITH CONFINEMENT

I. G. BROWN, D. L. DIMOCK, E. MAZZUCATO,* M. A. ROTHMAN,
R. M. SINCLAIR AND K. M. YOUNG
PLASMA PHYSICS LABORATORY, PRINCETON UNIVERSITY,
PRINCETON, N.J., UNITED STATES OF AMERICA

Abstract

EXPERIMENTAL STUDIES OF ANOMALOUS RESISTIVITY AND THE ASSOCIATION OF FLUCTUATIONS AND COLLISION FREQUENCY WITH CONFINEMENT. Results on the properties of ohmically heated plasmas in the C stellarator are given for a new collisionless regime and for the transition region between collisional and collisionless plasmas. In these experiments confinement times can exceed the "Bohm time" by a factor of 5. Detailed probe measurements have identified two instabilities which contribute to the plasma loss. Thomson scattering of laser light has been used to check the conductivity temperature, with densities from 4×10^{11} to 10^{13} cm^{-3}, and for some interesting regimes an anomalous resistivity is found.

Fluctuations characteristic of the current-drive drift instability (the Kadomtsev mode) are found when $u/v_i \geqslant 1$ and $k_{\|} \lambda_e > 1$ (where u is the electron drift velocity, v_i the ion thermal velocity, $k_{\|}$ is the parallel wave number, and λ_e the collision mean free path). For this case, the outward flux obtained from correlation of Langmuir probe fluctuations is sufficient to provide the observed loss rate. With increased shear the confinement improves by a factor of 3. For the high-density, low-temperature regime with $u/v_i < 1$ and $k_{\|} \lambda_e \ll 1$, fluctuations characteristic of a curvature-driven resistive ballooning mode are found and here the fluctuations are insufficient to account for the loss rate.

The Thomson scattering measurements show that for $u/v_e < 0.02$ the temperatures obtained from Thomson scattering agree very closely with the conductivity temperatures. (Here v_e is the electron thermal velocity.) However, in the range $0.02 < u/v_e < 0.1$, the laser-determined temperature rises steadily to v almost three times the conductivity temperature, indicating an anomalous resistivity.

Studies of the transition region from short to moderately long collision mean free paths have been extended by combining ohmic heating with ion-cyclotron resonance heating. The electrons can be heated by Landay dampening of the ion cyclotron waves to about 100 eV at densities of 10^{13} cm^{-3} (with ion temperatures, T_i, about 500 eV), and to 70 eV at 10^{11} cm^{-3} (with $T_i < 2\ T_e$). As λ_e is increased up to 50 axial lengths, the ratio of the observed confinement times to the computed Bohm times is a monotonically increasing function of the product of λ_e and the rotational transform, rising from unity to a maximum observed value of 5.

1. INTRODUCTION

In the past it was shown that for ohmically-heated discharges in the C stellarator the plasma loss is at the Bohm rate or faster [1]. These results were obtained under collisional conditions, defined in this case to mean that the electron mean free path is less than the axial machine

---

* Present address: Laboratorio Gas Ionizzati, CNEN, Frascati, Italy.

Note: We define $v_{eth} \equiv (3kT_{\perp}/m_e)^{1/2}$, where $kT_{\perp}$ is the perpendicular electron temperature. In the fluctuation experiments we define $v_i \equiv (2kT/M_i)^{1/2}$, where kT is the ion temperature, assumed to be the same as the conductivity temperature.

length, $\lambda_e < L$. The experiments discussed in this paper are directed toward an understanding of this rapid loss by i) investigating the conductivity and its relation to the electron temperature, ii) examining the role of coherent low-frequency fluctuations in the loss and relating the fluctuations to instabilities predicted by established theory, and iii) determining the increase in the ratio of the observed containment time to the calculated Bohm confinement time τ/τ_{Bohm} for plasmas as a function of λ_e. For $\lambda_e > L$, an increase in τ/τ_{Bohm} is observed both in cases where the electron drift velocity u_e due to the ohmic current is greater than or less than the ion thermal velocity v_i.

The anomalous component of the conductivity has been obtained from detailed spatial analysis of the perpendicular temperature, which together with the density distribution is found from the Thomson scattering of ruby-laser light. These measurements have been made over a wide range of the ratio of u_e/v_{eth} (v_{eth} being the electron thermal velocity). The conductivity obtained from the Spitzer relation [2] for this temperature is then compared with the measured conductivity. The existence of an anomalous component of the resistivity and the relation of its onset to u_e/v_{eth}, M_i, and Z, the average ionic charge, are considered in Sec. 2.

Probe measurements of large-amplitude, low-frequency coherent fluctuations [3] have been extended to consider their effect on plasma confinement when $u_e/v_i < 1$, which corresponds approximately to $\lambda_e < L$. These fluctuations exhibit potential variations $e\phi' \sim kT_e$ and density variations of approximately 20%. Measurements in the presence of a sheared field produced by an $\ell = 3$ helical winding indicate that the fluctuations produce only a part of the observed loss. Detailed modal identification indicates agreement between the observed fluctuation properties and those predicted for the resistive gravitational mode assuming the weak-shear, weakly-positive $\int d\ell/B$ properties applicable to this stellarator. These results are discussed in Sec. 3.

The previous identification [3] of the coherent fluctuations with the current-driven drift instability, and the relation of these fluctuations to the observed plasma loss rate, when $u_e/v_i > 1$, suggests the possibility of reducing the loss rate by applying shear to localize the modes. In Sec. 4 we discuss an experiment in which we observe an increase of τ/τ_{Bohm} to about 3 when shear is applied. A further experiment where one can achieve a range of λ_e from $\lambda_e < L$ to $\lambda_e >> L$ by making use of electron Landau damping of ion cyclotron waves to heat the plasma is discussed in Sec. 5. Values of τ/τ_{Bohm} up to about 5 are observed.

The Model C stellarator, with ohmic heating and with ion cyclotron heating, has been described previously [4], [5]. Two $\ell = 3$ windings, one on each end, provide rotational transform and shear. The experiments make use of plasmas with densities $2 \times 10^{12}\ cm^{-3} \lesssim n_e \lesssim 2 \times 10^{13}\ cm^{-3}$ and ohmic current $100\ A \lesssim I_{OH} \lesssim 2000\ A$ and electron temperatures $5\ eV \lesssim kT_e \lesssim 100\ eV$. For the ion cyclotron wave heating of the electrons, low currents ($I_{OH} \simeq 30$ A) were used at lower densities ($n_e \sim 10^{11}\ cm^{-3}$).

2. EXPERIMENTS ON ANOMALOUS CONDUCTIVITY
(D. Dimock and E. Mazzucato)

A series of Thomson scattering measurements on hydrogen plasmas has been reported earlier [6]. From these measurements it was found that under some conditions the plasma exhibited an anomalously high resistivity. Investigating plasmas with a variety of densities, temperatures, plasma diameters, rotational transforms, current densities, and time dependence of current density, it was found that an anomalous resistivity is, among the above variables, a function only of the ratio of electron drift velocity u_e to electron thermal velocity v_{eth}. These measurements have now been extended to investigate the dependence of the anomalous resistivity on magnetic field strength, ion mass, and ion charge.

The measuring apparatus consists of a ruby laser emitting approximately 50 joules in 1 millisecond. The beam passes through the plasma perpendicular to the magnetic field and is focussed to a spot of about 1-mm diameter in the plasma. Light scattered from a 1-cm length of the focal region of the beam at 90° to the beam and to the magnetic field is collected by the f:3 input of a seven-channel monochromator. The entire apparatus can be moved to scan across a diameter of the plasma, the direction of scanning being parallel to the laser beam.

The plasmas investigated were in the normal ohmic heating regime, with densities of 10^{12} to 10^{13} cm^{-3} and electron temperatures of 20 to 150 eV. Plasma diameters were 7.5 to 12.5 cm and the rotational transform at the plasma surface was 0.6 to 1.2 radians. Ohmic heating currents ranged from 0.8 to 2.5 kA. The measurements were made after the first 3 milliseconds, at times when the density had fallen to between 0.5 and 0.1 of the peak density.

For each time and spatial position, measurements are made at 14 wavelengths at ~ 25 Å intervals. These are then fitted by the method of least squares to a Maxwell-Boltzmann velocity distribution to yield temperature and density at each measured point across the plasma diameter.

A range of values of u_e/v_{eth} could be explored under one set of discharge conditions by measuring at different times during the density decay under constant plasma current conditions. By varying the current and initial gas pressure, the same values of u_e/v_{eth} could then be achieved with different values of n_e and T_e. From the temperature profile as a function of radius we can derive the appropriate mean temperature to compare with the measured electrical conductivity σ_{cond}. This temperature is $T_\perp = [\int_0^{r_0} T^{3/2}\, r\,dr / \int_0^{r_0} r\,dr]^{2/3}$. The conductivity to be expected from theory [2], assuming that $T_\parallel = T_\perp$, is $\sigma_{scat} \propto T_\perp^{3/2}$.

In Fig. 1 $\sigma_{scat}/\sigma_{cond}$ is plotted against u_e/v_{eth} for a number of discharges in hydrogen at two values of confining field and for deuterium and helium discharges. For the times in the discharges at which the helium measurements were made, previous work has shown that the helium is almost completely twice ionized. From Fig. 1 it is clear that we have good agreement with conductivity theory for $u_e/v_{eth} < 0.02$. The effect of reducing the magnetic field is to enhance the anomalous part of the conductivity, but the onset with increasing u_e/v_{eth} is not changed. The hydrogen and deuterium points exhibit no difference in onset or magnitude of the anomaly, indicating that the phenomenon is mass-independent. The helium points show an onset at approximately twice the value of u_e/v_{eth}, suggesting a dependence on ion charge.

A lack of mass-dependence and the presence of a Z-dependence suggest that the phenomenon is dependent on electron-ion collisions. However, at the onset the electrons are gaining only about 1% of their rms thermal velocity, from the electric field, in the mean electron-ion collision time. Thus it seems very unlikely that this represents an effect of electron runaways, or that there exists any large difference between $T_\perp$ and $T_\parallel$.

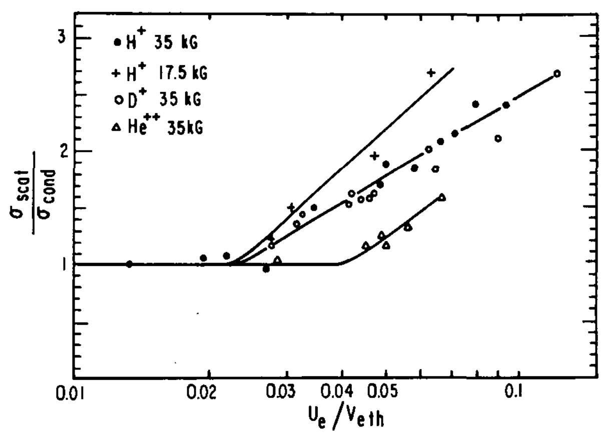

FIG. 1. Ratio of measured to theoretical plasma resistivity as a function of the ratio of electron drift to thermal velocity.

Although our data provide no immediate explanation of the anomalous resistivity, they do seem to eliminate or make improbable some explanations. Recognizing that the phenomenon is a reduction in current below the level to be expected for a given voltage, we can examine two limiting cases. The first is that all the current-carrying electrons are subject uniformly to some force which opposes their drift motion in the direction of the electric field. In this case a large part of the ohmic heating energy input is being delivered to the source of this impeding force. If we consider a typical case with a plasma current half of that anticipated, then half the power is going into the anomalous part of the plasma resistance. This represents a very large power input, capable of providing the entire thermal energy content of the plasma in a time of the order of 200 microseconds. It seems unlikely that this much power is being fed directly into the plasma turbulence, assuming small-amplitude theory.

The second case is that some fraction of the electrons is completely prevented from participating in this drift motion, but the remainder of the electrons are left unimpeded. In this case the power is dissipated in ohmic heating by the remainder of the electrons. This could arise, for instance, from electrons being trapped by potential fluctuations in the plasma. This would require that of the order of half of the current-carrying electrons be trapped, requiring potentials of several kT/e, which is larger than is generally observed.

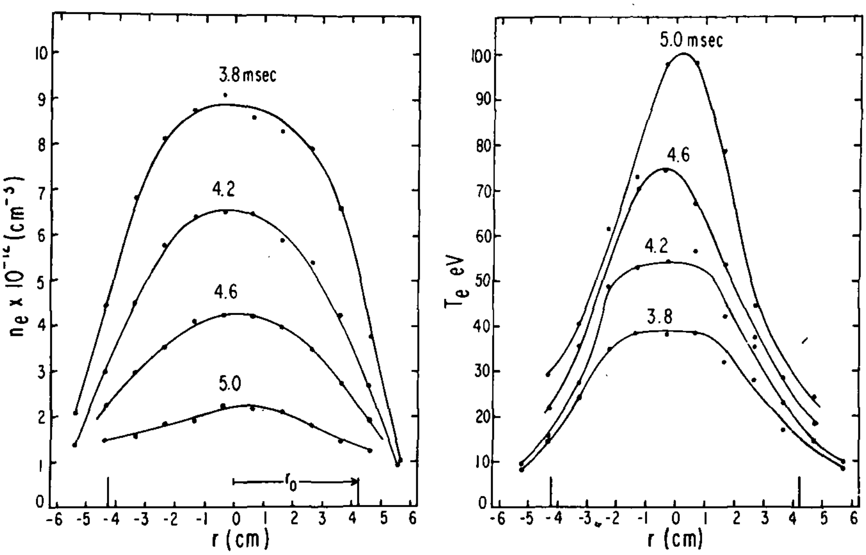

FIG. 2. n_e and T_e as a function of radius for four times in one discharge.

The question of whether the current reduction is uniform across the aperture of the plasma can be only partly answered by examination of Fig. 2, which presents the n_e and T_e profiles measured by Thomson scattering in a deuterium discharge at 35 kG at four different times during the discharge. It can be seen from the behavior of T_e vs radius and time that if the current is localized spatially it must be localized in the center of the discharge, since the temperature profiles are peaked in this region and become more so with increasing time. The current cannot be entirely concentrated in the center of the plasma, since this would imply that the plasma, from about two-thirds of the radius outward, offered a very high resistance, which would mean that there could be no toroidal equilibrium in this region and therefore that the observed pressure gradients in this region could not be supported.

Although the above could be construed as evidence against a wave-current interaction as an explanation of the anomaly, in the next section we shall see that waves are observed in just the region of the anomaly, suggesting that the difficulty lies in our lack of understanding of the wave-current interaction.

3. FLUCTUATION MEASUREMENTS (K. M. Young)

3.1 Turbulent flux and plasma loss rate from coherent fluctuations

The turbulent flux of plasma across the magnetic field, measured locally for coherent modes by a technique discussed in Ref. 3, is compared to the particle loss rate in Fig. 3 for ohmically-heated discharges. The particle loss rate was measured either by flux-measuring grid-electrode collector assemblies located in the divertor [7], or deduced from the density decay rate measured by microwave interferometers corrected as well as possible for neutral particle influx [8]. The solid line is the predicted relationship for a rectangular density distribution if the fluctuations are responsible for the plasma loss and the loss is uniform over the surface. The dashed line indicates data obtained previously with $\ell = 2$ helical transform [3] under conditions where $u_e/v_i > 1$. A confirmatory point with $\ell = 3$ transform is also shown. This result indicates clearly that the fluctuations are sufficient to provide the plasma loss in the regime where $u_e/v_i > 1$, thereby justifying the experiment reported in Sec. 4 on the effect of shear on confinement.

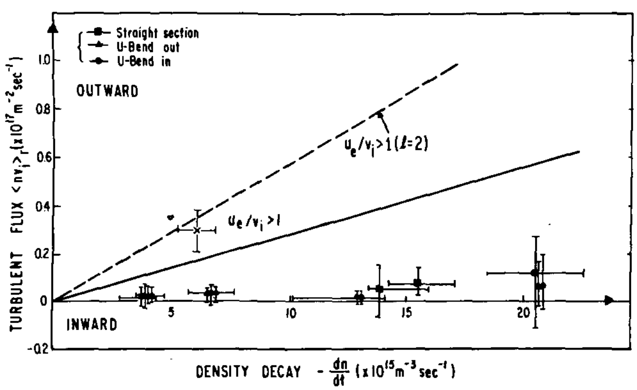

FIG. 3. The turbulent flux from coherent fluctuations shown as a function of the observed density decay rate. The solid line shows the predicted curve if the loss is wholly due to the fluctuations assuming a rectangular density profile and assuming that there is a uniform flux across the surface. The dashed line shows the dependence obtained for $u_e/v_i > 1$ [3]. The data points are for $u_e/v_i \leq 1$ for different locations in the stellarator.

The bulk of the data points are obtained for $u_e/v_i \lesssim 1$. These points are obtained with probes in the straight section of the vacuum vessel and also on the inside and outside at the center of one U bend. No significant difference is observed in the outward flux among these locations (nor was any significant difference in fluctuation amplitude observed), suggesting that a strongly ballooning mode is not responsible for the loss. In these data the observed loss rate can be as much as three times the computed Bohm rate: the observed flux is always directed outward and can never provide more than 50% of the observed loss rate. These results are consistent with the earlier interpretation from macroscopic measurements, which was that the resistive lack of equilibrium is responsible for the loss [9], [10].

3.2 Mode identification for $u_e/v_i \lesssim 1$

For $u_e/v_i \lesssim 1$, detailed examination of the low-m coherent fluctuations indicates that they are localized within a few millimeters about the rational magnetic surfaces. The azimuthal phase velocity of the fluctuations changes direction from the electron diamagnetic drift to the ion drift direction as u_e/v_i decreases through unity. The measured values of the radial electric field show that the fluctuations move slowly in the ∇p_i direction with respect to the plasma for $u_e/v_i \lesssim 1$. The amplitude variation parallel to B is less than 30% and the fluctuations of the azimuthal component of magnetic field, B'_θ, are proportional to $\phi' n_o$.

We find that these properties are consistent with theoretical predictions for the curvature-driven resistive mode [11 - 13] in the C stellarator. For conditions of weak shear and weakly positive unstable $\int d\ell/B$ applicable to the stellarator, the dispersion relation for this mode, neglecting finite Larmor radius effects, is

$$\left(1 - \frac{h}{h_o} y - y^3\right) = h_o^{-1/4} \frac{1}{k_y L_s} \left(\frac{\omega'}{\omega_o}\right)^{1/2} y^{5/2} \tag{1}$$

The normalized growth rate is , $y \equiv s/(\omega_o h_o^{1/2})$, where $\omega_o^2 \equiv 2v_i^2/aR$, s being the growth rate, R being the major radius of curvature, and a the density decay length. L_s is the shear length ($1/L_s \equiv r/L\, d\iota/dr$), $\omega' \equiv \omega_e \omega_i/\nu_{ei}$, where ω_e and ω_i are the electron and ion gyrofrequencies and ν_{ei} is the electron collision frequency. The quantity h_o is

$$h_o \equiv \left[\frac{m^2 L_R^2}{8\pi^2 r^2} \frac{\omega_o}{\omega'}\right]^{2/3} \tag{2}$$

where L_R is the curvature length $(2\pi L/\iota)$ and h is the effective well depth, given approximately by $h \simeq -2 \times 10^{-2}$ in this case. The dispersion relation, Eq. (1), assumes that $s \gg \omega^*$, the electron diamagnetic drift frequency, which is justified for this high-density, low-temperature regime. The appearance of this mode is very weakly ballooning, the predicted variation in growth rate along the magnetic field being about 15%. The real part of the frequency, crudely estimated from finite Larmor effects in the absence of shear [11], predicts that the wave moves in the ion drift direction with a velocity comparable to the observed value. One can also derive the dependence $B'_\theta \propto n_o \phi'$ assuming limited amplitude of the fluctuations [7].

These results indicate a close agreement between the experimental observations and theoretical predictions for the curvature-driven resistive mode in a short mean free path regime of the stellarator. In the absence of current, this instability may remain the cause of plasma loss even when the mean free path becomes longer than the machine length.

4. EFFECT OF SHEAR ON CONFINEMENT IN OHMICALLY-HEATED DISCHARGES ($u/v_i > 1$) (K. M. Young)

Increasing the externally applied transform, either sheared or shear-free, had little or no effect on ohmic-heated discharges with about 2 kA of current and with density about 10^{13} cm^{-3} [9]. Studies with magnetic probes indicated that the transform due to the current distribution reduced the externally applied shear. Experiments were then performed at lower ohmic heating currents (maximum $I_{OH} \approx 500$ A) which were programmed to decrease at about the density decay rate so that u_e/v_i was maintained at a value only slightly greater than unity. The current-driven drift mode could then exist and shear could also be applied. Results of this experiment are shown in Fig. 4, where the normalized confinement time is shown as a function of the rotational transform and shear (on a nonlinear scale) computed

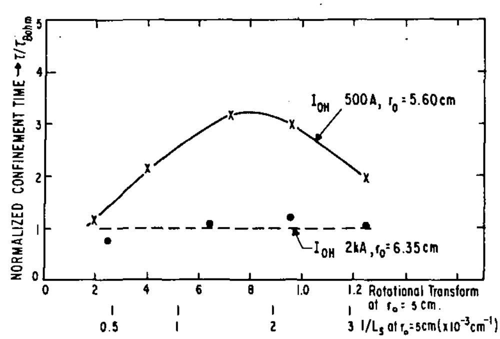

FIG. 4. The confinement time, normalized to the Bohm time, as a function of the transform, and shear, in the ℓ = 3 helical winding. The temperature varies by less than 20% in either set of data. The data are for the condition $u_e/v_i > 1$.

at 5-cm radius. The confinement time was deduced from the particle flux to the divertor, in conjunction with probe measurements of the radial density distribution, and was also checked by comparing with the microwave density decay rate corrected for influx of particles [8]. While the high-current ($I_{OH} \approx 2$ kA) data indicated no dependence on shear or transform, in the case of the lower current ($I_{OH} \lesssim 500$ A), there is an increase in containment time as the rotational transform (and also the shear) is increased. For these discharges the temperature (measured from the conductivity) is nearly constant. The increased confinement time as the shear is increased is in qualitative agreement with expectation [14], but the decrease in the time constant at high values of transform is not understood. Similar effects are also observed for plasmas heated by ion cyclotron waves (Sec. 5) and in gun-produced plasmas [15]. For the case of ohmically-heated discharges, it is possible that low-m kink instabilities could lead to the loss [4], but an additional possibility is defects in the magnetic field. These defects could be in the form of coil misalignment or in the form of magnetic islands [16,17]. However, application of transverse fields which correspond to various possible misalignments, and which calculations show lead to island formation [18], does not change the observed confinement time until this field is nearly an order of magnitude larger than that corresponding to any misalignment known to be present. The possibility that the long time constant, $\tau \simeq 3\ \tau_{Bohm}$, could be in part due to the presence of fast electrons cannot be ignored. A crude experiment inserting a 2.5 mm diameter probe all the way to the center of the plasma, to stop any fast component, suggests, however, that τ reaches at least twice τ_{Bohm}.

Under conditions at which the best confinement was observed ($\tau \simeq 3\ \tau_{Bohm}$), the fluctuations are observed to move in the electron drift direction and are about one-half the amplitude observed when the Bohm diffusion rate is observed. In addition, the radial localization of the coherent modes is less than 5 mm compared with the values of 5 - 10 mm previously reported for the $\ell = 2$ helical transform [3]. Though these results are consistent with the inference that shear provides a decrease in the turbulent diffusion rate, only a complete turbulent flux measurement can prove this point.

5. CONTAINMENT STUDIES OVER A WIDE RANGE OF λ_e FROM ION CYCLOTRON HEATING (I. G. Brown, M. A. Rothman, and R. M. Sinclair)

If the resistive instabilities play a role in the anomalous loss of current-free plasmas (in the sense that $u_e/v_i < 1$), the containment time should become longer as the mean free path becomes long compared with the axial machine length. By heating the electrons with ion cyclotron waves at low densities and making use of the ability to heat ions and electrons independently, it is now possible to study the confinement of such plasmas over a broader range of parameters (and in particular to $\lambda_e >> L$) than in previously reported experiments [5].

The toroidal plasma is formed by an ohmic heating current (typically a few hundred amperes to several kiloamperes for $n \gtrsim 10^{12}\ cm^{-3}$, or ~ 30 A for $n \sim 10^{11}\ cm^{-3}$), such that $u_e/v_i \lesssim 1$. The confining magnetic field at a Stix coil, installed in a straight section of the stellarator, is adjusted for optimum coupling of energy into ion cyclotron waves [19]; the field adjacent to this section is separately controlled to vary the ion and electron heating [20]. The electrons are heated over this range of parameters principally by Landau damping of the waves [21]; the ions are heated at a magnetic beach by cyclotron damping [22]. We have found it possible to use this method to heat the electrons at densities as low as $10^{11}\ cm^{-3}$ [23]. The radius used was the maximum available (6.1 cm), since the power to the plasma (hence the temperature) is a sensitive function of radius [22].

The electron temperature was obtained from the conductivity for the dc ohmic heating current, which continued to flow during and after ICRH. The ICRH raised kT_e to $\lesssim 100$ eV at the highest density, and to $\lesssim 70$ eV at $10^{11}\ cm^{-3}$. The perpendicular ion temperature was found from the diamagnetic pressure and kT_e [24]; this could only be done accurately for $n \gtrsim 10^{12}\ cm^{-3}$; at $10^{11}\ cm^{-3}$ we can only say that $kT_i < 2\ kT_e$. The flux of particles entering the divertor, from which the confinement time τ was calculated, was measured with the flux collectors located in the divertor.

After the end of the ICRH pulse, the plasma cooled in about one millisecond to the initial temperature. We observed an increase in plasma density following ICRH, comparable to the initial density. We assume this is due to ionization of the unavoidable fraction of neutral gas remaining at the time ICRH is applied. The magnitudes of the density increase, and the cooling time of the plasma, are what would be expected if all the electrons are characterized by the kT_e calculated from the conductivity and are being cooled by the neutral gas.

Measurements made before, and as a function of time after, ICRH yielded a number of values of τ/τ_{Bohm} and λ_e for each discharge. This method for obtaining a range of values of λ_e has the obvious disadvantage that the important parameters T_e and τ are changing rapidly during the measuring period. This means, for example, that plasma arriving at the divertor collectors at a given instant has left the main discharge at an earlier time when the temperature was higher than that measured at the arrival time. Corrections for this and related effects are estimated to be small, and do not change the conclusions. Aside from the systematic errors associated with transient measurements, uncertainties in the actual measurements of temperatures, etc., alone could account for ~ ±30% fluctuation in the value of τ/τ_{Bohm}. The method does, however, provide us with information for the important case where $\lambda_e > L$ but $u_e/v_i < 1$, which can be compared with the results of Sec. 4.

We found empirically that plotting τ/τ_{Bohm} vs $\lambda_e \iota$ made the results for various discharges most nearly coincide. This suggests that the pertinent parameter is the ratio of λ_e to a connection length $(2\pi L/\iota)$. Values of ι at the nominal aperture between 0.3 rad and 1.5 rad were used. (The minimum value is enough to assure equilibrium [4].)

Typical values of τ/τ_{Bohm} as a function of $\lambda_e \iota$ are given in Fig. 5. (Similar results, with more scatter, were obtained with hydrogen at half the confining field.) For $\lambda_e << L$, τ/τ_{Bohm} was independent of λ_e and ι. As λ_e was increased so that $\lambda_e \iota \sim L$ (1 rad), an increase in τ/τ_{Bohm} was noted. A peak value of five for τ/τ_{Bohm} was observed.

A parametric analysis showed that the scatter of the results evident in Fig. 5 is not due to any further systematic dependence on T_e, n, or ι. Any one collection of data showed small scatter, while those taken weeks apart showed more. The slow variation of τ/τ_{Bohm} with λ_e, coupled with this scatter, does mean that any further dependence of τ/τ_{Bohm} on ι could be masked by the small range of ι available. We cannot thus definitely exclude any further dependence on ι beyond that envisaged in treating $\lambda_e \iota$ as the relevant parameter.

For values of $n \gtrsim 10^{12}$ cm^{-3}, the ohmic heating current was varied by an order of magnitude, increasing kT_e before ICRH. This produced no consistent change in the dependence of τ/τ_{Bohm} on $\lambda_e \iota$. In this same range, where measurements of kT_i were possible, we were able to hold kT_e constant and vary kT_i from $kT_e/2$ to 10 kT_e, producing a change in the ion relaxation time from ~ 20 μsec to ~ 2 milliseconds, or from 10^{-2} τ to 2τ. This also produced no consistent change in τ/τ_{Bohm}, showing that the anisotropic ion velocity distribution produced by ICRH does not affect the plasma containment (for $\lambda_e \lesssim L$). This is in agreement with the results of Pease et al. [5]. The maximum ion temperature attained (averaged around the torus) was kT_i = 550 eV [25].

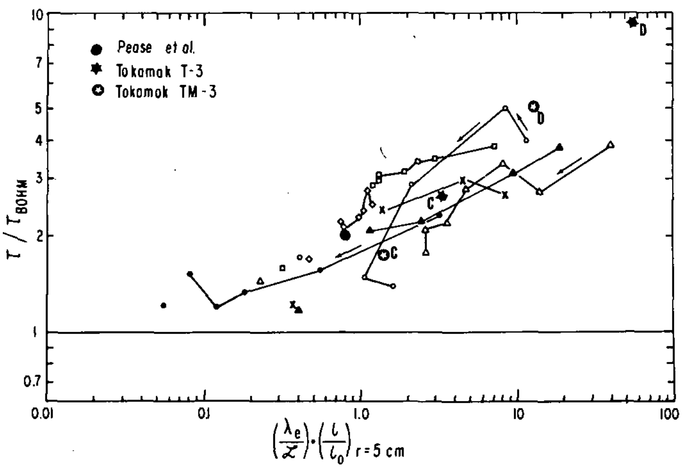

FIG. 5. Ratio of observed confinement time to the calculated Bohm time, measured before and after ICRH in a number of deuterium discharges, versus mean free path (in units of the axial length) times rotational transform at 5.0 cm radius caused by an ℓ = 3 helical winding (in units of ι_0 = 0.30 π). Each symbol identifies a separate discharge; the unconnected points are taken before ICRH, and those connected by lines show the results as the plasma cools after ICRH. [The Tokamak points are calculated taking kT_e from plasma conductivity measurements ("C") and, for contrast, from diamagnetic measurements ("D"); the transform for these points is caused by an ohmic heating current, and is calculated at the measured plasma radius. The axial length used is that of the appropriate device.]

The only consistent deviation from this simple dependence of τ/τ_{Bohm} on $\lambda_e \iota$ was at large values of λ_e and ι. In Fig. 6 we show the dependence of τ/τ_{Bohm} on ι, for data taken from a number of separate discharges with various ranges of λ_e. We see that τ/τ_{Bohm} increases with ι for $\lambda_e \gtrsim L$. At the longest λ_e it shows a reduction at large ι, similar to that discussed in the previous section.

We have searched for possible alternative explanations of these results. One possibility that we cannot exclude is that a fraction of the electrons may be heated by the ICRH to a higher temperature than the rest. For example, electrons travelling with the phase velocity of the ion cyclotron waves would have ~ 400 eV of energy. Such a fraction could account for most (or all) of the observed increase in conductivity, and for the ionization following ICRH; its cooling time (at 400 eV) by electron-electron collisions would be ~ 1 millisecond at the lowest value of n_e used. We do find that the observed cooling time is approximately inversely proportional to the density increase over a factor of four (1/2 to 2 msec), consistent with cooling by electron-neutral collisions of a plasma at the observed conductivity temperature; this limited range does not allow us to exclude the possibility of a hot component. If indeed the distribution function is strongly non-Maxwellian, then the concept of the Bohm time becomes ambiguous. In particular, if the relevant measure of mean particle energy to be used in calculating τ_{Bohm} is biased towards the low-energy end of the distribution, then τ_{Bohm} is underestimated by using the conductivity temperature; the data points of Fig. 5 should be shifted down and to the left.

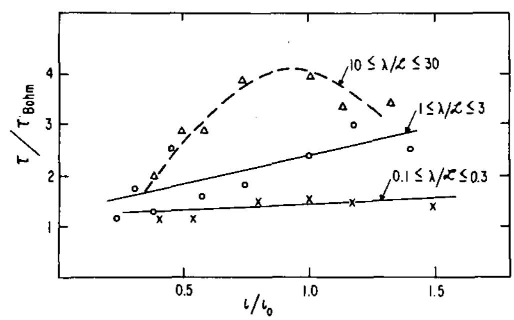

FIG. 6. Values of τ/τ_{Bohm} versus rotational transform from a number of separate discharges with λ_e in the indicated intervals. (Each point is the average of about 20 measurements.)

In Fig. 5 we also show some representative points from other experiments. That of Pease et al. [5] was obtained by methods similar to those of the present work. Those for the Tokamak devices were inferred from representative data published by Artsimovich et al. [26]. From the latter data we could calculate the electron temperature in two different ways: It was taken to be either that determined from the gross plasma conductivity, or that calculated from the diamagnetic pressure. Both of these calculations could be considered consistent with our results, since using a larger kT_e increases both λ_e and τ/τ_{Bohm}.

6. SUMMARY AND CONCLUSIONS

The experiments discussed in this paper have been directed toward elucidation of the anomalous plasma loss in the C stellarator. The experiments all make use of ohmic heating to form the plasma, but we find that the detailed properties observed depend markedly on the ratio of the current drift velocity to the particle thermal velocities. As u_e/v_i becomes greater than unity with ohmic heating, the plasmas become collisionless in the sense that $\lambda_e \gtrsim L$. Alternatively, the collisionless regime has been attained by Landau damping of ion cyclotron waves by the electrons with $u_e/v_i < 1$.

Examination of the perpendicular electron temperature and density distribution by Thomson scattering of ruby-laser light indicates that for $u_e/v_{eth} \lesssim 0.02$, the temperature obtained from the conductivity is in agreement with the averaged perpendicular temperature. This result confirms Spitzer's theoretical derivation [2] of the conductivity, and is also in agreement with many other temperature-measuring techniques discussed in Ref. 4.

However, for $u_e/v_{eth} > 0.02$, there is a discrepancy between the measured conductivity and that predicted by the measured perpendicular temperature. As much as half of the plasma resistance is anomalous. For hydrogen $u_e/v_{eth} > 0.02$ is equivalent to $u_e/v_i \gtrsim 1$, and this is the case for which large-amplitude coherent fluctuations observed in the plasma were identified previously with the current-driven drift mode [3]. This suggests that the anomalous resistivity is associated with this mode. A detailed comparison of the onset of this mode with the onset of the anomalous resistivity must await the results of theoretical work now in progress. The experimental agreement for hydrogen and deuterium is good, but measurements of the fluctuations and turbulent transport have not yet been made in helium plasmas.

In the region of $u_e/v_i < 1$, the experimental data on the coherent fluctuations can best be related to a mildly ballooning resistive gravitational mode. The experiments also show that only a small fraction of the plasma loss is associated with the fluctuations. Under these conditions, the interaction between the ohmic heating current and the turbulence may be less than that for a current-driven mode, yielding conductivity values of the temperature which are more nearly correct.

The mode identification of the fluctuations with the current-driven drift instability led to an experiment to determine whether shear could reduce the plasma loss rate for this mode. For a relatively small amount of shear, $L_s \simeq 0.9$ m, the ratio of $\tau/\tau_{Bohm} \simeq 3$ is in qualitative agreement with Kadomtsev and Pogutse's predictions [14] about the effect of radial localization of the mode on the diffusion rate. For low ohmic currents but high electron temperatures obtained by Landau damping of ion cyclotron waves, a similar ratio τ/τ_{Bohm} was obtained, as well as an indication of a dependence on rotational transform (or shear). For both of these methods of forming the hot plasma, there is a reduction in confinement time if the helical transform is increased further which may be associated with a deterioration of the quality of the magnetic surfaces.

The studies using ICRH show that for $\lambda_e \lesssim L$, the confinement time is given by the Bohm formula using the electron temperature, independent of the ion temperature. The ratio of τ/τ_{Bohm} increases slowly with $\lambda_e\,\iota$ for $\lambda_e \gtrsim L$. The principal uncertainty in the interpretation of this increase in τ/τ_{Bohm} remains associated with the details of the electron velocity distribution following ICRH.

This work was performed under the auspices of the U. S. Atomic Energy Commission, Contract AT(30-1)-1238.

REFERENCES

[1] BISHOP, A.S., HINNOV, E., "Plasma Physics and Controlled Nuclear Fusion Research" (IAEA, Vienna, 1966), Vol. II, p. 673.

[2] SPITZER, L., JR., "Physics of Fully Ionized Gases" (Interscience, New York, 1962), p. 139.

[3] YOUNG, K.M., Phys. Fluids 10 (1967) 213.

[4] SINCLAIR, R.M., YOSHIKAWA, S., HARRIES, W.L., YOUNG, K.M., WEIMER, K.E., JOHNSON, J.L., Phys. Fluids 8 (1965) 118.

[5] PEASE, R.S., YOSHIKAWA, S., EUBANK, H.P., Phys. Fluids 10 (1967) 2059.

[6] DIMOCK, D., MAZZUCATO, E., Phys. Rev. Letters 20 (1968) 713.

[7] YOUNG, K.M., Ph.D. Thesis, Princeton University (1968).

[8] HARRIES, W.L., KESSLER, J.O., SINCLAIR, R.M., YOSHIKAWA, S., Phys. Fluids 7 (1964) 151.

[9] YOSHIKAWA, S., YOUNG, K.M., SINCLAIR, R.M., HARRIES, W.L. Plasma Physics Laboratory MATT-282 (1962).

[10] YOUNG, K.M., YOSHIKAWA, S., SINCLAIR, R.M., Phys. Fluids 9 (1966) 1447.

[11] COPPI, B., ROSENBLUTH, M.N., "Plasma Physics and Controlled Nuclear Fusion Research" (IAEA, Vienna, 1966), Vol. I, p. 617.

[12] FURTH, H.P., KILLEEN, J., ROSENBLUTH, M.N., COPPI, B., in "Plasma Physics and Controlled Nuclear Fusion Research" (IAEA, Vienna, 1966), Vol. I, p. 103.

[13] YOSHIKAWA, S., Bull. Am. Phys. Soc. 12 (1967) 805.

[14] KADOMTSEV, B.B., POGUTSE, O.P., Kurchatov Institute Report IAE-1227 (1966) [English translation: Culham Laboratory Report CLM-Trans 11 (1967)].

[15] GROVE, D.J., MESERVEY, E.B., STODIEK, W., YOUNG, K.M., this meeting CN-24/D-2.

[16] KERST, D.W., J. Nucl. Energy Pt. C, 4 (1962) 253.

[17] SOLOV'EV, L.S., Doklady Akademi Nauk, SSSR 168 (1966) 76.

[18] *SHEFFIELD, G., Princeton Plasma Physics Laboratory* MATT-Q-24, (1967) p. 335.

[19] ROTHMAN, M.A., SINCLAIR, R.M., BROWN, I.G., Bull. Am. Phys. Soc. 13 (1968) 286.

[20] YOSHIKAWA, S., SINCLAIR, R.M., ROTHMAN, M.A., "Plasma Physics and Controlled Nuclear Fusion Research" (IAEA, Vienna, 1966), Vol. II, p. 925.

[21] YOSHIKAWA, S., YAMATO, H., Phys. Fluids 9 (1966) 1814.

[22] STIX, T.H., The Theory of Plasma Waves (McGraw-Hill Book Co., Inc., New York, 1962).

[23] SINCLAIR, R.M., ROTHMAN, M.A., BROWN, I.G., Bull. Am. Phys. Soc. 13 (1968) 286.

[24] ROTHMAN, M.A., Plasma Physics 10 (1968) 86.

[25] ROTHMAN, M.A., SINCLAIR, R.M., BROWN, I.G., Bull. Am. Phys. Soc. 13 (1968) 870.

[26] ARTSIMOVICH, L.A., BOBROVSKI, G.A., MIRNOV, C.V., RAZUMOVA, K.A., STRELKOV, V.S., Atomnaya Energiya 22 (1967) 259.

DISCUSSION

D.A. SHCHEGLOV: What was the relationship between the electron-cyclotron and the plasma frequencies in those experiments where anomalous resistance was observed?

R.M. SINCLAIR: At B = 35 kG, Ω_e was 6.2×10^{11} c/s and ω_{pe} was 2.8×10^{10} c/s.

CONFINEMENT OF CONTACT-IONIZED BARIUM PLASMA IN THE WENDELSTEIN STELLARATOR W II*

E. BERKL, D. ECKHARTT, G. v. GIERKE, G. GRIEGER, E. HINNOV**,
K. U. v. HAGENOW AND W. OHLENDORF
INSTITUT FÜR PLASMAPHYSIK, GARCHING, MUNICH,
FEDERAL REPUBLIC OF GERMANY

Abstract

CONFINEMENT OF CONTACT-IONIZED BARIUM PLASMA IN THE WENDELSTEIN STELLARATOR W II.
The confinement of low-β plasmas in a stellarator magnetic field has been studied experimentally as a continuation of our previous work. A new stellarator, W II, allows d.c. operation. It has circular shape, avoids interruptions of the helical windings generating an $\ell = 2$ helical field, and possesses five-fold rotational symmetry. It has practically no shear but a small average magnetic well, 3% in depth. Barium plasma was produced by contact ionization on a radiation-heated tantalum sphere located on or near the magnetic axis. Measurements of the density distribution were performed for various values of the magnetic field, the angle of rotational transform and the magnitude of the input ion flux. The ion density was determined by two independent methods, namely (i) by Langmuir probes and (ii) by resonance fluorescence. The measured relation between input ion flux and peak ion density is in agreement with numerical calculations of this dependence assuming resistive diffusion across a stellarator magnetic field and recombination on the surfaces of the emitter and its supporting wire as well as on the surfaces of any probe introduced into the plasma. This confirms earlier measurements done in the apparatus W Ib. For the higher emitter temperature assumed in the calculations the flux lost on the emitter is negligibly small compared to the flux radially outwards. It has also been found that for input ion flux and main magnetic field kept constant the peak ion density decreases markedly whenever $\iota/2\pi$ is a rational fraction.

Introduction

Previous experiments on the confinement of a Cs plasma in the Wendelstein stellarator W Ib [1, 2, 3] gave evidence that - in comparison to "pump-out" - the plasma loss rate only slightly exceeds that expected for resistive diffusion (including the factor $(1 + ŧ^{-2})$ for stellarator confinement [4]) and recombination on the emitter and the probes. This statement holds after a critical revision of the previous results based on current knowledge [5, 6] ($\iota/2\pi$ is here denoted by ŧ).
However, the uncertainty introduced by the use of probes for density measurement, the relatively short duration of 0.8 sec of the magnetic field pulse, the time dependence of the emitter temperature, the complicated magnetic field structure of the W Ib stellarator and the restriction on plasma radius required a new experiment in order to put the results on a safer ground.

---

* This work was performed under the terms of the agreement between the Institut für Plasmaphysik GmbH, Garching near Munich, and Euratom to conduct joint research in the field of plasma physics.

** On leave from Princeton University, USA.

Therefore, a new stellarator, W II, has been built. This is a circular torus with a comparatively large aspect ratio of 0.1 and the highest degree of symmetry achievable for a $\ell = 2$ stellarator. It has practically no shear, but does possess a small average magnetic well about 3 % in depth. Steady-state operation can be achieved for 20 sec or more. Observation ports as large as consistent with these requirements have been provided to allow spectroscopic investigations in addition to the diagnostic techniques previously used.

Experimental Arrangement

The stellarator W II (fig. 1) is a circular torus with radius of curvature R = 50 cm and an effective tube diameter 2r = 12 cm. The main field is produced by 44 coils, equally spaced and connected in series. The maximum field strength is 9 kG d.c. or about 15 kG pulsed. The helical windings are of the type $\ell = 2$, and are wrapped uniformly around and directly upon the vacuum tube with a field period of five. The only deviation from five-fold rotational symmetry is caused by the current leads.
The requirements of symmetry unfortunately limit the location and size of the observation ports.

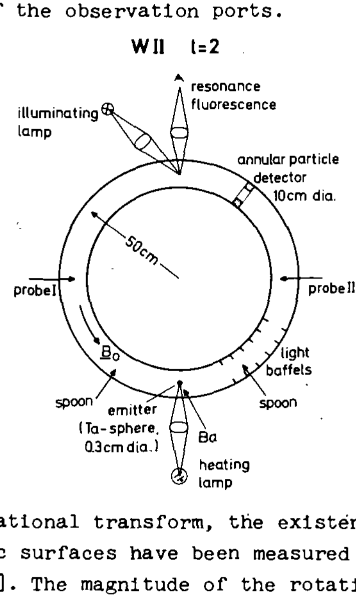

FIG. 1. Schematic drawing of the stellarator W II.

The rotational transform, the existence and the shape of the magnetic surfaces have been measured by means of a pulsed electron beam [7]. The magnitude of the rotational transform agrees closely with calculations [8], as shown in fig. 2. The magnetic surfaces are nearly elliptical in cross-section. In the range of $\iota = \frac{\iota}{2\pi}$ investigated the ratio of the two axes of the ellipses can be approximated by the formula

$$\frac{a}{b} = 1.14 + 1.46\,\iota$$

So far only magnetic fields of 5 and 7.5 kG have been used. The maximum rotational transform for these cases are ι = 0.5 and ι = 0.22 respectively. The plasma diameter is limited by the magnetic surface tangent to an annular particle detector with an inner radius

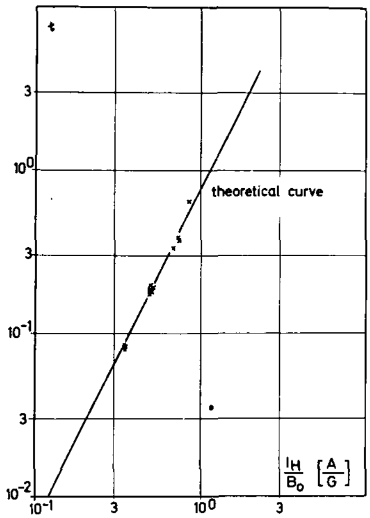

FIG. 2. Rotational transform, ι, vs the ratio between the current in the helical windings and the strength of the main magnetic field, measured by means of a pulsed electron beam. The calculated curve is shown for comparison.

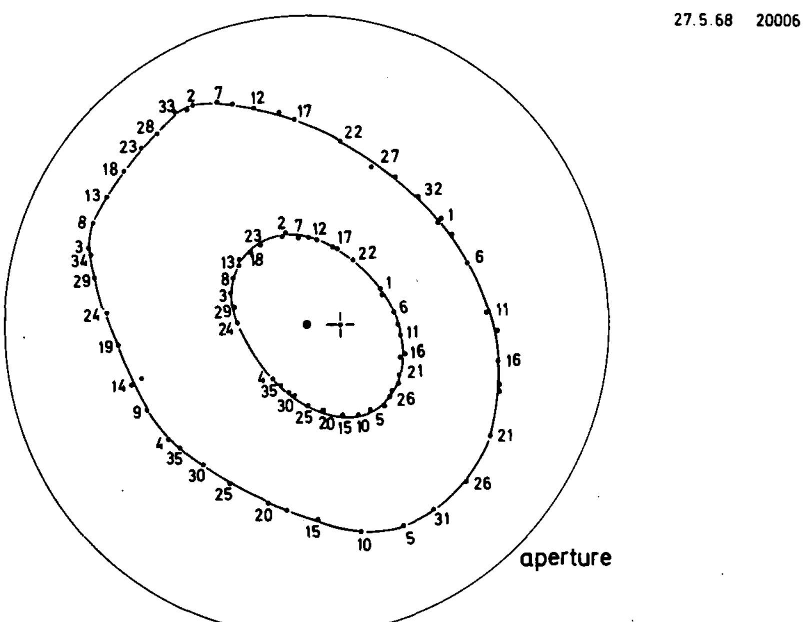

FIG. 2a. An example of the drift surfaces in the stellarator W II found by the use of a pulsed electron beam.

of $r_p = 5$ cm. This yields an effective aperture with the radius $r_{eff} = 5.0 - 1.65\,t$ cm.
Ba plasma is produced by contact ionization on a Tantalum sphere of 3 mm diameter. The sphere was suspended by a Tungsten wire of 50 µm diameter on or near the magnetic axis. It was heated to a temperature of about 2150 °K by focussing a 6.5 kW high pressure Xe arc upon its surface. The measured current of thermally emitted electrons allowed the formation of an electron sheath up to densities of about $3 \cdot 10^9$ cm^{-3}. Higher temperatures could not be achieved by this means because of the limited solid angle available.
Two removable spoon probes are arranged on either side of the emitter. With the help of these probes the total input flux of ions, Φ_B, could be determined from the ion saturation current also in the presence of the magnetic field. The ion density was measured in two different ways. (i) Probes could be introduced 90° azimuthally displaced from the plasma source. The probe tips were 30 µm in diameter and 3 - 5 mm in length. The probe shafts had a diameter of 0.1 mm. The probes were biased with respect to the emitter. The ion density has been evaluated in the usual way from the probe signal except that an "increased sensitivity factor" of 2.5 was taken into account [9, 10].
(ii) At 180° around the machine the density was measured by the method of resonance fluorescence [11]. A capillary high pressure Xe lamp was used to excite the Ba^+ resonance lines. The spatial resolution used was about 2.5 x 2.5 x 12 mm^3 with the long dimension orientated parallel to the main magnetic field. Horizontal scans could be made by shifting the illuminating lamp and vertical scans by deflecting the image of the stellarator by means of a variprism [12]. The particle detector (fig. 10) was intended to measure the flux leaving the confinement region. It was of the double-double probe type described previously [13]. The sensitive parts of the particle detector were divided into four segments, each consisting of three azimuthal strips of 2 mm radial extension.

Experimental Results and Discussion

Two main relationships were subject to experimental investigation: (i) the peak particle density as function of the input ion flux, Φ_B, for fixed magnetic fields; and (ii) the dependence of the peak ion density on t with input flux and main magnetic field kept constant. For some of the parameters particle density profiles were determined and the influence of the presence of a probe within the plasma on the ion density studied.

The experimental results are compared with a theoretical model which considers resistive diffusion across the stellarator magnetic field in the approximation of small ι and recombination on the emitter and its supporting wire as the dominant loss processes. If probes are introduced into the plasma the losses on their surfaces are also taken into account. This model has been found to describe successfully the experimental results obtained with the W Ib stellarator [6] and has been modified only for the different parameters present in this experiment. The curves shown for comparison with the experimental results are calculated for emitter temperatures of 2320 $^{\circ}$K, i.e. U_{th} = 0.2 V, and 2100 $^{\circ}$K, i.e. U_{th} = 0.18 V. In the former case the flux lost by recombination on the emitter is small compared to the flux lost by diffusion and therefore has only a minor influence on the peak particle density, except for the highest values of ι and n.

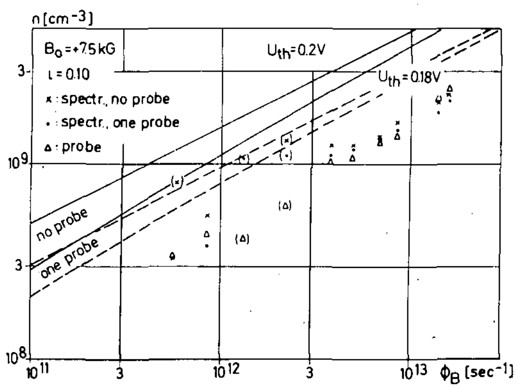

FIG. 3. Peak ion density vs input ion flux measured by resonance fluorescence and by probe for B_0 = 5 kG and ι = 0.10. Calculated curves for U_{th} = 0.2 V and 0.18 V respectively are shown for comparison.

Figs 3 - 5 give the dependence of the measured density on the input flux for different parameters. There are three different measurements of the density: a) by resonance fluorescence with no probe introduced into the plasma; b) by resonance fluorescence with one probe in the plasma; and c) by the probe itself. The measured points follow a $n \sim \sqrt{\Phi_B}$ dependence as expected for the model discussed above, except for a few points shown in brackets. With the latter points there exists some uncertainty with respect to the experimental parameters present during the measurement. The absolute density is smaller by a factor of 2 or 3 than the one calculated for U_{th} = 0.2 V but exceeds the Bohm value by two orders of magnitude for $\Phi_B = 10^{12}$ sec^{-1}. If the loss rates are that small, the introduction of an obstacle into the plasma should reduce the density considerably. This effect is realized by introducing a probe into the plasma, i.e. a glass-covered wire of 0.01 cm outer diameter. In this case the density as measured by resonance fluorescence is reduced by 20 - 30 %, in agreement with the calculations. The residual disagreement between the density measured and calculated might find its explanation in the fact that the temperature of the emitter was only 2150 °K i.e. $U_{th} \approx 0.18$ V yielding a much larger recombination coefficient. On the other hand, the appropriate value of the work function of Ta for these operating conditions is not known to us and seems to be in disagreement with the usual assumptions. This involves some uncertainties in the flux lost by surface recombination and will be subject to further investigations. It was in fact a surprising result that Ta could be used so effectively to produce a Ba plasma.

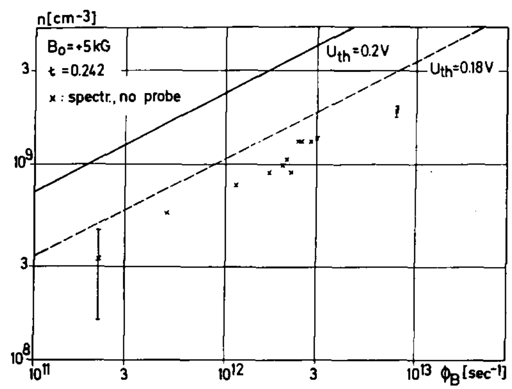

FIG.4. Peak ion density vs. input ion flux measured by resonance fluorescence for B_0 = 5 kG and ι = 0.242. Calculated curves for U_{th} = 0.2 V and 0.18 V respectively are shown for comparison.

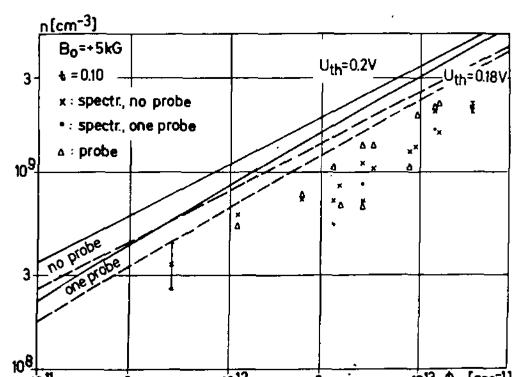

FIG.5. Peak ion density vs. input ion flux measured by resonance fluorescence and by probe for B_0 = 7.5 kG and ι = 0.10. Calculated curves for U_{th} = 0.2 V and 0.18 V respectively are shown for comparison.

The increase in density when increasing the magnetic field strength from 5 to 7.5 kG is calculated to be 40 %. An increase of roughly this magnitude was observed by resonance fluorescence measurements at higher fluxes. At lower input fluxes the experimental error is of the same order as the effect expected.

In figs 6-8 the dependence of the peak ion density on t is shown. It can be seen that above a certain t the density rises steeply. This critical value of t decreases with increasing Φ_B and increasing B which might be explained in terms of thermalization of the plasma and supports earlier explanations [2]. It should also be emphasized that for small values of t it is not permitted to neglect the ion inertia terms as has been done in the calculations.

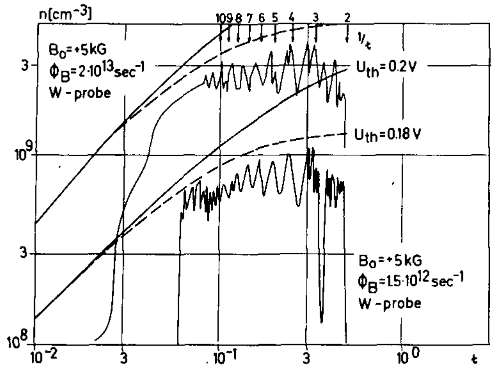

FIG.6. Peak ion density vs t measured by probe for B_0 = 5 kG and Φ_B = 1.5 · $10^{12}\,s^{-1}$ and Φ_B = $2\times10^{13}\,s^{-1}$ respectively. For comparison calculated curves are shown for U_{th} = 0.2 V and 0.18 V respectively.

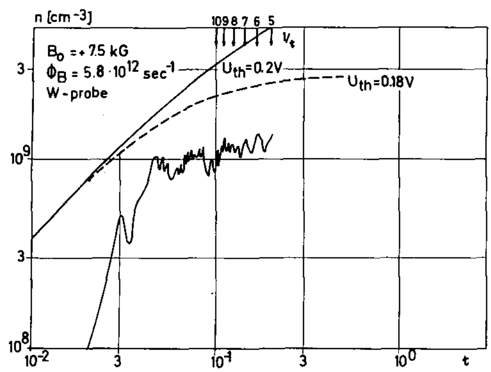

FIG.7. Peak ion density vs. t measured by resonance fluorescence for B_0 = 5 kG and Φ_B = $9.5\times10^{12}\,s^{-1}$. For comparison calculated curves are shown for U_{th} = 0.2 V and 0.18 V respectively.

For larger t the density shows discrete maxima and minima. Within the experimental error the minima occur if $1/t$ is a rational number+), some of them being indicated on the top of the figures.

+) The term "rational number" in this connection should be understood as $1/t = \frac{m}{n}$ with m, n being not too large integers.

Unfortunately, no precise statement can be made about this fact, since the currents of the generators showed some fluctuations with time and could not be measured with sufficient precision to reduce the error in ι below 3-4 %. That the fine structure of the confinement properties could be observed so clearly is ascribed to the fact that the W II device has practically no shear. In this case ι becomes rational for a large part of the plasma cross-section simultaneously. When ι

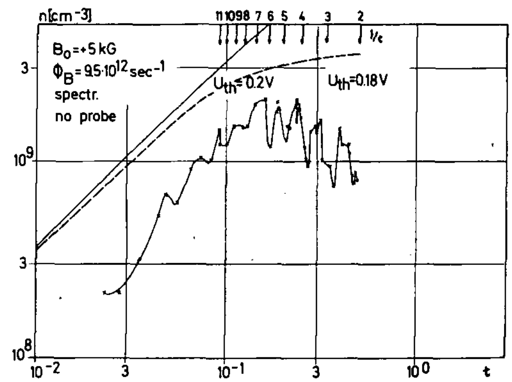

FIG.8. Peak ion density vs. ι measured by probe for B_0 = 7.5 kG and Φ_B = 5.8 x 10^{12} s^{-1}. Calculated curves for U_{th} = 0.2 V and 0.18 V, respectively, are shown for comparison.

is a rational fraction magnetic surfaces are no longer defined since the magnetic lines close upon themselves after a certain number of revolutions around the machine. In this case the condition $\nabla_{\parallel} p = 0$ no longer requires that the pressure is constant on the magnetic surfaces but only along the individual closed lines. Equilibrium between plasma pressure and magnetic field forces in such degenerate cases requires $p = f(q)$ where $q = \oint \frac{dl}{B}$. In general surfaces of constant q will differ from the magnetic surfaces (as defined by a slight change of ι) but it has been found by numerical calculations that closed q-surfaces in fact exist in W II in the immediate neighbourhood of the magnetic surfaces, at least for ι = 0.5. Therefore, the appearance of such drastic changes of the confinement properties are not to be expected simply on the basis of the absence of well-defined magnetic surfaces. It is not clear, on the other hand, how the stability is affected if ι becomes a rational fraction particularly as the device has negative V'- properties. One possible explanation for the observation might be found in the development of convective cells if ι is rational since the supporting wire of the emitter - even though it was very thin - might influence the potential on those magnetic lines which pass through or near it. In contrast, if magnetic surfaces exist, i.e. if ι is an irrational fraction, these surfaces must closely agree with the surfaces of constant potential, prohibiting the generation of convective cells oriented perpendicular to the magnetic surfaces. All these possibilities are being investigated both theoretically and experimentally.

As far as the maxima of n are concerned, they follow closely the calculated curve if one uses the actual temperature of the emitter (0.18 V) except for the highest values of ι where the deviation seems to become larger.

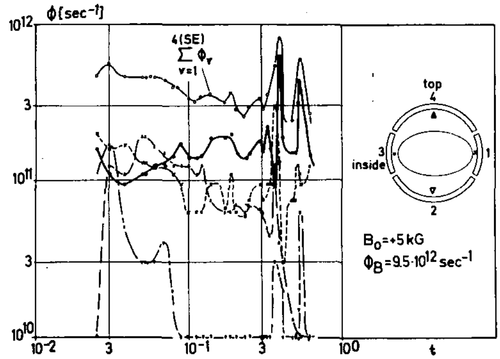

FIG. 9. Fluxes to the individual segments of the particle detector and the sum of these fluxes vs . ι for B_0 = 5 kG and Φ_B = 9.5 × 10^{12} s^{-1}. No probe was present within the plasma. These data were taken simultaneously with the ones shown in Fig. 7. For the meaning of the symbols see insert.

In fig. 9 the ion flux collected by the particle detector vs. ι is plotted. These data were taken simultaneously with the ones shown in fig. 7. No probe was present within the plasma in this case. It can be observed that for increasing ι the plasma is lost preferentially in the plane of the torus towards the segments 1 and 3, which is in agreement with the orientation of the elliptical cross section of the magnetic surfaces as shown in the insert of fig. 9. Upon reversing the direction of the helical currents the orientation of the ellipse is rotated by 90° and the plasma is found to be lost towards the segments 2 and 4. Furthermore, by comparison with fig. 7 it can be seen that the flux found at the particle detector increases if the centre density decreases. It has not yet been investigated, however, why the direction of the increased loss flux is not always the same but depends very sensitively on the magnitude of ι . The answer might, perhaps, be found in a change of the orientation of convective cells possibly generated by the presence of the wire suspending the emitter. The total flux found on both sides of the detector is only about 10 % of the input ion flux. The flux reaching the wall of the vacuum chamber should be negligibly small as the flux decreases sharply in the radial direction (see fig. 11). There use has been made of the radial splitting of the sensitive segments of the particle detector. These results probably find their explanation in a larger recombination on the emitter and, preferentially, on the suspending wire than assumed. This is supported by the observation that there is only a small change of the signal detected by the particle detector if a probe is introduced into the plasma. Further experimental investigations of this effect are planned. If only the main magnetic field is switched on (τ = 0) the plasma is lost preferentially in the outward direction (Fig.12). In that case no signal is found on the inner segments of the detector.

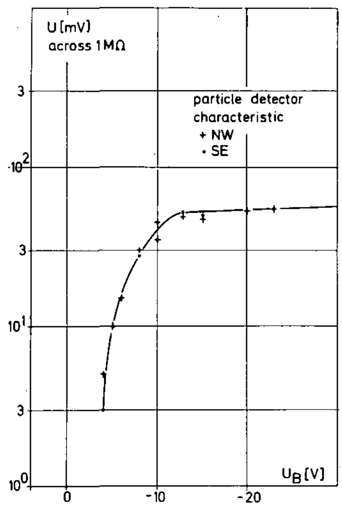

FIG.10. Characteristic of the particle detector. The electron-collecting grids were always electrically connected with the wall of the vacuum chamber.

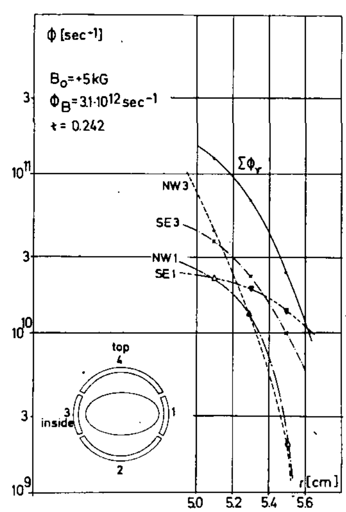

FIG.11. Radial dependence of the flux collected by the particle detector. Use has been made in this case of the radial splitting of the individual segments.

In fig. 13 a profile of particle density is shown for a case with the emitter positioned 7 mm off the magnetic axis. The profile was measured by probe and by resonance fluorescence without the probe. One observes fair agreement between both curves. The dip in the centre is produced by the probe acting as a particle sink and could be observed by resonance fluorescence+) as well.

The measured amplitude of the fluctuations is less than 1 % of the total density if t is carefully adjusted for optimum conditions. This holds for regions around the plasma centre and for a cut-off frequency of the probe circuit of 500 kHz (see fig. 14). No

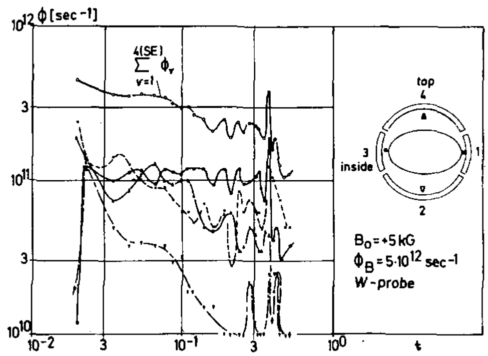

FIG. 12. Fluxes to the individual segments of the particle detector and the sum of these fluxes vs. t for B_0 = 5 kG and $\Phi_B = 5 \times 10^{12}\,s^{-1}$. In this case a probe was introduced into the plasma.

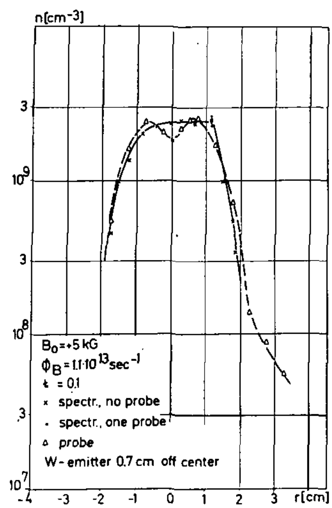

FIG. 13. Profile of particle density measured by resonance fluorescence without any probe being present within the plasma except for one point showing the reduction in central density when introducing the probe and by probe. The position of the emitter was 7 mm off axis, B_0 = 5 kG, $\Phi_B = 1.1 \times 10^{13}\,s^{-1}$.

+) An additional result of this investigation is that this type of probes, if evaluated as described above, shows close agreement with the density measured by resonance fluorescence not only in Q-machines but also in closed configurations outside the emitter region.

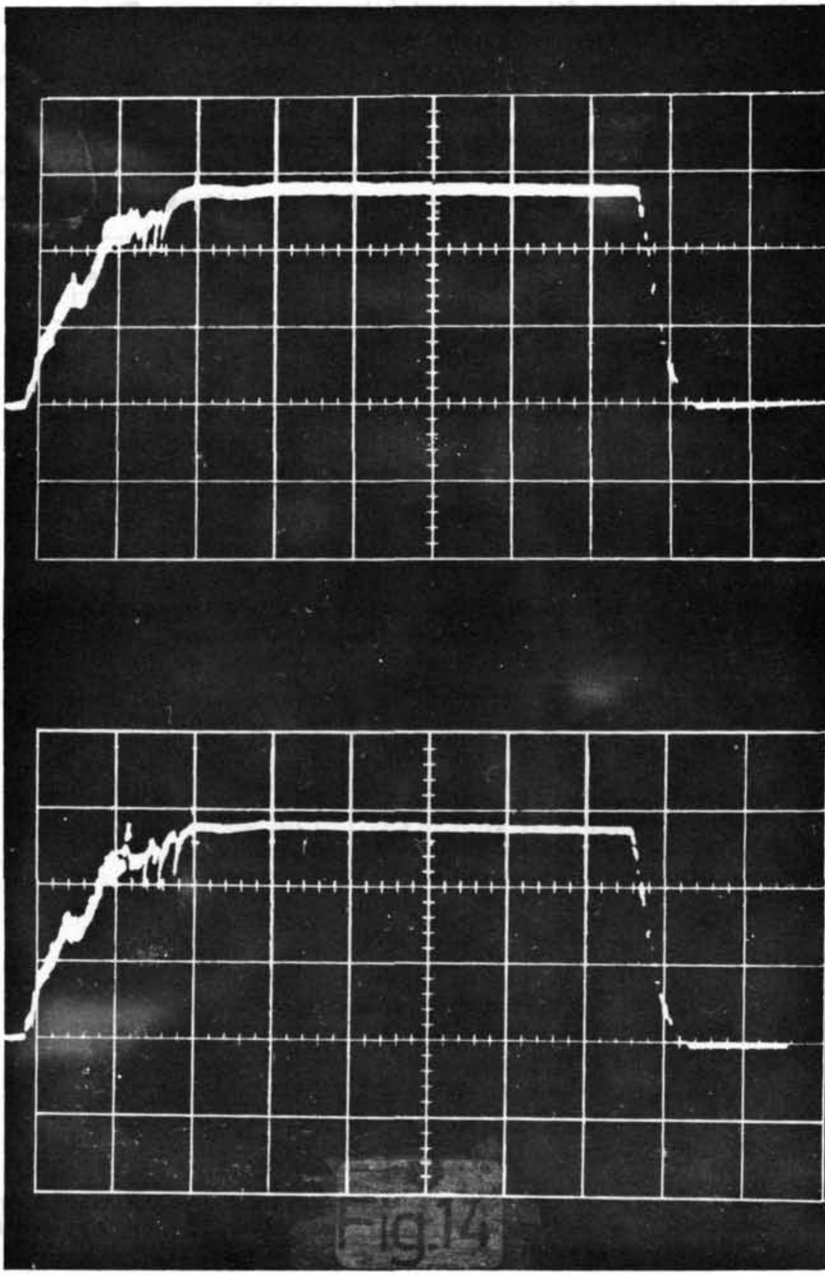

FIG. 14. Example of the probe signal for a case with carefully adjusted ϵ. The sweep is 5 s per division. On the lower picture a low pass filter with a cut-off frequency of 30 kHz has been used. The upper picture is taken without such a filter, the cut-off frequency of the probe circuit being 500 kHz. Small residual oscillations observed in this case are identified as pick up from a radio station located nearby and operating at ν = 800 kHz.

particular investigations were performed on fluctuations in the region of steep density gradients. For values of ι other than optimum, low-frequency fluctuations of 0.1 - 500 Hz were observed which fall into the same frequency range as the current fluctuations of the generators. Therefore, these fluctuations are believed to be fluctuations of the confinement properties with fluctuating ι . This is supported by the additional observations that:
a) quiescent plasma conditions could also be found for n being a minimum as function of ι , and b) rapid changes of the orientation of the loss fluxes as indicated by the signals of the particle detector were observed.

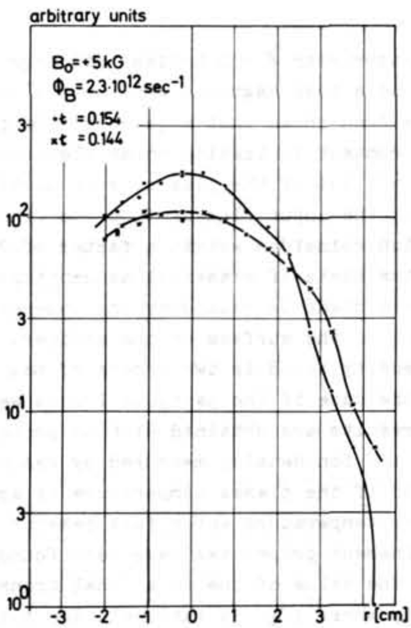

FIG.15. Comparison of two profiles of particle density for identical B_0 = 5 kG and $\Phi_B = 2.3 \times 10^{12}\ s^{-1}$ but for different ι being 0.154 and 0.144 (~ 1/7) respectively.

In fig. 15 two profiles of particle density are compared, one taken for n being a maximum (ι = 0.154) and one for the adjoining minimum (ι = 0.144 ~ 1/7). One sees that the profiles are quite different in shape, so that fluctuations in ι should yield considerable fluctuations in n. Some of the profiles taken preferentially at higher densities were integrated over the plasma volume and this number divided by the input flux. The confinement time obtained this way is of the order of 1 sec which is about a factor of 2 shorter than that calculated. Again this might be caused by a recombining flux larger than assumed in the calculations.

For the low temperature of the emitter and the parameters present in this experiment no strong dependence of the peak ion density on the correction fields is expected according to our earlier explanations [2]. This is in agreement with observations carried out at $B = 5$ kG and $\Phi_B > 1.9 \cdot 10^{12}$ sec^{-1}.
The highest density investigated is just below the limit where, even for larger values of ι, the ion inertia, which has been neglected in the calculations, should strongly influence the confinement properties and therefore the peak density [6].

Summary

A circular stellarator with $\ell = 2$ helical windings yielding practically no shear but a mean magnetic well of 3 % depth has been built. It has been shown that a quiescent Ba plasma can be established by contact ionization on an electron-emitting Ta sphere covering only 0.1 % of the plasma cross section. Over 2 orders of magnitude of the input flux of ions one finds an $n \sim \sqrt{\Phi_B}$ dependence which coincides within a factor of 2 with curves calculated on the basis of classical assumptions only. The residual discrepancy might be caused by the underestimation of the flux recombining on the surface of the emitter. For $\Phi_B = 10^{12}$ sec^{-1} the density found is two orders of magnitude higher than would be the case if the particle losses were governed by "pump-out". These results are obtained with no probe present within the plasma and the ion density measured by resonance fluorescence, they hold if the plasma temperature is assumed to be equal to the emitter temperature which fact remains still to be measured. The confinement properties have been found to be strongly dependent on the value of the rotational transform, showing minima probably where $1/\iota$ is rational. The maxima in between follow closely the theoretical curve if one uses $U_{th} = 0.18$ V which is close to the actual temperature of the emitter. Confinement times of the order of 1 sec are observed. Finally, it should be mentioned once more that the ionizing properties of Tantalum surfaces require detailed investigation as considerable deviations from the "equilibrium model" seem to be indicated.

Acknowledgement

We wish to thank Prof. A. Schlüter for many helpful discussions. For technical help, for scientific discussions, numerical calculations, evaluations and drawings we are indebted to so many people that it is impossible to enumerate all of them individually.

Without their enthusiastic help it would have been impossible to perform this work in such a short time. Special thanks are due to the house Osram, and the DVL Institut für Raumsimulation, which provided us with high-pressure Xenon lamps in a very critical phase of the experiment.

REFERENCES

[1] ECKHARTT, D., v. GIERKE, G., GRIEGER, G., in Plasma Physics and Controlled Nuclear Fusion Research (Proc. Conf. Culham, 1965) 2, IAEA, Vienna (1966) 719.

[2] ECKHARTT, D., v. GIERKE, G., GRIEGER, G., Institut für Plasmaphysik Report IPP 2/52 (1966).

[3] BERKL, E., ECKHARTT, D., v. GIERKE, G., GRIEGER, G., Phys. Rev. Letters 17 (1966) 906.

[4] PFIRSCH, D., SCHLÜTER, A., Max-Planck-Institut Report MPI-PA-7/62.

[5] BERKL, E., v. GIERKE, G., GRIEGER, G., Institut für Plasmaphysik Report IPP 2/69 (1968).

[6] v. GIERKE, G., GRIEGER, G., v. HAGENOW, K.U., Institut für Plasmaphysik Report IPP 2/70 (1968).

[7] to be published.

[8] to be published.

[9] HASHMI, M., van der HOUVEN van OORDT, A.J., WEGROWE, J.-G., 2nd European Conf. on Controll. Fusion and Plasma Physics, Stockholm (1967). (To be published in Plasma Physics).

[10] La FRAMBOISE, J.G., Institute for Aerospace Studies, University of Toronto, UTIAS Rep. No.100.

[11] RYNN, N., HINNOV, E., JOHNSON, L.C., Rev. scient. Instrum. 38 10 (1967) 1378.

[12] HIRSCHBERG, J.H., Journal Appl. Opt. 4, No.6 (1965) 759.

[13] D'ANGELO, N., DIMOCK, D., FUJITA, J., GRIEGER, G., HASHMI, M., STODIEK, W., in Ionization Phenomena in Gases, (Proc. 6th Int. Conf., Paris, 1963) 1 (1964) 399.

DISCUSSION

R.M. SINCLAIR: Is the dependence on rotational transform that you observe consistent with your earlier results (obtained two years ago) concerning the dependence of confinement on transverse field?

G. GRIEGER: The results are consistent with our earlier ones. Owing to the relatively low temperature of the emitter (2150°K), there should be only a weak dependence of the confinement on transverse fields, as long as the displacement of the magnetic axis does not become large compared with the diameter of the emitter.

S. YOSHIKAWA: Existing experimental data do not show L^2 dependence above $L/2\pi = 0.1$. Although recombination may explain this behaviour, we cannot at present rule out the additional loss. Do you agree?

G. GRIEGER: Yes, I agree. However, I would like to point out that, under the conditions of the experiment, the factor by which the cross-field losses might exceed resistive diffusion cannot be a very large one (as indicated in the figures).

S. YOSHIKAWA: What is the agreement or the difference between calculated and experimental density profiles?

G. GRIEGER: The density profile is determined by recombination on the support of the emitter and diffusion across the field. However, the recombination is difficult to take into account accurately. Estimates show rough agreement with the observed density profile.

A. GIBSON: What limit can you place on the amplitude of the fluctuations observed?

G. GRIEGER: If ι is properly adjusted to optimum conditions, $\Delta n/n$ should not exceed about 1%.

ИССЛЕДОВАНИЕ КВАЗИПОСТОЯННЫХ ЭЛЕКТРИЧЕСКИХ ПОЛЕЙ И ФЛУКТУАЦИЙ ПЛАЗМЫ В СТЕЛЛАРАТОРЕ Л-1

М.С.БЕРЕЖЕЦКИЙ, С.Е.ГРЕБЕНЩИКОВ,
И.А.КОССЫЙ, Ю.И.НЕЧАЕВ, М.С.РАБИНОВИЧ,
И.С.СБИТНИКОВА и И.С.ШПИГЕЛЬ
ФИЗИЧЕСКИЙ ИНСТИТУТ им.П.Н.ЛЕБЕДЕВА
АН СССР, МОСКВА,
СССР

Abstract — Аннотация

INVESTIGATION OF QUASI-STATIONARY ELECTRIC FIELDS AND PLASMA FLUCTUATIONS IN THE L-1 STELLARATOR. The authors present the results of L-1 stellarator experiments relating to the quasi-stationary electric fields and the fluctuations in a low-density collisionless plasma produced by external injection. The experiments bring out the important role played by the structure of the magnetic surfaces in plasma diffusion in the stellarator. The importance of the fine structure of the surfaces is established. The appearance of magnetic islands affects the macroscopic parameters of the plasma (containment time, potential). The plasma lifetime depends to a large extent on the rotational transform of the field lines. Investigation of the fluctuations shows that density and potential fluctuations with frequencies $f < 100$ kc/s occur in the plasma. The frequency spectrum and modes of these fluctuations are a function of the rotational transform of the field lines. Measurements of the radial plasma flux due to the fluctuations (based on the value of $\langle \tilde{n} \tilde{E} \rangle$) do not indicate any connection between the observed plasma losses and the fluctuations. The measurements show that in the case of closed magnetic surfaces the plasma acquires negative potential with respect to the chamber walls. The strength of the potential depends on the magnetic field intensity and on the rotational transform of the field lines. The observed correlation between plasma potential and plasma lifetime in the trap suggests that there is a particle escape mechanism associated with the absence of complete plasma equilibrium in the magnetic field of the stellarator.

ИССЛЕДОВАНИЕ КВАЗИПОСТОЯННЫХ ЭЛЕКТРИЧЕСКИХ ПОЛЕЙ И ФЛУКТУАЦИЙ ПЛАЗМЫ В СТЕЛЛАРАТОРЕ Л-1. Приводятся результаты экспериментов, выполненных на стеллараторе Л-1, по исследованию квазипостоянных электрических полей и флуктуаций в бесстолкновительной плазме низкого давления, создаваемой методом внешней инжекции. Эксперименты показали существенную роль структуры магнитных поверхностей в диффузии плазмы в стеллараторе. Установлено существенное значение тонкой структуры поверхностей. Появление так называемых магнитных розеток или островов сказывается на макроскопических параметрах плазмы (время удержания, потенциал). Время жизни плазмы зависит от величины вращательного преобразования силовых линий. Исследование флуктуаций показало, что в плазме существуют колебания плотности и потенциала с частотами $f < 100$ кгц. Спектр частот и моды возникающих колебаний являются функцией вращательного преобразования силовых линий. Измерения радиального потока плазмы вследствие флуктуаций (по величине $\langle \tilde{n} \tilde{E} \rangle$ не позволили связать наблюдаемые потери плазмы с наличием флуктуаций. Измерения показали, что в случае существования замкнутых магнитных поверхностей плазма принимает отрицательный потенциал относительно стенок камеры. Величина установившегося потенциала зависит от напряженности магнитного поля и величины вращательного преобразования силовых линий. Наблюдаемая корреляция между величиной потенциала плазмы и ее временем жизни в ловушке позволяет предположить, что существует какой-то механизм ухода частиц, связанный с отсутствием полного равновесия плазмы в стеллараторном магнитном поле.

1. ВВЕДЕНИЕ

В экспериментах [1, 2], выполненных ранее на стеллараторе "Ливень-1", исследовалось влияние винтовых магнитных полей на удержание плазмы низкого давления ($\beta \ll \beta_{\text{крит.}}$). Плазма создавалась методом внешней инжекции и являлась бессоударительной – длины пробега частиц были порядка 100 периметров установки. В этих экспериментах было показано существенное влияние винтовых полей на удержание плазмы. Наряду с этим было установлено, что время жизни плазмы в ловушке не определяется классической столкновительной диффузией, превышая ее приблизительно в 10^3 раз. Однако в отличие от экспериментов на стеллараторах С, В-3, где исследовалось удержание сравнительно плотной плазмы [3 – 5], создаваемой методом омической ионизации и нагрева, время жизни плазмы в установке "Ливень" не определяется формулой Бома для аномальной диффузии. Хотя в наших экспериментах [2] время жизни зависит линейно от напряженности магнитного поля, но оно также существенным образом является функцией угла вращательного преобразования ι силовых линий. При $\iota \simeq \pi$ коэффициент диффузии становится почти на порядок меньше бомовского.

Данная работа посвящена дальнейшему изучению удержания бесстолкновительной плазмы низкого давления и исследованию различных процессов, которые, в принципе, могли бы быть ответственными за уход плазмы из ловушки.

Одна из возможных причин аномальной диффузии плазмы в магнитном поле связана с раскачкой в плазме неустойчивостей из-за наличия градиента плотности и температуры. В наших условиях, когда частоты столкновений невелики ($\nu_e \ll k_z\nu_{Te}$, $\omega > \nu_i$), можно ожидать, по-видимому, развития лишь бесстолкновительных дрейфовых неустойчивостей. Имеющийся в стеллараторе шир $\theta = (r\Delta\iota/L) \sim 10^{-2}$ достаточен для подавления крупномасштабных высокочастотных ($\omega > k_z\nu_{Te}$) колебаний $\left(\theta > \frac{\rho_i}{a}\sqrt{\frac{m}{M}},\ \frac{a}{R}\sqrt{\frac{m}{M}}\right)$. Однако данной величины шира недостаточно для подавления низкочастотных колебаний в области $k_z\nu_{Ti} < \omega < k_z\nu_{Te}$, поскольку $\theta < (\rho_i/a)$. В связи с этим представляет несомненный интерес изучение флуктуаций в плазме, удерживаемой в стеллараторном магнитном поле.

Возникающие в плазме квазипостоянные электрические поля, их знак и величина, по-видимому, однозначно связаны с условиями удер-

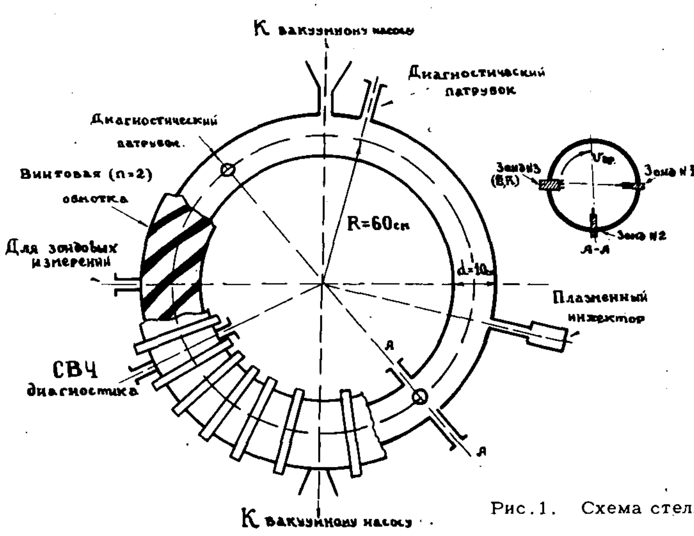

Рис.1. Схема стелларатора "Ливень-1".

жания заряженных частиц в ловушке. Если изучение флуктуаций в плазме может ответить на вопрос, не являются ли неустойчивости причиной аномально быстрого ухода плазмы из стелларатора, то изучение квазипостоянных полей, вероятно, поможет понять, не связан ли такой уход с отсутствием равновесия плазмы в магнитном поле. В настоящее время обе причины являются, по-существу, равновероятными, поскольку исследования этих вопросов на всех существующих стеллараторах находятся в начальной стадии.

В данной работе содержатся результаты экспериментов по изучению квазипостоянных электрических полей и флуктуаций в плазме низкого давления, создаваемой методом внешней инжекции и их связи с временем жизни плазмы. Эксперименты проводились на установке "Л-1", являющейся двухзаходным ($l = 2$) стелларатором, параметры и конструкция которого приведены в работе [6]. Параметры плазмы те же, что описаны в работе [2] (начальная плотность плазмы $n_0 \sim 5\cdot 10^{10}$, $T_e \sim 5 \div 10$ эв). На рис.1 приведено схематическое устройство стелларатора Л-1 и размещение диагностической аппаратуры.

2. ИССЛЕДОВАНИЕ ФЛУКТУАЦИЙ ПЛАЗМЫ В СТЕЛЛАРАТОРЕ

Уже в прежних экспериментах на стеллараторе Л-1 было установлено [2], что в распадающейся плазме низкого давления возникают низкочастотные колебания, однако подробного изучения их не проводилось. Ниже излагаются результаты дальнейших экспериментов по изучению характера возникающих колебаний (амплитуд, мод и частотных спектров).

Измерения колебаний плотности проводились с помощью одиночных ленгмюровских зондов диаметром $d = 0{,}1$ мм и длиной $l = 2 \div 5$ мм. Для наименьшего возмущения плазмы зондами измерения проводились обычно по ионному току насыщения. Анализ спектра колебаний проводился с помощью специальной электронно-оптической системы [7], позволяющей по полученным осциллограммам получать спектр одиночного процесса.

Проведенные измерения показали, что через некоторое время после инжекции в плазме раскачиваются низкочастотные колебания, верхняя частота спектра которых лежит в области 100 кгц. При этом отсутствуют сколько-нибудь заметные высокочастотные колебания в полосе частот до 5 Мгц.

Для того чтобы оценить поперечные размеры возникающих в плазме флуктуаций, измерения проводились одновременно двумя зондами, расположенными в одном сечении камеры (рис.1). Зонд №1 длиной 5 мм располагался на горизонтальном радиусе сечения с внешней стороны тора, в точке, где наблюдается максимальная амплитуда колебаний при данном значении величины ϵ[1]. Зонд №2 длиной 2 мм помещался с нижней стороны тора на угловом расстоянии 90° от первого зонда и перемещался вдоль малого радиуса тора в вертикальном направлении с шагом 2 мм. Измерения показали, что существует область с радиальной шириной около 10 мм, в которой сигналы с обоих зондов хорошо совпадают друг с другом, но сдвинуты один относительно другого по фазе.

---

[1] Параметр ϵ является отношением амплитуды основной гармоники винтового поля $H_{2\perp}$ к величине продольного поля на оси тора H_0 и связан следующим образом с углом преобразования силовых линий $\iota \simeq \pi N \epsilon^2 (1 + 2\alpha^2 r^2)$, где $N = 7$ – число шагов винтовой обмотки на длине тора, а $\alpha = (2\pi/L_\perp) \sim 0{,}12$ – величина, обратная шагу винтовой обмотки $L_\perp$.

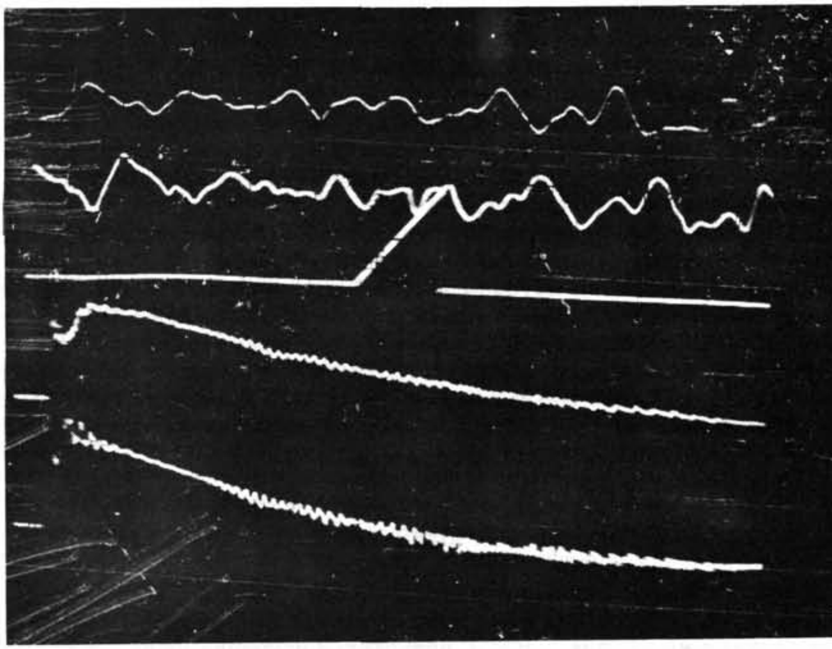

Рис.2. Осциллограммы колебаний плотности на двух азимутах ($\Delta\varphi = 90°$) в одном сечении камеры H_0 = 5 кэ: 1,4 – ионный ток зонда № 1; 2,5 – ионный ток зонда № 2; 3 – момент включения быстрой развертки.
r_1 = 15 мм; r_2 = 17 мм.

На рис.2 приведена типичная осциллограмма зондовых сигналов при $\epsilon = 0{,}33$. На 4 и 5 лучах осциллографа – зондовые сигналы при длительности развертки 2,5 мсек. На 1 и 2 лучах – участок зондового сигнала спустя 1,2 мсек после момента инжекции (длительность развертки 250 мксек). На третьем луче показан момент включения быстрой развертки. Измеряя сдвиг сигналов во времени, можно оценить азимутальную фазовую скорость флуктуаций и направление их распространения. На рис.3 приведена серия совмещенных по фазе осциллограмм. Поскольку сигналы существенно не синусоидальны и имеют характерные особенности, в большинстве случаев совмещение сигналов по фазе не представляло труда. Сдвиг сигналов по времени в среднем равен 20 мксек. Поскольку размеры большого зонда (5 мм) соизмеримы с радиальными размерами области корреляции ($\approx$ 10 мм), на нем происходило некоторое пространственное усреднение колебаний по сравнению с зондом № 2, что видно по осциллограммам рис.2 и 3.

Вычисленная азимутальная фазовая скорость колебаний лежит в пределах $1 \div 1{,}5 \cdot 10^5$ см/сек, а направление их распространения совпадает с направлением ларморовского вращения электронов. Оценка величины скорости ларморовского дрейфа для нашего случая $V_\perp = cT_e/eHL_\perp$, где $L_\perp$ – радиальный размер неоднородности плазмы, дает также значение $1 \div 2 \cdot 10^5$ см/сек, что не противоречит предположению, что наблюдаемые флуктуации связаны с возбуждением дрейфовых волн. Однако такой же эффект может иметь место при вращении плазмы в скрещенных электрическом и магнитном полях в присутствии каких-либо неоднородностей

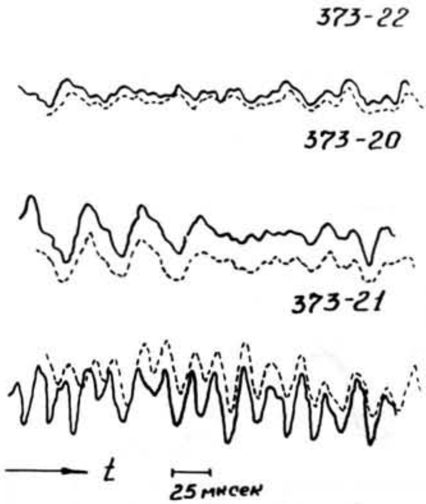

Рис.3. Осциллограммы с зондов № 1 и № 2, совмещенные по фазе. Сплошная кривая — зонд № 1.

плотности по сечению. Та же величина скорости азимутального дрейфа может быть получена при величине радиального электрического поля напряженностью ~5 в/см. Как будет показано ниже, в нашем случае действительно существуют радиальные электрические поля напряженностью несколько вольт на сантиметр.

Из осциллограмм рис.2 и 3 видно, что сдвиги по времени между сигналами обоих зондов оказываются соизмеримыми с характерными временами флуктуаций, т.е. азимутальная протяженность неоднородности соизмерима с расстоянием между зондами (~2 см). Периоды появления характерных флуктуаций при $\epsilon = 0{,}33$ оказываются в два или четыре раза меньше периода вращения, соответствующего измеренной скорости дрейфа, т.е. основными методами возмущения плотности являются $m = 2$ и $m = 4$. Это обстоятельство может быть объяснено, если учесть, что при $\epsilon = 0{,}33$ средний угол преобразования поворота $\iota \sim \pi$ и силовые линии замыкаются через два оборота. На рис.4 приведен спектр частот флуктуации, усредненный по 9 осциллограммам флуктуаций плотности, полученных в идентичных условиях. Видно, что имеются две области частот ($f_2 \simeq 25$ Кгц и $f_4 \simeq 50$ Кгц), соответствующих определенным выше модам колебаний.

Подобные измерения были проведены и при других значениях преобразования поворота: $\iota = \pi/2 (\epsilon = 0{,}27)$ и $\iota = 4\pi/3 (\epsilon = 0{,}39)$. При этом также наблюдались радиальные области, в которых оба зонда регистрировали идентичные, но сдвинутые по времени колебания. В отличие от случая $\epsilon = 0{,}33$ основными модами наблюдаемых колебаний были соответственно четвертая и третья.

Таким образом, видно, что структура магнитного поля оказывает существенное влияние на характер возникающих колебаний. Радиальный размер флуктуаций ~1 см, а азимутальный — порядка нескольких сантиметров и меняется в зависимости от моды возбуждаемых колебаний. Поскольку номер моды связан с резонансными значениями угла преобразования поворота, можно предположить, что продольная длина

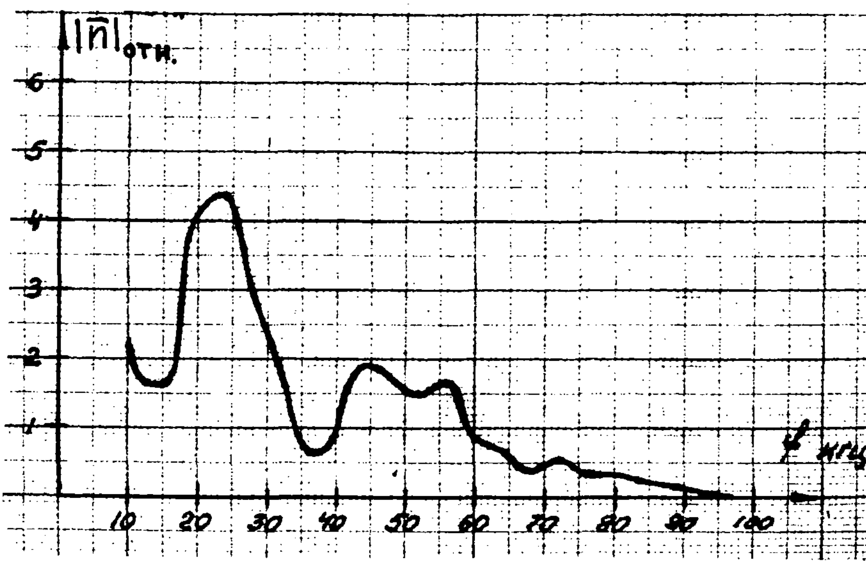

Рис.4. Спектр колебаний плотности плазмы.

колебаний велика и сравнима с продольными размерами системы, т.е. наблюдаемые низкочастотные колебания плотности являются длинноволновыми.

Колебания изучались при различных значениях напряженности магнитного поля. Как показали измерения, хотя характер спектра несколько меняется, верхняя частота колебаний с точностью $20 \div 30\%$ оставалась неизменной при изменении напряженности магнитного поля в 3 раза — от 2,5 до 7,5 кэ. Максимальная амплитуда колебаний плотности не превосходила $10 - 20\%$.

Флуктуации электрического поля в плазме также являются низкочастотными. Пространственная структура этих флуктуаций и соотношение между радиальной E_r и азимутальными E_φ составляющими вектора напряженности электрического поля (точнее, между нормальной по отношению к магнитной поверхности E_n и тангенциальной E_t составляющими поля) еще не исследованы. Амплитуда наблюдаемых колебаний $\tilde{E}$ не превышает 1 в/см.

На основании выполненных экспериментов пока не представляется возможным сделать заключение о природе возникающих колебаний. Наличие радиального электрического поля, неоднородного по радиусу, приводящего к общему вращению плазмы, затрудняет идентификацию существующих колебаний.

Основной вопрос, возникающий при исследовании колебаний плазмы в ловушке, заключается в том, в какой мере наблюдаемые флуктуации плазмы ответственны за аномальную диффузию плазмы.

Изучение колебаний плазмы в течение длительного времени (несколько месяцев) показало, что их амплитуда не остается постоянной. Она изменяется со временем вследствие каких-то пока еще не выясненных причин. Однако при этом не наблюдалось сколько-нибудь заметного изменения времени жизни плазмы.

Для количественного определения диффузионного потока частиц, вызванного колебаниями плазмы, были проведены измерения величины $\langle \widetilde{E}_\varphi \widetilde{n} \rangle$ на одном азимуте сечения камеры с внутренней стороны тора. Два зонда длиной ~2,5 мм, расположенных друг от друга на расстоянии 5 мм, измеряли азимутальную составляющую флуктуирующего электрического поля $\widetilde{E}_\varphi$. Между ними, но на расстоянии 5 мм по оси Z, от плоскости, в которой лежат эти зонды, находился третий зонд, измеряющий флуктуации плотности плазмы $\widetilde{n}$. Для колебаний с продольной длиной волны, большей, чем 5 мм, можно было считать, что измерения плотности и электрического поля проводятся в одной точке.

Зонды могли перемещаться по радиусу. В результате обработки полученных осциллограмм определялся радиальный поток $q_r = 10^8 \frac{\langle \widetilde{E}_\varphi \widetilde{n} \rangle}{H}$. Измеренная величина потока не может объяснить наблюдаемого в эксперименте времени жизни плазмы и должна была приводить к временам удержания, примерно на порядок превышающие реально наблюдаемые. Окончательный ответ на вопрос об общем потоке частиц, вызываемом колебаниями, можно будет дать лишь после выполнения измерений на различных азимутах в плоскости сечения камеры. Строго говоря, измерения должны быть выполнены по некоторому замкнутому контуру, охватывающему плазму.

На основании этих предварительных экспериментов можно высказать предположение о том, что потери частиц, вызванные наблюдаемыми в плазме флуктуациями, не являются, по-видимому, определяющими и существует какая-то другая причина аномальной диффузии плазмы в стеллараторе.

3. КВАЗИПОСТОЯННЫЕ ЭЛЕКТРИЧЕСКИЕ ПОЛЯ И ВРЕМЯ ЖИЗНИ ПЛАЗМЫ

Измерение потенциала плазмы производилось с помощью одиночных зондов. "Плавающий" потенциал плазмы измерялся обычными цилиндрическими зондами. Из обработки их зондовой характеристики возможно получение также истинного потенциала пространства. Однако, из-за сильного влияния магнитного поля на форму зондовой характеристики, точность таких измерений становится недостаточной. Поэтому для этих измерений потенциала был применен эмитирующий зонд. Суть метода заключается в следующем. В заданной точке размещается вольфрамовая нить, используемая в холодном или накаленном состоянии в качестве зонда. Этот зонд, во втором случае, при определенном соотношении разности потенциалов зонд-плазма, может эмитировать электроны. Снимаются характеристики холодного и накаленного зонда. Точка разветвления обеих характеристик определяет потенциал плазмы.

Этот метод измерения потенциала плазмы в магнитном поле является, по-видимому, более надежным и точным, чем его определение по точке перегиба зондовой характеристики. Для того чтобы зонд не возмущал плазмы, он постоянно был "плавающим", и лишь в момент измерений на него импульсно подавалось напряжение. При работе зонда в эмитирующем режиме вблизи него создавалось локальное возмущение магнитного поля, обусловленное током накала. Однако из-за малости возникающего магнитного поля $< 10^{-3} H_0$ и его локальности, оно практически не оказывало влияния ни на форму магнитных поверхностей стелларатора, ни на движение частиц плазмы вблизи зонда.

Измерения потенциала плазмы в стеллараторе показали, что плазма заряжена отрицательно, причем абсолютная величина потенциала плазмы относительно стенок вакуумной камеры достигает величины ~25 – 30 в. Установление потенциала происходит за время, соизмеримое с длительностью заполнения ловушки плазмой, ≃100 мксек. Его спад происходит существенно медленнее. На рис.5 приведены зависимости от времени

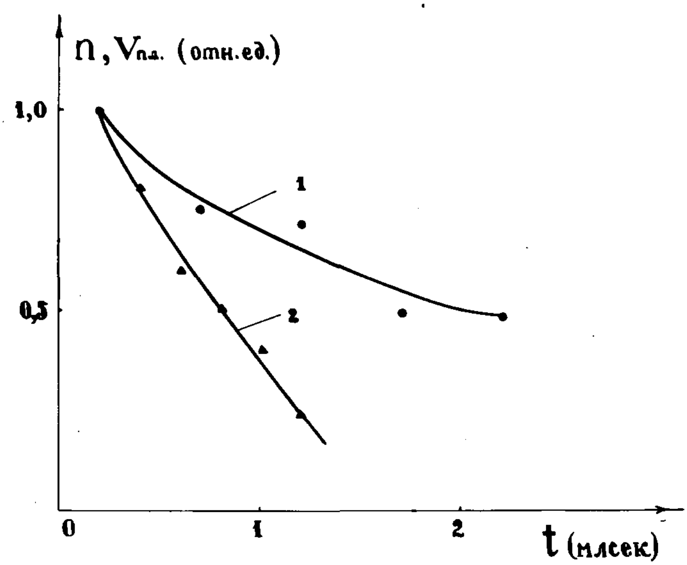

Рис.5. Измерение во времени концентрации плазмы (кривая 2) и плазменного потенциала (кривая 1); H_0 = 3,7 кэ; ϵ = 0,39.

относительных величин плотности и потенциала в центральной части камеры при H = 3,7 кэ и ϵ = 0,39. Из рис.5 видно, что постоянная спада потенциала приблизительно в 3 раза больше постоянной спада плотности, т.е. за время жизни плазмы потенциал меняется относительно слабо. Распределения потенциала по радиусу показывают, что его абсолютная величина спадает от центра камеры к стенкам, т.е. в плазме существует квазипостоянное радиальное электрическое поле напряженностью несколько вольт на сантиметр.

Таким образом, в стеллараторе в начальные моменты времени в результате преимущественного ухода ионов возникает электрическое радиальное поле определенной величины. В дальнейшем устанавливается практически амбиполярный уход частиц плазмы.

Представляло определенный интерес исследовать, как зависит возникающий потенциал плазмы от свойств удерживающего магнитного поля. В связи с этим были проведены измерения зависимости потенциала плазмы от напряженности магнитного поля H_0 и величины ϵ.

На рис.6 приведена зависимость потенциала плазмы вблизи оси тора (r = 10 мм) от напряженности продольного магнитного поля H_0(ϵ=0,39) через 200 мксек после инжекции. Как видно из графика, величина потенциала увеличивается с ростом магнитного поля. Распределение потенциала по сечению при этом меняется незначительно. Подобные зависимости сохраняются для всех моментов времени. Заметим, что время жизни плазмы также возрастает с увеличением магнитного поля [2]. Зави-

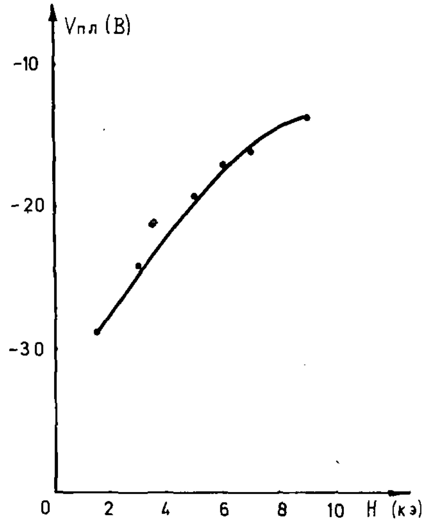

Рис.6. Зависимость потенциала плазмы от напряженности продольного магнитного поля; $\epsilon = 0{,}39$; $r = 10$ мм.

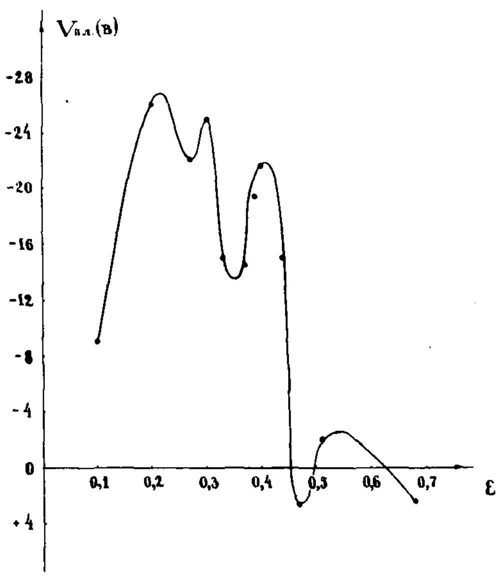

Рис.7. Зависимость плазменного потенциала от ϵ, $H_0 = 4$ кэ.

симость потенциала плазмы от параметра ϵ приведена на рис.7. Вначале с увеличением винтовых полей происходит рост потенциала плазмы, затем он замедляется. На кривой, в области резонансных значений ϵ при $\iota = (k/m)2\pi$; k и m — целые числа, имеются характерные провалы. При $\epsilon = 0{,}44$ потенциал начинает резко уменьшаться и затем меняет свой знак. При больших значениях ϵ имеются два участка, где потенциал плазмы положителен. Как показали измерения [8], именно в этих областях значений винтовых полей внутри камеры отсутствуют замкнутые магнитные поверхности. В отсутствие винтовых полей ($\epsilon = 0$) потенциал плазмы также положителен.

В том случае, когда внутри камеры стелларатора существуют замкнутые магнитные поверхности, потенциал плазмы всегда отрицателен и, наоборот, при отсутствии замкнутых магнитных поверхностей плазма принимает положительный потенциал, поскольку в данном случае имеется преимущественный уход электронов вдоль силовых линий.

В целом зависимость величины потенциала от ϵ напоминает полученную ранее [2] кривую зависимости времени жизни плазмы от этого параметра. Впоследствии метод СВЧ-измерения плотности на стелларa-

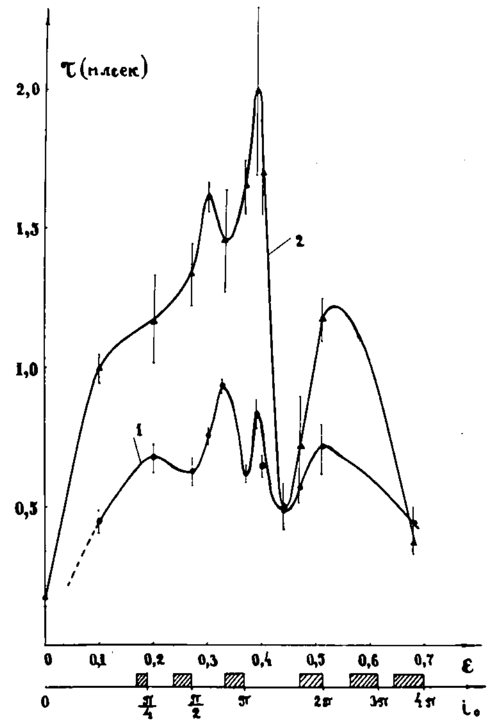

Рис.8. Зависимость времени удержания плазмы от величины ϵ: кривая 1 – H_0 = 4 кэ; кривая 2 – H_0 = 7 кэ.

торе Л-1 был модернизирован, что позволило существенно увеличить точность и надежность измерения времени жизни плазмы. Результаты более детальных измерений зависимости времени удержания плазмы от величины винтового поля приведены на рис.8. Наряду со шкалой ϵ, на рисунке по оси ординат отложен соответствующий угол преобразования поворота на оси стелларатора ι_0. Заштрихованные области показывают расчетные значения ϵ для $0 \leq r \leq 3$, при которых происходит вырождение магнитных поверхностей и замыкание силовых линий самих на себя. В этих случаях при наличии соответствующих (резонансных) возмущений происходит расщепление магнитных поверхностей и образование так называемых розеток или магнитных островов. Размеры розеток определяются амплитудой соответствующих возмущений магнитного поля. На графике отмечены лишь местоположения резонансов низших порядков m = 1, 2, 4. Из рис.8 видно, что время жизни в области $\epsilon = 0 \div 0{,}4$, т.е. там, где существуют замкнутые магнитные поверхности, имеет тенденцию к росту. При $\epsilon = 0{,}47$, вследствие резонанса первого рода ($\iota = 2\pi$) происходит сильное возмущение поверхностей. Смещение магнитной оси при этом, по-видимому, настолько велико, что силовые линии, образующие поверхности вблизи оси, начинают пересекать стенки вакуумной камеры и уходят из объема ловушки. При $\epsilon > 0{,}6$ трудно выделить какое-либо одно возмущение, так как за счет возрастания градиента угла прокручивания резонансные области начинают перекрываться и наблюдаемое здесь разрушение поверхностей может являться следствием воздействия нескольких резонансных возмущений. В тех областях *значений ϵ ($\epsilon \sim 0{,}47$ и $\epsilon > 0{,}6$), где время жизни плазмы резко уменьша*ется и не зависит от напряженности магнитного поля, в этих условиях время жизни плазмы соответствует нескольким временам пролета ионов вдоль оси системы. Это согласуется с результатами магнитных измерений, показывающих уход силовых линий из объема камеры за несколько оборотов.

Провал на кривых в области $\epsilon = 0{,}33 - 0{,}37$ происходит в области резонансов второго рода. Экспериментально [8] было обнаружено, что в этом случае имеет место образование двух розеток на магнитных поверхностях с радиальными размерами $\Delta r \sim 1$ см. Розетки появляются на оси при $\epsilon = 0{,}37$ и затем сдвигаются на радиус ~ 3 см при $\epsilon = 0{,}33$. Заметим, что для такого возмущения магнитных поверхностей достаточно очень незначительных аплитуд возмущающего поля. Так, для случая резонанса второго рода ($m = 2$) амплитуда соответствующей гармоники возмущающего поля $\tilde{H}$ согласно [9] равна $\tilde{H}_2/H_0 = (\Delta r^2/2rL)\,\Delta\iota$, где Δr – размер магнитной ячейки, r – средний радиус ограничивающей магнитной поверхности, L – длина установки, а $\Delta\iota$ – приращение угла прокручивания силовых линий на размер порядка r. Оценка показывает, что для образования в стеллараторе Л-1 наблюдаемых розеток в области второго резонанса достаточно возмущения с амплитудой $\tilde{H}_2 \sim 10^{-4} H_0$. Как видим, столь малые возмущения поля оказывают существенное влияние на макроскопические параметры плазмы.

Провалы на рис.7 и 8 при $\epsilon = 0{,}27$ соответствуют по расчету резонансу 4-го рода $\left(\iota = \frac{2\pi}{4}\right)$, однако при данном ϵ на установке не производилось измерение формы магнитных поверхностей и размер магнитных розеток не известен.

При магнитных измерениях [8] были обнаружены розетки на внешних поверхностях при резонансе третьего рода $\epsilon = 0{,}39$. Ширину этих розеток не удалось замерить экспериментально, поскольку она, по-видимому, была меньше или порядка размеров измерительного зонда. В этих исследованиях не удалось обнаружить заметное влияние этого возмущения магнитных поверхностей на время жизни плазмы. Не наблюдается также влияния третьего резонанса при $\iota = 2\pi/3$. Необходимо отметить, что провалы на кривых $\tau(\epsilon)$ и $V(\epsilon)$ не совсем точно соответствуют положению резонансов на шкале ϵ, рассчитанных теоретически и подтвержденных по магнитным измерениям с электронным пучком. Так, например, провал на рис.8 в области резонанса первого рода ($\epsilon \sim 0{,}47$) несколько смещен в область меньших углов преобразования поворота. Положение провала при резонансе второго рода меняется при измерении напряженности магнитного поля H_0. Форма кривых зависимости потенциала от ϵ (рис.7) для различных моментов времени также несколько деформируется. Пока не имеется объяснения этого эффекта. Для его выяснения необходимо, по-видимому, проведение более детальных измерений, в частности, с большим количеством точек по ϵ.

Проведенные измерения показывают, что форма стеллараторных магнитных поверхностей оказывает существенное влияние на удерживающие свойства ловушки. Необходимым условием, конечно, является существование замкнутых магнитных поверхностей, ибо поведение плазмы качественно меняется в области разрушенных магнитных поверхностей. Однако тонкая структура магнитных поверхностей, размеры возникающих розеток также оказывают существенное влияние на время удержания плазмы. Как видно из рис.8, появление розеток на магнитных поверхностях, уменьшая время жизни плазмы, нарушает рост времени удержания плазмы с увеличением угла прокручивания и его градиента. Приведенные экспериментальные данные указывают на необходимость увеличения, по крайней мере на порядок, точности создания стеллараторного магнитного поля, доведя ее до величины $(\Delta\tilde{H}/H) < 10^{-5}$.

Связь между временем жизни плазмы и величиной возникающего радиального электрического поля указывает на то, что последнее оказывает существенное влияние на удержание плазмы в ловушке. Величина электрического поля настолько велика, что заметно влияет на движение ионов в ловушке. Так, за счет дрейфа ионов в скрещенных полях для них возникает дополнительный угол прокручивания ι_E, совпадающий по порядку величины с углом преобразования поворота в стеллараторном поле и, в зависимости от знака продольной скорости иона, увеличивающий или уменьшающий угол преобразования, обусловленный винтовыми обмотками. (Так, например, $\iota_E \approx \pm\pi$ при $E \sim 5$ в/см и $H \sim 5$ кэ). То, что величина потенциала плазмы зависит от удерживающих свойств магнитного поля, указывает, что возникающее электрическое поле является в некотором смысле равновесным и необходимым для удержания плазмы.

Попытка расчета равновесного электрического поля в стеллараторе была предпринята в работе [10]. Хотя в работе допущен целый ряд упрощений, в ней было получено, что равновесный потенциал плазмы является функцией напряженности магнитного поля и угла преобразования. Качественно изученные в эксперименте данные не противоречат выводам данной работы.

С другой стороны, пока еще не исследован вопрос о том, является ли вектор напряженности электрического поля нормальным по отношению к магнитным поверхностям и насколько электрические эквипотенциали отличаются от магнитных поверхностей. При несовпадении эквипотенциалей с магнитными поверхностями в плазме появятся дополнительные дрейфы частиц поперек силовых линий. В какой мере эти дрейфы будут скомпенсированы и не приведут ли они к уходу частиц плазмы на стенки, пока еще не ясно. Этот вопрос нуждается в детальном экспериментальном и теоретическом исследовании.

Возникновение в начальные моменты времени квазипостоянного электрического поля, величина которого коррелирует с последующим временем удержания плазмы, и его связь с удерживающими свойствами магнитного поля позволяют высказать предположение, что в данном случае отсутствует истинное равновесие. Если эта гипотеза верна, то, как показывают эксперименты, равновесие плазмы в ловушке уменьшается с ростом напряженности магнитного поля и угла преобразования силовых линий (или его градиента). И, наоборот, наличие розеток на магнитных поверхностях по каким-то причинам ухудшает равновесие плазмы в ловушке.

4. ЗАКЛЮЧЕНИЕ

Эксперименты по удержанию плазмы низкого давления ($\beta \leq 10^{-6}$) в стеллараторе Л-1 показали существенную роль структуры магнитных поверхностей на диффузию плазмы. При этом оказалось важным не только само существование замкнутых поверхностей, но и их тонкая структура. Появление так называемых магнитных розеток или островов сказывается на макроскопических параметрах плазмы (время удержания, потенциал).

Время жизни плазмы в стеллараторе Л-1 зависит от преобразования поворота силовых линий. Оно резко увеличивается с ростом винтовых полей вплоть до углов прокручивания $\iota \simeq \pi/2$, далее за счет появления магнитных розеток при резонансах низшего порядка происходят резкие спады, приводящие к среднему замедлению его роста. Влияние магнитных розеток на диффузию плазмы несколько уменьшается с ростом напряженности магнитного поля.

Исследования показали, что в плазме возникают низкочастотные (порядка десятков килогерц) колебания. Наличие в стеллараторе радиального электрического поля приводит к вращению плазмы как целого со скоростями $\sim 10^5$ см/сек, что затрудняет установить природу возникающих в плазме флуктуаций. Азимутальные моды наблюдаемых колебаний однозначно связаны с углом преобразования поворота силовых линий и равны или кратны номеру резонанса на магнитных поверхностях. На основании предварительных экспериментов по измерению радиального потока плазмы вследствие флуктуации (по величине $\langle \tilde{E}_\varphi \tilde{n} \rangle$ можно предположить, что вклад колебаний в диффузию сравнительно мал и не может объяснить наблюдаемых времен жизни плазмы. Окончательный ответ на вопрос о влиянии колебаний на диффузию плазмы остается пока открытым и необходимы дальнейшие исследования.

Как показали измерения, в случае существования замкнутых магнитных поверхностей, плазма принимает отрицательный потенциал относительно стенок камеры. Возникающее радиальное электрическое поле должно при этом оказывать существенное влияние на движение в магнитном поле. Наблюдаемая корреляция между величиной потенциала плазмы и ее временем жизни в ловушке позволяет предположить, что существует какой-то механизм ухода частиц, связанный с отсутствием полного равновесия плазмы в стеллараторном магнитном поле. Для подтверждения высказанных выше предположений необходимо проведение дальнейших экспериментов.

Таким образом, на основании описанных выше экспериментов и их обсуждения не представляется возможным сделать вывод о механизме, приводящем к повышенной диффузии плазмы в стеллараторе Л-1. Данные эксперимента еще раз подтвердили, что существенную роль в удержании плазмы играет качество магнитного поля и его тонкая структура.

В заключение авторы считают своим приятным долгом выразить благодарность И.С.Данилкину, Л.М.Коврижных и А.А.Рухадзе за полезные дискуссии при обсуждении результатов эксперимента. Авторы благодарят также Л.М.Аносову, С.Н.Греппова и О.И.Назаренко за помощь в проведении экспериментов.

ЛИТЕРАТУРА

[1] БАТАНОВ, Г.М., БЕРЕЖЕЦКИЙ, М.С., ГРЕБЕНЩИКОВ, С.Е., ЗВЕРЕВ, Н.М., ПОПРЯДУХИН, А.П., РАБИНОВИЧ, М.С., СБИТНИКОВА, И.С., ШПИГЕЛЬ, И.С., ДАН СССР 160 № 6 (1965).

[2] АКУЛИНА, Д.К., БАТАНОВ, Г.М., БЕРЕЖЕЦКИЙ, М.С., ГРЕБЕНЩИКОВ, С.Е., РАБИНОВИЧ, М.С., СБИТНИКОВА, И.С., ШПИГЕЛЬ, И.С., Plasma Phys. and Contr. Nucl. Fusion Res. (Proc. Conf., Culham, 1965) IAEA 2 (1966) 733.

[3] STODICK, W., ELLIS, R.A., GORMAN, J.G., Nucl. Fusion, Suppl.I.

[4] REASE, R.S., YOSHIKAWA, S., EUBANK, H.P., Phys. Fl. 9 (1966) 2059.

[5] STODICK, W., GROVE, D.J., KESSLER, J.O., Plasma Phys. and Contr. Nucl. Fusion Res. (Proc. Conf., Culham) 2 (1966) 687.

[6] БЕРЕЖЕЦКИЙ, М.С., ГРЕБЕНЩИКОВ, С.Е., ЗВЕРЕВ, Н.М., ШПИГЕЛЬ, И.С., Труды ФИАН, XXXII (1965) 20.

[7] НЕЧАЕВ, Ю.И., ШПИГЕЛЬ, И.С., ПТЭ (в печати).

[8] БЕРЕЖЕЦКИЙ, М.С., ГРЕБЕНЩИКОВ, С.Е., ПОПРЯДУХИН, А.П., ШПИГЕЛЬ, И.С., ЖТФ, XXXV, вып.12 (1965) 2167.

[9] СОЛОВЬЕВ, Л.С., ШАФРАНОВ, В.Д., "Вопросы теории плазмы", вып.5, 3, Атомиздат, 1967.

[10] BISHOP, A.S., SMITH, C.G., Phys. Fl. 9 (1966) 1380.

ТУРБУЛЕНТНАЯ ПЛАЗМА В СТЕЛЛАРАТОРЕ; МАСС-ЭНЕРГЕТИЧЕСКИЕ ИССЛЕДОВАНИЯ ПЛАЗМЫ, ЗАХВАЧЕННОЙ В АПЕРТУРУ ДИВЕРТОРА ПРИ ИНЖЕКЦИИ ЧЕРЕЗ МАГНИТНУЮ ЩЕЛЬ

П.Я.БУРЧЕНКО, Б.Т.ВАСИЛЕНКО, Е.Д.ВОЛКОВ,
О.С.ПАВЛИЧЕНКО, В.А.ПОТАПЕНКО,
В.А.РУДАКОВ, Ф.Ф.ТЕРЕЩЕНКО, В.Т.ТОЛОК,
В.М.ЗАЛКИНД, В.Г.ЗЫКОВ, В.И.КАРПУХИН
и Н.И.РУДНЕВ
ФИЗИКО-ТЕХНИЧЕСКИЙ ИНСТИТУТ АН УССР,
ХАРЬКОВ,
СССР

Abstract — Аннотация

TURBULENT PLASMA IN A STELLARATOR AND MASS-ENERGY INVESTIGATIONS OF A PLASMA TRAPPED IN A DIVERTOR APERTURE DURING INJECTION THROUGH A MAGNETIC SLIT. 1. The authors report investigations concerning the current-induced heating and containment of a plasma in the "Sirius" stellarator. Particular attention is paid to those oscillatory processes in the plasma which might be important in determining both the heating efficiency and the rate of energy and particle loss. After adjusting the magnetic system of the stellarator by multipole transmission of an electron beam, the authors investigate the dependence of the plasma decay rate on the initial plasma density, the intensity of the containing field and the current. It is shown that the stellarator functions as a trap only when the gas-kinetic pressure of the plasma $nkT < \beta H^2/8$, the plasma decay time as determined by interferometer measurements being directly proportional to the intensity of the magnetic field and inversely proportional to the electron temperature. This relationship may be due to drift instabilities. Investigations of low-frequency oscillations using Langmuir probes show that in a plasma produced by a current discharge oscillations with frequencies $\omega \sim (cT/eH)(n'/n)$ are indeed excited. The spectra of these oscillations are derived and the dependence of the frequency on the magnetic field intensity and the temperature is found. Investigations of the current-induced heating of the plasma in a stellarator, for widely varying values of the electric field induced in the plasma column, show that there are regions of highly anomalous electrical conductivity. In these regions microwave and X-ray emission are observed, together with a large difference in temperature as determined by measuring the conductivity of the plasma and the diamagnetic effect. These observations cannot be explained on the basis of the classical collisional theory of current-induced heating. Thus, it is shown that during the formation and heating of a plasma in a stellarator collective oscillations are excited over a wide range of frequencies. Complete understanding of the processes of energy input and loss can be achieved only if one takes into account these phenomena, which are still insufficiently understood by the theoreticians. 2. Using a Thomson mass spectrograph and a time-of-flight mass spectrometer, the authors investigate the energy spectra, mass composition and other parameters of a plasma trapped in a divertor aperture during injection through a magnetic slit from a coaxial plasma gun (magnetic field intensity in the divertor mirrors 1.5 - 20 kOe). It is shown that there is a magnetic field intensity (8 - 12 kOe) at which capture of the hydrogen ions along the magnetic field lines near the axis is optimized. Optimum capture of high-energy hydrogen ions occurs for approximately the same range of magnetic field intensities.

ТУРБУЛЕНТНАЯ ПЛАЗМА В СТЕЛЛАРАТОРЕ; МАСС-ЭНЕРГЕТИЧЕСКИЕ ИССЛЕДОВАНИЯ ПЛАЗМЫ, ЗАХВАЧЕННОЙ В АПЕРТУРУ ДИВЕРТОРА ПРИ ИНЖЕКЦИИ ЧЕРЕЗ МАГНИТНУЮ ЩЕЛЬ. I. Приводятся результаты исследований токового нагрева и удержания плазмы в стеллараторе "Сириус". Особое внимание уделялось изучению колебательных процессов в плазме, которые могут в значительной степени определять как эффективность нагрева, так и скорость потерь энергии и частиц. После настройки магнитной системы стелларатора при помощи методики многократного прохождения электронного пучка были проведены исследования зависимости скорости распада плазмы от ее начальной плотности, величины удерживающего поля и тока. Показано, что стелларатор работает как ловушка только в том случае, когда газокинетическое давление плазмы $nkT < \beta_e \frac{H^2}{8\pi}$. Время распада плазмы, определенное по интерферометрическим измерениям, оказывается прямо пропорциональным величине магнитного поля и обратно пропорциональным электронной температуре. Такой ход зависимости может быть обусловлен дрейфовыми неустойчивостями. Исследования низкочастотных колебаний, проведенные при помощи ленгмюровских зондов, показали, что в плазме токового разряда действительно имеет место возбуждение колебаний с частотами $\omega \sim \frac{cT}{eH} \cdot \frac{n'}{n}$. Построены спектры этих колебаний и найдены зависимости частоты от величины магнитного поля и температуры. Исследования токового нагрева плазмы в стеллараторе, проведенные в широкой области изменения электрического поля, индуцируемого в плазменном шнуре, показали, что имеются области значительной аномалии электропроводности. В этих областях наблюдаются микроволновые и рентгеновские излучения, а также большое различие в температурах, определенных по проводимости и диамагнитному эффекту плазмы. Наблюдаемые эффекты не могут быть объяснены на основе классической столкновительной теории токового нагрева. Показано, что в процессе создания и нагрева плазмы в стеллараторе в ней наблюдается возбуждение коллективных колебаний в широкой области частот. Полное понимание процессов ввода и потерь энергии может быть достигнуто только при учете этих еще недостаточно понятных теоретически явлений.

II. С помощью масс-спектрографа Томсона и пролетного масс-спектрометра исследовались энергетические спектры, массовый состав и другие параметры плазмы, захваченной в апертуру дивертора при внешней инжекции через его магнитную щель из коаксиальной плазменной пушки. Измерения проводились при напряженности магнитного поля в пробках дивертора 1,5 – 20 кэ. Показано, что имеется оптимальная напряженность магнитного поля (8 – 12 кэ), при которой происходит наилучший захват ионов водорода на приосевые силовые линии магнитного поля. Примерно в том же диапазоне магнитных полей происходит наилучший захват высокоэнергетичных ионов водорода.

I. ТУРБУЛЕНТНАЯ ПЛАЗМА В СТЕЛЛАРАТОРЕ

Исследования удержания плазмы в стеллараторах показали, что скорость ухода заряженных частиц в процессе омического нагрева аномально велика и по порядку величины совпадает с бомовской [1, 2]. Более того, на стеллараторах "В-3" и "С-1" было обнаружено, что наложение поля винтовых обмоток практически не влияет на скорость распада плазмы омического разряда [3].

Аномально высокие скорости потерь могут быть вызваны следующими причинами: 1) недостаточно точной настройкой магнитной системы сталларатора, 2) потерей равновесия плазменного шнура, 3) возбуждением в плазме в процессе нагрева длинноволновых низкочастотных колебаний.

В данной части излагаются результаты экспериментов, связанных с изучением колебательных процессов в плазме, которые оказывают существенное влияние на скорости нагрева плазмы и ее потерь из ловушки.

Эксперименты проводились на стеллараторе "Сириус" [4], схематический вид которого показан на рис.1. Основные параметры приведены ниже:

1) удерживающее магнитное поле	H = 20 кэ
2) винтовое поле, 2 обмотки	$l = 3$
3) диаметр вакуумной камеры	d = 10 см
4) аксиальная длина камеры	L = 600 см
5) предельный ток Шафранова-Крускала	I = 4 ка
6) равновесное	$\beta_e = 3 \cdot 10^{-4}$
7) устойчивое	$\beta_c = 5 \cdot 10^{-3}$

Магнитная система этой ловушки была предварительно отъюстирована при помощи методики многократного прохождения электронного пучка [5].

Угол преобразования на длине машины i, измеренный на границе ограничивающей диафрагмы диаметром 52 мм при выбранном варианте питания, составляет 100°, а соответствующая величина шира – 0,02.

Нагрев плазмы производится при помощи омического разряда (длительность импульса тока – 1 мсек). Давление нейтрального гелия изменялось от $2 \cdot 10^{-5}$ до $5 \cdot 10^{-4}$ мм рт.ст., напряженность электрического поля E – от 0,08 до 0,4 в/см, магнитное поле – от 4 до 15 кэ.

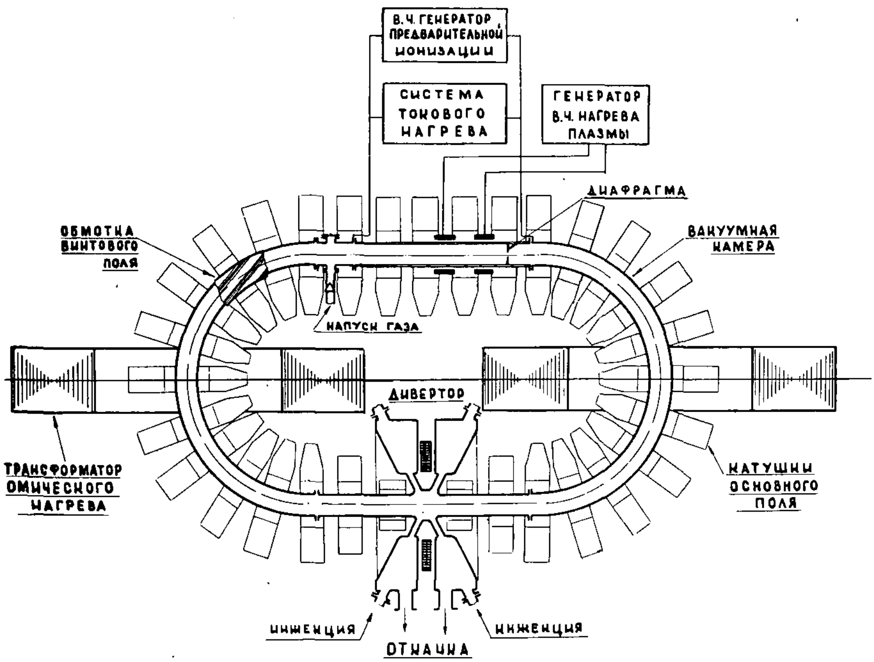

Рис.1. Схематический вид стелларатора "Сириус".

В процессе экспериментов регистрировались: ток в плазменном шнуре, напряжение на обходе камеры, ход плотности во времени, диамагнетизм плазмы, распределение плотности по сечению плазменного шнура, флуктуации плавающего потенциала, рентгеновское и микроволновое излучения. Теоретические исследования показывают, что в системах с малым широм наиболее существенный вклад в турбулентную диффузию должны вносить дрейфовые колебания неоднородной плазмы [6, 7]. Изучение низкочастотных колебаний плазмы проводилось при помощи ленгмюровских зондов, расположенных на границе плазменного шнура. Типичная осциллограмма сигнала флуктуаций плавающего потенциала приведена на рис.2.

Изучение спектральных свойств этих случайных колебаний производилось путем определения автокорреляционной функции

$$R(\tau) = \lim_{T \to \infty} \frac{1}{T} \int_{-T}^{T} x(t) \cdot x(t-\tau)\, dt$$

и вычисления спектральной плотности процесса

$$S(\omega) = \frac{1}{\pi}\int_{-\infty}^{\infty} R(\tau)\, e^{-i\omega\tau}\, d\tau$$

Наблюдаемые колебания нестационарны (математическое ожидание процесса зависит от времени), поэтому выполнялось предварительное центрирование сигнала путем вычитания оценки текущего значения математического ожидания, определяемого по промежуткам времени $\sim 0{,}02\, t_p$ (время реализации равно длительности импульса омического нагрева $t_p = t_{о.н.}$). Указанная величина интервала усреднения при вычислении оценки математического ожидания определялась путем минимизации дисперсии центрируемого процесса. Вычисление корреляционной функции и спектральной плотности производилось на ЭВМ.

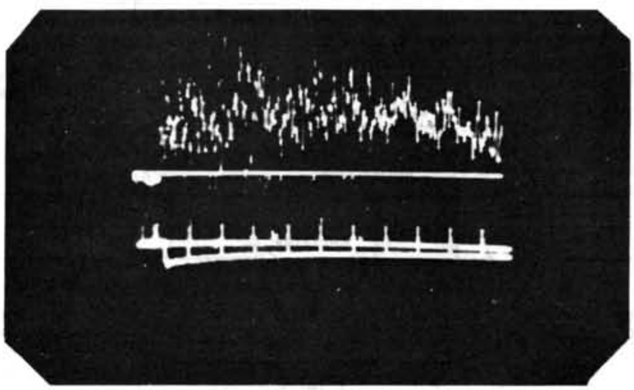

Рис.2. Осциллограммы сигналов флуктуаций плавающего потенциала и напряжения на обходе камеры. Расстояние между метками – 100 мксек.

Оценки спектральной плотности показали, что наиболее существенный вклад в спектр вносят колебания с частотами, лежащими в диапазоне 20 ÷ 100 кгц. Это обстоятельство позволило производить вычисления оценок значений корреляционной функции и спектральной плотности путем усреднения по промежуткам времени $\tau^* = 0{,}2\, t_p$. Связанное с этим уширение спектра не играет существенной роли, так как его величина $\Delta f = 1/\tau^* = 5$ кгц мала по сравнению с наиболее существенными частотами в спектре. На рис.3 приведена спектрограмма сигнала флуктуаций плавающего потенциала, полученного при концентрации плазмы $n_e = 10^{14}$ см$^{-3}$.

Изучение спектров колебаний показало, что основная частота зависит от величины магнитного поля, температуры плазмы и ее плотности. При плотности плазмы $n_e \geq 8{\cdot}10^{13}$ см$^{-3}$ спектры колебаний оказываются почти невоспроизводимыми от разряда к разряду. При меньших концентрациях спектрограммы воспроизводятся, а основная частота в спектре зависит от величины удерживающего магнитного поля (рис.4).

Измерения спектра флуктуаций плавающего потенциала во времени совместно с диамагнитизмом показали, что частота колебаний оказывается пропорциональной температуре плазмы (рис.5).

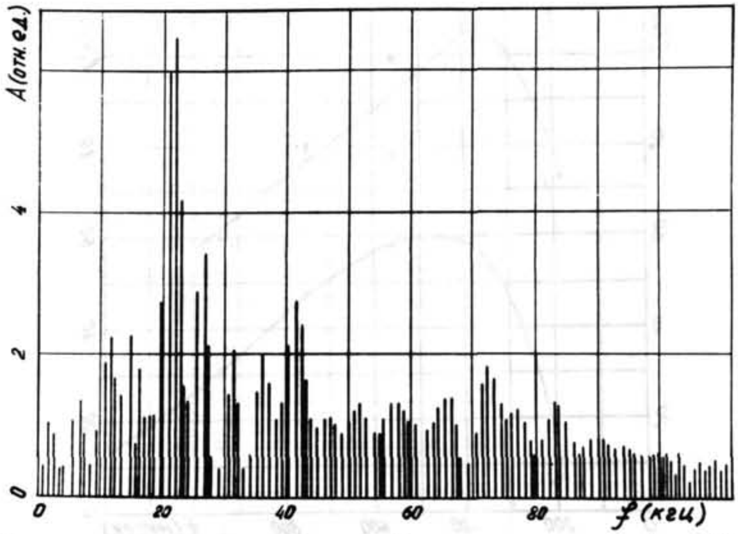

Рис.3. Спектрограмма сигнала флуктуаций плавающего потенциала ($n_e = 10^{14}$ см$^{-3}$, E = 0,3 в/см, H = 16 кэ).

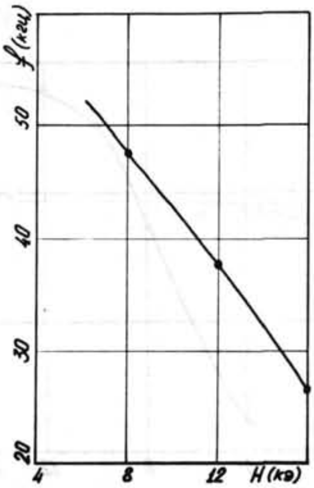

Рис.4. Зависимость частоты флуктуаций от напряженности удерживающего магнитного поля ($n_e = 4\cdot10^{13}$ см$^{-3}$, E = 0,15 в/см).

При учете поведения температуры с изменением магнитного поля (рис.6) получено, что частота колебаний практически линейно зависит от отношения температуры плазмы к напряженности магнитного поля при плотности $n_e < 8\cdot10^{13}$ см$^{-3}$ (рис.7).

Оценка дрейфовых частот

$$\omega = k_y \frac{cT}{eH} \cdot \frac{\nabla n_e}{n_e}$$

для имеющихся экспериментальных значений температуры плазмы, магнитного поля и градиента плотности дают данные, довольно хорошо совпа-

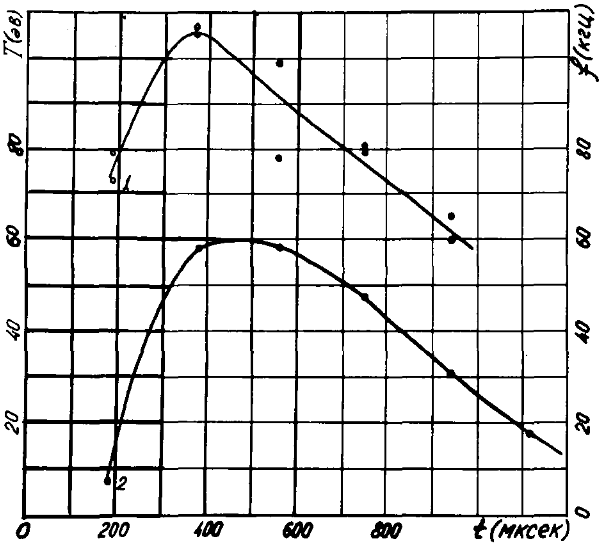

Рис.5. Поведение частоты флуктуаций плавающего потенциала и температуры плазмы во времени: 1 – частота; 2 – температура.

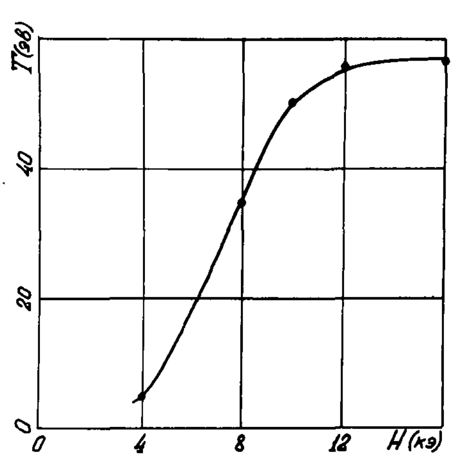

Рис.6. Зависимость температуры плазмы от напряженности магнитного поля ($n_e = 4 \cdot 10^{13}$ см$^{-3}$, $E = 0{,}15$ в/см).

дающие с наблюдаемыми частотами. На рис.7 пунктирными линиями обозначены дрейфовые частоты, рассчитанные для мод $m = 2$ и $m = 3$. Экспериментальные точки укладываются, в основном, между этими линиями.

Следует отметить, что в области рабочих параметров, где имеются различия между температурами, измеренными по диамагнетизму и проводимости плазмы, частота следует зависимости T/H, если в расчетах используется диамагнитная температура.

Измерения функции взаимной корреляции сигналов с зондов, расположенных вдоль магнитного поля, показали, что возмущения потенциала сильно скоррелированы, т.е. возмущения сильно вытянуты вдоль магнитного поля. Измерения взаимной корреляции сигналов с двух зондов, расположенных по азимуту на границе плазменного шнура (расстояние между зондами – 2 см), дают значения скорости распространения возмущения $V_s = 8{\cdot}10^4 \div 6{\cdot}10^5$ см·сек$^{-1}$. При постоянной напряженности магнитного поля характер изменения азимутальной скорости подобен характеру изменения температуры.

Одновременные измерения частоты колебаний и скорости их распространения позволяют оценить k_y; эти оценки показали, что наблюдается хорошее согласие определенного таким образом k_y с вычисленным из соотношения $k_y = m/r_0$ с $m = 2 \div 3$.

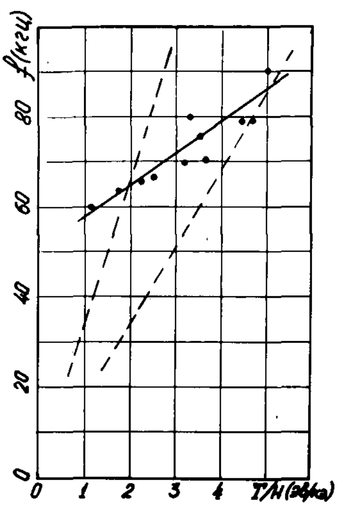

Рис.7. Зависимость частоты флуктуаций плавающего потенциала от отношения T/H.

Учитывая то, что частота столкновений $\nu_{ei} \gg \omega$, можно предположить, что в данном случае наблюдается дрейфоводиссипативная неустойчивость, скорость потерь при которой порядка бомовской [8].

Как уже отмечалось, при плотности плазмы $n_e \geq 8{\cdot}10^{13}$ см$^{-3}$ результаты измерений флуктуаций плавающего потенциала оказываются невоспроизводимыми от разряда к разряду. Такая же картина наблюдается при работе с выключенными винтовыми обмотками, т.е. в случае, когда угол преобразования $i = 0$.

С другой стороны, измерения скорости распада плазмы в зависимости от величины магнитного поля при $i = 0$ показали, что постоянная времени распада τ (время уменьшения концентрации в e раз) практически не зависит от H в широкой области изменения концентрации и определяется, по-видимому, дрейфом заряженных частиц в скрещенных магнитном и электрическом полях.

Измерения скорости распада при наличии винтового поля ($i = 100°$) дают такие же результаты для плазмы с концентрацией электронов $n_e > 8{\cdot}10^{13}$ см$^{-3}$. При снижении n_e наблюдается линейная зависимость постоянной времени распада от величины удерживающего магнитного поля. На рис.8 показана зависимость τ(H) при $i = 0°$ и $i = 100°$ и различных концентрациях плазмы.

Одновременные измерения скорости распада плазмы и диамагнетизма показали, что линейная зависимость $\tau(H)$ наблюдается в том случае, когда во время импульса нагрева выполняется условие

$$nk\,T_D < \beta_e \frac{H^2}{8\pi}$$

где

$$\beta_e = 2^{3-2n}\,\frac{q-2n+4}{q}\cdot\frac{i^2}{\pi L}\;r_0$$

а q берется из соотношения, которым апроксимируется давление в плазме

$$P = P_0\left\{1 - \left(\frac{r}{r_0}\right)^q\right\}$$

Таким образом, при нарушении условия равновесия, т.е. при $nk\,T_D > \beta_e \frac{H^2}{8\pi}$, скорость распада, как и в случае $i = 0$, не зависит от величины магнитного поля, а флуктуации потенциала становятся невоспроизводимыми. При выполнении условия равновесия $nk\,T_D < \beta_e \frac{H^2}{8\pi}$ имеются четко выраженные дрейфовые колебания, которые, по-видимому, и приводят к турбулентной диффузии.

Коллективные колебания определяют в значительной степени и эффективность поглощения энергии в плазме омического разряда. Известно, что неизотермическая плазма ($T_e \gg T_i$) в электрическом поле неустойчива по отношению к возбуждению ионно-звуковых и ленгмюровских колебаний [9, 10]. Возбуждением именно этих колебаний были качественно объяснены результаты исследований аномалии сопротивления плазмы в надкритических электрических полях [11 – 13]. Теоретические исследования, использованные для объяснения данного эффекта, были выполнены для случая, когда можно пренебречь влиянием удерживающего магнитного поля, т.е. для случая

$$H_0 \ll (4\pi m_e c^2 n_e)^{1/2} \quad [14-16]$$

Однако, исследования омического разряда в замкнутой магнитной ловушке показали, что даже при $E \leq E_k$ и $H_0 \gg (4\pi m_e c^2 n_e)^{1/2}$ сопротивление плазмы может оказаться аномально большим [17]. Эти данные, как было показано в работе [18], находятся в качественном соответствии с представлениями об изотропизации ускоренных электронов на колебаниях, возбуждаемых при аномальном эффекте Допплера. Однако, отсутствие микроволновых и рентгеновских измерений не позволяет трактовать результаты работы [17] более определенно.

Исследования омического разряда в стеллараторе "Сириус", проведенные при большой концентрации ($n_e > 5{\cdot}10^{13}$ см$^{-3}$) и напряженности электрического поля $E \simeq 0{,}08 \div 0{,}4$ в/см, показали, что процесс нагрева довольно хорошо описывается столкновительным механизмом. Температура плазмы, вычисленная по проводимости T_σ, при этом в пределах погрешностей измерений совпадает с температурой, рассчитанной по диамагнитным измерениям T_D. При $n_e < 5 \cdot 10^{13}$ см$^{-3}$ и тех же напряженностях электрического поля поведение разряда существенно изменяется. Вместе с появлением рентгеновского и микроволнового излучений нарушается равенство между T_σ и T_D. При этом отклонение T_σ от T_D наблюдается в той же области E/E_k, где имеется возрастание сопротивления (рис.9). Следует отметить, что эффект роста сопротивления в той же области изменения E/E_k был обнаружен в прямолинейном разряде в 1961 году [19].

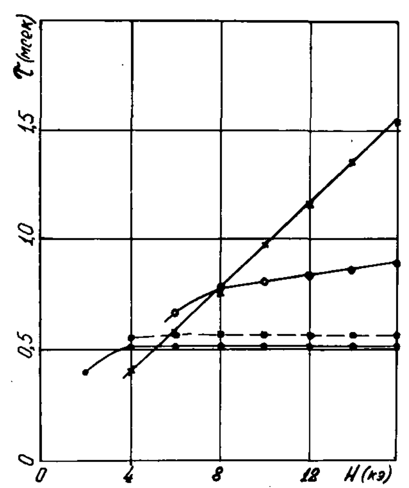

Рис.8. Зависимость постоянной распада плазмы от напряженности магнитного поля при $E = 0{,}15$ в/см и различных концентрациях плазмы:

■ = $2 \cdot 10^{13}$ см$^{-3}$, i = 0;
● = 10^{14} см$^{-3}$, i = 100°;
○ = $8 \cdot 10^{13}$ см$^{-3}$, i = 100°;
× = $2 \cdot 10^{13}$ см$^{-3}$, i = 100°;

Различие в температурах, рассчитанных по диамагнетизму и проводимости, существенно зависит от магнитного поля. На рис.10 показана диамагнитная температура в зависимости от концентрации плазмы при E = Const. Параметром этих кривых служит величина магнитного поля.

Зависимость T_D/T_σ от H при наличии микроволнового и рентгеновского излучений, казалось бы, дает возможность объяснения полученных результатов на основе возбуждения резонанса

$$\omega - n\omega_H - k_z V_z = 0 \text{ с } n < 0$$

Однако, значительная аномалия сопротивления, наблюдаемая при $\omega_H < \omega_0$, не может быть объяснена ни указанным механизмом, ни раскачкой ионно-звуковой неустойчивости, если приложенное электрическое поле оказывается меньше критического поля Драйсера.

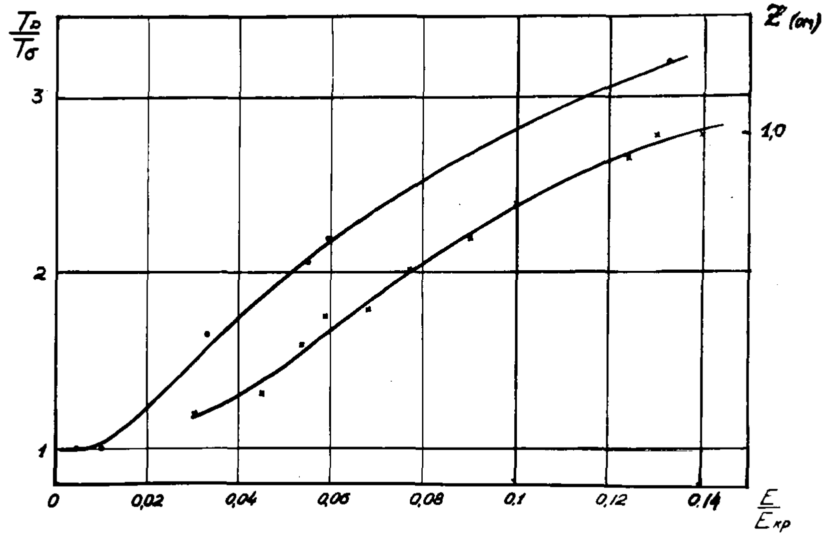

Рис.9. Зависимость T_D/T_σ и сопротивления плазмы z от отношения E/E_k.

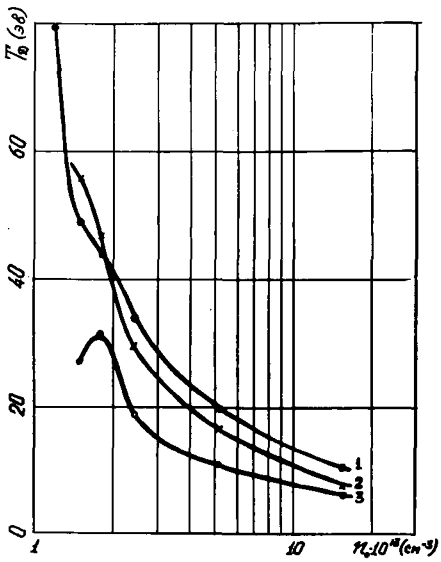

Рис.10. Зависимость диамагнитной температуры от концентрации плазмы при различных магнитных полях и E = const:
1 – 16 кэ; 2 – 12 кэ; 3 – 8 кэ.

II. МАСС-ЭНЕРГЕТИЧЕСКИЕ ИССЛЕДОВАНИЯ ПЛАЗМЫ, ЗАХВАЧЕННОЙ В АПЕРТУРУ ДИВЕРТОРА ПРИ ИНЖЕКЦИИ ЧЕРЕЗ МАГНИТНУЮ ЩЕЛЬ

Выполненные ранее эксперименты по исследованию возможности инжекции плазмы в стелларатор через щели дивертора [20] показали, что значительная часть плазмы успешно захватывается внутри апертуры дивертора и распространяется вдоль силовых линий магнитного поля в противоположных направлениях. Было показано также, что количество захваченной плазмы максимально при напряженности магнитного поля от 8 до 15 кэ. Выше и ниже этих значений число захваченных в апертуру частиц уменьшается.

В данной работе исследовались энергетические спектры, массовый состав и другие параметры плазмы, захваченной в апертуру дивертора при внешней инжекции через его магнитную щель из коаксиальной плазменной пушки, в зависимости от напряженности магнитного поля и режима работы пушки.

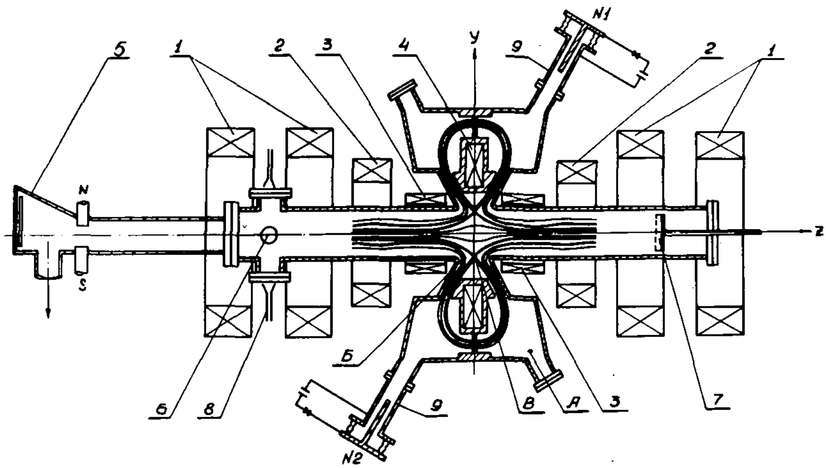

Рис.11. Принципиальная схема установки:
1,2,3 – положительные катушки; 4 – отрицательная катушка; 5 – масс-спектрограф; 6 – радиальный зонд; 7 – плазмоскоп; 8 – интерферометр; 9 – источники плазмы.

Эксперименты проводились на установке, описанной в работах [20, 24]. На торце вакуумной камеры вблизи магнитной оси размещался масс-спектрограф Томсона и пролетный масс-спектрометр (рис.11). Первым прибором исследовался интегральный спектр, как массовый, так и энергетический, вторым – пространственная структура сгустка [21, 22]. Масс-спектрограф можно было передвигать по радиусу в пределах $r = \pm 1{,}2$ см, что давало возможность исследовать плазму в любой точке ограниченной апертурой системы. Следует отметить, что приборы были расположены на расстоянии $L = 60$ см от последней магнитной катушки, т.е. в области слабого рассеянного магнитного поля, порядка нескольких гаусс, так что влиянием этого поля на анализаторы можно было пренебречь. Кроме того, все величины, пропорциональные плотности частиц водородного компонента плазмы, несколько занижены вследствие ухода по силовым линиям магнитного поля легкого компонента плазмы на конце соленоида.

Из многих экспериментальных работ, в которых проводились подобные исследования плазменных сгустков, генерируемых коаксиальными источниками, известно, что их структура зависит от режима источника и в особенности от задержки между напуском газа в межэлектродные промежутки и подачей напряжения на них. Режим работы источника выбирался таким образом, чтобы при максимальных напряженностях магнитного поля частицы водорода в захваченной плазме имели максимальное значение энергии и возможно большее процентное содержание относительно общего числа частиц. Исследования проводились в широком интервале задержек между моментами напуска газа и подачей напряжения на электроды инжектора (τ = 260 ÷ 360 мксек) и при значениях напряженности магнитного поля 1,5 ÷ 20 кэ.

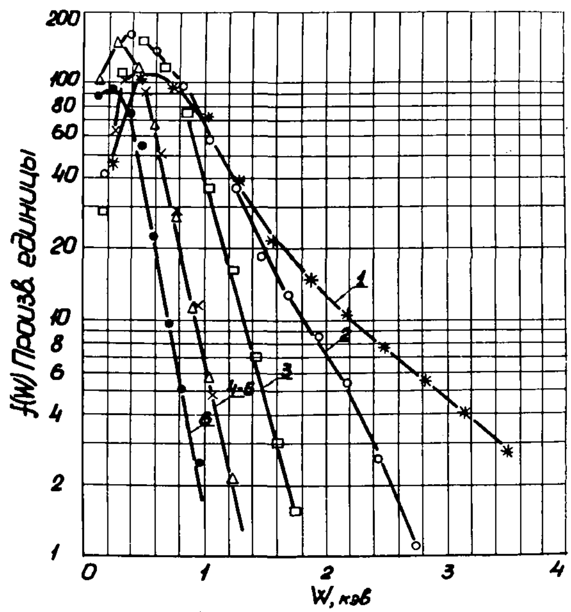

Рис.12. Функции распределения ионов водорода по энергиям для постоянных значений задержки:
1 – τ = 260 мксек; 2 – τ = 285 мксек; 3 – τ = 300 мксек; 4,5 – τ = 320÷360 мксек; 6 – τ = 400 мксек.

Рис.12 иллюстрирует распределение ионов водорода по энергиям при напряженности магнитного поля (в пробке) 15 кэ. Параметром кривых выбрана задержка τ. С уменьшением задержки растет как количество частиц в максимуме функции распределения, так и количество высокоэнергетичных частиц. Но уже при задержке τ = 260 мксек максимальная энергия захваченных частиц продолжает расти, а количество частиц средней энергии уменьшается.

Для выбора оптимального режима источника интересно было исследовать относительное содержание водорода и примесей в широком интервале значений магнитного поля и различных режимов источников. На рис.13 приведено процентное содержание водорода в зависимости от напряженности магнитного поля для двух наиболее интересных режимов источника плазмы (τ = 285 мксек, τ = 300 мксек). Пунктирная линия соответствует тому значению относительного содержания ионов водорода, которое дает сам источник. Кубиками обозначено значение водорода в процентах на диверторной поверхности.

Низкий процент содержания водорода в захваченной плазме для малых напряженностей магнитного поля можно объяснить следующим образом. При слабых полях величина поперечной составляющей рассеянного поля в области инжекции небольшая, что дает возможность плазменному сгустку беспрепятственно входить в щель дивертора, но при выходе из щели сгусток снова попадает в область поперечного магнитного поля, напряженность которого равна нескольким сотням эрстед. Поэтому плазма свободно проникает поперек магнитного поля, ударяется о противоположную стенку камеры и выбивает примеси. Частицы, регистрируемые анализатором, имеют вторичное происхождение. По-видимому, часть плазмы при слабых полях ударяется о стенки щели дивертора, загрязняется и свободно проникает в систему. С ростом же поля процентное содержание водорода растет. Это указывает на то, что свободное

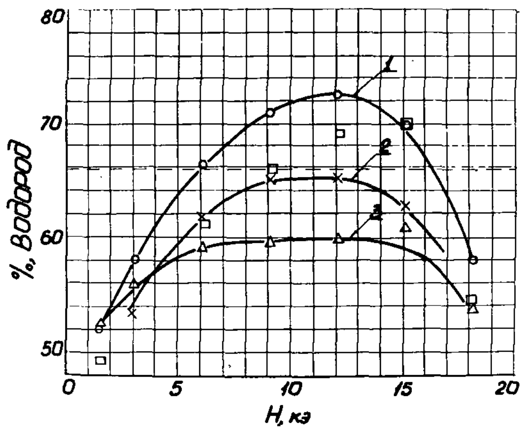

Рис.13. Процентное содержание водорода относительно количества всех частиц, захваченных в систему, в зависимости от напряженности магнитного поля:
1 – (-z), τ = 300 мксек; 2 – (+z), τ = 300 мксек; 3 – (-z), τ = 285 мксек; □ – (-z) – диверторная линия; r = + 12 мм.

проникновение плазмы поперек поля на выходе из щели дивертора затрудняется, и количество захваченных ионов водорода приближается к значению, инжектируемому самим источником.

В области полей H = 9 ÷ 13 кэ наблюдается максимальный захват водорода. Однако, при дальнейшем увеличении поля процентное содержание водорода уменьшается; такой ход кривых, по-видимому, объясняется тем, что непосредственно в области инжекции (между щелью дивертора и источником) при напряженностях магнитного поля выше 13 кэ амплитуда напряженности рассеянного магнитного поля имеет большую величину ($H_z \approx 1$ кэ), что может привести к значительному искажению первоначальной структуры сгустка и уменьшить плотность прошедшей через щель плазмы.

Принимая во внимание растекания по силовым линиям магнитного поля преимущественно легкого компонента плазмы [23], можно предположить, что при больших напряженностях магнитного поля происходит обеднение сгустка водородом на рассеянном поперечном поле в пространстве между источником и щелью дивертора, и поэтому наблюдается относительное уменьшение количества ионов водорода.

На рис.14 показаны функции распределения ионов водорода по энергиям, полученные при τ = 285 мксек и при постоянных значениях напряженностей магнитного поля, из которых следует, что с ростом магнитного поля кривые сдвигаются в область больших энергий. Для напряженности магнитного поля H = 12 кэ рост энергии прекращается. Максимум кривой f(w) начинает уменьшаться и одновременно наблюдается обратный ход кривых функций распределения.

Рис.15 аналогичен рис.14, но характеризует энергетическое распределение ионов водорода, движущихся в направлении,совпадающем с направлением инжекции +z. Характерно, что в направлении +z уже при малых магнитных полях (1,5 ÷ 6 кгс) наблюдается захват на силовые

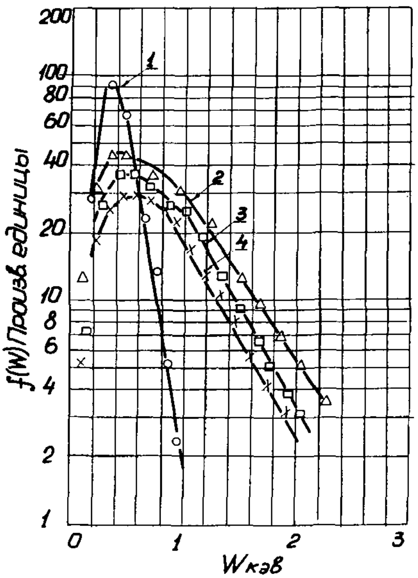

Рис.14. Функции распределения по энергиям ионов водорода захваченной плазмы в направлении -z, τ = 285 мксек:
1 – 1,5 кэ; 2 – 9 кэ; 3 – 12 кэ; 4 – 15 кэ.

линии частиц водорода наибольшей энергии (до 4 кэв). При более высоких магнитных полях энергия частиц уменьшается, и при H = 18 кэ она не превышает 2 кэв. Средняя энергия находится на уровне 0,6 кэв. В направлении – z максимальная энергия частиц не превышает 2 кэв, но количество частиц средней энергии уменьшается быстрее, чем количество быстрых частиц.

На рис.16 кривые 1 и 2 иллюстрируют функции распределения ионов водорода, которые генерирует источник в двух режимах (τ = 285 мксек и τ = 300 мксек, H = 0). Кривые 3 и 4 получены для ионов водорода, движущихся вдоль оси, при инжекции через щель дивертора в тех же режимах источника и при H = 9 кэ (кривая 4) и H = 6 кэ (кривая 3).

Из рис.16 видно, что в обоих режимах при инжекции через дивертор происходит потеря наиболее быстрых ионов водорода, хотя в данном случае магнитное поле было выбрано отптимальным для прохождения высокоэнергетичных частиц. При всех других напряженностях магнитного поля потеря высокоэнергетичных частиц еще более существенна.

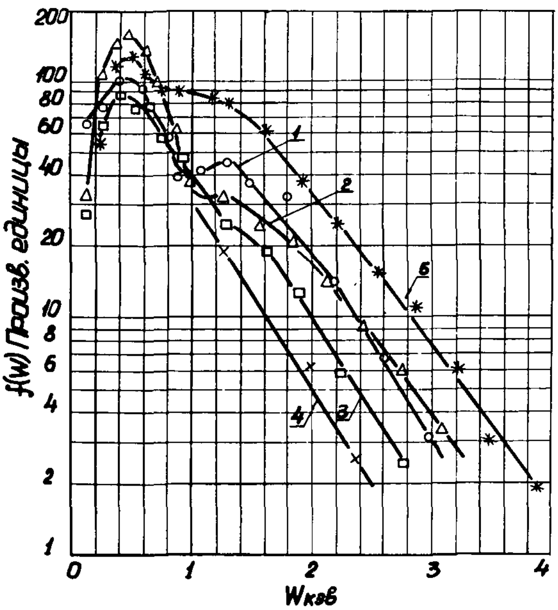

Рис.15. Функции распределения по энергиям ионов водорода захваченной плазмы в направлении +z, τ = 285 мксек:
1 – 1,5 кэ; 2 – 3 кэ; 3 – 12 кэ; 4 – 18 кэ; 5 – 6 кэ.

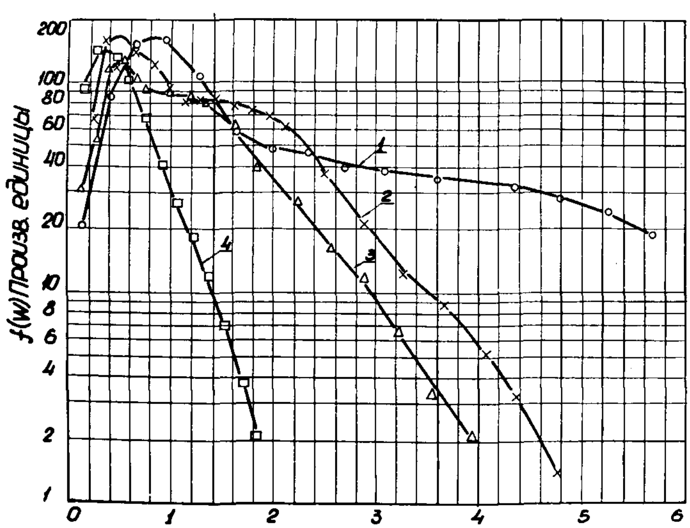

Рис.16. Сравнение функций распределения ионов водорода захваченной плазмы и функций распределения самого источника:
1,2 – H = 0, τ = 285 мксек и 300 мксек соответственно; 3 – H = 6 кэ, τ = 285 мксек;
4 – H = 9 кэ, τ = 300 мксек.

Можно высказать следующие предположения по поводу потери частиц с высокими энергиями.

При малых напряженностях магнитного поля высокоэнергетичные частицы проходят свободно поперек магнитного поля и гибнут на стенке вакуумной камеры, частично проходя в противоположную щель дивертора. При большом магнитном поле, ввиду их малой плотности, они не могут проникнуть поперек силовых линий рассеянного магнитного поля в пространстве между источниками и щелью дивертора, уходят на стенки по силовым линиям и гибнут в диверторе в месте инжекции.

Некоторые измерения массового состава и пространственной структуры сгустка, движущегося в направлении оси z, исследовались также пролетным масс-спектрометром [22], в котором с помощью модулятора на короткое время (0,2 – 0,5 мксек) снималось напряжение с запирающего электрода и, таким образом, формировался узкий пакет частиц, разрешающийся по массам на пролетной длине анализатора (53 см). Сигнал с модулятора одновременно с сигналом регистрирующего ФЭУ подавался на вход осциллографа. Таким образом, можно было точно измерять время пролета пучка частиц и определить m/z.

Из-за интегрирования модулирующего импульса в измерительных цепях не было возможности сделать его достаточно узким, поэтому водородный пик сливался с импульсом модулятора и разрешить его не удалось. Однако, относительное количество водорода было определено с помощью масс-спектрометра Томсона. Более тяжелые массы разрешались довольно четко.

Пространственная структура сгустка исследовалась путем подачи модулирующего импульса в различные моменты времени относительно момента запуска инжектора. Измерения пролетным масс-спектрометром в совокупности с измерениями масс-спектрометром Томсона позволили определить относительное количество ионов разного сорта, имеющих одинаковую энергию. Например, при напряженности магнитного поля 8 кэ среди частиц, обладающих энергией поступательного движения 375 эв, содержится ионов водорода 70%, ионов C^{++++} – 9%, C^{+++} – 6%, C^{++} – 6%, O^{++} – 6%, C^{+} – 1,8%, Fe^{++} – 1,2%. Среди частиц с энергией 750 эв наблюдались ионы H^{+}, O^{+++}, O^{++}, C^{+}, O^{+}, F^{+}, Cu^{++}, Fe^{+}.

Необходимо заметить, что в экспериментах не удалось обнаружить ионов примесей с энергией выше 1,2 кэв, движущихся в направлении $\pm z$, хотя инжектор такие ионы генерировал. Этих ионов не было обнаружено как на оси, так и в пределах радиуса 12 мм, т.е. в пределах апертуры дивертора. По-видимому, высокоэнергетичные примеси свободно проходят через поперечное магнитное поле. Часть из них попадает в противоположную щель дивертора, а часть ударяется в противоположную стенку вакуумной камеры.

Проведенные исследования массового состава и энергетического спектра ионов плазмы, инжектированной через щели и движущейся вдоль продольной оси дивертора, показали, что имеется оптимальная напряженность магнитного поля, при которой наблюдается наибольший процент захвата ионов водорода на приосевые силовые линии. Примерно в том же диапазоне магнитных полей происходит наилучший захват высокоэнергетичных ионов водорода. Однако, наиболее энергетичные ионы водорода (с энергией выше 4 кэв) и высокоэнергетичные ионы примесей (с энергией выше 1,2 кэв) в апертуру дивертора не захватываются и, вероятно, теряют свою энергию при взаимодействии со стенками камеры в щели или же гибнут у стенки, пересекая поперечное магнитное поле.

При инжекции в магнитное поле с напряженностью выше оптимальной происходит также уменьшение общего количества захваченных внутри апертуры ионов водорода. Для улучшения захвата инжектированной плазмы, по-видимому, целесообразно использовать некоторые усовершенствования метода инжекции плазмы в стелларатор через дивертор. В частности, возможно применение сшивания выведенного в дивертор магнитного потока с магнитным полем плазмовода [25], а также использование поляризационного взаимодействия встречных плазменных потоков в поперечном магнитном поле [26].

ЛИТЕРАТУРА

[1] COOR, T., CUNNINGHAM, S.P., ELLIS, R.A., HEALD, M.A., KRANZ, A.Z., Phys. Fluids 1 1 (1958) 411.
[2] ELLIS, R.A., GOLDBERG, L.P., GORMAN, J.G., Phys. Fluids 3 3 (1960) 468.
[3] БЛИНОВ, П.И., ГАВРИЛОВ, Б.И., ЧЕРЕМНЫХ, П.А., ЯШИН, Н.М., Атомная энергия 20 (1966) 310.
[4] БИРЮКОВ, О.В., БУРЧЕНКО, П.Я., ВАСИЛЕНКО, Б.Т., ВОЛКОВ, Е.Д., ГЕОРГИЕВСКИЙ, А.В., ЛОГИНОВ, А.С., НИКОЛАЕВ, Р.М., САШЕНКО, Ю.В., СУПРУНЕНКО, В.А., ТОЛОК, В.Т., Атомная энергия 23 2(1967) 99.
[5] БУРЧЕНКО, П.Я., ВАСИЛЕНКО, Б.Т., ВОЛКОВ, Е.Д., НИКОЛАЕВ, Р.М., СЕБКО, В.П., ПОТАПЕНКО, В.А., Атомная энергия 23 2(1967) 135.
[6] МИХАЙЛОВСКИЙ, А.Б., В сб. "Вопросы теории плазмы", Госатомиздат, М., 1963, стр.141.
[7] ТИМОФЕЕВ, А.В., ДАН СССР 152 1(1963) 84.
[8] МОИСЕЕВ, С.С., САГДЕЕВ, Р.З., ЖЭТФ 44 2(1963) 763.
[9] ГОРДЕЕВ, Г.В., ЖЭТФ 27 (1954) 1924.
[10] ФАЙНБЕРГ, Я.Б., В сб. "Физика плазмы и проблемы управляемого термоядерного синтеза" 2 Изд. АН УССР, Киев, 1963, стр.88.
[11] СУПРУНЕНКО, В.А., ФАЙНБЕРГ, Я.Б., ТОЛОК, В.Т., СУХОМЛИН, Е.А., РЕВА, Н.И., БУРЧЕНКО, П.Я., РУДНЕВ, Н.И., ВОЛКОВ, Е.Д., Атомная энергия 14 4(1963) 349.
[12] БУРЧЕНКО, П.Я., ВАСИЛЕНКО, Б.Т., ВОЛКОВ, Е.Д., НИКОЛАЕВ, Р.М., ПОТАПЕНКО, В.А., ТОЛОК, В.Т., ЖЭТФ (Письма) 3 6(1966) 243.
[13] ДЕМИДОВ, Б.А., ЕЛАГИН, Н.И., ФАНЧЕНКО, Д.С., ДАН СССР 174 2(1967) 327.
[14] FIELD, E.C., et al., Phys. Fluids 7 (1964) 1937.
[15] РУДАКОВ, Л.И., КОРАБЛЕВ, Л.В., ЖЭТФ 50 (1966) 220.
[16] КОВРИЖНЫХ, Л.М., ЖЭТФ 51 6(1966) 1795.
[17] АРЦИМОВИЧ, Л.А., БОБРОВСКИЙ, Г.А., МИРОНОВ, С.В., РАЗУМОВА, К.А., СТРЕЛКОВ, В.С., Атомная энергия 22 4(1967) 259.
[18] КАДОМЦЕВ, Б.Б., ПОГУЦЕ, О.П., ЖЭТФ 53 6(1967) 2025.
[19] СУПРУНЕНКО, В.А., СУХОМЛИН, Е.А., ВОЛКОВ, Е.Д., РУДНЕВ, Н.И., ЖТФ 31 9(1961) 1057.
[20] ЗЫКОВ, В.Г., РУДНЕВ, Н.И., Доклад № THaC2 на II Европ. конф. по физике плазмы, Стокгольм, 1967.
[21] КОНОВАЛОВ, И.И., КРУПНИК, Л.И., ОНИЩЕНКО, И.И., ШУЛИКА, Н.Т., Сб. "Диагностика плазмы", Госатомиздат, М., 1963, стр.154.
[22] КАЛМЫКОВ, А.А., ТИМОФЕЕВ, А.Д., ПАНКРАТЬЕВ, Ю.Л., НОЗДРАЧЕВ, М.Е., Сб. "Физика плазмы и проблемы управляемого термоядерного синтеза", Изд. АН УССР, Киев, вып.4, 1965, стр.241.
[23] ДЕМИДЕНКО, И.И., ПАДАЛКА, В.Г., САФРОНОВ, Б.Г., СИНЕЛЬНИКОВ, К.Д., ЖТФ 34 6(1964) 1183.
[24] БИРЮКОВ, О.В., ГЕОРГИЕВСКИЙ, А.В., ЗИСЕР, В.Е., КРАВЧИН, Б.В., КИТАЕВСКИЙ, Л.Х., ПОГОЖЕВ, Д.П., СЕРГЕЕВ, Ю.Ф., Атомная энергия 23 2(1967) 136.
[25] ГЕОРГИЕВСКИЙ, А.В., БИРЮКОВ, О.В., ДИКИЙ, А.Г., ЗИСЕР, В.Е., ПЕЛЕТМИНСКАЯ, В.Г., Атомная энергия 24 1(1968) 61.
[26] ЗЫКОВ, В.Г., СИНИЦА, Н.Г., СТЕПАНЕНКО, И.А., ТОЛОК, В.Т., СИНЕЛЬНИКОВ, К.Д., ЖТФ 34 8(1964) 1417.

DISCUSSION

A. GIBSON: What theoretical derivation was used to obtain the value of β_e given in your paper?

E.D. VOLKOV: We used the following expression:

$$\beta_e = 2^{3-2n} \frac{q - 2n+4}{q} \frac{i^2}{\pi L} r_0$$

where q was derived from the approximate expression for the pressure $P = P_0\{1 - (r/r_0)^q\}$.

A. GIBSON: Did you observe in your experiments any dependence of β_e on the applied transverse magnetic field?

E.D. VOLKOV: We did not carry out any experiments with transverse fields.

УДЕРЖАНИЕ ПЛАЗМЫ В СТЕЛЛАРАТОРЕ ПРИ РАЗЛИЧНЫХ ЗНАЧЕНИЯХ ДЛИНЫ СВОБОДНОГО ПРОБЕГА

В.Н.БОЧАРОВ, В.И.ВОЛОСОВ, А.В.КОМИН,
В.М.ПАНАСЮК и Ю.Н.ЮДИН
ИНСТИТУТ ЯДЕРНОЙ ФИЗИКИ СИБИРСКОГО
ОТДЕЛЕНИЯ АН СССР, НОВОСИБИРСК,
СССР

Abstract — Аннотация

PLASMA CONTAINMENT IN A STELLARATOR FOR DIFFERENT FREE PATH LENGTHS. The authors investigate experimentally plasma decay in a stellarator with the following parameters: radius of the device R = 50 cm; chamber radius r = 5 cm; angle of inclination of the helical winding 45°; $\ell = 3$. According to theory the maximum angle of the curved field trajectory $i = 4\pi$; the measured value $i \cong \pi$. To heat the electrons and produce the plasma the authors employ the "stochastic heating" method, in which a high-frequency voltage is applied across one or several sections of the metallic chamber (f = 5 Mc/s; $U_{h.f} = 40$ V). The parameters of the plasma produced by this method are: $n = 10^9$ cm^{-3}; $T_e = 30 - 300$ eV; neutral atom density $10^{11} - 10^{15}$ cm^{-3}. The plasma decay is studied after the high-frequency generator has been switched off and the electrons have cooled to 5-10 eV. Densities of $10^9 - 10^6$ cm^{-3} are measured by means of a u.h.f. resonator. The experiments are carried out with argon and helium. The plasma decay time reduced to a constant separatrix radius $\tau' = \tau(r/r_c)^2$, where r_c is the true separatrix radius. When the electron free paths are relatively short (less than or of the same order as the perimeter of the system), the approximate empirical formula $\tau' = k\epsilon^2 H_p^2$ can be used, where ϵ is the ratio of the helical winding current to the toroidal winding current and H is the longitudinal field. The resulting dependence of the plasma lifetime on the magnetic field and on ϵ^2 (ϵ^2 being proportional to the shear) is of the same order of magnitude as the diffusion coefficient determined by the universal (drift) instability. Correlation measurements with the help of nv-probes show that oscillations with frequencies close to the drift frequency are present in the plasma.

УДЕРЖАНИЕ ПЛАЗМЫ В СТЕЛЛАРАТОРЕ ПРИ РАЗЛИЧНЫХ ЗНАЧЕНИЯХ ДЛИНЫ СВОБОДНОГО ПРОБЕГА. Проводились эксперименты по изучению процесса распада плазмы в стеллараторе с параметрами: радиус установки R = 50 см; радиус камеры r = 5 см; угол наклона винтовой обмотки 45°; $l = 3$. Максимальный угол прокручивания силовой линии, согласно теории, равен $i = 4\pi$, а измеренное значение $i \approx \pi$. Для нагрева электронов и создания плазмы использовался метод "стохастического нагрева", при котором ВЧ-напряжение приложено к одному или нескольким разрезам металлической камеры (f = 5 Мгц, $U_{ВЧ} = 40$в). Параметры полученной этим методом плазмы: $n = 10^9$ см$^{-3}$; $T_e = 30-300$ эв; плотность нейтральных атомов от 10^{11} до 10^{15} см$^{-3}$. Распад плазмы изучался после выключения ВЧ-генератора и остывания электронов до энергии 5-10 эв. Плотность измерялась от 10^9 до 10^6 см$^{-3}$ при помощи СВЧ-резонатора. Эксперименты были выполнены на аргоне и гелии. Время распада плазмы, приведенное к постоянному радиусу сепаратриссы $\tau' = \tau(r/r_c)^2$; r_c – истинный радиус сепаратриссы; в случае относительно малых пробегов электронов (меньше или порядка периметра системы) можно аппроксимировать эмпирической формулой $\tau' = K\epsilon^2 H^2 p$, где ϵ – отношение тока винтовой обмотки к току тороидальной, H – продольное поле. Полученная зависимость времени жизни плазмы от магнитного поля и ϵ^2 (величина ϵ^2 пропорциональна ширу) соответствует, по порядку величины, коэффициенту диффузии, определяемому универсальной (дрейфовой) неустойчивостью. Корреляционные измерения, проведенные с помощью nv-зондов, показали наличие в плазме колебаний с частотами, близкими к дрейфовой частоте.

Одним из методов изучения свойств термоядерной плазмы в замкнутых магнитных ловушках является моделирование при помощи относительно холодной и редкой плазмы, в которой при соответствующем выборе параметров должны наблюдаться те же закономерности, что и в горячей "термоядерной" плазме. Модельный эксперимент позволяет изучить свойства плазмы в зависимости как от структуры магнитного поля – величины шира θ и угла прокручивания i, глубины магнитной ямы V', величины магнитного поля или точнее ρ_Λ/r (r – поперечный размер системы),– так и от параметров плазмы – отношения длины свободного пробега λ к периметру системы $S \approx 2\pi R$, отношения температуры ионов T_i к электронной T_e, отношения размера дебаевского радиуса r_D к размерам системы и т.д. При этом лишь немногие параметры, например, $\beta = 8\pi nT/H^2$, поддаются моделированию в ограниченной области ($\beta < 10^{-4}$-10^{-6}).

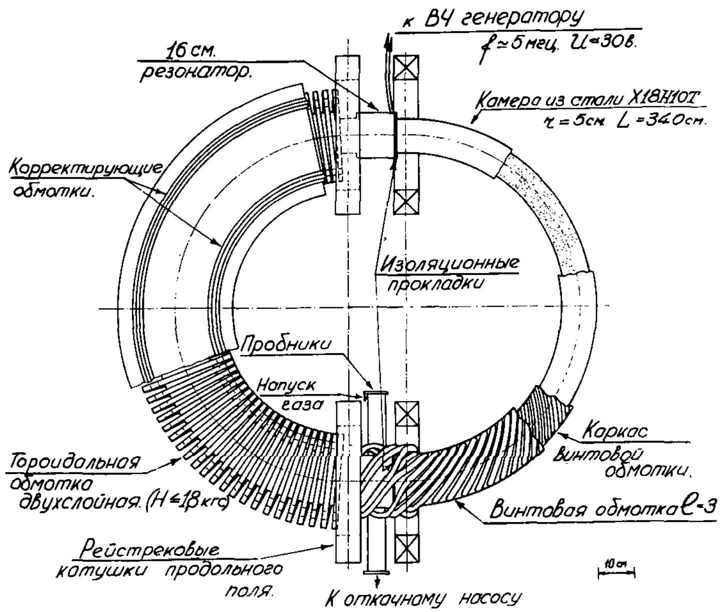

Рис.1. Схематический разрез стелларатора.

В данной работе была сделана попытка провести изучение свойств плазмы при низких температурах электронов и относительно низкой плотности плазмы, которая ограничена снизу условием, что дебаевский радиус должен быть много меньше поперечных размеров системы. Снижение требований к параметрам плазмы позволило применять для ее создания и нагрева довольно простой метод стохастического нагрева. При использовании этого метода можно было в процессе эксперимента независимо менять каждый из следующих параметров: отношение пробега к периметру, шир или угол прокручивания, магнитное поле, массу ионов и ряд других.

Несмотря на то, что некоторые из подобных экспериментов проводились ранее в других лабораториях [1 – 3], результаты, полученные в данной работе, относятся к более широкому кругу параметров, что позволяет сделать ряд интересных обобщений.

ОПИСАНИЕ УСТАНОВКИ

Магнитная ловушка типа "стелларатор" с 3-х заходной винтовой обмоткой была построена в ИЯФ СО АН СССР в 1967 году. Особенностью установки является наличие винтовой обмотки на прямолинейных участках, что позволяет работать без цилиндрителей и получить дополнительное вращательное преобразование. Радиус установки – 50 см, радиус камеры – 5 см, средний радиус винтовой обмотки – 6,7 см, длина прямолинейных участков – 16 см и осевая длина камеры – 346 см. При угле наклона винтовой обмотки ~45° полное число периодов обмотки $N=8\frac{2}{3}$ (по 1/3 на прямолинейном участке), см. рис.1. Расчеты, аналогичные расчетам Гибсона [4], дают максимальное вращательное преобразование $i \approx 4\pi$. Реальное максимальное вращательное преобразование меньше ($\sim\pi$) за счет возмущений, вносимых прямолинейными участками и неоднородностями винтового и продольного полей на прямолинейном участке. Продольное магнитное поле в постоянном режиме может достигать 2 кэ, а в импульсном режиме – 6 кэ (длительность импульса 1 сек) при максимальном значении шира. Для компенсации обратного тока и неточностей установки тороидальной обмотки использовались корректирующие обмотки, дающие произвольную компоненту магнитного поля в плоскости, перпендикулярной продольному полю. В экспериментах величина корректирующего поля была ~1% от основного. Предельный вакуум в системе был равен $\sim 3\cdot 10^{-7}$ тор. Давление нейтрального газа в экспериментах менялось от 10^{-6} до 10^{-1} тор.

МЕТОД СОЗДАНИЯ ПЛАЗМЫ

Создание плазмы и нагрев электронов осуществлялись методом стохастического нагрева. К разрезу металлической вакуумной камеры (рис.1) прикладывалось ВЧ-напряжение с частотой порядка нескольких мегагерц; электроны, образующиеся в объеме при ионизации остаточного газа, нагреваются до энергии W_{max}, определяемой условиями нарушения стохастичности [5]:

$$W_{max} = (RfU/5S)^{2/3}$$

где R – радиус установки; f – частота в Мгц, U – амплитуда ВЧ-напряжения в вольтах, S – число разрезов. Для нашего эксперимента при $f = 5$ Мгц, $U_{ВЧ} = 40$ в и $S = 2$ получаем $W_{max} = 100$ эв. С другой стороны, необходимо выполнить условие, определяющее вхождение частиц в режим ускорения $f^2 l^2 < 150\ U$; l – размер области локализации ускоряющего поля ($l \geq r$).

Приведенные выше оценки позволяют найти оптимальную частоту f_0 ВЧ-генератора, для нашего эксперимента $f_0 \approx 3-10$ Мгц. Максимальная плотность плазмы, которая может быть получена этим методом, ограничена условием равенства скин-слоя поперечному размеру плазмы

$$r < \frac{c}{\omega_p} = \left(\frac{mc^2}{4\pi n e^2}\right)^{1/2}$$

максимальная плотность плазмы в экспериментах достигла 10^9 см$^{-3}$; приведенная выше оценка дает $n \leq 10^{10}$ см$^{-3}$.

ЭКСПЕРИМЕНТАЛЬНЫЕ РЕЗУЛЬТАТЫ

Диффузия плазмы изучалась в режиме распада, после выключения ВЧ-генератора (длительность ВЧ-импульсов – 1-10мсек, частота повторения – 50 гц). Оценки и эксперимент показывают, что при этом электроны в плазме относительно быстро остывают до энергии ~ 5-10 эв за счет неупругих соударений, после чего время остывания резко возрастает, так как неупругие соударения при этих энергиях практически отсутствуют, а упругие соударения дают время остывания в $3\ M_i/8m$ раз больше при тех же сечениях [6]. Средняя энергия ионов при этом много ниже электронной. Оценки показывают, что ионы могут нагреваться за счет стационарных или переменных электрических полей до энергии не выше 0,1 эв.

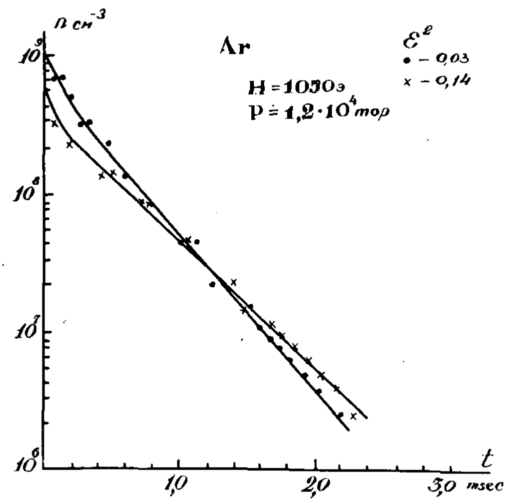

Рис.2. Типичная кривая распада плотности плазмы для A_r.

Средняя энергия электронов в режиме распада измерялась с помощью многосеточного зонда через 0,3, 0,6 и 1,2 мсек после начала распада. Разброс по энергии в этих точках не превышал 20%, что свидетельствует о том, что плазма практически не остывает за время распада. При различных параметрах плазмы для гелия и аргона была получена средняя энергия $T_e \approx 7 \pm 2$ эв.

С помощью 16-см резонатора, помещенного в одном из прямолинейных участков установки, измерялась плотность плазмы в процессе ее распада. Типичная кривая распада приведена на рис.2. Начальный участок кривой связан с быстрой диффузией и остыванием электронов от 30-100 до 5-10 эв. Прямолинейный участок функции $\ln n(t)$ использовался для определения τ распада. Наличие прямолинейного участка на кривых $\ln n(t)$ вплоть до вакуума 10^{-3} - 10^{-2} тор является косвенным доказательством постоянства T_e в процессе распада. Кроме τ, можно ввести величину τ' (аналогично [2]), которая равна τ, если средний радиус сепаратриссы r_c больше радиуса камеры r, и равна $\tau(r_c/r)^2$, если $r_c < r$.

Радиус сепаратриссы r_c может быть определен по Гибсону [4]. В действительности, за счет неидеальности магнитного поля величина r_c меньше и определяется по перегибу кривой $\tau(\epsilon^2)$; определенное таким образом

r_c удовлетворительно совпадает с теоретическим значением r_c при $i \approx \pi$. Коэффициент диффузии D может быть определен из τ' распада: $D = (r/2,4)^2(\tau')^{-1}$, если процесс ионизации не дает существенного вклада за время распада. Для нашего случая $r = 5$ см. Однако, более правильно брать средний радиус последней вписанной в камеру поверхности, для которой $r \approx 4$ см. Оценки времени максвеллизации показали, что оно много больше как времени ионизации, так и времени распада, т.е. поправки, связанные с ионизацией, не существенны.

Зависимость τ и τ' от отношения тока винтовой обмотки ($I_в$) к току тороидальной (I_T) приведена на рис.3 и 4. Для удобства сравнения с теорией на рисунках приведен параметр ϵ, определяющий отношение амплитуды винтового поля к продольному (см., например,[1]), который равен в нашем случае $\epsilon = 0,17\, I_в/I_T$. Заметим, что $i \approx 3,8\, \pi N^3 \epsilon^2 r_c^2 R^{-2}$, $\theta \approx r_c i/\pi R$. Время τ' линейно зависит от ϵ^2 для различных значений вакуума и магнитного поля. Отклонение от этого закона наблюдается лишь при достаточно высоком вакууме $p \leq 5 \cdot 10^{-5}$ тор.

Взаимодействие плазмы с нейтральным газом приводит к увеличению τ' (см. рис.5) в довольно широких пределах по λ_{en}/S от 10^{-2} до 10; λ_{en} – пробег электронов, S – периметр установки. При давлении газа выше, чем $\sim 3 \cdot 10^{-3}$ тор, τ' начинает убывать. Это падение, по-видимому, объясняется влиянием классической диффузии. Для сравнения на рис.5 приведены значения τ' для классической и бомовской диффузии. Заметим, что при достаточно плохом вакууме, при условии

$$(\omega_{He}\tau_{en})(\omega_{Hi}\tau_{in}) \leq \frac{4\pi^2}{i^2} \cdot \frac{R}{r}$$

коэффициент классической диффузии в стеллараторе определяется без поправок, связанных с величиной $4\pi^2/i^2$.

Постоянное магнитное поле в экспериментах изменялось от 300 до 1200 эрстед. Зависимость τ от H приведена на рис.6. Большинство экспериментальных точек ложится на кривую $\tau \sim H^2$.

С увеличением массы иона τ несколько возрастает, но четкой зависимости $\tau \sim \sqrt{M_i}$ (как это предсказывает теория) не наблюдается.

На основании приведенных выше экспериментальных данных, время распада плазмы (при $\lambda_{en} \leq S$) можно аппроксимировать эмпирической формулой:

$$\tau' \approx K\epsilon^2 H^n F(p) \approx K\epsilon^2 H^2 p$$

где K – постоянная, зависящая от параметров плазмы; $n = 2 \pm 0,2$.

Распад плазмы сопровождается колебаниями с частотами в интервале 1-50 кгц (причем наибольшая амплитуда колебаний соответствует частотам ~5-10 кгц). Оценки показывают, что эти частоты близки к дрейфовым $\omega = \frac{cT_e}{eH} \cdot \frac{1}{r\lambda_\varphi}$, которые равны в нашем случае приблизительно 10 кгц для основной моды колебаний.

Корреляционные измерения величины nV, проведенные с помощью нескольких зондов (диаметр зонда-шарика 3 мм), помещенных в плазму на различных азимутах, дали для величины $m = 2\pi r/\lambda_\varphi$ значения от 1 до 3. Те же измерения для λ_r дали размер порядка 5-10 мм. Типичные осциллограммы, полученные с 5 зондов, расположенных на одной магнитной поверхности по азимуту через 60°, приведены на рис.7.

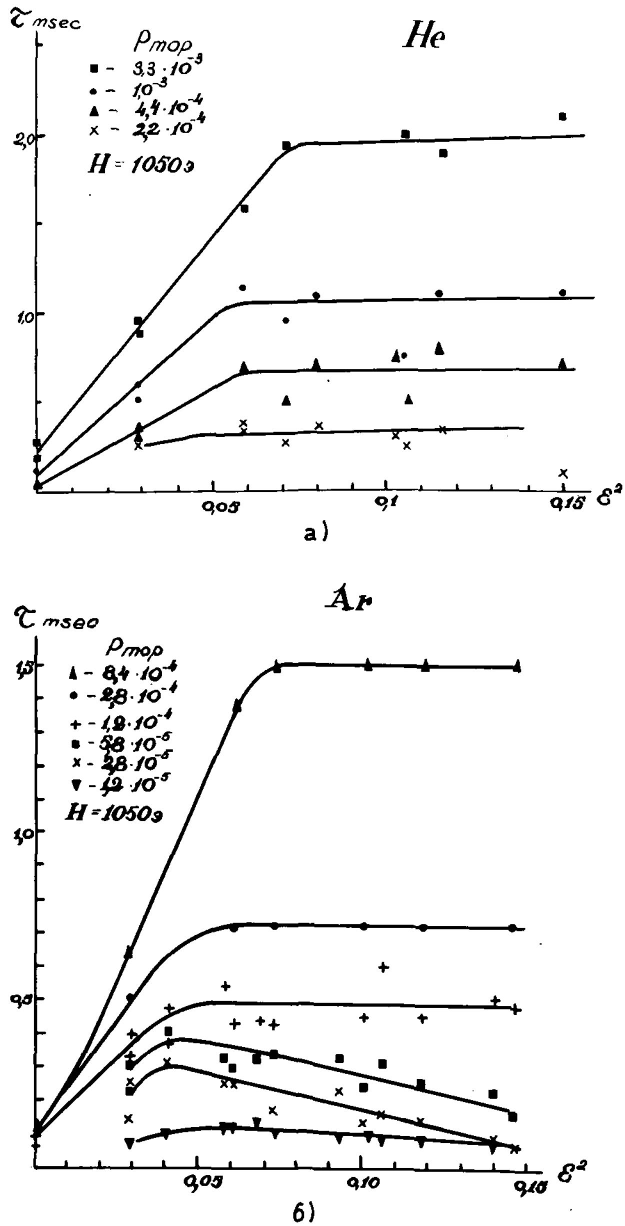

Рис.3. Зависимость времени жизни плазмы от $\epsilon^2 (\epsilon \sim I_B)$, H= 1050 э: а) – H_e; б) – A_r.

Колебания плотности на кривых распада плазмы наблюдаются вплоть до плотности n_e, соответствующей $r_D \approx$ 1-2 см. При этом скорость распада не меняется (см. рис.8). Это, по-видимому, подтверждает тот факт, что поперечная длина волны колебаний, вызывающих диффузию, не менее 1-2 см.

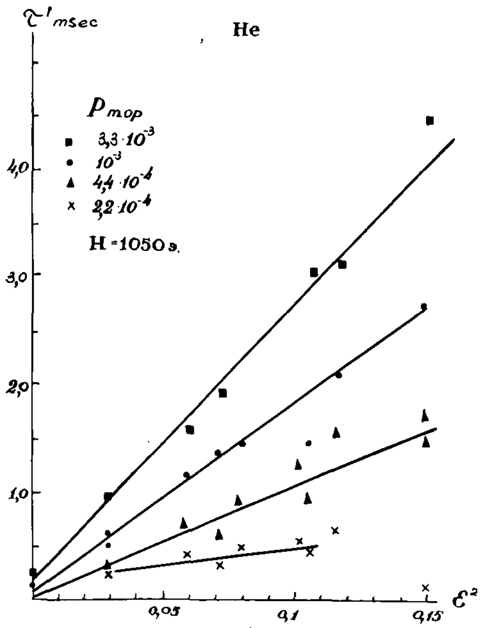

а)

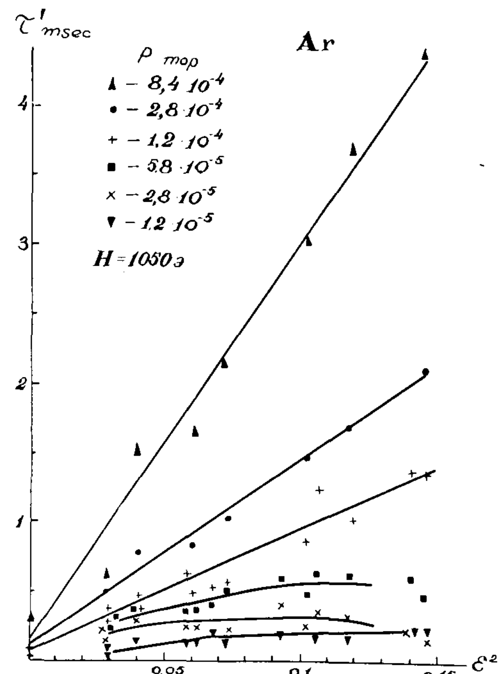

б)

Рис.4. Зависимость приведенного времени жизни плазмы от ϵ^2, H = 1050 э: а) – H_e; б) – A_r.

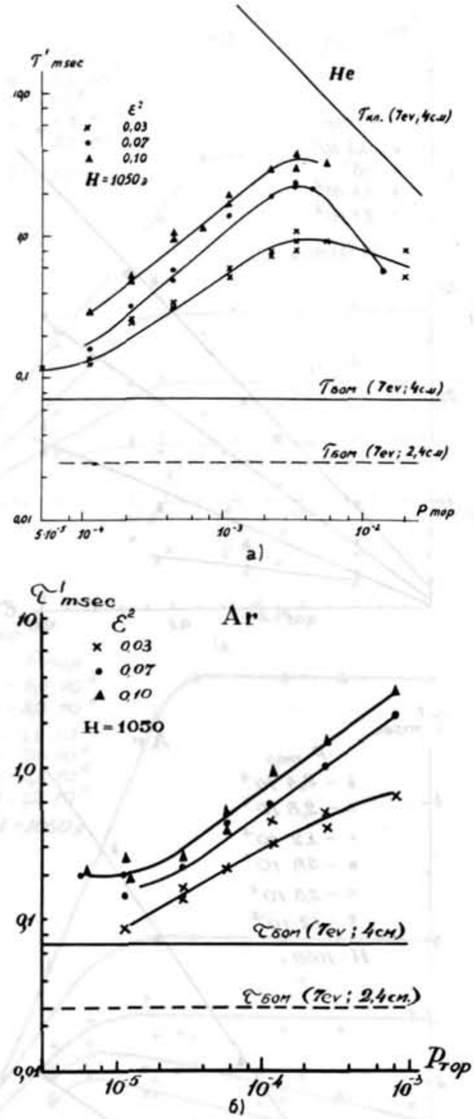

Рис.5. Зависимость приведенного времени жизни от давления нейтрального газа, H = 1050 э: а) – H_e; б) – A_r.

Амплитуда колебаний, нормированная на среднюю плотность плазмы, уменьшалась с увеличением давления от $3 \cdot 10^{-5}$ до 10^{-3} тор приблизительно в 2 раза и практически не зависела от величины магнитного поля.

ОБСУЖДЕНИЕ

1. Экспериментально измеренная зависимость времени жизни и коэффициента диффузии от шира и магнитного поля соответствует по порядку величины коэффициенту диффузии, определяемому универсальной

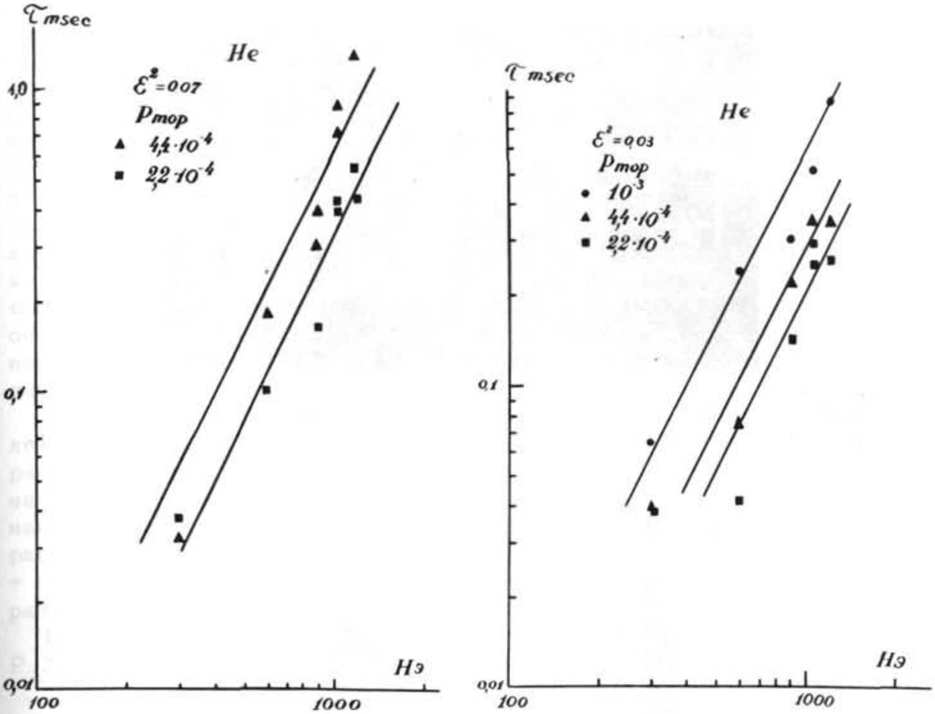

Рис.6. Зависимость времени жизни плазмы от величины продольного магнитного поля для H_e.

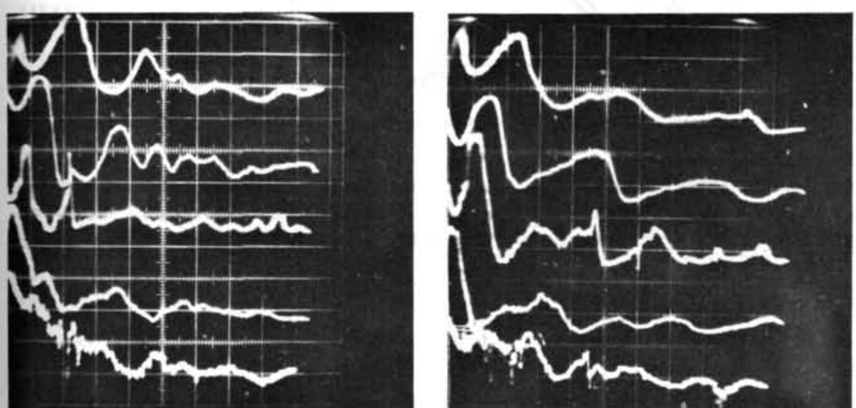

а) б)

Рис.7. Корреляция токов на зонды, расположенные в поперечном сечении магнитной поверхности; развертка 50 мксек-см; $p = 10^{-3}$ тор; $\epsilon^2 = 0{,}07$; A_r: а) H = 600 э; б) 900 э.

(дрейфовой) неустойчивостью [7,8]. С увеличением шира уменьшается характерный размер турбулентных пульсаций и диффузия падает. С другой стороны, ион-нейтральные столкновения оказывают стабилизирующее действие на неустойчивость, что соответствует уменьшению коэффициента диффузии с увеличением плотности.

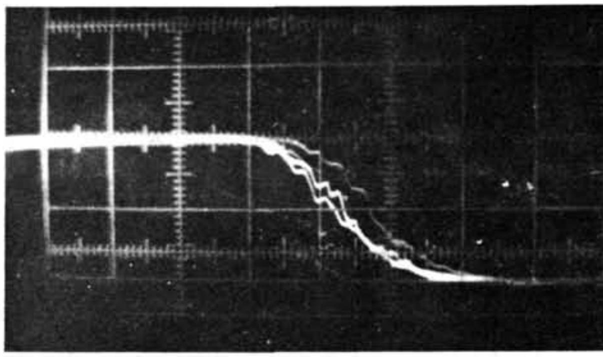

Рис.8. Типичная осциллограмма распада плотности плазмы для H_e; развертка 0,5 мксек/см; интервал плотностей – от $3 \cdot 10^7$ до $1 \cdot 10^6$ см$^{-3}$; H = 1050 э; p = $1,2 \cdot 10^{-4}$ тор; $\epsilon^2 = 0,14$.

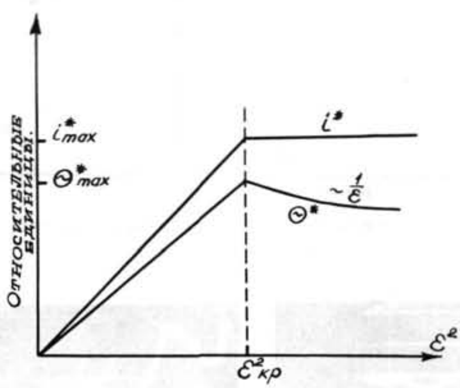

Рис.9. Зависимость i и θ от ϵ^2.

Неустойчивость на запертых частицах [9], по-видимому, не может быть причиной наблюдавшейся аномальной диффузии. Критерий полного подавления этой неустойчивости, в соответствии с [10], имеет вид

$$\frac{\nu_e}{\epsilon_T} \frac{r}{v_{Te}\,\theta\sqrt{\epsilon_T}} \geq 0,1\left(\frac{m_e}{m_i}\right)^{1/3} \cdot \frac{T_i}{T_e}\ ;\ \epsilon_T \approx r/R$$

Для аргона при учете электрон-нейтральных соударений эта оценка дает давление $\sim 10^{-7}$ тор, что на четыре порядка отличается от давления, при котором измеренный коэффициент диффузии приближается к классическому (см. рис.5б).

2. Большой интерес представляет зависимость времени распада плазмы от величины шира ϵ^2. Время τ', введение которого вызвано необходимостью учитывать реальные размеры сепаратриссы, линейно зависит от ϵ^2. Однако, поведение плазмы должно определяться не ϵ^2 – в некотором смысле формальным параметром, а углом прокручивания i или широм θ на поверхности реальной сепаратриссы. Зависимость этих вели-

чин от ϵ^2 приведена на рис.9; при $\epsilon^2 < \epsilon^2_{кр}$, i и θ пропорциональны ϵ^2, при $\epsilon^2 > \epsilon^2_{кр}$, i — слабо растет в соответствии с [4], а θ убывает приблизительно как ϵ^{-1}. Графики i и θ оказываются подобными графику реального времени удержания (рис.3). Можно предположить, что по каким-то причинам диффузионный размер при вписывании сепаратриссы в камеру не изменяется. Таким диффузионным размером может быть полный размер камеры (например, за счет того, что небольшое количество плазмы находится за сепаратриссой) или размер некоторого наружного слоя плазмы, в котором происходит диффузия. В этом случае диффузия определяется величиной τ (а не τ') и величина D обратно пропорциональна i или θ в соответствии с рис.3. Это объяснение не претендует на строгость, но оно позволяет наметить некоторые контрольные эксперименты для выяснения процессов, происходящих при диффузии, а также показывает, что диффузия в стеллараторе является достаточно сложным процессом.

3. Приведенные выше выражения, связывающие τ' с магнитным полем и величиной ϵ^2, несколько отличаются от результатов, полученных ранее в ФИАН (СССР) и Принстоне (США) [1 - 3]. Так, например, ранее наблюдалась линейная зависимость τ от магнитного поля, а не квадратичная (см. рис.6); другим был характер зависимости от ϵ (или от θ). Это расхождение можно объяснить тем, что детальное изучение зависимости τ от ϵ, H и p было проведено нами при $\lambda/S < 10$, тогда как большинство ранее описанных экспериментов проводилось при $\lambda/S > 10$.

В заключение авторы выражают глубокую благодарность А.А.Галееву и Р.З.Сагдееву за внимание к работе и ценные советы.

ЛИТЕРАТУРА

[1] АКУЛИНА, Д.К., БАТАНОВ, Г.М. и др., Plasma Physics and Controlled Nuclear Fusion Research, Conf. Proc. (Culham, 1965) IAEA, Vienna 2 1966, p. 733.
[2] ELLIS, B., Confinement of Injected Plasma in the Etude Stellarator, Доклад на Конф. по замкнутым системам, Принстон, июнь 1967.
[3] STODIEK, W., GROVE, D. and KESSLER, J.O., Plasma Physics and Controlled Nuclear Fusion Research, Conf. Proc. (Culham, 1965) IAEA, Vienna 2 1966, p. 687.
[4] GIBSON, A., Phys. Fluids 10 7 (1967) 1553.
[5] ВОЛОСОВ, В.И., КОМИН, А.В., ЖТФ 5 (1968).
[6] МАК-ДАНИЕЛЬ, И., Процессы столкновений в ионизованных газах, Москва, 1967, стр. 32.
[7] ГАЛЕЕВ, А.А., МОИСЕЕВ, С.С., САГДЕЕВ, Р.З., Атомная энергия 15 (1963) 451.
[8] КАДОМЦЕВ, Б.Б., ПОГУЦЕ, О.П., Вопросы теории плазмы 5 Москва, 1967, стр. 340.
[9] КАДОМЦЕВ, Б.Б., ПОГУЦЕ, О.П., ЖЭТФ 51 (1966) 1734.
[10] ГАЛЕЕВ, А.А., САГДЕЕВ, Р.З., ДАН СССР, 1 июня 1968 г. (в печати).

DISCUSSION

S. YOSHIKAWA: What was the accuracy of your electron temperature measurements at such a low density? It is remarkable (in view of the presence of oxygen, etc.) that T_e remains at 7 eV for the duration of the plasma.

V.I. VOLOSOV: The electron energy distribution function was studied with the aid of a multigrid analyser. The measurements were accurate to within ±2 eV. Estimates have shown that the presence of oxygen could not affect electron cooling.

S. YOSHIKAWA: Electrons with an energy of 7 eV and a Maxwellian distribution may not be sufficient to cause ionization, but runaway (high-energy) electrons may cause ionization which increases the density decay time.

V.I. VOLOSOV: Measurements showed that there were no electrons with energies higher than 15 eV in this experiment.

S.J. BUCHSBAUM: Would you not expect diffusional cooling in the afterglow?

V.I. VOLOSOV: We observed plasma cooling only with an extremely poor vacuum ($\sim 10^{-2}$ mmHg); the shape of the associated decay curves changed and the decay "tail" had a very gentle slope.

EXPERIMENTS ON PLASMA INJECTION, HEATING AND CONFINEMENT IN STELLARATORS

J. H. ADLAM, D. E. T. F. ASHBY, R. J. BICKERTON, J. N. BURCHAM,
M. FRIEDMAN, S. M. HAMBERGER, E. S. HOTSTON, D. J. LEES,
A. MALEIN, P. REYNOLDS, P. A. SHATFORD AND B. M. WHITE
UKAEA, CULHAM LABORATORY, ABINGDON, BERKS, UNITED KINGDOM

Abstract

EXPERIMENTS ON PLASMA INJECTION, HEATING AND CONFINEMENT IN STELLARATORS. A simple plasma accelerator that injects plasma across a magnetic field is described. It consists of two disc-shaped electrodes in the magnetic field of a long solenoid with additional helical (ℓ = 3) windings. Gas is supplied from hydrogen-loaded titanium electrodes. An artificial line is discharged across these electrodes producing a plasma stream which crosses the magnetic field as well as spreading along the field lines. Typical parameters in the experiments to be described are an ion energy of 30 eV, a pulse length of 50 μs, a total number of ions of $\sim 6 \times 10^{15}$ in a field of 3 kG.

This system has been used to inject plasma into two stellarators. The first uses a silica torus of 10 cm bore, 65 cm major diameter and an axial field of $\sim$3 kG. External helical windings (ℓ = 3) provide a maximum rotational transform of $\sim 120°$. Plasma is injected into this first stellarator, enabling the initial preheat voltage pulse to break down a hydrogen gas background (pressure $\sim 10^{-4}$ torr). The resulting plasma is then heated to kilovolt temperatures by inducing in it a large axial electric field (greatly exceeding the critical field for runaway). The current which flows for 1 μs is a uni-directional pulse of $\sim 10^4$ A. Large-amplitude electrostatic waves are excited; the collisionless damping of these waves leads to rapid heating of both electrons and ions.

In a second stellarator, the helical winding has a minor radius of 9 cm and major radius of 40 cm. The pulsed magnetic field is $\sim$3 kG and ℓ = 3 windings give a rotational transform of 220° and a shear parameter $\theta \sim 6 \times 10^{-2}$. Experimental results indicate that the injected plasma is confined in this stellarator for periods of up to 15 Bohm times.

1. INTRODUCTION

Low-β toroidal plasma containment systems appear the most promising as potential thermonuclear reactors [1]. For such reactors we cannot envisage solid conductors buried in the plasma, and so we are led to systems of the stellarator type in which the confining magnetic fields are produced solely by currents in external conductors. Such fields have no simple symmetry and consequently it cannot be proved analytically or by computation that closed magnetic surfaces and particle-drift surfaces exist to the accuracy required for a fusion machine. However, in a recent experiment [2] Gibson has shown that β-particles produced by the radioactive decay of tritium gas are contained in an ℓ = 3 toroidal stellarator for more than 10^7 transits, (i.e. adequate for thermonuclear purposes). Gibson and Mason have also shown by computation [3] that the loss cone in a stellarator is more serious than was thought hitherto [4], but that nevertheless adequate confinement for fusion can be achieved. In this work the effect of an ambipolar electric field on particle orbits was ignored. It is widely believed that the inclusion of this effect will improve the particle confinement but this remains unproven. Thus we have grounds for believing that an adequate plasma equilibrium can be achieved in a stellarator although clearly much remains to be done on the subject.

The remaining major problems are those of plasma injection, plasma heating and confinement. Note that containment for ~ 100 Bohm times is sufficient for a fusion reactor [1]; that no stability theory exists which takes full account of the field geometry in a stellarator; but that results obtained in simpler geometries suggest that adequate stability is possible in a high-shear stellarator [5].

In this paper we describe the progress of experimental work at Culham on these three problems, plasma injection, heating and confinement.

2. PLASMA INJECTION

The acceleration of plasma and its subsequent injection into various configurations of magnetic field have been extensively studied in the last decade. The plasma accelerators commonly used for injection are limited to pulsed operation because they depend on a moving current sheet to act as a piston (e.g., the Marshall [6] and thetatron [7] injectors). In contrast the injector to be described here [8] is essentially a d.c. device, i.e. although in practice it is pulsed, in principle its duration can be unlimited. Another novel feature is that its operation depends upon the magnetic field of the plasma trap itself and hence it produces a polarized stream, which moves across the field lines. The injector has a comparatively high electrical impedance and is normally used at a current of order 100 A, whereas most other accelerators require currents of 1-100 kA. The energy input is correspondingly low, and in the experiments to be described is typically one joule. It is physically compact and at present is used to produce $\sim 6 \times 10^{15}$ ions with energies ~ 50 eV.

2.1. Construction of injector

Figure 1 shows the injector schematically and illustrates its mode of operation. Two disc-shaped electrodes are set in a uniform magnetic field so that the discharge current flowing between them is orthogonal to the magnetic field. The electrodes are made of hydrogen-loaded titanium and are fed with current from an artificial line. The direction of current flow is such that the magnetic force $\vec{j} \times \vec{B}$ drives the plasma way from the electrodes and their supports and across the magnetic field.

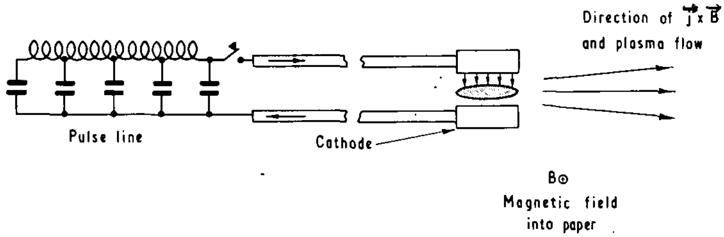

FIG.1. Schematic of plasma injector illustrating its mode of operation.

2.2. Operation of injector

Although the detailed operation of the injector is complex and not fully understood, the following general points can be made:

(a) the maximum energy the ions can acquire is approximately V electron volts where V is the voltage drop across the discharge.
(b) conservation of momentum together with condition (a) implies that the electrode spacing is approximately equal to the ion gyro-radius for ions of energy eV.

The artificial line driving the discharge is charged to 1200 V, has an effective impedance of 13 Ω, and a pulse time of 50 μs. To initiate the discharge in the injector, a negative pulse of 15 kV is applied to a trigger pin set in the cathode.

The injector is tested by firing it transversely into a 15 cm-diameter glass vacuum vessel set in a 2 metre long solenoid which produces field strengths of up to 3 kG. Helical $\ell = 3$ stabilizing windings are located at a radius of 10 cm with a field period of 34 cm and carry currents of up to 40 kA. The injection of plasma into this system has been studied using ion probes [9], an ion energy analyser [9], and a plasmascope [10]. Probe measurements show that with the ℓ-windings energized, approximately 30% of the plasma produced by the gun is trapped by the magnetic field. With no current in the ℓ-windings, the trapping efficiency is reduced, and the plasma density shows wild fluctuations and becomes highly irreproducible. This behaviour is presumably due to instability in the unsheared magnetic field. With a 5 mm spacing between the disc electrodes and with a 3 kG field from the solenoid, the trapped plasma has an ion temperature of $\sim$30 eV and an electron temperature of $\sim$20 eV. Figure 2 shows plasmascope photographs taken end-on to the solenoid. The characteristic trefoil shape of the separatrix for $\ell = 3$ magnetic surfaces is clearly shown.

No direct information on the percentage of impurity ions in the plasma is available, but measurements [8] of ion gyro-radii indicate that the ions are predominantly protons. It should be noted that the electrodes show no sign of damage or melting after many thousands of discharges.

Our results show that the method of plasma production using a quasi-d.c. plasma injector offers interesting possibilities for filling traps with plasma.

3. PLASMA HEATING

Since the pioneering work of Adlam [11] and Zavoisky [12], it has been known that it is possible to deposit energy into a plasma extremely rapidly through the process of turbulent heating. In this process, a large current is passed through the plasma such that strong electrostatic instabilities are excited. The particle scattering in the resultant electric microfields leads to rapid heating and to a high plasma resistivity.

We report here the results of experiments on the TWIST apparatus which is an $\ell = 3$ toroidal stellarator with facilities for turbulent heating. These results are concerned mainly with the properties of the heating process rather than the subsequent containment of the heated plasma. As

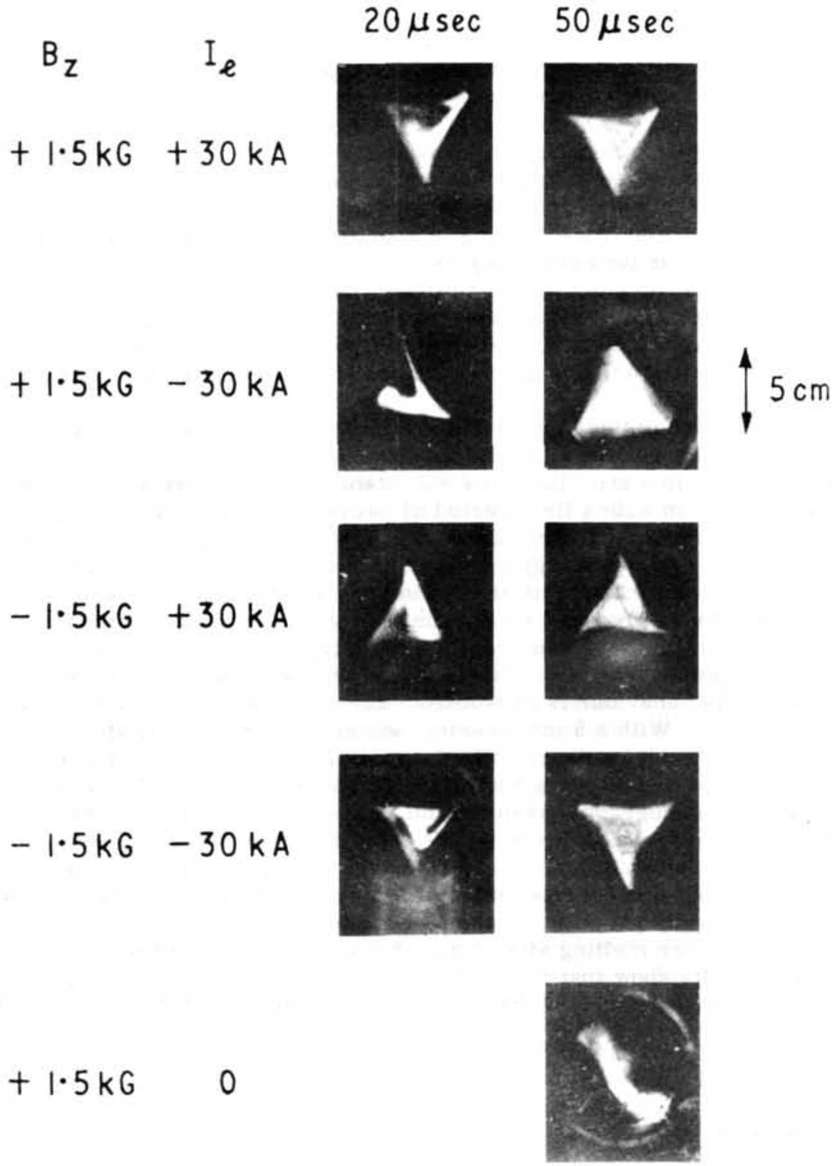

FIG. 2. Plasmascope photographs of plasma injected into a straight stellarator showing trefoil shape of separatrix.

will be seen, the strength of the magnetic field (≤ 3 kG) in this stellarator is not adequate to contain the large plasma pressure produced by the heating pulse. Thus the chief function of the stellarator fields in the present study is to enable a suitably low-density initial plasma to be established in the torus prior to the application of turbulent heating.

3.1. Apparatus

The discharge chamber consists of a single-piece-fused silica toroid. Its dimension and the main parameters of the TWIST apparatus are given in Table 1. The axial magnetic field is produced by a single turn coaxial loop (Fig. 3), which is energized by a 4000 μF capacitor bank via a low inductance concentric line and pulse transformer. The time to peak current is 0.3 msec, and the decay time constant is 1.5 ms. The ℓ = 3 helical windings are made from 1.2 cm diameter solid copper bars and are energized from a separate capacitor bank with a current pulse synchronized with that of the B_z field.

The electric field used to drive currents around the torus both for plasma preparation and its subsequent turbulent heating are electromagnetically induced by currents in a close-fitting primary winding (Fig. 4). This winding consists of 16 equally spaced parallel wires wound circumferentially on the torus and divided into four quadrants. Current is fed into the four gaps via low-inductance transmission lines. The turbulent heating pulse is obtained by the simultaneous discharge into each of the four gaps of a low-inductance 0.28 μF, 60 kV capacitor through a pressurized spark gap. The current pulse is reduced to a single half-cycle by non-linear resistors in series with each capacitor, thus allowing plasma containment to be measured within 1 μs after the heating pulse. The fast capacitors are usually charged to a maximum of 45 kV; the pulse duration is ~1 μs, and the peak secondary voltage around the plasma loop is ~60 kV.

The pre-heat pulse is induced using the same primary windings that are used for the heating pulse, sufficient decoupling being provided by LC

TABLE I. DIMENSIONS AND PARAMETERS OF TWIST AND PROTO-CLEO

	TWIST	PROTO-CLEO
Major radius R	32 cm	40 cm
ℓ-winding minor radius (ℓ = 3)	10 cm	9 cm
Separatrix radius r_m (trefoil apex)	4.5 cm	5 cm
Computed rotational transform per field period at separatrix (i_k)	30°	32°
Number of field periods	4	7
ℓ-winding current	20 kA	15 kA
Toroidal magnetic field B_z	3 kG	3 kG
Shear length $L_s = \frac{2\pi R}{i}$ (i is the total rotational transform at the separatrix)	100 cm	75 cm
$\Theta = r_m/L_s$	1/20	1/15
Useful time duration of magnetic fields	~100 μs	~10 ms

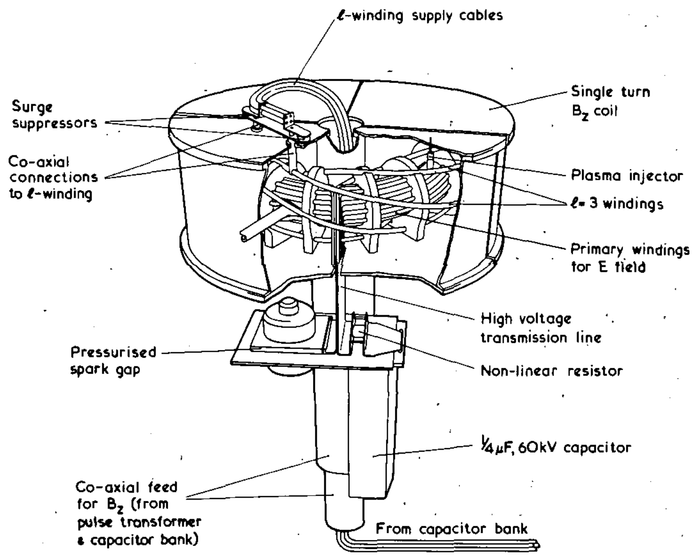

FIG. 3. Arrangement of TWIST apparatus (Principal components only).

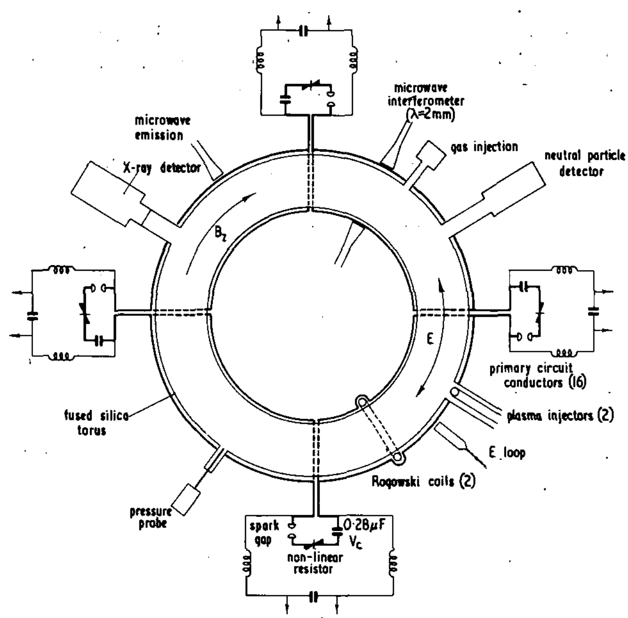

FIG. 4. Schematic showing heating circuit and diagnostics used in TWIST.

filters to prevent the higher frequency high voltage pulse appearing across the pre-heat supply. The secondary voltage induced during the pre-heat is 200 V, the gas current is typically ~300 A, and lasts for ~60 μs. To ensure a reproducible working pressure, the gas is admitted to the vacuum system from a fixed volume by a fast-acting, magnetically-operated valve.

Between shots the base pressure is $\sim 10^{-6}$ torr. The gas is pre-ionised by introducing plasma from two injectors of the type described earlier. With this arrangement it is possible to get reliable breakdown in hydrogen for pressures $\gtrsim 10^{-4}$ torr. Figure 5 shows the operating sequence and typical waveforms during the various stages of the experiment.

3.2. Experimental results

The existence of strong electrostatic turbulence is indicated by a high level of electromagnetic radiation at frequencies around the electron plasma frequency ω_{pe}. The radiation is detected by a waveguide aerial coupled to appropriate broad-band crystals. The emission is unpolarized and corresponds to $\sim 10^{-2}$ watt/cm^2 for the 3cm band.

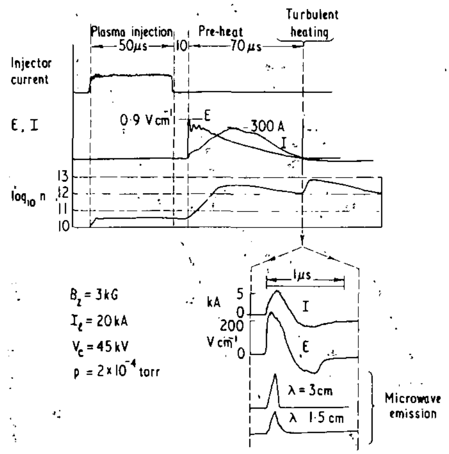

FIG. 5. Operating sequence for TWIST, showing typical waveforms under standard conditions: B_z = 3 kG, ℓ-winding current 20 kA, V_c = 45 kV, pressure = 10^{-4} torr H_2.

The plasma resistance is measured from the ratio E/I when dI/dt = 0, i.e. at peak current. (E is the applied electric field and I the discharge current.) This measurement has been made over several decades of initial plasma density and with gas fillings of hydrogen, argon and xenon. The plasma density is determined from the phase change of a 2mm microwave beam traversing the discharge. Although the gas is not fully ionized, consideration of ionization rates shows that no significant change in plasma density can occur during the times of interest (i.e. $< 0.4\ \mu$s). The measured resistance values [13] are shown in Fig. 6. They are consistent both in magnitude and in the dependence on plasma density and ion mass with the following formula derived from Buneman's [14] work on the conductivity of a plasma in which the two-stream instability is occurring,

$$\sigma(\text{esu}) = \frac{\omega_{pe}^2}{4\pi}\,\tau_{\text{eff}} \approx \frac{1}{2}\left(\frac{M}{m}\right)^{1/3}\omega_{pe} \qquad (1)$$

where τ_{eff} is the effective 90° scattering time for electrons. It should be noted that the electric fields used in these experiments ($100 < E < 500$ V cm^{-1})

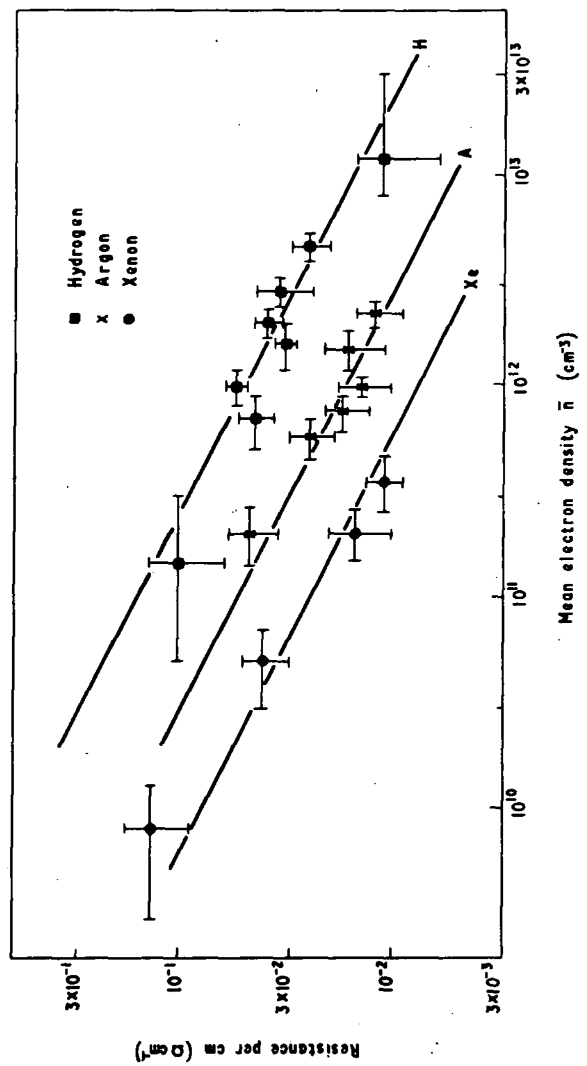

FIG. 6. Variation of measured resistance per cm of plasma column with density for various gases.

are appreciably greater than those used by Demidov et al. [15] under otherwise similar conditions. Figure 7 compares our results with those of Demidov et al.

Both direct and indirect measurements of plasma pressure show that the electrical energy dissipated appears as thermal energy in the plasma. For example, with $E = 300$ volts cm^{-1}, $n = 1.5 \times 10^{12}$ cm^{-3}, a piezo-electric pressure probe [16] shows a maximum particle energy density in the plasma of approximately 2×10^{16} eV cm^{-3} at $t = 0.2$ μs which is in close agreement with the electrical energy dissipated in the current pulse. X-rays are emitted both during the pulse, with a pronounced peak at maximum

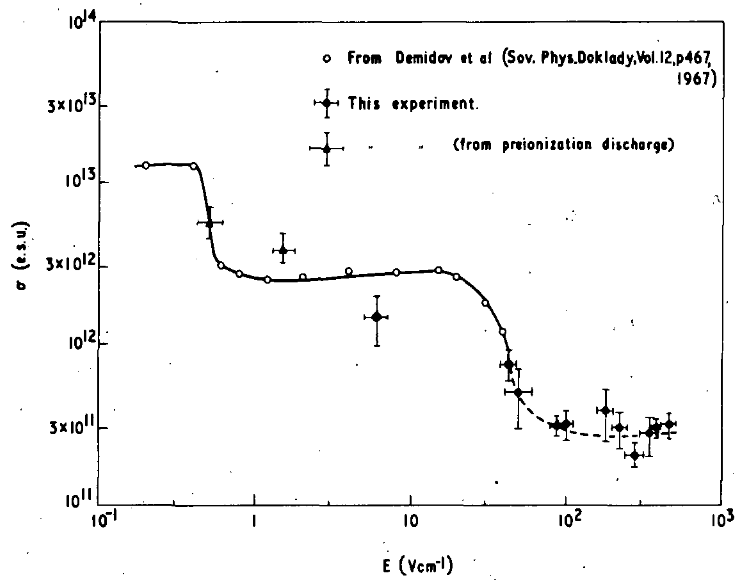

FIG. 7. Variation of plasma conductivity with electric field for hydrogen with electron density $\bar{n}_e \approx 10^{12}$ cm^{-3}.

current, and for 2-3 μs after the pulse. Absorber measurements are consistent with bombardment of the walls by electrons with temperature approximately 10 keV. In some earlier experiments [17] conducted at a higher gas pressure (2×10^{-3} torr) in a system without ℓ-windings we also observed a large flux of fast neutrals with energies up to 3 keV. From the absolute flux of neutrals with an energy of 2 keV, we estimated the ion temperature to be approximately 0.7 keV. In these earlier experiments the charge exchange time (10^{-7} s) was less than the heating time so that, with the lower neutral density now prevailing, we would expect a somewhat higher ion temperature. Note that with a magnetic field strength of 3 kG the value of β produced by the turbulent heating can easily be as high as 10%. Although, at present, such high values are not obtainable by injection methods, in stellarators they are of critical importance from the viewpoint of a fusion reactor. If the heating pulse is shorter than the Bohm time corresponding to the final temperature, no substantial plasma loss should occur during the turbulent phase.

In summary, these experiments have established the effectiveness of turbulent heating in a toroidal stellarator, confirmed the theoretical scaling law for the turbulent conductivity and shown that ions as well as electrons are heated. Although it seems improbable that turbulent heating will be a practical way to start up a fusion reactor, it is nevertheless a powerful technique for filling experimental stellarators with interesting plasma.

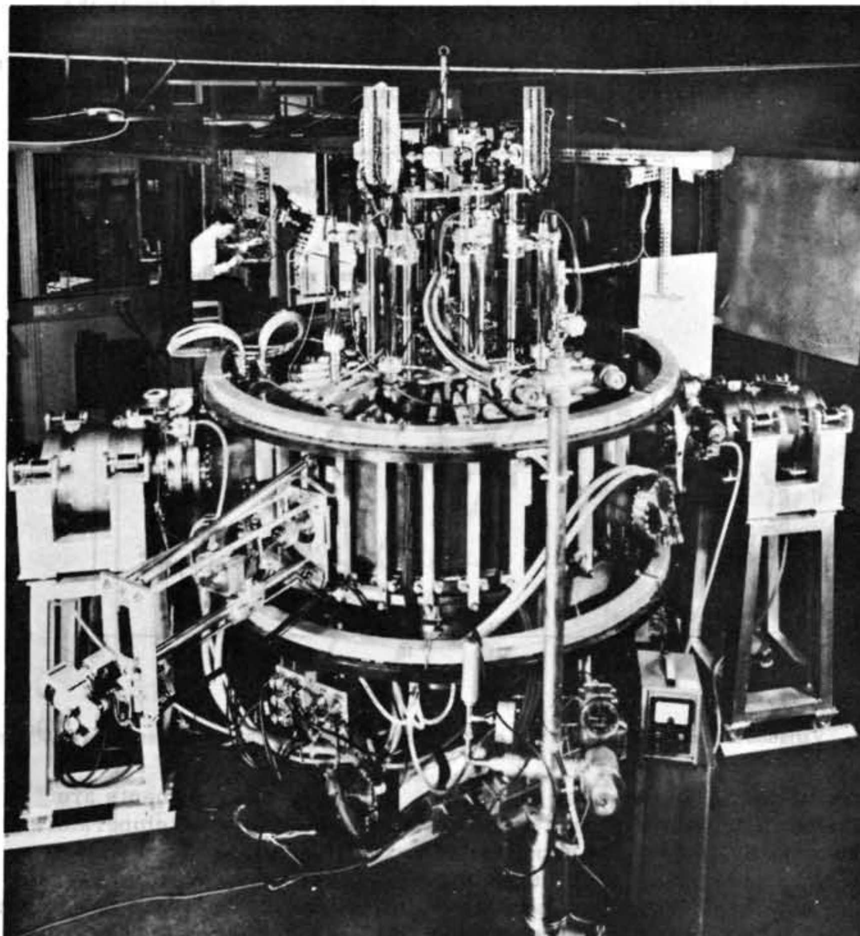

FIG. 8. General view of PROTO-CLEO stellarator.

4. PLASMA CONFINEMENT

The PROTO-CLEO apparatus has been built to study the confinement of plasma injected into a high-shear toroidal stellarator.

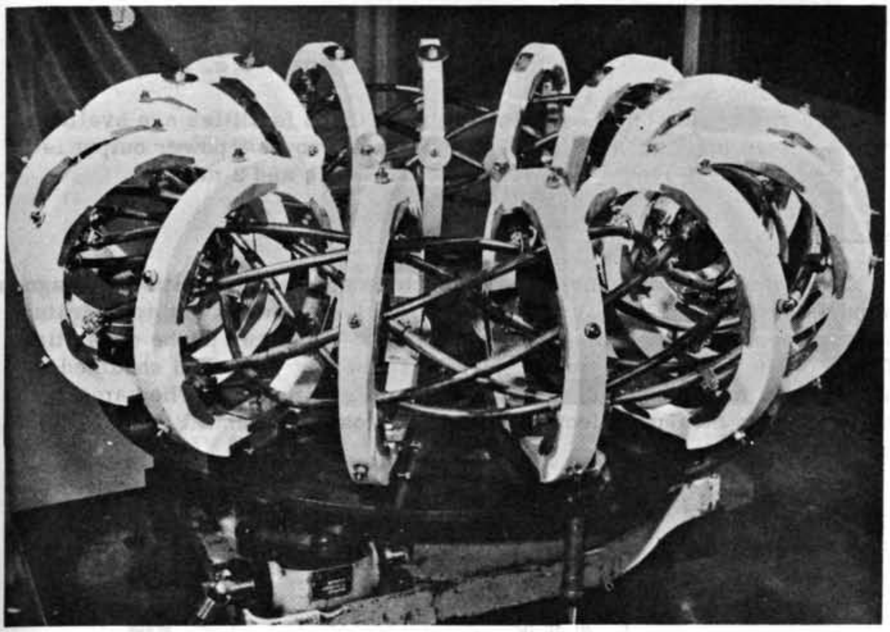

FIG. 9. PROTO-CLEO ℓ-windings before mounting in vacuum envelope.

4.1. Apparatus

A general view of the apparatus is shown in Fig. 8. Details of the $\ell = 3$ helical winding construction are seen in Fig. 9. The 1.2 cm diameter copper conductors which make up the winding are supported by 15 ceramic rings and are located with a positional accuracy of $\pm$ 0.025 cm. The current feeds are made coaxial to minimize the magnetic field perturbation.

The stainless steel vacuum tank is a toroid with a 40 cm square cross-section. Titanium filaments can be moved into the centre of the ℓ-windings for gettering the system. Background pumping of the tank is by two sputter ion pumps. With gettered walls at room temperature, the base pressure is 2×10^{-8} torr.

The B_z coil system consists of 30 single-turn demountable square coils carrying a current of up to 20 kA. The maximum measured magnetic field error of the B_z is $\pm$ 0.1% at the separatrix.

The B_z coils and the ℓ-windings are connected in series so that their fields vary in unison. They are energized by a capacitor bank made up of 500 V, 500μF electrolytic capacitors, with a total capacitance of 1.25 F. It is subdivided into 20 units each switched by a thyristor [18] and clamped by a silicon diode.

A small vertical magnetic field can be applied using the Helmholtz coils visible in Fig. 8, which can produce an average magnetic well [19] with a depth of $\sim$10% and reduced shear.

4.2. Plasma production

PROTO-CLEO is filled with plasma by the quasi-d.c. injector described earlier.

Electron cyclotron resonance heating (ECRH) facilities are available from a pulsed magnetron (9.45 GHz). Peak microwave power output is 4 kW and the pulse length is variable between 1 μs and 2 ms.

4.3. Diagnostics

The general arrangement of the machine and the disposition of diagnostic ports are shown in Fig. 10. Time resolved density and temperature measurements are made using a swept double Langmuir probe consisting of two 0.75 mm diameter tungsten wires spaced by 7 mm and sheathed in thin glass (1 mm diameter) to within 7 mm of their ends. The same probe can be used to measure electric fields and floating potential in the plasma.

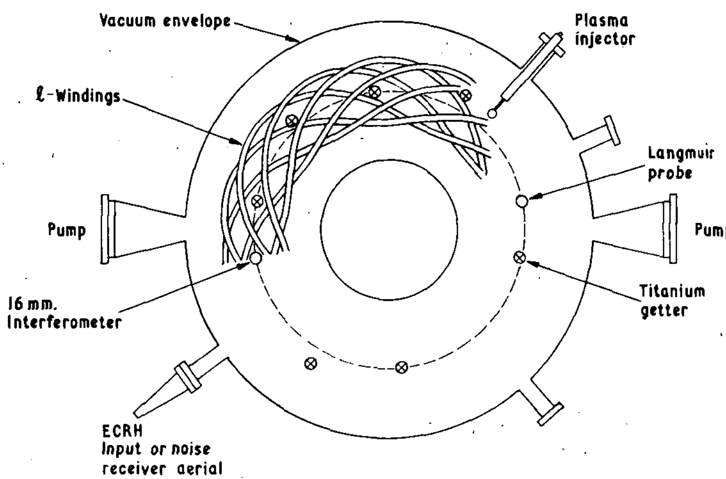

FIG. 10. Schematic view of PROTO-CLEO stellarator showing diagnostic positions.

The average plasma density is measured with a 16 mm wavelength version of the microwave interferometer developed by Hotston and Seidl [20].

An estimate of the electron temperature can be made by measuring the microwave noise emitted by the plasma. This is detected by an aerial close to the plasma (Fig. 10), coupled to a superhet receiver. The magnetic field varies by 15% across the confinement region and so allows plasma-generated radiation at frequencies less or equal to the upper hybrid frequency (Heald and Wharton 1965) [21] to escape through the density gradient at the edge of the plasma, provided that the wave is polarized with its electric vector perpendicular to B.

4.4. Results

All results unless otherwise stated were obtained under the standard conditions of Table 1. The decay of the plasma density as measured by the double probe and by the microwave interferometer is shown in Fig. 11.

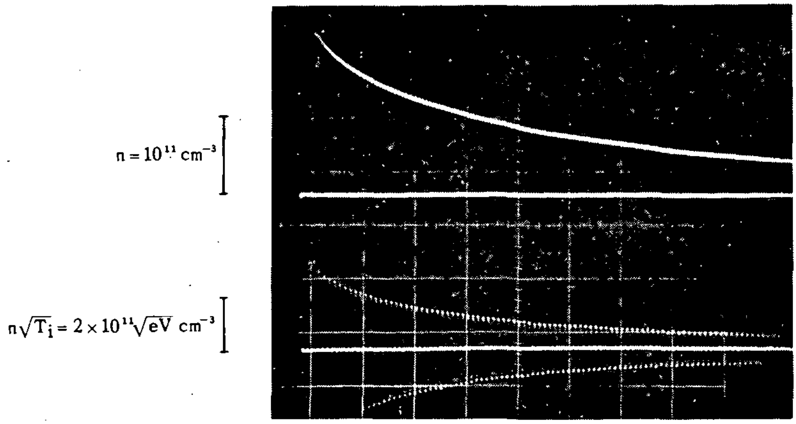

FIG. 11. Oscillograms of density decay. Upper trace: microwave interferometer phase change; lower trace: flux to a modulated double probe at 2.5 cm radius; time axis: 1 ms per division.

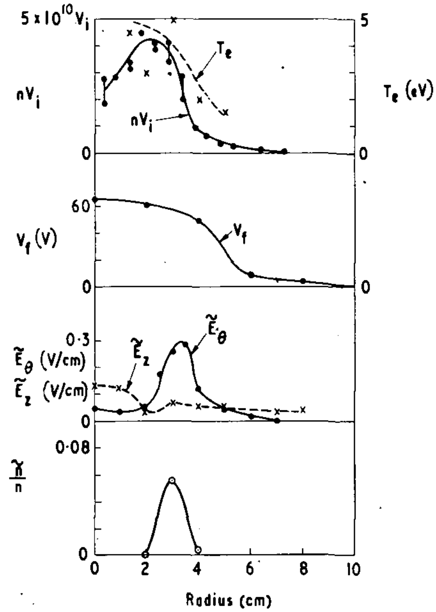

FIG. 12. Radial profiles of plasma parameters measured under the standard conditions: (a) (nv_i) and T_e determined by double probe; (b) floating potential Vf ; (c) average peak to peak fluctuations of aximuthal electric field $\tilde{E}_\theta$ and axial electric field $\tilde{E}_z$; (d) peak to peak density fluctuation n as a fraction of the maximum density; (a) measured 1 ms after injection, (b) - (d) measured 2 ms after injection.

The two signals agree in shape and they show a smooth density decay from an initial peak density of $\sim 10^{11}$ cm^{-3} with a time constant ~ 5 ms. The electron temperature decays slowly from an initial value of 5 eV; after 5 ms it reaches ~ 2 eV. The radial density distribution determined from double-probe measurements is shown in Fig. 12a. Note that the maximum density gradient occurs in the outer 2 cm, the region of high shear and large rotational transform. The electron temperature varies less rapidly with radius, decreasing from 5 eV on the axis to ~ 2 eV at the edge of the plasma.

Figure 12b shows the variation of floating potential (V_f) with radius. The plasma has a positive centre and the potential difference between the axis and the edge of the plasma (separatrix) is ~ 3 (kT_e/e).

Fluctuations in azimuthal (E_θ) and axial electric field (E_z), are observed (averaged over the probe spacing) in the frequency range 10-100 kHz; no well defined frequencies are apparent. The average peak-to-peak value of fluctuations is recorded; the radial variation is shown in Fig. 12c. $\tilde{E}_\theta$

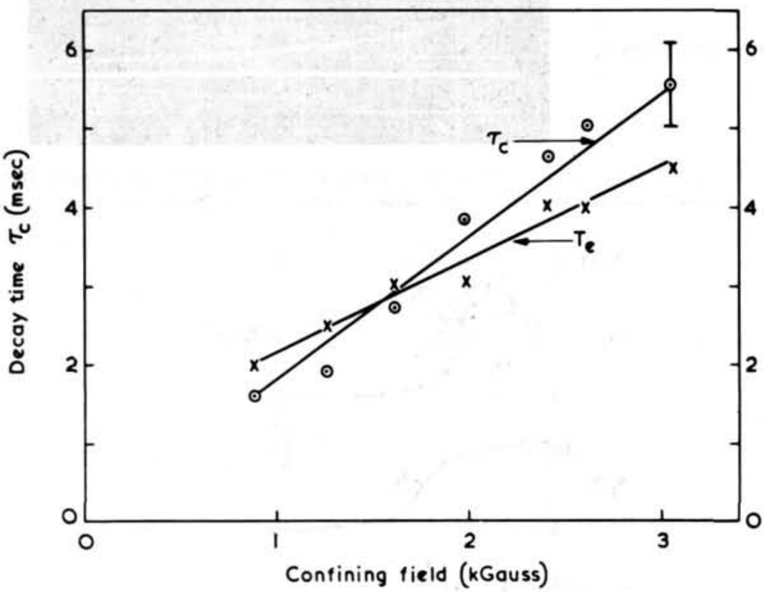

FIG. 13. Density e-folding time τ_c and electron temperature T_e (measured 1 ms after injection) as a function of confining field, B_0. The ℓ-winding current I_ℓ is adjusted so that B_0/I_ℓ is constant, i.e. constant shear.

varies from ~ 50 mVcm^{-1} near the magnetic axis to a maximum value of ~ 300 mVcm^{-1} in the region of steep density gradient at which $\tilde{E}_z$ is about an order of magnitude smaller. Density fluctuations occur in the same frequency range (Fig. 12d), and reach a peak-to-peak value of 5% in the region of steep density gradient. These observations are consistent with an instability occurring where there is a large gradient in density and are characterized by $\lambda_\perp \leq 1$ cm across the field, $\lambda_\parallel \geq 10\ \lambda_\perp$ and potential fluctuations $\sim (1/10)$ (kT_e/e).

The microwave noise was measured with the local oscillator of the receiver set at frequencies of 8.0, 8.5, 9.0, 10.0 GHz and with $B_z = 3$ kG. The noise was most intense at 8.5 GHz; Fig. 15 shows a typical oscillogram of the receiver output. The electron temperature is determined by assuming that the noise is black-body radiation. The noise output at 8.0 GHz is similar to that in Fig. 15, save that the radiation temperature is somewhat lower. At 9.0 GHz there is an initial burst of radiation corresponding to $T_e = 9$ eV decaying to 0.3 eV or less in 1 ms. Note that, as the plasma density decays, the hybrid frequency drops until it is below the

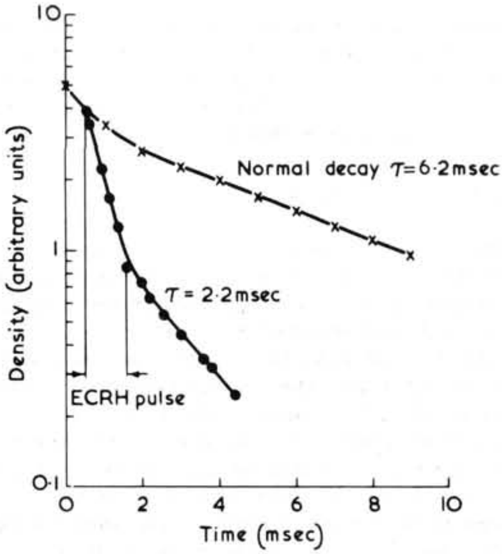

FIG. 14. Time variation of density when 2 kW ECRH pulse applied to injected plasma for 1 ms, compared with normal decay.

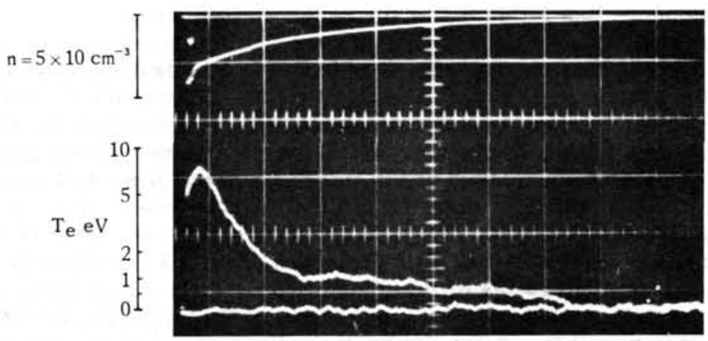

FIG. 15. Oscillograms of microwave noise emitted from plasma.
Upper trace: density decay from microwave interferometer with density scale shown; lower trace: output of superhet receiver. Local oscillator frequency 8.54 G Hz. The scale on the left indicates the value of T_e assuming black body radiation; time axis: 1 ms per division.

receiver frequency. Since the plasma should not be an effective radiator at frequencies above the upper-hybrid resonance, we would expect the behaviour that we observe, namely, a reduction in noise temperature as the receiver frequency is increased. Thus the noise temperatures indicated in Fig. 15 represent lower limits to the true values.

The variation of density decay time τ_C with confining field strength at constant shear is shown in Figure 13. We see that it is proportional to B. However, the operation of the injector depends on the trap field, and the electron temperature measured after 1 ms is also found to be linearly dependent on B.

The effect of a 2 kW, 1 ms ECRH heating pulse on the plasma density decay is shown in Fig. 14. The density decays rapidly during the heating pulse with a time constant of $\sim 300\ \mu s$. There is no indication of a transient density rise which would be expected if the initial plasma were only weakly ionized. After the microwave power is turned off, the decay time increases to ~ 2 ms. The double probe measurements show that the electron temperature after microwave heating is ~ 10 eV.

4.5. Discussion of confinement results

Transverse injection of plasma into a stellarator from a small injector placed outside the separatrix has been shown to be feasible. Plasma is captured in the absence of any pre-ionization in the confinement region.

Under the standard conditions of Table I, the plasma has a sharply defined edge at a radius r of 3.5 cm. Taking into account the azimuthal position of the probe relative to the ℓ-windings, this is consistent with the computed radial position of the trefoil apex at 5 cm.

The rate of decay of density and the electron temperature vary during the lifetime of the plasma. For one set of data at t = 0.5 ms, the decay time $\tau_C \simeq 2.8$ ms, and $T_e \simeq 4.5$ eV while at t = 5 ms, $\tau_C = 7.2$ ms and $T_e = 2.3$ eV. These results show a substantial improvement over the Bohm time $\tau_B = \pi r^2 eB/kT_e$; thus for t = 0.5 ms, $\tau_C/\tau_B \simeq 10$ and for t = 5 ms, $\tau_C/\tau_B \simeq 14$. If the microwave noise temperatures are used rather than the Langmuir probe values, then at t = 0.5 ms, $\tau_C/\tau_B \simeq 15$ and for t = 5 ms, $\tau_C/\tau_B \simeq 6$. This last value is clearly too low since by that time the upper hybrid frequency has fallen below the receiver frequency.

At present it is not possible to be sure that the density decay time is a true measure of particle containment since some ionization may be taking place in the plasma. However, the fact that the plasma density shows no transient increase when the microwave heating pulse is applied, suggests that the neutral density in the plasma is low and ionization negligible.

The electron temperature of the trapped plasma depends linearly on the confining field B, and hence the Bohm time is independent of B. Since the average confinement time τ_C is observed to increase linearly with B, the ratio τ_C/τ_B also increases with B from ~ 8 at B = 1 kG to ~ 20 at B = 3 kG.

The microwave heating of the plasma resulted in a rapid loss of plasma during the heating pulse. No measurements of T_e during the heating pulse have yet been possible. After the heating, the remaining plasma has a higher decay rate than before, and also a higher electron temperature (~ 10 eV). The improvement over the Bohm time therefore still remains at approximately 10.

The plasma exhibits fluctuations of electric field and density in the outer region where the maximum density gradient occurs. The radial plasma flux Γ due to these fluctuations is

$$\Gamma \approx \frac{(\widetilde{E}_\theta \cdot \widetilde{n})}{8B}\, \alpha$$

where α (≤ 1) is the correlation coefficient.

Taking $\widetilde{E}_\theta \simeq 0.30$ V/cm and $\widetilde{n} \simeq 0.05\, n_0$ from Fig. 12 (where peak-to-peak values are given) then the calculated loss rate Γ is about half the observed rate if $\alpha \sim 1$. Thus the fluctuations remain a possible cause of the particle loss.

The 'classical' containment time for the plasma may be calculated from the work of Gibson and Mason [3], i.e. taking into account the detailed particle orbits, ignoring the ambipolar electric field, but assuming the loss rate to be the slowest of the respective ion and electron rates. Under our conditions, the collision rate is high enough so that localized particle diffusion is not important. Instead, the loss of blocked particles is dominant as first discussed by Galeev and Sagdeev [22], leading to a diffusion coefficient independent of the plasma density:

$$D \simeq \frac{4\pi^{\frac{3}{2}}}{i} \frac{\rho_e}{R} \frac{kT_e}{eB}$$

where ρ_e is the electron gyro-radius, and R is the major radius of the plasma. With our parameters this leads to a containment time of $\sim$ 50 ms. Note that in this model the electrons diffuse more slowly than the ions and so one would expect the plasma centre to be negatively charged – in fact it is positively charged.

The sign of this charge and the magnitude of the potential difference between the axis and the separatrix ($\sim 3\ kT_e/e$) suggest that the electrons are contained solely by electrostatic forces (i.e. "held in by the ions"). The electrons must therefore be free to move radially faster than the ions. This might be due either to poor containment of magnetic field lines (failure to form surfaces) or to the presence of a high-frequency instability $\omega_{ci} < \omega < \omega_{ce}$, which would lead to relatively free flow of electrons across the magnetic field.

5. CONCLUSIONS

1. A quasi-d.c. plasma injector has been developed and shown to be an effective means for filling stellarators.
2. Turbulent heating has been shown to produce hot plasma ($\beta \sim 10\%$) in a stellarator device. A theoretical scaling law for the turbulent electrical conductivity has been confirmed, and it has also been shown that ion-heating takes place.
3. Experiments on the containment of plasma injected into a toroidal stellarator have shown confinement times up to $\sim$ 15 times the Bohm value. This is in qualitative agreement with similar work by Akulina et al. [23] and by Ellis and Eubank [24]. At present we have insufficient data to decide on the relative importance of shear, rotational transform, collision rates and other factors.

ACKNOWLEDGEMENTS

The authors gratefully acknowledge the assistance of Messrs D. A. Aldcroft, P. Richold, S.J. Turley, D.R.A. Webb and Mr. P.A. Worsnop's engineering team in this work. We also thank Dr. R.S. Pease for his advice and encouragement throughout.

REFERENCES

[1] CARRUTHERS, R., DAVENPORT, P.A., MITCHELL, J.T.D., The economic generation of power from thermonuclear reactors, Culham Report CLM R85 (1967).
[2] GIBSON, A., HUGILL, J., REID, G.W., ROWE, R.A., SANDERS, B.C., (these Proceedings).
[3] GIBSON, A., MASON, D.W., Binary collision losses in stellarators, Culham Preprint P 173.

[4] BISHOP, A.S., SMITH, C.G., Physics Fluids 9 (1966) 1380.
[5] BICKERTON, R.J., GIBSON, A., Physics Fluids 10 (1967) 682.
[6] MARSHALL, J., Physics Fluids 3 (1960) 134.
[7] ALLEN, T.K., COX, A.J., SPALDING, I.J., in Plasma Physics and Controlled Nuclear Fusion Research (Proc. Conf. Culham, 1965) 2, IAEA, Vienna (1965) 427.
[8] ASHBY, D.E.T.F., Plasma Physics 10 (1968) 665.
[9] ASHBY, D.E.T.F., GOODING, T.J., HAYWORTH, B.R., LARSON, A.V., A.I. A.A. Journal 3 (1965) 1140.
[10] KRUPNIK, L.I., SHULIKA, N.G., 'Plasma Diagnostics' State Publishing House of Literature of Atomic Sciences and Technology Moscow, Translation AEC-tr-6578 (1963).
[11] ADLAM, J., HOLMES, L.S., in Plasma Physics and Controlled Nuclear Fusion Research (Proc.Conf. Salzburg, 1961), Nucl.Fusion, Suppl.-Part 3 (1963) 1121 (Abstract); Nucl.Fusion 3 (1963) 62 (Full paper).
[12] BABYKIN, M.V., ZAVOISKY, E.K., RUDAKOV, L.I., SKORYUPIN, V.A., Nucl.Fusion, Suppl.-Part 3 (1963) 1073; ZAVOISKY, E.K., Atomn.Energ. 14 (1963) 57.
[13] HAMBERGER, S.M., FRIEDMAN, M., Culham Preprint P177 (1968).
[14] BUNEMAN, O., Phys.Rev. 115 (1959) 503.
[15] DEMIDOV, B.A., ELAGIN, N.I., FANCHENKO, S.D., Soviet Phys.Dokl. 12 (1967) 467.
[16] FRIEDMAN, M., Plasma Physics 10 (1968) 561.
[17] HAMBERGER, S.M., MALEIN, A., ADLAM, J.H., FRIEDMAN, M., Phys.Rev.Lett. 19 (1967) 350.
[18] PEDLEY, T.R., VARLEY, G.L., Proc. 5th Symp. Fusion Technology, Oxford (July 1968).
[19] TAYLOR, J.B., Physics Fluids 6 (1963) 1529.
[20] HOTSTON, E., SEIDL, M., J. scient. Instrum. 42 (1965) 225.
[21] HEALD, M., WHARTON, C., Plasma Diagnostics with Microwaves, sec. 1.4.9., Wiley New York (1965).
[22] GALEEV, A.A., SAGDEEV, R.Z., Zh.eksp.teor.Fiz. 53 (1967) 348; Soviet Phys. JETP 26 (1968) 233.
[23] AKULINA, D.K., BATANOV, G.M., BEREZHETSKY, M.S., GREBENSCHIKOV, S.E., RABINOVICH, M.S., SBITNIKOVA, I.S., SHPIEGEL, I.S., in Plasma Physics and Controlled Nuclear Fusion Research (Proc. Conf.Culham, 1965) 2, IAEA, Vienna (1966) 733.
[24] ELLIS, R.A., EUBANK, H.P., Physics Fluids 11 (1968) 1109.

NOTE ADDED IN PROOF

Since writing this paper it has been found that the number of shots which can be obtained from the plasma gun depends on the type of vacuum system in which it is used. In an oil diffusion pumped system with a base pressure of 10^{-6} Torr no limit has been found to the number of shots. In the Proto-Cleo vacuum system pumped by titanium sputter ion pumps and getters, with a base pressure of 10^{-8} Torr, the number of shots is limited to about 100. Experiments to elucidate this behaviour are underway.

DISCUSSION

V.N. TSYTOVICH: How good was the thermal isolation of the plasma during turbulent heating?

R.J. BICKERTON: Piezo-electric probe and soft X-ray analysis shows that there is no serious loss of energy from the plasma during the heating pulse.

V.N. TSYTOVICH: Did you observe microwave emission during turbulent heating – and, if so, in what frequency range?

R.J. BICKERTON: Strong, unpolarized microwave emission in the neighbourhood of the plasma frequency was observed during the heating pulse.

COMPUTER SIMULATION OF PLASMA CONFINEMENT IN A STELLARATOR

C. G. SMITH
PLASMA PHYSICS LABORATORY, PRINCETON UNIVERSITY,
PRINCETON, N. J.
AND
A. S. BISHOP
UNITED STATES ATOMIC ENERGY COMMISSION, UNITED STATES OF AMERICA

Abstract

COMPUTER SIMULATION OF PLASMA CONFINEMENT IN A STELLARATOR. The time-dependent approach to, and stability of, low-density equilibria in toroidal geometry is studied by simultaneously integrating the guiding-center equations of motion for a vast number of particles characterized by a distribution of parallel and perpendicular energies and initial positions. A static magnetic field which models the major effect of stellarator helical windings is used for the calculation, but the self-consistent, time-evolving electric fields are included in the dynamics. Axial symmetry is imposed, but motions parallel to the magnetic field are treated since these are projected on the cross-sectional plane by the rotational transform. Consequently the effect of mirroring and of a parallel electric field are included. In particular, the motion of electrons along field lines to cancel the charge imbalance due to curvature drifts is explicitly treated. In the single calculation performed thus far, the development of azimuthally asymmetric potential surfaces has been observed. This is primarily an m = 1 perturbation, the energy of which undergoes growth on the order of a Bohm confinement time and then slight decay thereafter. The long time evolution occurs in the up-down (with respect to the toroidal plane) asymmetry; the in-out asymmetry, after an initial flip of sign, persists in a fashion which reinforces the trapping of electrons by the toroidal structure of the magnetic field. Superimposed are fluctuations with a period equal to the time required for electrons to move from the top to bottom of the machine by streaming along the field lines. The outward transport of electrons by $\vec{E} \times \vec{B}$ drifts is small.

INTRODUCTION

Once the need for rotational transform in stellarator configurations was seen [1], the question of confinement was soon felt to be of less interest than that of hydromagnetic stability. Recently, it has come to be appreciated that the problem of single-particle containment in closed systems warrants further, detailed study.

In the drift approximation, particles appear to flow along lines of force, but these are not identical to those of the vacuum magnetic field and are different for particles of different energy and magnetic moment [2]. Thus, the question of the possible nonexistence of flux surfaces for the vacuum field [3] translates directly to the possibility of nonclosure of trajectory surfaces for the particle (beyond the simple loss by flow along noncontained vacuum lines).

There is now the recognition that variations in field strength along the magnetic line, as small as they may be in toroidal configurations, still are quite important because, by their ability to trap, these force one to view the plasma as composed of distinct classes of particles [4]. For example, there are three categories of particles in a stellarator, one of which can drift out beyond the separatrix no matter how large the magnetic field strength [5].

One consequence has been the requirement to reexamine the question of stability, but now from a microscopic point of view. As a practical matter, the shift of particle surfaces off magnetic surfaces may be of numerical significance for certain regions of phase space. Then "scrape-off" by a vacuum vessel wall will lead to a "loss-cone" depletion similar to that of open-ended systems, and velocity-space relaxation processes triggered by the subsequent instability can produce a continuous loss of plasma [6]. Less traumatic micro-instabilites are possible because of steep gradients which may appear in phase space at the boundary between trajectories of different topologies [7]. Trapping, by disrupting communication along the line of force, can be crucial for instabilities which, from the hydromagnetic point of view, are thought to be easily stabilized [8]. Finally, it should be noted that the shift of particle and magnetic surfaces increases the step length for random walks and thereby modifies the diffusion coefficient [9].

Because of the difference in m/e among species, guiding-center calculations predict charge separation, so that the self-consistent electric fields must be included in the dynamics. Although the impact is certain to be significant, little effort has been directed to this problem, and results are meager. Attention usually is focused on the famous $\vec{E} \times \vec{B}$ drift, but the role of $E_{\parallel}$ in determining the extent of trapping should not be overlooked.

The calculation of stationary equilibria is a nonlinear problem and is likely to require numerical work. Once completed, the results must then be tested for stability. If a major computing program is to be undertaken, it seems preferable to consider the initial-value problem and cover both aspects at once.

In this paper we study the time-dependent approach to, and stability of, low-density (specifically, the zero β, collisionless regime) equilibria in toroidal geometry with the self-consistent, time-evolving electric potential. Due to the limited computer capacity presently available, axial symmetry is imposed. Full three-dimensional perturbations of the potential are therefore disallowed, and a model magnetic field must be used to simulate the major effects of stellarator helical windings. However, motions parallel to the line of force are treated, and an $E_{\parallel}$ is permitted in the model.

One disadvantage of performing a "computer experiment" is that a considerable expenditure is required to survey the parameter space routinely scanned in laboratory experiments. This, however, is compensated by the diagnostics and the wealth of detailed information obtainable.

THE MODEL

The evolution of the distribution function is obtained by integrating forward in time the guiding-center drift equations [10] for a representative set of particles. When specialized to the case of a static vacuum magnetic field and first-order electric field, these equations read, in the leading approximation, as follows:

$$\frac{d\vec{r}}{dt} = v_{\parallel}\vec{n} + \vec{V} \pm \frac{1}{\Omega_{\pm} B}\left(\frac{\mu B}{m_{\pm}} + v_{\parallel}^2\right)\vec{n} \times \nabla B$$

$$\frac{dv_{\parallel}}{dt} = -\frac{1}{m_{\pm}}\vec{n}\cdot\nabla(\mu B \pm e\Phi) + \frac{v_{\parallel}}{B}\vec{V}\cdot\nabla B$$

$$\frac{d\mu}{dt} = 0$$

where $\pm$ denotes the species (electron or ion) of charge $\pm e$ and mass $m_{\pm}$. The magnetic field is denoted by $\vec{B}$, its unit tangent vector by $\vec{n}$, and $\Omega = eB/mc$ is the gyrofrequency. The $\vec{E} \times \vec{B}$ drift is expressed as

$$\vec{V} \equiv -\frac{c}{B}\nabla\Phi \times \vec{n}$$

Field quantities may be evaluated at $\vec{r}$, although properly it is the position of the guiding center rather than of the particle. The magnetic moment, μ, is defined in terms of the perpendicular energy. In this paper, the expression "perpendicular velocity" will always mean simply the square root of μ in the units of velocity, according to the definition

$$v_{\perp}^2 \equiv \frac{2\mu B_o}{m}$$

where B_o is a reference field strength to be introduced later, and $v_{\parallel}$ is essentially the microscopic velocity parallel to the line of force. The above set of equations displays the following integral of the combined zeroth- plus first-order motion for the case of a static electric field

$$\frac{d}{dt}\left(\frac{1}{2}mv_{\parallel}^2 + \mu B \pm e\Phi\right) = 0$$

The energy of the $\vec{E} \times \vec{B}$ drift is absent from the above expression since it is taken to be second order. This is dictated by the expectation that the potential will change by kT in a distance on the order of the plasma column radius, r_o, allowing one to obtain the following estimate

$$V \sim \frac{c}{B}\frac{kT/e}{r_o} \sim \frac{v_{th}/\Omega}{r_o}\, v_{th}$$

where $v_{th} \equiv (kT/m)^{1/2}$ is the thermal speed typical of the zero-order motion. Thus V is smaller by the ratio of the gyro-radius to the tube radius.

The electric potential, Φ , is obtained in a self-consistent manner from the evolving charge distribution through Poisson's equation

$$\nabla^2 \Phi = -4\pi n_o e \sum_{\pm} \pm \frac{2\pi B}{m_\pm} \iint f_\pm \, d\mu \, dv_\parallel$$

where n_o provides a density scaling for the distribution function $f(\vec{r}, \mu, v_\parallel, t)$. Moments of the distribution are obtained by partial summation over the representative set of particles. The spatial density of particles is given, correct through first order, by the density of guiding centers (this is not necessarily true of the higher moments) [11] .

The coordinate system, $\vec{r} = (r, \phi, z)$, is taken to be a curved cylindrical system centered about the minor axis of the torus. The metric is

$$(d\ell)^2 = (dr)^2 + (rd\phi)^2 + [1 + (r/R) \cos \phi]^2 (dz)^2$$

where R is the major radius. The position in the cross-sectional plane of the plasma column is given by (r, ϕ), with r the distance from the minor axis and ϕ measured from the toroidal plane to the outside. Axial symmetry is to be imposed, so that no quantities vary with z , which measures distance along the minor axis.

The imposed magnetic field is that employed by Knorr [12] to study stellarator equilibria,

$$\vec{B} = B_o [1 + (r/R) \cos \phi]^{-1} \left\{ 0, \frac{\iota}{2\pi} \frac{r}{R} [1 - (r/R)^2]^{-1/2}, 1 \right\}$$

consisting of a main axial confining field B_z with toroidal structure and a B_ϕ to provide rotational transform. Since the field is not curl free, the transform angle, $\iota(r)$, should be identified as arising from internal plasma currents as in the Tokomak device. The approach we take here, however, is to use it to model the major effect of stellarator multipolar windings. The resulting drift equations are interpreted as representing the average motion in the asymptotic limit of a large number of helical field periods once around the machine [13] . This model neglects the class of very low parallel velocity particles which are trapped within a helical field period [5] . The flux surfaces are concentric circles centered about the minor axis, and V'' is favorable for MHD stability.

The model is treated in the thin tube or small aspect ratio limit, $r/R << 1$. Thus we take

$$B \approx B_o [1 - (r/R) \cos \phi]$$

$$n_\phi \approx \frac{\iota}{2\pi} \frac{r}{R}$$

$$n_z \approx 1$$

Drifts perpendicular to and mirroring along the lines of force arise from the toroidal structure, while the role of B_ϕ is only to provide rotation about the minor axis. ($v_{\parallel} n_\phi$ projects the motion along the line of force onto the cross-sectional plane. In this connection, azimuthal variations of $\Phi(r, \phi)$ project back along the line, causing a perturbation in $E_{\parallel}$ with wave number

$$k_{\parallel} = m \frac{\iota}{2\pi R}$$

where m is the azimuthal mode number.)

The thin tube limit permits the potential to be solved for in reciprocal powers of R, according to the scheme,

$$\nabla_o^2 \Phi_n = -\sigma_n$$

where

$$\nabla_o^2 \equiv \frac{1}{r} \frac{\partial}{\partial r}\left(r \frac{\partial}{\partial r}\right) + \frac{\partial^2}{r^2 \partial\phi^2}$$

and the sources for the first few terms are

$$\sigma_o = 4\pi n_o e \sum_{\pm} \pm \pi \iint f_{\pm} \, dv_{\perp}^2 \, dv_{\parallel}$$

$$\sigma_1 = \frac{r}{R}\left(- \cos\phi \, \sigma_o + \cos\phi \frac{\partial \Phi_o}{r \partial r} - \sin\phi \frac{\partial \Phi_o}{r^2 \partial\phi}\right)$$

Only the contribution of the azimuthally symmetric portion of the charge density to the cosine amplitude of the $m = 1$ mode is of consequence.

A vacuum vessel wall at $r = r_o$ sets the boundary condition for the problem. There the potential is required to go to zero. Furthermore, the wall acts as an adsorber; particles reaching $r = r_o$ are removed from the calculation. This is a gross simplification of actual events at the boundary. In devices with an aperture limiter or a divertor, adsorption is concentrated at one point along z. The plasma column sits well off from the conducting wall, and the potential tends to float at the edge.

NUMERICAL TECHNIQUES

A Fortran code has been written for the IBM 7094 computer, for which the computing time is of the order of 35 hours per case. Reduced to its utmost simplicity, the program first advances at constant potential a vast number of particles forward through a short time step, then calculates the density and corrects the potential. This is repeated for a large number of time steps.

The integration scheme used is a second-order, Adams-Bashforth predictor-corrector [14]. If the set of guiding-center equations is written as $dr/dt = v(r,t)$ and n denotes evaluation at the n^{th} time step, then a prediction of r based on the past history is obtained from the explicit relation

$$r'_{n+1} = r_n + \frac{\Delta t}{2}(3v_n - v_{n-1})$$

while a corrected value is obtained by one iteration of the implicit relation

$$r_{n+1} = r_n + \frac{\Delta t}{2}(v'_{n+1} + v_n)$$

Comparison of the predicted and corrected result (which measures the *truncation error*) allows the program to dynamically check for each particle the appropriateness of the chosen time step, Δt. This scheme requires two solutions of Poisson's equation per time step.

The spatial density is obtained by counting from the representative set those particles residing within a given cell on a grid structure in the (r, ϕ) plane. Because the elemental area is $r\,dr\,d\phi$, it is desirable to establish a uniform grid in the (r^2, ϕ) plane so that the cells are of equal weight. A further refinement to obtaining smooth density profiles is to distribute (for the purpose of counting only) a particle among the four adjacent cells according to the area overlap of a cell centered about the particle with respect to the fixed cells. For the calculations reported here, a 12 by 12 grid was chosen.

Solving Poisson's equation requires some caution in order to minimize collisional effects. The discreteness of the model (cell structure and a finite number of particles) tends to produce the effect of close encounters. A direct numerical attack of finite-differencing the Laplacian operator requires, in the interest of accuracy, cells of small dimensions. Holding the total number of particles (and hence the computing time) fixed, this implies a small number of particles per cell. Hence, density fluctuations tend to be large and the potential will not be a smooth function of the spatial coordinates. This difficulty may be circumvented by the following scheme [15]. Poisson's equation is first Fourier analyzed with respect to the azimuthal coordinate ϕ. The solution of the resulting system of ordinary differential equations in the radial coordinate is expressed in terms of integrals of the charge density with kernels which are simple powers of r. The charge density is given a global representation, and the integrations are then performed analytically. The representation chosen here is a polynomial in r^2 multiplied by r^m for the m^{th} mode, and the coefficients are determined numerically by a least-squares fit to the data (thus providing a smoothing operation on the statistical fluctuations).

Details (particularly side conditions for the fit) as well as numerical examples may be found in the reference cited above. For the calculations reported here, a sixth-degree polynomial was taken, and only the first six Fourier modes retained. (Note that taking a fewer number of modes than that allowed by the number of cells itself constitutes a least-squares fit of the azimuthal dependence.)

Great care must be exercised in preparing the initial state to avoid persistence of the initial conditions. What is required is a delicate mixture of randomization (to reduce correlations) and microscopic detailed balance (to provide uniformity). The following procedure was adopted in preparing a uniform, Maxwellian distribution function. Each cell in the (r^2, ϕ) plane was quartered, and to each of the sub-cells was assigned 50 particles per species. Two tables of 25 entries were prepared with values of $v_{\parallel}$ and $v_{\perp}$. These were obtained by taking the appropriate distribution function $f(v)$ (with $v > 0$) normalized to 25 and calculating the mean value of v for successive intervals Δv defined by unit area under the distribution curve. The coordinates for two particles were selected by

(a) Picking $v_{\perp}$ sequentially from its table, restarting from the beginning when moving to a new sub-cell, and assigning to both,

(b) Picking $|v_{\parallel}|$ randomly from its table, provided that the particular value had not been previously picked within the sub-cell, and assigning plus and minus values among the two particles, and

(c) Independently picking r^2 and ϕ randomly so as to be located within the sub-cell.

(Random selection is based on a computer program which generates a random sequence of numbers uniformly distributed in the interval (0,1).) Plots of data in the $v_{\parallel}$, $v_{\perp}$ plane, to be presented in the next section, will therefore show remnants of a grid structure (particularly as $v_{\perp}$ is a constant), and for this reason its origin has been explained in such detail here.

The total number of particles initially in the calculation is $2 \times 12 \times 12 \times 200 = 57{,}600$. Such a large number is required in order to keep collisions out of the problem--that is, to obtain solutions of Poisson's equation free of close encounter potentials. To the degree that one is unsuccessful in reducing the statistical fluctuations, an upper limit is placed to the allowable values of the scaling density, n_o. This is symptomatic of the approach to a high-density regime, in which quasi-neutrality is assumed and the potential is determined from the dynamics so as to insure its maintenance.

RESULTS

Only a single case (Case 3) for the complete problem has thus far been run. It corresponds to the situation of a hot plasma

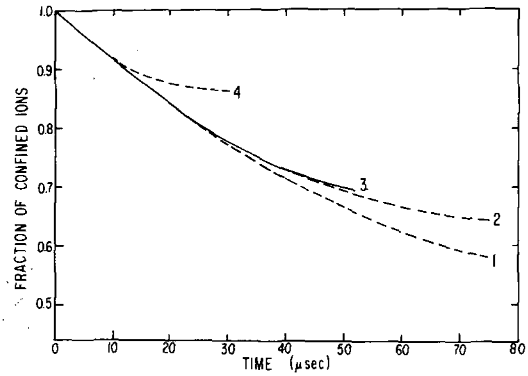

FIG. 1. Loss of ions as a function of time for cases: (1) no electric fields, (2) radial field only, $n_0 = 10^8$, (4) radial field only, $n_0 = 10^9$, and (3) complete model, $n_0 = 10^8$.

($kT_+ = kT_- = 1$ keV) at very low density ($n_0 = 10^8$ cm^{-3}) immersed in a strong magnetic field ($B_0 = 30$ kG). Dimensions are those appropriate for the Model C stellarator ($R = 100$ cm, $r_0 = 5$ cm), and the effect of an $\ell = 2$ helical winding is simulated ($\iota = \pi/4$). A realistic mass ratio ($m_+/m_- = 1837$) was used in the calculations. The choice of parameters provides for 50 ion gyro-radii across the plasma column but, because of the low density, only 4 Debye lengths. The initial condition is a spatially uniform, Maxwellian plasma at zero potential.

Confinement is shown in Figs 1 and 2, the first of which presents a comparison with the results of three special cases. These were obtained under the restriction of either no electric field altogether or only a radial field, and the electron dynamics was ignored. Loss takes place on the drift time scale; the Bohm time in this instance is 23 μsec.

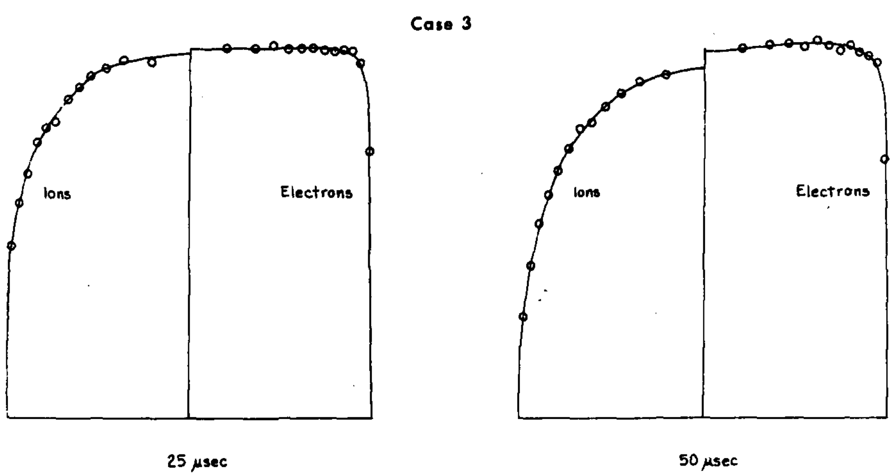

FIG. 2. Radial density profiles (azimuthally averaged).

In the absence of electric fields we can identify two classes of particles. Those with at least moderate values of parallel energy may freely circulate along the line of force; the trajectory closes on itself, but with an excursion of the drift surface away from the flux surface given by

$$\Delta r \approx -\left(1 + 2\frac{v_{\parallel}^2}{v_{\perp}^2}\right)\frac{2\pi}{\iota}\frac{v_{\perp}}{v_{\parallel}}\frac{v_{\perp}}{\Omega}$$

The magnitude increases as $v_{\parallel}$ decreases until particles become trapped to the outside by the toroidal structure of the magnetic field strength, whereupon the magnitude begins to decrease as

$$\Delta r \approx -\frac{4\pi}{\iota}\frac{R}{r}\frac{v_{\parallel}}{v_{\perp}}\frac{v_{\perp}}{\Omega}$$

(Δr is defined as the change in r from one crossing of the toroidal plane to the next; the expressions are in the limit of $\Delta r/r << 1.$) The maximum excursion occurs at the phase space boundary

$$\left(\frac{v_{\parallel}}{v_{\perp}}\right)^2 \approx 2\frac{r}{R}$$

between the two types of trajectories and is given by

$$(\Delta r)_{max} \approx -\frac{2\pi}{\iota}\left(2\frac{R}{r}\right)^{1/2}\frac{v_{\perp}}{\Omega}$$

For ions in the work reported here, the excursion at thermal velocities is nearly a third of the tube diameter and at maximum value exceeds it. Thus a sizeable fraction of ions will be scraped off at the boundary, which accounts for the loss observed in the data. Excursions in the electron orbit are smaller by the factor 43.

The preferential loss of ions creates a potential well (hill for electrons) tending to prevent further loss. The depth observed for $n_o=10^8$ is only a fraction of thermal energy, whereas at the higher density (Case 4) it nearly equals kT. Ideally, electrons flow along the line so as to cancel any charge imbalance caused by the ion drift. Then the $\vec{E} \times \vec{B}$ drift is in the flux surface and provides rotation which either supplements or detracts, depending on the sign of $v_{\parallel}$, that provided by the transform. Although V is first order, n_ϕ is small by the aspect ratio, and the two rotations may be comparable, as is the case for the ions here.

Without the proper parallel electron motion $\vec{E} \times \vec{B}$ drift off the flux surface is possible. It is larger than the ∇B drift if the azimuthal variation of the potential exceeds

$$\left(\frac{1}{m}\frac{r}{R}\right)\frac{kT}{e}$$

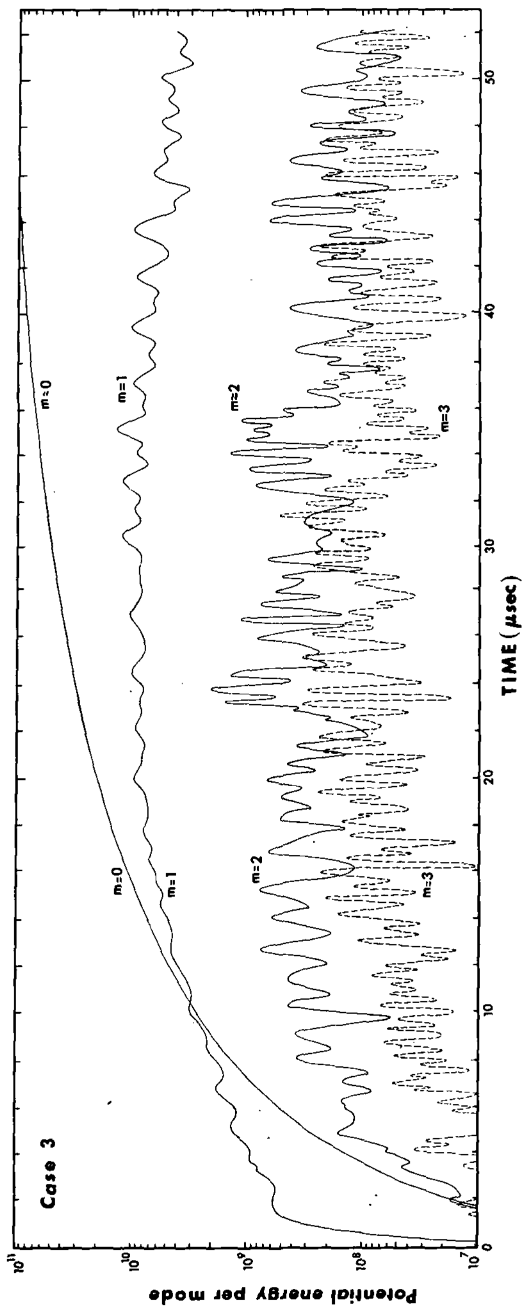

FIG. 3. Evolution of the potential energy in the first few azimuthal modes.

where m is the mode number. If the variation exceeds

$$\left(\frac{\iota}{2\pi}\frac{r}{\Omega/v_{th}}\frac{r}{R}\right)\frac{kT}{e}$$

(the coefficient is the order of ten for electrons in the numerical work), particles tend to follow the contours of constant potential. While the loss of electrons solely as the result of direct $\vec{E} \times \vec{B}$ outward streaming seems remote, the emphasis has been misplaced here. The potential variations should first be viewed along the lines, where, by trapping particles, they are seen to spoil the benefits of rotational transform. If a particle can be localized, a substantially smaller electric field can be effective in causing rapid loss of particles. In fact, the ∇B drift (which is independent of mass for particles of the same energy) is sufficient.

The major result of the numerical work is the demonstration that disruptive potential variations along the line of force may be created and maintained, even in the collisionless regime.

The development of the potential is shown in Figs 3 and 4. The latter shows the equipotential contours in the cross-sectional plane at 1 μsec intervals (every fifth time step). The orientation is that the toroidal plane is horizontal and the major axis to the left; the ion drift is down.

The energy of the $m = 0$ mode rises on the drift time scale as ions are scraped off at the boundary and levels off when the well depth is sufficient to prevent further loss. The downward drift of the ions suddenly creates an $m = 1$ charge imbalance. The initial quick rise is halted in 2 μsec, the time required for electrons to get from the top of the machine to the bottom by free streaming along the line. But rather than reversing itself, the energy continues to grow, now on a longer time scale, reaches a plateau, and then decays somewhat. The energy in the $m = 2$ mode also shows growth and then decay; curiously, the data suggest a shift of the frequency of the oscillations to a higher value midway through the run. The energy in the remaining modes successively falls off, and that of $m = 6$ would not appear in Fig. 3.

The $m = 1$ mode involves two amplitudes: the in-out and the up-down distortion. The long-time evolution of the energy is due mostly to the behavior of the up-down distortion; the in-out amplitude, after a time for adjustment, is relatively stationary.

Ions as a whole shift in the down and out direction, and the electrons essentially follow along. The leading-order description for the electrons,

$$\frac{\partial f}{\partial t} + v_{\parallel}\vec{n}\cdot\nabla f - \frac{1}{m}\vec{n}\cdot\nabla(\mu B - e\Phi)\frac{\partial f}{\partial v_{\parallel}} = 0$$

may be used on the short-time scale of equilibration along the line, with the ions fixed because their motion is on a much longer time scale. The magnetic field strength appears to the electrons as a static potential

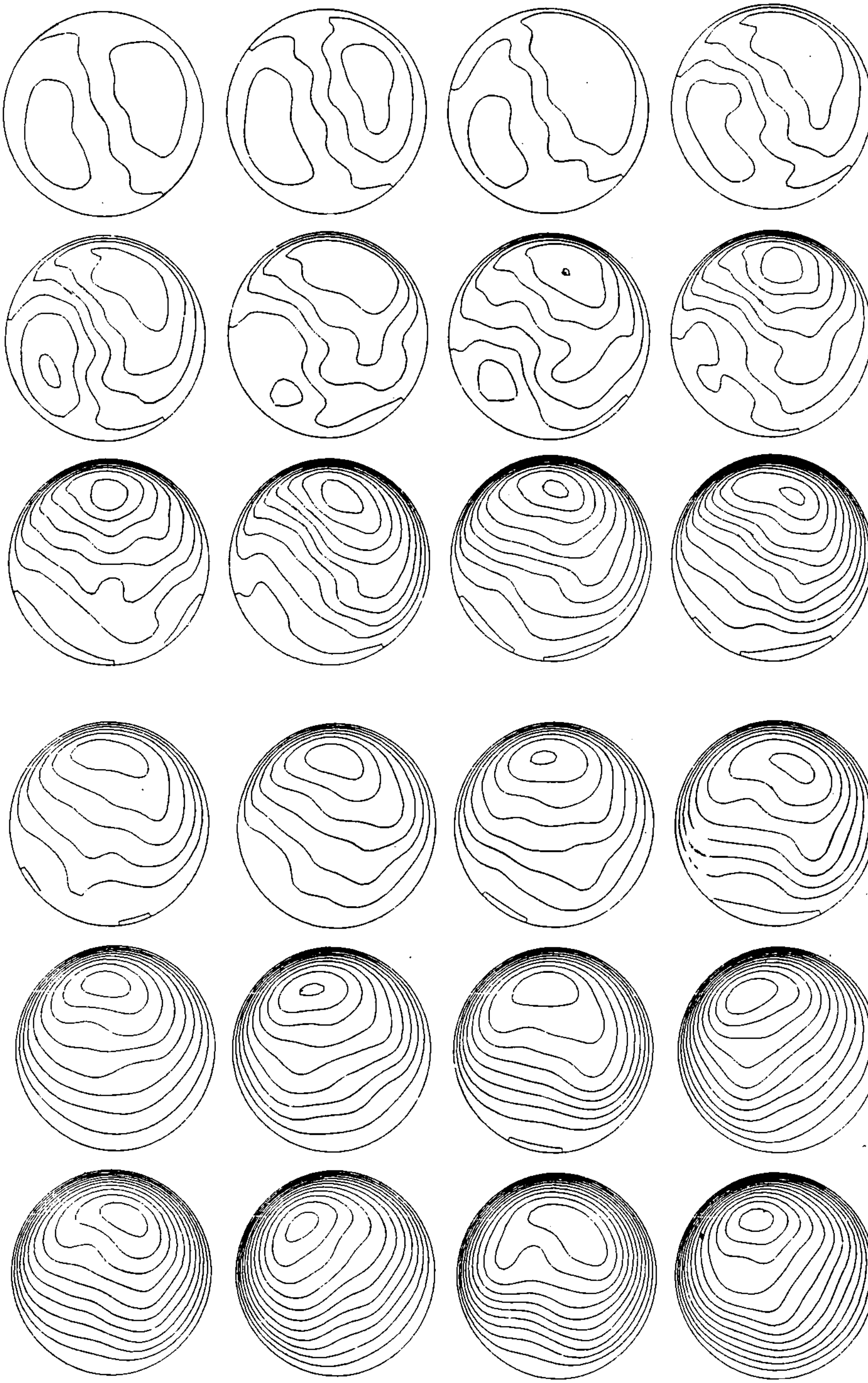

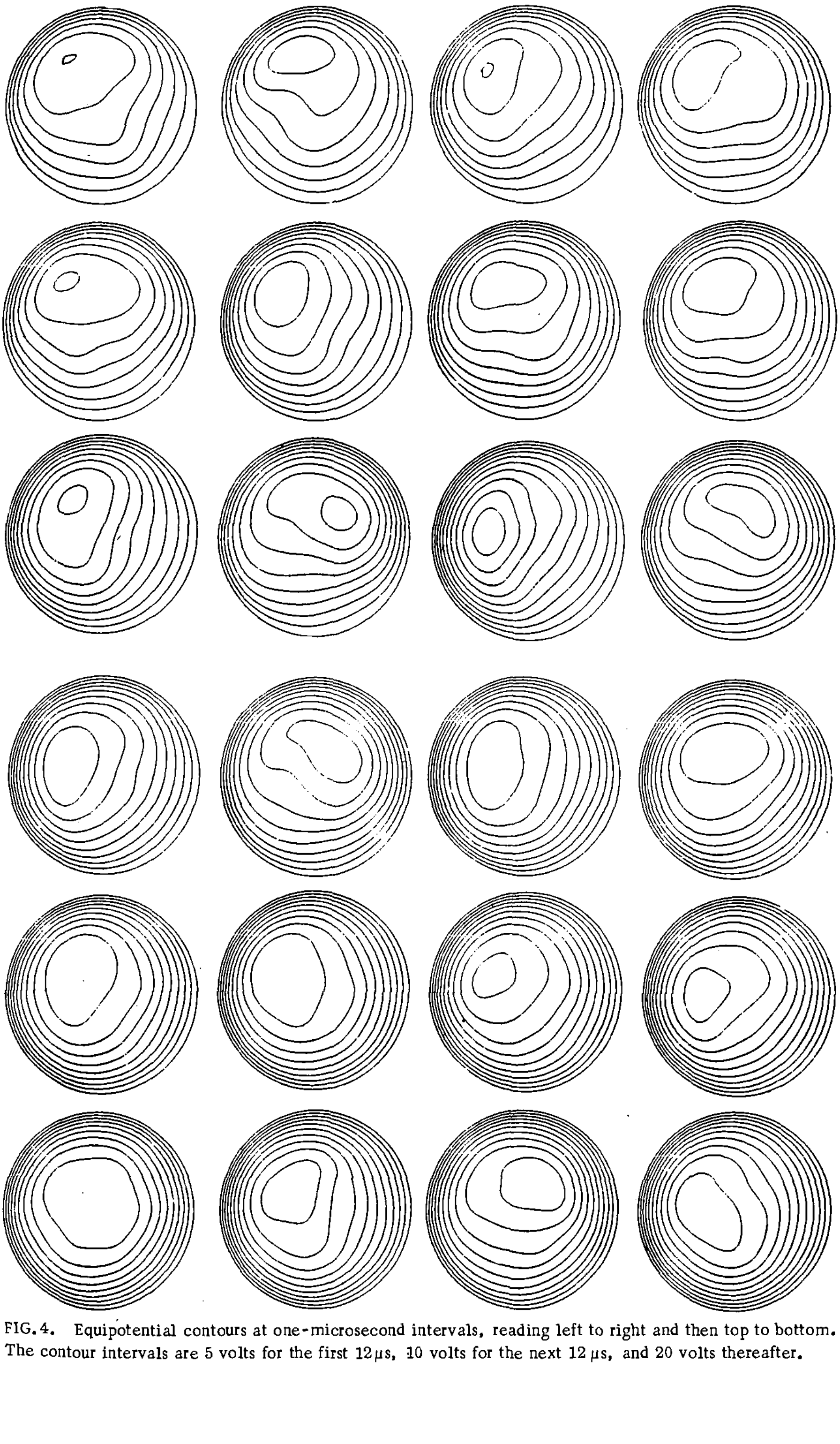

FIG. 4. Equipotential contours at one-microsecond intervals, reading left to right and then top to bottom. The contour intervals are 5 volts for the first 12 μs, 10 volts for the next 12 μs, and 20 volts thereafter.

and hence a fixed charge distribution. In a sense there are two ion charge distributions for the electrons to chase after.

In the first several microseconds the electric potential develops an in-out distortion (negative to the outside) which opposes the "magnetic potential"

$$\frac{r}{R} \frac{\mu B_o}{e} \cos \phi$$

and tends to present the electrons with a force-free situation. This is disrupted by the downward drift of ions, and thereupon the up-down

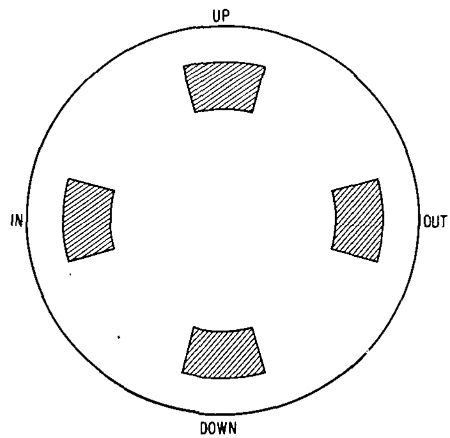

FIG. 5. Regions in configuration space from which velocity distributions are constructed.

distortion progressively becomes dominant. This in time diminishes, however, as the ion loss is completed. Then what remains is a basic in-out asymmetry which appears to persist. Now, though, it reinforces for the electrons (negative to the inside) the effect of the magnetic field structure.

Because of the imposition of axial symmetry,

$$\vec{n} \cdot \nabla = n_\phi \frac{\partial}{r \partial \phi}$$

and the electron description looks like the equation for one-dimension plasma oscillations, modified by the introduction of an applied potential. However, Poisson's equation does not look one-dimensional in ϕ (because of the r dependence and the metric) so that the analogy is not perfect. Nevertheless, what is observed here must be a nonlinear oscillation similar to the type considered by Bernstein, Greene, and Kruskal [16].

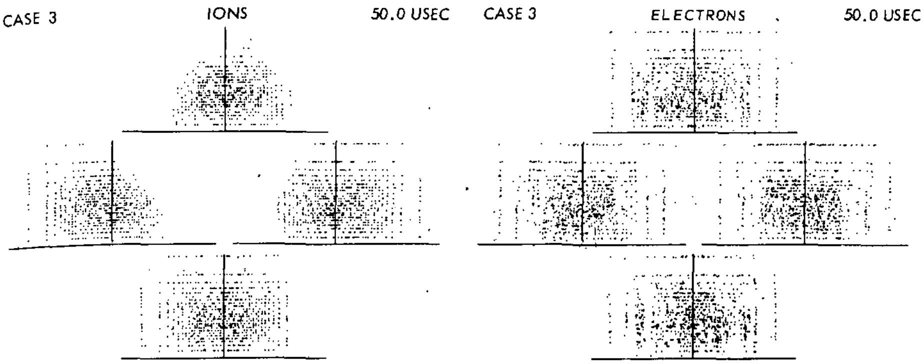

FIG. 6. Sample points in the ($v_\perp$, $v_\parallel$) plane for ions (left) and electrons (right).

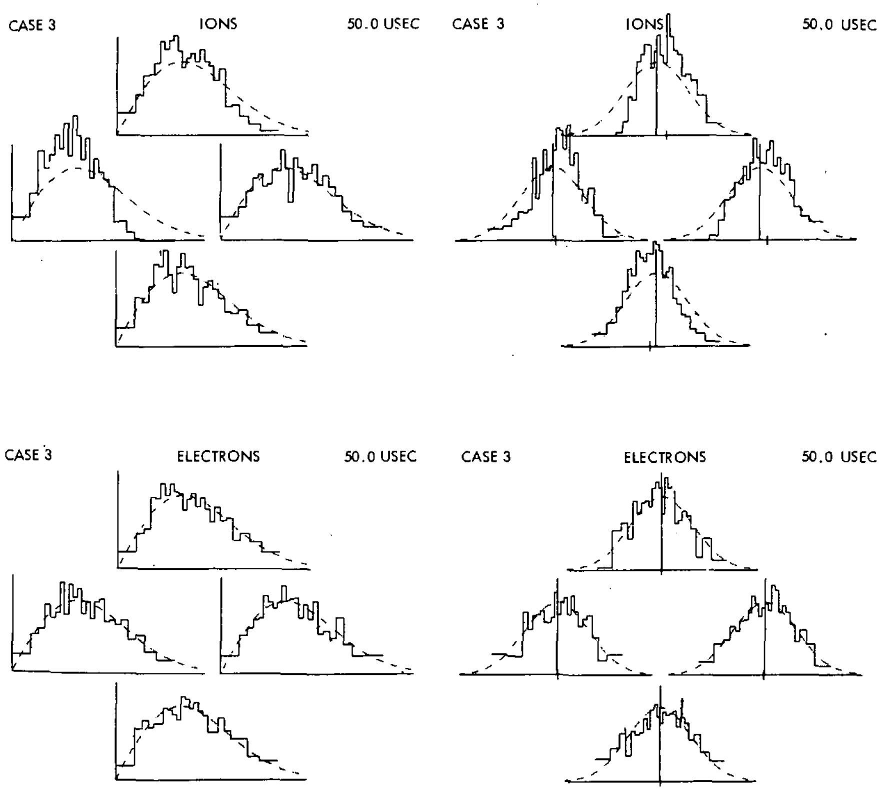

FIG. 7. Velocity distribution functions $f_\perp$ (left) and $f_\parallel$ (right) for ions (a) and electrons (b).

One interesting feature of the present results, in contrast to other observations of stable, nonlinear waves [17], is that these apparently can be maintained without gross distortion of the distribution function from the Maxwellian.

Velocity distributions at four selected points in space have been determined by sampling particles found in the cross-hatched areas shown in Fig. 5. Again the orientation is that the toroidal plane is horizontal with the major axis to the left and the main confining field out of the diagram. The spatial arrangement is maintained in the subsequent figures. The radii were chosen so that the areas of the annuli stand in the ratio 1:1:1. Positive $v_{\parallel}$ is motion in the direction of $\vec{B}$ (counter-clockwise rotation in the cross-sectional plane).

Figure 6 shows the individual points of the sampled particles in the $(v_{\perp}, v_{\parallel})$ plane at a given instant, $t = 50$ μsec. (The reason for the grid-like structure is explained towards the end of the preceding section.) The ion data show the phase space depletion by scrape-off of certain trajectories with large excursions from the flux surface. The feature of the electron data is the mixing of parallel velocities due to acceleration by the parallel electric field. There is perhaps a suggestion of some structure, holes appearing internally in the distribution, but this remains unsubstantiated.

The distributions of one velocity coordinate, integrated over the second, are presented in Fig. 7, with the Maxwellian shown for comparison by the dashed curves. The depletion shows up in the ion distribution functions as a truncation of the tail and a non-zero value of $\langle v_{\parallel} \rangle$ (indicated by the tick mark on the abscissa). The electron distribution functions, on the other hand, are relatively free of major defects.

ACKNOWLEDGMENTS

Stimulating discussions with Drs. E. A. Frieman, H. P. Furth, J. L. Johnson, and J. M. Greene are gratefully acknowledged. We are extremely indebted to Mr. J. Peoples for his painstaking preparation of the graphic material.

This work was performed under the auspices of the United States Atomic Energy Commission, Contract No. AT(30-1)-1238, and made use of computer facilities supported in part by National Science Foundation Grant NSF-GP579.

CONCLUSIONS

Numerical experiments have demonstrated that stable potential variations along magnetic lines of force can be maintained in the collisionless regime. Those observed reinforce the trapping of electrons by the toroidal structure of the magnetic field, causing a larger fraction of the electron component of a plasma to experience unfavorable curvature exclusively. Instabilities whose suppression requires good communication along the line must be reexamined in the light of this result.

REFERENCES

[1] SPITZER, L. Jr., The stellarator concept, Phys. Fluids 1 4 (1958) 253.

[2] MOROZOV, A.I., SOLOV'EV, L.S., Integrals of the drift equations, Doklady Akad. Nauk SSSR 128 3 (1959) 506.

[3] SOLOV'EV, L.S., SHAFRANOV, V.D., Perturbation of magnetic surfaces, Symp. on Exp. and Theo. Aspects of Toroidal Confinement, Princeton (1966).

[4] GRAD, H., Toroidal containment of a plasma, Phys. Fluids 10 1 (1967) 137.

[5] GIBSON, A., TAYLOR, J.B., Single particle motion in toroidal stellarator fields, Phys. Fluids 10 12 (1967) 2653.

[6] BISHOP, A.S., SMITH, C.G., Microscopic treatment of classical containment in the stellarator, Phys. Fluids 9 7 (1966) 1380.

[7] BERK, H.L., GALEEV, A.A., Velocity space instabilities in a toroidal geometry, Phys. Fluids 10 2 (1967) 441.

[8] KADOMTSEV, B.B., POGUTSE, O. P., Plasma instability due to particle trapping in a toroidal geometry, Zh. Eksp. Teor. Fiz. 51 6 (1966) 1734.

[9] GALEEV, A.A., SAGDEEV, R.Z., Transport phenomena in a collisionless plasma in a toroidal system, Zh. Eksp. Teor. Fiz. 53 1 (1967) 348.

[10] NORTHROP, T.G., The guiding center approximation to charged particle motion, Annals Phys. 15 1 (1961) 79.

[11] NORTHROP, T.G., The Adiabatic Motion of Charged Particles, Interscience, New York (1963).

[12] KNORR, G., Equilibrium of a toroidal plasma with finite resistivity and inertia, Phys. Fluids 8, 7 (1965) 1334.

[13] SMITH, C.G., Guiding center drifts in the stellarator, Bull. Am. Phys. Soc. 12 5 (1967) 764.

[14] RALSTON, A., A First Course in Numerical Analysis, McGraw-Hill, New York (1965).

[15] SMITH, C.G., On the numerical solution of Poisson's equation, Proc. Symp. on Computer Simulation of Plasma and Many-Body Problems, Williamsburg, NASA SP-153 (1967) 63.

[16] BERNSTEIN, I.B., GREENE, J.M., KRUSKAL, M.D., Exact nonlinear plasma oscillations, Phys. Rev. 108 3 (1957) 546.

[17] ROBERTS, K.V., BERK, H.L., Nonlinear evolution of a two-stream instability, Phys. Rev. Lett. 19 6 (1967) 297.

DISCUSSION

A. GIBSON: Your work does not include "localized particles" mirrored in the gradients of the helical field of a stellarator. Would you expect the inclusion of this group to modify your results, especially by permitting the escape of electrons during the initial stages?

C. G. SMITH: In order to describe the magnetic field for which "localized particles" are possible one requires three dimensions. If the electric potential is also allowed to have three-dimensional variations, I would expect considerable modification in the results (hopefully, the observation of pump-out). I consider this extension of the model to be more important than the inclusion of the "localized particles". Of course, my expectation of greater complexity in the potential and your discovery of the "localized particles" both rest on the existence of gradients along the helical co-ordinate and the removal of symmetry.

A. V. KOMIN: What are the operating memory and the computation speed of your computer?

C. G. SMITH: The computer used in this work was an IBM 7094. It has a basic machine cycle time of 2 μs. Many operations are performed at the rate of 0.25×10^6 s^{-1}, but floating point arithmetic is somewhat slower. Since the data are much larger than the high-speed memory capacity, an important consideration is the transfer rate to secondary storage. In this work, the medium was magnetic tape with a transfer rate of 15 000 words per second.

A. V. KOMIN: What is the time necessary for computing one variant and the density at the end of the computation?

C. G. SMITH: A time step for advancing the particle co-ordinates requires slightly more than six minutes. The time required to calculate the density and solve for the potential is negligible in comparison.

S. J. BUCHSBAUM: How much computer time does a typical run require?

C. G. SMITH: Approximately 35 hours per case for the complete model. For the dashed data curves in Fig. 1 the electron dynamics was ignored and the running time was much shorter.

Yu. N. DNESTROVSKY: Is the time step chosen by you sufficient to describe the oscillations of the higher harmonics?

C. G. SMITH: The m = 0, 1, 2, 3 modes are faithfully described by the chosen time step, but the higher harmonics are probably not. The energy of these modes, however, is quite small.

DRIFT WAVES AND NON-LINEAR PHENOMENA

(Session E)

Chairman: B. BRUNELLI

Papers E-1 to E-7 were presented
by F.F. CHEN as Rapporteur

FINITE ION LARMOR RADIUS AND ION-ION COLLISION EFFECTS ON EQUILIBRIUM, CRITICAL FLUCTUATION AND DRIFT-WAVE STATES OF ALKALI-METAL PLASMAS

T.K. CHU, H.W. HENDEL,* R.W. MOTLEY, F. PERKINS, P.A. POLITZER, T.H. STIX AND S. VON GOELER
PLASMA PHYSICS LABORATORY, PRINCETON UNIVERSITY,
PRINCETON, N.J., UNITED STATES OF AMERICA

Abstract

FINITE ION LARMOR RADIUS AND ION-ION COLLISION EFFECTS ON EQUILIBRIUM, CRITICAL FLUCTUATIONS AND DRIFT-WAVE STATES OF ALKALI-METAL PLASMAS. Recent experiments and theories show that the effects of finite Larmor radius and ion-ion collisions, i.e. ion transverse viscosity, play a major role in determining the equilibrium state, and the linear stabilization and nonlinear amplitude saturation of the collisional drift-wave state in alkali-metal plasmas.

While the Q machine is one of the most elementary devices used in plasma research, nevertheless diffusion of plasma from this device is still incompletely understood. In confirmation of the equilibrium model, which is based on the balance of end-wall recombination and electron flow, are measurements at high density, $n_i > 10^{11}\,cm^{-3}$: (a) The observed variation of density with input atom flux ($n_i^2 \sim \phi$), and (b) the chopped-input measurements of plasma lifetime, τ ($\tau = 1/\alpha_w n_i$, $\alpha_w \equiv$ wall recombination coefficient). Paradoxical are the observations that (a) $\tau \approx$ constant for $n_i < 10^{11}\,cm^{-3}$; (b) The radial loss to an absorber placed many density-profile decay lengths, ℓ, away from the plasma axis can be 30-50% of the total loss; (c) ℓ does not vary with temperature as expected ($\ell^2 \neq D/\alpha_w n_i$); and (d) ℓ lies in the range of 1-2 times the ion Larmor radius. In progress is an experimental program to reduce plasma convection due to end-plate temperature gradients, and a theoretical program in which transverse ion viscosity effects are included in the diffusion calculation. Results from this program will be related to the phenomena cited above.

Detailed observations of collisional drift-waves in alkali-metal plasmas have confirmed the parametric dependence of ω and $\vec{k}$ on magnetic field strength and plasma temperature. Furthermore, the wave amplitude is observed to vary with mode number, magnetic field strength, plasma temperature and density, and ion mass as does the calculated linear-theory growth rate, provided ion transverse viscosity is included in the theory. Nonlinear theory predicts limit cycle behaviour (amplitude saturation) and wave-induced transport in qualitative agreement with experimental observations. Critical fluctuations, from the critical magnetic field B_c of onset to $B \leq B_c/2$, i.e. in the stable regime, are identified by: (a) The presence of enhanced thermal fluctuations at the drift-wave eigenfrequency; (b) The dependence of fluctuation amplitude on calculated linear growth rate γ as a function of both B and radial position; (c) The dependence of fluctuation amplitude on the noise amplitude, $A \propto A_{noise}$ when the noise is varied externally.

Amplitudes of critical fluctuations in the stable regime and finite drift-wave amplitudes after onset agree with an amplitude master-equation of the Landau-Kadomtsev type, $\partial A/\partial t = 0 = \lambda A + CA_{noise} - \alpha A^3$.

1. PLASMA LOSS IN THE STABLE STATE

1.1. Introduction

Although the Q machine is one of the most elementary plasma traps, the loss of plasma from this device is still incompletely understood. Several studies have shown that, while the plasma lifetime

* On leave from RCA-Laboratories, Princeton, N.J.

at high densities follows roughly the classical model (where plasma losses result from end-plate recombination and Coulomb collisions) [1-3] at low densities anomalous losses appear [3-7]. For instance, measurements with an atomic beam chopped [6] have shown that the plasma lifetime never exceeds 20 msec ($\tau = 10\,\tau_{Bohm}$) although the classical model would predict much longer times (> 1 sec) at the lowest densities.

In this paper, we report and discuss further work to explain the anomalous loss. The experimental work is designed to distinguish which of the several modes of anomalous loss is dominant: ion transport resulting from 1) oscillations, 2) radial diffusion, 3) end-plate or volume recombination, and 4) dc convective motions. The theoretical work is an investigation of the importance of ion collisional viscosity for radial plasma diffusion.

1.2. The experiments

The experimental apparatus was the Princeton Q-3 machine shown in Fig. 1. The source of cesium ions was a 1.0 mm diameter hole in the center of one of the hot tungsten end-plates. The plasma profiles were measured midway between the hot plates with a Langmuir probe (tip size: 0.075 length; 0.0075 cm diam.). The radial flux of ions leaving the column was measured with a biased (-20V) split ring collector (see Fig. 2) which extended 1-2 mm inside the heat shield. The current collected by this ring was compared with the total ion current measured by a 'flux' plate covering the plasma area.

For confining fields below ~ 7 kG, there is very little noise in the plasma ($\Delta n/n < 0.01$), and oscillations cannot cause significant ion transport in this regime.

1.3. Results

An early set of profiles, taken with uniformly ($\pm 10^{\circ}$ K), but not necessarily symmetrically, heated end-plates, is shown in Fig. 1. The plasma density increases with magnetic field and is compressed towards the center of the plate. If one assumes a Bessel function solution in the source-free region of the form $n^2 = n_o^2 K_o(r/R)$, where K_o is a modified Bessel function of the second kind and R the relaxation length, one measures values of R between 1 and 2 times the ion cyclotron radius, as shown in Fig. 2. On the basis of similar data D'Angelo and Rynn concluded that diffusion was caused by electron-ion collisions, because the measured R is also close to the theoretical value for classical diffusion, $R = (D_\perp/\alpha n)^{1/2}$, where $D_\perp$ is the electron-ion diffusion coefficient, and α the (wall) recombination coefficient.

We do not believe that this data can be interpreted simply in terms of classical diffusion. First, the confinement time, for $n < 10^{11}$ cm^{-3}, is constant [3,6] rather than varying as $1/n$. Second, the plasma column does not seem to broaden (see Fig. 2) as the end-plate temperature is increased from 2200° K to 2500° K. Third, theory would predict that most of the ions would be lost by recombination since $R << R_o$ (column radius). However, the guard ring data, Fig. 3, show that 1/3 to 1/2 of the total ion flux is collected at the column edge, strongly indicating a radial loss.

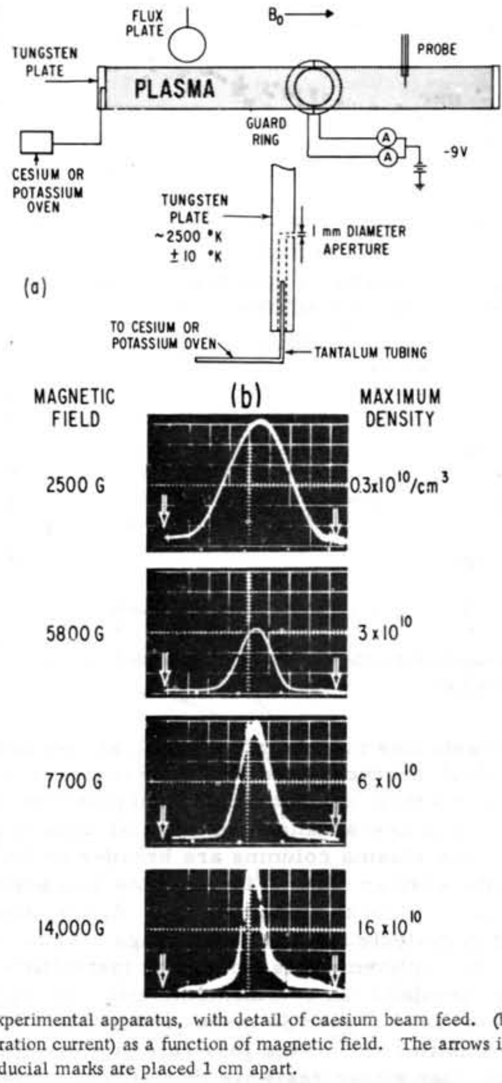

FIG. 1. (a) Sketch of experimental apparatus, with detail of caesium beam feed. (b) Radial caesium plasma profiles (ion saturation current) as a function of magnetic field. The arrows indicate the edge of the hot plate. The fiducial marks are placed 1 cm apart.

The nature of this radial loss remains obscure. Since for moderate magnetic fields, B ~ 6 kG., both n and ∇n are extremely small near the outer edge of the column; no simple diffusion mechanism can be expected to apply. In this region it is likely that the plasma is lost by convection [8-11], i.e., by $\vec{E} \times \vec{B}$ drifts resulting from non-axisymmetric temperature gradients on the hot end-plates. Floating potential profiles, which show closed equipotential surfaces near the center but not near the edge of the column, support this view.

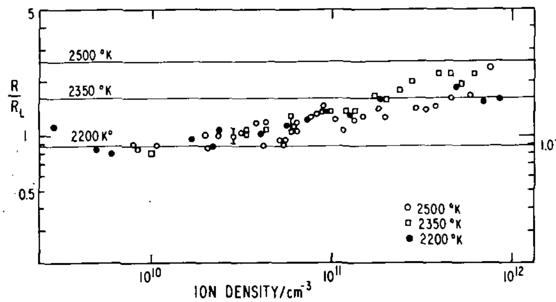

FIG. 2. Relaxation length R relative to the ion cyclotron radius R_L as a function of plasma density. The data were obtained with various magnetic fields between 2 and 15 kG.

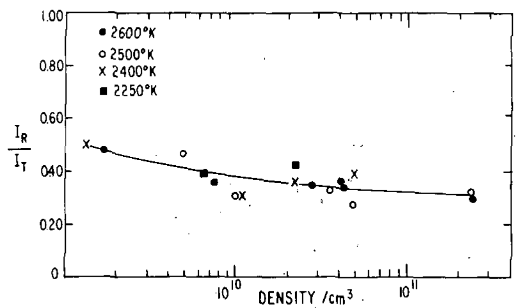

FIG. 3. Ratio of guard ring current to the total ion current as a function of density in a caesium plasma. The magnetic field was 5.3 kG.

To investigate this mechanism of ion loss, we designed a hollow tungsten plate, which produces circular, concentric isotherms (and hence circular, concentric equipotentials) and precludes ion drift out of the column. With this new arrangement, similar density profiles have been measured. The plasma columns are broader (~ 50 %) but more symmetric than the earlier data. Floating potential surfaces appear to be closed within 2-3 mm of the plasma edge. Again, about 40 % of the total ion current is collected by the guard rings. At high magnetic fields (above 4-8 kG), the confinement is limited by instabilities. However, below instability threshold the confinement, although slightly longer, still cannot be increased beyond 30 msec, independent of plasma density. That is, at low densities (10^{10}), the loss rate is more than an order of magnitude larger than either resistive diffusion of surface recombination.

1.4. Effect of ion viscosity on plasma profiles and loss rates

The theoretical work consists of solving numerically the ion radial diffusion equations including ion collisional viscosity and assuming isothermal end-plates. In an electron-rich Q machine, ion diffusion can proceed independently of electron diffusion since electrons from the hot end-plates provide charge neutrality. This calculation, which is an improvement in the classical model, is relevant to the high-density regime; like other classical effects, ion collisional viscosity predicts a density-dependent plasma lifetime that is not observed at low densities. This radial diffusion equation is

$$\frac{16kTc^2}{e^2B^2}\frac{\partial^2}{\partial\xi^2}\,\xi^2\,\mu_\perp\frac{\partial^2}{\partial\xi^2}\,\ell n(n^2) - 4\eta_\perp\frac{kTc^2}{B^2}\frac{\partial}{\partial\xi}\,\xi\frac{\partial}{\partial\xi}\,n^2 = S-\alpha n^2 \qquad (1)$$

where

$$\mu_\perp = \frac{nkT\nu_{ii}}{4\Omega_i^2}\;;\qquad \nu_{ii} = \frac{8\sqrt{\pi}}{5}\,\frac{ne^4\,\ell n\,\Lambda}{M_i^{1/2}\,(kT)^{3/2}}$$

$$\Omega_i = eB/M_i c\;;\qquad \eta_\perp = \frac{4\sqrt{2\pi}\,m_e^{1/2}\,e^2\,\ell n\Lambda}{3(kT)^{3/2}}$$

and $\xi = r^2$, S is the plasma source, α is the end-plate recombination coefficient, and M_i, m denote the ion and electron masses, respectively. Two boundary conditions, the plasma density and velocity at the plasma edge, were not known in advance and were fitted to the experimental profile. Figure 4 presents a comparison between measured and calculated profiles for a high magnetic field (5650 gauss).

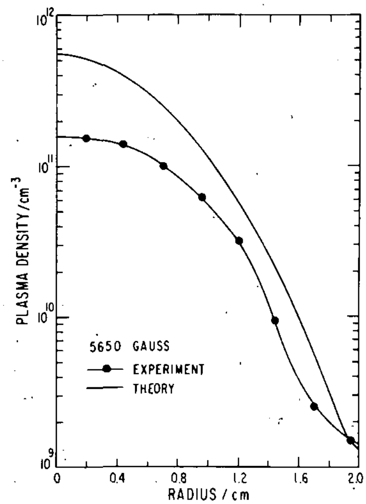

FIG. 4. A comparison between calculated and observed plasma density profiles. The theoretical calculation assumed isothermal endplates while the experiment had a radial temperature gradient of ~ + 50°K/cm.

There is qualitative agreement between the profiles, but this agreement is probably caused by the fact that end-plate recombination is the dominant loss mechanism in both theory and experiment. At low magnetic fields (2 kG) almost two orders of magnitude separate the predicted ($n = 3 \times 10^{11}$ cm^{-3}) and observed ($n = 5 \times 10^{9}$ cm^{-3}) central densities.

Qualitatively, ion viscosity forces the plasma to rotate rigidly, except near the boundary; its effect on the radial diffusion is small.

1.5. Conclusion

We conclude that in the stable low-density regime the plasma loss rate cannot be explained by electron-ion collisions, ion-ion collisions, convective dc drifts, or end-plate recombination.

2. DRIFT-WAVE STATE AND CRITICAL FLUCTUATIONS*

2.1. Introduction

Collisional drift waves [12] can arise in fully ionized, magnetically confined, low-β plasmas as a result of the combined effects of density gradient, ion inertia, and electron parallel motion. Finite ion inertia causes the transverse ion motion to differ from the corresponding electron motion (and the drift-wave phase velocity from the diamagnetic velocity), while the electrons, through collisions with ions (parallel resistivity), make available the free energy (density gradient) for spontaneous excitation. Alkali-metal plasmas, produced in Q-devices designed to separate density- and temperature-gradient regions, are suitable for drift-wave study since the plasma is near thermal equilibrium and the only known excitation mechanism for instability in the pertinent region is the density gradient.

For perturbations of infinitesimal amplitude with longitudinal and perpendicular wavelength $\lambda_{\parallel}$ and $\lambda_{\perp}$, wave growth depends on the transport rate of electrons over $\lambda_{\parallel}$. Diffusion over $\lambda_{\perp}$ due to ion-ion collisions supresses the incipient instability by equalizing local density deviations. (Transverse electron-ion diffusion also tends to suppress instability, but is smaller by $(m_e/b^2 M_i)^{1/2}$, $b = \frac{1}{2} k_{\perp}^2 r_L^2$.) Marginal stability occurs when the transport rate of electrons over $\lambda_{\parallel}$ balances that of ions over $\lambda_{\perp}$. Furthermore, because of the existence of such a marginal or critical point, critical fluctuations, i.e., enhanced thermal fluctuations at the drift-wave frequency, can be observed in the stable regime. In the unstable regime, the finite-amplitude wave produces radial transport above the classical level. The observed amplitude saturation of the unstable wave can be attributed to alteration of the density profile by such diffusive transport, but mode-mode coupling appears to be a more plausible explanation.

2.2. Linear regime

Theoretical analysis of collisional drift waves is based on the ion and electron fluid equations with the following assumptions:

---

* This work was done on Q-1. The ions are produced by atomic beams incident on the entire ionizer plates, different from the method used in Part 1.

(a) the wave electric field is given by $\vec{E} = -\vec{\nabla}\phi$;

(b) the magnetic field, $\vec{B} = B\vec{z}$, is uniform and static;

(c) $\omega << \Omega_i = eB/M_i c$;

(d) $v_{i\parallel} = \partial v_{i\perp}/\partial z = 0$;

(e) ion temperature changes due to compressive effects may be neglected;

(f) $-dn_o/n_o dx$ = constant ;

(g) $r_L << (-n_o/n'_o)$, r_L being the ion Larmor radius.

Linear stability analysis based on these assumptions yields the amplitude equation:

$$a(\omega, \vec{k})\, A = 0 \qquad (2)$$

where A is the instability amplitude, $a(\omega, \vec{k}) = 0$ is the linear dispersion relation [13] essentially represented by $a \sim \omega - \omega_o - i\gamma$, with ω_o the real part of the wave frequency, and where the growth rate, γ , can be positive or negative, as determined by the plasma parameters. Adopting the scaling $\omega \sim k_y v_d \sim b^2 \nu_{ii}/4 \sim b\Omega_i \omega/2\nu_{ii}$, where $v_d = -(kTc/eB)(n'_o/n_o)$ and

$$b = \frac{1}{2}k_\perp^2 r_L^2 ,$$

the condition $\gamma = 0$ for long axial wavelength [14] $\lambda_\parallel$ is given by the balance of the transport rates for electrons and ions over the longitudinal and transverse wavelengths, respectively:

$$V_{e\parallel}/\lambda_\parallel - V_{i\perp}/\lambda_\perp = 0, \qquad \text{with} \qquad V_{e\parallel} = \left(\frac{1}{n}\right) D_\parallel \nabla_\parallel n \qquad \text{and}$$

$$V_{i\perp} = \frac{1}{e^2 nB^2}\left[\nabla_\perp \cdot \mu_\perp \cdot \nabla_\perp\right]\left(\frac{\nabla_\perp p}{n}\right)$$

where $D_\parallel = (KT/m_e \nu_{ei})$ and $\mu_\perp \approx n_o KT\nu_{ii}/4\Omega_i^2$.

We note that the ion diffusion velocity $V_{i\perp}$ contains effects of ion-ion collisions and finite ion Larmor radius. The stability criterion may be written, equivalently, as:

$$\frac{k_\perp}{B} > \left(\frac{4e^4 k_\parallel^2}{c^4 M_i^2 KT\ m_e \nu_{ei} \nu_{ii}}\right)^{1/4} \alpha \left(\frac{T}{n_o}\right)^{1/2} \frac{1}{M_i^{3/8}} \qquad (3)$$

Azimuthal modes m ($m \to k_y r$, $k_\perp^2 \approx k_x^2 + k_y^2$) are therefore successively stabilized with decreasing magnetic field for given temperature, density, and ion mass. Equation (3) states that the observed frequency does not scale as $1/B$, since the mode number m of the dominant mode should change with B. We note that, in addition, ω changes with the growth rate as well. Parametric dependences of ω and $\underline{k}$ are compared with experimental results [13] in Fig. 5. At the saturation stage the finite-amplitude drift wave is

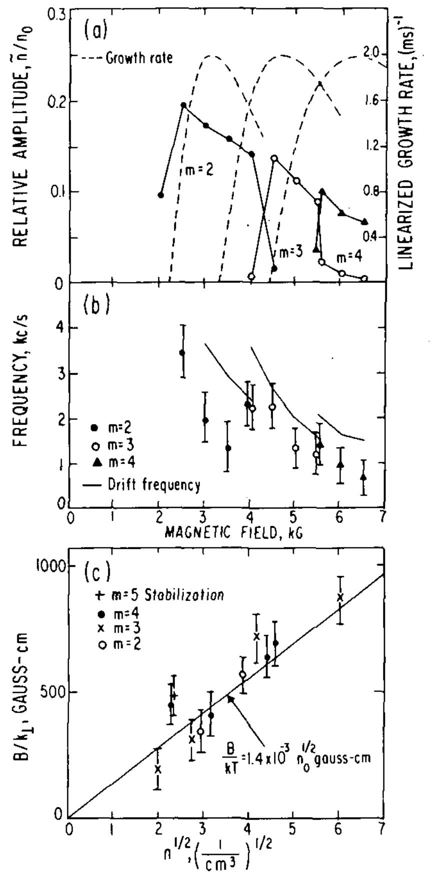

FIG. 5. (a) Observed wave amplitude and theoretical growth rate as function of magnetic field. The absolute value of magnetic field for the theoretical (slab model) curve has been scaled by a factor of ~ 1.5. $\tilde{n}/n_0$ is the ratio of wave amplitude to centre density. (b) Comparison of oscillation frequency (after subtraction of Doppler shift) with drift-wave frequency. The drift-wave frequency is computed from experimental values of k_y, T, $\nabla n_0/n_0$. Potassium plasma, $n_0 = 1.2 \times 10^{11}$ cm^{-3}, T = 2800°K. (c) Ratio of magnetic field to perpendicular wave number vs square root of density, for stabilization points of several modes. Theory gives proportionality factor of 9.7×10^{-4} gauss-cm.

found to be nearly sinusoidal, i.e., one mode is dominant. Furthermore, agreement of experimentally observed stabilization with Eq. (3), as a function of T and M_i, has also been observed [14].

2.3. Critical fluctuations

When effects of excitation are included, Eq. (1) becomes

$$f = aA \tag{4}$$

Forming the quadratic from (4), we obtain the following amplitude equation

$$|A^2| = |f^2/a^2| \tag{5}$$

For an externally applied disturbance, f is prescribed. For thermal fluctuations, f represents the random ion-fluid stress (associated with ion-ion collisions) and the random electron parallel current (associated with electron-ion collisions). The (quadratic) correlation of the random quantities $\langle f(\vec{r}_1, t_1) f(\vec{r}_2, t_2)\rangle$ can be calculated from fluctuation theory [15].

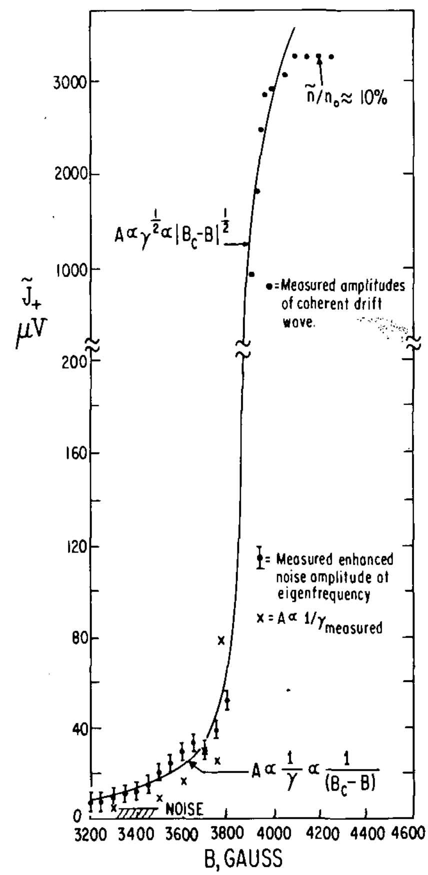

FIG. 6. Ion saturation current amplitudes vs B. Lower part: critical fluctuation amplitude. Upper part: drift-wave amplitude. Caesium, T = 2750°K, $n_{0\ centre} \simeq 10^{11}\ cm^{-3}$ at 4 kG, radial position = 0.65 mm, $R_{load} = 10^6\ \Omega$.

The amplitude equation (5) (or its ensemble average) gives the wave amplitude in response to excitation. In the stable regime near instability onset, i.e., when $a(\omega, \vec{k})$ in (5) approaches zero, background fluctuation amplitudes at the drift-wave frequency are greatly enhanced. Such critical ion-saturation-current fluctuations, measured with Langmuir probes, are shown [16] in Fig. 6. The plasma noise power was found to maximize when the load resistance was matched to the plasma resistance obtained independently from the probe characteristic. The ion current fluctuation (noise) level measured adjacent to, but off, the eigenfrequency, is comparable to that obtained from $\langle f^2 \rangle$, i.e., the Nyquist level. In Fig. 7 the amplitude of critical current fluctuations at the eigenfrequency is shown as a function of radial position. Maximum wave amplitude occurs at a radial position of maximum linear growth rate, or, in the stable regime, of minimum linear damping rate. The noise level indicated is nearly independent of radial position.

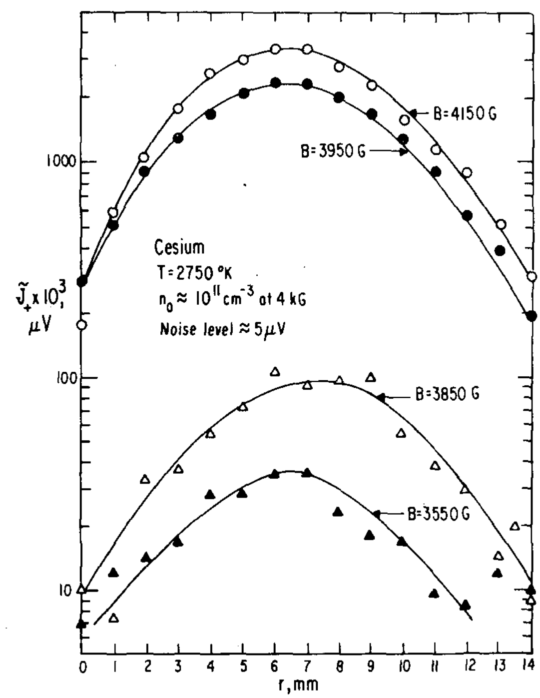

FIG. 7. Ion saturation current amplitude of critical fluctuation (in the stable regime) and of drift wave vs radial position.

2.4. Wave-associated transport

Experimentally, large enhanced plasma loss [17] is observed after wave destabilization. For a wave of ~10% relative amplitude, radial plasma transport (one order of magnitude above classical transport) measured from wave parameters is ~1/10 of the Bohm value

(Fig. 8). This transport results from the phase difference between the plasma potential wave, ϕ, and the density wave, $\tilde{n}$, Fig. 8. The measured plasma transport for a steady-state finite-amplitude wave is in qualitative agreement with nonlinear mode-coupling calculations [18].

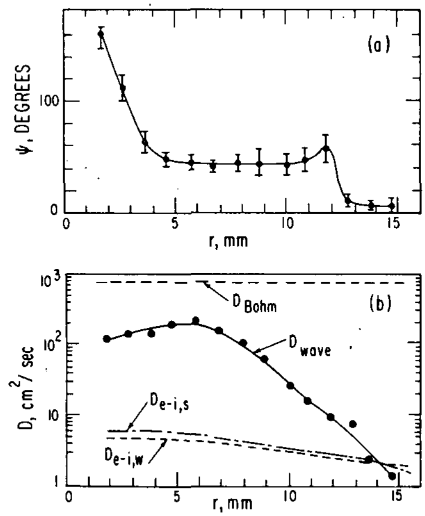

FIG. 8. (a) Measured phase angle ψ by which the density wave leads the potential wave. (b) Comparison of diffusion coefficients.

2.5. Amplitude saturation

Wave growth in the vicinity [19] of $\gamma = 0$ is also affected by coupling between modes. Representing the wave amplitude by

$$A = A_1 e^{i(k_y y + k_z z - \omega t)} + A_2 e^{2i(k_y y + k_z z - \omega t)} + \text{complex conjugate} \tag{6}$$

and collecting coefficients of each Fourier component from the non-linear equations containing linear and quadratic elements, we obtain the following coupled amplitude equations [18],

$$a A_1 + b A_2 A_1^* = f_1 \tag{7}$$

$$c A_2 + d A_1 A_1 = f_2 \tag{8}$$

For completeness, we include both excitation terms f_1 and f_2 for the respective Fourier components. In (7) and (8), $a(\omega, \vec{k}) = 0$ and $c(\omega, \vec{k}) = 0$ give linear dispersion relations for the fundamental and the second harmonic, respectively, and $b(\omega, \vec{k})$ and $d(\omega, \vec{k})$ are mode-coupling coefficients. In the absence of excitations, (7) and (8) give

$$|A_1^2| = \frac{ac}{bd} \tag{9}$$

Equation (9) can be interpreted as a dispersion relation for non-linear waves, in which the wave-envelope magnitude appears as a parameter. The sign of the imaginary part of ω indicates nonlinear stability or damping. When (9) is satisfied for $|A_1|^2 \neq 0$ and for real ω, the behavior described is that of a limit cycle, i.e., a finite-amplitude steady-state oscillation.

2.6. Master equation

In the stable region away from onset, the mode-coupling terms in (8) can be neglected and the amplitude is given as in (5) by $A_1 \approx f_1/a$. For a frequency-independent (white noise) excitation spectrum, A_1 will be enhanced at the drift-wave frequency, $\omega = \omega_o$, leaving $a \sim \omega - (\omega_o + i\gamma) \sim \gamma$, and

$$| A_1 | \sim \frac{1}{\gamma} \tag{10}$$

The solution of Eq. (9) will also require $\omega \approx \omega_o$, and in this unstable region

$$| A_1 |^2 \sim \gamma \tag{11}$$

An amplitude master-equation covering both the damped and the nonlinear regimes may be derived from (7) and (8). Their simultaneous solution is

$$a A_1 - \frac{bd}{c} A_1^* A_1^2 = f_1 - \frac{b}{c} f_2 A_1^* \tag{12}$$

Separating (12) into real and imaginary parts, one of these will be satisfied by $\mathrm{Re}\,\omega \approx \omega_o$. The other part will specify $\mathrm{Im}\,\omega$. Replacing $\mathrm{Im}\,\omega$ by $\partial / \partial t$, this second equation reads

$$\frac{\partial}{\partial t} | A | = \gamma | A | + \text{const} | f_1 | + \text{const} | A |^3 \tag{13}$$

Similar amplitude master equations have been given by Landau [20] and Kadomtsev [21]. The amplitude behavior expressed by (10), (11), and (13) is seen in Fig. 6 to agree with the experiment. In addition, experiments have verified the dependence of the critical fluctuation amplitude on externally-applied noise [16].

2.7. Conclusion

Stabilizing effects of ion-ion collisions and finite ion Larmor radius suppress growth of density-gradient-driven collisional drift waves so that negative growth rate results when plasma parameters, such as magnetic field, density, or temperature, are below (or above) their critical values. At stabilization, the parametric dependence of ω and $\vec{k}$ is measured to be in agreement with linear theory. In the linearly stable regime, critical fluctuations at the drift-wave frequency are observed. The amplitude dependence of critical fluctuations on the linear damping rate ($\gamma < 0$) and on thermal or externally applied noise level, as well as the amplitude dependence of the drift wave on linear growth rate ($\gamma > 0$) in the unstable regime adjacent to onset, are found in agreement with an amplitude master-equation:

$$\frac{\partial A}{\partial t} = \gamma A + C A_{noise} - \alpha A^3$$

obtained from nonlinear calculations based on mode-mode coupling. Radial plasma transport, ~10% of the Bohm value, is measured for a steady-state wave of ~10% relative amplitude. This transport is a direct consequence of the n-ϕ phase difference. The measured transport is in qualitative agreement with nonlinear calculations.

Acknowledgment

This work was performed under the auspices of the U.S. Atomic Energy Commission, Contract No. AT(30-1)-1238.

REFERENCES

[1] D'ANGELO, N., and RYNN, N., Phys. Fluids 4 (1961) 1303.
[2] VON GOELER, S., Phys. Fluids 7 (1964) 463.
[3] MOTLEY, R. W., Phys. Fluids 8 (1965) 205.
[4] EASTLUND, B. J., Phys. Fluids 9 (1966) 161.
[5] BUCHELNIKOVA, N. A., Nucl. Fusion 6 (1966) 122.
[6] VON GOELER, S., and MOTLEY, R. W., Phys. Fluids 10 (1967) 1361.
[7] CHEN, F. F., and MOSHER, D., Phys. Rev. Letters 18 (1967) 639.
[8] SHEPHERD, L. T., Bull. Am. Phys. Soc. 10 (1965) 213.
[9] HARTMAN, C. W., and MUNGER, R. H., private communication.
[10] CHEN, F. F., Phys. Fluids 9 (1966) 2534.
[11] VON GOELER, S., and MOTLEY, R. W. Proc. of Conference on Physics of Quiescent Plasmas, Laboratorio Gas Ionizzati, Frascati, Italy (1967) p. 243.
[12] MOISEEV, S. S., SAGDEEV, R. Z., Zh. Eksperim i Teor. Fiz. 44 (1963) 763 [Soviet Phys.—JETP 17 (1963) 515].
CHEN, F. F., Phys. Fluids 7 (1964) 949.
GALEEV, A. A., MOISEEV, S. S., SAGDEEV, R. Z., Atomnaya Energiya 15 (1963) 451 [J. Nucl. Energy, Pt. C 6 (1964) 645].
MIKHAILOVSKII, A. B., POGUTSE, O. P., Dokl. Akad. Nauk SSR 156 (1964) 64 [Soviet Phys.—Doklady 9 (1964) 379].
COPPI, B., HENDEL, H. W., PERKINS, F., POLITZER, P. A., Proc. of Conference on Physics of Quiescent Plasmas, Laboratorio Gas Ionizzati, Frascati, Italy, Pt. 1 (1967) p. 201.
[13] HENDEL, H. W., COPPI, B., PERKINS, F., POLITZER, P. A., Phys. Rev. Letters 18 (1967) 439.
[14] HENDEL, H. W., CHU, T. K., POLITZER, P. A., Princeton Plasma Physics Laboratory MATT-586 (1968).

[15] LANDAU, L. D., LIFSHITZ, E. M., JETP 32 (1957) 618 [Soviet Phys.—JETP 5 (1957) 512].

[16] HENDEL, H. W., CHU, T. K., APS Los Alamos Meeting (June 1968).

[17] CHU, T. K., HENDEL, H. W., POLITZER, P. A., Phys. Rev. Letters 19 (1967) 1110.

[18] STIX, T. H., Princeton Plasma Physics Laboratory MATT-558 (1968).

[19] At maximum saturation-amplitude stage, results of a nonlinear theory by T. H. Dupree, Massachusetts Institute of Technology Report, 1968, based on incoherent scattering of particle orbits by waves, agree with experimental amplitudes.

[20] LANDAU, L. D., Acad. Sci. URSS 44 (1944) 311.

[21] KADOMTSEV, B. B., Plasma Turbulence, Academic Press, New York (1965).

EFFECT OF SHEAR AND CONNECTION LENGTH ON DRIFT WAVES AND PLASMA CONFINEMENT *

F. F. CHEN, D. MOSHER † AND K. C. ROGERS ‡
PLASMA PHYSICS LABORATORY, PRINCETON UNIVERSITY,
PRINCETON, N. J., UNITED STATES OF AMERICA

Abstract

EFFECT OF SHEAR AND CONNECTION LENGTH ON DRIFT WAVES AND PLASMA CONFINEMENT. We have investigated separately the effectiveness of shear and of short connection length on drift instabilities in a 0.22 eV thermally-ionized, 3-meter long potassium plasma. These experiments were carried out with T_i/T_e and ρ_i/R in a regime comparable to what would obtain in a fusion reactor. In the density range $n = 10^9 - 10^{11}$ cm^{-3}, we cover the transition from collisionless to collisional excitation of drift waves; ion viscosity is important only at highest densities studied.

By tailoring the radial electric field, it is possible to produce quiescence, turbulence, or single modes. Shear is applied by passing current through a 1-cm diam. hard core along the axis. Both turbulent and coherent drift waves are stabilized by shear of order $\theta \sim 0.05$, in fair agreement with the theory of Krall and Rosenbluth. However, at large shear, small-amplitude coherent oscillations reappear unexpectedly.

At zero shear, $D_\perp$ is 2-3 times the Bohm diffusion coefficient; at maximum shear, $D_\perp$ is decreased a factor of 5-30 to 2-3 times the classical value. At least half of $D_\perp$, however, is not connected with oscillations at all; it is due to the d.c. drifts in weak asymmetric electric fields produced by temperature variations at the end plate. The twisting of the equipotentials into spirals and thus symmetrization of the E fields has been observed in detail experimentally. A finite-Larmor-radius theory for the effect of shear in reducing the radial drift is found to be in agreement with the observed reduction in $D_\perp$.

Short connection length is achieved by internal current loops providing a B_z opposing the main B_z, thus creating stagnation points lying on the axis. In the vicinity of each ring, the plasma is bent around the ring and is stabilized by both minimum-$\bar{B}$ and viscous damping. The rings are spaced 75-180 cm apart, and between rings the field is uniform. Thus, instabilities are restricted to those with short $\lambda_{\parallel}$. We find that the oscillation level is greatly reduced by current in the rings.

We conclude that 1) radial electric fields affect not only the frequencies but also the excitation thresholds of drift waves; 2) it is easy, with small shear or minimum-$\bar{B}$, to reduce oscillations to a level at which they contribute negligibly to anomalous transport; and 3) the primary loss mechanism is steady convection along asymmetric equipotentials, and large shear can reduce the loss rate by twisting the equipotentials into long spirals.

1. INTRODUCTION AND APPARATUS

Drift waves in an inhomogeneous plasma can be stabilized by a) magnetic or velocity shear and b) minimum-$\bar{B}$ with short connection length between regions of favorable curvature. In this paper we summarize four experiments designed to test separately the effectiveness of each method in suppressing oscillations and decreasing anomalous plasma transport. The experiments were carried out in a thermally ionized potassium plasma (Q machine) in which currents and mass flow along $\mathbf{B}$ were carefully minimized. A diagram of the machine in the shear configuration is shown in Fig. 1. The 326-cm length of the plasma between the hot plates allows waves of small $k_{\parallel}$ to grow in spite of

* Supported under the auspices of the US Atomic Energy Commission.
† Present address: Los Alamos Scientific Laboratory, Los Alamos, New Mexico.
‡ Permanent address: Stevens Institute of Technology, Hoboken, N.J.

line-tying by the electron sheaths at each end plate [1]. At 4 kG, the ion gyroradius r_L is 0.1 cm, so that there are 5 - 10 gyroradii in a density scale length r_0 in the hard-core configuration; the ratio r_L/r_0 is comparable to that in the present generation of multipoles. By varying the density n, the mean free path can be varied from 100 cm down to less than 1 cm.

In thermionic plasmas the radial electric field E_r is primarily determined by the equation

$$j_T \exp(e\phi/KT) = \frac{1}{4} n v_e \tag{1}$$

expressing the balance between random electron current striking the end plates and the thermionically emitted current, attenuated by the Coulomb barrier of the sheath. Here j_T is the Richardson current $j_T = AT^2 \exp(-e\phi_w/KT)$, and ϕ is the (negative) potential drop from the end plate surface to the sheath edge. Since n varies with radius, so will ϕ. The resulting E_r causes a plasma rotation which Doppler shifts the electron diamagnetic velocity $\vec{v}_{De} \equiv -(KT/eB)(n'/n)\,\vec{\theta}$ to *zero in the laboratory frame and the ion diamagnetic velocity* $\vec{v}_{Di} = -\vec{v}_{De}$ to $2\vec{v}_{Di}$. However, deviations from this "normal" E_r occur when small temperature gradients in the end plates cause large variations in j_T, and when ion-ion collisions allow a nonvanishing mobility across $\vec{B}$. These effects are important in understanding the results which follow.

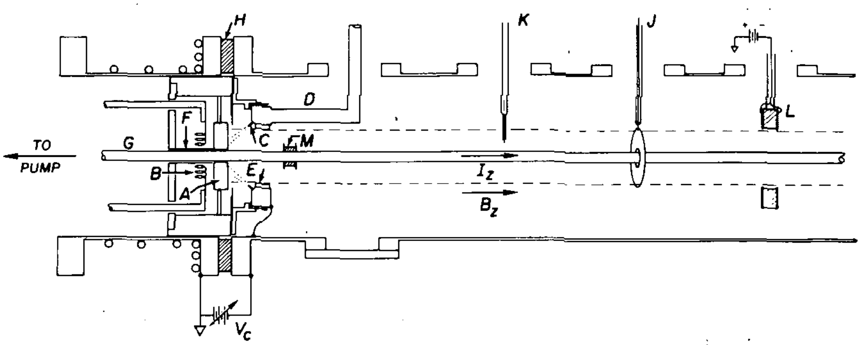

FIG. 1. Schematic diagram showing one end of the hard-core Q machine; the other end is identical and is located 3 metres away. The tungsten hot plate A is heated to 2550°K by electron bombardment from the filament B. Neutral potassium atoms impinging on A are collimated by 16 small pipes C emanating from an annular chamber fed by the heated pipe D. The plasma aperture is defined by the limiter E. The grounded molybdenum tube F prevents fast electrons from entering the plasma. The hard core G is a water-cooled, anodized aluminium tube 1 cm in diameter threaded through 1.3 cm diameter holes in the hot plates and kept straight by 500 kg of tension. The ceramic break H allows the vacuum chamber, including the aperture limiter E, to be biased at a potential V_C relative to the grounded hot plates. The collector J measures the total flux of ions emitted from the hot plate; J is split so as to be removable. K is a typical Langmuir probe. L is a plasma catcher for measuring the radial losses to the outside. The inner limiter M can also be used to measure losses to the inside and to set the plasma potential at the inner boundary. The plasma diameter is 5.08 cm, and all positions are approximately to scale, except that L is normally at the midplane of the machine.

2. ANOMALOUS TRANSPORT BY PLASMA CONVECTION

When the neutral input flux Φ_{in} is kept constant, we have previously reported [2] that the plasma density increases by more than an order of magnitude as the hard-core current I_s is increased to its maximum value of 4 kA d.c. This effect is illustrated in Fig. 2, which shows the increase in n with I_s. The curve n_{osc} is a lower limit on the density expected if losses were due to oscillations alone; this limit is obtained from the oscillation amplitude n_1 and the assumption that n_1 and potential ϕ_1 are 90° out of phase. It is seen that above $I_s = 200$ A, the density is limited by a shear-dependent loss mechanism not related to oscillations.

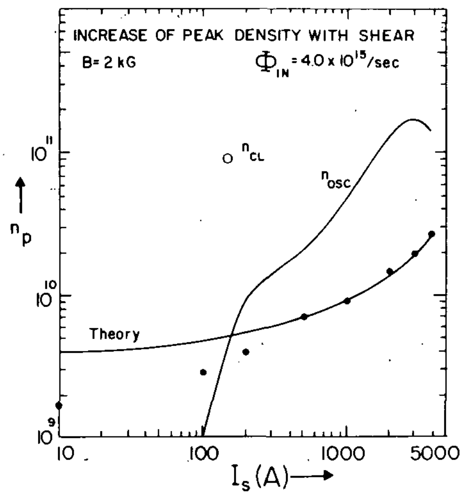

FIG. 2. Increase of peak density n_p with current in the hard core. The point n_{c1} is the density expected from classical processes alone (resistive diffusion and end-plate recombination).

Such a mechanism is the steady convection of plasma along equipotentials which are not concentric with the plasma. According to Eq. (1), asymmetries in the distribution of plasma potential ϕ can arise from azimuthal gradients in end-plate temperature T and hence in j_T. This effect has been verified by direct pyrometric measurements ($\Delta T \approx \pm 15°$ K in our case). When shear is applied, the radially varying rotational transform causes the equipotentials to be twisted into long spirals, as shown in Fig. 3, because potential is approximately constant along a line of force. This has the effect of symmetrizing the drift surfaces, and ions must $\vec{E} \times \vec{B}$ drift a longer distance to change radial position. [Note that electrons are not confined because of the Simon short-circuit effect and need only satisfy Eq. (1).]

The existence of spiral convective cells is revealed by radial scans of probe floating potential, as shown in Fig. 4 for two values of I_s. These patterns are steady and reproducible. The spacing Δr between spiral arms is found to vary as r^3, as expected from theory.

By probing the entire cross section, one can plot the equipotential contours shown in Fig. 5 for two different distances from the hot plate. These observations confirm the existence of spiral convective patterns in the presence of shear. We next compute the increase in confinement time arising from this effect.

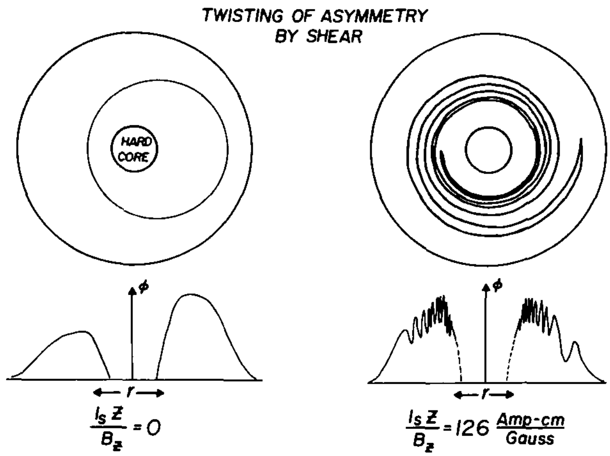

FIG. 3. Schematic of how an equipotential contour with an m = 1 asymmetry can be twisted into a spiral by shear, characterized by the parameter $I_s z/B_z$, where z is the axial separation between the two cross-sections depicted. Radial profiles of plasma potential ϕ are shown below. In double-ended operation, the spirals from each end plate are superimposed.

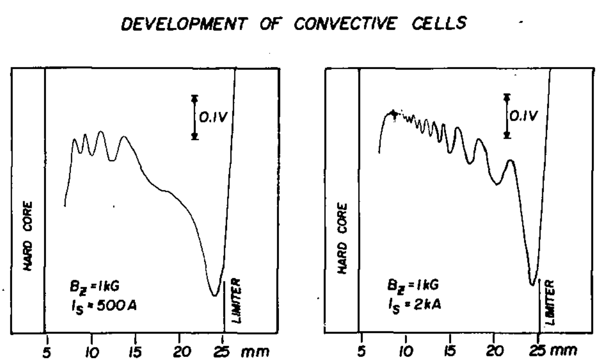

FIG. 4. Radial profiles of probe floating potential at midplane of machine in simple-ended operation. Peak density was about $10^{10}\,\text{cm}^{-3}$.

If r_L were zero, one can show that the radial component v_r of ion drift velocity is not changed by shear, since the increase in path length is exactly cancelled by an increase in drift velocity due to the steepening of potential gradients when the spiral patterns develop. However, when the wavelength Δr of the sinusoidal potential variations in Fig. 4 becomes smaller than r_L, an ion samples different electric fields in each gyration; and its guiding center suffers a decrease in drift velocity. We have computed the guiding-center motion for arbitrary $\Delta r/r_L$ by expanding the ion equation of motion in a sheared field in the small parameter $\epsilon \equiv r_L \; \partial\eta/\partial r$, where $\eta \equiv e\phi/KT = \eta_o(r) + \eta_1(r,\theta)$, η_o being the symmetric part and η_1 the asymmetric part of the potential. From Fig. 4 it is seen that $r_L \; d\eta_o/dr$ is small because η_o, though of O(1), is slowly varying; and $r_L \; \partial\eta_1/dr$ is small because $\eta_1 << 1$, though it is rapidly varying. After integrating over a Maxwellian distribution, we find

$$v_r = \frac{E_\theta}{B_z} \exp - \left[\frac{1}{4} \frac{mz}{r} \frac{r_L}{r} \frac{B_\theta}{B_z} \right]^2 \tag{2}$$

where E_θ is the azimuthal electric field at an end plate due to an asymmetry of the form $\sin m\theta$, and the exponential factor expresses the decrease in v_r at a distance z from one end plate due to shear and finite r_L.

To compute the loss rate we assume that ions have a high probability P of being lost to the limiter or to the hard core if they reach $r = r_2$ or $r = r_1$, respectively, where r_1 and r_2 are about a Larmor diameter away from the actual boundaries; and we integrate $n v_r$ for outgoing particles over θ and z at these radii. We also assume that the equipotentials that reach r_1 and r_2 are easily populated from those that do not; a few collisions are sufficient to do this when the asymmetry is large. A typical result is shown as the "theory" curve on Fig. 2. The slope of this curve depends on the ratio of losses at r_1 to those at r_2; for the measured ratio the fit is good. The absolute magnitude of n_p depends on P and some form factors; it is also in good agreement with experiment.

We conclude that at high shear the anomalous loss can be entirely attributed to steady convection. At zero shear, convective losses are about equal to losses connected with oscillations.

3. EFFECT OF RADIAL ELECTRIC FIELDS ON DRIFT WAVES

The low-frequency oscillations in our machine are generally turbulent, with a continuous spectrum up to ~ 5 kHz. To recover the coherent oscillations of Hendel et al. [3], we have a) removed the hard core and the hole in the end plates, b) changed the collimation of K atoms to have a peak on the axis, c) increased n_p to the 10^{11} cm^{-3} range, and d) insulated the vacuum chamber and added the limiter E (Fig. 1) so that a variable potential V_c could be applied to the edge of the plasma. This oscillation amplitude vs V_c is shown in Fig. 6. With the normal bias $V_c = 0$, large turbulent fluctuations always appear. For $V_c < 0$, these fluctuations increase, and the plasma suffers "pumpout." For a range of V_c the plasma is quiescent ($n_1/n_0 < 1\%$). At a critical V_c, in this case about +2 V, coherent oscillations set in. As V_c is further increased, these oscillations change frequency, sometimes undergo a mode switch, and then become noisy. The quiescent range of V_c narrows and disappears with increasing B. The coherent waves are generally m = 1 or m = 2 modes with amplitude maximum

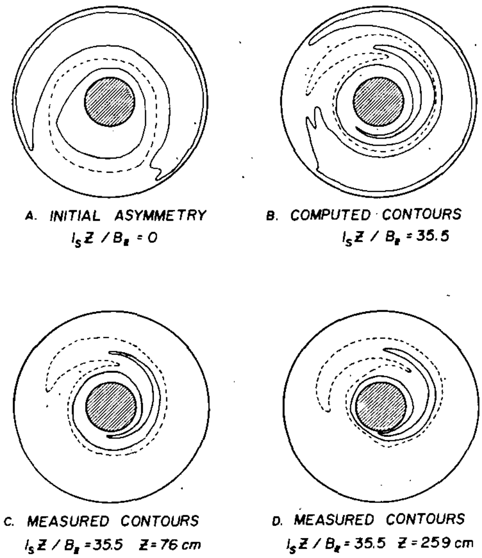

FIG. 5. Equipotential contours (A) measured with $I_s = 0$, (B) computed from (A) with a rotational transform corresponding to $I_s z/B_z = 35.5$ A-cm/G, (C) measured at z = 76 cm, and (D) measured at z = 259 cm with I_s adjusted to keep $I_s z/B_z$ constant. Some equipotentials are shown dashed for clarity. The slight difference between (C) and (D) is caused by diffusion.

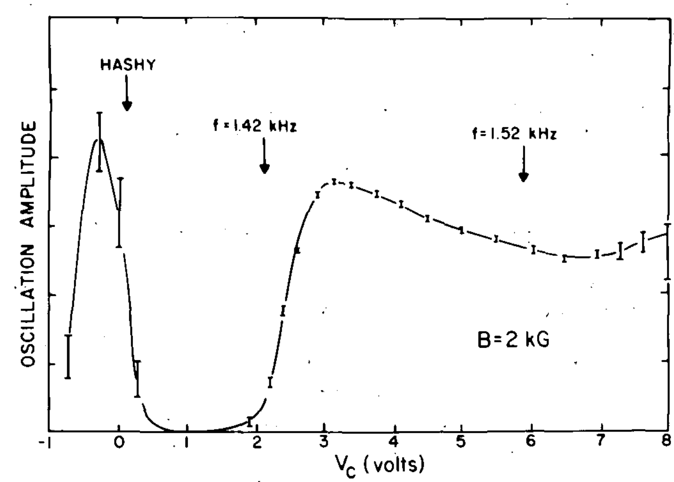

FIG. 6. Amplitude of oscillations on probe current vs vacuum chamber bias V_C. The decrease in amplitude at $V_C < 0$ is due to loss of plasma density.

at the midplane and zero at the end plates. They have an unmeasurably small $n_1 - \phi_1$ phase shift and have little effect on the plasma density. The steady-state amplitude n_1/n_0 varies from 0.01 to 0.3, depending on factors such as V_c.

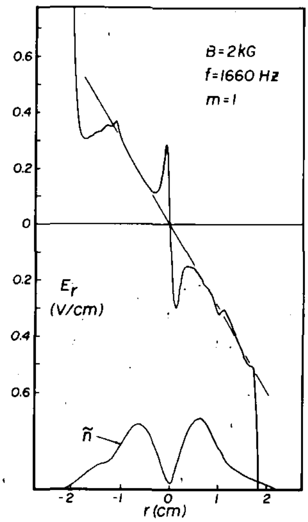

FIG. 7. Direct measurement of the radial profile of E_r in the plasma. Deviation from the solid line through the origin indicates deviation from solid-body rotation. The amplitude distribution of the oscillation is shown below.

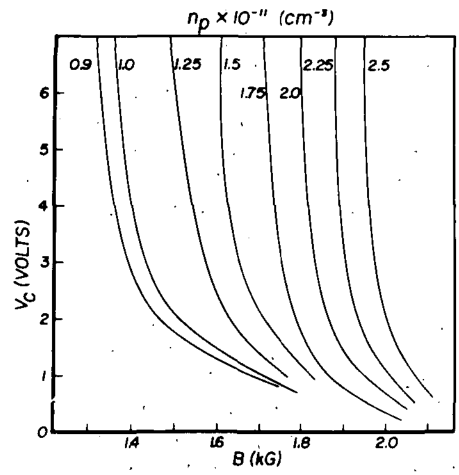

FIG. 8. Variation of the threshold value of V_c with B at various peak densities n_p. Waves can be excited by either increasing B at fixed V_c or increasing V_c at fixed B.

When V_c is varied, the radial electric field E_r in the plasma is changed from that given by Eq. (1) because of the finite ion mobility. We have measured E_r directly by a new technique employing synchronous detection of floating potential signals when the plasma is displaced by ~ 1 mm at a frequency of 17 Hz by means of auxiliary coils. Figure 7 shows an example of such a measurement. It is seen that there is a region in which $E_r \propto r$; that is, there is no velocity shear; and the oscillation is peaked there. This appears to be a necessary requirement for coherent waves. In the case of Fig. 7, the end plates were cooler at the center than at the edge and we had $E_r > 0$; the wave velocity in the E = 0 frame was then $v_{De}/2$, in agreement with the results of Hendel et al. [3]. However, when $E_r < 0$ was achieved by preferentially heating the center of the end plates, there was no longer agreement with the drift-wave velocity, a result previously reported by Hartman [4].

Figure 8 shows the voltage V_c at onset of oscillations vs B for various densities. The curves approach a critical field B_c asymptotically. If $B_c/k_\perp$ is plotted against $n^{1/2}$, as done by Chu et al. [5], there is agreement with their results. The bending of the curves of Fig. 8 toward higher B at low V_c is an indication of stabilization by shear in the $\vec{E} \times \vec{B}$ drift velocity. We conclude that $E_r(r)$ has a profound effect on both the frequency and the excitation of drift waves.

4. DRIFT WAVE STABILIZATION BY MAGNETIC SHEAR

4.1. Turbulent oscillations

We have previously [2, 6] reported on the stabilization of turbulent oscillations occurring at low density ($n < 10^{10}$) with the vacuum chamber grounded. These oscillations had largest amplitudes on the inside gradient (near the hard core) but were pushed to the outside gradient, reduced in amplitude, and localized radially by the application of several kA of current I_s. Measurements with an electronic correlator showed that these fluctuations propagated at the proper velocity for drift waves in the E = 0 frame, and that the $n_1 - \phi_1$ phase shift was unmeasurably small. Figure 9 shows further observations indicating that the stabilizing effect of I_s is not monotonic. Reappearance of oscillations at high shear was unexpected, as was the large amount of shear needed to suppress all oscillations.

4.2 Sinusoidal oscillations

By adjusting the biases on the outer limiter E and inner limiter M (Fig. 1), we can now produce clean oscillations occurring (at $I_s = 0$) on either the outer or inner density gradient. Examples of these are shown in Figs 10 and 11, respectively. The outside waves are usually $m = 7$ or 8 and prefer $B \approx 3$ kG, in contrast to $m = 1$ or 2 and $B \approx 2$ kG for the gentler gradients of Sec. 3. These waves are line-tied at the end plates and have a single maximum near the midplane. The $n_1 - \phi_1$ phase shift is zero. In the E = 0 frame, the wave velocity $\omega/k_\perp$ is about $0.3\ v_{De}$; this agrees with the computed dispersion relation [7] if the finiteness of $k_\perp^2 r_L^2$ is further taken into account. Furthermore, $\omega/k_\perp$ is closer to v_{De} if V_c is close to threshold. The inside oscillations are generally $m = 1$. The wave velocity in the E = 0 frame is $1.5\ v_{Di}$ if the Doppler shift is computed with the value of E_r at the amplitude maximum; however, as seen on Fig. 11, E_r varies rapidly on the scale length of r_L, and the wave velocity is probably affected by the nonuniformity in E. The $n_1 - \phi_1$ phase shift is nearly 180°, with ϕ_1 slightly leading; this suggests that the inside waves are FLR-stabilized flute modes.

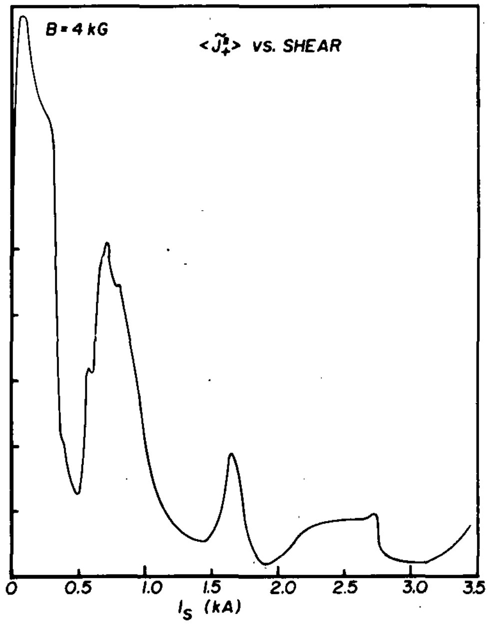

FIG. 9. Mean square oscillation amplitude at a fixed radius as a function of hard-core current.

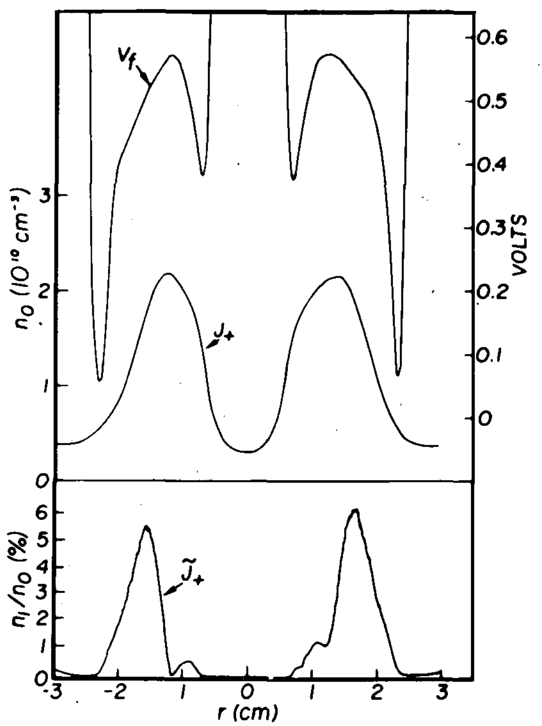

FIG. 10. Amplitude, density, and potential distributions for a 3520 Hz, m = 10 sinusoidal oscillation occurring on the outside gradient at B = 3 kG, I_s = 0.

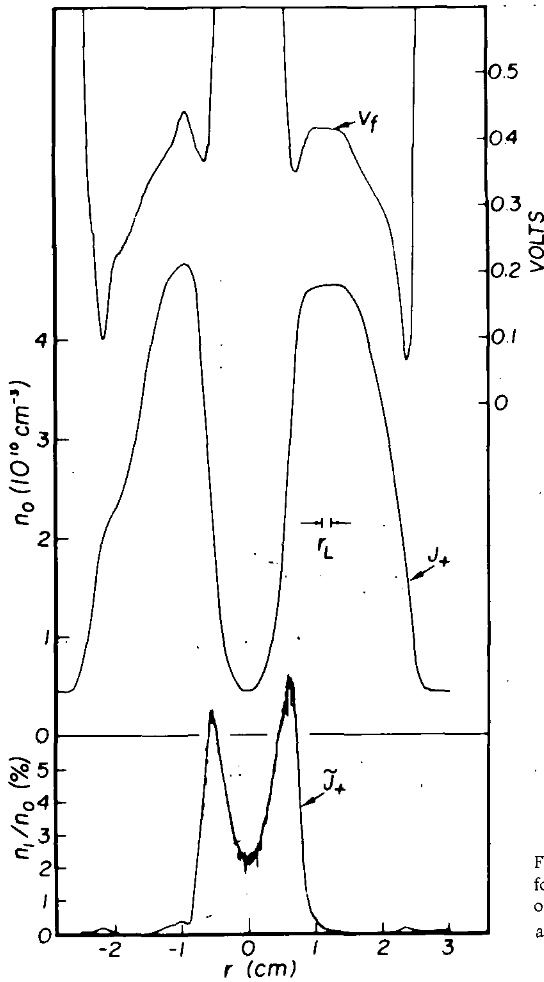

FIG. 11. Amplitude and density distributions for a 5200 Hz, m = 1 sinusoidal oscillation occurring on the inside gradient at B = 3 kG, I_S = 0.

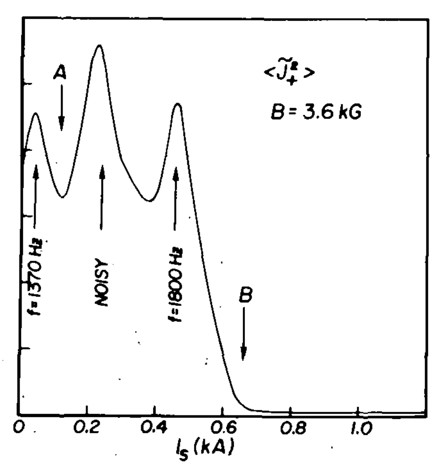

FIG. 12. Mean square oscillation amplitude vs hard-core current for coherent modes on outside density gradient.

When shear is applied to the waves on the outside gradient, the variation of oscillation amplitude with I_s is similar to that shown in Fig. 9 for turbulent waves, except that the first peak at low shear often exhibits fine structure, as shown in Fig. 12. The mode switch

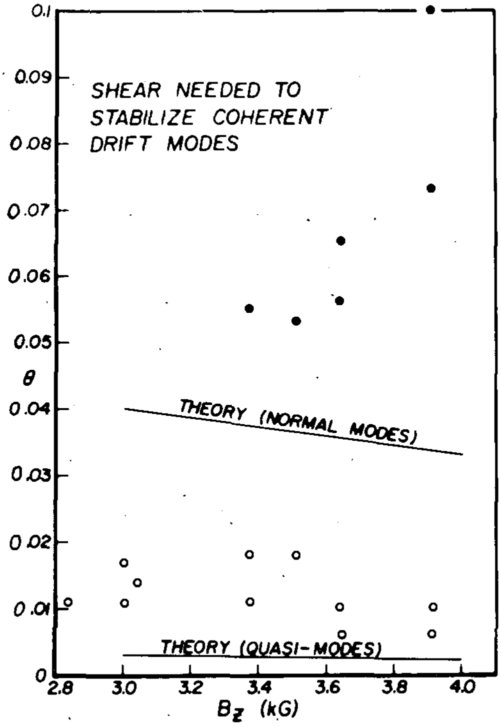

FIG. 13. Shear parameter θ required to stabilize coherent drift modes. The open points refer to point A of Fig. 12; the solid points to point B. The value of θ was taken at the radius of maximum oscillation amplitude, with r_0 defined by $n'_0/n_0 = -2r/r_0^2$. The theoretical values are computed from Krall and Rosenbluth (upper line) and Coppi et al. (lower line). For the latter we have taken the number N of e-foldings to be 3 and have used the measured value of $k_y v_D$.

at point A is probably caused by the change in E_r brought on by shear; the oscillation amplitude does not decrease greatly until point B. The shear parameters θ, defined by

$$\theta = \int_{r+r_o/2}^{r-r_o/2} \frac{\partial}{\partial r} \left[\frac{B_\theta(r)}{r B_z} \right] r\,dr$$

corresponding to points A and B are plotted in Fig. 13 for m = 7 and m = 8 modes at various B_z. Comparison is made with the two most relevant theories: that of Krall and Rosenbluth [8] for collisionless normal modes,

$$\theta_{crit} = r_L / 2 r_o \tag{3}$$

and that of Coppi et al. [9] for resistive quasi-modes,

$$\theta_{crit} = \frac{1}{3M} \left(\frac{m}{M} \frac{\nu_{ei}}{k_y v_D} \right)^{1/2} \tag{4}$$

Since Eq. (3) predicts a higher value of θ than Eq. (4), the latter is irrelevant; at any rate, we do not observe the large radial propagation velocity expected of quasi-modes. Collisions are expected to raise the value of θ given by Eq. (3) only slightly. Since Eq. (3) is accurate only to within a factor of 2 or 3, there is agreement with the solid points on Fig. 13.

The waves which reappear at high shear (Fig. 9) are $m = 1$ modes with a sawtooth wave form and $f \approx 370$ Hz. Their $k_{\parallel}$ is difficult to measure because of the large shear. Since the electric field pattern (Fig. 5) is so complicated, the Doppler shift is difficult to compute. In one case we found $\omega/k_{\perp} = 0.55 \pm 0.11\ v_{De}$ by averaging E_r measured at four azimuths. We calculate that the excitation of either flute or drift modes by the centrifugal force due to plasma rotation and line curvature is weaker than the excitation of ordinary resistive drift waves. We conjecture that these high-shear modes are Kelvin-Helmholtz instabilities connected with the spiral convective patterns of Sec. 2. The amplitudes are so small that these modes have no measurable effect on plasma confinement.

We conclude that our stabilization results for single modes are in agreement with theory, within the accuracy of existing theories.

5. STABILIZATION BY DAWSON RINGS

To test stabilization by short convection length, we have added internal reverse-current loops to the machine with solid end plates and no hard core, as shown in Fig. 14. As pointed out by Dawson [10], this configuration has favorable $\int d\ell/B$ everywhere. The field configuration at $B_z = 2$ kG, with $I_D = 22.6$ kA-turns in the Dawson rings, is shown in Fig. 15. In addition to minimum-$\overline{B}$ stabilization in the neighborhood of each coil, one expects viscous stabilization, since the ratio of r_L to plasma thickness d in the "bridge" region is only about 0.3.

Density profiles with the ring on and off are shown in Fig. 16. By means of obstacles inserted into the plasma (Fig. 14), we have determined that the large density near the axis with the coil on must, in the absence of oscillations, come from collisional diffusion in the bridge region. The fast diffusion there unfortunately also shortens the plasma lifetime, so that a direct comparison of oscillation levels with the coils on and off cannot be made.

Figure 17 shows the stabilization of an $m = 2$, $f = 3.4$ kHz drift wave at 2 kG. However, the corresponding density profiles (Fig. 18) show a factor of 5 decrease in density and, presumably, of plasma lifetime. The increased loss rate is due partly to collisional diffusion in the bridge region and partly to stray fields from the return leads, as

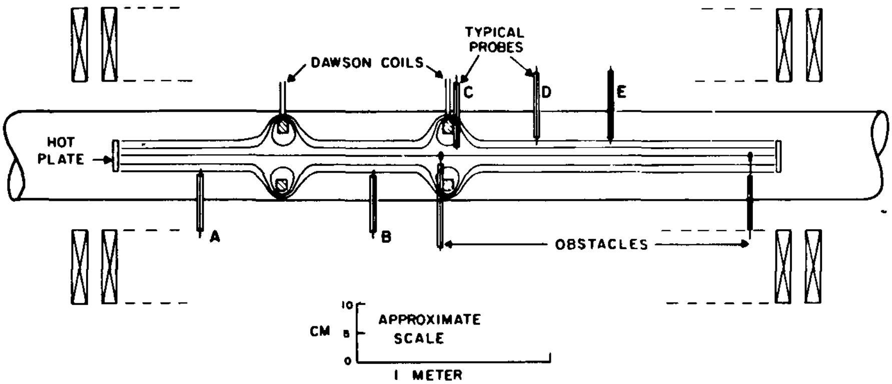

FIG. 14. Machine configuration for the Dawson ring experiment.

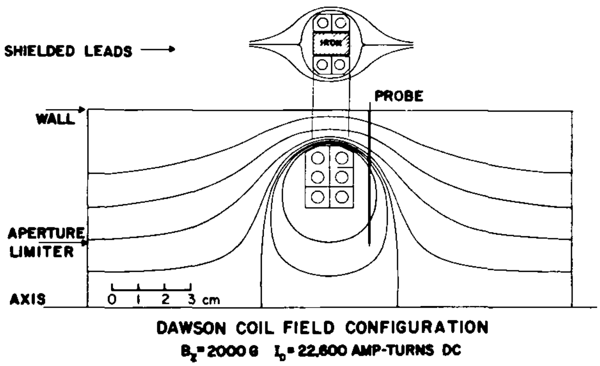

FIG. 15. Field lines around a Dawson ring in normal operation. The insert shows a top view of the computed field configuration around the leads, which are magnetically shielded with the help of an iron insert.

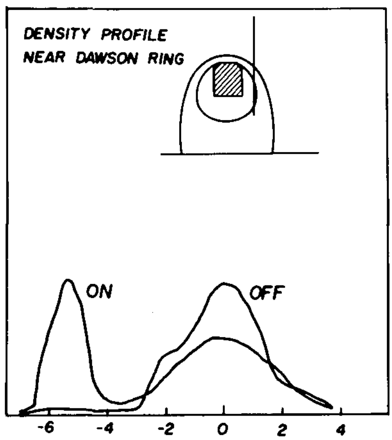

FIG. 16. Density profiles near the Dawson ring with the ring current on and off, taken with a probe in the position shown.

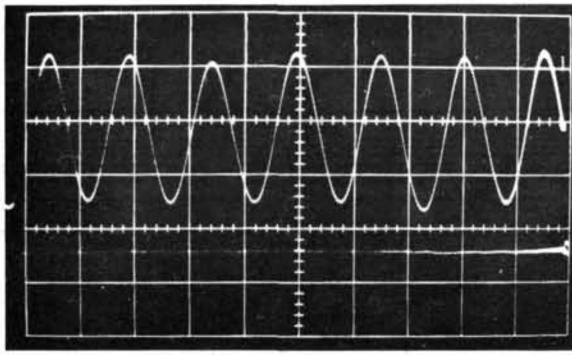

FIG. 17. Top trace: drift wave with Dawson ring off. Bottom trace: probe signal with same gain with Dawson ring on. Ac coupled; 200 μs/cm. Probe E (Fig. 14).

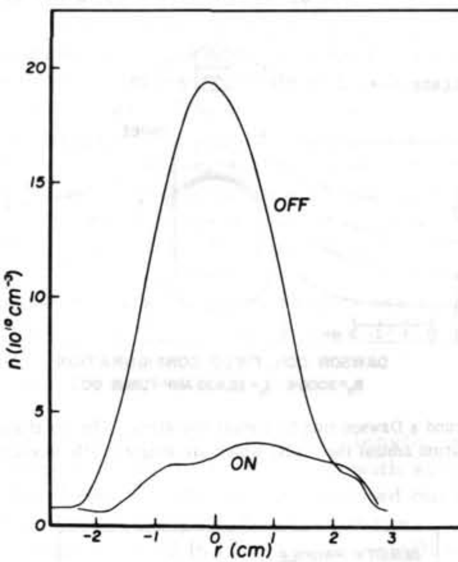

FIG. 18. Density profiles corresponding to Fig. 17. Probe D (Fig. 14).

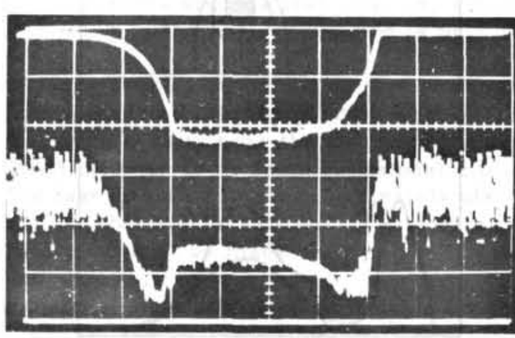

FIG. 19. Top trace: Dawson ring current, 20 kA-turns/cm, increasing downwards. Bottom trace: probe current at r = 1.5 cm, d.c.-coupled (baseline is at bottom). Sweep: 20 ms/cm, from right to left. Low density during rise and fall of current is due to the field lines intersecting the Dawson ring.

determined by reversing the sign of I_D. To reduce the diffusion loss, we increased B_z to 3.24 kG and pulsed I_D to 44 kA-turns for 0.1 sec. The oscillations were turbulent at this B_z. A typical pulse is shown in Fig. 19. Probe D (Fig. 14) was placed on the density gradient of both the "off" and "on" profiles. It is seen from the profiles of Fig. 20 that although the density decrease was only a factor of 2, the decrease in n_1/n_0 was as much as a factor of 20. No further improvement was observed by using probe B (Fig. 14), located in a shorter section of the machine between two rings. Since a large reduction in oscillation level always accompanies the firing of the Dawson rings, we conclude that this is an efficient method for stabilizing drift waves. However, we were unable to increase the plasma lifetime.

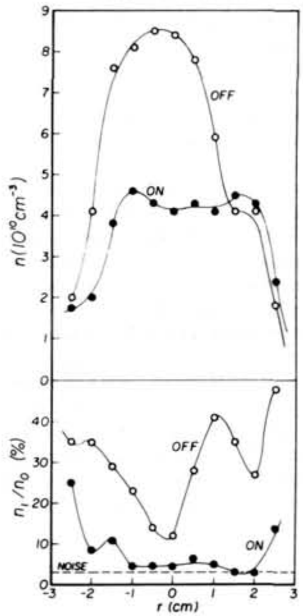

FIG. 20. Profiles of density and oscillation amplitude with B_z = 3240 G, I_D = 0, and 44 kA-turns.

REFERENCES

[1] CHEN, F. F., J. Nucl. Energy, Pt C, 7 (1965) 399.

[2] CHEN, F. F., MOSHER, D., Phys. Rev. Letters 18 (1967) 639.

[3] HENDEL, H. W., COPPI, B., PERKINS, F., POLITZER, P. A. Phys. Rev. Letters 18 (1967) 439.

[4] HARTMAN, C. W., MUNGER, R. H., Proceedings of the Conference on Physics of Quiescent Plasmas, Frascati, Italy, Pt. 1 (1967) 49.

[5] CHU, T. K., et al., Paper CN-24/E-1, this conference, Fig. 5c.

[6] CHEN, F. F., Proceedings of the Conference on Physics of Quiescent Plasmas, Frascati, Italy, Pt. 1 (1967) 145.

[7] CHEN, F. F., Phys. Fluids 10 (1967) 1647.

[8] KRALL, N. A., ROSENBLUTH, M. N., Phys. Fluids 8 (1965) 1488.

[9] COPPI, B., LAVAL, G., PELLAT, R., ROSENBLUTH, M. N., Nucl. Fusion 6 (1966) 261.

[10] DAWSON, J., private communication.

EXPERIMENTAL STUDY OF THE EFFECT OF RADIAL ELECTRIC FIELDS ON THE STABILITY OF A MAGNETICALLY CONFINED PLASMA

L. ENRIQUES, A. M. LEVINE AND G. B. RIGHETTI
LABORATORI GAS IONIZZATI (ASSOCIAZIONE EURATOM-CNEN)
FRASCATI, ROME, ITALY

Abstract

EXPERIMENTAL STUDY OF THE EFFECT OF RADIAL ELECTRIC FIELDS ON THE STABILITY OF A MAGNETICALLY CONFINED PLASMA. Low-frequency, spontaneous, electrostatic oscillations propagating azimuthally in low-β, magnetically confined plasma columns, have been studied in many devices. In most of these experiments, the peak amplitude of the observed oscillations has been in a region where both radial density gradients and radial electric fields existed. To separate these two effects we studied the behaviour of the coherent oscillations of an alkali plasma in conditions where the radial electric field could be externally controlled.

The experiments were performed in a single-ended, large-diameter (8 cm), alkali plasma (Q-machine). To achieve an adjustable electric field, the hot end-plate was split into two concentric parts separated by a small gap. By applying a steady voltage between these sections, an adjustable electric field is observed down the 90-cm length of the plasma column. For low applied voltages the plasma was quiescent.

When the voltage was increased above a threshold value (between 0.05 and 0.5 V), low-frequency (1 - 10 kHz) coherent oscillations were observed. In this case, the electric-field drift velocity was much greater than the density-gradient drift velocity. The oscillations propagated azimuthally in the $\vec{E}\times\vec{B}$ direction and formed a standing wave in the radial direction. For a given azimuthal mode number, the frequency was proportional to the applied voltage. Potential and density fluctuations were out of phase, suggesting that this is a flute-type mode, perhaps driven by shear in azimuthal velocity.

At higher applied voltages (1 - 3 V), the density gradient in the centre part of the plasma increased noticeably. In this region there was a strong density gradient, but a comparatively small electric field. Here, a different kind of azimuthally propagating, coherent, low-frequency (1 - 3 kHz) oscillation was observed. In this case, density and potential oscillations were in phase, suggesting some form of drift wave.

1. INTRODUCTION

Both non-uniform radial electric fields and radial density gradients affect the stability of magnetized plasma columns. In most experiments it is difficult to separate these two effects. In this work we studied the behaviour of the spontaneous coherent oscillations of an alkali plasma, in conditions where the radial electric field could be externally controlled. Two different modes of oscillation were found. The first is localized in a region where the electric field drift velocity is much greater than the density-gradient drift velocity. We believe this may be a flute-type mode driven by shear in the azimuthal velocity [1, 2]. The second mode is localized in a zone of large density gradient but comparatively small electric field. We believe this oscillation is related to the density-gradient drift wave studied extensively by Buchelnikova, Hendel and others [3-6].

In the next section some of the details of the experimental arrangement are described. In sections 3 and 4 we describe the behaviour of the "electric-field" mode and the "density-gradient" mode. Section 5 contains a discussion of these results.

2. EXPERIMENTAL DETAILS

This experiment was performed in large-diameter (8 cm) caesium and potassium plasma columns 90 cm long (a "Q-machine") [7, 8]. The density (n) was in the range of 10^9 - 10^{11} cm^{-3} and the magnetic field (B) was between 2 and 7 kG. A single end-plate was heated to approximately 2000°K by thermal radiation from a surrounding hot cylinder. By proper design of the screens in the back of the plate, the radiation losses can be adjusted to obtain a uniform temperature profile. The cold end-plate terminating the plasma column was normally biased to collect ions.

In these experiments, a controllable electric field was required. To achieve this, the hot plate was split into two concentric sections. The inner plate had a radius of 2.0 cm. The annular plate had an inner radius of 2.2 cm and an outer one of 4.0 cm. With the two plates grounded together, the plasma was quiescent with reasonably uniform density and potential, except for small changes in the "gap" region.

When the outer plate was grounded and a d.c. voltage applied to the inner one, a radial electric field was observed down the entire length of the plasma column. The potential differences measured in the plasma were approximately equal to the applied voltages. No experimental difference was observed if the role of the two plates was reversed; that is, if the inner was grounded and the outer biased. The applied voltages also had an effect on the density gradients present throughout the plasma. As will be discussed later, this feature enabled us to observe oscillations in a region of "weak" electric field and "strong" density gradient.

Most of the measurements described below were made with Langmuir probes 5 mm long and 0.4 mm in diameter, aligned along the magnetic field. The results presented have been checked with different probes of varying sizes and shapes, with no significant differences observed.

Within a single run, all measurements were quite reproducible. There were, however, small changes in the exact shape of the radial density and potential profiles each time the plate structure was rebuilt. Unless otherwise stated, the results quoted below did not depend on these changes.

3. ELECTRIC FIELD MODE

When the voltage applied between the two sections of the split end-plate was increased above a threshold value (typically between 0.05 and 0.5 V), coherent, nearly sinusoidal oscillations were observed on both the ion current and floating voltage of a probe. As previously reported [9], these oscillations propagated azimuthally in the direction of the $\vec{E} \times \vec{B}$ drift. The observed frequency (usually between 1 and 10 kHz) for a given azimuthal mode number was proportional to the applied voltage. Normally, only one mode was observed at a time.

In Fig. 1 we show some actual data obtained in a potassium plasma at $n = 5 \times 10^9$ cm^{-3}, and B = 2.5 kG, with an applied voltage (- 0.65 V) well above the threshold value. These measurements were made approximately 50 cm away from the hot plate. The top two traces display the ion current collected by a negatively biased probe, and the floating voltage as a function of radial position. The probe was mechanically driven across the plasma with the radial displacement known to within 0.02 cm.

From curves such as these we may compute the observed electric fields. In these measurements we have found peak electric fields of approximately 1 V/cm, an order of magnitude larger than was found in the runs reported in a preliminary note [9]. This difference might have been due to insufficient accuracy in monitoring the probe displacement in those earlier runs. As a result, the electric fields reported earlier were an average value taken over a scale length larger than the true spatial variation.

For conditions in which the oscillations were observed, the peak electric-field drift velocities [$\vec{v}_E = c\,\vec{E}\times\vec{B}/B^2$] were of the order of the ion thermal velocity. The azimuthal phase velocity of the waves was in the same direction as, but less than, the peak electric-field drift velocity.

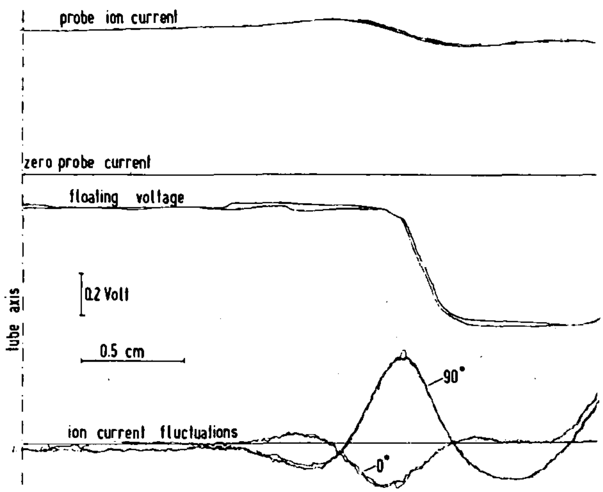

FIG. 1. Radial dependence of the "electric-field" mode. Top trace: probe ion current (arbitrary units). Centre trace: floating voltage. Note that the voltage axis is reversed in this figure. Bottom trace: quadrature components of the ion current fluctuations (arbitrary units). Plasma parameters: potassium; $B = 2.5$ kG, $n = 5 \times 10^9$ cm^{-3} ; applied voltage = -0.65 V; oscillation frequency = 2.1 kHz.

From the profile of the ion current collected by a negatively biased probe, we may estimate the scale length for the density gradient. In the case shown in Fig. 1, the density gradient was quite small, $n(dn/dr)^{-1} \approx 2.2$ cm. In other runs the density variations were larger. However, in all cases in which oscillations were observed, the peak density-gradient drift velocity [$\vec{v}_n = (ckT/eB)(1/n)(dn/dr)$] was at least a factor of two lower than the peak electric-field drift velocity.

Also shown in Fig. 1 is data concerning the amplitude and phase of the fluctuations in ion current as a function of radial position. This information was obtained by using the oscillations on a remote fixed probe as the reference for a lock-in amplifier. The output of this phase synchronous detector is the product (averaged over 30 ms) of the signal amplitude and the cosine of the phase shift between the signal and the reference. This is the 0° trace shown in Fig. 1. Then the phase of the reference signal was delayed by 90° and the measurement repeated (the 90° trace in Fig. 1). This information was used to calculate the amplitude and phase of the oscillations as a function of radial position. A typical result for both ion current and floating potential fluctuations is shown in Fig. 2. This data was taken in a caesium plasma at $n = 4 \times 10^{10}$ cm^{-3}, B = 3.5 kG and with an applied voltage of -0.6 V. The potential fluctuation measurements were made using a shielded probe with the shield driven by a unity-gain amplifier.

From these curves one may obtain the following information. First, the position of maximum oscillation amplitude normally does not coincide with the position of the maximum electric field. The node (or exact

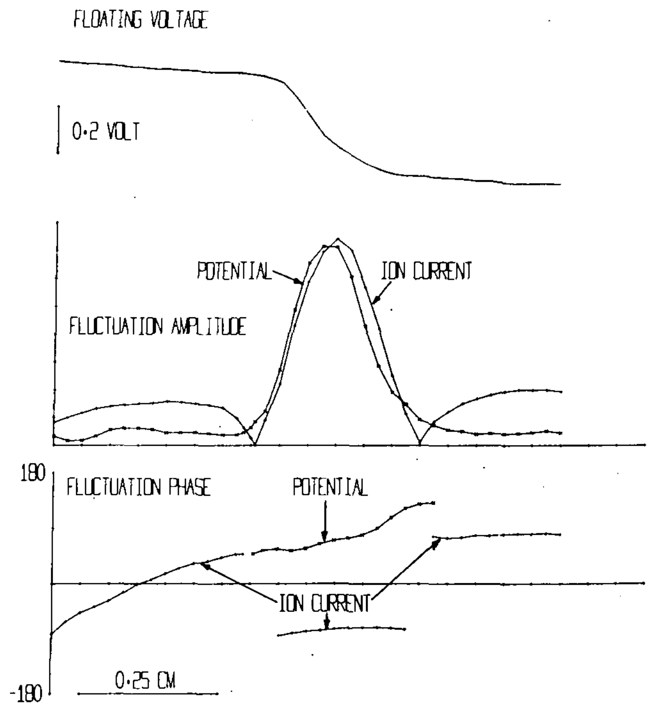

FIG. 2. Radial dependence of the analysed data for the "electric-field" mode. Top trace: floating voltage. Centre trace: fluctuation amplitude (arbitrary units). Both potential and ion current fluctuations are displayed. Bottom trace: fluctuation phase. Phases are plotted only when amplitude exceeds 0.6 division. Plasma parameters: caesium; B = 3.5 kG; $n = 4 \times 10^{10}$ cm^{-3}; applied voltage = -0.6 V; oscillation frequency = 4.3 kHz. The tube axis is off scale 1.5 cm from the right-hand side.

zero) shown in the current fluctuations occurs in almost all cases. That these are genuine nodes may be seen from Fig. 1, where the quadrature components of the fluctuating current are observed to cross at the zero line. The second relative minimum is usually not an exact zero. Between these two minima the amplitude varies rapidly with position, but the phase is roughly constant. Thus the wave is predominantly a standing wave in the radial direction. As mentioned earlier, these waves propagate in the aximuthal direction.

For the case in Fig. 2, the maximum fluctuation amplitude of the ion current is approximately 15% rms, while the maximum of the potential fluctuations is 80 mV rms. The phase shift between the potential fluctuations and density (i.e. ion current) fluctuations in the electric-field region is approximately 150°, with the potential fluctuations leading. That is, the density and potential fluctuations are out of phase. This suggests that the parallel wavelength is very long. We know that the parallel wavelength is much larger than the perpendicular wavelength, but we do not at present have careful measurements on its precise value.

The voltage threshold in this experiment was typically between 0.05 and 0.5 V, both for positive and negative applied voltage. The exact value varied from run to run. From experiments on electron cyclotron resonance heating [10] it is known that the threshold voltage increases with increasing electron temperature. Furthermore, the threshold voltage appears to be insensitive to density variations.

To summarize the features of the "electric field" mode; above a threshold voltage we observed coherent oscillations in both ion saturation current and floating potential. For a given azimuthal mode number, the frequency of these oscillations was proportional to the applied voltage. The oscillations were localized in a region of the plasma where there was a strong non-uniform electric field and a small density gradient. A standing wave was set up in the radial direction with a propagating wave in the $\vec{E} \times \vec{B}$ direction. Potential and density fluctuations were out of phase.

4. DENSITY-GRADIENT MODE

When the applied voltage was increased to comparatively high values (1 - 3 V), with the inner section of the plate positive, the density gradient in the centre part of the plasma column increased noticeably. Such a situation is shown in Fig. 3 for a caesium plasma at $n = 10^{10}$ cm^{-3} and $B = 3.5$ kG. Here, for an applied voltage of + 2.2 V, we find a region in the plasma with a density-gradient scale length of 0.7 cm and an electric field of approximately 0.1 V/cm. These values are typical for this mode. At the edge of this region, there is a large drop in potential. Observe that this situation is similar to the one found in a conventional Q-machine, where a drop in potential, of the opposite polarity, is associated with the edge of the plate.

Under these conditions, as shown in Fig. 3, we observed oscillations in the density-gradient region. The frequency of these oscillations (1-3 kHz) was not proportional to the applied voltage, but depended on the density gradients and electric fields in the region of the maximum oscillation amplitude. Unlike the "electric-field" mode, this mode had potential fluctuations that were approximately in phase with the density fluctuations. The fluctuation amplitudes for both density and potential were approximately 15% rms.

It should be noted that these oscillations also had a well-defined threshold voltage. In this case, increasing the applied voltage primarily increased the density gradient, while having only a small effect on the electric field found in the region of the oscillations. Furthermore, we observed this oscillation only when the density was decreasing outwards.

5. DISCUSSION

The observation that the "electric-field" mode has density and potential fluctuations out of phase strongly suggests that this is some form of flute instability, perhaps driven by the shear in azimuthal velocity. All our observations have been consistent with this hypothesis. The problem of the flute mode in a non-uniform electric field has been considered theoretically by Rosenbluth and Simon [1]. They conclude that the system is stable when some appropriate average electric-field drift velocity is less than the density-gradient drift. Although we have observed little change in the threshold condition in runs with greatly differing density gradients, we have never observed this mode when the density-gradient drift was greater than the electric-field drift. Therefore, our results are not in contradiction with their theory.

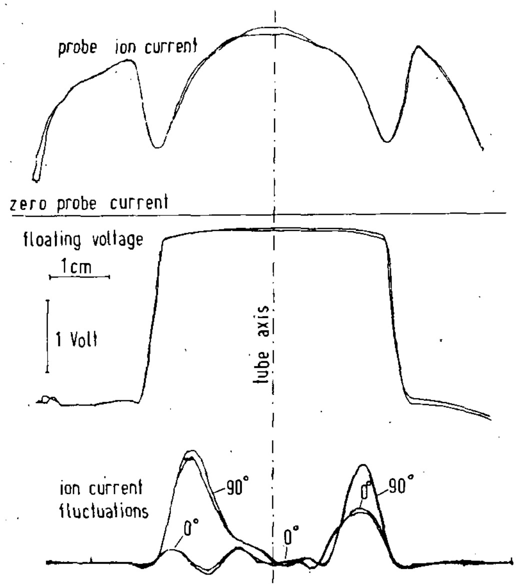

FIG. 3. Radial dependence of the "density-gradient" mode. Top trace: probe ion current (arbitrary units). Centre trace: floating voltage. Bottom trace: quadrature components of the ion current fluctuations (arbitrary units). Plasma parameters: caesium; B = 3.5 kG; $n = 10^{10}$ cm^{-3}; applied voltage = 2.2 V; oscillation frequency = 2.2 kHz.

The fact that the azimuthal phase velocity for this mode is less than the peak electric-field drift velocity is not surprising, for two reasons. First, the maximum amplitude of the oscillations is not located at the electric-field maximum, and second, the finite ion Larmor radius ($\sim$0.1 cm) should introduce an averaging out over the observed field. As for the threshold, in the experiment we measured a threshold voltage. Because of the non-uniformity of the electric field, it is difficult to say if there was a threshold electric field, or if, as has been suggested by certain theories [11], higher derivatives of the electric field were important.

In a recent experiment, Kent [2] identified the "edge" oscillations in a Q-machine as a flute instability driven by a shear in azimuthal velocity. Although the de-stabilizing mechanisms are similar, our experiment differs in that we were not looking at the edge of the column (a region of large temperature and density gradients as well as electric fields) but within the column, in a region of controllable electric field.

Let us now discuss the "density-gradient" mode described in section 4. It is clear from the data presented that this mode is quite different from the "electric-field" mode described above. The most important of these differences is that the density and potential oscillations are in phase, a fact which suggests some form of drift wave. While many authors have studied density-gradient drift waves (e.g. [4-6]), the most extensive observations on coherent oscillations with a peak amplitude not at the edge of the column have been reported by Hendel [3]. Our work differs in that we were operating with only one hot plate and at lower densities. At our densities ($n = 10^9$ - 10^{10} cm^{-3}), ion-ion collisions should not be as important as in the Hendel experiments.

There remain two unexplained features of our results. One is that we did not succeed in observing a coherent density-gradient mode when the density decreased towards the axis. The second, and more important, is that we observed a clear threshold that appeared to be related to increasing density gradient. It has been suggested by certain theoretical works [11] that, in a slab geometry, a linearly varying electric field can stabilize a drift wave if the density gradient is not too large. This may be the mechanism that determined our threshold.

CONCLUSION

The results that are reported in this paper indicate that both a non-uniform radial electric field and a radial density gradient can induce coherent, nearly sinusoidal oscillations in a magnetized plasma column.

ACKNOWLEDGEMENTS

The authors wish to thank Dr. A. Nocentini and Dr. M. Dobrowolny for helpful discussions, and Dr. G. Kent, Dr. F.F. Chen, and Dr. F. Sisto for making unpublished results available to us. The able assistance of Mr. W. Bozzolan and Mr. S. Viselli in operating the Q-machine is gratefully acknowledged.

REFERENCES

[1] ROSENBLUTH, M.N., SIMON, A., Physics Fluids 8 (1965) 1300.
[2] KENT, G., Thesis, City University of New York (1968).
[3] HENDEL, H.W., POLITZER, P.A., Proc. Conf. Physics of Quiescent Plasmas 1 (Frascati, 1967), 181.
[4] BUCHELNIKOVA, N.S., Nucl. Fusion 4 (1964) 165.
[5] LASHINSKY, H., Phys. Rev. Lett. 12 (1964) 121.
[6] LITTLE, P.F., BARRETT, P.S., Proc. Conf. Physics of Quiescent Plasmas 1 (Frascati, 1967) 173.
[7] RYNN, N., D'ANGELO, N., Rev. scient. Instrum. 31 (1960) 1326.
[8] ENRIQUES, L., GAROSI, F., NERI, A., Proc. Conf. Physics of Quiescent Plasmas 2 (Frascati, 1967) 627.
[9] ENRIQUES, L., LEVINE, A.M., RIGHETTI, G.B., Plasma Physics 10 (1968) 641.
[10] SISTO, F., Thesis, University of Rome (1968).
[11] NOCENTINI, A., private communication.

SUPRESSION OF DRIFT WAVE IN A CAESIUM PLASMA BY EXTERNALLY APPLIED ALTERNATING-CURRENT ELECTRIC FIELDS *

R. ITATANI AND T. OBIKI
DEPARTMENT OF ELECTRONICS, KYOTO UNIVERSITY, KYOTO
AND
N. TAKAHASHI
INSTITUTE OF PLASMA PHYSICS, NAGOYA UNIVERSITY, NAGOYA, JAPAN

Abstract

SUPPRESSION OF DRIFT WAVE IN A CAESIUM PLASMA BY EXTERNALLY APPLIED ALTERNATING-CURRENT ELECTRIC FIELDS. An experimental study of suppression of drift waves by superimposition of a.c. electric fields is reported. The experiment was carried out with a caesium plasma called TP-C machine at the Institute of Plasma Physics, Nagoya University. The plasma is about 1 m long and 2 cm in diameter. Plasma densities range from 1×10^8 to 3×10^{10} cm^{-3}, plasma temperatures from 2000 to 3000°K, and magnetic fields from 1.4 to 2.8 kG. A meshed grid, movable along the plasma column, divides the plasma into two regions; region I bounded by the ionizer plate and the grid, and region II by the grid and the end of the vacuum vessel. Movable Langmuir probes are equipped to measure plasma parameters and to pick up oscillations.

Oscillations, having a fine spectrum and regarded as drift waves, of fundamental frequencies of about 10 kHz are excited spontaneously under two operating conditions of the ionizer; one is a low-power operation that yields an ion-rich sheath at the ionizer plate and another is a high-power operation that forms a nearly neutral sheath (slighly electron-rich or not).

When an a.c. voltage of frequencies higher than those of the drift waves is applied to the grid and exceeds about a few tens of volts, the intensities of the waves decrease more than 20 db and their frequencies shift slightly with the increase in the applied voltage in both cases, and this suppression effect is more drastic in region II. In the case of the d.c. bias, according to the sheath condition, ion-rich or nearly neutral, the positive or negative bias of the grid is effective to stabilize the waves. The plasma length affects such stabilizations only in the case of the high-power operation. The stabilizing effect of the a.c. voltage is more efficient than that of the d.c. bias, although both the effects seem qualitatively equivalent. This surplus effect of the a.c. voltage for stabilizations may be due to the asynchronous quenching phenomenon as a result of non-linear interactions of the drift waves with the induced perturbations like the ion acoustic waves excited by the grid.

Drift waves in a caesium plasma are stabilized by placing a.c. electric fields parallel to magnetic fields through a meshed grid immersed in the plasma. This stabilization may be caused partly by a bias effect due to rectifying characteristics of a plasma sheath and partly by some non-linear processes due to couplings between drift waves and applied perturbations like ion acoustic waves.

Some coupling phenomena are also observed when the frequencies of the applied perturbations are close to those of the drift waves.

---

* This work was carried under the Collaborating Research Program at the Institute of Plasma Physics, Nagoya University, Nagoya.

INTRODUCTION

In this paper we describe some results that were obtained during experimental investigations of the interactions between spontaneously excited drift waves and externally applied a.c. electric fields in a weak inhomogeneous, fully ionized plasma column confined by a static magnetic field. The possibility of stabilizing the drift-waves by means of external a.c. fields is presented.

It has been reported that the drift wave [1] can be stabilized by virtue of the arrangement of magnetic-field configurations [2], boundary conditions of a plasma column [3], and the column length [4].

There have been theoretical works on the problem of stabilizing the drift wave by means of non-linear processes. Dupree [5] has shown the case where the drift wave could be suppressed by imposing high-frequency noise fields perpendicular to the magnetic fields; Fainberg and Shapiro [6], Amano [7], imposed high-frequency electric fields parallel to the magnetic fields; and Krall [8] has described the case of phase mixing. Thomassen [9] has conducted an experiment according to the reference [5], and observed the quenching of low-frequency noises in a sodium plasma.

We have applied low-frequency electric fields (the frequency was comparable to the drift-wave frequency, in contrast to the above-mentioned theories [5-7]), parallel to the magnetic field, and observed the couplings between drift waves and applied perturbations.

The experiment was carried out with a thermal caesium plasma device, called the TP-C machine at the Institute of Plasma Physics, Nagoya University.

EXPERIMENTAL APPARATUS

A schematic diagram of the experimental apparatus is shown in Fig. 1. The plasma was produced by the contact ionization of a collimated beam of caesium atoms on a hot tantalum plate heated at 1500-2300° K, which gives a plasma density of 1×10^8 - 3×10^{10} cm^{-3} at a background pressure of about 10^{-6} mm Hg or less. The plasma column was about 1 m long and 2 cm in diam. A uniform magnetic field of 1.4 - 2.8 kG was applied over the experimental region. A meshed grid was used throughout this work in order to introduce external fields into the plasma. The grid, fabricated with molybdenum wires of 0.2 mm diam. spaced 1.5 mm apart, and 4 cm in total diameter, was placed in the plasma with its plane normal to the magnetic field. A continuous sinusoidal signal from an external oscillator of 1-500 kHz and 0-40 V in peak-to-peak value was applied to the grid biased with a negative or a positive d.c. voltage (-40 V to + 40 V) with respect to the hot plate. The grid divides the plasma into two regions; region I, bounded by the grid and the hot plate, and region II by the grid and the end of the vacuum vessel. In region I, a radially movable plane Langmuir probe, P_I, and a probe P_{II} fixed to the grid and separated by 5.5 cm from the grid, were placed with their plane normal to the magnetic field. In region II, an axially movable probe, P_{III}, was placed so that the probe was on the edge of the plasma column where the density gradient might be regarded as largest. In each region the plasma parameters, such as the density, electron temperature, and the spectrum of the oscillations, were somewhat different. So the experiment was done in both regions.

EXPERIMENTAL RESULTS

In this machine some regular fluctuations were observed, which have fine spectra with several peaks and occur under two different operating conditions of the plasma source, a hot plate and a caesium boiler. One type of oscillation occurs at low temperatures of the hot plate (called low-power operation), and the other at a higher temperature (high-power operation). The former evidently corresponds to the ion-rich sheath condition at the hot plate and the latter seems to correspond to the nearly neutral sheath condition.

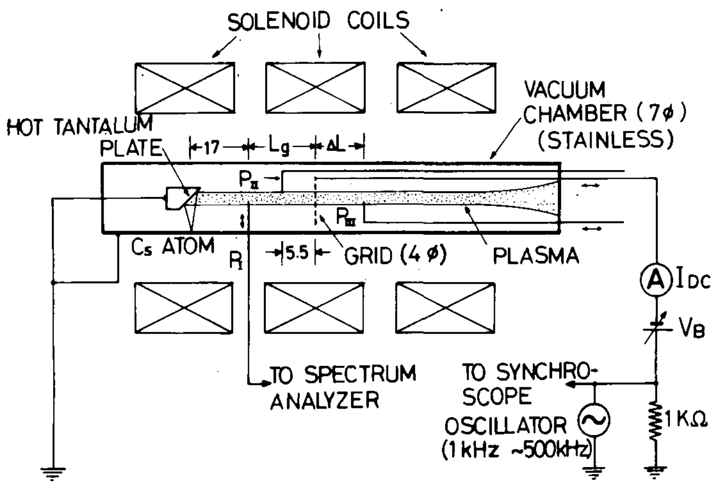

FIG. 1. Schematic diagram of the experimental device (TP-C machine). All dimensions are in centimetres.

The induced perturbations in the plasma by the a.c. voltage applied to the grid consist of ion acoustic waves (k = 0) and the impedance drop due to the electric current in the plasma (k = 0). The former is more intensive in region II and the latter in region I.

The plasma density and the density profile across the plasma column are hardly affected in region I, but appreciably so in region II by a grid bias and/or an applied a.c. voltage to the grid.

1. Waves under ion-rich condition

When the input power of the ionizer is 600 W or less, the plasma with a density of 3×10^8 cm^{-3} and a temperature of 2000°K is generated in the confining magnetic field of 1.4 - 2.1 kG. Low-frequency oscillations, having a spectrum of one or three peaks, are observed as shown in Fig. 2-a(A).

These waves, with an amplitude of 10-100 mV ($e\varphi/kT$ = 0.05 - 0.5), have a wave vector nearly perpendicular to the magnetic field, and are localized in regions where the density gradient is large.

The frequency of the oscillations is about 12 kHz, and approximately inversely proportional to the magnetic field strength. The drift-wave frequency, calculated from the theory taking into account the finite

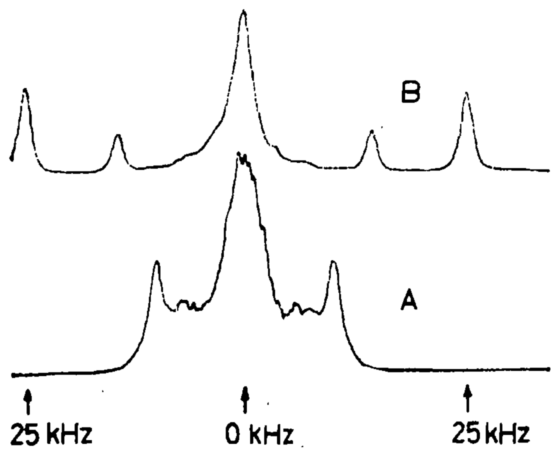

FIG. 2-a. (A) Spectrum of the drift wave at the low-power operation. N ~ 5×10^8 cm^{-3}, B = 1.44 kG, V_{ac} = 0 V, V_{dc} = -5 V. (B) Spectrum of the drift wave after the a.c. signal was applied; f_e = 25 kHz, V_{ac} = 34 V. The probe P_I was used.

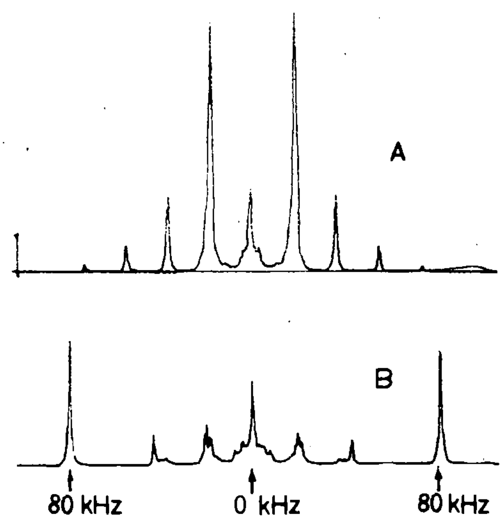

FIG. 2-b. (A) Spectrum of the low-frequency oscillation at the high-power operation: N ~ 3×10^{10} cm^{-3}, B = 2.1 kG, V_{dc} = -4.5 V. (B) Spectrum after the a.c. signal was applied; V_{ac} = 60 V, f_e = 80 kHz. The probe P_I was used.

Larmor radius [10], should be modified by the azimuthal plasma drift caused by the radial electric field existing in the plasma. Thus, the drift-wave frequency calculated with the measured parameters in the experiment becomes 11-15 kHz. This value almost agrees with the observed frequencies.

The amplitude of the waves decrease when a positive voltage is applied to the grid. This stabilizing effect of the positive d.c. bias is well known as a short-circuit of drift waves [3]. When the a.c. voltage is applied instead of d.c., the amplitude decreases are also observed in the same fashion as those of the d.c. voltage, as shown in Fig. 3-a. The stabilizing

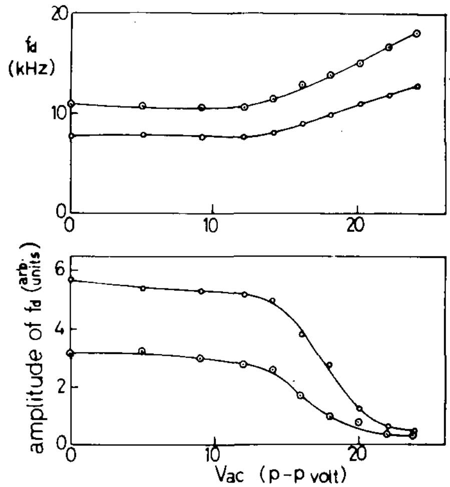

FIG. 3-a. Amplitude and frequency of the drift wave versus external a. c. signal amplitude. The probe P_I was used at the low-power operation: N ~ 10^8 cm^{-3}, B = 2.1 kG, V_{dc} = -5 V, f_e = 400 kHz. The blank point and the dotted point represent the first and the second peaks of the spectrum.

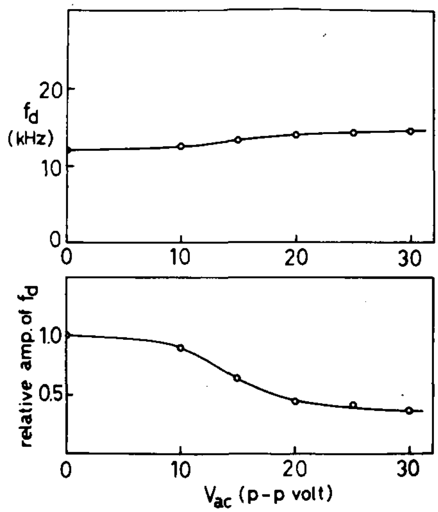

FIG. 3-b. Amplitude and frequency of the drift wave versus external a. c. signal intensity when keeping the d. c. grid current constant at I_{dc} = 20 μA. The grid bias voltage was gradually decreased with the increase of V_{ac}. The machine was under the low-power operation: B = 1.4 kG, N ~ 10^8 cm^{-3}, f_e = 25 kHz. P_I was used.

effect on drift waves does not depend upon the frequency of the applied perturbation, which are higher than that of the drift wave. As is well known, an a.c. voltage applied to the grid causes the electron current to increase because of rectifying characteristics of the sheath. This increase in the d.c. current may have the same effect with the d.c. bias to the waves. To check this, the amplitude of the waves to the same grid current are plotted to the applied a.c. voltage in Fig. 3-b. This means that the average conductivity of the sheath is kept constant. According to the increase of the a.c. voltage, the amplitude of the drift waves decreases in spite of the same d.c. current. This suggests that the applied a.c. voltage causes surplus suppression to the drift waves. The surplus effect of the a.c. voltage may be attributed to some non-linear properties of the plasma bulk, such as couplings between waves as shown below, or asynchronous quenchings found with respect to ion waves [11], because the non-linear properties of the sheath were taken into account by keeping the d.c. current of the grid constant.

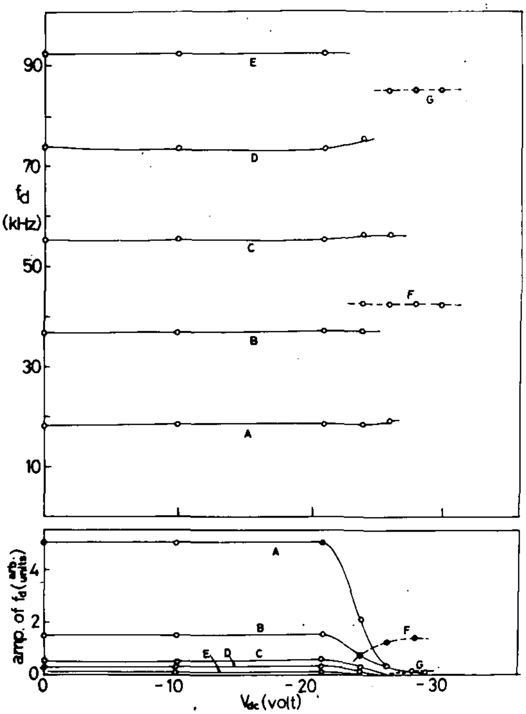

FIG. 4. Amplitude and frequency of the low-frequency oscillation versus d.c. bias voltage of the grid at the high-power operation; $N \sim 3 \times 10^{10}$ cm^{-3} , $B = 2.1$ kG. A, B, C, D, and E curves correspond to the order of the harmonics of the low-frequency oscillation; m = 1, 2, ..., 5, respectively. F and G curves correspond to the first and the second harmonics of the oscillation after the mode change took place.

This suppression effect of the a.c. voltage is insensitive to the plasma length ($L \cong 1$ m), and the negatively biased grid has no force to suppress the drift waves.

2. Waves under nearly neutral condition

When the input power of the ionizer is 1.0 - 1.2 kW, and the plasma with densities of 3×10^{10} cm^{-3} and temperatures of 2500°K is generated in the magnetic field of 2.0 - 2.8 kG, a very fine spectrum of low-frequency oscillations, shown in Fig. 2-b(A), is observed on the floating potential of the Langmuir probes, and the saturation ion and electron current towards the Langmuir probes.

These oscillations do not diminish when a positive bias is applied to the grid, but are stabilized when a negative bias is applied. The a.c. voltage applied to the grid is also effective in suppressing the oscillations. The stabilizing effects of the d.c. and a.c. voltages are compared in Figs 4 and 5. Similar to the above case, more effective suppressions are obtained by the a.c. voltage than by the d.c. In all cases, the amplitude reduction accompanies the frequency shift.

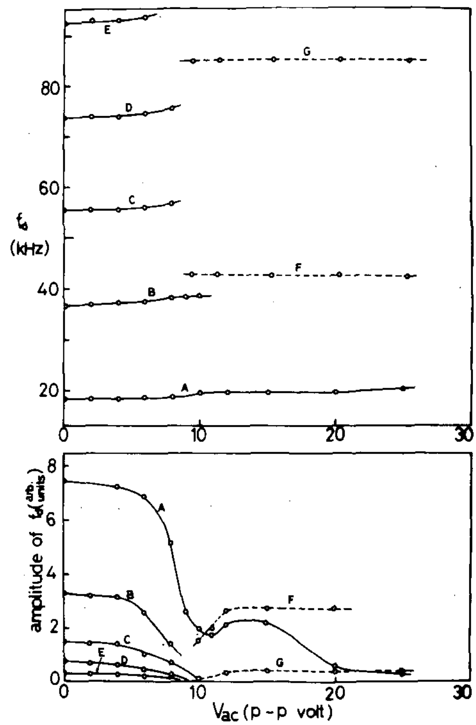

FIG. 5. Amplitude and frequency of the low-frequency oscillation versus a.c. signal amplitude. For the rest of legend see Fig. 4.

The plasma length, the distance between the ionizer plate and the grid, affects these suppressions as shown in Fig. 6. When the length is shorter than about 24 cm, the stabilization by the grid is very effective. Beyond this length, it becomes ineffective.

This oscillation which has frequency of about 17 kHz seems to be the drift wave, because of its intensity profile across the plasma column and the phase relation around the column. On the other hand, the frequency is not always inversely proportional to the magnetic field intensity. In addition, a sudden change of the mode of the oscillations is sometimes observed. This causes a decay of the existing oscillations and a generation of a new mode of oscillations. This is shown with dashed lines in Figs 4 and 5.

This behaviour of the oscillations suggests that the negative bias as well as the a.c. voltage work to shorten the axial wave-length of the drift waves. If so, the fact that the available length of the suppression is 24 cm fits the stability criterion of Lashinsky [4]. The effect of the negative bias is, however, inconsistent with the previous works [3], if the oscillations mentioned here are the drift waves.

3. Waves in region II

Under both operation conditions, the waves in region II are suppressed almost completely by the a.c. voltage, and this fact is independent of the plasma length between the grid and the cold end of the vacuum vessel. The plasma in region II is governed by the grid potential, because the plasma flows from region I to region II through the grid. The plasma density in region II decreases with a positive and a negative bias of the grid, and reaches maximum value almost at the floating potential of the grid. Then the application of the a.c. voltage causes density reduction of the plasma in region II. The rate of the damping of the wave is, however, far larger than that of the reduction of the plasma density.

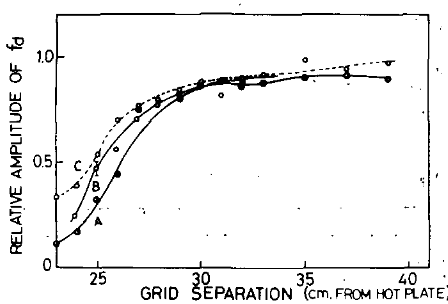

FIG. 6. Relations between the quenching effect on the low-frequency oscillation by the a.c. signal or the d.c. bias and the plasma column length. The machine was under the high-power operation; $N \sim 3 \times 10^{10}$ cm^{-3}, B = 2.1 kG. The curve A represents the case where V_{ac} = 64 V, f_e = 80 kHz was applied to the grid; the curve B represents V_{dc} = -15 V, V_{ac} = 0 V; the curve C represents V_{ac} = 23 V, which gives the d.c. grid current, I_{dc} = 50 μA. The probe P_I was used.

4. Coupling phenomena

When the applied signal frequency is close to the drift-wave frequency, the strong coupling between them is observed. The coupling between drift waves and ion acoustic waves, both excited spontaneously, has been reported by Ishii [12]. In our experiment, the combination frequencies $2f_d - f_e$ and $2|f_e - f_d|$, where f_d is the frequency of the drift wave and f_e that of the applied signal, are observed, whether $f_d > f_e$ or $f_d < f_e$.

When the intensity of the applied perturbation is nearly equal to that of the drift wave, and $|f_d - f_e|$ is reduced to zero, both signals disappear almost completely from the response of the spectrum analyser at one edge of the plasma column, intensified mutually at the other edge.

This phenomenon is attributed to the interference between the induced perturbation and a drift wave so that the phase of the drift wave is locked to that of the applied perturbation, and their plane of the polarization of the oscillation is so fixed to the vacuum vessel that both signals are cancelled out at the plasma edge where the surface length of the column along the axis is at a minimum. This fixing of the plane of the polarization seems to result from the asymmetry of the machine, which has the hot plate placed at an angle of 45° to the axis, and then the surface length is different around the column. These must be also due to the non-linear coupling between them.

SUMMARY

Low-frequency oscillations regarded as drift waves in a caesium plasma are stabilized by the a.c. voltage applied to the grid immersed in the plasma. This stabilization is caused partly by a bias effect of the grid owing to the rectifying characteristics of the sheath, and partly by some processes like non-linear couplings between instabilities and applied perturbations through the grid. This explanation seems true because coupling phenomena between drift waves and ion acoustic waves with wave vectors parallel to the magnetic field have been observed for certain.

ACKNOWLEDGEMENTS

We would like to thank Professor K. Takayama at the Institute of Plasma Physics, Nagoya University, for his continuous support; Professor Y. Otani, Electrical Engineering, Kyoto University, for his kind encouragement; and Dr. J. Dawson, Plasma Physics Laboratory, Princeton University, for his interesting suggestion and discussion. We wish also to express our appreciation to Dr. K. Nishikawa, Dr. T. Amano, and Dr. H. Momota, for valuable discussions and theoretical support, to Dr. H. Ikezi for valuable suggestions of measurements and arrangements of the experiment, and the members of TP-C Group for their support.

REFERENCES

[1] RUDAKOV, L.I., SAGDEEV, R.Z., DAN SSSR 138 (1961) 581 (translation: Soviet Phys. Doklady 6 (1961) 415); LASHINSKY, H., Phys. Rev. Lett. 12 (1964) 121.
[2] CHEN, F.F., MOSHER, D., Phys. Rev. Lett. 18 (1967) 639.
DECKER, J.A. Jr. et al., Physics Fluids 10 (1967) 2442.
[3] CHEN, F.F., J. nucl. Energy Pt. C7 (1965) 399; Physics Fluids 8 (1965) 752.
[4] LASHINSKY, H., Phys. Rev. Lett. 13 (1964) 47.
[5] DUPREE, T.H., Physics Fluids 10 (1967) 1049.
[6] FAINBERG, Ya.B., SHAPIRO, V.D., Zh. eksp. teor. Fiz. 52 (1967) 293 (translation: Soviet Phys. JETP 25 (1967) 189).
[7] AMANO, T., Private communication.
[8] KRALL, N.A., Phys. Rev. 158 (1967) 138.
[9] THOMASSEN, K.I., Phys. Lett. 26A (1967) 22.
[10] KADOMTSEV, B.B., "Drift Instability of a Plasma", Plasma Turbulence, Academic Press, London (1965) Ch. IV.
[11] OBIKI, T., ITATANI, R., OTANI, Y., Phys. Rev. Letters 20 (1968) 184.
[12] ISHII, S., J. Phys. Soc. Japan 23 (1967) 464.

ONDES ACOUSTIQUES IONIQUES DANS UN MAGNETOPLASMA ALCALIN

H. J. DOUCET ET D. GRESILLON
LABORATOIRE DE PHYSIQUE DES MILIEUX IONISES,
ECOLE POLYTECHNIQUE, PARIS, FRANCE

Abstract — Résumé

ION ACOUSTIC WAVES IN AN ALKALI MAGNETO-PLASMA. By a series of experiments on ion wave propagation in a magneto-plasma of caesium ionized by surface ionization, the authors studied the effects due to collisions between ions and neutral particles, the mean plasma velocity, the ratio $\theta = T_e/T_i$ of electron and ion temperatures and the non-linear behaviour of a collisionless plasma.

In a machine called OPS using direct injection of caesium illuminating one emitter the effect of collisions between neutrals and ions has been studied. The ratio $\theta = T_e/T_i$ of the electron and ion temperatures which is an important parameter for the propagation and damping of the ion waves can be easily modified by injection of helium into the machine. The variations of phase velocity and damping as functions of the frequency for different pressures of injected neutral gas show a change in the ion temperature, the mean plasma velocity and a continuous transition from the Landau damping to the collisionnal damping.

A separation of the two zones, the first one where the ions are cooled and the other where the wave is propagating, allows the study of the Landau damping and the measurement of the ratio θ.

A non-linear damping of the ion wave has been observed and studied. The classical Landau damping is found for the lower frequency range but as the distance of propagation is of the order of or larger than half a wavelength, the measured damping becomes less than the Landau damping rate, and amplitude modulation is observed. The pseudo-wavelength and the modulation rate are bound by the period and amplitude of the wave as is foreseen by a non-linear theory. We observed that the wave behaviour is similar to the effect obtained in mixing the ion wave and a fast wave which has been found in the experiments.

ONDES ACOUSTIQUES IONIQUES DANS UN MAGNETOPLASMA ALCALIN. Par une série d'expériences de propagation d'ondes ioniques dans un magnétoplasma de césium ionisé par contact, les auteurs ont étudié les effets qui sont liés aux collisions ions-neutres, à la vitesse moyenne du plasma, au rapport des températures électronique et ionique T_e/T_i et au caractère non linéaire d'un plasma sans collisions.

Dans une machine nommée OPS, fonctionnant en injection directe de césium sur un seul émetteur, l'effet des collisions ion-neutre a été étudié. Le rapport T_e/T_i des températures électroniques et ioniques, paramètre important pour la propagation et l'amortissement des ondes ioniques, peut être aisément modifié en injectant de l'hélium dans la machine. Les variations de la vitesse de phase et de l'amortissement en fonction de la fréquence pour différentes pressions de gaz neutre injecté montrent une modification de la température ionique et de la vitesse moyenne du plasma, et une transition continue de l'amortissement Landau à l'amortissement collisionnel.

Une séparation des zones de refroidissement des ions et de propagation de l'onde permet l'étude de l'amortissement Landau et la mesure du rapport T_e/T_i.

Un amortissement non linéaire de l'onde ionique a été observé et étudié. L'amortissement Landau classique est obtenu pour les basses fréquences mais dès que la distance de propagation est supérieure ou égale à une demi-longueur d'onde environ, l'amortissement obtenu devient inférieur à l'amortissement Landau et une oscillation de l'amplitude de l'onde est observée. La « pseudo-longueur» d'onde et l'amplitude de cette variation sont liées à la période et à l'amplitude de l'onde comme le prévoit une théorie non linéaire. On montre que l'effet produit est analogue à celui d'un mélange de l'onde ionique avec un mode rapide observé expérimentalement.

1. PROPAGATION D'ONDES IONIQUES DANS UN PLASMA DE CESIUM EN PRESENCE DE GAZ NEUTRE

Afin de vérifier de façon décisive l'amortissement sans collisions des ondes ioniques, il faut pouvoir mesurer et, si possible, modifier le rapport $\theta = T_e/T_i$ des températures électronique et ionique.

On peut espérer refroidir les ions par collisions ion-neutre [1], mais l'introduction d'un gaz neutre dans un plasma ionisé par contact modifie également d'autres grandeurs caractéristiques telles que la densité électronique et la vitesse moyenne du plasma. Il faudra donc tenir compte de ces variations et des autres types d'amortissement.

La mesure des températures électronique et ionique peut s'effectuer en utilisant un analyseur électrostatique à condition de s'affranchir des effets de recouvrement de césium qui perturbent gravement les mesures classiques de température électronique par sonde de Langmuir.

1.1. Amortissement collisionnel

Les collisions ion-neutre vont introduire, outre l'amortissement Landau, un amortissement collisionnel qui va rapidement devenir prépondérant.

Cet amortissement a été décrit [2] par un modèle fluide. On peut retrouver les résultats, très simplement, en utilisant les équations de continuité du nombre des particules et de la quantité de mouvement, écrites séparément pour les ions et pour les électrons, puis couplées par l'équation de Poisson. Les échanges de quantités de mouvement sont représentés par l'introduction de deux fréquences de collisions élastiques, ν_{en} et ν_{in}, des électrons et des ions avec les neutres.

L'équation de dispersion d'une onde de compression progressive dans l'espace de fréquence angulaire ω et de nombre d'onde k s'écrit [3] sous la forme générale suivante:

$$1 = \frac{\pi_e^2}{\omega^2 + i\nu_{en}\,\omega - k^2 V_e^2} + \frac{\pi_i^2}{\omega^2 + i\nu_{in}\,\omega - k^2 V_i^2}$$

π_e et π_i étant respectivement les fréquences plasma des électrons et des ions, V_e et V_i leurs vitesses thermiques. La vitesse de phase est alors:

$$v_\varphi = \frac{\omega}{\operatorname{Re} k} = \sqrt{2}\, V_s \left[1 + \left(1 + \frac{\nu_c^2}{\omega^2}\right)^{\frac{1}{2}}\right]^{-\frac{1}{2}}$$

et le taux d'amortissement:

$$\beta = \operatorname{Im} k = \frac{\omega}{\sqrt{2}\, V_s} \left[\left(1 + \frac{\nu_c^2}{\omega^2}\right)^{\frac{1}{2}} - 1\right]^{\frac{1}{2}}$$

expressions dans lesquelles ν_c et V_s, fréquence de collision et vitesse de phase classique des ondes ioniques, sont les moyennes pondérées par les masses des fréquences de collisions et des carrés des vitesses thermiques des électrons et des ions.

1.2. Vitesse moyenne du plasma – Effet Doppler

Un plasma de césium ionisé par contact sur un émetteur présente une vitesse moyenne v_p qui est de l'ordre de grandeur de la vitesse thermique des ions, vitesse non négligeable devant la vitesse de phase des ondes ioniques. Il en résulte un effet Doppler important.

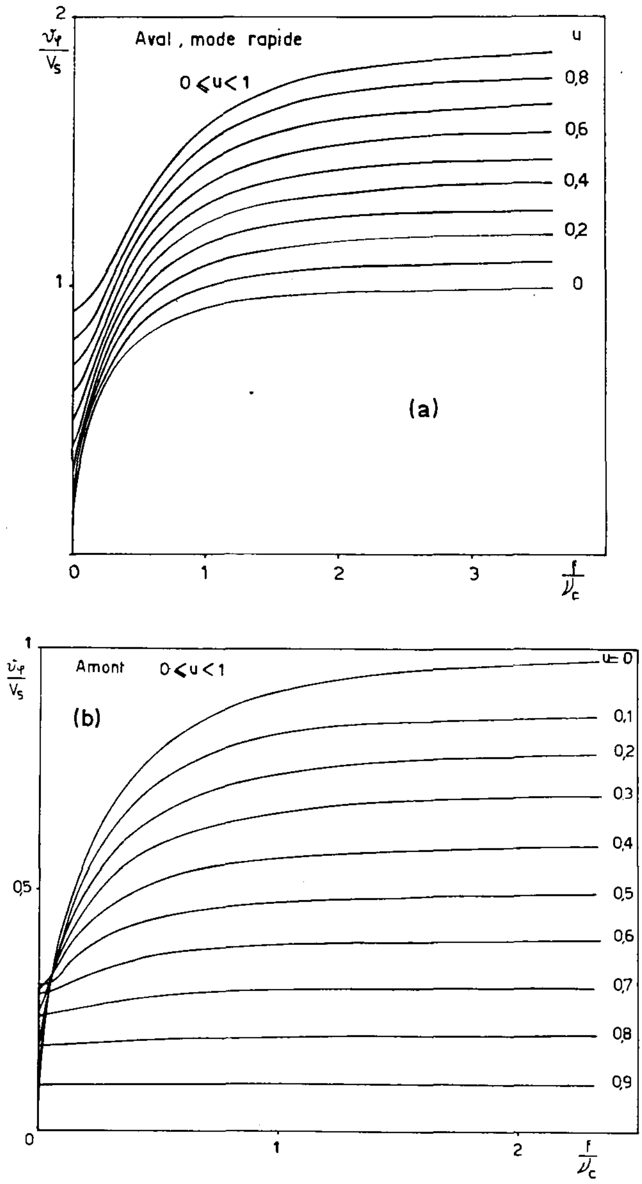

FIG. 1. Variations de la vitesse de phase réduite v_φ/V_s en fonction de la fréquence réduite f/ν_c pour différentes valeurs de la vitesse moyenne réduite du plasma $u = v_p/V_s$; a) onde aval, b) onde amont.

En supposant une vitesse moyenne des électrons égale à celle des ions et sans champ électrique statique, les grandeurs d'ordre 0 (densités, vitesses moyennes, etc.) sont des fonctions d'espace en raison des collisions. On suppose les variations assez faibles pour ne pas tenir compte des gradients de densité et des divergences des vitesses moyennes.

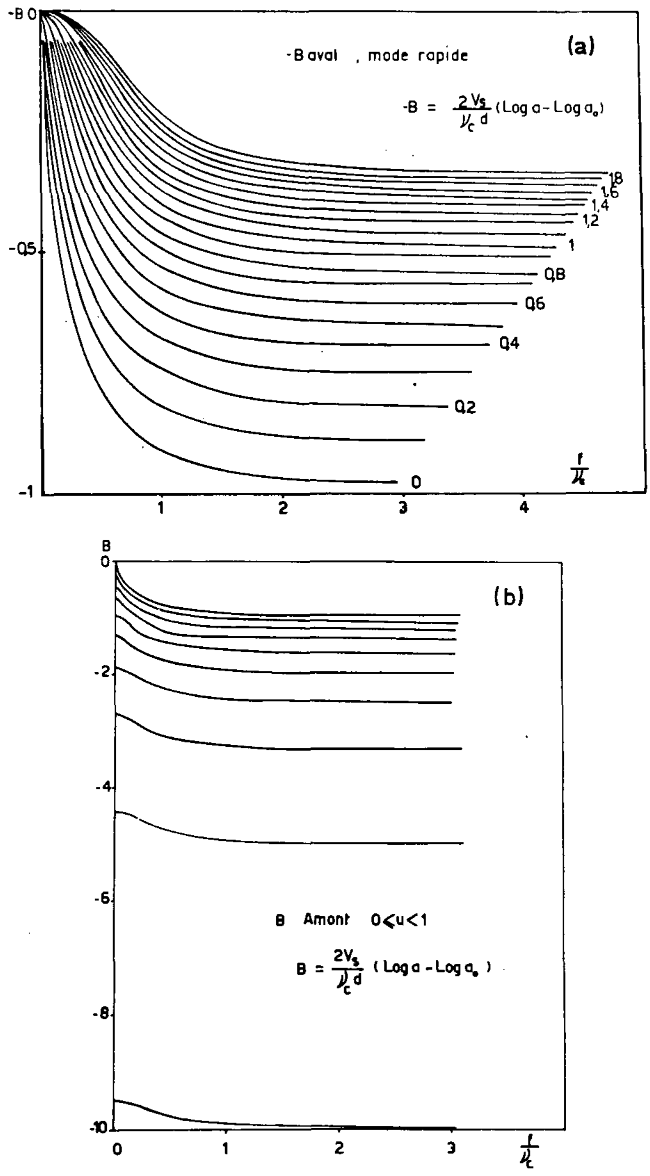

FIG. 2. Variations du coefficient d'amortissement B en fonction de la fréquence réduite f/ν_c pour différentes valeurs de la vitesse moyenne réduite du plasma $u = v_p/V_s$; a) onde aval, b) onde amont.

La relation générale de dispersion [3] s'écrit alors:

$$1 = \frac{\pi_i^2}{g_i} + \frac{\pi_e^2}{g_e} \quad \text{avec:}$$

$$g_e = (\omega_2 - kv_p)^2 + i\,\nu_{en}(\omega_2 - kv_p) - k^2 V_e^2$$

$$g_i = (\omega_2 - kv_p)^2 + i\,\nu_{in}(\omega_2 - kv_p) - k^2 V_i^2$$

L'onde se propageant dans le plasma n'a plus la fréquence réelle injectée ω_2, mais la fréquence complexe $\omega_1 = \omega_2 - kv_p = \Omega - i\beta v_p$ où le nombre d'onde $k = \alpha + i\beta$.

La résolution en basse fréquence suivant le procédé décrit dans [3] conduit avec les variables réduites:

- fréquence réduite $y = \Omega/\nu_c$,
- vitesse de phase réduite $x = v_\varphi/V_s$,
- vitesse moyenne réduite $u = v_p/V_s$

à l'équation de dispersion:

$$y^2 = \frac{x(x-u)[(u^2+1)x - u(u^2-1)]}{4(1+u-x)(1-u+x)[ux-(u^2-1)]^2}$$

et au taux d'amortissement:

$$\beta = \frac{\nu_c B}{2\,V_s} \quad \text{avec:} \quad B = \frac{x-u}{u(x-u)+1}$$

Les variations de la vitesse de phase réduite et du terme d'amortissement B en fonction de la fréquence sont présentées aux figures 1 et 2 pour les ondes aval et amont pour différentes valeurs de la vitesse moyenne du plasma.

1.3. Résultats expérimentaux

Le plasma utilisé est celui de la machine OPS essentiellement constituée d'un émetteur en tantale chauffé par bombardement électronique sur lequel on injecte du césium à l'aide d'un tube relié à un réservoir à température contrôlée, situé à l'extérieur de la machine. Un cylindre de plasma de 3 cm de diamètre est confiné par un champ magnétique maximal de 2, 3 kG. La plasma est limité à une longueur maximale de 80 cm par une plaque froide.

Deux grilles constituées par des fils de cuivre de 60 μm de diamètre espacées de 1 mm sont placées perpendiculairement au champ magnétique et séparées par une distance variable de 2 à 40 cm.

Les courbes de dispersion et d'amortissement obtenues sont présentées dans les figures 3 et 4, pour une distance de propagation d = 10 cm et pour quatre valeurs de la pression: $P_1 = 5 \times 10^{-6}$ torr de gaz résiduels, $P_2 = 2 \times 10^{-3}$ torr, $P_3 = 5 \times 10^{-3}$ torr et $P_4 = 6,5 \times 10^{-3}$ torr d'hélium.

De ces courbes de dispersion et d'amortissement on peut déduire pour chaque valeur de la pression:

- la vitesse moyenne du plasma;
- la vitesse de phase des ondes ioniques et par suite la température des ions;
- la fréquence de collision ion-neutre.

Les éléments dont l'interprétation est la plus simple sont les parties asymptotiques dans lesquelles les fréquences de collision n'interviennent pas. Cette partie asymptotique des courbes n'est obtenue que pour les vitesses de phase aval, ce qui détermine $a = V_s(1+u)$.

Si on admet que l'excitation des grilles est aussi efficace pour une onde amont que pour une onde aval, on peut terminer le calcul en utilisant la limite basse fréquence du rapport des amplitudes des ondes aval et amont.

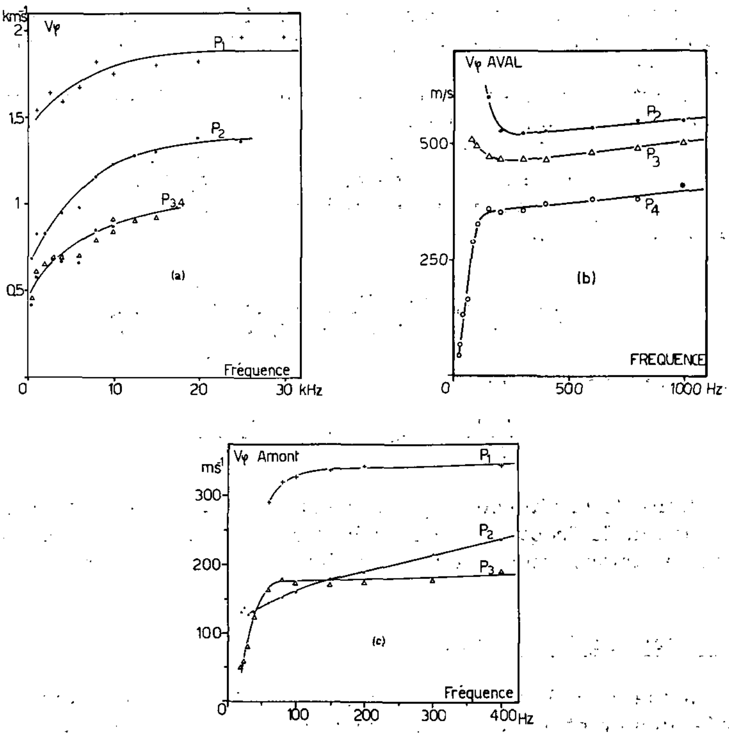

FIG. 3. Vitesse de phase mesurée en fonction de la fréquence pour différentes valeurs de la pression d'hélium; a) onde aval, b) onde aval en très basse fréquence, c) onde amont.

Cette hypothèse n'est pas très justifiée car nous avons observé que la grille fonctionne comme une valve, si bien que l'excitation aval est plus efficace que l'excitation amont. Si η est le rapport des pentes des caractéristiques de la densité entre grilles en fonction de leurs tensions de polarisation, le logarithme b du rapport des limites basse fréquence des amplitudes de l'onde pour les modes aval et amont devient:

$$b = \frac{1}{1-\omega^2}\frac{\nu_c d}{V_s} + \log \eta$$

Les mesures de a, b et η, connaissant d, et l'estimation de ν_c permet de calculer V_s et v_p pour chaque valeur de la pression.

Le tableau I présente les valeurs obtenues, le calcul de la température ionique étant fait à l'aide du rapport θ des températures électronique et ionique, en supposant que le coefficient de compression des ions est $\gamma_i = 3$ et en admettant la valeur limite $\eta = 1$.

La courbe 5 montre les valeurs de la température ionique mesurée en fonction de la pression à l'aide d'un analyseur électrostatique. Les points marqués par un cercle figurant les valeurs obtenues par mesure de propagation d'onde en supposant $T_e = T_i = T_{émetteur}$ pour le vide limite. La courbe en trait plein correspond à une section efficace de collision Cs^+- He de $\sigma_{in} = 6,7 \times 10^{-15}$ cm^2.

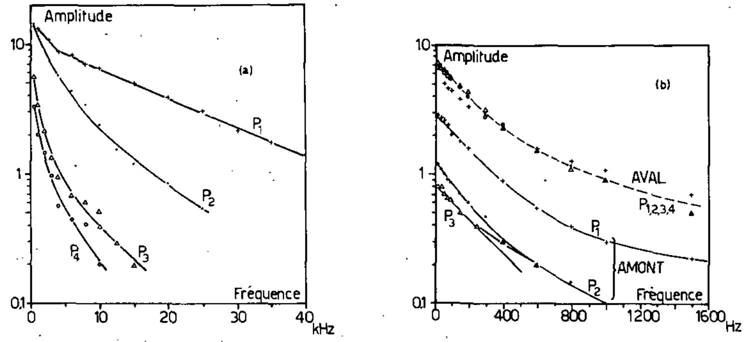

FIG. 4. Amplitude de l'onde détectée en fonction de la fréquence pour différentes valeurs de la pression d'hélium; a) onde aval, b) onde amont et aval en très basse fréquence.

TABLEAU I. VALEURS DE LA VITESSE DE PHASE, DE LA VITESSE MOYENNE DU PLASMA ET DE LA TEMPERATURE DES IONS DEDUITES DES FIGURES 3 ET 4

P hélium (torr)	ν_c (kHz)	a (m/s)	V_s (m/s)	v_p (m/s)	$1/\theta = T_i/T_e$	T_i (°K)
$5\cdot10^{-6}$	0,5	1820	922	896	1	2200
$2\cdot10^{-3}$	14	1350	830	529	0,75	1640
$5\cdot10^{-3}$	35	880	649	232	0,33	720

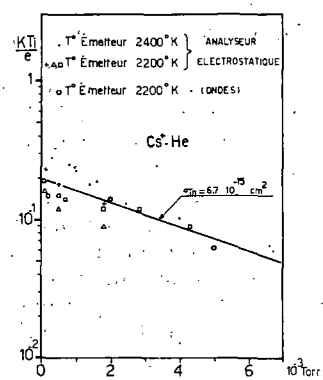

FIG. 5. Température des ions en fonction de la pression d'hélium. Les cercles indiquent les valeurs obtenues à partir des expériences de propagations d'onde ionique.

Dans ces conditions, en utilisant un résultat classique de la théorie cinétique [4], pour $T_e = T_i = T_{\text{émetteur}}$, la vitesse de phase devient:

$$v_\varphi = A\left(1,45 + \frac{v_p}{A} + \frac{0,36}{1,45 + v_p/A}\right)$$

où $A = (2\ KT/m_i)^{\frac{1}{2}}$ qui, pour $T = 1930°K$ et $v_p = 896$ m/s, donne $v_\varphi = 1730$ m/s pour 1820 m/s mesuré.

En conclusion, l'introduction d'un gaz neutre dans une machine à plasma de césium:

- modifie la vitesse moyenne du plasma;
- introduit un amortissement collisionnel qui devient rapidement un amortissement supérieur à l'amortissement Landau;
- refroidit les ions par collisions ions-neutres.

La vitesse moyenne du plasma, la vitesse de phase et l'amortissement des ondes ioniques sont en accord raisonnable avec la théorie macroscopique présentée ci-dessus.

Par contre, en très basse fréquence (fig. 3b) la vitesse de phase du mode aval présente une augmentation nette et reproductible qui n'est pas expliquée par le modèle théorique simple utilisé.

2. MESURE DES TEMPERATURES ELECTRONIQUE ET IONIQUE – AMORTISSEMENT LANDAU

L'introduction d'un gaz neutre dans un plasma de césium permet de refroidir les ions. Cependant, l'étude de l'amortissement Landau n'est possible que si l'amortissement collisionnel est très faible. Pour obtenir ces conditions, nous avons séparé la région de refroidissement dans la machine de la zone de propagation à l'aide d'un pompage différentiel assurant une décade de différence de pression entre ces deux zones.

D'autre part, pour éviter de tenir compte de la vitesse moyenne du plasma, nous utilisons une densité assez importante de l'ordre de 10^9 p/cm^3 devant l'émetteur dont la température est maintenue assez faible (2100°K).

Dans ces conditions, la gaine électronique accélératrice des ions est faible et on peut négliger la vitesse moyenne du plasma devant la vitesse de phase des ondes.

Pour mesurer les températures ionique et électronique, nous avons mis au point un analyseur électrostatique dont la grille d'analyse est formée d'une plaque de cuivre percée de trous de 10 μm de diamètre distants de 50 μm. Le collecteur est polarisé de façon à analyser successivement les fonctions de distribution des ions et des électrons. L'ensemble est placé dans un four chauffé à 400°C, température nécessaire pour éviter un effet de recouvrement de césium sur la grille d'analyse qui apporterait une erreur importante sur la mesure de température électronique.

L'équation de dispersion classique [5] des ondes ioniques obtenues à partir des équations de Vlasov appliquées aux ions et aux électrons, équations couplées par l'équation de Poisson, est:

$$Z'\left(\theta^{-\frac{1}{2}}\sqrt{\frac{m_e}{m_i}}\,\xi\right) + \theta\, Z'(\xi) = \frac{k^2}{k_D^2}$$

où ξ est la vitesse complexe : $\xi = \omega/kA$, $Z_2(\xi)$ est la fonction de dispersion plasma [6] et $k_D^2 = (\pi_i^2/A^2)(1/\theta)$.

La figure 6 montre les variations de la vitesse de phase et de la distance d'amortissement δ, distance au bout de laquelle l'amplitude de l'onde est réduite d'un facteur e, en fonction du rapport θ des températures électronique et ionique.

Pour une pression de l'ordre de 10^{-5} torr, on obtient par exemple une température électronique correspondant à KT_e = 0, 19 eV et une température ionique à KT_i = 0, 31 eV, mesurées par l'analyseur

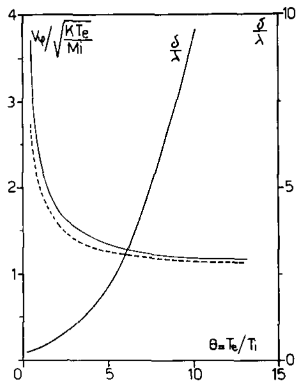

FIG. 6. Variations de la vitesse de phase et de l'amortissement en fonction du rapport des températures électronique et ionique (théorie cinétique).

électrostatique. La théorie ci-dessus fournit dans ces conditions δ/λ = 0, 29 et une vitesse de phase de 1, 17 km/s, alors que la courbe d'amortissement conduit à une valeur expérimentale δ/λ = 0, 30 et une vitesse de phase variant de 1 km/s à 1, 4 km/s entre 8 kHz et 15 kHz. Cette variation de vitesse peut être due en partie aux collisions sur les neutres qui, malgré le pompage différentiel, ne sont pas complètement éliminées.

En conclusion, les mesures de températures électronique et ionique par analyseur électrostatique, bien que peu précises et facilement faussées par des effets de recouvrement de césium, permettent de confirmer les valeurs de l'amortissement sans collisions données par la théorie cinétique.

Une étude systématique en fonction du rapport θ est difficile, car l'amortissement collisionnel devient très vite prépondérant à basse fréquence. A fréquence plus élevée, on quitte rapidement le régime d'amortissement linéaire. Cependant une variation du taux d'amortissement pour des valeurs de θ variant de 1 à 3 a été observée entre 5 et 20 kHz en refroidissant des ions potassium et césium avec de l'argon [7].

3. AMORTISSEMENT NON LINEAIRE

L'amortissement Landau, basé sur une théorie linéaire, suppose que la fonction de distribution des ions n'est pas notablement modifiée par l'onde ionique.

Un amortissement non linéaire de l'onde de compression électronique a été observé [8] et décrit à l'aide d'une théorie quasi linéaire [9] et de calculs numériques sur machine [10]. Dans tous les cas, on trouve, pour une onde de grande amplitude, une modulation oscillante de l'amplitude de l'onde et un amortissement plus faible que l'amortissement linéaire.

Un amortissement d'apparence analogue a été observé sur les ondes ioniques de grande amplitude [11] et [12]. Les figures 7 et 8 présentent un exemple de variations de l'amplitude du signal détecté en fonction de la distance pour plusieurs valeurs de l'amplitude et de la fréquence du signal d'excitation.

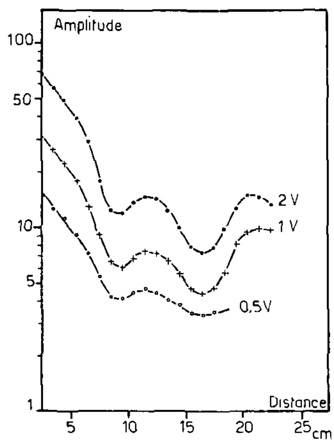

FIG. 7. Variations de l'amplitude du signal détecté en fonction de la distance pour différentes valeurs de l'amplitude crête-crête de la tension appliquée pour une fréquence de 30 kHz.

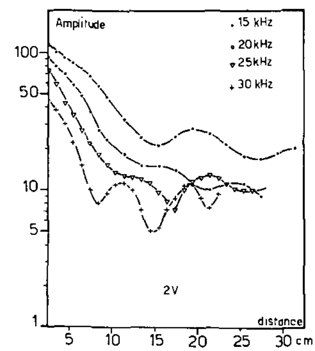

FIG. 8. Variations de l'amplitude du signal détecté en fonction de la distance pour différentes valeurs de la fréquence avec une tension appliquée crête-crête de 2 V.

De même que pour l'onde électronique, on observe une modulation oscillante de l'amplitude du signal détecté. La «pseudo-longueur» d'onde est bien proportionnelle à l'inverse de la fréquence et l'amplitude de la modulation à la racine carrée de l'amplitude du signal d'excitation. Dans le cas de nos expériences, l'amplitude moyenne ne decroît que très lentement avec la distance, ainsi que le prévoit la théorie non linéaire, par opposition avec les expériences présentées dans la référence 12.

La théorie non linéaire de l'amortissement sans collisions des ondes ioniques pourrait donc sembler expliquer la plupart des résultats expérimentaux. Cependant, quelques points restent obscurs:

1. Dans une théorie non linéaire, la position du premier minimum, ou la distance à laquelle l'amortissement s'écarte des valeurs prévues par la théorie de Landau pour les faibles amplitudes, est caractéristique du temps de relaxation des particules résonantes dans le puits de potentiel de l'onde. Ce temps [9]

$$\tau = \sqrt{\frac{m}{eEk}}$$

doit donc être proportionnel à l'inverse de la racine carrée du potentiel appliqué. Cette dépendance est assez bien observée pour les ondes électroniques [8]. Par contre, la figure 7 montre que la position du premier minimum pour l'onde ionique est indépendante de l'amplitude du signal appliqué.

2. L'oscillation d'amplitude semble dépendre de la densité du plasma entre les grilles. Une suppression des effets non linéaires peut être attendue lorsque la densité est suffisante pour que les collisions ion-ion maintiennent, malgré l'amortissement Landau, une fonction de distribution maxwellienne pour les ions. Or, l'effet de densité s'observe à des densités beaucoup plus basses : en effet, pour que les collisions ion-ion interviennent, il faudrait une fréquence de collisions ion-ion de l'ordre de 10 kHz au moins, ce qui conduit, pour une température de 2200°K, à une densité supérieure à $2 \cdot 10^{10}$ p/cm^3, et dans toutes nos expériences de propagation la densité est toujours restée bien inférieure à 10^9 p/cm .

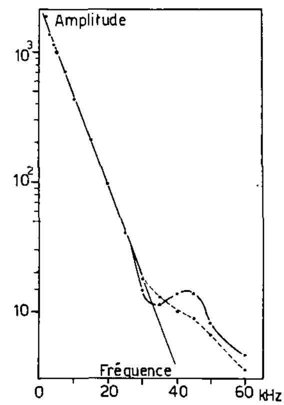

FIG. 9. Variation de l'amplitude du signal détecté en fonction de la fréquence. La courbe en trait plein représente l'amplitude du signal mélangé (onde entretenue); la courbe en pointillé représente l'amplitude du signal ionique seul.

Une autre explication partielle possible de la nature oscillante de l'onde peut être proposée. Nous avons observé [3] au-dessus de la fréquence plasma des ions l'existence de deux modes simultanés ayant des vitesses de phase différentes:

- l'onde ionique, dont la vitesse de phase augmente légèrement avec la fréquence au-dessus de la fréquence plasma des ions;
- une onde rapide, dont la vitesse est de 5 à 10 fois supérieure à celle de l'onde ionique.

Ces deux signaux se composent pour donner une nature oscillante de l'amplitude de l'onde qui explique l'indépendance du premier minimum avec l'amplitude du signal d'excitation et la proportionnalité de la «pseudo-longueur» d'onde avec l'inverse de la fréquence de l'onde.

La figure 9 montre, en fonction de la fréquence, les variations expérimentales de l'amplitude des signaux pulsés détectés à l'aide d'un Princeton Applied Research Waveform Eductor.

La courbe en trait plein montre les variations du signal entretenu et la courbe en pointillé les variations du signal ionique pulsé seul qui présente donc encore ici un écart notable par rapport aux valeurs prévues par l'amortissement linéaire de Landau. Cette variation d'amplitude est conforme aux résultats d'un calcul numérique effectué par Armstrong [14] pour l'amortissement non linéaire d'une onde ionique à partir d'un modèle utilisant une équation de Vlasov pour la fonction de distribution des ions et un modèle fluide pour les électrons.

En conclusion, l'amortissement des signaux détectés en fonction de la distance ou de la fréquence produit un effet assez semblable à celui de l'amortissement sans collisions des ondes électroniques de grande amplitude. Une autre interprétation est possible car une propagation au-dessus de la fréquence plasma des ions peut produire, par mélange d'ondes de vitesses différentes, en effet très analogue.

REMERCIEMENTS

Nous exprimons nos remerciements aux Dr I. Alexeff, T.P. Armstrong et Nguyen Quang Dong pour de fructueuses discussions des effets non linéaires, au Dr Haug pour nous avoir signalé la possibilité de mesurer la température ionique par analyseur électrostatique, et à M. Rouillé pour son intelligente et active participation aux expériences.

Ce travail a pu être réalisé grâce au concours financier de l'Ecole polytechnique, de la DRME et de l'Euratom.

REFERENCES

[1] BLAU, F.P., GUILINO, E., HASHINI, M., D'ANGELO, N., First European Conf. Controlled Fusion and Plasma Physics, Munich (1966) CONF.66 1041; Physics of Quiescent Plasmas (Proc. Conf. Frascati, 1967) 1, (1967) 79.

[2] HATTA, Y., SATO, N., in Phenomena in Ionized Gases (Proc. 5th Int. Conf., Munich, 1961) 1 (1962) 478; ALEXEFF, I., JONES, W.D., Therm. Div. semiann. Prog. Rep., ORNL 3652 (1964) 56.

[3] DOUCET, H., JONES, W.D., C.r. hebd. Séanc. Acad. Sci., Paris 260 (1965) 3577-79.

[4] WONG, A.Y., MOTLEY, R.W., D'ANGELO, N., Phys. Rev. 133 A (1964) 436-42.

[5] FRIED, B.D., GOULD, R.W., Physics Fluids 4 (1961) 139-47.

[6] FRIED, B.D., CONTE, S.D., The Plasma Dispersion Function, Academic Press, New York (1961).

[7] ANDERSEN, H.K., D'ANGELO, N., JENSEN, V.O., MICHELSEN, P., NIELSEN, P., Effects of ion-atom collisions on the propagation and damping of ion-acoustic waves (à paraître).

[8] MALMBERG, J.H., WHARTON, C.B., Phys. Rev. Lett. 19 (1967) 775-78.

[9] O'NEIL, T., Physics Fluids 8 (1965) 2255-62; AL'TSHUL, L.M., KARPMAN, V.J., Zh. éksp. teor. Fiz. 49 (1965) 515-28; Soviet Phys. JETP 22 (1966) 361-74.

[10] GARY, S.P., Physics Fluids 10 (1967) 570-81; ARMSTRONG, T.P., Physics Fluids 10 (1967) 1269-80.

[11] DOUCET, H.J., GRESILLON, D., Phys. Lett. 25 A (1967) 697-98.

[12] SATO, N., IKEZI, H., YAMASHITA, Y., TAKAHASHI, N., Phys. Lett. 26 A (1968) 437-38; Phys. Rev. Lett. 20 (1968) 837-39.

[13] DOUCET, H., GRESILLON, D., Propagation d'ondes ioniques au voisinage de la fréquence plasma des ions, Rapp. PMI-374 (juin 1968).

[14] ARMSTRONG, T.P., Communication privée, mai 1968.

DISCUSSION

S.J. BUCHSBAUM: When helium is introduced into a Q-machine, is the resulting drop in ion temperature uniform along the axis?

H.J. DOUCET: In our experiment the cooling and propagation zones are separated. In the propagation zone, cooling of the ions by collision is negligible and the ion temperature is a constant.

NON-LINEAR DRIFT WAVES IN A PLASMA WITH A TEMPERATURE GRADIENT *

V. N. ORAEVSKY**, H. TASSO AND H. WOBIG
INSTITUT FÜR PLASMAPHYSIK, GARCHING, MUNICH,
FEDERAL REPUBLIC OF GERMANY

Abstract

NON-LINEAR DRIFT WAVES IN A PLASMA WITH A TEMPERATURE GRADIENT. In a low-β plasma slab we consider stationary drift waves with an electrostatic potential of the type $\varphi(y-ut, x, z)$, where x is the co-ordinate in the direction of the equilibrium gradients, and z is the co-ordinate along the magnetic field. We assume the x-dependence of the varying quantities to be small, the ion temperature to be much smaller than the electron temperature, and make use of the two-fluid theory neglecting the dissipative effects. We take into account the electron temperature gradient as was done previously, but add the dispersive effects due to the ion inertia perpendicular to $\vec{B}$. The final equation is similar to the Korteweg-de Vries equation. It has as solutions a general non-linear wave, a solitary wave and an exact sinus wave. The two last solutions are due to the temperature gradient.

In the dissipative case, resistivity alone does not allow periodic solutions if solutions of the type $\varphi(y-ut + \alpha z)$ are considered. The x-dependence of potential and density fluctuations seems to be essential for the calculation of the diffusion averaged over one period of oscillation.

In a small-β plasma slab we examined stationary drift waves with an electrostatic potential of the type $\varphi(y-ut, x, z)$, where x is the co-ordinate in the direction of the equilibrium gradients, and Z is the co-ordinate along the magnetic field. We assumed the x-dependence of the varying quantities to be small – in fact in this case it does not essentially change the results – the ion temperature T_i to be much smaller than the electron temperature T_e, and we made use of the two-fluid theory, neglecting the dissipative effects. We took into account the electron temperature gradient as done previously [1], but we added the dispersive effects coming from the ion inertia perpendicular to $\vec{B}$.

Our basic equations are:

$$\frac{\partial n_e}{\partial t} + \frac{\vec{E} \times \vec{B}}{B^2} \cdot \nabla n_e + \frac{\partial}{\partial z} n_e v_{ze} = 0 \tag{1}$$

$$\frac{\partial n_i}{\partial t} + \frac{\vec{E} \times \vec{B}}{B^2} \cdot \nabla n_i + \operatorname{div} n_i \vec{v}_{i1} = 0 \tag{2}$$

$$\operatorname{div} n_i v_{i1} = \frac{M_i}{e B^2} \frac{\partial}{\partial y} n_i \frac{\partial^2 \varphi}{\partial t \partial y} \tag{3}$$

* This work was performed under the terms of the agreement on association between the Institut für Plasmaphysik and Euratom.

** On leave from the Institute of Physics of the Academy of Sciences of the Ukrainian SSR, Kiev, USSR.

which is the inertial correction to the perpendicular motion of the ions.

$$n_i = n_e \tag{4}$$

and

$$n_e = n_0(x)e^{-\frac{e\varphi}{kT_e(x)}} \tag{5}$$

which comes from the motion of the electrons along $\vec{B}$, neglecting their inertia and other resonance effects.

These equations are valid in the usual domain,

$$k_{\parallel} v_{thi} < \omega < k_{\parallel} v_{the}$$

Let us now find solutions of the type $\varphi(y-ut, x, z)$ and substitute φ in Eq.(2) for n_i and div $n_i\vec{v}_{i1}$ using Eqs (3), (4), (5). We then get the following equation:

$$\frac{uen_0}{kT}\frac{\partial\varphi}{\partial y} + \frac{1}{B}\frac{\partial\varphi}{\partial y}\left(n_0' - \frac{en_0}{kT}\frac{T_e'}{T}\varphi\right) - \frac{Mun_0}{eB^2}\left(\frac{\partial^3\varphi}{\partial y^3} - \frac{e}{kT_e}\frac{\partial\varphi}{\partial y}\frac{\partial^2\varphi}{\partial y^2}\right) = 0 \tag{6}$$

The first two terms have already been found in Ref. [1], where the temperature gradient gives a Burgers-type term. The third term is a dispersive one analogous to the case of the Korteweg-de Vries equation, and is due to the inertia of the ions perpendicular to $\vec{B}$. Equation (6) can be written formally:

$$\frac{\partial\varphi}{\partial y}(a + b\varphi) = c\left(\frac{\partial^3\varphi}{\partial y^3} - \frac{e}{kT_e}\frac{\partial\varphi}{\partial y}\frac{\partial^2\varphi}{\partial y^2}\right) \tag{6'}$$

where x serves as a parameter. y does not appear in Eq.(6) and therefore one can reduce the order denoting

$$\frac{\partial\varphi}{\partial y} = V(\varphi); \quad \frac{\partial^2\varphi}{\partial y^2} = VV', \quad \frac{\partial^3\varphi}{\partial y^3} = V^2V'' + VV'^2$$

and becomes

$$(V^2)'' - \frac{e}{kT_e}(V^2)' = \frac{2}{c}(a + b\varphi)$$

the solution of which is

$$\left(\frac{\partial\varphi}{\partial y}\right)^2 = \alpha\frac{kT_e}{e}e^{\frac{e\varphi}{kT_e}} + \beta\varphi + \frac{\gamma}{2}\varphi^2 + \delta \tag{7}$$

where α, δ are arbitrary constants,

$$\beta = -2\,\frac{eB^2}{Mu}\left[u + \frac{kT_e}{eB}\left(\frac{n_0'}{n_0} + \frac{T_e'}{T_e}\right)\right]$$

$$\gamma = -2\,\frac{T_e'}{T_e}\,\frac{eB}{Mu}$$

Using the diagram method as in Ref. [2], Eq. (7) yields many possible waves:

(a) 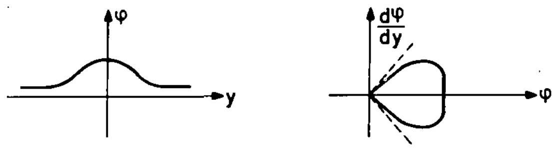

(a) The solitary wave when $\gamma < 0$

(b) 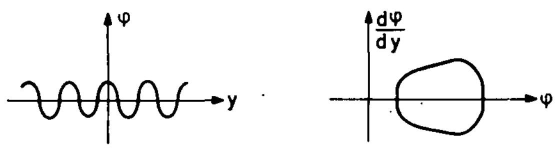

(b) Periodic waves in general

(c) Sinus waves due to the existence of even a small temperature gradient when $\alpha = \beta = 0$
In this case $\varphi = \varphi_{max} \sin \sigma y$ is a solution

$$\sigma^2 = \frac{1}{a_i^2}\,\frac{d\,\mathrm{Log}\,T_e}{d\,\mathrm{Log}\,n_0}\;\frac{1}{1 + \dfrac{d\,\mathrm{Log}\,T_e}{d\,\mathrm{Log}\,n_0}}\,, \quad a_i^2 = \frac{M\,T_e}{e^2B^2} \tag{8}$$

In cylindrical geometry $\sigma^2 = m^2/r^2$; this imposes a restriction on the radius of the plasma for the existence of the wave.

Resistive case. Periodic solutions and diffusion

If we consider solutions of the type $\varphi(y-ut+\alpha z)$ and $n(y-ut+\alpha z)$ Eqs (5) and (6) now become:

$$n = n_0(x)\exp\left[-\frac{e\varphi}{kT_e} + \eta\frac{\psi}{kT_e}\right] \tag{9}$$

$$-n_0u\left[-\frac{e}{kT_e}\frac{\partial\varphi}{\partial y} + \frac{\eta}{kT_e}\frac{\partial\psi}{\partial y}\right] + \frac{n_0'}{B}\frac{\partial\varphi}{\partial y} - \frac{Mun_0}{eB^2}\left[\frac{\partial^3\varphi}{\partial y^3} - \frac{\partial^2\varphi}{\partial y^2}\left(\frac{e}{kT}\frac{\partial\varphi}{\partial y} - \frac{\eta}{kT}\frac{\partial\psi}{\partial y}\right)\right] = 0$$

(10)

where η is the resistivity and $\frac{\partial\psi}{\partial z} = n\,v_z$

We must also take $\operatorname{div}\vec{j} = 0$

$$\alpha^2\frac{\partial\psi}{\partial y} + \frac{Mu}{eB^2}\,n\,\frac{\partial^2\varphi}{\partial y^2} = \text{const} \tag{11}$$

The diffusion in one period of oscillation is given by $\oint n(\partial\varphi/\partial y)\,dy$. It is easy to show from Eq. (10) that $\oint n(\partial\varphi/\partial y)dy = 0$. This supposes that the system possesses periodic solutions. In fact there is no periodic solution of Eqs(10) and (11). This is shown by integrating Eq. (10) over one period. It then follows that $\oint (\partial^2\varphi/\partial y^2)(\partial\psi/\partial y)\,dy = 0$, which is in contradiction with condition (11).

The introduction of finite ion temperature does not change the result. The presence of viscosity, if it allows periodic solutions, still gives either no diffusion, or a small diffusion. But the x-dependence of φ and ψ could completely change the problem.

CONCLUSION

(a) The two-fluid theory gives interesting results on non-linear drift waves in the non-dissipative case, these being associated with a gradient in the electron temperature.
(b) In the dissipative case, we believe that the x-dependence of the varying quantities of the wave is essential for calculating the diffusion.

REFERENCES

[1] TASSO, H., Phys. Lett. 24A 11(1967)618.
[2] SAGDEEV, R.Z., Rev. Plasma Phys. (LEONTOVICH, M.A., Ed.) 4 (1966) 23.

DISCUSSION

H. TASSO: I should like to make two comments regarding this paper, of which I am a co-author. In considering the problem of the existence of periodic waves (non-linear drift waves) one should take into account as far as possible the inertial term.

When calculating the diffusion due to the wave, I think it is essential to take into account the x-dependence of the density and the electrostatic potential.

F.F. CHEN: I agree with both points. The mathematical existence or non-existence of periodic solutions seems to depend on higher-order terms in the expansion of ion orbits in powers of r_L/R; I gained this impression in a conversation with Stix, who was to present this Rapporteur's paper. The estimates of transport rates in both your work and that of Stix (paper CN-24/E-1) suffer from crude assumptions regarding the x-dependence.

DIFFUSION AND RECOMBINATION IN A Q-DEVICE *

M. HASHMI, A. J. VAN DER HOUVEN VAN OORDT AND
J.-G. WEGROWE
INSTITUT FÜR PLASMAPHYSIK, GARCHING, MUNICH,
FEDERAL REPUBLIC OF GERMANY

Abstract

DIFFUSION AND RECOMBINATION IN A Q-DEVICE. To determine the diffusion coefficient perpendicular to the magnetic field $\vec{B}$ in a Q-device, the particle losses (||B) at the hot end plates should be known. Assuming resistive diffusion, the "equilibrium" theory predicts for strong magnetic fields that the dominant loss process should be recombination at the hot end plates.

Attempts were made to verify the "equilibrium" theory. For plasma densities $n \leq 10^{11} cm^{-3}$, the particle losses were found to be much larger than expected from the theory. A $j_0 \sim n$ dependence instead of $j_0 \sim n^2$ was observed, j_0 being the incoming neutral flux. However, j_0 was determined indirectly in these experiments by just measuring the total ion flux φ. Moreover, no conclusive information was available regarding the nature of these additional losses, i.e. whether the particles are lost parallel or perpendicular to the magnetic field.

In the present work measurements are performed in a singly ionized barium plasma of a Q-device (BARBARA) by varying the atomic flux, magnetic field, plate temperature, ion temperature, degree of ionization and mode of operation (single- or double-ended). The central part of the hot end plate is "illuminated" by an atomic beam of barium. The plasma density distribution is measured by Langmuir probes, microwave cavity, and resonance fluorescence scattering (λ = 4554 Å) methods, whose reliability has been checked. The spectroscopic method is now also extended to the barium atoms (λ = 5535 Å), allowing us to perform the hitherto lacking direct measurement of j_0. Further, the total ion input flux and the outgoing flux normal to $\vec{B}$ are also measured. Moreover, analysis of the radial density profiles outside the "illuminated" region is also made as a function of B.

These measurements give a possibility of a step-by-step determination of the article losses perpendicular and parallel to $\vec{B}$ separately.

1. INTRODUCTION

There is a lack of agreement between theory and experiment on the nature of particle losses in a Q-device.

Assuming classical diffusion [5], the "equilibrium" theory [1] predicts the surface recombination at the hot end-plates to be the dominant loss process at strong magnetic fields, yielding a $j_0 \sim n^2$ dependence having the exact form of

$$j_0 = \frac{v_+ v_-}{8\ \mathrm{RiLa}}\, n^2$$

j_0 and n are the atomic flux ($cm^{-2} s^{-1}$) striking the end-plate and the plasma density (cm^{-3}) respectively, v_+ and v_- being the ion and the electron thermal velocities, Ri and La the Richardson current and Langmuir function.

* This work was performed under the terms of the agreement between the Institut für Plasmaphysik GmbH, Munich-Garching, and Euratom to conduct joint research in the field of plasma physics.

On the other hand, several experiments, measuring the total number of ions coming into the plasma per second, Φ_i, and the density, n, by using different diagnostic techniques, have yielded a $\Phi_i \sim n$ dependence for $n \leqslant 2 \times 10^{11}$ cm^{-3}. Relating Φ_i to j_0 by $\Phi_i = \gamma j_0 A$ (where A is the effective plasma cross-section and $\gamma = La/1+La$), these experiments have shown particle losses much larger than those predicted by the "equilibrium" theory and give a $j_0 \sim n$ dependence instead of $j_0 \sim n^2$[2-4]. However, the nature of these additional losses could not be decided from these measurements. One could only conclude that either the losses at the surface of the hot end-plates are larger than those predicted by the "equilibrium" theory or the losses across the magnetic field are larger than those given by classical diffusion. This enhanced diffusion may be described, for instance, by Bohm's coefficient, as it has been observed in Q-devices; however, not under "quiescent" conditions (relative density fluctuations $\tilde{n}/n \leqslant 0.05$) [6-9].

Regarding enhanced losses on the surface of the end-plates, there are two possibilities. Firstly, the ionization on the end plates may not follow the Langmuir function. To explain a $j_0 \sim n$ dependence, the ionization should then depend upon the number of particles striking the end-plates. Secondly, the number of ions per second that overcome the sheath and reach the end-plates may be larger than that predicted by the "equilibrium" theory. This is only possible when the actual particle energy reaches the sheath potential [10].

It must be mentioned here that the charge exchange [11] should not contribute appreciably to particle losses in a barium plasma, the vapour pressure being very low and the vacuum vessel usually cooled.

To decide from the above-mentioned possibilities, in the present experiment the total particle losses and the diffusion across the magnetic field B were determined in the "quiescent" state of the plasma. In addition, the diffusion across B in a "non-quiescent" state ($\tilde{n}/n \geqslant 0.1$) and its correlation with the amplitude of the oscillations were investigated.

To measure directly the absolute density distribution of the atomic beam, the method of resonance fluorescence scattering of light by barium atoms was employed. The same method, applied to the ions, supplemented by microwave and Langmuir probes, was used to measure the absolute density distribution of the plasma as a function of B. Moreover, a metallic disc and a ring were provided to measure $\Phi_i(s^{-1})$ and $\Phi_R(s^{-1})$, the latter being the number of outgoing particles perpendicular to B.

2. EXPERIMENTAL SET-UP

The measurements were performed in a singly ionized barium plasma of the Q-device BARBARA [12]. The length of the plasma column was 50 cm. The magnetic field B could be varied up to 10 kG. The machine could be operated double-ended (D.E.) (both the end-plates hot and grounded) as well as single-ended (S.E.) (only one end-plate hot). The latter permits the cold end-plate to have a negative or positive bias, or to be kept floating or grounded. The end-plates could be heated up to 2800°K. Tungstan end-plates 3.2 cm in diam. were used whose absolute temperature calibration was done by measuring the spectral emission of light. The temperature difference from centre to edge was found to be about 1%. The plasma was produced by "illuminating" only the central region of one of the hot end-plates by means of a finely collimated atomic beam coming from the oven-collimator system. Its absolute density distribution was measured by resonance fluorescense scattering method (γ = 5535 Å) as a function of oven temperature, T_0, and of the distance from the oven-collimator system. The half-width, 2 R_0, at the position of the end-plate was found to be 6 mm[13]. The plasma density was measured by resonance fluorescence scattering of light by the ions (γ = 4554 and 4934 Å) from a volume of about 2×10^{-3} cm^3, by a microwave cavity (TM_{010} mode), and by a cylindrical Langmuir probe ($\sim 10^{-2}$ cm^2). The reliability of these methods with an accuracy of 30% has already been established in an earlier experiment [12]. The spectroscopic and the probe measurements were made at the midplane of the device, whereas the microwave cavity was located between the midplane and an end-plate. Φ_i and Φ_R were measured at the midplane by temporarily inserting the metallic disc into the plasma and the ring concentric to the end-plates and collecting the ion saturation current. The diameter of the disc was 45 mm, whereas the inner and outer diameters of the ring were 28 and 36 mm. In addition, the total number of ions per second coming to the negatively biased cold end-plate, Φ_P, was measured in S. E. The base pressure was in the 10^{-6} to 10^{-7} torr range.

3. RESULTS AND DISCUSSION

3.1. "Quiescent" state of plasma

Figure 1 shows the plasma peak density n as a function of j_0. The dashed line in D. E. represents the "equilibrium" theory ($j_0 \sim n^2$) for 2100°K. The dotted line in S. E. shows the curve for enhanced losses as described by Bohm's diffusion [1] coefficient. The experiments exhibit a $j_0 \sim$ n behaviour. The magnitude of the discrepancy between the experiments and the "equilibrium" theory is seen in Fig. 1. This confirms our earlier measurements of $\Phi_i \sim n$, with fully "illuminated" end-plate, independent of all the operating conditions for $n \leqslant 2 \times 10^{11}$ cm^{-3} [4]. Moreover, under the same operating conditions, the ratio Φ_i/n of our earlier and present experiments turns out to be the same.

The behaviour of the probability of ionization γ is directly verified under various operating conditions as shown in Fig. 2. The normalized values of $\int j_0(r) r\, dr$ and Φ_i show identical behaviour, confirming that, at different plate temperatures, γ is independent of the number of particles per second striking the end-plate. The absolute value of γ was found to be roughly in agreement with the theoretical value.

This excludes the supposition that the deviation between the experiments and the "equilibrium" theory might be due to an irregular behaviour of the ionization on the end-plates.

Since the magnitude of total losses was approximately that of Bohm diffusion as shown in Fig. 1, it may be thought that these additional losses take place across B. To investigate this, we measured the broadening of the radial density profiles as a function of B. Figure 3 shows the atomic

---

[1] Bohm diffusion is calculated by assuming longitudinal velocity of ions equal to the axial thermal velocity and a ratio of neutral beam width to end-plate diameter, $\varphi = 0.25$; classical diffusion and volume recombination (α) with $\varphi = 0.25$ and $\alpha_{eq.} = 5 \times 10^{-9}$ cm^3/s [14].

density profile and a typical plasma density profile; the error in abscissa being ± 0.5 mm. The ratio of the half-width of plasma profile to half-width of neutral profile (R_+/R_0) as a function of B is shown in Fig. 4 under various operating conditions. The peak density for these measurements remained below 10^{10} cm^{-3}. The solid and dotted curves represent the broadening by classical and Bohm diffusions, respectively.

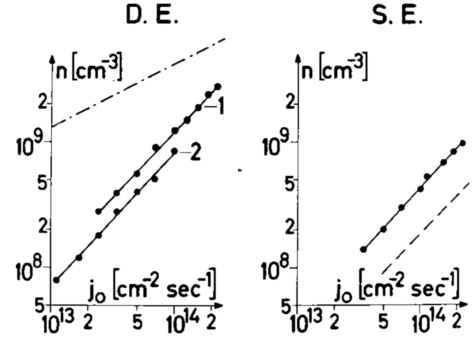

FIG. 1. Peak density n vs j_0 curves. B = 5.7 kG
D. E.: T_p = 2400°K (1) S. E.: T_p = 2400°K
T_p = 2100°K (2)
----: Bohm diffusion*
-·-·-·-· : Equilibrium theory for T_p = 2100°K
* See footnote in main text

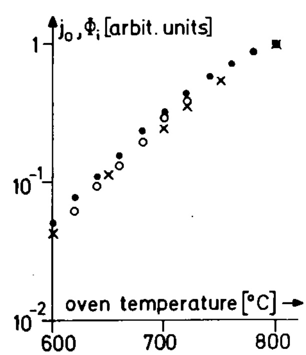

FIG. 2. Normalized j_0 and Φ_i vs. T_{oven} curves
• : $\int j_0(r)\,r\,dr$
× : Φ_i at T_p = 2400°K
O : Φ_i at T_p = 2100°K

It may be postulated now that, in spite of the absence of an appreciable broadening of the profiles, the particle losses take place across B. To show that this is not so, we used a metallic ring. Unfortunately, a "background" plasma was usually present (Fig. 3). We made sure that the "background" did not originate from the collimator. Its magnitude varied with the operating conditions. Φ_R was found to be independent of B and a function of "background". When the background was low, Φ_R/Φ_i was found to be 0.2 and under worst conditions it was 0.5.

This point was further investigated by measuring Φ_i and Φ_p. Both were found to be identical showing that:

(a) No particles are lost outside the plate radius; and

(b) The flux measured by the ring is collected only by that part of its area which overlaps with the end-plates.

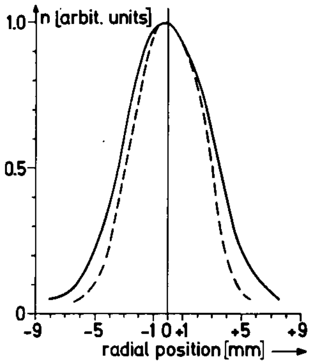

FIG. 3. Normalized radial density profiles in "quiescent" state
——— Profile of plasma
----- Profile of atomic beam

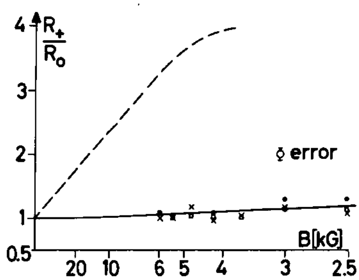

FIG. 4. Relative broadening of the density profiles, R_+/R_0, as a function of 1/B
$2R_0$ = Half width of atomic beam = 6 mm
$2R_+$ = Half width of plasma profile
x, □, O correspond to different operating conditions
——— Broadening due to classical diffusion and recombination*
----- Broadening due to Bohm diffusion*
* See footnote on page -

Thus, the measurements of the broadening of the profiles show that the losses across B are not compatible with enhanced diffusion and are compatible with classical diffusion. This is further supported by the independence of Φ_i/n on the atomic beam width as mentioned above. The comparison of Φ_R and Φ_i, and the equality of Φ_p and Φ_i exclude such loss mechanism across B as postulated above.

3.2. "Non-Quiescent" state of plasma

The question of correlation between the amplitude of coherent low-frequency electrostatic osciallations and diffusion across B has been the subject of a number of investigations [7, 9].

Besides the "quiescent" state, we could excite a "non-quiescent" state in which osciallations of fundamental frequency 3 kHz were observed. In S.E. this was achieved by grounding the cold end-plate or drawing the electron saturation current; in D.E. by a slight inequality between the end-plate temperatures.

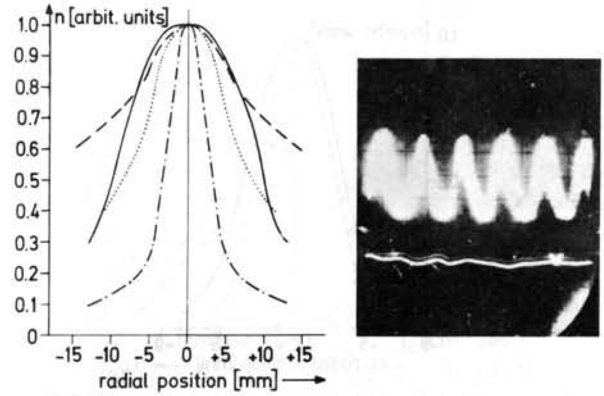

FIG. 5. Normalized radial density profiles in "quiescent" and "non-quiescent" states in S. E. operation

. -. -. -. - "quiescent" state

. . . . cold end-plate grounded

-------- cold end-plate drawing electron saturation current

——— Bohm diffusion *

The oscillogram shows the amplitude of oscillations in "quiescent" (lower signal) and "non-quiescent" (upper curve) states.

* See footnote on page -

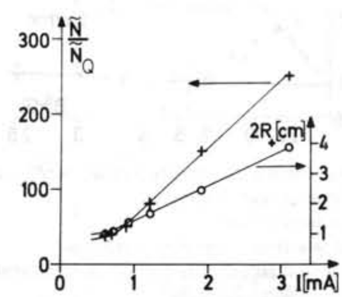

FIG. 6. Relative density oscillations (+) and broadening of the density profiles (o) as a function of electron current.

$2R_+$ = Half-width of plasma profile

$\tilde{N}$ = $\tilde{n}/n$ in "non-quiescent" state

$\tilde{N}_Q$ = $\tilde{n}/n$ in "quiescent" state

Figure 5 shows the radial density profiles in "quiescent" and "non-quiescent" states. The profile due to Bohm diffusion is also shown. In the quiescent state, the plasma density profile is comparable with the neutral density profile, while in the "non-quiescent" state it broadens and the peak density decreases. We never observed the broadening of the profile without the appearance of the above-mentioned oscillations. Figure 6 shows the relative density fluctuations and the half-width of the plasma density profiles as a function of currents drawn by the end-plate. It is seen that the amplitude of oscillations as well as the half-width of the plasma density profiles increases with the current, reaching the value corresponding to Bohm's diffusion coefficient. The nature of the wave is still being investigated.

4. CONCLUSIONS

The results of our experiments demonstrate that in the "quiescent" state the discrepancy between the "equilibrium" theory and the experiments is neither due to an irregular behaviour of the ionization on the end-plate nor to particle losses across B, which are found to be negligibly small. The only factor with which we are left now is an enhanced recombination at the end-plates. It should be mentioned here that Ref. [10] seems to describe the enhanced recombination adequately.

Further, in a collisionless plasma, coherent oscillations have an influence on the diffusion coefficient across B which may reach Bohm's diffusion coefficient depending upon the amplitude of the oscillations.

REFERENCES

[1] GOELER, S. von, Physics Fluids 7 (1964) 463.
[2] MOTLEY, R. W., Physics Fluids 8 (1965) 205.
[3] ECKHARTT, D., GRIEGER, G., GUILINO, E., HASHMI, M., unpublished (1964).
[4] HASHMI, M., HOUVEN VAN OORDT, A.J. van der, WEGROWE, J.-G., 2nd Europ Conf. Controlled Fusion and Plasma Physics, Stockholm, (1967) (to be published in Plasma Physics).
[5] D'ANGELO, N., RYNN, N., Physics Fluids 4 (1961) 1303.
[6] RYNN, N., Physics Fluids 7 (1964) 1084.
[7] BUCHELNIKOVA, N.S., SALINOV, R.A., EIDELMAN, Yu.I., Physics of Quiescent Plasmas, (Proc. Conf. Frascati, 1967) 1 (1967) 129.
[8] JOSEPHY, K., EASTLUND, B.J., MARSHALL, T.C., Physics of Quiescent Plasmas, (Proc. Conf. Frascati, 1967) 1 (1967) 271.
[9] HENDEL, H.W., COPPI, B., PERKINS, F., POLITZER, P.A., Phys. Rev. Lett. 18 (1967) 439.
[10] HOUVEN VAN OORDT, A.J. van der, To be published.
[11] DREICER, H., HENDERSON, D.B., Phys. Rev. Lett. 20 (1968) 374.
[12] HASHMI, M., HOUVEN VAN OORDT, A.J. van der, WEGROWE, J.-G., (to be published in Nuclear Fusion).
[13] HASHMI, M., HOUVEN VAN OORDT, A.J. van der, IPP-Report 2/66, March 1968.
[14] WEGROWE, J.-G., (to be published).

THEORY AND MEASUREMENT OF THE PERTURBATION IN THE ELECTRON VELOCITY DISTRIBUTION CAUSED BY A LANDAU DAMPED WAVE *

J. H. MALMBERG
GULF GENERAL ATOMIC INC., SAN DIEGO, CALIF.
AND
UNIVERSITY OF CALIFORNIA, SAN DIEGO, LA JOLLA, CALIF.
T. H. JENSEN
GULF GENERAL ATOMIC INC., SAN DIEGO, CALIF.
AND
T. M. O'NEIL
UNIVERSITY OF CALIFORNIA, SAN DIEGO, LA JOLLA, CALIF.
UNITED STATES OF AMERICA

Abstract

THEORY AND MEASUREMENT OF THE PERTURBATION IN THE ELECTRON VELOCITY DISTRIBUTION CAUSED BY A LANDAU DAMPED WAVE. The Landau damping of an electron plasma wave in a collisionless plasma produces a perturbation in the electron velocity distribution function. The first-order theory of Landau predicts presistent high-frequency oscillations in the distribution function, but no change in the time-averaged distribution. Using a procedure analogous to quasi-linear theory we have carried this calculation to one higher order in the amplitude of the electric field and obtained the perturbation in the time-averaged distribution function. The perturbation is proportional to the square of the electric field and is resonant near the phase velocity of the wave. We have tested this theory experimentally by direct measurement of the time-averaged perturbation in the electron velocity distribution. Prior experiments testing the linear and non-linear theory of plasma waves, using the same plasma, provide detailed evidence that the plasma matches the assumptions of the theory. For the present experiment, a Landau damped wave is launched in the plasma and electrons near the resonant velocity are allowed to escape from the plasma. Their velocity distribution is measured with an electrostatic analyser. The results agree with theory.

I. INTRODUCTION

The linear theory[1] for longitudinal electron waves in a plasma has been known for a long time and this theory has been confirmed experimentally[2-6]. When this theory is carried to higher orders in the wave electric potential, φ, a number of new phenomena appear. This paper deals with the changes in the time-averaged velocity distribution caused by a single wave. In first order this change is zero, but there is a non-zero change in second order. In the limit of many waves with random phases, quasi-linear theory,[7] which predicts the change in the velocity distribution caused by the waves, is expected to become valid. Thus the subject of this paper is closely related to quasi-linear theory; it is of the same order in φ, namely second, but here the effect of a single wave is investigated rather than the effect of many waves.

* This research was sponsored by the Defense Atomic Support Agency under Contract DASA01-68-C-0091.

For the experiment, the plasma is produced in a duoplasmatron arc source and drifts from it into a homogeneous magnetic field, forming a plasma column. The downstream end of the column is terminated by a negatively charged plate. The most energetic electrons escape the plasma and enter an electron energy analyzer mounted behind a hole in the end plate. A probe connected to an r.f. transmitter launches a damped electrostatic wave in the plasma. The transmitter is set at a series of fixed frequencies and for each the wave number and damping of the wave are measured. The waves cause a change in the time-averaged velocity distribution of the electrons, and this change is measured by means of the electron analyzer. Since the wave phase velocity changes with applied frequency, all the measurements can be made as a function of wave phase velocity.

The theory predicts that the main change in the velocity distribution occurs close to the phase velocity of the wave, and this is found experimentally. The theory also predicts that the change in the velocity distribution is proportional to φ^2 and this was established experimentally over a wide range. The measurements also show that the increase in resonant electron kinetic energy agrees in absolute magnitude with the original wave energy.

II. THEORY

We consider a long, axially symmetric plasma column immersed in a strong homogeneous magnetic field, and bounded by a cylindrical conductor. The plasma axis is taken to define the z-direction and the position of the transmitter probe to define the point $z = 0$. The plasma source is located many Landau damping lengths to the left of the transmitter (i.e., at $z = -\infty$) and the velocity analyzer many Landau damping lengths to the right of the transmitter (i.e., at $z = +\infty$).

Because of the strong magnetic field [i.e., $eB/mc > (4\pi ne^2/m)^{\frac{1}{2}}$], the electrons are constrained to move along the field lines, and their dynamics can be described by the one dimensional Vlasov equation

$$\frac{\partial f}{\partial t} + v_z \frac{\partial f}{\partial z} - \frac{e}{m}\frac{\partial \varphi}{\partial z}\frac{\partial f}{\partial v_z} = 0 \tag{1}$$

where f is the electron distribution, φ is the electric potential, and e and m are the electron charge and mass, respectively. This equation must be solved in conjunction with Poisson's equation

$$\frac{\partial^2 \varphi}{\partial z^2} + \frac{1}{r^2}\frac{\partial^2 \varphi}{\partial \theta^2} + \frac{1}{r}\frac{\partial}{\partial r}\ r\frac{\partial \varphi}{\partial r} = 4\pi e\left[n_i(r) - \int_{-\infty}^{\infty} dvf\right] \tag{2}$$

where n_i is the ion-density and the coordinates (r,θ) are the polar coordinates in the plane perpendicular to the plasma axis, that is, perpendicular to the z-axis. We will solve Eqs (1) and (2) by a perturbation expansion carried to second order in the wave amplitude.

If the transmitter probe is driven at frequency ω, the linear plasma response will be of the form

$$\begin{aligned}\varphi(z,r,\theta,t) &= \varphi_\omega(z,r,\theta)e^{i\omega t} + \text{C.C.}\\ \delta f(v_z,z,r,\theta,t) &= \delta f_\omega(v_z,z,r,\theta)e^{i\omega t} + \text{C.C.}\end{aligned} \tag{3}$$

where we have set $f = f_o + \delta f$ and C.C. stands for complex conjugate. The quantities δf_ω and φ_ω are related through the linearized Vlasov equation

$$i\omega f_\omega + v_z \frac{\partial}{\partial z} \delta f_\omega - \frac{e}{m} \frac{\partial \varphi_\omega}{\partial z} \frac{\partial f_o}{\partial v_z} = 0 \qquad (4)$$

which has the solution

$$\delta f_\omega = \frac{e}{m} \frac{\partial f_o}{\partial v_z} \frac{1}{v_z} \int_{-\infty}^{z} dz' \varphi_\omega(z') e^{i\omega/v_z (z'-z)} \qquad (5)$$

The general solution for φ_ω will be a sum of eigenmodes for the system

$$\varphi_\omega(r,z,\theta) = \sum_{n,m} \varphi_{nm}(\omega) \psi_{nm}(r,z) e^{im\theta} \qquad (6)$$

where the quantities $\varphi_{nm}(\omega)$ are coupling constants expressing the extent to which each mode is excited by the transmitter probe. The indices (n,m) are the radial and azimuthal mode numbers for the normalized eigenmodes ψ_{nm}.

To obtain the second-order correction to the time average distribution, f_o, we can take the time average of Eq. (1)

$$v_z \frac{\partial f_o}{\partial z} = \frac{e}{m} \left[\frac{\partial \varphi_{-\omega}}{\partial z} \frac{\partial f_\omega}{\partial v_z} + \text{C.C.} \right] \qquad (7)$$

where the right-hand side is to be evaluated by substituting the linear expressions for φ_ω and δf_ω. When this procedure has been carried out Eq. (7) is formally identical to the well-known quasi-linear diffusion equation. Conceptually, however, it is different from the quasi-linear equation. Since only a single wave is present (or more important, a single phase), the diffusion predicted by Eq. (7) is fake (or reversible) diffusion as opposed to the irreversible diffusion introduced by the random phase approximation of quasi-linear theory.

The analyzer current can now be calculated. The transmitter probe is chopped at 100 kc/sec and the analyzer current drives a coherent detector operated at the chopping frequency. So the detector output measures the difference between the analyzer current when the transmitter is on and when it is off. Since the analyzer admits only those electrons with axial velocity greater than a variable cut off velocity v_c, the coherent analyzer current is

$$I_{\text{coh.}}(v_c) = e \int_0^{r_o} r dr \int_0^{2\pi} d\theta \int_{v_c}^{\infty} dv_z\, v_z \left[f_o(z = +\infty) - f_o(z = -\infty) \right] \qquad (8)$$

where r_o is the radius of the analyzer aperture (centered on the plasma axis) and $[f_o(z = +\infty) - f_o(z = -\infty)]$ is to be calculated assuming the transmitter is on. Evaluating this latter quantity by integrating Eq. (7) from $z = -\infty$ to $z + \infty$ and substituting the result in Eq. (8) yields

$$I_{coh.}(v_c) = \frac{e^2}{m}\int_0^{r_o} r\,dr \int_0^{2\pi} d\theta \int_{-\infty}^{+\infty} dz \int_{v_c}^{\infty} \frac{\partial}{\partial v_z}\left[\frac{\partial \varphi_{-\omega}}{\partial z}\,\delta f_\omega + \text{C.C}\right] \quad (9)$$

Carrying out the v_z-integration gives the result

$$I_{coh.}(v_c) = -\frac{e^2}{m}\int_0^{r_o} r\,dr \int_0^{2\pi} d\theta \int_{-\infty}^{+\infty} dz \left[\frac{\partial \varphi_{-\omega}}{\partial z}\,\delta f_\omega(v_c) + \text{C.C.}\right] \quad (10)$$

Replacing $\varphi_{-\omega}$ and δf_ω in this equation by the general expressions given earlier [see Eqs (5) and (6)] would yield a series of terms representing the contributions of the various modes to the analyzer current. As will be shown shortly, the contribution to the coherent current from a weakly damped mode is peaked near the phase velocity of the mode, with the width of the peak proportional to the damping rate. Since the θ-independent lowest order radial mode (i.e., $n = 0$, $m = 0$) is essentially the only weakly damped mode, we need only retain this mode to investigate the peak which is observed in the coherent analyzer current. In fact, we have shown experimentally, by an interference technique which cancels this mode and thereby destroys the peak, that this mode is indeed responsible for the peak (see Sec. III). As has been shown previously,[3,4] this lowest order mode is asymptotically of the form

$$\varphi_\omega = \varphi_o\ \psi_o(r)\begin{cases} e^{-ik_R z + k_I z} & z \gtrsim L_D \\ e^{ik_R z - k_I z} & z \lesssim -L_D \end{cases} \quad (11)$$

where the theoretically predicted values of k_R and k_I agree with the experimental values, (i.e., an asymptotic form applies in each direction at distances large compared to the Debye length, L_D). The function $\psi_o(r)$ is normalized to unity at $r = 0$.

Because the radius, r_o, of the analyzer aperture is much smaller than the characteristic radius of the eigenmode $\psi_o(r)$, we may evaluate $\psi_o(r)$ at $r = 0$ where it is normalized to unity. Also, since the velocity analyzer only looks at positive velocities and the peak in the analyzer current is located close to the phase velocity of the mode producing the peak, we need only retain that part of the lowest order mode traveling to the right, that is, the upper term in Eq. (11). Substituting this term into Eqs (5) and (10) yields the result

$$I_{coh.}(v_c) = -\frac{e^3}{m^2}\,\pi r_o^2 k_R^2 \varphi_o^2 \left(\frac{\partial f_o}{\partial v}\right)_{v=v_c} \int_0^{\infty} dz \quad (12)$$
$$\times \left[\frac{e^{2k_I z} - e^{ik_R z - i\frac{\omega}{v_c} z + k_I z}}{i\omega - ik_R v_c + k_I v_c} + \text{C.C.}\right]$$

Carrying out the remaining z-integration reduces Eq. (12) to the final result

$$I_{coh.}(v_c) = -\frac{e^3}{m^2} \frac{\pi r_o^2 k_R^2 \varphi_o^2}{(\omega - k_R v_c)^2 + (k_I v_c)^2} v_c \left(\frac{\partial f_o}{\partial v}\right)_{v=v_c} \tag{13}$$

If we had retained the exact, rather than asymptotic, form of the lowest mode in Eq. (11), the resonant denominator in Eq. (13) would simply have been replaced by the Landau dielectric function,[1] $|\epsilon(k,kv_c|^2$, which reduces to the expression in Eq. (13) near the phase velocity of the mode. We have written out the theory including the lower term in Eq. (11) and shown by numerical computations that its contribution is insignificant.

The total power of the lowest order mode is transformed to kinetic energy of resonant electrons since the wave is damped within the length of the plasma column. The difference between the kinetic energy of the resonant electrons entering the analyzer per unit time when the transmitter is on and their kinetic energy when it is off is

$$P_A = \pi r_o^2 \int \frac{m}{2} v^3 \, \Delta f_o(v) dv$$

where $\Delta f_o = f_o(z=+\infty) - f_o(z=-\infty)$ and the velocity integral is to be extended only over the resonance peak. (Of course the higher order modes and the near field give contribution to the coherent current at lower velocities.) Since

$$\frac{dI_{coh.}(v)}{dv} = - v\Delta f(v)\pi r_o^2 e$$

one obtains by integration by parts

$$P_A = \frac{1}{e}\int I_{coh.}(\mathcal{E})d\mathcal{E} \tag{14}$$

where $\mathcal{E} = \frac{1}{2} mv^2$.

The total power, P_T, transmitted downstream in the mode under consideration, can be measured. Since the radial profile of the power flow is proportional to $n(r)\,|\psi_o(r)|^2$, where $n(r)$ is particle density profile and $\psi_o(r)$, is the radial dependence of the eigenfunction, one obtains

$$P_A = P_T \, \pi r_o^2 \frac{n(0)\,|\psi_o(0)|^2}{\int_0^\infty 2\pi r n(r)\,|\psi_o(r)|^2} \tag{15}$$

Here, the fact that r_o is small compared to the characteristic radius of $\psi_o(r)$, is used. The function $n(r)$ is measured and $\psi_o(r)$ is calculated in connection with the calculation of the dispersion curve for the waves. Also P_T and the integral of Eq. (14) are measured. Thus, Eqs (14) and (15) are subject to experimental test.

III. EXPERIMENT

The machine with which the experiments are done has been described previously.[3-8] A few minor modifications have been made for the present experiment. In Fig. 1 is shown a schematic of the machine. The plasma source is a duoplasmatron and the gas used is hydrogen. The plasma forms a 200 cm long column in a homogeneous magnetic field of 240 G. The plasma column is surrounded by a slotted stainless steel tube with an inside radius of 5.2 cm. The slots allow us to put probes into the plasma and move them axially the full length of the machine. An annular permanent magnet which locally establishes a magnetic cusp field is placed just outside the duoplamatron. A separately biased cylindrical electrode is placed near the cusp magnet. When the bias is properly adjusted, this combination reduces radial diffusion of the plasma for reasons that are not clearly understood.

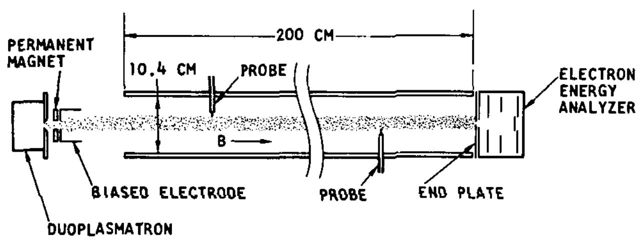

FIG. 1. Schematic of the apparatus.

At the downstream end, the plasma is terminated by a negatively charged metal plate. Sufficiently energetic electrons may escape the plasma and enter an electron analyzer through a hole with a diameter of 1.5 mm in the center of the plate. The electron analyzer (which is also immersed in the magnetic field which confines the plasma column) is shown in Fig. 2. Electrons with parallel kinetic energy large enough to pass the potential barrier in the plane of the discriminator electrode will be collected by the collector. Since the beam diameter is small compared to the diameter of the hole in the discriminator electrode, the resolution of the analyzer is satisfactory (about 1%) even though the height of the potential barrier in the plane of the analyzer electrode depends on the radius. (For a small given beam diameter, the resolution of the analyzer improves as the size of the hole in the discriminator electrode is increased.) One big advantage of using a discriminator electrode with a hole instead of a grid is that metal surfaces tend to be covered with an insulating film,(probably pumpoil) which has been observed to charge electrically when placed in the electron beam. The electron analyzer measures parallel kinetic energy of electrons referred to ground potential. If the space potential in the plasma is different from ground potential, which is generally the case, the parallel kinetic energy of an electron when it is in the plasma is different from the energy measured by the analyzer. This difference is the space potential of the plasma. Thus, fluctuations in the space potential will appear as a limitation to the resolution of the analyzer.

The potential rise created by the repeller electrode rejects ions from the plasma which enter the analyzer. The collector-guard ring arrangement is designed so that secondary photoelectrons from the discriminator electrode cannot reach the collector since they must follow magnetic field lines. Since the potential in the plane of the discriminator electrode at the axis is not identical with the potential of the discriminator electrode, the analyzer was calibrated with an electron beam. The calibration agrees with the calculated result.

The velocity distribution of the electrons is very close to Maxwellian with a temperature of $kT_e = 6.2$ eV. The electron density is $2.5 \times 10^8 cm^{-3}$ at the axis and drops smoothly to zero at the wall with a half-maximum-radius of about 1.5 cm. The background pressure is $\sim 1 \times 10^{-5}$ Torr (mostly H_2). Hence the Debye length is about 1 mm; the electron mean free path for electron-ion collisions is of the order of 1000 m and for electron-neutral collisions is of the order of 40 m. For the present experiment, the plasma is collisionless in the sense of the theory.

When an r.f. voltage is applied to a probe inserted into this plasma, electron plasma waves are excited which propagate in both directions along the plasma column. While many eigenmodes of the plasma are excited, only

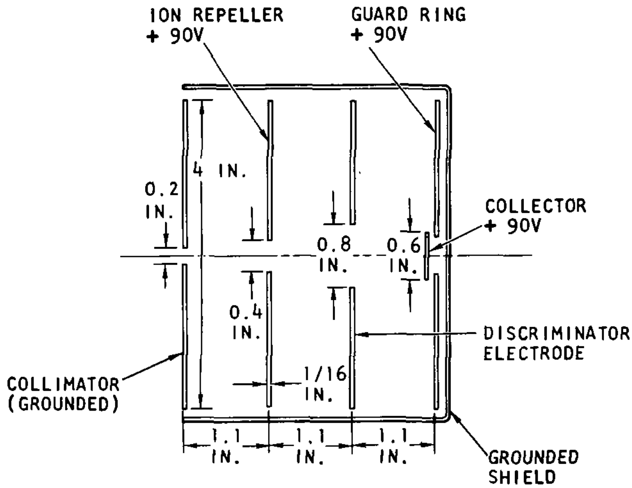

FIG. 2. Schematic of electron analyser.

the lowest radial and azimuthal eigenmode is observable for appreciable distances from the antenna when the frequency is sufficiently high, since all higher modes are very heavily damped. In previous experiments[4] we have measured the dispersion of these waves, and found that it is accurately predicted by the theory of Landau modified to account for the finite radial geometry of the system. The damping of these waves has also been measured[2-4] and it was shown that heavy exponential damping is observed, even though collisional damping is negligible under these circumstances; that the damping is caused by electrons traveling at the phase velocity of the wave; and that the magnitude of the damping, its dependence on phase velocity, and its dependence on plasma temperature are accurately predicted by the theory of Landau. Thus electron plasma waves in this machine are very well understood.

The dispersion curve depends only on the radial density profile and on the temperature and the central density of the plasma. Thus from a measured dispersion curve and radial profile the temperature and central density may be deduced, (both to a precision of about 5%). The temperature can also be deduced independently from the damping data, also with a precision of about 5%. A third temperature is obtained by direct measurement of the tail of the velocity distribution function using the electron analyzer. Over the range of this measurement ($3kT_e$ to $8kT_e$) the distribution is accurately Maxwellian and again a 5% precision for the temperature is obtained. These three "temperatures" will agree only if the distribution function is a Maxwellian since each depends on a different aspect of the distribution function. All three measurements give $kT_e = 6.2$ eV within 5%.

The density measurement applies to a particular position along the plasma column. Actually, the density on the axis is decreasing in the downstream direction and the density profile broadens. This in turn means that the dispersion curve changes with distance along the plasma column. By measurement of the dispersion curve at various positions, it was found that the density on the axis is decreasing by about 20% per 100 cm. For the measurements presented in this paper the effects due to this density gradient can be neglected.

The measurements of the perturbation in the velocity distribution caused by a Landau damped wave, were made in the following way. A wave is launched from a transmitter probe placed about the middle of the plasma column, typically so that the probe tip is 1 cm from the plasma axis. The probe is a .1 mm tungsten wire; 2 mm at the end of the wire is exposed. The rest is covered first with glass, then with a stainless steel tube and then again glass, so that, except for the exposed tip, it forms an insulated coaxial line. This coaxial line is connected to a 50 Ω r.f. transmitter, which is chopped on and off at a frequency of 100 kc. The frequency range used is 125-165 Mc/s. The r.m.s. r.f. voltage applied to the probe varies from 0.5 to 8 V. The collector current from the electron analyzer is applied to a coherent detector locked on the signal that chops the transmitter. Thus the output of the coherent detector is proportional to the coherent analyzer current, that is, the difference between the analyzer current when the transmitter is on and when it is off. The output of the coherent detector is connected to the y-input of an x-y recorder. The x-input is connected to the analyzer electrode voltage. This voltage, which controls the analyzer cut-off energy, (and hence v_c), is swept slowly. A typical recorder curve is given in Fig. 3. This curve exhibits a resonance structure.

Since $k_I/k_R \ll 1$, Eq. (13) predicts a resonance shape multiplied by a rather slowly varying function, $v_c(\partial f_o/\partial v)_{v=v_c}$, so qualitative agreement with theory is immediately apparent. It was assumed in the derivation of Eq. (13) that only the lowest order mode contributed to the resonance. We have demonstrated experimentally that neither higher order modes nor the near field contribute appreciably to the shape of the curve in Fig. 3. Two transmitter probes were placed about 4 cm apart. They were connected to the same transmitter but in the coax line to one of the probes was placed a phase shifter and a variable attenuator. The relative phase and amplitude between the r.f. applied to the two probes was adjusted such that the downstream wave transmitted by the first probe was nearly cancelled by the wave transmitted by the second probe. The coherent current observed when both probes were connected was about 15% of the coherent current observed when either probe was disconnected. Furthermore, with both probes connected, the coherent current increases by a factor of about 10 when the distance between the probes was increased by one-half wavelength; in this case the two waves interfered constructively rather than destructively. This interference of waves takes place only for the lowest mode and not for near fields or higher modes launched by the probes. Therefore the coherent current observed is mainly due to the lowest mode.

From Eq. (13), the coherent current, $I_{coh.}$ has its maximum at roughly the energy, $\mathcal{E} \sim \frac{1}{2}\, m(\omega/k_R)^2$. The exact energy can be calculated from Eq. (13) since the distribution function is known. Using the measured values of k_I/k_R and a temperature of 6.2 eV, the theory predicts the solid curve of Fig. 4 for the position of the maximum as a function of the "phase velocity energy," $\frac{1}{2}\, m(\omega/k_R)^2$. Also shown in Fig. 4 are the corresponding experimental results. The analyzer energies have been adjusted by a constant to allow for the space potential of the plasma, which is not known a priori. For Fig. 4 the space potential used is -12.7 V to ground, which is close to the best fit. The high energy data of Fig. 4 correspond to low frequencies. For even lower frequencies the waves become so lightly damped that the wave extends over a considerable length of the plasma column. In such cases the finite density gradient mentioned earlier becomes important

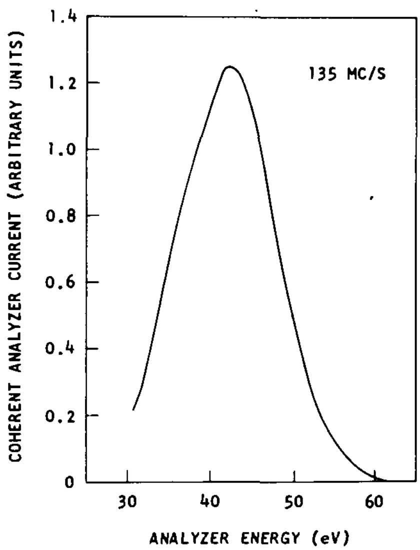

FIG. 3. Coherent current vs analyser energy. The analyser energies are corrected for plasma potential.

since the phase velocity then becomes a function of position. A WKB approximation to this problem was worked out, and this latter calculation fits the experimental data at low frequencies. For the results for the restricted frequency range presented in Fig. 4, however, the incorporation of the finite density gradient does not have any appreciable effect.

Equation (13) predicts that the coherent current is proportional to the square of the potential amplitude of the wave, φ_0^2, which in turn is proportional to the probe voltage squared. The data of Fig. 5 show that the coherent current maximum is proportional to φ_0^2, as expected. It was also found that the shape of the coherent current vs analyzer voltage was independent of the probe voltage (except at very high probe voltages).

Equations (14) and (15) were confirmed experimentally. These equations relate the increase in resonant electron kinetic energy to the original wave power. To find the total wave power, P_T, launched in the downstream direction by the transmitter probe, it is necessary to know the probe-plasma wave coupling constant (i.e., to know as a function of frequency the relation between the plasma wave power and the r.f. probe voltage). We assume that the coupling constant from the transmitter probe signal to a plasma wave is equal to the coupling constant from a plasma wave to this same probe used as a receiver. The total attenuation from a transmitter probe to a receiver probe, placed a reasonable distance apart, is the sum

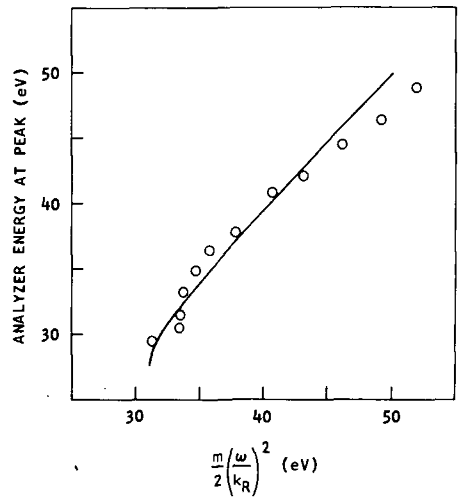

FIG. 4. Analyser energy at coherent current maximum vs (1/2)m $(\omega/k)^2$. The solid curve is the theoretical curve. The experimental points are adjusted for plasma potential.

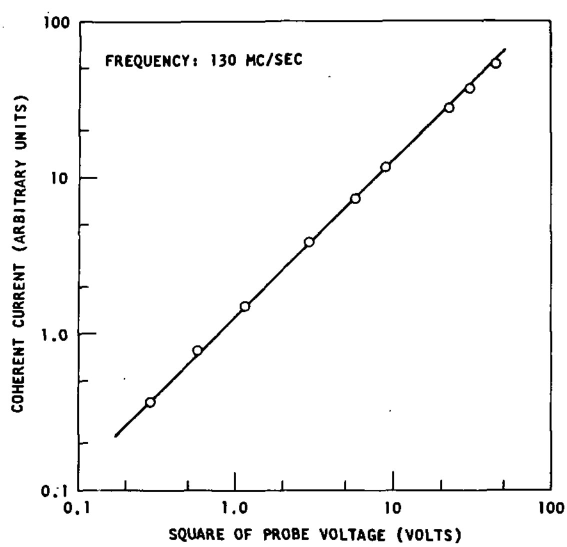

FIG. 5. Maximum coherent current vs square of probe voltage.

of three parts: namely, the attenuation of each of the probes in coupling to the plasma wave and the attenuation of the wave traveling through the plasma between the probes. The last part can be evaluated from a measurement of the damping coefficient and the distance between the probes. Using three probes, this measurement is made for 3 pairs. Three equations with 3 unknowns, namely the probe attenuations, are obtained, and the coupling constants can be deduced. Thus, when the voltage on the transmitter probe is measured, the total power in the launched wave can be found. We have used this method for determining wave power in two prior experiments[9-10] in which the result was checked by independent measurements and satisfactory agreement was obtained. It should be noted that the power, P_T, is the power in the lowest order mode. As an example, 4 V (r.m.s.) r.f. at 130 Mc/s was measured on a transmitter probe for which the attenuation was measured to be 43 db. The total wave power launched is $P_T = 16 \times 10^{-6}$ W. By numerical integration, the integral in Eq. (15) was evaluated using the measured radial density profile and $\psi_o(r)$ (which comes from the numerical dispersion curve calculation). The radius of the hole through which electrons enter the analyzer is known, and Eq. (15) gives $P_A = 10^{-7}$ W. The integral in Eq. (14) was also integrated numerically using the measured resonance curve. This yields a value for P_A' of 1.2×10^{-7} W. An evaluation of possible errors in the measurements gives an uncertainty of about 3 db, so the close agreement between these two numbers is somewhat fortuitous.

The width of the resonance curves is within a factor of two of that predicted by Eq.(13). At low frequencies the observed widths are about a factor of 2 bigger than the ones given by Eq.(13), while at high frequencies the discrepancy is smaller. We have studied experimentally a number of possible causes for this discrepancy. One possibility was that plasma noise was large enough to produce appreciable velocity space diffusion. In order to test this idea, noise in a broad band around the transmitter frequency was launched from another probe. The power per unit bandwidth of transmitted noise was several times the natural plasma noise (as monitored by a receiver probe in the spatial region of interest). Since this increase of background noise had no effect on the coherent current, it was concluded that the background noise played no important role in the experiment.

Another possibility investigated was that the broadening of the resonance was caused by low frequency density fluctuations. This is ruled out experimentally as follows. Since the transmitter frequency is fixed, when the density fluctuates, the result is a time variation in the wavelength of the wave. The density fluctuations were found by measuring fluctuations in the wave number at 0 - 1 Mhz with an interferometer. It was found that these fluctuations are too small to explain the broadening.

In all likelihood the observed broadening is caused by fluctuations in the plasma potential; as mentioned previously, such fluctuations will appear as a limitation on the resolution of the analyzer. The fluctuations in the analyzer current, as observed on an oscilloscope, are comparable to the average current. This means that the fluctuations of the plasma potential are comparable to the electron temperature, and hence that the effective resolution of the analyzer is of order kT_e, which agrees with the observed widths. Fluctuations of a similar magnitude are inferred from probe measurements. This limitation on the analyzer resolution has prevented us from measuring the dependence of the resonance width on k_I.

IV. CONCLUSION

The perturbation in the time-averaged electron velocity distribution caused by a Landau damped electrostatic wave can be calculated using a second order perturbation theory, formally identical to quasi-linear theory. The theory predicts that this perturbation in the velocity distribution is resonant near the phase velocity of the wave, that its amplitude is proportional to the square of the wave amplitude, and that the width of the resonance is proportional to the wave damping coefficient.

The experimental results agree with the theory. The measurements show that the perturbation is resonant near the phase velocity of the transmitted wave, that it is proportional to the square of the wave amplitude and that the absolute magnitude of the perturbation accounts for the dissipated wave energy. The measured resonance widths agree with theory within a factor of two. The instrumental resolution is insufficient to make a closer comparison.

ACKNOWLEDGMENT

It is a pleasure to acknowledge the contributions and excellent assistance of Charles D. Moore to the experimental work and of Paul Vidmar to the computing work.

REFERENCES

[1] LANDAU, L., J. Phys. 10 1 (1946) 45.

[2] MALMBERG, J. H. and WHARTON, C. B., Phys. Rev. Letters 13 6 (1964) 184.

[3] MALMBERG, J.H., WHARTON, C. B., and DRUMMOND, W. E., Plasma Physics and Controlled Nuclear Fusion Research, (International Atomic Energy Agency, Vienna) I (1965) 485.

[4] MALMBERG, J. H. and WHARTON, C. B., Phys. Rev. Letters 17 4 (1966) 175.

[5] VAN HOVEN, G., Phys. Rev. Letters 17 4 (1966) 169.

[6] DERFLER, H. and SIMONEN, T. C., Phys. Rev.Letters 17 4 (1966) 172.

[7] DRUMMOND, W. E. and PINES, D., Nuclear Fusion, Part 3 (1962 Supplement) 1049.

[8] MALMBERG, J. H., CARLSON, N. W., WHARTON, C. B., and DRUMMOND, W. E., Proc. 6th Int. Sur Les Phenomènes D'Ionisation Dans Les Gaz, Paris 4 (1963) 229.

[9] MALMBERG, J. H. and WHARTON, C. B., Phys. Rev. Letters 19 14 (1967) 775.

[10] WHARTON, C. B. and MALMBERG, J. H., "Microwave scattering from plasma waves," Gulf General Atomic Report GA-8178 (to be published in Phys. Fluids).

DISCUSSION

E. CANOBBIO: Up to what value of the applied field can the second-order expansion which you use be considered valid?

J.H. MALMBERG: The theory should be valid until the wave amplitude is sufficient for large-amplitude effects to appear in the wave damping; i.e. until $(1/v_p k_i)\,(ekE/m)^{\frac{1}{2}} \gtrsim (2\pi)^{\frac{1}{2}}$.

E. CANOBBIO: Have you any experimental evidence of this limit?

J.H. MALMBERG: When the amplitude attains approximately this level, large-amplitude effects appear in the damping, and the shape of the perturbation in the velocity distribution begins to change.

PROCESSUS NON LINEAIRES

R. CANO, C. ETIEVANT, I. FIDONE, G. LAVAL, J. OLIVAIN,
R. PELLAT, M. PERULLI ET B. ZANFAGNA
ASSOCIATION EURATOM-CEA, FONTENAY-AUX-ROSES, FRANCE

Abstract — Résumé

NON-LINEAR PROCESSES. The experiments described in this paper show that there are two types of non-linear three-wave processes:

A. Disintegration of an electron plasma wave. In a plasma column of a density of 10^8 to 10^9 electrons/cm^3, an electron temperature of the order of several eV, a length of 60 cm, a radius of 1 cm, which is confined by a magnetic field of 2500 G, a monochromatic electron plasma wave of frequency f_1 is excited. A noise spectrum in a frequency band always below f_1 due to the disintegration of this wave is observed. The resonance relations are verified. The threshold level and the energy transfer lengths are measured. The results of measurement show that the mechanism of disintegration should be interpreted without making use of the random-phase hypothesis. The shape of the spectrum is explained by varying the interaction coefficient as a function of the different phase velocities. In the same way, the parameter amplification of a wave pre-excited at one of the disintegration spectrum frequencies is studied.

B. Non-linear generation of an electromagnetic wave. In a plasma with an electron density between 10^9 and 10^{11} electrons/cm^3, which is confined by a magnetic field of the order of 4000 G and generated by a stationary high-frequency discharge, the interaction of two microwave beams propagated perpendicularly to the confining magnetic field and polarized both according to ordinary and extraordinary modes is brought about. The intersection of these beams defines the volume of interaction in which the third wave is generated. Two processes were studied, depending on the polarization of the two primary waves: (OX. O') and (OO', X).

The measurements show that the conditions of resonance imposed on the frequencies and propagation vectors are satisfied. The power released is compared with the theoretical value. The polarization of the generated wave is in accordance with that expected from the structure of the interaction matrix.

PROCESSUS NON LINEAIRES. Les expériences décrites dans ce mémoire mettent en évidence deux types de processus non linéaires à trois ondes:

A. Désintégration d'une onde plasma électronique. Dans une colonne de plasma d'une densité de 10^8 à 10^9 el/cm^3, d'une température électronique de l'ordre de quelques eV, d'une longueur de 60 cm, d'un rayon de 1 cm, confinée par uu champ magnétique de 2500 G, on excite une onde plasma électronique monochromatique, de fréquence f_1. On observe un spectre de bruit dans une bande de fréquence toujours inférieure à f_1 engendré par la désintégration de cette onde. Les relations de résonance sont vérifiées. On mesure le niveau du seuil et les longueurs de transfert d'énergie. Les résultats de mesure montrent que le mécanisme de désintégration doit être interprété sans faire appel à l'hypothèse des phases aléatoires. La forme du spectre s'explique par la variation du coefficient d'interaction en fonction des différentes vitesses de phase. On étudie également l'amplification paramétrique d'une onde pré-excitée à l'une des fréquences du spectre de désintégration.

B. Génération non linéaire d'une onde électromagnétique. Dans un plasma de densité électronique comprise entre 10^9 et 10^{11} el/cm^3, confiné par un champ magnétique de l'ordre de 4000 G et créé par une décharge haute fréquence stationnaire, on fait interagir deux faisceaux de micro-ondes se propageant perpendiculairement au champ magnétique de confinement et polarisés, soit selon le mode ordinaire, soit selon le mode extraordinaire. L'intersection de ces faisceaux définit le volume d'interaction dans lequel est engendrée la troisième onde. Deux processus ont été étudiés, dépendant de la polarisation des deux ondes primaires: (OX, O') et (OO', X).

Les mesures montrent que les conditions de résonance sur les fréquences et les vecteurs de propagation sont vérifiées. La puissance émise est comparée avec la valeur théorique. La polarisation de l'onde engendrée est conforme à celle prévue par la structure de la matrice d'interaction.

A. DESINTEGRATION D'UNE ONDE PLASMA ELECTRONIQUE [1]

A-1. Théorie

Dans une colonne de plasma homogène sans collisions, en géométrie cylindrique, on étudie la désintégration d'une onde plasma électronique se propageant le long d'un champ magnétique fort ($\omega_{pe} \leq \omega_{ce}$). Les ondes engendrées par cette désintégration sont également, comme le montrent les résultats expérimentaux, des ondes plasma électroniques. Par ce point l'expérience présentée diffère d'autres travaux effectués sur la désintégration d'une onde [2 ; 3 ; 4 ; 5 ; 6].

Dans la phase initiale du mécanisme, les ondes engendrées ont une amplitude suffisamment faible pour que la désintégration puisse apparaître comme une superposition de mécanismes élémentaires d'interaction à trois ondes complètement indépendants les uns des autres. D'autre part, pendant cette phase initiale, on peut considérer que l'onde primaire conserve une amplitude E_{1r} sensiblement constante. Dans ces conditions, l'évolution spatiale des amplitudes E_2 et E_3 de deux ondes en interaction s'écrit :

$$\frac{\partial E_{2,3}(z)}{\partial z} = -\left(\gamma_{2,3} + i\,\Delta k_{2,3}\right) E_{2,3}(z) + V_{2,3}\, E_1 E^{*}_{3,2}(z) \tag{1}$$

où γ_j est l'amortissement linéaire spatial, Δk_j le défaut de résonance, V_j le coefficient d'interaction d'expression [1 ; 7]

$$V_j = \frac{e}{2M}\,\frac{k_j^{3}}{P_j}\,\omega_{pe}^{2}\left(\prod_{n=1}^{3}\frac{1}{\omega_n}\right)\sum_{\nu=1}^{3}\frac{k_\nu}{\omega_\nu}\,\alpha_j$$

avec P_j constante numérique définie par les conditions de raccordement et

$$\alpha_j = \frac{\int_0^a J_{m_1}(P_1 r)\, J_{m_2}(P_2 r)\, J_{m_3}(P_3 r)\, r\, dr}{\mathcal{N}_j}$$

a : rayon du plasma, $\mathcal{N}_j$: coefficient d'orthonormalisation des fonctions de Bessel [1].

Les équations (1) sont écrites en supposant que les conditions de quasi résonance suivantes sont satisfaites :

$$\begin{aligned} &\omega_1 = \omega_2 + \omega_3 \\ &m_1 = m_2 + m_3 \\ &k_1(\omega_1) = k_2(\omega_2) + k_3(\omega_3) + \sum \Delta k_j \\ &D(\omega_j, k_j) = 0 \end{aligned} \tag{2}$$

---

[1] Ces résultats constituent une partie du travail de Thèse de M. Pérulli [1].

où $D(\omega_j, k_j) = 0$ est la relation de dispersion linéaire des ondes plasma électroniques :

$$\omega_j^2 = \frac{k_j^2 \, \omega_{pe}^2}{k_j^2 + P_j^2} \tag{3}$$

Les solutions des équations (1) ont un comportement spatial du type $e^{S_\pm z}$ avec :

$$2 S_\pm = -\left[\gamma_2 + \gamma_3 + i\left(\Delta k_2 - \Delta k_3\right)\right] \pm \left\{\left[\gamma_3 - \gamma_2 - i\left(\Delta k_2 + \Delta k_3\right)\right]^2 + 4 V_2 V_3 |E_1|^2\right\}^{1/2} \tag{4}$$

On voit sur l'expression (4) que la solution S_+ permet une croissance spatiale si :

$$|E_1|^2 > |E_1|_o^2 = \frac{\gamma_2 \gamma_3}{V_2 V_3}\left[1 + \frac{(\Delta k_2 + \Delta k_3)^2}{(\gamma_2 + \gamma_3)^2}\right] \tag{5}$$

Très au-dessus du seuil d'instabilité $|E_1|_o$, la longueur de croissance spatiale L satisfait à la relation :

$$L |E_1| = \left(V_2 V_3\right)^{-1/2} \tag{6}$$

Dans ce cas on a également la relation :

$$\frac{|E_2|}{|E_3|} \sim \left(\frac{k_2}{k_3}\right)^{3/2} \tag{7}$$

qui montre que l'onde de fréquence plus élevée est de plus grande amplitude.

Il est à remarquer qu'un mécanisme d'interaction à trois ondes résonnant (c'est-à-dire pour lequel $\Delta k_{2,3} = 0$) n'est pas possible si les trois ondes appartiennent à la même branche de la courbe de dispersion. Le mécanisme de désintégration doit donc faire apparaître dans le spectre engendré des ondes appartenant à des branches différentes.

Cette remarque s'applique également au mécanisme d'amplification paramétrique, c'est-à-dire à la situation décrite ci-dessus dans laquelle l'une des ondes, E_2 par exemple, est préexcitée. En l'absence de l'onde pompe E_1, l'onde E_2 se propage avec son amortissement naturel γ_2. En présence de l'onde pompe E_1, l'onde E_2 se propage avec le taux de croissance S_+ défini par l'équation (4).

A - 2. Description du Plasma

La désintégration d'une onde plasma électronique a été étudiée dans l'expérience représentée schématiquement Fig. 1. Un plasma de densité de l'ordre de 10^9 el/cm^3 diffuse le long d'un champ magnétique uniforme ($B_o >$ 2 000 Gauss) à partir d'une source (du type décharge Reflex). Les mesures présentées ont été effectuées dans un plasma de Xénon de température $T_e \sim 1$ à 2 eV. Entre la source de plasma et le collecteur s'établit un gradient longitudinal de densité de l'ordre de 1 % par cm.

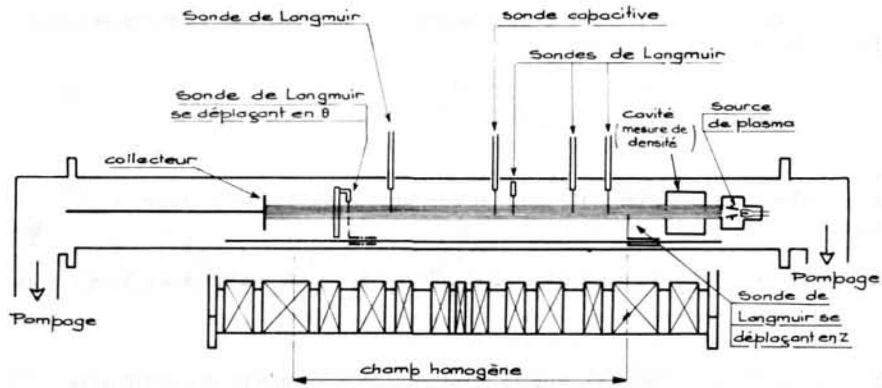

FIG. 1. Schéma de principe du dispositif expérimental EOS.

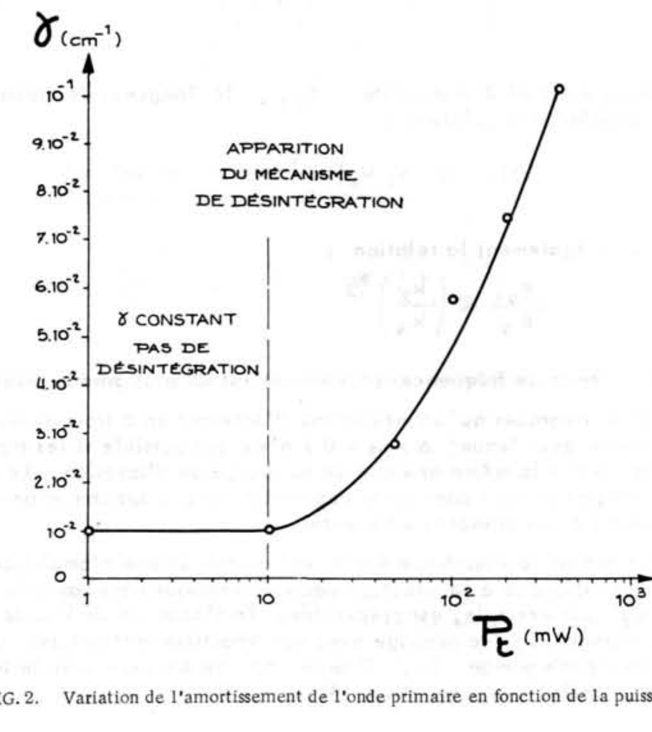

FIG. 2. Variation de l'amortissement de l'onde primaire en fonction de la puissance.

A - 3. Résultats Expérimentaux

Une onde plasma électronique est excitée dans le plasma à fréquence fixe à l'aide d'une sonde émettrice reliée à un oscillateur dont on fait varier la puissance. La variation de l'amplitude de l'onde est mesurée le long de la colonne de plasma à l'aide d'une sonde mobile. La Figure 2 montre que lorsque la puissance du générateur est suffisamment faible, le taux d'amortissement de l'onde reste constant et compatible avec la théorie de Landau.

Dans ce régime, les analyses de spectre montrent que l'onde reste monochromatique au cours de sa propagation. Au delà d'une valeur critique, le taux d'amortissement croît rapidement avec la puissance délivrée par le générateur. La Figure 3 représente une série de spectres relevés le long de l'axe, lorsque la puissance du générateur est supérieure à cette valeur critique.

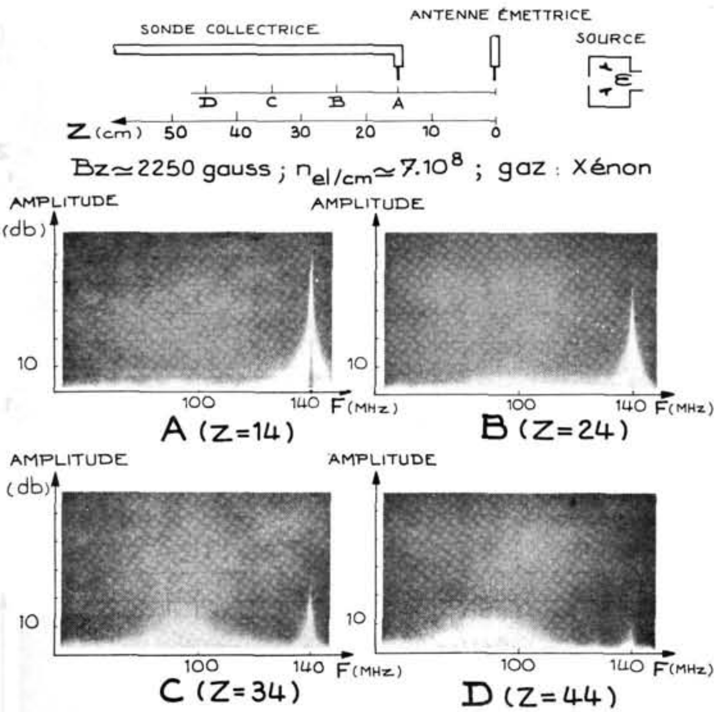

FIG. 3. Evolution le long de l'axe Z de l'onde primaire et du spectre de désintégration.

Sur ces spectres, on voit, d'une part *la raie correspondant à l'onde initiale* (ici 140 Mc/s) dont l'amplitude décroît rapidement le long de Z, et d'autre part on observe l'apparition d'un spectre de désintégration dans un domaine de fréquences inférieures à F_1.

Conditions de résonance

A l'aide de filtres accordables à bande étroite (5 à 10 % de la fréquence centrale), des paquets d'ondes *sont sélectionnés dans le spectre de désintégration et leur structure spatiale est explorée* par le déplacement de la sonde réceptrice.

La Figure 4 montre des exemples de mesures de longueur d'onde (obtenues par interférométrie avec un signal de référence donné par une sonde fixe) : la fréquence de l'onde primaire est 160 Mc/s et les fréquences des deux ondes conjuguées sélectionnées dans le spectre de désintégration sont 70 Mc/s et 90 Mc/s.

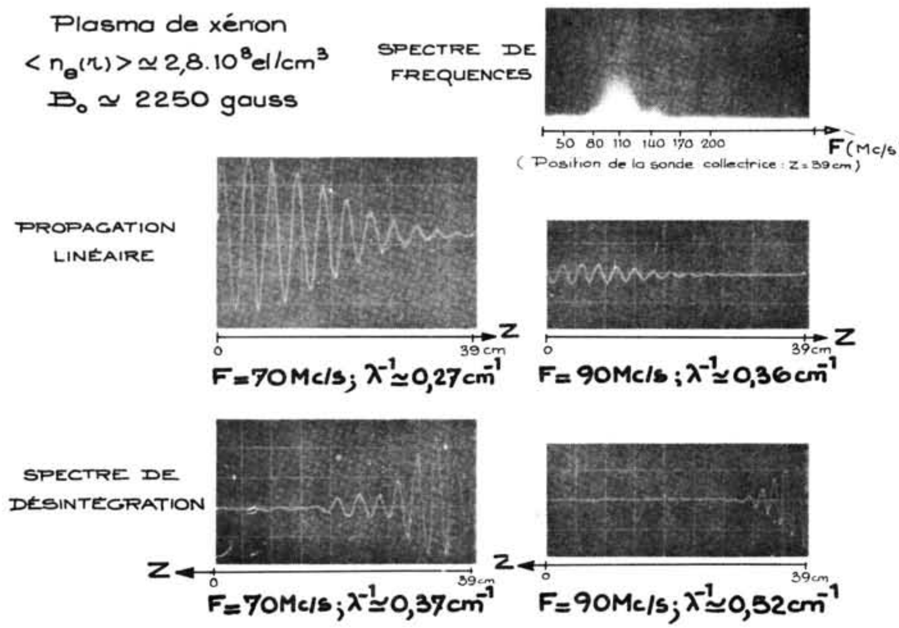

FIG. 4. Mesure de longueurs d'ondes longitudinales.

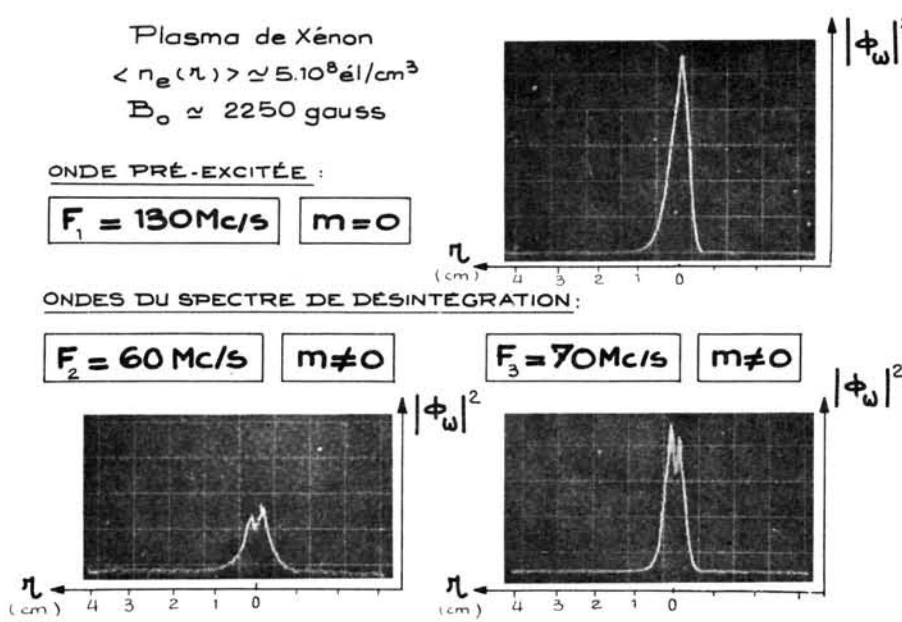

FIG. 5. Profil radial du potentiel fluctuant.

On constate que les ondes du spectre de désintégration ont des longueurs d'onde qui les placent sur des branches de la relation de dispersion différentes de l'onde qui se désintègre [8].

Une exploration radiale du potentiel oscillant à l'aide d'une sonde (Figure 5) permet de confirmer la présence de modes d'ordre plus élevé dans le spectre de désintégration. L'onde primaire de fréquence 130 Mc/s a un profil $|\phi_\omega|^2$ présentant un maximum sur l'axe (caractéristique d'un mode m = 0). Les profils $|\phi_\omega|^2$ des deux ondes de désintégration analysées à 60 Mc/s et 70 Mc/s présentent un creux sur l'axe (caractéristique de modes $m \neq 0$).

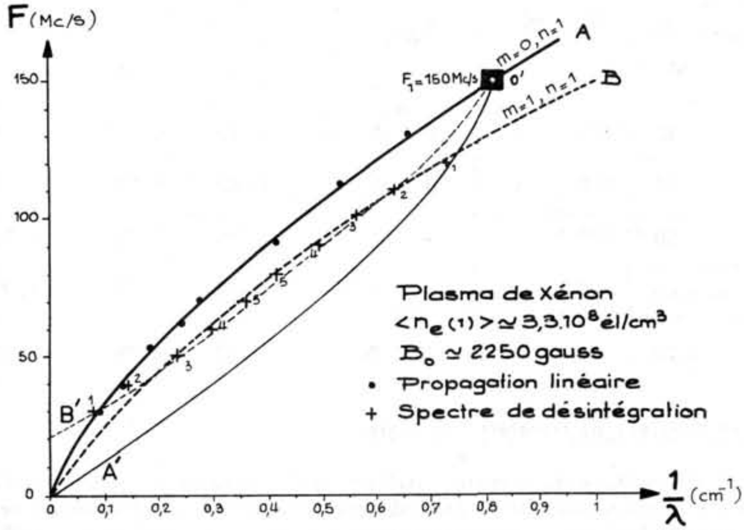

FIG. 6. Courbe de dispersion des ondes engendrées.

Pour vérifier les conditions de résonance sur les fréquences et sur les longueurs d'onde (équations 2), on utilise une méthode graphique représentée Figure 6. Les branches A et B sont les courbes de dispersion des modes (m = 0 ; n = 1) et (m = 1 ; n = 1) respectivement.

L'onde primaire dont on étudie la désintégration a pour fréquence F_1 = 150 Mc/s et sa structure spatiale correspond à un mode (m = 0 ; n = 1) dont le point représentatif O' est situé sur la branche A.

Il est simple de vérifier que les conditions de résonance ($\Delta k = 0$ dans les équations (2)) sont satisfaites aux points d'intersection des branches A et B avec les branches A' et B' déduites de A et B par une symétrie par rapport au point O, suivie d'une translation de vecteur $\overrightarrow{OO'}$.

Les mesures de longueurs d'onde dans le spectre de désintégration sont portées sur la même figure. On remarque que ces points se placent soit sur la branche A (m = 0 ; n = 1), soit sur la branche B (m = 1 ; n = 1).

Les grandeurs caractéristiques de chaque couple d'ondes conjuguées ($F_1 = F_2 + F_3$), repéré par un numéro sur la Figure 6, sont portées dans le tableau I. La dernière colonne de ce tableau indique le défaut de résonance. Celui-ci reste de l'ordre de quelques pour cent, ce qui constitue une vérification des relations de résonance.

TABLEAU I. GRANDEURS CARACTERISTIQUES DE CHAQUE COUPLE D'ONDES CONJUGUEES

$$\text{Onde primaire} \begin{cases} F_1 = 150\ \text{Mc/s} \\ \lambda_1^{-1} \simeq 0{,}80\ \text{cm}^{-1} \\ m_1 = 0 \end{cases}$$

Numéro du couple de fréquences conjuguées	Fréquences conjuguées F_2 Mc/s	F_3 Mc/s	Nombre d'onde azimutal m_2	m_3	Inverse de la longueur d'onde longitudinale λ_2^{-1} cm^{-1}	λ_3^{-1} cm^{-1}	Résultante $\lambda_2^{-1}+\lambda_3^{-1}$ cm^{-1}	Défaut de résonance $\frac{\Delta k}{k}$
1	30	120	0	0	0,083	0,73	0,813	1,3%
2	40	110	0	0	0,14	0,63	0,77	4 %
3	50	100	-	-	0, 23	0,56	0,79	1,3%
4	60	90	-	1	0,30	0,49	0,79	1,3%
5	70	80	1	1	0,36	0,42	0,78	2,5%

Seuil et longueur de transfert d'énergie

L'amplitude du potentiel oscillant a été mesurée en valeur absolue à l'aide d'une sonde capacitive préalablement étalonnée à la fréquence de travail. Les seuils d'instabilité ainsi mesurés sont en accord satisfaisant (30 % près) avec les valeurs théoriques déduites de la relation (5).

Les valeurs correspondantes du rapport de la densité oscillante à la densité moyenne sont de l'ordre de 10^{-3} à 10^{-2}.

On a porté sur la Figure 7 les taux de croissance spatiale des ondes de désintégration, pour différentes puissances P_t transmises à la sonde par le générateur. On a contrôlé que P_t est proportionnel à $|E_1|^2$, ce qui permet d'interpréter les résultats de la Figure 8 comme une vérification de la relation (6).

Amplification paramétrique

L'ensemble des résultats précédents semble confirmer la validité du modèle théorique décrivant la désintégration comme une superposition de processus indépendants d'interaction résonnante à trois ondes. Pour une amplitude A_1 de l'onde primaire, supérieure au seuil, l'amplification paramétrique d'une onde de fréquence F_2, préexcitée dans la bande de fréquences du spectre de désintégration, apporte une confirmation directe des hypothèses précédentes. Sur la Figure 9 ($A_1 \neq 0$) on voit émerger du spectre de désintégration les deux raies conjuguées de fréquences F_2 et $F_3 = F_1 - F_2$. Cette observation montre que parmi les modes excités directement à la fréquence F_2 existe celui dont la structure spatiale est compatible avec l'ensemble des conditions de résonance. Des mesures directes de longueur d'onde à la fréquence F_2 confirment que seul ce mode est amplifié.

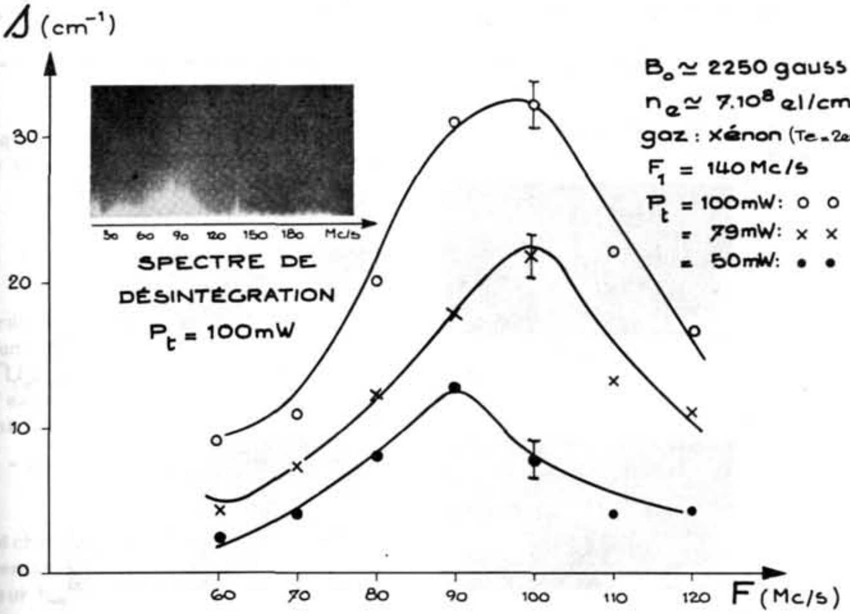

FIG. 7. Taux de croissance spatiale du spectre de désintégration pour differentes puissances de l'onde initiale F_1.

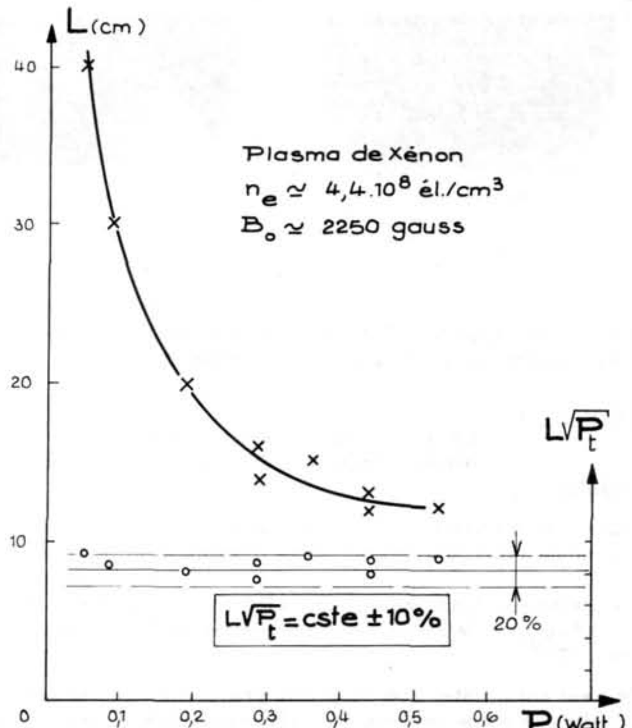

FIG. 8. Variation de la longueur de transfert d'énergie en fonction de la puissance transmise.

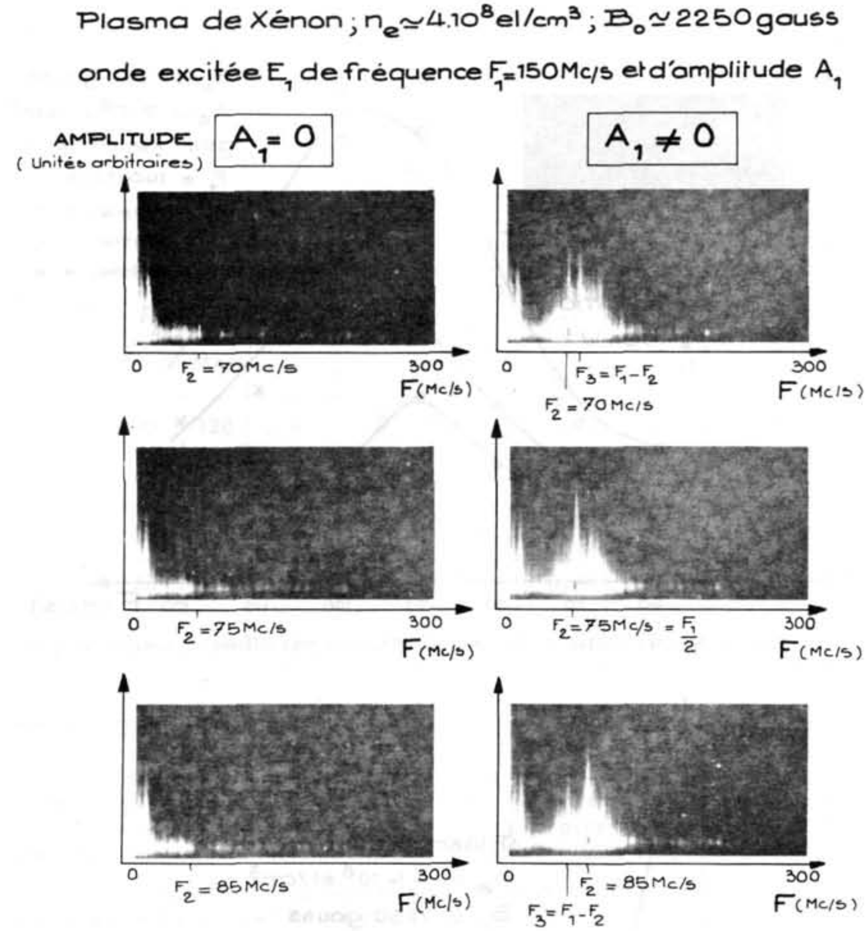

FIG. 9. Amplification paramétrique.

Les mesures du gain de l'amplification paramétrique vérifient la relation (7) et expliquent la forme du spectre de désintégration.

A - 4. Conclusions

La théorie de l'interaction non linéaire de trois ondes plasma électroniques a reçu une confirmation expérimentale satisfaisante.

On remarque également que l'amplification paramétrique a permis d'exciter des modes possédant une structure spatiale d'ordre élevé ($m \neq 0$; $n > 1$).

On constate qu'une onde plasma électronique peut être instable non linéairement même pour de très faibles amplitudes de l'oscillation (n_1/n_o de l'ordre de 10^{-3}).

On peut enfin noter que, malgré sa grande largeur, le spectre de désintégration, dans sa phase initiale de croissance, s'interprète sans faire appel à l'hypothèse des phases aléatoires.

B. GENERATION NON LINEAIRE D'UNE ONDE ELECTROMAGNETIQUE

B-1. Introduction

On envoie deux faisceaux d'ondes électromagnétiques dans un plasma, perpendiculairement au champ magnétique de confinement. On étudie l'interaction non linéaire qui se produit dans le volume de plasma commun aux deux faisceaux, dans les deux cas suivants :

- Interaction non linéaire d'une onde ordinaire O et d'une onde extraordinaire X.
- Interaction non linéaire de deux ondes ordinaires.

La théorie faite en plasma froid [10] prévoit la création d'une onde ordinaire dans le premier cas (XO , O') et celle d'une onde extraordinaire dans le second cas (OO', X). On a montré, à l'aide de la théorie cinétique [11] décrivant correctement les effets thermiques, que pour le plasma de l'expérience considérée ($T_e \sim$ quelques eV), la théorie en plasma froid est justifiée.

B - 2. Dispositif expérimental

La Figure 10 représente la section de mesures. Le plasma est un plasma d'Argon formé par une décharge haute fréquence ($F = 20$ MHz ; $P \lesssim 800$ Watts) permanente. La densité électronique, contôlée par le débit de gaz ou la puissance du générateur Haute Fréquence, est comprise entre 10^9 électrons/cm^3 et quelques 10^{11}.

Un faisceau de micro-ondes, de faible puissance, focalisé, de fréquence comprise entre 8 GHz et 13 GHz et polarisé selon le mode extraordinaire permet de mesurer le profil de densité du plasma.

Le champ magnétique de confinement ($B_o \leqslant 6 \times 10^3$ Gauss) est homogène à 1 % le long de l'axe, mais varie de 10 % sur le diamètre du plasma ($\sim$ 10 cm).

Les deux faisceaux micro-ondes sont produits, l'un par un klystron de fréquence fixe ($F_1 = 8{,}8$ GHz ; $P \leqslant 6$ Watts), l'autre par un klystron de fréquence variable suivi d'un T.O.P. (CSF , F 4 056) délivrant une puissance de 6 Watts à 8 GHz et de 2 Watts à 10 GHz. Des lentilles convergentes de Téflon concentrent la puissance des deux faisceaux sur des diamètres respectifs de 4 et 7 cm (à 3 db). Dans toutes les expériences, l'angle Θ_{12} entre les deux faisceaux est de 45 degrés.

L'onde électromagnétique de fréquence $F_3 = F_1 + F_2$ créée par interaction non linéaire est détectée par un cornet récepteur, dont l'axe peut être déplacé angulairement afin de mesurer la direction d'émission. Le guide reliant le cornet au récepteur est adapté à la fréquence F_3 et sert en même temps de filtre pour éliminer les ondes primaires. On utilise un récepteur superhétérodyne suivi d'un amplificateur sélectif ($F = 10^3$ Hz), l'une des deux sources étant modulée à cette fréquence. La puissance minimum détectable de l'ensemble est de 2×10^{-12} Watts.

B-3. Interaction d'une onde extraordinaire de fréquence F_x et d'une onde ordinaire de fréquence F_o : (XO , O')

La Figure 11 a représente un exemple d'enregistrement de la puissance émise à fréquence $F_x + F_o$; ($F_x = 8{,}8$ GHz et $F_o = 8{,}6$ GHz), lorsqu'on fait varier l'intensité du champ magnétique mesurée par β ($\beta = F_c/F_x$ où F_c est la fréquence cyclotronique électronique). On

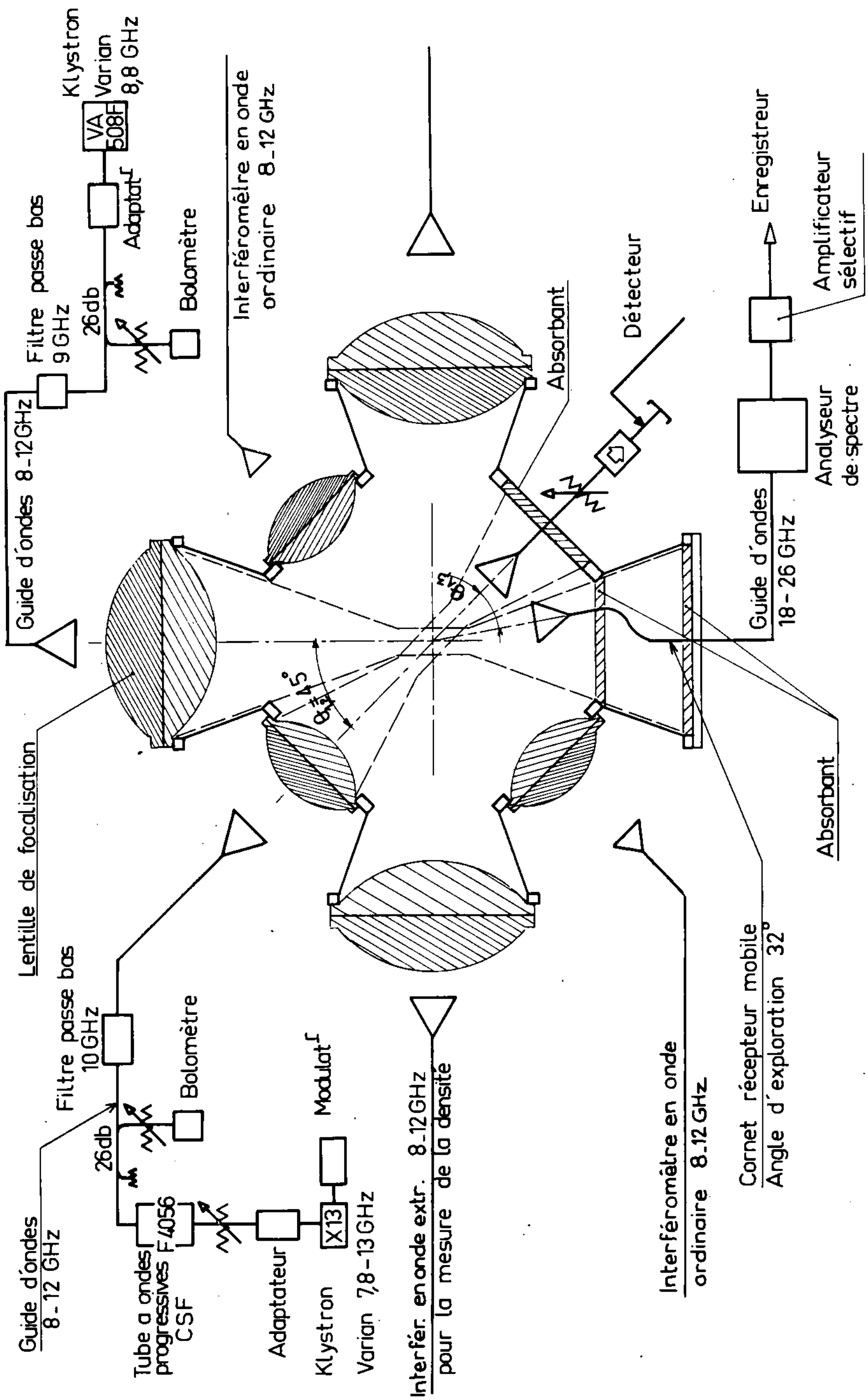

FIG. 10. Section de mesure.

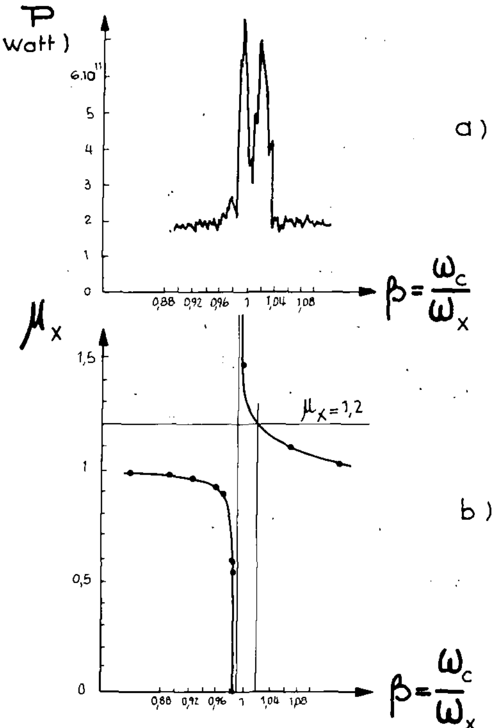

FIG. 11. Interaction (X0, 0') — Puissance (a) et μ_X (b) en fonction de β.

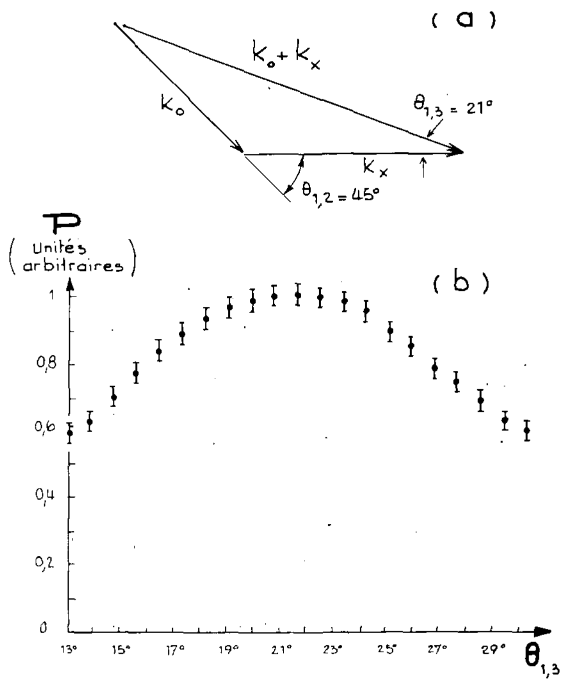

FIG. 12. Puissance en fonction de $\theta_{1,3}$.

remarque la présence de deux pics d'émission (de 2 à 3 % de largeur et dont les maximas peuvent être repérés avec une précision de l'ordre de 10^{-3}). On mesure la direction de l'émission en se calant sur l'un des pics et en déplaçant angulairement le cornet récepteur. L'émission présente un maximum pour $\theta = 21°$ avec une largeur à mi-hauteur d'environ 20° (Fig. 12b). Connaissant les angles θ_{12} et θ_{13} il est possible de construire le triangle de résonance entre les vecteurs d'onde (Fig. 12a). Les modules des vecteurs $\vec{k}_o$ et $\vec{k}_x$ sont déduits de mesures par interférométrie du déphasage subi par chacune des deux ondes primaires (X , O) lors de la traversée du plasma. La Figure 11b représente un exemple de la variation de l'indice μ_x de l'onde extraordinaire, déduit d'une telle mesure.

La Figure 12a montre que la règle de sélection des vecteurs d'onde $\vec{k}_{o'} = \vec{k}_x + \vec{k}_o$ est bien vérifiée dans la limite de précision des mesures (± 2 % pour l'amplitude des k , ± 5 % pour l'angle θ_{13} correspondant au maximum de la courbe de la Figure 12b).

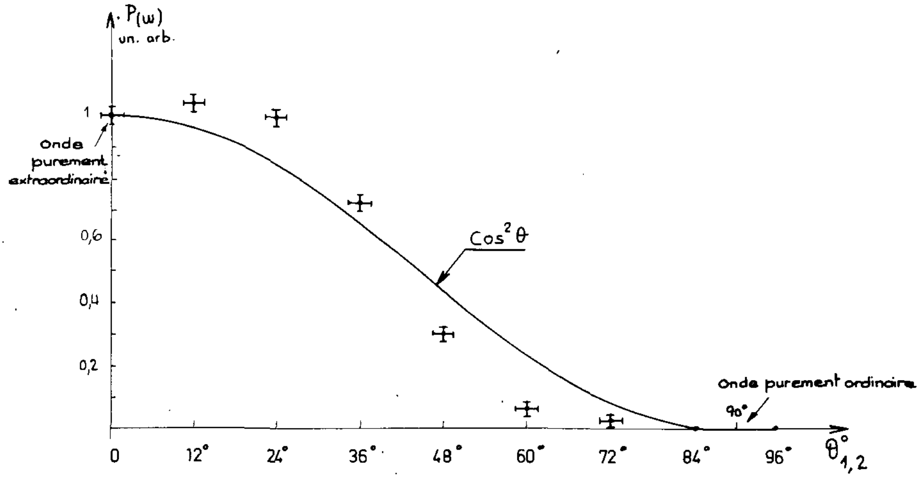

FIG. 13. Puissance de l'onde secondaire en fonction de la polarisation de l'une des deux ondes primaires.

On vérifie successivement deux propriétés de l'interaction étudiée :

a) La relation entre les polarisations des trois ondes

La Figure 13 représente la puissance de l'onde engendrée, polarisée suivant le mode ordinaire, lorsqu'on fait tourner la direction de polarisation de l'une des ondes primaires, tous les autres paramètres restant fixes. On observe une puissance maximale lorsque l'une des ondes primaires est ordinaire et l'autre extraordinaire ; cette puissance s'annule lorsque les deux ondes sont ordinaires ce qui vérifie la règle (XO , O').

b) Le coefficient d'interaction

Conformément aux notations de l'étude théorique [10], l'intensité du vecteur de Poynting de l'onde engendrée est reliée aux intensités S_1 et S_2 des deux ondes incidentes par le facteur sans dimension :

$$Q = \frac{2}{\pi} \left(\frac{m}{e}\right)^2 \frac{c^5}{R_o^2} \frac{S_3}{S_1 S_2}$$

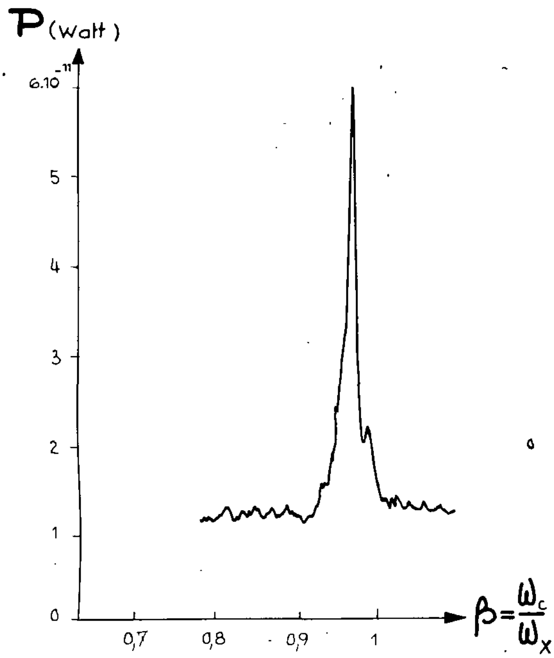

FIG. 14. Interaction (00', X) - Puissance de l'onde secondaire en fonction du champ magnétique.

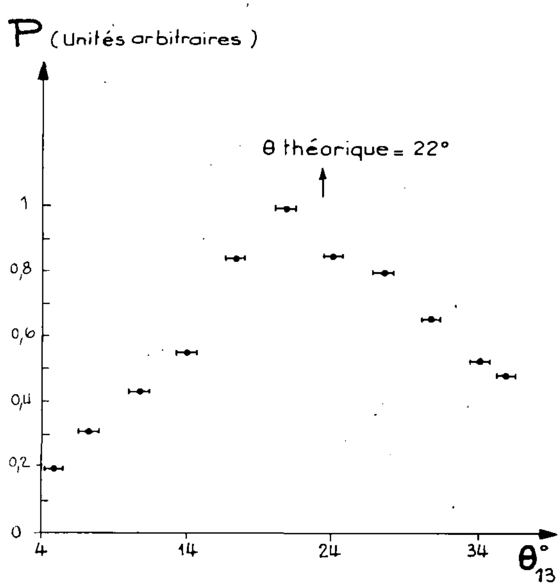

FIG. 15. Interaction (00', X) - Variation de la puissance de l'onde secondaire en fonction de l'angle de sortie.

où R_0 est la longueur moyenne d'interaction. On mesure directement les puissances transportées par chacune des trois ondes, ce qui permet de déduire des valeurs expérimentales de Q. Ces valeurs sont en accord, à un facteur 2 près, avec celles déduites de la théorie [10].

B - 4. Interaction de deux ondes ordinaires (OO', X)

Les deux faisceaux incidents sont polarisés selon le mode ordinaire. La Figure 14 représente un exemple d'enregistrement de la puissance émise dans le mode extraordinaire en fonction de l'intensité de champ magnétique (on remarque la présence d'un pic principal et d'un pic secondaire dans la plupart des résultats). La mesure de la répartition angulaire de la puissance émise (Fig. 15) met en évidence un maximum au voisinage de la valeur $\theta_{13} = 22°$ prévue par le calcul.

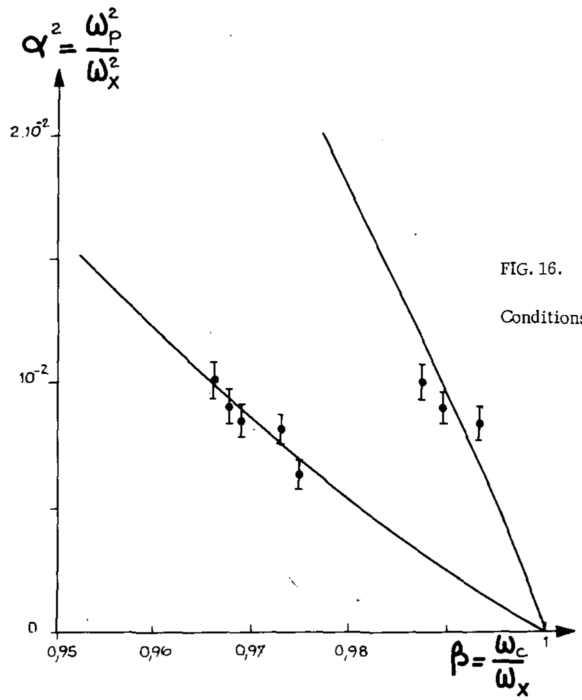

FIG. 16. Interaction (00', X)

Conditions de résonance: $\begin{cases} \omega_X = \omega_0 + \omega_0' \\ \vec{k}_X = \vec{k}_0 + \vec{k}_0' \end{cases}$

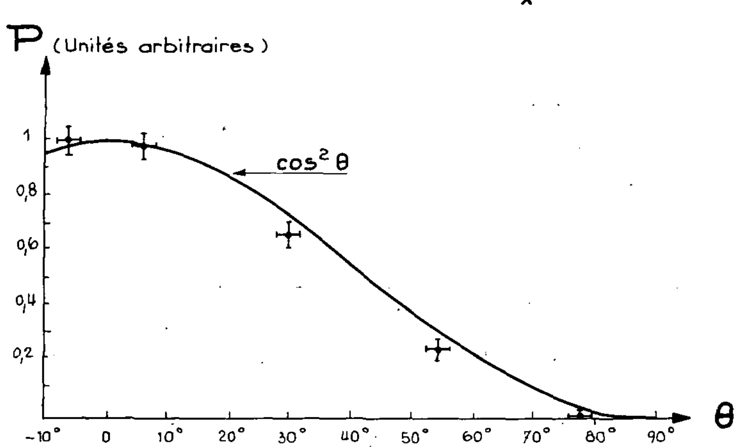

FIG. 17. Interaction (00', X) - Puissance de l'onde secondaire en fonction de la polarisation d'une des deux ondes primaires.

Pour des valeurs fixes de θ_{12} (θ_{12} = 45°) et de θ_{13}(θ_{13} = 22°), les conditions de résonance sont vérifiées analytiquement dans le plan (α^2,β) sur les deux branches de courbes représentées en trait plein Figure 16 ($\alpha = \omega_p / \omega_x$; $\beta = \omega_c / \omega_x$). Les points correspondent aux deux pics relevés sur des enregistrements analogues à celui de la Figure 14. Les mesures de α sont faites par interférométrie avec le faisceau auxiliaire d'ondes extraordinaires en transmission et en réflexion /13/. Les propriétés de la matrice d'interaction (polarisations, coefficient d'interaction) ont été également vérifiées. La Figure 17 représente la variation de la puissance reçue dans le mode extraordinaire lorsqu'on fait tourner la direction de la polarisation de l'une des deux ondes incidentes. On constate que la puissance est maximale lorsque ces deux ondes sont ordinaires (θ = 0) et nulle lorsque l'une des deux est extraordinaire (θ = 90°). Ce qui vérifie la règle (OO' , X).

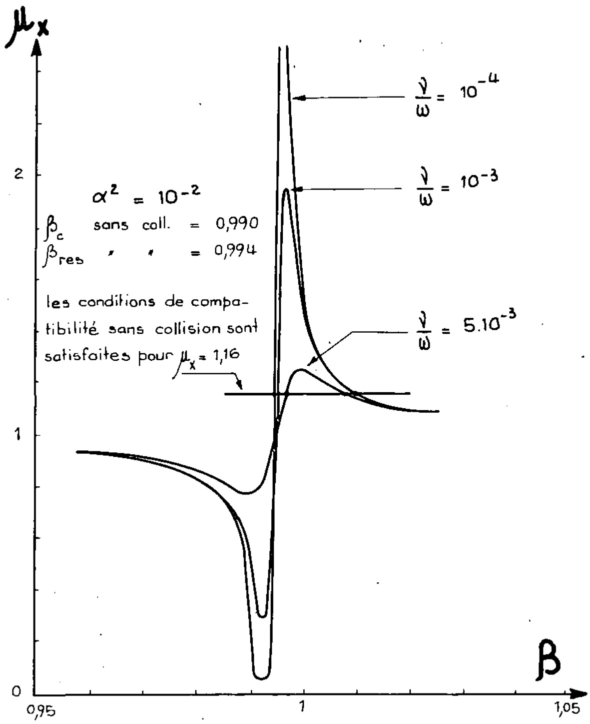

FIG. 18. μ_X en fonction de β.

Le coefficient d'interaction défini au paragraphe B-3 a été mesuré et se trouve dans tous les cas en accord , à un facteur 2 près, avec la valeur théorique.

B-5. Discussion des résultats et Conclusion

Dans les deux cas d'interaction étudiés (X O, O') et (OO', X) , on observe l'apparition de deux pics d'émission à des valeurs très voisines de $\beta = \omega_c / \omega_x$. Dans un modèle de plasma "froid", non collisionnel, la branche asymptotique de l'indice μ_x de l'onde extraordinaire permet de prévoir l'un des deux pics (Fig. 11 b). Si l'on tient compte des collisions (les fréquences de collisions électron-ion et électron-neutre sont de l'ordre de 10^{-3} fois les fréquences étudiées), la discontinuité de l'indice μ_x à la fréquence hybride haute est remplacée par une branche continue (Fig.18). Cette branche rend possible l'apparition d'un second pic d'émission, compatible avec les résultats expérimentaux (Fig. 11 a et 14). Cette explication est celle actuellement proposée pour interpréter le dédoublement du pic d'émission.

La vérification de la condition de résonance, c'est-à-dire, la fermeture du triangle ($\vec{k}_1$, $\vec{k}_2$, $\vec{k}_3$) nécessite un certain nombre de commentaires :

. L'angle θ_{13} correspond au maximum des pics d'émission (Fig. 12b et 15) est en très bon accord (± 1 %) avec la valeur permettant la fermeture du triangle de résonance dans un milieu homogène.

Pour expliquer la largeur angulaire des pics d'émission, on peut remarquer que :

Les profils radiaux de densité et de champ magnétique entraînent une variation des indices de propagation dans la région d'interaction.

Le nombre de demi-longeurs d'onde des faisceaux primaires à l'intérieur de la colonne de plasma est faible (entre trois et six).

La région d'interaction est relativement proche (de l'ordre de 10 cm) du cornet récepteur et les Figures 12b et 15 ne sont donc pas à proprement parler des diagrammes de rayonnement.

En conclusion, malgré certaines difficultés expérimentales que nous venons de souligner, les résultats exposés mettent en évidence la création d'une onde électromagnétique par interaction non linéaire résonnante de deux ondes électromagnétiques. Les relations entre les polarisations des trois ondes ont été très bien vérifiées et l'ordre de grandeur des coefficients d'interaction mesurés est en accord avec les résultats théoriques.

REFERENCES

[1] PERULLI M. - Thèse de Doctorat d'Etat, Faculté des Sciences de Paris, Juillet 1968.

[2] STERN R.A., TZOAR N. - Phys. Review Letters 17, 903 (1966).

[3] MESSIAN A.M., VANDENPLAS P.E. - Phys. Letters 25 A n° 4, 339 (1967).

[4] CONSTANTIN A., LEPRINCE P., POINTU A.M., POMEAU Y., Journal de Physique, supt. n° 4, Avril 1968.

[5] HIROE S., IKEGAMI H. - Rapport Nagoya IPPJ 60, Nov. 1967.

[6] FEDORCHENKO V.D., MURATOV V.I., RUTKEVITCH B.N. - Nuclear Fusion, vol. 8 n° 1, April 1968.

[7] ETIEVANT C., FIDONE I., LAVAL G., OLIVAIN J., PELLAT R., PERULLI M. - C.R. Acad. Sc. de Paris T. 263, 19-21 Juillet 1966.

[8] PERULLI M., LAVAL G., PELLAT R. - C.R. Acad. Sc. de Paris, à paraître.

[9] PERULLI M., LAVAL G., PELLAT R. - C.R. Acad. Sc. de Paris, à paraître.

[10] ETIEVANT C., FIDONE I., OSSAKOW S., OZIZMIR E., SU C. - MATT-566, Jan. 1968, à paraître dans Phys. Fluids.

[11] CANO R., ETIEVANT C., FIDONE I., GRANATA G. - Rapport EUR-CEA-FC 478 (1968).

[12] LEIBA E. - C.R. VIIIème Conf. Phenomena in Ionized Gases, Vienna, Sept. 1967, 402.

[13] TULLE P.A., ZANFAGNA B. - C.R. Acad. Sc. de Paris, à paraître.

DISCUSSION

V.N. TSYTOVICH: Theory usually predicts the effects of non-linear wave phase variations in decay interactions. Have you measured the phase relations of the waves during their interaction?

C. ETIEVANT: The measurement you propose is very difficult to make owing to the presence of plasma density fluctuations, which themselves result in phase variations. For this reason we have not been able to perform this measurement.

RELATION DE DISPERSION DES FLUCTUATIONS DEDUITE DES MESURES DE FONCTIONS DE CORRELATION CARACTERISTIQUES DE LA DIFFUSION TURBULENTE D'UN PLASMA D'HYDROGENE

M. BERNARD, G. BRIFFOD, R. FRANK, M. GREGOIRE ET J. WEISSE
CEA, CENTRE D'ETUDES NUCLEAIRES DE SACLAY, FRANCE

Abstract — Résumé

FLUCTUATION DISPERSION RELATION DEDUCED FROM CORRELATION FUNCTION MEASUREMENTS: CHARACTERISTICS OF THE TURBULENT DIFFUSION OF A HYDROGEN PLASMA. The fluctuations present in the plasma column obtained by diffusion in the DAPHNIS experiment are characterized by a continuous frequency spectrum similar to a noise spectrum whose cut-off frequency is much lower than the gyromagnetic frequency of the ions. To identify the instabilities causing these fluctuations, and to determine their role in the turbulent diffusion of the plasma, one has to use correlation methods. The authors have measured correlation functions of the type

$$C_{xy}(\tau, r, \theta, z) = \frac{1}{T}\int_0^T X(t,0,0,0)Y(t+\tau, r, \theta, z)\,dt$$

where x and y may be respectively, the fluctuating density, the fluctuating floating potential or the fluctuating field.

From a knowledge of these functions it is possible to deduce: (a) Correlation times τ_c and lengths ℓ_c, which are quantities characteristic of the turbulence; (b) The energy spectrum of the fluctuations; (c) The experimental dispersion relation of the instabilities; (d) The values of the fluxes $\langle nv_r\rangle = \left\langle n\frac{E_\theta}{B_0}\right\rangle$ indicating turbulent diffusion.

Examination of the dispersion relations reveals a number of points that are in agreement with the theory of drift instabilities. In particular, propagation is essentially azimuthal ($k_\perp/k_\parallel \gg 1$) and the dependence $\omega(k)$ is linear, corresponding to a phase velocity of the same order of magnitude as the electron drift velocities. It should also be noted that most of the energy of the fluctuations is localized in the modes m = 1, 2, 3 and that increases in the applied magnetic field transfer this energy to modes of an increasingly high order.

The values of the fluxes $\left\langle n\frac{E_\theta}{B_0}\right\rangle$ have to be compared with values which were obtained earlier by average measurements of density gradient and flux (by means of Langmuir probes and plasma eaters); these indicated diffusion ten times less than Bohm diffusion. The diffusion coefficients deduced from the correlation times, $D_\perp = \langle E_\theta^2\rangle\tau_c/B_0^2$, are also compared with those obtained earlier.

The authors are extending these results to higher magnetic field and density values, and studying the effect of magnetic shear on the reduction of these fluctuations and the resulting turbulent diffusion.

RELATION DE DISPERSION DES FLUCTUATIONS DEDUITE DES MESURES DE FONCTIONS DE CORRELATION - CARACTERISTIQUES DE LA DIFFUSION TURBULENTE D'UN PLASMA D'HYDROGENE. Les fluctuations présentes dans la colonne de plasma obtenue par diffusion dans l'expérience DAPHNIS sont caractérisées par un spectre continu de fréquences analogue à celui d'un bruit dont la fréquence de coupure est très inférieure à la fréquence gyromagnétique des ions. Afin d'identifier les instabilités qui sont à l'origine de ces fluctuations et de préciser leur rôle dans la diffusion turbulente du plasma, il faut faire appel à des méthodes de corrélation. Les auteurs ont mesuré des fonctions de corrélation du type

$$C_{xy}(\tau, r, \theta, z) = \frac{1}{T}\int_0^T X(t,0,0,0)\,Y(t+\tau, r, \theta, z)\,dt$$

où x et y peuvent être la densité, le potentiel flottant ou le champ électrique fluctuant.

De la connaissance de ces fonctions, ils ont pu déduire a) des temps τ_C et des longueurs ℓ_C de corrélation, grandeurs caractéristiques de la turbulence; b) le spectre d'énergie des fluctuations; c) la relation de dispersion expérimentale des instabilités; d) les valeurs des flux $\langle n v_r \rangle = \left\langle n \frac{E_\theta}{B_0} \right\rangle$ significatives de la diffusion turbulente.

L'examen des relations de dispersion fait apparaître un certain nombre de points conformes à la théorie des instabilités de dérive. En particulier, la propagation est essentiellement azimutale ($k_\perp/k_\parallel \gg 1$) et la dépendance $\omega(k)$ est linéaire, correspondant à une vitesse de phase de l'ordre des vitesses de dérive électroniques. Il est à noter également que la plus grande partie de l'énergie des fluctuations est localisée dans les modes m = 1, 2, 3 et que l'augmentation du champ magnétique appliqué transfère cette énergie à des modes d'ordre de plus en plus élevé.

Les valeurs des flux $\left\langle n \frac{E_\theta}{B_0} \right\rangle$ sont à comparer à des valeurs précédemment obtenues par des mesures moyennes de gradient de densité et de flux (au moyen de sondes de Langmuir et de plasma-eater) et qui avaient mis en évidence une diffusion dix fois inférieure à celle de Bohm. On comparera aussi les coefficients de diffusion déduits des temps de corrélation $D_\perp = \langle E_\theta^2 \rangle \tau_C/B_0^2$, à ceux qui ont été obtenues précédemment.

Une extension de ces résultats à des valeurs de champ magnétique et de densité plus élevées est en cours, ainsi que l'étude de l'effet du cisaillement magnétique sur la réduction de ces fluctuations et de la diffusion turbulente qui en résulte.

Dans les études de la diffusion des particules à travers les lignes du champ magnétique, le problème essentiel est celui de la relation entre les fluctuations et les pertes de particules. Dans les plasmas turbulents où les grandeurs fluctuantes se présentent sous la forme d'un bruit à large bande, l'identification des fluctuations qui sont à l'origine des mécanismes de pertes est très difficile à partir de la seule connaissance de leur spectre de fréquence. Pour essayer de mesurer des grandeurs physiques qui permettent à la fois de caractériser les fluctuations observées et de les relier aux pertes de particules, nous avons développé des méthodes fondées sur les propriétés des fonctions de corrélation. A partir des mesures des fonctions d'auto et d'intercorrélation des variables fluctuantes, il est possible de définir les fluctuations par des caractéristiques précises telles que : la densité spectrale d'énergie du bruit, les temps et longueur de corrélation, la relation de dispersion D (ω, k), et de relier ces caractéristiques au coefficient de diffusion.

Dans le présent travail, nous avons utilisé ces méthodes pour l'étude des fluctuations à basse fréquence observées dans le plasma de diffusion obtenu dans l'expérience "Daphnis". Il existe plusieurs mécanismes d'instabilité susceptibles de donner naissance aux fluctuations observées. Les conditions expérimentales qui seront précisées dans la première partie ont été choisies de façon à éviter les instabilités dues à la courbure des lignes de champ magnétique, à la présence d'un courant ou d'électrons rapides le long des lignes de champ.

Dans la deuxième partie, nous présenterons les résultats obtenus à partir des méthodes de corrélation pour caractériser et identifier les fluctuations. Certains de ces résultats, en particulier la variation radiale de l'amplitude des modes, la relation de dispersion azimutale linéaire, soulignent l'importance des effets liés aux vitesses de dérive.

Dans la troisième partie, nous donnerons les résultats des mesures des pertes radiales. Le coefficient de diffusion défini à partir des caractéristiques des fluctuations $D = \left(\langle E_\theta^2 \rangle / B^2\right) \tau_c$ rend bien compte des pertes observées et mesurées par d'autres méthodes.

1. CONDITIONS EXPERIMENTALES

1.1. Description de l'expérience "Daphnis" (fig. 1)

L'expérience "Daphnis" a déjà été décrite précédemment /1/, nous ne rappellerons donc que les conditions expérimentales nécessaires à la discussion de l'étude qui suit.

Le gaz neutre est introduit à l'une des extrémités de l'expérience dans une source coaxiale à cathode chaude où il est ionisé. Le plasma d'hydrogène ainsi produit diffuse le long des lignes de champ magnétique B et se recombine à l'autre extrémité de l'enceinte. Comme le plasma

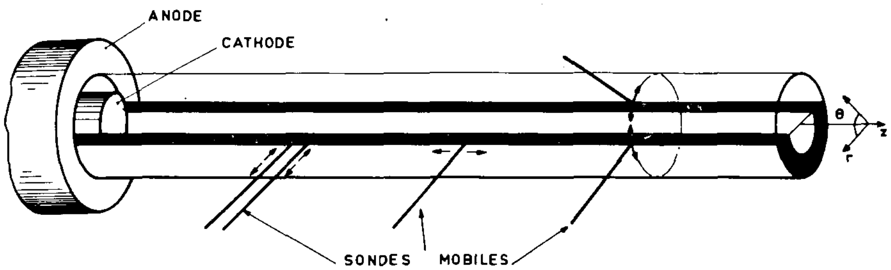

Pression de travail	:	5.10^{-4}	—	5.10^{-3}	. torr
B_z uniforme	:	0	—	3000	. gauss
Densité n	:	10^{11}	—	10^{12}	. cm^{-3}

FIG. 1. Schéma de principe de l'expérience.

diffuse, le courant macroscopique, le long des lignes de champ, est nul, ce qui permet d'éviter les instabilités dues à la présence d'un courant parallèle à B. Le champ magnétique est uniforme dans tout le volume pour éliminer les effets de courbure qui peuvent donner naissance à des instabilités en "flûte" et donc à des pertes de particules par convection. Les conditions d'ionisation du gaz neutre dans la source ont été particulièrement soignées, de façon à obtenir un plasma homogène et le minimum d'électrons rapides dans la région de diffusion. Les mesures sont faites à environ un mètre de la source dans une enceinte équipée de sondes réglables dans les trois directions.

1.2. Caractéristiques du plasma de diffusion

Dans les conditions de fonctionnement normales citées ci-dessus, les caractéristiques du plasma sont les suivantes : pression dans la chambre de mesure 5.10^{-3} - 10^{-4} Torr, densité 5.10^{10} - 5.10^{12} $e.cm^{-3}$, champ magnétique 0-3 kG, température électronique 2-15 eV, température ionique 0,5 eV.

Nous avons représenté sur la fig. 2 une variation typique de la densité en fonction du rayon. La position radiale du maximum de densité est fixée par le diamètre des électrodes coaxiales de la source. Ce paramètre

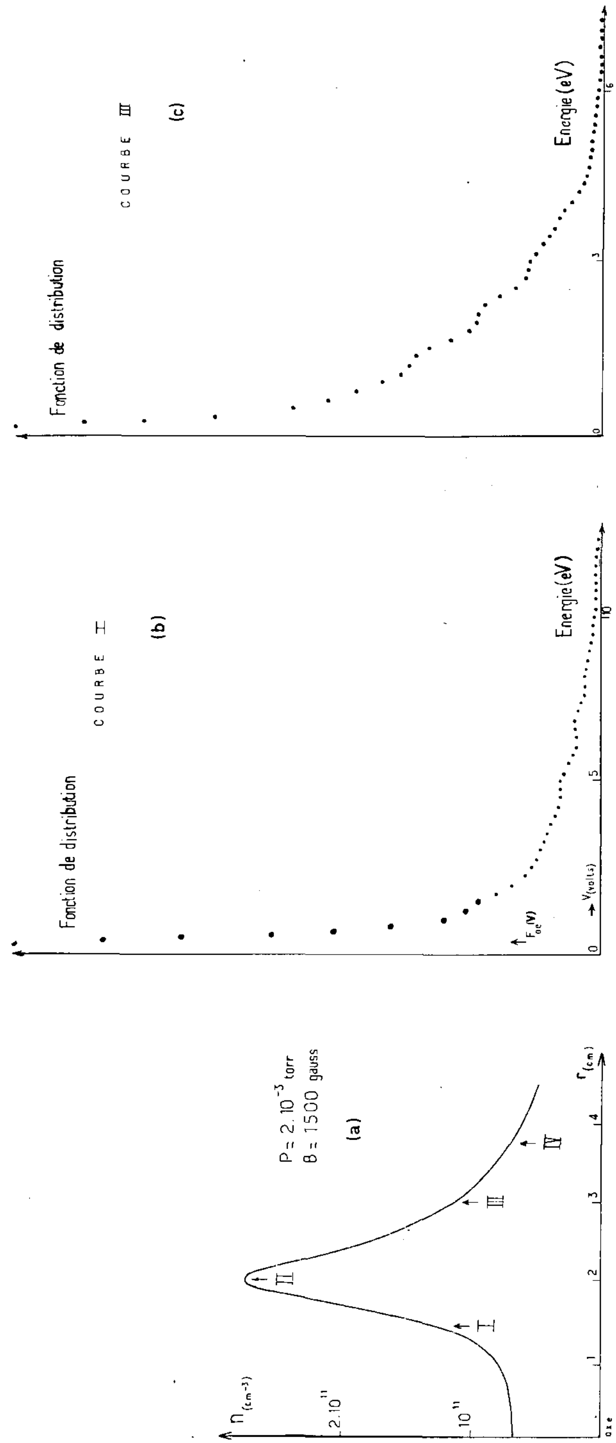
Fonction de distribution
COURBE III
(c)
Energie (eV)
Fonction de distribution
COURBE I
(b)
Energie (eV)
P = 2.10^-3 torr
B = 1500 gauss
(a)
I
II
III
IV
2.10^11
10^11
axe

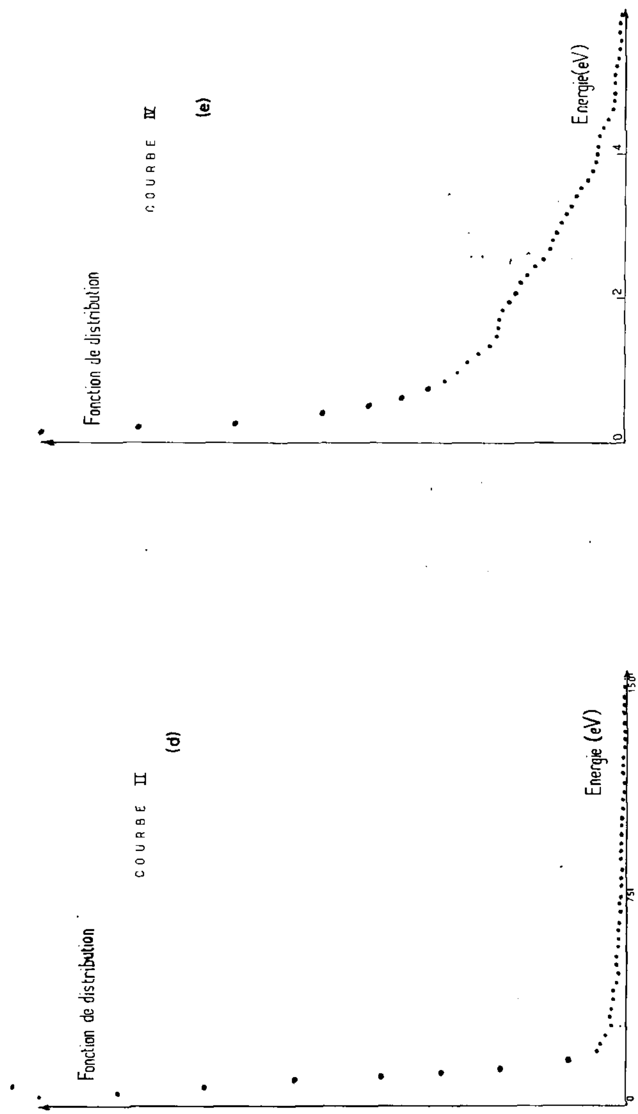

FIG. 2. Mesure de la fonction de distribution en énergie en fonction du rayon.

géométrique réglable est important car il permet de définir deux régions dans le plasma :

- la région extérieure de la colonne où le gradient de densité est négatif $\nabla n < 0$ et dans laquelle les forces de pression et centrifuge sont de même sens $-\nabla p \cdot \frac{v^2}{R} > 0$
- la région intérieure de la colonne où le gradient de densité est positif $\nabla n > 0$ et les forces précédentes de signe opposé. Dans cette partie du plasma les instabilités en "flûte" dues à la force centrifuge $\frac{Mv^2}{R} \sim \frac{ME^2}{B^2}\frac{1}{R}$ ne peuvent pas se développer /2/.

La forme de la fonction de distribution des vitesses électroniques $F_0(v)$ est une caractéristique très importante du plasma. Nous l'avons mesurée à l'aide d'une sonde à séparation électrostatique spécialement conçue à cet effet /3/. La variation de $F_0(v)$ dans la direction radiale est donnée sur la fig. 2. On peut remarquer que $F_0(v)$ est toujours monotone, ce qui exclut la possibilité d'exciter des instabilités liées à un excès d'électrons rapides.

2. IDENTIFICATION DES FLUCTUATIONS

Pour les conditions expérimentales précédentes, le plasma de diffusion obtenu est le siège de fluctuations à basse fréquence $\omega < \omega_{ci}$. Ces fluctuations sont caractérisées par un spectre de fréquences continu à large bande. A partir de la seule connaissance de ce spectre, il n'est pas possible d'identifier les instabilités qui sont à l'origine des fluctuations observées. Pour cette raison, nous avons développé des méthodes de corrélation.

2. 1. Etudes des fluctuations par la méthode des fonctions de corrélation

Soit $X(t,\ell)$ une variable aléatoire stationnaire, sa fonction d'auto-corrélation s'écrit :

$$C_{\ell\ell}(\tau) = \frac{1}{T}\int_0^T X(t,\ell)\, X(t+\tau,\ell)\, dt$$

La fonction d'auto-corrélation $C(\tau)$ admet pour transformée de Fourier la fonction $G(\omega)$ représentant la densité spectrale d'énergie (théorème de Wiener-Khintchine)

$$G(\omega) = \int_0^\infty C(\tau) \cos \omega\tau \, d\tau$$

Ce résultat classique fournit une méthode expérimentale précise pour atteindre le spectre de puissance des fluctuations $G(\omega)$ à partir de la mesure des fonctions d'auto-corrélation et le calcul de leur transformée de Fourier /4/. Cette relation n'utilise que l'hypothèse de stationnarité.

La fonction d'intercorrélation $C(\tau,\lambda)$ de la variable mesurée en deux points distants de λ et sa transformée de Fourier $G'(\omega)$ s'écrivent :

$$C_{\ell,\ell+\lambda} = \frac{1}{T}\int_0^T X(t,\ell)\cdot X(t+\tau,\ell+\lambda)\, dt \quad ; \quad G'(\omega) = \int_0^\infty C_{\ell,\ell+\lambda}\, e^{i\omega\tau} d\tau$$

Considérons la variable $X(t,\ell)$ comme une somme d'ondes planes se propageant dans le plasma

$$X(t,\ell) = \int_0^{\infty} A(\omega)\, e^{ik(\omega)\ell} \cdot e^{i\omega t}\, d\omega$$

Dans ce cas $G'(\omega)$ se met sous la forme :

$$G'(\omega) = G(\omega)\, e^{ik(\omega)\lambda}$$

ce qui entraîne que $G'(\omega)$ a pour module le spectre d'énergie défini précédemment et pour argument la fonction $k(\omega)\,\lambda$. Expérimentalement la mesure de la fonction d'intercorrélation $C_{\ell,\ell+\lambda}$ et le calcul de sa transformée de Fourier permettra donc :

- de vérifier l'hypothèse de la propagation si $|G'(\omega)| = G(\omega)$
- d'atteindre la fonction $k(\omega)\,\lambda$ dont on déduit la relation de dispersion.

Les grandeurs fluctuantes sont mesurées à l'aide de sondes électrostatiques déplaçables dans les trois directions r, θ, z. Les fonctions d'auto et d'intercorrélation sont données par un corrélateur multicanal travaillant en temps réel et dont la bande passante est de 400 kHz. /5/ . Ces fonctions sont définies par 159 points, c'est-à-dire 159 valeurs discrètes de la variable τ. La valeur minimum de l'échelon élémentaire $\Delta\tau$ est de 0,5 μs. Les données numériques fournies par le corrélateur sont traduites sur bandes perforées. L'analyse de Fourier des fonctions de corrélation est effectuée à l'aide d'un calculateur digital. La précision de cette transformation, c'est-à-dire la précision obtenue sur le spectre de Fourier, dépend du nombre de points qui définissent les fonctions de corrélation. Nous avons pu l'augmenter en associant plusieurs valeurs de $\Delta\tau$ élémentaire pour chaque courbe.

2. 2. Fonctions d'autocorrélation - Etude de la densité spectrale d'énergie en fonction du rayon

Les fonctions d'autocorrélation mesurées aux points r, θ, z — $r, \theta+\Delta\theta, z$ — $r, \theta, z+\Delta z$ sont identiques, ce qui signifie que la turbulence est homogène dans les directions θ (fig. 5) et z. Par contre, ce résultat n'est pas vérifié dans la direction r.

Pour préciser les caractéristiques radiales des fluctuations, nous avons étudié en fonction du rayon la déformation de la fonction d'autocorrélation et du spectre d'énergie correspondant $G(\omega)$ de la densité fluctuante mesurée localement à l'aide de sondes. La figure 3 donne six spectres d'énergie normalisés correspondant à six points de mesure . L'examen de ces courbes montre que la forme de ce spectre dépend du profil radial de la densité. Dans les régions à faible gradient ∇n, c'est-à-dire au voisinage de l'axe et à l'extérieur de la colonne, la densité spectrale d'énergie des fluctuations est une fonction décroissante monotone de la fréquence - positions 1 et 6 -. Par contre, dans les régions à fort gradient, la densité d'énergie des fluctuations est localisée. On observe des raies larges dans certains intervalles de fréquences - positions 2, 4, 5-.

(a)

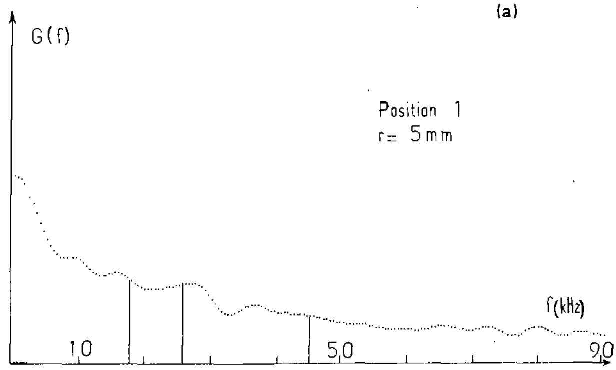
G(f)
Position 1
r= 5mm
f(kHz)
10
50
90

(b)

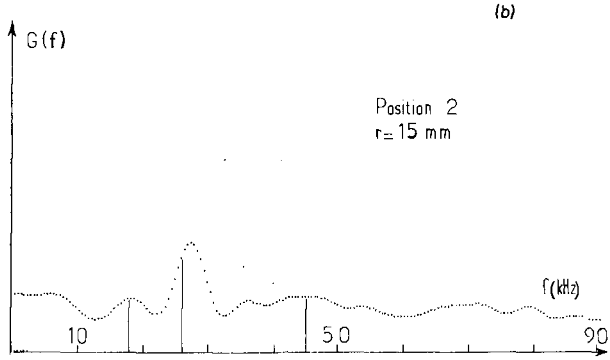
G(f)
Position 2
r=15 mm
f(kHz)
10
50
90

(c)

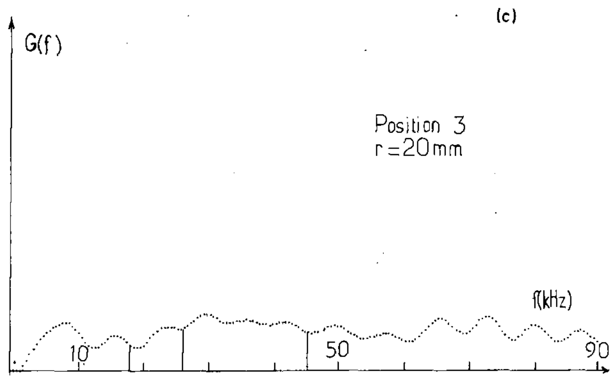
G(f)
Position 3
r=20mm
f(kHz)
10
50
90

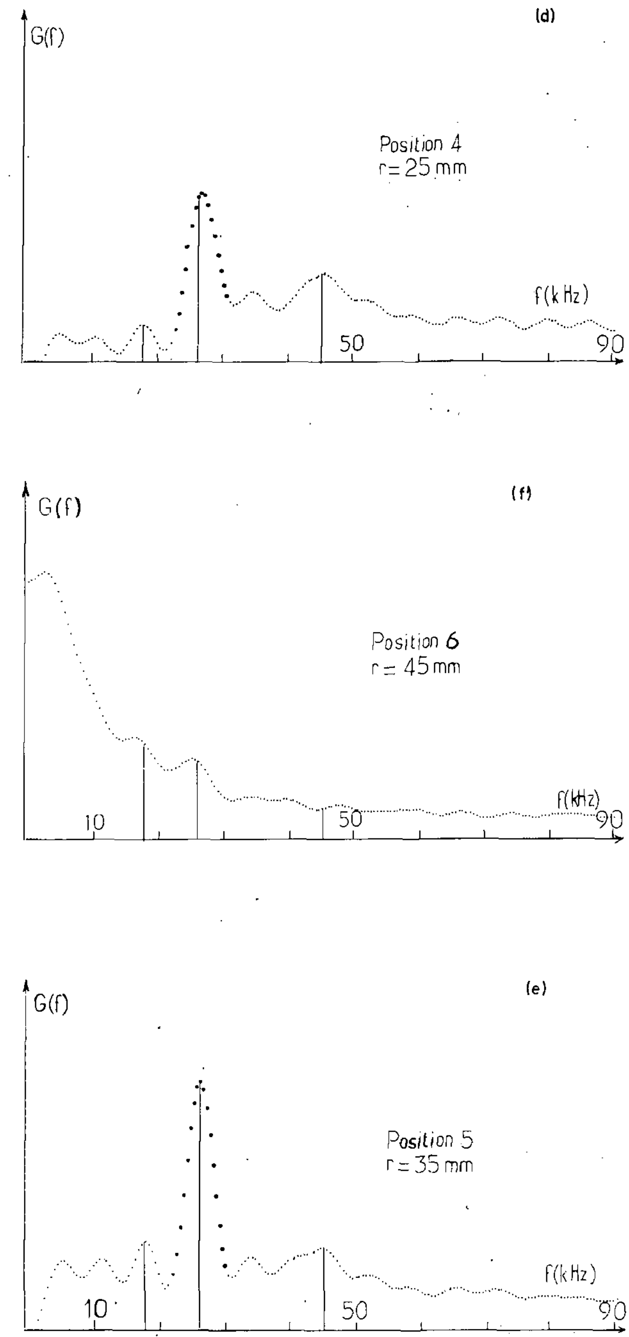

FIG. 3. Spectres de puissance.

Au maximum de densité, les raies du spectre disparaissent - position 3 -. Le rôle du gradient de densité apparaît de façon plus significative sur la fig. 4, où l'on a représenté la variation de puissance de trois fréquences significatives du spectre. On constate en particulier que les modes choisis, 18-26-45 kHz, sont localisés dans les régions où le gradient de densité est important. L'extension radiale de ces modes Λ_r est de l'ordre de la distance caractéristique du gradient de densité. Il est important de remarquer que, bien que le plasma soit creux, les fluctuations sont excitées de la même manière à l'intérieur et à l'extérieur de la colonne, ce qui exclut la possibilité d'interpréter ces résultats à partir d'instabilités du type flûte.

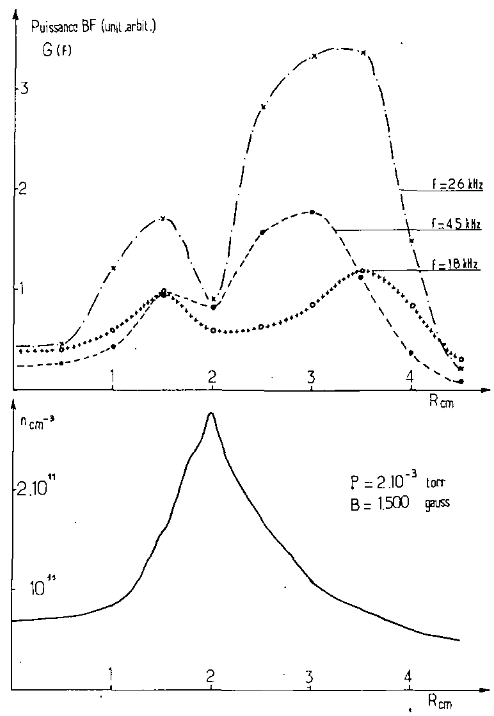

FIG. 4. Localisation radiale des modes.

2. 3. Fonctions d'intercorrélation - Relation de dispersion des fluctuations

Nous avons vu que, dans le cas où l'hypothèse de propagation plane est vérifiée, on peut déduire la relation de dispersion $k(\omega)$ du calcul de la transformée de Fourier $G'(\omega)$ de la fonction d'intercorrélation.

La figure 5 donne un ensemble de résultats obtenus sur deux sondes placées respectivement aux points r, θ, z et $r, \theta+\Delta\theta, z$ c'est-à-dire les deux fonctions d'autocorrélation, la fonction d'intercorrélation, les deux spectres $G(\omega)$ correspondant à la transformée de Fourier des autocorrélations et le module $|G'(\omega)|$ de la transformée de Fourier de l'intercorrélation.

De la comparaison de ces trois dernières courbes, on peut tirer deux conclusions importantes :

- d'une part, l'identité des deux spectres confirme l'hypothèse d'homogénéité en θ .
- d'autre part, et surtout, l'identité de $G(\omega)$ et de $|G'(\omega)|$ permet effectivement de représenter les fluctuations de densité sous la forme d'une somme d'ondes planes

$$n(t) = \int A(\omega, r)\, e^{i(\omega t - m\theta - kz)}\, d\omega$$

où $A(\omega, r)$ est une fonction réelle.

La figure 6 complète ces résultats par le tracé de l'argument $k(\omega)\lambda = m(\omega)\Delta\theta$ de $G'(\omega)$ c'est-à-dire la relation de dispersion locale des fluctuations dans la direction azimutale. Cette relation est linéaire et s'écrit en introduisant le rayon r correspondant au point de mesure

$$f = \frac{m}{2\pi r} v_0$$

où v_0 est la vitesse de transport des fluctuations.

La courbe n° 2, relevée à l'extérieur du plasma pour un rayon r = 2,2cm, correspond à une vitesse de phase des fluctuations de 2,3 · 10^3 m/s. La courbe n°1, obtenue à l'intérieur du plasma, pour un rayon r = 1,2 cm, donne une vitesse v_0 de 10^3 m/s.

Ces mesures font apparaître plusieurs points importants :

- d'une part, les fluctuations sont de même nature à l'intérieur et à l'extérieur de la colonne. Leur relation de dispersion est en effet toujours approximativement linéaire ;
- d'autre part, ces fluctuations se propagent dans le même sens quel que soit le signe du gradient. Ceci souligne l'importance du champ électrique radial sur la détermination de cette vitesse /6/.

2.4. Discussion

Les instabilités qui peuvent rendre compte des caractéristiques des fluctuations étudiées doivent, comme nous venons de le voir :

- être excitées indépendamment du signe du gradient de densité ∇n ;
- être localisées dans les régions où ∇n est important ;
- avoir une relation de dispersion linéaire, avec une vitesse de propagation plus grande à l'extérieur qu'à l'intérieur de la colonne.

Ces caractéristiques sont très proches de celles des instabilités de dérive. En effet, dans cette expérience, le champ magnétique est uniforme, le plasma collisionnel $(\nu > k_y v_D)$, sa fonction de distribution monotone et le rayon de Larmor des ions a_i inférieur aux dimensions caractéristiques du gradient de densité ∇n et de l'extension des modes $\lambda_r\, (k_\perp^2 a_i^2 < 1)$.

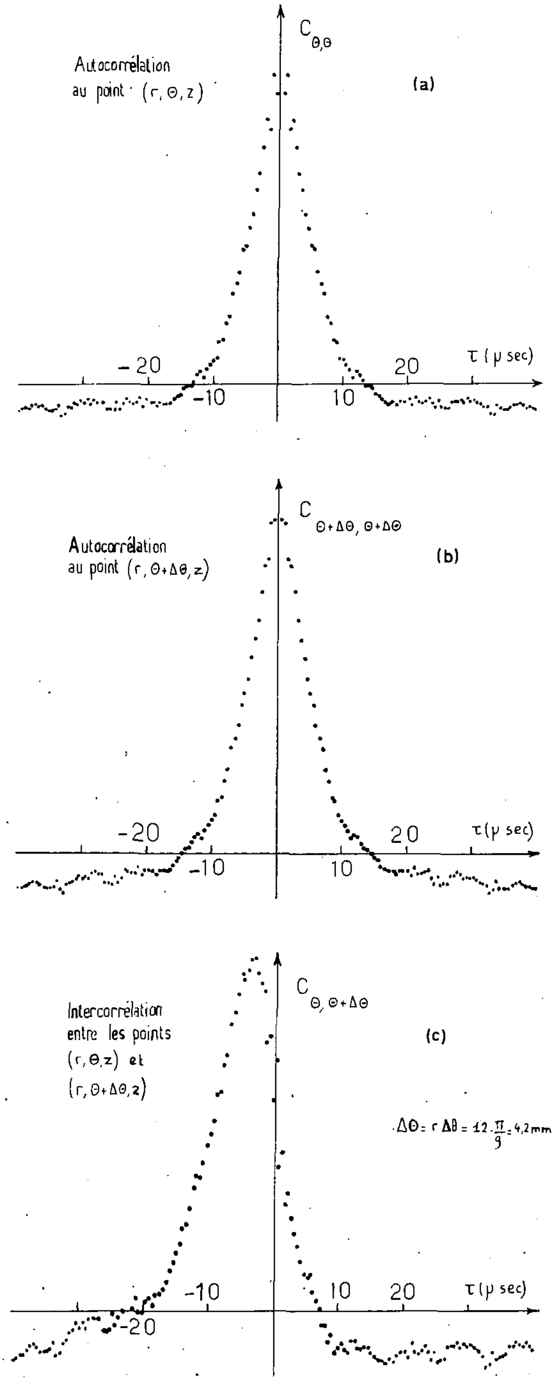

$C_{\Theta,\Theta}$
Autocorrélation au point (r, Θ, z)
(a)
τ (μ sec)
-20
-10
10
20
$C_{\Theta+\Delta\Theta,\Theta+\Delta\Theta}$
Autocorrélation au point $(r, \Theta+\Delta\Theta, z)$
(b)
τ (μ sec)
-20
-10
10
20
$C_{\Theta,\Theta+\Delta\Theta}$
Intercorrélation entre les points (r, Θ, z) et $(r, \Theta+\Delta\Theta, z)$
(c)
$\Delta\Theta = r\,\Delta\theta = 12 \cdot \frac{\pi}{9} = 4{,}2$ mm
τ (μ sec)
-20
-10
10
20

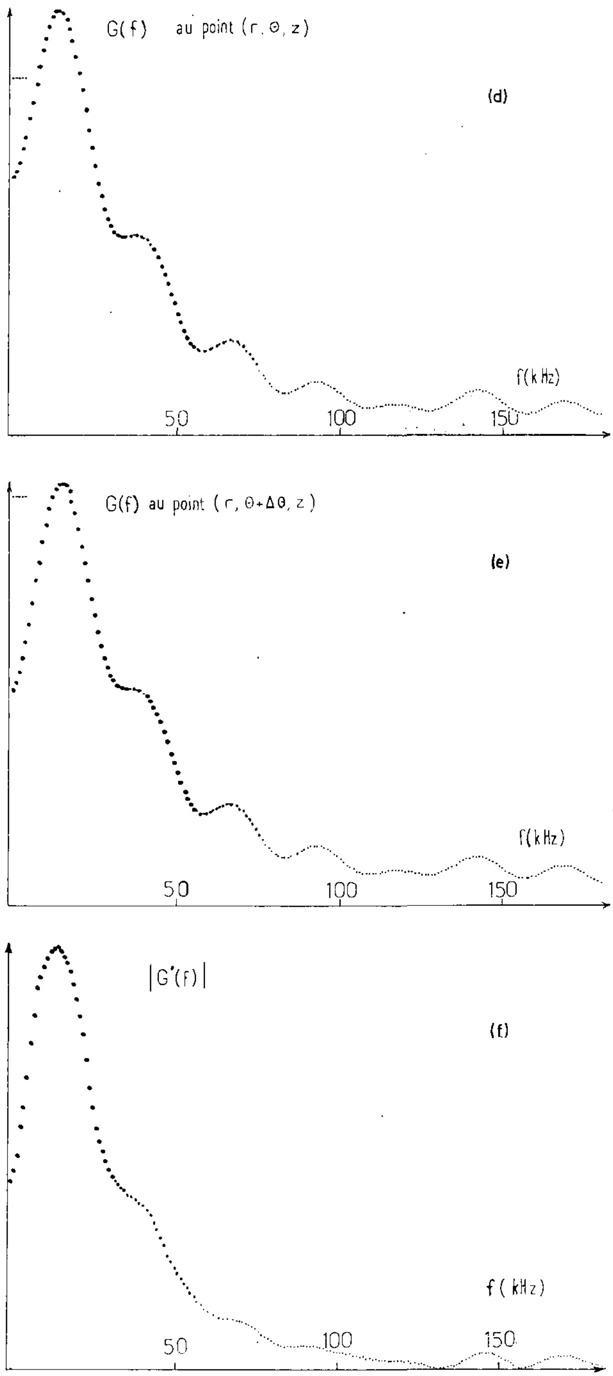

FIG. 5. Homogénéité et propagation plane azimutales.

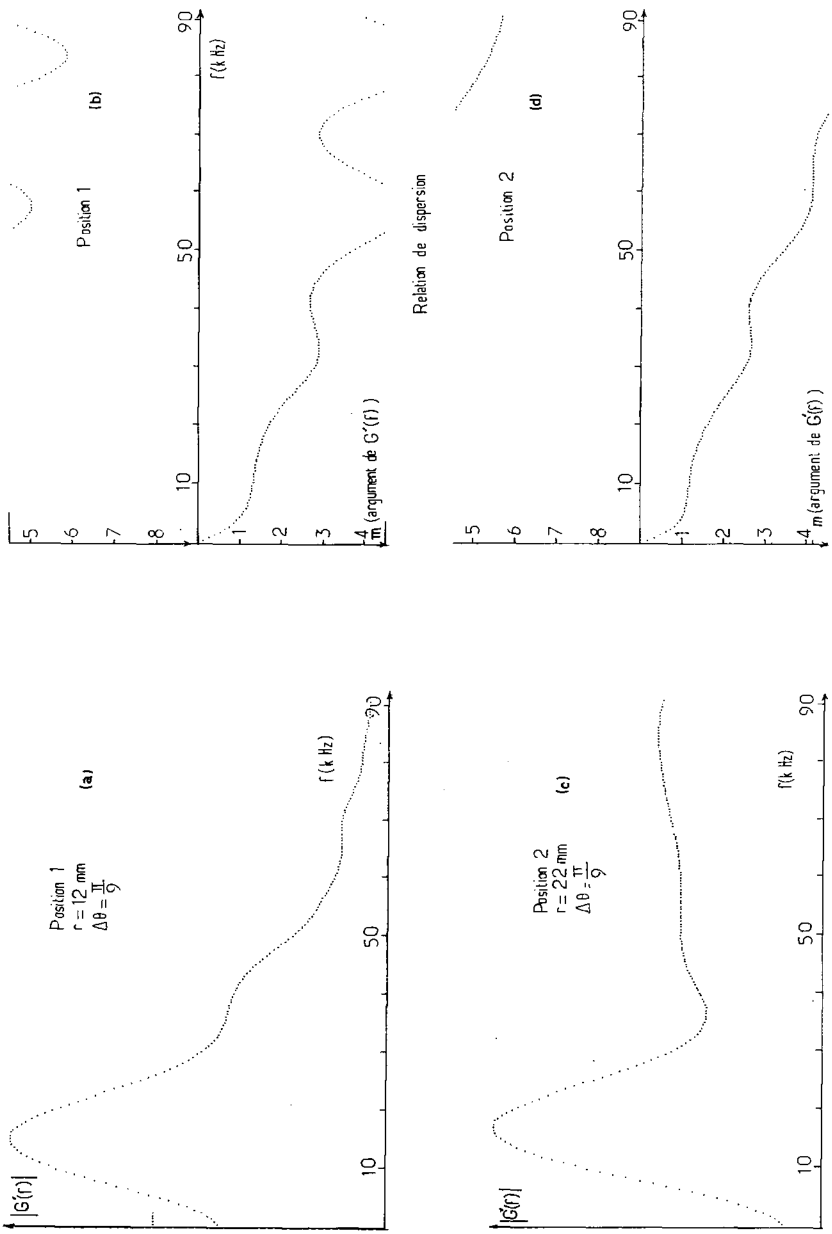

FIG. 6. Module et argument de G'(f) - relation de dispersion (à gauche: intérieur; à droite: extérieur).

Dans ce cas, l'instabilité de dérive résistive peut se développer avec une pulsation et un taux de croissance maximum de l'ordre de

$$\gamma \sim \omega^* \sim \frac{1}{2} k_y v_D = \frac{1}{2} \frac{m}{r} v_D \qquad ; \qquad v_D = \frac{kT_e}{eB} \frac{\nabla n}{n}$$

où v_D est la vitesse diamagnétique du plasma /7/, /8/. Le critère d'instabilité ne dépend pas du signe de ∇n, le taux de croissance est maximum pour le maximum de ∇n et la relation de dispersion est linéaire. Expérimentalement, la distance radiale λ_r sur laquelle les modes sont excités détermine assez bien la distance caractéristique du gradient - voir fig. 4 -. Lorsque B = 1 kG, λ_r = 2,5cm, Te = 2 eV au centre du gradient, ce qui donne, pour la vitesse diamagnétique $v_D \sim 2.10^3$ m/s et pour la vitesse de phase des ondes v_φ

$$v_\varphi = \frac{\omega^* r}{m} = 0,5\, v_D \simeq 10^3 \text{ m/s}$$

Si l'on compare cette vitesse à la vitesse de propagation v_o obtenue par la relation de dispersion expérimentale - fig. 6 -, on constate :

- que dans la région extérieure du plasma où $\nabla n < 0$, v_φ est approximativement deux fois plus petit que v_o (fig. 6 - position 2) ;
- que dans la région intérieure où $\nabla n > 0$, v_o et v_φ sont sensiblement de la même valeur mais de signes opposés. En effet, l'inversion du gradient de densité ne s'accompagne pas d'une inversion du sens de propagation des fluctuations comme le montre la relation de dispersion (fig. 6 - position 1).

Ceci peut s'expliquer par la présence du champ électrique radial qui produit une rotation d'ensemble du plasma /9/. La vitesse de transport des fluctuations devient alors :

$$v'_{\varphi\,ext} = \frac{E_r}{B} + \frac{1}{2} v_D \qquad \text{pour} \quad \nabla n < 0 \qquad \text{extérieur}$$

$$v'_{\varphi\,int} = \frac{E_r}{B} - \frac{1}{2} v_D \qquad \text{pour} \quad \nabla n > 0 \qquad \text{intérieur.}$$

Nous n'avons pas un ensemble complet de mesures de E_r qui est difficile à déterminer. Nous l'avons mesuré pour B = 1 kG, en utilisant deux méthodes : d'une part à partir du potentiel flottant en le corrigeant par la température T_e, d'autre part à l'aide de la sonde à séparation électrostatique qui permet de mieux approcher le potentiel plasma. La variation du potentiel sur la distance caractéristique du gradient λ_r donne pour le champ électrique radial 2 V/cm et pour les vitesses :

v'_φ ext. = 3.10^3 m/sec pour $\nabla n < 0$

v'_φ int. = 10^3 m/sec pour $\nabla n > 0$

ce qui est en bon accord avec les vitesses v_o déduites des relations de dispersion expérimentales :

v_o ext. = $2,3.10^3$ m/sec pour $\nabla n < 0$

v_o int. = 10^3 m/sec pour $\nabla n > 0$

L'autre point intéressant est la comparaison entre les longueurs d'onde théoriques et expérimentales. Le spectre de puissance montre qu'une grande partie de l'énergie des fluctuations est centrée autour de la fréquence f = 26 kHz. La longueur d'onde, calculée à partir de la relation de dispersion pour cette fréquence caractéristique,donne :

$$\lambda_y = \frac{V_D}{2f^*} \simeq 3,8 \text{ cm.}$$

Le point $\tau = 0$ de la fonction d'intercorrélation azimutale $C_{\theta,\theta+\Delta\theta}(\tau)$ est la valeur du produit $\langle n_\theta(t) \cdot n_{\theta+\Delta\theta}(t)\rangle$. La variation de ce produit pour différentes valeurs de $\Delta\theta$ donne la longueur de corrélation azimutale des fluctuations λ_c. Au rayon R = 2, 2 cm, $\lambda_c \simeq 4,2$ cm.

Lorsque le champ magnétique augmente, les longueurs d'onde plus courtes sont excitées /10/ d'après la relation

$$k_{y\,max} \propto B\left(\frac{T}{n}\right)^{\frac{1}{2}}$$

Dans l'intervalle de variation de B considéré 0, 75 à 2, 5 kG, la vitesse diamagnétique V_D et la température T_e varient peu, ce qui donne une relation de la forme $\dfrac{\omega^*}{B} \approx C^{te}$

Nous avons porté sur la figure 7 le temps de corrélation des fluctuations du champ électrique et de la densité. La relation $B\tau_c \approx C^{te}$ est assez bien satisfaite.

Les instabilités de dérive résistive rendent donc bien compte des fluctuations observées lorsque l'on fait intervenir le champ électrique radial du plasma. Des mesures plus complètes de la relation de dispersion en fonction du rayon et du champ magnétique sont en cours pour obtenir une comparaison quantitative plus fine entre ces résultats et le modèle théorique des instabilités de dérive résistive.

3. RELATION FLUCTUATIONS - DIFFUSION

Lorsqu'on s'éloigne des régions où le gradient de densité est important, les fonctions de corrélation et les spectres d'énergie correspondants G (ω) deviennent des fonctions décroissantes et monotones. On peut dans ces conditions définir un temps de corrélation des fluctuations

$$\tau_c = \frac{1}{\langle n_0\rangle^2}\int_0^\infty C(\tau)\, d\tau$$

et relier ces fluctuations au coefficient de diffusion /11/

$$D_{f\perp} = \left(\langle E_\theta^2\rangle / B^2\right)\tau_c$$

La courbe expérimentale $D_{f\perp}(B)$ obtenue à partir de la mesure du temps de corrélation τ_{cE} du champ électrique fluctuant et de sa valeur quadratique moyenne$(\langle E_\theta^2\rangle)$ est donnée sur la figure 7. En valeur absolue $D_{f\perp}$ est inférieur au coefficient de Bohm défini comme

$$D_{Bohm} = \frac{1}{16}\,\frac{KT_e}{eB}$$

Le domaine de variation du champ magnétique est trop étroit pour conclure sur la dépendance de $D_{f\perp}$ en fonction de B . On peut toutefois remarquer que dans cet intervalle cette relation est sensiblement de la forme $D \approx B^{-1}$.

Sur cette même figure 7, nous avons représenté la valeur expérimentale du coefficient de diffusion $D_{M\perp}$ obtenu à partir de la mesure du flux $\langle n E_\theta \rangle$ et de la relation $\langle n E_\theta \rangle = D_{M_\perp} \nabla n$ /12/.

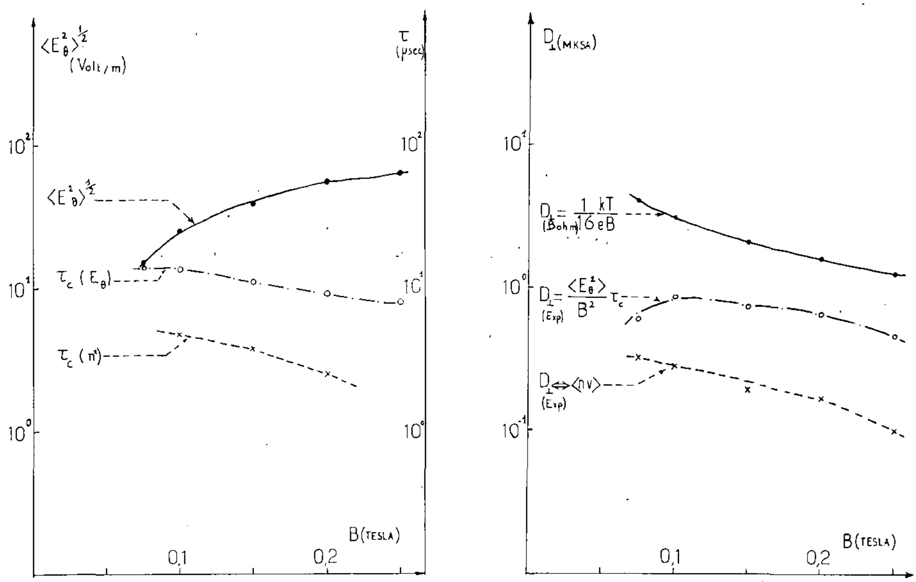

FIG. 7. a) Caractéristiques du champ F_θ fluctuant; b) coéfficient de diffusion $D_\perp$.

Ce coefficient de diffusion $D_{M\perp}$ est légèrement inférieur au précédent $D_{f\perp}$ d'un facteur 3 ou 4. Des pertes estimées par ces deux méthodes sont toutefois du même ordre de grandeur et comparables à celles mesurées précédemment dans des conditions expérimentales semblables à partir de la mesure du flux longitudinal par un "plasma eater" /1/

$$D_{exp} \simeq 0{,}1 \; D_{Bohm}$$

Il est intéressant, en s'appuyant sur le modèle des instabilités de dérive résistive discuté précédemment, de comparer la valeur expérimentale du coefficient de diffusion $D_{f\perp}$ à celle donnée théoriquement /13/

$$D_{\perp\,theor} = \frac{\langle E_\theta^2 \rangle}{B^2}\,\tau_c \quad \text{avec} \quad \frac{\langle E_\theta^2 \rangle^{1/2}}{B} \approx v_D$$

et τ_c est l'inverse du temps de montée de l'instabilité, c'est-à-dire

$$\tau_c^{-1} \approx \gamma \approx \omega_R^* = \frac{1}{2}\, k_y v_D$$

Avec cette hypothèse et en prenant pour ω^*, la pulsation correspondant à la fréquence du spectre d'énergie $G(\omega)$ sur laquelle est centrée la plus grande partie de l'énergie des fluctuations, $f^* = 26$ kHz, on obtient $\tau_c = (2\pi f^*)^{-1} = 6\,\mu s$. Ce temps est comparable au temps de corrélation τ_{CE} mesuré. Par contre, la vitesse fluctuante mesurée expérimentalement $V_f = \frac{\langle E_\theta^2 \rangle^{1/2}}{B} = 2 \sim 1,5.10^2$ m/s est inférieure d'un ordre de grandeur à la vitesse théorique égale à $V_D \simeq 2.10^3$ m/s . Si l'on estime cette vitesse fluctuante à partir de la relation $V_n \tau^{-1} = \frac{V_n^2}{\lambda_\perp}$ en prenant les valeurs expérimentales de $\tau \sim 10\,\mu s$, $\lambda_\perp \sim \lambda_r = 2,5$ cm (extension des modes) /7/, on obtient également une vitesse dix fois supérieure à celle mesurée expérimentalement. Cette remarque confirme le fait que le coefficient de diffusion mesuré est inférieur à celui de Bohm.

REMERCIEMENTS

Nous tenons à remercier MM. J.P. BUSSAC, M. TOUZEAU pour leur collaboration à ce travail et MM. G. LAVAL, D. LEPECHINSKY, R. PELLAT et P. ROLLAND pour leurs commentaires sur certains aspects théoriques des instabilités de dérive.

REFERENCES

/1/ BERNARD M., BRIFFOD G., GREGOIRE M., WEISSE J., Proc. of Conf. on Quiescent Plasmas, Frascati (1967), part. 1.

/2/ ROSENBLUTH M.N., KRALL N.A., ROSTOKER N., Conf. Salzbourg (Sept. 1961) - Nuclear Fusion (1962), part 1.

/3/ - BERNARD M., BRIFFOD G., GREGOIRE M., WEISSE J., 7th Int. Conf. on Ionized Gases - Belgrade (1965).
- FRANK R., Thèse, Faculté d'Orsay, France (1968).

/4/ - BEREZIN A.B., BULYGINSKY D.G., VILOJVNAS M.I., RODICHKIN V.A., 8th Int. Conf. on Ionized Gases, Vienne, (1967).
- CHUNG K., ROSE D.J., Appl. Phys. Let., Vol. 11, N°8 (Oct. 1967).
- BUCHELNIKOVA N.S., SALIMOV R.A., EDELMAN J.J., 8th Int. Conf. on Ionized Gases, Vienne, (Sept. 1967).

/5/ MAX J., BERTHIER D., CHEVALIER H., C.E.N. Grenoble (France).

/6/ HENDEL H.W., POLITSER P.A., Proc. of Conf. on Quiescent Plasmas, Frascati (1967), part 1.

/7/ MOISEEV S.S., SAGDEEV R.Z., Zh. Te. Fi., Vol. 34, N°2 (1964).

/8/ CHEN F.F., Phys. of Fluids, Vol. 8, N° 7, (July 1965).

/9/ LEGARDEUR R., LEPECHINSKY D., ROLLAND P., C.E.N. de Saclay, IGn/RT/594 (to be published in Phys. of Fluids).

/10/ - LAVAL G., PELLAT R., Proc. of Conf. on Quiescent Plasmas, Frascati (1967), part 1.

- COPPI B., HENDEL H.W., PERKINS F., POLITZER P.A., Proc. of Conf. on Quiescent Plasmas, Frascati (1967), part 1.

/11/ SPITZER L., Phys. of Fluids, 3 (1960), p. 659.

/12/ BOL K., ELLIS R., Princeton Annual Report (1966) MATT Q. 24 p. 31.

/13/ DUPREE T.H., 9th Annual Meeting of A.P.S., Austin (Texas), Nov. 8-11, 1967.

SOME INVESTIGATIONS OF NON-LINEAR PLASMA BEHAVIOUR ON ONE-DIMENSIONAL PLASMA MODELS

J.M. DAWSON AND C.G. HSI
PLASMA PHYSICS LABORATORY, PRINCETON UNIVERSITY,
PRINCETON, N.J., UNITED STATES OF AMERICA
AND
R. SHANNY
SPACE SCIENCES LABORATORY, GENERAL ELECTRIC COMPANY,
KING OF PRUSSIA, PA., UNITED STATES OF AMERICA

Abstract

SOME INVESTIGATIONS OF NON-LINEAR PLASMA BEHAVIOUR ON ONE-DIMENSIONAL PLASMA MODELS. Earlier calculations on the two-stream instability using the sheet model are extended. Vortexes in phase space similar to those found by Roberts and Berk are found. A new finite-size particle model is developed to reduce collisional effects. This model suppresses the short-wavelength field fluctuations while leaving the long-wavelength collective modes unaffected. The turbulence generated by a small bump in the tail of the distribution function is investigated on this model. It is found here as in the sheet model calculations that a hot Maxwellian tail is formed which co-exists with the main plasma for a very long time.

1. INTRODUCTION

In an earlier work [1] a number of non-linear phenomena were investigated on the charge sheet model. It is the purpose of this paper to describe some work which has grown out of these calculations. This work includes new calculations on the sheet model, the development of a finite-size particle model which it is hoped will eliminate some of the shortcomings of the sheet model, and comparison of results from this new model with those from the sheet model for the problem of the instability due to a weak beam passing through the plasma. It should be possible to extend the methods used in the new model to two- and three-dimensional models. Before describing these calculations we shall summarize the previous calculations, as they motivated much of this extension. We shall then describe the new model and discuss the results of the calculations.

In the earlier works [1, 2], four problems were investigated:

(a) The damping of a large-amplitude wave,

(b) Mode coupling by non-linear Landau damping,

(c) Emission and absorption of waves due to sheet encounters,

and

(d) The turbulence generated by a weak bump in the tail of the distribution function.

For the first of these problems, the damping of a large-amplitude wave, it was found that the initial damping was much larger than that predicted by linearized theory. The enhancement of the damping was due to the acceleration of particles, with initial velocities much slower than the wave velocity, up to velocities equal to or greater than its phase velocity. Particles whose velocity differs from the phase velocity of the wave by as much as Δv,

$$\Delta v = \sqrt{2 \frac{eE}{mk}}$$

can be so affected. Since generally the number of slow particles rises rapidly with decreasing velocity, the number of such particles which can be accelerated rises rapidly with E and so does the damping. The results of the numerical experiment and a rough theory for the effect can be found in Ref. [1].

The second investigation was that of mode-mode coupling by the mechanism of non-linear Landau damping. In this investigation it was found that a number of effects could dominate non-linear Landau damping [3]; the second was the strong acceleration of particles similar to that found in the first investigation. When precautions were taken so as to avoid these effects, the theory was verified.

The third experiment involved the collisional damping and emission of waves due to particle encounters. Here the theory of Birmingham, Dawson, and Kulsrud [4] was verified. Their calculation is similar to that used in the theory of weak turbulence, and so this experiment verifies that theory at least for the low level of fluctuations involved. The result of these experiments can be found in Ref. [2].

The fourth experiment investigated the turbulence generated by a weak beam passing through the plasma. The bump flattened out rapidly (time scale $20\,\omega_p^{-1}$) as predicted by quasilinear theory. However, it continued to evolve so that by the time $t \approx 150\ \omega_p^{-1}$, the tail had a more or less Maxwellian shape at a temperature determined by the initial beam energy. The plasma thus contained two components, a hot tail and a cold main plasma. These two components coexisted for a long period of time ($t > 300\,\omega_p^{-1}$). Particles with much higher energy than the initial beam energy were produced (energies up to four times the mean beam energy were observed).

At the same time, the waves with phase velocities living in the tail acquired mean energies equal to the temperature of the tail. Thus the hot tail and the associated waves seemed to come to a quasi-thermal equilibrium. The waves showed rapid fluctuations in their energy. It appeared that Cherenkov emission and absorption played a strong role in these fluctuations and in establishing the thermal equilibrium of the tail particles among themselves. Details of this investigation can be found in Ref. [1].

2. THE FINITE-SIZE PARTICLE MODEL

2.1. The model

In the experiment on mode-mode coupling it was found that damping of the waves due to particle encounters could mask the effect being investigated. This damping is a collisional damping due to the use of discrete particles. Because the computer can only handle a few thousand particles, the graininess due to the particles is rather large and the associated collisional effects are overemphasized. For one-dimensional models this effect is not too serious because to a large extent collisions in one dimension do not alter the distribution function [5, 6, 7]. For two-and three-dimensional models, however, it would be very serious, as already observed by Hockney [8]. Even in one dimension it did cause trouble for the mode coupling experiment. We should like to eliminate such collisional effects while keeping the collective effects associated with wavelengths longer than a Debye length.

Towards this goal we have developed a new one-dimensional model involving finite-size particles which to a large extent suppress the density fluctuations and E fields for short wavelengths and the associated collisional effects. The model consists of a large number of negative charge clouds embedded in a uniform fixed neutralizing background. Our method is somewhat related to that used by Hockney [8] and Birdsall [9] for two- and three-dimensional models, although our procedure is quite different.

First, we essentially take the charge density due to one of the clouds to be given by

$$\rho(x,t) = -\frac{\sigma \exp[-(x-x_i)^2/2a^2]}{\sqrt{2\pi}\, a} \tag{1}$$

where x_i is the central position of the ith cloud, $-\sigma$ is the total charge on the cloud, and a is its half width. We shall use the Fourier analysis of the electric field in determining the motion of the particles. Thus we proceed as follows.

First, if we Fourier analyze ρ, we find

$$\rho(k,t) = -\frac{\sigma \exp[-(k^2a^2/2) + ikx_i]}{\sqrt{2\pi}} \tag{2}$$

and the associated electric field

$$E(k,t) = -\frac{4\pi\sigma i \exp[-(k^2a^2/2) + ikx_i]}{k\sqrt{2\pi}} \tag{3}$$

The force on particle j due to particle i is given by

$$F_{ji} = \int_{-\infty}^{-\infty} E_i(x)\rho_j(x)\,dx = \frac{2\sigma^2 i}{\sqrt{2\pi}\, a} \int \frac{\exp\left[ik(x_i - x) - \frac{k^2a^2}{2} - \frac{(x-x_j)^2}{2a^2}\right]}{k}\, dk\, dx \tag{4}$$

$$F_{ji} = 2\sigma^2 i \int \frac{e^{ik(x_i - x_j) - k^2a^2}}{k}\, dk$$

We observe that this force has the same functional form as the E field at x_j due to a particle at x_i with a half-width of $\sqrt{2}$ a and a charge of σ.

Now rather than using the force law given by (4), we take the force law to be given by a finite Fourier sum

$$F_{ji} = F_o \sum_{-k_{max}}^{k_{max}} \frac{\left[e^{ik(x_i - x_j) - k^2 a^2} - \delta_{n,o}\right]}{k} \tag{5}$$

where $k = nk_{min}$, n is an integer, $\delta_{n,0}$ is the Kronecker delta, and k_{min} is the spacing in k. We must choose the size of the sytem so that this is an accurate description of the force law. Introducing the maximum wave number k_{max} says that we are considering wavelengths such that $\lambda \geqq 2\pi/k_{max}$. This is necessary since we can only handle a finite number of modes. However, as we have already stated, we are interested in suppressing the noise in the short-wavelength modes, and so this is to some extent desirable. Further, since their amplitudes fall off exponentially, higher modes do not count for much provided k_{max} a is larger than one. This cutoff does mean that the charge shape is not exactly Gaussian, but its deviations are small.

The force on particle i due to all other particles is thus taken to be given by

$$F_i = m\ddot{x}_i = \sum_{-k_{max}}^{k_{max}} \frac{A e^{-k^2 a^2}}{k} \left[e^{-ikx_i} - \delta_{n,o}\right] \sum_j e^{ikx_j} \tag{6}$$

(i can be included in the second sum because there is no self force on i). To advance the particles in time, we assume that during a time step the force can be computed as if the particles move uniformly. We further assume that $k_{max}\Delta t$ is small or that a particle moves only a small fraction of the shortest wavelength considered. Thus we can approximate (6) during a time step by

$$m\ddot{x}_i = \sum_{-k_{max}}^{k_{max}} \frac{A e^{-k^2 a^2}}{k} \left[e^{-ikx_i(t)} - \delta_{n,o}\right]\left[1 - ikv_i(t)\tau - \frac{k^2 v_i^2(t)\tau^2}{2}\right] \tag{7}$$

$$\sum_j e^{ikx_j(t)}\left[1 + ikv_j(t)\tau - \frac{k^2 v_j^2(t)\tau^2}{2}\right]$$

where τ is the elapsed time from the start of the time step at t. We may integrate Eq.(7) to obtain

$$v_i(t+\Delta t) - v_i(t) = \sum_{-k_{max}}^{k_{max}} \frac{A e^{-k^2 a^2}}{mk} \left[e^{-ikx_i(t)} - \delta_{n,o} \right] \left\{ \left(\Delta t - \frac{ikv_i(t)\Delta t^2}{2} - \frac{k^2 v_i^2(t)\Delta t^3}{6} \right) \cdot \left(\sum_j e^{ikx_j(t)} \right) + \left(\frac{ik\Delta t^2}{2} + \frac{k^2 v_i(t)\Delta t^3}{3} \right) \cdot \left(\sum_j e^{ikx_j(t)} v_j(t) \right) - \frac{k^2 \Delta t^3}{6} \sum_j v_j^2(t) e^{ikx_j(t)} \right\} \tag{8}$$

$$x_i(t+\Delta t) - x_i(t) - v_i \Delta t = \sum_{-k_{max}}^{k_{max}} \frac{A e^{-k^2 a^2}}{mk} \left[e^{-ikx_i(t)} - \delta_{n,o} \right] \cdot \left\{ \left(\frac{\Delta t^2}{2} - \frac{ikv_i(t)\Delta t^3}{6} - \frac{k^2 v_i^2(t)\Delta t^4}{24} \right) \cdot \sum_j e^{ikx_j(t)} + \left(\frac{ik\Delta t^3}{6} + \frac{k^2 v_i(t)\Delta t^4}{12} \right) \cdot \sum_j v_j(t) e^{ikx_j(t)} - \frac{k^2 \Delta t^4}{24} \sum_j v_j^2(t) e^{ikx_j(t)} \right\} \tag{9}$$

Equations [8] and [9] look relatively complex, and one may wonder if we are not losing rather than gaining by this technique. In this connection we should note the following. First, the sums on j are independent of i and can thus be evaluated once and for all particles. Each sum on j must be evaluated for every k considered. Thus, if there are N particles and M modes we must evaluate NM terms. If we had computed particle interactions directly there would be $N^2/2$ terms. Thus, if M is much smaller than the number of particles, we gain by this technique. In general, we wish to keep only a few modes, the long-wavelength collective modes which are important to the problem under investigation. Thus M should be much smaller than N. Further, the particles must more or less represent the full distribution function, whereas the modes only have to represent the spatial part of the disturbance. Thus by this argument also, we require many more particles than modes.

By including the time dependences of the particle positions in Eq. (7), we complicate Eqs (8) and (9). However, by doing this we greatly improve the accuracy of the method and allow ourselves to take larger time steps. This more than compensates for the added computations as far as running time is concerned.

This method is also very flexible in that we can easily change the size of the particles and the number of modes we keep, so as to check whether or not these cause important changes in the results. Further, since this method involves exact dynamics of particles interacting through a modified Coulomb force law, conservation of energy is a good check on calculation. Errors due to using finite spatial grids do not enter. Finally, it should be possible to extend this method to two and three dimensions. Our present method of calculating appears to be somewhat slow for such problems. However, it appears that some modifications in the procedure can reduce the computing time from one which goes like NM to one which goes like $N + M^2$, which will substantially reduce the computation time. We are presently investigating this possibility.

2.2. Investigation of fluctuations about thermal equilibrium

The first problem we investigated with the finite-size particle model was the fluctuations about thermal equilibrium to see if they behaved as expected. Figure 1 shows a plot of the amplitude of the rms electric field fluctuations vs mode number for charge clouds with $a = 2\lambda_D$ (λ_D is the Debye length), and with $k_{max}\lambda_D$ equal to 2. The solid curve is the theoretically predicted curve for Gaussian charge clouds. This curve is predicted from the formula

$$P(E_k)\,dE_k \propto e^{-\psi_k(E_k)/KT}\,dE_k \tag{10}$$

where $P(E_k)$ is the probability of finding the electric field in dE_k about the value E_k, and ψ_k is the work required to create the fluctuations E_k; ψ_k is given by

$$\psi_k = \frac{E_k^2 L}{16\pi}\left(1 + k^2\lambda_D^2\, e^{k^2a^2}\right) \tag{11}$$

(L is the length of the system). The first term on the right is the energy in the electric field, the second term is that required to compress the gas of cloud centers isothermally to the required density.

The average value of $E_k^2 L$ obtained from Eqs (10) and (11) is

$$\left\langle \frac{E_k^2 L}{8\pi} \right\rangle = \frac{KT}{2\left\{1 + k^2\lambda_D^2\, e^{k^2a^2}\right\}} \tag{12}$$

The upper dashed curve in Fig. 1 is that predicted for sheets, i.e. a equals zero. The points are those obtained from the numerical experiment. They agree quite well with the theoretically predicted values. There are some deviations for small mode numbers, but this is most likely due to the fact that the initial conditions do not start these modes out with energy KT, and they take a long time to relax to their thermal value (the averages used here are time averages).

As can be seen from Fig. 1, the theoretical fluctuations at long wavelengths are hardly affected by the use of finite-size particles while those at short wavelengths are strongly suppressed as expected. We have run other cases with different values of a and always find similar agreement.

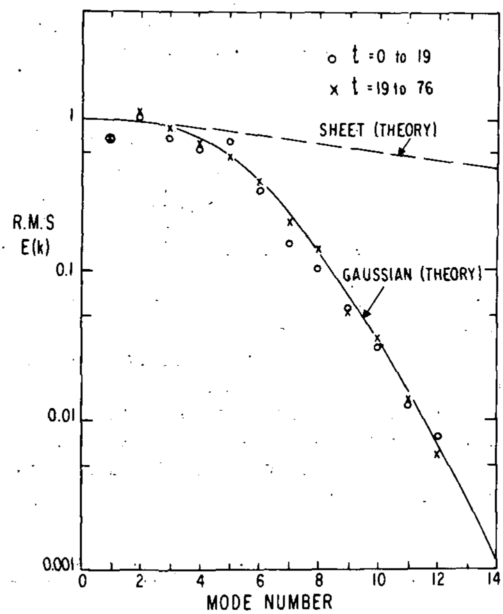

FIG. 1. rms E-field vs mode number.

Another interesting thing we can do is derive the dispersion relation for the finite-size particle model. The collisionless Boltzman equation for these particles is given by

$$\frac{\partial f}{\partial t} + v\frac{\partial f}{\partial x} + \frac{F}{m}\frac{\partial f}{\partial v} = 0 \tag{13}$$

where f(x, v) is the distribution function of cloud centre and velocities. The force on the particles obtained by integrating $E(\xi)\rho(\xi, x)$ over ξ, x is the position of the center of the charge cloud,

$$F(x) = 4\pi\sigma^2 i \int \frac{dk\, e^{-ikx-k^2a^2}}{\sqrt{2\pi}\, k} \int f(k, v)\, dv \tag{14}$$

This is the same expression one obtains for point particles except for the factor $\exp(-k^2a^2)$. If we linearize Eq.(13) and Fourier analyze Eqs(13) and (14) in space and time, we obtain

$$f(k, \omega) = \frac{i F(k, \omega)\, \partial f\, \partial/\partial v}{m(\omega + kv - i\epsilon)} \tag{15}$$

$$kF = 4\pi\sigma^2 e^{-k^2a^2} \int f(k, v)\, dv \tag{16}$$

Here ϵ is a small damping which has been added to determine the direction of integration around the poles. Substituting Eq.(15) into Eq.(16) we obtain the dispersion relation

$$1 = \frac{4\pi\sigma^2}{mk} e^{-k^2a^2} \int \frac{\partial f_o / \partial v \, dv}{(\omega + kv - i\epsilon)} \tag{17}$$

This is the same as the usual dispersion relation except for the factor $\exp(-k^2a^2)$. Thus the long-wavelength modes are unaffected while the short-wavelength modes are strongly modified.

3. INVESTIGATIONS OF THE TWO-STREAM INSTABILITY

We have carried on the investigation of the two-stream instability started in Ref.[1] in two ways. First, we have looked at the instability produced by a weak beam with no initial velocity spread on the sheet model. We have also investigated this problem on the finite-size particle model and find substantial agreement when the particles are not too large. Second, we have investigated the problem of the weak bump in the tail of the distribution on the finite-size particle model and have compared the results with the earlier sheet model results. Again we find substantial agreement; a long hot tail is formed which coexists with the main plasma which is much colder. The long-wavelength modes again show rapid fluctuations in energy.

Let us now discuss the instability produced by a weak cold beam passing through a warm plasma.

3.1. The cold beam for the sheet plasma

The situation which was investigated was the following: The plasma contained 2000 sheets, one-fifth of the particles were in the beam, there were twenty particles per Debye length in the main plasma, and the beam velocity was four times the thermal velocity. The whole distribution is shifted in velocity by $-0.8\ v_T$ so that the system has no net momentum or current. Figure 2 shows a sampling of plots of the particle positions in phase (x, v) space for the times $\omega_p t = 0, 1, 2, \ldots, 60$. Time runs from left to right and top to bottom. The vertical axis is v and the horizontal one x in each figure. The striking thing in these figures is the production of holes or vortex in phase space. The production of such holes in phase space has been extensively discussed by Roberts and Berk [10] for the water bag model. The interesting thing about these holes is their persistence; there are still well-defined holes after $\omega_p t$ equals 60 (we have seen them to $\omega_p t = 70$).

Such vortex-type motions are not contained in quasilinear theory. They appear to have a relatively long life here and perhaps should be treated as some type of individual entity, just as waves are. It remains to be seen how important such things will be for two- and three-dimensional motions. However, vortex-type motions (though not in phase space) have been observed in a number of two dimensional models [9, 11, 12]; they have also been seen in auroral displays. It is certain that vortexes must play an important role in many types of plasma turbulence, just as they do in hydrodynamic turbulence.

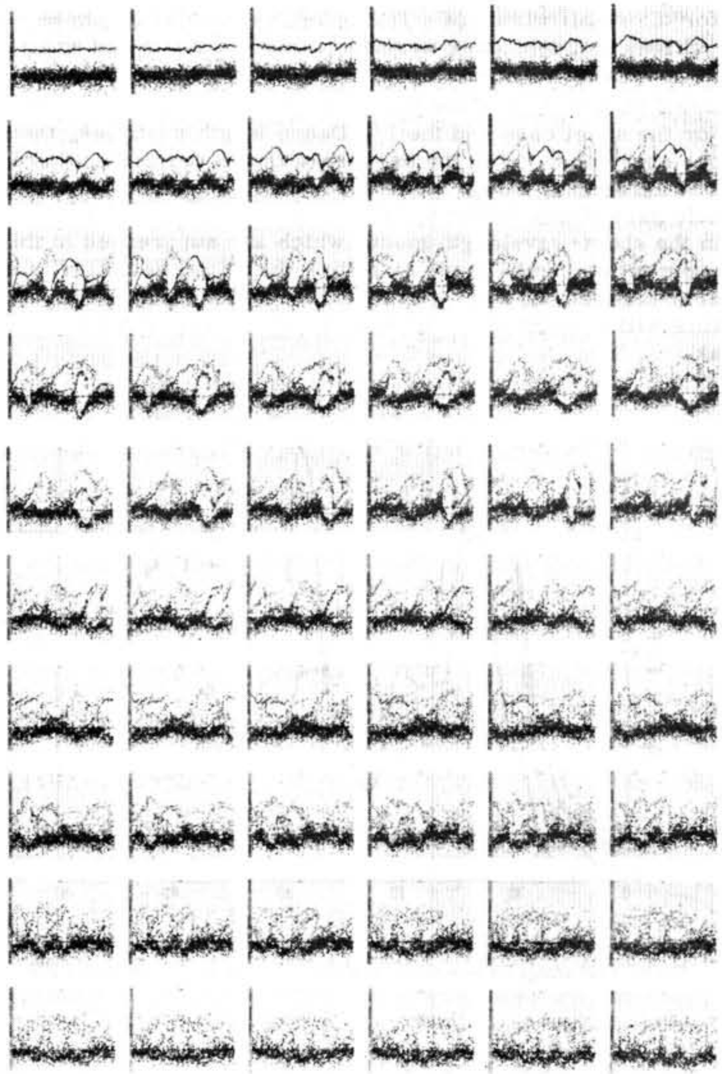

FIG. 2. Vortexes for two-stream instability; sheet model.

3.2. The weak cold beam for finite-size particles

We have also investigated this instability on the finite-size particle model. This was done primarily to compare results with the sheet model case. For this experiment, systems containing 1000 particles were used; one-fifth of them were in the beam. There were twenty particles per Debye length, the beam was cold and had a velocity of four times thermal velocity (again shifting the velocities of all particles so there is no net current). Runs were made with particles of one-half, one, and two Debye lengths for their half widths ($a = 1/2\ \lambda_D, \lambda_D, 2\lambda_D$). For all three runs the initial positions and velocities were the same. A short run was made with the sheet model with identical initial conditions for comparison.

Figure 3 shows plots of the total electric field energy for these four runs. For the sheet case and the 1/2 Debye length particles, there is quite close agreement. For the one Debye length particles, there is still pretty good agreement though some differences appear. However, an appreciable part of this difference can be attributed to the electric field energy in the short-wavelength modes which are suppressed in this case. A rough correction can be made by adding the initial deviation in electric field energy between the $a = \lambda_D$ case and the sheet case, to the $a = \lambda_D$ case. This will account for about half the difference at the time of the first peak.

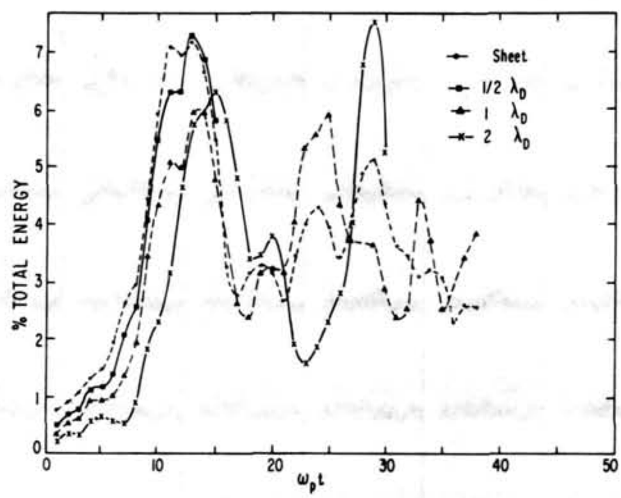

FIG. 3. Electric field energy for two-stream instability; comparison for particles of different sizes.

TABLE I. GROWTH RATES FOR MODES 1-4, VARIOUS PARTICLE SIZES

a/λ_D	Mode Number 1	2	3	4
0	0.163	0.255	0.250	0.148
0.5	0.163	0.255	0.243	0.125
1.0	0.163	0.250	0.220	0.058
2.0	0.162	0.233	0.114	0.002

When one comes to the two Debye length size particles, a qualitative change takes place, in that the first peak in the electric field energy is appreciably reduced and the second peak is much larger. This difference is probably due to the fact that the size of the particle affects the growth rate of mode three. Table I lists the growth rates for all four cases for modes 1-4.

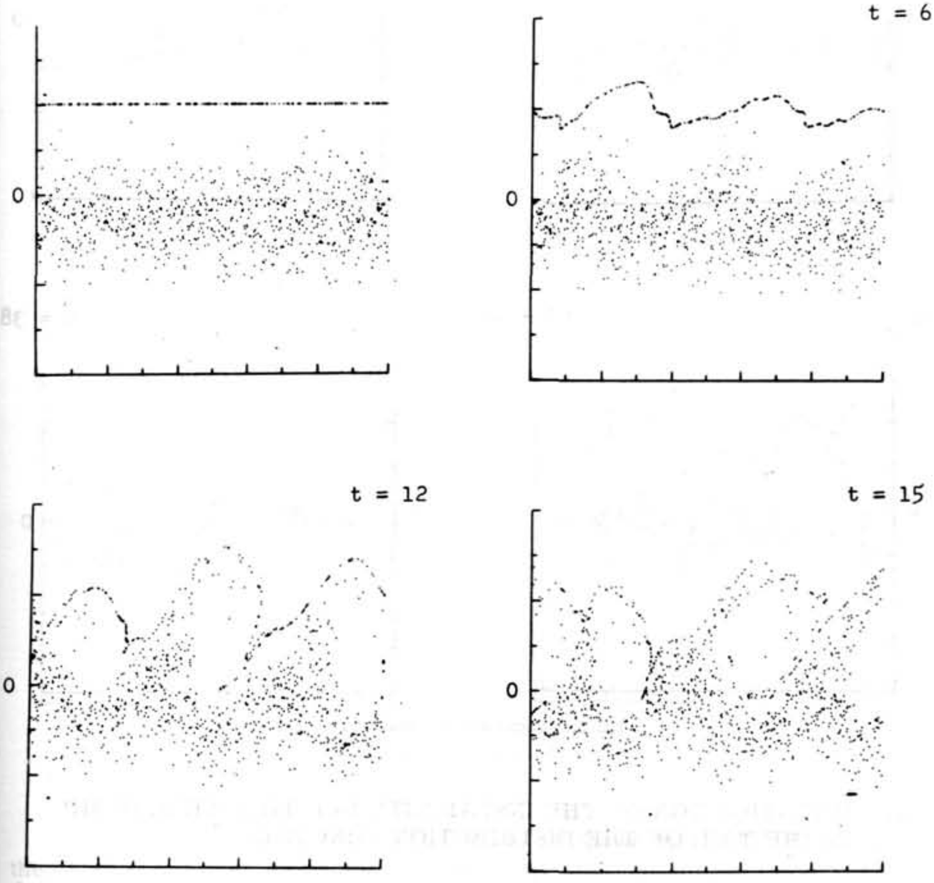

FIG. 4. Vortexes in xv space for $a = \lambda_D/2$.

Figures 4, 5, and 6 show phase space plots of the particle positions for various times. The initial conditions are the same for all cases so that the t = 0 plot for a equals $1/2\ \lambda_D$ would apply to all cases. The plots for $1/2\ \lambda_D$ and $1\ \lambda_D$ are strikingly similar, both as to the number of vortexes formed [3] and their shape at $\omega_p t = 6, 12, 15$. For the case of the equal to $2\ \lambda_D$, however, only two vortexes are formed, and thus there is a qualitative difference. This more or less shows that mode three was effectively stabilized by the finite size of the particle and that this led to the qualitative difference in electric field energy between this case and the others. If more modes had been unstable, say 5 to 10, it is likely that the difference would not have been so great.

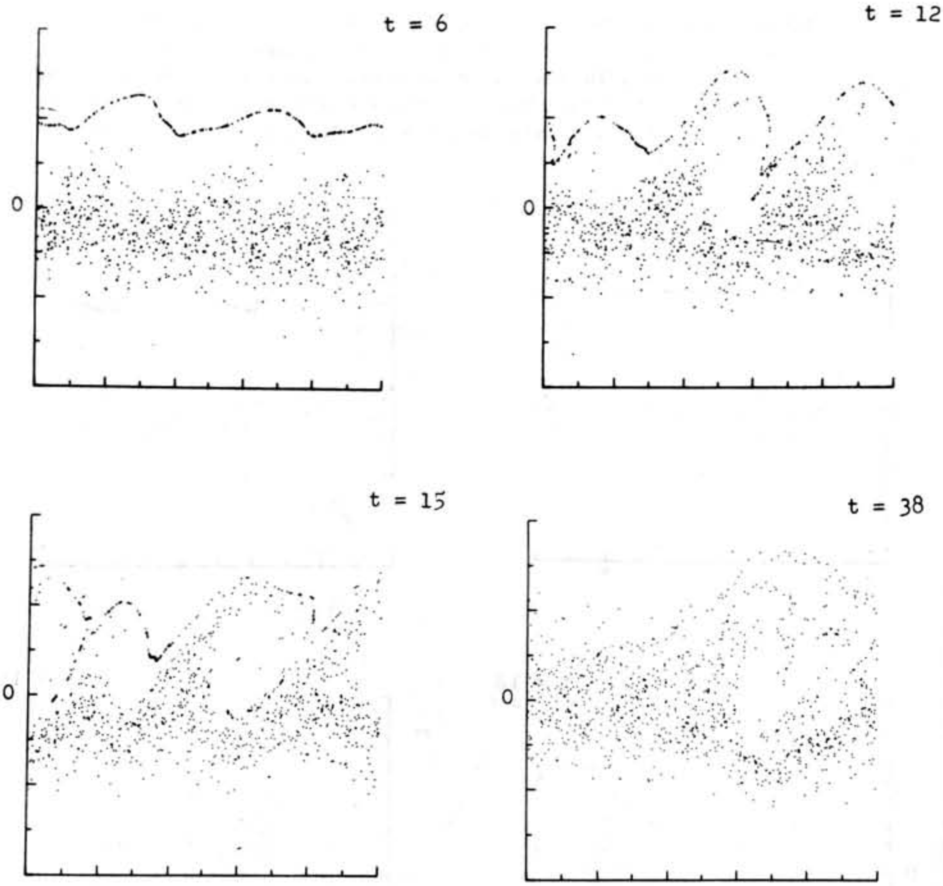

FIG. 5. Vortexes in xv space for $a = \lambda_D$.

4. INVESTIGATION OF THE INSTABILITY DUE TO A WEAK BUMP IN THE TAIL OF THE DISTRIBUTION FUNCTION

A third problem which has been investigated on the finite-size particle model is that of the instability due to a weak bump in the tail of the distribution function. This problem was investigated on the sheet model, and some interesting results were found which are summarized in the introduction. The purpose of redoing this problem on the finite-size particle model was to see if softening the collisions altered these results. It has been found that the results are essentially unaltered.

The case which was run was that of a 1000-particle system with ten particles per Debye length. The beam contained 10% of the particles and had a mean velocity of four times the thermal velocity. The spread in velocity for the beam was the thermal velocity. The velocity of all particles was shifted by $-0.4\ v_T$ so as to give no net current. The particles had half-widths, a, of two Debye lengths. Initially the most unstable mode was mode four.

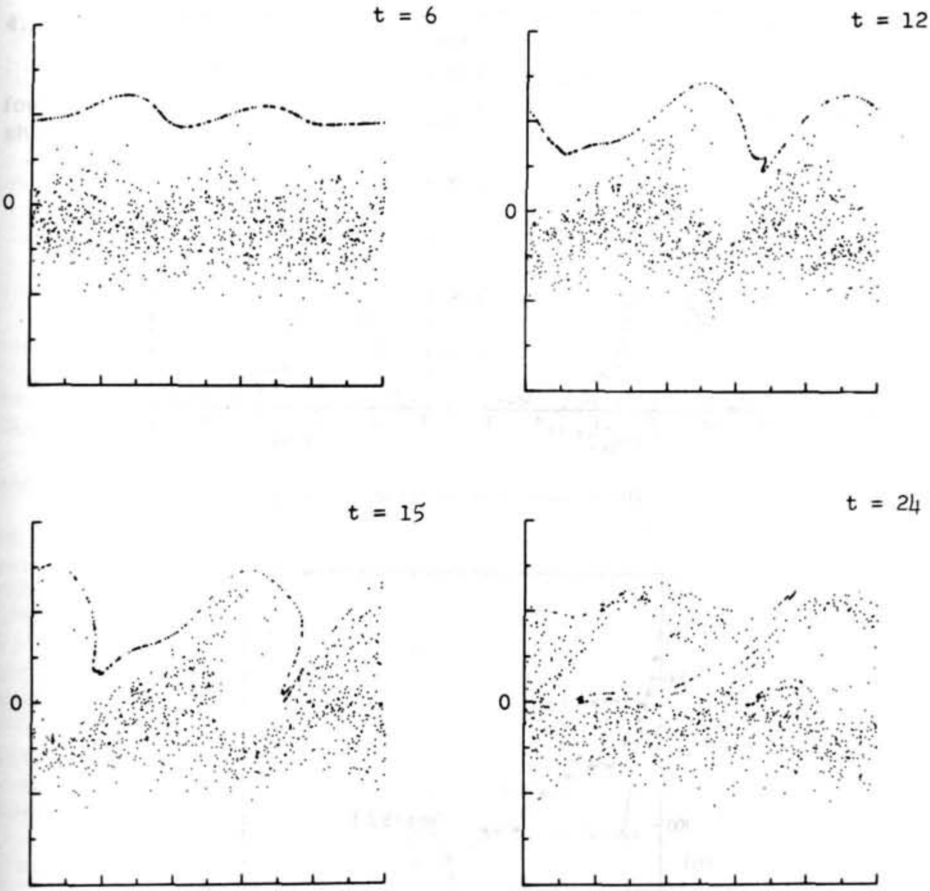

FIG. 6. Vortexes in xv space for a = $2\lambda_D$.

The initial bumps rapidly flattened out as shown in Fig. 7. The tail then slowly extended itself and developed into the Maxwellian shape shown in Fig. 8. This figure shows the log of the distribution function versus velocity squared (shifted by 0.4 v_T to center it with the main Maxwellian) at $\omega_p t$ equals 174 (this is a short-time average of the distribution, averaged over $\Delta t \omega_p$ = 12). The two components of the plasma are clearly shown by the two straight lines. The temperature of the hot component is about eight times that for the cold. The energy contained in the tail is roughly equal to that contained in the initial bump. The tail contains about 15% more particles than it did at time zero (the tail being taken as those particles with velocities greater than twice the thermal velocity). Particles in the tail extend out to 6.9 times the thermal velocity (v_T) at this time. Initially, there was one particle beyond 5.7 v_T.

Figure 9 shows a plot of the average electric field energy versus mode number. The low mode numbers are strongly excited. The average energy at the peak is 7 KT which is roughly the temperature of the tail.

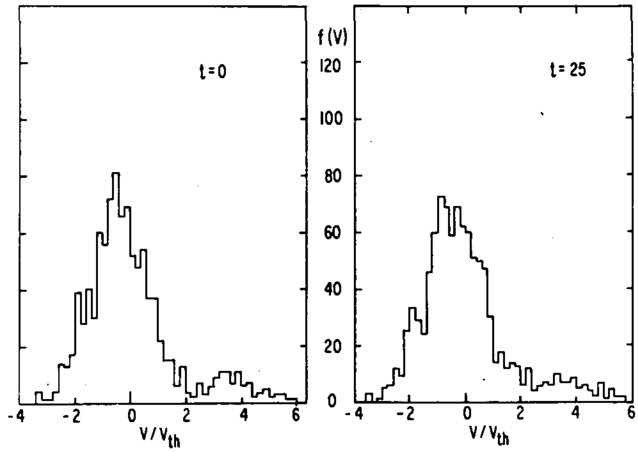

FIG. 7. Distribution function at t = 0 and 25.

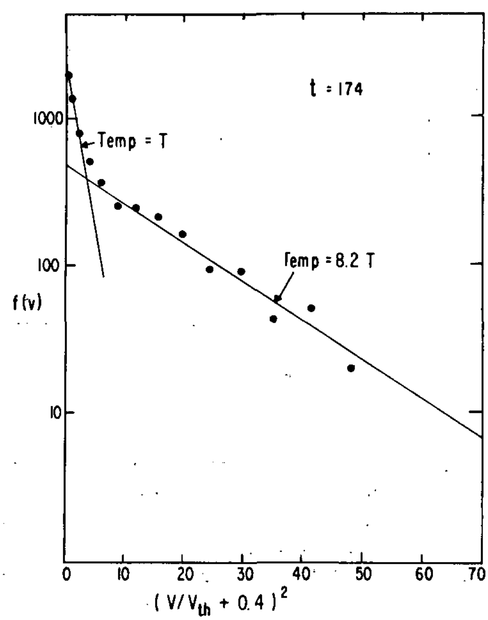

FIG. 8. Two-temperature distribution function.

The electric field energy for mode 4 is plotted vs time in Fig. 10. It shows rapid time variations. Some of this is due to the energy oscillating back and forth between the electric field and the mass motion of the particles (this goes at a frequency of 2 ω_p). However, it is also clear that the wave energy is rapidly changing on a time scale of about 10 ω_p^{-1}. This result is in agreement with the earlier sheet model results.

4.1. Comparison with the sheet model calculation

The results just described are essentially in agreement with those found for the sheet model. The cases run were slightly different. For the sheet model the system contained 2000 particles with 20 particles per

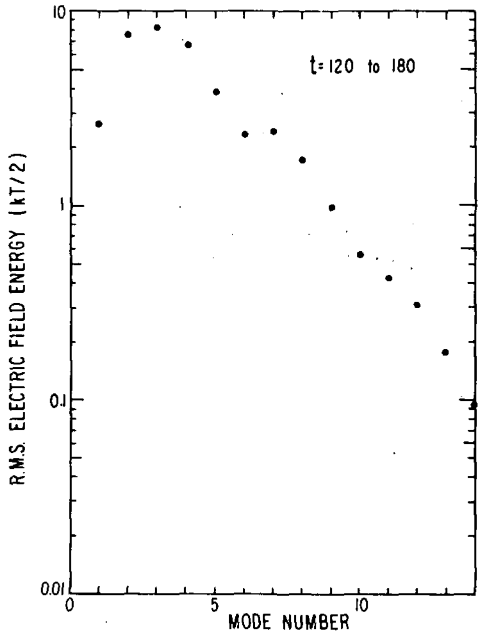

FIG. 9. Electric field energy vs mode number.

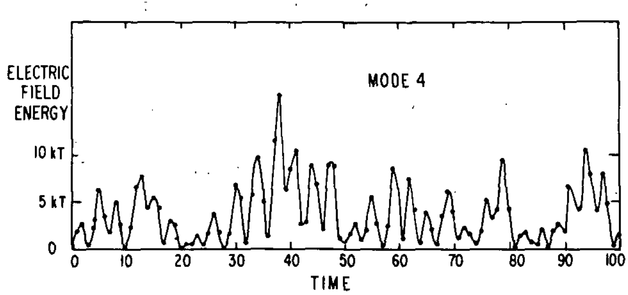

FIG. 10. Fluctuations in electric field energy vs time.

Debye length. The beam contained 5% of the particles rather than the 10% used here. The beam velocity was 3.7 v_T. Initially there were no particles beyond 4.5 v_T for the sheet case whereas for this calculation there were particles all the way out to 5.7 v_T at t equals zero. For the sheet model calculations the mean wave energy for waves with phase velocities lying in the tail was roughly given by the temperature of the tail. The same is found here. Also the waves showed the same kind of rapid fluctuations as are shown in Fig. 10. For the sheet case we interpreted this as resulting from Cherenkov emission and absorption of waves by the fast particles. The same process takes place here; fast moving clouds of charge also will emit waves. The rate of emission is, however, reduced by the factor $\exp\{-2\,\omega_p^2 a^2/v^2\}$. The finite-size particles reduce the collisional effects between the cold particles and hence any influence this would have on the formation and decay of the tail. However, the size does not materially affect the behaviour of the long-wavelength modes. Since we do not expect the short-wavelength modes to play much of a role here, the results should not be greatly affected, as seems to be the case.

In the sheet calculation the tail became Maxwellian after about $\omega_p t$ equal to 150; this is about the same as the time observed here. With the lower energy (10 particles per Debye length) for the finite-particle case, we might have expected somewhat faster relaxation. However, the finite size certainly should slow down the process. If we assume the thermalization comes about due to Cherenkov emission and absorption of waves by the fast particles, then the time should be $\exp\{2\,\omega_p^2 a^2/v_H^2\}$ times longer where v_H is the velocity of the hot particles. Taking a to equal $2\lambda_D$ and v_H to equal $4\,v_T$, this factor is 1.7. For the sheet model, somewhat higher-energy particles were observed (out to 7.8 v_T) but this was only after a very long time ($\omega_p t \approx 300$). For the sheet model, a somewhat larger number of cold particles were drawn into the tail (a 50% increase versus 15% here). This might have been due to the larger fluctuations at short wavelengths for the sheet model, it might be due to the fact that we used a 10% beam here, or both things may play a role.

4.2. Vortexes

We looked for vortexes for the smooth bump-in-tail problem by making phase space plots like those shown before. These plots did not show any pronounced indication of the vortexes found for the 20% cold beam. Thus, the spreading of the beam in velocity and the reduction of its strength greatly reduce or eliminate the vortexes. This trend has also been seen by Morse [13] and is to be expected [14].

ACKNOWLEDGEMENTS

This work was performed under the auspices of the US Atomic Energy Commission, Contract No. AT(30-1)-1238.

REFERENCES

[1] DAWSON, J.M., SHANNY, R., Princeton Plasma Physics Report, MATT-568, submitted to Physics of Fluids for publication.

[2] DAWSON, J.M., SHANNY, R., BIRMINGHAM, T.J., Princeton Plasma Physics Report, MATT-596, submitted to Physics of Fluids for publication.

[3] Sheet encounters do not change the distribution function in one dimension; because of conservation of energy and momentum they can, however, damp a wave (see Ref.[2]).

[4] BIRMINGHAM, T.J., DAWSON, J.M., KULSRUD, R., Physics Fluids 9 (1966) 2014.

[5] WEINSTEIN, R.H., FUX, M.R., Bull. Am. phys. Soc. 12 (1967) 806.

[6] DAWSON, J.M., Physics Fluids 7 (1964) 419.

[7] SMITH, C., DAWSON, J.M., Princeton Plasma Physics Report, MATT-151 (1963); also SMITH, C., Ph. D. Thesis, Princeton University (1963).

[8] HOCKNEY, R., Physics Fluids 9 (1966) 1826.
[9] BIRDSALL, K.V., FUSS, D., Bull. Am. phys. Soc. 11 (1968) 283.
[10] ROBERTS, K.V., BERK, H.L., Phys. Rev. Lett. 19 (1967) 297; also Physics Fluids 10 (1967) 1595.
[11] LEVY, R.H., HOCKNEY, R.W., Physics Fluids 11 (1968) 766.
[12] BYERS, J.A., Physics Fluids 9 (1966) 1038.
[13] MORSE, R.L., Private communication.
[14] ONEIL, T.M., MALBERY, J.H., General Atomic Report GA-8253 (1967).

DISCUSSION

E. CANOBBIO: What happens to the exclusion principle in phase space in the case of Gaussian particles? Are there any quantum-like effects?

J.M. DAWSON: The flow in phase space (x, v space, where x is the position of the centre of the particle and v is its velocity) satisfies Liouville's theorem. However, the particles are allowed to pass freely through one another, so there is no exclusion in this sense. We use a finite, discrete set of k's, so that the problem is quantized in that sense.

B. BRUNELLI (Chairman): How powerful does the computer have to be for extension of the numerical experiments to two and three dimensions?

J.M. DAWSON: In the one-dimensional case it takes about two minutes for a time of ω_p^{-1} (1000 particles, 20 modes). The calculation is proportional to the number of particles multiplied by the number of modes. For two dimensions the situation is roughly the same and, since one probably needs more particles and more modes, computation is correspondingly slower. However, we believe that through the introduction of modifications the calculation can be made proportional to the number of particles plus the square of the number of modes. This should be much faster, and we can probably reduce it to a couple of minutes per ω_p^{-1}.

НЕЛИНЕЙНЫЕ ВОЛНОВЫЕ ЯВЛЕНИЯ В ВЫСОКОТЕМПЕРАТУРНОЙ ПЛАЗМЕ

К.С.КАРПЛЮК, Я.И.КОЛЕСНИЧЕНКО,
Э.Н.КРИВОРУЦКИЙ, В.Г.МАХАНЬКОВ,
В.Н.ОРАЕВСКИЙ, В.П.ПАВЛЕНКО
и В.Н.ЦЫТОВИЧ
ИНСТИТУТ ФИЗИКИ АН УССР, КИЕВ,
СССР

Abstract — Аннотация

NON-LINEAR WAVE PHENOMENA IN A HIGH-TEMPERATURE PLASMA. In most plasma experiments the non-linear plasma properties are very pronounced - hence the interest in non-linear plasma theory and particularly in the non-linear theory of the interaction of waves in a plasma. The study of wave interaction mechanisms is important from the point of view of understanding the many physical processes which occur in a high-temperature plasma (relaxation processes in an unstable plasma, propagation of collisionless shock waves, high-frequency stabilization of plasma instabilities, etc.). The authors of the present paper investigate two aspects of the theory of wave interaction:

1. The theory of wave interaction in bounded plasma systems;
2. The substantial change in the dispersion properties of drift oscillations in a plasma with high-frequency turbulence.

In most works on the theory of wave interaction in a plasma the calculations are based on the assumption of an unbounded plasma. In actual devices, however, the boundaries often affect wave propagation; this is reflected both in changes in the dispersion characteristics of the waves in an unbounded plasma and in the appearance of a new type of wave found only in bounded systems (surface waves).

In the first part of the paper the authors set forth the theory of wave interaction in a bounded plasma. The method employed enables one to take into account interactions of all types of wave - both space and surface. Particular attention is paid to the procedure for deriving equations for the interacting waves. With the help of these equations the authors consider a number of concrete three-plasmon interactions. The special features of the interaction of waves in a bounded plasma are also noted.

In most cases, together with the unbounded plasma approximation, works on non-linear plasma theory resort explicitly to the assumption that the individual wave interactions are independent. This assumption is not always valid. In the second part of the paper the authors consider cases where certain wave processes have a considerable effect on others. It is shown that the developed high-frequency turbulence of a plasma has a substantial effect on the spectrum and build-up of drift oscillations.

Even in cases of relatively weak turbulence there is a critical turbulence energy at which the stabilization of drift, hydrodynamic, kinetic and other instabilities becomes possible. The authors find a new class of non-linear drift instabilities occurring in a turbulent plasma.

НЕЛИНЕЙНЫЕ ВОЛНОВЫЕ ЯВЛЕНИЯ В ВЫСОКОТЕМПЕРАТУРНОЙ ПЛАЗМЕ. В большинстве плазменных экспериментов резко проявляются нелинейные свойства плазмы. Именно этим обусловлен интерес к теоретическим работам, в частности, к работам по нелинейной теории взаимодействия волн в плазме. Изучение механизмов взаимодействия волн важно для понимания физических процессов, происходящих в высокотемпературной плазме (в частности, таких, как релаксационные процессы в неустойчивой плазме, распространение бесстолкновительных ударных волн, высокочастотная стабилизация плазменных неустойчивостей и т.д.). В данной работе исследуются два аспекта теории взаимодействия волн. Рассмотрены: 1) теория взаимодействия волн в ограниченных плазменных системах; 2) существенное изменение дисперсионных свойств дрейфовых колебаний в плазме с высокочастотной турбулентностью. Обычно в работах по теории взаимодействия волн в плазме расчет ведется в приближении безграничной плазмы. Однако,в реальных установках часто сказывается влияние границ на распространение волн в плазме. Это влияние проявляется как в изменении дисперсионных характеристик волн, существующих в безграничной плазме, так и в появлении нового типа волн, присущего только ограниченным системам так называемых поверхностных волн. Излагается теория взаимодействия волн в ограниченной плазме. Используемая методика позволяет учитывать взаимодействия всех видов волн как объемных, так и поверхностных. Основное внимание уделяется процедуре вывода уравнений для взаимодействующих волн. С помощью полученных уравнений рассматриваются конкретные трехплазменные взаимодействия. Отмечены особенности взаимодействия волн в ограниченной плазме. Наряду с использованием приближения безграничной плазмы, обычно в работах по нелинейной теории плазмы явно или неявно используется предположение о независимости отдельных волновых взаимодействий, которое не всегда справедливо. Рассматриваются случаи, когда одни волновые процессы существенно влияют на другие. Показано, что развитая высокочастотная турбулентность плазмы существенно влияет на спектр и раскачку дрейфовых колебаний. Даже при относительно слабой турбулентности существует критическое значение энергии турбулентности, начиная с которого возможна стабилизация дрейфовых, а также других как гидродинамических, так и кинетических неустойчивостей. Найден новый класс нелинейно-дрейфовых неустойчивостей турбулентной плазмы.

1. ВЗАИМОДЕЙСТВИЕ ВОЛН В ОГРАНИЧЕННОЙ ПЛАЗМЕ

Запишем систему гидродинамических уравнений для плазмы совместно с уравнениями Максвелла (в случае слабой нелинейности) в следующем виде:

$$\left(i\frac{\partial}{\partial t} + \hat{H}_0\right)\psi + \hat{H}_1(\psi,\psi) = 0 \; ; \qquad (\text{I.I})$$

где ψ -вектор, описывающий состояние плазмы, $\hat{H}_0$ -линейный дифференциальный оператор с разрывными (на границе плазмы) коэффициентами, описывающий линейные колебания плазмы; $\hat{H}_1$ -квадратичный по ψ дифференциальный оператор, стремящийся к нулю при стремлении вектора ψ к ψ_0-вектору, который описывает равновесное состояние плазмы. Уравнение (I.I) совместно с соответствующими граничными условиями определяет вектор состояния ψ.

Учитывая слабую нелинейность, решение уравнения (I.I) можем находить методом теории возмущений [1-3]. Тогда в нулевом приближении зависимость вектора состояния от времени может быть выбрана в виде $exp\{-i\omega t\}$,и задача сводится к отысканию собственных значений оператора $\hat{H}_0$:

$$\left(\omega + \hat{H}_0\right)\psi_\omega^{(0)} = 0 \qquad (\text{I.2})$$

В первом приближении вектор состояния ψ можно представить в виде:

$$\psi = \sum C_{\omega'}(t)\,\psi_{\omega'}^{(0)} \qquad (I.3)$$

где $C_{\omega'}(t)$–амплитуды волн, медленно меняющиеся во времени.

Для получения уравнения, описывающего изменение во времени амплитуды волны C_{ω}, необходимо подставить (I.3) в (I.I), а затем спроектировать полученное уравнение на направление $\psi_{\omega}^{(0)}$. Проектирование можно осуществить умножением (I.I) скалярно на вектор $\tilde{\psi}_{\tilde{\omega}}^{(0)}$, который определяется сопряженными граничными условиями совместно с уравнением, эрмитово сопряженным к (I.2) [I].

$$(\tilde{\omega} + \hat{H}_0^{+})\tilde{\psi}_{\tilde{\omega}}^{(0)} = 0\,; \qquad (I.4)$$

После осуществления описанной процедуры получим динамическое уравнение, описывающее изменение во времени амплитуды $C_{\omega}(t)$, обусловленное взаимодействием волн (см.также [2 – 5].

$$\frac{\partial C_{\omega}}{\partial t} = -i\sum_{\omega_1\omega_2} V_{\omega\omega_1\omega_2}\, C_{\omega_1} C_{\omega_2} \qquad (I.5)$$

где

$$V_{\omega\omega_1\omega_2} = -\frac{(\tilde{\psi}_{\tilde{\omega}}^{(0)}, \hat{H}_1)}{(\tilde{\psi}_{\tilde{\omega}}^{(0)}, \psi_{\omega}^{(0)})} \qquad (I.6)$$

Применим описанный выше формализм к ряду конкретных примеров. Учитывая практическую важность цилиндрических систем и близких к ним тороидальных систем с малой тороидаль-

---

I) Для того, чтобы любая собственная функция $\tilde{\psi}_{\tilde{\omega}'}$ была ортогональная ко всем собственным функциям ψ_{ω}, за исключением $\psi_{\omega'}$, необходимо все собственные значения сопряженной задачи $\tilde{\omega}$ поставить в соответствие собственным значениям ω таким образом, чтобы $\tilde{\omega}' = \omega'^{*}$. Тогда системы функций ψ_{ω} и $\tilde{\psi}_{\tilde{\omega}}$ называются биортогональными.

ностью, всюду в дальнейшем рассмотрение будет проведено для цилиндрического плазменного столба в магнитном поле.

В качестве примера рассмотрим взаимодействие магнитогидродинамических волн в плазменном цилиндре, удерживаемом в вакууме продольным магнитным полем. Прежде всего необходимо решить линейную задачу. В силу цилиндрической симметрии зависимость собственных векторов от продольной и азимутальной координат выберем в виде $\exp\{ik_z z + im\varphi\}$. Тогда оператор $\hat{H}_0$ принимает вид:

I) <u>для внутренней области</u> (величины во внутренней области будем обозначать индексом "i"; в случае, когда это не вызовет недоразумений, этот индекс будем опускать).

$$\hat{H}_0^{(i)} = \begin{pmatrix} 0 & \frac{i}{r}\frac{\partial}{\partial r} r & -\frac{m}{r} & -k_z & 0 & 0 & 0 \\ iS^2\frac{\partial}{\partial r} & 0 & 0 & 0 & k_z V_A^2 & 0 & iV_A^2\frac{\partial}{\partial r} \\ -S^2\frac{m}{r} & 0 & 0 & 0 & 0 & k_z V_A^2 & -\frac{m}{r}V_A^2 \\ -k_z S^2 & 0 & 0 & 0 & 0 & 0 & 0 \\ 0 & k_z & 0 & 0 & 0 & 0 & 0 \\ 0 & 0 & k_z & 0 & 0 & 0 & 0 \\ 0 & \frac{i}{r}\frac{\partial}{\partial r} r & -\frac{m}{r} & 0 & 0 & 0 & 0 \end{pmatrix} \qquad (1.7)$$

Компоненты кэт-вектора Ψ связаны с магнитогидродинамическими величинами следующим образом:

$$\psi_1 = \frac{\rho}{\rho_0} \equiv n; \quad \psi_{2,3,4} = V_{r,\varphi,z}; \quad \psi_{5,6,7} = \frac{H_{r,\varphi,z}}{H_0^{(i)}} \equiv h_{r,\varphi,z}; \qquad (I.8)$$

где ρ, $\vec{H}$ -малые отклонения плотности и магнитного поля от своих равновесных значений ρ_0; $H_0^{(i)}$; $S^2 = \gamma\frac{p_0}{\rho_0}$; $V_A^2 = \frac{H_0^{(i)2}}{4\pi\rho_0}$; $\vec{V}$ -гидродинамическая скорость,

2) для внешней области (все величины во внешней области будем обозначать индексом "e").

$$\hat{H}_0^{(e)} = \begin{pmatrix} 0 & 0 & 0 & 0 & k_z c & -\frac{mc}{r} \\ 0 & 0 & 0 & -k_z c & 0 & -ic\frac{\partial}{\partial r} \\ 0 & 0 & 0 & \frac{mc}{r} & \frac{ic}{r}\frac{\partial}{\partial r}r & 0 \\ 0 & -k_z c & \frac{mc}{r} & 0 & 0 & 0 \\ k_z c & 0 & ic\frac{\partial}{\partial r} & 0 & 0 & 0 \\ -\frac{mc}{r} & -\frac{ic}{r}\frac{\partial}{\partial r}r & 0 & 0 & 0 & 0 \end{pmatrix} \qquad (I.9)$$

а компоненты вектора ψ связаны с электрическим и магнитными полями:

$$\psi_{1,2,3}^{(e)} = H_{r,\varphi,z}^{(e)} / H_0^{(e)} \equiv h_{r,\varphi,z}^{(e)}; \; \psi_{4,5,6}^{(e)} = E_{r,\varphi,z} / H_0^{(e)} \equiv e_{r,\varphi,z}^{(e)}, \qquad (I.10)$$

Уравнение (I.2) с оператором $\hat{H}_0$, который задается выражениями (I.7), (I.9), совместно с граничными условиями

$$\delta^2 n + V_A^2 h_z^{(i)} = V_A^{(e)2} h_z^{(e)}; \quad V_r = c\, e_\varphi^{(e)}; \quad e_z^{(e)} = 0 ; \qquad (I.11)$$

(где $V_A^{(e)2} = H_0^{(e)2} / 4\pi\rho_0$) определяет собственные функции и собственные значения линейной задачи. В граничных условиях все величины следует брать, вообще говоря, на смещенной границе плазмы $r = a + \xi$ (a-радиус плазменного шнура, ξ -смещение границы плазмы вследствие колебаний). Однако, в силу того, что мы рассматриваем однородную плазму с резкой границей, в граничных условиях (I.II) все величины берутся при $r = a$ [2].

Найдем эрмитово сопряженный оператор $\hat{H}_0^+$, используя хорошо известное определение:

$$(\chi, \hat{H}_0 \psi) = (\hat{H}_0^+ \chi, \psi) \qquad (I.12)$$

---

2) Тем не менее, колебания границы плазмы учитываются, поскольку V_r не равно нулю на равновесной границе.

Здесь ψ и χ -произвольные функции, удовлетворяющие соответственно граничным условиям (I.II) и сопряженным к ним; скалярное произведение определено обычным образом:

$$(\chi,\psi)=\frac{1}{V}\int\limits_V d\vec{z}\,\chi_i^*\psi_i\ ; \tag{I.13}$$

Подставляя выражения для $\hat{H}_o$ из (I.7) и (I.9) в (I.I2) и выполняя интегрирование по частям, получим:

$$(\chi,\hat{H}_o\psi)=(\hat{A}\chi,\psi)+i\oint\limits_{r=a}dz\,r\,d\varphi\Big\{c\Big[\chi_3^{(e)*}\psi_5^{(e)}+\chi_5^{(e)*}\psi_3^{(e)}\Big]- \tag{I.14}$$
$$-\Big[\chi_2^{(i)*}\big(S^2\psi_1^{(i)}+V_A^2\psi_7^{(i)}\big)+\big(\chi_1^{(i)*}+\chi_7^{(i)*}\big)\psi_2^{(i)}\Big]\Big\}\ ;$$

Учитывая (I.II), (I.I4), можно записать сопряженные граничные условия (являющиеся условием обращения в нуль поверхностного интеграла):

$$\chi_1^{(i)}+\chi_7^{(i)}=\chi_6^{(e)}\ ;\qquad V_A^{(e)2}\chi_2^{(i)}=c\chi_5^{(e)}\ ; \tag{I.15}$$

На классе функций, удовлетворяющих граничным условиям (I.I5), оператор $\hat{A}$ является оператором $\hat{H}_o^+$ и имеет вид:

I) <u>во внутренней области:</u>

$$\hat{H}_o^{(i)+}=\begin{pmatrix} 0 & i\frac{S^2}{r}\frac{\partial}{\partial r}r & -S^2\frac{m}{r} & -K_zS^2 & 0 & 0 & 0\\ i\frac{\partial}{\partial r} & 0 & 0 & 0 & K_z & 0 & i\frac{\partial}{\partial r}\\ -\frac{m}{r} & 0 & 0 & 0 & 0 & K_z & -\frac{m}{r}\\ -K_z & 0 & 0 & 0 & 0 & 0 & 0\\ 0 & K_zV_A^2 & 0 & 0 & 0 & 0 & 0\\ 0 & 0 & K_zV_A^2 & 0 & 0 & 0 & 0\\ 0 & i\frac{V_A^2}{r}\frac{\partial}{\partial r}r & -\frac{m}{r}V_A^2 & 0 & 0 & 0 & 0 \end{pmatrix} \tag{I.16}$$

2) <u>во внешней области</u> $\hat{H}_o^{(e)+}$ представляется матрицей (I.9).

Сравнивая выражения для $\hat{H}_o^+$ и $\hat{H}_o$ (см.(I.7),(I.9) и (I.II), (I,I5)) нетрудно установить справедливость следующего равенства:

$$\tilde{\psi}_{\tilde{\omega}}=\hat{\gamma}\,\psi_\omega \tag{I.17}$$

где

$$\gamma^{(i)} = \begin{pmatrix} \frac{S^2}{V_A^2} & 0 & 0 \\ 0 & \frac{\overleftrightarrow{1}}{V_A^2} & 0 \\ 0 & 0 & \overleftrightarrow{1} \end{pmatrix}; \quad \overleftrightarrow{1} = \begin{pmatrix} 1 & 0 & 0 \\ 0 & 1 & 0 \\ 0 & 0 & 1 \end{pmatrix}; \quad \gamma^{(e)}_{ik} = \delta_{ik} \qquad (I.18)$$

Нетрудно также получить систему собственных функций оператора $\hat{H}_0$. Для волн, не возмущающих плотность плазмы (альфвеновские волны), $\psi_\omega^{(e)} = 0$, а собственные функции во внутренней области в случае аксиально симметричной моды (m =0) такие:

$$n = h_r = h_z = 0; \quad V_r = V_z = 0; \quad h_\varphi = -\frac{k_z}{\omega} V_\varphi; \qquad (I.19)$$

$$V_\varphi = f(r) \exp\{-i\omega t + ik_z z\};$$

и в случае $m \neq 0$:

$$n = h_z = 0; \quad V_z = 0; \quad V_\varphi = \frac{i}{m}\frac{\partial}{\partial r}(rV_r); \quad h_r = -\frac{k_z}{\omega}V_r; \quad h_\varphi = -\frac{k_z}{\omega}V_\varphi; \qquad (I.20)$$

$$V_r = (r-a)\,g(r) \exp\{-i\omega t + ik_z z + im\varphi\};$$

где $f(r)$ и $g(r)$ –произвольные ограниченные функции r.

(собственные значения альфвеновских волн определяются таким же соотношением, как и для безграничной плазмы $\omega^2 = k_z^2 V_A^2$).

Для магнитозвуковых волн ($n \neq 0$) собственные функции определяются следующими соотношениями:

$$\left.\begin{aligned} V_r &= \frac{\alpha}{i\omega}\frac{\partial n}{\partial r}; \quad V_\varphi = \frac{\alpha m}{\omega r} n; \quad V_z = \frac{k_z}{\omega} S^2 n; \\ h_r &= i\frac{\alpha k_z}{\omega^2}\frac{\partial n}{\partial r}; \quad h_\varphi = -\frac{\alpha k_z m}{\omega^2 r} n; \quad h_z = \lambda n \end{aligned}\right\} \qquad (I.21)$$

$$\left.\begin{aligned} n &= C_1 J_m(|k_r| r) \exp\{-i\omega t + ik_z z + im\varphi\}; \quad \text{при } k_r^2 > 0 \\ n &= C_2 I_m(|k_r| r) \exp\{-i\omega t + ik_z z + im\varphi\}; \quad \text{при } k_r^2 < 0 \end{aligned}\right\} \qquad (I.22)$$

где

$$k_r^2 = \frac{(\omega^2 - k_z^2 V_A^2)(\omega^2 - k_z^2 S'^2)}{\omega^2 (V_A^2 + S^2) - k_z^2 V_A^2 S^2} \qquad (I.23)$$

$$\alpha = \frac{\omega^2 - k_z^2 S'^2}{k_r^2}; \quad \lambda = 1 - \frac{k_z^2 S^2}{\omega^2} \qquad (I.24)$$

J_m и I_m –обычная и модифицированная функции Бесселя.

Во внешней области компоненты вектора состояния такие:

$$h_r^{(e)} = -i\frac{k_z}{\varkappa^2}\frac{\partial h_z^{(e)}}{\partial r}; \quad h_\varphi^{(e)} = \frac{m}{r}\frac{k_z}{\varkappa^2}h_z^{(e)}; \quad e_r^{(e)} = \frac{m}{r}\frac{\omega}{\varkappa^2 c}h_z^{(e)}; \tag{I.25}$$

$$e_\varphi^{(e)} = \frac{i\omega}{c\varkappa^2}\frac{\partial h_z^{(e)}}{\partial r}; \quad e_z^{(e)} = 0; \quad h_z^{(e)} = C^{(e)}K_m(|\varkappa| r)\exp\{-i\omega t + ik_z z + im\varphi\};$$

где $K_m(|\varkappa| r)$ -функция Макдональда, $\varkappa^2 = k_z^2 - \frac{\omega^2}{c^2}$;

Сшивая с помощью граничных условий внутренние решения (I.2I), (I.22) с внешними решениями (I.25), получим уравнения, которые совместно с уравнением (I.23) полностью определяют дисперсию рассматриваемых волн [3]:

$$\frac{J_m'(|k_r|a)}{J_m(|k_r|a)} = \frac{(k_z^2 V_A^2 - \omega^2)K_m'(|\varkappa|a)}{|k_r|\varkappa V_A^{(e)2} K_m(|\varkappa|a)} \tag{I.26}$$

В (I.26), штрих означает дифференцирование по аргументу функции.

Приведем результаты анализа полученных уравнений [6]. При $k_r a \ll 1$ уравнение (I.26) описывает в случае $m \neq 0$ поверхностные волны с дисперсией.

$$\omega \simeq \pm\sqrt{2}\, k_z V_A \tag{I.27}$$

и в случае, когда $m = 0$ обьемные волны с дисперсией

$$\omega^2 \simeq k_z^2 S'^2 \tag{I.28}$$

При $k_r a \gg \max(m, 1)$ уравнение (I.26) совместно с (I.23) описывает обьемные волны с дисперсией:

$$\omega_{1,2} \simeq \pm k V_A; \quad \omega_{3,4} \simeq \pm k_z S; \quad k^2 \equiv k_r^2 + k_z^2; \tag{I.29}$$

Это обычная быстрая и медленная магнитозвуковая волны с тем отличием от безграничной плазмы, что k_r дискретно.

Полученные собственные значения совместно с (I.I9)-(I.23) полностью определяют собственные вектора $\psi_\omega^{(0)}$ оператора $\hat{H}_0$ и сопряженные к ним $\tilde{\psi}_\omega^{(0)}$.

---

3) В дальнейшем будем рассматривать $\beta \ll 1$. Тогда k_r^2 всегда положительная величина.

Как видно из (I.6), для вычисления матричного элемента необходимо найти ($\widetilde{\psi}^{(0)}_{\omega}, \hat{H}_1$), а также норму ($\widetilde{\psi}^{(0)}_{\omega}, \psi^{(0)}_{\omega}$). Выпишем явный вид $\hat{H}_1$,описывающего взаимодействия магнитогидродинамических волн.

$$\hat{H}_1 = \sum_{\sigma_1}\sum_{\sigma_2} C_{\sigma_1} C_{\sigma_2} \begin{pmatrix} i \operatorname{div} n_{\sigma_1} \vec{V}_{\sigma_2} \\ i(\vec{V}_{\sigma_1}\nabla)\vec{V}_{\sigma_2} + i n_{\sigma_1}\frac{\partial \vec{V}_{\sigma_2}}{\partial t} + iS^2(\gamma-1) n_{\sigma_1}\nabla n_{\sigma_2} + iV_A^2[\vec{h}_{\sigma_1}\times \operatorname{rot} \vec{h}_{\sigma_2}] \\ -i \operatorname{rot} \vec{V}_{\sigma_1} \times \vec{h}_{\sigma_2} \end{pmatrix} \qquad (I.30)$$

где $\sigma = \{\omega, m, k_z\}$

Используя (I.30), нетрудно найти явный вид матричных элементов $V_{\sigma\sigma_1\sigma_2}$. Матричный элемент, описывающий взаимодействие альфвеновских волн, так же как безграничной плазмы, равен нулю. Взаимодействие магнитозвуковой волны с альфвеновскими описывается матричным элементом:

$$V_{\sigma\sigma_1\sigma_2} = \frac{\sqrt{\omega_1\omega_2/\omega H_0^2}}{\prod_i (\widetilde{\psi}_i, \psi_i)^{1/2}} \frac{\alpha_1}{V_A^2\omega_1} \int_0^a dr \Big\{ \Big[V_{r_2}\Big(-im_2 V_\varphi^* - V_r^* + V_r^* r\frac{\partial}{\partial r}\Big) + V_\varphi^* \frac{\partial}{\partial r}(rV_{\varphi_2}) \Big] \frac{\partial n_1}{\partial r} -$$

$$- V_r^* V_{\varphi_2}\Big[(m_2-m_1)\frac{\partial n_1}{\partial r} + 2\frac{m_1}{r} n_1\Big] - V_\varphi^* V_{\varphi_2} n_1 \frac{m_1^2}{r} + m_1 \frac{\omega}{k_z}\Big(\frac{k_{z1}}{\omega_1} - \frac{k_{z2}}{\omega_2}\Big)\Big(mV_r^* + iV_\varphi^* r\frac{\partial}{\partial r}\Big) V_{r_2}\frac{n_1}{r} +$$

$$+ V_A^2 \frac{k_z}{\omega}\Big(\frac{k_{z2}}{\omega_2} - \frac{k_{z1}}{\omega_1}\Big)\Big(-imV_r^* + V_\varphi^* r\frac{\partial}{\partial r}\Big)\Big(V_{\varphi_2}\frac{\partial n_1}{\partial r}\Big) - rn_1\big(V_r^* V_{r_2} + V_\varphi^* V_{\varphi_2}\big) \times \qquad (I.31)$$

$$\Big[\frac{m_1 m_2}{r^2} + S^2\frac{k_{z1}k_{z2}}{\alpha_1}\Big(1+\frac{\omega}{\omega_2}\Big) + \frac{\omega_1\omega_2}{\alpha_1}(\lambda_1 - 1) + \lambda_1\frac{\omega\omega_1}{\alpha_1}\Big] +$$

$$+ V_A^2 \frac{k_{z1}k_{z2}}{\omega_1\omega_2}\Big(\frac{m_1}{r}V_r^* n_1 + iV_\varphi^*\frac{\partial n_1}{\partial r}\Big)\Big(i\frac{\partial}{\partial r}(rV_{\varphi_2}) + m_2 V_{r2}\Big)\Big\}$$

$$\text{Здесь:}\quad (\widetilde{\psi}_\omega, \psi_\omega)_A = \frac{4}{a^2 V_A^2}\int_0^a r\,dr\,(V_r^2 + V_\varphi^2) \qquad (1.32)$$

$$(\widetilde{\psi}_\omega, \psi_\omega)_{M,S} = \frac{2}{1 - k_z^2 V_A^2/\omega^2}\Big\{\Big(1 - \frac{2k_z^2 S^2}{\omega^2}\Big)\big(J_m'^2 - J_m J_m''\big) + \frac{1}{k_z a} J_m J_m'\Big\}; \qquad (1.33)$$

$$n_i = J_{m_i}(|k_{z_i}| r)$$

а V_r и V_φ определены (I.19) и (I.20). Следующий матричный элемент определяет взаимодействие альфвеновской с магнитозвуковыми волнами:

$$
\begin{aligned}
&V_{\sigma\sigma_1\sigma_2} = W_{\sigma\sigma_1\sigma_2} + W_{\sigma\sigma_2\sigma_1} \\
&W_{\sigma\sigma_1\sigma_2} = \frac{\sqrt{\omega_1\omega_2/\omega H_0^2}}{\prod_i(\tilde{\Psi}_i,\Psi_i)^{1/2}} \int_0^a r\,dr \Big\{ n_1\Big(iV_r^*\frac{\partial n_2}{\partial r} - \frac{m_2}{r}V_\varphi^* n_2\Big)\times \\
&\Big[\lambda_1\Big(\lambda_2+\alpha_2\frac{k_{z2}^2}{\omega_2}\Big) + \frac{\alpha_2}{V_A^2}\frac{\omega}{\omega_2}\Big(\lambda_1 + S^2\frac{k_{z1}k_{z2}}{\omega_1\omega_2}\Big) + \frac{\alpha_2}{V_A^2}\Big(\frac{\alpha_1 m_1 m_2}{\omega_1\omega_2 r^2} + \\
&+ S^2\frac{k_{z1}k_{z2}}{\omega_1\omega_2} - 1\Big)\Big] + \frac{\alpha_1\alpha_2}{V_A^2\omega_1\omega_2}\Big[-i\frac{m_1}{r^3}V_r^* n_1 n_2 + \frac{V_\varphi^*}{r}\frac{\partial n_1}{\partial r}\frac{\partial n_2}{\partial r}\Big] + \\
&+ \frac{\alpha_1\alpha_2}{V_A^2\omega_1\omega_2}\Big[\frac{\omega}{k_z}\Big(\frac{k_{z2}}{\omega_2} - \frac{k_{z1}}{\omega_1}\Big)\Big(-\frac{im}{r}V_r^* + V_\varphi^*\frac{\partial}{\partial r}\Big)\frac{n_2}{r}\frac{\partial n_1}{\partial r}\Big]\Big\}
\end{aligned}
\tag{I.34}
$$

И, наконец, матричный элемент, описывающий взаимодействие магнитозвуковых волн:

$$
\begin{aligned}
&W_{\sigma\sigma_1\sigma_2} = \frac{\sqrt{\omega_1\omega_2/\omega H_0^2}}{\prod_i(\tilde{\Psi}_i,\Psi_i)^{1/2}} \int_0^a r\,dr \Big\{ -n^* n_1 n_2 \Big[\beta\Big\langle \frac{m m_2}{r^2}\Big(\frac{\alpha_2}{\omega_2} + (\gamma-1)\frac{\alpha}{\omega}\Big) + \\
&+ S^2 k_z k_{z2}\Big(\frac{1}{\omega_2} + \frac{\gamma-1}{\omega}\Big)\Big\rangle + \frac{m_2}{\omega r^2}\Big(\lambda_2 + \frac{k_{z2}^2\alpha_2}{\omega_2^2}\Big)\Big(\alpha m\lambda_1 + S^2\alpha_1 m_1\frac{k_z k_{z1}}{\omega_1^2}\Big) + \\
&+ \frac{\alpha_2 m m_2}{\omega_2 r^2}\Big(\lambda_1 + S^2\frac{k_{z1}k_{z2}}{\omega_1\omega_2}\Big)\Big(\lambda + \frac{k_z^2\alpha}{\omega^2}\Big) + \frac{1}{V_A^2\omega}\Big(\frac{\alpha_1 m_1 m_2/r^2 + S^2 k_{z1}k_{z2}}{\omega_1\omega_2} - 1\Big)\times \\
&\Big(\frac{\alpha\alpha_2 m m_2}{r^2} + S^4 k_z k_{z2}\Big)\Big] - \frac{\partial n^*}{\partial r} n_1 \frac{\partial n_2}{\partial r}\frac{\alpha}{\omega}\Big[\frac{\alpha_2}{V_A^2\omega_1\omega_2}\Big(\alpha_1\frac{m_1 m_2}{r^2} + S^2 k_{z1}k_{z2}\Big) + \\
&+ \frac{1}{V_A^2}\big[S^2(\gamma-1) - \alpha_2\big] + \frac{k_z^2\alpha_2}{\omega\omega_2}\Big(\lambda_1 + S^2\frac{k_{z1}k_{z2}}{\omega_1\omega_2}\Big) + \lambda_1\alpha_2\frac{k_{z2}^2}{\omega_2^2} + \lambda_1\lambda_2\Big] + \\
&+ \frac{\alpha\alpha_1\alpha_2}{V_A^2\omega\omega_1}\Big[\frac{\partial n^*}{\partial r}\frac{\partial n_1}{\partial r}\frac{\partial^2 n_2}{\partial r^2} + \frac{\partial n^*}{\partial r} n_1 n_2\frac{m_1 m_2}{r^3} + n^*\frac{\partial n_1}{\partial r}\frac{\partial n_2}{\partial r}\frac{m m_2}{r^2}\Big] + \\
&+ \frac{\alpha_2}{\omega_2}\frac{n^*}{r}\frac{\partial}{\partial r}\Big(r n_1\frac{\partial n_2}{\partial r}\Big)\Big(\lambda\lambda_1 + S^2\lambda\frac{k_{z1}k_{z2}}{\omega_1\omega_2} + \beta\Big) + n^*\frac{\partial n_1}{\partial r}\frac{\partial n_2}{\partial r} S^2 k_z\frac{\alpha_1}{\omega\omega_1}\times \\
&\times\Big[\frac{k_{z1}}{\omega_1}\Big(\lambda_2 + \alpha_2\frac{k_{z2}^2}{\omega_2^2}\Big) + \beta\frac{k_{z2}}{\omega_2}\Big] + \frac{\alpha\alpha_1\alpha_2 m m_2 k_z}{\omega^2\omega_1\omega_2}\Big(\frac{k_{z2}}{\omega_2} - \frac{k_{z1}}{\omega_1}\Big)\Big(\frac{1}{r}\frac{\partial n^*}{\partial r} + \frac{n^*}{r}\frac{\partial}{\partial r}\Big)\Big(\frac{n_2}{r}\frac{\partial n_1}{\partial r}\Big)\Big\}
\end{aligned}
\tag{I.35}
$$

Можно показать, что матричные элементы, определяемые (I.31)–(I.35), удовлетворяют обычным свойствам симметрии [3].

Эти свойства симметрии матричных элементов позволяют получить кинетическое уравнение для волн (справедливое в приближении хаотических фаз), которое совпадает, в основном, по виду с соответствующим уравнением (см. [2-3] для безграничной плазмы.

Отметим, что для ограниченной плазмы закон сохранения проекции квазиимпульса на направление, в котором плазма ограничена, вообще говоря, не выполняется [7, 8]. Как видно из выражения для матричных элементов, в случае объемных волн, интегралы, стоящие в них, обладают резонансными свойствами. Они максимальны при $K_{\tau} = K_{\tau_1} + K_{\tau_2}$, т.е. для них приближенно выполняется закон сохранения квазиимпульса. Если же хоть одна из взаимодействующих волн-поверхностная, то интегралы такими свойствами не обладают. Поэтому во взаимодействиях с участием поверхностных волн закон сохранения квазиимпульса не выполняется.

Схемы возможных распадных процессов, связанных с магтогидродинамическими волнами и присущих только ограниченной плазме, приведены на рис.I. Как видно из этого рисунка, в ограниченной плазме появляется много новых каналов взаимодействий волн, играющих важную роль в установлении спектра колебаний.

2. ДРЕЙФОВЫЕ КОЛЕБАНИЯ ЗАМАГНИЧЕННОЙ ТУРБУЛЕНТНОЙ ПЛАЗМЫ

Обычно теория дрейфовых неустойчивостей не учитывает наличия высокочастотных турбулентных пульсаций в плазме. Однако, в силу нелинейной связанности различных типов волн в турбулентной плазме низкочастотные и, в частности, дрейфовые колебания могут зависеть от интенсивности высокочастотной турбулентности. Наибольший интерес для приложений представляют

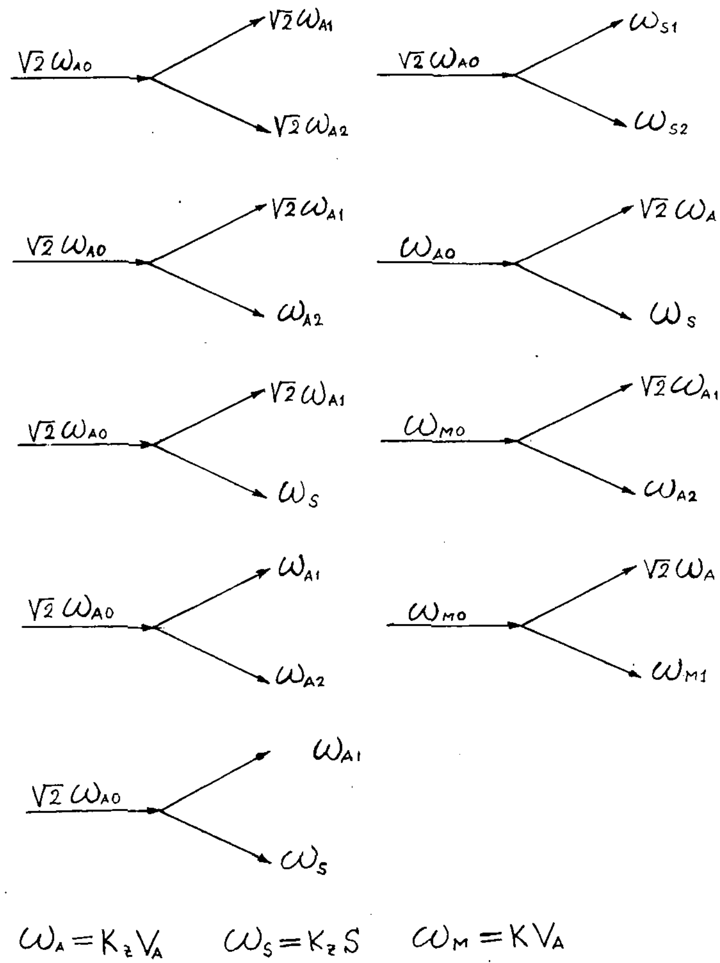

Рис.1. Схемы возможных распадных процессов, связанных с магнитогидродинамическими волнами и присущих только ограниченной плазме.

исследования апериодически раскачивающихся гидродинамических дрейфовых колебаний. Появление низкочастотных неустойчивостей плазмы из-за наличия высокочастотной турбулентности рассматривалось ранее в [9, 10]. В работе [11] был предложен общий метод, позволяющий исследовать дисперсионные свойства плазмы в условиях, когда высокочастотные пульсации сильно изменяют электромагнитные свойства в области низких частот. Простые физические аргументы показывают, что даже в условиях $\frac{W}{nT} \ll 1$, где W-плотность энергии высокочастотной турбулентности, изменение низкочастотных свойств плазмы может быть не малым. Действительно, хорошо известно, что наличие турбулентности приводит к возникновению эффективных турбулентных соударений частиц с волнами и волн между собой, зависящих от энергии турбулентности [12, 13]. В условиях $\frac{W}{nT} \ll 1$ эти эффективные частоты $\nu_1, \nu_2 \ldots$ много меньше частот турбулентных пульсации, однако они могут быть достаточно большими, если уровень турбулентности не очень низок. Для частот ω меньших, например, ν_1, можно ожидать коренного различия дисперсионных свойств турбулентной и нетурбулентной плазмы.

В слаботурбулентной плазме эффективные турбулентные столкновения, пропорциональные более высоким степеням энергии турбулентности, имеют меньшую частоту. В настоящей работе учтены турбулентные столкновения ν_1 первого порядка по энергии турбулентности (квазилинейные, распадные и другие нелинейные соударения) и ν_2 второго порядка по энергии турбулентности. Дрейфовые колебания плазмы исследуются в области частот $\nu_1 \gg \omega \gg \nu_2$. Эффективные частоты ν_1, ν_2 зависят не только от энергии турбулентности, но также и от $\omega, \vec{k}$-частот и волновых векторов дрейфовых колебаний. Проведенное исследование позволяет установить также, в какой области частот и энергии турбулентности $\nu_2 \ll \nu_1$. Это определяет границы применимости получаемых результатов. Предполагая, что электроны плазмы замагничены, используем для их описания дрейфовое кинетическое уравнение. Разобьем полную функцию распределения электронов, а также электрическое поле на турбулентные и регулярные составляющие

$$F^{(e)} = F_T^{(e)} + F_R^{(e)} \qquad \langle F_T^{(e)} \rangle = 0 \qquad (2.1)$$

$$\vec{E} = \vec{E}_T + \vec{E}_R \qquad \langle \vec{E}_T \rangle = 0 \qquad (2.2)$$

Легко получить уравнения для этих компонент. В исходном турбулентном состоянии $\vec{E}_k=0$ и, получаемые уравнения, описывающие турбулентное состояние плазмы, удовлетворены в силу стационарности спектра турбулентности и функций распределения частиц. Пусть $F_0^{(e)}$-регулярная часть функции распределения исходного турбулентного состояния. Для малых $\vec{E}_k$ будем искать отклик турбулентной плазмы на поле $\vec{E}_k$, возникающий из-за слабого изменения распределения частиц и распределения турбулентных пульсаций. Указанное уравнение для малых поправок может быть получено в общем виде. Используя далее в интеграле турбулентных соударений разложение по амплитуде турбулентных пульсаций с точностью до членов, пропорциональных W и W^2, получим довольно сложное интегродифференциальное уравнение для δF-отклонений распределения частиц от равновесных. Разложение по параметрам $\frac{\omega}{\omega_1}$ и $\frac{k}{k_1}$ (где ω_1 и k_1 частота и волновой вектор турбулентных пульсаций) позволяет решить это уравнение и найти тензор проницаемости турбулентной плазмы. Для колебаний, сохраняющих квазинейтральность, имеем

$$\varepsilon_k = \varepsilon_k^{(e)} + \varepsilon_k^{(i)} - 1 \tag{2.3}$$

где $\varepsilon_k^{(i)}$-ионная линейная проницаемость, $k=\{\vec{k},\omega\}$.

$$\varepsilon_k^{(e)} = 1 + \frac{4\pi e^2}{k^2}\,\frac{\int \frac{dV_z}{\omega - k_z V_z}\left[k_z \frac{\partial F_0}{\partial V_z}(1+\alpha_k) + \frac{k_y}{\omega_{He}}\frac{\partial F_0}{\partial x}\right]}{1 + \beta_k \int \frac{dV_z}{\omega - k_z V_z}\,\frac{\partial F_0}{\partial V_z}} \tag{2.4}$$

$$k_z = \frac{(\vec{k}\vec{H}_0)}{H_0} \qquad V_z = \frac{(\vec{V}\vec{H}_0)}{H_0}$$

$$\alpha_k = \int \alpha_{kk_1} W_{k_1} d\vec{k}_1 \qquad \beta_k = \int \beta_{kk_1} W_{k_1} d\vec{k}_1$$

$W=\int W_{k_1} d\vec{k}_1$; W_{k_1}-описывает спектр турбулентных пульсаций. В (2.4) учтены соударения ν_1 и отброшены ν_2 $(\omega \gg \nu_2)$. Коэффициенты α_{kk_1} и β_{kk_1} -довольно громоздкие выражения, зависящие также от типа турбулентных пульсаций.

Если, например, в плазме возбуждены интенсивные одномерные (вдоль $\vec{H}_0$) турбулентные ленгморовские пульсации, то при $\omega \ll k_z V_{Te}$

$$\mathcal{E}_k^{(e)} \simeq 1 + \frac{\omega_{oe}^2}{k^2 v_{Te}^2} \frac{1 + i\sqrt{\frac{\pi}{2}}\left(\omega - \omega_* + \omega_* \frac{\eta}{2}\right)\frac{1}{k_z V_{Te}}}{1 + g\left(1 + i\sqrt{\frac{\pi}{2}}\frac{\omega}{k_z V_{Te}}\right)} \qquad (2.6)$$

$$\omega_{oe}^2 = \frac{4\pi n_o e^2}{m_e} \qquad \omega_* = -\frac{k_y T_e}{m_i \omega_{H_i}} \frac{\partial \ln n_o}{\partial x} \qquad \eta = \frac{d \ln T_e}{d \ln n_o} \qquad (2.7)$$

$$g = -\frac{\pi e^2 k_z}{m_e^2 V_{Te}^2 \omega_{oe}} \int dk_1 \frac{1}{\omega - k_z V_g} \frac{\partial}{\partial k_1} W_{k_1} \qquad (2.8)$$

$V_g = \frac{3k_1 V_{Te}^2}{\omega_{oe}}$ -групповая скорость ленгмюровских волн. В пределе $g \to 0$ уравнение $\mathcal{E}_k = 0$ дает известные дисперсионные уравнения дрейфовых колебаний линейной теории [14-16]. Из (2.6) видно, что при $g \gg 1$ происходит стабилизация кинетической неустойчивости быстрой дрейфовой волны при

$$\eta > 2 \qquad (2.9)$$

Если $\omega \ll k_z V_g$, то при $\frac{W}{n_o T} \gg 12 \frac{V_{Te}^2}{V_\phi^2}$ $\left(V_\phi = \frac{\omega_{oe}}{k_1}\right)$ и $k_z V_s \ll \sqrt{g}\,\omega_*$ получим $\omega = \omega_* g$ т.е. существенное увеличение частоты дрейфовых колебаний. При $\omega \gg k_z V_g$ оказывается возможным возникновение новой нелинейной дрейфовой неустойчивости $\omega^3 = \frac{3}{4} k_z^2 V_{Te}^2 \omega_* \frac{W}{n_o T}$, если $\frac{W}{n_o T_e} \gg \frac{\omega_*^2}{k_z^2 V_{Te}^2}$. Следствием развития этой неустойчивости будет, однако, изменение распределения высокочастотных пульсаций в направлении неоднородности плазмы.

Если в плазме возбуждены непотенциальные (поперечные) пульсации на частотах, близких к ω_{oe}, то в гидродинамической области $\omega \gg k_z V_{Te}$ возможна стабилизация дрейфовых потенциальных и непотенциальных колебаний. Так, при $\omega \ll k V_{g_1}$

$V_{g_1} \simeq \frac{K_1 C^2}{\omega_{oe}} = \frac{C^2}{V_\phi}$ плазма устойчива относительно возбуждения дрейфовых колебаний, если

$$\frac{m_i}{m_e} \gg M \gg K_\perp^2 \frac{V_{T_i}^2}{\omega_{H_i}^2} \qquad (2.10)$$

$$M \simeq \frac{K_z^2 V_{Te}^2}{\omega^2} \frac{W}{4 n_0 T_e} \left(\frac{\lambda_1 \omega_{oe}}{c}\right)^2$$

λ_1-характерная длина волны пульсаций. При этом

$$\omega \simeq \omega_* \left[1 - \frac{W}{4 n_0 T_e} \left(\frac{\lambda_1 \omega_{oe}}{c}\right)^2\right]$$

При выполнении неравенств $\omega \ll K V_{g_1}$

$K_z V_{T_i} \ll \omega \ll K_z V_{T_e}$ дисперсионное уравнение принимает вид:

$$\frac{\omega_{oe}^2}{K^2 V_{Te}^2} \left[\frac{1 + i\sqrt{\frac{\pi}{2}}\left(\omega - \omega_*^{(e)} + \omega_*^{(e)} \frac{\eta}{2}\right)\frac{1}{K_z V_{Te}}}{1 - \frac{\omega_{oe}^2}{4 n_0 T_e}\int W_{K_1} \frac{d\vec{K}_1}{K_1^2}\left(1 + i\sqrt{\frac{\pi}{2}}\frac{\omega}{K_z V_{Te}}\right)} - \frac{\omega_*^{(e)}}{\omega}\right] - \frac{\omega_{oi}^2}{\omega^2}\frac{K_z^2}{K^2}\left(1 - \frac{\omega_*^{(i)}}{\omega}\right) = 0 \qquad (2.11)$$

$\omega_*^{(i)} = \frac{K_y n_0}{m_i \omega_{H_i}} \frac{\partial}{\partial x}(n_0 T_i)$ а $\omega_*^{(e)}$ – соответствует (2.7). Если $g_1 = \left(\frac{\lambda_1 \omega_{oe}}{c}\right)^2 \frac{W}{n_0 T_e} \gg 1$; $T_i = 0$, то

$$\omega = g_1 \omega_* \text{ ; при } \sqrt{g_1}\,\omega_* \gg K_z V_S \text{ ; } \left(V_S = \sqrt{\frac{T_e}{m_i}}\right)$$

дрейфовые колебания оказываются затухающими. Область существования температурно дрейфовой неустойчивости с $\eta \gg 1$; $\omega^3 = -K_z^2 V_S^2 \omega_*^{(i)}$ сдвигается в область очень больших η с ростом энергии турбулентности, а именно, $\eta \gg g$.

Исследование роли турбулентных соударений ν_2 позволило получить критерий, достаточный для применимости приведенных результатов

$$Max\left\{\omega, K V_g\right\} \gg \frac{K_1}{K}\omega_K^c \qquad (2.12)$$

где $\left(\omega_K^c\right)^{-1}$ – характерное время исчезновения корреляций высокочастотных турбулентных пульсаций

$$\omega_K^c = -\omega_{oe} \int \frac{W_{K_1} dK_1\, \varepsilon_L^{(i)}(K - K_1)}{4 n_0 T_e\, \varepsilon_L^{(e)}(K - K_1)} \qquad (2.13)$$

ЛИТЕРАТУРА

[1] ОРАЕВСКИЙ, В.Н., САГДЕЕВ, Р.З., ЖТФ 32 (1962) 1291.
[2] КАДОМЦЕВ, Б.Б., ПЕТВИАШВИЛИ, В.И., ЖЭТФ 43 (1962) 2234.
ГАЛЕЕВ, А.А., КАРПМАН, В.И., ЖЭТФ 44 (1963) 592.
[3] КЛИМОНТОВИЧ, Ю.Л., СИЛИН, В.П., ЖЭТФ 42 (1962) 286.
КОВРИЖНЫХ, Л.М., ЦЫТОВИЧ, В.Н., ЖЭТФ 46 (1964) 2213.
[4] SUDAN, R.N., CAVALIERE, A., ROSENBLUTH, M.N., Publ. Intern. Centre for Theoretical Physics, Trieste, 1966.
[5] КАРПЛЮК, К.С., ОРАЕВСКИЙ, В.Н., Доклад на Симпозиуме по ударным волнам (Новосибирск, 1967) ЖТФ 38 (1968) 8.
[6] КАРПЛЮК, К.С., КОЛЕСНИЧЕНКО, Я.И., ОРАЕВСКИЙ, В.Н., Укр. физ. журн., июль 1968.
[7] ИВАНОВ, А.А., РЮТОВ, Д.Д., ЖЭТФ 48 (1965) 684.
[8] РЮТОВ, Д.Д., ДАН СССР 164 (1965) 1273.
[9] ВЕДЕНОВ, А.А., РУДАКОВ, Л.И., ДАН СССР 159 (1964) 767.
[10] КОГАН, Е.Я., МОИСЕЕВ, С.С., ОРАЕВСКИЙ, В.Н., Прикл. мех. и техн. физ. №5 (1965).
[11] ЦЫТОВИЧ, В.Н., ДАН СССР, июнь (1968).
[12] ВЕДЕНОВ, А.А., ВЕЛИХОВ, Е.П., САГДЕЕВ, Р.З., Ядерный синтез 1 (1961) 81.
[13] DRUMMOND, W.E., Pines, Nuclear Fusion, Suppl., part III (1962) 1049.
[14] КАДОМЦЕВ, Б.Б., ТИМОФЕЕВ, А.В., ДАН СССР 146 (1962) 581.
[15] ГАЛЕЕВ, А.А., ОРАЕВСКИЙ, В.Н., САГДЕЕВ, Р.З., ЖЭТФ 44 (1963) 903.
[16] МИХАЙЛОВСКИЙ, А.Б., РУДАКОВ, Л.И., ЖЭТФ 44 (1963) 312.

NON-LINEAR INTERACTIONS OF POSITIVE AND NEGATIVE ENERGY MODES IN PLASMAS

M. N. ROSENBLUTH AND B. COPPI
PRINCETON UNIVERSITY,
AND
INSTITUTE FOR ADVANCED STUDY, PRINCETON, N.J.,
AND
R. N. SUDAN
CORNELL UNIVERSITY, ITHACA, N.Y.,
UNITED STATES OF AMERICA

Abstract

NON-LINEAR INTERACTIONS OF POSITIVE AND NEGATIVE ENERGY MODES IN PLASMAS. The effects of mode-mode coupling and non-linear Landau damping on stability are studied in the usual weak turbulence approximation.

It is shown that the multi-wave interaction can be explosively unstable when, for $\Sigma_{j=1}^{n} \vec{k}_j = 0$ and $\Sigma_{j=1}^{n} \omega_{\vec{k}_j} = 0$, we also have $S_1 = S_2 \ldots S_n$, where $S_j = (\partial\epsilon/\partial\omega_{\vec{k}_j})/|\partial\epsilon/\partial\omega_{\vec{k}_j}|$, n being the number of interacting waves.

Similarly, conditions under which the non-linear Landau scattering (two-wave particle interaction) can lead to instability are derived.

In the absence of a magnetic field the non-linear Landau scattering occurs for particles of velocity $\vec{v}$ such that $\omega_{\vec{k}'} + \omega_{\vec{k}''} + (\vec{k} + \vec{k}') \cdot \vec{v} = 0$ and the corresponding instability condition is $S_{\vec{k}}(\vec{k} + \vec{k}') \cdot \int (\partial f/\partial p) d^3 \vec{p} > 0$. For a plasma in a magnetic field, the resonance condition is $\omega_{\vec{k}} + \omega_{\vec{k}'} = \ell\Omega_c$, $\ell\Omega_c$ being a multiple of the cyclotron frequency, considering waves with $\vec{k} \cdot \vec{B} = 0$, so that all particles are simultaneously resonant.

The condition for explosive growth is $S_{\vec{k}} = S_{\vec{k}'}$ and $(\omega_{\vec{k}} + \omega_{\vec{k}'})\ S_{\vec{k}} \int (\partial f/\partial\epsilon) |V(E)|^2\ dE > 0$. Here the matrix element V(E) may be evaluated by using detailed balance with the simple process of single-particle scattering of waves.

A significant example analysed is that of a loss-cone distribution for a plasma in a magnetic field. This can have positive and negative energy modes, for which unstable three-wave and two-wave interactions can occur with growth rates which are appreciable for rather modest intensities. A mechanism of this type can be a possible explanation of bursts of radiation often associated with anisotropic plasmas. It is pointed out that these unstable non-linear interactions can be found in some cases for drift waves. In general, these results suggest that the usual quasi-linear perturbation theory may need modification to acquire the proper convergence properties.

1. INTRODUCTION

The concept of "negative energy" waves has proved useful in many areas of physics including the theory of microwave tubes [1]. In recent years it has received some attention in the literature of plasma physics [2-6]. Our objective in this paper is to examine the non-linear interaction of positive and negative energy electrostatic modes of a plasma immersed in a magnetic field. A system which is capable of positive and negative energy excitations can be shown to be unstable when selected interactions between modes, or between modes and the particle distribution are possible. Roughly speaking, negative energy modes grow by losing energy to positive energy modes or to the particles.

In section 2 of the present paper we state the definition of wave energy and momentum. We then consider a statistical ensemble of interacting modes. Starting from the "principle of microscopic detailed balance" we develop a kinetic equation for the density of these modes in wave-number space. A general treatment of both mode-mode coupling and interaction between modes and particles, the so-called non-linear Landau damping, is given. We derive the general conditions under which mode-mode and mode-particle interaction can lead to a non-linear instability. In addition, a simplified method to compute the relevant matrix interaction elements for non-linear Landau damping is given, via evaluation of the single particle wave scattering.

A statistical approach is no longer relevant when we have only a few large-amplitude modes. In this limit the relative phases between modes become important. The criterion for explosive interaction for such a triplet of modes and the critical initial amplitudes are given. By an explosive interaction is meant one in which the amplitudes reach infinity in a finite time.

In the remaining sections we apply the theory developed in section 2 to the high-frequency modes of a low-pressure plasma with a loss-cone distribution. In section 3 a particularly simple form of the dispersion relation for flute modes ($\omega > \Omega$ where Ω is the ion gyrofrequency) is derived by summing over all the harmonic terms. The existence of both positive and negative energy modes is established.

In section 4 we reconsider the flute modes discussed in section 3, to evaluate the matrix elements for non-linear Landau (inverse) damping and estimate a significant non-linear growth rate.

In section 5 we treat the non-linear coupling of a wave interacting with itself and with the particles.

In section 6 the non-linear three-wave interaction for these flute modes is analysed, and it is found that it can lead to a significantly rapid non-linear instability.

We summarize the main conclusions in section 7.

2. KINETIC EQUATION FOR WAVES

Wave energy and momentum

By computing the work done by an external agent in setting up a wave of a given amplitude in a medium it is straightforward to obtain the following well known expressions [7] for the wave energy and momentum,

$$U_{\vec{k}} = \frac{|E_{\vec{k}}|^2}{8\pi} \omega_{\vec{k}} \frac{\partial \epsilon}{\partial \omega_{\vec{k}}} \approx \omega_{\vec{k}} N_{\vec{k}} s_{\vec{k}} \tag{2.1}$$

$$P_{\vec{k}} = \frac{|E_{\vec{k}}|^2}{8\pi} \vec{k} \frac{\partial \epsilon}{\partial \omega_{\vec{k}}} = \vec{k} N_{\vec{k}} s_{\vec{k}} \tag{2.2}$$

In these expressions, $|E_{\vec{k}}|$ is the amplitude of an electrostatic wave, $N_{\vec{k}}$, the wave occupation number, is positive definite, ϵ is the real part of the dielectric constant, $\omega_{\vec{k}}$, the real part of the frequency, is a solution of

$$\epsilon(\vec{k}, \omega_{\vec{k}}) = 0$$

and

$$s_{\vec{k}} \equiv \sin \partial\epsilon / \partial\omega_{\vec{k}}$$

It is clear from the above definitions that the wave energy is not invariant to a Galilean transformation while both $N_{\vec{k}}$ and $s_{\vec{k}}$ are invariant. We anticipate therefore that the sign of $U_{\vec{k}}$ by itself will not determine, in later discussions, the nature of the wave interactions, without regard to the reference frame.

Development of wave kinetic equation

We adopt the "weak turbulence" approximation [8, 9] which assumes that the energy in the fluctuations is much smaller than the overall system energy. In this regime the wave occupation numbers $N_{\vec{k}}$ are good quasi-coordinates of the system. In this section we shall derive the kinetic equation for $N_{\vec{k}}$ without resorting to the Vlasov equation but from the principle of microscopic detailed balance. Of course, the Vlasov equation is needed in the actual calculation of the interaction matrix elements.

We shall begin by computing only the mode-mode coupling terms leaving the treatment of all wave-particle interactions towards the end of this section. Each triplet of interacting waves must satisfy the selection rules for resonant interaction viz.,

$$\vec{k} + \vec{k}' + \vec{k}'' = 0 \tag{2.3}$$

$$\omega_{\vec{k}} + \omega_{\vec{k}'} + \omega_{\vec{k}''} = 0 \tag{2.4}$$

The conservation of energy and momentum during the course of this interaction can be expressed through

$$\omega_{\vec{k}} s_{\vec{k}} \Delta N_{\vec{k}} + \omega_{\vec{k}'} s_{\vec{k}'} \Delta N_{\vec{k}'} + \omega_{\vec{k}''} s_{\vec{k}''} \Delta N_{\vec{k}''} = 0 \tag{2.5}$$

$$\vec{k} s_{\vec{k}} \Delta N_{\vec{k}} + \vec{k}' s_{\vec{k}'} \Delta N_{\vec{k}'} + \vec{k}'' s_{\vec{k}''} \Delta N_{\vec{k}''} = 0 \tag{2.6}$$

where $\Delta N_{\vec{k}}$ represents the change in the occupation number of the state $\vec{k}$ due to the interaction. To make Eqs (2.5) and (2.6) compatible with Eqs (2.3) and (2.4) we must have

$$s_{\vec{k}} \Delta N_{\vec{k}} = s_{\vec{k}'} \Delta N_{\vec{k}'} = s_{\vec{k}''} \Delta N_{\vec{k}''} \tag{2.7}$$

The principle of detailed balance gives

$$\frac{d}{dt} N_{\vec{k}} = \text{(Emission Process - Absorption Process)}$$

We recall that the transition probabilities for a process and its inverse are equal except for statistical factors arising from the Bose-Einstein statistics of the waves, i.e. the Einstein coefficients. We define $\hat{N}_{\vec{k}} = N_{\vec{k}} / \Delta N_{\vec{k}} |$ and let $W_{\vec{k}, \vec{k}', \vec{k}''}$ be the transition probability. Thus

$$\frac{d}{dt} \hat{N}_{\vec{k}} = \sum_{\vec{k}', \vec{k}''} W_{\vec{k}, \vec{k}', \vec{k}''} \Big\{ [\hat{N}_{\vec{k}} + \tfrac{1}{2}(1 + \Delta \hat{N}_{\vec{k}})] [\hat{N}_{\vec{k}'} + \tfrac{1}{2}(1 + \Delta \hat{N}_{\vec{k}'})] [\hat{N}_{\vec{k}''} + \tfrac{1}{2}(1 + \Delta \hat{N}_{\vec{k}''})] - [\hat{N}_{\vec{k}} + \tfrac{1}{2}(1 - \Delta \hat{N}_{\vec{k}})] [\hat{N}_{\vec{k}'} + \tfrac{1}{2}(1 - \Delta \hat{N}_{\vec{k}'})] [\hat{N}_{\vec{k}''} + \tfrac{1}{2}(1 - \Delta \hat{N}_{\vec{k}''})] \Big\} \delta_{-\vec{k}, \vec{k}' + \vec{k}''} \delta(\omega_{\vec{k}} + \omega_{\vec{k}'} + \omega_{\vec{k}''}) \tag{2.8}$$

Here the factors in $\frac{1}{2}(1 \pm \Delta \hat{N})$ result from the Bose statistics. The interaction matrix elements are defined as $|V_{\vec{k}, \vec{k}', \vec{k}''}|^2 = W_{\vec{k}, \vec{k}', \vec{k}''} / \Delta N_{\vec{k}}$ and taking the classical limit $\hat{N} \gg 1$, we obtain the well known kinetic equation [10-12]

$$\frac{d}{dt} N_{\vec{k}} = \sum_{\vec{k}', \vec{k}''} |V_{\vec{k}, \vec{k}', \vec{k}''}|^2 s_{\vec{k}} N_{\vec{k}} N_{\vec{k}'} N_{\vec{k}''} \left(\frac{s_{\vec{k}}}{N_{\vec{k}}} + \frac{s_{\vec{k}'}}{N_{\vec{k}'}} + \frac{s_{\vec{k}''}}{N_{\vec{k}''}} \right) \times \delta_{-\vec{k}, \vec{k}' + \vec{k}''} \delta(\omega_{\vec{k}} + \omega_{\vec{k}'} + \omega_{\vec{k}''}) \tag{2.9}$$

This derivation implies that $|V_{\vec{k}, \vec{k}', \vec{k}''}|$ be symmetric to mutual interchanges of $\vec{k}$, $\vec{k}'$ and $\vec{k}''$ for each three-wave interaction.

The remarkable thing to note about Eq.(2.9) is that if all interacting triplets obeyed the additional selection rule

$$s_{\vec{k}} = s_{\vec{k}'} = s_{\vec{k}''} \tag{2.10}$$

the non-linear terms of Eq.(2.9) would predict an explosive instability in which the wave amplitudes become infinite at a finite time. In the light of Eq.(2.4), we can interpret relation (2.10) to mean that the wave with the largest frequency must differ in the sign of its energy from the other two. If a positive-energy wave splits up into two negative-energy waves the amplitudes of all three waves grow because the positive wave grows by absorbing positive energy which is given up to the negative-energy waves as they increase in amplitude. Notice that the criterion (2.10) is frame-invariant.

The criterion (2.10) can be extended to any number of interacting waves, so that its equivalent when all $s_{\vec{k}}$ are equal, would give an explosive instability to all orders in $N_{\vec{k}}$. This clearly reveals a breakdown in the conventional perturbation procedure on which the "weak turbulence" approximation is based.

Large-amplitude wave interaction

When the amplitude of any particular triplet is much larger than the other waves it has to be treated independently and with due regard to phase differences [13, 14]. Extending the analysis of Armstrong et al.[13] for a single triplet we find that an explosive interaction occurs when the selection rule (2.10) is obeyed. However, when a frequency mismatch $\Delta\omega \equiv \omega' + \omega' + \omega''$ is present, an explosive interaction takes place only if the initial amplitude is above a certain critical threshold. For instance, if the amplitudes are all equal at $t = 0$, i.e. $\alpha_{\vec{k}} = \alpha_{\vec{k}'} = \alpha_{\vec{k}''}$, then

$$\alpha_{\vec{k}}\,(t = 0) > \frac{1}{6}\,\left|\frac{\Delta\omega}{V}\right| \tag{2.11}$$

for instability where α^2 is the energy density in the mode. Similar thresholds can be found for other cases.

Non-linear Landau damping

We now investigate the process by which two waves do not mix to give a third resonant mode but give rise to a virtual beat wave. In the absence of a magnetic field, this beat wave would interact with particles moving at the phase velocity of the beat wave through the usual process of Landau damping. This two-wave-particle process can, of course, be generalized to include several waves and particles. The contribution of this process to the wave kinetic equation can be obtained through perturbation theory, but its detailed calculation turns out to be very tedious because the theory has to be carried out to third order to account for all the terms contributing to this process. We shall develop the theory here as we did earlier for mode-mode coupling, by an application of the principle of detailed balance. Thus we calculate the scattering of wave $\vec{k}'$ by a dressed particle to a wave $\vec{k}''$. The condition for a particle in a strong magnetic field to be in resonance with waves $\vec{k}'$ and $\vec{k}''$, is

$$\omega' + \omega'' - (k'_{\parallel} + k''_{\parallel})\, v_{\parallel} = n\Omega \tag{2.12}$$

The conservation of energy and the parallel and transverse components of momentum are expressed through

$$\omega' s' \Delta N' + \omega'' s'' \Delta N'' + m v_{\parallel} \Delta v_{\parallel} + \Delta E_{\perp} = 0 \tag{2.13}$$

$$k'_{\parallel} s' \Delta N' + k''_{\parallel} s'' \Delta N'' + m \Delta v_{\parallel} = 0 \tag{2.14}$$

$$\vec{k}'_{\perp} s' \Delta N' + \vec{k}''_{\perp} s'' \Delta N'' + \Delta \vec{p}_{\perp} = 0 \tag{2.15}$$

We invoke the correspondence principle and note that quantum-mechanically $\Delta\hat{N}$ and $\Delta E_\perp/\Omega$ should be integral and hence the preceding relations imply

$$s''\Delta N'' = s'\Delta N' \tag{2.16}$$

$$\Delta E_\perp = -n\Omega s'\Delta N' \tag{2.17}$$

$$\Delta\vec{p}_\perp = -(\vec{k}'_\perp + \vec{k}''_\perp)s'\Delta N' \tag{2.18}$$

The principle of detailed balance applied to this process becomes (the primes denote dependence on $\vec{k}'$ and $\vec{k}''$):

$$\frac{d}{dt}\hat{N}'' = W_{\vec{k}',\vec{k}''}(E)\Big\{f(e)[\hat{N}'' + \tfrac{1}{2}(1+\Delta\hat{N}'')][\hat{N}' + \tfrac{1}{2}(1+\Delta\hat{N}')]$$
$$-f(E+\Delta E)[\hat{N}'' + \tfrac{1}{2}(1-\Delta\hat{N}'')][\hat{N}' + \tfrac{1}{2}(1-\Delta\hat{N}')]\Big\} \tag{2.19}$$

In writing Eq.(2.19) we are restricting the discussion to flute modes $k_\parallel = 0$ so that condition (2.12) involves all values of $v_\parallel$ and therefore all the particles. In addition we write E for $E_\perp$. In the classical limit $\Delta E \ll E$ and $\hat{N} \gg 1$ we obtain

$$\frac{d}{dt}\hat{N}'' = W_{\vec{k}',\vec{k}''}(E)\Big\{f(E)[\hat{N}'\Delta\hat{N}'' + \hat{N}''\Delta\hat{N}'] - \Delta E\,\frac{\partial f}{\partial E}\,\hat{N}''\hat{N}'\Big\} \tag{2.20}$$

In this equation the term $\hat{N}'\Delta\hat{N}'' + \hat{N}''\Delta\hat{N}'$ can be interpreted as wave scattering by particles and $-\Delta E\,\hat{N}'\hat{N}''\,\partial f/\partial E$ constitutes the non-linear Landau damping or growth. When the entire particle and wave population is taken into account the kinetic equation becomes

$$\frac{dN''}{dt} = \sum_{\vec{k}'}\int dE\,|V_{\vec{k}',\vec{k}''}(E)|^2\Big\{\frac{\partial f}{\partial E}(\omega'+\omega'')s''N'N''$$
$$+ f(E)(s'N' + s''N'')\Big\}\,\delta(\omega'+\omega''-n\Omega) \tag{2.21}$$

where $W_{\vec{k}',\vec{k}''}\,\Delta\hat{N}'' = W_{\vec{k}'',\vec{k}'}\,\Delta\hat{N}' = |V_{\vec{k}',\vec{k}''}(E)|^2$. Since the matrix elements for non-linear Landau damping and the wave scattering process are identical [22] we need only to consider the wave scattering process for computing $V_{\vec{k}',\vec{k}''}(E)$. A detailed example of this calculation is given in section 5.

From Eq.(2.21) it is evident that non-linear Landau growth occurs for

$$s' = s''$$

$$s'(\omega'+\omega'')\int dE\left(\frac{\partial f}{\partial E}\,|V_{\vec{k}',\vec{k}''}(E)|^2\right) > 0 \tag{2.22}$$

for $\omega'+\omega'' = n\Omega$.

Defining $\overline{\partial f}/\partial E \equiv \int (\partial f/\partial E)\,|V|^2\, dE$ we see four possible cases of explosive instability:

1) Two positive-energy waves with $|\omega'| + |\omega''| = n\Omega$ $\overline{\partial f}/\partial E > 0$.
2) Two negative-energy waves with $|\omega'| + |\omega''| = n\Omega$ $\overline{\partial f}/\partial E < 0$.

3) One negative and one positive-energy wave with $|\omega_+| - |\omega_-| = |n|\Omega$ and $\partial f/\partial E > 0$.

4) One negative and one positive-energy wave with $|\omega_-| - |\omega_+| = |n|\Omega$ and $\partial f/\partial E < 0$.

In the absence of a magnetic field a similar development provides the following conditions for instability

$$s' = s''$$

$$s'(\vec{k}+\vec{k}') \int \frac{\partial f}{\partial \vec{p}}\, |V_{\vec{k}'\vec{k}''}(p)|^2 d^3p > 0 \tag{2.23}$$

From the preceding results it is clear that $s'\,dN'/dt = s''dN''/dt$. In particular for the non-linear interaction of Langmuir waves $s' = -s''$ and the total number of waves is conserved [15, 16].

3. HIGH-FREQUENCY MODES FOR LOSS-CONE DISTRIBUTION

We now apply the theory developed in section 2 to a low-pressure magnetic-mirror confined plasma, in order to investigate any possible explosive wave interactions. Let us examine the electrostatic flute modes at high frequencies ($\Omega_e \gg \omega > \Omega_i$) and neglect the effects of magnetic curvature and density gradient. The fact that $k_\parallel = 0$, makes it possible to assume that these modes do not convect in a uniform field. Following Post and Rosenbluth [17] the dispersion relation for these electrostatic modes is given by (neglecting electron terms),

$$\epsilon(k,\omega) = 1 + \frac{\omega_p^2}{k^2} \int_0^\infty dv_\perp^2 \frac{\partial f}{\partial v_\perp^2} \sum_{n=-\infty}^{\infty} \frac{n}{\overline{\omega}-n}\, J_n^2\left(\frac{kv_\perp}{\Omega}\right) = 0 \tag{3.1}$$

where $\overline{\omega} = \omega/\Omega$ and ω_p is the plasma frequency. This notation is used throughout this paper and often the argument of the Bessel functions is contracted to just k.

In the limit of $\omega > \Omega$ it is possible to put this dispersion relation in a more convenient form by summing over all the harmonic terms. We shall indicate how this is done for a special distribution $f \sim \alpha^2 v_\perp^2 \exp[-\alpha v_\perp^2]$ which retains some of the features of a loss-cone distribution viz., the absence of particles around $v_\perp = 0$. From the identity

$$\oint_C \frac{d\nu}{\sin \pi\nu}\, \frac{J_\nu(z)J_{-\nu}(z)}{\nu-\overline{\omega}} = 0$$

where C is a contour whose radius $R \to \infty$, we may express

$$\sum_{n=-\infty}^{\infty} \frac{n}{\bar{\omega}-n} J_n^2(k) = \sum_{n=-\infty}^{\infty} \frac{(-1)^n J_n(k) J_{-n}(k)}{\bar{\omega}-n} = \frac{\pi\bar{\omega}}{\sin \pi\bar{\omega}} J_{\bar{\omega}}(k) J_{-\bar{\omega}}(k)$$

Substituting this result in the velocity integral of Eq.(3.1) we obtain on *using a Bessel function identity,*

$$\alpha^2 \frac{\partial}{\partial\alpha} \alpha \int_0^\infty dv_\perp^2 \, e^{-\alpha v_\perp^2} \left(\frac{2\bar{\omega}}{\sin \pi\bar{\omega}}\right) \int_0^{\pi/2} d\theta \, \cos(2\bar{\omega}\theta) J_0\left(\frac{2kv_\perp}{\Omega} \cos\theta\right)$$

$$= \left(\frac{2\bar{\omega}}{\sin \pi\bar{\omega}}\right) \alpha^2 \frac{\partial}{\partial\alpha} \int_0^{\pi/2} d\theta \, \cos(2\bar{\omega}\theta) \exp[-(k^2 \cos^2\theta/\alpha\Omega^2)]$$

In the limit $ka_i > 1$, $\bar{\omega} > 1$, the dominant contribution in the θ-integration comes from the region near $\theta \lesssim \pi/2$. Introduce $\theta = \pi/2 = \hat{\theta}$ and allow the lower limit to approach infinity. The integral is approximated by

$$\frac{k}{\Omega\sqrt{\alpha}} \int_0^\infty d\hat{\theta} \, \cos(\pi\bar{\omega} - 2\bar{\omega}\hat{\theta}) \exp[-(k^2\hat{\theta}^2/\alpha\Omega^2)]$$

$$= \cos(\pi\bar{\omega}) \, u_R(2\omega\sqrt{\alpha}/k) + \sin(\pi\bar{\omega}) u_I(2\omega\sqrt{\alpha}/k)$$

where

$$u_R(x) + iu_I(x) = \int_0^\infty dy \, \exp(ixy - y^2)$$

The dispersion relation becomes

$$\epsilon(k,\omega) = 1 + \frac{\omega_p^2}{k^2\lambda_D^2} \alpha \frac{\partial}{\partial\alpha} \left\{\frac{2\omega\sqrt{\alpha}}{k}\left[u_R\left(\frac{2\omega\sqrt{\alpha}}{k}\right) \operatorname{ctg}(\pi\bar{\omega}) + u_I\left(\frac{2\omega\sqrt{\alpha}}{k}\right)\right]\right\} \tag{3.2}$$

The function u is simply related to the conventional plasma dispersion function [18]. Notice that in this high-frequency limit the dispersion relation could be obtained immediately by replacing the pole contribution i in a straight-line orbit calculation with $\operatorname{ctg}(\pi\bar{\omega})$. It is possible to generalize this result to any loss-cone distribution. In this case

$$\epsilon(k,\omega) = 1 - \frac{1}{k^2\lambda_D^2}\left\{F_R\left(\frac{\omega}{k\bar{v}_i}\right) + \operatorname{ctg}(\pi\bar{\omega}) F_I\left(\frac{\omega}{k\bar{v}_i}\right)\right\} \tag{3.3}$$

where

$$F(\zeta) = -2\int_0^\infty d\xi \frac{\partial\psi}{\partial\xi}\frac{1}{(1-\xi/\zeta^2)^{\frac{1}{2}}}$$

$$\overline{v}_i^2 = \int_0^\infty dv_\parallel dv_\perp^2 f v_\perp^2 / \int_0^\infty dv_\parallel dv_\perp^2 f$$

and $\psi(\xi) = \psi_0 \int_{-\infty}^{\infty} dv_\parallel f(v_\perp^2, v_\parallel^2)$, ψ_0 is a normalization constant. In the limit $k^2\lambda_D^2 \ll 1$, we have

$$\mathrm{ctg}(\pi\overline{\omega}) = -F_R/F_I$$

In Fig. 1, $\eta = \mathrm{ctg}^{-1}(-F_R/F_I)$ is plotted as a function of $\omega/k\overline{v}_i$. The sign of the wave energy is mainly determined by the term $F_I(\partial/\partial\omega)\,\mathrm{ctg}(\pi\overline{\omega})$, hence by the sign of F_I. The transition from negative to positive energy occurs for $\eta \approx \pi$ Since the deviation of $\overline{\omega}$ from integral values is proportional to η it becomes a quantity of importance when attempting to satisfy the frequency selection rules.

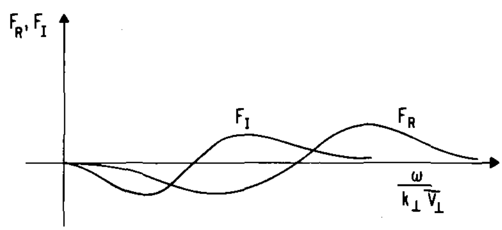

FIG. 1a. Typical profile of the functions F_I and F_R entering the dispersion relation for loss-cone distribution functions (section 3).

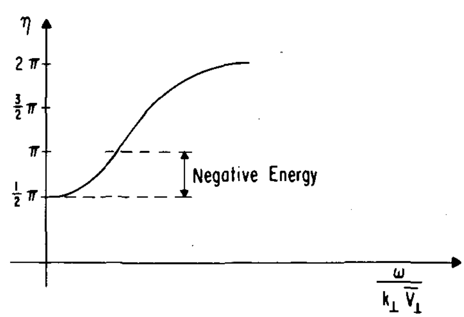

FIG. 1b. Approximate representation of the dispersion relation for loss-cone distribution functions showing the region where the energy wave is negative (section 3). Here $\eta = \pi(\omega/\Omega - \ell)$, and ℓ is an integer.

4. NON-LINEAR LANDAU DAMPING

Derivation of matrix elements $V_{\vec{k}',\vec{k}''}(E)$

Recalling the argument presented in section 2 the matrix elements for non-linear Landau damping are to be computed by the detailed evaluation of the scattering of the wave $\vec{k}'$ off a distribution f(E) where $\vec{k}''$ is the scattered wave vector. This scattering must be computed off a dressed particle as is well known from the scattering of electromagnetic waves by a plasma [19]. The initial distribution of the bare particle is represented by

$$f(t=0) = \frac{1}{(2\pi)^{3/2}} e^{-i\vec{k}\cdot\vec{x}_0} \delta(v_\parallel - v_{\parallel 0})\delta(v_\perp^2 - v_{\perp 0}^2)\delta(\theta - \theta_0) \tag{4.1}$$

We neglect the time of formation of the screening cloud and set $k_\parallel = 0$ and we let $\vec{k} = k\hat{e}_y$. The dressed particle distribution is found by regarding the bare particle distribution as the initial value in the linearized Vlasov equation, solving for f_k in terms of φ_k the Fourier-analysed potential and then eliminating φ_k through Poisson's equation which in the limit $k^2\lambda_D^2 \ll 1$ and $m_e/m_i \ll 1$ reduces to

$$\int d\theta \, dv_\perp^2 dv_\parallel f_{\vec{k}} = 0$$

In this manner the time-asymptotic dressed particle distribution is given by

$$f_{\vec{k}}(t) = \sum_m f_{\vec{k}}^{(m)}(t)$$

$$= \frac{1}{(2\pi)^{5/2}} \exp i\left\{-\vec{k}\cdot\vec{x}_0 + \frac{k}{\Omega}(v_{\perp 0}\sin\theta_0 - v_\perp \sin\theta)\right\} \sum_m e^{im(\theta - \theta_0 - \Omega t)}$$

$$\left\{ \delta(v_\perp^2 - v_{\perp 0}^2)\delta(v_\parallel - v_{\parallel 0}) - \frac{\dfrac{\partial f}{\partial v_\perp^2} J_m\left(\dfrac{kv_\perp}{\Omega}\right) J_m\left(\dfrac{kv_{\perp 0}}{\Omega}\right)}{\displaystyle\int dv_\perp^2 \frac{\partial f}{\partial v_\perp^2} J_m^2\left(\frac{kv_\perp}{\Omega}\right)} \right\} \tag{4.2}$$

Let us take the incident wave to be of amplitude $E_{\vec{k}'}$ at frequency ω' and our object is to derive the scattered $E_{\vec{k}'+\vec{k}}$ off the distribution $f_{\vec{k}}^{(m)}$. The linearized Vlasov equation gives us

$$\left(\frac{\partial}{\partial t} + \vec{v}\cdot\nabla + \Omega\frac{\partial}{\partial\theta}\right) f'' e^{i\omega'' t} = -\frac{e}{m_i}\left(\vec{E}_{\vec{k}'+\vec{k}} \cdot \frac{\partial}{\partial \vec{v}} f_0 + \vec{E}_{\vec{k}'} \cdot \frac{\partial}{\partial \vec{v}} f_{\vec{k}}^{(m)}\right) \tag{4.3}$$

where we have used a contracted notation: $f'' e^{i\omega'' t} \equiv f^{(m)}_{\vec{k}'+\vec{k}}, \omega'' = \omega' + m\Omega$, $\vec{k}'' = \vec{k} + \vec{k}'$. For the sake of simplicity we set $\vec{k}'$ parallel to $\vec{k}''$. We obtain f'' by integrating Eq.(4.3) over zero-order orbits. From the resulting expression for f'' the charge density ρ'' is computed via

$$\rho'' = e\int dv_\perp^2 \int dv_\parallel \int d\theta\, f''$$

Thus we get

$$\rho''_m(t) \equiv [\rho''(\varphi') + \rho'(\varphi'')]\, e^{-i(\omega'+m\Omega)t}$$

$$= \left\{ \frac{e^2}{m_i}\, \varphi'\, \frac{k'k''}{(2\pi)^{3/2}} \exp i\left[-\vec{k}\cdot\vec{x}_0 + \frac{kv_{\perp 0}}{\Omega} \sin\theta_0 - im\,\theta_0 \right] \right.$$

$$\left. \times \sum_\ell g^{\vec{k}'\vec{k}''}_{\ell m} + \frac{k''^2}{4\pi}\, \varphi''[1 - \epsilon(\vec{k}'', \omega' + m\Omega)] \right\} e^{-i(\omega'+m\Omega)t} \qquad (4.4)$$

where

$$g^{\vec{k}'\vec{k}''}_{\ell m} = \frac{1}{[\omega' + (m-\ell)\Omega]^2 - \Omega^2} \left\{ J_\ell\left(\frac{k''v_{\perp 0}}{\Omega}\right) J_{\ell - m}\left(\frac{k'v_{\perp 0}}{\Omega}\right) \right.$$

$$\left. - J_m\left(\frac{kv_{\perp 0}}{\Omega}\right) \frac{\int dv_\perp^2 \frac{\partial \bar{f}}{\partial v_\perp^2} J_\ell\left(\frac{k''v_\perp}{\Omega}\right) J_{\ell-m}\left(\frac{k'v_\perp}{\Omega}\right) J_m\left(\frac{kv_\perp}{\Omega}\right)}{\int dv_\perp^2 \frac{\partial \bar{f}}{\partial v_\perp^2} J_m^2\left(\frac{kv_\perp}{\Omega}\right)} \right\}$$

where $\vec{k} \equiv \vec{k}'' - \vec{k}'$ and $\bar{f}(v_\perp^2) \equiv \int dv_\parallel\, f(v_\perp^2, v_\parallel)$. We now write Poisson's equation as $k''^2\varphi'' = 4\pi\rho''$. Since ω'' is a wave of the system $\epsilon(\omega'', \vec{k}'') = 0$ we can express the slow variation of the wave amplitude by

$$i\frac{\partial\epsilon}{\partial\omega''}\, \frac{\partial\varphi''}{\partial t} + \frac{4\pi}{k''^2}\, \rho''(\varphi')e^{-i\Delta\omega t} = 0 \qquad (4.5)$$

where $\rho''(\varphi')$ is defined in Eq.(4.4) and $\Delta\omega = \omega' + m\Omega - \omega''$. We can now construct the expression for $dN''/dt = (k^2/8\pi)\,[\varphi''^* \,\partial\varphi''/\partial t + \varphi''\, \partial\varphi''^*/\partial t]\, \partial\epsilon/\partial\omega''$ out of the lowest order solution of Eq.(4.5)

$$\varphi'' = -\frac{4\pi\rho''(\varphi')}{k^2 \frac{\partial\epsilon}{\partial\omega''}\Delta\omega}\,(e^{-i\Delta\omega t} - 1)$$

to obtain

$$\frac{dN''}{dt} = \frac{4\pi}{k''^2 \left|\frac{\partial\epsilon}{\partial\omega''}\right|} \left|\rho''(\varphi')\right|^2 \frac{\sin \Delta\omega t}{\Delta\omega} \tag{4.6}$$

Finally we substitute for $\rho''(\varphi')$ from Eq.(4.4) and taking the limit $\Delta\omega t \rightarrow \infty$

$$\frac{dN''}{dt} = N' \int \frac{1}{n} \frac{\partial}{\partial v_{\perp 0}^2} \bar{f}_2 (v_{\perp 0}^2, v_{\parallel 0}) \left| V^{(m)}_{\vec{k}', \vec{k}''} (v_{\perp 0}) \right|^2 \delta(\omega'' - \omega' - m\Omega)$$

$$= (\omega'' - \omega') s'' N'' N' \Upsilon^{(m)}_{\vec{k}', \vec{k}''} \delta(\omega'' - \omega' - m\Omega) \tag{4.7}$$

where

$$\left| V^{(m)}_{\vec{k}', \vec{k}''} \right|^2 = \frac{\omega_{pi}^4}{\left|\frac{\partial\epsilon}{\partial\omega'} \frac{\partial\epsilon}{\partial\omega''}\right| n} \left(\sum_{\ell} g_{\ell m}^{\vec{k}' \vec{k}''} \right)^2$$

$$\Upsilon^{(m)}_{\vec{k}', \vec{k}''} = \frac{2}{n m_i} \int dv_{\perp 0}^2 \frac{\partial \bar{f}}{\partial v_{\perp 0}^2} (v_{\perp 0}^2) \left| V^{(m)}_{\vec{k}' \vec{k}''} (v_{\perp 0}) \right|^2$$

$$= \frac{\omega_{pi}^4}{\left|\frac{\partial\epsilon}{\partial\omega'} \frac{\partial\epsilon}{\partial\omega''}\right| n} \left(\frac{2}{m_i \bar{v}_i^2} \right) \sum_{\ell, s} \frac{1}{[(\omega'' - \ell\Omega)^2 - \Omega^2][(\omega'' - s\Omega)^2 - \Omega^2]}$$

$$\left\{ \int_0^\infty d\xi \left(\frac{\partial\psi}{\partial\xi}\right) J_\ell(k'') J_s(k') J_{\ell - m}(k') J_{s-m}(k') - \frac{\left[\int_0^\infty d\xi \left(\frac{\partial\psi}{\partial\xi}\right) J_\ell(k'') J_{\ell-m}(k') J_m(k)\right]\left[\int_0^\infty d\xi \left(\frac{\partial\psi}{\partial\xi}\right) J_s(k'') J_{s-m}(k') J_m(k)\right]}{\int_0^\infty d\xi \left(\frac{\partial\psi}{\partial\xi}\right) J_m^2(k\xi)} \right\}$$

Note that Υ is proportional to the $\partial\bar{f}/\partial E$ average of the matrix elements defined in section 2. In the above expressions we have employed the notation defined in section 3, n is the particle number density and the argument of the Bessel functions have been briefly indicated by k. It is possible to prove the symmetry relations

$$\sum_{\ell} g_{\ell,m}^{\vec{k}'\vec{k}''} = \sum_{j} g_{j,-m}^{\vec{k}''\vec{k}'} \tag{4.8}$$

which implies

$$\Upsilon_{\vec{k}',\vec{k}''}^{(m)} = \Upsilon_{\vec{k}'',\vec{k}'}^{(-m)}$$

and in consequence we have

$$\frac{dN'}{dt} = -(\omega''-\omega')\, s'\, N'\, N''\, \Upsilon_{\vec{k}',\vec{k}''}^{(m)}\, \delta(\omega''-\omega'-m\Omega) \tag{4.9}$$

From Eqs (4.7, 9) we can infer that if $\Upsilon>0$, instability can occur when the $\vec{k}''$ wave has positive frequency $\omega''>\omega'$ and is of positive energy while the $\vec{k}'$ wave is of negative energy. Referring to Fig.1, $\eta(k'')$ must lie between $3\pi/2$ and 2π, while $\eta(k')$ must lie between $\pi/2$ and π.

On the other hand if $\Upsilon<0$ the k'' wave with $|\omega''|>|\omega'|$ has to be of negative energy and the k' wave of positive energy. From Fig.1 we see that this is also possible although requiring $k'' \ggg k'$.

We see also from Fig.1 that it is impossible for two negative-energy waves to satisfy the resonance condition. While two positive-energy waves could satisfy the selection rules, it will turn out that $\overline{\partial f}/\partial E>0$ is not possible.

Growth due to non-linear Landau damping

We shall develop here an asymptotic evaluation of Υ and with its help estimate the non-linear growth for two interacting waves. As a first step we need to put the sum $\sum g_{\ell,m}^{\vec{k}'\vec{k}''}$ which occurs in the expression for Υ in a more tractable form. This involves a summation,

$$\begin{aligned}
\vartheta &\equiv \tfrac{1}{2}\sum_{\ell} J_{\ell}(k'')\,J_{\ell-m}(k')\left[\frac{1}{\overline{\omega}''-\ell-1}-\frac{1}{\overline{\omega}''-\ell+1}\right] \\
&= \frac{i^{-m}}{(2\pi)^2}\int_0^{\infty} d\lambda\,\sin\lambda \sum_{\ell}(-1)^{\ell} e^{i(\overline{\omega}''-\ell)\lambda}\int d\varphi \exp i\left[\frac{k''v_{\perp}}{\Omega}\cos\varphi+\ell\varphi\right] \\
&\quad\times\int d\varphi' \exp i\left[\frac{k''v_{\perp}}{\Omega}\cos\varphi'+(\ell-m)\varphi'\right] \\
&= \frac{i^{-m}}{(2\pi)}\int_0^{\infty} d\lambda\, e^{-i\overline{\omega}''\lambda}\sin\lambda\int d\varphi' \exp i\left[\frac{v_{\perp}}{\Omega}(k'-k''\cos\lambda)\cos\varphi'-k''\sin\lambda\cos\varphi'-im\varphi'\right]
\end{aligned}$$

In the large-m limit, i.e. $\bar{\omega}'' \gg 1$ and $\omega'' \gg k''\bar{v}_i$ as a positive-energy wave we can approximate the above integral. Since we expect no saddle points for large but finite λ, we let $\lambda \sim 1/\bar{\omega}'' \ll 1$ and expand to lowest order, ($|k| = |k''-k|$)

$$\vartheta = \frac{i^{-m}}{2\pi}\int d\varphi' \exp i\left[\frac{|k| v_\perp}{\Omega}\cos\varphi - im\,\varphi'\right]\int_0^\infty d\lambda\, e^{i\omega''\lambda}$$

$$\left\{\lambda - i\,\frac{k''v_\perp}{\Omega}\sin\varphi'\,\lambda^2 - \tfrac{1}{2}\,\frac{k''v_\perp}{\Omega}\left(\frac{k''v_\perp}{\Omega}\sin^2\varphi' - i\cos\varphi'\right)\lambda^3\right\}$$

$$= \frac{1}{\bar{\omega}''^2}\left[(1+\Delta)\,J_m\left(\frac{kv_\perp}{\Omega}\right) - \frac{3k''}{k\bar{\omega}''^2}\,v_\perp\,\frac{\partial}{\partial v_\perp}\,J_m\left(\frac{kv_\perp}{\Omega}\right)\right] \qquad (4.10)$$

where Δ is a coefficient that together with the term $(1+\Delta)J_m$ can be shown not to contribute to the final expression for Υ that we are seeking. We now define an expression R_m which determines the sign of Υ:

$$\frac{nR_m}{\bar{v}_i^2} \equiv \int_0^\infty dv_{\perp 0}^2\,\frac{\partial\bar{f}}{\partial v_0^2}\left(\sum_\ell g_{\ell,m}(v_{\perp 0})\right)^2$$

$$\equiv A - \frac{C^2}{D} \qquad (4.11)$$

where

$$\left(\sum_\ell g_{\ell,m}\right)^2 = \left\{\vartheta(v_{\perp 0}) - J_m(v_{\perp 0})\,\frac{\int_0^\infty dv_\perp^2\,\frac{\partial\bar{f}}{\partial v_\perp^2}\,J_m(v_\perp)\vartheta(v_\perp)}{\int_0^\infty dv_\perp^2\,\frac{\partial\bar{f}}{\partial v_\perp^2}\,J_m^2(v_\perp)}\right\}^2$$

$$A, C, D \equiv \int_0^\infty dv_\perp^2\,\frac{\partial\bar{f}}{\partial v_\perp^2}\left\{\vartheta^2(v_\perp),\ J_m(v_\perp)\vartheta(v_\perp),\ J_m^2(v_\perp)\right\}.$$

It is of interest to note that the effect of particle dressing is to introduce the term $-C^2/D$ which radically alters the results, nearly cancelling A and changing the character of $\partial\bar{f}/\partial E$ as we shall see. By adopting the distribution $f \sim \alpha^2 v_\perp^2 \exp[-\alpha v_\perp^2]$ used earlier in section 3 we are able to perform the velocity integration. In terms of $b \equiv k^2/2\alpha\Omega^2$ the quantity D equals

$$D = e^{-b}\,[(b+m)\,I_m(b) - b\,I_{m-1}(b)] \tag{4.11a}$$

$$D \approx \frac{1}{\sqrt{2\pi b}}\left(1 - \frac{m^2}{b}\right) e^{-m^2/2b}$$

in the large m and b limit. In the same limit A and C approximate to

$$A \approx \sqrt{\frac{b}{2\pi}}\left(1 + \frac{m^2}{b}\right) e^{-m^2/2b} \tag{4.11b}$$

$$C \approx \frac{1}{\sqrt{2\pi b}}\left[\frac{1}{8}\,\frac{m^4}{b^2} - \frac{2m^2}{b} + \frac{1}{2}\right] e^{-m^2/2b} \tag{4.11c}$$

When these approximations are substituted in the expression for R_m we obtain

$$R = -\left(\frac{\Omega}{\omega}\right)^8 \left(\frac{3k''}{k}\right)^2 e^{-m^2/2b}\left(\frac{b}{2\pi}\right)^{\frac{1}{2}}\left\{1 + \frac{m^2}{b}\,\frac{\left(\frac{1}{8}\,\frac{m^4}{b^2} - \frac{2m^2}{b} + \frac{1}{2}\right)^2}{b - m^2}\right\} \tag{4.12}$$

This result shows that for the asymptotic limit we have been able to treat R and hence the $\partial f/\partial E$ average of the matrix elements $\overline{\partial f/\partial E}$ is a small negative quantity which becomes positive only for b close to m^2. Thus only a very narrow region in k space viz. where $b \approxeq m^2$ is available for this instability because everywhere else the waves will be damped.

On the other hand, for the case in which the negative-energy wave has a higher frequency than the positive-energy wave, i.e. $|\omega_-| > |\omega_+|$ we need not be restricted to a narrow region for instability, as the matrix elements nearly always have the proper sign for instability. The non-linear growth rate γ_{NL} is computed as follows:

$$\frac{1}{N''}\frac{dN''}{dt} \equiv \gamma_{NL} = s'' \sum_{m,\vec{k}'} (\omega''-\omega')(N\,\Upsilon^{(m)}_{\vec{k}'\,\vec{k}''})\,\delta(\omega''-\omega' - m\Omega) \tag{4.13}$$

$$\approx \frac{m\Upsilon}{(d\omega/dk)\Delta k}\,\mathscr{E}$$

where $\mathscr{E} = \Sigma_{\vec{k}} N_{\vec{k}} \omega_{\vec{k}}$ is the wave energy density per unit volume, and Δk is the width of the spectrum. Substituting for Υ from Eqs (4.7) and (4.12) and assuming that a wide spectrum of waves has been excited ($k \sim \Delta k$, $\omega \approx k\bar{v}_i$), we obtain to within numerical factors,

$$\gamma_{NL} \sim \left(\frac{\mathscr{E}}{nT_i}\right) \left(\frac{\Omega}{\omega}\right)^3 \Omega \tag{4.14}$$

and T_i is the ion kinetic temperature.
The appropriate value of ω for a typical wave would depend on the solution of the kinetic equation and perhaps on the initial conditions. In view of the dependence of the growth rate on the frequency we might expect typically ω of a few times Ω_i although values as large as ω_{pi} are not excluded. This growth rate is comparable to that obtained from mode-mode coupling (section 6). If on the other hand a narrow spectrum of waves is excited at the right frequencies for interaction, then we may replace the delta function in Eq.(4.13) by $1/\gamma_{NL}$ and the appropriate growth rate becomes for $k \sim \Delta k \sim 1/a_i$

$$\gamma_N \sim \left(\frac{\mathscr{E}}{nT_i}\right)^{\frac{1}{2}} \left(\frac{\Omega}{\omega}\right)^{3/2} \Omega \tag{4.15}$$

Returning to the case $|\omega_-| < |\omega_+|$, is is clear from the preceding discussion that the spectrum of excited waves must be very narrow for growth to occur as most interactions are damping. An extreme limit of this behaviour is given by $b \sim m^2$ if somehow the strong interaction between these resonant waves becomes dominant. In the expression for R (4.12) the last term in the brackets acts as a resonant denominator and can therefore be set proportional to $1/\gamma_{NL}$. In this extreme narrow spectrum case the non-linear growth rate is

$$\gamma_{NL} \sim \left(\frac{\mathscr{E}}{nT_i}\right)^{1/3} \left(\frac{\Omega}{\omega}\right) \Omega \tag{4.16}$$

5. SELF-INTERACTION OF WAVES

If a wave has frequency $\omega = m\Omega/2$, then it can interact through non-linear Landau damping with itself to yield non-linear damping or instability. Such non-linear instability is perhaps of special interest, avoiding the necessity of speculating on the outcome of the solution of the kinetic equation[1]. We assume here that this process may be calculated as a limiting case of the two-wave non-linear Landau damping without worrying about the fact that the random phase approximation is no longer justified. It is perhaps conceivable that the phase of the matrix element could play a significant role which we have ignored.

[1] This treatment is closest to linear normal mode analysis on which stability theory is normally based.

Referring to Fig.1 we see two possible cases: (a) m even, the "zero-energy" wave which is a rather singular case which we do not consider in this paper and (b) m odd the positive energy modes with $\eta = 3\pi/2$ which we consider here.

Thus

$$2\omega = m\Omega \tag{5.1}$$

where m is an odd integer. The "virtual wave" will have 2k for the wave number. The kinetic equation takes the form

$$\frac{d}{dt} N_{\vec{k}} = (m\Omega s_{\vec{k}}) N_{\vec{k}}^2 \Upsilon_{2\vec{k}}^{(m)} \delta\left(\omega - \frac{m}{2}\Omega\right) \tag{5.2}$$

where

$$\Upsilon_{2\vec{k}}^{(m)} = 2 \frac{\omega_{pi}^4 R_m(2k)}{\left(\frac{\partial\epsilon}{\partial\omega}\right)^2 (nm_i \bar{v}_i^2 \Omega^4)} \tag{5.3}$$

The expression for the quantity ϑ defined in section 4 can be shown to reduce, in this case, to

$$\vartheta = \frac{2}{\pi} \int_0^{2\pi} d\varphi\, e^{-im\varphi} \int_0^{\infty} d\zeta\, \sin\zeta \cos\zeta \exp\left[-i2\frac{kv_\perp}{2\Omega} \sin\varphi \ \cos\zeta - \epsilon\zeta\right]$$

to be taken in the limit $\epsilon \to +0$. By a sequence of integration by parts the ζ integral turns out to be

$$\frac{1}{\hat{K}^2}\left\{ e^{-i\hat{K}} (1 + i\hat{K}) - 1 - [J_0(\hat{K}) + KJ_1(\hat{K}) - 1] \right\}$$

where $\hat{K} = (2kv_\perp/\Omega) \sin\varphi \equiv K \sin\varphi$. In the subsequent φ integration the term in square brackets does not contribute because it is even in φ and the result is

$$\vartheta = 4 \int_0^1 \mu\, d\mu\, J_m(\mu K) \tag{5.4}$$

In the large m limit we may proceed as in section 4 for the special distribution $v_\perp^2 \exp[-\alpha v_\perp^2]$ to evaluate R_m to be:

$$R_m \approx \frac{1}{\bar{b}}\left\{ e^{-m^2/2\bar{b}} - \frac{m^2}{\bar{b}} \int_{m^2/2\bar{b}}^{\infty} d\zeta\, e^{-\zeta}/\zeta - \sqrt{\frac{2\pi}{b}} \frac{[1 - m^2/2b]^2}{1 - m^2/\bar{b}} \right\} \tag{5.5}$$

where $m^2/\bar{b} = 2\alpha\omega^2/k^2$. The wave frequency is to be chosen such that $\eta = \pi(\omega/\Omega - \ell\Omega) = 3\pi/2$ which has positive-wave energy. But $m^2/\bar{b} = 1$ corresponds to the region where the wave energy changes sign (Fig.1). Thus the wave frequency for which $\eta = 3\pi/2$ is such that R_m is negative and the interaction leads to damping. To avoid the high m limit we have used Eq.(4.4) and numerically evaluated R_m, as well as the roots of Eq.(5.7) and the corresponding value for $\partial\epsilon/\partial\omega$ for finite values of $m = 3, 5...$ Except for a narrow band where $m^2 \approx \bar{b}$ we find that R_m is almost always negative as in the high m limit. Since it is also found that the energy $\omega\, \partial\epsilon/\partial\omega$ is positive ($\epsilon = 0$), we conclude that no self-interaction is unstable in the absence of a density gradient. In this range of m, but for large b, R_m is independent of m and approximates to

$$R \approx -\frac{1}{2\bar{b}}\left(1 + \sqrt{\frac{2\pi}{b}}\right) \text{ as in Eq.(4.12).} \tag{5.6}$$

As R_m is almost always negative, unstable self-interaction is only possible if negative-energy waves can be made self-interacting. This is possible if we consider a plasma with a density gradient perpendicular to $\vec{B}$ and $\vec{k}$. The extended dispersion relation now becomes

$$\epsilon(k,\omega) = b\left(\frac{\lambda_{Di}^2}{a_i^2} + \frac{m_e}{m_i}\right) - \frac{\sqrt{b}}{\bar{\omega}}\left[\frac{a_i}{\sqrt{2}n}\,\frac{dn}{dx}\,\frac{k}{|k|}\right]$$

$$- \frac{2\bar{\omega}}{\sin(\pi\bar{\omega})}\, b\, \frac{\partial}{\partial b}\int_0^{\pi/2} d\varphi \cos(2\bar{\omega}\varphi) e^{-2b\cos^2\varphi} \tag{5.7}$$

and requires that the quantity in square brackets be positive such that

$$\frac{a_i}{n}\left|\frac{dn}{dx}\right| > \sqrt{\frac{b}{2}}\left(\frac{\lambda_{Di}^2}{a_i^2} + \frac{m_e}{m_i}\right) \tag{5.8}$$

The inclusion of the Debye length and density gradient terms does not affect our previous evaluation of the matrix elements provided they are less than unity. Under these restrictions (5.7) has a solution for $b \gg 1$. Performing the integral over φ in this limit we obtain for $\bar{\omega} = \frac{1}{2}$,

$$b\left(\frac{m_e}{m_i} + \frac{\Omega^2}{\omega_{pi}^2}\right) - \sqrt{2b}\,\frac{a_i}{n}\left|\frac{dn}{dx}\right| + \frac{1}{4b} = 0 \tag{5.9}$$

The condition for instability is therefore that the density gradient be sufficient for the wave to exist since if $b = b_0$ is a solution of $\epsilon = 0$ then for $\bar{\omega} = \frac{1}{2}$

$$\frac{\partial\epsilon}{\partial\omega} \approx -\frac{1}{2}\left(\frac{\pi}{2}\right)^{3/2} \frac{1}{\sqrt{b_0}} < 0$$

This condition is

$$\frac{a_i}{n}\left|\frac{dn}{dx}\right| > \frac{2}{3^{3/4}}\left(\frac{m_e}{m_i} + \frac{\Omega^2}{\omega_{pi}^2}\right)^{3/4} \tag{5.10}$$

The condition for non-linear self-interaction instability (5.10) does not differ very much from the linear stability limit. However, we can demonstrate that there is a narrow band where only the non-linear instability exists. Defining

$$\Lambda_0 \equiv \left(\frac{m_e}{m_i} + \frac{\Omega^2}{\omega_{pi}^2}\right)$$

$$\Psi \equiv \frac{\frac{a_i}{} \sqrt{2}}{n}\left|\frac{dn}{dx}\right|$$

and performing the integral in Eq.(5.7) in the large b limit, we obtain

$$\Lambda(\Psi, b, \bar{\omega}) \equiv \frac{\Phi}{\sqrt{b}} - \frac{\bar{\omega}^2}{b} - \frac{1}{2b^{3/2}}\sqrt{\frac{\pi}{2}}\;\bar{\omega}\;\mathrm{ctg}\;\pi\bar{\omega} = \Lambda_0 \tag{5.11}$$

The non-linear instability condition (6.8) is obtained by requiring that for $\bar{\omega} = \frac{1}{2}$ the maximum of Λ with respect to b, be larger than Λ_0, i.e.

$$\mathrm{Max}_b\; \Lambda(\Psi, b, \bar{\omega} = \tfrac{1}{2}) > \Lambda_0 \tag{5.12}$$

On the other hand, the condition for linear instability is given by

$$\mathrm{Min}_{\bar{\omega}}\; \{\mathrm{Max}_b \Lambda(\Psi, b, \bar{\omega})\} > \Lambda_0 \tag{5.13}$$

Since Λ is a monotonic function of Ψ and $\mathrm{Max}_b\; \Lambda(\Psi, b, \bar{\omega} = \frac{1}{2}) >$ $\mathrm{Min}_{\bar{\omega}}\; \{\mathrm{Max}_b\; \Lambda(\Psi, b, \bar{\omega})\}$ it follows that linear instability requires larger values of Ψ than non-linear instability.

Note that as Ψ is increased to the linear stability limit, the non-linear growth rate becomes infinite due to the factor $(\partial\epsilon/\partial\omega)^{-1}$.

6. EVALUATION OF MODE-MODE COUPLING EFFECTS

Selection rules

Referring to the high-frequency modes discussed in section 3, we are now interested in evaluating the effects of their mode-mode coupling. As a first step we analyse the selection rules for non-linear growth for all possible types of interacting waves [20]. Here all frequencies are taken positive.

a) A positive-energy wave decaying into two of negative energy; $\omega_+ = \omega'_- + \omega''_-$. This implies (see Fig.1) that $\omega/k > \omega'/k'$ and $\omega/k > \omega''/k''$, while at the same time $\vec{k} = \vec{k}' + \vec{k}''$. These conditions are satisfied if $\vec{k}'$ and $\vec{k}''$ are opposite in sign so that $k < k', k''$.

b) A negative-energy wave decaying into two of positive energy; $\omega_- = \omega'_+ + \omega''_+$. Then $\omega/k < \omega'/k'$, $\omega/k < \omega''/k''$ or $k'k'' < (k-k')(k-k'')$, a condition which is clearly impossible. This interaction is ruled out.

c) Arguing in the same manner it can be shown that the interactions $\omega_+ = \omega'_+ + \omega''_+$, $\omega_+ = \omega'_+ + \omega''_-$ and $\omega_- = \omega'_- + \omega''_-$, $\omega_- = \omega'_- + \omega''_+$ are possible non-explosive interactions.

Calculation of matrix element $V_{\vec{k},\vec{k}',\vec{k}''}$

We adopt the standard method of calculating $V_{\vec{k},\vec{k}',\vec{k}''}$ based on a perturbation theory of the Vlasov equation in which the distribution function is expanded in powers of a given, small, arbitrary electric field $\vec{E}(\vec{r}, t)$. According to this theory the matrix elements are given by [16]

$$V_{\vec{k},\vec{k}',\vec{k}''} = \frac{s_{\vec{k}} \dfrac{k^2}{8\pi} \epsilon^{(2)}(\vec{k}', \vec{k}'')}{\left| \dfrac{k^2}{8\pi} \dfrac{\partial\epsilon}{\partial\omega_{\vec{k}}} \dfrac{k'^2}{8\pi} \dfrac{\partial\epsilon}{\partial\omega_{\vec{k}'}} \dfrac{k''^2}{8\pi} \dfrac{\partial\epsilon}{\partial\omega_{\vec{k}''}} \right|^{\frac{1}{2}}}$$

where the second-order dielectric constant $\epsilon^{(2)}$ is related to the second-order charge density through the relation

$$\epsilon^{(2)}(\vec{k}', \vec{k}'')\tilde{\phi}_{\vec{k}'} \tilde{\phi}_{\vec{k}''} \delta_{-\vec{k},\vec{k}'+\vec{k}''} = -\frac{4\pi}{k^2} \sum_j e_j \int f^{(2)}_{\vec{k},j} d^3v \equiv -\frac{4\pi}{k^2} \rho^{(2)}_{\vec{k}}$$

$\tilde{\phi}_{\vec{k}}$ is the amplitude of lowest-order potential wave. To compute $\epsilon^{(2)}(\vec{k}', \vec{k}'')$, an integration over orbits gives:

$$f^{(2)}_{\vec{k}} = i \frac{e}{m_i} \int_{-\infty}^{t} dt' \left[\phi_{\vec{k}'} \vec{k}' \cdot \frac{\partial}{\partial \vec{v}} f^{(1)}_{\vec{k}''} + \phi_{\vec{k}''} \vec{k}'' \cdot \frac{\partial}{\partial \vec{v}} f^{(1)}_{\vec{k}'} \right] \tag{6.1}$$

By a sequence of algebraic manipulations we are enabled to put $\epsilon^{(2)}(\vec{k}', \vec{k}'')$ in the form

$$\frac{k^2}{4\pi} \epsilon^{(2)}(\vec{k}'; \vec{k}'') = \frac{e^3}{m_i^2 \Omega^2} kk'k'' \int_0^\infty dv_\perp^2 \frac{\partial f}{\partial v_\perp^2} \sum_{\ell, m, n} J_\ell(k) J_\ell(k'') J_n(k')$$

$$\frac{\delta_{m+n,-\ell}}{(\bar{\omega} - \ell)^2 - 1} \left\{ \frac{n/k''}{\bar{\omega}'' - n} + \frac{m/k'}{\bar{\omega}' - m} \right\} \tag{6.2a}$$

where the arguments of the Bessel functions are in fact $kv_\perp/\Omega$. This expression for $\epsilon^{(2)}$ is still not ideal for computing $V_{\vec{k},\vec{k}',\vec{k}''}$ nor are all the symmetry properties of $\epsilon^{(2)}$ immediately evident. We have been able to obtain a particularly transparent expression for $\epsilon^{(2)}$ in the limit of $\omega \gg \Omega$ by summing over all the harmonic terms. The result is

$$\frac{k^2}{4\pi}\,\epsilon^{(2)}(\vec{k}',\vec{k}'') = \frac{e^3}{m^2}\,kk'k''\{P+\pi[R'\operatorname{ctg}\pi\bar{\omega}'+R\operatorname{ctg}\pi\bar{\omega}+R''\operatorname{ctg}\pi\bar{\omega}'']\} \tag{6.2b}$$

where P is the principal part of the integral:

$$\int_{-\infty}^{\infty}\int_{-\infty}^{\infty} dv_x dv_y v_y \frac{\partial f}{\partial v^2}\left[(\omega+kv_y)(\omega'+k'v_y)(\omega''+k''v_y)\right]^{-1}$$

and R, R', and R'' are the respective pole contributions. Again, the only difference from the non-magnetic case is the replacement of i by ctg $\pi\bar{\omega}$ in the resonances. In this form $V_{\vec{k},\vec{k}',\vec{k}''}$ is manifestly symmetric to all interchanges of k, k' and k''.

Non-linear growth rate

We now estimate the non-linear growth rate of the instability due to the interaction process (a). Let ω be of positive energy and both ω' and ω'' be of negative energy so that $\omega''> k\bar{v}_i$ and $\omega'<k'\bar{v}_i$, $\omega''<k''\bar{v}_i$. For the special loss-cone distribution of section 3 we obtain

$$k^2\epsilon^{(2)} \sim \left(\frac{e}{T_i}\right) kk'\left(\frac{\omega_{pi}^2}{\omega^2}\right)\left(\frac{\omega'\sqrt{\alpha}}{k}\right)\pi\ \operatorname{ctg}(\pi\bar{\omega}')$$

with the kinetic temperature $T_i = m_i/\alpha$. Since the possible singularities of $\operatorname{ctg}(\pi\omega')$ will be eventually cancelled by those in $\partial\epsilon/\partial\omega$, we set $\operatorname{ctn}\pi\omega \sim 1$ to get a rough estimate of $V_{\vec{k},\vec{k}',\vec{k}''}$.

Processes of type (c) can also take place with equal probability but their general effect will be to redistribute the energy gained through process (a) among waves of the same type of energy. Since the matrix elements for the stable and unstable interactions are comparable and the regions in k-space involved are also comparable we can reasonably conclude that type (a) interactions cause the system to go explosively unstable.

The non-linear growth rate can be computed in the same manner as in section 4. If it is assumed that the spectrum of excited waves is broad then

$$\gamma_{NL} \approx \left(\frac{\mathscr{E}}{nT_i}\right)\frac{\Omega^2}{\omega} \tag{6.3}$$

a result very comparable to the non-linear Landau damping. For this estimate we have assumed $\omega \sim k\bar{v}_i$ as in previous order-of-magnitude evaluations.

On the other hand, if it is assumed that the wave energy is concentrated in a few modes, then as in section 4 we may approximate the delta function in the kinetic equation by $1/\gamma_{NL}$ and the growth rate is given by

$$\gamma_{NL} \approx \left(\frac{\mathscr{E}}{nT_i}\right)^{\frac{1}{2}} \left(\frac{\Omega^3}{\omega}\right)^{\frac{1}{2}} \tag{6.4}$$

7. CONCLUSION

We summarize the main conclusions of this paper as follows:

i) The criterion for an explosive instability from wave-wave interaction is $s = s' = s''$.

ii) The criterion for an explosive instability from the non-linear Landau process is $s' = s''$ and

(a) $$(\omega' + \omega'')s' \int dE \, \frac{\partial f}{\partial E} \, |V_{k', k''}(E)|^2 > 0$$

in the case with magnetic field, i.e. $\omega' + \omega'' = n\Omega$.

(b) $$(k' + k'')s' \int d^3p \, \frac{\partial f}{\partial p} \, |V_{k', k''}(p)|^2 > 0$$

where there is no magnetic field.

iii) The principle of microscopic detailed balance is shown to provide a convenient method to generate the kinetic equation for waves. A new method of computing matrix elements for non-linear Landau damping from the process of wave scattering by dressed particles is developed.

iv) The application of this theory to the high-frequency flute modes of a mirror confined plasma shows that both 3-wave mode coupling and non-linear Landau damping can lead to non-linear wave growth. Matrix elements for this case are evaluated and growth rates are given.

v) A special case of non-linear Landau damping occurs when the two waves are the same. We show that this self-interaction non-linear instability does not in general occur for loss-cone distributions, but does occur in the presence of a density gradient somewhat less than the critical value for the linear drift loss-cone instability.

vi) From these considerations it is clear that we would not expect "weak turbulence" to occur in mirror confined plasmas as non-linear terms are destabilizing, but rather a rapid increase in the level of fluctuations followed by a relaxation process in which the plasma attains a new equilibrium, probably by quasi-linearly expelling particles into the loss cone. This may well explain the phenomena of bursts of radiation and particles at the harmonics of the ion gyro-frequency often observed in mirror machines [21].

ACKNOWLEDGEMENTS

We wish to thank Gary M.Walters for his collaboration and many interesting discussions. Special thanks are also due to Herbert Fishman for his help and for programming the numerical work.

Work performed under the auspices of the US Atomic Energy Commission, Contract AT(30-1)-3927.

The contribution of R.N.S. was supported in part by the National Science Foundation, Atmospheric Sciences Section, Grant GA-989.

REFERENCES

[1] LOUISELL, W.H., PIERCE, J., Proc. Inst. Radio Engrs 43 (1955) 425.
[2] KADOMTSEV, B.B., MIKHAILOVSKII, A.B., TIMOFEEV, A.V., Zh. eksp. teor. Fiz. 47 (1965) 2266. [English translation: Soviet Phys. JETP 20 (1965) 1517.]
[3] BERS, A., GRUBER, S., Appl. Phys. Lett. 6 (1965) 27.
[4] DIKASOV, V.M., RUDAKOV, L.I., RYUTOV, D.D., Zh. eksp. teor. Fiz. 48 (1965) 913. [English translation: Soviet Phys. JETP 21 (1966) 608.]
[5] HALL, L.S., HECKROTTE, W., Physics Fluids 9 (1966) 1496.
[6] TIMOFEEV, A.V., Zh. eksp. teor. Fiz. Letters 4 (1966) 48. [English translation: Soviet Phys. JETP 4 (1966) 32.]
[7] STIX, T.H., The Theory of Plasma Waves, McGraw-Hill, New York (1963) 46.
[8] SAGDEEV, R.Z., GALEEV, A.A., Paper IC/66/64, International Centre for Theoretical Physics, Trieste (1966).
[9] KADOMTSEV, B.B., Plasma Turbulence, Academic Press, London (1965) 31.
[10] CAMAC, M., KANTROVITZ, A.R., LITVAK, M.N., PATRICK, R.M., PETSCHEK, H.E. in Plasma Physics and Controlled Nuclear Fusion (Proc. Conf. Salzburg, 1961) Nucl. Fusion, Suppl. Part 3 (1962) 423.
[11] GALEEV, A.A., KARPMAN, V.I., Zh. eksp. teor. Fiz. 44 (1963) 592. [English translation: Soviet Phys. JETP 17 (1963) 403.]
[12] KADOMTSEV, B.B., PETVIASHVILI, V.I., Zh. eksp. teor. Fiz. 43 (1962) 2234. [English translation: Soviet Phys. JETP 16 (1963) 1578.]
[13] ARMSTRONG, I.A., BLOEMBERGEN, N., DUCUING, J., PERSHAN, P.S., Phys. Rev. 127 (1962) 1918.
[14] ORAEVSKII, V.N., SAGDEEV, R.Z., Zh. techn. Fiz. 32 (1962) 1291. [English translation: Soviet Phys. Tech. Phys. 7 (1963) 355.]
[15] ALTSHUL, L.M., KARPMAN, V.I., Zh. eksp. teor. Fiz. 47 (1964) 1552. [English translation: Soviet Phys. JETP 20 (1965) 1043.]
[16] GALEEV, A.A., KARPMAN, V.I., SAGDEEV, R.Z., Nucl. Fusion 5 (1965) 20.
[17] POST, R.F., ROSENBLUTH, M.N., Physics Fluids 9 (1966) 730.
[18] FRIED, B.D., CONTE, S., Plasma Dispersion Function, Academic Press, New York (1961).
[19] ROSENBLUTH, M.N., ROSTOKER, N., Physics Fluids 5 (1962) 776.
[20] A discussion of this condition, with reference to the two-stream instability has been given in Ref.[4] and recently also by AAMODT, R.E., SLOAN, M.L., Phys. Rev. Lett. 19 (1967) 1227.
[21] KUO, L.G., MURPHY, E.G., PETRAVIC, M., SWEETMAN, D.B., Physics Fluids 7 (1964) 988.
[22] Following completion of this paper we have learned that this point of view has been previously exploited by KOVRIZHNYKH, L.M. (EUR-CEA-258-1964), and has been used by L.M. KOVRIZHNYKH and V.N. TSYTOVICH in subsequent papers [e.g. Soviet Phys. JETP 19 (1964) 1494] to discuss similar questions, e.g. beam stability problems, Langmuir waves, etc.

DISCUSSION

V.N. TSYTOVICH: How did you obtain the results for a narrow spectrum?

R.N. SUDAN: They were obtained from the same kinetic equations, except that in making the estimate for γ_{NL} the non-linear growth rate, $\delta(\omega' + \omega'' - mQ)$, is approximated by $1/\gamma_{NL}$.

V.N. TSYTOVICH: Does non-linear Landau damping also lead to explosive instabilities? If so, what is the physical cause?

R.N. SUDAN: Non-linear Landau damping does indeed give rise to an explosive growth, provided the criteria given in the paper are satisfied. For a certain choice of frequencies the total action is conserved, but when the explosive criterion is satisfied this is not so, because in this case $dN'/dt = dN''/dt$.

V.G. MAKHANKOV: What was the time dependence of the energy density for explosive processes?

R.N. SUDAN: If the interacting waves are taken to be linearly stable, it is easy to show that in an explosive interaction $N_k(t) \sim N(t=0)/[1 - \alpha t N(t=0)]$ where $\alpha N_0 = 1/\gamma_{NL}$. A slightly more complicated expression is obtained when the linear growth rate is taken into account.

V.G. MAKHANKOV: Did you take into account the influence of pair collisions in considering non-linear collisions?

R.N. SUDAN: No, we did not feel that they would affect our calculations significantly.

INSTABILITES NON LINEAIRES DANS UN PLASMA INHOMOGENE

B. COPPI*, G. LAVAL, R. PELLAT ET TU KHIET**
ASSOCIATION EURATOM-CEA,
FONTENAY-AUX-ROSES, FRANCE

Abstract — Résumé

NON-LINEAR INSTABILITIES IN AN INHOMOGENEOUS PLASMA. The low-frequency drift modes of a low-pressure isothermal inhomogeneous plasma can be stabilized if the shear of the magnetic field lines exceeds a critical value given by the expression $r/L_s = (1/2\sqrt{2})(a/r)$, where L_s is the shear length, r the characteristic length of density variation, and a the ion Larmor radius.

The authors first show that, even if $r/L_s < (1/2\sqrt{2})(a/r)$, it is possible to achieve a substantial reduction in the rate of growth of the modes and thereby satisfy the conditions for applying the theory of weak turbulence. If $a/r \ll 1$, the normal modes are very easily stabilized, but convective perturbations are known to persist and these can become amplified by propagating in the direction of the density gradient. These perturbations can be excited only by thermal fluctuations, which are explicitly calculated. The maximum amplitude of the relative density fluctuations are then deduced.

If the plasma is fairly dense, weak shear is sufficient to maintain these fluctuations at a level at which the resulting diffusion is negligible. In both these cases of weak turbulence, however, non-linear instability may arise and cause diffusion that is far more substantial than the linear theories predict. On the one hand, the authors note that the energy of the drift waves is negative if their phase velocity parallel to the magnetic field is greater than the thermal velocity of the electrons, and discuss the development of the non-linear instability which results as a function of shear. On the other hand, they show that non-linear reflection of the convective perturbations may occur before they reach the region where they would be absorbed by the ion Landau effect. They estimate the threshold which the amplitude of the initial perturbations must pass for a non-linear instability to develop.

INSTABILITES NON LINEAIRES DANS UN PLASMA INHOMOGENE. Les modes de dérive B.F. d'un plasma inhomogène, isotherme et à faible pression peuvent être stabilisés si le cisaillement des lignes du champ magnétique dépasse une valeur critique donnée par $r/L_s = (1/2\sqrt{2})(a/r)$ où L_s est la distance du cisaillement, r la longueur caractéristique de variation de la densité et a le rayon de Larmor des ions. Les auteurs montrent d'abord que même si $r/L_s < (1/2\sqrt{2})(a/r)$, on peut obtenir une réduction notable du taux de croissance des modes et remplir ainsi les conditions d'application de la théorie de la turbulence faible. Si $a/r \ll 1$, les modes normaux seront très facilement stabilisés, mais on sait qu'il subsistera des perturbations convectives qui pourront s'amplifier en se propageant dans la direction du gradient de densité. Ces perturbations ne peuvent être excitées que par les fluctuations thermiques que les auteurs calculent explicitement. Ils en déduisent l'amplitude maximale des fluctuations relatives de la densité. Si le plasma est assez dense, un faible cisaillement suffit alors à les maintenir à un niveau tel que la diffusion résultante soit négligeable. Toutefois, dans ces deux cas de turbulence faible, il peut apparaître une instabilité non linéaire qui entraîne une diffusion beaucoup plus importante que ne le laissent prévoir les théories linéaires. En effet, les auteurs constatent d'abord que l'énergie des ondes de dérive est négative si leur vitesse de phase parallèle au champ magnétique est supérieure à la vitesse thermique électronique. Ils discutent le développement de l'instabilité non linéaire qui en résultera en fonction du cisaillement. D'autre part, ils montrent qu'il peut y avoir réflexion non linéaire des perturbations convectives avant qu'elles n'atteignent la région où elles seront absorbées par effet Landau des ions. Ils estiment le seuil que doit dépasser l'amplitude des perturbations initiales pour qu'une instabilité non linéaire se développe.

---

* The Institute for Advanced Study, Princeton, N.J., USA.

** Laboratoire de physique des plasmas, Faculté des sciences d'Orsay, France.

I. INTRODUCTION

En raison des conséquences qu'elle peut avoir pour le confinement, la diffusion due aux instabilités de dérive a fait l'objet de nombreux travaux théoriques tout au moins dans le cas des plasmas de $\beta > \frac{m}{M}$ [1; 2; 3; 4]. Cette condition supprime en effet les modes de taux de croissance fort, ce qui permet d'étudier la diffusion dans le cadre des équations de la turbulence faible. Mais cette condition n'est pas vérifiée dans les conditions expérimentales actuelles où les plasmas sont toujours de très faible pression ($\beta \lesssim 10^{-4}$).

Cela ne signifie pas que, dans ces expériences, la turbulence due aux ondes de dérive doive être forte et la diffusion rapide. La théorie montre, en effet, que l'on peut stabiliser ces ondes, notamment par un cisaillement suffisant des lignes de force [5 - 6]. Les critères de stabilisation par cisaillement sont de deux sortes. Les uns concernent la stabilisation des modes normaux localisés par une variation radiale du gradient de densité [5] ; lorsque le cisaillement est suffisant pour supprimer les modes instables, le plasma peut rester localement instable et amplifier des paquets d'onde : on obtient ainsi d'autres critères de stabilité [6] en imposant que cette amplification ne dépasse pas un certain nombre, n_o, d'exponentiations. La détermination de ce nombre n_o sera l'objet principal de notre étude.

Dans une première partie, on précise le rôle stabilisant du cisaillement sur les modes localisés, en calculant explicitement le taux de croissance des modes. On montre que le taux de croissance peut être très réduit par rapport au cas sans cisaillement, ce qui permet a priori d'étudier l'interaction non linéaire de ces modes dans le cadre d'une théorie de turbulence faible : on dérive formellement en Annexe I les équations adaptées à l'étude non linéaire des modes localisés. On constate cependant que l'amplitude des modes les plus instables ne peut être limitée par couplage de modes résonnants.

Dans le cas où le critère de stabilisation des modes est satisfait, on analyse la propagation et l'amplification des modes convectifs excités par les fluctuations thermiques du plasma. On en déduit que n_o doit être grand (donc le cisaillement faible) pour que les modes convectifs aient une amplitude dangereuse pour le confinement.

On montre ensuite qu'un mécanisme de réflexion non linéaire de paquets d'ondes permet de déclencher une instabilité non linéaire. Le calcul du seuil de cette instabilité conduit à fixer $n_o \simeq 1$ dans les critères de stabilité pour les modes convectifs.

La même conclusion est obtenue par l'analyse d'une instabilité non linéaire due au couplage résonnant d'ondes de dérive ayant des énergies de signes différents.

II. MODES NORMAUX LOCALISES

Soit un plasma isotherme, sans collisions, inhomogène dans la direction $\overline{OX}$, confiné par un champ magnétique $\overline{B} = B_o\,(\overline{e}_z + \frac{x}{L_s}\,\overline{e}_y\,)$ où la composante du champ dans la direction $\overline{OY}$ représente l'effet du cisaillement des lignes de forces. On suppose que les vitesses de dérive $V_{i,e}$ des ions et des électrons sont maximales au point $x = 0$, $V_{i,e} = V_{i,e}\left[1 - \frac{x^2}{2r^2}\right]$ avec $1/r = \frac{d}{dx}\, \mathrm{Log}\, n /_{x=0}$ où n est la densité. On fait l'hypothèse que ce plasma est de faible pression ($\beta < m/M$), ce qui correspond aux résultats expérimentaux actuels des machines toroïdales. Dans ces conditions, après analyse de Fourier suivant $\overline{OY}$ et $\overline{OZ}$, le potentiel électrostatique ϕ des ondes de dérive est solution de l'équation différentielle :

$$\frac{\omega-\omega_0}{\omega}\left[I_1(b)-I_0(b)\right]e^{-b}\frac{a^2}{2}\frac{d^2\phi}{dx^2} + \frac{\omega_0}{\omega}\left[1+W_e-I_0 e^{-b}\right]\frac{x^2}{r^2}\phi + D\phi = 0 \tag{1}$$

avec $D \equiv 2 - \frac{\omega+\omega_0}{\omega}(1+W_e) - \frac{\omega-\omega_0}{\omega} I_0(b)e^{-b}(1+W_i)$

où $\omega_0 = K_y V_e^0$, $b = \frac{K_y^2 a^2}{2}$, a étant le rayon de Larmor moyen des ions

$$W_{i,e} \equiv -(\pi)^{1/2}\int_{-\infty}^{+\infty}\frac{x e^{-x^2}dx}{x+(\omega-i\varepsilon)/K_{/\!/}V_{th\,i,e}} \; ; \; K_{/\!/} = \frac{\overline{K}\cdot\overline{B}}{B} \; ;$$

$V_{th\,i,e}$, vitesses thermiques des ions et des électrons.

La condition de stabilité des modes normaux localisés s'écrit [5] :

$$L_s/r < 2\sqrt{2}\; r/a \tag{2}$$

Lorsque cette condition est satisfaite, on ne peut localiser les solutions de l'équation (1) dans un domaine en x où l'effet Landau des ions soit négligeable et tous les modes sont fortement amortis. Le modèle analysé simule une configuration toroïdale : L_s/r est un nombre qui caractérise le cisaillement ($L_s \rightarrow \frac{r_0}{R}\frac{d\iota}{dr}$ où r_0 est la distance radiale du point de localisation, R le grand rayon du tore, ι l'angle de transformation rotationnelle) ; il ne dépend que de la configuration magnétique et varie de l'ordre de 30 pour un lévitron à 100 pour un Tokomac ou un Stellerator à fort "shear". Le critère (2) est donc difficile à satisfaire expérimentalement car il impose un grand nombre de rayons de Larmor des ions dans l'échelle caractéristique du gradient de densité. Il semble nécessaire d'étudier le rôle d'un cisaillement insuffisant pour stabiliser linéairement tous les modes ($L_s/r > 2\sqrt{2}\; r/a$), mais suffisant pour limiter non linéairement leur amplitude. On peut d'ailleurs remarquer qu'en l'absence de cisaillement le β des plasmas toroïdaux actuels serait trop faible pour réduire la turbulence due aux ondes de dérive à un niveau entraînant une faible diffusion. Nous supposons donc que le critère (2) n'est pas satisfait, mais que L_s/r reste inférieur ou de l'ordre de $(M/m)^{1/2}$ pour éviter l'apparition d'instabilités non linéaires dues aux modes convectifs (sections IV et V).

Pour ces valeurs du cisaillement, l'extension radiale de la région "fluide" ($\omega_0 \gtrsim \frac{K\cdot B}{B} V_{the}$), à taux de croissance local fort, reste inférieure ou de l'ordre du rayon de Larmor des ions. Les points tournants de la solution B.k.W. de l'équation (1) sont localisés dans la région résonnante pour les électrons ($\omega \ll \frac{K\cdot B}{B} V_{the}$) ; ils ont pour abscisse $\pm x_0$, avec :

$$x_0 = r\left[\frac{\omega}{\omega_0 I_0(b)e^{-b}}\left(2 - \frac{\omega-\omega_0}{\omega}I_0(b)e^{-b}\right)\right]^{1/2} \tag{3}$$

La valeur minimale Δ de x_o, qui correspond aux modes les plus localisés $\left(\phi(x) \sim \exp -(x/\Delta)^2\right)$ est donnée par l'expression :

$$\Delta^4 = \frac{(ar)^2\left[1+I_o(b)\,e^{-b}\right]\left[I_o(b)-I_1(b)\right]}{I_o(b)\left[2-I_o(b)\,e^{-b}\right]} \tag{4}$$

Le taux de croissance γ s'obtient par un calcul de perturbation qui tient compte de W_z. En ordre de grandeur, on peut prévoir pour les modes à $k_z \sim 0$, qui sont de taux de croissance maximum :

$$\gamma \sim \frac{L_s}{x_o}\,\frac{\omega^2(\omega+\omega_o)}{\omega_o K_y\ V_{the}\ I_o e^{-b}} \tag{5}$$

Cette formule, qui pour $b \lesssim 1$ s'écrit : $\gamma/\omega_o b \sim \frac{a L_s}{r x_o}\left(\frac{m}{M}\right)^{1/2}$ montre que le taux de croissance est particulièrement réduit pour les modes de grande extension et pour tous les modes si les ions ont un nombre atomique A élevé. Des calculs numériques ont confirmé ces résultats puisque, pour le mode $\phi \sim \exp-(x/\Delta)^2$ et pour $b = 1$, on a obtenu $\gamma/\omega = 0{,}2$, avec $r/a = 10$, $L_s/r = 140$ pour $A = 40$.

Remarquons enfin une propriété importante des modes : la valeur moyenne de la longueur d'onde radiale diminue avec l'extension du mode, puisque d'après (1) :

$$\frac{\langle K_x\rangle^2 a^2}{2} \simeq \left(\frac{x_o}{r}\right)^2 \frac{\omega_o}{\omega_o-\omega}\left[1-I_1/I_o\right]^{-1} \tag{6}$$

D'après les résultats obtenus pour le taux de croissance, on peut a priori chercher une limitation non linéaire de l'amplitude des modes instables dans le cadre d'une théorie de turbulence faible. On rappelle toutefois que la théorie classique repose sur un développement en série de Fourier pour les variables d'espace et néglige les effets convectifs dus à l'inhomogénéité. On trouvera en Annexe I une dérivation formelle des équations de faible turbulence adaptées à l'étude des modes.

En l'absence de cisaillement et pour des plasmas de $\beta > m/M$, la théorie non linéaire a été faite pour des paquets d'onde [2 ; 3 ; 4]. On peut justifier cette hypothèse en remarquant que le taux de croissance d'un paquet d'ondes est pratiquement constant à l'échelle de la localisation des modes : il en résulte que l'exponentiation est grande entre les points tournants et que l'équilibre du bruit peut être local. Le niveau de fluctuations est alors contrôlé par les ondes ($K_x a \sim K_y a \sim 1$) car le taux de croissance dépend peu de K_x pour $K_y a \sim 1$ et la matrice d'interaction est proportionnelle à K_x^2 [4].

Pour $\beta < m/M$, avec les valeurs de cisaillement que l'on considère $\left[\frac{r}{a} < \frac{L_s}{r} < \left(\frac{M}{m}\right)^{1/2}\right]$ l'amplification d'un paquet d'ondes est faible entre deux réflections aux points tournants et un mode peut se former dans une phase de croissance linéaire. Considérons plus particulièrement un mode ω de faible extension ($x_o \sim \Delta$) et de taux de croissance fort ($K_y a \sim 1$). Sa probabilité d'interaction non linéaire avec un autre mode ω' de faible extension est négligeable car on a nécessairement $\omega \simeq \omega'$ puisque pour ces deux modes $K_y, K'_y \gg \frac{\partial}{\partial x}$. Ce mode peut également se dissocier en deux modes de grande extension mais, contrairement au cas sans cisaillement avec $\beta > m/M$, ces modes ont un taux de croissance négligeable (5) et leur niveau d'excitation reste trop faible pour limiter la croissance des modes de courte extension.

III. MODES CONVECTIFS

Si le cisaillement satisfait à la condition (1) les modes normaux sont amortis. Le plasma reste cependant "localement" instable et l'on peut prévoir [6] que pour des valeurs trop faibles du cisaillement ($\left(\frac{m}{M}\right)^{1/2} < \frac{L_s}{r} < \frac{r}{a}$) certains modes convectifs seront suffisamment amplifiés pour interagir non linéairement entre eux. Nous nous limitons à l'étude des modes tels que $b \equiv \frac{a^2}{2}\left(K_y^2 - \frac{\partial^2}{\partial x^2}\right) \lesssim 1$ (ces modes jouant un rôle essentiel dans la diffusion) avec l'hypothèse supplémentaire que $K_y^2 < \frac{\partial^2}{\partial x^2}$, qui permet de contrôler la validité de l'approximation B.K.W. Ces modes satisfont à l'équation différentielle :

$$\frac{a^2}{2}\frac{d^2\phi}{dx^2} + \left[W_i - \frac{\omega + \omega_o}{\omega - \omega_o} W_e - \frac{K_y^2 a^2}{2}\right]\phi = 0 \tag{7}$$

qui s'obtient à partir de (1) en négligeant la dépendance spatiale de la vitesse de dérive devant celle des fonctions $W_{i,e}$ d'argument $K_{/\!/} = \frac{K_y(x-X)}{L_s}$. Pour le domaine de propagation résonnant ($V_{thi} < \omega/K_{/\!/} < V_{the}$) et dans l'approximation locale, l'équation (7) peut s'écrire :

$$K_x^2 \; a^2 = \frac{(x-X)^2 V_{the}^2}{L_s^2 \; V_e^2} - \frac{\delta\omega}{K_y V_e}\left[1 + i\sqrt{\pi}\,\frac{L_s V_e}{|x-X| V_{the}}\,\frac{K_y}{|K_y|}\right] - K_y^2 a^2 \tag{8}$$

D'après cette expression, on doit choisir $\frac{\delta\omega}{K_y V_e} > 0$ pour assurer la propagation aux petites valeurs de $x - X$; la vitesse de groupe, $V_G = -\frac{\partial\omega}{\partial K_x}$ est donc de signe opposé à $\mathrm{Im}\, K_x$ ce qui montre qu'un paquet d'ondes localement instable est amplifié quelque soit le sens de sa propagation en x. Pour les valeurs de x telles que $|x - X| \gtrsim \frac{a L_s}{2r}$ un paquet d'ondes est rapidement absorbé par l'effet Landau des ions. Pour étudier la propagation pour les valeurs $|x - X| \lesssim \left(\frac{m}{M}\right)^{1/2} \frac{a L_s}{2r}$ où l'approximation BKW n'est plus justifiée, on a résolu numériquement l'équation (7) en imposant à la solution d'être une onde transmise se propageant vers $x \to \infty$. On a obtenu pour tous les paquets d'ondes un coefficient de réflexion proche de 0,5. A cette occasion, on a également vérifié les résultats obtenus analytiquement [6] et constaté que l'amplification maximale est obtenue pour $K_x \gtrsim K_y$; l'amplification des paquets d'onde avec $K_x \lesssim K_y$ pourrait être a priori plus grande, mais le domaine de propagation est très réduit pour un plasma isotherme et le résultat numérique est identique. En résumé, dans le cadre de la théorie linéaire, toute perturbation apparaissant dans un domaine en x défini par $|x - X| \lesssim a L_s/2r$ sera amplifié d'un facteur $\exp(2n_o)$, au plus, avant d'être absorbée par l'effet Landau des ions ; n_o est défini comme $\int \frac{\gamma(x)dx}{V_{gr}}$, l'intégrale étant prise entre l'effet Landau des ions et le point de réflexion.

Les perturbations naturelles du plasma sont dues aux fluctuations thermiques ; pour les calculer, on doit tenir compte du caractère discret des particules et introduire la fonction de distribution fine :
$\nu = \Sigma\, \delta(\bar{r} - \bar{r}_i)\, \delta(\bar{v} - \bar{v}_i)$ où $(\bar{r}_i, \bar{v}_i)$ sont les positions et vitesses des particules à l'instant t ; la fonction de distribution à une particule est définie à partir d'une moyenne d'ensemble, $f = \langle \nu \rangle$, faite sur $(\bar{r}_i, \bar{v}_i)$. A l'ordre le plus bas en champ électrique, la fluctuation microscopique de densité $\delta\nu = \nu - f$ est solution de l'équation :

$$\frac{d}{dt}(\delta\nu) = -\frac{q}{m}\, \nabla\phi \cdot \frac{\partial f}{\partial \bar{v}} \tag{9}$$

où $\frac{d}{dt}$ est l'opérateur de dérivation le long des trajectoires non perturbées.

Si l'on caractérise ensuite l'amplitude du champ électrique fluctuant par sa fluctuation quadratique moyenne I_K par unité de volume :

$$I_K = \frac{|\phi_K|^2}{V} \qquad \phi_K = \int_V \phi(\bar{r})\, \exp(i\bar{K}\bar{r})\, d\bar{r} \tag{10}$$

on obtient pour I_K l'équation de transport suivante :

$$\frac{\partial I_K}{\partial t} + \frac{\partial}{\partial x}\left(V_{gr} I_K\right) = 2\gamma_K I_K + \frac{4\pi^2 T^2}{e^2 n \frac{\partial D}{\partial \omega}} \int f(v)\, \delta(\omega + K_{/\!/} V_{/\!/})\, dv \tag{11}$$

valable dans le domaine $V_{thi} < \frac{\omega}{K_{/\!/}} < V_{the}$; D a été précédemment défini (1).

Pour résoudre l'équation (11) on se donne une valeur réelle de K_x et on intègre dans la région d'amplification en tenant compte de la dépendance de γ en fonction de x (celle de V_{gr} est négligeable), et des conditions aux limites ; on obtient pour l'amplitude maximale en régime stationnaire :

$$I_K = \frac{4\pi^2 T^2}{e^2 n} \frac{\exp(4n_o) - 1}{\left[2 - I_o e^{-b}\right]\left[1 - I_o e^{-b}\right]} \tag{12}$$

Ce qui donne pour $K_\perp a \sim 1$, $\Delta K_{/\!/} \sim \frac{1}{r}$, $n_o > 1$

$$\frac{e^2\phi^2}{T^2} \sim \frac{\exp(4n_o)}{n a^2 r} \tag{13}$$

$n a^2 r$ est a priori un nombre très grand, surtout si le champ magnétique est faible, le plasma de grandes dimensions et la densité élevée ; les fluctuations thermiques restent donc négligeables ; il en est de même du coefficient de diffusion obtenu à partir d'un calcul de flux :

$$< n v_x > = \frac{1}{V} \int \frac{n E_y}{B} d\bar{r} \tag{14}$$

et qui est en ordre de grandeur donné par l'expression :

$$D \sim \frac{a V thi}{(n a^3)} \exp(4 n_o) \tag{15}$$

Par un calcul négligeant les effets non linéaires, D ne serait important que dans la mesure où $\exp(4n_o)$ serait de l'ordre de $(n a^3)$; la valeur de L_s/r correspondante pourrait être ainsi d'un ordre de grandeur plus petite que la valeur $(M/m)^{1/2}$ admise généralement et dépendrait d'autres paramètres de l'équilibre.

IV. REFLEXIONS NON LINEAIRES

En fait, si les fluctuations thermiques sont négligeables, on doit inclure dans l'équation d'évolution de I_K, les termes de couplage résonnants et non résonnants (effet Landau non linéaire). Cette équation peut alors s'écrire :

$$\frac{\partial I_K}{\partial t} + \frac{\partial}{\partial x}\left(V_{gr} I_K\right) = 2\gamma_K I_K + \int dK' dK'' \left|V_{K,K',K''}\right|^2 I_{K'} I_{K''} \,\delta(K-K'-K'')\,\delta(\omega_K - \omega_{K'} - \omega_{K''})$$
$$+ \int dK' \, W_{K,K'} \, I_K I_{K'} \tag{16}$$

Le second terme proportionnel à $I_{K'} I_{K''}$ correspond à la création de l'onde K par couplage non linéaire des ondes K', K''. Le dernier terme regroupe les termes de désintégration et d'effet Landau non linéaire proportionnels à I_K.

L'équation (16) met en évidence des mécanismes d'instabilité non linéaires qui permettent de déterminer n_o : dans ce chapitre, on analyse plus particulièrement l'effet d'une réflexion non linéaire ; celle-ci se produit lorsque le couplage de deux ondes de vitesses de groupe de même signe donne une troisième onde de vitesse de groupe de signe opposé.

Au voisinage de la région de forte absorption par effet Landau des ions, d'abscisse $x = \frac{K_z}{K_y} L_s + \frac{a L_s}{2r}$, l'onde K est, avant amplification, de très faible amplitude. Le seul terme non négligeable de l'équation (16) peut être le terme de création, dans la mesure où les ondes K' et K" sont créées en des points différents et de grande amplitude au point considéré. En dehors de cette région, on supposera $I_K, I_{K'}, I_{K''} \ll \gamma |V|^{-2}$ ce qui permettra de négliger tous les termes non linéaires.

Puisqu'une onde se réfléchit linéairement au point d'abscisse $x = -\frac{K_z}{K_y} L_s + \left(\frac{m}{M}\right)^{1/2} \frac{a L_s}{2r}$, on dispose d'éléments suffisants pour étudier un couplage d'ondes pouvant conduire à une instabilité non linéaire. Sur la Figure 1, on a seulement indiqué les points de réflexion linéaire (d'abscisse x_1, x_2, x_3) des ondes considérées. On a

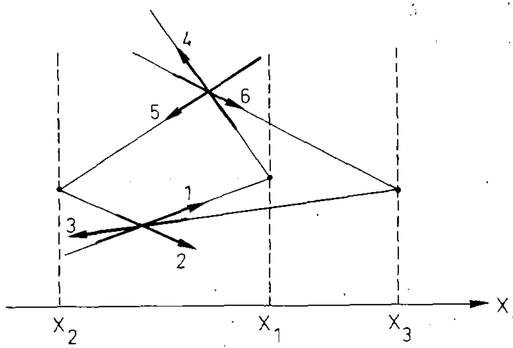

FIG. 1. Points de réflexion linéaire d'un couplage d'ondes.

fait l'hypothèse, justifiée par la suite, que les points d'absorption de l'onde 5 sont à droite de x_1. On voit que si l'onde 4 a une grande amplitude, elle génère l'onde 6 par couplage avec l'onde 5 au voisinage de x_2 et l'onde 5 par couplage avec l'onde 6 au voisinage de x_1. Les ondes 5 et 6 sont amplifiées, réfléchies pour donner les ondes 2 et 3 qui génèrent 1 par couplage ; celle-ci est amplifiée et se réfléchit pour renforcer l'onde 4.

Dans les équations d'évolution des amplitudes, on conserve le terme de création pour les ondes incidentes (1 ; 5 ; 6) mais ce terme peut être négligé pour les ondes réfléchies (2 ; 3 ; 4) ; on obtient ainsi pour les ondes 1 et 4 à titre d'exemple les équations :

$$\begin{cases} \dfrac{\partial N_1}{\partial t} + V^1_{gr} \dfrac{\partial N_1}{\partial x} = 2 \gamma^1 N_1 + V^2 N_2 N_3 \\[2ex] \dfrac{\partial N_4}{\partial t} - V^1_{gr} \dfrac{\partial N_4}{\partial x} = 2 \gamma^1 N_4 \end{cases} \tag{17}$$

avec la définition $N_K = I_K \left(\frac{\partial D}{\partial \omega}\right) \simeq I_K / K_y V_e$, qui permet d'obtenir des coefficients de couplage V^2 égaux pour les trois ondes en interaction. D'après le schéma précédent, la réflexion linéaire permet au terme source, $V^2 N_2 N_3$, de ne pas s'annuler au point où N_1 s'annule. En supposant le coefficient de réflexion égal à l'unité pour simplifier les calculs, on peut écrire les conditions aux limites, pour les ondes 1 et 4 ; 2 et 5 ; et 3 et 6 :

$$\begin{aligned} N_1(x_1) &= N_4(x_1) \quad ; \quad N_1(x_2) = 0 \\ N_2(x_2) &= N_5(x_2) \quad ; \quad N_5(x_1) = 0 \\ N_3(x_3) &= N_6(x_3) \quad ; \quad N_6(x_2) = 0 \end{aligned} \tag{18}$$

Pour trouver le seuil d'instabilité non linéaire, on cherche la solution stationnaire des équations (17) puis on montre que le système d'ondes est instable si le niveau de fluctuations dépasse celui défini par l'état stationnaire. Au point de vue physique, l'état stationnaire correspond au cas où l'amplification linéaire compense exactement la perte d'énergie due au faible coefficient de réflexion non linéaire. Pour alléger les calculs, on remplace $\gamma^1(x)$ dans les équations (17) par sa valeur moyenne ; on introduit alors la notation :

$$n_1 = (X_1 - X_2)\lambda_1 = \frac{1}{V^1_{gr}} \int_{X_2}^{X_1} \gamma^1(x)\,dx \qquad (19)$$

avec des définitions analogues pour n_2 et n_3. On déduit alors de l'éq.(17):

$$N_1^\circ(X_1) = \frac{V^2 N_5(X_2) N_6(X_3)}{2(\lambda_1 + \lambda_3 - \lambda_2)} \exp 2(n_1 + n_3) \qquad (20)$$

$$N_6^\circ(x) = \int_{X_2}^{X} dx' \frac{|V|^2}{V^6_{gr}} N_4(x') N_5(x') \exp - \lambda_3 (x - x') \qquad (21)$$

La contribution à l'intégrale vient essentiellement des valeurs de X proches de X_2. Or, pour X proche de X_2, $N_5^\circ(X) = N_5^\circ(X_2)\exp - \lambda_2(X - X_2)$; on en déduit,

$$N_6^\circ(X_3) = \frac{|V|^2 N_5(x_2) N_1(x_1)}{2V^6_{gr}(\lambda_1 + \lambda_2 + \lambda_3)} \exp 2(n_1 + n_3) ; N_5^\circ(x_2) = \frac{|V|^2 N_1(X_1) N_6(X_3)}{2V^2_{gr}(\lambda_2 + \lambda_3 - \lambda_1)} \exp 2n_2 \qquad (22)$$

et, en combinant ces résultats, les expressions $N_1^\circ, N_5^\circ, N_6^\circ$, telles que par exemple:

$$N_1^\circ(X_1) = \frac{2}{|V|^2} \left[V^2_{gr} V^6_{gr} (\lambda_1 + \lambda_2 + \lambda_3)(\lambda_2 + \lambda_3 - \lambda_1) \right]^{1/2} \exp - (n_1 + n_2 + n_3) \qquad (23)$$

On a supposé dans ces calculs $\lambda_1 \sim \lambda_2 \sim \lambda_3$, $|X_1 - X_2| \gg |X_3 - X_1|$. En ordre de grandeur, les amplitudes des ondes dans l'état stationnaire ne dépassent pas $\gamma|V|^2 \exp - n_0$ même après réflexion linéaire et réamplification, ce qui correspond à une très faible perturbation de densité si $n_0 > 1$.

Pour étudier la stabilité de l'état stationnaire, on pose $N_1 = N_1^0 + \tilde{N}_1$ et on linéarise le système (17), ce qui permet de chercher des solutions ayant un comportement temporel en exp st:

$$\begin{cases} V^1_{gr} \dfrac{\partial \tilde{N}_1}{\partial x} = (2\gamma^1 - s)\tilde{N}_1 + V^2(\tilde{N}_2 N_3^\circ + N_2^\circ \tilde{N}_3) \\ -V^1_{gr} \dfrac{\partial \tilde{N}_4}{\partial x} = (2\gamma^1 - s)\tilde{N}_4 \end{cases} \qquad (24)$$

et des équations analogues pour $\tilde{N}_2, \tilde{N}_3$.

Si on suppose a priori $s \ll \gamma$, on peut résoudre le système précédent (24) par la méthode déjà utilisée pour la recherche de l'état stationnaire ; on obtient :

$$\frac{\left[1-\exp-(\sigma_1+\sigma_2)\Delta\right]\left[1-\exp-(\sigma_1+\sigma_2)\Delta\right]}{\left[\exp-(\sigma_1+\sigma_2)\Delta+\exp-(\sigma_1+\sigma_3)\Delta\right]\left[\exp-(\sigma_1+\sigma_3)\Delta+\exp-(\sigma_2+\sigma_3)\Delta\right]}=1 \tag{25}$$

où l'on a posé $\sigma_i = s/V_{gr}^i \quad \Delta = X_1 - X_2$

On montre facilement que l'équation (25) possède une racine réelle positive : $s \simeq V_{gr}^2 (X_1 - X_2)$, telle que $s \ll \gamma$ si $n_o > 1$. L'état stationnaire est donc instable, le coefficient de réflexion non linéaire augmente avec l'amplitude des ondes et le système évolue vers un état d'amplitude plus élevé. Le processus se poursuit jusqu'à ce que les termes non linéaires négligés, proportionnels à I_K (16), termes qui ne sont pas définis positifs, puissent limiter l'amplitude. Si l'amplitude de la perturbation initiale dépasse le seuil d'instabilité, le système est porté dans un état de turbulence où les fluctuations atteignent nécessairement un niveau relativement élevé donné par $< N_i > \sim < \gamma^i >/|V|^2$.

Pour assurer la stabilité, il faut que le seuil soit suffisamment élevé, c'est-à-dire voisin de l'état de saturation des amplitudes. Dans les critères de stabilité vis-à-vis des paquets d'ondes, la valeur de n_o ne doit pas être déterminée à partir des fluctuations thermiques. D'après les équations (22), $N_i \sim \gamma |V|^{-2} \exp - n_i$, il faut donc choisir $n_i \sim 1$; puisque n_i est donné par $n_i = \int \frac{\gamma^i(x)}{V_{gr}^i}$, la condition pour que cette intégrale soit de l'ordre de l'unité correspond à

$$\frac{r}{L_s} \gtrsim K_x a \left(\frac{m}{M}\right)^{1/2} \quad \text{avec} \left(K_x a \lesssim 1\right) \tag{26}$$

comme on l'a montré dans la référence [6].

Il reste à démontrer explicitement la possibilité de réaliser le couplage d'ondes considéré. On doit d'abord satisfaire aux règles de sélection sur les nombre d'onde et les fréquences :

$$K_3 = K_1 + K_2 \quad ; \quad \omega_3 = \omega_1 + \omega_2$$

où, pour les ondes étudiées, $\omega = - K_y V_e (1 - K_x^2 a^2)$; remarquons que les règles de sélection pour le couplage des ondes réfléchies sont automatiquement satisfaites puisque ω est paire en Kx . Si l'on pose $U_i = K_{yi}/K_{xi}$ on déduit des relations précédentes :

$$(U_1 - U_2) K_{x1} = K_{x3} (U_3 - U_2) \,;\, (U_2 - U_1) K_{x2} = (U_3 - U_1) K_{x3} \tag{27}$$

U_1, U_2, U_3 étant liées par l'équation :

$$(U_1 - U_2)(U_2 - U_3)(U_3 - U_1)(U_1 + U_2 + U_3) = 0$$

On peut se donner a priori K_{x3}, U_2 et U_3; on en déduit les autres inconnues par la relation $U_1 + U_2 + U_3 = 0$, qui correspond au seul couplage intéressant. On remarque alors que deux ondes ayant des vitesse de groupe de même signe se couplent pour donner une troisième onde dont la vitesse de groupe est opposée.

En tenant compte des règles de sélection, on voit que la matrice d'interaction dont l'expression est donnée en Annexe I peut s'écrire, pour les ondes étudiées :

$$|V_{123}|^2 \, \delta(\omega_1 + \omega_2 - \omega_3) = \frac{18 (K_{x3})^5 a^2}{V_e B^2} \, \frac{U_3^2 (U_2 + 2U_1)(U_1 + 2U_2)}{(U_1 - U_2)^2} \, \delta(U_1 + U_2 + U_3) \tag{28}$$

Dans les équations d'évolution portant sur N_i, $|V|^2$ est alors donné par :

$$|V|^2 = \left| \frac{K_{y2} \, K_{y3}}{K_{y1}} V_e \right| |V_{123}|^2 \, \delta(\omega_1 + \omega_2 - \omega_3) \tag{29}$$

On doit aussi montrer qu'on peut choisir la disposition des points de réflexion et d'absorption de la Figure 1 ; posant $\hat{X}_i = -\left(\frac{K_z}{K_y}\right) L_s = X_i - \left(\frac{m}{M}\right)^{1/2} \frac{a L_s}{2r}$ on doit donc vérifier que $\hat{X}_1 > \hat{X}_2$ et $\hat{X}_3 > \hat{X}_2$.
On peut supposer $K_{z3} = X_3 = 0$ et, si on tient compte de la relation entre le les U_i, on obtient $\hat{X}_1 = \hat{X}_2 \frac{U_2 + 2U_1}{U_1 (U_1 + 2U_2)}$; on choisit alors :

$$\hat{X}_2 < 0 \; ; \; U_1 > U_2 > 0 \quad \text{avec} \quad -\frac{a L_s}{2r} \ll \hat{X}_2 < -\frac{a L_s}{2r}\left(\frac{m}{M}\right)^{1/2} \tag{30}$$

Dans le cas d'un système toroïdal, $K_y \rightarrow m/r_o$, $K_z \rightarrow P/R$; alors, $\hat{X}_2 \sim \left(P_2/m_2\right) \left(\frac{di}{dr_o}\right)^{-1}$ et la double inégalité (30) devient :

$$\left(\frac{m}{M}\right)^{1/2} \frac{aR}{2rr_o} < P_2/m_2 < \frac{aR}{2rr_o} \tag{31}$$

V. INTERACTION D'ONDES D'ENERGIE POSITIVE ET D'ENERGIE NEGATIVE

On sait que le couplage résonnant d'une onde (ω, K) d'énergie négative et de deux ondes (ω', K'); (ω'', K'') d'énergie positive peut également être la cause d'une instabilité non linéaire [7 ; 8 ; 9]. Si $\varepsilon(\omega, K)$ est la constante diélectrique du plasma, l'énergie d'une onde a le signe de $\omega \frac{\partial \varepsilon}{\partial \omega}$. Pour les ondes de dérive : $K^2 \lambda_D^2 \, \varepsilon(\omega, K) \equiv D$ où λ_D est la longueur de Debye ; D a été précédemment défini (1). Dans le cas où l'on se limite à l'étude des ondes telles que $b < |W_e|$, on obtient :

$$\omega \frac{\partial \varepsilon}{\partial \omega} = \frac{\omega}{K^2 \lambda_D^2} \, \frac{\partial D}{\partial \omega} \simeq -W_e \tag{32}$$

ce qui montre que l'énergie d'une onde de dérive est positive ou négative suivant que la vitesse de phase $\omega/K_{\parallel}$ est plus petite ($W_e \simeq -1$) ou plus grande ($W_e > 0$) que la vitesse thermique électronique. Le choix que l'on a fait, $b < |W_e|$, est nécessaire pour assurer la réalité de la fréquence des ondes dans le domaine fluide ($\omega/K_{\parallel} > V_{the}$). D'après (32), la condition d'existence des ondes d'énergie négative se réduit à $L/r > (M/m)^{1/2} \frac{1}{K_y a}$ dans un système toroïdal où les lignes de force ont une longueur finie L ; dans une configuration avec cisaillement des lignes de force, il faut a priori que $L_s/r > (M/m)^{1/2}$, condition qui peut être vérifiée dans le Stellerator C par exemple.

Commençons par l'étude d'une configuration sans cisaillement. Pour que le couplage résonnant soit possible, il faut satisfaire aux règles de sélection habituelles : $\omega = \omega' + \omega''$, $K = K' + K''$ et pour que ce couplage conduise à une instabilité, on doit choisir $\omega > \omega'$, $\omega'' > 0$.

Si v'_φ et v''_φ sont les vitesses de phase des ondes K', K'' le long du champ magnétique, les règles de sélection imposent que $v'_\varphi v''_\varphi < 0$. D'autre part, si l'on tient compte des relations de dispersion des différentes ondes, respectivement :

$$\omega = -\omega_0 \left(1 + 2\frac{\bar{b}}{W_e}\right); \; \omega' = -\omega'_0 (1 - 2\bar{b}'); \; \omega'' = -\omega''_0 (1 - 2\bar{b}'')$$

où l'on a posé : $\bar{b} \equiv b - \frac{1}{2}\left[\frac{K_{\parallel} V_{thi}}{\omega_0}\right]^2$, la règle de sélection en fréquence devient :

$$K_y \frac{b}{W_e} = -\left(K'_y \bar{b}' + K''_y \bar{b}''\right) \tag{33}$$

Puisque $\bar{b} \sim b > 0$, d'après la relation (33) il faut que $\bar{b}'$ ou $\bar{b}'' < 0$: les ondes K' et K'' ont donc des longueurs d'ondes parallèles au champ magnétique relativement courtes ; l'une de ces ondes au moins est légèrement amortie. Il peut en résulter un seuil pour l'instabilité non linéaire étudiée, mais le taux d'amortissement de l'onde K' ou K'' pouvant être très petit, on suppose que les ondes en interaction sont initialement excitées au-dessus du seuil.

Dans l'équation cinétique de l'Annexe I, on peut vérifier que tous les termes non linéaires qui décrivent l'interaction résonnante des ondes K, K', K'' sont définis positifs (contrairement au cas habituel où les énergies des ondes sont de même signe). Si un spectre assez large de ces ondes a été excité, cette équation permet de calculer l'ordre de grandeur du taux de croissance de l'instabilité non linéaire qui en résulte :

$$\gamma_{NL} \sim \omega_0 b \left(\frac{\tilde{V}_E}{V_e}\right)^2 \tag{34}$$

Pour évaluer γ_{NL} on a utilisé l'expression donnée en Annexe I, en remplaçant $\frac{\partial \omega}{\partial K} \Delta K$ par $b\,\omega_0$ et choisi $K_x \sim K_y$, $|\bar{b}'| \sim |\bar{b}''| \sim b$; $V_E = \frac{K_x \tilde{\Phi}}{B}$.

On peut exprimer également $\frac{V_E}{V_e}$ en fonction de la fluctuation relative de densité $\frac{\tilde{n}}{n}$ puisque : $\frac{V_E}{V_e} \sim K_x r \frac{e\tilde{\phi}}{T} = K_x r \frac{\tilde{n}}{n}$.

Si, par contre, un spectre d'ondes étroit est excité, on doit utiliser les équations d'interaction de trois ondes cohérentes mais le taux de croissance peut également être évalué en remplaçant $\delta(\omega - \omega' - \omega'')$ par γ_{NL}^{-1} dans l'équation cinétique :

$$\gamma_{NL} \sim \omega_o b \left(\frac{V_E}{V_e} \right) \tag{35}$$

Le taux de croissance est donc d'autant plus rapide que la densité fluctuante est plus grande (la validité de la théorie impose cependant la limitation $\gamma < \omega_o b$). On remarque également que cette instabilité non linéaire intéresse un domaine de l'espace des K beaucoup plus étendu que celui des modes linéairement instables.

Il est intéressant d'évaluer le cisaillement nécessaire pour supprimer l'instabilité non linéaire. Dans ce cas, on doit tenir compte de la convection dans l'espace des $K_{/\!/}$ puisque $K_{/\!/}(x) = K_y \frac{x}{L_s} + K_{/\!/}(o)$. On peut imposer a priori comme condition suffisante de stabilité que l'onde d'énergie négative sorte de la région de propagation fluide ($\omega > K_{/\!/} V_{the}$) en un temps plus court que γ_{NL}^{-1} . En choisissant le taux de croissance le plus rapide (35) on obtient :

$$\frac{r}{L_s} < \frac{1}{K_x a} \left(\frac{m}{M} \right)^{1/2} \left(b \frac{\tilde{V}_E}{V_e} \right) \tag{36}$$

Considérant cette formule, il semble que pour des valeurs suffisamment élevées de la densité fluctuante on doive imposer des cisaillements très élevés. En fait, les ondes d'énergie négative disparaissent si $\frac{L_s}{r} \lesssim \left(\frac{M}{m} \right)^{1/2}$ qui apparaît ainsi comme la véritable condition suffisante de stabilité.

Un autre exemple d'onde de dérive électronique d'énergie négative a récemment été trouvé dans des configurations asymétriques telles que les multipoles où l'intensité du champ magnétique varie le long de la ligne de force [10]. Pour une configuration de ce type, on avait précédemment démontré [11] qu'une résonance onde-particules apparaît lorsque la fréquence d'une onde est celle des particules trappées dans les minima de champ magnétique. Dans de nombreux cas d'un intérêt pratique [11 , 12], cet effet réduit l'espace des vitesses intéressé par une résonance, par comparaison avec un plasma en champ magnétique constant. Il a été démontré, en particulier [10], que cet effet peut être simulé, si l'on suppose que la fonction de distribution a un plateau à l'origine, ce qui revient à introduire dans l'équation (1) un W_e effectif tel que pour $\omega < K_{/\!/} V_{the}$, $W_e = -1 - \frac{\omega^2}{(K_{/\!/} V_{the})}$. On suppose la direction d'asymétrie suivant OY et $K_{/\!/} = 1/L$ où L est la distance entre un minimum et un maximum de champ magnétique (L est ordinairement appelé la longueur de connection). En utilisant l'équation (1) avec ces hypothèses, on obtient pour $\omega < \omega_o, b > 1$, la constante diélectrique :

$$\varepsilon(\omega, K) = \frac{1}{(K\lambda_D)^2}\left\{2 + \frac{\omega_o\omega}{(K_{/\!/}V_{the})^2} - \frac{\omega_o}{\omega}\frac{1}{\sqrt{2\pi b}}\right\} \tag{37}$$

La relation de dispersion $\varepsilon = 0$ met en évidence deux ondes :

$$\omega\pm = \frac{(K_{/\!/}V_{the})^2}{\omega_o}\left\{-1 \pm \left(1 - \frac{1}{\sqrt{2\pi b}}\left(\frac{\omega_o}{K_{/\!/}V_{the}}\right)^2\right)^{1/2}\right\} \tag{38}$$

Ces deux ondes sont instables si : $\omega_o > K_{/\!/}V_{the}(2\pi b)^{1/4}$.

Dans le cas opposé où $K_{/\!/} < \omega_o < K_{/\!/}V_{the}(2\pi b)^{1/4}$, ω est une onde d'énergie négative et l'on peut réaliser une interaction non linéaire instable en la couplant à deux ondes ω_+ d'énergie positive. On constate ainsi que le domaine d'existence des ondes non linéairement instables peut être plus étendu que celui des ondes linéairement instables, notamment dans le cas $b \gg 1$.

CONCLUSION

Nous avons montré que l'approximation locale n'était pas suffisante pour la théorie non linéaire des instabilités de dérive d'un plasma inhomogène dans un champ magnétique avec cisaillement des lignes de force.

Si $\frac{a}{r} > \frac{r}{L_s} > \left(\frac{m}{M}\right)^{1/2}$, le plasma est stable vis-à-vis des perturbations convectives et le taux de croissance des modes normaux localisés est réduit par le cisaillement ; néanmoins l'amplitude des modes de taux de croissance maximal ne peut être limitée en restant dans le cadre de la théorie de la turbulence faible.

Si $\frac{r}{L_s} < \left(\frac{m}{M}\right)^{1/2}$, l'amplitude des perturbations convectives ne sera pas déterminée par le bruit thermique, car une instabilité non linéaire porte le système dans un état de turbulence indépendant des conditions initiales d'excitation. Il convient donc de prendre un coefficient d'amplification de l'ordre de l'unité dans les critères de stabilité vis-à-vis des perturbations convectives.

ANNEXE I

Equations de la Turbulence Faible pour les Modes Localisés

On conserve le développement de Fourier pour les variables y, z mais on projette le potentiel électrique sur les modes normaux linéaires en ce qui concerne la dépendance en x ; on pose donc : $\phi = \sum_m \alpha_m \phi_m$ où ϕ_m est la solution normalisée de l'équation (1) ; l'indice m caractérise les nombres d'onde K_y et K_z aussi bien que le nombre de nœuds de la solution B.K.W. Les perturbations de densité à l'ordre 2 et 3 par rapport au potentiel électrique s'écrivent respectivement :

$$n^2(K,\omega) = \frac{en}{T} \sum_{\substack{\omega=\omega_1+\omega_2 \\ K=K_1+K_2}} \sum_{m_1,m_2} \alpha_{m_1 m_2} \hat{V}_2(K,\omega;K_1,\omega_1;K_2,\omega_2)\phi_{m_1}\phi_{m_2}$$

$$n^3(K,\omega) = \frac{en}{T} \sum_{\substack{\omega=\omega_1+\omega_2+\omega_3 \\ K=K_1+K_2+K_3}} \sum_{m_1,m_2,m_3} \alpha_{m_1}\alpha_{m_2}\alpha_{m_3} \hat{V}_3(K,\omega;K_1,\omega_1;K_2,\omega_2;K_3,\omega_3)\phi_{m1}\phi_{m2}\phi_{m3}$$

où $\hat{V}_2$ et $\hat{V}_3$ sont des opérateurs symétrisés portant sur la variable x . Si l'on introduit également l'opérateur $\hat{D}(K,\omega,x)$ tel que l'équation (1) s'écrive : $\hat{D}\phi = 0$, l'équation cinétique des amplitudes α_n dans l'approximation des phases aléatoires prend la forme suivante :

$$<\phi_m \frac{\partial \hat{D}}{\partial \omega_m} \phi_m>\left\{ \frac{\partial |\alpha_m|^2}{\partial t} - 2\gamma_m |\alpha_m|^2 \right\} =$$

$$I_m\Bigg\{ \sum_{K=K_1+K_2} \left| <\phi_m \hat{V}_2(K,\omega_m;K_1,\omega_{m_1};K_2,\omega_{m2})\phi_{m_1}\phi_{m2}> \right|^2 \frac{|\alpha_{m_1}|^2|\alpha_{m_2}|^2}{<\phi_m \hat{D}(-K,-\omega_{m_1}-\omega_{m_2})\phi_m>}$$

$$+ 2\sum_{K=K_1+K_2} <\phi_{m_1}\hat{V}_2(K_1,K_1-2K_2)\phi_m\phi^*_{m2}><\phi_m\hat{V}_2(K,K_1,K_2)\phi_{m_1}\phi_{m_2}> \frac{|\alpha_m|^2|\alpha_{m2}|^2}{<\phi_{m_1}\hat{D}(K_1;\omega_m-\omega_{m2})\phi_{m_1}>}$$

$$+ \sum_{m_1} <\phi_m \hat{V}_3(K,\omega_m;K_1,\omega_{m_1};-K,-\omega_m;-K_1,-\omega_{m_1})\phi^*_m\phi_{m_1}\phi^*_{m_1}>|\alpha_m|^2|\alpha_{m_1}|^2 \Bigg\}$$

où l'on a introduit la notation de produit scalaire : $<f,g> = \int f^* g\, dx$.

Lorsqu'il y a couplage de modes résonnants, on doit substituer à $<\varphi_m \hat{D}(K,\omega_i+\omega_j)\phi_m>$ l'expression $<\phi_m \frac{\partial \hat{D}}{\partial \omega}\phi_m>(\omega_i+\omega_j-\omega_m-i\varepsilon)$. Dans les termes de diffusion des ondes par les particules, $\omega_i+\omega_j$ est très inférieur à ω_m , la dépendance de $\hat{D}$ en fonction de x est négligeable et cet opérateur se réduit à un scalaire.

Pour les modes en interaction dont la dépendance radiale satisfait à l'approximation B.K.W., les opérateurs $\hat{V}_2$ et $\hat{V}_3$ se réduisent à des scalaires et s'identifient avec les expressions obtenues dans l'approximation locale [4]. Pour les interactions résonnantes, on obtient notamment :

$$|\hat{V}_2|^2 = |V|^2 \left(\frac{\partial D}{\partial \omega}\right)^2$$

avec, dans le cas où $b \lesssim 1$, $\omega < K_{/\!/} V_{the}$: $\frac{\partial D}{\partial \omega} \sim \omega^{-1}$ et

$$|V|^2 \equiv \frac{2a^4}{B^2}\left[(K_{x2}K_{y3})^2+(K_{x3}K_{y2})^2\right]\left[K^2_{x_2}+K^2_{y2}-K^2_{x3}-K^2_{y3}\right]^2$$

D'après l'équation cinétique, on peut également estimer dans l'approximation locale, l'ordre de grandeur du taux de croissance (ou d'amortissement) non linéaire :

$$\gamma_{NL} \sim \frac{|\phi|^2 \, |V|^2}{\frac{\partial \omega}{\partial K} \Delta K}$$

où ΔK est le domaine d'extension en K des modes qui participent à l'interaction.

REFERENCES

[1] GALEEV A.A. - JETP 17, 1292 (1963)

[2] KADOMTSEV B.B. - JETP 18, 847 (1964)

[3] GALEEV A.A. et RUDAKOV I.- JETP 18, 444 (1964)

[4] SAGDEEV R.Z. and GALEEV A.A. - International Center for Theoretical Physics, Report IC/66/64, pages 131-139, Trieste (1966)

[5] KRALL N.A. and ROSENBLUTH M.N. - Phys. Fluids 8, 1488 (1965)

[6] COPPI B., LAVAL G., PELLAT R. et ROSENBLUTH M.N. - Nuclear Fusion 6, 261 (1966)

[7] KADOMTSEV B.B., MIKHAILOVSKII A.B. et TIMOFEEV A.V. - JETP 20, 1517 (1965)

[8] DIKASOV V.M., RUDAKOV L.I., RYUTOV D.D. - JETP 21, 608 (1966)

[9] COPPI B., ROSENBLUTH M.N. et SUDAN R.N. - Princeton University, Report MATT-529 (1967), non publié

[10] COPPI B., ROSENBLUTH M.N. and RUTHERFORD P. - Princeton University Report MATT-611 (1968), soumis à Phys. Rev. Letters

[11] COPPI B., LAVAL G., PELLAT R. and ROSENBLUTH M.N. - Plasma Physics 10, 1 (1968)

[12] RUTHERFORD P. and FRIEMAN E.A. - Phys. Fluids 11, 569 (1968)

DISCUSSION

E. MINARDI: How were the thermal fluctuations computed?

G. LAVAL: They were computed by a test particle method which can be applied to systems out of equilibrium and to unstable systems.

THE INFLUENCE OF ELECTRICAL RESISTIVITY ON THE MHD STABILITY OF STATIONARY EQUILIBRIA

H. FRIEDEL* AND P. UNTEREGGER
INSTITUTE FOR THEORETICAL PHYSICS, UNIVERSITY OF INNSBRUCK, INNSBRUCK, AUSTRIA

Abstract

THE INFLUENCE OF ELECTRICAL RESISTIVITY ON THE MHD STABILITY OF STATIONARY EQUILIBRIA. A general class of equilibrium configurations with a zero-order fluid velocity is investigated using a method similar to that of Coppi. The hydromagnetic system under consideration is characterized by finite electrical conductivity, zero viscosity and zero thermal conductivity. Using a Lagrangian description, an equation of motion governing small displacements of the system about the equilibrium is found. Furthermore, general criteria determining the influence of electrical resistivity on modes stable or marginally stable in the non-dissipative case are derived. For infinite electrical conductivity we get agreement with the results found by Frieman and Coppi. Finally, a general formalism for treating instability problems with arbitrary dissipative effects is presented.

1. INTRODUCTION

One method that has been proposed for studying the stability of non-dissipative hydromagnetic systems is the "normal mode" analysis and the corresponding energy principle technique [1]. In the present paper a similar procedure based on a perturbation method is used to investigate the influence of finite electrical resistivity on the stability behaviour of stationary equilibria.

Originally Coppi [2] started stability investigations of dissipative, but static hydromagnetic systems in a quite general fashion irrespective of special configurations. The hydromagnetic stability of stationary, rather than static equilibria without dissipation, on the other hand, was first studied by Frieman and Rotenberg [3]. The purpose of this paper is the examination of a general class of MHD configurations including dissipation and a zero-order fluid velocity distribution.

The hydromagnetic system under investigation is characterized by finite electrical conductivity, zero viscosity and zero thermal conductivity. Using a Lagrangian description, an equation of motion governing small displacements about a given equilibrium configuration is derived. Under the further assumption of small constant electrical resistivity some general critera determining the influence of electrical resistivity on modes that are stable or marginally stable in the non-dissipative case, are presented.

---

* Deceased 1967.

2. THE BASIC FLUID EQUATIONS

We consider a hydromagnetic system represented by the following set of equations written in dimensionless form (throughout this paper we use rationalized Gaussian units with c = 1):

$$\rho \frac{d\vec{v}}{dt} + \nabla p - (\mathrm{curl}\,\vec{B}) \times \vec{B} = 0 \tag{1}$$

$$\frac{\partial \rho}{\partial t} + \nabla \cdot (\rho \vec{v}) = 0 \tag{2}$$

$$\frac{dp}{dt} - \frac{\gamma p}{\rho}\frac{d\rho}{dt} = (\gamma - 1)\eta(\mathrm{curl}\,\vec{B})^2 \tag{3}$$

$$\frac{\partial \vec{B}}{\partial t} - \mathrm{curl}(\vec{v} \times \vec{B}) = -\,\mathrm{curl}(\eta\ \mathrm{curl}\,\vec{B}) \tag{4}$$

where $\vec{v}$ is the fluid velocity, ρ the mass density, p the fluid pressure, $\vec{B}$ the magnetic field made dimensionless by the characteristic values v^0, ρ^0, p^0 and B^0, respectively, $\gamma = c_p/c_v$ the adiabatic exponent, and η the dimensionless electrical resistivity (= reciprocal magnetic Reynolds number). The original set of Eqs (1) - (4) contained two numbers, the pressure coefficient N_p and the Cowling number Co. Without loss of generality we eliminated these two numbers by means of the transformations

$$p \to N_p p, \qquad \vec{B} \to \mathrm{Co}^{1/2}\vec{B} \tag{5}$$

The only transport coefficient in the fluid equations is the scalar electrical resitivity η. In particular, the thermal conductivity and the viscosity were assumed to be negligible. The corresponding set of equations describing the given stationary equilibrium configuration is obtained from Eqs (1) - (4) by setting all the partial time derivatives equal to zero. The equilibrium quantities $\vec{v}_0$, ρ_0, p_0 and $\vec{B}_0$, respectively, are well-known functions of the equilibrium position vector $\vec{r}_0$ only.

3. THE EQUATION OF MOTION FOR SMALL DISPLACEMENTS

To be able, in principle, to follow in time any small motion about the equilibrium state it is convenient to adopt a Lagrangian description of the fluid motion. Accordingly, all quantities are now considered to be functions of $\vec{r}_0$, the initial location of a fluid element at time t = 0, and of t, the time. Let the Lagrangian displacement vector $\vec{\xi}$ be defined by

$$\vec{r} = \vec{r}_0 + \vec{\xi}(\vec{r}_0, t) \tag{6}$$

where $\vec{r}$ is the location of the fluid element at time t, i.e. the perturbed position vector. Clearly, $\vec{\xi}(\vec{r}_0, t = 0)$ is equal to zero. For deriving first-order expressions in $\vec{\xi}$ for the perturbed quantities u_1, i.e. for ρ_1, p_1 and $\vec{B}_1$, respectively, we use the relations

$$\vec{v} = \vec{v}_0 + (\vec{v}_0 \cdot \nabla_0)\vec{\xi} + \frac{\partial \vec{\xi}}{\partial t} \tag{7a}$$

$$\nabla = \nabla_0 - \nabla_0 \vec{\xi} \cdot \nabla_0 \tag{7b}$$

$$\nabla \frac{d}{dt} - \frac{d}{dt} \nabla = \nabla \vec{v} \cdot \nabla \tag{7c}$$

In the non-dissipative case the first-order perturbed quantities u_1 can be explicitly expressed as functions of $\vec{\xi}$. What we do is to separate u_1 in a non-dissipative part and a part $\tilde{u}$ depending on the resistivity η.

Retaining only the first-order terms in $\vec{\xi}$, we obtain

$$\rho_1 = - \rho_0 \nabla_0 \cdot \vec{\xi} \tag{8a}$$

$$p_1 = - \gamma p_0 \nabla_0 \cdot \vec{\xi} - \tilde{p}(\eta) \tag{8b}$$

$$\vec{B}_1 = (\vec{B}_0 \cdot \nabla_0)\vec{\xi} - \vec{B}_0 \nabla_0 \cdot \vec{\xi} + \tilde{\vec{B}}(\eta) \tag{8c}$$

The dissipative parts $\tilde{p}(\eta)$ and $\tilde{\vec{B}}(\eta)$ are implicitly given by the equations:

$$- \gamma \rho_0^{\gamma-1} \cdot \tilde{p} \frac{d\rho_0}{dt} + \rho_0^{-\gamma} \frac{d\tilde{p}}{dt} = (\gamma - 1)[\eta \rho^{-\gamma} (\mathrm{curl}\, \vec{B})^2]_1 \tag{9a}$$

$$\frac{d\tilde{\vec{B}}}{dt} + (\nabla_0 \cdot \vec{v}_0)\tilde{\vec{B}} - (\tilde{\vec{B}} \cdot \nabla_0)\vec{v}_0 = - [\mathrm{curl}(\eta\; \mathrm{curl}\, \vec{B})]_1 \tag{9b}$$

where the symbol $[\;\;]_1$ means a collection of first-order perturbed quantities.

Finally, the linearized equation of motion, which follows from Eq. (1), taking into account Eqs (8) and the equilibrium equations, becomes

$$\rho_0 \frac{\partial^2 \vec{\xi}}{\partial t^2} + 2\rho_0 (\vec{v}_0 \cdot \nabla_0)\frac{\partial \vec{\xi}}{\partial t} - F\{\vec{\xi}\} = G\{\tilde{\vec{B}}, \tilde{p}\} \tag{10}$$

with

$$F\{\vec{\xi}\} = \nabla_0 \cdot [\gamma p_0 \nabla_0 \cdot \vec{\xi} + (\vec{\xi} \cdot \nabla_0)p_0] - \vec{B}_0 \times (\nabla_0 \times \vec{Q}) - \vec{Q} \times (\nabla_0 \times \vec{B}_0)$$
$$+ \nabla_0[\rho_0 \vec{\xi}(\vec{v}_0 \cdot \nabla_0)\vec{v}_0 - \rho_0 \vec{v}_0 (\vec{v}_0 \cdot \nabla_0)\vec{\xi}] \tag{11a}$$

$$G\{\tilde{\vec{B}}, \tilde{p}\} = \nabla_0 \tilde{p} + (\nabla_0 \times \vec{B}_0) \times \tilde{\vec{B}} + (\nabla_0 \times \tilde{\vec{B}}) \times \vec{B}_0 \tag{11b}$$

and

$$\vec{Q} = \nabla_0 \times (\vec{\xi} \times \vec{B}_0) \tag{11c}$$

Note that $F\{\vec{\xi}\}$, which is a linear function in $\vec{\xi}$ and its spatial derivatives, depends only on $\vec{\xi}$ and not on $\dot{\vec{\xi}}$, where the dot indicates differentiation with respect to time. With appropriate initial and boundary conditions, Eq. (10) determines the displacement vector $\vec{\xi}$. Furthermore, Eqs (8) then determine the perturbed field quantities.

In the absence of dissipation, which means $G\{\tilde{\vec{B}}, \tilde{p}\} = 0$, Eq. (10) agrees with the corresponding equation of motion found by Frieman and Rotenberg [3].

4. STABILITY ANALYSIS AND EFFECTS OF ELECTRICAL RESISTIVITY

Let us now examine the influence of small constant electrical resistivity ($\eta \ll 1$) on the stability behaviour of stationary equilibria by means of a perturbation technique. For simplicity we assume $\tilde{p} = 0$. Since the time does not appear explicitly in Eq. (10), we seek normal mode solutions of the form

$$\vec{\xi}(\vec{r}_0, t) = \vec{\xi}(\vec{r}_0)e^{i\omega t} \equiv \vec{\xi}^{\,0} e^{i\omega t} \tag{12}$$

Consequently, the equation of motion (10) reduces to

$$-\omega^2 \rho_0 \vec{\xi}^{\,0} + 2i\omega\rho_0(\vec{v}_0 \cdot \nabla_0)\vec{\xi}^{\,0} - F\{\vec{\xi}^{\,0}\} = G\{\tilde{\vec{B}}^{\,0}\} \tag{13}$$

if

$$\tilde{\vec{B}}(\vec{r}_0, t) = \tilde{\vec{B}}(\vec{r}_0)e^{i\omega t} = \tilde{\vec{B}}^{\,0} e^{i\omega t} \tag{14}$$

The validity of this last condition can be shown by the consistency of the following expansions:

$$\begin{aligned} \vec{\xi}^{\,0} &= \vec{\xi}_0 + \eta\vec{\xi}_1 + \eta^2\vec{\xi}_2 + \ldots \\ \omega &= \omega_0 + \eta\omega_1 + \eta^2\omega_2 + \ldots \\ \tilde{\vec{B}}^{\,0} &= \eta\tilde{\vec{B}}_1 + \eta^2\tilde{\vec{B}}_2 + \ldots \end{aligned} \tag{15}$$

Hence, to zero-order in η, Eq. (13) becomes

$$\omega_0^2\rho_0\vec{\xi}_0 - 2i\omega_0\rho_0(\vec{v}_0 \cdot \nabla_0)\vec{\xi}_0 + F\{\vec{\xi}_0\} = 0 \tag{16}$$

For the following it is important to show the self-adjointness of the two operators $i\rho_0(\vec{v}_0 \cdot \nabla_0)$ and F, respectively. This property could be proved directly by a number of integrations by parts. If we multiply Eq. (16) by the conjugate complex vector $\vec{\xi}_0^*$ and integrate over the fluid volume, we obtain

$$\omega_0^2\langle\rho_0\vec{\xi}_0^* \cdot \vec{\xi}_0\rangle - 2i\omega_0\langle\vec{\xi}_0^* \cdot \rho_0(\vec{v}_0 \cdot \nabla_0)\vec{\xi}_0\rangle + \langle\vec{\xi}_0^* \cdot F\{\vec{\xi}_0\}\rangle = 0 \tag{17}$$

Since we can rewrite the second term in this equation as surface integral, which vanishes as ρ_0 vanishes at the fluid-vacuum interface by virtue of the boundary conditions, we get the relation

$$\omega_0^2\langle\rho_0\vec{\xi}_0^* \cdot \vec{\xi}_0\rangle + \langle\vec{\xi}_0^* \cdot F\{\vec{\xi}_0\}\rangle = 0 \tag{18}$$

showing that ω_0^2 must always be real. Consequently, the velocity field in this case may not lead to the phenomenon of overstability. From Eq.(18) the zero-order stability criterium

$$\frac{\langle \vec{\xi}_0^* \cdot F\{\vec{\xi}_0\}\rangle}{\langle \rho_0 \vec{\xi}_0^* \cdot \vec{\xi}_0 \rangle} < 0 \tag{19}$$

follows immediately. As was to be expected, this result agrees with the criterium first found by Frieman and Rotenberg [3]. For marginally stable modes ($\omega_0 = 0$), Eq.(17) reduces to $F\{\vec{\xi}_0\} = 0$. Continuing, we will investigate the first-order influence of electrical resistivity on stable zero-order modes ($\omega_0^2 > 0$).

To first order in η, Eq.(13) can be written in the form

$$-\omega_0^2 \rho_0 \vec{\xi}_1 - 2\omega_0\omega_1\rho_0\vec{\xi}_0 + 2i\omega_0\rho_0(\vec{v}_0 \cdot \nabla_0)\vec{\xi}_1 + 2i\omega_1\rho_0(\vec{v}_0 \cdot \nabla_0)\vec{\xi}_0 - F\{\vec{\xi}_1\} = G_1\{\vec{\xi}_0\} \tag{20}$$

where

$$G_1\{\vec{\xi}_0\} = (\nabla_0 \times \vec{B}_0) \times \tilde{\vec{B}}_1 + (\nabla_0 \times \tilde{\vec{B}}_1) \times \vec{B}_0 \tag{21}$$

Multiplying Eq.(20) by $\vec{\xi}_0^*$ and using the self-adjointness property of the operators, we obtain by integration over the fluid volume

$$-2\omega_0\omega_1\langle \rho_0 \vec{\xi}_0^* \cdot \vec{\xi}_0 \rangle + 2i\omega_0 \langle \vec{\xi}_0^* \cdot \rho_0(\vec{v}_0 \cdot \nabla_0)\vec{\xi}_0 \rangle - \langle \vec{\xi}_0^* \cdot G_1\{\vec{\xi}_0\}\rangle = 0 \tag{22}$$

The second term again vanishes for the same reason as above and so we find, on solving for ω_1^2:

$$\omega_1^2 = -\frac{\langle \vec{\xi}_0^* \cdot G_1\{\vec{\xi}_0\}\rangle}{2\omega_0 \langle \rho_0 \vec{\xi}_0^* \cdot \vec{\xi}_0 \rangle} \tag{23}$$

Contrary to zero-order, in the first order there might be overstable modes, if $\langle \vec{\xi}_0^* \cdot G_1\{\vec{\xi}_0\}\rangle$ is a complex number. The perturbed modes are unstable, if this inner product is purely imaginary and $\langle \vec{\xi}_0^* \cdot G_1\{\vec{\xi}_0\}\rangle < 0$. Otherwise the perturbed modes are stable.

Finally, let us proceed examining the influence of resistivity to first order on marginally stable ($\omega_0 = 0$) zero-order modes. To this end we first must look for the fastest growth-rate ω_f. Thus, we choose as expansion parameter $\lambda = \eta^\epsilon$ instead of η. From the structure of Eq.(20) we draw the conclusion $\omega_f = \eta^{1/2}\omega_1$, i.e. $\epsilon_{min} = 1/2$. The expansions (15) are now replaced by

$$\begin{aligned} \tilde{\vec{u}} &= \tilde{\vec{u}}_0 + \lambda \tilde{\vec{u}}_1 + \lambda^2 \tilde{\vec{u}}_2 + \dots \\ \omega &= \lambda\omega_1 + \lambda^2 \omega_2 + \dots \end{aligned} \tag{24}$$

To first order in λ, we get

$$2i\omega_1\rho_0(\vec{v}_0 \cdot \nabla_0)\vec{\xi}_0 - F\{\vec{\xi}_0\} = 0 \tag{25}$$

Up to second order in λ, Eq.(13) may be written as

$$-\omega_1^2\rho_0\vec{\xi}_0 + 2i\omega_2\rho_0(\vec{v}_0\cdot\nabla_0)\vec{\xi}_0 + 2i\omega_1\rho_0(\vec{v}_0\cdot\nabla_0)\vec{\xi}_1 - F\{\vec{\xi}_2\} = G_2\{\vec{\xi}_0\} \tag{26}$$

with

$$G_2\{\vec{\xi}_0\} = (\nabla_0\times\vec{B}_0)\times\tilde{\vec{B}}_2 + (\nabla_0\times\tilde{\vec{B}}_2)\times\vec{B}_0 \tag{27}$$

In a similar way as before we obtain, on solving for ω_1^2:

$$\omega_1^2 = -\frac{\langle\vec{\xi}_0^*\cdot G_2\{\vec{\xi}_0\}\rangle}{\langle\rho_0\vec{\xi}_0^*\cdot\vec{\xi}_0\rangle} \tag{28}$$

Consequently, the answer to the question of the stability of the system developed depends on the largest finite value of $\langle\vec{\xi}_0^*\cdot G_2\{\vec{\xi}_0\}\rangle$. If this expression is an imaginary quantity, we get overstable modes. For the case that it is real and positive, the hydromagnetic system is unstable.

5. SUMMARY

The general analysis given in the preceding sections is an extension of the investigations performed by Frieman and Rotenberg [3] ($\sigma = \infty$, $\vec{v}_0 \neq 0$) as well as by Coppi [2] ($\sigma \neq \infty$, $\vec{v}_0 = 0$). The basis of this analysis is an equilibrium configuration with a zero-order velocity field, which modifies the result obtained by Coppi. The first-order information on the influence of small constant electrical resistivity on the stability behaviour of a system stable or marginally stable in zero order is contained within the value ω_1^2 given explicitly as function of $\vec{\xi}_0$.

ACKNOWLEDGEMENTS

The research reported in this paper has been sponsored in part by the United States Government under Contract no. F6105267-C-0014. One of the authors (P.U.) is very grateful to all the members of the theoretical Plasma Physics Division for many fruitful discussions and suggestions, particularly Professor F. Cap.

REFERENCES

[1] BERNSTEIN, I.B., FRIEMAN, E.A., KRUSKAL, M.D., KULSRUD, R.M., Proc. R. Soc. A 244 (1958) 17.
[2] COPPI, B., in Proc. 7th Lockheed Symp. on MHD, Stanford University (1963).
[3] FRIEMAN, E., ROTENBERG, M., Rev. mod. Phys. 32 (1960) 898.

DISCUSSION

B. COPPI: How do the results which you obtained when considering marginally stable hydromagnetic modes compare with those obtained when analysing (in the absence of resistivity) modes that are far from marginal stability?

P. UNTEREGGER: We have not yet investigated this problem in detail. Within the framework of our theory, however, it should be possible to answer this question to zeroth order in the resistivity η.

H. TASSO: Since this method does not give you new modes, I do not understand how you can obtain instabilities in the case where $v_0 = 0$.

P. UNTEREGGER: To first order in the resistivity η we do get overstable modes, whereas to zeroth order in η overstability cannot occur (for the case $v_0 \neq 0$).

TOROIDAL CONFINEMENT IV (THEORY), LASER-PRODUCED PLASMAS, ASTRON

(Session F)

Chairman: M. RABINOVICH

Papers F-6 to F-8 were presented by R. PAPOULAR as Rapporteur.

LOW-FREQUENCY PLASMA LOSS MECHANISMS IN MHD-STABILIZED TORUSES

H. P. FURTH AND M. N. ROSENBLUTH*
PLASMA PHYSICS LABORATORY, PRINCETON UNIVERSITY,
PRINCETON, N.J., UNITED STATES OF AMERICA

Abstract

LOW-FREQUENCY PLASMA LOSS MECHANISMS IN MHD-STABILIZED TORUSES. Anomalous plasma losses can occur even in the absence of apparent fluctuations, through the mechanism of large single-particle excursions in spatially irregular quasistatic magnetic and electric fields. The conservation of the second adiabatic invariant J provides the basis for a general analysis of these low-frequency mechanisms.

In sheared magnetic fields, the presence of a regular electrostatic potential $e\Phi_0 > kTr_0/R_0$, constant on magnetic surfaces, is sufficient to suppress single-particle excursions in both axisymmetric and stellarator geometry. The effect on particle excursions of irregular electrostatic potentials is investigated and in the limit of small gyroradii and strong shear is found to be comparable to the effect of non-symmetric (stellarator) geometry. Magnetic trapping of particles lends itself to self-consistent irregular potentials (convective cells), while electrostatic trapping leads to a stable drift mode, and to the possibility of convective cells.

Shearless magnetic wells (multipoles), are unstable against growth of MHD convective cells. For small plasma potentials, however, the instability goes to short wavelength where the MHD approximation breaks down. Small gyroradii and deep magnetic wells are found to be favourable to the suppression of particle convection.

1. INTRODUCTION

Anomalous plasma transport by fluctuations in the drift-frequency range has received extensive theoretical treatment, and has been shown in some instances to account for experimental toroidal-confinement results. In several recent torus experiments [1-4] with moderately collisionless plasmas, however, the magnitude of the observed fluctuations is clearly insufficient to account for the measured rate of radial plasma transport.

High-frequency oscillations, beyond the range of conventional Langmuir-probe measurement, can be ruled out on energetic grounds [5] as possible causes of Bohmlike diffusion rates. In low-frequency loss mechanisms, on the other hand, the Bohm diffusion constant tends to emerge naturally as the basic dimensional parameter. When such processes control the plasma lifetime, they are not recognized as "fluctuations," but as changes in the plasma equilibrium.

In the present paper, we survey the possibilities for low-frequency plasma transport. For simplicity, we confine ourselves here to the collisionless case (though small collisional effects can be important [6-7] and may play a key role in some present-day torus experiments). By "low-frequency loss mechanisms," we shall mean primarily that

---

* Also, Institute for Advanced Study, Princeton, N.J.

ω is much smaller than the bounce frequency of either trapped electrons or ions, so that the second adiabatic invariant J is conserved. This conservation of J provides a unifying point of view, from which we can approach both the single-particle and collective low-frequency behavior of the plasma.

In Sec. 2 we review the problem of single-particle drift motion under the influence of torus magnetic fields and regular electrostatic potentials (conforming to the magnetic surfaces). In Sec. 3, we treat sheared magnetic fields and irregular electrostatic potentials. In Sec. 4, we treat convective cells in shearless magnetic fields (e.g., multipoles).

We conclude that low-frequency irregular electrostatic potentials could be responsible for Bohmlike rates of plasma loss in some present-day torus experiments. Suppression of these loss mechanisms is favored by small ion gyroradii, strong shear, good minimum-average-B properties, and moderate regular plasma potentials. In the sheared-field case, the avoidance of magnetic particle trapping is also fairly effective against low-frequency transport.

2. TOROIDAL MAGNETIC FIELD CONFIGURATIONS WITH REGULAR ELECTROSTATIC POTENTIALS

2.1. Axisymmetric case

For axisymmetric torus (levitron, tokamak, multipole) the conservation of canonical angular momentum $p_\phi = (mv_\phi + e/c\, A_\phi)R$ in the toroidal direction permits a simple and exact analysis of particle orbits. Any particle excursion from its initial flux surface corresponds to a variation of A_ϕ. The maximum possible excursion [8] is thus the particle gyroradius in the poloidal magnetic field component (the curl of A_ϕ). Within these bounds, particles that are trapped magnetically execute a periodic motion along field lines, the projection of their guiding-center motion onto a constant-ϕ plane being the familiar banana [9](Fig. 1).

If the poloidal magnetic field component is very weak (small rotational transform), the ion bananas may intersect the plasma boundary. The barely trapped ions, which have the largest bananas, are then lost preferentially, giving rise to the concept of a "loss cone" for toruses [10]. For practical torus parameters, however, electrons are not lost in this way; and so a negative electrostatic potential well develops.

By a simple analysis, we can work out the explicit banana orbit in the presence of a regular electrostatic potential [11] Φ_o (constant on the magnetic surfaces) plus an irregular potential contribution $\Phi_1(r,\theta)$. The equations for conservation of energy and canonical angular momentum are then

$$\mu\Delta B + e\Delta\Phi_1 + \frac{1}{2}m(v_\parallel^2 - v_{\parallel o}^2) + e\Phi_o' r_1 + \frac{1}{2}e\Phi_o'' r_1^2 = 0 \qquad (1)$$

$$(mv_\parallel \cos\alpha + \frac{e}{c}A_\phi)(R_o + \Delta R) = mv_{\parallel o}\cos\alpha_o R_o \qquad (2)$$

where r_1 refers to a small particle excursion from an initial magnetic surface r_o; the Δ's refer to parameter variation within the surface, along the trajectory; and the null subscripts refer to the mirror point of a trapped particle, where r_1 and the Δ's vanish. We have used $v_\phi = v_\parallel \cos\alpha$, where $\alpha = \tan^{-1}(r_o \iota / 2\pi R)$. In terms of the rotational transform ι, we identify

$$A_\phi = \frac{B_o r_o}{2\pi R_o} \int dr_1 \, \iota$$

where B_o is the mean toroidal magnetic field. The gyrofrequency in the poloidal field component is then $\omega_c = (B_o e/mc)(r_o \iota/2\pi R_o)$. Since the rotational transform, rather than the shear, is the basic factor controlling the banana size, we will for simplicity neglect shear-effects in what follows.

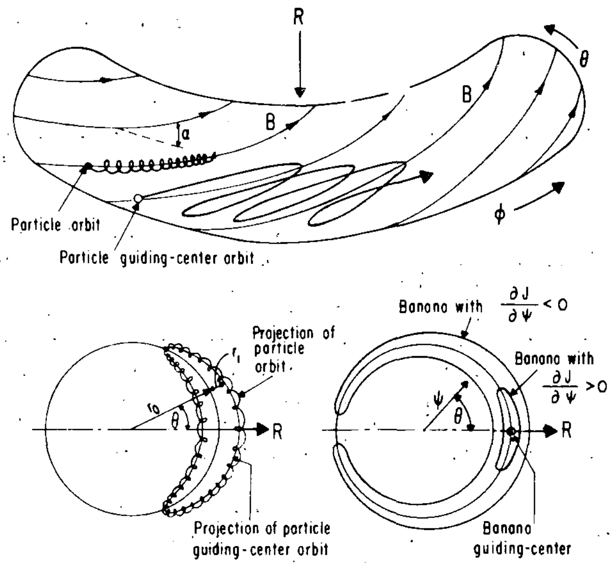

FIG. 1. Particle orbits and guiding-centre orbits (bananas) in an axisymmetric torus.

The condition for mirroring is, from (1) and (2), that the r_1 term should vanish,

$$v_{\parallel o} = \frac{e\Phi_o'}{m\omega_c} \cos\alpha \tag{3}$$

The equation for the banana orbit is then found to be

$$r_1^2 = \frac{-\frac{\Delta B}{B_o} m v_{\perp o}^2 + 2\frac{\Delta R}{R_o} m v_{\parallel o}^2 - 2e\Delta\Phi_1}{m\omega_c^2 \cos^{-2}\alpha + e\Phi_o''} \tag{4}$$

We shall make use of the $\Delta\Phi_1$ term in Sec. 3, but ignore it at present. Taking ι to be small, reduces (4) to the simple form

$$r_1^2 = \frac{\Delta R}{R_o} \frac{m(v_{\perp o}^2 + 2v_{\| o}^2)}{m\omega_c^2 + e\Phi_o''} \tag{4'}$$

By comparison, the excursions of untrapped particles (non-vanishing r_1-term in the orbit equation) are typically much smaller

$$r_1 = -\frac{\Delta R}{2R_o} \frac{m(v_{\perp o}^2 + 2v_{\| o}^2)}{m\omega_c v_{\| o} - e\Phi_o'} \tag{5}$$

The excursion of a barely untrapped particle approaches one half that of a barely trapped one.

For $\Phi_o \equiv 0$, the maximum possible excursion of any particle is thus roughly the gyroradius in the poloidal field component, reduced by $(r_o/R_o)^{1/2}$. For electrons, it is then generally easy to satisfy $r_1 \ll r_o$. If there is a loss of ions, it gives rise, by Poisson's equation, to a potential well $e\Phi_o'' > 0$, which acts directly to reduce the ion banana size in Eq. (4). There is also an indirect effect, through Eq. (3), which says that for sufficiently large $e\Phi_o'$ of either sign, the $v_{\| o}$ required of mirroring particles can be pushed sufficiently far into the tail of the distribution function to make the fraction of trapped ions negligible. From these considerations it follows that a potential well for ions, of order $e\Phi_o > kT_i r_o/R_o$, is always sufficient to suppress the particle excursions: through Eq. (4), if $e\Phi_o'' \gtrsim m\omega_{ci}^2$, and through Eq. (3), in the case of very small rotational transform or weak magnetic field.

In the special case of pure poloidal field we have $\alpha = \pi/2$, and the guiding center displacement r_1 then vanishes. The maximum particle excursion is then simply its gyroradius.

We turn now to the conservation of J, which for nearly closed orbits (bananas, or untrapped particle orbits around the torus on nearly rational magnetic surfaces), has the form:

$$J = \oint d\ell \cdot \{\vec{v} + \frac{e}{mc}\vec{A}\} \tag{6}$$

The second term vanishes for the trapped particles.

For J to be conserved, we assume that the gyroradius r_g is small relative to r_o, and that $e\Phi \ll kTr_o/r_g$. The drift motion of the bananas must lie on the constant-J surfaces, which in the axisymmetric case are identical with the flux surfaces. This information is already contained in the stronger constraint of p_ϕ-conservation, and thus J-conservation is redundant in the axisymmetric case. The rate of banana drift

$\omega_d = \langle v_\phi \rangle / R_o$ around the torus [12] is, however, given conveniently by differentiating J with respect to the flux coordinate ψ (which corresponds to $R_o A_\phi$),

$$\omega_d = -\frac{c}{e}\frac{\partial J}{\partial \psi}\Big/\frac{\partial J}{\partial W} = -\frac{mc}{e}\frac{\frac{\partial}{\partial \psi}\oint d\ell\, v_\parallel}{\oint d\ell / v_\parallel}$$

$$\approx -\frac{\oint d\chi \frac{\partial}{\partial \psi}\left(\frac{Bc}{B_\perp^2}\sqrt{2(W-\mu B - e\Phi)}\right)}{\oint d\chi \frac{Be}{B_\perp^2}\frac{1}{\sqrt{2(W-\mu B - e\Phi)}}} \tag{7}$$

Here, $B_\perp$ is the poloidal magnetic field component, and $d\chi = B_\perp\, d\ell_\perp$. The toroidal drift arises because the three-dimensional particle orbit, of which the closed banana is the two-dimensional projection, does not in general close perfectly on itself after a cycle. This non-closure, and the resultant toroidal drift ω_d, has two contributing factors: the gradient in $\mu B + e\Phi$ arising from $\partial B/\partial \Psi$ and $\partial \Phi/\partial \Psi$; and the gradient in the length $\oint d\ell$ between mirror points, arising from shear.

The effect of the gradients in B and Φ always dominates for those particles which (a) have null $v_\parallel$ or (b) are barely trapped. With $\Phi \equiv 0$, the standard toroidal drift pattern is that for tokamaks, where the null-$v_\parallel$ particles have $\partial J/\partial \Psi > 0$ (unfavorable ∇B-drift) the barely trapped particles have $\partial J/\partial \psi < 0$ (favorable ∇B-drift) and there is thus always an intermediate class with $\partial J/\partial \psi \approx 0$. (With outward-decreasing rotational transform, the effect of shear on $\partial J/\partial \psi$ is in the positive direction, i.e., lengthening $\oint d\ell$.) In levitrons, on the other hand, it is possible to have $\partial J/\partial \psi > 0$ for all the trapped particles. In multipoles, the null-$v_\parallel$ particles have $\partial J/\partial \psi < 0$ and the barely trapped ones have $\partial J/\partial \psi > 0$; but with special shaping of the flux bridge [13] all particles can have $\partial J/\partial \psi < 0$. This can also be done, in a narrow band of flux surfaces, for the spherator type of levitron. Alternatively, it is possible on a fairly wide band of flux surfaces to have virtually no particle trapping at all in an appropriately shaped levitron.

2.2. Helically symmetric case

An infinite straight stellarator can have an ignorable helical coordinate $\theta' = \theta + kz$, with which is associated the conservation of helical canonical momentum $p_{\theta'}$. In that case, exactly the same treatment applies as in the case of axisymmetry: the trapped particles execute bananas that drift along the ignorable coordinate at rates proportional to $\partial J/\partial \psi$; and in the limit of null gyroradius all the particle orbits lie exactly on the magnetic surfaces.

In the straight stellarator, the null-$v_{\parallel}$ particles have $\partial J/\partial\psi > \theta$ and the barely trapped ones have $\partial J/\partial\psi < 0$, so that there is always a class of $\partial J/\partial\psi \approx 0$ particles, as in the tokamak. The rotational transform, as seen in the (θ, r)-frame increases outward, but the transform as seen from the (θ', r)-frame decreases outward, and since this is the frame in which the mirror points are stationary, the effect of shear on $\partial J/\partial\psi$ is positive, as in the tokamak.

2.3. Nonsymmetric case

When there is no ignorable coordinate, and canonical momentum conservation thus fails, we must turn to J-conservation [14] as in Eq. (6), to place bounds on particle excursions. In the limit of null gyroradius the excursions of untrapped particles from the flux surfaces still tend towards zero, since the $A_{\parallel}$-term in (6) then dominates. (There is, of course, an untrapped-particle-surface-break-up problem, related to the magnetic-surface problem itself [15-17]). The trapped-particle bananas, on the other hand, drift on constant-J surfaces that need have no relation at all to the flux surfaces, since for the trapped particles the $A_{\parallel}$-term in (6) disappears. This null-gyroradius behavior is rather ominous, since it remains the same for reactors as for present-day experiments of a given geometry, and is also the same for electrons and ions.

To estimate the magnitude ψ_1 of banana excursions [6] from flux surfaces ψ_o, we consider a symmetric configuration, having ignorable coordinate θ' and adiabatic invariant J_o, plus weak desymmetrizing variations ΔB and $\Delta\Phi_1$ along θ'. The constant-J condition then prescribes the banana guiding-center orbit:

$$\psi_1 \frac{\partial J_o}{\partial\psi} + \frac{1}{2}\psi_1^2 \frac{\partial^2 J_o}{\partial\psi^2} = \oint \frac{d\ell}{mv_{\parallel}} (\mu\Delta B + e\Delta\Phi_1) \tag{8}$$

The banana drifts along θ'; and when there is a θ'-dependent variation in $\mu\Delta B + e\Delta\Phi_1$ averaged over the banana, it can then become trapped, and will thus trace out a "superbanana" orbit (Fig. 2). At a turning point in this orbit, we have $\partial J_o/\partial\psi = 0$, and the excursion given by

$$\psi_1^2 = \frac{\frac{2}{m}\oint \frac{d\ell}{v_{\parallel}} (\mu\Delta B + e\Delta\Phi_1)}{\partial^2 J_o/\partial\psi^2} \tag{9}$$

The results for the superbanana orbit are entirely analogous to those obtained earlier for the banana orbit. The low-ω_d bananas are preferentially trapped. The untrapped bananas typically have much smaller excursions,

$$\psi_1 = \frac{\frac{1}{m}\oint \frac{d\ell}{v_{\parallel}} (\mu\Delta B + e\Delta\Phi_1)}{\partial J_o/\partial\psi} \tag{10}$$

The barely untrapped bananas approach half the excursion of the barely trapped bananas. [The maximum ω_d for which trapping occurs is derived from $(\partial J/\partial\psi_{max} = 1/2\,\psi_{1\,max}\,\partial^2 J_o/\partial\psi^2)$.] In the present section, we will neglect $\Delta\Phi_1$ and consider superbananas caused by nonsymmetric field configurations. The case of principal interest is the toroidal stellarator with helical windings [14, 16, 18]. For large aspect ratio R_o/r_o, we can take the straight stellarator of Sec.2.2 as the basic symmetric configuration, which is perturbed by a weak variation in B due to the variation in ΔR. The above analysis then applies. Stellarator windings with high ℓ are very unfavorable [18], since $\partial J_o/\partial\psi$ then is small

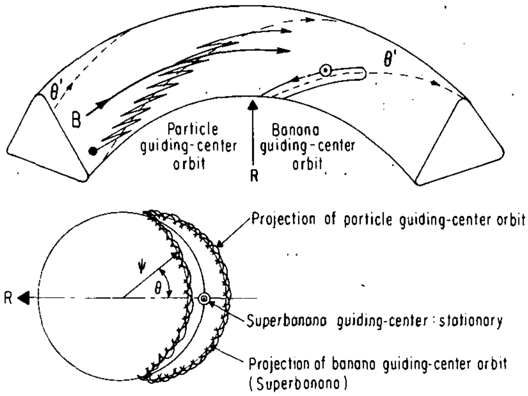

FIG. 2. Particle guiding-centre orbits and banana guiding-centre orbits (superbananas) in a stellarator.

except for the edge of the confinement region. On the other hand, a strong $\ell = 1$ component favors large $\partial J_o/\partial\psi$ throughout and can make the linear stellarator resistant to symmetry-spoiling by the toroidal curvature.

A general cure for the superbanana problem can be found in terms of an electrostatic potential [6] of either sign. If the electrostatic well is much greater than the variation of μB over the confinement region, then $\partial J_o/\partial\psi$ can be made altogether positive for one particle species and altogether negative for the other, thus eliminating banana-trapping. This is analogous to the elimination of trapped particles, by way of Eq. (3); but the magnitude of potential required is only $e\Phi_o > kT\,\Delta B/B$, which is far more lenient than (3) in the small-gyroradius, large-rotational-transform limit.

The class of particles that lack a unique J-value deserves special comment. These are particles with a mirror point lying very near to some local field maximum B_{max}, which are sometimes reflected and sometimes passed, depending on banana position. These non-J-conserving particles are embedded between two classes of J-conserving particles. The latter cannot become non-J-conserving, and therefore, by Liouville's theorem, the non-J-conserving particles cannot become J-conserving. The conservation of nonconservation then limits these particles to a locus of $\mu B_{max} + e\Phi_o = constant$, which will lie within the confinement region when $e\Phi_o > kT\Delta B/B$, as before.

3. SHEARED MAGNETIC FIELDS AND IRREGULAR ELECTROSTATIC POTENTIALS

3.1. Existence of potential variations on magnetic surfaces

In a finitely sheared magnetic field, infinite-conductivity hydromagnetic modes are energetically excluded at low β, which is the case we consider here. In this case, the presence of irregular electrostatic potentials Φ_1 on the magnetic surfaces is necessarily accompanied by potential drops of order Φ_1 along magnetic field lines. Such a situation may seem paradoxical for a collisionless (hence, "infinite-conductivity") plasma; however, we know from Ref. 19 how to construct special distribution functions $f(v_{\|})$ giving self-consistent static solutions for arbitrary Φ_1.

In the limit of short Debye length, the condition we must meet is

$$\int d v_{\|} \, f_+ \left(\frac{1}{2} m v_{\|}^2 + e \Phi_1\right) - \int d v_{\|} \, f_- \left(\frac{1}{2} m v_{\|}^2 - e \Phi_1\right) = 0 \qquad (11)$$

which is to hold identically over some range of Φ_1. For nearly Maxwellian distributions, with $e \Phi_1 \ll kT$, this becomes simply

$$\int d v_{\|} \, f'_+ \left(\frac{1}{2} m v_{\|}^2\right) + \int d v_{\|} \, f'_- \left(\frac{1}{2} m v_{\|}^2\right) = 0 \qquad (12)$$

In other words, the ions or electrons, or both, must have a deficiency of low-$v_{\|}$ particles. For finite $e \Phi_1$, Eq. (11) can be solved by a Laplace-transform method [19] and leads to a similar prescription for $f(v_{\|})$. A moderate departure from the Maxwellian is sufficient as long as we restrict ourselves to $e \Phi_1 < kT$, which we shall do in what follows.

We note that local scarcities of low-$v_{\|}$ particles can arise as a property of the equilibrium (and this is clearly shown in the calculations of Ref. 20). Such scarcities can also arise in the course of a perturbation that acts differently on trapped and untrapped particles [21]. Non-Maxwellian configurations of this kind could give rise to fast-growing instabilities; but in the context of the present paper we concern ourselves only with the consequences for low-frequency modes.

We will consider, first of all, what effect an irregular potential in the range $e \Phi_1 < kT$ can have on single-particle motion.

3.2. Potentials with one ignorable coordinate: untrapped E-bananas

If we take a magnetic field configuration having two ignorable coordinates (e.g., an infinite linear form of the levitron), and add a potential Φ_1 with one helical ignorable coordinate θ', then the particle excursions are rather similar to those described in Sec. 2.1. Naively, one might have supposed that low-$v_{\|}$ particles would drift along constant-Φ_1 surfaces, just as one might have supposed in Sec. 2.1 that they would drift along constant-B surfaces. What prevents this from happening in either case is the trapping of the low-$v_{\parallel}$ particles by the same gradient in Φ or μB that is responsible for their excursions.

To help visualize the analogy between B-bananas and E-bananas, we begin with the special case where z is the ignorable coordinate (Fig. 3) and $v_z = v_{\parallel} \cos \alpha$. Then p_z is conserved, and we go back to Eqs (1) and (2) with $\Delta B = \Delta R = 0$, and the ϕ-coordinate replaced by z. The condition for mirror-trapping is still Eq. (3) and from (4) we have left

$$r_1^2 = \frac{-2 e \Delta \Phi_1}{m\omega_c^2 \cos^{-2}\alpha + e \Phi_o''} \tag{13}$$

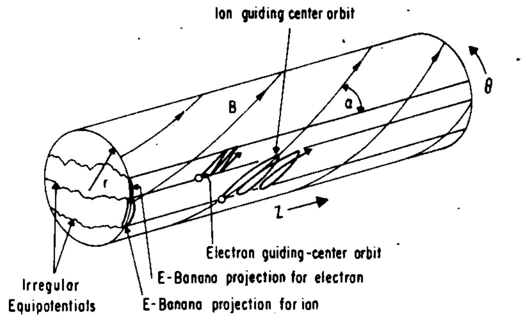

FIG. 3. Particle guiding-centre orbits (E-bananas) in a cylindrical sheared-field configuration with irregular electrostatic potentials $\Phi_1(r, \theta)$.

For $\Delta\Phi_1 < kT$, the case of present interest, the banana size is less than the gyroradius taken in the poloidal field component. An important point to note is that: in electrostatic trapping, ions and electrons are trapped separately, in adjacent regions along a given field line. Ions are trapped on the $\Delta\Phi_1 < 0$ side of the mirror point, and electrons on the $\Delta\Phi_1 > 0$ side.

More generally, when Φ_1 has a helical ignorable coordinate θ', we can carry through the same analysis, using conservation of $p_{\theta'}$. The banana size is then at most of the order of the gyroradius taken in the magnetic-field component transverse to the ignorable coordinate. This suggests that the most dangerous choice of θ' on a given flux surface is along the local magnetic field lines. Then the transverse magnetic field vanishes locally, and $A_{\theta'}$ becomes of order r_1^2/L_s, rather than r_1, where L_s is the shear length.

We will carry out the relevant banana analysis in the plane case, with a principal magnetic field B_z, with z as the ignorable coordinate, y as the coordinate across flux surfaces, and $B_x(y) = 0$ at $y = 0$. We then find for the trapped-particle excursions in a potential $\Phi = \Phi_o(y) + \Delta\Phi_1(x,y)$, and in the frame where $\Phi_o'(y) = 0$ at $y = 0$, so that $v_{\parallel o} = 0$,

$$-e\Delta\Phi_1 = \frac{y^2}{2} e \Phi_o'' + \frac{y^4}{4}\left[m(\omega_c')^2 + \frac{1}{6}\Phi''''\right] \tag{14}$$

For $\Phi_o \equiv 0$, the maximum excursion is

$$y_{max} = \left[\frac{-4 e \Delta \Phi_{1 max}}{m(\omega_c')^2} \right]^{1/4} \sim (r_g L_s)^{1/2} \qquad (15)$$

where $\omega_c' = e B_x / mc$, and r_g is the gyroradius taken in the B_z-field for a particle energy $e\Delta\Phi_{1 max}$ which can be no greater than kT. As in the familiar case of B-bananas in low-rotational-transform toruses, we thus find that the E-banana size can exceed r_g considerably, though going to zero for null r_g. The peculiarity of the worst E-bananas in sheared field is that they vanish only with $r_g^{1/2}$.

From the preceding it is easy to generalize to the case of a magnetic-field configuration with one ignorable coordinate (tokamak, levitron) and a potential Φ_1 with the same ignorable coordinate. This simple case of additive electric-magnetic trapping is covered by the full Eq. (4). The self-consistent dynamic plasma behavior for this type of magnetic field and potential has been explored by computer in Ref. 20.

3.3. Formation of superbananas in the presence of irregular electrostatic potentials

Noting the similarity of E-bananas and B-bananas, we can now proceed to investigate the process of banana trapping (superbanana formation) in more general terms than in Sec. 2.3, including the effect of irregular electrostatic potentials. In this way all particle excursion mechanisms of interest in the low-frequency range are covered. The six basic types of orbit are given in Table I. (In addition there are, of course, mixed cases, like the example at the end of the previous section, where the trapping role is played by a superposition of electric and magnetic fields.)

The following basic rules apply:

(a) Configurations with two ignorable coordinates (including magnetic and electrostatic fields) have no trapping and no bananas.

(b) The introduction of B-trapping or E-trapping implies loss of at least one ignorable coordinate. The trapped particles make banana orbits, which are restricted to drifting along the remaining ignorable coordinate.

(c) There can be either B-trapping or E-trapping of the B-banana or E-banana, and this implies the elimination of both ignorable coordinates. The particle executes its banana orbit at thermal velocity, and the banana executes the superbanana orbit at drift velocity. The superbanana does not move at all.

(d) The low-$v_{\parallel}$ particles are most readily trapped into bananas, and the low-ω_d bananas most readily into superbananas. The banana size depends on the gyro-

TABLE I. COMPLETE TABLE OF BANANAS

Ignorable Coordinate	Banana Species	Habitat
2	No bananas	Linear discharge or hard-core geometry with regular potential.
1	B-banana	Tokamak, levitron, multipole, with ϕ-independent potential; linear θ'-independent stellarator with θ'-independent potential.
1	E-banana	Linear discharge or hard-core geometry with θ'-independent potential.
0	B-trapped B-banana	Toroidal stellarator.
0	E-trapped B-banana	Finite-amplitude trapped-particle instability.
0	B-trapped E-banana	Large-amplitude trapped-particle instability.
0	E-trapped E-banana	Finite-amplitude electrostatic trapped particle modes.

radius, but the superbanana size depends only on the geometry and relative magnitude of fields.

(e) B-trapped ions and electrons are trapped in the same place, but E-trapped ions and electrons are trapped in adjacent sections of a field line. B-trapped ion and electron bananas are trapped in the same place, but E-trapped ion and electron bananas are trapped in adjacent sections of the erstwhile ignorable coordinate.

In looking for particle loss mechanisms that involve irregular electrostatic potentials, we must focus attention, first of all, on the trapped particles [the untrapped ones being protected from loss by the

$A_{\|}$-term in Eq. (6)]. Among the bananas, the trapped ones will have the largest excursions in irregular potentials [see Eqs (9) and (10)]. The subject of particle loss by convective cells in sheared field is then closely connected with the three types of electric superbanana.

3.4. E-trapped B-bananas

The trapped-particle instability [21] can be a low-frequency, purely growing mode, and is thus a natural model for a self-consistent convective cell. This mode conserves J, and is most easily analyzed in terms of the J-properties of the configuration [13].

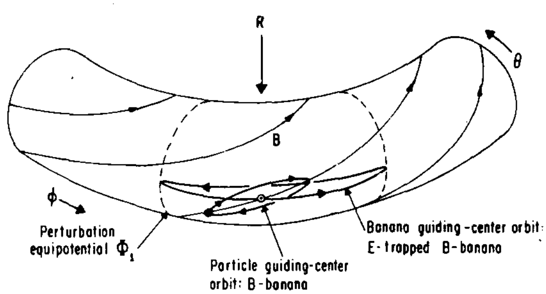

FIG. 4. Trapped-particle instability in tokamak geometry, showing finite-amplitude effect on banana guiding-centre motion: the E-trapped B-banana.

Taking as a concrete example the trapped-particle mode in the tokamak geometry (Fig. 4), we have B-bananas drifting along ϕ and interacting with a perturbation potential $\Phi_1 = \Phi_1(\psi,\theta)\, e^{im\phi}$, which displaces them in ψ. For $\partial J/\partial\psi > 0$, the sign of ω_d is such that this banana displacement gives a charge separation self-consistent, through Poisson's equation, with the potential Φ_1. To obtain a solution, one therefore takes a potential variation in θ such that the displacement of those bananas having $\partial J/\partial\psi > 0$ is emphasized; that is to say, Φ_1 is peaked near the tips of such bananas, where it has a strong influence on their drifts [cf. Eq. (8)]. From the point of view of energetics, we confirm that $\partial J/\partial\psi > 0$ corresponds to a reduction of banana energy with outward displacement [12], favoring the growth of such a mode. If $\partial J/\partial\psi \gtrsim 0$, the growth rate is small, giving a nearly static convective cell.

We now consider what a finite-amplitude convective cell of this kind implies for particle transport. The untrapped particles are prevented by their J-conservation from having any excursion in ψ. The bananas with large $\partial J/\partial\psi$ are slightly displaced, according to Eq. (10), taken with $\Delta B = 0$. It is only the trapped bananas that have excursions

$$\psi_1^2 = \frac{\frac{2}{m}\oint \frac{d\ell}{v_{\|}}\, e\,\Phi_1}{\partial^2 J/\partial\psi^2} \tag{16}$$

which can be considerable even for small $e\,\Phi_1 << kT$.

Thus we see that the real danger of the trapped-particle convective cell lies in the formation of E-trapped B-bananas for the low-ω_d particles. In the absence of a regular potential Φ_o, these excursions are just as serious as those of the B-trapped B-bananas in the stellarator. One may indeed say that an axisymmetric torus (tokamak, levitron) which permits a trapped-particle convective cell to grow is automatically downgraded to stellarator symmetry as far as the single-particle excursions are concerned.

The addition of a regular potential Φ_o does not stabilize the trapped-particle mode until Φ_o is so large as to untrap all the ions [see Eq. (3)], in which case it can also induce new instabilities [22]. A much smaller Φ_o, of order kTr_o/R_o, is however sufficient to prevent $\partial J/\partial\psi \approx 0$ for all bananas, thus eliminating the easily E-trapped B-bananas, and limiting the maximum excursions that any particles can have in the trapped-particle mode. The role played here by Φ_o is exactly as in the stellarator, where it is also unnecessary to eliminate the trapped ions, but useful to eliminate the B-trapped B-bananas.

3.5. B-trapped E-bananas

Continuing with the analogy between excursions in the trapped-particle mode and ordinary stellarator excursions, we recall that in the limit of sufficiently low aspect ratio ($R_o/r_o \to 1$) the R-dependence of the toroidal magnetic field does not merely trap the B-bananas but actually traps the particles. In the same way, when the perturbation potential Φ_1 becomes finite, the trapped-particle mode progresses from E-trapping of B-bananas to E-trapping of particles. The resultant E-bananas must drift orthogonal to the drift of the B-bananas, and cease to contribute to the growth of the mode. (The particles having the largest excursion will now be the B-trapped E-bananas.)

An effective upper limit on the amplitude of the standard trapped-particle mode is thus set by the transition from magnetic to electrostatic particle trapping, which occurs for $e\,\Phi_1 \sim kTr_o/R_o$.

3.6. E-trapped E-bananas

In a configuration with negligible magnetic trapping (a linear levitron or a toroidal one with appropriate field shaping) there can be no trapped-particle instability of the standard type; but there can still be a purely electrostatic trapped-particle mode.

We consider a plane model, with a basic magnetic field B_z and a finite electrostatic potential $\Phi_T(z)$, which is periodic in z and traps the low-$v_{\parallel}$ particles electrostatically. We assume that $e\,\Phi_T \ll kT$, so that the equilibrium condition is simply given by Eq. (12). We will assume a B_x-component of the magnetic field, so that a perturbation $\Phi_1 = \Phi_1(z)\,e^{i(kx+\omega t)}$ does not give rise to a displacement across flux for the untrapped particles — just as in the case of a sheared field. From Sec. 3.1., we know also that the potential $\Phi_T(z)$ by itself cannot give rise to any trapped or untrapped particle drift in the y-direction, even in the presence of the B_x-component. We also allow for a gradient $\partial B/\partial y$ by introducing a drift velocity v_d, which we take simply to be constant for each species.

The problem is analyzed in the same manner as in Ref. 13 for B-trapped particles. The distinctive feature of the E-trapped case is that each particle species now sees a different average perturbation

$$\langle \Phi_{1j} \rangle = \frac{\oint dz \dfrac{\Phi_1}{\sqrt{W - e_j \Phi_T}}}{\oint dz \dfrac{1}{\sqrt{W - e_j \Phi_T}}} \tag{17}$$

where the integral is taken between the turning points appropriate for each species ($j = \pm$). The resultant dispersion relation is

$$\int_{e\Phi_T}^{e\Phi_{T\,max}} dW \frac{\langle \Phi_{1+} \rangle \left(\omega \dfrac{\partial f_{o+}}{\partial W} - \dfrac{kc}{eB_z} \dfrac{\partial f_{o+}}{\partial y} \right)}{\sqrt{W - e\Phi_T}\,(\omega - k v_d)} + \int_{-e\Phi_T}^{e\Phi_{T\,max}} dW \frac{\langle \Phi_{1-} \rangle \left(\omega \dfrac{\partial f_{o-}}{\partial W} + \dfrac{kc}{eB_z} \dfrac{\partial f_{o-}}{\partial y} \right)}{\sqrt{W + e\Phi_T}\,(\omega + k v_d)} = 0 \tag{18}$$

The potential Φ_T is a function of z, and Eq. (18) must be satisfied for all z. The quantities $\langle \Phi_{1j} \rangle$ are functions only of W, as defined in Eq. (17). The two integrals represent the contributions of the trapped ions and electrons, the contributions of the untrapped particles (their displacement along magnetic field) having been eliminated with the help of the zero-order condition Eq. (12).

For $e\Phi_T \ll kT$, it is consistent with the condition (12) to assume that $\partial f/\partial W$ and $\partial f_o/\partial y$ are constant in the small velocity range occupied by the trapped particles. With this simplification, two types of solution for Eq. (18) can be seen by inspection.

(A) There is a stable mode for $\omega = \omega^* = (kc/eB_z)(\partial f_o/\partial y)(\partial f_o/\partial W)^{-1}$, with ϕ_1 taken to be odd about the maximum of Φ_T (the point about which the electrons are trapped), so that $\langle \Phi_{1-} \rangle$ vanishes identically. (Example: $\Phi_o = \Phi_{o\,max} \cos 2k_o z$, $\Phi_1 = \Phi_{1\,max} \sin k_o z$.) In this mode, the electrons are not displaced at all, and the ions carry a stable wave at something like the ion drift frequency. A similar solution is obtained with the roles of ions and electrons interchanged. We note that the drift velocity v_d has no effect on the waves.

(B) If $v_d < 0$, corresponding to an unfavorable magnetic-field gradient, there can also be an electrostatic trapped-particle instability. The disappearance of the untrapped-particle contribution in (18) means that the trapped particles are untied from any flute-inhibition by currents along magnetic field. The constraint that now inhibits flutes is that the electrons and ions are trapped in adjacent regions along magnetic field, and thus flutelike plasma displacements tend to violate the charge-neutrality condition (18). An unstable mode must therefore have the property of displacing the trapped electrons and ions together in the intermediate region where their orbits overlap, while avoiding a net displacement of either species at the top and bottom of the Φ_T well. This prescription can be carried out straight-forwardly for multistep models of Φ_T, and Eq. (18) then reduces to

$$\frac{\omega - \omega^*}{\omega - kv_d} + \frac{\omega + \omega^*}{\omega + kv_d} = 0 \qquad (18')$$

so that $\omega = (\omega^* kv_d)^{1/2}$, a result similar to that for the magnetic trapped-particle instability. The idealizations involved in the present treatment make it somewhat difficult, however, to assess the relative practical importance of the electrostatic and magnetic trapped-particle modes.

3.7. Discussion

From the results of Secs. 2 and 3, we can see qualitatively, first of all, that self-consistent equilibria can exist, both in symmetric and nonsymmetric toruses with sheared field. In Sec. 2 we have shown that a regular potential $e\Phi_0 >> kT\,r_0/R_0$ is sufficient to restrict the particle orbit to the vicinity of the magnetic surfaces. In general, the particle density distribution over a magnetic surface may not tend to be uniform, giving rise to charge separation and a self-consistent potential $e\Phi_1$. As we have seen in Sec. 3, if this potential does not exceed $kT\,r_0/R_0$, it will not spoil the restriction of particle orbits to flux surfaces. This will clearly be the case, for example, when $T_e \lesssim T_i\,r_0/R_0$, since $e\Phi_1$ cannot exceed kT_e.

We note next, that even strong magnetic shear does not provide protection against further perturbations Φ_1 — that is to say, neighboring equilibria in the form of irregular convective cells. All that is required is a distribution function deficient in low-$v_{\parallel}$ particles — and even a Maxwellian starting distribution function can be given local deficiencies in low-$v_{\parallel}$ particles through the preferred transport of the trapped particles.

The latter process occurs spontaneously in the standard trapped-particle mode, which is therefore a useful self-consistent model for convective cells in a sheared field. One should note, however, that only the magnetic trapping is an essential feature for such convective cells: the driving of the trapped-particle mode by an unfavorable gradient of J is incidental, and can be replaced by other driving mechanisms [23]. It seems, moreover, that electrostatic trapping can also give rise to slow-growing instabilities.

The appearance of irregular potentials $e\Phi_1 \sim kT\,r_0/R_0$ (such as one might expect from trapped-particle modes) seems at first sight to imply Bohm-like rates of plasma transport: $D \sim \Phi_1 c/B \sim (r_0/R_0) kT\,c/eB$. Fortunately, we have seen in Sec. 3 that in sheared fields the particles are not in general lost due to the presence of such potentials. If there is a strong shear and the ion gyroradius is small, the untrapped particles cannot be transported appreciably across magnetic surfaces, and the E-bananas are also small. If there is a regular plasma potential $e\Phi_o > kT\, r_o/R_o$, sufficient to insure $\partial J/\partial\psi \neq 0$, the E-trapping of B-bananas (or E-bananas) can be eliminated. In present-day experiments, of course, these conditions may not be met to a sufficient extent. In particular, the requirement for small E-bananas, as given in Eq. (15), would appear to be seldom met.

Once the banana-size problem is removed by sufficiently strong magnetic field and shear, the experimental study of the special levitron configuration with minimal magnetic trapping becomes of considerable interest, since the electrostatic trapping effects can then be studied by themselves.

4. CONVECTIVE CELLS IN UNSHEARED MAGNETIC FIELD CONFIGURATIONS

4.1. Single-particle motion in irregular electrostatic potentials

Taking the multipole torus [3,4] as our typical example of an unsheared toroidal confinement geometry, we consider the particle motion in a potential $\Phi = \Phi_o(\psi) + \Phi_1(\psi,\phi)$ which is constant along the (closed) magnetic-field lines, but is irregular in its dependence on the other two coordinates. Canonical momentum conservation then fails, and we turn next to Eq. (6), noting that $A_{\|}$ vanishes for the closed-line multipole. The J for both trapped and untrapped particles is given by the first term in (6).

For $e\Phi_1$ of order $\lesssim kT$, this flutelike electrostatic perturbation has an effect on the particle excursions which we have already described in Eqs. (8)-(10). Those trapped-particle bananas, or untrapped-particle loops around the minor circumference, for which $\partial J/\partial\psi \approx 0$ readily become trapped in Φ_1, and then drift back and forth cyclically in the ϕ-direction. The others drift around the torus on orbits that are merely displaced somewhat by the presence of Φ_1. For Φ_1 of order $>> kT$ the Φ-term becomes dominant in J, and all particles drift along the constant-Φ surfaces. This is the situation when Φ_1 corresponds to hydromagnetic disturbances, which fall typically into the range $kT << e\Phi_1 \lesssim kT\, r_o/r_{gi}$. At the upper end, where the convective velocity approaches v_{sound}, the J-conservation itself fails for the ions.

4.2. Pseudohydromagnetic equation for closed-line configurations

In turning to the subject of convective cells, that is, self-consistent steady-state solutions with irregular potentials, it is of interest to begin at the hydromagnetic level. In closed-line geometries, such disturbances are not excluded by the magnetic-field structure, and indeed they are frequently produced in experiments: either in the form of the flute instability; or by virtue of dynamic plasma-injection methods; or by flow to plasma-intercepting mechanical supports.

In order to describe this motion, it is useful to seek an approximation where the χ-coordinate (along the poloidal magnetic field) has been integrated out, and we are left with a simple two-dimensional flow of plasma-filled flux tubes. We begin with the full hydromagnetic equations:

$$\frac{\partial \rho}{\partial t} + \nabla \cdot (\rho \vec{v}) = 0 \tag{19}$$

$$\frac{\partial p}{\partial t} + \vec{v} \cdot \nabla p + \gamma p \nabla \cdot \vec{v} = 0 \tag{20}$$

$$\rho\left[\frac{\partial \vec{v}}{\partial t} + (\vec{v} \cdot \nabla)\vec{v}\right] = -\nabla p + \vec{j} \times \vec{B} \tag{21}$$

We will treat the linear multipole case (where z replaces ϕ), and therefore redefine ψ in this section to mean poloidal flux per unit length in z. We write $\vec{v} = \nabla \Phi \times \vec{B}/B^2 + \vec{v}_{\parallel} \vec{B}/B$, with $\Phi = \Phi(\psi, z)$, so that $v_\psi = -\partial\Phi/B\partial z$ and $v_z = \partial\Phi/\partial\psi$. Equations (19) and (20) then take form.

$$\frac{\partial M}{\partial t} + \frac{\partial \Phi}{\partial \psi}\frac{\partial M}{\partial z} - \frac{\partial \Phi}{\partial z}\frac{\partial M}{\partial \psi} = 0 \tag{22}$$

$$\frac{\partial P}{\partial t} + \frac{\partial \Phi}{\partial \psi}\frac{\partial P}{\partial z} - \frac{\partial \Phi}{\partial z}\frac{\partial P}{\partial \psi} = 0 \tag{23}$$

where $M = \rho \int d\ell/B$ and $P = (\int d\ell/B)^\gamma$. To eliminate the χ-dependence from Eq. (21), we need to make an approximation: we neglect those terms in $(\vec{v} \cdot \nabla)\vec{v}$ involving $v_{\parallel}$. This means that we lose the inertial effects arising from whatever rearrangement of plasma within a flux tube is required as it moves along the ψ-coordinate. The "pseudohydromagnetic equation" so obtained obviously breaks down near the multipole separatrix, but so does the entire hydromagnetic treatment, since r_g becomes large in the same region.

We thus obtain from Eq. (21), by taking $\int d\ell[(\vec{B} \cdot \nabla) j_{\parallel}]/B^2 = 0$, the equation of motion

$$\begin{aligned}
&\frac{\partial}{\partial \psi}\left(M \frac{\partial^2 \Phi}{\partial \psi \partial t}\right) + \frac{\partial}{\partial z}\left(M_3 \frac{\partial^2 \Phi}{\partial z \partial t}\right) + \\
&+ \frac{\partial}{\partial \psi}\left[M\left(\frac{\partial \Phi}{\partial \psi}\frac{\partial^2 \Phi}{\partial \psi \partial z} - \frac{\partial \Phi}{\partial z}\frac{\partial^2 \Phi}{\partial \psi^2}\right)\right] + \\
&+ \frac{\partial}{\partial z}\left[M_3\left\{\left(\frac{\partial \Phi}{\partial \psi}\frac{\partial^2 \Phi}{\partial z^2} - \frac{\partial \Phi}{\partial z}\frac{\partial^2 \Phi}{\partial \psi dz}\right) - \frac{1}{4}\frac{\partial \log U_3}{\partial \psi}\left(\frac{\partial \Phi}{\partial z}\right)^2\right\}\right] \\
&= -\frac{\partial P}{\partial z} U^{-\gamma} \frac{\partial U}{\partial \psi}
\end{aligned} \tag{24}$$

where $U = \int d\ell/B$ and $U_3 = \int d\ell/B^3$ are functions only of ψ, while M, P, and $M_3 = \rho \int d\ell/B^3$ are functions of ψ, z, and t. The boundary condition is typically that Φ should be finite and constant in z at some boundary or at infinity.

4.3. Hydromagnetic convective cells

The Eqs (22)-(24) can be simplified and solved by a number of approaches. The case U = constant (uniform magnetic field) has been discussed by Poukey [24]. An analysis that approximates nonuniform U by a gravitational potential has been carried out by Yoshikawa and Barrault [25], to show the existence of stationary hydromagnetic convective cells. [We note in passing that the assumption of particular relations between U_3 and U is sufficient to allow Eq. (24) to be reduced to second order for the static case.]

For present purposes, we will use a static potential model

$$\Phi = \Phi_o(\psi) + \Phi_1(\psi)\, e^{ikz}$$

with $\Phi_1 << \Phi_o$, and look for the solutions of Eqs (22)-(24). From (22) and (23) it follows that any static solution has the form $M = M(\Phi)$, $P = P(\Phi)$. For (24) we now have

$$\frac{d^2 S_1}{d\psi^2} - S_1\left[k^2\,\frac{U_3}{U} + \frac{d^3 S_o/d\psi^3}{d S_o/d\psi} - U^{-\gamma}\,\frac{dP}{dS_o}\,\frac{dU}{dS_o}\right] = 0 \qquad (25)$$

where we have introduced $S = \int M^{1/2}\, d\Phi$, so that $S_o = \int M^{1/2}(\Phi_o)\, d\Phi_o$, $S_1 = M^{1/2}(\Phi_o)\,\Phi_1$. The meaning of $(\nabla S/B)^2$ is, of course, the kinetic energy of a flux tube.

Solutions to Eq. (25) represent possible neighboring equilibrium states, and are therefore all valid models for static convective cells. It is, however, important to distinguish between $\omega = 0$ solutions that represent true marginal-stability points (with unstable growth for slightly different choice of k) and $\omega = 0$ solutions that are simply stable waves seen in an appropriately moving coordinate system. The former type of convective cell is far more interesting, since it is likely to appear spontaneously. In the next section, where we consider this problem for a simplified gravitational-type well, we find for wells that are even in ψ with flows that are odd in ψ that the $\omega = 0$ solutions do indeed represent marginal stability. This is the case that we shall assume in the present discussions. It should be noted, however, that the detailed shape of the profile at the $S_o' = 0$ point can play a critical role, and that it is therefore unfortunate that the hydromagnetic analysis breaks down, for multipoles, at just this point. The situation is similar to that for the tearing mode [26] in this respect, and suggests the need for a more sophisticated analysis in the region where the magnetic field has its null.

For U = constant, we see that (25) reduces to the marginal-stability equation for the ordinary hydrodynamic shear-flow problem. The marginal wavelength k_o^{-1} is typically of the order of the shear-layer thickness, and the perturbation S_1 extends over the layer, without interior nodes. (This marginal stability problem is mathematically the same as that for the tearing mode, with the shear-flow term $S_o'''/S_o' < 0$ corresponding to $B_o''/B_o < 0$.)

For U $\neq$ constant, the magnitude of the pressure term in (26) relative to the shear-flow term is characterized by the Richardson number [27]

$$J_R = \frac{v^2_{sound}}{(dv_{zo}/dr)^2 R_c r_o} \rightarrow \frac{g\, d \log \rho / dx}{(dv_{zo}/dr)^2} \tag{26}$$

$$\sim \left(\frac{kT}{e\Phi_o}\right)^2 \frac{r_o^3}{r_{gi}^2 R_c}$$

We use r_o now to mean the pressure scale height and R_c is the scale height of the magnetic well.

In the flute-destabilizing case $dP/dU < 0$, the pressure term in (25) typically has opposite sign from the shear-flow term, and forces k_o^2 toward smaller values. The possibility of a marginal stability solution is eliminated when J_R is greater than of order unity.

In the flute-stabilizing case, $dP/dU > 0$, the pressure term typically has the same sign as the shear-flow term; it forces k_o^2 toward larger values, and introduces perturbations S_1 with multiple nodes. Thus we have the ironic result that stable magnetic wells (e.g., multipoles) lend themselves particularly well to convective cells. Actually, however, the forcing of k_o^2 toward large values is a stabilizing effect, since eventually the simple MHD analysis becomes invalid. This limit is discussed in Sec. 4.5.

We note that the convective cells discussed here are analogous to the Kelvin-Helmholtz instability [27] of classical hydrodynamics.* Wind blowing over water represents a shear flow in a stable gravitational well. Without surface tension (which corresponds loosely to finite-r_{gi} stabilization) sufficiently short wavelengths are unstable at any wind velocity. With surface tension, there is a minimum wind velocity before perturbations are expected to appear. The familiar experimental verification of this effect lends plausibility to the present interpretation of convective cells in multipole toruses.

4.4. Equivalent gravitational model

In order to simplify the time-dependent convective cell problem, without changing its essential character, it is convenient to go to plane geometry, in a constant B_y-field and use a gravitational field which is a

* The detailed mathematical results given in Ref. 27 are, however, quite different from those we obtain here, since uniform gravity has an effect that is qualitatively different from that of a two-sided gravitational well.

function of x. The $\omega = 0$ equation that corresponds to Eq. (25) then may be written

$$\frac{d^2 S_1}{dx^2} - S_1 \left[k^2 + \frac{d^3 S_o/dx^3}{d S_o/dx} - \frac{g\, d\rho/dx}{S_o^2} \right] = 0 \qquad (27)$$

where $v_{zo} = \rho^{-1/2}\, d S_o/dx$ and $v_{x1} = \rho^{-1/2} S_1 ik$

A corresponding equation for nonstatic perturbations $v_{x1} e^{i(kz+\omega t)}$ is

$$\frac{d^2 v_{x1}}{dx^2} - v_{x1} \left[k^2 - \frac{k}{\omega - k v_{zo}} \frac{d^2 v_{zo}}{dx^2} - \frac{k^2 G}{(\omega - k v_{zo})^2} \right] = 0 \qquad (28)$$

where we have used the simplifying model that ρ = constant, but $G = (g/\rho)\, d\rho/dx$, which corresponds to $v^2_{sound}/r_o R_c$, is still taken to be an arbitrary function of x.

In the standard problem of interest, $G > 0$ represents a localized flute-stabilizing well and is even in x, with a null at $x = 0$; while v_{zo} represents the flow associated with some potential of the plasma in the well, and is odd in x. The shear-flow term in $d^2 v_{zo}/dx^2$ has much the same type of effect as the G-term, but is generally smaller for cases of interest, and especially for small v_{zo}. We will assume here that G/v^2_{zo} is well-behaved near $x = 0$.

To show that there are unstable modes bordering on the $\omega = 0$ solutions of Eq. (28), is trivial in the case of even solutions. Expanding in ω and $\delta k = k - k_o$, one then finds that there is a purely growing mode with $i\omega = O(\delta k)$ for negative δk; that is, on the long-wavelength side of the marginal wavelength.

To illustrate the complete dispersion relation, it is convenient to adopt a specific x-dependence

$$v_{zo} = v'x, \quad G = G_2 x^2 \qquad (29)$$

Eq. (28) then takes the form of the Whittaker equation

$$\frac{d^2 v_{x1}}{dz^2} - v_{x1} \left(\frac{1}{4} - \frac{\epsilon}{z} + \frac{\mu^2 - \frac{1}{4}}{z^2} \right) = 0 \qquad (30)$$

where $z = 2(\gamma - ikx)(\kappa/k)(1 - k^2/\kappa^2)^{1/2}$, and $\gamma = i\omega/v'$, $\kappa^2 = G_2/(v')^2$, $\epsilon = \gamma(\kappa/k)(1 - k^2/\kappa^2)^{1/2}$, $\mu^2 = \frac{1}{4} + \gamma^2\kappa^2/k^2$. The boundary condition is $v_{x1} = 0$ at $x_b = \pm x_o$, corresponding to $z_b = \pm i z_o + \tilde{\gamma}$, where $z_o = 2x_o\kappa(1 - k^2/\kappa^2)^{1/2}$, $\tilde{\gamma} = 2\gamma(\kappa/k)(1 - k^2/\kappa^2)^{1/2}$.

The two solutions of (30) are $\psi_{\pm} = e^{-z/2}\, z^{\pm\mu+1/2} F(\pm\mu-\epsilon+1/2\, |\pm 2\mu+1|z)$, where F is the confluent hypergeometric function. We will treat the case $z_o >> 1$, which is of principal interest for strong gravitational wells and weak flows. Using the asymptotic form of F we then find the eigenvalue condition:

$$|z_b|^{-2\epsilon} e^{\tilde{\gamma}} \sin\{z_o + 2\epsilon \tan^{-1}(\tilde{\gamma}/z_o) - \epsilon\pi\} + \frac{\Gamma(1/2+\mu-\epsilon)}{\Gamma(1/2+\mu+\epsilon)} \sin \pi(1/2-\mu+\epsilon) = 0 \qquad (31)$$

The $\omega = 0$ solutions of (30) simply have the eigenvalue condition $z_o = n\pi$, with odd and even integral values of n corresponding respectively to the cosine and sine solutions. Examining (31) in the vicinity of $\gamma = 0$, gives us $\delta z_o = z_o - n\pi$, and we find

$$\begin{aligned} \delta z_o &= 2\pi\epsilon, & n \text{ odd} \\ &= -2\pi\epsilon^2 \log z_o, & n \text{ even} \end{aligned} \qquad (32)$$

Thus we verify that the unstable neighboring mode of the cosine solution lies at larger wavelengths; and we find that for the sine solution the instability lies on the short-wavelength side, and has a growth rate $i\omega = O(\delta k^{1/2})$.

Since $\epsilon < 1$ always holds in the range of interest, we simplify (31) to the form

$$z_o^{-2\epsilon} \sin z_o + \pi\epsilon = 0 \qquad (33)$$

The instability appears in the intervals $\pi < z_o < 2\pi$, $3\pi < z_o < 4\pi$, etc.; and the maximum of ϵ is roughly $\epsilon_{max} \sim 1/2 \log \log z_o / \log z_o < 0.2$. The highest growth rate is found for $k^2 = \kappa^2/2$, and is given very roughly by

$$i\omega = v'\delta \sim \frac{v'}{4 \log \kappa x_o} \qquad (34)$$

The simple model (29) that we have used here illustrates some of the basic points mentioned earlier. The "shear-flow term" in d^2v_{zo}/dx^2 vanishes identically here, without eliminating the shear-flow instability. The G-term gives the important effects, and for low streaming velocities pushes the wavelength toward small values since we have $k^2 + n^2\pi^2/4x_o^2 \approx \kappa^2$. The Richardson number J_R is identified as $\kappa^2 x^2$.

4.5. Finite gyroradius effects

For plasma potentials Φ_o that are not large compared with kT, we expect to enter the finite-gyroradius regime, which has been studied in Ref. 28. The $\omega = 0$ equation retains the exact form (26); however, with a modified interpretation of S :

$$\begin{aligned} v_{zo} &= \rho^{-1/2}(1 - dp_o/ne\, d\Phi_o)^{-1/2}\, S_o \\ v_{x1} &= \rho^{-1/2}(1 - dp_o/ne\, d\Phi_o)^{-1/2}\, S_1 ik \end{aligned} \qquad (35)$$

The important point here is that for $dp_o/ne\, d\Phi_o > 1$, the g-term in Eq. (26) changes sign. This will happen if the sign of the electrostatic potential is such as to help balance the ion pressure, and the magnitude of the potential is $e\Phi_o < kT$. A flute-stable well, with $gd\rho/dx > 0$, then tends to drive k_o^2 to small values in Eq. (26), and in fact can easily eliminate the possibility of marginal stability solutions since J_R is typically very large compared with unity.

If the sign of the electrostatic potential is such as to repel the ions, then the finite-gyroradius effect does not alter the eigenvalue problem posed by Eq. (26). Also, one can still show that there are unstable neighboring modes. In that case, however, k_o^2 is driven to large values for $gd\rho/dx > 0$, with the limit $(k_o r_{gi})^2 \rightarrow J_R (r_{gi}/r_o)^2 \rightarrow 1$ being reached when $e\Phi_o < kT(r_o/R_c)^{1/2}$; and thus for still smaller Φ_o the analysis breaks down.

4.6. Discussion

For closed magnetic field lines, much more dangerous convective cells can occur than in sheared magnetic fields. Both trapped and untrapped particles are susceptible to convection, and will be convected along constant-Φ lines if $e\Phi_1 >> kT$, which is possible in the absence of shear. Furthermore, "MHD-stable" closed-line configurations are always unstable against the growth of convective cells if there is any plasma potential and if one remains within the framework of the simple MHD theory.

This unfavorable theoretical picture probably applies quite well to the dynamic injection stage of present-day multipole experiments [3,4] where there are large directed plasma velocities. On the other hand, as soon as the plasma potential subsides below kT, it is more difficult to see, in terms of the preceding analysis, how any substantial plasma loss by convective cells could take place.

This is already clear from an energetic argument. The Richardson number J_R of Eq. (27) gives a convenient comparison between the energy required to displace fluid in a favorable gravitational well, and the energy available from the plasma flow to drive such a displacement [27]. For $J_R << 1$ the situation is "energetically" unstable. For large J_R, we have found in Secs. 4.3 and 4.4 that the instability can persist (actually becoming somewhat localized near the null of G, where J_R remains small). In this limit, however, the transport of the bulk plasma out of the well is energetically impossible. (Reverting to the analogy given in Sec 4.3, we would say that, while even a gentle wind can cause waves, it takes a very strong wind before the water is lost.) It thus appears from Eq. (27) that important plasma losses are ruled out for $e\Phi_o < kT$, as long as we also have $r_{gi} < r_o^{3/2}/R_c^{1/2}$.

We conclude that a multipole configuration with a deep magnetic well, small ion gyroradius, and potentials not exceeding kT should be relatively invulnerable to the Kelvin-Helmholtz type of convective cell. These conditions may not, however, be met to a sufficient extent in some present-day experiments.

In Sec. 3, we have featured the trapped-particle mode as a model for convection in sheared fields. This type of instability, of course, is also possible in unsheared configurations [13, 23], particularly if driven by effects other than $\partial J/\partial\psi > 0$. Conversely, one may assume that the Kelvin-Helmholtz type of convective cell, discussed in the present section for closed field lines, will persist at least in weak shear. The subject of low-frequency loss mechanisms thus appears to offer a fertile ground for further theoretical investigation — and perhaps even for explanation of the experimental anomalies.

5. ACKNOWLEDGMENTS

We wish to thank our colleagues in Novosibirsk, particularly Drs. R. Z. Sagdeev and A. A. Galeev, for many valuable discussions clarifying the single-particle containment problem. Several novel suggestions by Dr. G. P. Fyurs, however, have not been fully understood at the time of writing.

We are indebted to Dr. S. Yoshikawa for pointing out the importance of the convective-cell problem in toroidal confinement. We also acknowledge the help of Dr. P. Rutherford. We thank Dr. H. Grad for stimulating discussions.

This work was performed under the auspices of the U. S. Atomic Energy Commission, Contract No. AT(30-1)-1238.

Note added in proof: We would like to refer to the closely related work of Dr. A. P. Popryadukhin which is to published in the Soviet Journal of Technical Physics.

REFERENCES

[1] YOSHIKAWA, S. et al., 3rd Conf. on Plasma Physics and Controlled Nuc. Fusion Research, CN-24/C-7, Novosibirsk (1968).

[2] ELLIS, R.A., Jr., EUBANK, H.P., Phys. Fluids 11 (1968) 1109; ELLIS, R.A., Jr., BOL, K., STIX, T.H., Phys. Fluids 10 (1967) 2095.

[3] KERST, D. et al., 3rd Conf. on Plasma Phys. and Controlled Nuc. Fusion Research, CN-24/C-1, Novosibirsk (1968).

[4] OHKAWA, T. et al., 3rd Conf. on Plasma Phys. and Controlled Nuc. Fusion Research, CN-24/C-2, Novosibirsk (1968).

[5] ROSENBLUTH, M.N., Proceedings of Intl. Sym. on Contemp. Physics, Trieste (1968).

[6] GALEEV, A.A., SAGDEEV, R.Z., FYURS, G.P., Culham Lab. Translation CTO/489 (1968).

[7] COPPI, B., ROSENBLUTH, M.N., Plasma Phys. and Controlled Nuc. Fusion Research I, Vienna, I.A.E.A. (1966) 617.

[8] TAMM, I.E., Plasma Phys. and the Problem of CTR, I (Pergamon, 1961) 35.

[9] MOROZOV, A.I., SOLOVEV, L.S., Soviet Phys, Doklady, 4 (1959) 1031.

[10] BISHOP, A.S., SMITH, C.G., Phys. Fluids 9 (1966) 1380.

[11] BERK, H.L., GALEEV, A.A., Phys. Fluids 10 (1967) 441.

[12] HASTIE, R.J., TAYLOR, J.B., HAAS, F.A., Annals of Physics 41 (1967) 302.

[13] ROSENBLUTH, M.N., Phys. Fluids 11 (1968) 869.

[14] MOROZOV, A.I., SOLOVEV, L.S., Soviet Physics, Tech. Phys. 5 (1960) 250.

[15] GRAD, H., Phys. Fluids 10 (1967) 137.

[16] POPRYADUKHIN, A.P., Plasma Physics (J. Nuc. Energy Pt. C) 8 (1966) 169.

[17] ROSENBLUTH, M.N., SAGDEEV, R.Z., TAYLOR, J.B., ZASLAVSKI, G.M., Nuc. Fusion 6 (1967) 297.

[18] GIBSON, A., TAYLOR, J.B., Phys. Fluids 10 (1967) 2653.

[19] BERNSTEIN, I.B., GREENE, J.M., KRUSKAL, M.D., Phys. Rev. 108 (1957) 546.

[20] SMITH, C.G., BISHOP, A.S., 3rd Conf. on Plasma Phys. and Controlled Nuc. Fusion Research, CN-24/D-9, Novosibirsk (1968).

[21] KADOMTSEV, B.B., POGUTSE, O., J. Exp. and Theor. Phys. (U.S.S.R.) 51 (1966) 1734.

[22] GALEEV, A.A., SAGDEEV, R.Z., WONG, H.V., Phys. Fluids 10 (1967) 1535.

[23] RUTHERFORD, P. et al., 3rd Conf. on Plasma Phys. and Controlled Nuc. Fusion Research, CN-24/C-5, Novosibirsk (1968).

[24] POUKEY, J.W., Phys. Fluids 10 (1967) 2253.

[25] YOSHIKAWA, S., BARRAULT, M.R., Princeton Plasma Physics Laboratory MATT-626 (1968).

[26] FURTH, H.P., KILLEEN, J., ROSENBLUTH, M.N., Phys. Fluids 6 (1963) 459.

[27] CHANDRASEKHAR, S., Hydrodynamic and Hydromagnetic Stability (Oxford 1961).

[28] ROSENBLUTH, M.N., SIMON, A., Phys. Fluids 8 (1965) 1300.

DISCUSSION

M.B. GOTTLIEB: What would be the effect, under reactor conditions, of the collisional processes you discussed in your oral presentation?

H.P. FURTH: In open-ended reactors, the confinement time is typically one ion-scattering time, τ_c, and the reactor temperature must accordingly be very high. In a toroidal system that has maximum ion excursions, S_{max}, the confinement time will be at least $\tau_c(r/S_{max})^2$, so that the required operating temperature can be moderately low (say 30 keV) for well-designed toruses with values r/S_{max} of the order of ten or more.

This is the reactor picture if one assumes that the main loss problem arises from perturbations which (like the ones discussed in our paper) disturb static symmetry. Of course, fluctuations may also be important in promoting plasma loss.

The type of excursion which is important in producing diffusion depends on the collision time. If $\tau_c \gg \tau_{Bohm}$, then super-bananas are important, and the confinement is controlled by $\tau \gtrsim \tau_c(r/S_{max})^2$, as already mentioned. For smaller τ_c, the important excursions are always those super-bananas or bananas whose period approximates to τ_c; and the resulting estimate of containment time is more optimistic - namely $\tau \sim \tau_{Bohm}$.

CONFIGURATIONS DU TYPE STELLARATOR AVEC PUITS MOYEN ET CISAILLEMENT DES LIGNES MAGNETIQUES

C. GOURDON, D. MARTY, E.K. MASCHKE ET J.P. DUMONT*
ASSOCIATION EURATOM-CEA SUR LA FUSION
FONTENAY-AUX-ROSES, FRANCE

Abstract — Résumé

CONFIGURATIONS OF THE STELLARATOR TYPE WITH MEAN WELL AND SHEAR. The configurations studied are defined in terms of conductors and currents. The magnetic lines or trajectories are then integrated numerically by means of an IBM 360-75 computer.

The authors show that it is possible to obtain simultaneously, in a magnetic configuration of the Stellarator type, a mean magnetic well and substantial shear. The type of configuration in which the authors are interested consists of three basic fields: an azimuthal field (B_φ = const/r); a multipolar field produced by helicoidal conductors (ℓ = order of multipolarity, $m = d\theta/d\varphi$); and a vertical correcting field (B_z).

A comparison is made between configurations of the types $\ell = 2$, $\ell = 3$, $\ell = 4$, with different values of m. The authors demonstrate the advantages of configurations produced by helicoidal conductors through which currents pass in the same direction.

A typical $\ell = 4$, $m = 3$ configuration is presented in detail. For this configuration, the depth of the mean well is 20%, the communication length is about 20 times the plasma radius, and the shear length in the region of poor curvature is five times the plasma radius.

The authors show in particular how magnetic well depth and rate of shear vary with variations in the amplitude of the vertical correcting field.

The authors study the appearance of islands of surface degeneration due to the resonance of certain closed magnetic lines with perturbations of the configuration as a result of possible constructional defects. The number of islands and their dimensions are related to periodicity and amplitude of the perturbations.

The precession surfaces are also studied, the movement of the charged particles being calculated in the guiding-centre approximation. This study will make it possible to determine the importance of the problem of trapped particles which do not execute a complete revolution.

CONFIGURATIONS DU TYPE STELLARATOR AVEC PUITS MOYEN ET CISAILLEMENT DES LIGNES MAGNETIQUES. Les auteurs définissent les configurations étudiées par la donnée des conducteurs et des courants. Ils procèdent ensuite à une intégration numérique des lignes magnétiques ou des trajectoires sur un ordinateur IBM 360-75.

Ils montrent qu'il est possible d'obtenir, dans une configuration magnétique du type Stellarator, en même temps un puits magnétique moyen et un important cisaillement des lignes magnétiques. La classe des configurations auxquelles ils s'intéressent est constituée de trois champs élémentaires: un champ azimutal B_φ = cte/r, un champ multipolaire créé par des conducteurs hélicoïdaux (ℓ = ordre de multipolarité; $m = d\theta/d\varphi$) et un champ correcteur vertical B_Z. Ils comparent des configurations des types $\ell = 2$, $\ell = 3$, $\ell = 4$ avec diverses valeurs de m. Ils montrent l'intérêt que présentent des configurations constituées à l'aide de conducteurs hélicoïdaux parcourus par des courants de même sens et présentent en détail une configuration typique $\ell = 4$, $m = 3$. Pour cette configuration, la profondeur du puits moyen est de 20%, la longueur de communication est d'environ 20 fois le rayon du plasma et la longueur de cisaillement vaut, dans la région de mauvaise courbure, cinq fois le rayon du plasma. Les auteurs montrent en particulier comment la profondeur du puits magnétique et le taux de cisaillement varient lorsque l'on fait varier l'amplitude du champ correcteur vertical.

Ils étudient l'apparition d'îlots de dégénérescence des surfaces par suite de la résonance de certaines lignes magnétiques fermées avec des perturbations de la configuration provenant de défauts éventuels de réalisation. Le nombre des îlots et leurs dimensions sont en relation avec la périodicité et l'amplitude des perturbations.

Parallèlement, les auteurs entreprennent une étude des surfaces de précession, le mouvement des particules chargées étant calculé dans l'approximation du centre guide. Cette étude permettra de préciser l'importance du problème des particules piégées qui n'effectuent pas une révolution complète.

I. INTRODUCTION

De nombreux travaux théoriques ont été récemment consacrés à l'étude des configurations magnétiques toroïdales du type Stellarator. La destruction des surfaces magnétiques extérieures due à la courbure du tore a été calculée analytiquement et numériquement [1] ; [2] ; [3]. Ces travaux ont montré une limitation sérieuse de l'angle de transformation rotationnelle maximum. Des perturbations des surfaces causées par les défauts de construction ont été étudiées [3]. Enfin, des configurations nouvelles ont été proposées qui permettent d'obtenir simultanément un puits magnétique moyen et un cisaillement important des lignes de force [4] ; [5] ; [6].

Nous présentons ici les résultats d'une étude systématique sur ces configurations. Cette étude comporte trois parties : 1) Une analyse complète des configurations de différents ordres multipolaires qui a permis de distinguer une nouvelle classe de configurations que nous appelons TORSATRON et qui présente des propriétés intéressantes concernant la stabilité d'un plasma.
2) Une étude de l'effet des perturbations sur les surfaces magnétiques.
3) Une étude du confinement individuel des particules.

Ce travail est fait par intégration numérique, sur ordinateur, des lignes magnétiques et des trajectoires de particules, le champ magnétique étant calculé à partir de la donnée des conducteurs.

II. PROPRIETES DES CONFIGURATIONS MAGNETIQUES

II-1. Répartition des courants et définition des paramètres

a) Deux propriétés sont importantes pour la stabilité du plasma : le cisaillement des lignes de force et l'existence d'un puits magnétique moyen. Dans cette étude, nous avons calculé, sur chaque surface magnétique, l'angle de transformation rotationnelle moyen ι et la dérivée V' du volume par rapport au flux

$$\iota = \lim_{m \to \infty} \frac{1}{m} \sum_{k=1}^{m} \iota_K \qquad V' = \lim_{m \to \infty} \frac{1}{m} \sum_{K=1}^{m} \oint \frac{d\ell}{B}$$

Dans certains cas on calcule l'angle de transformation rotationnelle par période de champ ι_p dont la variation donne une idée du cisaillement local.

b) Les configurations étudiées sont constituées par la superposition de trois champs magnétiques (Fig. 1 - a) :
- Un champ azimutal $B_\varphi = {}^{cst}/_r$
- Un champ multipolaire d'ordre ℓ créé par des conducteurs hélicoïdaux sur la surface d'un tore
- Un champ vertical uniforme B_z.

Le champ multipolaire peut être créé de deux façons (Fig. 1 b) :
1) Par $2 \times \ell$ hélices parcourues par des courants de sens alterné. Nous appelons ces configurations STELLARATORS CLASSIQUES.
2) Par ℓ hélices parcourues par des courants de même sens. Nous appelons ces configurations TORSATRONS.

---
* Société d'études techniques et d'entreprises générales (SODETEG).

Dans ce dernier cas, les courants hélicoïdaux de même sens créent un champ vertical B_z qui doit être compensé de façon à obtenir des surfaces magnétiques fermées. Dans la suite, les champs multipolaires torsatrons seront toujours supposés être compensés par un champ :

$$B_{z_{comp}} = - \frac{1}{2\pi} \int_0^{2\pi} d\varphi \cdot B_{z_{Hélice}}(\rho = 0)$$

Un champ correcteur B_z supplémentaire permet d'ajuster la position des surfaces magnétiques de façon à ce que soit obtenu un puits magnétique moyen.

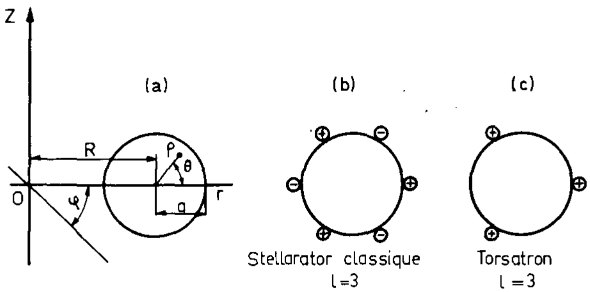

FIG. 1. a) Système de référence. b) et c) Comparaison de la création du champ multipolaire dans le stellarator classique et dans le torsatron.

c) Il n'est pas possible, dans le cas des configurations toroïdales non axisymétriques, de démontrer analytiquement l'existence de surfaces magnétiques. Toutefois, si une intégration numérique précise et prolongée montre que les lignes magnétiques restent sur une surface avec une approximation qui correspond à la précision du calcul, nous concluons à l'existence de celle-ci. Typiquement, dans nos calculs, la précision est de l'ordre de $\Delta x / L = 10^{-6}$ où L est la longueur intégrée de la ligne.

II-2. Résultats obtenus avec des conducteurs multipolaires-circulaires (m = 1)

Une étude comparative complète entre les configurations STELLARATOR CLASSIQUE non corrigées et corrigées d'une part, et les configurations TORSATRON non corrigées et corrigées d'autre part, a été réalisée pour $\ell = 2$; $\ell = 3$; $\ell = 4$ et $\ell = 6$ avec des conducteurs hélicoïdaux particuliers qui sont des cercles de Villarceau. Ces cercles inscrits sur le tore peuvent être considérés dans le système de référence (ρ , θ, φ) comme des hélices à pas variable qui font un petit tour pour un grand tour du tore $m \equiv d\theta/d\varphi = 1$. Dans ce cas particulier, le champ magnétique multipolaire s'exprime simplement au moyen d'intégrales elliptiques, ce qui permet un calcul numérique rapide et précis. Les caractéristiques essentielles des configurations torsatron sont parfaitement mises en évidence avec ce type simple de conducteur et les conclusions de la comparaison faite ici s'appliquent qualitativement avec des conducteurs hélicoïdaux $m = 2$; 3 ; 4 etc .

Nous donnons à titre d'exemple une description détaillée des configurations $\ell = 3$.

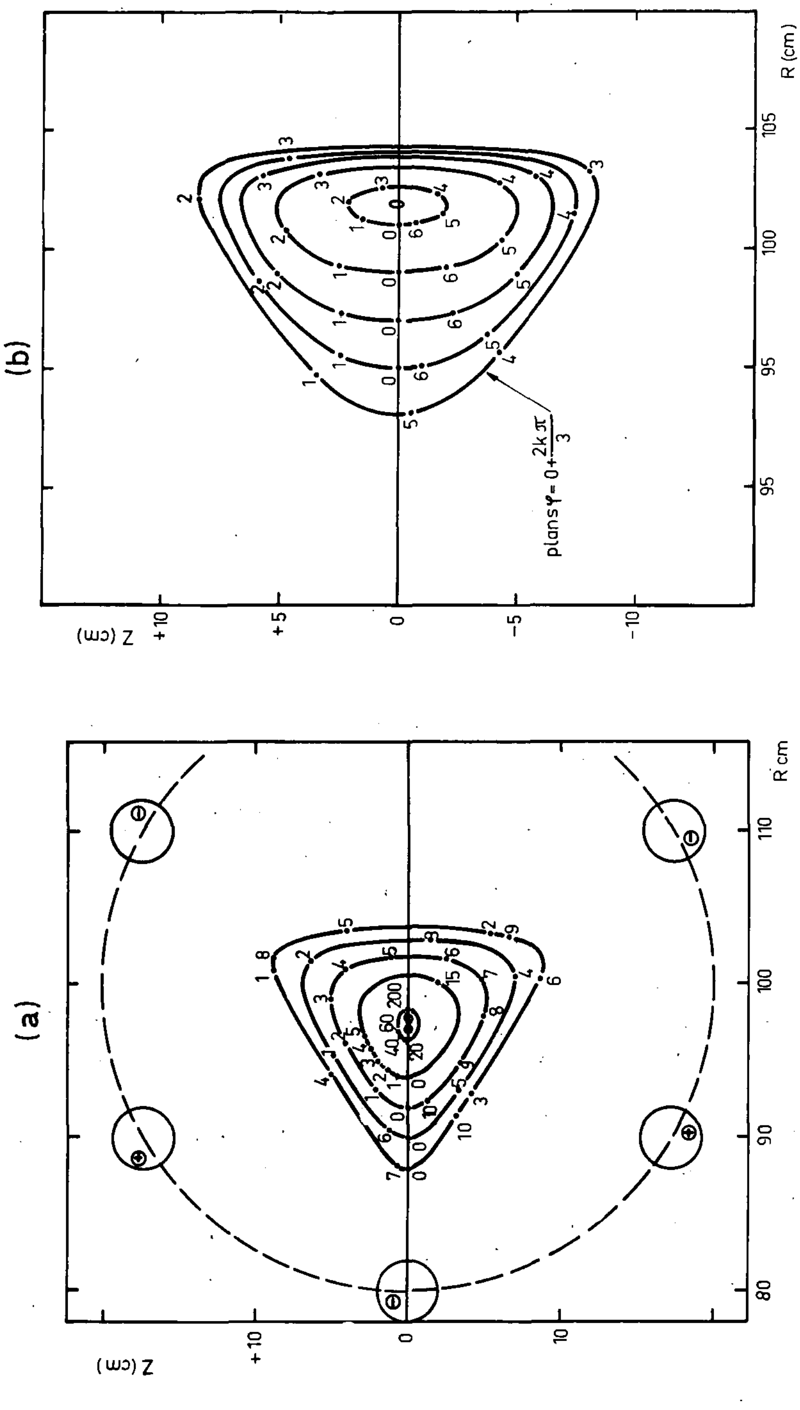

FIG. 2. Configuration stellarator classique $\ell = 3$, $m = 1$ (six cercles de Villarceau): a) sans champ B_Z correcteur; b) avec champ correcteur.

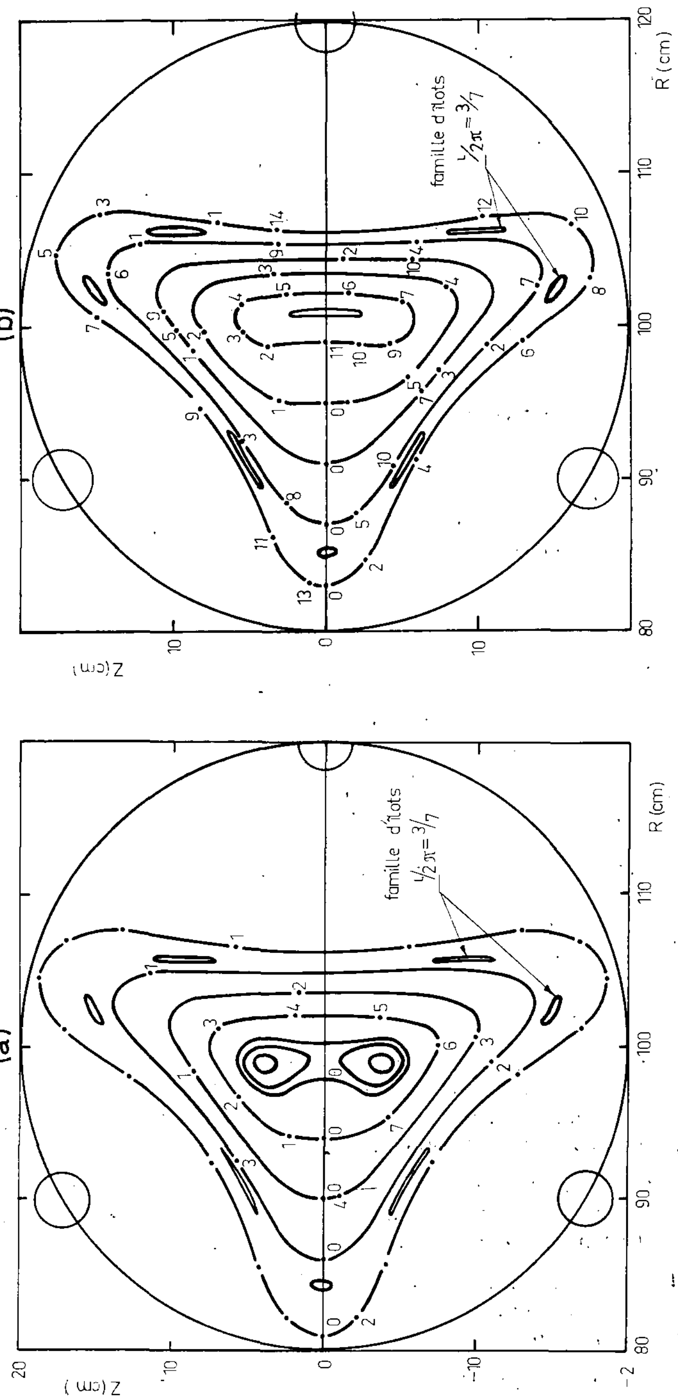

FIG. 3. Configuration torsatron $\ell = 3$, $m = 1$ (trois cercles de Villarceau): a) sans champ B_z correcteur; b) avec champ correcteur optimal.

a) Stellarator classique $\ell = 3$; $m = 1$

La Figure 2a représente l'intersection de la famille de surfaces magnétiques par le plan méridien $\varphi = 0$, pour une configuration $\ell = 3$ sans champ correcteur. On remarque la présence, au centre, d'une petite séparatrice avec deux axes magnétiques. Une telle structure avait été trouvée théoriquement par ALEKSIN [7]. Cette singularité n'existe pas dans un stellarator droit, elle est due à la courbure du tore et elle ne tourne pas, d'après les observations faites dans des plans méridiens successifs autour du tore. Les sections droites des surfaces extérieures sont triangulaires et tournent avec les conducteurs hélicoïdaux. La transformation rotationnelle est nulle sur la séparatrice interne et elle croît jusqu'aux environs de $\iota/2\pi = 0,3$ sur les bords du volume utile. La quantité V' croît légèrement du centre vers l'extérieur.

Si l'on ajoute à cette configuration un champ correcteur vertical B_z la séparatrice interne disparaît ; on n'observe plus qu'un seul axe magnétique (Fig. 2b). Pour une valeur convenable de B_z on obtient un puits magnétique moyen mais la transformation rotationnelle sur l'axe magnétique augmente, elle devient pratiquement constante dans tout le volume utile et il n'y a plus de cisaillement des lignes magnétiques - sauf, peut-être, tout à fait sur l'extérieur du volume utile.

b) Torsatron $\ell = 3$; $m = 1$

La Figure 3a est relative à la configuration $\ell = 3$ du type torsatron réalisée avec trois cercles de Villarceau parcourus par des courants de même sens. On observe une séparatrice interne qui renferme une partie notable du volume utile. Ici encore, la séparatrice interne ne tourne pas lorsqu'on fait un tour autour du tore. Pour la configuration non corrigée, la transformation rotationnelle vaut zero sur la séparatrice interne et monte rapidement vers l'extérieur jusqu'à $\iota/2\pi \sim 0,5$. Il n'y a pratiquement pas de puits magnétique moyen ($\sim$ 2 %).

Si on ajoute un champ correcteur B_z, le volume interne à la séparatrice diminue. Pour une valeur convenable de B_z la séparatrice interne disparaît et il y a un seul axe magnétique sur lequel la transformation rotationelle est nulle (Fig. 3b).

c) Configuration torsatron avec $\ell = 4$ et $\ell = 6$

Dans les configurations torsatron, le sens d'enroulement des conducteurs hélicoïdaux est tel que la composante azimutale du champ qu'ils créent s'ajoute au champ azimutal principal. La Figure 4 précise quelle est, dans ces conditions la position des surfaces magnétiques par rapport aux conducteurs hélicoïdaux. Pour les configurations $\ell = 3$; 4 ; 6 non corrigées, il existe une séparatrice interne qui renferme une fraction d'autant plus élevée du volume que ℓ est plus grand (10 % pour $\ell = 3$; 65 % pour $\ell = 6$).

Sur la Figure 5, nous avons résumé les propriétés essentielles des configurations étudiées. Pour chaque configuration on donne ι et V' en fonction du volume normalisé au volume utile total.

Les torsatrons sans correction présentent une séparatrice interne renfermant un volume important. Le volume interne à cette séparatrice se réduit progressivement au fur et à mesure que l'on améliore le puits magnétique moyen

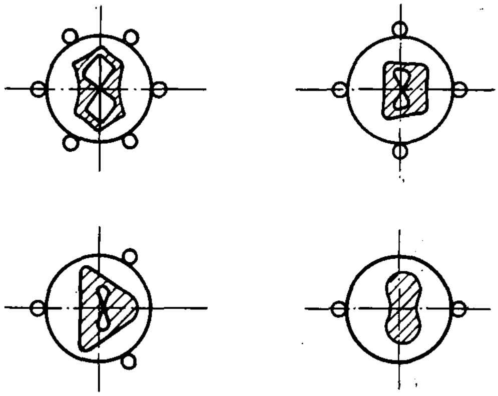

FIG. 4. Position des surfaces magnetiques par rapport aux conducteurs hélicoïdaux dans les configurations torsatron non corrigées pour $\ell = 2$, $\ell = 3$, $\ell = 4$, $\ell = 6$.

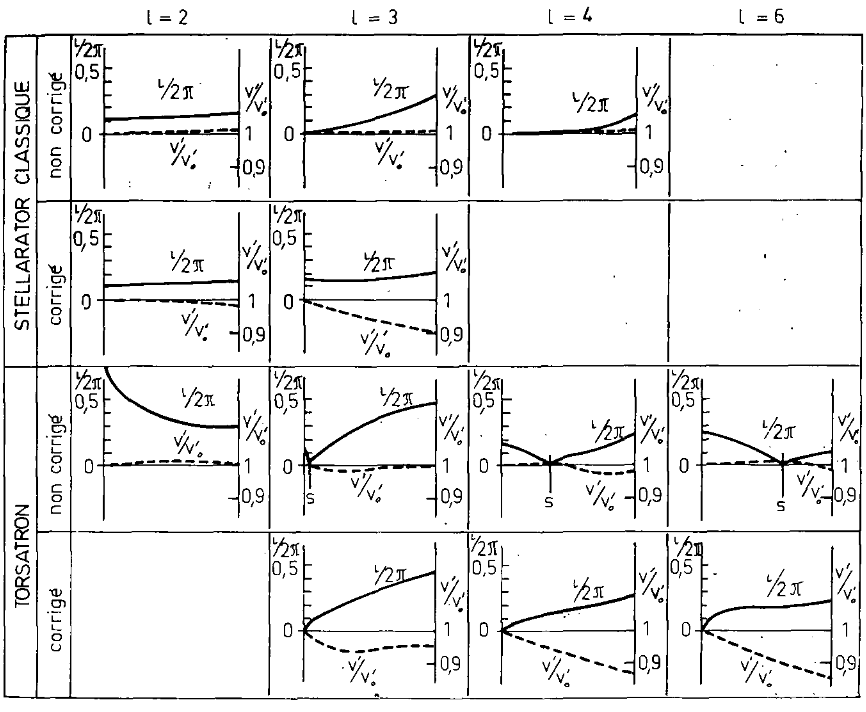

FIG. 5. Variation de $\iota/2\pi$ et v'/v'_0 en fonction de Ψ/Ψ_{max} pour les diverses configurations étudiées avec des conducteurs multipolaires circulaires.

par addition du champ correcteur B_z. Pour la valeur de B_z qui fait juste disparaitre la séparatrice, on obtient une configuration qui possède à la fois un puits magnétique moyen et un cisaillement important des lignes de force dans tout le volume utile. A cause de cette propriété commune, les torsatrons constituent une classe de configurations distincte de celle des stellarators classiques.

TABLEAU I. PARAMETRES PRINCIPAUX DES CONFIGURATIONS m = 3 ETUDIEES

		V_{utile}	$\Delta V'/V'_o$	$(\iota/2\pi)$	$Q = \frac{\overline{P}}{R} \times \Delta\,(\iota/2\pi)$	$\eta = \frac{B_{max}}{B_{min}}$
R/a = 4,44	Stellarator classique $\ell = 3$ m = 3 non corrigé	$0{,}103\,R^3$	-0,001	0,75	0,055	1,20
	Torsatron $\ell = 3$ m = 3 non corrigé	$0{,}4\,R^3$	-0,015	0,82	0,12	1,5
	Torsatron $\ell = 3$ m = 3 corrigé	$0{,}25\,R^3$	-0,095	0,53	0,06	1,33
	Torsatron $\ell = 4$ m = 3 non corrigé	$0{,}7\,R^3$	-0,020	0,75	0,14	1,8
	Torsatron $\ell = 4$ m = 3 corrigé	$0{,}5\,R^3$	-0,180	0,44	0,066	1,52
R/a = 10	Torsatron $\ell = 4$ m = 3 non corrigé	$0{,}05\,R^3$	-0,003	0,86	0,043	1,12
	Torsatron $\ell = 4$ m = 3 corrigé	$0{,}047\,R^3$	-0,05	0,77	0,038	1,12

TABLEAU II. COURANT DANS LES BOBINES B_φ ET DANS LES ENROULEMENTS HELICOIDAUX

		Ampère Tours Totaux Bobines $B\varphi$ $A_{TB} = I_B \times N_B$	Ampères Tours Totaux Hélices $A_{TH} = I_H \times \ell \times m$	Ampère par conducteur hélicoïdal
R/a = 4,44	Stellarator classique $\ell = 3$ m = 3	5 B.R		± 0,25 B.R
	Torsatron $\ell = 3$ m = 3	2,5 B.R	2,5 B.R	0,278 B.R
	Torsatron $\ell = 4$ m = 3	3,025 B.R	1,975 B.R	0,1646 B.R
R/a = 10	Torsatron $\ell = 4$ m = 3	4 B.R	1 B.R	0,0833 B.R

II-3. Résultats obtenus avec des conducteurs multipolaires hélicoïdaux ($m>1$)

Pour augmenter la valeur de la transformation rotationnelle et le cisaillement des lignes magnétiques, il est nécessaire d'utiliser des enroulements multipolaires plus serrés ($m = 2$; 3; 4....).

Nous avons constaté que pour $m > 3$, la valeur de $\iota/2\pi$ sur la dernière surface fermée n'augmente pratiquement plus avec m.

Nous avons étudié en détail les configurations stellarator classique et torsatron pour $\ell = 3$; $m = 3$ avec un rapport d'aspect $R/a = 4{,}44$ ainsi que les configurations torsatron $\ell = 4$; $m = 3$ avec les rapports d'aspect $R/a = 4{,}44$ et $R/a = 10$.

Nous donnons dans le tableau n° I, pour chacune de ces configurations, la valeur des paramètres suivants : v_u = volume utile à l'intérieur de la dernière surface magnétique fermée; $\Delta V/V_o$ = profondeur du puits magnétique moyen ; valeur moyenne de $\iota/2\pi$ sur la dernière surface magnétique fermée.

Ces valeurs correspondent, dans chaque cas, à une optimisation du rapport des amplitudes du champ multipolaire et du champ azimutal. Nous donnons dans le tableau n° II les valeurs des courants respectivement dans les bobines du B_φ principal et dans les enroulements hélicoïdaux.

Pour pouvoir comparer qualitativement les différentes configurations étudiées du point de vue du cisaillement des lignes magnétiques, nous définissons un facteur de qualité $Q = (\bar{\rho}/R) \times \Delta(\iota/2\pi)$ où $\Delta(\iota/2\pi)$ est la valeur moyenne de $\iota/2\pi$ sur la dernière surface magnétique fermée et $\bar{\rho}$ le rayon moyen de celle-ci.

Le " facteur de qualité ", Q, est tiré de l'expression du paramètre de cisaillement $\theta = \rho^2/R \times \frac{d\,\iota/2\pi}{d\rho}$ en écrivant $\rho = \bar{\rho}$ et en prenant la valeur moyenne de $d(\iota/2\pi)/d\rho$ dans le volume utile, à savoir $\Delta(\iota/2\pi)/\bar{\rho}$

On doit remarquer que les valeurs locales de θ peuvent être beaucoup plus élevées que la valeur de Q. Par exemple, pour la configuration torsatron corrigé $\ell = 4$; $m = 3$, on trouve dans la mauvaise courbure $\theta = 0{,}24$. Nous donnons (Fig. 6), à titre d'exemple pour cette dernière configuration, les valeurs de $\iota/2\pi$ et de θ moyennes sur une période de champ dans la mauvaise courbure. L'on se rappelle que, pour cette configuration particulière, la profondeur relative de puits magnétique moyen est de 18 %.

III. EFFETS DES PERTURBATIONS - FORMATION D'ILOTS

III-1. Remarques Générales

Lors de l'étude détaillée de la structure magnétique d'une configuration, on rencontre certaines lignes de force particulières, fermées au bout d'un petit nombre de tours du tore, et qui se comportent comme des axes magnétiques secondaires. Au voisinage de ces lignes, il existe une structure tubulaire des surfaces magnétiques. L'intersection de ces surfaces particulières avec un plan méridien φ = cste se présente sous forme d'une chaîne d'îlots qui s'intercale entre des surfaces non perturbées. Le nombre I des îlots d'une chaîne est lié au nombre P de périodes de la configuration magnétique et à l'angle de transformation rotationnelle par la relation

$I = K \frac{P}{(\iota/2\pi)}$ où K est le plus petit nombre entier tel que I soit entier.

Ces structures peuvent apparaître dans des configurations perturbées. On sait que dans ce cas la largeur $\Delta\rho$ de la région perturbée est liée à l'amplitude ΔB de la perturbation et au cisaillement $d\iota/d\rho$ par $\Delta\rho \propto \sqrt{\Delta B/(d\iota/d\rho)}$ /8/.

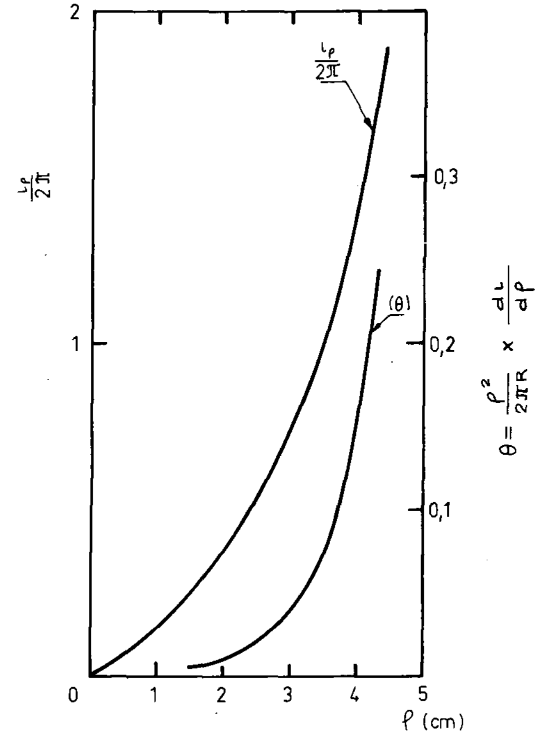

FIG. 6. Etude de la transformation rotationnelle et du paramètre de cisaillement locaux dans la mauvaise courbure pour la configuration torsatron $\ell = 4$, $m = 3$ corrigée.

Nous distinguerons deux catégories d'îlots suivant leur mode de création :

III-2. <u>Ilots naturels</u> Il s'agit d'îlots qui apparaissent dans une configuration non perturbée. Dans les configurations possédant un nombre faible de périodes, par exemple $\ell = 2$; $m = 1$, ces îlots peuvent prendre des dimensions notables $\Delta\rho/a \sim 0{,}05$. Par contre dans les configurations qui nous intéressent ici, à savoir $\ell = 3$; $m = 3$ et $\ell = 4$; $m = 3$, ces îlots naturels sont toujours très petits $\Delta\rho/a \sim 0{,}01$.

III-3. <u>Ilots de perturbation</u> Ces îlots apparaissent en présence de défauts technologiques de réalisation ou en présence de champs perturbateurs extérieurs. Nous étudions ici l'effet de certains défauts de réalisation. Nous distinguerons deux catégories de défauts :

a) Les déplacements d'ensemble qui correspondent à un mauvais positionnement, l'un par rapport à l'autre, des champs multipolaires et azimutaux.
b) Les défauts locaux aléatoires sur les bobines B_φ ou les hélices.

III-3-1. Déplacements d'Ensemble

Le déplacement relatif peut être décomposé en une rotation autour de OZ, une translation parallèlement à OZ, une translation perpendiculairement à OZ, et une inclinaison d'un angle α de l'axe de référence du champ B_z par rapport à l'axe de référence du système hélicoïdal. Seuls ces deux derniers déplacements apportent des perturbations. Nous étudions ici, à titre d'exemple, le déplacement angulaire α.

En présence d'une telle perturbation, la périodicité de la configuration est ramenée à $P = 1$. On doit donc s'attendre à voir apparaître une famille de deux îlots au voisinage de $\iota/2\pi = \frac{1}{2}$, de trois îlots au voisinage de $\iota/2\pi = \frac{1}{3}$, etc ...

La Figure 7a montre le voisinage de $\iota/2\pi = \frac{1}{2}$ dans une configuration Torsatron $\ell = 3$ $m = 3$; avec $\alpha = 3$ minutes d'arc. On constate que la largeur des ilots est proportionnelle à $\sqrt{\alpha}$. La taille des îlots diminue vers l'intérieur de la configuration et nous n'en avons pas observé pour $\iota/2\pi < \frac{1}{4}$. D'autre part, même lorsque les îlots sont larges ($\Delta\rho > 1$ cm), pourvu qu'il n'y ait pas recouvrement entre deux familles d'îlots voisines, les lignes magnétiques sont confinées de façon stable sur les îlots.

On doit noter que la présence du champ magnétique terrestre correspond à une déformation d'ensemble non négligeable qui peut donner naissance à des îlots de plusieurs millimètres de largeur sur une configuration avec un niveau de champ moyen de 5 kG.

Pour limiter les déplacements d'ensemble, on réalisera le champ à l'aide d'une série de bobines situées dans des plans méridiens. Ces bobines seront positionnées individuellement par rapport aux enroulements hélicoïdaux. Il subsistera néanmoins des erreurs aléatoires locales de positionnement.

III-3-2. Défauts locaux aléatoires

Ces défauts correspondent à des perturbations sensiblement moins dangereuses que les déplacements d'ensemble étudiés dans le paragraphe précédent. Nous étudierons ici à titre d'exemple les effets des erreurs de position Δz des bobines créant le champ azimutal B_φ. Les autres déplacements possibles donnent, pour des écarts mécaniques comparables, des effets quantitativement équivalents.

La configuration de référence, pour cette étude, est une configuration torsatron $\ell = 4$ $m = 3$ dans laquelle le champ azimutal B_φ est créé par un ensemble de 24 bobines régulièrement espacées en φ.

Dans le cas de déplacements Δz_i des différentes bobines ($i = 1 ; \ldots 24$) on peut décomposer la perturbation résultante en série de Fourrier en φ. Le terme fondamental (valeur moyenne de Δz_i) représente un déplacement d'ensemble qui n'apporte pas de perturbation. Le premier harmonique ($P = 1$) correspond à un déplacement d'ensemble du type étudié au paragraphe précédent.

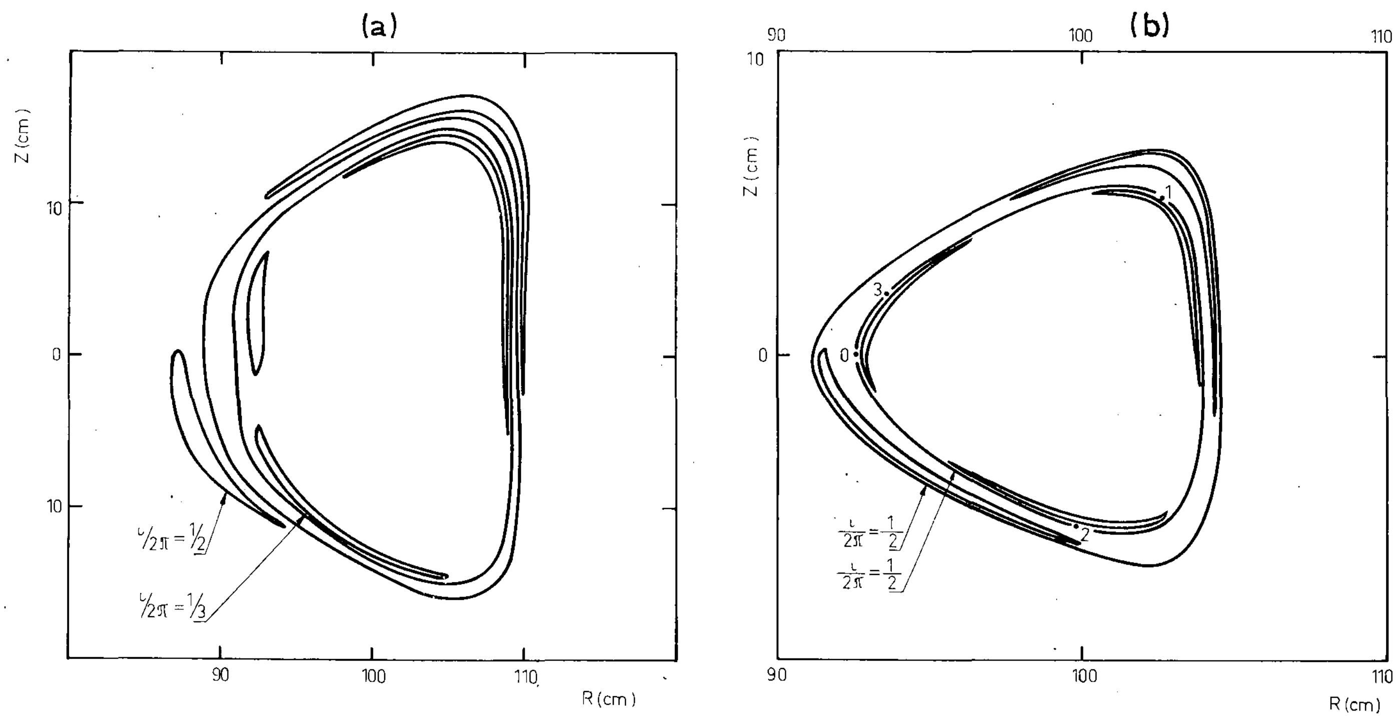

FIG. 7. Famille d'îlots apparaissant par suite d'un déplacement d'ensemble (Oz, Oz') = 10^{-3} de l'axe de référence du champ B_φ par rapport à l'axe du tore: a) sur la configuration $\ell = 3$, m = 3 torsatron corrigée; b) sur la configuration stellarator classique $\ell = 3$, m = 3.

En déplaçant une seule bobine de ΔZ, l'harmonique $P = 1$ est dominant et on voit apparaître trois îlots au voisinage de $\iota/2\pi = \frac{1}{3}$ et quatre îlots au voisinage de $\iota/2\pi = \frac{1}{4}$. La largeur de ces îlots varie comme $\sqrt{\Delta Z}$ et vaut 1 cm pour $\Delta Z = 2$ mm pour $\iota/2\pi = \frac{1}{3}$. Si on déplace de la même quantité ΔZ deux bobines diamétralement opposées ($P = 2$) on voit apparaître un nombre d'îlots double mais leur largeur est réduite d'un facteur 2.

Dans le cas de déplacements aléatoires de toutes les bobines, la décomposition contient en général plusieurs harmoniques dont les amplitudes sont d'un ordre de grandeur inférieur à l'amplitude moyenne des écarts ΔZ_i. Nous avons constaté que c'est la période du premier harmonique d'amplitude non négligeable qui détermine le nombre d'ilots. On a trouvé des îlots avec une largeur de l'ordre du millimètre pour une amplitude moyenne des écarts de quelques dixièmes de millimètre.

III-3-3. Comparaison des effets des perturbations sur diverses configurations

L'étude comparative des diverses configurations, du point de vue de leur sensibilité aux perturbations, a montré qu'elles y étaient toutes sensibles. Cette étude a permis de dégager les conclusions générales suivantes :

Nous avons trouvé des chaînes d'îlots correspondant à $\iota/2\pi = \frac{1}{2}$; $\frac{2}{5}$; $\frac{1}{3}$; $\frac{2}{7}$; $\frac{1}{4}$. Nous avons constaté que les surfaces externes étaient les plus sensibles aux perturbations. En particulier, nous n'avons pas trouvé d'îlot dans la partie centrale du volume utile ($\iota/2\pi < 1/4$) pour les configurations $\ell = 3$ $m = 3$ et $\ell = 4$ $m = 4$.
Ce phénomène est à rapprocher de la destruction des surfaces extérieures par effet de courbure.

Le nombre des îlots sur chaque chaîne correspond à la formule donnée au paragraphe III-1 où P est la périodicité de la configuration perturbée.

La variation de largeur des îlots le long d'une chaîne est bien représentée par $\Delta\rho \propto \left(\frac{d\iota_p}{d\rho}\right)^{-1/2}$ où ι_p est la valeur locale de la transformation rotationnelle définie au paragraphe II-1.

D'une façon plus globale, on constate que la largeur moyenne $\Delta\rho$ des îlots dans la région extérieure de la configuration varie comme $(\Delta\iota/\bar{\rho})^{-1/2}$; il en résulte que $\Delta\rho/\bar{\rho} \propto Q^{-1/2}$ où Q est le facteur de qualité défini au paragraphe II-3.

Nous donnons, à titre d'exemple, sur la Figure 7(a-b), la comparaison des effets d'un déplacement d'ensemble $OZ, OZ' = \alpha = 10^{-3}$ sur les configurations $\ell = 3$ $m = 3$ Stellarator classique et Torsatron corrigé. Nous constatons que les effets sont du même ordre de grandeur. La valeur $\Delta\rho/\bar{\rho}$ est toutefois deux fois plus faible dans le cas du Stellarator classique. Ceci tient au fait que dans cette configuration la totalité du cisaillement est pratiquement localisée au voisinage des surfaces externes.

IV. ETUDE DU CONFINEMENT DES PARTICULES

L'étude du confinement des particules est faite par intégration numérique de la trajectoire du centre guide dans l'approximation du mouvement adiabatique. Cette étude montre l'existence de particules piégées et permet de déterminer l'angle solide de perte perpendiculaire en chaque point du volume utile.

L'effet de miroir longitudinal qui conduit à l'existence de particules piégées et à l'existence d'un cône de perte perpendiculaire est caractérisé sur chaque surface magnétique par la valeur du rapport de miroir maximum $\eta = B_{max}/B_{min}$.

Pour la configuration Stellarator classique $\ell = 3$; $m = 3$ avec $R/a = 4{,}44$, η vaut 1,20 sur la dernière surface magnétique fermée.

Pour le Torsatron corrigé $\ell = 4$ $m = 3$ $R/a = 4{,}44$, η atteint la valeur 1,53 .

Nous avons reporté dans le tableau I la valeur de η pour certaines configurations étudiées.

Si l'on tient compte de la variation spatiale du rapport de miroir à l'intérieur du volume utile et si l'on admet un profil de densité raisonnable, on constate que 10 % d'une population initialement maxwellienne subit l'effet de miroir dans le stellarator classique et que la proportion atteint 20 % dans le torsatron $\ell = 4$.

REFERENCES

[1] ROSENBLUTH M.N., SAGDEEV R.Z., TAYLOR J.B. et ZASLAVSKY G.M. - Nuclear Fusion 6 (1966) 297.

[2] FILONENKO N.N., SAGDEEV R.Z., et SASLAVSKY G.M. - Nuclear Fusion 7 (1967) 253 .

[3] GIBSON A - Physics of Fluids 10 (1967) 1553 .

[4] GOURDON C., MARTY D. et VUILLEMIN M. - Bull. Am. Phys. Soc. 13 (1968) 287.

[5] FURTH H.P., JOHNSON J.L. et SHEFFIELD G.V. Bull. Am. Phys. Soc. 13 (1968) 287.

[6] FREIS R.P., HARTMAN C.W. et KILLEEN J. Bull. Am. Phys. Soc. 13 (1968) 276.

[7] ALEKSIN V.F. - Compte Rendus de la 3ème conférence sur la Physique des plasmas et réactions thermonucleaires contrôlées, Kharkov, 1962, p. 216 , Editeur K.D. Sinelnikov.

[8] Voir par exemple :
MOROZOV A.I. et SOLIVIEV L.S. - Geometrija magnitonogo polja (Geometrie du champ magnétique), Voprosy teorii plazmy 2, Gosatomizdat, Moscou 1963, Editeur Leontovich, M.A.

DISCUSSION

A. GIBSON: In your oral presentation, you showed two examples of the effect of a relative tilt between the toroidal and helical fields. In the first, the surfaces were almost entirely fragmented, while in the second only the outer layers were destroyed. What was the difference between these two cases?

C.H. GOURDON: The first slide, which is reproduced below and in which the surfaces are almost entirely fragmented, corresponds to a perturbation (OZ, OZ') $= \alpha = 30$ minutes of arc. The second slide (Fig. 7b in the paper) corresponds to (OZ, OZ') = 3 minutes of arc. In the case of very small angles the surfaces are not completely fragmented, but islands with widths proportional to $\sqrt{\alpha}$ appear.

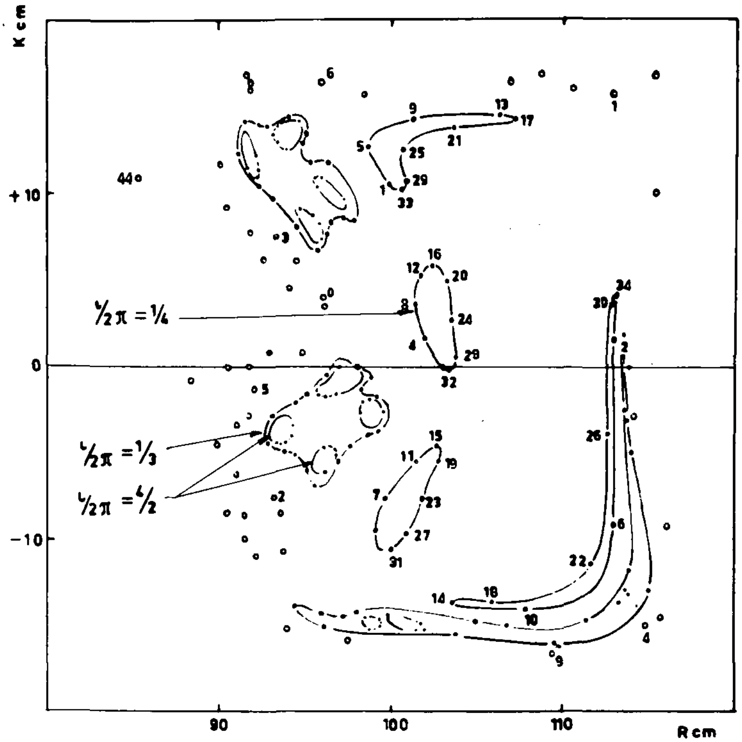

CONFIGURATION OCTOPOLAIRE DE RÉFÉRENCE

PERTUBATION (OZ, O'Z') = 30 minutes d'Arc

A. GIBSON: Does the complete fragmentation of the surfaces which occurred because of a tilt in a system with three unidirectional helical currents also occur for a similar tilt in a system with six currents of alternate size?

C.H. GOURDON: Whatever the configuration (stellarator or torsatron), the magnetic surfaces are destroyed at high values of α. Destruction proceeds with increasing α, beginning with the outer layers, and is more rapid in cases of weak shear. With equal shear the two configurations are equally sensitive.

УСТОЙЧИВОСТЬ ПЛАЗМЫ В ДВУХЗАХОДНОМ ПОЛЕ С ВИНТОВОЙ СИММЕТРИЕЙ

С.Е.РОСИНСКИЙ, В.Г.РУХЛИН и А.А.РУХАДЗЕ
ФИЗИЧЕСКИЙ ИНСТИТУТ им.П.Н.ЛЕБЕДЕВА
АН СССР, МОСКВА,
СССР

Abstract — Аннотация

STABILITY OF A PLASMA IN A STRAIGHT TWO-TURN FIELD WITH HELICAL SYMMETRY. We consider the problem of stable containment of a plasma in a magnetic field with helical symmetry. Using the collisionless kinetic equation of Vlasov, we examine the potential oscillations of a low-pressure plasma in conditions such that perturbation of the vacuum equilibrium magnetic field by the plasma can be neglected. We consider instabilities developing in times short enough so that particle blockage effects are not significant, and also instabilities governed largely by the presence of blocked particles. Particular attention is given to elucidating the effects of complex geometry, especially the influence of local shear and variable curvature on instability growth. Analyses of oscillation stability have shown that oscillations which are not too highly localized (developing in times small compared with the time of particle transit over a distance equivalent to the helical winding pitch) are well stabilized by mean square local shear. This stabilizing effect is much stronger than the square of mean shear which stabilizes strongly localized oscillations. In these conditions the flute instability does not show up at all. The oscillations can be unstable only as a result of the Larmor drift of the particles, when the increment of unstable perturbations is small compared with the Larmor drift frequency. However, these instabilities are not dangerous either, since they are easily stabilized by mean square local shear. Particle blockage and variable curvature of the lines of force of the magnetic field result in a number of new instabilities, apart from those already found in the work of Kadomtsev et al. and Rosenbluth et al. Some of these are hydrodynamic and can be stabilized by shear. When we allow for the thermal velocity spread of the particles a number of kinetic instabilities appear, some of which are in fact difficult to deal with because they are not adequately stabilized by shear.

УСТОЙЧИВОСТЬ ПЛАЗМЫ В ДВУХЗАХОДНОМ ПОЛЕ С ВИНТОВОЙ СИММЕТРИЕЙ. С помощью бесстолкновительного кинетического уравнения исследуются потенциальные колебания плазмы в прямом двухзаходном поле с винтовой симметрией. В системах рассматриваемого типа наиболее опасными являются неустойчивые колебания с частотами, малыми по сравнению с частотой колебаний запертых частиц между пробками магнитного поля, и с продольными длинами волн, большими по сравнению с шагом токовой обмотки. Помимо неустойчивости на запертых частицах, найденной в работе Кадомцева и Погуце, показано существование обычной желобковой неустойчивости, обусловленной дрейфом запертых частиц и обладающей большим инкрементом. Эта неустойчивость может быть стабилизирована широм и конечным ларморовским радиусом ионов. Показано, что в магнитном поле с периодической кривизной резонансное взаимодействие квазипериодического движения частиц с нормальными колебаниями плазмы приводит к раскачке этих колебаний. При этом резонансное взаимодействие чисто периодического движения запертых частиц также приводит к кинетическим неустойчивостям, но с гораздо меньшими инкрементами. Если фазовая скорость волны вдоль средней силовой линии магнитного поля становится меньше продольной скорости медленнопролетных частиц, то инкременты обычных кинетических неустойчивостей значительно уменьшаются. Кроме того, исследованы новые неустойчивые спектры, существенно обусловленные эффектом запертости частиц, а также получены критерии стабилизации широм и конечным ларморовским радиусом таких неустойчивых колебаний.

1. ВВЕДЕНИЕ

В последнее время возрос интерес к теории колебаний и устойчивости плазмы в системах со сложной геометрией магнитного поля (то-есть обладающих переменной кривизной силовых линий, гофрировкой, вращательным преобразованием и тороидальностью). Это связано с тем,что большинство экспериментов сейчас проводится именно на установках со сложной конфигурацией силовых линий магнитного поля (Токамак, стелларатор и др.),поскольку в системах с относительно простой конфигурацией магнитного поля,как показывали многочисленные исследования, возникают неустойчивости, приводящие к развалу плазмы.

Как известно,в системах с неоднородностью вдоль магнитного поля существуют две группы частиц, существенно отличающиеся по характеру движения: запертые частицы, совершающие колебания между магнитными пробками, и пролетные частицы, которые свободно движутся вдоль силовых линий магнитного поля. Соответственно этому могут развиваться физически различные типы неустойчивых колебаний,связанные с эффектом запертости частиц[1] и резонансным взаимодействием между волной и квазипериодическим движением пролетных частиц [2] , между волной и колебаниями запертых частиц и,наконец, между волной и средним движением медленнопролетных частиц.В работах [1,2] рассматривались лишь отдельные упрощенные задачи, выявляющие тот или иной определенный эффект.Например, в работе [1] полностью пренебрегалось продольным движением пролетных частиц, а в работе [2] рассматривалось модельное магнитное поле в плоской геометрии.

В настоящей работе исследуются колебания плазмы в конкретном магнитном поле, созданном двумя винтовыми обмотками с противоположными направлениями токов в них (прямое двухзаходное поле). На примере этого поля,обладающего периодической кривизной, гофрировкой и средним углом прокручивания силовых линий, исследуются колебания плазмы, которые могут иметь место в реальных установках.

В §§2,3 рассмотрено равновесное состояние плазмы в таком поле и получены уравнения малых колебаний. В §4 проводится исследование решений этих уравнений в различных областях частот.

Следует отметить,что помимо обычного (черенковского) резонансного взаимодействия волны с продольным движением частиц и известного резонанса,обусловленного периодической кривизной магнитного поля[2], в системах рассматриваемого типа возникают резонансы другого характера, обусловленные как колебательным движением запертых частиц, так и квазипериодическим движением пролетных частиц. Это,в свою очередь, приводит к новым типам кинетических неустойчивостей, причем характер той или иной неустойчивости определяется областью частот колебаний. Если частота колебаний велика по сравнению со всеми характерными частотами движения частиц (точнее, ведущих центров),то резонансные эффекты экспоненциально малы и различие в характере движения пролетных и запертых частиц не проявляется. В области промежуточных частот (частота велика по сравнению с характерной частотой колебаний запертых частиц, но мала по сравнению с обратным временем прохождения быстропролетной частицей расстояния, равного пространственному периоду изменения магнитного поля) сказывается резонанс, обусловленный наличием периодической кривизны[2] ,а также резонанс,связанный с периодическим изменением продольной скорости быстропролетных частиц. Наконец,в области самых низких частот начинают играть роль резонансы на запертых и медленнопролетных частицах.

Это физическое различие в характере движения частиц приводит к необходимости различного аналитического описания в зависимости от частоты исследуемых колебаний. Исследование колебаний на устойчивость удобно, как обычно, проводить в трех областях частот в зависимости от соотношения между фазовой скоростью волны ($\omega/\bar{k}_{\parallel}$) и тепловыми скоростями частиц.

Для выявления наиболее опасных неустойчивостей и возможности их стабилизации мы зададимся определенными параметрами, характерными для существующих установок (стелларатор типа "Ливень" ФИАН): малый радиус тора r_0 =2см, большой радиус тора R_0 =60см, параметр $\mathcal{E}$ (см.ниже) $\simeq$ 0,3, плотность частиц N =10^{11} см$^{-3}$, температура T =15 эв ($T_e \simeq T_i$),напряженность магнитного поля $B_0 \approx 5.10^3$ э, число витков токовой обмотки n=7. Отметим,что хотя изложенная теория относится к прямой системе, ввиду малости тороидального отношения ($\frac{r_0}{R_0} \sim \mathcal{E}\rho^2$, $\rho \sim n\frac{r_0}{R_0}$) приводимые нами оценки могут быть качественно применимы и для такой тороидальной системы.

При исследовании устойчивости особое внимание будет уделено возникновению и стабилизации неустойчивых спектров колебаний, не имеющих места в системах с простой конфигурацией силовых линий магнитного поля, а известные в таких системах неустойчивые спектры (и условия их стабилизации), которые также могут иметь место в рассматриваемой нами системе, будут вынесены в сводную таблицу, приведенную в конце статьи.

2. РАВНОВЕСНОЕ СОСТОЯНИЕ

Рассмотрим равновесное состояние плазмы в прямом двухзаходном винтовом поле, которое в цилиндрической системе координат записывается в виде [3]

$$B_r = 2\mathcal{E}B_0 I_2' \sin 2\theta;\quad B_\varphi = 2\mathcal{E}B_0\frac{I_2}{\rho}\cos 2\theta;\quad B_z = B_0\left[1 - 2\mathcal{E}I_2\cos 2\theta\right] \tag{2.1}$$

где $\theta = \varphi - \alpha z$, $\mathcal{E}$ - безразмерный параметр, $\rho = \alpha r$, $\alpha = \frac{2\pi}{L_{об}}$, $L_{об}$ - шаг токовой обмотки, а $I_2 = I_2(2\rho)$ - функция Бесселя от мнимого аргумента.

Рассматривая плазму низкого давления, будем пренебрегать поправками к вакуумному магнитному полю. В дальнейшем нам будет удобно ввести систему координат $\{x^1, x^2, x^3\}$, связанную с магнитной поверхностью, поэтому в качестве координаты x^1 выберем координату магнитной поверхности

$$\Psi = r\sqrt{1 - 2\varepsilon \frac{I_2'}{\rho}\cos 2\theta} \qquad (2.2)$$

Вторую и третью координаты выберем из тех соображений, чтобы, во-первых, силовые линии на магнитной поверхности были прямыми и, во-вторых, по одной из переменных, например, x^2, любая физическая величина была бы периодической функцией. За координату x^2 примем θ, а для нахождения третьей координаты x^3 будем исходить из уравнения силовой линии в координатах $\{\Psi, \theta, z\}$ на магнитной поверхности

$$\frac{d\theta}{B^\theta} = \frac{dz}{B^z} \qquad (2.3)$$

где $B^i = \vec{B}\,\nabla x^i$ – контравариантные компоненты вектора магнитного поля. Используя (2.2), величины B^θ и B^z можно выразить только через θ и Ψ, а потому, интегрируя (2.3), получим

$$z - \int \frac{B^z}{B^\theta}\, d\theta = \mathrm{Const} \qquad (2.4)$$

Разбивая $\frac{B^z}{B^\theta}$ на постоянную и переменную части и вводя новую координату $x^3 = \xi = z - \int \widetilde{\frac{B^z}{B^\theta}}\, d\theta$, уравнение (2.4) в переменных (Ψ, θ, ξ) приведем к уравнению прямых силовых линий на магнитной поверхности

$$\theta - \mu^{-1}\xi = \mathrm{const} \qquad (2.5)$$

где $\mu^{-1}(\Psi) = \frac{1}{2\pi}\int_0^{2\pi} \frac{B^z}{B^\theta}\, d\theta = \overline{\frac{B^z}{B^\theta}}$. Во введенной системе координат метрический тензор g_{ij} и контравариантные компоненты магнитного поля имеют вид:

$$g_{ij}=\begin{pmatrix} \alpha_1^2+(1+\rho^2)\alpha_3^2; & g_{21}; & g_{31} \\ \alpha_1\alpha_2+(1+\rho^2)\alpha_3\alpha_4; & \frac{\rho^2}{\alpha^2}+\alpha_2^2+(1+\rho^2)\alpha_4^2+2\frac{\rho^2}{\alpha}\alpha_4; & g_{32} \\ (1+\rho^2)\alpha_3; & \frac{\rho^2}{\alpha}+(1+\rho^2)\alpha_4 & 1+\rho^2 \end{pmatrix} \tag{2.6}$$

$$B^i=\{B^\psi,B^\theta,B^z\}=\left\{0,\alpha\left(\frac{B_\varphi}{\rho}-B_z\right),\frac{B^\theta}{\mu}\right\}$$

где $\alpha_1=\left(\frac{\partial z}{\partial\psi}\right)_\theta$; $\alpha_2=\left(\frac{\partial z}{\partial\theta}\right)_\psi$; $\alpha_3=\left(\frac{\partial z}{\partial\psi}\right)_{\theta,\xi}$; $\alpha_4=\left(\frac{\partial z}{\partial\theta}\right)_{\psi,\xi}$

Равновесная функция распределения для ионов и электронов удовлетворяет стационарному кинетическому уравнению

$$\vec{v}\nabla f^0+[\vec{v}\cdot\vec{\Omega}]\frac{\partial}{\partial\vec{v}}f^0=0 \tag{2.7}$$

Далее удобно будет связать систему координат в пространстве скоростей с силовой линией магнитного поля, положив:

$$\vec{v}=v_\parallel\vec{\tau}_0+v_\perp(\vec{\tau}_1\cos\varphi+\vec{\tau}_2\sin\varphi), \tag{2.8}$$

где $\vec{\tau}_0=\frac{\vec{B}}{B}$, а $\vec{\tau}_1$ и $\vec{\tau}_2$ – ортогональные орты в плоскости, перпендикулярной к силовой линии, φ –азимут в этой плоскости. Одной из точных характеристик уравнения (2.7) является $v^2=Const$. Для нахождения другой характеристики возьмем первую контравариантную компоненту от векторного уравнения движения $d\vec{r}=\vec{v}dt$. Полагая $\vec{\tau}_1=\frac{\nabla\psi}{|\nabla\psi|}$, получим

$$d\psi=\vec{v}\nabla\psi dt=v_\perp|\nabla\psi|\cos\varphi dt$$

В приближении слабой неоднородности, когда ларморовский радиус частиц мал по сравнению с характерным масштабом неоднородности равновесных функций, $d\varphi\simeq-\Omega dt$, а ψ и $v_\perp$ мало меняются вдоль траекторий частиц. Учитывая это, получим следующую приближенную характеристику:

$$\psi^*=\psi+\frac{v_\perp}{\Omega}|\nabla\psi|\sin\varphi\simeq Const \tag{2.9}$$

Тогда в качестве равновесной функции можно взять функцию от характеристик v^2 и ψ^*, близкую к локальному максвелловскому распределению F^0:

$$f^0 = f^0(v^2, \psi^*) \approx \left(1 + \frac{v_\perp \sin\varphi}{\Omega} |\nabla\psi| \frac{\partial^0}{\partial\psi}\right) F^0(v^2, \psi) \qquad (2.10)$$

где $$\frac{\partial^0}{\partial\psi} = \frac{\partial T}{\partial\psi}\frac{\partial}{\partial T} + \frac{\partial N}{\partial\psi}\frac{\partial}{\partial N}$$

Выбор равновесной функции в виде (2.10) физически соответствует тому, что давление плазмы $P = \sum NT$ на данной магнитной поверхности почти постоянно и отвечает гидродинамическому условию равновесия.

3. УРАВНЕНИЕ МАЛЫХ КОЛЕБАНИЙ

Для рассматриваемой нами плазмы низкого давления колебания поля можно считать потенциальными, т.е. $\vec{E} = -\nabla\varphi$. Возмущенная функция распределения при этом определяется как решение линеаризованного кинетического уравнения:

$$\left\{\frac{\partial}{\partial t} + \vec{v}\nabla + [\vec{v} \times \vec{\Omega}]\frac{\partial}{\partial\vec{v}}\right\} f = \frac{e}{m}\nabla\varphi \frac{\partial f^0}{\partial\vec{v}} \qquad (3.1)$$

Ввиду того, что равновесные величины не являются функциями ξ, а по θ должно быть все периодично, возмущенные потенциал и функцию распределения можно представить в виде:

$$\varphi = \sum_\ell \int dk \exp(ik\psi + i\ell\theta + ik_\xi \xi - i\omega t)\, \varphi_\ell(k,\omega) \qquad (3.2)$$

$$f_\ell = \sum_\ell \int dk \exp(ik\psi + i\ell\theta + ik_\xi \xi - i\omega t)\, f_\ell(\vec{v}, \psi, \theta, k, \omega)$$

Здесь компоненты Фурье возмущенной функции распределения определяются по формуле:

$$f_\ell = -\frac{e}{T}\varphi\left\{1 + i\left[\omega - \frac{k^* v_T^2}{\Omega}\frac{\partial^0}{\partial\psi}\right]\int_0^\infty d\tau \exp(i\omega\tau + ik_i\Delta x^i)\right\} F_0 \qquad (3.3)$$

где $k^* = k[\vec{\tau}_0 \cdot \nabla\psi]$, $k_i = \{k, \ell, k_\xi\}$, $\tau = -\Delta t$, а $\Delta x^i = \{\Delta\psi, \Delta\theta, \Delta\xi\}$ – изменение координат частицы при движении вдоль траектории за время Δt. Для нахождения Δx^i необходимо решить систему уравнений движения. В сильном магнитном поле движение частиц носит дрейфовый характер, и изменение координат частицы записывается в виде

$$\Delta X^i = \Delta \bar{X}^i + \frac{v_\perp}{\Omega}\left(\tau_1^{\,i}\Delta\cos\varphi + \tau_2^{\,i}\Delta\sin\varphi\right) \qquad (3.4)$$

где смещение координаты $\bar{X}_i$ ведущего центра частицы определяется решением системы уравнений в дрейфовом приближении (черту усреднения для простоты опускаем)

$$\frac{dX^i}{dt} = v_\parallel \tau_0^{\,i} + \frac{v_\perp^2 + 2v_\parallel^2}{2\Omega}\left[\vec{\tau}_0 \nabla \ln B\right]^i \qquad (3.5)$$

$$v^2 = const, \quad \mu_0 = \frac{v_\perp^2}{B} = const$$

Здесь μ_0 - поперечный адиабатический инвариант.

Систему уравнений (3.5) будем решать при условии малости параметра[1] $\mathcal{E}$. В разложении модуля поля B можно ограничиться при этом членами $\sim\mathcal{E}$. Тогда из двух последних уравнений (3.5) получим следующую зависимость скорости продольного движения частицы вдоль траектории от координат:

$$v_\parallel = \sigma v_{\parallel 0}\sqrt{1 - \varkappa^{-2}\sin^2\theta}, \qquad (3.6)$$

где $v_{\parallel 0} = \sqrt{v^2 - \mu_0 B_{min}}$, $\varkappa^{-2} = 4\mathcal{E}\mu_0 B I_2 / v_{\parallel 0}^2$, $B_{min} = B(\theta=0)$, $\sigma = \mathrm{sgn}\, v_\parallel$

Из формулы (3.6) вытекает, что значение $\varkappa = 1$ разделяет частицы на запертые и пролетные. При $\varkappa < 1$ частицы движутся в ограниченных областях по θ, совершая колебания с амплитудой $\theta_0 = \arcsin\varkappa$ около точек $\theta = \pi m$, $m = 0, \pm 1 \ldots$ и периодом

$$T_3 = \frac{4}{\alpha v_{\parallel 0}}\varkappa K(\varkappa) \qquad (3.7)$$

где $K(\varkappa)$ - полный эллиптический интеграл первого рода. Продольная скорость запертых частиц мала по сравнению с поперечной ($v_\parallel \lesssim \sqrt{\mathcal{E} I_2}\, v_\perp$). При $\varkappa > 1$ частицы движутся всегда в

[1] Если учесть, что плазма находится в области, ограниченной сепаратриссой магнитного поля, то для реальных установок ($\mathcal{E}\sim 0{,}3$) сепаратрисса лежит на расстоянии $\rho \sim 1$ (см., например, работы [3] стр. 42) и можно ограничиться рассмотрением расстояний $\rho \lesssim 1$. При этом $I_2(2\rho) < 1$.

одном направлении ($\sigma = const$), причем удвоенный период изменения их продольной скорости

$$T_{np} = \frac{4}{\alpha v_{\parallel 0}} K(\varkappa^{-1}) \tag{3.8}$$

непосредственно переходит в период колебаний запертых частиц при $\varkappa < 1$.

Возмущенный потенциал ϕ удовлетворяет уравнению

$$\Delta \phi = 4\pi \sum e \int f d\vec{v} \tag{3.9}$$

Здесь и ниже знак $\sum$ означает суммирование по сортам частиц.

Подставляя выражение для возмущенной функции распределения (3.2) в уравнение (3.9), получим интегродифференциальное уравнение для Ф

$$\Delta \phi = \sum \sum_{\ell} \int dk e^{ik_i x^i} \phi_\ell(k, k_\xi, \omega) K(\omega, \ell, k, k_\xi, \psi, \theta)$$
$$K = \frac{4\pi e^2 N}{T} \left[1 + \frac{i}{N}\left(\omega - \frac{k^* v_T^2}{\Omega}\frac{\partial^0}{\partial \psi}\right)\right] \int d\vec{v} F^0 \int_0^\infty d\tau e^{i\omega\tau + ik_i \Delta x^i} \tag{3.10}$$

Нам будет удобнее перейти от интегродифференциального уравнения к системе зацепляющихся уравнений. Для этого проинтегрируем уравнение (3.10) по углу θ с весом $e^{-i\ell\theta}$ и воспользуемся тем, что ядро $K(\theta)$ периодично по θ с периодом π. Соответствующую систему уравнений в приближении квазинейтральности возмущений можно привести к виду

$$\sum \sum_{\nu} \int dk\, e^{ik\psi}_{+\pi/2} K_\nu(\ell + 2\nu)\, \phi(\ell + 2\nu) = 0$$
$$K_\nu = \frac{1}{\pi} \int_{-\pi/2} d\theta K(\theta) e^{2i\nu\theta} \tag{3.11}$$

В формуле (3.11) мы перешли от суммирования по ℓ к суммированию по $\nu = \frac{\ell - \ell'}{2}$ и опустили штрих у ℓ'.

Для нахождения явного вида K_ν необходимо знать решения системы уравнений (3.5), которые существенно определяются характерными временами процесса, или, другими словами, частотами рассматриваемых колебаний. Из формул (3.7) и (3.8) следует, что характерное время прохождения запертыми и медленно-пролетными частицами $(\varkappa \sim 1)$ расстояния $L_{об} = \frac{2\pi}{\alpha}$ между двумя последовательными максимумами поля порядка $\sim \frac{1}{\alpha v_T \sqrt{\varepsilon I_2}}$ (т.к. их продольные скорости $v_\parallel \sim v_\perp \sqrt{\varepsilon I_2} \sim v_T \sqrt{\varepsilon I_2}$, где $v_T = \sqrt{\frac{T}{m}}$), тогда как соответствующее время для быстропролетных частиц $\sim \frac{1}{\alpha v_T}$ (так как для них $v_\parallel \sim v_\perp$). Наличие таких характерных времен позволяет нам легко получить коэффициенты K_γ в следующих областях частот: а) $\omega \gg \alpha v_T$; в) $\alpha v_T \sqrt{\varepsilon I_2} \ll \omega \ll \alpha v_T$; с) $\omega \ll \alpha v_T \sqrt{\varepsilon I_2}$.

а) В области высоких частот $\omega \gg \alpha v_T$ не проявляется существенного различия между запертыми и пролетными частицами, поскольку за времена $\Delta t \sim \frac{1}{\omega} \ll \frac{1}{\alpha v_T}$ продольные скорости всех частиц мало меняются. Решая первое уравнение системы (3.5) путем разложения по малому параметру $\Delta t = t' - t = -\tau$ (с точностью до членов второго порядка), получим

$$\Delta X^i = -v_\parallel \tau_0^i \tau - \frac{v_\perp^2 + 2v_\parallel^2}{2\Omega}[\vec{\tau}_0 \nabla \ln B] + \frac{\tau^2}{2}\left[v_\parallel^2 \frac{\partial \tau_0^i}{\partial \theta} - v_\perp^2 \tau_0^i \frac{\partial \ln B}{\partial \theta}\right]\tau_0^2 \tag{3.12}$$

Подстановка выражения (3.12) в формулу (3.10) дает нам выражение для K_γ в рассматриваемой области частот:

$$K_\gamma = \frac{\omega_L^2}{v_T^2}\left[\delta_{\gamma 0} - \frac{\hat{1}}{\pi N}\int_{-\pi/2}^{\pi/2} d\theta\, e^{-2i\gamma\theta} \sum_n \int d\vec{v}\, \frac{J_n^2 F^0}{\tilde{\omega}}\left(1 + i\alpha\, \frac{v_\parallel^2 \frac{\partial K_\parallel}{\partial \theta} - v_\perp^2 K_\parallel \frac{\partial \ln B}{\partial \theta}}{\tilde{\omega}^2}\right)\right] \tag{3.13}$$

где $\tilde{\omega} = \omega - n\Omega - K_\parallel v_\parallel - \frac{K_B (v_\perp^2 + 2v_\parallel^2)}{2\Omega R}$; $K_\parallel = K_i \tau_0^i$; $K_B = K_i[\vec{\tau}_0 \nabla \ln B]R$, $R^{-1} = |[\vec{\tau}_0 \nabla \ln B]|$ – радиус кривизны силовых линий, $\hat{1} = 1 - \frac{K^* v_T^2}{\omega\Omega}\frac{\partial^0}{\partial \psi}$, $J_n = J_n(z)$, $z = K_\perp v_\perp / \Omega$.

в) В промежуточной области частот $\alpha v_T \sqrt{\varepsilon I_2} < \omega < \alpha v_T$ различие в характере движения частиц оказывается уже существенным. Поэтому решение системы уравнений (3.8) для запертых (медленнопролетных) частиц отличается от решения для быстропролетных частиц. Для запертых и медленнопролетных частиц изменение продольной скорости попрежнему мало и, следовательно, справедливо решение (3.12). При нахождении решения системы уравнений (3.5) для быстропролетных частиц поступим следующим образом. В первом приближении по отношению лармоpo вского радиуса к характерному размеру неоднородности поля изменение координат при движении частицы можно представить в виде $\Delta X^{i}=(\Delta X^{i})_{\parallel}+(\Delta X^{i})_{gr}$, где $(\Delta X^{i})_{\parallel}$ определяется продольным движением частицы,а $(\Delta X^{i})_{gr}$ – смещение из-за магнитного дрейфа. Тогда решение уравнения для $(\Delta\theta)_{\parallel}$ можно записать в неявном виде:

$$\Delta t=-\frac{1}{\alpha v_{\parallel 0}}\left\{\int_{\theta}^{\theta+(\Delta\theta)_{\parallel}}\frac{d\theta'}{\sqrt{1-x^{-2}\sin^2\theta'}}-\varepsilon\frac{I_2}{\rho^2}\left[\sin\left(2\theta+(\Delta\theta)_{\parallel}\right)-\sin 2\theta\right]\right\} \tag{3.14}$$

Используя формулы разложения эллиптических функций в ряды Фурье [4] , получим

$$(\Delta\theta)_{\parallel}=\sigma\omega_{np}\tau+\left(2q-\varepsilon\frac{I_2}{\rho^2}\right)\left[\sin 2(\theta+\sigma\omega_{np}\tau)-\sin 2\theta\right],$$

где $\omega_{np}=\frac{2\pi}{T_{np}}$; $q=\exp\left(-\pi\frac{K'(x^{-1})}{K(x^{-1})}\right)$. После этого решение системы уравнений (3.5) принимает вид:

$$\begin{aligned}
\Delta\psi &= \sigma\varepsilon\alpha\frac{2v^2-v_\perp^2}{\Omega\,\omega_{np}}\frac{I_2}{\rho^2}\left[\cos 2(\theta-\sigma\omega_{np}\tau)-\cos 2\theta\right]\\
\Delta\theta &= \sigma\omega_{np}\tau-\frac{\varepsilon\alpha^2}{2}\left[\left(\varepsilon f_2-4q\frac{I_2'}{\rho}\right)\frac{2v^2-v_\perp^2}{2\Omega}-8\varepsilon I_2 I_2'\frac{v^2}{\rho\Omega}\right]\tau+\\
&+\left(2q-\varepsilon\frac{I_2}{\rho^2}+\varepsilon\alpha\frac{2v^2-v_\perp^2}{\rho\Omega v_{\parallel}}I_2'\right)\left[\sin(2\theta-2\omega_{np}\tau\sigma)-\sin 2\theta\right]\\
\Delta\xi &= \mu^{-1}(\Delta\theta)_{\parallel}-\varepsilon^2\alpha\frac{2v^2-v_\perp^2}{4\Omega}f_3\tau
\end{aligned} \tag{3.15}$$

Здесь $\mu^{-1}=\frac{1-\bar{i}}{\alpha}$, $\bar{i}=\frac{\varepsilon^2}{\rho}\frac{d}{d\rho}\frac{I_2 I_2'}{\rho}$ – средний угол прокручивания силовых линий магнитного поля, $f_{2,3}=f_{2,3}(\rho)$ – сложные функции ρ, явный вид которых нам не понадобится,но при $\rho\lesssim 1$ они положительны и порядка единицы.

Так как решение для запертых и медленнопролетных частиц отличается от решения для быстропролетных частиц (вид подинтегральной функции в формуле (3.10) в областях $\varkappa\sim 1$ и $\varkappa\gg 1$ различен),то возникает неопределенность в пределах интегрирования (т.е. граничное значение $\varkappa$,разделяющее области применимости формул (3.12) и (3.15),неопределенно). Эту неопределенность можно устранить,если произвести оценку вклада той и другой области в окончательный результат. Оказывается,что ввиду относительно малого числа запертых и медленнопролетных частиц по сравнению с быстропролетными, а также ввиду того,что магнитный дрейф запертых и медленно-пролетных частиц носит локальный характер (т.е. зависит от θ), вклад их пренебрежимо мал. Кроме того,так как формулы (3.15) имеют довольно широкую область применимости (разложение в ряд Фурье эллиптических функций хорошо сходится вплоть до $\varkappa \sim 1$),то в формуле (3.10) можно ограничиться учетом только пролетных частиц и во всей области интегрирования использовать решение системы уравнений (3.5) в виде (3.15). Тогда выражение для K_ν в области промежуточных частот $\alpha v_T\sqrt{\varepsilon I_2} < \omega < \alpha v_T$ запишется в виде:

$$K_\nu = \frac{\omega_L^2}{v_T^2}\Big[\delta_{\nu 0} - \frac{1}{N}\sum_{p,n}\int_{\varkappa>1} d\vec{v}\,\tilde{\omega}^{-1} J_n^2 F^0 J_p(z_1) J_{p+\nu}(z_1) e^{-i\nu\xi}\Big] \tag{3.16}$$

Здесь $\bar{K}_\parallel = K_\xi + \ell\mu$

$$\tilde{\omega} = \omega - n\Omega - \bar{\omega}_{dr} - (\bar{K}_\parallel - 2p\alpha)v_\parallel$$

$$z_1^2 = \Big[-\Big(2q - \varepsilon\frac{I_2}{\rho^2}\Big)\frac{\bar{K}_\parallel}{\alpha} + \varepsilon\alpha\frac{2v^2 - v_\perp^2}{4\Omega v_\parallel}\frac{I_2'}{\rho}\ell\Big]^2 + \varepsilon^2\Big(\frac{2v^2 - v_\perp^2}{4\Omega v_\parallel}\Big)^2\frac{I_2^2}{\rho^4}K^2,$$

$$\xi = \operatorname{arctg}\frac{\varepsilon I_2 K(2v^2 - v_\perp^2)/2\Omega\rho^2}{-2\Big(2q - \varepsilon\frac{I_2}{\rho^2}\Big)v_\parallel\frac{\bar{K}_\parallel}{\alpha} + \varepsilon\alpha\ell I_2'(2v^2 - v_\perp^2)/2\Omega\rho}$$

$$\bar{\omega}_{dr} = \varepsilon\alpha\Big\{\Big[\frac{\varepsilon}{2}(\alpha f_2\ell + f_3K_\xi) - 2\alpha q\frac{I_2'}{\rho}\ell\Big]\frac{2v^2 - v_\perp^2}{2\Omega} - 4\varepsilon\alpha\ell I_2 I_2'\frac{v^2}{\rho\Omega}\Big\}$$

c) Наконец, в области низких частот $\omega < \alpha v_T\sqrt{\varepsilon I_2}$ основные эффекты проявляются за времена, большие по сравнению с периодом движения частиц. Особенно сильно за такие времена сказывается различие в характере движения ведущих центров запертых и пролетных частиц вдоль силовых линий магнитного поля. Движение захваченных частиц,совершающих много колебаний между локальными пробками магнитного поля, можно аппроксимировать гармоническими колебаниями около положений равновесия $\bar{\Theta}=\pi m$ $(m=0,\pm 1 \ldots)$ с амплитудой $\Theta_0=\arcsin \varkappa$ и периодом T_3. Точное решение уравнений (3.5), выраженное через эллиптические функции и разложенное в тригонометрический ряд по параметру $q<1$, показывает, что такая аппроксимация законна для всех $\varkappa$, не очень близких к единице. Однако, это не существенно, поскольку узкая область значений $\varkappa \approx 1$ дает пренебрежимо малый вклад при интегрировании по $\varkappa$ в выражении для K_ν. Решение системы (3.5) для движения пролетных частиц вдоль магнитного поля можно получить аналогично тому, как это было сделано в пункте в).

При интегрировании дрейфовых членов в (3.5) можно произвести усреднение по соответствующим периодам запертых и пролетных частиц, как это было сделано в работе [1] для захваченных частиц. В результате получим следующее решение системы (3.5)

$$\Delta\Psi=0, \quad \Delta\xi^{3,np}=\mu^{-1}(\Delta\Theta)_{\parallel}^{3,np},$$
$$\Delta\Theta^{3,np}=(\Delta\Theta)_{\parallel}^{3,np}+\alpha^2\,\frac{2v_\parallel^2+v_\perp^2}{2\Omega}\,\gamma\varepsilon\frac{I_2'}{\rho}\tau\,\Theta^{3,np}, \tag{3.17}$$

где $(\Delta\Theta)_{\parallel}^{3}=\pi m-\Theta+\Theta_0\sin(\sigma\omega_3\tau+\beta_m)$,

$$(\Delta\Theta)_{\parallel}^{np}=\sigma\omega_{np}\tau+\left(2q-\varepsilon\frac{I_2}{\rho}\right)\left[\sin 2(\sigma\omega_{np}\tau+\Theta)-\sin 2\Theta\right];$$

$$Q^3=2\frac{E(\varkappa)}{K(\varkappa)}-1, \quad Q^{np}=1-2\varkappa^2\left[1-\frac{E(\varkappa^{-1})}{K(\varkappa^{-1})}\right], \quad \beta_m=\arcsin\frac{\Theta-\pi m}{\Theta_0}$$

$E(\varkappa)$ - полный эллиптический интеграл второго рода. После подстановки (3.17) в формулу (3.10), выражение для K_ν в области $\omega<\alpha v_T\sqrt{\varepsilon I_2}$ приводится к виду:

$$K_\nu=\frac{\omega_L^2}{v_T^2}\left\{\delta_{\nu 0}-\frac{1}{N}\frac{2}{\pi}\int_{-\pi/2}^{\pi/2}d\theta\, e^{2i\nu\theta}\sum_{n,p,\lambda}\left[\int_{\varkappa<1}d\vec{v}\, e^{-i\beta_0\lambda}J_n^2F^0\times\right.\right.$$
$$\times\frac{J_p(z_3)J_{p+\lambda}(z_3)(\omega-n\Omega-\omega_{dp}^3)}{(\omega-n\Omega-\omega_{dp}^3)^2-p^2\omega_3^2}+\int_{\varkappa>1}d\vec{v}\,e^{-2i\lambda\theta}J_n^2F^0\frac{J_p(z_{np})J_{p+\lambda}(z_{np})(\omega-n\Omega-\omega_{dp}^{np})}{(\omega-n\Omega-\omega_{dp}^{np})^2-\left(\frac{K_\parallel}{\alpha}-2p\right)^2\omega_{np}^2} \tag{3.18}$$

где $\omega_{gp}^{з,пр} = -2\varepsilon\alpha^2 \frac{2v^2 - v_\perp^2}{\Omega} \frac{I_2'}{\rho} Q_1^{з,пр}$, $z_з = \frac{\bar{k}_\parallel}{\alpha}\theta_0$, $z_{пр} = \frac{\bar{k}_\parallel}{\alpha}\left(2q - \varepsilon\frac{I_2}{\rho^2}\right)$

При интегрировании по скоростям в формулах (3.I3) и (3.I8) надо перейти от $v_\parallel$ к переменной x по формуле

$$dv_\parallel = v_\perp \sqrt{4\varepsilon I_2}\, \frac{x\,dx}{\sqrt{x^2 - \sin^2\theta}}$$

4. СПЕКТРЫ КОЛЕБАНИЙ. УСТОЙЧИВОСТЬ ПЛАЗМЫ

Полученная в §3 система зацепляющихся уравнений(3.II) для компонент Фурье возмущенного потенциала $\Phi_{\ell+2\nu}$ и выражения (3.I3), (3.I6),(3.I8) для коэффициентов K_ν этой системы позволяют исследовать вопрос об устойчивости потенциальных колебаний плазмы,помещенной в прямое двухзаходное поле с винтовой симметрией. В общем случае нахождение решения бесконечной системы зацепляющихся уравнений ничем не проще решения интегро-дифференциального уравнения. Но,как показывает анализ коэффициентов K_ν, в наиболее интересном случае не слишком малых длин волн вдоль средней силовой линии магнитного поля $(\bar{K}_\parallel < \alpha)$ система (3.II) расцепляется и сводится к системе трех однородных уравнений относительно Φ_ℓ и $\Phi_{\ell\pm2}$. При этом искомое дисперсионное уравнение получается из условия разрешимости этой системы и может быть записано в виде

$$K_0(\ell) - \frac{K_{+1}(\ell+2)K_{-1}(\ell)}{K_0(\ell+2)} - \frac{K_{-1}(\ell-2)K_{+1}(\ell)}{K_0(\ell-2)} = 0 \qquad (4.I)$$

Строго говоря,уравнение (4.I) справедливо только в нулевом пределе геометрической оптики $(K\Delta X \to \infty)$,где ΔX - область локализации колебаний. При исследовании сильно локализованных колебаний $(K\Delta X \sim 1)$ необходимо вместо алгебраического уравнения (4.I) писать соответствующее ему дифференциальное уравнение,что делается простой заменой $K \to -i\frac{\partial}{\partial X}$

Уравнение (4.I) имеет существенно различный вид в зависимости от соотношения между фазовой скоростью волны вдоль усредненной силовой линии магнитного поля $(\omega/\bar{k}_{\parallel})$ и тепловыми скоростями частиц. Поэтому разумно разбить всю область исследуемых частот на три: I) $\omega > k_{\parallel} v_{Te}$; 2) $k_{\parallel} v_{Ti} < \omega < k_{\parallel} v_{Te}$; 3) $\omega < k_{\parallel} v_{Ti}$. Уравнение в любой из этих областей имеет вид

$$\mathcal{D} = \mathcal{D}' + i\sqrt{\frac{\pi}{2}}\,\mathcal{D}'' = 0 \tag{4.2}$$

где эрмитова часть $\mathcal{D}'$ существенно различна в каждой из этих областей, тогда как антиэрмитова часть $\mathcal{D}''$ сильно меняется внутри одной области в зависимости от соотношений между ω и T_{np}^{-1}, T_3^{-1}. I) $\underline{\omega > k_{\parallel} v_{Te}}$. В этой области частот выражения для $\mathcal{D}'$ и $\mathcal{D}''$ имеют вид:

$$\mathcal{D}' = \left(1 - \frac{\omega_{pi}}{\omega}\right) k_{\perp}^2 \rho_i^2 \frac{T_e}{T_i} - \left(1 - \frac{\omega_{pe}}{\omega}\right) \frac{\bar{k}_{\parallel}^2 v_{Te}^2}{\omega^2} - \frac{\Omega_1}{\omega} + \frac{W}{\omega^2} \tag{4.3}$$

$$\mathcal{D}'' = \begin{cases} 0 \ (\text{экспоненциально мало}), & \omega > \alpha v_{Te}; \\ -2\varepsilon \bar{I}_2 \dfrac{\omega_{1e}^{H}(\omega - \omega_{pi})}{\omega - \omega_{pe}} \hat{1}_e \dfrac{\alpha v_{Te}}{\omega^2}, & \alpha v_{Te}\sqrt{\varepsilon \bar{I}_2} < \omega < \alpha v_{Te}; \\ \dfrac{\omega_{1i}^{H}(\omega - \omega_{pi})}{\omega(\omega - \omega_{pe})} \hat{1}_e \left[\left\langle \dfrac{\omega^3}{\omega_{3e}^3} J_1(2\theta_0) \Pi_{0,0}^3 \right\rangle + \left\langle \dfrac{\omega^3}{4\omega_{bpe}^3} \Pi_{0e}^{np} \right\rangle\right], & \alpha v_{Ti} < \omega < \alpha v_{Te}\sqrt{\varepsilon \bar{I}_2}; \\ \dfrac{T_e}{T_i} \hat{1}_i \varepsilon^2 \bar{I}_2^{-2} \dfrac{\alpha^3 v_{Ti}^3}{\omega^3}, & \alpha v_{Ti}\sqrt{\varepsilon \bar{I}_2} < \omega < \alpha v_{Ti}; \\ 2\dfrac{T_e}{T_i} \hat{1}_i \dfrac{k_{\parallel}^2}{\alpha^2} \left\langle \dfrac{\omega^3}{\omega_{3i}^3} \theta_0^2 \left(\Pi_{0,0}^3 - \Pi_{2,0}^{np}\right)\right\rangle, & \omega < \alpha v_{Ti}\sqrt{\varepsilon \bar{I}_2}; \end{cases} \tag{4.4}$$

где
$$\Omega_1 = \begin{cases} 0 & \text{при } \omega > \alpha v_{Te}\sqrt{\varepsilon \bar{I}_2} \text{ и } \omega < \alpha v_{Ti}\sqrt{\varepsilon \bar{I}_2}; \\ \omega_{3e}^{H} \omega_{1e}^{H} \left\langle J_0^2(2\theta_0) \Pi_{01}^3 \right\rangle & \text{при } \sqrt{\varepsilon \bar{I}_2}\,\alpha v_{Ti} < \omega < \sqrt{\varepsilon \bar{I}_2}\,\alpha v_{Te}, \end{cases}$$

$$W = \begin{cases} \left(1 + \dfrac{T_e}{T_i}\right)\omega_{pi}\left(\omega_{0i}^{H} - 2\bar{I}_2 \omega_{1i}^{H}\right), & \omega > \alpha v_{Te}, \\ -4\langle q \rangle \omega_{pe} \omega_{1e}^{H} \varepsilon + \left(1 + \dfrac{T_e}{T_i}\right)\omega_{pi}\left(\omega_{0i}^{H} - 2\bar{I}_2 \omega_{1i}^{H} \varepsilon\right), & \alpha v_{Te}\sqrt{\varepsilon \bar{I}_2} < \omega < \alpha v_{Te}, \\ \omega_{pe}\left[\omega_{3e}^{H} + \varepsilon \dfrac{T_i}{T_e} \omega_{1e}^{H} \left\langle J_0(2\theta_0) \Pi_{01}^3 \right\rangle\right], & \alpha v_{Ti}\sqrt{\varepsilon \bar{I}_2} < \omega < \alpha v_{Te}\sqrt{\varepsilon \bar{I}_2} \\ \left(1 + \dfrac{T_e}{T_i}\right)\omega_{pi}\left(\omega_{3i}^{H} + \omega_{npi}^{H}\right); & \omega < \sqrt{\varepsilon \bar{I}_2}\,\alpha v_{Ti} \end{cases}$$

$$\omega_p = \frac{\ell v_T^2}{\psi \Omega}\frac{\partial \ln NT}{\partial \psi},\quad \omega_0^{M} = -\frac{\varepsilon^2 \alpha v_T^2}{\Omega}\left(K_\xi f_3 + \alpha \ell f_2\right),\quad \omega_1^{M} = -4\alpha^2\varepsilon\frac{\ell v_T^2}{\Omega}\frac{I_2'}{\rho}$$

$$\Pi_{\lambda,\nu}^{3} = \frac{2}{\pi}\int_0^{\theta_0} d\theta\,\frac{\cos(2\nu\theta + \lambda\beta_0)}{\sqrt{x^2 - \sin^2\theta}},\quad \Pi_m^{np} = \frac{2}{\pi}\int_0^{\pi/2} d\theta\,\frac{\cos 2m\theta}{\sqrt{x^2 - \sin^2\theta}}$$

$$\omega_{3,np}^{M} = 6\varepsilon\alpha^2\,\frac{\ell v_T^2}{\Omega}\frac{I_2'}{\rho}\left\langle Q^{3,np}\,\Pi_{0,0}^{3,np}\right\rangle$$

$$\langle f_3\rangle = \sqrt{\varepsilon I_2}\int_0^1 f_3\,dx^2;\qquad \langle f_{np}\rangle = \sqrt{\varepsilon I_2}\int_1^\infty \frac{dx^2}{\left(1+4x^2\varepsilon I_2\right)^{5/2}}$$

Здесь и в дальнейшем под $K_\parallel$ будет пониматься $\overline{K_\parallel}$.

Ввиду того, что антиэрмитовская часть уравнения (4.2) мала, основные спектры частот колебаний определяются как решения уравнения

$$\mathcal{D}' = \left(1 - \frac{\omega_{pi}}{\omega}\right)K_\perp^2\rho_i^2\frac{T_e}{T_i} - \left(1 - \frac{\omega_{pe}}{\omega}\right)\frac{K_\parallel^2 v_{Te}^2}{\omega^2} - \frac{\Omega_1}{\omega} + \frac{W}{\omega^2} = 0 \qquad (4.5)$$

Анализ возможных спектров уравнения (4.5) начнем с исследования желобковых неустойчивостей, обусловленных кривизной магнитного поля. В зависимости от области частот колебаний в рассматриваемой системе с переменной кривизной силовых линий магнитного поля может проявляться как средний дрейф частиц, обусловленный средней кривизной $\bar{R}^{-1} \sim \alpha\varepsilon^2\rho^3$, так и локальный, определяемый локальной кривизной силовых линий $\tilde{R}^{-1} \sim \alpha\varepsilon\rho$. При этом среднюю кривизну поля чувствуют в основном быстропролетные частицы, тогда как запертые и медленнопролетные частицы ощущают в первую очередь влияние локальной кривизны магнитного поля. Сильно запертые $x \ll 1$ и быстропролетные $x \gg 1$ частицы в основном находятся в области неблагоприятной кривизны магнитного поля и могут привести к желобковым неустойчивостям, в то время как слабозапертые и медленнопролетные частицы основную часть времени проводят в области благоприятной кривизны, а потому оказывают некоторое стабилизирующее влияние.

Замечая, что в области частот $\omega > \alpha v_{Te}\sqrt{\varepsilon I_2}$ и $\omega < \alpha v_{Ti}\sqrt{\varepsilon I_2}$ величина $\Omega_1 = 0$, а последний член в уравнении (4.5) равен

$$W = K_\perp^2 \rho_i^2 \frac{v_{Ti}}{a R_{эфф}} \left(1 + \frac{T_e}{T_i}\right) \quad (4.6)$$

где $a = \left|\frac{d \ln NT}{d\psi}\right|^{-1}$, $R_{эфф}$ - эффективный радиус кривизны, различный в разных областях частот, легко видеть, что уравнение (4.5) описывает обычные желобковые колебания плазмы, инкремент развития и условие стабилизации широм которых имеют вид[5]

$$\gamma_{max} \simeq \frac{v_{Ti}}{\sqrt{a R_{эфф}}} \left(1 + \frac{T_e}{T_i}\right) \quad (4.7)$$

$$\Theta = a \left|\frac{K_\parallel'}{K_\theta}\right| > 4 \frac{a}{R_{эфф}} \sqrt{\frac{m}{M}} \quad (4.8)$$

Подставляя в определение Θ значение продольного волнового числа $K_\parallel = -\alpha\left[\ell + \frac{K_\xi}{\alpha}(1 - \bar{i})\right]$ и производя дифференцирование среднего угла прокручивания $\bar{i}$ (см.(3.15)) по магнитной поверхности ψ, получим (при $\rho \ll 1$)

$$\Theta \approx 2\alpha a \varepsilon^2 \rho^2 \quad (4.9)$$

В области высоких частот $\omega > \alpha v_{Te}$ эффективный радиус кривизны по порядку величины совпадает со средним радиусом $\bar{R}$, и поэтому желобковые неустойчивости легко стабилизированы широм; критерий стабилизации (4.8) при этом сводится к неравенству $\rho\sqrt{\frac{m}{M}} < 1$. Более того, эта неустойчивость вообще не может развиваться в реальной установке, поскольку она возможна лишь на больших расстояниях от оси системы $r \gg a\sqrt{\frac{m}{M}}$ (когда член с магнитным дрейфом в уравнении(4.5)может сравниться с членом $K_\perp^2\rho_i^2$), где фактически отсутствует плазма.

Желобковая неустойчивость реально может иметь место лишь в области низких частот $\omega < \alpha v_{Ti}\sqrt{\varepsilon I_2}$, когда магнитный дрейф обусловлен в основном движением сильнозапертых частиц, а слабозапертые и медленнопролетные частицы дают стабилизирующий (но малый) вклад в эффективную кривизну. Эффективный радиус кривизны в данном случае порядка $\frac{\tilde{R}}{\sqrt{\varepsilon I_2}}$, так как число запертых частиц в $\sqrt{\varepsilon I_2}$ раз меньше полного числа частиц. Он равен

$$R_{эфф} = \tilde{R}\frac{1}{q_1\sqrt{\varepsilon I_2}}, \quad \tilde{R}^{-1} = \alpha\varepsilon\rho$$

$$q_1 = \frac{12}{\pi}\frac{I_2}{\rho^2}\int_0^1 d\varkappa^2\left[2E-K+\frac{\varkappa^2K+2(E-K)}{(\varkappa^2+4\varepsilon I_2)^{5/2}}\right]$$

Подставляя это значение $R_{эфф}$ и Θ из (4.9) в формулы (4.7) и(4.8), находим инкремент развития и критерий стабилизации широм желобковой неустойчивости в области частот $\omega<\alpha v_{T_i}\sqrt{\varepsilon I_2}$

$$\gamma = \frac{v_{T_i}}{\sqrt{a\tilde{R}}}\left(q_1\sqrt{\varepsilon I_2}\right)^{1/2} \tag{4.10}$$

$$\Theta > 4\frac{a}{\tilde{R}}\sqrt{\frac{m}{M}}\sqrt{\varepsilon I_2}\,q_1 \quad \left(\text{т.е. } \varepsilon \gtrsim \frac{m}{M}\right) \tag{4.11}$$

Условие (4.11) показывает, что в реальных установках ($\varepsilon\sim0,3$) рассмотренная неустойчивость легко стабилизируется широм.

Как следует из определения W, в области частот $\alpha v_{T_e}\sqrt{\varepsilon I_2}<\omega<\alpha v_{T_e}$ при условии $\langle q\rangle > \varepsilon$ величина $W<0$. Это объясняется тем, что при условии $\langle q\rangle > \varepsilon$ вклад от дрейфа слабопролетных частиц, проводящих большую часть времени в поле с благоприятной кривизной, превосходит вклад от дрейфа быстропролетных частиц, определяемого неблагоприятной средней кривизной (напомним, что вклад запертых электронов в этой области частот пренебрежимо мал). При этом возможна неустойчивость, аналогичная рассмотренной в работе Коппи и др.[2] в поле с периодической кривизной, но с благоприятной средней кривизной силовых линий магнитного поля. Эта неустойчивость носит кинетический характер и может приводить к раскачке колебаний с частотой

$$\omega \simeq -\alpha v_{T_i}\frac{\varepsilon\rho}{k_\perp q_1} < \omega_{pi} \tag{4.12}$$

и инкрементом развития

$$\gamma = \frac{\varepsilon}{2}I_2\alpha v_{T_e}\frac{T_i}{T_e}\frac{1}{\langle q\rangle} \tag{4.13}$$

Физическая природа этой неустойчивости заключается в резонансном взаимодействии быстропролетных электронов с волной в поле с периодической кривизной силовых линий. Критерий стабилизации широм рассматриваемой неустойчивости можно получить из того условия, что для ее существования член от продольного движения электронов $\frac{k_\parallel^2 v_{Te}^2}{\omega^2}$ в уравнении (4.5) не должен превосходить члена от инерции ионов $k_\perp^2 \rho_i^2 \left(1 - \frac{\omega_{pi}}{\omega}\right)$

Это дает следующий критерий стабилизации широм

$$\Theta > \frac{\rho_i}{a} \sqrt{\frac{m T_i}{M T_e}}\, k_\perp \rho_i \qquad (4.14)$$

Условие (4.14) хорошо выполнено в установках, в которых $\theta \gtrsim 10^{-3}$.

Если, наконец, учесть, что и при частотах $\alpha v_{Ti} \sqrt{\varepsilon I_2} < \omega < \alpha v_{Te} \sqrt{\varepsilon I_2}$ желобковые колебания оказываются устойчивыми (так как наряду с членом $\frac{W}{\omega^2}$ в уравнении (4.5) появляется член $\frac{\Omega_1}{\omega}$, благодаря которому спектр становится вещественным), то можно сделать заключение, что желобковые неустойчивости во всех практически важных случаях застабилизированы.

Переходя к исследованию дрейфовых колебаний, мы можем отбросить в уравнении (4.5) малые члены, определяемые магнитным дрейфом частиц. Тогда независимо от соотношения между частотой колебаний и обратным временем пролета частиц расстояния между локальными магнитными пробками уравнение (4.5) сводится к уравнению:

$$\left(1 - \frac{\omega_{pi}}{\omega}\right) \frac{T_e}{T_i} k_\perp^2 \rho_i^2 - \left(1 - \frac{\omega_{pe}}{\omega}\right) \frac{k_\parallel^2 v_{Te}^2}{\omega^2} = 0 \qquad (4.15)$$

Если в случае простой геометрии магнитного поля (в отсутствие запертых частиц и периодической кривизны) в рассматриваемой области частот $\omega > k_\parallel v_{Te}$ антиэрмитовская часть уравнения (4.2), а, следовательно, и инкременты возможных кинетических неустойчивостей экспоненциально малы, то в данном магнитном поле наряду с известными гидродинамическими неустойчивостями, описываемыми уравнением (4.I5), возможна не экспоненциально малая кинетическая раскачка колебаний, связанная с резонансным взаимодействием запертых частиц и пролетных частиц с волной.

Исследуем сначала один из таких спектров, который лежит в области высоких частот $\omega > \omega_p$ и определяется формулой

$$\omega^2 = \frac{k_\parallel^2 v_{Te}^2}{k_\perp^2 \rho_i^2} \frac{T_i}{T_e} \tag{4.I6}$$

Используя явный вид $\mathcal{D}''$, получим мнимую добавку к частоте $\gamma = -\frac{\mathcal{D}''}{\partial \mathcal{D}'/\partial \omega}$, которая оказывается положительной лишь в области частот $\alpha v_{Te} \sqrt{\varepsilon I_2} < \omega < \alpha v_{Te}$ и равной

$$\gamma = 4\sqrt{\frac{\pi}{2}}\, \alpha v_{Ti} \frac{\alpha^2 |\ell|}{k_\perp |k_\parallel|} \varepsilon^2 \frac{I_2 I_2'}{\rho} \tag{4.I7}$$

Механизм такой неустойчивости аналогичен механизму неустойчивости, рассмотренной в работе [2], и объясняется резонансным взаимодействием волны с квазипериодическим движением пролетных частиц (электронов) в поле с переменной кривизной. Инкремент (4.I7) при этом существенно определяется локальным (меняющимся вдоль силовой линии магнитного поля) магнитным дрейфом ω_i^M ионов. Так как локальное рассмотрение справедливо при условии, когда область локализации колебаний не мала по сравнению с характерным размером неоднородности плазмы, то для получения критерия стабилизации рассмотренной неустойчивости широм следует исходить из условий применимости формул (4.I6).(4.I7), полагая в них $k_\parallel \simeq k_\parallel' a = k_\perp \theta$. При этом, учитывая, что рассмотренный выше спектр неустойчив только при не слишком больших частотах $\omega < \alpha v_{Te}$, а по условию рассмотрения $\omega \ll \Omega_i$, получим следующий критерий стабилизации широм

$$\Theta > \min\left\{\alpha \rho_i \sqrt{\frac{T_e}{T_i}};\ \sqrt{\frac{m}{M}}\right\} \tag{4.I8}$$

Эта неустойчивость является наиболее опасной в рассматриваемой области частот $\omega > k_\parallel v_{Te}$, т.к., во-первых, максимальный инкремент $\gamma_{max} \sim \alpha v_{T_i} \sim \omega_{p_i}$ (для существующих установок $\gamma_{max} \sim 10^5$ сек$^{-1}$) достаточно велик и, во-вторых, она плохо стабилизируется широм (для приводимой нами установки $\theta \sim 10^{-3}$, а $\alpha\rho_i \sim \sqrt{\frac{m}{M}} 10^{-2}$, т.е. условие (4.18) не выполняется).

Рассмотрим теперь дрейфовые колебания с частотами $\omega \sim \omega_p$. Если продольные длины волн не очень велики $k_\perp^2 \rho_i^2 \frac{T_e}{T_i} \gg \frac{k_\parallel^2 v_{T_e}^2}{\omega_{p_i}^2}$, то решение уравнения (4.15) имеет вид

$$\omega = \omega_{p_i}\left[1 + \left(\frac{T_i}{T_e} + \frac{d\ln N T_e}{d\ln N T_i}\right)\frac{k_\parallel^2 v_{T_e}^2}{\omega_{p_i}^2 k_\perp^2 \rho_i^2}\right] \tag{4.19}$$

Здесь оставлено малое слагаемое в квадратных скобках, существенное для определения инкремента нарастания колебаний, который в разных областях частот имеет различный вид и определяется выражениями:

$$\gamma = \begin{cases} 8\sqrt{\frac{\pi}{2}}\varepsilon^2 I_2 I_2' \alpha v_{T_e} \frac{k_\parallel^2 v_{T_e}^2}{\omega^2 k_\perp^4 \rho_i^4}\left(\frac{T_i}{T_e} + \frac{d\ln N T_e}{d\ln N T_i}\right)^{1/2} \frac{\alpha\, d\psi}{d\ln N T_i}, & \alpha v_{T_e}\sqrt{\varepsilon I_2} < \omega < \alpha v_{T_e} \\ 4\sqrt{\frac{\pi}{2}} \frac{\omega^2}{\alpha v_{T_e}} \frac{k_\parallel^2}{\alpha^2} \frac{1}{k_\perp^2 \rho_i^2} \frac{I_2'}{I_2} q_2 \left(\frac{T_i}{T_e} + \frac{d\ln N T_e}{d\ln N T_i}\right)^{3/2} \frac{\alpha\, d\psi}{d\ln N T_i}, & \alpha v_{T_i} < \omega < \alpha v_{T_e}\sqrt{\varepsilon I_2} \\ -\sqrt{\frac{\pi}{2}}\alpha v_{T_i} \frac{\alpha^2 v_{T_i}^2}{\omega^2 k_\perp^2 \rho_i^2} \varepsilon^2 I_2^2 \left(1 - \frac{d\ln N T_i}{d\ln N T_i}\right)^{3/2}, & \sqrt{\varepsilon I_2}\,\alpha v_{T_i} < \omega < \alpha v_{T_i} \\ -\sqrt{\frac{\pi}{2}}\alpha v_{T_i} \frac{k_\parallel^2}{\alpha^2} \frac{\omega^4}{\alpha^4 v_{T_i}^4 \varepsilon I_2} \frac{q_3}{k_\perp^2 \rho_i^2}\left(1 - \frac{d\ln N T_i}{d\ln N T_i}\right)^{-3/2}, & \omega < \alpha v_{T_i}\sqrt{\varepsilon I_2} \end{cases} \tag{4.20}$$

где

$$q_2 = \frac{4}{\pi^4}\left[\int_0^1 d\varkappa^2 K^4(\varkappa)\, J_1(2\theta_0) + \frac{1}{4}\int_1^\infty \frac{K^4(\varkappa^{-1})}{\varkappa^3} d\varkappa^2\right]$$

$$q_3 = \frac{4}{\pi^9}\int_0^1 d\varkappa^2 \int_0^{\theta_0} \frac{\theta^2 d\theta}{\sqrt{\varkappa^2 - \sin^2\theta}} K^3(\varkappa)$$

Из формул (4.20) следует, что при условии $\frac{T_i}{T_e} + \frac{d\ln N T_e}{d\ln N T_i}^{-3/2} < 0$ в плазме возможна неустойчивость в области частот $\alpha v_{T_e}\sqrt{\varepsilon I_2} > \omega \sim \omega_{p} \gg \alpha v_{T_i}$, обусловленная резонансным взаимодействием запертых электронов с волной. Инкремент этой неустойчивости определяется локальным дрейфом ионов. Для колебаний в области $\alpha v_{T_i}\sqrt{\varepsilon I_2} < \omega \sim \omega_{p_i} < \alpha v_{T_i}$ неустойчивость возникает при $\frac{d\ln T_i}{d\ln N} > 0$ и обусловлена резонансным взаимодействием квазипериодического движения пролетных частиц (ионов) с волной.

В областях частот $\omega \gg \alpha v_{T_e}\sqrt{\varepsilon I_2}$ и $\omega < \alpha v_{T_i}\sqrt{\varepsilon I_2}$ также возможны неустойчивости в условиях, когда $\frac{d\ln T_i}{d\ln N} < 0$. В области $\omega > \alpha v_{T_e}\sqrt{\varepsilon I_2}$ неустойчивость обусловлена резонансным взаимодействием квазипериодического движения пролетных электронов с волной и имеет место при условии $\frac{T_i}{T_e} + \frac{d\ln N T_e^{1/2}}{d\ln N T_i} < 0$, а в области $\omega < \alpha v_{T_i}\sqrt{\varepsilon I_2}$ колебания неустойчивы, если $-1 < \frac{d\ln T_i}{d\ln N} < 0$. Неустойчивость в этом последнем случае обусловлена резонансом волны с колебаниями запертых ионов.

Наконец, отметим, что рассмотренные дрейфовые неустойчивости стабилизируются при нарушении неравенства $k_\perp^2 \rho_i^2 \frac{T_e}{T_i} \gg \frac{k_\parallel^2 v_{T_e}^2}{\omega^2}$. Условие стабилизации при этом имеет вид

$$\Theta > \frac{\rho_i}{a}\sqrt{\frac{m}{M}}\,k_\perp \rho_i \qquad (4.21)$$

Это условие, как уже отмечалось (см. (4.14)), для имеющихся в настоящее время установок ($\theta \sim 10^{-3}$) хорошо выполняется.

Если выполнено обратное неравенство $\frac{T_e}{T_i}k_\perp^2\rho_i^2 \ll \frac{k_\parallel^2 v_{T_e}^2}{\omega^2}$, то спектр частот близок к частоте лармоdoровского дрейфа электронов

$$\omega = \omega_{pe}\left[1 + \left(\frac{T_e}{T_i} + \frac{d\ln N T_i}{d\ln N T_e}\right)k_\perp^2 \rho_i^2 \frac{\omega_{pe}^2}{k_\parallel^2 v_{T_e}^2}\right] \qquad (4.22)$$

а инкремент неустойчивости определяется выражениями

$$\gamma = \begin{cases} \sqrt{\frac{\pi}{2}}\,8\varepsilon^2 I_2 I_2'\left(1 - \frac{d\ln N T_e^{1/2}}{d\ln N T_e}\right)\frac{T_i}{T_e}\frac{\alpha v_{T_e}}{k_\perp^2\rho_i^2}\frac{\alpha\, d\nu}{d\ln N T_e}, & \alpha v_{T_e}\sqrt{\varepsilon I_2} < \omega < \alpha v_{T_e} \\ \sqrt{\frac{\pi}{2}}\frac{I_2'}{2 I_2}\frac{\omega^4}{\alpha^3 v_{T_e}^3}\left(1 - \frac{d\ln N T_e^{3/2}}{d\ln N T_e}\right)\frac{T_i^2}{T_e^2}\frac{q_2}{k_\perp^2\rho_i^2}\frac{\alpha\, d\nu}{d\ln N T_e}, & \alpha v_{T_i} < \omega < \alpha v_{T_e}\sqrt{\varepsilon I_2} \\ \sqrt{\frac{\pi}{2}}\,\varepsilon^2 I_2^2\left(\frac{T_e}{T_i} + \frac{d\ln N T_i^{3/2}}{d\ln N T_e}\right)\frac{\alpha^3 v_{T_i}^3}{k_\parallel^2 v_{T_e}^2}, & \sqrt{\varepsilon I_2}\,\alpha v_{T_i} < \omega < \alpha v_{T_i} \\ \sqrt{\frac{\pi}{2}}\frac{q_3}{2\varepsilon I_2}\left(\frac{T_e}{T_i} + \frac{d\ln N T_i^{-3/2}}{d\ln N T_e}\right)\frac{\omega^6}{\alpha^5 v_{T_i}^5}\frac{m T_i}{M T_e}, & \omega < \alpha v_{T_i}\sqrt{\varepsilon I_2} \end{cases} \qquad (4.23)$$

Формулы (4.23) показывают, что колебания с частотами $\omega > \alpha v_{T_i}$ неустойчивы только в плазме с $-1 < \frac{d\ln T_e}{d\ln N} < 0$, в то время как для колебаний с частотами $\omega < \alpha v_{T_i}$ условия неустойчивостей более реальны: $\frac{T_e}{T_i} + \frac{d\ln N T_i^{3/2}}{d\ln N T_e} > 0$ при $\omega > \alpha v_{T_i}\sqrt{\varepsilon I_2}$ и $\frac{T_e}{T_i} + \frac{d\ln N T_i^{-3/2}}{d\ln N T_e} > 0$ при $\omega < \alpha v_{T_i}\sqrt{\varepsilon I_2}$. Критерий стабилизации рассмотренных неустойчивостей вытекает из условия нарушения неравенства $\omega \simeq \omega_{pe} > k_{\parallel} v_{Te}$ и имеет вид

$$\Theta > \frac{\rho_i}{a}\sqrt{\frac{m}{M}\frac{T_e}{T_i}} \qquad (4.24)$$

В установках, для которых мы приводим оценки ($\Theta \sim 10^{-3}$),это условие стабилизации находится на грани выполнимости, поскольку $\frac{\rho_i}{a}\sqrt{\frac{m}{M}} \sim 10^{-3}$.

Помимо рассмотренных спектров в неизотермической плазме с горячими ионами ($T_i \gg T_e$) существует решение уравнения(4.15)

$$\omega = -\frac{k_{\parallel}^2 v_{Te}^2}{\omega_{pi} k_{\perp}^2 \rho_i^2}\frac{T_i}{T_e} \qquad (4.25)$$

удовлетворяющее условию $\omega_{pi} \gg \omega \gg \omega_{pe}$.Анализ уравнения(4.2) показывает,что рассматриваемые колебания могут оказаться неустойчивыми,если частота лежит в области $\omega < \alpha v_{Ti}$,причем при $\omega \sim \alpha v_{Ti}\sqrt{\varepsilon I_2}$ неустойчивость имеет место только в плазме, в которой $-1 < \frac{d\ln T_i}{d\ln N} < -\frac{2}{3}$, и инкремент ее развития равен

$$\gamma = \varepsilon^2 I_2^2 k_{\perp}^2 \rho_i^2 \frac{T_i}{T_e}\frac{\alpha^3 v_{Ti}^3}{\omega^2}\left|\frac{d\ln N T_i^{3/2}}{d\ln N T_i}\right| \qquad (4.26)$$

В более реальных условиях развивается неустойчивость в области $\omega < \alpha v_{Ti}\sqrt{\varepsilon I_2}$.Инкремент развития неустойчивости при этом определяется выражением

$$\gamma = -\frac{q_3}{2\varepsilon I_2}\frac{\omega^4}{\alpha^3 v_{Ti}^3}\frac{k_{\parallel}^2}{\alpha^2}(k_{\perp}\rho_i)^2\frac{T_i}{T_e}\frac{d\ln N T_i^{-3/2}}{d\ln N T_i} \qquad (4.27)$$

а условие ее существования имеет вид $\frac{d\ln T_i}{d\ln N} > \frac{2}{3}$

Исходя из того,что эти колебания могут быть неустойчивыми только в случае,когда выполнено условие $\omega < \omega_{pi}$,находим критерий их стабилизации широм

$$\Theta > \frac{\rho_i}{a}\sqrt{\frac{m}{M}}\, k_{\perp}\rho_i \qquad (4.28)$$

который,как уже отмечалось, хорошо выполняется для реальных установок.

2. $k_\parallel v_{Ti} < \omega < k_\parallel v_{Te}$. В этой области частот уравнение колебаний (4.2) имеет вид

$$1-\frac{\omega_{ne}}{\omega}+\left(1-\frac{\omega_{pi}}{\omega}\right)\left(\frac{T_e}{T_i}k_\perp^2\rho_i^2-\frac{k_\parallel^2 v_s^2}{\omega^2}-\frac{\Omega_2}{\omega}\right)+ \tag{4.29}$$

$$+\frac{\omega_{pi}\,\omega_{3i}^M}{\omega^2}\left(1+\frac{T_e}{T_i}\right)+\hat{1}_e\left\langle\frac{\omega^2}{\frac{k_\parallel^2}{\alpha^2}\omega_{npe}^2}\Pi_0^{np}\right\rangle+i\sqrt{\frac{\pi}{2}}\,\mathcal{D}''=0$$

где

$$v_s=\sqrt{\frac{T_e}{M}}$$

$$\Omega_2=\begin{cases}\omega_{oi}^M-2I_2\,\omega_{ii}^M\varepsilon, & \omega>\alpha v_{Ti}\\ 2\langle q\rangle\,\omega_{ii}^M, & \alpha v_{Ti}\sqrt{\varepsilon I_2}<\omega<\alpha v_{Ti}\\ \omega_{npi}^M, & \omega<\alpha v_{Ti}\sqrt{\varepsilon I_2}\end{cases}$$

$$\mathcal{D}''=\begin{cases}\hat{1}_e\dfrac{\omega}{|k_\parallel|v_{Te}} & \omega>k_\parallel v_{Te}\sqrt{\varepsilon I_2},\ \alpha v_{Ti}\sqrt{\varepsilon I_2}\\ \hat{1}_e\left\langle\dfrac{\omega^3}{\left(\frac{|k_\parallel|}{\alpha}\omega_{npe}\right)^3}\Pi_0^{np}\right\rangle, & \alpha v_{Ti}\sqrt{\varepsilon I_2}<\omega<k_\parallel v_{Te}\sqrt{\varepsilon I_2}\\ \hat{1}_e\left\langle\dfrac{\omega^3}{\left(\frac{|k_\parallel|}{\alpha}\omega_{npe}\right)^3}\Pi_0^{np}\right\rangle+\dfrac{T_e}{T_e}\hat{1}_i\left\langle\dfrac{\omega^3 k_\parallel^2}{\omega_{3i}^3\alpha^2}\Theta_0^2\left(\Pi_{0,0}^3-\Pi_{2,0}^3\right)\right\rangle, & \omega<k_\parallel v_{Te}\sqrt{\varepsilon I_2},\ \omega<\alpha v_{Ti}\sqrt{\varepsilon I_2}\end{cases}$$

Предпоследний член в эрмитовой части уравнения (4.29) определяется магнитным дрейфом запертых частиц и присутствует в уравнении только при $\omega<\alpha v_{Ti}\sqrt{\varepsilon I_2}$. Последний же член в эрмитовой части обусловлен продольным движением медленнопролетных частиц ($\kappa\sim 1$) и учитывается в уравнении лишь в области частот $\omega<k_\parallel v_{Te}\sqrt{\varepsilon I_2}$. Наличие этого члена приводит к появлению существенно новых гидродинамически неустойчивых спектров колебаний. Действительно, если в плазме $\frac{d\ln T}{d\ln N}\gg 1$, то уравнение (4.29) при $\omega\ll\omega_{ne}$ сводится к виду:

$$1+\frac{k_\parallel^2 v_{Ti}^2}{\omega^2}\frac{d\ln T_i}{d\ln N}-\frac{\omega^2}{k_\parallel^2 v_{Te}^2}\frac{q_4}{\sqrt{\varepsilon I_2}}\frac{d\ln T_e}{d\ln N}=0 \tag{4.30}$$

и имеет следующие решения

$$\omega_\pm^2=\sqrt{\varepsilon I_2}\,\frac{k_\parallel^2 v_{Te}^2}{2q_4}\frac{d\ln N}{d\ln T_e}\left[1\pm\sqrt{1+4\frac{mT_i}{MT_e}\frac{d\ln T_e}{d\ln T_i}\left(\frac{d\ln T_i}{d\ln N}\right)^2\frac{q_4}{\sqrt{\varepsilon I_2}}}\right] \tag{4.31}$$

где

$$q_\gamma = \frac{2}{\pi^3}\int_0^1 dx^2 \frac{K^3(x)}{\sqrt{x^2+4\varepsilon I_2}}$$

Видно,что наличие медленнопролетных частиц в системе приводит к искажению известной дрейфово-температурной неустойчивости со спектром

$$\omega^2 = -k_\parallel^2 v_s^2 \frac{d\ln T_i}{d\ln N} \tag{4.32}$$

который получается как предельное значение ω_-^2 при формальном стремлении величины q_γ к нулю в (4.31). Кроме того, в установках с $\frac{d\ln T_e}{d\ln N} < 0$ появляется существенно новый неустойчивый спектр $\omega^2 = \omega_r^2 < 0$. Критерий стабилизации широм рассмотренной неустойчивости имеет вид

$$\Theta > \frac{\rho_i}{a}\left(\frac{T_e}{T_i}\frac{m}{M}\frac{q_\gamma}{\sqrt{\varepsilon I_2}}\right)^{1/2}\left(\frac{d\ln N}{d\ln T}\right)^{3/2} \tag{4.33}$$

и вытекает из того,что при его выполнении последним членом в уравнении (4.30),ответственным за неустойчивость,можно пренебречь. Критерий (4.33) является значительно более слабым,чем критерий стабилизации дрейфово-температурной неустойчивости (4.32) ($\Theta > \frac{\rho_i}{a}\sqrt{\frac{T_e}{T_i}}\left(\frac{d\ln N}{d\ln T}\right)^{3/2}$ см.,например,[6]).

Если же,напротив, магнитный дрейф не мал,то,удерживая в уравнении (4.29) члены, обусловленные магнитным дрейфом частиц, находим следующее неустойчивое решение

$$\omega^3 = \frac{1}{2} k_\parallel^2 v_{Te}^2 \left[\Omega_2 + \omega_{3i}^M\left(1+\frac{T_e}{T_i}\right)\right]\frac{T_i}{T_e}\frac{\sqrt{\varepsilon I_2}}{q_\gamma} \tag{4.34}$$

Критерий стабилизации этой неустойчивости можно получить из тех же соображений,что и выше, и имеет вид

$$\Theta > \frac{\rho_i}{a}\sqrt{\frac{m}{M}}\left(\frac{a}{R_{эф}\,\varepsilon I_2}\right)^{1/4} \tag{4.35}$$

Этот критерий,как и (4.24), находится на грани выполнимости, поскольку для реальных установок $\left(\frac{a}{R_{эф}\,\varepsilon I_2}\right)^{1/4} \sim 1$.

Эффект запертости частиц проявляется не только в появлении новых гидродинамически неустойчивых спектров,но и в искажении обычных кинетически неустойчивых спектров. Так в области $\omega < k_\parallel v_{Te} \sqrt{\varepsilon I_2}$ в уравнении (4.29) изменяется антиэрмитовская часть $\mathcal{D}''$,что приводит к изменению инкрементов,хорошо известных в поле с простой геометрией кинетических неустойчивостей. Для дрейфовых колебаний с частотой

$$\omega = \omega_{ne} \ (1 - \Delta)$$

$$\Delta = \left(1 + \frac{T_i}{T_e} \frac{d\ln N T_i}{d\ln N}\right)\left(\frac{T_e}{T_i} k_\perp^2 \rho_i^2 - \frac{k_\parallel^2 v_s^2}{\omega^2} - \frac{\Omega_q}{\omega}\right) + \frac{\omega_{pi}\, \omega_{Di}^M}{\omega^2}\left(1 + \frac{T_e}{T_i}\right) \quad (4.34)$$

инкремент неустойчивости в зависимости от области частот имеет различный вид и определяется выражениями

$$\gamma = \begin{cases} \sqrt{\dfrac{\pi}{2}} \dfrac{\omega^2}{|k_\parallel| v_{Te}} \left(\Delta - \dfrac{1}{2} \dfrac{d\ln T_e}{d\ln N}\right), & \omega > k_\parallel v_{Te} \sqrt{\varepsilon I_2},\ \alpha v_{Ti} \sqrt{\varepsilon I_2} \\ \sqrt{\dfrac{\pi}{2}} \dfrac{4}{\pi} \dfrac{1}{\varepsilon I_2} \dfrac{\omega^4}{(|k_\parallel| v_{Te})^3} \left(\Delta - \dfrac{3}{2} \dfrac{d\ln T_e}{d\ln N}\right), & \alpha v_{Ti} \sqrt{\varepsilon I_2} < \omega < k_\parallel v_{Te} \sqrt{\varepsilon I_2} \\ \sqrt{\dfrac{\pi}{2}} \dfrac{4}{\pi \varepsilon I_2} \dfrac{\omega^4}{(|k_\parallel| v_{Te})^3} \left(\Delta - \dfrac{3}{2} \dfrac{d\ln T_e}{d\ln N}\right) - \dfrac{q_3 k_\parallel^2 \omega^4}{\varepsilon I_2 \alpha^5 v_{Ti}^3} \left(1 + \dfrac{T_i}{T_e} \dfrac{d\ln N T_i}{d\ln N}\right)^{-3/2}, & \omega < \alpha v_{Ti} \sqrt{\varepsilon I_2},\ \omega < k_\parallel v_{Te} \sqrt{\varepsilon I_2} \end{cases} \quad (4.35)$$

Из приведенных формул следует,что в области частот $\omega > k_\parallel v_{Te} \sqrt{\varepsilon I_2}$ выражение для инкремента развития неустойчивости совпадает с соответствующим выражением в поле с простой конфигурацией силовых линий, с той лишь разницей,что магнитный дрейф ионов дает различный вклад в зависимости от соотношения между частотой колебаний ω и двумя характерными обратными временами движения ионов. Если выполнено соотношение $\omega > \alpha v_{Ti}$,то основной вклад в инкремент дает средний дрейф быстропролетных ионов; если $\sqrt{\varepsilon I_2}\, \alpha v_{Ti} < \omega < \alpha v_{Ti}$, то наряду со средним дрейфом быстропролетных ионов,сказывается локальный дрейф медленнопролетных ионов и,наконец, в области частот $\omega < \alpha v_{Ti} \sqrt{\varepsilon I_2}$ определяющим является локальный дрейф запертых электронов и ионов. Критерий стабилизации рассматриваемой неустойчивости в области частот $\omega > k_\parallel v_{Te} \sqrt{\varepsilon I_2}$

вытекает из условия нарушения неравенства $\omega \approx \omega_{*e} > k_\parallel v_{Ti} (k_\perp \rho_i)^{-1}$ и имеет вид

$$\theta > \frac{\rho_i}{a} \frac{T_e}{T_i} k_\perp \rho_i \qquad (4.36)$$

В существующих установках ($\theta \sim 10^{-3}$) этот критерий выполняется плохо (так как правая часть неравенства даже для самых длинноволновых колебаний $\gtrsim 10^{-3}$). В области частот $\omega \approx \omega_{ne} < k_\parallel v_{Te} \sqrt{\varepsilon I_2}$ инкремент развития неустойчивости,как следует из формулы (4.35),уменьшается в отношении $\left(\frac{\omega}{k_\parallel v_{Te}\sqrt{\varepsilon I_2}}\right)^2$; однако,критерий стабилизации по-прежнему определяется формулой (4.36). Если при этом частота колебаний $\omega < \alpha v_{Ti} \sqrt{\varepsilon I_2}$ то для плазмы,в которой $\frac{d\ln T}{d\ln N} < \frac{2}{3}\left(1 + \frac{T_e}{T_i}\right)$, в инкременте нарастания появляется стабилизирующая добавка,обусловленная резонансным взаимодействием запертых ионов с волной. При выполнении условия $\frac{k_\parallel^5}{\alpha^5} \gtrsim \frac{v_{Ti}^3}{v_{Te}^3}$ эта добавка приводит к полной стабилизации колебаний.Если учесть,что $\omega < \alpha v_{Ti} \sqrt{\varepsilon I_2}$ а $k_\perp \rho_i < \alpha a \frac{T_e}{T_i} \sqrt{\varepsilon I_2}$,то отсюда непосредственно получаем следующий критерий стабилизации неустойчивости широм

$$\theta > \frac{\rho_i}{a} \frac{T_e}{T_i} \left(\frac{m}{M} \frac{T_i}{T_e}\right)^{0,3} \frac{1}{\sqrt{\varepsilon I_2}} \qquad (4.37)$$

который для реальных систем также плохо выполняется,как и (4.36). С другой стороны, если в плазме выполнено обратное неравенство $\frac{d\ln T}{d\ln N} > \frac{2}{3}\left(1 + \frac{T_e}{T_i}\right)$, то в области частот $\omega < \alpha v_{Ti} \sqrt{\varepsilon I_2}$ добавка к инкременту, обусловленная резонансом запертых частиц с волной,может привести к новой неустойчивости,критерий стабилизации которой определяется формулой (4.36). Так как в реальных условиях $k_\perp \rho_i \gtrsim \alpha a \frac{T_e}{T_i} \sqrt{\varepsilon I_2}$ $k_\perp \rho_i > \frac{\rho_i}{a} \sim 5.10^{-2}$, $\alpha a \sqrt{\varepsilon I_2} \sim 10^{-2}$, то-есть $\omega > \alpha v_{Ti} \sqrt{\varepsilon I_2}$, то отмеченные выше эффекты, обусловленные резонансным взаимодействием запертых частиц с волной, в установках могут не проявляться.

В неизотермической плазме ($T_e \gg T_i$) существуют, как известно [1], еще две ветви кинетически неустойчивых колебаний, спектры частот которых определяются выражениями

$$\omega_\pm = \frac{1}{2}\,\omega_{ne} \pm \sqrt{\frac{1}{4}\omega_{ne}^2 + k_\parallel^2 v_s^2} \tag{4.38}$$

В области $\omega > k_\parallel v_{Te}\sqrt{\varepsilon I_2}$ инкременты развития условия неустойчивости и критерий стабилизации широм таких колебаний хорошо известны [1]. Если же $\omega < k_\parallel v_{Te}\sqrt{\varepsilon I_2}$, то, помимо уменьшения инкремента в $\left(\frac{\omega}{k_\parallel v_{Te}\sqrt{\varepsilon I_2}}\right)^2$ раз, для колебаний с частотой $\omega = \omega_+$ изменяется условие неустойчивости $\frac{d\ln T_e}{d\ln N} > \frac{2}{3}$. Критерий стабилизации широм этой неустойчивости, также как и известных дрейфово-температурных неустойчивостей (см. таблицу) в существующих установках не выполняется.

3. $\underline{\omega < k_\parallel v_{Ti}}$. Известно, что в системах с простой конфигурацией силовых линий магнитного поля колебания в области частот $\omega < k_\parallel v_{Ti}$ отсутствуют (имеет место дебаевская экранировка поля). Наличие в системе захваченных частиц, как было показано в работе Кадомцева и Погуце [1], приводит к появлению неустойчивых колебаний, обусловленных магнитным дрейфом захваченных частиц. Эта неустойчивость, как показывает анализ общего уравнения, лежит в области частот $\omega < k_\parallel v_{Ti}\sqrt{\varepsilon I_2}$ (колебания с частотами $\omega > k_\parallel v_{Ti}\sqrt{\varepsilon I_2}$ отсутствуют из-за дебаевской экранировки поля). Уравнение колебаний при этом имеет вид

$$1+\frac{T_i}{T_e}-\frac{6}{\pi}\sqrt{\varepsilon I_2}\,\frac{\omega_{pi}}{\omega}k_\perp^2\rho_i^2+\frac{\omega_{pi}\,\omega_{si}^{T}}{\omega^2}\left(1+\frac{T_e}{T_i}\right)-\frac{\omega\,\omega_{pi}}{k_\parallel^2 v_{Ti}^2}\,\frac{d\ln NT_i^{-1}}{d\ln NT_i}\,\frac{q_r}{\sqrt{\varepsilon I_2}}$$

$$-i\sqrt{\frac{\pi}{2}}\,\frac{\omega_{pi}}{\omega}\left(\frac{\omega}{|k_\parallel| v_{Ti}}\right)^3\frac{q_5}{\varepsilon I_2}\,\frac{d\ln NT_i^{-3/2}}{d\ln NT_i} \tag{4.39}$$

где $q_5 = 2\pi^{-4}\int_0^1 d\varkappa^2 K^4(\varkappa)$. Для достаточно больших $k_\parallel$ последним членом в эрмитовой части можно пренебречь. Пренебрегая также членом, связанным с инерцией ионов, получим гидродинамически неустойчивый спектр, обусловленный дрейфом запертых частиц [1].

$$\omega^2 = -|\omega_{pi}| \frac{|e|}{\Psi'} \rho_i \frac{v_{Ti}}{R} \sqrt{E I_2}\, q_1^3 \frac{1 + T_e/T_i}{1 + T_i/T_e} \tag{4.40}$$

где $q_1^3 = \frac{12}{\pi} \frac{\bar{I}_2'}{\beta}\int_0^1 d\varkappa^2 (2E-K)$ определяется вкладом только запертых частиц и отличается от q_1 лишь на малую величину, обусловленную вкладом медленнопролетных частиц. Хотя инкремент этой неустойчивости меньше инкремента обычной желобковой неустойчивости, она гораздо опаснее, так как не может быть застабилизирована широм. Учет конечного ларморовского радиуса ионов приводит к стабилизации этой неустойчивости при условии

$$(k_\perp \rho_i)^4 > \frac{a}{R}\left(1 + \frac{T_e}{T_i}\right)\frac{\pi^2}{9}\frac{q_1^3}{\sqrt{E I_2}} \cdot \left(1 + \frac{T_i}{T_e}\right) \tag{4.41}$$

Однако, неравенство (4.41) для реальных установок плохо выполняется. Если даже предположить, что условие (4.41) выполнено и спектр колебаний вещественен, учет черенковского поглощения на медленнопролетных частицах приводит к кинетической неустойчивости с инкрементом

$$\gamma \simeq -\sqrt{\frac{\pi}{2}} \frac{\omega^4}{(|k_\parallel| v_{Ti})^3} \frac{d\ln N T_i^{-3/2}}{d\ln N T_i} \frac{\pi}{6} \frac{q_5}{k_\perp^2 \rho_i^2 (E I_2)^{3/2}} \tag{4.42}$$

которая развивается при условии $-1 < \frac{d\ln N}{d\ln T_i} < \frac{3}{2}$.

Кинетическая неустойчивость, как гидродинамическая, не может быть застабилизирована широм. Именно поэтому она также представляется нам весьма опасной.

Наконец, заметим, что в области наиболее опасных длинноволновых колебаний, когда условие (4.41) не выполняемо, можно

ТАБЛИЦА 1.

$$\omega >> k_\parallel v_{Te}$$

№№	Спектры частот	Условие существования	Механизм неустойчивости	Стабилизация широм
I.	$\omega^2 = \frac{v_{Ti}^2}{R_{эф}}\left(1+\frac{T_e}{T_i}\right)\frac{\partial \ln N T_i}{\partial \psi}$ $R_{эф}^{-1} = \alpha\varepsilon\rho\sqrt{\varepsilon I_2}$	$\omega < \alpha v_{Ti}\sqrt{\varepsilon I_2}$	дрейф запертых частиц	$\Theta > 4\frac{a}{R_{эф}}\sqrt{\frac{m}{M}}$ $(\varepsilon > \frac{m}{M})$
2.	$\omega \approx -\alpha v_{Ti}\varepsilon\rho(k_\perp\rho_i)^{-1}$ $\omega \lesssim \omega_p$ $\gamma \approx \alpha v_{Te}\sqrt{\varepsilon I_2}\frac{T_i}{T_e}$	$\alpha v_{Te}\sqrt{\varepsilon I_2} < \omega < \alpha v_{Te}$	резонанс пролетных электронов с волной	$\Theta > \frac{\rho_i}{a}\sqrt{\frac{m T_i}{M T_e}}k_\perp\rho_i$
3.	$\omega^2 = \frac{k_\parallel^2 v_{Te}^2}{k_\perp^2\rho_i^2}\frac{T_i}{T_e}$ $\gamma \approx \varepsilon^2\rho^3\alpha v_{Ti}\frac{\alpha}{k_\parallel}$	$\alpha v_{Te}\sqrt{\varepsilon I_2} < \omega < \alpha v_{Te}$	резонанс пролетных электронов с волной	$\Theta > \min\left(\sqrt{\frac{m}{M}}, \alpha\rho_i\right)$
4.	$\omega = \omega_{pi}$ $k_\perp^2\rho_i^2 > \frac{k_\parallel^2 v_{Te}^2}{\omega^2}\frac{T_i}{T_e}$ $\gamma \approx -\varepsilon^2\rho^3\alpha v_{Te}a\frac{k_\parallel^2 v_{Te}^2}{\omega^2}\times\left[\frac{T_i}{T_e}+\frac{\partial \ln N T_e^{1/2}}{\partial \ln N T_i}\right]$	$\alpha v_{Te}\sqrt{\varepsilon I_2} < \omega < \alpha v_{Te}$; $\frac{T_i}{T_e}+\frac{\partial \ln N T_e^{1/2}}{\partial \ln N T_i} < 0$	резонанс пролетных электронов с волной	$\Theta > \frac{\rho_i}{a}\sqrt{\frac{m}{M}}k_\perp\rho_i$
	$\gamma \approx -\frac{\omega^2 k_\parallel^2}{\alpha^3 v_{Te}}\left(\frac{T_i}{T_e}+\frac{\partial \ln N T_e^{-3/2}}{\partial \ln N T_i}\right)\frac{1}{k_\perp^2\rho_i^2}$	$\alpha v_{Ti} < \omega < \alpha v_{Te}\sqrt{\varepsilon I_2}$ $\left(\frac{T_i}{T_e}+\frac{\partial \ln N T_e^{-3/2}}{\partial \ln N T_i}\right) < 0$	резонанс запертых и медленнопролетных электронов с волной	
	$\gamma \simeq -\varepsilon^2\rho^3\frac{\alpha^3 v_{Ti}^3}{\omega^2}\left(1-\frac{\partial \ln N T_i^{3/2}}{\partial \ln N T_i}\right)$	$\alpha v_{Ti}\sqrt{\varepsilon I_2} < \omega < \alpha v_{Ti}$ $\frac{\partial \ln T_i}{\partial \ln N} > 0$	резонанс пролетных ионов с волной	
	$\gamma \approx -\frac{\omega^4 k_\parallel^2}{\alpha^5 v_{Ti}^3}\left(1-\frac{\partial \ln N T_i^{-3/2}}{\partial \ln N T_i}\right)\cdot\left(\varepsilon I_2 k_\perp^2\rho_i^2\right)^{-1}$	$\omega < \alpha v_{Ti}\sqrt{\varepsilon I_2}$ $-1 < \frac{\partial \ln T_i}{\partial \ln N} < 0$	резонанс запертых ионов с волной	

ТАБЛИЦА I (продолжение)

№№	Спектры частот	Условие существования	Механизм неустойчивостей	Стабилизация широм
5.	$\omega = \omega_{pe}$	$k_\perp^2\rho_i^2 < \frac{k_\parallel^2 v_{Te}^2}{\omega^2}\frac{T_i}{T_e}$		$\Theta > \frac{\rho_i}{a}\sqrt{\frac{m}{M}\frac{T_e}{T_i}}$
	$\gamma \approx -\frac{\alpha^2 v_{Te} a \varepsilon^2 \rho^3}{2 k_\perp^2 \rho_i^2}\frac{\partial \ln T_e}{\partial \ln N T_e}$;	$\alpha v_{Te}\sqrt{\varepsilon I_2} < \omega < \alpha v_{Te}$ $-1 < \frac{\partial \ln T_e}{\partial \ln N} < 0$	резонанс пролетных электронов с волной	
	$\gamma \approx -\frac{\alpha v_{Te}\omega^4}{\alpha^4 v_{Te}^4}\frac{T_i}{T_e}\frac{1}{k_\perp^2\rho_i^2}\frac{\partial \ln T_e}{\partial \ln N T_e}$;	$\alpha v_{Ti} < \omega < \alpha v_{Te}\sqrt{\varepsilon I_2}$ $-1 < \frac{\partial \ln T_e}{\partial \ln N} < 0$	резонанс на запертых электронах	
	$\gamma = \alpha v_{Ti}\frac{m T_i}{M T_e}\frac{\alpha^2\varepsilon^2\rho^4}{k_\parallel^2}\left[\frac{T_e}{T_i}+\frac{\partial \ln N T_i}{\partial \ln N T_e}\right]^{3/2}$;	$\alpha v_{Ti}\sqrt{\varepsilon I_2} < \omega < \alpha v_{Ti}$ $\frac{T_e}{T_i}+\frac{\partial \ln N T_i}{\partial \ln N T_e}^{3/2} > 0$	резонанс на пролетных ионах	
	$\gamma \approx \frac{m}{M}\frac{\omega^6}{\alpha^5 v_{Ti}^5 \varepsilon I_2}\left(1+\frac{T_i}{T_e}\frac{\partial \ln N T_i}{\partial \ln N T_e}\right)^{-3/2}$;	$\omega < \alpha v_{Ti}\,\varepsilon I_2$ $\frac{T_e}{T_i}+\frac{\partial \ln N T_i}{\partial \ln N T_e}^{-3/2} > 0$	резонанс на запертых ионах	
6.	$\omega = -\frac{k_\parallel^2 v_{Te}^2}{\omega_{pi}}\frac{T_i}{T_e}\frac{1}{k_\perp^2\rho_i^2}$;	$T_e \gg T_i$		$\Theta > \frac{\rho_i}{a}\sqrt{\frac{m}{M}}\,k_\perp\rho_i$
	$\gamma \simeq -\frac{\alpha^3 v_{Ti}^3}{\omega^2}\varepsilon^2\rho^4\frac{T_i}{T_e}\frac{\partial \ln N T_i}{\partial \ln N T_i}^{3/2}\cdot k_\perp^2\rho_i^2$.	$\alpha v_{Ti}\sqrt{\varepsilon I_2} < \omega < \alpha v_{Ti}$ $-1 < \frac{\partial \ln T_i}{\partial \ln N} < -\frac{2}{3}$	резонанс на пролетных ионах	$\Theta > \frac{\rho_i}{a}\sqrt{\frac{m}{M}\alpha a}\,k_\perp\rho_i$
	$\gamma = -\frac{\omega^4}{\alpha^3 v_{Ti}^3}\frac{T_i}{T_e}\frac{k_\parallel^2}{\alpha^2}\frac{k_\perp^2\rho_i^2}{\varepsilon I_2}\frac{\partial \ln N T_i}{\partial \ln N T_i}^{3/2}$;	$\omega < \alpha v_{Ti}\sqrt{\varepsilon I_2}$ $\frac{\partial \ln T_i}{\partial \ln N} > \frac{3}{2}$	резонанс на запертых ионах	$\Theta > \alpha\rho_i k_\perp\rho_i \times \sqrt{\varepsilon^{1/2}\frac{m}{M}}$
7.	$\omega^2 = -\frac{k_\parallel^2 v_{Te}^2}{k_\perp^2\rho_i^2}\frac{\partial \ln N T_e}{\partial \ln N T_i}$	$\omega < \omega_p$ $k_\perp^2\rho_i^2 > \frac{4a}{R_{эф}}$		$\Theta > \frac{\rho_i}{a}\sqrt{\frac{m}{M}}\,k_\perp\rho_i$
8.	$\omega^3 = \omega_{pe} k_\parallel^2 v_{Te}^2 \frac{T_i}{T_e}$	$T_e \gg T_i$		$\Theta > \sqrt{\frac{m}{M}}\frac{\rho_i}{a}$

ТАБЛИЦА II.

$$K_{\parallel} v_{Ti} < \omega < K_{\parallel} v_{Te}$$

№№	Спектры частот	Условие существования	Механизм неустойчивости	Стабилизация широм
1.	$\omega_+^2 = K_{\parallel}^2 v_{Te}^2 \sqrt{\varepsilon I_2}\,\frac{\partial \ln N}{\partial \ln T_e}$	$\omega < K_{\parallel} v_{Te}\alpha\sqrt{\varepsilon I_2}$ $\omega < \omega_{ne}$; $\frac{d \ln T_e}{d \ln N} > \frac{1}{\sqrt{\varepsilon I_2}}$	—	$\Theta > \frac{\rho_i}{a}\sqrt{\frac{m\,T_e}{M\,T_i\sqrt{\varepsilon I_2}}}\left(\frac{\partial \ln N}{\partial \ln T_e}\right)^{3/2}$
	$\omega_-^2 = -K_{\parallel}^2 v_s^2 \frac{\partial \ln T_i}{\partial \ln N}$;	$\omega < \omega_{ne}$ $\frac{\partial \ln T_e}{\partial \ln N} \gg 1$	—	$\Theta > \frac{\rho_i}{a}\sqrt{\frac{T_e}{T_i}}\left(\frac{\partial \ln N}{\partial \ln T_e}\right)^{3/2}$
2.	$\omega^2 = -K_{\parallel}^2 v_s^2 \omega_{pi}$	$\omega > \omega_{ne}$ $\frac{\partial \ln T_i}{\partial \ln N} \gg 1$		$\Theta > \frac{\rho_i}{a}\frac{T_e}{T_i}$
3.	$\omega = -\frac{K_{\parallel}^2 v_{Ti}^2}{\omega_{ne}}$	$T_e \gg T_i$ $\omega < \omega_{ne}$		
	$\gamma_1 = \frac{\omega^2}{K_{\parallel} v_{Te}}\left(1 - \frac{1}{2}\frac{\partial \ln T_e}{\partial \ln N}\right)$;	$\omega \gg K_{\parallel} v_{Te}\alpha\sqrt{\varepsilon I_2}$ $\omega \gg \alpha v_{Ti}\sqrt{\varepsilon I_2}$ $\frac{\partial \ln T_e}{\partial \ln N} > 2$	резонанс на медленнопролетных электронах	$\Theta > \frac{\rho_i}{a}\sqrt{\frac{T_e}{T_i}}$
	$\gamma_2 = \frac{\omega^2}{K_{\parallel} v_{Te}}\left(1 - \frac{3}{2}\frac{\partial \ln T_e}{\partial \ln N}\right)$;	$\alpha v_{Ti} < \frac{\omega}{\sqrt{\varepsilon I_2}} < K_{\parallel} v_{Te}$ $\frac{\partial \ln T_e}{\partial \ln N} > \frac{2}{3}$	резонанс на медленнопролетных электронах и запертых ионах	$\Theta > \frac{\rho_i}{a}\sqrt{\frac{M}{m}\varepsilon\frac{T_e}{T_i}}$
	$\gamma_3 = \gamma_2 - \frac{\omega^4 \alpha a}{\alpha^3 v_{Ti}^3}\,\frac{K_{\parallel}^4}{\alpha^4 K_{\perp}^2 \rho_i^2}$,	$\frac{\partial \ln T_e}{\partial \ln N} > \frac{2}{3}$		$\Theta > \min\left(\alpha\rho_i\sqrt{\frac{M}{m}\varepsilon};\ K\rho_i v_{\varepsilon}\right)$
4.	$\omega_\pm = \pm \lvert K_{\parallel}\rvert v_s$	$T_e \gg T_i$		$\Theta > \frac{\rho_i}{a}\frac{\partial \ln T_e}{\partial \ln N}$
	$\gamma_1 = \mp K_{\parallel} v_{Te}\,\frac{\omega^2}{K_{\parallel}^2 v_{Te}^2}\,\frac{\rho_i}{a}\sqrt{\frac{T_i}{T_e}}\,\frac{\partial \ln T_e}{\partial \ln N}$	$\omega > \omega_{ne}$ $\omega > K_{\parallel} v_{Te}\sqrt{\varepsilon I_2}$	резонанс на медленно пролетных электронах	
	$\gamma_2 \approx \gamma_1\,\frac{\omega^2}{K_{\parallel}^2 v_{Te}^2\,\varepsilon I_2}$			

ТАБЛИЦА II (продолжение)

№№	Спектры частот	Условие существования	Механизм неустойчивости	Стабилизация широм
5.	$\omega \simeq \omega_{ne}$			
	$\gamma_1 = \frac{\omega^2}{k_\parallel v_{Te}}\left(\Delta_1 - \frac{1}{2}\frac{\partial \ln T_e}{\partial \ln N}\right)$	$\omega \gg k_\parallel v_{Te}\sqrt{\varepsilon I_2}$ $\omega \gg \alpha v_{Ti}\sqrt{\varepsilon I_2}$		$\Theta > \frac{\rho_i}{a}\frac{T_e}{T_i}$
	$\gamma_2 = \frac{\omega^4}{k_\parallel^3 v_{Te}\varepsilon I_2}\left(\Delta_2 - \frac{3}{2}\frac{\partial \ln T_e}{\partial \ln N}\right)$;	$\alpha v_{Ti} < \frac{\omega}{\sqrt{\varepsilon I_2}} < k_\parallel v_{Te}$	резонанс на медленно пролетных электронах	$\Theta > \frac{\rho_i}{a}\frac{1}{\alpha a}\sqrt{\frac{m}{M}\frac{T_e}{T_i}}$
	$\gamma_3 = \gamma_2 - \frac{k_\parallel^2\omega^4}{\alpha^5 v_{Ti}^3\sqrt{\varepsilon I_2}}\left(1 - \frac{T_i}{T_e}\frac{\partial \ln NT_i}{\partial \ln NT_i}\right)^{3/2}$;	$\omega < \alpha v_{Ti}\sqrt{\varepsilon I_2}$ $\omega < k_\parallel v_{Te}\sqrt{\varepsilon I_2}$	резонансы на медленно пролетных электронах и запертых ионах	$\Theta > \min\left(\frac{\rho_i}{a}\frac{T_e}{T_i}, \left(\frac{m}{M}\right)^{0,3}\frac{\rho_i}{a\sqrt{\varepsilon I_2}}\right)$
6.	$\omega^2 = -\frac{v_{Ti}^2}{a R_{эф}} k_\perp^2\rho_i^2\frac{\partial \ln T_i}{\partial \ln N}$; $R_{эф}^{-1} = \begin{cases} \varepsilon^2\rho^3\alpha & \text{при } \omega > \alpha v_{Ti}; \\ \varepsilon^{3/2}\rho^2\alpha & \text{при } \omega < \alpha v_{Ti}; \end{cases}$	$\left(1 - k_\perp^2\rho_i^2\frac{\partial \ln T_i}{\partial \ln N}\right) < 4\frac{a}{R_{эф}}\frac{\partial \ln T_i}{\partial \ln N}$ $\frac{\partial \ln T_i}{\partial \ln N} \gg 1$		$\Theta > \frac{\rho_i}{\sqrt{a R_{эф}}}\sqrt{\frac{\partial \ln T_i}{\partial \ln N}}$
7.	$\omega^3 \simeq k_\parallel^2 v_{Te}^2 k_\perp\rho_i\frac{v_{Ti}}{R_{эф}}\sqrt{\varepsilon}\rho$ $R_{эф}^{-1} = \begin{cases} \varepsilon^2\rho^3\alpha & \text{при } \omega > \alpha v_{Ti} \\ \varepsilon^{3/2}\rho^2\alpha & \text{при } \omega < \alpha v_{Ti} \end{cases}$	$\omega < k_\parallel v_{Te}\sqrt{\varepsilon I_2}$ $\frac{\partial \ln T_e}{\partial \ln N} \gg 1$		$\Theta > \frac{\rho_i}{a}\sqrt{\frac{m}{M}}\sqrt[4]{\frac{a}{R_{эф}}\varepsilon I_2} \times \left(\frac{\partial \ln T_e}{\partial \ln N}\right)^{3/4}$

$$\Delta_1 = k_\perp^2\rho_i^2\frac{T_e}{T_i} - \frac{k_\parallel^2 v_s^2}{\omega^2} - \varepsilon^2\rho^4\alpha a\frac{T_i}{T_e}$$

$$\Delta_2 = \Delta_1 + \varepsilon^{3/2}\rho^2\alpha a\frac{T_e^2}{T_e^2}$$

получить еще один гидродинамически неустойчивый спектр,обусловленный характером движения медленнопролетных частиц:

$$\omega^3 = -k_\parallel^2 v_{Ti}^2 \frac{\ell}{\Psi} \rho_i \frac{v_{Ti}}{R} \frac{d\ln N T_i}{d\ln N T_i^{-1}} \left(1 + \frac{T_e}{T_i}\right)^2 \frac{q_1^3}{q_4} \varepsilon I_2 \left(1 + \frac{T_i}{T_e}\right)^{-1} \quad (4.43)$$

Эта неустойчивость существует только при достаточно малых $k_\parallel$,когда предпоследний член в уравнении (4.40) превосходит единицу.Поэтому она может быть застабилизирована широм при условии

$$\theta > \frac{\rho_i}{a} \left(1 + \frac{T_i}{T_e}\right)^{-1} \quad (4.44)$$

Как уже отмечалось выше, это условие в существующих установках не выполняется. В отличие от неустойчивости (4.40)колебания со спектром(4.43) неустойчивы как в области с неблагоприятной,так и в области с благоприятной кривизной удерживающего поля.

5. ЗАКЛЮЧЕНИЕ

Проведенный нами анализ устойчивости малых возмущений в плазме, помещенной в двухзаходное магнитное поле с винтовой симметрией,показал,что наиболее опасными остаются,в основном, уже известные неустойчивости:гидродинамическая неустойчивость (типа желобковой) на запертых частицах[1],которая хотя имеет и небольшой инкремент,но в принципе не может быть застабилизирована широм,дрейфово-температурные и кинетические неустойчивости,для стабилизации которых необходим достаточно большой шир ($\theta > \frac{\rho_i}{a} \frac{d\ln T}{d\ln N}$ при $\frac{d\ln T}{d\ln N} \gg 1$,либо $\theta > \frac{\rho_i}{a} \sqrt{\frac{T_e}{T_i}}$ при $T_e \gg T_i$). Такой шир пока еще не получен в реальных установках.Из найденных нами новых неустойчивостей наиболее опасной является кинетическая неустойчивость,обусловленная резонансом быстропролетных электронов с волной.Эта неустойчивость имеет достаточно большой инкремент (4.17),по порядку величины сравнимый с дрейфовой частотой,и не стабилизируется широм,который достигнут в существующих установках на сегодняшний день.

ТАБЛИЦА III

$\omega \ll k_\parallel v_{Ti}$

№№	Спектры частот	Условие существования	Механизмы неустойчивости	Стабилизация широм
I.	$\omega^2 \approx -k_\perp^2\rho_i^2 \frac{v_{Ti}^2}{aR}\varepsilon^{3/2}\rho_i^2$	$\omega \ll k_\parallel v_{Ti}\sqrt{\varepsilon I_1}$ $k_\perp^2\rho_i^2 < \sqrt{\alpha a\sqrt{\varepsilon}}$	Дрейф запертых частиц	отсутствует
2.	$\omega \approx k_\perp^3\rho_i^3 \frac{v_{Ti}}{a}\sqrt{\varepsilon I_2}\left(1+\frac{T_i}{T_e}\right)^{-1}$ $\gamma = \frac{\omega^4}{(k_\parallel v_{Ti})^3}\frac{1}{k_\perp^2\rho_i^2(\sqrt{\varepsilon I_2})^3}\frac{\partial \ln T_i^{3/2}N}{\partial \ln N T_i}$	$\omega \ll k_\parallel v_{Ti}\sqrt{\varepsilon I_2}$; $k_\perp^4\rho_i^4 > a\alpha\sqrt{\varepsilon}$		отсутствует
3.	$\omega^3 \approx -k_\parallel^2 v_{Ti}^2\varepsilon^2\rho^3\alpha v_{Ti} k_\perp\rho_i$;	$\omega < k_\parallel v_{Ti}\sqrt{\varepsilon I_2}$, $\Theta > \frac{\rho_i}{a}\left(1+\frac{T_i}{T_e}\right)^{-1}$.		

Как показывают оценки, для стабилизации широм всех рассмотренных нами низкочастотных длинноволновых колебаний (за исключением неустойчивости на запертых частицах [1]) в термоядерной плазме ($T \sim 10^4$ эв, $B_0 \sim 10^5$ эрстед, $N \sim 10^{15}$ см$^{-3}$) необходимо построить двухзаходный стелларатор с параметрами $R_0 = 2 \div 3$ м, $r_0 = 0,5$ м, $\varepsilon = 0,3$, $h = 5 \div 6$.

ЛИТЕРАТУРА

[1] КАДОМЦЕВ, Б.Б., ПОГУЦЕ, О.П., сб. "Вопросы теории плазмы" вып.5, М., Госатомиздат, 1967.

[2] КОППИ, Б., РОЗЕНБЛЮТ, М., Препринт № 21-102,1967.

[3] МОРОЗОВ, А.И., СОЛОВЬВ, Л.С., Сб. "Вопросы теории плазмы" вып. 2, М., Госатомиздат, 1963.

[4] ГРАДШТЕЙН, И.С., РЫЖИК, И.М., "Таблицы интегралов", М., Физматгиз, 1962.

[5] МИХАЙЛОВСКАЯ, Л.В., МИХАЙЛОВСКИЙ, А.Б., Ядерный синтез 5 (1965) 234.

[6] РУХАДЗЕ, А.А., СИЛИН, В.П., Кинетическая теория дрейфово-диссипативных неустойчивостей (Доклад на конференции в Принстоне, 1966) УФН 95 № 2 (1968).

DISCUSSION

B. COPPI: Could you give more information about the kinetic instability of slowly moving particles which you have found?

A.A. RUKHADZE: If you mean the instability whose spectrum I discussed in my oral presentation, its nature consists in the resonance interaction of fast moving electrons with a wave in a field with periodic curvature, a mechanism similar to that which has been considered by you and Rosenbluth. Moreover, there are other kinetic instability mechanisms which consist of resonance interaction of the wave with oscillations of the trapped particles and with the average motion of the slowly moving particles (Cherenkov effect).

A MAXIMUM-B STELLERATOR

S. FISHER, H. GRAD, Y. SONE AND J. STAPLES
COURANT INSTITUTE OF MATHEMATICAL SCIENCES
NEW YORK UNIVERSITY, NEW YORK, N.Y.,
UNITED STATES OF AMERICA

Abstract

A MAXIMUM-B STELLERATOR. Every toroidal plasma is a hybrid combination of mirror machine and torus. Approximately half the plasma consists of trapped particles. Towards the outer edge, the population becomes almost entirely trapped (circulating particles are preferentially scraped off). A toroidal plasma in equilibrium cannot be isotropic, and towards the edge the anisotropy becomes more pronounced. In most geometries there will be holes in phase space which are qualitatively similar to a loss cone. The geometry we propose is one in which these mirror attributes are planned rather than accidental. The maximum-B criterion enjoys all known advantages of minimum-B (with respect to micro- and macro-stability as well as containment) and is much more easily realized practically. In particular, it can be achieved in a torus without internal conductors.

One representation is as a modification of an $\ell = 3$ Stellerator. Qualitatively, there is an outer shell which is comparable to a mirror machine, and an inner toroidal core. Compared to a mirror machine this offers the interesting possibility of cutting particle losses by a large factor in a familiar range of densities and temperatures. Compared to a Stellarator, it offers the possibility of achieving mirror machine (or much better than mirror machine) parameters in a toroidal geometry.

There are many mechanisms which can lead to "Bohm" diffusion including non-collective orbit drifts and lack of equilibrium as well as a variety of different instabilities. It is not known at the present time under what conditions each of these mechanisms is applicable or potentially dangerous. The outer shell of the maximum-B configuration should be free of this phenomenon as in any conventional mirror machine. The large flat field region in the center should be relatively free of all micro-instability. Containment of particles (a possible source of Bohm diffusion) is secured by the maximum-B property. Also, a stable outer shell should exert an inhibiting effect on whatever specifically toroidal ills the interior is subject to.

We discuss the status of the theory of this type of geometry with regard to magnetic field configuration, orbits, equilibrium (scalar pressure and anisotropic), and a modicum of stability, primarily in a straight version.

1. INTRODUCTION

Our purpose in this paper is to discuss the features of a certain class of toroidal containment geometries which are advantageous with respect to orbits, equilibrium, and macro-stability[1]. A great deal of attention has been paid to plasma micro-stability. While this is, no doubt, important, the significance of simple orbit containment and static equilibrium is at least equal in importance, and in the present state of the art for toroidal confinement, it is considerably more urgent.

In most toroidal configurations some 20% to 90% of the plasma consists of trapped orbits. The containment of circulating orbits is related to flux surfaces. It has been recently recognized that containment of the large trapped segment of the plasma population can be completely unrelated to flux surfaces [2]. Also, numerical calculation of the trapped particle drift surfaces is at least two orders of magnitude larger than that of flux surfaces. Additional complications are the presence of a class of circulating particles which border on being trapped [3] and several classes of transitional trapped particles which can change their trapped state [2]. The latter orbits can cover an appreciable part of phase space and are not simply described by either flux or drift surfaces.

It is axiomatic that an exact equilibrium can never be produced; there will be a residual level of fluctuation which depends on the details of injection, unless this is lost by dissipation. But in some cases there is an irreducible lower level for the fluctuations, independent of how much care is used to create the plasma and regardless of dissipation; mathematically, there is no equilibrium that the plasma can try to approach [2].

It is interesting to compare a mirror machine with a torus in this context. In most mirror machines the orbit problem is relatively simple. Questions of equilibrium, fluctuations caused by imperfect injection, and macro-stability are all reduced by line-tying and the free communication with the outside world. There remains an easily identified dominant physical effect, the loss cone. In a torus no dominant phenomenon can be identified at the present time. It is not clear what part of the plasma loss can be attributed to direct orbit loss, lack of equilibrium, incidental fluctuations left by imperfect injection, macro- or various forms of micro-instability (including loss cone), and a variety of "anomalous" diffusion mechanisms. We shall concentrate, in this paper, on the more primitive of these physical mechanisms.

2. MAXIMUM-B STELLERATOR CONFIGURATIONS

It is necessary to distinguish three distinct magnetic well concepts[1].

Min-B_1: A magnetic configuration in which the plasma ends at a flux surface on which $\partial|B|/\partial n > 0$.

Min-B_2: A magnetic configuration in which the plasma is contained in a region of nested, monotonically increasing $|B|$-contours.

Max-B: The plasma is contained within a $|B|$-contour on which the value of $|B|$ is larger than any value in the interior of the plasma (there can be other local maxima as well as minima and other stationary points in the plasma).

Min-B_1 was originally introduced as a stability criterion for a field-excluding scalar pressure plasma [4]; it is in

[1] Sometimes $V'' < 0$ is also called a "magnetic well." This concept has no connection with orbit containment and only a tenuous connection with stability (cf. Appendix).

this case a necessary and sufficient condition for stability. Min-B_2 was originally introduced to contain Taylor's special guiding-center anisotropic distribution, $f(\varepsilon,\mu)$ with $\partial f/\partial\varepsilon < 0$ [5]. Max-B was introduced [6] as a relaxation of Taylor's containment criterion, Min-B_2.

Min-B_1 cannot be satisfied on any smooth flux surface, whether mirror or torus [4] (this theorem led to the Cusped Geometry). Min-B_2 can be satisfied in a mirror but, apparently, not in a toroidal vacuum field. Max-B can be easily satisfied in either a mirror or a torus.

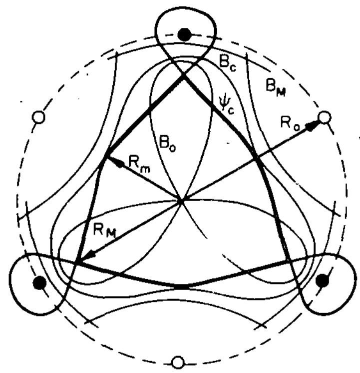

FIG. 1. Hexapole field configuration.

Min-B_1 is also a sufficient condition for stability of a general scalar pressure equilibrium [7]; but it represents only a qualitative tendency since, in this case, it can never be satisfied. When combined with the requirement that $|B|$ not vanish, in order to encourage mirror containment [8], it is even more qualitative, since an anisotropic plasma does not end at a flux surface. Neither Min-B_2 nor Max-B has been related to stability in any way. In particular, the belief that Min-B is a stability criterion which can be achieved in a mirror but not in a torus results simply from blending several different criteria.

The simplest prototype of a Max-B torus is a straight version, periodic in z, composed of a uniform z-field B_o plus a helical field of order $N \geq 3$ (hexapole or higher; 2N is the total number of coils) [1]. The dominant features, shown in Fig. 1 for N = 3, are a separatrix, ψ_c, (heavy solid line) which encloses a family of flux surfaces and is surrounded by a simple closed $|B|$-contour, B_c. If we consider the plasma to end at B_c, there are trapped orbits between B_c and ψ_c and a combination of trapped and circulating particles within ψ_c. There is a field minimum, $B_m < B_o$, inside each of the three lobes $|B| = B_o$. B_M represents the largest simple $|B|$-contour which encloses the plasma, but not the coils. If the plasma is limited to a small flux surface, we have a conventional Stellerator; if it extends beyond the coils, we have a helically modified multipole.

There are two basic dimensionless parameters which describe such a field (in addition to N). We take them to be the helical pitch

$$x = kR_o = 2\pi R_o/L \qquad (2.1)$$

(R_o is the coil radius and L is the axial period for a single coil) and

$$\alpha = \frac{\mu_o I_1}{2\pi R_o B_o} = \frac{I_1}{I_o} \qquad (2.2)$$

the ratio of the helical current in one wire, I_1, to the "toroidal" current in an axial length $2\pi R_o$.

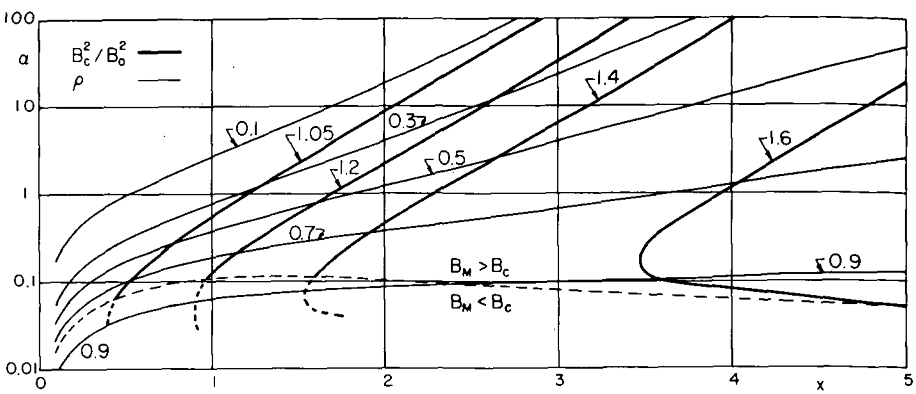

FIG. 2. Hexapole parameter variation.

Some of the interesting parameter variations are shown in Fig. 2. For all α and x we have $B_c^2/B_o^2 < 1.633$. But slightly smaller values, e.g. $B_c^2/B_o^2 > 1.4$, can be attained for a wide range of α and x. The size of the flux region is described by $\rho = R_M/R_o$ (cf. Figs. 1 and 2). The dashed line in Fig. 2 separates a region ($B_M > B_c$) where the B_c contour surrounds the entire flux region from another region ($B_M < B_c$ below the dashed line) where the useful flux region has to be reduced in order to be entirely contained within a $|B|$-contour. There are several other "well-depth" parameters viz. B_o/B_m and B_M/B_o which can take quite large values, and a parameter R_m/R_M which describes the shape of the separatrix; these will be described elsewhere. Fig. 1 is drawn for the values N = 3, x = 2, ρ = 0.8, $B_c^2/B_o^2 = 1.46$, $B_M^2/B_o^2 = 2.65$, $B_m^2/B_o^2 = 0.279$. The question of optimizing containment with respect to the various well-depths and flux properties is premature at this time. But it is clear that there is a wide range of relevant parameters in which a significant well-depth and a sizeable flux region are simultaneously possible.

The asymptotic behavior for large x, keeping $R_M/R_o = \rho$ and N fixed is given by

$$\begin{aligned} \psi_c &\sim \frac{1}{2} x^2(\rho^2 - 2\rho/Nx) \\ \beta = \alpha Nx &\sim \frac{1}{2} \rho^{1/2} \exp[Nx(1-\rho)] \\ B_m^2/B_o^2 &\sim 0 \\ B_c^2/B_o^2 &\sim 1.633 \\ B_M^2/B_o^2 &\sim \beta^2 \end{aligned} \tag{2.3}$$

Since Nx is the number of positive helical coils in an axial length $2\pi R$, β is the ratio of the "total" helical to toroidal current in a given axial length.

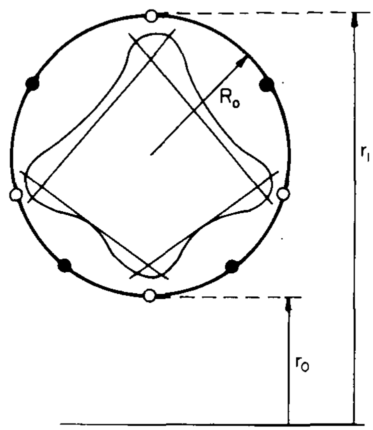

FIG. 3. Toroidal octupole

There are many more parameters to consider when this helical field is bent into an actual torus. There is not only the obvious aspect ratio of the torus but the shape of the minor cross-section (a circle, R_o, as in Fig. 3, is not necessarily optimal); also, not only does α vary with the distance r from the axis, but the pitch, x, and coil density, $N/2\pi R_o$, may vary with r. For even a large aspect ratio quadrupole it has been found that the useable flux area is seriously reduced. But it is easy to show that a finite aspect torus with large value of Nx can be just as effective as the straight configuration. The asymptotic formulas (2.3) carry over if we interpret x, α, ν = Nx to be local values (functions of r); x(r) is the tangent of the pitch angle, $\alpha \sim r$, and $\nu(r)$ is the density of positive coils per $2\pi R_o$ of axial length (α is also normalized to $2\pi R_o$ of axial length).

To insure axial symmetry, we must have $\nu r/x$ = const. We find that the separatrix is (asymptotically) a simple closed curve if ψ_c is constant in r. To lowest order, taking $\rho \sim 1$ and $\psi_c \sim \frac{1}{2} x^2$, this implies constant pitch angle x. Thus the optimal coil density, ν, varies as $1/r$ (an intuitive result).

The asymptotic value of $B_c^2 = 1.633\ B_o^2$ cannot be kept constant since $B_o \sim \frac{1}{r}$. But the gradient of $|B|$ is very large in the limit of large Nx; therefore there is a $|B|$-contour which closely surrounds the separtrix.

Using the more exact formulas (2.3) in an appropriate toroidal form for a toroidal aspect ratio two (i.e. $r_1/r_o = 2$ in Fig. 3--the toroidal field varies by a factor two), together with a nominal value $N = 4$ (octupole) and $x = 3$, we find a ψ_c which is completely enclosed within a $|B|$-contour such that x ranges between 2.7 and 3.4, ρ between 0.8 and 0.9, and ν between 8.5 and 17 (as r varies by a factor 2). The nominal value $Nx \sim 12$ is probably large enough for the asymptotic formulas to be fairly accurate, but some numerical calculation is necessary to verify and extend these results. A thin region in the neighborhood of the separatrix can be expected to behave stochastically [9].

The influence on these vacuum Max-B fields of finite β plasma equilibria, both scalar pressure and anisotropic, will be published elsewhere.

3. CONTAINMENT

We give a summary of the status of the relevant theory under the headings, Orbits, Equilibrium, and Diffusion. The question of stability is touched on briefly in the Conclusion.

Orbits

The most primitive question with regard to containment involves individual particle orbits, assuming that the field is known. There are many classes of orbits, each with its own distinct requirements. The two main categories are circulating particles whose confinement is related to flux surfaces and trapped particles which may be similarly guided by drift surfaces. In an asymmetric field (such as a Stellerator) the trapped drift surfaces are quite distinct from flux surfaces, even in the limit of vanishing gyro radius, and the study of flux surfaces alone ignores an important component of a toroidal plasma. At a given location, the ratio of trapped to total density (for an isotropic distribution) is $(1 - B/B_1)^{1/2}$, where B is the local value of B and B_1 is the maximum on the given flux surface. The trapped population is always appreciable, and in a multipole it is even most of the plasma.

In addition to the basic classes, trapped and circulating, there are transitional orbits. Circulating particles which border on being trapped are not confined to a flux surface or a drift surface, and every cross-over from one trapped state to another yields trapped orbits which are not confined to a drift surface. The latter class of orbits has the disturbing property that a <u>finite</u> portion of phase space can be covered ergodically in the limit of vanishing gyro radius [10].

Consider the different trapped states I, II', and II" in Fig. 4. In an asymmetric field, the cross-over value B_o will vary from line to line on a drift surface. The adiabatic invariant $J = \int V_{\parallel} ds$ which defines a drift surface is a local invariant only. A particle which drifts from state II to state I and then back to state II will not return to the same drift surface or value of J. Since there is an essentially random choice between II' and II", it is clear that the path is ergodic for all drift surfaces which touch a given cross-over value $\varepsilon/\mu = B_o$. This gives a finite ergodic volume in phase space, unless the field is symmetric by reflection through a plane.

A cruder but much simpler containment mechanism than drift surfaces is a magnetic well. A particle with $\varepsilon/\mu < B_1$ cannot reach a position where a field has the value B_1. This is true whether there are drift surfaces or cross-over and ergodic regions, or transitions from circulating to trapped.

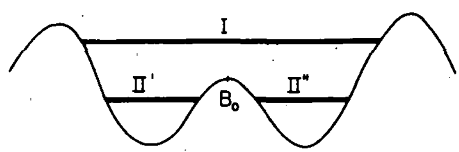

FIG. 4. Trapped states.

In comparison with the single family of flux surfaces, there is a family of distinct drift surfaces for each ε/μ in the absence of an electrostatic field, and a separate family for ε and μ individually in the presence of a field. With the added complication of a number of different trapped states to consider, we see the enormous gain in simplicity of containment with a well to counterbalance the reduction in flexibility.

The question of resonances of fields and orbits is quite complex. The size of the resonance regions must be distinguished from containment effectiveness. In this connection, we must also distinguish the problem of flux surfaces and guiding-center orbits from that of finite but small gyro radius orbits. The mathematical characterization is by a plane map for the magnetic field problem and for any order in a guiding-center orbit expansion. Any closed invariant curve guarantees absolute containment of the interior, no matter how wide the interior resonances may be. Physically, a flux line cannot cross a closed flux surface, nor can a guiding-center orbit cross a guiding-center drift surface. But the exact orbit equations involve a four-dimensional map. Although it can be proved that, under perturbation, a finite part of the four-dimensional phase space is absolutely contained on a family of invariant surfaces [11], there is no simple implication with regard to containment in the omitted resonant regions in this case.

For example, in an axially symmetric mirror, finite orbits yield a two-dimensional map. Thus resonances do not necessarily imply losses. But in an asymmetric mirror, the map is four-dimensional. With finite orbits, there is a set of everywhere dense (though possibly very thin) loss cones.

Explicit flux or guiding-center surfaces are usually found only when there is an ignorable coordinate. But one can also find asymptotically ignorable coordinates in an expansion. This occurs, e.g., in a "Stellerator" expansion in which a finite rotational transform is built up from a large number of identical segments, each with a small transform. The same is true of the large Nx limit described in Sec. 2. Such asymptotically ignorable limits are characterized by transendentally thin resonances which are invisible to an expansion. It should be pointed out that such an approximately ignorable coordinate applies only to the magnetic field, to definitely circulating particles, and, in general, to any

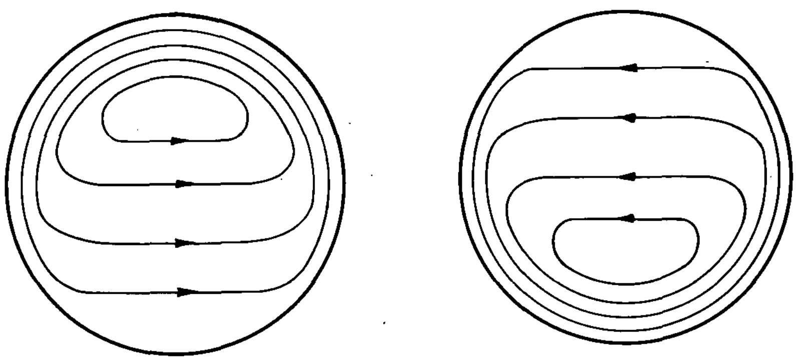

FIG. 5. Ion and electron drift surfaces.

quantity which samples the entire magnetic line. Trapped particle drift surfaces are localized and remain distinct from flux surfaces even in the limit of vanishing gyro radius.

An expansion can miss resonance regions even when they are not transcendentally thin. A perturbation by an amount δ from a symmetric configuration will normally give rise to resonances which are algebraically thin in δ. But a expansion in $(r-r_o)/\delta$ (or r/δ) about a non-resonant location r_o (or about the axis) will miss all resonances.

In the finite toroidal aspect, large x expansion of Sec. 2, the rotational transform is very small at a distance from the coils. Particles will be confined to surfaces which arise from ∇B drifts in the interior and from the rotational transform near the coils, somewhat as shown in Fig. 5.

If a straight helical field is bent into a large aspect torus, the full Max-B region is not required for confinement. Trapped particle drift "ribbons" will be only slightly perturbed by the toroidal curvature. Higher order trapped orbits, transitional orbits, and barely circulating orbits introduced by the perturbation will be found in a possibly ergodic region; but this region is bounded on one side by safely trapped particles, and on the other by safely circulating particles. One can therefore guess that a large aspect torus might be safely contained by a quadrupole field without Max-B properties.

We have carefully avoided mention of electric fields up to now. In principle they can be included in the orbit analysis or numerical calculation, provided that they are known. Circulating particles are relatively insensitive to electric fields; (the primary effect is to change the rotational transform). But trapped particles can be extremely sensitive to electric fields. For example, consider a configuration with contained drift surfaces in the absence of E. To lowest order, electrons and ions follow the same drift surfaces, but with opposite orientation. A small electric field will distort the electron and ion drift surfaces oppositely. An E x B field large enough to dominate the ∇B drift constrains the trapped ions and electrons to flux (i.e. equipotential) surfaces, but now with the same orientation. Between these extremes, the electric field must be such as to completely open up either the ion or electron drift surfaces. The worst situation, apparently, is with E x B drifts comparable to ∇B drifts. Electric fields of this magnitude are almost inevitable in a torus, although they may be shorted out in a mirror.

To summarize, absolute or high order orbit containment in a torus requires either an ignorable (or asymptotically ignorable) coordinate or a magnetic well. Otherwise, only zero or first order confinement can be verified (even though high order confinement is frequently verifiable in <u>part</u> of phase space). There is high order containment of trapped particles in a well (with a suitably cut-off loss cone distribution). Good containment could also be accomplished, in principle, by designing suitable drift surfaces, but such a calculation would be enormous. Circulating particles are contained to high order if the border between trapped and circulating is taken care of (at the separatrix and elsewhere); this is done simply only by a well.

Equilibrium

Almost the entire equilibrium theory in containment geometries is obtained from the zero order guiding-center theory (and the important special case, scalar pressure MHD)[2]. Given the guiding-center distributions, $f_{\pm}(\varepsilon,\mu,\psi)$ (ψ represents one or two flux coordinates), we construct a charge neutralization potential $\phi(B,\psi)$ by solving a nonlinear integral equation, after which $p_{\perp}(B,\psi)$ and $p_{\parallel}(B,\psi)$ can be evaluated and the problem reduces to a system of partial differential equations. These equations are elliptic provided that a local stability requirement is met [12].

---

[2] For a comprehensive survey see [12].

The equations fail to have solutions in a toroidal geometry unless one of the following conditions is met [2]:

$$\begin{array}{ll} \text{a)} & \text{ignorable coordinate} \\ \text{b)} & \text{closed magnetic lines} \\ \text{c)} & f(\varepsilon,\mu) \text{ independent of } \psi \\ \text{d)} & \text{piecewise constant pressure } p_i \text{ or } f_i(\varepsilon,\mu). \end{array} \qquad (3.1)$$

Formal asymptotic expansions can also be obtained if there is an asymptotically ignorable coordinate.

The mathematical breakdown when the above conditions are met should be physically evidenced by anomalously large parallel current. Such islands of large $J_{\parallel}$ have been observed[3]. At very low β (such as in the aforementioned experiment), there may be no consequences other than large current. At higher β, electric fluctuations and instabilities should be induced by the large $J_{\parallel}$.

It is interesting to compare a mirror machine with a torus in this context. A scalar pressure mirror machine with $J_{\parallel} = 0$ at the ends (no line-tying) requires special pressure profiles to be in equilibrium [13]. But it is always possible to redistribute the pressure values to make it into an equilibrium ($p \sim \int d\ell/B$). Similarly, only special guiding-center distributions will be in equilibrium when placed in a mirror with insulated ends [6]. In this case it is not known whether every "incorrect" distribution function can be shifted into an equilibrium. In a general asymmetric torus with shear, there are only very special pressure profiles (step-functions) and very special distributions [$f(\varepsilon,\mu)$] which are in equilibrium. In this case an "incorrect" distribution cannot be rearranged to reach equilibrium.

In a mirror with line tying, any pressure profile or distribution function is compatible with equilibrium. The fact that there is no line tying in a torus is perhaps the single most important qualitative difference from a mirror. There are many physical signals which propagate along magnetic lines--Alfvén waves, electrostatic potential, guiding-center orbits, etc. Whether subject to the experimenter's control or not, this information has access to the outside of the plasma in a mirror but not in a torus.

A related but independent effect involving charge neutrality also arises from imperfect creation of the plasma. A magnetic line which almost closes presents two points which are distant when measured along the line but are nearby across the field. Electrostatic potential propagates along the line to establish charge neutrality. In equilibrium, the potential is obtained as the solution of an integral equation and is a function of B alone on a given flux surface. The values of ϕ at the two nearby ends of the magnetic line hardly differ, and no significant perpendicular fields arise. In a transient problem, large perpendicular fields can arise, and the reaction of the system, through E x B, has no direct

---

[3] University of Wisconsin Multipole, D. Kerst, private communication.

relation to the causal mechanism which propagates along the line. Thus we can expect enhanced fluctuations near a resonance even in cases (such as axial symmetry) where a true equilibrium can exist.

The Max-B drift surfaces of Fig. 5 present a special problem. The ion and electron distribution functions must be constant on their respective drift surfaces. The only distribution functions that can maintain charge neutrality are $f_{\pm}(\varepsilon,\mu)$, independent of the drift surface coordinate. Another distribution might give rise to a dipole electric field; if the resultant E x B were to dominate the ∇B drift, the ion and electron drift surfaces would again coincide and might look like Fig. 6.

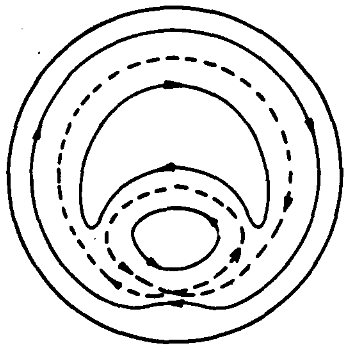

FIG. 6. Electric field drift surfaces.

In any problem in which ∇B makes a significant contribution to the drift surfaces (e.g. with small rotational transform) the only compatible equilibrium distribution is $f(\varepsilon,\mu)$ independent of flux coordinate. Conversely, if we do not set up this precise distribution function, any equilibrium with small magnetic rotational transform must be dominated by induced electric fields. In a case with ergodic drift surfaces, there is a clear mechanism to produce $f(\varepsilon,\mu)$. In a case such as Fig. 5, the resolution is through electric fields; it is not clear why they should be static.

The special distribution, $f(\varepsilon,\mu)$, is compatible with first order drifts. There is virtually no other first order equilibrium theory which includes particle drifts. It is clear that there are no general equilibria with finite gyro radius. In a simple mirror without axial symmetry there is an everywhere dense loss cone! This might cause little experimental difficulty; but it makes theory exceedingly difficult. The most useful theoretical expedient may be a formal expansion with an asymptotically ignorable coordinate. The proper interpretation of such a result is that, even though no true solution exists, one would expect that this formal "solution," taken as an initial value, would persist for some time. Whether the result is valuable or not depends on the time scale of the experiment.

To summarize, no equilibrium analysis beyond first order has been done (except in geometries which are too simple to contain plasma). A first order theory exists only for the distribution $f(\varepsilon,\mu)$ and (partially) for axial symmetry. The possibilities for zero order theory are only slightly more general (3.1). To resolve the nonexistent zero order solutions would require going to at least second order. The result would presumably be very large instead of infinite currents. Strict equilibria probably do not exist except in very special cases. The crucial problem is to try to estimate how long an approximate equilibrium can persist, and to estimate the level of fluctuations. No conventional stability analysis can be attempted except in the cases listed in (3.1).

In the straight Max-B configuration, equilibria can be computed for any guiding-center distribution $f(\varepsilon,\mu,\psi)$. For example, $a(\psi)f(\varepsilon) + b(\psi)g(\varepsilon,\mu)$ allows a transition from an isotropic core to a loss cone distribution in the mirror region. In a general toroidal version only $f(\varepsilon,\mu)$ or piecewise constant $f_i(\varepsilon,\mu)$ can be used. But with many periodic sections, asymptotic expansions of equilibria can be carried out in as much generality as for the straight configuration [14], [15].

Diffusion

A diffusion process results from a random walk. If δ is the step size and ν the step frequency, the diffusion coefficient $D \sim \delta^2\nu$, and the containment time is $\tau \sim R^2/D = R^2/\delta^2\nu$ (R is the radius of the plasma). In "classical" diffusion $\delta \sim \lambda$ (Larmor radius) and $\nu \sim \nu_c$ (collision frequency), giving $D_c \sim \lambda^2\nu_c$. In "Bohm" diffusion $\delta \sim \lambda$ but $\nu \sim \omega_c$ (cyclotron frequency), thus $D_B \sim \lambda^2\omega_c$.

Particle loss from a drift surface which intersects the wall is a direct rather than a random walk. But converting the containment time $\tau \sim R/v_d$ ($v_d \sim \lambda v_{th}/R$) into an equivalent diffusion coefficient gives exactly D_B.

We wish to estimate the "anomalous" diffusion which is produced by a number of mechanisms which alter the basic random (or direct) walk. In addition to the collision frequency ν_c and cyclotron frequency ω_c, we shall consider the drift frequency $\nu_d \sim v_d/R$ and the transit frequency $\nu_t \sim v_{th}/R$; (we use ν_t to represent a bounce frequency between mirrors as well as a transit frequency, once around the torus). We shall assume that ν_c, $\nu_d \ll \nu_t \ll \omega_c$, but allow ν_c/ν_d to be arbitrary ($\omega_c\nu_d \sim \nu_t^2$).

First consider collisions which alter the trapped state of a particle. Suppose there are two sets of trapped drift surfaces which differ finitely; i.e. two drift surfaces through the same point will diverge by an appreciable fraction of R. If $\nu_c \ll \nu_d$, a particle will be lost after a finite number of collisions; by finite we mean a number which depends solely on the geometry of the drift surfaces; in particular, it does not increase as $\lambda \to 0$. The containment time is $1/\nu_c$, thus $D \sim (\nu_c/\nu_d)D_B$. If $\nu_c \gg \nu_d$, the random walk has step size $\delta = v_d/v_c$ and step frequency v_c; we have $D \sim (v_d/v_c)D_B$. We can combine the results, for arbitrary v_c/v_d in the form $D \sim \alpha D_B$ where α is the smaller of v_c/v_d and v_d/v_c; we have $D \gg D_c$ for all parameter values. D is comparable to D_B if $v_d \sim v_c$. There is, of course, an omitted geometrical factor which depends on the divergence between the two sets of drift surfaces.

For a trapped-circulating transition, we compare drift surfaces with flux surfaces. For $v_c \ll v_d$ the situation is exactly the same as for a trapped-trapped transition. For $v_c \gg v_d$ the situation is different. It takes a shorter time, $1/v_t$, to cover a flux surface, than to cover a drift surface, $1/v_d$. The process is a random walk from one flux surface to another, the step being a short segment of a drift surface. Since a borderline trapped particle is approximately ergodic on a flux surface, grazing collisions are relatively ineffective, and v_c must be reduced by a factor log Λ. For $v_c \sim v_d$ we estimate $D \sim D_B$.

We see that the trapped-circulating transition can be somewhat less effective than the trapped-trapped, but a more important consideration might be the relative divergence between sets of drift surfaces as compared to drift and flux surfaces. Note that this effect is quite distinct from that found in axial symmetry where the divergence ("banana" thickness) becomes small with λ.

Next we turn to the effect of ergodic drift surfaces. If the ergodic region reaches the wall we have $D \sim D_B$, with a numerical factor that depends on the magnetic geometry alone (and, in principle, can be calculated exactly). If the ergodic regions do not touch the wall, we may have enhanced collisional diffusion. For $v_c \gg v_d$, there is no enhancement, $D \sim D_c$. For $v_c \ll v_d$ a simple estimate yields $D \sim (n/\log \Lambda)D_c$ where n is the thickness of the ergodic layer in Larmor radii. This is probably not significant.

In a Max-B configuration with large Nx, Fig. 5, we have a thin outer shell which a particle passes through quickly, and a large inner region where the drift is slow. A simple estimate shows that collisions in the outer shell are more effective. Because of the short residence time, the local diffusion coefficient is reduced by a factor d/R (d is the layer thickness), but the net effect is to reduce the (classical) containment time of the entire plasma by a factor d/R. If in varying the magnetic field one were to keep d a finite multiple of λ, the effective diffusion coefficient would appear to scale as 1/B.

In the zero order guiding-center theory, $E + u \times B = 0$, magnetic surfaces are preserved by any motion. To next order one finds a flux mis-match in a magnetic line, on circling the torus, which is on the order of λ [from curl $(E + u \times B) \neq 0$]. This random walk, with step size $\delta \sim \lambda$ and step frequency v_t yields $D \sim (v_t/v_c)D_c \sim (v_t/\omega_c)D_B$; we have $D_c \ll D \ll D_B$.

As described previously, we can expect to find a fluctuating perpendicular electric field of order $E \sim kT/er$ between the two ends of a magnetic line which misses being closed by an amount r. We estimate

$$\langle E^2 \rangle = \frac{1}{R}\int E^2 dr$$

where at each resonance r is cut off at a value λ; thus $\langle E^2 \rangle \sim k^2T^2/e^2R\lambda$. From the formula $D \sim \langle E^2 \rangle / B^2\nu_t$ (which assumes that E is uncorrelated after a circuit $1/\nu_t$ around the torus), we find $D \sim D_B$. This mechanism is applicable to any system with shear, axially symmetric or not.

In the MHD theory, $J_\parallel$ propagates along a line as an Alfven wave. Estimating $E_\perp \sim k_\perp(kT/e)$ and $J_\perp \sim k_\perp p/B$, a simple calculation gives the estimate

$$J_\parallel / J_\perp \sim k_\perp \lambda / \beta^{1/2}$$

We conclude that large $J_\parallel$ (as a consequence of resonances) can give rise to $\langle E_\perp^2 \rangle$ of a magnitude to produce significant diffusion (as in the previous calculation). But conversely, $E_\perp$ arising from almost closed lines can be expected to give rise to very large $J_\parallel$ even in an axially symmetric geometry.

Some of the diffusion coefficients are the same for ions and electrons (e.g. D_B); others are not. A balance will be reached by some kind of ambipolar mechanism; but this can be very complex if several competing processes act at one time.

With ingenuity one can certainly find many more "anomalous" diffusion effects. In a given situation there may be a dozen different diffusion coefficients, each effective in a certain part of physical of phase space. No experimental scaling law is by itself sufficient to identify a loss mechanism. It is unlikely that all of these effects will be important in any given experiment; but it is also quite likely that each mechanism will be observable in <u>some</u> experiment.

Each one of these effects can be pinned down to, say within one order of magnitude, but only after a large scale theoretical program (for each). It is probably up to experiment to try to determine whether only a small number of these possibilities actually dominate containment.

4. CONCLUSION

The toroidal Max-B configuration possesses a number of attractive features with regard to containment. Orbits are very well confined through a combination of flux surfaces and a deep magnetic well. Equilibrium features are quite good as a consequence of the well and approximately ignorable coordinate (taking many periodic sections).

The general nature of the field is such as to promote macro-stability[4]. There is no trouble stabilizing near the axis (cf. Appendix). Further out, the well and substantial shear offer a strong tendency toward stability. For the outer mirror layer, we may refer to established experimental mirror machine practice.

High frequency micro-stability in the flux surface region is likely to be quite good because the anisotropy can be much smaller than in a mirror machine. Low frequency drift stability or instability cannot be reliably predicted in any hot plasma at this time. There is also no reliable way of predicting the magnitude of any "anomalous" or "Bohm" diffusion since this is an essentially empirical concept. As a specifically toroidal phenomenon, we can guess that Bohm diffusion is related to the fact that magnetic lines and particle orbits have no direct communication with the exterior of the plasma. We have seen that this has a very pronounced effect on the possibility of obtaining an equilibrium, on the sensitivity to small errors in injection, and, of course, on stability. All these effects are sufficiently reduced in a mirror machine to reveal the loss cone as the dominant loss mechanism. Empirically, one can create a hot, moderately dense, quiescent plasma in a mirror. It would seem reasonable to expect that a toroidal, approximately isotropic plasma which is surrounded by and in intimate contact with such a quiescent "grounded" loss cone plasma would relatively quiet. On the other hand, the interior which is relatively free of loss cones, should not be restricted in density (e.g. measured in ω_p/ω_c) as is the outer blanket.

The Max-B configuration is fully competitive with axially symmetric toroidal configurations. With a number of periodic sections, the helical field presents an asymptotically ignorable coordinate. In addition there is a deep vacuum magnetic well without levitated or supported conductors, and a tranquilizing enveloping mirror plasma.

We have given a highly qualitative evaluation of this configuration. The reason is that the best present combination of theoretical and experimental knowledge is incapable of predicting the performance of <u>any</u> projected toroidal device with an uncertainty less than <u>some</u> two orders of magnitude.

APPENDIX. Generalized Interchange Stability

In the variational formulation of guiding-center stability, a variation is defined by a displacement of the magnetic lines together with a variation of the distribution function on each line. For a given magnetic field displacement, the energy is minimized by a <u>pessimistic</u> variation of the distribution function. <u>On a magnetic</u> line of finite length, the pessimistic variation is given by assigning a given value of f to an ε-contour of constant area [$J = \int V_{\parallel} ds$ = const.][16].

---

[4] Several specific indications are presented in [14].

But in an infinite uniform field, the pessimistic variation is given by the constraint ε = const. instead of J = const. [12]. More generally, on a line of infinite length but in a nonuniform field, the pessimistic variation is given by the constraint

$$\begin{aligned} J &= \text{const. for trapped particles} \\ \varepsilon &= \text{const. for non-trapped particles.} \end{aligned} \qquad (A.1)$$

It can be shown that the apparent discontinuity in the constraint is unessential (to be published).

There is a similar analysis in scalar pressure MHD. Given a magnetic line displacement, the pessimistic displacement of plasma along the line is such as to yield p = const. For a line of finite length, the constant value of p is related to the volume change by the constant entropy η. But, if the line has infinite length, any finite perturbed portion of the line is connected to an essentially infinite reservoir, and the constraint becomes p = const. instead of η = const. In the case of finite length (mirror machine or torus with closed lines), interchange stability is determined by the (necessary and sufficient) criterion

$$q'(pq^{\gamma})' > 0 \,, \quad \text{or} \quad q'(p'/p + \gamma q'/q) > 0 \qquad (A.2)$$

where $q = \int d\ell/B = V'(\psi)$ is the volume of a flux tube.

In a torus with shear, there is no proper interchange which leaves the magnetic field unchanged. But near a shear-free region, $V'(\psi) \sim 0$, or near a magnetic axis, one can construct an approximate interchange. The magnetic line is infinitely long and one obtains

$$q'p' > 0 \qquad (A.3)$$

(or $V'' < 0$) corresponding to a pressure constraint instead of (A.2) for an entropy constraint [17].

The finite length magnetic line criterion (A.2) is more easily satisfied then (A.3); in particular the interior of the plasma can be stabilized by merely taking p' small, no matter what sign $q' = V''$ has. The guiding-center criterion is always of this type, even with the more relaxed constraint, (A.1), for infinite line length. The qualitative reason is that trapped particles are not concerned with the extent of the magnetic line.

For an isotropic distribution $f = \sigma(\psi)\hat{f}(\varepsilon)$, an elementary calculation (similar to formula (8.2) in [6]) yields the generalized interchange stability criterion

$$\sigma Q_T - \sigma' R > 0 \qquad (A.4)$$

where

$$Q_T = -\int_T (\partial\varepsilon/\partial\psi)^2\ \hat{f}'(\varepsilon)\,dJd\mu > 0 \quad . \qquad (A.5)$$

is integrated over trapped orbits only and

$$R = \int (\partial\varepsilon/\partial\psi)\hat{f}(\varepsilon)\,dJd\mu \qquad (A.6)$$

is integrated over all phase space. At low β an elementary calculation shows that $R = -\hat{p}q'(\psi)$. The second term of (A.4) corresponds to the MHD V'' criterion for a generalized interchange. The first term in (A.4) gives the guiding-center modification; we recall that guiding-center stability of a scalar pressure equilibrium is easier to achieve than MHD stability of the same equilibrium. In particular, stability is assured near the axis if $|\sigma'|$ is sufficiently small no matter what sign R or V'' has. As was previously found in mirror machines [6], macro-stabilization of the center of a plasma is relatively easy.

We remark that lack of communication of trapped particles along magnetic lines leads to improved macro-stability, even though it may possibly weaken micro-stability.

The work presented here was supported by the U.S. Atomic Energy Commission under Contract No. AT(30-1)-1480.

R E F E R E N C E S

[1] Grad, H., Phys. Rev. Letters 18 (1967) 585.

[2] Grad, H., Phys. Fluids 10 (1967) 137.

[3] Bishop, A. S. and Smith, C. G., Phys. Fluids 9 (1966) 1380.

[4] Grad, H., Motion and stability of free surfaces, WASH 289 (1955) 115.

[5] Taylor, J. B., Phys. Fluids 6 (1963) 1529.

[6] Grad, H., Stability of mirror machines, Plasma Physics and Controlled Nuclear Fusion, II, IAEA Vienna (1966) 161.

[7] Bernstein, I. B., et. al., Proc. Roy. Soc. A244 (1958) 17.

[8] Grad, H., Marphology of stable geometries, TID 7536 (1957) 196.

[9] Filonenko, N. N., Sagdeev, R. Z., Zaslavsky, G. M., Nucl. Fusion 7 (1967) 253.

[10] Grad , H. Anomalous particle losses in toroidal and complex mirror geometries, Bull. Amer. Phys. Soc., Ser. II, 13 (1968) 298.

[11] Arnold, V., Usp. Mat. Nauk USSR 18, Ser. 5 (113)(1963) 13; also Moser, J., Math. Ann. 169 (1967) 136.

[12] Grad, H., The guiding center plasma, Symp. Appl. Math. XVIII, Amer. Math. Soc. (1967) 162.

[13] Grad, H., Phys. Fluids 7 (1964) 1283.

[14] Blank, A. A., Grad, H., and Weitzner, H., Toroidal high-β equilibria, Paper CN-24/K-6, 3rd Conf. on Plasma Phys. and Controlled Nucl. Fusion Res.

[15] Johnson, J. L., Morse, R. L., and Riesenfeld, W. B., Hydromagnetic equilibrium of a thin-skin finite beta toroidal plasma, Los Alamos Sci. Lab. Rep. LA-3770, Paper B2 (1967).

[16] Grad, H., Phys. Fluids 9 (1966) 225.

[17] Greene, J. M. and Johnson, J. L., Phys. Fluids 5 (1962) 510; also Mercier, C., Nucl. Fusion Suppl., Part II, (1962) 801.

DISCUSSION

H.P. FURTH: I agree with Dr. Grad that one of the most striking experimental facts of controlled fusion research is the contrast between high anomalous cross-field diffusion in toruses and low anomalous cross-field diffusion in open-ended systems. Dr. Grad seems to attribute this contrast to the difference in magnetic-field topology and geometry. In my opinion, the real cause of the contrast may be that in typical torus experiments there are very many collision times, while in open-ended experiments there is automatically less than a collision time. Thus, the torus experiments labour under the great burden of limiting the particle excursions to very small steps, if diffusion is to be small. This type of consideration leads naturally to Bohm-like diffusion rates when the collision time is shorter than the Bohm time.

Incidentally, if this explanation is correct, it implies that Dr. Grad's proposed confinement geometry will not have very unique properties. His scheme requires that the outer region should have a long collision time. Under this condition, there may not be a problem of Bohm-like diffusion in the first place.

H. GRAD: This difference of opinion will probably be resolved only with the passage of time, since the present evidence is inconclusive. However, the stellerator experiment at Princeton, which exhibits a lifetime of 5 × Bohm in about one collision time, casts some doubt on Dr. Furth's hypothesis.

R.S. PEASE: You say in the abstract "the outer shell of the maximum-B configuration should be free of this phenomenon ("Bohm" diffusion) as in any conventional mirror-machine". What is the basis of this statement?

H. GRAD: The statement is based on the assumption that this mirror-machine plasma shell will have the same properties as a conventional mirror-machine.

PRODUCTION OF A DENSE DEUTERIUM PLASMA IN A STRONG MAGNETIC FIELD BY A GIANT LASER PULSE (HOT-ICE EXPERIMENT)

U. ASCOLI-BARTOLI, B. BRUNELLI, A. CARUSO, A. DE ANGELIS, G. GATTI, R. GRATTON, F. PARLANGE AND H. SALZMANN
LABORATORI GAS IONIZZATI (ASSOCIAZIONE EURATOM-CNEN), FRASCATI, ROME, ITALY

Abstract

PRODUCTION OF A DENSE DEUTERIUM PLASMA IN A STRONG MAGNETIC FIELD BY A GIANT LASER PULSE (HOT-ICE EXPERIMENT). An experiment of plasma production by means of a short-duration giant laser pulse, focused on a deuterium pellet, is described. The plasma can be produced in a pre-existing strong magnetic field parallel to the optical axis. The deuterium targets are produced with a cryostat and injected in such a way that they pass very close to the optical axis. The total number of deuterons in a single target is about 5×10^{17}.

The results reported here are mainly concerned with the production of plasma in absence of a magnetic field. There are indications that, at least during a period of around 30 to 40 nsec, the system consists of two phases: a "high"-density phase with a density of the order of solid state and a temperature of about 4 eV, whose outer layers are heated by the laser and continuously expand, forming a "low"-density phase with a density of about 10^{19} cm^{-3} and a temperature of approximately 100 to 200 eV. Furthermore, the high-density phase is – as a reaction to this process – strongly accelerated in the direction of the laser light. Preliminary measurements with a strong magnetic field have been carried out.

1. DESCRIPTION OF EXPERIMENT

The idea of the "hot-ice" [1] experiment is to produce a plasma cloud in a vacuum environment by ionizing small solid deuterium targets with a focused laser beam. Furthermore, it is intended to study the interaction of a strong magnetic field with this plasma.

The parameters of the laser and of the targets are respectively:

(a) Laser: the Q-switched (Kerr cell) Neodimium laser consists of an oscillator and three amplifiers. The characteristics of the giant pulse are:

Total energy	50 J
Pulse duration	30 ns
Mean power	1.7 GW
Peak power	3.4 GW
Focal spot diameter (f = 12 cm)	$\approx 5 \times 10^{-2}$ cm
Mean energy flux in the focal region	$\approx 0.9 \times 10^{19}$ erg s^{-1} cm^{-2}

(b) Solid deuterium targets (of cylindrical form):

Diameter	2×10^{-2} cm
Length	2.5×10^{-2} cm
Average number of deuterons per target	5×10^{17}

The targets are produced one by one in a helium-cooled solidifier and ejected towards the focal spot along reasonably reproducible trajectories perpendicular to the laser optical axis [2]. All targets which cross the focal spot (the probability is about 0.3) pass through two optical reference beams. The switching-on sequence of the optical pumping, the magnetic field and the Kerr-cell is related to the interruptions of these beams. When the target is just in the focal spot, the laser is Q-switched and the magnetic field has reached its peak value.

The magnetic field is parallel to the optical axis and the maximum peak value is 450 kG [3]. To increase the action of the field, a hollow, stainless-steel cylinder (i.d. = 5.0 mm and o.d. = 8.0 mm) is introduced into the single-turn coil [4]. The rise-time of the magnetic field is slow

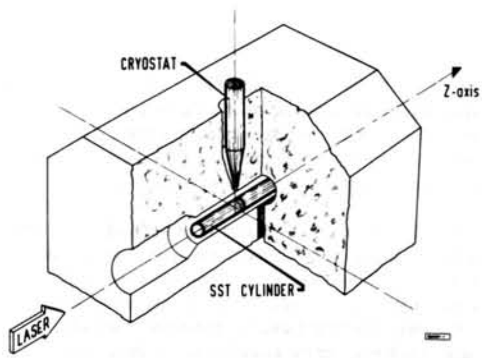

FIG. 1. The central region of the experiment.

enough (60 μs) to ensure penetration through the cylinder, which, on the other hand, behaves like a high conductivity wall with respect to the fast magnetic field variation produced by the plasma expansion. In this way the magnetic field outside the plasma can reach values considerably higher than the pre-established one.

The coil and the steel cylinder are split in two halves, separated by a 1.5-mm gap, which allows lateral observation of the plasma in the focal spot region. The central zone of the experiment is shown in Fig. 1.

2. EXPERIMENTAL RESULTS WITHOUT MAGNETIC FIELD

The following diagnostics were used:

2.1. Streak photography of the light emitted by the plasma in the visible region.

2.2. Intensity measurements in the visible region by means of phototubes.

2.3. Measurements of the time of flight of the ions emitted in the forward direction.

2.4. Measurement of the waveform of the laser pulse before and beyond the target.

2.1. Streak photography of the light emitted by the plasma

Sweep velocities of 60 ns/cm and 30 ns/cm were used; the entrance slit is about 2 cm long with a typical width of 0.25 mm.

An enlarged image of the region of interest is formed on the slit. The plasma can be observed laterally, i.e. perpendicular to the optical axis, or axially.

2.1.1. Lateral observations

To observe the motion of the luminous region along the axis, the slit was placed parallel to the optical axis. The visible region is limited by the width of the gap between the two halves of the steel cylinder. A typical

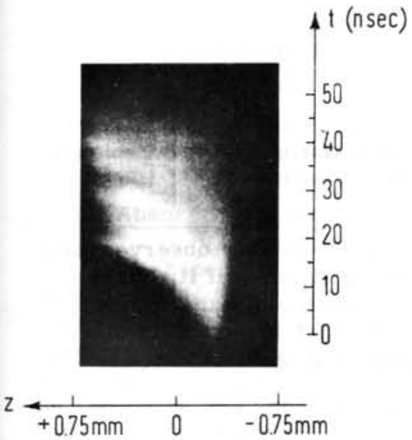

FIG. 2. Axial behaviour of the plasma; slit of the camera parallel to the axis; side view.

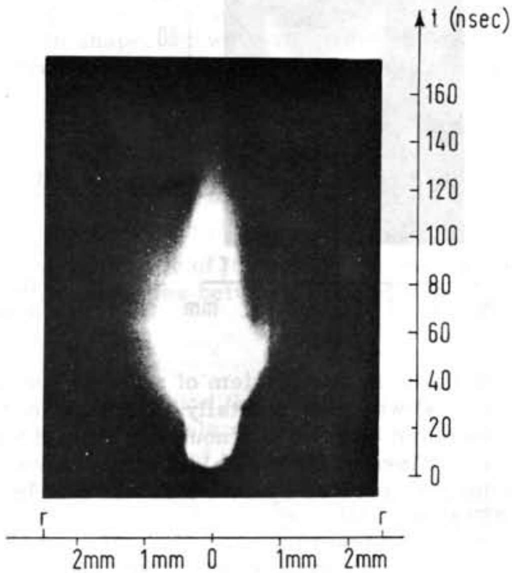

FIG. 3. Radial behaviour of the plasma: slit of the camera perpendicular to the axis (in the median plane); side view.

picture is shown in Fig. 2. The luminous region begins more or less in the middle of the gap (in the point where the target is hit). The subsequent behaviour is strongly asymmetric with respect to this point, in the sense that almost all the ligth comes from a region that is accelerated in the direction of the laser beam, while no light is observed from the region between the middle point and the laser. On the other hand, the radial motion of the luminous region was observed by placing the slit perpendicular to the optical axis for three different positions with respect to the median plane of the gap.

In Fig. 3 the radial behaviour on the median plane is shown, and an analogous behaviour is observed if the slit is moved from the median plane away from the laser. However, if the slit is moved towards the laser, a lower light intensity (about one order of magnitude) is observed, just at the limit of detectability.

2.1.2. Axial observations

These measurements were carried out with two different optical systems with considerably different apertures but similar enlargements.

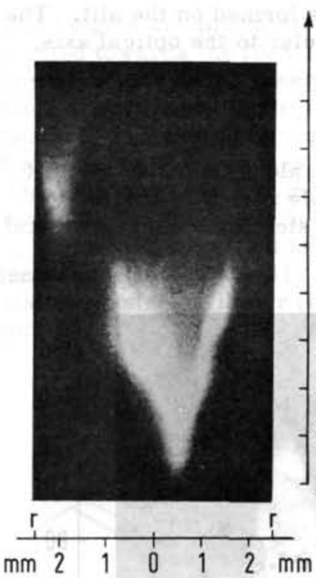

FIG. 4. Radial behaviour of the plasma; end view; lower-aperture optical system.

With the optical system of smaller aperture, the behaviour observed (see Fig. 4) was fundamentally analogous to that of Fig. 3, even if it should be noted that the luminous region in the central zone of the discharge, i.e. close to the optical axis, disappears after about 40 ns. With the larger aperture system a rather fast luminous front is observed (see Fig. 5a).

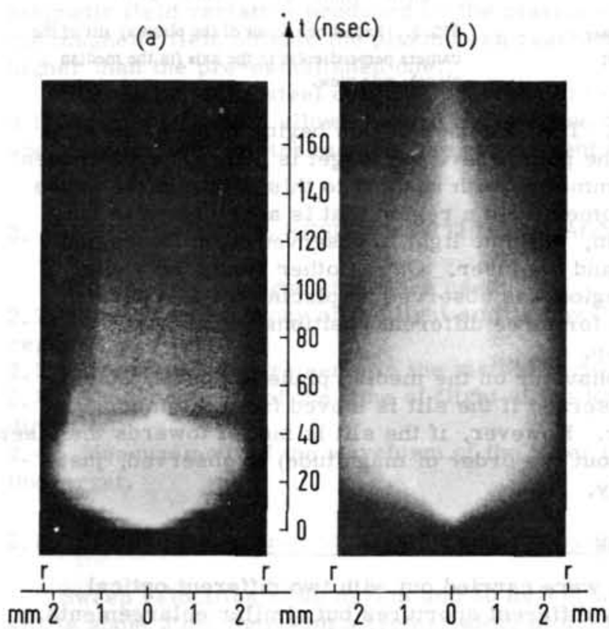

FIG. 5. Radial behaviour of the plasma; end view; larger-aperture optical system:

(a) B = 0
(b) B = 250 kG.

2.2. Measurements of the emitted light intensity in the visible region [5]

These measurements were carried out with a set of phototubes and light-pipes, observing an enlarged side-on view of the region of interest, limited by a vertical slit. An interference filter (5890 Å) was introduced in the optical path. By comparison with a carbon arc we obtained absolute values for the intensity.

The slit is placed to observe a region shifted 0.7 mm away from the median plane toward the laser; in this way the brightest region recorded in the streak pictures is excluded from observation.

The signals, roughly triangular in shape, show a half-width of about 70 ns. The maximum intensity corresponds to that emitted by an optically thin plasma, having a density of 5×10^{18} cm^{-3} and a temperature of the order of 10^2 eV.

2.3. Measurements of the time of flight of the ions emitted in the forward direction

The time of flight is measured at a distance of 200 cm. Velocities between 10^7 and 2×10^7 cm s^{-1} were found (i.e. energies between 100 and 400 eV).

2.4. Absorption of the Laser light

The shape of the laser pulse before and behind the plasma region was recorded by two fast photodiodes. The signals show that, when the target is hit, a strong attenuation and distortion of the central zone of the laser pulse, takes place. The initial and final parts of the pulse, however, remain practically unchanged. The time during which the pulse is distorted is around 30 to 40 ns, and the pulse may prove to have decreased by up to 50% during this period, with considerable variations between the different shots.

3. INTERPRETATION OF THE RESULTS

It must be emphasized that the preliminary nature of the results still leaves many important questions to be answered. Nevertheless, it is possible to interpret the given results according to the theoretical model described in Ref. [6].

The essential point is the simultaneous existence, at least for times of the order of 10^{-8} s, of two different phases: (a) a "low-density" phase, with a temperature of the order of 10^2 eV and a density of the order of 10^{19} cm^{-3}, which is ejected continuously towards the laser from the exposed surface of the target; (b) a "high-density" phase, in practice the target itself, first compressed and heated up to a temperature of some electron volts as a reaction on the emission of the "low-density" phase, and then, for the same reason, accelerated as a whole in the direction of the laser light.

According to the theoretical predictions it is to be expected that the high-density phase will be considerably brighter (from 10 to 100 times) and therefore easier to detect. The photograph of Fig. 2 is then simply interpreted by assuming that only the high-density phase is visible. From the acceleration undergone by this phase the pressure acting on the surface exposed to the light can be deduced, and can be evaluated to be of the order of 10^{12} erg cm^{-3}, which is in full agreement with the value anticipated by the theoretical model mentioned (note that this pressure is three orders of magnitude larger than the radiation pressure).

The radial behaviour of the high-density phase is shown in Figs 3 and 4. A radial expansion takes place with typical velocities of 2×10^6 cm s^{-1}, corresponding to a temperature of about 4 eV. The density can therefore be evaluated and results are approximately those of the density of solids. These values are in remarkable agreement with the theoretical predictions.

It should be mentioned that, according to the theoretical model adopted, the high-density phase should disappear within a time of 30 ns except for a fraction which escapes the laser action because of the radial expansion. This makes possible a meaningful interpretation of the photograph given in Fig. 4: in fact, the central region of the "dense" phase disappears after a time around 40 ns, while the expanding lateral regions remain visible longer. It should be observed that in Fig. 5a (and 5b) these lateral regions are not visible. This is due to an enlargement of the focal spot (a focusing lens with longer focal length was used in the shots corresponding to these pictures); as a consequence, the quantity of matter escaping the laser action is strongly reduced. Also the absorption measurements carried out with the double photodiode system show that no opaque matter is present in the laser path for longer than 30 to 40 ns.

As far as the low-density phase is concerned, observations with the streak camera are only possible if the aperture of the optical system is enlarged considerably. This has been done in the measurements reported in Fig. 5a; a luminous front is visible, expanding with a velocity corresponding to some units in 10^7 cm s^{-1} which corresponds to some hundreds of electron volts. This front becomes invisible if neutral filters are inserted, while a central luminous region, which can be identified with the high-density region, remains visible.

Another way to reveal the existence of the low-density phase suggested by the theory, is to measure the light intensity emitted by the region between the median plane and the laser by means of phototubes. This region cannot be occupied by the high-density phase. As reported before, an intensity in accordance with that of a plasma having the expected characteristics, was found.

4. MEASUREMENTS IN THE PRESENCE OF A MAGNETIC FIELD

Preliminary measurements were carried out in the presence of a magnetic field of 250 kG.

The most evident effect was an increase of about a factor 10 in the luminosity of the low-density phase; both the streak camera, and the phototube-measurements, show that this increase lasts for more than 100 ns (see Fig. 5b). Moreover, the diameter of the luminous region is about one millimetre, which seems to indicate the presence of an interesting confinement process. It is still too early for a discussion of the oscillograms obtained with a set of magnetic probes placed between the plasma and the steel cylinder. The behaviour of the high-density phase seems to be practically unaffected by the presence of a magnetic field.

5. CONCLUDING REMARKS

The reported results show that when a very intense laser beam is focused on a solid target, plasma is emitted by the surface exposed to the laser, while the rest of the target is correspondingly compressed and accelerated as a whole in the direction of the laser beam. Of course, if the laser pulse lasts long enough, this "high-density phase" disappears except for that fraction which escapes the laser action, owing to the radial expansion.

In the described experiment, the high-density phase has a temperature of ≈ 4 eV, and a density near to that of solids; this phase strongly radiates in the visible region. The intensity of the radiation from the emitted plasma is much lower. The experimental results for this phase are in good agreement with the theoretical prediction of a density of 10^{19} cm^{-3} and a temperature of 200 eV.

The magnetic field, as indicated by the first observations, seems to have some confining effect on the emitted plasma, whose density is somewhat increased.

ACKNOWLEDGEMENTS

We express our sincere thanks to the members of our technical staff, particularly to Mr. A. Cecchini for the design and the construction of the cryostat, to Mr. E. Grilli for his work on the Laser, to Mr. L. Lovisetto for his contribution in making the magnetic field generator and to Mr. M. Tabellini for carrying out the optical measurements.

REFERENCES

[1] ASCOLI-BARTOLI, U., DE MICHELIS, C., MAZZUCCATO, E., "The hot-ice experiment", Plasma Physics and Controlled Nuclear Fusion Research (Proc. Symp. Culham, 1965) 2, IAEA, Vienna (1966) 941-51.

[2] CECCHINI, A., DE ANGELIS, A., GRATTON, R., Int. Rep. Laboratori Gas Ionizzati 68/8 (1968).

[3] BRUNELLI, B., LOVISETTO, L., PARLANGE, F., Int. Rep. Laboratori Gas Ionizzati 68/18 (1968).

[4] CAVALIERE, A., GIUPPONI, P., GRATTON, R., Phys. Lett. 25A (1967).

[5] GRIEM, H.R., Plasma Spectroscopy, McGraw-Hill (1964) 288, 309.

[6] CARUSO, A., GRATTON, R., Int. Rep. Laboratori Gas Ionizzati 68/2 (1968).

DISCUSSION

C. YAMANAKA: In the Frascati experiment, the particle size is almost equal to that of the laser spot. What is the neutral density in such a case?

A. CARUSO: The presence of neutrals at the end of the laser pulse depends essentially on the relative dimensions of the laser spot and of the target, and on the duration of the laser pulse. We have derived formulas for these conditions in a paper to be published in "Plasma Physics".

P. VASSEUR: Working with the same assumptions as those adopted by the Frascati group, we have irradiated a metal target having a thickness of the order of 0.1 - 10 μm and have have found that, for an energy of 2-3 J, a 1-μm aluminium target completely absorbs this energy and that the thickness of the zone where the interaction (plasma + high-density gas) occurs is of the same order of magnitude.

I imagine this is due to the existence of neutrals in the interaction zone.

PRODUCTION AND MAGNETIC FIELD CONFINEMENT OF LASER-IRRADIATED SOLID PARTICLE PLASMAS *

A. F. HAUGHT, D. H. POLK AND W. J. FADER
UNITED AIRCRAFT RESEARCH LABORATORIES
EAST HARTFORD, CONN., UNITED STATES OF AMERICA

Abstract

PRODUCTION AND MAGNETIC FIELD CONFINEMENT OF LASER-IRRADIATED SOLID PARTICLE PLASMAS. The focused high-intensity beam from a Q-spoiled laser has been used to form a high-temperature, high-density plasma from a single 10-20 micron radius solid particle of lithium hydride which is electrically suspended in a vacuum environment free of all material supports. Time-resolved charge collection measurements of the freely expanding plasma have shown that a high degree of ionization of the 10^{15} atoms in the lithium hydride particle can be achieved and that the plasma produced is essentially spherically symmetric in density over the full 4 π solid angle. Time-of-flight studies of the plasma expansion have shown that average electron and ion energies exceeding 200 electron volts are obtained and that the plasma expansion rate, like the plasma density, is spherically symmetric. No charge separation or separation of the lithium and hydrogen ions is observed in the expanding plasma. Numerical calculations of the plasma formation and expansion have been made using a one-dimensional spherical hydrodynamic model and, on the basis of the results obtained, an integrated similarity model has been developed for calculations of the plasma time history and energy over the range of conditions employed in the experiments. These calculations, which include the effects of laser pulse time history, fraction of the incident beam occupied by the expanding plasma, radial density and velocity gradients within the plasma, and spatial distribution of the incident laser energy, give results for the plasma radial density distribution, velocity profile, and plasma energy in good agreement with those determined experimentally over the full range of the present measurements. Measurements have been carried out to examine the interaction of these laser-produced plasmas with mirror, cusp, and minimum-B magnetic fields. Experiments with mirror and minimum-B magnetic fields up to 8 kG show that plasmas with densities of 10^{12}-10^{13} cm^{-3} are confined for times of 5 μs (mirror) and 10 μs (minimum-B) and that a measurable amount of plasma is still present within the containment volume at times as late as 20 μs (mirror) and 100 μs (minimum-B), compared with the 0.3 μs "lifetime" associated with the free plasma expansion. The plasma decay rate in the 8 kG minimum-B magnetic field is consistent with that for Coulomb collisional scattering loss into the magnetic-field loss cones.

1. INTRODUCTION

Three configurations have been utilized for the production of plasmas by laser radiation. In the first of these, the laser radiation is focused within a homogeneous medium, and the ionization and plasma production occur in the high-intensity region of the lens focus. Such experiments have been carried out in gases, liquids, and more recently, in solids. This geometry ensures that the medium from which the plasma is formed occupies the entire region of the lens focus and, with solids, liquids, or gases at pressures greater than one atmosphere, leads to plasma densities in excess of

---

* The free plasma production studies were supported in part by the Air Force Office of Scientific Research, Contract F44620-67-C-0082. Portions of the magnetic field interaction investigations were supported by the US Atomic Energy Commission, Contract AT(30-1)-3578.

10^{19} cm^{-3}. As a consequence of the high plasma density and the complete filling of the focal volume, the fraction of laser beam energy absorbed can be as high as 90 percent. Although the surrounding medium restricts the expansion of the hot plasma, the plasma is rapidly cooled by the adjacent medium, and the inertial constraint interferes with studies of the confinement properties of magnetic fields of less than megagauss intensity. To eliminate the effects of the surrounding medium, plasmas have been formed in vacuum by laser irradiation of a thin foil or solid surface. With this geometry, however, large numbers of neutral atoms are observed to boil off the heated focal region after the laser heating, and the degree of ionization averaged over all of the vaporized material is relatively low. In addition, for magnetic field confinement studies, the presence of the solid surface in the region to be occupied by the plasma is undesirable. The studies of this paper are concerned with the third laser heating geometry in which a small solid particle suspended in a vacuum environment is irradiated with a high-intensity laser pulse to produce an isolated plasma either (a) freely expanding or (b) within a confining magnetic field for examination of the plasma-magnetic field interaction. The number of atoms in the plasma is controlled by the particle size used and, by optimizing the particle size for the laser beam power and pulse duration employed in the present experiments, average plasma energies of 200 eV/particle are obtained. With reasonable future developments in laser capabilities it appears that plasmas comprising 10^{17}-10^{18} particles at an average energy of 10 kilovolts can be produced using this technique.

2. PLASMA PRODUCTION

Particles of lithium hydride from which the plasma is formed are electrodynamically suspended in vacuum in the electric field produced by the cubical array of electrodes shown in Fig. 1. [1,2,3] The particles are stored in an injector located within the vacuum system and are mechanically projected up into the suspension region by means of spring wire. Electrons emitted from a hot filament charge the particles as they enter the suspension volume. Those particles with the proper charge to mass ratio are captured by the suspension electric fields. By adjustment of the applied ac potentials and of dc potentials applied individually to the six electrodes, all but one of the particles is ejected from the suspension field, and the remaining particle is positioned within the suspension volume at the point where the particle orbit is a minimum. By means of three orthogonal slides, the suspension electrode array is then moved so that the particle, in its minimum orbit, is located within the lens focal region. Upon removal of the suspension electric fields to provide a field free environment, the giant pulse beam from a Q-spoiled ruby laser is focused onto the particle, vaporizing the particle and ionizing and heating the resulting gas to form a high-temperature, high-density plasma.

In the present system, a development of that described in Refs. 1 and 2, the suspension electrodes are spaced 10 cm apart, providing a 1 liter free volume for the plasma expansion. Magnet coils located immediately behind each of the six suspension electrodes are used to generate mirror, cusp, or minimum-B magnetic fields at center field strengths up to 10 kG for plasma confinement investigations. A Korad K-1500 oscillator-amplifier ruby laser with an output pulse of 1 GW peak power, 10-15 nsec half-width, and 1 mrad half-power beam divergence is employed in the present studies. A two-direction telemicroscope viewing system, with which the particle is observed along two orthogonal axes, is used to position the suspended particle within the laser beam focal region previously determined from the burn spot produced by the focused beam on a movable (and removable) metal surface. Using a technique first applied by Lubin, [4] the size of the suspended particle is determined in each experiment from the diffraction pattern of the particle in an auxiliary He-Ne laser beam. As applied in the present experiments, the diffraction pattern technique permits selection of those particles most closely approximating a spherical shape and provides an accurate measure of the characteristic dimension of the irregularly faceted particle from which the initial particle volume, and therefore atom number, can be determined within a factor of two.

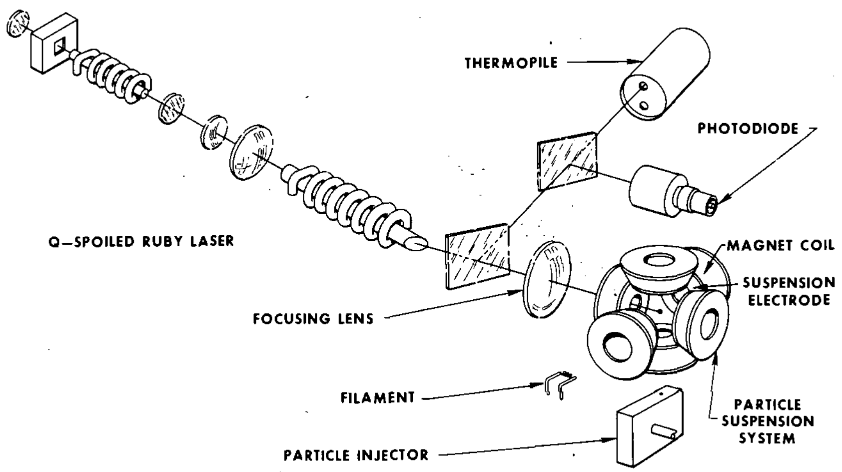

FIG. 1. Particle plasma apparatus.

2.1 Free Plasma Expansion - Theory

Upon irradiation with the focused laser beam, the suspended lithium hydride particle is vaporized, and the atoms in the resulting gas are ionized and heated to form a high-temperature, high-density plasma. Since the plasma is produced in a vacuum, it immediately begins to expand in response to pressure forces developed within it. This expansion lowers the plasma density, decreasing the plasma absorption coefficient and eventually terminating the heating by the laser pulse. Models of the plasma formation and growth have been developed to follow in detail the plasma time history and to determine the optimum experimental conditions for the plasma production. The hydrodynamic equations for the plasma expansion, taking into account a time-dependent uniform energy input to the plasma from the laser beam, have been solved numerically by dividing the plasma into a series of concentric spherical shells and computing the density, expansion velocity, and temperature within each shell [5]. From the results of these calculations, very early in the heating, when the plasma energy is less than 10 percent of its final value, the temperature becomes uniform throughout the plasma, the density assumes a Gaussian radial profile with a maximum at the plasma center, and the velocity increases linearly from zero at the plasma center to its value at the plasma boundary. The persistence of these radial distributions during the subsequent heating and expansion of the plasma suggest an integrated similarity model in which the asymptotic forms of the density and velocity profiles determined from the hydrodynamic model are assumed throughout the plasma growth, and the expansion equations are simplified by integration over the plasma volume. During the initial stages, when the assumed similarity conditions do not strictly apply, the energy absorbed is small, and any discrepancies resulting from the use of this model do not materially affect the results obtained. The expansion time history and values of plasma energy calculated with the integrated similarity model and the hydrodynamic model are virtually indistinguishable over the entire range of conditions of experimental interest, justifying the use of the simpler integrated similarity model for extensive calculations with different values of the experimental parameters. The integrated similarity model employed for these calculations is a generalized form of that first formulated by Basov and Krokhin [6] and by Dawson [7] and further developed by Haught and Polk [1,2]. In its present generalized form, the model incorporates the plasma density profile obtained from the hydrodynamic calculations and takes into account both the Gaussian radial distribution of the laser beam flux in the focal region and the chord paths of the radiation through the spherical plasma.

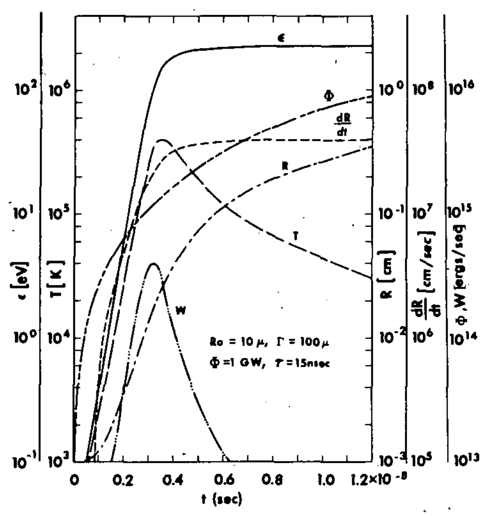

FIG. 2. Plasma time history - integrated similarity model.

Using this integrated similarity model, the time dependent plasma expansion rate, dR/dt, temperature, T, average plasma energy, ϵ, and laser power absorbed, W, have been calculated for different values of the laser pulse peak power, Φ, pulse duration, τ, initial particle size, R_0, and focal spot radius, Γ. The free expansion time history given by the integrated similarity model (and the hydrodynamic model as well) for the representative parameters of Fig. 2 is typical of the results obtained over the entire range of initial conditions examined. The time development of such plasmas is discussed at length in Refs 1, 2, and 5; it is significant, however, to note that as a result of the rapid plasma expansion the peak plasma temperature in free expansion corresponds to only 1/5 the average energy of the plasma and essentially all of the plasma energy is in the form of kinetic energy of radial expansion before the plasma radius exceeds 0.2 cm ($100\,R_0$). For plasma confinement investigations, therefore, it is necessary that the plasma expansion be stopped and the radial kinetic energy be recovered as plasma thermal energy.

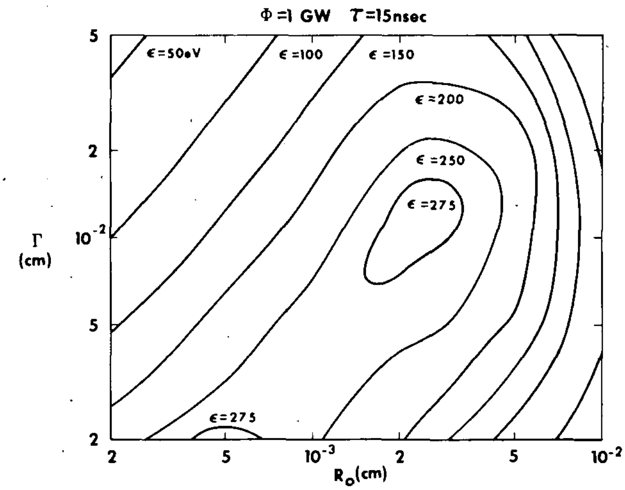

FIG. 3. Plasma energy surface - integrated similarity model.

Calculations of the plasma energy for a given laser beam power and pulse duration have been carried out over a range of initial particle radii and focal spot dimensions to establish the experimental conditions required for maximum plasma energy and to determine the limits on the total number of ions which can be produced at this energy. Such calculations yield a characteristic plasma energy surface (ϵ vs R_0, Γ) like that shown in Fig. 3. Energy surface calculations carried out for different laser beam powers and pulse durations all display the ridge region, evident in Fig. 3, within which the plasma energy is a maximum and away from which the plasma energy decreases rapidly. This maximum energy region is characterized by the two conditions.

$$2R_0 \le \Gamma \le 5R_0$$
$$R_0(\mu) \le 2.5\,[\Phi(\mathrm{MW})]^{2/9}[\tau(\mathrm{nsec})]^{1/2}$$

and within this region the plasma energy obtained is given by

$$\epsilon_{max}(\mathrm{eV}) = 108\,[\Phi(\mathrm{MW})]^{1/3}\,[\tau(\mathrm{nsec})]^{-1/2}$$

Within the maximum heating region, the energy input efficiency from the laser beam to the plasma is an optimum (30 percent) when the initial particle size has the maximum value given by the relation above. These relations are an accurate fit (± 15 percent) to the calculated energy and maximum particle radius values over the entire range of conditions examined, 20 MW $\leq \Phi \leq$ 1000 GW and 0.1 nsec $\leq \tau \leq$ 50 nsec. While increased laser power permits the use of larger particles and yields higher plasma energies, the pulse duration and focal spot dimensions must be adjusted for the best compromise of plasma energy, ion number, and experimental convenience required in a given application.

2.2 Free Plasma Expansion - Experimental

Charge collector diagnostics have been used to measure the ionization and spherical symmetry of plasmas produced by laser beam irradiation of single 10-20 μ radius lithium hydride particles. Using six charge collectors, simultaneous observations were made of the charge density of the expanding plasma in six directions relative to the laser beam axis. The charge collection (and thus the amount of plasma expanding) in the direction of the laser beam is somewhat lower than observed in the other directions. The maximum difference, however, is less than a factor of two, and the charge density distribution in the expanding plasma is essentially spherically symmetric. Using two charge collectors located on the same radial line at different distances from the plasma origin, measurements of the time delay between the arrival of the plasma at the two probes can be used to determine the plasma expansion velocity. Using three pairs of probes, simultaneous time-of-flight measurements were made of the plasma expansion in three directions relative to the laser beam. Within 10 percent, the plasma time of flight in the three directions is the same, and the expansion velocity of the plasma is also spherically symmetric. These results establish that the freely expanding plasma produced in the experiments is essentially spherically symmetric in both density and expansion velocity despite the unidirectional energy input to the plasma and justify the simplifying assumption of spherical symmetry employed in the theoretical models.

From Fig. 3, after the plasma radius exceeds $\sim 10^{-1}$ cm, the plasma temperature is greatly decreased from its peak value, the expansion velocity reaches its asymptotic value, and nearly all of the plasma energy is in the form of kinetic energy of radial expansion. As a result, since the plasma density and velocity profiles are unchanging with time, the energy of the plasma ions and electrons is uniquely determined by the asymptotic expansion velocity of the plasma boundary. Measurements of the plasma expansion velocity have been made and used to determine the average plasma energy (total energy divided by the number of electrons and ions in the plasma) for a number of different experimental conditions with the results shown in Table I. The agreement between the theoretically predicted energies and those experimentally obtained for the three widely different conditions of laser power and beam divergence provides strong support for the validity of the hydrodynamic and integrated similarity models of the plasma formation and growth.

TABLE I. Plasma energies for different values of laser parameters and focal spot radius

LASER POWER (MW)	LASER DURATION (nsec)	FOCAL RADIUS, Γ (μ)	PARTICLE RADIUS, Ro (μ)	EXPERIMENTAL		THEORETICAL AVERAGE ENERGY (eV)
				EXPANSION VELOCITY (cm/sec)	AVERAGE ENERGY (eV)	
30	10	400	10	1×10^7	15	11
20	20	60	10	2×10^7	60	65
300	15	100	15	4×10^7	210	190

3. MAGNETIC FIELD CONFINEMENT INVESTIGATIONS

The laser irradiated single particle plasma is a spherically expanding free plasma, produced in vacuum with no supports, background gas, net mass motion, or net currents present. As a result, this plasma is particularly suitable for studying the interaction of a plasma with magnetic containment fields. With megagauss magnetic fields, pressure balance for the several hundred electron volt plasmas of the present experiments would be obtained at a plasma density greater than 10^{19} cm^{-3}. At these densities, the plasma is still opaque to the laser beam, and a much larger fraction of the total laser beam energy would be absorbed, giving rise to a plasma energy greater than that of the freely expanding plasma. However, the production of megagauss magnetic fields is a difficult problem in itself and, as a result, a second regime of interest has been investigated in the studies reported here. In these studies, the plasma is allowed to expand in magnetic fields of kilogauss field strength and is trapped at a density of $\sim 10^{13}$ cm^{-3}. Such experiments permit the examination of the capture, thermalization, and subsequent decay of an initially spherical radially expanding plasma in mirror, cusp, and minimum-B containment fields.

3.1 Magnetic Field Interaction - Theory

Studies of the deceleration of a laser-irradiated particle plasma expanding in an applied magnetic field have been made by explicitly calculating the perturbation of the magnetic field by the expanding plasma [8] and incorporating the resulting magnetic force and ohmic dissipation terms in the equations for the hydrodynamic model of the plasma motion. In this analysis, anisotropy of the electrical conductivity and longitudinal or axial motion of the plasma are both neglected and only the motion of the plasma at the midplane where the plasma-field coupling is strongest is calculated. Despite the obvious limitation of the approximate model, these calculations do give a physical picture of the processes by which the transverse expansion of a laser produced plasma is stopped by a magnetic field. Since the interaction of the plasma with the magnetic field occurs while the plasma is small compared with the radius of curvature of the mirror and minimum-B containment fields employed in the experimental studies, for mathematical convenience an initially uniform magnetic field was assumed in the calculations. The calculated time history of the plasma expansion in a 10 kG magnetic field is shown in Fig. 4 for a 290 eV/particle plasma. The solid curves represent the plasma temperature, average energy, outer boundary velocity, and plasma radius for zero field, while the dashed curves indicate the time dependence of the same variables for this plasma in an applied field of 10 kG. Early in the plasma development, the plasma energy density (kinetic plus thermal) is large compared with the energy density of the magnetic field, and the calculated plasma energy and initial motion are unaffected by the presence of the field. As a result, the plasma energy absorption and early time development are identical with those for the case of no magnetic field, and the measurements and calculation for the spherical free plasma expansion define the initial conditions for the plasma interaction with the magnetic field.

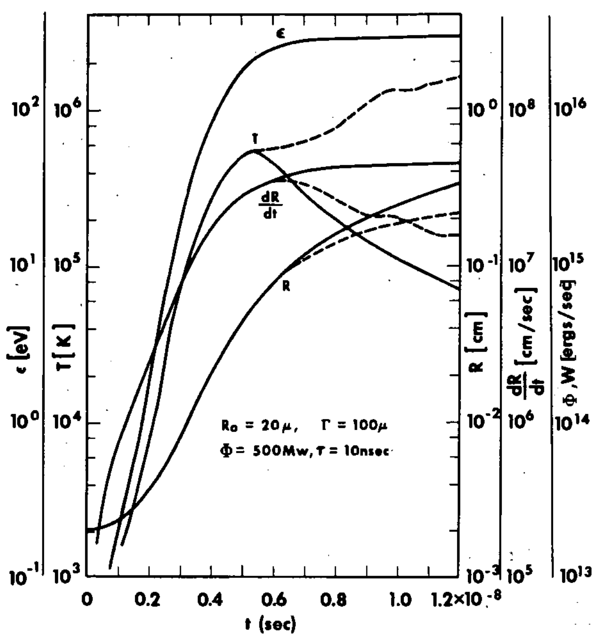

FIG. 4. Plasma time history in 10 kG magnetic field.

The plasma expansion continues as a free expansion until the purely hydrodynamic terms in the equation governing its motion have decreased to values comparable with the magnetic forces and ohmic dissipation terms. At this point, while the plasma motion parallel to the field continues unimpeded, the plasma-magnetic field coupling acts to decelerate the transverse expansion of the plasma. The deceleration is greatest near the plasma boundary where both the magnetic field and the induced current density are largest. The plasma interior, on the other hand, continues to move as in a free expansion since the magnetic field and the current density within the plasma are small. The calculated plasma density and temperature profiles in the midplane are shown in Fig. 5 at four different times for the plasma of Fig. 4 in a 10 kG magnetic field. The plasma density, temperature, and velocity in the interior region are initially identical with those calculated for the corresponding zero field expansion. As the plasma boundary is slowed, the interior regions overtake it, producing a region of high density in which the plasma temperature increases to a value comparable with

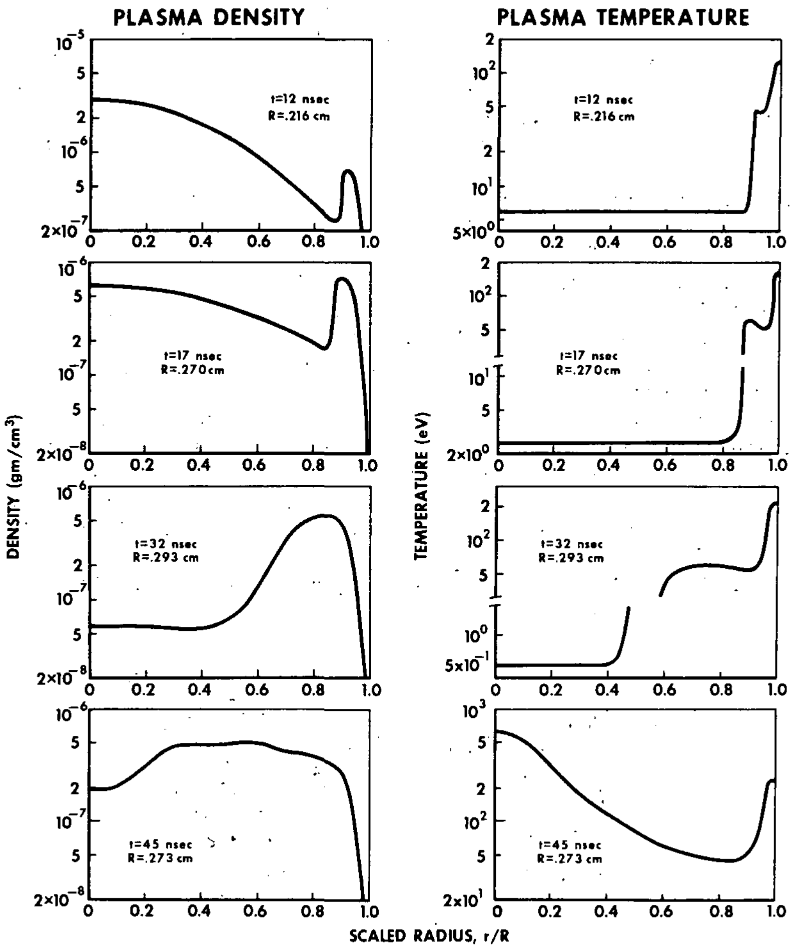

FIG. 5. Plasma deceleration in a uniform magnetic field B = 10 kG.

the average plasma energy. It is the temperature of the region near the plasma boundary which is plotted as the dotted curve in Fig. 4. The rise in plasma temperature accompanying the development of the hollow plasma shell is principally the result of compression of the plasma. Ohmic heating of the plasma by currents in the shell is of minor importance since the plasma resistivity, and hence the ohmic dissipation, decreases with increasing temperature. Corresponding to the large positive density gradient shown at 32 nsec, there is a positive pressure gradient which causes the plasma to flow back toward the center. Since the field at this time has been virtually excluded from the plasma interior, this flow is relatively unimpeded, and in the subsequent motion the plasma tends toward a uniform density distribution within its maximum expansion radius of ~ 0.3 cm.

3.2 Magnetic Field Confinement Investigations - Experimental

For experimental studies of the magnetic field containment of these laser produced plasmas, the plasma is formed in place at the center of a confinement field. Coils, with which simple mirror and minimum-B magnetic fields can be generated, are incorporated into the suspension electrode assembly (See Figs 1 and 6). The coils are connected in pairs and are powered by three independent ignitron-switched capacitor bank power supplies. With currents in the same direction in two opposite coils, a mirror magnetic field in any one of three orthogonal directions can be produced. Using all six coils, one coil pair connected to form a simple mirror field and the other two pairs of coils connected to produce opposed cusps, a minimum-B magnetic field is produced. In Fig. 6 directions are identified which, along with "up" and "down" are used to define the location of the charge collector and time-of-flight diagnostics and the orientation of the magnetic fields in the experiments. In each case in the experimental results which follow, the magnetic field axis is in the North-South direction. With the particle suspended at the lens focus, the magnetic field is turned on. The suspension voltages are then removed, and the particle is irradiated with the laser beam, producing the plasma which then expands within the magnetic confinement field. From the results of the magnetic field interaction calculations, the plasma energy absorption and formation takes place while the plasma is so small that no appreciable deceleration of the plasma by the magnetic field occurs. The plasma develops as if the magnetic field were not present, and the spherical field-free plasma expansion forms the initial conditions for the plasma interaction with the magnetic field.

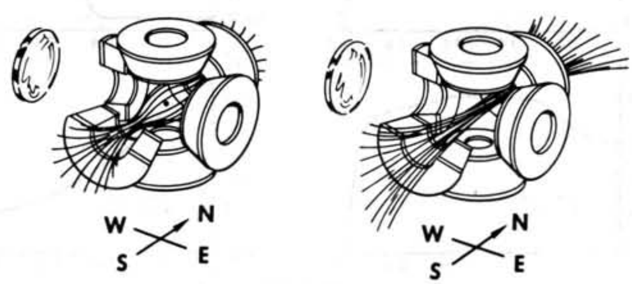

FIG. 6. Magnetic field geometries - mirror and minimum-B.

Charge collector measurements have been made to examine the amount of plasma leaving the magnetic confinement field in different directions relative to the magnetic field axis. The results of such experiments with 8 kG simple mirror and minimum-B magnetic fields are shown in Fig. 7 and compared with the free plasma expansion. In these experiments the mirror ratio is 4.3, and the magnetic field intensity given is that at the center where the plasma production and initial magnetic field interaction occur. The charge collector probes register the ion flux through the probe aperture (apertures of all probes equal), and, for a given probe, the integrated charge collection recorded as a voltage signal on a capacitor represents the amount of plasma which has expanded in the collection solid angle of that probe. Six charge collectors were used in these experiments, one (South) viewing the plasma along the magnetic field axis and the other five observing the plasma in directions transverse to the magnetic field. With no magnetic field, the integrated charge collection as a function of time is the same (within a factor of two) for each of the six probes--the essentially spherically symmetric density distribution associated with the free plasma expansion. With either a simple mirror or a minimum-B magnetic field, a significant alteration in the expanding plasma symmetry develops, the asymmetry increasing with increasing field strength. The charge collection and thus the plasma flux in the direction of the magnetic field axis is greatly increased compared with the zero field case, and plasma is observed over an interval of many microseconds in contrast to the less than one-half microsecond collection time for the free plasma expansion. Associated with the increased plasma flux along the magnetic field axis, the charge collection observed transverse to the magnetic field is greatly reduced. Both the strong asymmetry in the direction of the magnetic field loss cones and the increase in collection time show that the major fraction of the initially expanding plasma was trapped within the magnetic field and only gradually escaped.

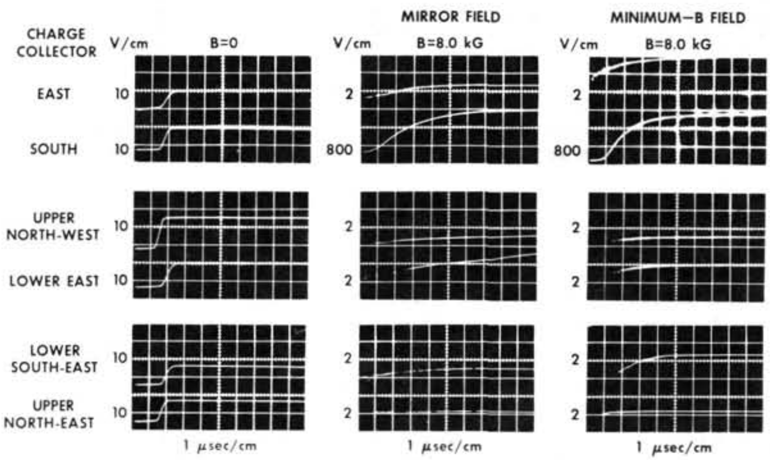

FIG. 7. Plasma expansion symmetry.

The cross field plasma loss has been examined using a modified version of the charge collector probes employed for the measurements of Fig. 7. The modified probes are apertured to restrict their collection solid angle and receive only plasma which has expanded directly across the magnetic field. From measurements with these probes, the cross field plasma loss is less than one-tenth that inferred from the non-directional probe results of Fig. 7. Integration of the plasma flux distribution over solid angle shows that less than one percent of the plasma in these experiments escapes from the containment region along directions transverse to the magnetic field while the remaining 99 percent leaves within the magnetic field loss cones. This result applies directly to the minimum-B magnetic field experiments. With the simple mirror field, the amplitudes of the signals received by most of the cross-field probes are the same as observed in the minimum-B experiments. However, late in the plasma decay a sudden large increase in the plasma flux is often detected by one or more of the probes in a given experiment. The large plasma flux is detected by different cross-field probes in different experiments. While conclusions from the limited data now available can only be tentative, it appears that this random large charge collection is the result of flute-like plasma losses across the magnetic field in the case of the simple mirror. The random large plasma flux transverse to the magnetic field is not observed in experiments with minimum-B magnetic fields at the higher field strengths ($\geq$ 5 kG) indicating that the flute-like behavior obtained in the simple mirror field is suppressed for sufficiently large positive field gradients in the minimum-B geometry.

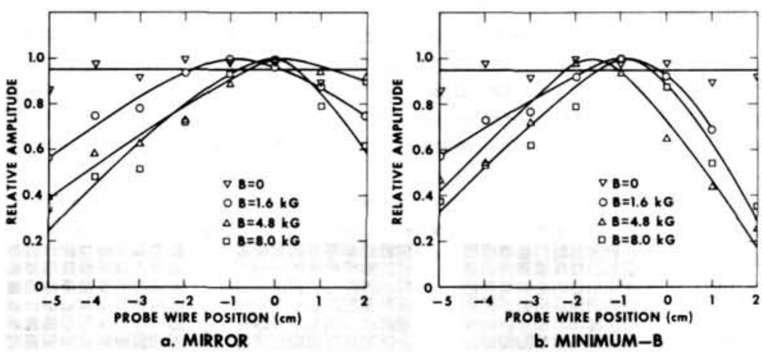

FIG. 8. Comb probe measurements.

A comb probe, consisting of a series of 8 negatively biased bare wire charge collectors, each 0.5 cm long and spaced one cm apart on a line normal to the magnetic field axis at a distance of 30 cm from the plasma origin, was used to examine the distribution of the plasma flux in the mirror loss cone. As shown in Fig. 8, with no magnetic field, the integrated ion charge collected by each of the comb probe wires was virtually identical--the uniform plasma flux of the free expansion plasma. To the extent that the plasma escaping out the mirror loss cones in the magnetic field containment experiments follows the magnetic field lines, the distribution of plasma measured by the comb probe should serve as a measure of the transverse spatial extent of the confined plasma within the magnetic field. For an axially symmetric magnetic field, the transverse radial dimensions of the plasma following a given flux is inversely proportional to the square root of the local magnetic field intensity. At the location of the comb probe, the magnetic field on the mirror axis is 2×10^{-2} that at the plasma origin, and each cm displacement of a charge collector wire away from the magnetic field axis corresponds to 0.14 cm at the center of the magnetic field. From the results of Fig. 8, with both simple mirror and minimum-B magnetic fields the charge collection at the comb probe is definitely peaked along the mirror axis, and the collection width is slightly decreased with increasing magnetic fields up to 8 kG. With an 8 kG simple mirror field, the half intensity radius of the plasma flux at the comb probe is 4 cm, corresponding to a transverse expansion of the plasma within the magnetic field of 0.6 cm.

This result is in remarkable agreement with the 0.3 cm value of the maximum plasma radius calculated in Fig. 4, particularly in view of the limitations of the theoretical model and the blurring of the measured plasma boundary due to the finite ion gyration radius of the escaping ions at the comb probe. With an 8 kG *minimum*-B magnetic field, the measured half intensity radius corresponds to a plasma radius within the field of 0.4 cm, and the transverse expansion of the plasma is apparently more restricted than for a simple mirror.

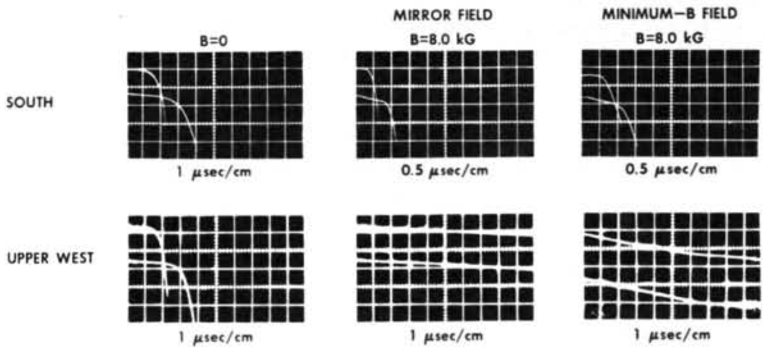

FIG. 9. Plasma expansion velocity.

Time-of-flight measurements of the plasma expansion rate have been made for the free plasma expansion and for the plasma expansion in mirror and minimum-B magnetic fields to examine the escape velocity associated with the loss cone and the cross field plasma decay. The results obtained for measurements along (South) and across (Upper West) the magnetic field are shown in Fig. 9. In these experiments the arrival times of the plasma at two probes located on the same radial line at different distances from the plasma origin are recorded, and the plasma expansion velocity is determined from the ratio of the probe separation to the plasma time of flight. With no magnetic field, the plasma time of flight, and therefore the plasma expansion velocity, is very nearly the same for both of these directions--the essentially spherically symmetric expansion of the free plasma. With a mirror magnetic field, as the field strength is increased, the plasma expansion velocity in the direction of the magnetic field axis is greatly increased (note change of time scale in Fig. 9) while the expansion velocity across the magnetic field is greatly reduced compared with field-free expansion of a plasma of the same energy. The same effect, only more pronounced, is observed with a minimum-B magnetic field. These results support the conclusion that the action of the magnetic field is to constrain the transverse expansion of the plasma, in agreement with the magnetic field interaction calculations and with the results of the comb probe measurements. This constraint maintains the plasma pressure at a higher value for a longer time than in the free expansion case, resulting in a larger plasma expansion velocity in the direction of the magnetic field. Were the magnetic field to result in a purely one-dimensional expansion without changing the plasma density profile, since the plasma energy is fixed, the plasma outer boundary velocity would be increased by a factor of $\sqrt{3}$ over that for a spherical expansion. Experimentally the velocity increase with the magnetic field is a factor of ~ 2, indicating that the plasma-magnetic field interaction has resulted in a one dimensional-like expansion having a somewhat altered density profile.

The charge collector and time-of-flight diagnostics examine the plasma after it has left the magnetic field interaction volume. While the results of Figs. 7 and 8 show that plasma has been contained by the magnetic field, to examine this point further microwave measurements of the plasma density decay within the magnetic field have been carried out. A simple 6 mm microwave interferometer was employed, and measurements were made of the amplitude and phase shift of the microwave signal transmitted through the plasma. For the free plasma expansion, the plasma growth and time development are known. Calculations were therefore carried out to predict the transmitted amplitude and phase shift signals as a function of plasma radius for comparison with the measured free plasma expansion signals. Initially the plasma is small compared with the microwave beam radius, and the plasma intercepts only a small fraction of microwave beam. As the plasma grows, it intercepts a larger and larger portion of the microwave beam, reducing the transmitted signal. With continued expansion, the plasma density drops to a value below cutoff, and a transmitted signal is again observed giving the upper curve of Fig. 10a. Similarly, from the combined effects of attenuation and phase shift by the plasma, an interference signal can be calculated and has the form shown in the lower curve of Fig. 10a. From these calculations, the transmitted amplitude departs from zero as the plasma density decreases below 3×10^{13} cm^{-3}, and the final phase shift maximum occurs at a plasma line of sight density of 10^{13} cm^{-2}. While the details of the amplitude and phase shift signals are affected by an applied magnetic field, the densities associated with the onset of transmission and with the final phase shift maximum are values which can be employed for measurements even in the presence of a magnetic field. The calculated curves were compared with experimental measured phase shift and transmitted amplitude signals as a function of time for a free plasma expansion. For a constant velocity plasma expansion, which from Fig. 2 develops very early in the plasma history, the plasma radius and experimental elapsed time are directly related by the plasma expansion velocity. With such scaling, it is observed that the transmitted amplitude and phase shift signals duplicate those calculated for the free plasma expansion, supporting the identification of the onset of transmission and the final phase shift maximum with specific values of the plasma density.

Experiments were carried out using this microwave system to examine the plasma density decay in both simple mirror and minimum-B magnetic fields, giving results such as shown in Fig. 11. With no magnetic field present, the free expansion amplitude and phase shift signals show that the plasma density decreases to a value below 3×10^{13} cm^{-3} in a time of 0.05 microseconds and measurable plasma is observed for a time of only 0.4 microseconds. With a simple mirror magnetic field, both of these times are increased with increasing field strength. In an 8 kG mirror magnetic field, the plasma lifetime (time for which the plasma density exceeds 3×10^{13} cm^{-3}) is 5 microseconds and measurable plasma is observed for a time of more than 16 microseconds. With a minimum-B magnetic field of 5 kG, the plasma lifetime is even greater: a plasma density of 3×10^{13} cm^{-3} is contained within the magnetic field for a time of 10 microseconds and measurable plasma is still present for as long as 80 microseconds. Increasing the minimum-B magnetic field strength from 5 kG to 8 kG does not, however, serve to further increase the plasma lifetime.

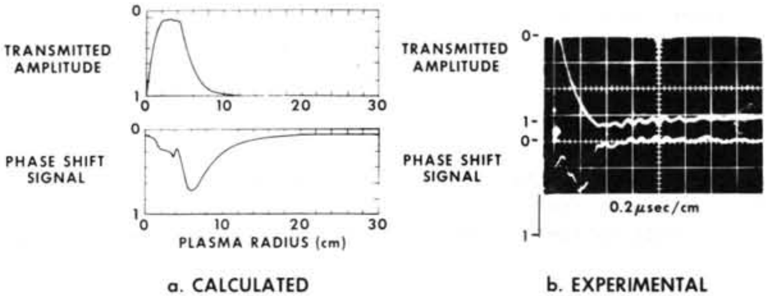

FIG. 10. Microwave interferometer diagnostics - free plasma expansion.

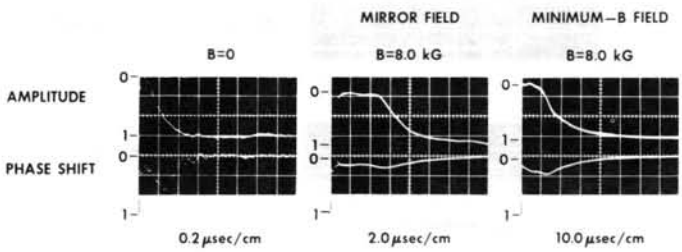

FIG. 11. Plasma density decay.

To determine the degree of thermalization obtained in the trapped plasma, a retarding potential probe has been used to measure the ion energies escaping out the magnetic containment field mirror loss cones at late times. The first grid within the probe is biased negative to extract the electrons from the ions in the plasma entering the probe aperture. A second grid has applied to it a 1-MHz, sinusoidal ion retarding potential, varying from zero to a positive peak voltage, which modulates the ion current to the plate. A third grounded screen grid isolates the ion collector plate from the 1 MHz signal on the retarding potential grid, and the ion collector plate of the probe is biased slightly negative to ensure complete collection of all ions passed by the grid network.

In general, the ions which arrive first at the probe have been hydrodynamically accelerated in the plasma expansion and have energies exceeding the peak retarding potential. As a result, the plate current is initially unperturbed by the retarding potential and is a measure of the ions which, in the initial plasma, have velocities lying within the mirror loss cones. At later times the energy of the escaping ions decreases, thermalization occurs, and the ion current to the plate is cut off during the portion of each cycle of the retarding potential for which the voltage exceeds the ion energy. The maximum energy of the escaping ions can be determined directly from the measured time interval during which the plate current is cut off. Using this probe, initial measurements, such as those in Fig. 10, show that the ions escaping out the loss cones of a minimum-B magnetic field of 4.9 kilogauss center field strength have energies up to 75Z eV (where Z is the maximum charge state of the ions in the plasma) at times as late as 15 microseconds after the plasma generation. Although the ionization state of the ions in the plasma is not known, the plasma is at least singly ionized. On that basis, the energy of the ions escaping along the magnetic field axis after 10 μ sec ranges up to 75 eV, whereas the ion energy for the equivalent ($\epsilon \sim$ 100 eV) plasma in free expansion would be less than 15 eV at these late times. These results, while preliminary, are a direct measure of the energy of the contained plasma and indicate that, upon confinement by the magnetic field, the plasma has been thermalized, in agreement with the theoretical calculations of the plasma-magnetic field interactions.

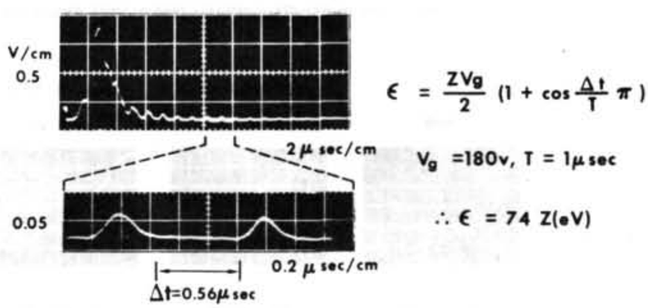

FIG. 12. Retarding potential probe ion energy measurements.

The scattering loss lifetime for the contained plasma can be calculated from the measured plasma density and energy. For a 3 x 10^{13} cm^{-3} plasma of hydrogen ions and singly ionized lithium at a temperature of ~ 50 eV, the average plasma energy evaluated from the measurements of Fig. 12, the Coulomb scattering loss lifetime in a short mirror magnetic field (mirror ratio 4) is 13 μ sec, a result in reasonable agreement with the 10 μ sec lifetime measured in the minimum-B magnetic field. If higher ionization state lithium ions are present, the plasma temperature determined from the retardation probe measurements ($\sim \frac{2}{3}$ x 75Z eV) is higher and the ion density evaluated from the microwave diagnostics ($n_e/\bar{Z}$) is lower, resulting in a collisional scattering lifetime little changed from that calculated for hydrogen ions and singly charge lithium. It appears, therefore, that the plasmas in these experiments are thermalized upon capture by the magnetic field and have a lifetime limited only by Coulomb collisional scattering into the magnetic field mirror loss cones. Since the Coulomb scattering loss lifetime is the maximum plasma lifetime which can be obtained for a given plasma density and temperature in an open-ended field geometry, this result explains why increasing the minimum-B magnetic field above 5 kG did not serve to increase the experimental plasma lifetime.

4. SUMMARY

Laser beam irradiation of solid lithium hydride particles has been used to form isolated, high-density, high-temperature plasmas in vacuum either (a) freely expanding or (b) within confining magnetic fields. The plasmas produced in free expansion are spherically symmetric in both density and expansion velocity and have average electron and ion energies up to 200 eV. Magnetic field interaction studies show that these plasmas, produced in simple mirror or minimum-B containment fields of up to 8 kG center field strength, are trapped and thermalized and, in a minimum-B magnetic field of greater than 5 kG, are confined with a lifetime limited only by Coulomb collisional scattering into the magnetic field loss cones. With reasonable future developments in laser capabilities, it appears that plasmas comprising 10^{17}-10^{18} ions and electrons of an average energy of 10 keV can be produced by this technique. On the basis of these results, laser irradiated solid particle plasmas provide a particularly interesting plasma source both for thermonuclear test devices and for general studies of plasma-magnetic field interactions. Currently in progress are mass spectrometer measurements to determine the ion species present in the confined plasma, flux coil studies of the early plasma-magnetic field interaction, and modifications to the laser system to produce average plasma energies in excess of 1 keV for studies of plasma trapping, thermalization, and confinement under conditions where Coulomb scattering losses do not limit the plasma lifetime to the $\sim 10\mu$ sec of the present experiments.

5. ACKNOWLEDGMENTS

We would like to acknowledge the contributions of Lawrence M. Lidsky of MIT and Ira B. Bernstein of Yale University with whom we have had many fruitful discussions throughout the course of this work.

6. REFERENCES

[1] HAUGHT, A. F., POLK, D. H., "Plasma Physics and Controlled Nuclear Fusion Research," Conf. Proc., Culham, Sept., 1965, IAEA, Vienna, 1966, Vol. II, p. 953.

[2] HAUGHT, A. F., POLK, D. H., Phys. Fluids 9 10 (1966) 2047.

[3] WUERKER, R. F., GOLDENBERG, H. M., LANGMUIR, R. V., J. Appl. Phys. 30 (1959) 441.

[4] LUBIN, M., U. of Rochester, private communication.

[5] FADER, W. J., "Hydrodynamic Model of a Spherical Plasma Produced by Q-Spoiled Laser Irradiation of a Solid Particle," to be published in the Phys. of Fluids.

[6] BASOV, N. G., KROKHIN, O. N., Proc. of the Conference on Quantum Electronics, Paris, 1963.

[7] DAWSON, J. M., Phys. Fluids 7 (1964) 981.

[8] BERNSTEIN, I. B., FADER, W. J., "Expansion of a Resistive Plasma in a Magnetic Field, " to be published in the Phys. of Fluids.

DISCUSSION

D. A. PANOV: Was there any evidence of loss-cone instability?

A. F. HAUGHT: For the conditions of our experiments ($n_i \sim 3 \times 10^{13}$, $T_i \sim 50$ eV, $B \sim 8$ kG, mirror ratio ~ 4, and mirror length ~ 10 cm) the ratio of the Larmor radius to the mirror length is about 100, while for the convective loss-cone instability of Post and Rosenbluth a ratio of ~ 200 is required. In agreement with this, no evidence for the loss cone instability was observed in the experiments, although other stability factors may well have been present.

C. YAMANAKA: We have observed soft X-ray emission in similar experiments. Have you made such observations?

A. F. HAUGHT: Yes, soft X-ray signals from these plasmas have been measured using a thin-foil scintillator detection system. However, at the temperatures of our present experiments, interfering line radiation from ionized lithium is also present, and the signals obtained cannot be interpreted in terms of an electron temperature for the plasma.

S. J. BUCHSBAUM: What fraction of laser energy gets converted into kinetic energy of particles?

A. F. HAUGHT: In our present experiments about 1-2% of the incident laser energy is absorbed by the plasma (see, for example, Fig. 2). However, by selecting the experimental particle radius and focal spot size conditions in accordance with the equations given in the paper, it is possible to obtain a laser energy transfer efficiency as high as 30%.

S. J. BUCHSBAUM: What limits the optimum efficiency to 30%?

A. F. HAUGHT: The conditions given in the paper and the optimum efficiency of 30% are determined on the basis of the additional requirement that the energy per particle in the plasma be maximized for the given laser beam power and pulse duration. The total number of particles in the plasma is limited by this requirement. Therefore, initially the solid particle does not occupy the full area of the laser beam focal spot and later, as the plasma expands, it rapidly becomes transparent to the laser radiation, both effects resulting in a maximum energy coupling of 30%. If, however, sufficient laser power becomes available, so that it is no longer necessary to maximize the energy per particle in the plasma for interesting experiments, then the number of particles in the plasma can be increased and essentially all the laser pulse energy can be coupled into the plasma.

P. VANDENPLAS: Have you considered accelerating the laser slightly at $t = 0$ so as to defocus the laser beam after the plasma has been formed, thereby increasing the section of the laser beam as the plasma expands? Such time-dependent defocusing might increase the efficiency of conversion of laser energy into plasma kinetic energy.

A. F. HAUGHT: If the laser beam is defocused after the plasma has been formed, the beam intensity in the focal spot is reduced and, to the extent that the defocused beam does not pass through the plasma or passes through the lower-density, weakly absorbing outer portion of the plasma, the energy absorption by the plasma is lowered.

It is possible that controlled time variation of the focal spot size during the irradiation of the plasma would result in an increase in the plasma energy for a given laser pulse, but this increase would in general be slight and would not justify the experimental complexity required. As a result, no such experiments are planned at any of the laboratories working with laser-produced plasmas.

V.N. TSYTOVICH: What is the role of turbulent heating in a laser-produced plasma?

J.M. DAWSON: Perhaps I might answer this question.

If one uses very short pulses, so that the plasma remains over-dense (maximum $\omega_p > \omega$ during the pulse), the laser light penetrates the plasma to the point where $\omega = \omega_p$. At that point coupling between the laser light and the longitudinal plasma oscillations can easily take place. One can readily obtain a greatly enhanced resistivity at this point; a type of turbulent heating can take place there. Even without enhanced resistivity, calculations we have carried out at Princeton indicate that with such short pulses strong absorption can be obtained at temperatures up to 10 keV, and with enhanced resistivity much higher temperatures should be possible.

HEATING AND CONFINEMENT STUDIES OF LASER-IRRADIATED SOLID-PARTICLE PLASMAS

M. J. LUBIN, H. S. DUNN AND W. FRIEDMAN
MECHANICAL AND AEROSPACE SCIENCES DEPARTMENT
UNIVERSITY OF ROCHESTER, ROCHESTER, N. Y.,
UNITED STATES OF AMERICA

Abstract

HEATING AND CONFINEMENT STUDIES OF LASER-IRRADIATED SOLID-PARTICLE PLASMAS. The plasma formed by vaporization of a small solid particle of lithium hydride, electrodynamically suspended in hard vacuum, with a "tailored" laser pulse is studied. It is shown that proper shaping of the initial leading edge of the laser pulse such that the particle is completely vaporized prior to the main heating and subsequent expansion leads to enhanced energy absorption. At peak laser powers of 1.51×10^9 W the peak measured temperatures in the expanding plasma, with no confining magnetic field, are in excess of 160 eV, while the measured average energies per particle in a fully ionized symmetrically expanding plasma containing 10^{16} ions, are 1 keV. Temperature measurements are carried out by light scattering and expansion energy is obtained using integrated charge collection probes and a 5.3 mm microwave interferometer.

Preliminary work on the interaction of this expanding plasma with a uniform magnetic field is presented. We examine the theoretical radiation expected in the case of weak interaction with the uniform field. In particular, the radiation intensity is presented for (a) the dipole radiation due to surface currents during the initial stages of expansion, (b) cyclotron surface radiation and (c) the volume cyclotron radiation during the later stages of the plasma expansion. A comparison of far infrared and millimeter measurements displays reasonable agreement with the predicted development in time of the plasma radiation.

Results of initial confinement studies in a non-zero minimum B magnetic field generated by a "baseball winding" are presented. Measurement of containment times with a microwave interferometer and flux probes indicate that densities of 10^{13} cm^{-3} are retained in a volume of 30 cm^3 for times in excess of 400 μs, in a 20 kG field. Of particular interest is the apparent flute-like behaviour at fields below 8 kG.

I. INTRODUCTION

Investigations of the production and containment of the plasma produced by the irradiation of a small particle of deuterium or lithium hydride by the energy contained in a pulse of laser radiation are at present in progress in a number of experimental devices (1-6).

A theoretical description of the plasma obtained by focused laser radiation on the LiH pellet in a vacuum background has been discussed in the literature and consists of a fluid dynamic solution to the expansion of a small plasma sphere, initially cold, into vacuum (13, 14). The sphere of compressible plasma is heated by the incident laser radiation leading to time dependent energy absorption described by a high frequency absorption coefficient (7, 8). The resulting plasma expansion may be approximated by a similarity solution in which the radial density profile in the similarity parameter r/R remains invariant (1). The major portion of the absorbed energy is converted into ordered energy of expansion and subsequent cooling of the plasma sphere, (Fig. 1).

In section II we briefly describe the experimental apparatus in which the "free expansion" studies on the irradiation of particles of lithium hydride by our group have been carried out. Brief consideration is given to the time dependent absorption of the incident radiation by the solid prior to full development of the plasma state. Treatment of the initial vaporization stage of the solid by a strong laser driven shock wave yields a working criterion for estimating the duration and amplitude of the initial vaporization pulse

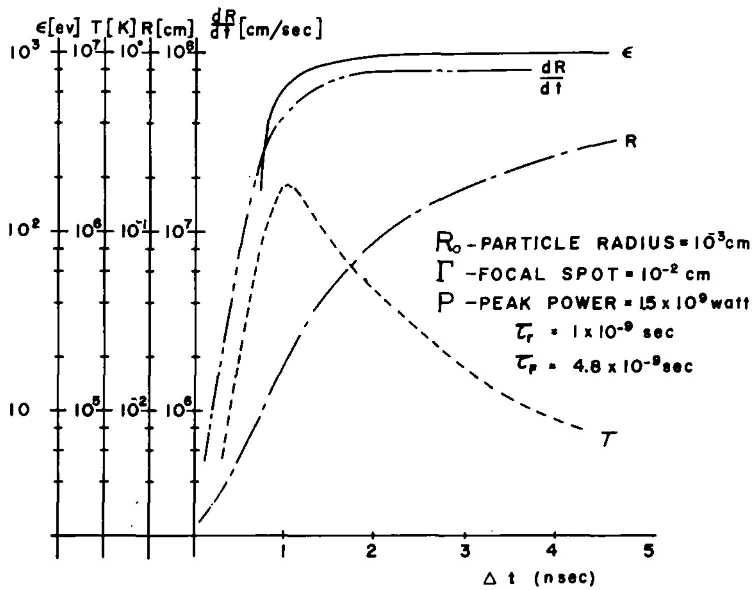

FIG. 1. Heating and expansion of lithium hydride plasma drop by a 1×10^{-9} second rise and 4.8×10^{-9} second fall laser pulse at 6943 Å.

prior to the main heating pulse. These free expansion measurements include peak electron temperature and ion temperature, electron density and average energy per particle.

In section III we present our current experimental and theoretical results of the interaction of this expanding plasma sphere with a uniform magnetic field. Measurements of the infrared radiation during the initial stages of expansion indicate the existence of induced currents whose time history and spectral radiation intensity is computed and compared with the available experimental data. The intermediate stage of expansion is characterized by surface cyclotron radiation due to partial larmor orbits of the expanding electrons. The relaxation time of the magnetic field into the plasma volume is calculated from a solution to the diffusion equation with time-varying conductivity utilizing the dipole radiation approximation. Finally the volume cyclotron radiation is presented which occurs after complete infusion of the uniform magnetic field into the plasma volume.

In section IV, our containment studies of this laser produced plasma in a minimum B field produced by a baseball winding are described. Of particular interest here is the apparent existence of flute-like behavior which together with particle scattering into the loss cause appears to limit the confinement times to those measured in our experiments.

II. FREE EXPANSION EXPERIMENTS

The experimental apparatus is shown schematically in Fig. 2a,b. Initially the particles from which the plasma is produced are injected into the chamber from below the electrodynamic suspension cage. The details of this type of suspension system are fully described in reference 1 and 9. Background pressure in the vacuum chamber during the experiment is 2×10^{-8}mm Hg. Approximately thirty particles are caught in stable orbits at a frequency of 14 cps in the vicinity of the geometric center of the suspension array. Adjustment of the DC bias on each of the eight suspension plates allows each particle to be measured by positioning a portion of its orbit in the collimated beam of a 1/10 milliwatt CW He-Ne laser. The resulting Fraunhoffer diffraction pattern is then monitored by a single photomultiplier tube or photographed as in Fig. 3. In this manner particle size can be determined to within a few percent and the total number of available electrons and ions compared with the experimentally determined numbers of electrons and ions yielding a measure of the degree of ionization. A single particle having the required dimensions and symmetry for the specific experiment is selected and the remainder ejected from the cage. The particle is then positioned at the focal spot of a meniscus lens which concentrates the incident giant pulsed radiation in the focal volume through which the particle passes in its orbit. The photomultiplier then triggers the laser which is delayed until the particle passes through the center of the focal spot. Simultaneously the electrodes of the suspension system are shorted to ground in less than one microsecond by light activated silicon controlled switches. The electrode surfaces act as limiters to the plasma volume.

Initially a single pulse of laser radiation with a peak power of 600 megawatts lasting for nine nanoseconds at the half power points was used for the free expansion energy coupling measurements. However, a measurable asymmetry was noticed in the time of arrival studies at distances as close as 15 mm. from the plasma center. Using biased wires as time of arrival charge collectors, it was observed that the plasma expanded up to 1.8 times faster in the forward direction toward the laser radiation than in the backward direction. We postulated that due to the interaction of the incident radiation with the solid pellet the plasma on the front surface was being preferentially heated leading to a colder plasma on the far side away from the incident radiation. More over the integrated time rate of charge collection Q_c was erratic indicating incomplete ionization of the solid particle. This occurred predominantly at particle sizes larger than 65 microns radius. These considerations led us to first heat the solid pellet with a prepulse of amplitude P_h and duration T sufficient to completely vaporize the LiH particle but not

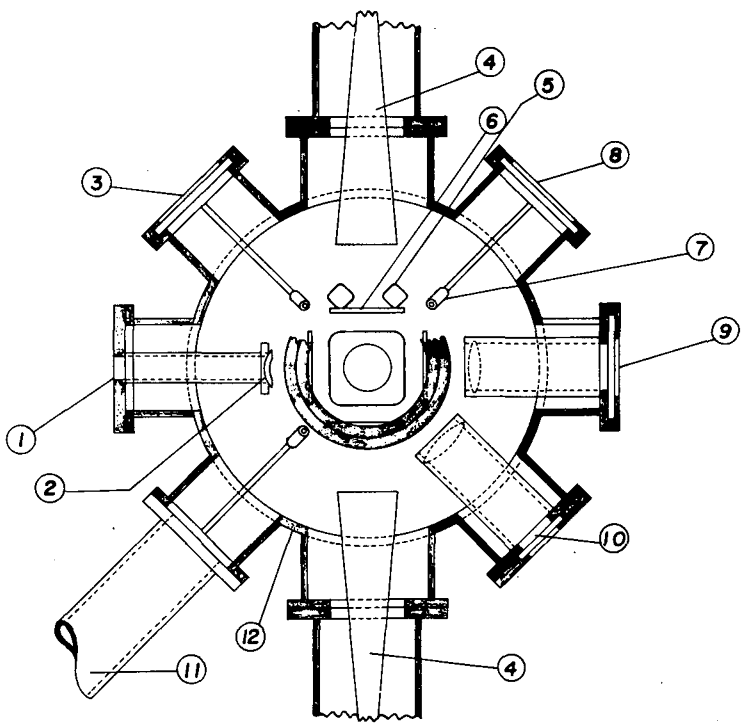

FIG. 2a. Schematic drawing of experimental apparatus: (1) incident laser direction; (2) meniscus focusing lens; (3) light scattering and diffraction measurement port; (4) mm. interferometer; (5) minimum "B" coil; (6) suspension electrodes; (7) time of flight collectors; (8) submillimetre interferometer port; (9) pulse transmission measurement; (10) scattering port; (11) submillimetre detector; (12) vacuum chamber.

significantly heat the resulting plasma. Following the initial vaporization pulse, during which the cold plasma has slightly expanded, the main plasma heating pulse is then applied. Although the vaporization of solid matter by laser radiation is not well understood, the following assumptions were made to determine the amplitude and duration of the vaporization pulse. Energy in excess of the binding energy of the LiH molecule must be supplied over a time no shorter than that required for a strong acoustic disturbance (shock wave) to traverse the pellet. For a LiH particle 20 microns in diameter, allowing for a coupling efficiency of one percent, the resulting laser power must be on the order of 5 megawatts lasting for 2 nanoseconds. A typical oscilloscope trace of the leading edge of the main plasma heating pulse preceded by a seven megawatt vaporization tail is shown in Fig. 4. The vaporization leading edge was produced by inserting a partially transmitting Pockel's cell at the output of the oscillator cavity which is delayed with respect to the main Q-switched oscillator pulse. A marked improve-

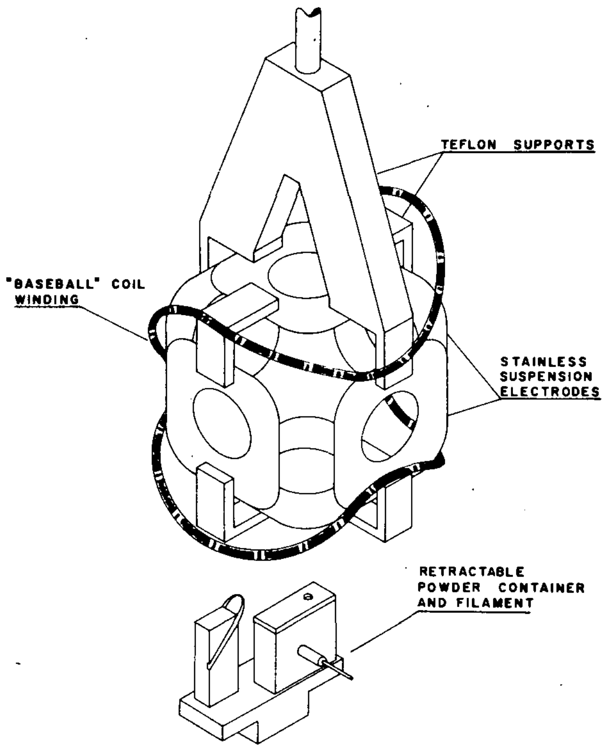

FIG. 2b. Suspension electrode schematic.

ment in the near field expansion symmetry as well as the deduced average energy per particle was immediately observed. The chief results presented in this report were obtained utilizing a Q-switched ruby oscillator-amplifier combination for both vaporization and heating giving a main plasma heating pulse of 1.51×10^9 watts peak power in a pulse width of 4 nanoseconds.

Time of flight charged particle collectors consisting of grided probes were used to determine (a) the far field symmetry of the plasma expansion, (b) the average energy per particle, and (c) the total number of electrons and ions in the freely expanding plasma. All the results contained in the present investigation were obtained with the charged particle collectors biased to collect ions only, (Fig. 5). The collected current is integrated in time at the detector to yield a value of total collected charge at any time. This total collected charge Q_c is then compared with the theoretical value of Q_c obtained from the similarity expansion model as shown in Fig. 6. Once the symmetry of the expansion was achieved by using the technique of tailoring the laser pulse, the total number of charged particles in the plasma can be obtained by integrating Q_c over the surface of the expanding plasma.

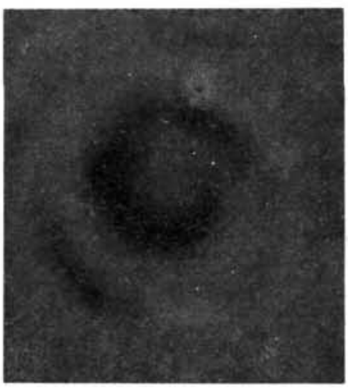

FIG. 3. Fraunhoffer diffraction pattern of a 26-micron suspended particle.

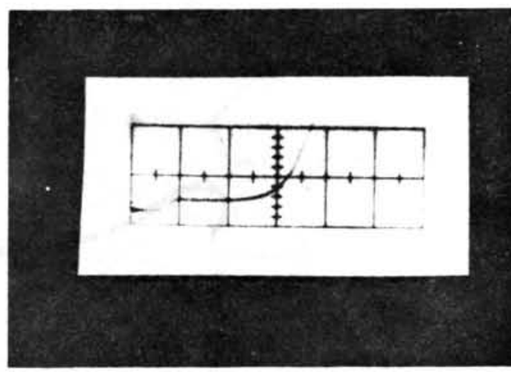

FIG. 4. Laser pulse leading edge showing initial vaporization tail. 1.5×10^{-9} s/division.

The electron and ion temperatures are measured by light scattering off of the expanding plasma volume utilizing a Q-switched ruby laser with an output of 100 MW and a pulse duration of 15×10^{-9}sec. As the electron number densities are very high during the period of peak temperature, the scattered spectra is predominantly determined by collective effects. For example, the characteristic scattering parameter defined by:

$$\alpha = \frac{\lambda_o}{\lambda_D}\left[4\pi \sin\frac{\Theta}{2}\right]^{-1}$$

λ_o - incident wave length

λ_D - debye length

Θ - scattering angle

which is effectively the ratio of the fluctuation wave length to the Debye length, is often in excess of 5. In this case, the collective effects between particles give rise to two important modes of oscillation, a central ion acoustic mode, strongly Laudau-damped with a half width determined by the ion temperature, and the plasma lines which represent the electron component of the density fluctuation. The distance of these lines from the center of the scattered spectrum is given by the dispersion relation for longitudinal plasma oscillations:

$$\Delta\lambda = \frac{\lambda_0}{2\pi c}\left[\omega_p^2 + \frac{3kT_e}{m}\left(\frac{4\pi}{\lambda_0}\sin\frac{\theta}{2}\right)^2\right]^{1/2} \quad \text{(Ångström)}$$

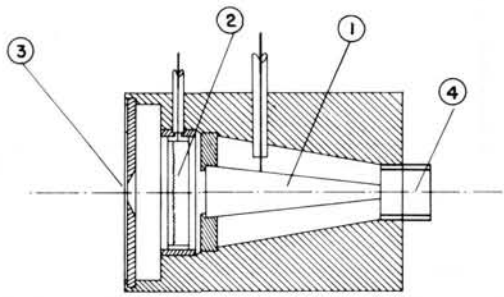

FIG. 5. Integrating charge collector. (1) 50 Ω transmission line; (2) screen; (3) 2 mm aperture; (4) 50 Ω BNC connector.

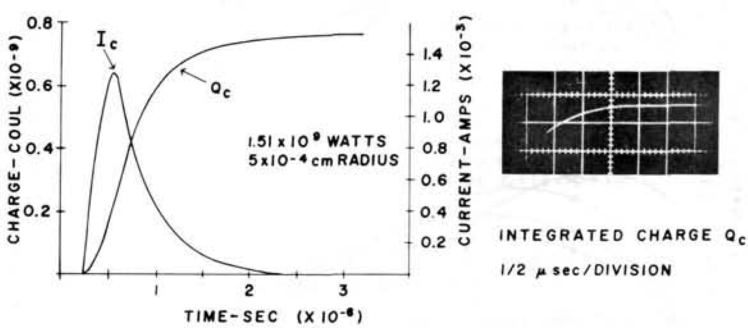

FIG. 6. Theoretical and experimental integrated charge collection.

Incident scattering radiation is focused down to a volume in the center of the plasma of 10^{-6} cm^3. Two plates of filter glass placed at the brewster angle absorb the transmitted laser light. The scattered light is collimated into a seven-sided pyramid whose surface is constructed of front surface mirrors. The light from each flat surface is directed through an interference filter to a photomultiplier tube. The scattered spectra are then compared with a single-set of theoretical spectra computed as in[10], resulting in a determination of both T_e and n_e. An example of the scattered spectra is shown in Fig. 7. Fig. 8 and 9 show the theoretically calculated curves for average energy per particle and

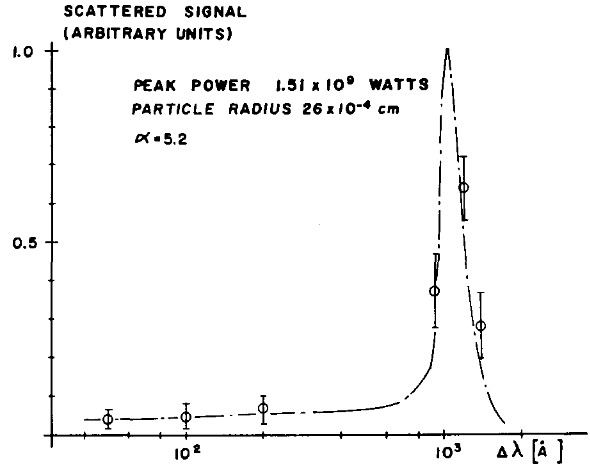

FIG. 7. Spectra of scattered light at peak temperature in free expansion.

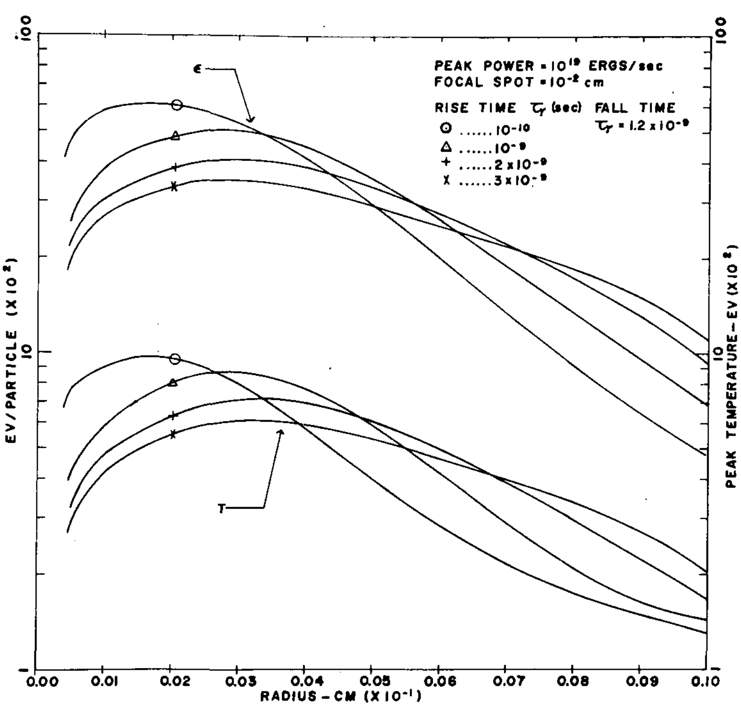

FIG. 8. Theoretical average energy per particle (ϵ) and peak temperature (T) vs particle size of LiH for a particular peak laser power with varying pulse shape (τ_r).

peak temperature as a function of particle size and peak power. The laser pulse is characterized by a modified Gaussian leading and trailing edge in a manner similar to ref. (1). The experimental free expansion results can be summarized by the data presented in Fig. 10. Here a comparison is made of the peak temperature and the average energy per particle with the calculated results from the free expansion analysis. While the temperature appears to be consistent with the theoretical model, the lower average energy at the larger particle size suggests that perhaps the heating at larger particle sizes is not as well understood. This trend toward lower energy per particle for large pellets has been observed at lower laser powers as well(6).

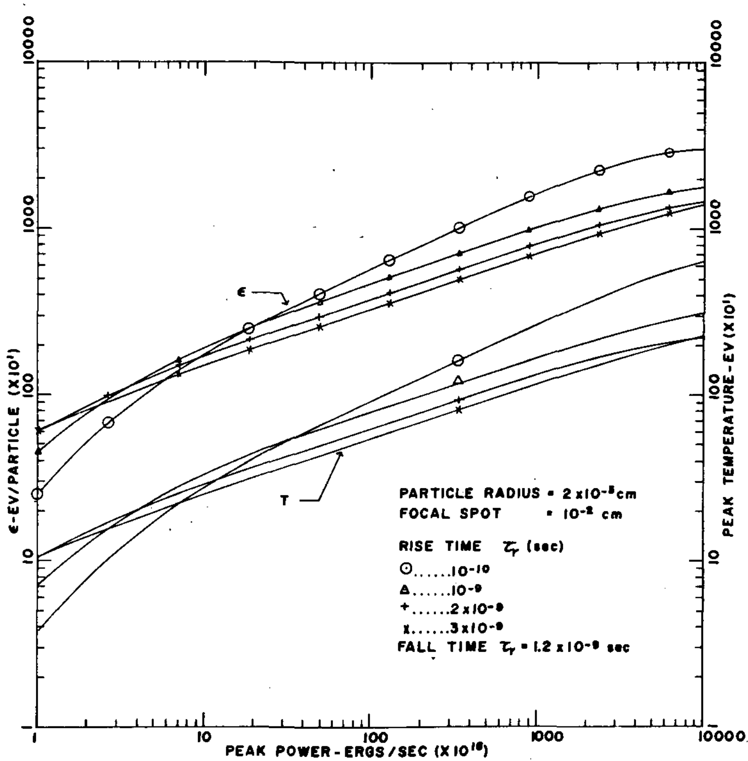

FIG. 9. Theoretical average energy per particle (ε) and peak temperature (T) vs varying peak laser power for a particular particle size.

III. UNIFORM FIELD STUDIES

In this section we discuss some of the radiative phenomena caused by the expansion of the laser-produced plasma in a uniform magnetic field as shown in Fig. 11. Immediately following the vaporization of the pellet the resulting plasma is "cold" and will have a low electrical conductivity. Consequently any magnetic field permeating the plasma during this stage of the expansion will not be affected by the presence of the plasma sphere. As the plasma absorbs energy from the laser pulse, the temperature increases very rapidly. The increasing conductivity results in compression of the magnetic

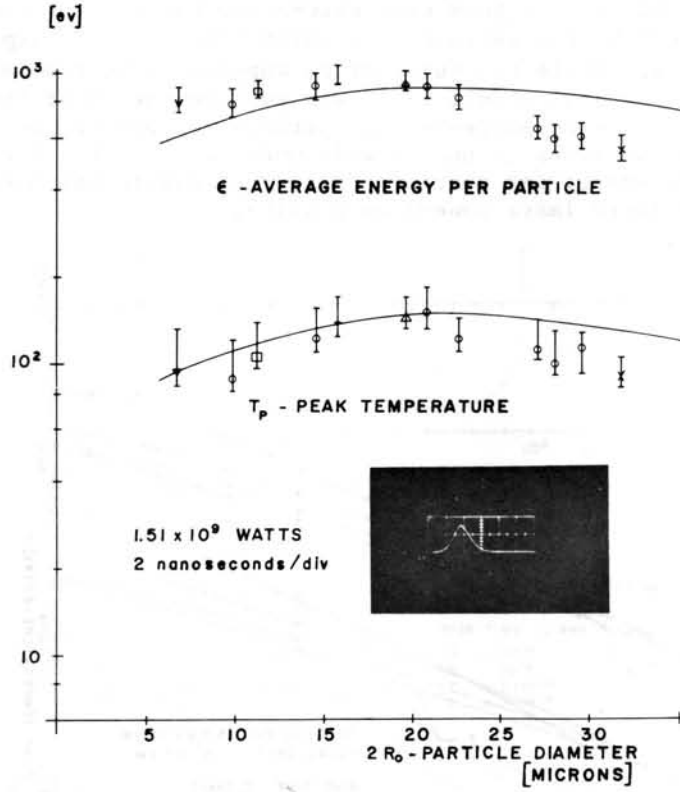

FIG. 10. A comparison of experimentally determined average energy per particle (ϵ) and peak temperature (T_p) with the theoretical model.

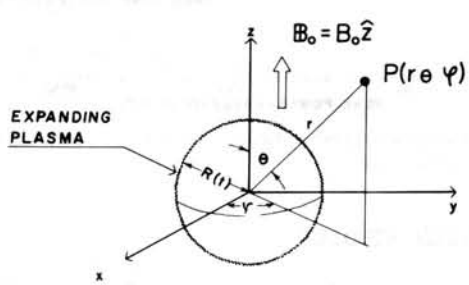

FIG. 11. Expansion of the plasma in a weak uniform magnetic field.

field as the plasma expands inducing currents resulting in time dependent dipole radiation. The shortest wave-length of this type of radiation will be on the order of the size of the plasma sphere at this point in time. As the plasma expansion continues past the point at which energy absorption terminates the temperature decreases as $T \sim r^{-2}$ and the field again permeates the cooling plasma volume. At this point the dipole like radiation falls to zero and one can expect volume cyclotron radiation to be observed. During the intermediate stage while the field is beginning to penetrate the expanding plasma, a contribution due to surface cyclotron radiation, that is, radiation due to electrons being reflected back into the plasma by the external magnetic field, is also a possible contribution to the total radiation spectrum. The radiation measurements presented here were carried out using a sub-millimeter detector with measurable wave length response from 70 microns to 8 mm. combined with a rise time of less than 4×10^{-9}sec. All measurements were in the direction $\theta = \frac{\pi}{2}$.

(a) Dipole Radiation: The equations governing the fields are

$$\begin{aligned} \nabla \times \vec{E} &= \frac{1}{c}\frac{\partial \vec{B}}{\partial t} \\ \nabla \times \vec{B} &= 4\pi \vec{J} + \frac{1}{c}\frac{\partial \vec{E}}{\partial t} \\ \vec{J} &= \sigma\left(\vec{E} + \frac{1}{c}\vec{u}\times\vec{B}\right) \end{aligned} \qquad (1)$$

The solution of the resulting quasi-static problem along with a discussion of the assumption of scalar conductivity is presented in ref. (11). Assuming a radial velocity

$$\vec{u} = \frac{r}{R}\frac{dR}{dt}\,\hat{r} \qquad (2a)$$

which implies a spherically symmetric expansion essentially unaffected by the field, the driving term causing the induced currents is

$$-\frac{r}{R}\frac{dR}{dt} B_0 \sin\theta\ \hat{\varphi} \qquad (2b)$$

Consequently the fields external to the plasma $(r > R)$ will always have a dipole structure.

With the introduction of the stream function ψ, the relevant fields are defined by

$$B_r = \frac{1}{r^2 \sin\theta}\frac{\partial \psi}{\partial \theta} \qquad (3a)$$

$$B_\theta = -\frac{1}{r\sin\theta}\frac{\partial \psi}{\partial r} \qquad (3b)$$

$$E_\varphi = -\frac{1}{r\sin\theta}\frac{\partial \psi}{\partial t} \qquad (3c)$$

where the governing equation for ψ is:

$$\frac{\partial^2\psi}{\partial r^2} - \frac{2\psi}{r^2} = \frac{4\pi r}{C^2}\left[\frac{\partial\psi}{\partial t} + \frac{1}{R}\frac{dR}{dt}\left(r\frac{\partial\psi}{\partial r}\right)\right] \tag{3d}$$

In equation (3d), the stream function ψ includes both the induced and the externally applied magnetic field. From reference 11 the solution of this problem subject to the initial condition that the external field permeates the plasma at time t = 0 is

$$\psi(r,\theta,t) = \frac{B_0\sin^2\theta}{2}\left[r^2 - \frac{\chi(t)}{r}\right] \tag{4a}$$

where the first term denotes the external field and the second term, the induced field, is for r $\geq$ R,

$$\chi(t) = 6\hat{R}(\tau)\int_0^\tau d\tau' \sum_1^\infty \frac{e^{-n^2\pi^2(\tau-\tau')}}{n^2\pi^2}\frac{d}{d\tau'}\hat{R}^2(\tau') \tag{4b}$$

The dimensionless time τ appearing in equation (4b) is defined by

$$\tau = \int_{t_i}^{t}\frac{C^2\,dt'}{4\pi\sigma R^2} \tag{4c}$$

and $\hat{R}(\tau)$ is the plasma radius R as a function of τ.

Before proceeding with an analysis of equations (4), let us return for a moment to the radiation fields. For the region outside the expanding plasma (r > R), a solution of equations (1) with displacement current retained is, in terms of the stream function ψ,

$$\psi = -\frac{B_0\sin^2\theta}{2}\left[\frac{1}{r}F(t-r/c) + \frac{1}{c}F'(t-r/c)\right] \tag{5a}$$

where F is an arbitrary function of the retarded time (t-r/c). When the radial coordinate r is small, say comparable with $R(t)$, the function F(t-r/c) may be expanded in the series

$$\psi = -\frac{B_0\sin^2\theta}{2r}\left[F(t) - \frac{1}{2}\frac{r^2}{C^2}F''(t) + \ldots\right] \tag{5b}$$

Since the displacement current has already been neglected for the analysis when r < R, it is consistent to omit the second term in the above equation because it is small compared with F(t). In this case, F(t) becomes equal to the expression $\chi(t)$ defined by equation (4b).

In terms of F(t), the radial component of the Poynting vector is

$$S_r = \frac{C B_o^2 \sin^2\theta}{16\pi r^2}\left(\frac{F}{r^2} + \frac{F'}{rc} + \frac{F''}{c^2}\right)\left(\frac{F'}{r} + \frac{F''}{c}\right) \tag{6}$$

where the primes on F denote differentiation with respect to the argument (t-r/c).

To proceed further, it is necessary to simplify equation (4b). The dimensionless time τ defined by equation (4c) may be written as

$$\tau = \int_{R_i}^{R} \frac{c^2 \, dR'}{4\pi\sigma R^2 \dot{R}} \tag{7a}$$

where R_i denotes the initial radius. The integrand of equation (7a) has been plotted versus R in Fig. 12 using the computed time history of the plasma expansion for a typical case. The exact shape of the curve will of course depend upon the details of the heating process but general features of the curve should not change appreciably. Setting the integrand of equation (7a) equal to f(R), we see that the approximate formula

$$f(R) = \frac{R_m c^2}{\dot{R}_o \sigma_o R_o^3 4\pi}\left[\frac{R}{R_m} + \frac{1}{2}\left(\frac{R_m}{R}\right)^2\right] \tag{7b}$$

fits the curve well for R > .04cm. The symbol Rm denotes the value of radius at which the minimum of f(R) occurs. The fact that f(R) varies linearly with radius for large R is not surprising since σR^3 is constant in the asymptotic portion of the expansion. The zero subscript denotes values measured during free expansion of the plasma.

Performing the integration of equation (7a), we obtain*

$$\tau \approx 1.85 \times 10^4 \left[\left(\frac{R}{R_m}\right)^2 - \left(\frac{R_m}{R}\right) + 23.8\right] \tag{8}$$

For values of radius less than 2.5 cm., it is found that τ is less than or equal to 1/10. From equation (4b), it is observed that this value of τ corresponds to the e-folding time of the n=1 mode. In other words, the time τ =1/10 describes the life-time of the induced fields.

---

* Numerical values listed here are representative of the particular case where radiation was measured. For details, see reference(12).

From equation (4b), after an integration by parts:

$$F(t) = 6\hat{R}(\tau)\left\{ \frac{d\hat{R}^2(\tau)}{d\tau} \sum_1^{\infty} \frac{1}{n^4\pi^4} - \frac{d\hat{R}^2(0)}{d\tau} \sum_1^{\infty} \frac{e^{-n^2\pi^2\tau}}{n^4\pi^4} - \int_0^{\tau} d\tau' \sum_1^{\infty} \frac{e^{-n^2\pi^2(\tau-\tau')}}{n^4\pi^4} \frac{d^2\hat{R}^2(\tau')}{d\tau'} \right\} \quad (9a)$$

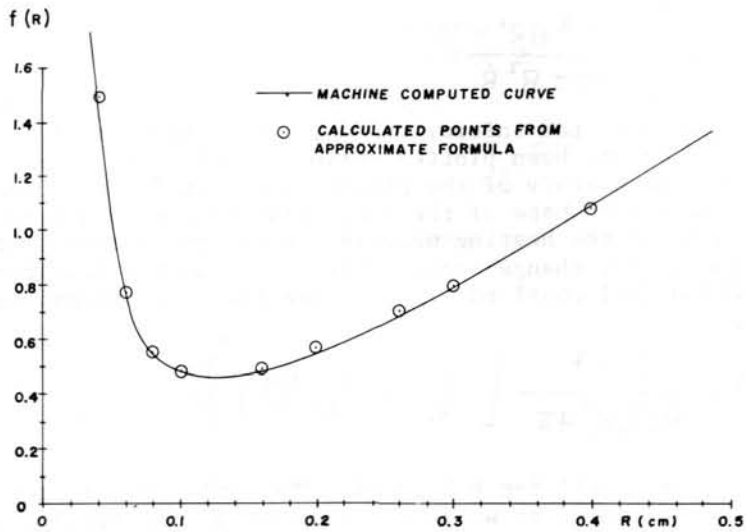

FIG. 12. Approximation to Eq. (7a).

Since τ is small during the radiation process, it is convenient to use an alternate form of the sum appearing in equation (9a), namely,

$$\sum_1^{\infty} \frac{e^{-n^2\pi^2\tau}}{n^4\pi^4} = \frac{1}{90} - \frac{\tau}{6} - \frac{\tau^2}{4} + \frac{2}{3\pi^{1/2}}\tau^{3/2} + J \quad (9b)$$

where J is given by the asymptotic formula:

$$J \sim \frac{\tau^{7/2}}{\pi^{1/2}} \sum_1^{\infty} \frac{e^{-n^2/\tau}}{n^4} \quad (9c)$$

For $\tau \leq 1/10$, it is apparent that the first four terms of equation (9b) are a good approximation. For the initial stages of the expansion where τ is very small, only the first term of equation (9b) is important so that:

$$F(t) \simeq \frac{d\hat{R}^2(0)}{d\tau} R(t)\tau(t) \tag{10a}$$

From equation (6), the far field radiated power can then be calculated using the formula,

$$S_r = \frac{B_0^2 \sin^2\theta}{16\pi c^2 r^2}(F'')^2 \tag{10b}$$

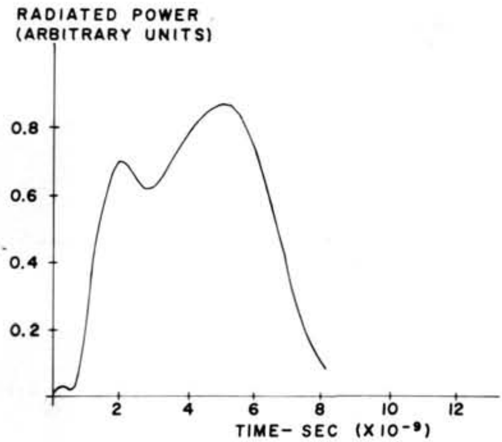

FIG. 13. Computed radiation intensity due to dipole currents over the bandwidth of the infrared detector.

For larger values of τ, it is convenient to return to equation (4b) since in this case,

$$\frac{d\hat{R}^2(\tau)}{d\tau} = \text{constant}$$

The intensity of dipole radiation into a solid angle will be

$$dI = S_r r^2 d\Omega$$

Consequently the measured radiation intensity will vary as B_0^2. The computed radiation intensity from the integral of equation (6) into the infrared detector is shown in Fig. 13, while the measured radiation in the $\pi/2$ direction is shown in Fig. 14. It is apparent that although the general form of the radiation pulse can be explained by the above considerations the magnitude does not scale exactly as B_0^2 but as B_0^{α} with α varying between one and two.

(b) Cyclotron Radiation: It is shown in ref. (12) that the volume cyclotron radiation varies also as B_0^2. Specifically

$$dI_c = \frac{e^4 B_0^2 n_e kT R^3(t)}{m^3 c^5} d\Omega \tag{11}$$

The contribution to the radiation intensity due to electrons describing partial lamor orbits before returning to the plasma volume is, in the case of a $\pi/2$ measurement, given by[12]:

$$dI_p \approx \frac{1}{10} \frac{e^3 B_0 n_e R^2(t) \pi^3}{m c^4} \left(\frac{2kT_e}{m\pi}\right)^{3/2} d\Omega \tag{12}$$

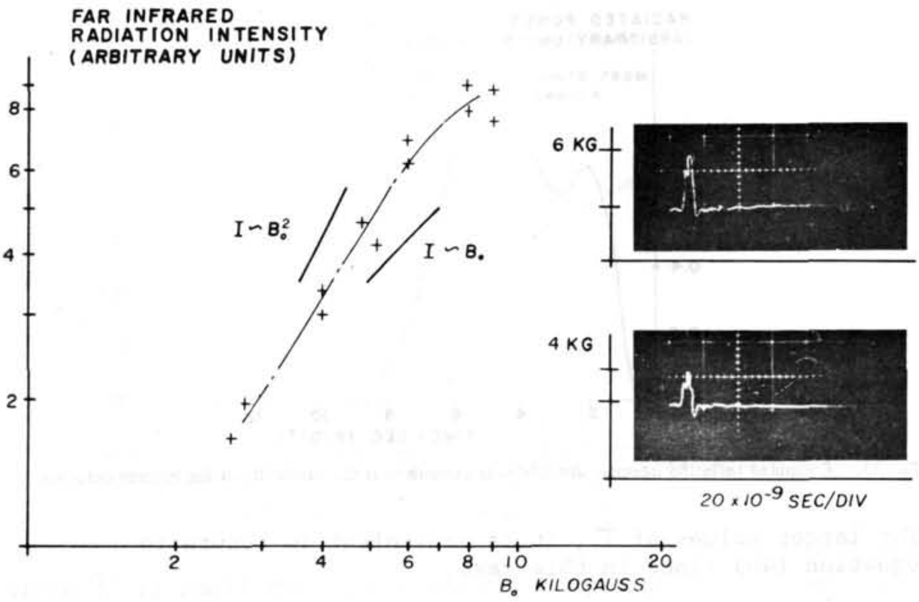

FIG. 14. Measured values of far infrared radiation intensity in a uniform magnetic field.

with the majority of the radiation being in the neighborhood of the first and second harmonics of the cyclotron frequency. This surface cyclotron radiation varies as B_0 and the ratio of volume to surface cyclotron radiation varies as $B_0^{-1/3}$ during the early stages of the infusion of the magnetic field into the plasma volume. We would expect then that as the magnetic field is increased the surface cyclotron radiation could predominate. This is offered as a tentative explanation for the trend of radiation intensity toward a linear dependence on at the higher values of magnetic field.

As both the surface and volume cyclotron radiation are functions of the electron temperature, the time history and extent of the interaction of the expanding plasma with the field can be inferred from the spectral intensity measurements in the neighborhood of the cyclotron frequency using equations (11) and (12). These studies are presently being pursued.

IV. CONFINEMENT STUDIES

Preliminary studies on the confinement of this plasma, produced inside of a non-zero minimum B magnetic field, have been undertaken. The magnetic field configuration is shown in Fig. 2 and the measured surfaces of constant "minimum B" are shown in Fig. 15. The field coil is driven from two actively crowbarred capacitor banks to provide a smooth cur-

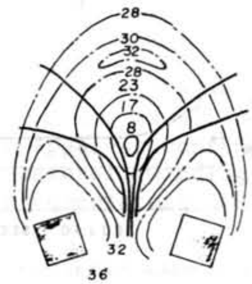

14 CENTIMETER "BASEBALL"
WINDING

FIG. 15. Surfaces of constant minimum B in the nine-turn winding.

rent pulse essentially constant over a time exceeding 900 microseconds. Measurements of the electron density of the confined plasma were carried out using two focused interferometers at wave lengths of 5.3mm. and 0.337mm. Representative transmission measurements are shown in Fig. 16.

Ion probes were placed in a direction transverse to the field lines two centimeters from the center of the well. The suspension electrodes were spaced 10 cm. between opposing faces. All the confinement experiments were done with pellets of LiH varying in size between 20 and 26 microns yielding approximately 10^{15} electrons in the fully ionized plasma. The probes consisted of a thin wire protruding one millimeter from an insulating teflon sleeve shielded in a thin braid. The braid sleeve was grounded simultaneously with the suspension electrodes. A negative potential of 50 volts applied to symmetrically placed probes was sufficient to block the electrons and collect ions only as indicated by no measurable change in collected ion signal when higher voltage was used. Oscilloscope traces from the three probes placed along the azimuth of the well volume are shown in Fig. 17. It is observed that, at this value of magnetic field, the initial burst of plasma across the well in all directions is followed approximately 10 microseconds later by an asymmetric flute-like behavior in the direction of probe 1 and 2. At the opposite side of the trap no secondary burst is observed. For higher values of

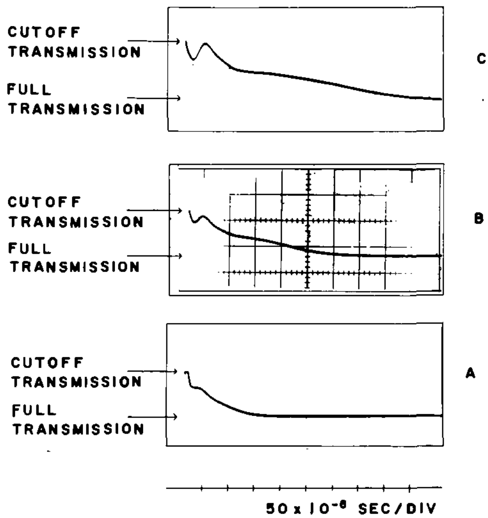

FIG. 16. 5.3-mm transmission measurements at (A) 8 kG; (B) 13 kG; (C) 19 kG.

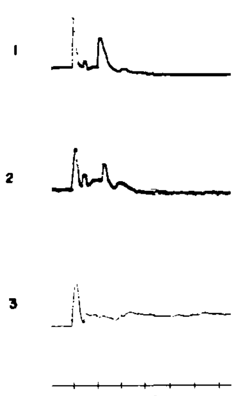

FIG. 17. Collected probe current along the azimuth of the well. Probes (1) and (2) are 30° apart, two centimetres from the centre of the well. Probe (3) is 180° away from probe (1).

magnetic field this behavior vanishes and only a single burst of current, decreasing in amplitude as the field is increased, is observed along all position on the azimuth.

The gross time history of the electron density over an estimated plasma volume of $30cm^3$ can be inferred from the microwave measurements. These indicate the presence of an electron density in excess of 2×10^{13} for 45 microseconds decreasing to approximately 2×10^{12} in 400 microseconds. If this decay were totally due to scattering into the loss cone it would suggest a thermalized ion temperature of approximately 860 ev which compares favorably with the average energy per particle for this case of 900 ev. At best approximately one percent of the plasma remains in the well for this amount of time.

V. CONCLUSION

The present study indicates that at high laser powers and short pulse widths, the plasma temperature and average energy per particle in the freely expanding plasma approach the values predicted from the continuum fluid model[1, 13, 14].

Preliminary results on the interaction of the expanding plasma with a uniform field show strong evidence for heating of the expanding plasma by azimuthal currents during the early expansion. There is not as yet sufficient experimental evidence to explain the apparent confinement in a minimum B geometry produced by a baseball winding as no direct measurement of electron or ion temperature has been made.

VI. ACKNOWLEDGEMENTS

This work was supported in part by the National Science Foundation under grants GK-861 and GK-2266, and in part by the Air Force Office of Scientific Research, grant 1279-67.

REFERENCES

(1) Haught, A.F., Polk, D.H., Phys. Fluids 9 (1966), 2047.

(2) Faugeras, P.E., Mattioli, M., Papoular, R., Optical Measurements on Laser Produced Plasmas, Euratom Rept., EUR-CEA-FC-467.

(3) Atkinson, D., Avivi, P., Francis, G., Millar, W. and Saunders, P., Bull. Am. Phys. Soc. 13 (1968), 320.

(4) Pack, J.L., George, T.V., Engelhardt, A.G., Bull. Am. Phys. Soc. 13 (1968), 320.

(5) Cavaliere, A., Giupponi, P., Gratton, R., Phys. Letters 25A (1967), 636.

(6) Lubin, M.J., Bull. Am. Phys. Soc. 13 (1968), 320.

(7) Dawson, J., Oberman, C., Phys. Fluids 5 (1962), 517.

(8) Dawson, J., Kaw, P., Green, B., "Laser Production of Plasmas", American Inst. for Aeronautics and Astronautics, Los-Angeles, Cal., June 24, 1968.

(9) Wuerrer, R.F., Goldenberg, H.M., Langmuir, R.V., Journ. Appl. Phys., 30 (1959), 441.

(10) Kegel, W.H., Inst. für Plasmaphysik Rept. IPP 6/34, Garching Bei München.

(11) Haught, A.F., Polk, D.H., Fader, W.J., United Aircraft Research Laboratories Rept. UARL F920365-6, NYO-3578-6, June 1967.

(12) Lubin, M.J., Dunn, H.S., University of Rochester, College of Eng. and Appl. Sci., Mech. and Aerospace Sciences, Rept. No. 4.

(13) Basov, N.G., Krokhin, O.N., Proceedings of the Conference on Quantum Electronics, Paris, 1963.

(14) Dawson, J.M., Phys. Fluids 7 (1964), 981.

DISCUSSION

G. V. SKLIZKOV: Could we have some information about the temperature of 1000 eV referred to in this paper?

M. J. LUBIN: the figure you have mentioned represents translational energy and not temperature. The temperature measurements, carried out by scattering, yield values of the order of 100 eV during peak temperature. However, it has been pointed out by Haught that these measurements are suspect because the total scattered spectra from the expanding plasma cannot be uniquely determined in terms both of number density and of temperature, and in fact a great deal of care must be exercised in interpreting the free-expansion temperature measurements deduced from scattering.

DISCUSSION

on papers CN-24/F-6 to CN-24/F-8

T. CONSOLI: I should like to make a general comment on the use of laser pre-ionized plasmas in a magnetic configuration. In his review paper, Mr. Papoular said that 10^{17} ions with an energy of 10 keV would be extremely interesting from the point of view of constructing a thermonuclear reactor. An order-of-magnitude calculation gives us an energy of the order of 500 J in the laser beam.

In our opinion there is another mehtod, which consists in producing the plasma by means of a lower-power laser and then using high-frequency heating. That is what we are doing at Saclay; starting with a 50-eV plasma produced by focusing a laser on a solid deuterium target, we raise the energy of some of the ions to 20 keV with an energy of 100 J in the high-frequency (1250 Mc/s) field pulse.

G. V. SKLIZKOV: I should like to draw attention to the possiblity of heating matter to thermonuclear temperatures by directing a laser beam onto a massive target.

R. PAPOULAR (Rapporteur): I agree that this new method is an important one, but in my opinion it requires laser performances that are as yet uncommon.

THEORETICAL AND EXPERIMENTAL RESULTS ON THE TRAPPING AND BEHAVIOUR OF THE E-LAYER IN THE ASTRON*

J. W. BEAL, M. BRETTSCHNEIDER, N. C. CHRISTOFILOS, R. E. HESTER, W. A. S. LAMB, W. A. SHERWOOD, R. L. SPOERLEIN, P. B. WEISS AND R. E. WRIGHT
LAWRENCE RADIATION LABORATORY, UNIVERSITY OF CALIFORNIA, LIVERMORE, CALIF., UNITED STATES OF AMERICA

Abstract

THEORETICAL AND EXPERIMENTAL RESULTS ON THE TRAPPING AND BEHAVIOUR OF THE E-LAYER IN THE ASTRON. The injection of 300 A of 3.8-MeV electrons into the Astron solenoid has resulted in the trapping of sufficient electrons to form an E-layer with strong diamagnetic effect.

Low-frequency stable precessional oscillations of the E-layer have been observed during the initial operation of the Astron facility. The precession frequency ω_p is the difference between the gyrofrequency (ω_c) and betatron frequency ω_c (1-n/2) of the E-layer where n = ($R\partial B/B\partial r$) of the confining mirror field. The magnetic field of the E-layer generates image currents in the walls of the tank, which in turn generate a field with positive gradient which is proportional to the loading factor (ζ) of the E-layer (ζ is defined as the ratio of the self-field of the E-layer to the external confining field B_0). When the loading factor ζ exceeds a certain threshold (ζ_c) the sense of the precession is reversed, and theory predicts that the motion is stable in agreement with the experiment.

The field generated by an E-layer of moderate thickness has been calculated. The image currents, the positive field index, and the threshold value of the loading factor ζ are calculated as a functio of the tank wall and the E-layer radius. The image currents provide a minimum-B field which tends to center the E-layer about the axis of symmetry of the tank.

The experimentally observed value of ζ exceeds the calculated threshold ζ_c but as electrons are lost by scattering in the residual gas the loading factor is gradually diminished. When ζ reaches the calculated value of ζ_c the net value of the field index becomes zero, an integral resonance occurs, and theory predicts that the E-layer will be "dumped" promptly. The "dump" is experimentally observed at the calculated value of ζ_c.

1. INTRODUCTION

In the Astron concept, a layer of relativistic particles, the E-layer, provides the solution for both the magnetic confinement and heating of the plasma to fusion temperature. The currents of rotating relativistic particles at a sufficient level can create a magnetic field configuration with a unique property, namely, a magnetic well with closed magnetic lines (Fig. 1). The closed lines provide confinement of plasmas with isotropic pressure while, for properly designed configurations, the destabilizing curvature drifts inherent in line closure tend to be overcome at every point along the lines by the favorable magnetic gradient drift prevailing within the closed magnetic well.

Thus hydromagnetic instabilities, the low-frequency universal instabilities observed in toroidal confinement and high-frequency microinstabilities due to the loss cone in open-ended confinement, should be suppressed at the same time.

* Work performed under the auspices of the US Atomic Energy Commission.

The combination of the currents of the confined plasma and the E-layer currents could extend considerably the volume of the closed magnetic well. If such a configuration is perfectly stable and diffusion losses do not exceed 10 to 100 times classical diffusion losses, a relativisitic electron E-layer (of energy 50 to 100 MeV) could provide plasma confinement and heating to fusion temperature [1], as it was originally proposed [2]. Since that time, experiments in toroidal confinement revealed the existence of the so-called Bohm diffusion which at plasma parameters suitable for a fusion reactor is a million times faster than classical diffusion. Since the exact nature of

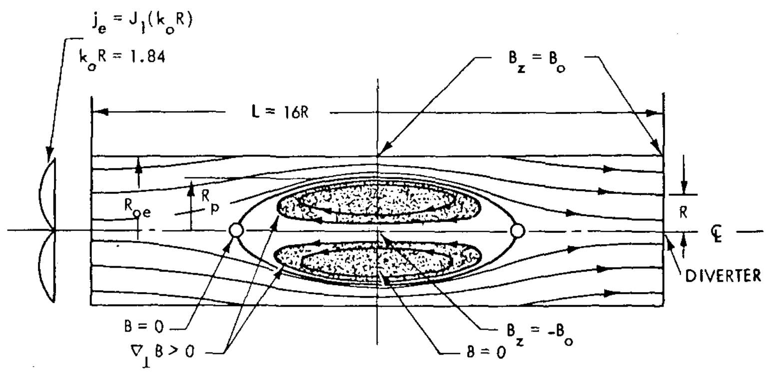

FIG. 1. E-layer configuration. Plasma confinement volume is in shaded area.

Bohm diffusion is not known as yet, there are speculations that even axisymmetric magnetic wells such as the magnetic well created by the combination of the E-layer and plasma currents would suffer from anomalous diffusion, limiting the plasma lifetime to 10 to 100 Bohm lifetimes. It is obvious that if these speculations prove correct, an electron E-layer cannot provide adequate plasma confinement. Bohm confinement time is proportional to (BR^2), where B is the confining magnetic field and R is the plasma radius, while the plasma confinement time allowed by fusion energy release is proportional to B^{-2}. Thus the ratio of the allowed plasma confinement time to Bohm confinement time is inversely proportional to B^3R^2. For confinement times approaching hundred Bohm confinement times and reasonable values of the magnetic field, the product BR is of the order of 10^7 (gauss cm) requiring an energy of the E-layer particles of a few GeV [3]. It is obvious that synchrotron radiation losses preclude the use of relativistic electrons as E-layer particles. Hence relativistic protons are the obvious choice if anomalous diffusion prevails. The relativistic proton E-layer was proposed several months ago [3]. In a relativistic proton E-layer plasma, confinement can be limited to the volume defined by the closed magnetic well created by the E-layer. The plasma thickness is 50 to 100 ion gyroradii, thus limiting anomalous diffusion. At the same time the E-layer protons can heat the plasma to fusion temperature even under conditions of anomalous diffusion. When the plasma is confined within the closed magnetic well, created by the E-layer, it could create transverse forces (m = 1 mode) which would tend to drive the E-layer off its axis toward the wall. Therefore, a positive restoring force is required which tends to center the E-layer at the axis of symmetry of the vacuum chamber. Such a restoring force is provided by the image currents created by the E-layer in the walls of the tank, which in turn generate a field with positive field gradient n, where $n = R\partial B/B\partial R$. The positive field gradient generated by the image currents of the E-layer is proportional to the diamagnetic strength or loading factor (ζ) of the E-layer. When the loading factor ζ exceeds a certain threshold (ζ_c) the positive gradient created by the image currents becomes equal and opposite to the negative gradient of the external mirror field confining the E-layer. Thus for E-layer strength $\zeta > \zeta_c$, the E-layer floats in an effective minimum-B field created by its own image currents. The higher the level of the E-layer, the stronger the restoring force is which tends to center the E-layer at the axis of symmetry of the confining vacuum tank. Because of the rotation of the electrons, any radial force creates a precession of the E-layer which is in the direction of the rotation of the electrons when the field gradient is negative. When the loading factor ζ exceeds the threshold ζ_c and the gradient becomes positive, the sense of the precession is reversed and theory predicts [4] that the motion is stable, which is in agreement with experimental observations. When the precession is forward, theory predicts [4] instability. Experimental observations, however, indicate that depending on the shape of the confining mirror field, this motion can be either stable or unstable.

In the following section the analytical solution is given for the self-magnetic field of the E-layer. The radial and axial current distribution are approximately represented by the functions $J_1(k_0r)$ and $\sin^2 kz$ respectively, which are the first terms of an expansion in Bessel and trigonometric functions of any arbitrary current distribution. The experimentally achieved E-layer current distributions are very similar to the assumed approximation. In section III the image currents of the E-layer are calculated and the value of the positive gradient is calculated as a function of the loading factor ζ, the geometry of the confining walls and the ratio of the radius to the length of the E-layer.

In section IV experimental results are compared with theory. The experimental results confirm the theoretical prediction that the precessional frequency is a linear function of the loading factor of the E-layer and agree quantitatively within 10%, which is considered an excellent agreement in view of the approximations made in the current distribution of the E-layer in order to simplify the solution of the field equations.

II. SOLUTION FOR THE SELF-MAGNETIC FIELD OF AN E-LAYER CONFINED BETWEEN TWO COAXIAL CYLINDERS

The E-layer is confined between two coaxial cylinders of radius R_w and R_c respectively. The mean radius of the E-layer is R and the current distribution is extended radially from a radius R_i to R_0. The functional dependence of the E-layer current distribution (j_e) is

$$j_e = j_0 \cdot J_1 (k_0 r) \sin^2 (kz/2) \qquad \text{(II.1)}$$

in the region

$$r < R_0, z > 0$$

$$r > R_1, z < L$$

and zero outside this region. The value of k_0 depends on the thickness of the E-layer, while k_0R_i and k_0R_0 are adjacent zeroes of the J_1 Bessel function. The value of $k = 2\pi/L$.

The vector potential generated by the E-layer current is

$$A_\theta = \frac{\eta_0}{2k_0}\bar{B}_0 J_1(k_0 r)\left[1+\frac{k^2}{k_0^2}\right] - \frac{\eta_0}{2k_0} B_0 J_1(k_0 r)\cos(kz)$$

$$+\left[\frac{\eta_a}{k} I_1(kr) + \frac{\eta_i}{k} K_1(kr)\right]\cos(kz) \qquad \text{(II.2)}$$

where

$$\eta_0 = \frac{\zeta}{\left(1+\frac{k^2}{k_0^2}\right)\left[J_0(kR_0) - J_0(kR_i)\right]} \qquad \text{(II.3)}$$

$B_0 = \gamma mc^2/Re$ and ζ is the loading factor of the E-layer.

Outside the E-layer ($r > R_0$) the solution for the vector potential in the absence of walls is

$$A_\theta = \frac{c_1}{r} + c_2\frac{r}{2} + \eta_v K_1(kr)\cos(kz) \qquad \text{(II.4)}$$

In the region $r < R_1$ the solution is

$$A_\theta = c_3\frac{r}{2} + \eta_c I_1(kr)\cos(kz). \qquad \text{(II.5)}$$

The components of the magnetic field which are independent of z do not create gradients. Thus we restrict ourselves to calculate the components of the field which depend on sin (kz) or cos (kz). The four constants η_a, η_i, η_v, η_c are determined by matching the two field components B_z and B_r at $r = R_i$ and $r = R_0$.

The result is

$$\eta_a = \eta_0\frac{\pi}{4}(kR_0) K_1(kR_0) J_0(k_0 R_0) \qquad \text{(II.6)}$$

$$\eta_i = \eta_0\frac{\pi}{4}(kR_i) I_1(kR_i) J_0(kR_i) \qquad \text{(II.7)}$$

$$\eta_v = \eta_0\frac{\pi}{4}\left[(kR_0) I_1(kR_0) J_0(k_0R_0) - (kR_i) I_1(kR_i) J_0(k_0R_i)\right] \qquad \text{(II.8)}$$

$$\eta_c = \eta_0\frac{\pi}{4}\left[(kR_0) K_1(kR_0) J_0(k_0R_0) - (kR_i) K_1(kR_i) J_0(k_0R_i)\right] \qquad \text{(II.9)}$$

III. CALCULATION OF THE FIELDS GENERATED BY THE IMAGE CURRENTS

In the experiments to date the E-layer lifetime is limited to several milliseconds. Thus the magnetic field is confined between two coaxial cylinder of radius R_w and R_c.

Image currents are generated in the two cylindrical surfaces which in turn generate a magnetic field with components:

(a) Outer cylinder

$$B_{zi} = \eta_w I_0(kr)\cos(kz) \qquad \text{(III.1)}$$

$$B_{ri} = \eta_w I_1(kr)\sin(kz) \qquad \text{(III.2)}$$

(b) Inner cylinder

$$B_{zi} = \eta_r K_0(kr)\cos(kz) \tag{III.3}$$

$$B_{ri} = -\eta_r K_1(kr)\sin(kz) \tag{III.4}$$

The constants η_w and η_r are determined by the boundary condition that the radial component of the magnetic field is zero at the walls. Thus

$$\eta_w = -\eta_v \frac{K_1(kR_w)}{I_1(kR_w)} \tag{III.5}$$

$$\eta_r = -\eta_c \frac{I_1(kR_c)}{K_1(kR_c)} \tag{III.6}$$

If the E-layer moves off-axis, its field follows the motion. In any such motion it is assumed that the thickness remains undistorted while its mean orbit R is distorted as $\xi e^{i\theta}$, where ξ is the maximum radial displacement. The off-axis displacement of the E-layer generates new image currents. Since its motion changes the value of the radial component of the magnetic field at the walls by

$$\tilde{B} = \left(\frac{\partial B_r}{\partial r}\right)\xi \tag{III.7}$$

where $\partial B_r/\partial r$ is evaluated at the tank walls. Since B_r should remain zero at the walls, new image currents are created with the following components.

(a) Outer wall

$$\tilde{B}_z = \tilde{\eta}_w I_1(kr)\cos(kz)\, e^{i\theta} \tag{III.8}$$

$$\tilde{B}_r = \tilde{\eta}_w I_1'(kr)\sin(kz)\, e^{i\theta} \tag{III.9}$$

$$\tilde{B}_\theta = \tilde{\eta}_w i \frac{I_1(kr)}{kr}\sin(kz)\, e^{i\theta} \tag{III.10}$$

(b) Inner wall

$$\tilde{B}_z = \tilde{\eta}_r K_1(kr)\cos(kz)\, e^{i\theta} \tag{III.11}$$

$$\tilde{B}_r = \tilde{\eta}_r K_1'(kr)\sin(kz)\, e^{i\theta} \tag{III.12}$$

$$\tilde{B}_\theta = \tilde{\eta}_r i \frac{K_1(kr)}{kr}\sin(kz)\, e^{i\theta} \tag{III.13}$$

The constants $\tilde{\eta}_w$ and $\tilde{\eta}_r$ are determined by the boundary conditions that the radial component of the field is zero at the tank walls, namely

$$\tilde{\eta}_w = -\eta_w(k\xi) \tag{III.14}$$

$$\tilde{\eta}_r = -\eta_r(k\xi) \tag{III.15}$$

Under the assumption that the radial current distribution of the E-layer is not distorted during the displacement ξ, because the self-field gradient is much higher than the image current field gradient, we can treat the E-layer as a super particle and calculate its betatron motion from the radial component of the linearized radial equation of motion,

$$\gamma m\left(\ddot{\xi} + \frac{\bar{v}_\theta^2}{R^2}\,\xi\right) = -\frac{\bar{v}_\theta}{c}\left[e\xi\,\frac{\partial B_z}{\partial r} + e\tilde{B}_z + e\xi\left(\frac{\partial B_z}{\partial r}\right)_m\right] \tag{III.16}$$

where $(\partial B_z/\partial r)_m$ is the gradient of the external confining mirror field. We define

$$\eta_m \equiv \frac{R}{B_0}\left(\frac{\partial B_z}{\partial r}\right)_m \tag{III.17}$$

$$\eta_i \equiv \frac{R}{B_0}\left[\frac{\partial B_z}{\partial r} + \frac{\tilde{B}_z}{\xi}\right] \tag{III.18}$$

$$\xi = \xi_0 e^{-i\omega t + i\theta} \tag{III.19}$$

Substituting in Eq. (III.16) we find

$$\omega^2 = \omega_c^2\,(1 + \eta_i + \eta_m) \tag{III.20}$$

Since $\eta_i + \eta_m << 1$

$$\omega = \omega_c\left(1 + \frac{\eta_m + \eta_i}{2}\right) \tag{III.21}$$

The field η_m index is negative because the external field is a mirror field. The field index η_i, however, is positive. The precession frequency is

$$\omega_p = \omega_c\left(\frac{|\eta_m| - \eta_i}{2}\right) \tag{III.22}$$

When $|\eta_m| < \eta_i$ the precession is backward (opposite to the motion of the electrons). There is general agreement that this motion is stable. In addition, it provides an effective minimum-B confinement for the E-layer. Since the field index η_i is proportional to the loading factor (ζ) of the E-layer, the focusing effect of the image currents becomes stronger as the E-layer builds up. The value of η_i is

$$\eta_i = \frac{\zeta\,(kR)^2\,(\psi_1 + \psi_2)}{4\left(1 + \frac{k^2}{k_0^2}\right)\left[J_0(k_0R_0) - J_0(k_0R_i)\right]} \tag{III.23}$$

where

$$\psi_1 = \frac{\pi}{2}\,\phi_1\left[\frac{R_0}{R}\,I_1(kR_0)\,J_0(k_0R_0) - \frac{R_i}{R}\,I_1(kR_i)\,J_0(k_0R_i)\right]\,I_1(kR) \tag{III.24}$$

$$\psi_2 = \frac{\pi}{2}\,\phi_2\left[\frac{R_0}{R}\,K_1(KR_0)\,J_0(k_0R_0) - \frac{R_i}{R}\,K_1(kR_i)\,J_0(k_0R_i)\right]\,K_1(kR) \tag{III.25}$$

and

$$\phi_1 = \frac{K_1(kR_w)}{I_1(kR_w)} - \frac{K_1'(kR_w)}{I_1'(kR_w)} \tag{III.26}$$

$$\phi_2 = \frac{I_1(kR_c)}{K_1(kR_c)} - \frac{I_1'(kR_c)}{K_1'(kR_c)} \tag{III.27}$$

In the function ϕ_1 the first term on the right-hand side is the contribution from the gradient of the axisymmetric image currents in the outer wall while the second term is the contribution from the image currents created by the off-axis motion of the E-layer. The function ϕ_2 represents the contribution of the image currents in the inner wall.

In a very thick E-layer ($R_i = 0$) the function $\phi_2 = 0$ and the focusing is achieved by the image current of the outer wall only.

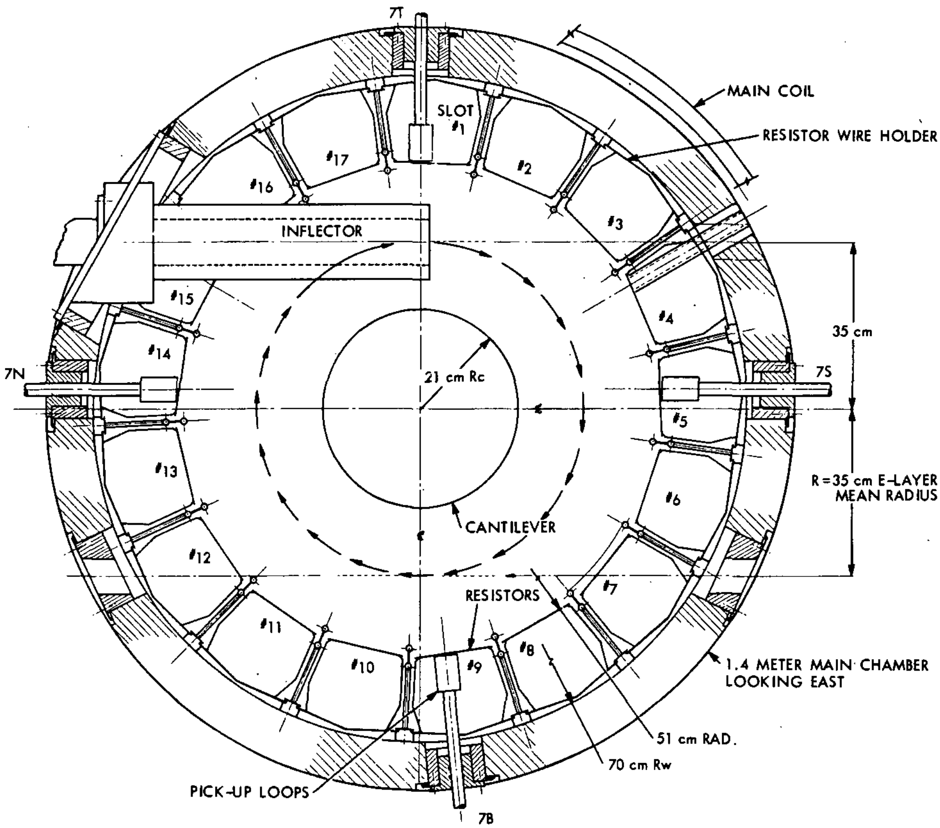

FIG. 2. Cross-section of the Astron tank.

IV. EXPERIMENTAL OBSERVATIONS

The Astron facility was shut down recently for several months for the installation of new precision tanks and coils. It was expected that among other improvements the precision alignment possible with the new tanks (± 250 microns from a reference axis) and similar accuracy in the location of the coils will result in the reduction of magnetic field inhomogeneities.

Experiments with the new facility started on February 19, 1968.

The results reported here were obtained in the first five days of operation, i.e. February 19 through 23.

The diagnostics used for the observations described in this report are pick-up loops located behind the resistive wires (Fig. 2). Each loop is a coil of 125 turns with total effective area of 1250 cm. The signal in the loops is proportional to B_e (B_e the magnetic field of the E-layer). These loops are located every 25.4 cm along the tank at the position N (Fig. 2). At some locations, up to four coils can be placed as shown in Fig. 2.

The observations in these experiments were limited to measurements of E-layer lifetime and observations of the precession phenomena as a function of the loading factor ζ of the E-layer. The direction of the precession is observed by comparing the phase of precession in the coils 7N (N for north) and 7T (T for top) located 90° apart in azimuth as shown in Fig. 2.

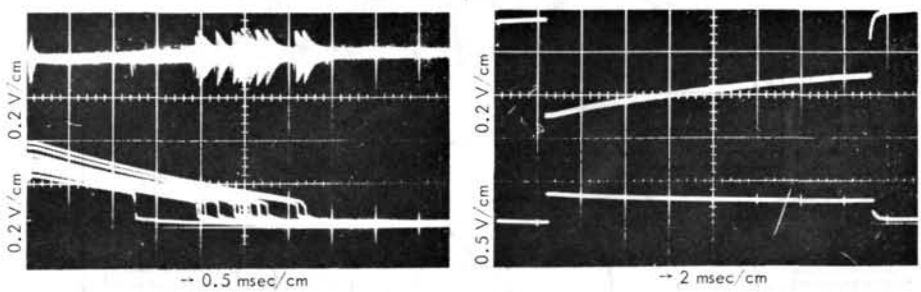

LOOP 8 N, PRESSURE 10 MICRONS H_2
TOP TRACE $\dot{B}$
BOTTOM TRACE $\int \dot{B}$

LOOP 8 N, PRESSURE 1 MICRON H_2
DOUBLE PULSE, BOTH TRACES $\int \dot{B}$
HALF-LIFE 12 msec

FIG. 3. E-layer current versus time and precession oscillations.

Observations of the E-layer precession were aimed to verify that at a critical loading factor $\zeta = \zeta_c$ when the dump occurs the precession frequency goes through zero, that for $\zeta > \zeta_c$ the precession is backward, that the precession frequency varies linearly with the loading factor ζ, and to compare quantitatively theoretical values with experimental results.

In Fig. 3a the traces of $\dot{B}$ and $\int \dot{B}$ are shown, indicating an E-layer halflife of 2 msec. Trapping was achieved at 10 microns of background hydrogen pressure. The symmetry plane of the E-layer is located 200 cm from the injector point. Approximately 15% of the E-layer survives the integral resonance. The surviving part of the E-layer precesses violently, as can be seen in the top trace.

In the next oscillogram in Fig. 3b, the current per centimeter of the E-layer formed in 1 micron of H_2 is shown. Trapping is achieved by preionizing the gas by a previous electron pulse injected 1.5 msec before the trapped pulse. The measured E-layer halflife is 12 msec.

In Fig. 4 the axial distribution of the axial component of the magnetic field of the E-layer at the radius of the loops is shown. Previous analysis [5] has shown that the axial current distribution of the E-layer is the same as the field distribution between the half-amplitude points (110 cm apart in Fig. 4). This observation indicates that in the approximation of the axial current distribution with $\sin^2$ (kz) the argument kR = 1. This in turn allowed the calibration of the signal observed in the loops. The result is 20 A/volt ± 3%.[1] Thus in Fig. 3a the peak E-layer current per centimeter is 8 A/cm, and in Fig. 3b is 10 A/cm. The corresponding values of ζ were 2.8% and 3.5%.[2] It should be noted that for the first time it is observed that the trapping efficiency at 1 micron of hydrogen is the same as at 10 microns.

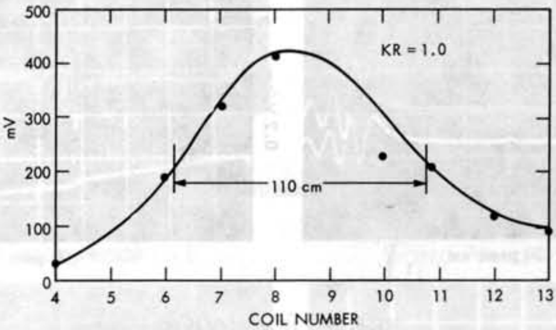

FIG. 4. Axial distribution of E-layer current.

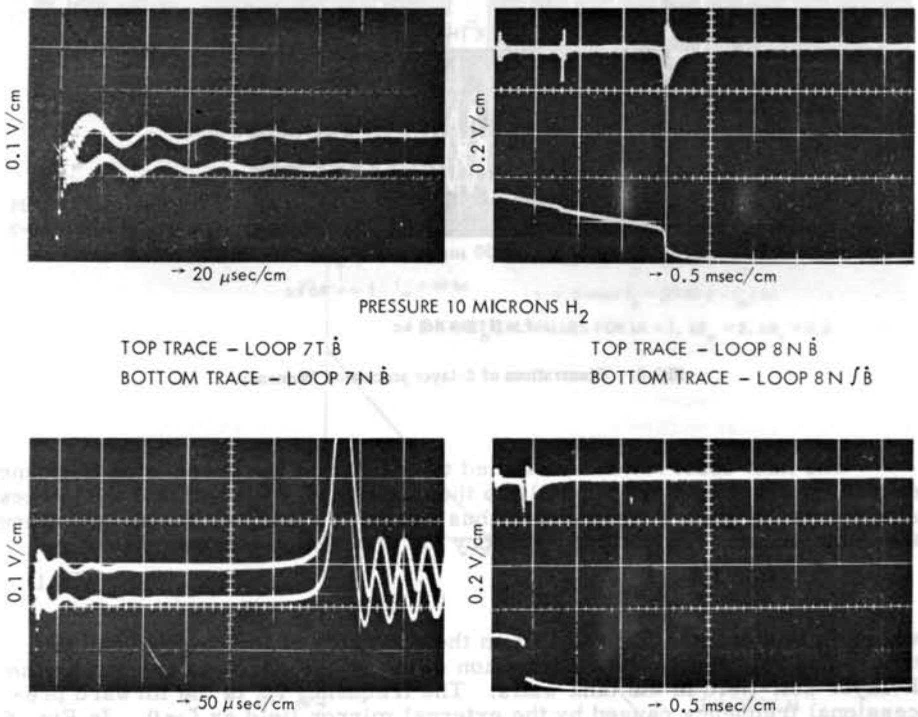

FIG. 5. Phase comparison of E-layer precessions before and after the dump.

[1] Experimental calibration of the loops with a mock-up E-layer resulted in the same value.

[2] The maximum value of ζ achieved to date is 6% [6].

In Fig. 5, in the oscillograms at the left, the phase of the precession in the loops 7N and 7T are compared. Initially when $\zeta > \zeta_c$, the E-layer precesses backwards. Following the "dump," however, the surviving E-layer precesses forward.

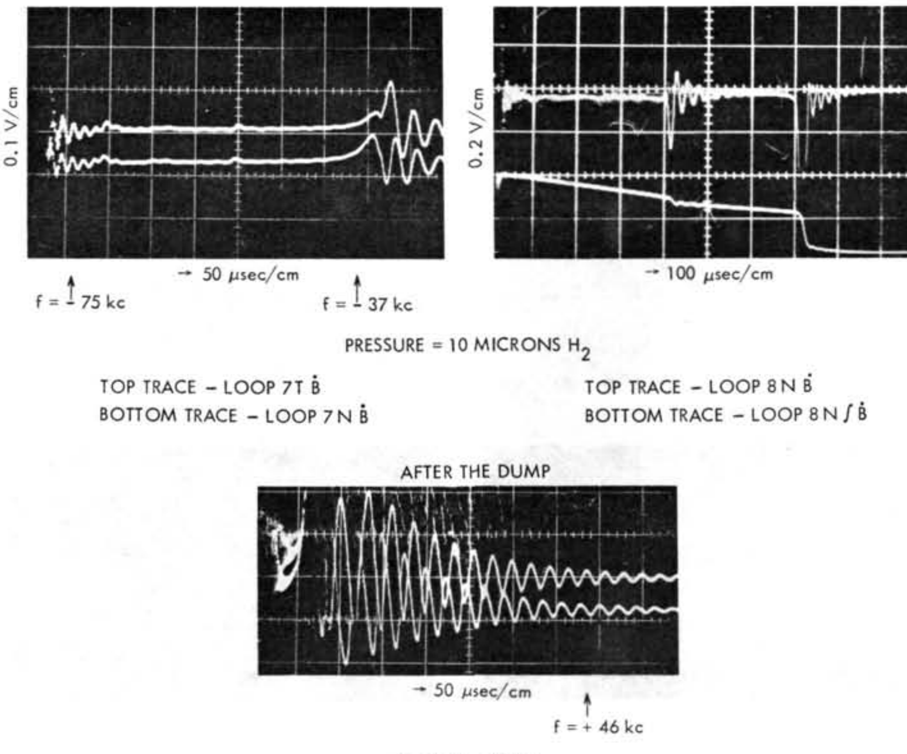

FIG. 6. Observations of E-layer precession frequency.

The next observation was aimed to verify that the precession frequency decreases linearly proportionally to the quantity $(\zeta - \zeta_c)$ and that the precession frequency goes through zero, thus causing an integral resonance, when the dump occurs. According to theory the precession frequency is

$$f_p = f_0 \zeta - f_m \tag{IV.1}$$

where f_0 is a constant, depending on the geometry of the E-layer and the tanks, and represents the contribution of the image currents created by the E-layer self-field in the tank walls. The frequency f_m is the forward precessional frequency caused by the external mirror field as $\zeta \to 0$. In Fig. 6 in the bottom oscillogram the frequency f_m is measured. In the top oscillograms the precession frequency is measured at two values of ζ. The second excitation of E-layer precession is caused by a small loss of E-layer electrons (probably caused by an internal integral resonance). Another two observations are shown in Fig. 7. In all three cases, the functional dependence of the precessional frequency is in good agreement with Eq. (IV.1).

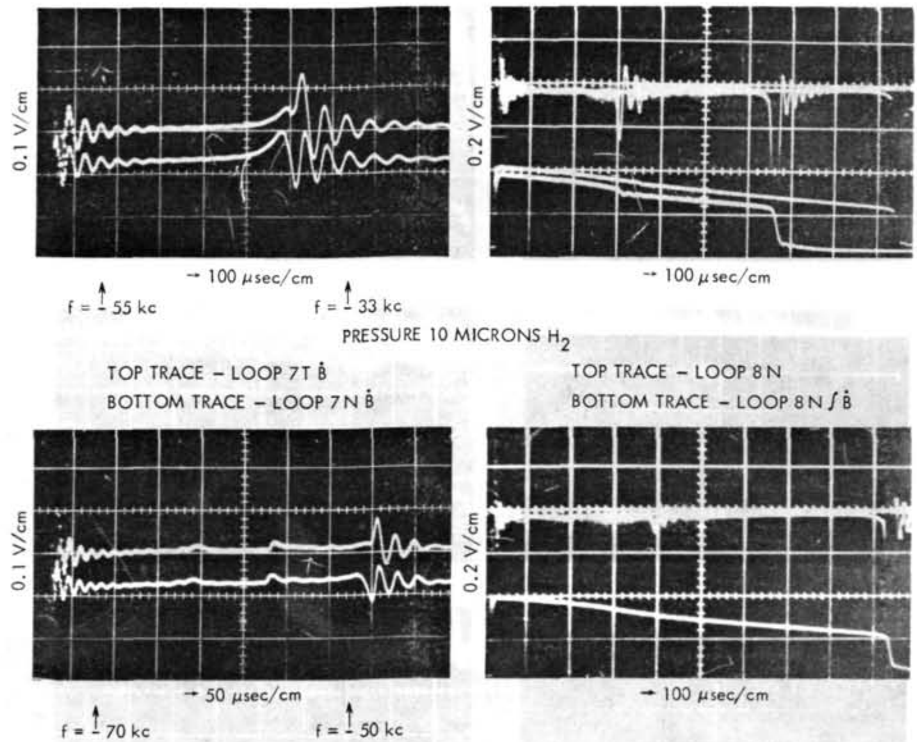

FIG. 7. Observations of E-layer precession frequency.

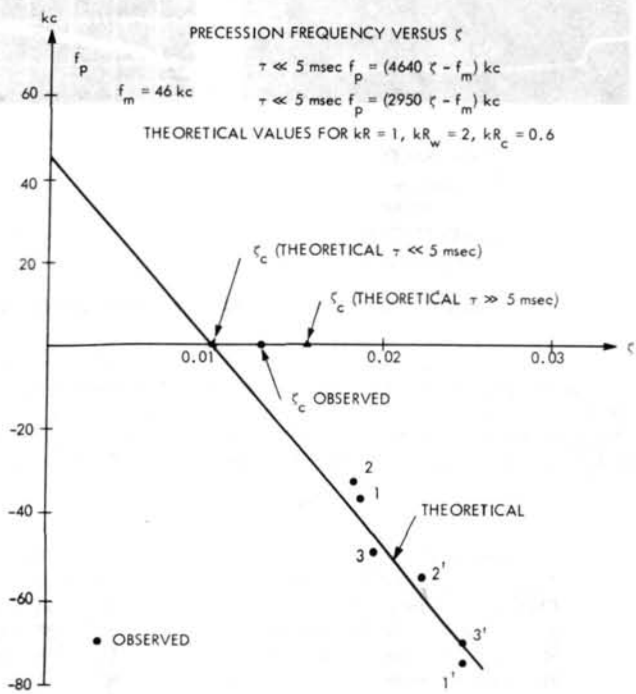

FIG. 8. Comparison of theoretical and experimental values of precession frequency of the E-layer.

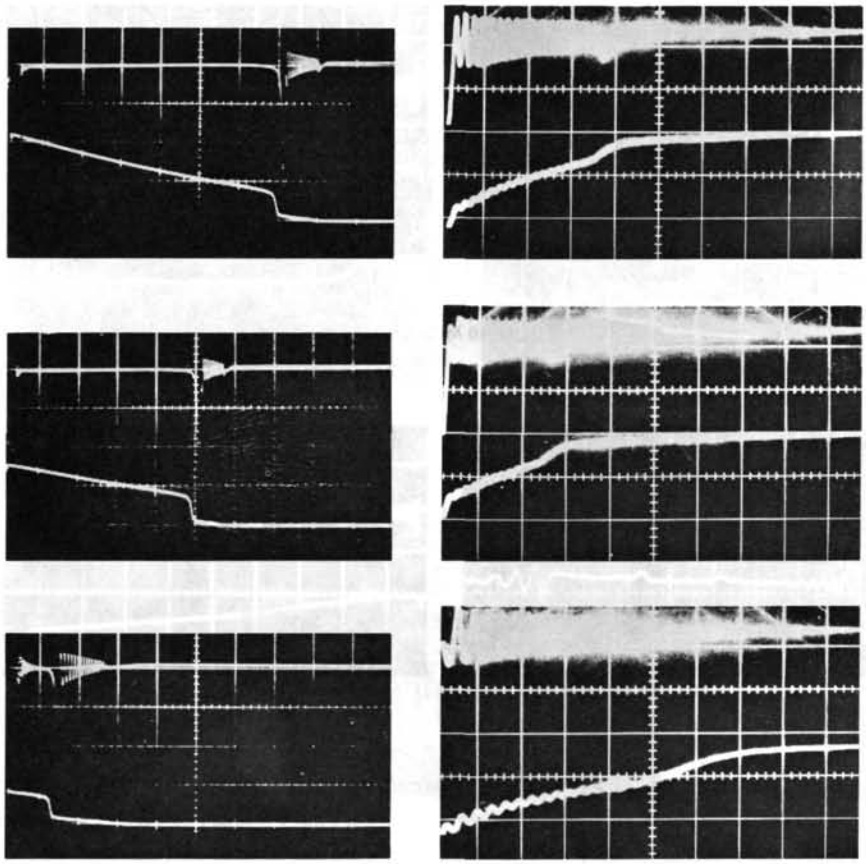

LOOP 8N

UPPER TRACES
$\dot{B}$ 200 mV/cm
200 μsec/cm
LOWER TRACES
$\int \dot{B}\,dt$ 200 mV/cm

UPPER TRACES
$\dot{B}$ 100 mV/cm
50 μsec/cm
LOWER TRACES
$\int \dot{B}\,dt$ - 20 mV/cm

FIG. 9. Precession oscillations following the dump (growing oscillations).

Finally, an analysis of the results was carried out to verify the extent of the quantitative agreement between the theoretical calculation of the precessional frequency and the observed values. The value of field index of the field generated by the image currents is calculated from Eqs. (III.23) through (III.27). The values of the E-layer and wall parameters are:

$$kR = 1, \; k = 2\pi/L$$

Length of E-layer	$L = 220$ cm
Mean radius of E-layer	$R = 35$ cm
Outer radius of E-layer	$R_0 = 41$ cm
Inner radius of E-layer	$R_i = 29$ cm
Radius of outer tank wall	$R_w = 70$ cm
Radius of inner tank wall	$R_c = 21$ cm

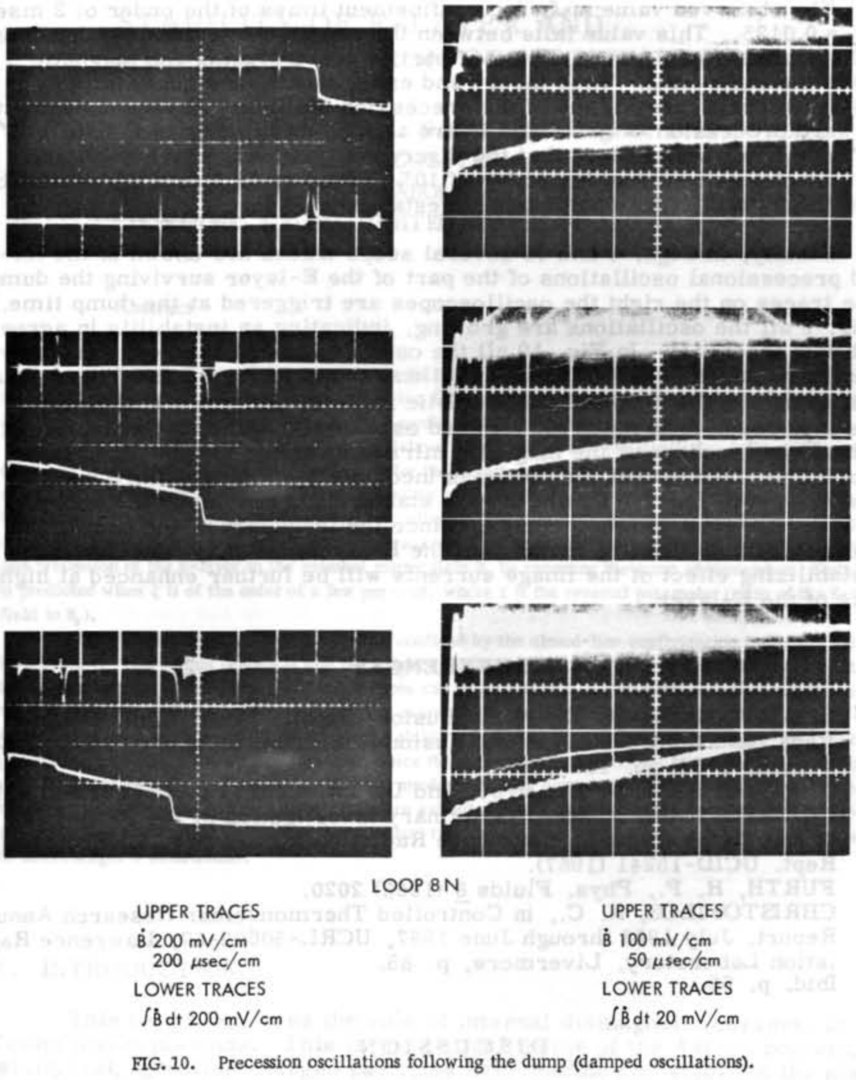

FIG. 10. Precession oscillations following the dump (damped oscillations).

The values of the function J_0 (k_0R_0) and J_0 (k_0R_i) are -0.25 and +0.30 respectively.

The first term on the right-hand side in Eq. (III.27) represents the contribution from the axisymmetric image current in the inner wall of the tank. Since the thickness of this wall is only 0.5 cm, this contribution disappears for E-layer confinement times of several milliseconds. Therefore, the precession frequency has been calculated for two cases with and without this term. The results are shown in Fig. 8. The precession frequency as calculated for confinement time $\tau \ll 5$ msec is plotted as a function of the E-layer loading factor ζ. The frequency goes through zero at $\zeta_c = 0.01$. For long confinement times, $\zeta_c = 0.015$. In both cases, the value of the forward precession frequency f_m = 46 kc has been measured experimentally as $\zeta \to 0$.

The observed value of ζ_c for confinement times of the order of 2 msec is $\zeta_c = 0.0125$. This value falls between the two theoretical values for short and long confinement time because of partial penetration of the magnetic field in the inner wall. Thus theory and experiments are quantitatively in good agreement. The values of the precession frequency observed during the backward precession (Figs. 6 and 7) are also plotted in Fig. 8 (points 1, 1', 2, 2', 3, 3'). We observe that the discrepancy between theoretical and experimental values is of the order of 10%. Thus an excellent agreement between theory and experiment has been established.

Finally, in Figs. 9 and 10 several scope traces are shown of the forward precessional oscillations of the part of the E-layer surviving the dump. In the traces on the right the oscilloscopes are triggered at the dump time. In Fig. 9 all the oscillations are growing, indicating an instability in agreement with theory [4]. In Fig. 10 all the oscillations are damped. The only parameter change between the observations shown in Fig. 9 and Fig. 10 is a small change of the shape of the magnetic mirror confining the E-layer. Since it is possible to make the forward oscillations stable or unstable just by changing the shape of the magnetic mirror, an effect not predicted theoretically, it appears that the theory is incomplete. The backward oscillations, however, for $\zeta > \zeta_c$ are always stable, in agreement with theory. The decay constant is 2 to 3 cycles. Since the frequency of the oscillation increases with the loading factor ζ of the E-layer, we may conclude that the stabilizing effect of the image currents will be further enhanced at higher levels of the E-layer.

REFERENCES

[1] CHRISTOFILOS, N. C., Nucl. Fusion, Suppl., Proc. Conf. Plasma Phys. and Controlled Nuclear Fusion Research, Salzburg, 1961 (IAEA, Vienna, 1962) pp. 159-168.

[2] CHRISTOFILOS, N. C., Proc. 2nd UN Int. Conf. PUAE 32 (1958) 279.

[3] CHRISTOFILOS, N. C., Preliminary Investigation of the Properties of a Scaled-up Astron, Lawrence Radiation Laboratory, Livermore, Rept. UCID-15241 (1967).

[4] FURTH, H. P., Phys. Fluids 8 (1965) 2020.

[5] CHRISTOFILOS, N. C., in Controlled Thermonuclear Research Annual Report, July 1966 through June 1967, UCRL-50002-67, Lawrence Radiation Laboratory, Livermore, p. 85.

[6] Ibid. p. 66.

DISCUSSION

V. G. MAKHANKOV: Have you observed effects associated with negative mass instability?

N. C. CHRISTOFILOS: Yes, the instability grows during injection of the electrons (0.3 μsec) and is subsequently self-quenched. The decay time is a fraction of a microsecond.

V. G. MAKHANKOV: Does this instability depend on the distance between the inner tank wall and the E-layer?

N. C. CHRISTOFILOS: No, it does not.

V. G. MAKHANKOV: What you have said about data on negative mass instability is very encouraging. However, these data conflict with current theory, since azimuthal instability necessarily leads to strong synchrotron emission and to synchrotron instability (see, for example, Briggs: IEEE Proceedings, 1968).

STABILITY OF E-LAYER AND PLASMA IN ASTRON CONFIGURATIONS *

G. BENFORD, D.L. BOOK, N.C. CHRISTOFILOS, T.K. FOWLER, V.K. NEIL AND L.D. PEARLSTEIN
LAWRENCE RADIATION LABORATORY, UNIVERSITY OF CALIFORNIA, LIVERMORE, CALIF., UNITED STATES OF AMERICA

Abstract

STABILITY OF E-LAYER AND PLASMA IN ASTRON CONFIGURATIONS. Stability criteria are derived for Astron configurations, including stability of the E-layer alone, E-layer beam-plasma interaction, and stability of plasma confined in a reversed-field configuration created by the E-layer.

It is shown that energy spread among E-layer electrons has a strong stabilizing influence on modes driven by the E-layer, as was shown previously for the negative mass and tearing modes. For example, energy spread strongly attenuates a beam-plasma instability in which the E-layer excites hybrid oscillations in a background plasma so that weak effects such as collisions can eliminate the residual instability. Another stabilizing mechanism is image currents in the tank walls. These stabilize a mode due to wall resistivity and precession of the E-layer in the external mirror field B_0 by reversing the sense of precession. Stability is predicted when ζ is of the order of a few per cent, where ζ is the reversal parameter (ratio of the E-layer field to B_0).

Low-frequency stability of the plasma confined by the closed-line configuration inside the E-layer is examined. The unique feature is that the magnetic gradient drift is favourable everywhere along the closed lines. Consequently, $\oint d\ell/B$ stable configurations can be constructed in which this favourable drift overcomes the bad curvature drift due to line closure. For example, in the limit of small aspect ratio elliptical field lines lead to zero average drifts and marginal stability. Reducing the curvature in the strong-field region (flattening) produces a stable configuration. Since the unfavourable drift occurs in the weak field region and only for particles of "large" parallel velocities, modes driven by particles stalling in this bad field region do not occur. Moreover, current distributions are exhibited which have favourable average drift everywhere along the line eliminating the bulk of the universal type instabilities. The limiting plasma pressure stable to interchanges is determined.

1. INTRODUCTION

This paper concerns the role of internal diamagnetic currents in confining fusion plasmas. This is the central theme of the Astron concept, in which fast, gyrating charged particles help confine and stabilize the plasma and also heat it [1]. In this, Astron differs from low-β toroidal and mirror confinement systems which rely solely on external focussing fields, but it has some features in common with internal current systems such as Tokamak. In the latter class of systems, and in Astron, one attempts to transfer the stability problem from the plasma proper to an internal current which can be stabilized by means not applicable to the plasma in the absence of this current. For example, in Tokamak the plasma is shear-stabilized by an ohmic heating current which is in turn focussed by its own images in the walls.

The distincitive feature of the Astron concept is that the function of carrying the internal current is divorced from the plasma itself and is given to an independent element, namely, the fast gyrating charge distribution,

* Work performed under the auspices of the U.S. Atomic Energy Commission.

called an E-layer. In this way, it should be possible to optimize independently the properties of the fusion plasma, in which the particle density must be large, and properties of the E-layer, in which the current density must be large for confinement and the energy density should be large for heating. As one can also separate the heating and confinement functions of the E-layer if necessary, here we shall only concern ourselves with the important question of stable confinement. With the primary objective of looking ahead to the fusion applications of the Astron concept, we shall for the most part limit the discussion to the final E-layer and plasma configuration rather than injection methods, though of course adequate stability must be maintained during injection and much of the analysis here applies to that phase, also.

For confinement purposes, the optimum E-layer is that which carries sufficient current to confine the plasma stably and yet is itself stable. A current of charges flowing through a plasma might be expected to be more stable the lower the charge density. This suggests a large E-layer velocity which also reduces the loss of E-layer particles by Coulomb collisions.

Thus, for a given current, the E-layer lifetime due to instability and collisions should increase with particle energy. The lifetime determines the power input. Since we are concerned here with E-layer diamagnetic fields comparable to the external field, the stored kinetic and field energy corresponding to a given layer current are comparable and are approximately the same whatever carries the current. Hence the power required to sustain a full E-layer of any composition, just this stored energy divided by the lifetime, should decrease with increasing energy up to energies such that radiative losses or inelastic collisions dominate.

This holds true into the relativistic regime, where the current versus particle density is maximum. The magnetic field of an E-layer with comparable thickness and radius R is just the external field times $\zeta = (\omega_{pE}^2/\omega_{cE}^2)(v^2/c^2)(\delta/R)$ where ω_{pE} and ω_{cE} are the (relativistic) plasma and cyclotron frequencies and v is the particle velocity. At relativistic velocities ($v = c$), ζ for a thick layer reduces to $\omega_{pE}^2/\omega_{cE}^2$, which must be order unity if the E-layer field is to compete with the external field. Collective motion in the thick E-layer is only just coming into importance at this density level.

Such considerations led originally to the idea of using relativistic electrons up to about 50-100 MeV limited by synchrotron radiation [1a]. More recently it has been shown that inelastic processes for BeV protons are compatible with their use in an E-layer and would provide much larger plasma confinement volumes [1c]. On the other hand, if the stability picture turns out favorably, the electrons or much lower energy protons or other ions would suffice should that prove desirable for other reasons. We have kept in mind this broad range of possibilities in doing the analysis.

Besides E-layer stability, the other major consideration is what combination of E-layer and external magnetic field is best for plasma confinement. The unique feature of imbedding the current inside the plasma is that the magnetic field increases outward independently of the field line curvature. Thus, for example, an E-layer confined between mirror coils creates an axially symmetric minimum-B field and a closed chain of these produces a minimum-B torus [1b], neither of which is possible with externally produced fields alone. These possibilities, for which the E-layer field is less than the external mirror field, are least demanding on E-layer stability; density levels already achieved experimentally in thin electron layers ($\omega_{pE}^2 \sim 0.3\ \omega_{cE}^2$) would probably suffice.

Here, as in the original concept, we shall consider E-layers strong enough to reverse the field and thereby produce a pattern of closed magnetic lines, as shown in Fig. 1. Because all the closed lines are at least partially imbedded in the layer, the favorable gradient inside the layer helps overcome the destabilizing effect of line closure, which contributes unfavorably to the drift of particles with large velocity $v_{\parallel}$ parallel to the lines. Shear stabilization could be added with the addition of a conductor along the axis, the result being essentially a Levitron with strong minimum-B and an aspect ratio of unity. On the other hand, if the plasma is imbedded wholly within the layer and if the E-layer current is hollowed out where plasma is located, the very strong field gradient due to the outwardly increasing E-layer current is sufficient to overcome the curvature effects.

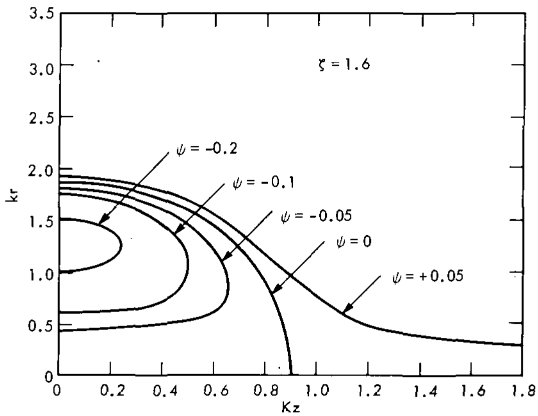

FIG. 1. Plot of the field lines, which are level lines of the flux function ψ defined in the text, for a reversal parameter ζ = 1: 6.

It is this hollow confinement configuration which we shall analyze here as representative of the virtues and problems of the Astron concept. We shall emphasize self-consistency by examining many aspects of the problem rather than fine details. We consider in subsequent sections reverse-field equilibria, stability of the layer,. stability of the plasma, and their coupling. The result is an example configuration of a plasma of appreciable beta imbedded in an E-layer, with many features favorable toward stability.

2. SOME STABLE E-LAYERS

In this section we consider just the E-layer, together with a cold background of opposite sign to neutralize the layer. These layers could be utilized in any of the confinement geometries in the Introduction.

In order to proceed from the most stable possible situations, we first consider E-layer phase space distributions which are thermodynamically stable, aside from coupling to the walls and cold background. We take the external mirror field confining the layer to be axially symmetric, and let the distribution be a monotone decreasing function of ξ, the sum of energy and canonical angular momentum given by

$$\xi = (p^2 c^2 + m^2 c^4)^{1/2} + \alpha\left(rp_\theta + \frac{q}{c}\psi\right) + q\phi - mc^2 \tag{1}$$

where $\vec{p}$ is the kinetic momentum; $\psi = rA_\theta(r,z)$ is the total flux function for external, layer and plasma fields; q and m are the charge and mass of E-layer particles; $\phi(r,z)$ is the electrostatic potential; and α is a parameter with dimensions of frequency. It is convenient to regard ξ as a function of

$$\vec{u} = \vec{p} + \hat{\theta}\, m\gamma_r r\alpha \tag{2}$$

$$\gamma_r = \left[(p^2/m^2c^2) + 1\right]^{1/2} \tag{3}$$

Then at a fixed position in space, ξ is minimal at $\vec{u} = 0$ and increases with $|\vec{u}|$, anistropically except in the non-relativistic limit where

$$\xi_{\text{non-rel}} \to (u^2/2m) + U(r,z) \tag{4}$$

$$U = \alpha\,(q/c)\psi - 1/2\; mr^2\alpha^2 + q\phi \tag{5}$$

Thus, non-relativistically, $f_0(\xi)$ describes a "rigid rotor" rotating at frequency α.

Monotone decreasing functions of ξ $(\partial f_0/\partial\xi < 0)$ are stable if the walls are good conductors, aside from coupling to the background charges. Monotone functions are also confined, after field reversal. If $\partial f_0/\partial\xi < 0$ and U increases outward from a point, the density $\int d\vec{p}\, f_0$ is peaked at this point. Before reversal, this point lies on the axis where the most probable momentum is zero, which is inconsistent with mirror confinement of the layer on account of collisions. But after reversal, the density peaks off axis where the most probable momentum $(\vec{u} = 0)$ is $\vec{p} = -\hat{\theta} m\ \gamma_r r\alpha$. This is large for the large values of α corresponding to big orbits, as in an E-layer. Note that, inasmuch as the most probable momentum has the same sign at all r, most of the particles included in the monotone distribution $f_0(\xi)$ rotate in the same sense whether or not the field is reversed. Current at an inner radius is mainly due to eccentric orbits with foci further out. Also, the sign of α for confinement is determined $(q\alpha > 0)$ and corresponds to the sense of E-layer praticle rotation in the external field. The same qualitative features hold relativistically, though the arithmetic is complicated by the fact that the shells of constant ξ are no longer simply spheres in $\vec{u}$-space.

Stability of the monotone functions of ξ in the absence of wall resistivity and coupling to the background follows from the fact that, with these restrictions, one is free to rotate with the layer, where $\partial f_0/\partial\xi < 0$ appears as a monotone function of the energy only [non-relativistically, compare Eq. (4)]. This eliminates the negative mass (or diochotron) instability associated with the layer rotation [2] and also modes associated with the overlap of cyclotron orbits which occur in "loss cone" distributions. In fact, these instabilities are "overkilled," which will turn out to leave room for useful departures from the monotone state when a hot plasma is added (or during buildup). The thermodynamic proof follows the usual lines [3]. From a linear combination of entropy and the total particle and field energy and angular momentum, one can construct a "free energy function" which is minimized by $f_0(\xi)$ and which is a constant of the motion aside from energy transfer to the background and to the walls if they are not perfectly conducting.

If the wall conductivity is poor, the passive walls absorb energy through eddy currents, which accounts for the growth of various negative energy modes in monoenergetic beams. Also, the layer modes can couple to the background through plasma oscillations and through the tearing mode.

It has been shown that tearing is suppressed by sufficient energy spread transverse to the layer currents if the layer is not too long [4]. As we shall see, energy spread in the layer also destroys unstable coupling to a resistive wall, and it can weaken the growth rate of beam-plasma oscillations to the point that wall resistivity prevents growth. Before proceeding to verify these points and to consider the effects of adding a hot plasma, we digress to arrive at configurations of interest.

3. REVERSED-FIELD EQUILIBRIA

To relate $f_0(\xi)$ to E-layer confinement, we must make the E-layer current and the flux function ψ consistent with each other. The current has only a θ-component, of the form

$$j = \int d\vec{p}\,(qp_\theta/m\gamma_r)f_0(\xi) = rF(r,\psi) \tag{6}$$

$$j_{\text{non-rel}} \rightarrow -qr\alpha\, n_0(r,z) = -qr\alpha \int d\vec{u}\; f_0\left[(u^2/2m) + U\right] \tag{7}$$

Some non-relativistic examples are the Maxwellian,

$$f_0 \propto \exp(-\xi/T)$$

$$j_{\text{non-rel}} = -\, n_0\, r\alpha\, q \exp(-U/T) \tag{8}$$

and the "waterbag" model,

$$f_0 \propto n_0\, \theta\,(U_0 - \xi)$$

$$j_{\text{non-rel}} = -\, n_0\, r\alpha\, q\left[(U_0 - U)/T_0\right]^{3/2} \theta\,(U_0 - U) \tag{9}$$

where $T_0 = U_0 - U_{min}$ and $\theta(x) = 1$ if $x > 0$, and $\theta = 0$ if $x < 0$. Note that derivatives of j in Eq. (9) are continuous, since the first factor vanishes where the derivative of the step function is singular. Note also that the lines of constant E-layer density are not ψ level lines; for example, in Eq. (7) this is because of the centrifugal and potential energy in U.

The field satisfies

$$\mathcal{O}\psi \equiv -\frac{c}{4\pi}\left(\frac{\partial}{\partial r}\frac{1}{r}\frac{\partial\psi}{\partial r} + \frac{1}{r}\frac{\partial^2\psi}{\partial z^2}\right) = j(r,\psi) \tag{10}$$

Solving this equation involves the usual tedium of boundary value problems plus the fact that j depends on ψ, generally non-linearly. Solutions have been given for an infinitely long layer with uniform external field and no z-depedence by Tonks [5] and Enoch [6], and an analytic solution for distribution (7) by Harris [7]. Though exact solutions with z-dependence are more difficult to obtain, we can generate approximate solutions by taking advantage of the fact that ψ is fairly insensitive to details of j, and j is in turn fairly insenstive to details of $f_0(\xi)$. Thus, as a start, we can choose a ψ corresponding to the desired reverse-field configuration; choose a monotone function $f_0(\xi)$ with a few free parameters; and finally fit the corresponding j to ψ by Eq. (10). This solution can then be improved by a perturbation expansion. Let ψ_0 and j_0 represent suitable trail functions satisfying Eq. (10), and let

$$\psi = \psi_0 + \epsilon\psi_1 + \epsilon^2\psi_2 + \ldots \tag{11}$$

where ϵ is a small ordering parameter. Having chosen parameters of j determined from f_0 for a best fit to j_0, we now regard $(j - j_0)$ as first order in ϵ. Then, with primes denoting partial derivatives by ψ,

$$\mathcal{O}\psi_1 = j(r, \psi_0) - j_0 + \psi_1 j'(r, \psi_0) \tag{12}$$

$$\mathcal{O}\psi_2 = \frac{1}{2}\psi_1\, j''(r, \psi_0) + \psi_2 j'(r, \psi_0) \tag{13}$$

and so on.

The following trial function represents a thick layer with current density peaked in the midplane:

$$\psi_0 = \psi_M + \psi_E \tag{14}$$

$$\psi_M = \frac{1}{2} c_0 r^2 + \sum_{n=1}^{\infty} c_n r I_n(nKr)\cos(nKz) \tag{15}$$

$$\psi_E = -\zeta(B/k)\, rJ_1(kr)\left[(1 - a_1)\cos Kz + a_1 \cos 3Kz\right] \tag{16}$$

We let this hold radially out to the first zero of J_1. Here ψ_M represents the external mirror field and ψ_E the E-layer. This field has the property that the current, to which only ψ_E contributes, is zero on a rectangle with boundaries at $kr = 0$, $kr = 3.84$ (the first zero of J_1) and $Kz = \pm\pi/2$. Also, if we let $a_1 = 1/4$, the E-layer field ($B_{Ez} = 1/r \cdot \partial\psi_E/\partial r$, $B_{Er} = -1/r \cdot \partial\psi_E/\partial z$) is zero at the axial boundaries $Kz = \pm\pi/2$ so that in principle ψ_E can be matched to a coil at the radial boundary $kr = 3.84$.

In the important interior region where field lines close, these details of matching boundaries matter little. Also, the mirror field can be assumed gentle there, since coils outside the layer cannot produce field gradients over layer dimensions competitive with the internal field gradient of a strong current layer. Then ψ_0 can be approximated by

$$\begin{aligned}\psi_0 &\approx \frac{1}{2} R_M Br^2 - (R_M - 1)\frac{B}{K} rI_1(Kr)\cos Kz - \zeta\frac{B}{k} J_1(kr)\cos Kz \\ &\approx \frac{B}{2k^2}\left[-(\zeta - 1)(kr)^2 + \frac{1}{2}(\zeta - 1 + R_M)(kr)^2(Kz)^2 + \frac{1}{8}(\zeta - K^2/k^2)(kr)^4 + \ldots\right]\end{aligned} \tag{17}$$

where R_M is the external mirror ratio. In Fig. 1, the contours of constant ψ_0, **which** are the field lines, are plotted for a weak mirror, $R_M \to 1$. Self-consistent E-layer equilibria generated by the Layer computer code [8] produce field patterns much like those in the figure.

From Eq. (17), one finds that ψ_0 is minimal ($\vec{B} = 0$) at $z = 0$ and $r = r_0$ where

$$(kr_0)^2 = 4(\zeta - 1)/\left[\zeta - (K^2/k^2)\right] \tag{18}$$

The midplane crossing r_1 and the turning points of the outermost closed line ($\psi_0 = 0$) are

$$(kr_1)^2 = 8(\zeta - 1)/\left[\zeta - (K^2/k^2)\right] \tag{19}$$

$$(Kz)^2 = 2(\zeta - 1)/(\zeta - 1 + R_M) \tag{20}$$

These formulas are not reliable if $K \to k$. We see that the closed lines collapse to the axis at the onset of reversal ($\zeta = 1$), but begin to fill the current boundaries as ζ increases. If we had chosen to locate the current off-axis, say between two zeros of J_1, the closed lines would appear at this inner boundary.

The flux function can be further expanded around its minimum at $r = r_0$ [Eq. (18)] to see the structure of the inner closed lines. With $x = r - r_0$,

$$\psi_0 = \text{const} + a_x(kx)^2 + a_z(Kz)^2 + \ldots \tag{21}$$

$$a_x = 2(\zeta - 1) \tag{22}$$

$$a_z = 2(\zeta - 1)(\zeta - 1 + R_m)/(\zeta - K^2/k^2) \tag{23}$$

From this, we see that the ellipticity of the inner lines is determined by K/k.

To complete the derivation, we must fit some f_0 to ψ_0. The essential features, including the extent of reversal and the shape of the inner closed field lines, are determined by four relations given by Eq. (18), and by

$$\int d\vec{x} j = \int d\vec{x} j_0 \tag{24}$$

and by expanding Eq. (12) in x, z in order to match the two coefficients of x^2 and z^2 in Eq. (21), omitting the arbitrary constant. Three of the four necessary free parameters come from the magnitude, radius and mean location of f_0 in phase space [e.g. n_0, T and α in Eqs. (8) and (9)]. These may be regarded as determining the density, thickness and radius of the current layer. The remaining parameter determines the foreshortening and bulging out of the current profile as the layer "pinches" with increasing reversal. This determines the ellipticity of the field lines, which essentially follow the shape of the current, through K/k in the above formulas. Thus, the fourth relation is satisfied by varying K/k in the trial function. Boundary matching is approximately taken into account by the fact that Eq (21) is a power expansion of Eq. (17). Carrying the perturbation procedure further is generally unnecessary if the closed line region is of primary interest.

4. ADDITION OF A HOT PLASMA

We now consider how to hollow out a region of the E-layer in which to confine hot plasma, as indicated in the Introduction. In principle, this can be accomplished by subtracting two monotone functions f_{01} and f_{02} such as those discussed above. It is, of course, essential that the difference be nowhere negative. In practice, this is a strong constraint which more or less forces us to choose α the same in f_{01} and f_{02} and limits the extent to which the current can be suppressed. Also, note that the current centroid and the field minimum $r = r_0$ where the plasma should be located tend to be separated by the centrifugal force. While the current and ψ

level lines (field lines) begin to merge as ζ increases, this can never be complete and comes at the expense of decreasing α and hence increasing n_0 for the same current. Thus, it is not possible to remove the E-layer from the plasma region only. To depress the current there, it must be depressed somewhere else as well.

The least current is removed if we depress current in a shell which contains all or a portion of the plasma region. This could be accomplished, for example, with waterbag models. With the notation of Eq. (9), let

$$f_0 = C\theta(U_0 - \xi) - C_1\left[\theta(U_2 - \xi) - \theta(U_1 - \xi)\right] \tag{25}$$

where U_2 and U_1 are the values of U (or its relativistic counterpart) at the boundaries of the plasma or at some interior points. It is necessary that $C_1 \le C$ to insure $f_0 \ge 0$. The current is, non-relativistically,

$$\begin{aligned} j = -r\alpha q\Big\{ & C(T_0)^{3/2}\left[(U_0 - U)/T_0\right]^{3/2}\theta(U_0 - U) - C_1(T_2)^{3/2} \\ & \times\left[(U_2 - U)/T_2\right]^{3/2}\theta(U_2 - U) + C_1(T_1)^{3/2}\left[(U_1 - U)/T_1\right]\theta(U_1 - U)\Big\} \end{aligned} \tag{26}$$

From this we see that j is depressed in the region of the plasma by a fraction

$$\Delta j/j = C_1/C\left[(T_2^{3/2} - T_1^{3/2})/T_0^{3/2}\right] \tag{27}$$

again with the notation of Eq. (9).

As a typical case, let $\zeta = 1.6$ in which case $k r_1 \approx 1/2(3.84) \approx 2$ which lies near the current centroid and $T_j = U_j = U_{min} = U_j + 1/2\, m\, r_1^2\alpha^2$; $U_1 = -3/8\, m\, r_1^2\alpha^2$, and $U_0 = 0$. Then, $\Delta j/j \approx 1/2\,(C_1/C)$. Thus, through the freedom in C_1 we can comfortably remove up to about half of the E-layer current from the plasma region. A portion of this is to be replaced by plasma current, $j_p(\psi)$, which has a form $\propto r\, n_p(\psi)$. In principle it is necessary to redo the self-consistent perturbation calculation with j_p included in j in Eqs. (10)-(13). However, so long as the net current removed is not a big fraction of the whole, this is not essential.

The main effect is in the steep current gradient produced in the neighborhood of the plasma. Approximately, the difference is that in ψ_0 one should keep a non-linear term in the conic function on the right side of Eq. (21),

$$\psi_0 \approx \text{const} + A_1\left[a_x(kx)^2 + a_z(Kz)^2\right] + A_2\left[a_x(kx)^2 + a_z(Kz)^2\right]^n + \dots \tag{28}$$

for some $n > 1$. If $n = 1$, the current is uniform; the nonuniformity is reflected in $n > 1$. That the constant current term does not vanish completely reflects the fact that $\Delta j/j < 1$. For small j_2, $A_1 \approx 1 - \Delta j/j$ and $A_2 \propto \Delta j/j$. Depending on the plasma pressure profile, Eq. (28) could also involve a cross term, depending on the azimuthal angle in the elliptical coordinate system defined by the field lines. Having in mind roughly circular lines, we have dropped this term in order to display the essential features.

To add the hot plasma, approximately we need only increase Δj by j_p, with A_1 and A_2 altered accordingly. This neglects the effect of j_p in determining ψ which in turn determines the level lines of j_p. It is valid to do this if $\Delta j \ll j$.

5. STABILITY OF THE PLASMA

We now consider the stability of a finite-β plasma imbedded at the minimum of a field such as Eq. (28). Here we regard the E-layer as rigid (ψ_E constant). Coupling between the layer and the plasma is discussed in the next section.

The most important consideration is MHD stability, as a function of plasma β where $\beta = 8\pi p/B^2$, p being the plasma pressure. At low β, plasma located in the minimum-B region of ψ_0 should be adequately stable if the radius of the containment region is not too small. Universal modes are eliminated both by the short length of lines relative to the plasma radius [9], roughly 2π for circular geometry, and by the steep magnetic gradient. We will not consider these further, except to examine the effects of the few particles with large $v_\parallel$. Also, we shall not consider in this section plasma modes at the cyclotron frequency and above, which are not expected to cause appreciable diffusion in toroidal confinement [3].

To fix ideas, we first consider circular field lines, $a_x \approx a_z$, and we neglect E-layer "toroidal" effects. That is, x plays the role of a Cartesian coordinate, which is equivalent to replacing the toroidal current layer by a long cyclinder. We shall examine corrections to this model presently.

The model can be analyzed by a straightforward application of the energy principle [11], so long as we remember that the "external" E-layer field is not a vacuum field ($\nabla \times B \neq 0$). We consider displacements varying as $\vec{\xi}(r) \exp i(m\phi + k_z z)$ in a cylindrical coordinate system with the z-axis parallel to the E-layer current where $r^2 = x^2 + z^2$ in Eq. (28). In three interesting limits we find

$$\delta W = \frac{1}{2}\int d\vec{x}\, \frac{\xi_r^2}{4\pi\Gamma p + B^2}\left[4\pi p' + rB\frac{\partial}{\partial r}\left(\frac{B}{r}\right)\right]\left[\frac{\Gamma}{B}\, r\, \frac{\partial}{\partial r}\left(\frac{B}{r}\right) p - p'\right],\; m = 0 \tag{29}$$

$$\delta W = \frac{1}{2}\int d\vec{x}\left\{\frac{B^2}{4\pi}\frac{m^2}{r^2} - \frac{p'}{B^2}\left[4\pi p' + rB\frac{\partial}{\partial r}\left(\frac{B}{r}\right)\right]\right\}\xi_r^2,\quad k_z r \gg m \tag{30}$$

$$\delta W = \int \frac{d\vec{x}}{8\pi}\left\{Q^2 - \frac{\beta}{2(m/r)^2}\, Q_r^2\left(\frac{p'}{p}\right)^2\right\}\quad k_z r \ll m \tag{31}$$

Here B is the total field including plasma and E-layer and external fields, which has only an azimuthal component. Also $p' = \partial p/\partial r$, constant pV^Γ is the pressure law, and $Q = \nabla \times (\vec{\xi} \times \vec{B})$ is the magnetic field perturbation.

These limits correspond to interchange, "ballooning" and tearing modes, in that order. From Eq. (31), tearing instability of the plasma alone does not occur as $\beta > 1$ is required; we shall return to this matter in discussing coupling to the E-layer. In Eq. (29), the second factor in the integrand is positive, since $p' < 0$ (pressure is maximum at $r = 0$) and B increases at least linearly with r, for the field of Eq. (28). Thus the interchange stability criterion, to make $\delta W > 0$, becomes

$$4\pi p' + rB\frac{\partial}{\partial r}\left(\frac{B}{r}\right) > 0 \tag{32}$$

This condition is also sufficient, but not necessary, to make $\delta W > 0$ in Eq. (30). That is, pure interchange (m = 0) is the worst mode. Ballooning instability in the usual sense, meaning an interchange localized to a bad gradient region, does not occur as there are no bad regions. To bend the line ($m \neq 0$) merely costs energy, as in Eq. (30).

As Ohkawa has pointed out [12], if $B \propto r$ corresponding to a uniform current density [$A_2 = 0$ in ψ_0, Eq. (28)], Eq. (32) indicates neutral stability at zero pressure and instability for $p' \neq 0$. But if $B \propto r^n$ with $n > 1$, Eq. (32) indicates stability for finite plasma β. A convenient way to express the critical β is in terms of the total plasma and E-layer currents within the plasma containment region,

$$I_p = \int_0^r 2\pi r dr\, J_p \tag{33}$$

$$I_E = \int_0^r 2\pi r dr\, J_E \tag{34}$$

Then, from the equilibrium condition $p' = -J_p B$ and integrating $\nabla \times \vec{B} = 4\pi(\vec{J}_p + \vec{J}_E)$ in r, Eq. (32) can be written as

$$(\pi r^2 J_E - I_E) > I_p \tag{35}$$

In a rough sense, the left side can be interpreted as the current removed in hollowing out the E-layer and the right side is the plasma current introduced, independent of details of the size and profile of the hollow.

We now turn to corrections to this model. To obtain an estimate of the effects, we compute $\oint d\ell/B$ for lines departing from a circle by a small aspect ratio R_p/r_0, where R_p is the plasma radius and r_0 is radial position, given by Eq. (18). To isolate effects, we take uniform current density [$A_2 = 0$ in Eq. (28)] which we found to correspond to neutral stability for $p' \to 0$. The calculation is straightforward but tedious. From the flux function

$$\psi = r \int d\vec{x}\, \frac{j(\vec{x}')}{|\vec{x} - \vec{x}'|} \tag{36}$$

we extract the magnetic field from which we obtain

$$\frac{\delta \oint \frac{d\ell}{B}}{\oint \frac{d\ell}{B}} = -\frac{1}{64} \frac{R_p^2}{r_0^2} \tag{37}$$

Thus, the neglected toroidal curvature has a weak stabilizing influence.

The effects of line ellipticity have been calculated from the Vlasov equation, which also provides a check on the above results for circular lines. Standard integration techniques lead to

$$\begin{aligned} f_1 = {} & -e\frac{\partial f_0}{\partial \epsilon} \frac{E_z}{ik_z} - \left(c \frac{\partial f_0}{\partial \psi} \frac{k_z}{\omega} + e \frac{\partial f_0}{\partial \epsilon}\right) \int_{-\infty}^{t} \frac{ds}{w} \exp\left\{-i \int_s^{s'} \frac{ds''}{w} \left[\omega - k_z v_D(s)\right]\right\} \\ & \times \left\{\frac{E_z}{ik_z}\left(1 - \frac{k_z^2 v_\perp^2}{\omega_{ce}^2}\right) + w\left(\hat{b} \cdot \vec{E} - \hat{b} \cdot \nabla \frac{E_z}{ik_z}\right) + \frac{k_z v_\perp^2}{2\omega_c}\left(\hat{a} \cdot \vec{E} - \hat{a} \cdot \nabla \frac{E_z}{ik_z}\right)\right\} \end{aligned} \tag{38}$$

Here f_1 is the perturbation of the distribution function; $v_D(s)$ is the drift velocity; ϵ the particle kinetic energy; w and $v_\perp$ the parallel and perpendicular velocities; k_z the wavenumber in the $\hat{z}$ (current) direction; $\hat{b}$ the unit vector along the line; $\hat{a}$ the unit vector in the density gradient direction; and f_0 is the equilibrium distribution function. In deriving the above expression we have made the usual low-frequency assumption, i.e., $\omega \ll \omega_{ci}$ and $k_\perp a_i \ll 1$. There are some Larmor radius terms kept in anticipation of cancellations which occur in the perturbed charge density. Now in general $\vec{E} = -\nabla\phi - (i\omega/c)\vec{A}$; however, there are essentially three independent choices for $\vec{A}$. The choice $\vec{A} = \hat{b}(\hat{b} \cdot \vec{A})$ leads to ballooning, which is not considered here since the macroscopic drifts are constructed to be favorable everywhere along the line. The choice $\vec{A} = \hat{z}(\hat{z} \cdot \vec{A})$ leads to tearing modes which are stable, as discussed in Eq. (31). Finally, the choice $\vec{A} = \hat{a}(\hat{a} \cdot \vec{A})$ incorporates the effect of line bending on the interchange modes with which we are concerned. Inserting Eq. (38) in Maxwell's equations (Poisson's and the $\vec{j} \cdot \hat{a}$ equation) we obtain, in a straightforward manner, the relation

$$- \frac{\frac{\partial}{\partial\psi} \oint \frac{d\ell}{B}}{\int \frac{d\ell}{B}} > - \frac{\frac{\partial p}{\partial\psi} \oint \frac{d\ell}{B^2}}{\oint d\ell} \tag{39}$$

for stability. To determine the effects of departing from circularity, we again use a perturbative technique, i.e., we write

$$\psi = \frac{1}{27} B_0^3 \left[1 + \frac{3\epsilon^2}{2}\right]^{-3/2} r^3 (1 + \epsilon \cos^2\theta)^3, \quad \epsilon \ll 1 \tag{40}$$

and insert this in Eq. (39) to obtain

$$\frac{1}{3\psi} > - \frac{\partial p}{\partial\psi} \frac{8\pi}{B_0^2} \frac{1}{\psi^{4/3}} \left(1 - \frac{5}{9}\epsilon^2\right) \tag{41}$$

as a stability criterion. We have normalized the magnetic field energy integrated over all space to be the same for both ϵ finite and $\epsilon = 0$. It is immediately obvious that disturbing the lines in the prescribed fashion has a stabilizing influence.

Finally, we consider the effects of the high parallel velocities which have unfavorable drifts. It should be pointed out that since these particles circulate freely, trapped particle modes [13] should not be a problem. However, these particles do provide the energy to destabilize the drift mode. For this mode to go, it is necessary to slow down the phase velocity of the waves below that of the ion diamagnetic current velocity which generates the restraint

$$k_\perp^2 \lambda_{Di}^2 \approx \frac{\omega_{ci}^2}{\omega_{pi}^2} < \frac{\frac{\partial}{\partial\psi} \oint \frac{d\ell}{B}}{\oint \frac{d\ell}{B}} \frac{\partial p}{\partial\psi} \tag{42}$$

for stability, where ω_{pi} and ω_{ci} are the ion plasma and cyclotron frequencies. Thus, this mode only occurs for low density. Resonance of the wave with the bounce frequency of the particles also leads to this drift instability with the same density threshold.

6. STABILITY OF THE COMBINED SYSTEM

We conclude by considering the effect of E-layer dynamics on the foregoing stability analysis. In this, we can rely heavily on previously published work [4], [14].

The most important phenomena are likely to be tearing, at low frequency, and coupling with plasma oscillations. Now, we have seen that tearing of the plasma alone does not occur. It has also been shown that parallel pressure stabilizes tearing of the layer alone [4], and Morse has found by computer simulation that the layer tends to find this state [15]. The combined system is then also stable. At threshold ($\omega \to 0$), for a tearing perturbation the E-layer contributes a destabilizing negative term in the integrand of Eq. (31) which is, however, $< Q^2$ if the E-layer alone is stable. The plasma term is also negative, but $< Q^2$ by a factor of $\lesssim \beta/2$. Thus, while the destabilizing effects do add, a plasma with β a few tenths does not drive the E-layer unstable unless it is on the brink of instability by itself.

Turning to plasma oscillations, we consider coupling to the hybrid frequency as an example case. The approximate dispersion relation, corresponding to a perturbation $E_\theta \exp i\ell\theta$, is

$$b^+ + b^- = \frac{\omega_p^2}{\omega^2 - \omega_c^2} + K\,\omega_{pE}^2 \int \frac{d\Omega\, P(\Omega)}{(\omega - \ell\Omega)^2 - \Omega^2}. \tag{43}$$

The first term on the right represents either plasma ions or electrons, depending on the case of interest, ω_p and ω_c being the corresponding plasma and cyclotron frequencies. The second term on the right represents the E-layer. The factor contains relativistic effects. It may be positive or negative, depending on whether the energy is above or below the transition energy of accelerator terminology. The gyrofrequency Ω varies with particle constants of motion with a probability distribution $P(\Omega) \propto J(-\partial f_0/\partial\xi)$, where J is the Jacobian of transforming to ω_0 as a variable. The quantities b^+ and b^- which take account of the surrounding walls are related respectively to the H-wave impedance at the outer and inner boundaries of the current layer. They are calculated in Ref. [14] for an infinitely thin layer, but the effects of the walls will not be qualitatively different for a layer of reasonable thickness so long as E_θ varies slowly across the layer. In general, $b^+ + b^-$ will have a real part either $\lessgtr 0$, and an imaginary part arising from the resistance in the walls. The imaginary part is always > 0.

This dispersion relation yields many of the instabilities characteristic of monoenergetic beams if $P = \delta(\Omega - \Omega_0)$, depending on parameters. Thus $K < 0$ yields the negative mass instability [14], or the resistive wall instability if $\mathrm{Im}(b_+ + b_-) \neq 0$ [16]. The hybrid instability occurs if $\omega \approx (\omega_p^2 + \omega_c^2)^{1/2} \approx \rho\omega_0$. These instabilities tend to go away if $P(\Omega)$ has suffient spread and if the wall resistance term is large enough. The necessary condition is that the spread $\Delta\Omega > \gamma$, so that the singularities at $\omega = \ell\Omega$ merely contribute poles. This is not difficult to satisfy for a thick layer, where $\Delta\Omega$ can approach Ω and $\gamma < \omega_{pE} \lesssim \Omega$. Then the dispersion relation becomes

$$b_+ + b_- = \frac{\omega_p^2}{\omega^2 - \omega_c^2} + \frac{iK\pi\,\omega_{pE}^2}{2\,\Omega_0^2}\left[-\left.\frac{P(Q)}{Q}\right|_{Q=\frac{\Delta\Omega}{\Omega_0}} + \left.\frac{P(\Omega)}{Q}\right|_{Q=-\frac{\Delta\omega}{\Omega_0}} \right]. \tag{44}$$

where $\Delta\omega = \omega - n\Omega_0$ and Ω_0 is the mean frequency in the distribution. Now irrespective of the signs of K, $(b_+ + b_-)$ and P, there is no instability ($\mathrm{Im}\,\omega > 0$) if

$$\mathrm{Im}(b_+ + b_-) > \frac{\pi\omega_{pE}^2}{\Omega_0^2} \left| \frac{KP(Q)}{Q} \right| \tag{45}$$

For a relativistic E-layer, the right side of Eq. (45) is of order unity, and the left side can be quite large. By contrast with a slow beam, in which perturbation fields tend to be isolated to the beam and fall off like $r^{-\ell}$ the relativistic beam radiates fields to the walls, where they tend to pile up corresponding to $|b_\pm| > 1$. For the wall structure in the present Astron experiments, both the real and imaginary parts are of order unity for values of $\ell \lesssim 10$. For higher values resonances with the wall structure will be encountered. This and other refinements of beam-plasma interaction need much further study. We would expect, however, that we have examined the potentially worst cases. For example, while hollowing out the layer causes P to be negative for certain values of Ω, resistive wall stabilization also insures that this does not cause instability so long as the distribution removed is a smooth function of ξ.

ACKNOWLEDGMENT

We are grateful to Dr. W. A. Newcomb for much help with the calculations of Section V.

REFERENCES

[1] CHRISTOFILOS, N. C., Proc. 2nd UN Int. Conf. PUAE 32 (1958) 279; [1a] Nucl. Fusion 1962 Suppl., Pt. I, p. 159; [1b] Phys. Fluids 9 (1966) 1425; [1c] Lawrence Radiation Laboratory, Livermore, UCID-15241, Rev. I, Nov. 1967 and UCID-15282, Dec. 1967.

[2] NIELSEN, C. E., SESSLER, A. M., SYMON, K. B., Proc. Int. Conf. High Energy Accelerators and Instrumentation (CERN, Geneva, 1959), p. 239.

[3] FOWLER, T. K., Phys. Fluids 8 (1965) 459; (erratum) 8 (1965) 2120.

[4] NEIL, V. K., Phys. Fluids 5 (1962) 14.

[5] TONKS, L., Phys. Rev. 118 (1960) 390.

[6] ENOCH, J., Phys. Fluids 9 (1966) 299.

[7] Discussed in FURTH, H. P., Nucl. Fusion 1962 Suppl., Pt. I, p. 169.

[8] KILLEEN, J., ROMPEL, S. L., J. Comp. Phys. 1 (1966) 29.

[9] KRALL, N. A., ROSENBLUTH, M. N., Phys. Fluids 8 (1965) 1488.

[10] FOWLER, T. K. GUEST, G. E., Plasma Physics and Controlled Nuclear Fusion Research (IAEA, Vienna, 1966) Vol. I, p. 383.

[11] BERNSTEIN, I. B., et al., Proc. Roy. Soc. 244 (1957) 17.

[12] OHKAWA, T., private communication.

[13] ROSENBLUTH, M. N., private communication.

[14] BRIGGS, R. J., NEIL, V. K., Plasma Phys. 9 (1967) 209; also references therein.

[15] MORSE, R. L., Bull. Am. Phys. Soc. 13 (1968) 713.

[16] FURTH, H. P., Phys. Fluids 8 (1965) 220.

DISCUSSION

R. S. PEASE: You said in your oral presentation that stability calculations require that the E-layer electrons move in the high-field region. Does this not seriously increase the energy loss from synchrotron radiation?

T. K. FOWLER: For the model of plasma embedded in a fat E-layer, which I discussed, the particles are in a high field. But, as I said, I was not restricting myself to electrons. As a reactor, this model is in fact more appropriate for relativistic protons, for which there is no radiation problem.

H. P. FURTH: If I understood your oral presentation correctly, the hydromagnetic stability of the plasma that is to be contained by the Astron requires a "hollow" distribution of the relativistic electrons. It seems to me that this type of "hollow" is rather similar to what Seidl in Czechoslovakia and Volosov at Novosibirsk have studied, both theoretically and experimentally, and have found to be particularly unstable. What is the feature of your proposed design that leads you to conclude that the "hollow" will remain stable?

T. K. FOWLER: My model is that of a rigid rotor. The hole is a hole in energy in the frame of rotation. This is anisotropy in a sense different from the distributions of two different canonical momenta treated in other models (such as Coppi's) and no doubt in some other experiments. I am grateful to you for bringing up a similar point earlier in private discussions; this has given me time to give the question more thought, and I have come to the conclusion that the hole is an additional source of instability. However, the stability criterion is less severe than the ordinary tearing which was treated.

R. C. WINGERSON: The need for large currents in the Astron E-layer implies injection of excess charge. The greater the field reversal, the less communication between the E-layer and the end walls. Excess charge accumulation may lead to large DC electric fields. Should these not be considered in the analysis?

T. K. FOWLER: The confinement of the E-layer particles is open-ended. I do not see why large electrostatic fields should develop.

M. LESSEN: We have studied a closely related problem at Rochester; namely, the stability with respect to a travelling wave perturbation of a plane, thick E-layer having on both sides a plasma with embedded magnetic fields out to infinity. The perturbation wave number vector was generally taken non-parallel to the motion in the E-layer.

It was found that the E-layer is unstable with respect to both the symmetric (sausage) and the anti-symmetric (kink) modes of the disturbance. The growth rate decreased with increasing E-layer energy.

Since the disturbance phase velocity along the E-layer is generally higher than the velocity of propagation in the surrounding plasma, it appears as a wave train radiating out of the E-layer. If the disturbance occurs at a resonant frequency of the plasma it may be an attractive way to heat the plasma.